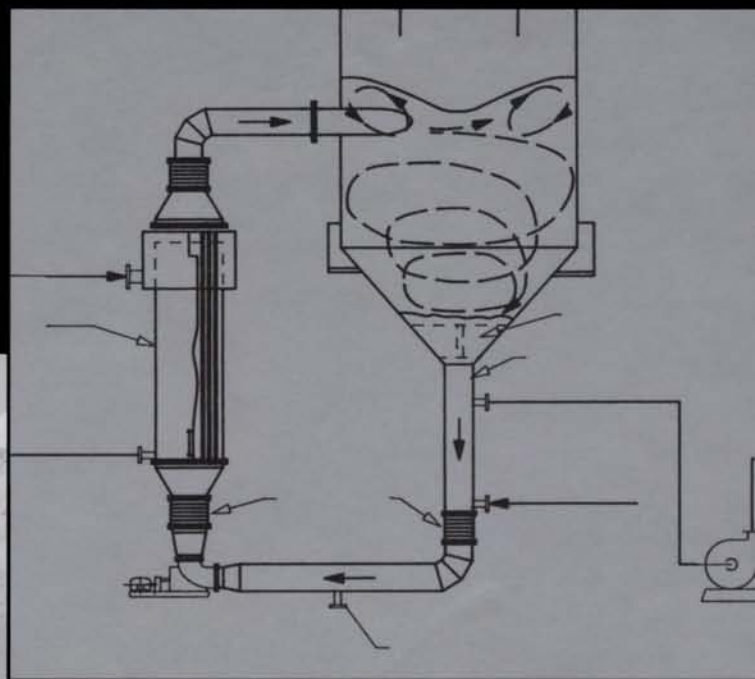


Handbook of Industrial Crystallization

Second Edition



Allan S. Myerson



Handbook of Industrial Crystallization

Second Edition

This Page Intentionally Left Blank

Handbook of Industrial Crystallization

Second Edition

Edited by

Allan S. Myerson

Professor of Chemical Engineering and
Dean, Armour College of Engineering
and Science
Illinois Institute of Technology

BUTTERWORTH
HEINEMANN

Boston • Oxford • Johannesburg • Melbourne • New Delhi • Singapore

Copyright © 2002 by Butterworth-Heinemann



A member of the Reed Elsevier group All rights reserved.

No part of this publication may be reproduced, stored in a retrieval system, or transmitted in any form or by any means, electronic, mechanical, photocopying, recording, or otherwise, without the prior written permission of the publisher.



Recognizing the importance of preserving what has been written, Butterworth-Heinemann prints its books on acid-free paper whenever possible.



Butterworth-Heinemann supports the efforts of American Forests and the Global ReLeaf program in its campaign for the betterment of trees, forests, and our environment.

Library of Congress Cataloging-in-Publication Data

Handbook of industrial crystallization / edited by
Allan S. Myerson.—2nd ed.

p. cm.

Includes bibliographical references and index.

ISBN 0-7506-7012-6 (alk. paper)

1. Crystallization—Industrial applications. I. Myerson,
Allan S., 1952-

TP156.C7 H36 2001

660'.284298—dc21

2001037405

British Library Cataloguing-in-Publication Data

A catalogue record for this book is available from the British Library.

The publisher offers special discounts on bulk orders of this book.
For information, please contact:

Manager of Special Sales
Butterworth-Heinemann
225 Wildwood Avenue
Woburn, MA 01801-2041
Tel: 781-904-2500
Fax: 781-904-2620

For information on all Butterworth-Heinemann publications
available, contact our World Wide Web home page
at: <http://www.bh.com>

10 9 8 7 6 5 4 3 2 1

Printed in the United States of America

Contributors

Stephen R. Anderson

DuPont Pharmaceuticals
Deepwater, New Jersey

Richard C. Bennett

Swenson Process Equipment Inc.
(Retired)
Harvey, Illinois

K.A. Berglund

Department of Chemical Engineering
Michigan State University
East Lansing, Michigan

H.C. Bülau

Gebr. Kaiser
Krefeld, Germany

Rajiv Ginde

International Specialty Products
Wayne, New Jersey

Daniel Green

DuPont
Central Research & Development
Wilmington, Delaware

Richard W. Hartel

Department of Food Science
University of Wisconsin-Madison
Madison, Wisconsin

Peter Karpinski

Novartis Pharmaceuticals
East Hanover, New Jersey

D.J. Kirwan

Department of Chemical Engineering
University of Virginia
Charlottesville, Virginia

Diana L. Klug

Boeing Company
Seattle, Washington

Paul Meenan

DuPont Pharmaceuticals
Deepwater, New Jersey

S.M. Miller

Eastman Chemicals
Kingsport, Tennessee

Allan S. Myerson

Department of Chemical Engineering
Illinois Institute of Technology
Chicago, Illinois

C.J. Orella

Merck Sharp & Dohme Research Laboratories
West Point, Pennsylvania

J.B. Rawlings

Department of Chemical Engineering
University of Minnesota
Minneapolis, Minnesota

Albert M. Schwartz

Abbott Laboratories
North Chicago, Illinois

C.W. Sink

Eastman Chemicals
Kingsport, Tennessee

J. Ulrich

Department of Chemical Engineering
Martin-Luther-University
Halle-Wittenberg
Halle, Germany

J.S. Wey

Eastman Chemicals
Rochester, New York

John Wiencek

Department of Chemical & Biochemical Engineering
University of Iowa
Iowa City, Iowa

This Page Intentionally Left Blank

Contents

PREFACE TO THE FIRST EDITION	xi	Nomenclature	63
		References	63
PREFACE TO THE SECOND EDITION	xiii		
CHAPTER 1 SOLUTIONS AND SOLUTION PROPERTIES	1	CHAPTER 3 THE INFLUENCE OF IMPURITIES AND SOLVENTS ON CRYSTALLIZATION	67
<i>Albert M. Schwartz and Allan S. Myerson</i>		<i>Paul A. Meenan, Stephen R. Anderson, and Diana L. Klug</i>	
1.1. Introduction and Motivation	1	3.1. Introduction	67
1.2. Units	1	3.2. Factors Determining Crystal Shape	67
1.3. Solubility of Inorganics	1	3.2.1. The Role of the Solid State in Shape Development	68
1.3.1. Basic Concepts	1	3.3. Influence of Solvents on Volume and Surface Diffusion Steps	70
1.3.2. Sparingly Soluble Species—Dilute Solutions	4	3.4. Structure of the Crystalline Interface	71
1.3.3. Concentrated Solutions	5	3.5. Factors Affecting Impurity Incorporation	72
1.4. Solubility of Organics	11	3.5.1. Equilibrium Separation	72
1.4.1. Thermodynamic Concepts and Ideal Solubility	11	3.5.2. Nonequilibrium Separation	74
1.4.2. Regular Solution Theory	13	3.5.3. Experimental Approaches to Distinguishing Impurity Retention Mechanism	78
1.4.3. Group Contribution Methods	14	3.6. Effect of Impurities on Crystal Growth Rate	80
1.4.4. Solubility in Mixed Solvents	14	3.6.1. Effect on the Movement of Steps	80
1.4.5. Measurement of Solubility	15	3.6.2. Impurity Adsorption Isotherms	82
1.5. Supersaturation and Metastability	16	3.6.3. Growth Models Based on Adsorption Isotherms	83
1.5.1. Units	16	3.7. Some Chemical Aspects of Solvent and Impurity Interactions	86
1.5.2. Metastability and the Metastable Limit	17	3.8. Tailor-Made Additives	90
1.5.3. Methods to Create Supersaturation	18	3.9. Effect of Solvents on Crystal Growth	93
1.6. Solution Properties	20	3.9.1. Role of the Solvent	93
1.6.1. Density	20	3.9.2. Jackson α -Factor	94
1.6.2. Viscosity	20	3.9.3. Effect of α -Factor on Growth Mechanism	95
1.6.3. Diffusivity	22	3.10. Summary	96
1.7. Thermal Properties	25	References	97
1.7.1. Heat Capacity	26		
1.7.2. Latent Heat	27	CHAPTER 4 ANALYSIS AND MEASUREMENT OF CRYSTALLIZATION UTILIZING THE POPULATION BALANCE	101
1.7.3. Heats of Mixing, Solution, and Crystallization	28	<i>K.A. Berglund</i>	
Nomenclature	29	4.1. Particle Size and Distribution	101
References	30	4.2. Measurement of Size Distribution	102
CHAPTER 2 CRYSTALS, CRYSTAL GROWTH, AND NUCLEATION	33	4.3. The Mixed Suspension, Mixed Product Removal (MSMPR) Formalism for the Population Balance	104
<i>Allan S. Myerson and Rajiv Ginde</i>		4.3.1. Mass Balance	106
2.1. Crystals	33	4.4. Generalized Population Balance	107
2.1.1. Lattices and Crystal Systems	33	4.5. Extension and Violations of the MSMPR Model	107
2.1.2. Miller Indices and Lattice Planes	35	4.5.1. Size-Dependent Crystal Growth	107
2.1.3. Crystal Structure and Bonding	35	4.5.2. Growth Rate Dispersion	108
2.1.4. Polymorphism	38	4.5.3. Methods to Treat Experimental Data	108
2.1.5. Isomorphism and Solid Solutions	40	4.5.4. Agglomeration	110
2.1.6. Imperfections in Crystals	40	4.5.5. Alteration of Residence Time Distribution to Control CSD	111
2.1.7. Crystal Habit	41	4.6. Summary	113
2.1.8. Prediction of Crystal Habit	42	Nomenclature	113
2.2. Nucleation	43	References	113
2.2.1. Homogeneous Nucleation	45		
2.2.2. Heterogeneous Nucleation	46	CHAPTER 5 CRYSTALLIZER SELECTION AND DESIGN	115
2.2.3. Secondary Nucleation	46	<i>Richard C. Bennett</i>	
2.2.4. Nucleation Kinetics	50	5.1. Fundamentals	115
2.2.5. Application to Industrial Crystallizers	52	5.1.1. Definition	115
2.3. Crystal Growth	53	5.1.2. Heat Effects in a Crystallization Process	115
2.3.1. Basic Concepts	53		
2.3.2. Theories of Crystal Growth	54		
2.3.3. Crystal Growth Kinetics	57		
2.3.4. Ostwald Ripening	61		
2.3.5. Size-Dependent Growth and Growth Rate Dispersion	62		

5.1.3. Yield of a Crystallization Process	116	6.6. Experimental Techniques	152
5.1.4. Fractional Crystallization	116	6.6.1. Supersaturation Measurements	152
5.1.5. Nucleation	117	6.6.2. Constant Composition Method	152
5.1.6. Population Density Balance	118	6.6.3. Critical Growth Rate Measurements	153
5.1.7. Crystal Size Distribution	118	6.6.4. 'Instantaneous' Mixing Devices	153
5.1.8. Crystal Weight Distribution	119	6.6.5. Sizing of Precipitates	153
5.1.9. Contact Nucleation	120	6.7. Modeling and Control of Crystal	
5.1.10. Crystallizers with Fines Removal	120	Size and CSD	154
5.1.11. Cyclic Behavior	122	6.7.1. Modeling of Crystal Size Distribution	154
5.2. Selection of a Crystallizer	123	6.7.2. Size Control	156
5.2.1. Information Required for Evaluation	123	6.8. Precipitation in Practice	157
5.2.2. Solubility	123	6.8.1. Continuous Precipitation	158
5.2.3. Scale of Operation	124	6.8.2. Batch Precipitation	158
5.2.4. Batch or Continuous Operation	124	6.9. Summary	158
5.2.5. Multistage Crystallizers	124	Nomenclature	159
5.2.6. Mechanical Vapor Recompression	126	References	159
5.2.7. Reactive Crystallizers	126		
5.3. Equipment Types	127	CHAPTER 7 MELT CRYSTALLIZATION	161
5.3.1. Batch Crystallizers	127	<i>J. Ulrich and H.C. Bülow</i>	
5.3.2. Fluidized Suspension Crystallizer	128	7.1. Definitions	161
5.3.3. Forced-Circulation Crystallizer	129	7.2. Benefits of Melt Crystallization	161
5.3.4. Draft Tube Baffle (DTB) Crystallizer	129	7.3. Phase Diagrams	162
5.3.5. Surface-Cooled Crystallizers	130	7.3.1. What to Learn from Phase Diagrams	162
5.3.6. Direct-Contact Refrigeration Crystallizers	131	7.3.2. How to Obtain Phase Diagrams	163
5.3.7. Teflon Tube Crystallizer	131	7.4. Crystallization Kinetics	163
5.3.8. Spray Crystallization	132	7.4.1. Importance of the Crystallization Kinetics to	
5.3.9. General Characteristics	133	Melt Crystallization	163
5.4. Crystallizer Design Procedure	133	7.4.2. Theoretical Approach to Crystallization	
5.5. Instrumentation and Control	136	Kinetics	164
5.5.1. Liquid Level Control	136	7.5. Solid Layer Crystallization	166
5.5.2. Absolute Pressure Control	136	7.5.1. Advantages	166
5.5.3. Magma (Slurry) Density Recorder Controller	136	7.5.2. Limitations	167
5.5.4. Steam Flow Recorder Controller	137	7.6. Suspension Crystallization	167
5.5.5. Feed-Flow Recording Controller	137	7.6.1. Advantages	167
5.5.6. Discharge Control	137	7.6.2. Limitations	167
5.5.7. Miscellaneous	137	7.7. Concepts of Existing Plants	167
5.5.8. Distributed Control Systems	137	7.7.1. Solid Layer Processes	167
5.5.9. Discharging	137	7.7.2. Suspension Process Concepts	171
5.5.10. Sampling	137	7.8. The Sweating Step	173
5.6. Crystallizer Costs	138	7.9. The Washing Step	174
Nomenclature	139	7.10. Continuous Plants	175
References	140	7.10.1. Advantages	175
CHAPTER 6 PRECIPITATION PROCESSES	141	7.10.2. Process Concepts	175
<i>P.H. Karpinski and J.S. Wey</i>		7.10.3. Problems	177
6.1. Introduction	141	7.10.4. Summary and a View to the Future	177
6.2. Physical and Thermodynamic Properties	141	References	177
6.2.1. Supersaturation Driving Force and Solubility	141		
6.2.2. The Gibbs-Thomson Equation and Surface Energy	142	CHAPTER 8 CRYSTALLIZER MIXING:	
6.2.3. Precipitation Diagrams	142	UNDERSTANDING AND MODELING	
6.2.4. Surface Chemistry and Colloid Stability	143	CRYSTALLIZER MIXING AND SUSPENSION FLOW	181
6.3. Nucleation Kinetics	143	<i>Daniel Green</i>	
6.3.1. Kinetics of Primary Nucleation	143	8.1. Introduction	181
6.3.2. Investigations of Nucleation Kinetics	144	8.2. Crystallizer Flows	181
6.4. Crystal Growth Kinetics	146	8.3. Distribution of Key Variables in Crystallizers	182
6.4.1. Growth Controlled by Mass Transport	146	8.4. Crystallizers	184
6.4.2. Growth Controlled by Surface Integration	146	8.4.1. Agitated Suspension	184
6.4.3. Growth Controlled by Combined Mechanisms	147	8.4.2. Fluidized Bed	187
6.4.4. Critical Growth Rate	147	8.4.3. Melt Crystallizers	188
6.4.5. Other Factors Affecting Crystal Growth	148	8.4.4. Feed Strategies	188
6.5. Other Processes Attributes in Precipitation	148	8.4.5. Agitators	188
6.5.1. Ostwald Ripening	148	8.5. Scale-Up	189
6.5.2. Aggregation	149	8.6. Modeling	191
6.5.3. Mixing	150	8.6.1. Experimental Modeling	191
		8.6.2. Computational Modeling	194

8.6.3. Impeller Treatment	195	CHAPTER 11 CRYSTALLIZATION IN THE PHARMACEUTICAL AND BIOPROCESSING INDUSTRIES	249
8.6.4. Treatment of Turbulence	195	<i>D.J. Kirwan and C.J. Orella</i>	
8.6.5. Modeling Multiphase Flow	195	11.1. The Role of Crystallization in Bioprocesses	249
8.6.6. Mixing Models	197	11.2. Solubility and the Creation of Supersaturation	249
8.6.7. Comprehensive Models	197	11.2.1. Temperature Effects on Solubility	250
8.7. Summary	197	11.2.2. pH Effects on Solubility	250
Acknowledgment	198	11.2.3. Reduction of Solubility with Anti-Solvents	251
References	198	11.2.4. Effects of Salts on Solubility	252
CHAPTER 9 CONTROL OF CRYSTALLIZATION PROCESSES	201	11.3. Control of Particle Size and Morphology	253
<i>J.B. Rawlings, C.W. Sink, and S.M. Miller</i>		11.3.1. Crystal Growth Kinetics	254
9.1. Introduction	201	11.3.2. Effects of Additives, Solvents, and Impurities	255
9.1.1. Overview	201	11.3.3. Nucleation and Seeding	256
9.1.2. Typical Crystallizer Design	202	11.4. The Purity of Biochemicals Produced by Crystallization	258
9.1.3. Measurements	202	11.4.1. Solvent Occlusion	258
9.1.4. Manipulated Variables	203	11.4.2. Incorporation of Solute Impurities	259
9.1.5. Control Algorithm	203	11.4.3. Co-Crystallization of Solutes and Polymorphs	260
9.2. Feedback Controllers	204	11.4.4. Improving Purity by Change of Crystal Form	260
9.2.1. Three Mode (PID) Controllers	204	11.5. Applications of Crystallization in the Pharmaceutical Industry	261
9.2.2. Stability Considerations	205	11.5.1. The Separation of Optical Isomers	261
9.2.3. Automatic/Manual Control Modes	206	11.5.2. Rapid Mixing and Rapid Precipitation	264
9.2.4. Tuning of PID Controllers	206	11.5.3. Ethanol Fractionation of Plasma Proteins	264
9.2.5. Further Feedback Control Techniques	207	Nomenclature	265
9.3. Industrial Crystallizer Control	209	Acknowledgment	266
9.3.1. Crystallizer Control Objectives	209	References	266
9.3.2. Continuous Crystallization Control	210	CHAPTER 12 CRYSTALLIZATION OF PROTEINS	267
9.3.3. Batch Crystallization Control	215	<i>John Wiencek</i>	
9.3.4. Sensor and Control Element Considerations	219	12.1. Introduction	267
9.4. Advanced Continuous Crystallizer Control	221	12.2. Protein Chemistry	269
9.4.1. Model Identification	221	12.2.1. Amino Acids and the Peptide Bond	269
9.4.2. Stability Considerations	222	12.2.2. Levels of Structure: Primary, Secondary, Tertiary, Quaternary	269
9.4.3. Feedback Controller Design	222	12.2.3. Ionizable Sidechains and Protein Net Charge	270
9.5. Advanced Batch Crystallizer Control	223	12.2.4. Disulfide Bonds as Crosslinkers within Proteins	270
9.5.1. Model Identification	224	12.2.5. Chemical Modifications of Proteins—Glycosylation, Lipidation, Phosphorylation	270
9.5.2. Optimal Open-Loop Control	224	12.2.6. Effectors	271
9.5.3. Feedback Controller Design	228	12.2.7. Determining Protein Concentration	271
Nomenclature	228	12.2.8. Protein Purity and Homogeneity	272
References	229	12.3. Variables Affecting Protein Solubility	274
CHAPTER 10 BATCH CRYSTALLIZATION	231	12.3.1. The Effect of pH on Protein Solubility	274
<i>J.S. Wey and P.H. Karpinski</i>		12.3.2. The Effect of Electrolyte on Protein Solubility	275
10.1. Introduction	231	12.3.3. The Effect of Anti-Solvents on Protein Solubility	276
10.2. Batch Crystallizers	231	12.3.4. The Effect of Soluble Synthetic Polymers on Protein Solubility	277
10.2.1. Laboratory Batch Crystallizers	231	12.3.5. The Effect of Pressure on Protein Solubility	277
10.2.2. Industrial Batch Crystallizers	233	12.3.6. The Effect of Temperature on Protein Solubility	277
10.3. Batch Crystallization Analysis	234	12.3.7. Case Studies in Lysozyme and the Generic Protein Phase Diagram	278
10.3.1. Batch Conservation Equations	234	12.4. Nucleation and Growth Mechanisms	280
10.3.2. CSD Analysis and Kinetic Studies	236	12.5. Physicochemical Measurements	280
10.4. Factors Affecting Batch Crystallization	238	12.5.1. Solubility Determination	280
10.4.1. Batch Cycle Time	238	12.5.2. Growth Rate Determination	280
10.4.2. Supersaturation Profile	239	12.6. Traditional Screening Tools	281
10.4.3. External Seeding	239	12.6.1. Vapor Diffusion Experiments	281
10.4.4. Fouling Control	241	12.6.2. Free Interface Diffusion	282
10.4.5. CSD Control	241	12.6.3. Dialysis	282
10.4.6. Growth Rate Dispersions	242	12.6.4. Batch Growth	283
10.4.7. Mixing	243	12.6.5. Seeding Techniques	283
10.5. Batch Crystallization Operations	244		
10.5.1. Cooling Crystallization	244		
10.5.2. Evaporative Crystallization	246		
10.5.3. Antisolvent Crystallization (Salting-Out)	246		
10.6. Summary	246		
Nomenclature	247		
References	248		

x CONTENTS

12.7. Summary	283	13.2.1. Control for Product Quality	290
Nomenclature	283	13.2.2. Control for Separation	292
Acknowledgment	284	13.3. Control to Prevent Crystallization	293
References	284	13.4. Factors Affecting Control of Crystallization	293
		13.4.1. Heat and Mass Transfer Rates	293
		13.4.2. Product Formulation	296
		13.4.3. Post-Processing Effects	297
CHAPTER 13 CRYSTALLIZATION IN FOODS	287	13.5. Summary	303
<i>Richard W. Hartel</i>		Acknowledgment	303
13.1. Controlling Crystallization in Foods	287	References	304
13.2. Control to Produce Desired Crystalline		INDEX	305
Structure	290		

Preface to the First Edition

Crystallization is a separation and purification process used in the production of a wide range of materials; from bulk commodity chemicals to specialty chemicals and pharmaceuticals. While the industrial practice of crystallization is quite old, many practitioners still treat it as an art. Many aspects of industrial crystallization have a well developed scientific basis and much progress has been made in recent years. Unfortunately, the number of researchers in the field is small, and this information is widely dispersed in the scientific and technical literature. This book will address this gap in the literature by providing a means for scientists or engineers to develop a basic understanding of industrial crystallization and provide the information necessary to begin work in the field, be it in design, research, or plant troubleshooting.

Of the eleven chapters in this book, the first two deal with fundamentals such as solubility, supersaturation, basic concepts in crystallography, nucleation, and crystal growth, and are aimed at

those with limited exposure in these areas. The second two chapters provide background in the important area of impurity crystal interactions, and an introduction to crystal size distribution measurements and the population balance method for modeling crystallization processes. These four chapters provide the background information that is needed to access and understand the technical literature, and are aimed at those individuals who have not been previously exposed to this material or who need a review.

The remaining seven chapters deal with individual topics important to industrial practice, such as design, mixing, precipitation, crystallizer control, and batch crystallization. In addition, topics that have become important in recent years, such as melt crystallization and the crystallization of biomolecules are also included. Each chapter is self-contained but assumes that the reader has knowledge of the fundamentals discussed in the first part of the book.

Allan S. Myerson

This Page Intentionally Left Blank

Preface to the Second Edition

Crystallization from solution and the melt continues to be an important separation and purification process in a wide variety of industries. Since the publication of this volume's first edition in 1993, interest in crystallization technology, particularly in the pharmaceutical and biotech industry, has increased dramatically. The first edition served as an introduction to the field and provided the information necessary to begin work in crystallization. This new edition incorporates and builds upon increased interest in crystallization and incorporates new material in a number of areas. This edition of the book includes a new chapter on crystallization of proteins (Chapter 12), a revised chapter on crystallization of pharmaceuticals (Chapter 11), and a new chapter in an area gaining

great importance: crystallization in the food industry (Chapter 13). Other topics that have become important in crystallization research and technology include molecular modeling applications, which are discussed in chapters 2 and 3, and computational fluid dynamics, which is discussed in Chapter 8 and precipitation which is discussed in a totally revised Chapter 6.

As in the first edition, the first four chapters provide an introduction to newcomers to the field, giving fundamental information and background needed to access and understand the field's technical literature. The remaining nine chapters deal with individual topics important to industrial crystallization and assume a working knowledge of the fundamentals presented in chapters 1–4.

Allan S. Myerson

This Page Intentionally Left Blank

SOLUTIONS AND SOLUTION PROPERTIES

Albert M. Schwartz and Allan S. Myerson

1.1. INTRODUCTION AND MOTIVATION

Crystallization is a separation and purification technique employed to produce a wide variety of materials. *Crystallization* may be defined as a phase change in which a crystalline product is obtained from a solution. A solution is a mixture of two or more species that form a homogeneous single phase. Solutions are normally thought of in terms of liquids, however, solutions may include solids and even gases. Typically, the term *solution* has come to mean a liquid solution consisting of a solvent, which is a liquid, and a solute, which is a solid, at the conditions of interest. The term *melt* is used to describe a material that is solid at normal conditions and is heated until it becomes a molten liquid. Melts may be pure materials, such as molten silicon used for wafers in semiconductors, or they may be mixtures of materials. In that sense, a homogeneous melt with more than one component is also a solution, however, it is normally referred to as a melt. A solution can also be gaseous; an example of this is a solution of a solid in a supercritical fluid.

Virtually all industrial crystallization processes involve solutions. The development, design, and control of any of these processes involve knowledge of a number of the properties of the solution. This chapter will present and explain solutions and solution properties, and relate these properties to industrial crystallization operations.

1.2. UNITS

Solutions are made up of two or more components of which one is the solvent and the other is the solute(s). There are a variety of ways to express the composition of a solution. If we consider the simple system of a solvent and a solute, its composition may be expressed in terms of mass fraction, mole fraction, or a variety of concentration units as shown in Table 1.1. The types of units that are commonly used can be divided into those that are ratios of the mass (or moles) of solute to the mass (or moles) of the solvent,

TABLE 1.1 Concentration Units

Type 1: Mass (or moles) solute/mass (or moles) solvent

Grams solute/100 grams solvent
Moles solute/100 grams solvent
Moles solute/1000 grams solvent—molal
lbm solute/lbm solvent
Moles solute/moles solvent

Type 2: Mass (or moles) solute/mass (or moles) solution

Grams solute/grams total Mass fraction
Moles solute/moles total Mole fraction

Type 3: Mass (or moles) solute/volume solution

Moles solute/liter of solution—molar
Grams solute/liter of solution
lbm solute/gallon solution

those that, are ratios of the mass (or moles) of the solute to the mass (or moles) of the solution, and those that are ratios of the mass (or moles) of the solute to the volume of the solution.

While all three units are commonly used, it is important to note that use of units of type 3, requires knowledge of the solution density to convert these units into those of the other types. In addition, type 3 units must be defined at a particular temperature since the volume of a solution is a function of temperature. The best units to use for solution preparation are mass of solute per mass of solvent. These units have no temperature dependence and solutions can be prepared simply by weighing each species. Conversion among mass (or mole) based units is also simple. Example 1.1 demonstrates conversion of units of all three types.

1.3. SOLUBILITY OF INORGANICS

1.3.1. BASIC CONCEPTS

A solution is formed by the addition of a solid solute to the solvent. The solid dissolves, forming the homogeneous solution. At a given temperature there is a maximum amount of solute that can dissolve in a given amount of solvent. When this maximum is reached the solution is said to be saturated. The amount of solute required to make a saturated solution at a given condition is called the *solubility*.

Solubilities of common materials vary widely, even when the materials appear to be similar. Table 1.2 lists the solubility of a number of inorganic species (Mullin 1997 and Myerson et al. 1990). The first five species all have calcium as the cation but their solubilities vary over several orders of magnitude. At 20°C the solubility of calcium hydroxide is 0.17 g/100 g water while that of calcium iodide is 204 g/100 g water. The same variation can be seen in the six sulfates listed in Table 1.2. Calcium sulfate has a solubility of 0.2 g/100 g water at 20°C while ammonium sulfate has a solubility of 75.4 g/100 g water.

TABLE 1.2 Solubilities of Inorganics at 20°C

Compound	Chemical Formula	Solubility (g anhydrous/100 g H ₂ O)
Calcium chloride	CaCl ₂	74.5
Calcium iodide	CaI ₂	204
Calcium nitrate	Ca(NO ₃) ₂	129
Calcium hydroxide	Ca(OH) ₂	0.17
Calcium sulfate	CaSO ₄	0.20
Ammonium sulfate	(NH ₄) ₂ SO ₄	75.4
Copper sulfate	CuSO ₄	20.7
Lithium sulfate	LiSO ₄	34
Magnesium sulfate	MgSO ₄	35.5
Silver sulfate	Ag ₂ SO ₄	0.7

(Based on data from Mullin 1997 and Myerson et al. 1990)

EXAMPLE 1.1**Conversion of Concentration Units**

Given: 1 molar solution of NaCl at 25 °C
 Density of solution = 1.042 g/cm³
 Molecular weight (MW) NaCl = 58.44

$$\begin{aligned}
 1 \text{ molar} &= \frac{1 \text{ mol NaCl}}{\text{liter of solution}} \frac{1 \text{ liter}}{1000 \text{ cm}^3} \frac{58.44 \text{ g NaCl}}{\text{mol NaCl}} \frac{1 \text{ cm}^3}{1.042 \text{ g}} \\
 &= \frac{0.056 \text{ g NaCl}}{\text{g solution}} \\
 &= 0.056 \text{ wt fraction NaCl} = 5.6 \text{ wt\% NaCl}
 \end{aligned}$$

$$\begin{aligned}
 \frac{0.056 \text{ g NaCl}}{\text{g solution}} &= \frac{0.056 \text{ g NaCl}}{0.944 \text{ g water} + 0.056 \text{ g NaCl}} \\
 &= 0.059 \text{ g NaCl/g water}
 \end{aligned}$$

$$\begin{aligned}
 0.056 \text{ wt fraction NaCl} &= \frac{0.056 \text{ g NaCl}}{0.944 \text{ g water} + 0.056 \text{ g NaCl}} \\
 &= \frac{\frac{0.056 \text{ g NaCl}}{58.44 \text{ g/g mol}}}{\frac{0.056 \text{ g NaCl}}{58.44 \text{ g/g mol}} + \frac{0.944 \text{ g water}}{18 \text{ g/g mol}}} \\
 &= 0.018 \text{ mol fraction NaCl}
 \end{aligned}$$

The solubility of materials depends on temperature. In the majority of cases the solubility increases with increasing temperature, although the rate of the increase varies widely from compound to compound. The solubility of several inorganics as a function of temperature are shown in Figure 1.1 (Mullin 1997). Sodium chloride is seen to have a relatively weak temperature dependence with the solubility changing from 35.7 to 39.8 g/100 g water over a 100 °C range. Potassium nitrate, on the other hand, changes from 13.4 to 247 g/100 g water over the same temperature range. This kind of information is very important in crystallization processes since it will determine the amount of cooling required to

yield a given amount of product and will in fact determine if cooling will provide a reasonable product yield.

Solubility can also decrease with increasing temperature with sparingly soluble materials. A good example of this is the calcium hydroxide water system shown in Figure 1.2.

The solubility of a compound in a particular solvent is part of that systems phase behavior and can be described graphically by a phase diagram. In phase diagrams of solid-liquid equilibria the mass fraction of the solid is usually plotted versus temperature. An example is Figure 1.3, which shows the phase diagram for the magnesium sulfate water system. This system demonstrates another common property of inorganic solids, the formation of *hydrates*. A *hydrate* is a solid formed upon crystallization from water that contains water molecules as part of its crystal structure. The chemical formula of a hydrate indicates the number of moles of water present per mole of the solute species by listing a stoichiometric number and water after the dot in the chemical formula. Many compounds that form hydrates form several with varying amounts of water. From the phase diagram (Figure 1.3) we can see that MgSO₄ forms four stable hydrates ranging from 12 mol of water/mol MgSO₄ to 1 mol of water/mol of MgSO₄. As is usual with hydrates, as the temperature rises, the number of moles of water in the stable hydrate declines and at some temperature the anhydrous material is the stable form.

The phase diagram contains much useful information. Referring to Figure 1.3, the line abcdef is the solubility or saturation line that defines a saturated solution at a given temperature. Line ab is the solubility line for the solvent (water) since when a solution in this region is cooled, ice crystallizes out and is in equilibrium with the solution. Point b marks what is known as the eutectic composition. At this composition, 0.165 weight fraction MgSO₄, if the solution is cooled both ice and MgSO₄ will separate as solids. The rest of the curve from b to f represents the solubility of MgSO₄ as a function of temperature. If we were to start with a solution at 100 °F and 25 wt% MgSO₄ (point A in Figure 1.3) and cool that solution, the solution would be saturated at the point where a vertical line from A crosses the saturation curve, which is at 80 °F. If the solution were cooled to 60 °F as shown in point D, the solution will have separated at equilibrium into solid MgSO₄ · 7H₂O and a saturated solution of the composition corresponding to point C.

The phase diagram also illustrates a general practice concerning hydrate solubility. The solubility of compounds that form hydrates

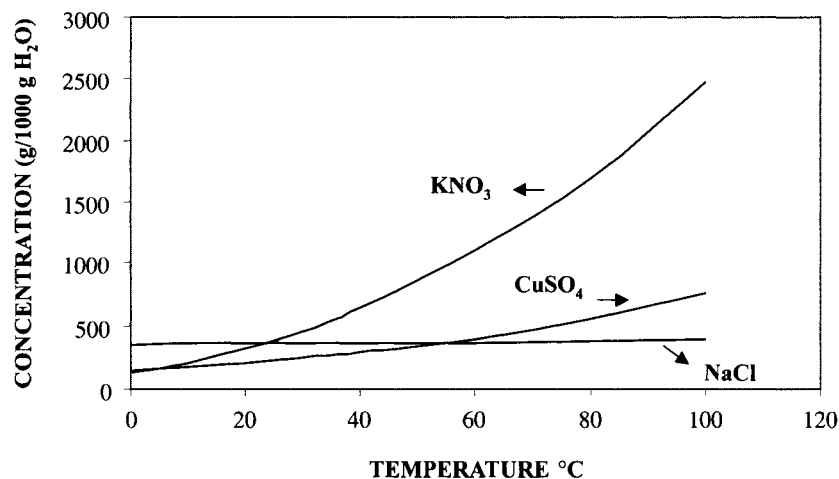


Figure 1.1 Solubility of KNO₃, CuSO₄, and NaCl in aqueous solution. (Data from Mullin 1997.)

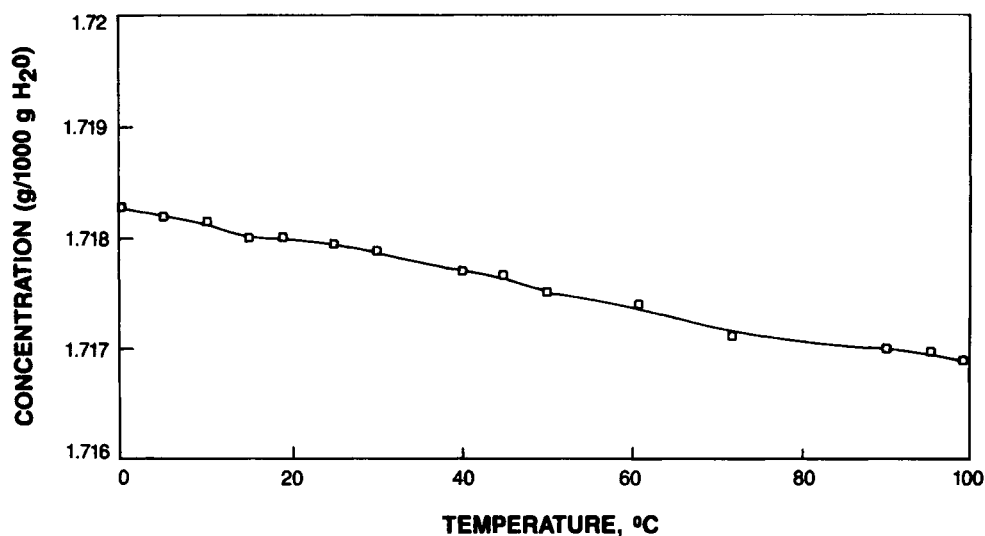


Figure 1.2 Solubility of calcium hydroxide in aqueous solution. (Data from Myerson et al. 1990.)

are usually given in terms of the anhydrous species. This saves much confusion when multiple stable hydrates can exist but requires that care be taken when performing mass balances or preparing solutions. Example 1.2 illustrates these types of calculations.

Phase diagrams can be significantly more complex than the example presented in Figure 1.3 and may involve additional stable phases and/or species. A number of references (Rosenberger 1981; Gordon 1968) discuss these issues in detail.

EXAMPLE 1.2 Calculations Involving Hydrates

Given solid $\text{MgSO}_4 \cdot 7\text{H}_2\text{O}$ prepare a saturated solution of MgSO_4 at 100°F .

(a) Looking at the phase diagram (Figure 1.3) the solubility of MgSO_4 at 100°F is 0.31 wt. fraction MgSO_4 (anhydrous) and the stable phase is $\text{MgSO}_4 \cdot 7\text{H}_2\text{O}$. First, calculate the amount of MgSO_4 (anhydrous) necessary to make a saturated solution at 100°F .

$$0.31 = x_f = \frac{\text{weight MgSO}_4 \text{ (g)}}{\text{weight MgSO}_4 \text{ (g)} + \text{weight H}_2\text{O (g)}} \quad (1)$$

Using a Basis: 1000 g H_2O , the weight of MgSO_4 (g) needed to make a saturated solution is 449 (g) MgSO_4 (anhydrous).

(b) Since the stable form of the MgSO_4 available is $\text{MgSO}_4 \cdot 7\text{H}_2\text{O}$, we must take into account the amount of water added to the solution from the MgSO_4 hydrate.

We first need to determine the amount of water added per gram of $\text{MgSO}_4 \cdot 7\text{H}_2\text{O}$. To do this we need to know the molecular masses of MgSO_4 , H_2O , and $\text{MgSO}_4 \cdot 7\text{H}_2\text{O}$. These are 120.37 g/gmol, 18.015 g/gmol, and 246.48 g/gmol, respectively.

$$x_{\text{MgSO}_4} = \frac{\text{wt. of MgSO}_4 \text{ in the hydrate}}{\text{wt. of MgSO}_4 \cdot 7\text{H}_2\text{O}} = \frac{120.37}{246.48} = 0.488 \quad (2)$$

$$x_{\text{H}_2\text{O}} = \frac{\text{wt. of H}_2\text{O in the hydrate}}{\text{wt. of MgSO}_4 \cdot 7\text{H}_2\text{O}} = \frac{126.11}{246.48} = 0.512 \quad (3)$$

Mass Balances:

$$\text{Total weight} = \text{wt. H}_2\text{O} + \text{wt. of MgSO}_4 \text{ in the hydrate} \quad (4)$$

$$0.31 \{\text{Total weight}\} = \text{wt. of MgSO}_4 \text{ in the hydrate} \quad (5)$$

$$0.69 \{\text{Total weight}\} = \text{wt. of H}_2\text{O in the hydrate} \\ + \text{wt. of H}_2\text{O solvent} \quad (6)$$

First we will examine equation (4) the total mass balance. Since we are using a basis of 1000 g of H_2O and the weight of MgSO_4 in the hydrate is equal to the weight of MgSO_4 (anhydrous) calculated in 1.2(a), the total weight of our system is 1449 g.

By substituting equations (2) and (3) into equations (5) and (6), respectively, we can solve for the amount of $\text{MgSO}_4 \cdot 7\text{H}_2\text{O}$ needed to make a saturated solution at 100°F .

$$0.31 \{1449 \text{ g}\} = 0.488 \{\text{wt. of MgSO}_4 \cdot 7\text{H}_2\text{O}\}$$

$$\text{wt. of MgSO}_4 \cdot 7\text{H}_2\text{O} = 920 \text{ g}$$

$$0.69 \{1449\} = \text{wt. H}_2\text{O solvent} + 0.512 \{\text{wt. of MgSO}_4 \cdot 7\text{H}_2\text{O}\}$$

$$0.69 \{1449\} = \text{wt. H}_2\text{O solvent} + 0.512 \{920 \text{ g}\}$$

$$\text{wt. H}_2\text{O solvent} = 529 \text{ g}$$

Therefore, in order to make a saturated solution of MgSO_4 at 100°F starting with $\text{MgSO}_4 \cdot 7\text{H}_2\text{O}$, we need to add 920 g of the hydrate to 529 g of H_2O .

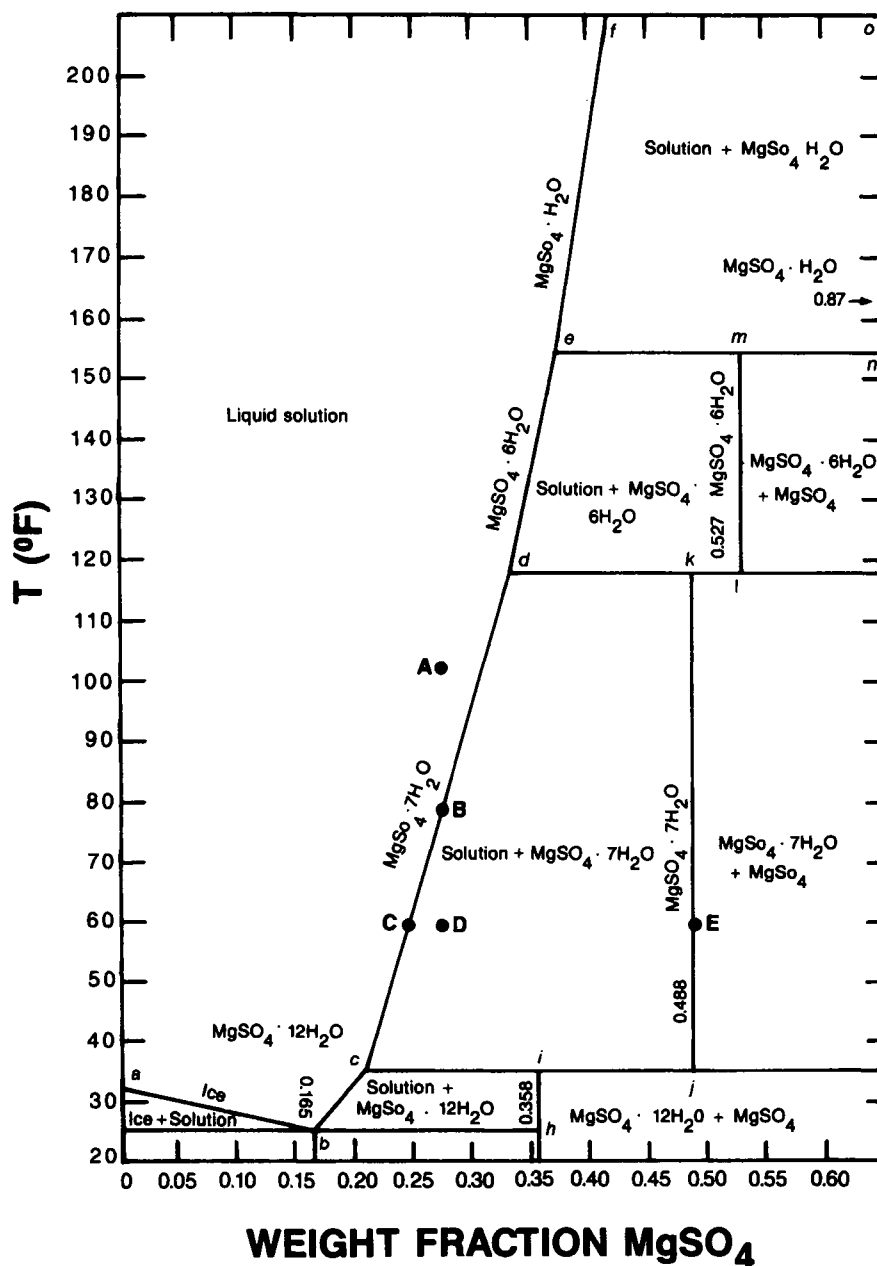


Figure 1.3 Phase diagram for $\text{MgSO}_4\text{--H}_2\text{O}$. (Reprinted by permission of John Wiley & Sons, Inc., from R.M. Felder and R.W. Rousseau (1986), *Elementary Principles of Chemical Processes*, 2nd ed., p. 259. © John Wiley and Sons, Inc.)

1.3.2. SPARINGLY SOLUBLE SPECIES—DILUTE SOLUTIONS

As we have seen in the previous section, the solubility of materials varies according to their chemical composition and with temperature. Solubility is also affected by the presence of additional species in the solution, by the pH, and by the use of different solvents (or solvent mixtures). When discussing inorganic species, the solvent is usually water, while with organics, the solvent can be water or a number of organic solvents, or solvent mixtures.

If we start with a sparingly soluble inorganic species such as silver chloride and add silver chloride to water in excess of the saturation concentration, we will eventually have equilibrium

between solid AgCl and the saturated solution. The AgCl is, as most of the common inorganics, an electrolyte and dissociates into its ionic constituents in solution. The dissociation reaction can be written as



The equilibrium constant for this reaction can be written as

$$K = (a_{\text{Ag}^+} a_{\text{Cl}^-}) / (a_{\text{AgCl}}) \quad (1.2)$$

where a denotes the activities of the species. If the solid AgCl is in its stable crystal form and at atmospheric pressure, it is at a

standard state and will have an activity of one. The equation can then be written as

$$K_{sp} = a^{\text{Ag}^+} a^{\text{Cl}^-} = \gamma^{\text{Ag}^+} (m_{\text{Ag}^+}) \gamma^{\text{Cl}^-} (m_{\text{Cl}^-}) \quad (1.3)$$

where γ is the activity coefficient of the species and m represents the concentrations in solution of the ions in molal units. For sparingly soluble species, such as AgCl, the activity coefficient can be assumed to be unity (using the asymmetric convention for activity coefficients) so that Eq. (1.3) reduces to

$$K_{sp} = [m_{\text{Ag}^+}][m_{\text{Cl}^-}] \quad (1.4)$$

This equation represents the solubility product of silver chloride. Solubility products are generally used to describe the solubility and equilibria of sparingly soluble salts in aqueous solutions. Solubility products of a number of substances are given in Table 1.3. It is important to remember that use of solubility product relations based on concentrations assumes that the solution is saturated, in equilibrium, and ideal (the activity coefficient is equal to one), and is therefore an approximation, except with very dilute solutions of one solute.

Eq. (1.4) can be used for electrolytes in which there is a 1:1 molar ratio of the anion and cation. For an electrolyte that consists of univalent and bivalent ions, such as silver sulfate, which dissociates into 2 mol of silver ion for each mole of sulfate ion, the solubility product equation would be written as

$$K_{sp} = (m_{\text{Ag}^+})^2 (m_{\text{SO}_4^{2-}}) \quad (1.5)$$

In the dissociation equation the concentration of the ions of each species are raised to the power of their stoichiometric number.

TABLE 1.3 Solubility Products

Substance	Solubility Product at 25 °C
Aluminum hydroxide	3.70×10^{-15}
Barium carbonate	2.58×10^{-9}
Barium chromate	1.17×10^{-10}
Barium fluoride	1.84×10^{-7}
Barium iodate monohydrate	1.67×10^{-9}
Barium sulfate	1.08×10^{-10}
Calcium carbonate (calcite)	3.36×10^{-9}
Calcium fluoride	3.45×10^{-11}
Calcium iodate hexahydrate	7.10×10^{-7}
Calcium oxalate monohydrate	2.32×10^{-9}
Calcium sulfate	4.93×10^{-5}
Cupric iodate monohydrate	6.94×10^{-8}
Cupric oxalate	4.43×10^{-10}
Cuprous bromide	6.27×10^{-9}
Cuprous chloride	1.72×10^{-7}
Cuprous iodide	1.27×10^{-12}
Ferric hydroxide	2.79×10^{-39}
Ferrous hydroxide	4.87×10^{-17}
Lead carbonate	7.40×10^{-14}
Lead sulfate	2.53×10^{-8}
Lithium carbonate	8.15×10^{-4}
Magnesium carbonate	6.82×10^{-6}
Magnesium fluoride	5.16×10^{-11}
Magnesium hydroxide	5.61×10^{-12}
Magnesium oxalate dihydrate	4.83×10^{-6}
Manganese carbonate	2.24×10^{-11}
Silver bromate	5.38×10^{-5}
Silver iodide	8.52×10^{-17}
Zinc hydroxide	3.00×10^{-17}

(Data from Lide 1998.)

The solubility product principle enables simple calculations to be made of the effect of other species on the solubility of a given substance and may be used to determine the species that will precipitate in an electrolyte mixture. One simple result of applying the solubility product principle is the common ion effect. This is the effect caused by the addition of an ionic species that has an ion in common with the species of interest. Since the solubility of a species is given by the product of the concentration of its ions, when the concentration of one type of ion increases, the concentration of the other must decline, or the overall concentration of that compound must decline. We can illustrate this simply by using our previous example of silver chloride. The solubility product of silver chloride at 25 °C is 1.56×10^{-10} . This means that at saturation we can dissolve 1.25×10^{-5} mol of AgCl/1000 g of water. If, however, we were to start with a solution that has a concentration of 1×10^{-5} molal NaCl (hence 1×10^{-5} molal Cl^-) the solubility product equation can be written in the form

$$K_{sp} = (m_{\text{Ag}^+})(m_{\text{Cl}^-}) = (x_{\text{Ag}^+})(x_{\text{Cl}^-} + 1 \times 10^{-5}) \quad (1.6)$$

$$K_{sp} = x^2 + 1 \times 10^{-5} x \quad (1.7)$$

where x is the amount of AgCl that can dissolve in the solution. Solving Eq. (1.7) results in $x = 0.725 \times 10^{-5}$ molal. The common ion effect has worked to decrease the solubility of the compound of interest. It is important to remember that this is true only for very dilute solutions. In more concentrated solutions, the activity coefficients are not unity and more complex electrical effects and complexation may occur. This is discussed in detail in the next section.

Another use of solubility products is the determination, in a mixture of slightly soluble materials, as to what material is likely to precipitate. This is done by looking at all the ion concentrations and calculating their products in all possible combinations. These are then compared with the solubility products that must already be known. This is useful in situations where scale formation is of interest, or in determining the behavior of slightly soluble mixtures.

1.3.3. CONCENTRATED SOLUTIONS

Unfortunately, like all easy to use principles, the solubility product principle is not generally applicable. At higher concentrations, electrical interactions, complex formation, and solution nonideality make the prediction of the effect of ionic species on the solubility of other ionic species much more complicated.

In the previous section we used the solubility product principle to calculate the effect of a common ion on the solubility of a sparingly soluble species. The common ion effect, however, is completely dominated by a more powerful effect when a large concentration of another electrolyte is present. In fact, the solubility of sparingly soluble materials increases with increasing ion concentration in solution. This is called the *salt effect* and is illustrated in Figures 1.4 through 1.6 where we see the increase in solubility of AgCl as a function of increasing concentrations of added electrolytes. We see this effect in both added salts with a common ion and without. This effect can also be induced by changing the pH of the solution since this changes the ion content of the solution.

The solubility of many inorganics in aqueous solution is available in the book by Linke and Seidell (1958). This reference also contains the solubilities of electrolytes in the presence of other species. As an example, Figure 1.7 shows the solubility of NaCl as a function of NaOH concentration. As a general rule, the solubility of most inorganics in water is available as a function of temperature. What is more difficult to find is the effect of other species on the solubility. If several other species are present the

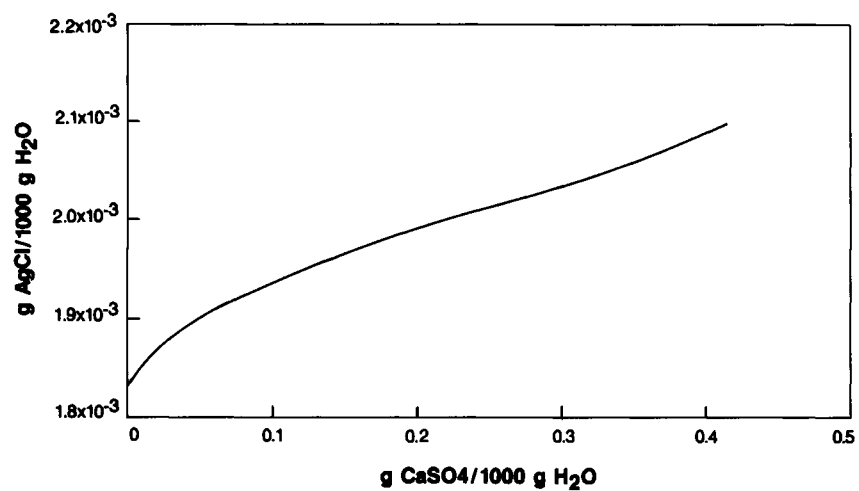


Figure 1.4 Solubility of AgCl in aqueous CaSO₄ solution at 25 °C. (Data from Linke and Seidell 1958, 1965.)

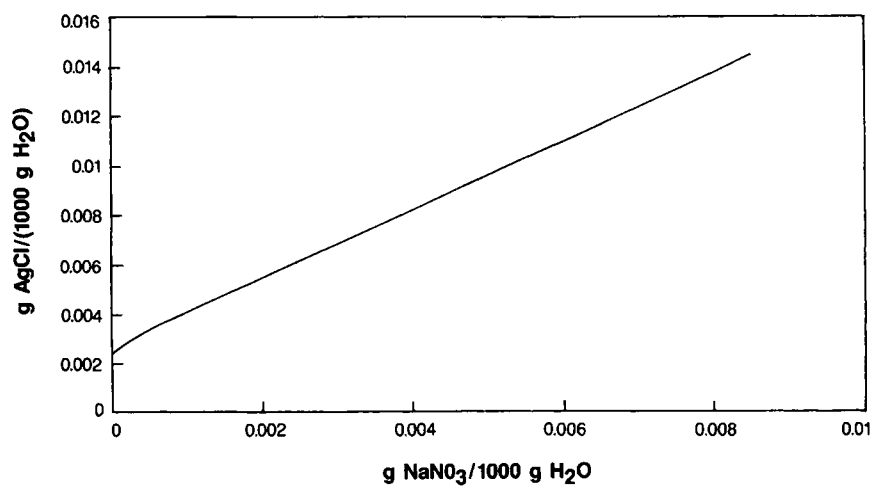


Figure 1.5 Solubility of AgCl in aqueous NaNO₃ solution at 30 °C. (Data from Linke and Seidell 1958, 1965.)

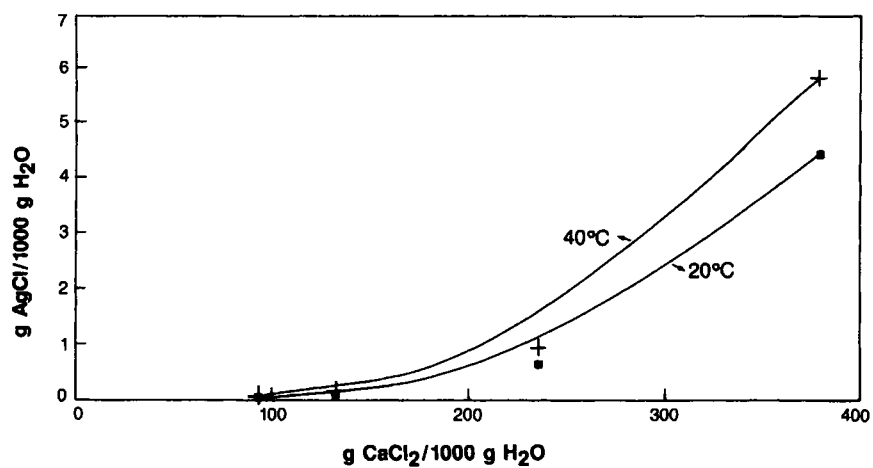


Figure 1.6 Solubility of AgCl in aqueous CaCl₂ solution. (Data from Linke and Seidell 1958, 1965.)

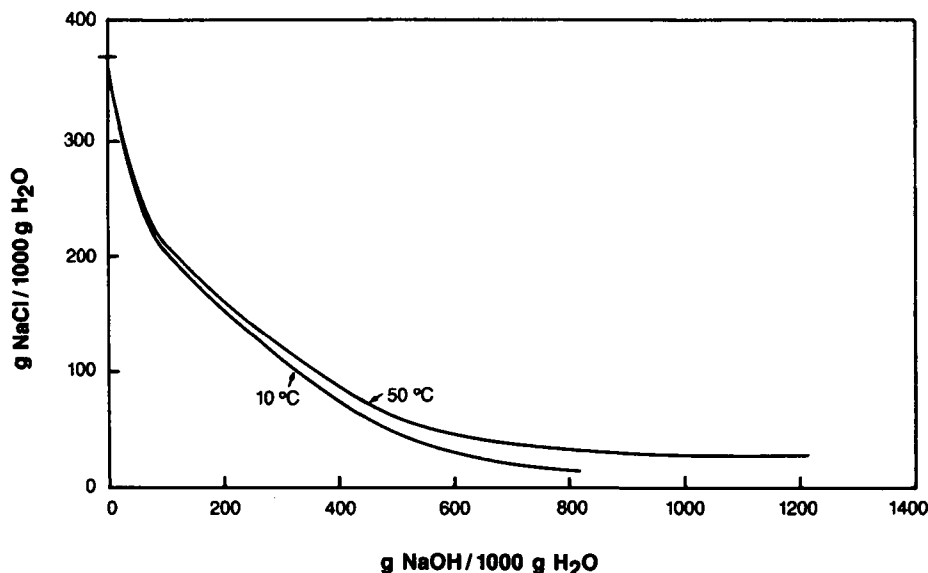


Figure 1.7 Solubility of NaCl in aqueous NaOH solution. (Data from Linke and Seidell 1958, 1965.)

data will usually not be available. Given this situation there are two alternatives. The first is to measure the solubility at the conditions and composition of interest. Experimental methods for solubility measurement will be discussed in Section 1.4.5. The second alternative is to calculate the solubility. This is a viable alternative when thermodynamic data are available for the pure components (in solution) making up the multicomponent mixture. An excellent reference for calculation techniques in this area is the *Handbook of Aqueous Electrolyte Thermodynamics* by Zemaitis et al. (1986). A simplified description of calculation techniques is presented in the next section.

Solution Thermodynamics. As we have seen previously, for a solution to be saturated it must be at equilibrium with the solid solute. Thermodynamically this means that the chemical potential of the solute in the solution is the same as the chemical potential of the species in the solid phase.

$$\mu_{i,\text{solid}} = \mu_{i,\text{solution}} \quad (1.8)$$

If the solute is an electrolyte that completely dissociates in solution (strong electrolyte), Eq. (1.8) can be rewritten as

$$\mu_{i,\text{solid}} = \nu_c \mu_c + \nu_a \mu_a \quad (1.9)$$

where ν_c and ν_a are the stoichiometric numbers, and μ_c and μ_a are the chemical potentials of the cation and anion, respectively. The chemical potential of a species is related to the species activity by

$$\mu_i(T) = \mu_{i(aq)}^0(T) + RT \ln(a_i) \quad (1.10)$$

where a_i is the activity of species i and $\mu_{i(aq)}^0$ is an arbitrary reference state chemical potential. The activity coefficient is defined as

$$\gamma_i = a_i/m_i \quad (1.11)$$

where m_i is the concentration in molal units. In electrolyte solutions, because of the condition of electroneutrality, the charges of the anion and cation will always balance. When a salt dissolves it

will dissociate into its component ions. This has led to the definition of a mean ionic activity coefficient and mean ionic molality defined as

$$\gamma_{\pm} = (\gamma_c^{\nu_c} \gamma_a^{\nu_a})^{1/\nu} \quad (1.12)$$

$$m_{\pm} = (m_c^{\nu_c} m_a^{\nu_a})^{1/\nu} \quad (1.13)$$

where the ν_c and ν_a are the stoichiometric number of ions of each type present in a given salt. The chemical potential for a salt can be written as

$$\mu_{\text{salt}(aq)} = \mu_{(aq)}^0 + \nu RT \ln(\gamma_{\pm} m_{\pm})^{\nu} \quad (1.14)$$

where $\mu_{(aq)}^0$ is the sum of the two ionic standard state chemical potentials and ν is the stoichiometric number of moles of ions in one mole of solid. In practice, experimental data are usually reported in terms of mean ionic activity coefficients. As we have discussed previously, various concentration units can be used. We have defined the activity coefficient of a molal scale. On a molar scale it is

$$y_i = \frac{a_i(c)}{(c_i)} \quad (1.15)$$

where y_i is the molar activity coefficient and c_i is the molar concentration. We can also define the activity coefficient on a mole fraction scale

$$f_i = \frac{a_i(x)}{x_i} \quad (1.16)$$

where f_i is the activity coefficient and x_i the mole fraction. Converting activity coefficients from one type of units to another is neither simple nor obvious. Equations that can be used for this conversion have been developed (Zemaitis et al. 1986) and appear below

$$f_{\pm} = (1.0 + 0.01M_s vm)\gamma_{\pm} \quad (1.17)$$

$$f_{\pm} = \frac{(\rho + 0.001c(vM_s - M))}{\rho_0} y_{\pm} \quad (1.18)$$

$$\gamma_{\pm} = \frac{(\rho - 0.001cM)}{\rho_0} y_{\pm} = \left(\frac{c}{m\rho_0}\right) y_{\pm} \quad (1.19)$$

$$y_{\pm} = (1 + 0.001mM) \left(\frac{\rho}{\rho_0}\right) \gamma_{\pm} = \left(\frac{m\rho_0}{c}\right) \gamma_{\pm} \quad (1.20)$$

where

v = stoichiometric number = $v_+ + v_-$
 ρ = solution density
 ρ_0 = solvent density
 M = molecular weight of the solute
 M_s = molecular weight of the solvent

Solubility of a Pure Component Strong Electrolyte. The calculation of the solubility of a pure component solid in solution requires that the mean ionic activity coefficient be known along with a thermodynamic solubility product (a solubility product based on activity). Thermodynamic solubility products can be calculated from standard state Gibbs free energy of formation data. If, for example, we wished to calculate the solubility of KCl in water at 25°C,



The equilibrium constant is given by equation.

$$K_{sp} = \frac{a_{\text{K}^+} a_{\text{Cl}^-}}{a_{\text{KCl}}} = (\gamma_{\text{K}^+} m_{\text{K}^+})(\gamma_{\text{Cl}^-} m_{\text{Cl}^-}) = \gamma_{\pm}^2 m_{\pm}^2 \quad (1.22)$$

The equilibrium constant is related to the Gibbs free energy of formation by the relation

$$K_{sp} = \exp(-\Delta G_{fo}/RT) \quad (1.23)$$

The free energy of formation of KCl can be written as

$$\Delta G_{fo} = \Delta G_{fo\text{K}^+} + \Delta G_{fo\text{Cl}^-} - \Delta G_{fo\text{KCl}} \quad (1.24)$$

Using data from the literature (Zemaitis et al. 1986) one finds,

$$\Delta G_{fo} = -1282 \text{ cal/g mol} \quad (1.25)$$

so that

$$K_{sp} = 8.704 \quad (1.26)$$

Employing this equilibrium constant and assuming an activity coefficient of 1 yields a solubility concentration of 2.95 molal. This compares with an experimental value (Linke and Seidell 1958) of 4.803 molal. Obviously assuming an activity coefficient of unity is a very poor approximation in this case and results in a large error.

The calculation of mean ionic activity coefficients can be complex and there are a number of methods available. Several

references (Zemaitis et al. 1986; Robinson and Stokes 1970; Guggenheim 1987) describe these various methods. The method of Bromley (1972, 1973, 1974) can be used up to a concentration of 6 molal and can be written as

$$\log \gamma_{\pm} = \frac{A|z^+z^-|\sqrt{I}}{1 + \sqrt{I}} + \frac{((0.06 + 0.6B)|z^+z^-|I)}{\left(1 + \frac{1.5}{|z^+z^-|}I\right)^2} + BI \quad (1.27)$$

where

γ_{\pm} = activity coefficient
 A = Debye-Hückel constant
 z = number of charges on the cation or anion
 I = ionic strength is $1/2\sum_i m_i z_i^2$
 B = constant for ion interaction

Values for the constant B are tabulated (Zemaitis et al. 1986) for a number of systems. For KCl, $B = 0.0240$. Employing Eq. (1.27), γ_{\pm} can be calculated as a function of m . This must be done until the product $\gamma_{\pm}^2 m^2 = K_{sp}$. For the KCl water system at 25°C, γ_{\pm} is given as a function of concentration in Table 1.4 along with $\gamma_{\pm}^2 m^2$. You can see that the resulting calculated solubility is approximately 5 molal, which compares reasonably well with the experimental value of 4.8 molal.

Electrolyte Mixtures. The calculation of the solubility of mixtures of strong electrolytes requires knowledge of the thermodynamic solubility product for all species that can precipitate and requires using an activity coefficient calculation method that takes into account ionic interactions. These techniques are well described in Zemaitis et al. (1986), however, we will discuss a simple case in this section.

The simplest case would be a calculation involving a single possible precipitating species. A good example is the effect of HCl on the solubility of KCl.

The thermodynamic solubility product K_{sp} for KCl is defined as

$$K_{sp} = (\gamma_{\text{K}^+} m_{\text{K}^+})(\gamma_{\text{Cl}^-} m_{\text{Cl}^-}) = \gamma_{\pm}^2 m^2 \quad (1.28)$$

In the previous example, we obtained K_{sp} from the Gibbs free energy data and used this to calculate the solubility of KCl. Normally for a common salt, solubility data is available. K_{sp} is,

TABLE 1.4 Calculated Activity Coefficients for KCl in Water at 25°C

m (molality)	γ_{\pm}	$m^2 \gamma^2$
0.01	0.901	8.11×10^{-6}
0.1	0.768	5.8×10^{-3}
1.0	0.603	0.364
1.5	0.582	0.762
2.0	0.573	1.31
2.5	0.569	2.02
3.0	0.569	2.91
3.5	0.572	4.01
4.0	0.577	5.32
4.5	0.584	6.91
5.0	0.592	8.76
$K_{sp} = 8.704$ from Gibbs free energy of formation		

(Data from Zemaitis et al. 1986.)

therefore, obtained from the experimental solubility data and activity coefficients. Using the experimental KCl solubility at 25°C (4.8 molal) and the Bromley activity coefficients yields a $K_{sp} = 8.01$. If we wish to calculate the KCl solubility in a 1 molal HCl solution, we can write the following equations

$$\frac{(\gamma_{K^+} m_{K^+})(\gamma_{Cl^-} m_{Cl^-})}{K_{sp}} = 1 \quad (1.29)$$

$$\begin{array}{ccccc} z_{K^+} m_{K^+} & + & z_{H^+} m_{H^+} & = & z_{Cl^-} m_{Cl^-} & + & z_{Cl^-} m_{Cl^-} \\ \text{(from KCl)} & & \text{(from HCl)} & & \text{(from KCl)} & & \text{(from HCl)} \end{array} \quad (1.30)$$

Eqs. (1.29) and (1.30) must be satisfied simultaneously for a fixed value of 1 molal HCl.

Using Bromley's method for multicomponent electrolytes

$$\log \gamma_i = \frac{-Az_i^2 \sqrt{I} + F_i}{1 + \sqrt{I}} \quad (1.31)$$

where

A = Hückel constant

I = ionic strength

i = any ion present

z_i = number of charges on ion i

F_i is an interaction parameter term

$$F_i = \sum B_{ij} z_i^2 m_j \quad (1.32)$$

where j indicates all ions of opposite charge to i

$$z_{ij} = \frac{z_i + z_j}{2} \quad (1.33)$$

where m_j = molality of ion j

$$B_{ij} = \frac{((0.06 + 0.6B)|z_i z_j|)}{\left(1 + \frac{1.5}{|z_i z_j|} I\right)^2} + B \quad (1.34)$$

Employing these equations the activity coefficient for K^+ and Cl^- are calculated as a function of KCl concentration at a fixed HCl concentration of 1 molar. These values along with the molalities of the ions are then substituted in Eq. (1.29) until it is an equality (within a desired error). The solubility of KCl in a 1 molal solution of HCl is found to be 3.73 molal, which compares with an experimental value of 3.92 molal. This calculation can then be repeated for other fixed HCl concentrations. Figure 1.8 compares the calculated and experimental values of KCl solubility over a range of HCl concentrations. Unfortunately, many systems of interest include species that form complexes, intermediates, and undissociated aqueous species. This greatly increases the complexity of solubility calculations because of the large number of possible species. In addition, mixtures with many species often include a number of species that may precipitate. These calculations are extremely tedious and time consuming to do by hand or to write a specific computer program for each application. Commercial software is available for calculations in complex electrolyte mixtures. The ProChem software developed by OLI Systems Inc. (Morris Plains, New Jersey) is an excellent example. The purpose of the package is to simultaneously consider the effects of the detailed reactions as well as the underlying species interactions

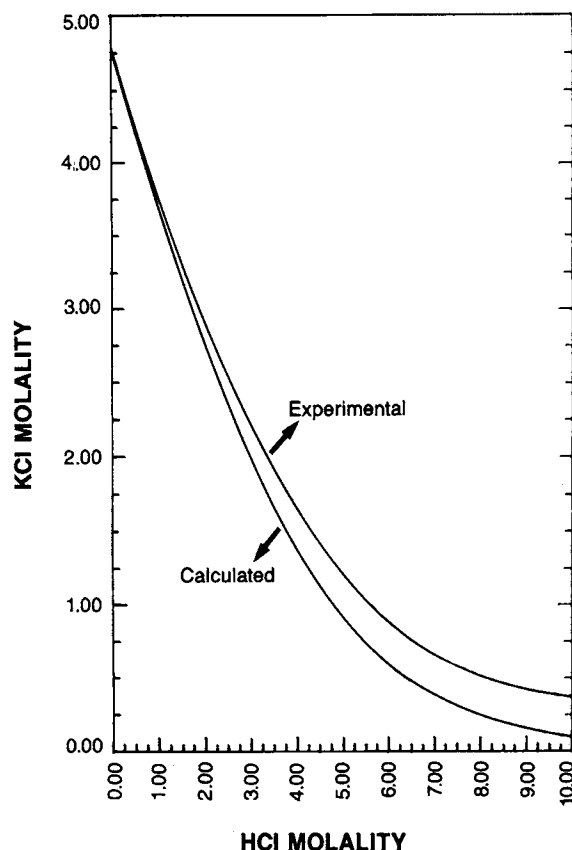


Figure 1.8 Calculated versus experimental KCl solubility in aqueous HCl solution at 25°C. (Reproduced from J.F. Zemaitis, Jr., D.M. Clark, M. Rafal, and N.C. Scrivner (1986), *Handbook of Aqueous Electrolyte Thermodynamics*, p. 284. Used by permission of the American Institute of Chemical Engineers. © 1986 AIChE.)

TABLE 1.5 Calculated Results for $Cr(OH)_3$ Solubility at 25°C

Equilibrium Constant	K (mol/kg)	
H_2O	9.94×10^{-15}	
$CrOH^{+2}$	1.30×10^{-10}	
$Cr(OH)_2^+$	2.72×10^{-9}	
$Cr(OH)_3$ (aq.)	2.03×10^{-6}	
$Cr(OH)_3$ (crystal)	6.44×10^{-31}	
$Cr(OH)_4^-$	1.67×10^{-5}	
$Cr_2(OH)_2^{+4}$	2.35×10^{-5}	
$Cr_3(OH)_4^{+5}$	2.52×10^{-7}	
Liquid phase pH = 10	Ionic strength = 1.01×10^{-2}	
Species	Moles	Activity Coefficient
H_2O	55.5	1.0
H^+	1.22×10^{-10}	0.904
OH^-	1.00×10^{-4}	0.902
Cr^{+3}	2.21×10^{-18}	0.397
$CrOH^{+2}$	9.32×10^{-13}	0.655
$Cr(OH)_2^+$	1.65×10^{-8}	0.899
$Cr(OH)_3$ (aq)	6.56×10^{-7}	1.0
$Cr(OH)_4^-$	3.95×10^{-6}	0.899
$Cr_2(OH)_2^{+4}$	2.98×10^{-21}	0.185
$Cr_3(OH)_4^{+5}$	4.48×10^{-22}	0.0725
Cl^-	1.00×10^{-2}	0.898
Na^+	1.01×10^{-2}	0.898

(Data from Zemaitis et al. 1986.)

that determine the actual activity coefficient values. Only by such a calculation can the solubility be determined.

A good example of the complexity of these calculations can be seen when looking at the solubility of $\text{Cr}(\text{OH})_3$. Simply assuming the dissociation reaction



and calculation a solubility using the K_{sp} obtained from Gibbs free energy of formation leads to serious error. That is because a number of other dissociation reactions and species are possible. These include: $\text{Cr}(\text{OH})_3$ (undissociated molecule in solution); $\text{Cr}(\text{OH})_4^-$; $\text{Cr}(\text{OH})_2^+$; $\text{Cr}(\text{OH})^{2+}$; $\text{Cr}_2(\text{OH})_4^{4+}$; and $\text{Cr}_3(\text{OH})_4^{5+}$.

Calculation of the solubility of $\text{Cr}(\text{OH})_3$ as a function of pH using HCl and NaOH to adjust the pH requires taking into account all species, equilibrium relationships, mass balance, and electroneutrality, as well as calculation of the ionic activity coefficients. The results of such a calculation (employing Prochem software) appears in Table 1.5 and Figures 1.9 and 1.10. Table 1.5 shows the results obtained at a pH of 10. Figure 1.9 gives the solubility results obtained from a series of calculations and also shows the concentration of the various species while Figure 1.10 compares the solubility obtained with that calculated from a solubility product. The solubility results obtained by the simple solubility product calculation are orders of magnitude less than those obtained by the complex calculation, demonstrating

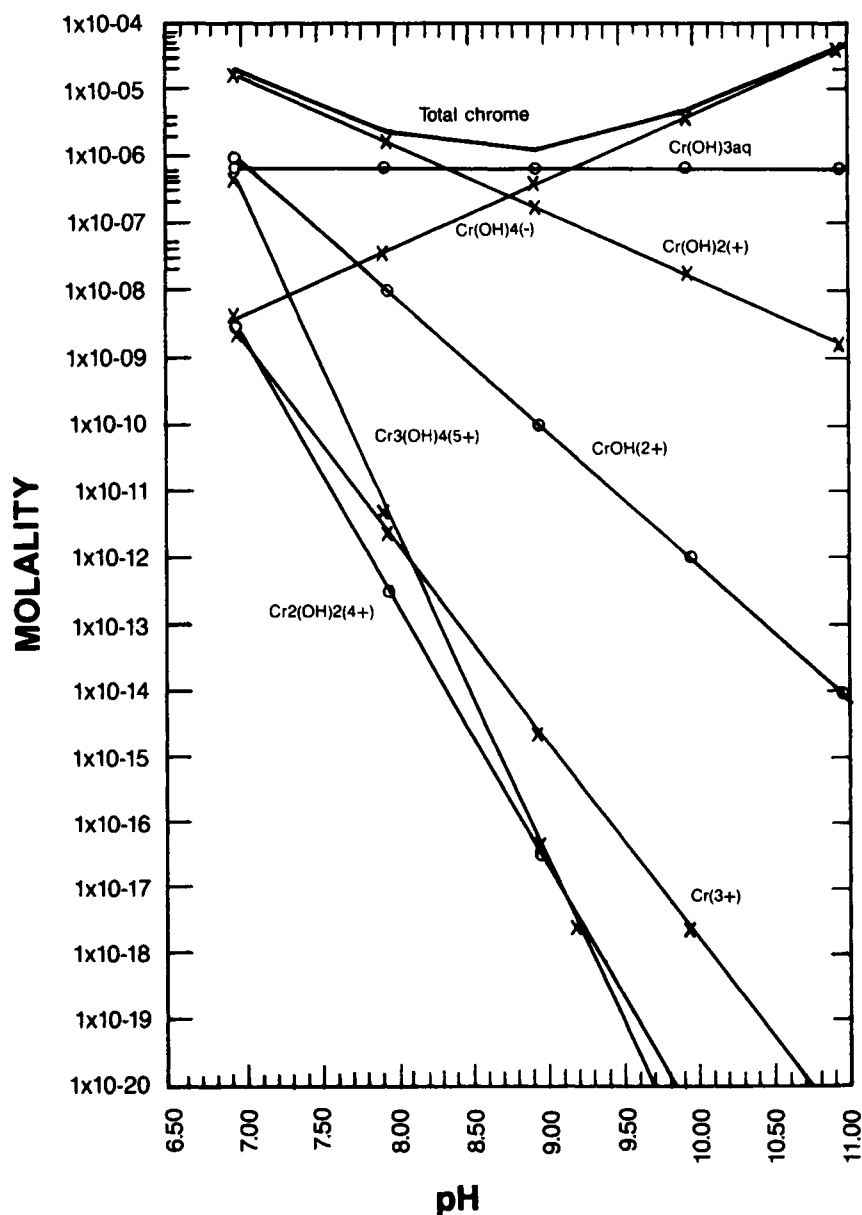


Figure 1.9 Chrome hydroxide solubility and speciation versus pH at 25 °C. (Reproduced from J.F. Zemaitis, Jr., D.M. Clark, M. Rafal, and N.C. Scrivner (1986), *Handbook of Aqueous Electrolyte Thermodynamics*, p. 661. Used by permission of the American Institute of Chemical Engineers. © 1986 AIChE.)

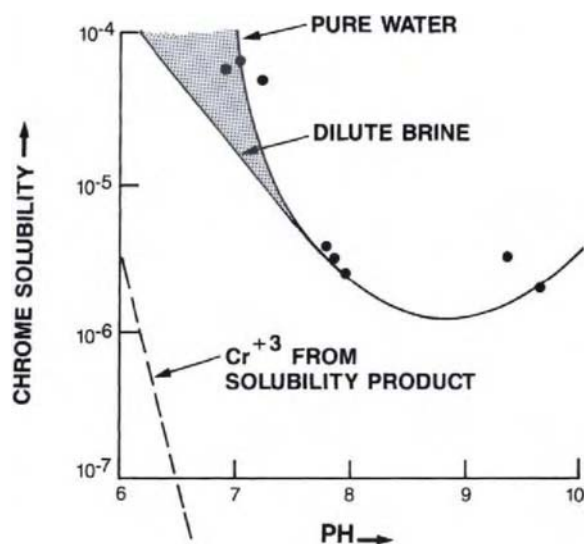


Figure 1.10 Chrome solubility versus pH. (Reproduced with permission of OLI Systems.)

the importance of considering all possible species in the calculation.

1.4. SOLUBILITY OF ORGANICS

In crystallization operations involving inorganic materials we virtually always employ water as the solvent, thus requiring solubility data on inorganic water systems. Since most inorganic materials are ionic, this means that dissociation reactions, ionic interactions, and pH play a major role in determining the solubility of a particular inorganic species in aqueous solution. When dealing with organic species (or inorganics in nonaqueous solvents) a wide variety of solvents and solvent mixtures can usually be employed. The interaction between the solute and the solvent determines the differences in solubility commonly observed for a given organic species in a number of different solvents. This is illustrated in Figures 1.11 and 1.12 for hexamethylene tetramine and adipic acid in several different solvents. In the development of crystallization processes this can be a powerful tool. In many cases the solvent chosen for a particular process is an arbitrary choice made in the laboratory with no thought of the downstream processing consequences. Many times, from a chemical synthesis or reaction point of view, a number of different solvents could be used with no significant change in product yield or quality. This means that the solubility and physical properties of the solvent (solubility as a function of temperature, absolute solubility, and vapor pressure) should be evaluated so that the solvent that provides the best characteristics for the crystallization step is chosen. This of course requires that the process development engineers be in contact with the synthetic organic chemists early in a process development.

In this section we will describe the basic principles required to estimate and calculate the solubility of an organic solute in different solvents and explain how to assess mixed solvents.

1.4.1. THERMODYNAMIC CONCEPTS AND IDEAL SOLUBILITY

As we have shown previously, the condition for equilibrium between a solid solute and a solvent is given by the relation

$$\mu_{i\text{solid}} = \mu_{i\text{solution}} \quad (1.36)$$

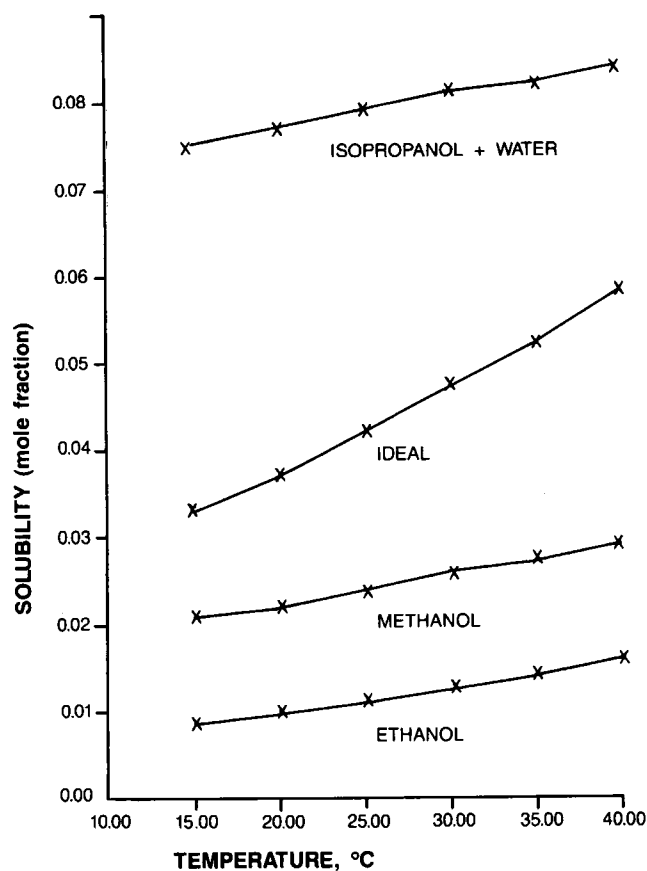


Figure 1.11 Solubility of hexamethylenetetramine in different solvents. (Reprinted with permission from S. Decker, W.P. Fan, and A.S. Myerson, "Solvent Selection and Batch Crystallization," *Ind. Eng. Chem. Fund.* 25, 925. © 1986 American Chemical Society.)

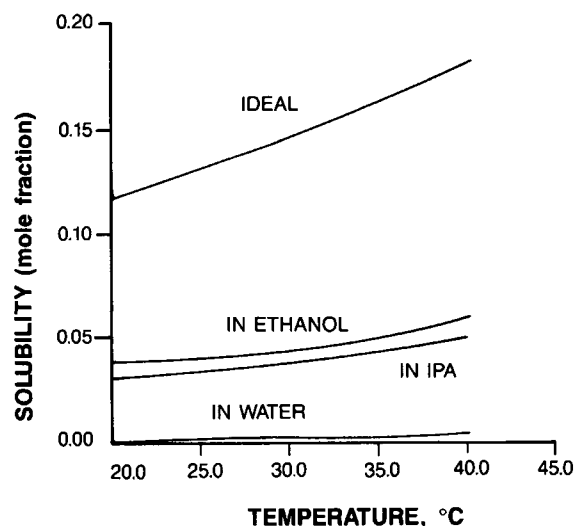


Figure 1.12 Solubility of adipic acid in different solvents. (Reprinted with permissions from S. Decker, W.P. Fan, and A.S. Myerson (1986), "Solvent Selection and Batch Crystallization," *Ind. Eng. Chem. Fund.* 25, 925. © 1986 American Chemical Society.)

12 SOLUTIONS AND SOLUTION PROPERTIES

A thermodynamic function known as the fugacity can be defined as

$$\mu_i - \mu_i^0 = RT \ln f_i/f_i^0 \quad (1.37)$$

Comparing Eq. (1.10) with Eq. (1.37) shows us that the activity $a_i = f_i/f_i^0$. Through a series of manipulations it can be shown (Prausnitz et al. 1999) that for phases in equilibrium

$$f_{\text{solid}} = f_{\text{solution}} \quad (1.38)$$

Eq. (1.38) will be more convenient for us to use in describing the solubility of organic solids in various solvents. The fugacity is often thought of as a "corrected pressure" and reduces to pressure when the solution is ideal. Eq. (1.38) can be rewritten as

$$f_{\text{solid}} = \gamma_2 x_2 f_2^0 \quad (1.39)$$

where

- f_2 = fugacity of the solid
- x_2 = mole fraction of the solute in the solution
- f_2^0 = standard state fugacity
- γ_2 = activity coefficient of the solute

or

$$x_2 = \frac{f_{\text{solid}}}{\gamma_2 f_2^0} \quad (1.40)$$

Eq. (1.40) is a general equation for the solubility of any solute in any solvent. We can see from this equation that the solubility depends on the activity coefficient and on the fugacity ratio f_2/f_2^0 . The standard state fugacity normally used for solid-liquid equilibrium is the fugacity of the pure solute in a subcooled liquid state below its melting point. We can simplify Eq. (1.40) further by assuming that our solid and subcooled liquid have small vapor pressures. We can then substitute vapor pressure for fugacity. If we further assume that the solute and solvent are chemically similar so that $\gamma_2 = 1$, then we can write

$$x_2 = \frac{P_{\text{solid}}^{\text{solute}}}{P_{\text{subcooled liquid}}^{\text{solute}}} \quad (1.41)$$

Eq. (1.41) gives the ideal solubility. Figure 1.13, an example phase diagram for a pure component, illustrates several points. First, we are interested in temperatures below the triple point since we are interested in conditions where the solute is a solid. Second, the subcooled liquid pressure is obtained by extrapolating the liquid-vapor line to the correct temperature.

Eq. (1.41) gives us two important pieces of information. The first is that the ideal solubility of the solute does not depend on the solvent chosen; the ideal solubility depends only on the solute properties. The second is that it shows the differences in the pure component phase diagrams that result from structural differences in materials will alter the triple point and hence the ideal solubility.

A general equation for the fugacity ratio is

$$\ln \frac{f_2}{f_{\text{subcooled liquid}}^{\text{solute}}} = \frac{\Delta H_{tp}}{R} \left(\frac{1}{T_{tp}} - \frac{1}{T} \right) - \frac{\Delta C_p}{R} \left(\ln \frac{T_{tp}}{T} - \frac{T_{tp}}{T} + 1 \right) - \frac{\Delta V}{RT} (P - P_{tp}) \quad (1.42)$$

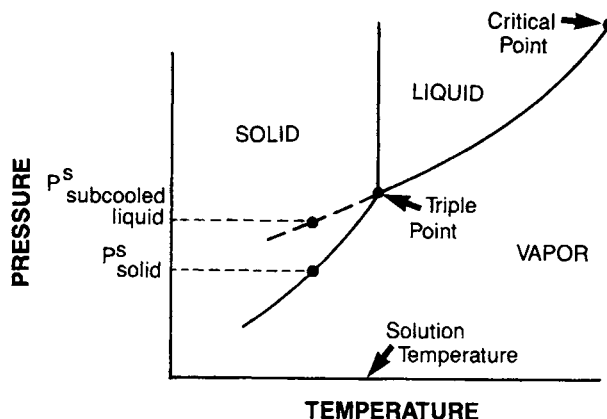


Figure 1.13 Schematic of a pure component phase diagram. (Reprinted by permission of Prentice Hall, Englewood Cliffs, New Jersey, from J.M. Prausnitz, R.N. Lichtenhaler, and E. Gomes de Azevedo, *Molecular Thermodynamics of Fluid-Phase Equilibria*, 2nd ed., © 1986, p. 417.)

where

- ΔH_{tp} = enthalpy change for the liquid solute transformation at the triple point
- T_{tp} = triple point temperature
- ΔC_p = difference between the C_p of the liquid and the solid
- ΔV = volume change

If substituted into Eq. (1.40) this yields the solubility equation

$$x_2 = \frac{1}{\gamma_2} \exp \left[\frac{\Delta H_{tp}}{R} \left(\frac{1}{T_{tp}} - \frac{1}{T} \right) - \frac{\Delta C_p}{R} \left(\ln \frac{T_{tp}}{T} - \frac{T_{tp}}{T} + 1 \right) - \frac{\Delta V}{RT} (P - P_{tp}) \right] \quad (1.43)$$

Eq. (1.43) is the most general form of the solubility equation. In most situations (though not all) the effect of pressure on solubility is negligible so that the last term on the right-hand side of the equation can be dropped. In addition, the heat capacity term can also usually be dropped from the equation. This yields

$$x_2 = \frac{1}{\gamma_2} \exp \left[\frac{\Delta H_{tp}}{R} \left(\frac{1}{T_{tp}} - \frac{1}{T} \right) \right] \quad (1.44)$$

or since

$$\Delta S = \Delta H_{tp}/T_{tp} \quad (1.45)$$

$$x_2 = \frac{1}{\gamma_2} \exp \left[\frac{\Delta S_{tp}}{R} (1 - T_{tp}/T) \right] \quad (1.46)$$

In many instances, the triple point temperature of a substance is not known. In those cases, the enthalpy of melting (fusion) and melting point temperature are used since they are usually close to the triple point temperature

$$x_2 = \frac{1}{\gamma_2} \exp \left[\frac{\Delta H_m}{R} \left(\frac{1}{T_m} - \frac{1}{T} \right) \right] \quad (1.47)$$

TABLE 1.6 Melting Temperature, Enthalpy of Melting, and Ideal Solubility of Organic Solutes at 25 °C

Substance	T_m (K)	ΔH_m (cal/mol)	Ideal Solubility (mol%)
<i>Ortho</i> -chloronitrobenzene	307.5	4546	79
<i>Meta</i> -chloronitrobenzene	317.6	4629	62
<i>Para</i> -chloronitrobenzene	356.7	4965	25
Napthalene	353.4	4494	31
Urea	406.0	3472	21
Phenol	314.1	2695	79
Anthracene	489.7	6898	1
Phenanthrene	369.5	4456	23
Biphenyl	342.2	4235	39

(Based on data from Walas 1985.)

For an ideal solution when the activity coefficient equation equals one, this reduces to

$$x_2 = \exp \left[\frac{\Delta H_m}{R} \left(\frac{1}{T_m} - \frac{1}{T} \right) \right] \quad (1.48)$$

Eq. (1.48) allows the simple calculation of ideal solubilities and can be used profitably to see the differences in solubility of chemically similar species with different structures. This is illustrated in Table 1.6 where calculated ideal solubilities are shown together with ΔH_m and T_m . Isomers of the same species can have widely different ideal solubilities based on changes in their physical properties, which relate back to their chemical structures. Eq. (1.48) also tells us that for an ideal solution, solubility increases with increasing temperature. The rate of increase is approximately proportional to the magnitude of the heat of fusion (melting). For materials with similar melting temperatures, the lower the heat of fusion, the higher the solubility. For materials with similar heats of fusion, the material with the lower melting temperature has the higher solubility. A good example of this is shown in Table 1.6 when looking at *ortho*-, *meta*-, and *para*-chloronitrobenzene. The lower melting *ortho* has an ideal solubility of 79 mol% compared with 25 mol% for the higher melting *para*. While Eq. (1.48) is useful for comparing relative solubilities of various solutes, it takes no account of the solvent used or solute-solvent interactions. To account for the role of the solvent, activity coefficients must be calculated.

1.4.2. REGULAR SOLUTION THEORY

In electrolytic solutions we were concerned with electrostatic interactions between ions in the solution and with the solvent (water). In solutions of nonelectrolytes we will be concerned with molecule-solvent interactions due to electrostatic forces, dispersion forces, and chemical forces.

Even though a solution contains no ions, electrostatic interactions can still be significant. This is because of a property called *polarity*. An electrically neutral molecule can have a dipole moment that is due to an asymmetric distribution of its electrical charge. This means that one end of the molecule is positive and the other end is negative. The dipole moment is defined by

$$\mu = el \quad (1.49)$$

where e is the magnitude of the electric charge and l is the distance between the two charges. The dipole moment is a measure of how polar a molecule is. As the dipole moment increases, the molecule

TABLE 1.7 Permanent Dipole Moments

Molecule	μ (Debyes)	Molecule	μ (Debyes)
CO	0.10	CH ₃ I	1.64
C ₃ H ₆	0.35	CH ₃ COOCH ₃	1.67
C ₆ H ₅ CH ₃	0.37	C ₂ H ₅ OH	1.70
PH ₃	0.55	H ₂ O	1.84
HBr	0.80	HF	1.91
CHCl ₃	1.05	C ₂ H ₅ F	1.92
(C ₂ H ₅) ₂ O	1.18	(CH ₃) ₂ CO	2.87
NH ₃	1.47	C ₆ H ₅ COCH ₃	3.00
C ₆ H ₅ NH ₂	1.48	C ₂ H ₅ NO ₂	3.70
C ₆ H ₅ Cl	1.55	CH ₃ CN	3.94
C ₂ H ₅ SH	1.56	CO(NH ₂) ₂	4.60
SO ₂	1.61	KBr	9.07

(Data from Prausnitz et al. 1986.)

is less symmetrical in terms of its electrical charge. A list of molecules and their dipole moments is given in Table 1.7. As you can see from the table, water is quite polar. There are also molecules with more complex charge distributions called *quadrupoles*, which also display this asymmetric charge behavior. This shows that even without ions, electrostatic interactions between polar solvent molecules and polar solute molecules will be of importance in activity coefficient calculations and will therefore affect the solubility.

Organic solutes and solvents are usually classified as polar or nonpolar, though, of course, there is a range of polarity. Nonpolar solutes and solvents also interact through forms of attraction and repulsion known as dispersion forces. Dispersion forces result from oscillations of electrons around the nucleus and have a rather complex explanation; however, it is sufficient to say that non-idealities can result from molecule-solvent interactions that result in values of the activity coefficient not equal to 1. An excellent reference in this area is the book of Prausnitz et al. (1999).

Generally, the activity coefficients are < 1 when polar interactions are important, with a resulting increase in solubility of compounds compared with the ideal solubility. The opposite is often true in nonpolar systems where dispersion forces are important, with the activity coefficients being > 1 . A variety of methods are used to calculate activity coefficients of solid solutes in solution. A frequently used method is that of Scatchard-Hildebrand, which is also known as "regular" solution theory (Prausnitz et al. 1999).

$$\ln \gamma_2 = \frac{V_2^L(\delta_1 - \delta_2)^2 \Phi_1^2}{RT} \quad (1.50)$$

where

V_2^L = molar volume of the subcooled liquid solute

δ_2 = solubility parameter of the subcooled liquid

δ_1 = solubility parameter of the solvent

Φ = volume fraction, or the solvent defined by

$$\Phi = \frac{x_1 V_1^L}{x_1 V_1^L + x_2 V_2^L} \quad (1.51)$$

The solubility parameters are defined by the relations

$$\delta_1 = \left(\frac{\Delta u_1^v}{v_1} \right)^{1/2} \quad \delta_2 = \left(\frac{\Delta u_2^v}{v_2} \right)^{1/2} \quad (1.52)$$

where Δu is the enthalpy of vaporization and v is the molar liquid volume. Solubility parameters for a number of solvents and solutes are given in Table 1.8. This method works moderately well at predicting solubilities in nonpolar materials. Calculated solubility

TABLE 1.8 Solubility Parameters at 25 °C

Substance	$\delta(\text{cal/cm}^3)^{1/2}$
Anthracene	9.9
Naphthalene	9.38
Phenanthrene	10.52
Acetic acid	10.05
Acetone	9.51
Aniline	11.46
1-Butanol	11.44
Carbon disulfide	9.86
Carbon tetrachloride	9.34
Chloroform	9.24
Cyclohexane	8.19
Cyclohexanol	11.4
Diethyl ether	7.54
Ethanol	12.92
<i>n</i> -Hexane	7.27
Methanol	14.51
Phenol	12.11
1-Propanol	12.05
2-Propanol	11.57
Perfluoro- <i>n</i> -heptane	6.0
Neopentane	6.2
Isopentane	6.8
<i>n</i> -Pentane	7.1
1-Hexene	7.3
<i>n</i> -Octane	7.5
<i>n</i> -Hexadecane	8.0
Ethyl benzene	8.8
Toluene	8.9
Benzene	9.2
Styrene	9.3
Tetrachloroethylene	9.3
Bromine	11.5

(Based on data from Prausnitz et al. 1986 and Walas 1985.)

results employing this theory are shown in Table 1.9 along with experimentally determined values. It is apparent that in many cases this theory predicts results very far from the experiment. A variety of modifications of the Scatchard-Hildebrand theory as well as other methods are available for activity coefficient calculations and are described by Walas (1985), Prausnitz et al. (1999), and Reid et al. (1987), however, no accurate general method is available for activity coefficient calculation of solid-solutes in liquids.

TABLE 1.9 Solubility of Naphthalene in Various Solvents by UNIFAC and Scatchard-Hildebrand Theory

Solvent	Solubility (mol%)		
	Experimental	UNIFAC	Scatchard-Hildebrand
Methanol	4.4	4.8	0.64
Ethanol	7.3	5.4	4.9
1-Propanol	9.4	9.3	11.3
2-Propanol	7.6	9.3	16.3
1-Butanol	11.6	11.1	18.8
<i>n</i> -Hexane	22.2	25.9	11.5
Cyclohexanol	22.5	20.5	20.0
Acetic acid	11.7	12.5	40.1
Acetone	37.8	35.8	42.2
Chloroform	47.3	47.0	37.8
Ideal solubility = 4.1 mol%			

(Data from Walas 1985.)

1.4.3. GROUP CONTRIBUTION METHODS

As we discussed in Section 1.3, on inorganic materials, industrial crystallization rarely takes place in systems that contain only the solute and solvent. In many situations, additional components are present in the solution that affect the solubility of the species of interest. With an organic solute, data for solubility in a particular solvent is often not available, while data for the effect of other species on the solubility is virtually nonexistent. This means that the only option available for determining solubility in a complex mixture of solute, solvent, and other components (impurities or by-products) is through calculation or experimental measurement. While experimental measurement is often necessary, estimation through calculation can be worthwhile.

The main methods available for the calculation of activity coefficients in multicomponent mixtures are called group *contribution methods*. This is because they are based on the idea of treating a molecule as a combination of functional groups and summing the contribution of the groups. This allows the calculation of properties for a large number of components from a limited number of groups. Two similar methods are used for these types of calculations, ASOG (analytical solution of groups) and UNIFAC (UNIQUAC functional group activity coefficient), and they are explained in detail in a number of references (Reid et al. 1987; Walas 1985; Kojima and Tochigi 1979; Fredenslund et al. 1977).

Both of these methods rely on the use of experimental activity coefficient data to obtain parameters that represent interaction between pairs of structural groups. These parameters are then combined to predict activity coefficients for complex species and mixtures of species made up from a number of these functional groups. An example of this would be the calculation of the behavior of a ternary system by employing data on the three possible binary pairs. Lists of parameters and detailed explanations of these calculations can be found in the references previously mentioned.

The groups contribution methods can also be used to calculate solubility in binary (solute-solvent) systems. A comparison of solubilities calculated employing the UNIFAC method with experimental values and values obtained from the Scatchard-Hildebrand theory is given in Table 1.9.

1.4.4. SOLUBILITY IN MIXED SOLVENTS

In looking for an appropriate solvent system for a particular solute to allow for the development of a crystallization process, often the desired properties cannot be obtained with the pure solvents that can be used. For a number of economic, safety, or product stability reasons, you may be forced to consider a small group of solvents. The solute might not have the desired solubility in any of these solvents, or if soluble, the solubility may not vary with temperature sufficiently to allow cooling crystallization. In these cases a possible solution is to use a solvent mixture to obtain the desired solution properties. The solubility of a species in a solvent mixture can significantly exceed the solubility of the species in either pure component solvent. This is illustrated in Figure 1.14 for the solute phenanthrene in the solvents cyclohexane and methyl iodide. Instead of a linear relation between the solvent composition and the solubility, the solubility has a maximum at a solvent composition of 0.33 wt% methyl iodide (solute-free basis). The large change in solubility with solvent composition can be very useful in crystallization processes. It provides a method other than temperature change to alter the solubility of the system. The solubility can be easily altered up or down by adding the appropriate solvent to the system. The method of changing solvent composition to induce crystallization will be discussed in more detail in Section 1.5.3.

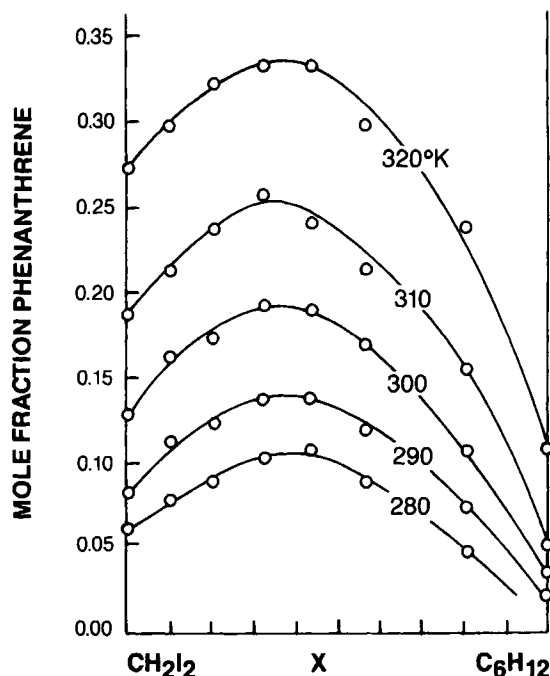


Figure 1.14 Solubility of phenanthrene in cyclohexane-methylene iodide mixtures. (Reprinted with permission from L.J. Gordon and R.L. Scott, "Enhanced Methylene Iodide Solubility in Solvent Mixtures. I. The System Phenanthrene-Cyclohexane-Methylene Iodide," *J. Am. Chem. Soc.* **74**, 4138. © 1952 American Chemical Society.)

Finding an appropriate mixed solvent system should not be done on a strictly trial and error basis. It should be examined systematically based on the binary solubility behavior of the solute in solvents of interest. It is important to remember that the mixed solvent system with the solute present must be miscible at the conditions of interest. The observed maximum in the solubility of solutes in mixtures is predicted by Scatchard-Hildebrand theory. Looking at Eq. (1.50) we see that when the solubility parameter of the solvent is the same as that of the subcooled liquid solute, the activity coefficient will be 1. This is the minimum value of the activity coefficient possible employing this relation. When the activity coefficient is equal to 1, the solubility of the solute is at a maximum. This then tells us that by picking two solvents with solubility parameters that are greater than and less than the solubility parameter of the solute, we can prepare a solvent mixture in which the solubility will be a maximum. As an example, let us look at the solute anthracene. Its solubility parameter is $9.9 \text{ (cal/cm}^3)^{1/2}$. Looking at Table 1.8, which lists solubility parameters for a number of common solvents, we see that ethanol and toluene have solubility parameters that bracket the value of anthracene. If we define a mean solubility parameter by the relation

$$\delta = \frac{\sum x_i V_i \delta_i}{\sum x_i V_i} \quad (1.53)$$

we can then calculate the solvent composition that will have the maximum solubility. This is a useful way to estimate the optimum solvent composition prior to experimental measurement. Examples of these calculations can be found in Walas (1985).

Another useful method is to employ the group contribution methods described in the previous section with data obtained on the binary pairs that make up the system.

Recently, Frank et al. (1999) presented a good review of these and other calculation-based methods to quickly screen solvents for use in organic solids crystallization processes.

1.4.5. MEASUREMENT OF SOLUBILITY

Accurate solubility data is a crucial part of the design, development, and operation of a crystallization process. When confronted with the need for accurate solubility data, it is often common to find that the data is not available for the solute at the conditions of interest. This is especially true for mixed and nonaqueous solvents, and for systems with more than one solute. In addition, most industrial crystallization processes involve solutions with impurities present. If it is desired to know the solubility of the solute in the actual working solution with all impurities present, it is very unlikely that data will be available in the literature. Methods for the calculation of solubility have been discussed previously. These can be quite useful, but often are not possible because of lack of adequate thermodynamic data. This means that the only method available to determine the needed information is solubility measurement.

The measurement of solubility appears to be quite simple, however, it is a measurement that can easily be done incorrectly, resulting in very large errors. Solubility should always be measured at a constant controlled temperature (isothermal) with agitation employed. A procedure for measuring solubility is given below:

1. To a jacketed or temperature-controlled vessel (temperature control should be 0.1°C or better), add a known mass of solvent.
2. Bring the solvent to the desired temperature. If the temperature is above room temperature or the solvent is organic, use a condenser to prevent evaporation.
3. Add the solute in excess (having determined the total mass added) and agitate the solution for a period of at least 4 h. A time period of 24 h is preferable.
4. Sample the solution and analyze for the solute concentration.

If solute analysis is not simple or accurate, step 4 can be replaced by filtering the solution, drying the remaining solid, and weighing. The amount of undissolved solute is subtracted from the total initially added. The long period of time is necessary because dissolution rates become very slow near saturation. If a short time period is used (1 h or less), the solubility will generally be underestimated.

If care is taken, data obtained using this procedure will be as accurate as the concentration measurement or weighing accuracy achieved.

Two common errors in solubility measurement that produce large errors involve using nonisothermal techniques. In one technique a solution of known concentration is made at a given temperature above room temperature and cooled until the first crystals appear. It is assumed that this temperature is the saturation temperature of the solution of the concentration initially prepared. This is incorrect. As we will see in Section 1.5, solutions become supersaturated (exceed their solubility concentration) before they crystallize. The temperature that the crystals appeared is likely to be significantly below the saturation temperature for that concentration so that the solubility has been significantly overestimated.

Another method that will result in error is to add a known amount of solute in excess to the solution and raise the temperature until it all dissolves. It is assumed that the temperature at which the last crystal disappears is the solubility temperature at the concentration of solution (total solute added per solvent in system). This is again incorrect because dissolution is not an instantaneous process and, in fact, becomes quite slow as the saturation

temperature is approached. This method will underestimate the solubility because the solution will have been heated above the saturation temperature.

Accurate solubility data is worth the time and trouble it will take to do the experiment correctly. Avoid the common errors discussed and be suspicious of data where the techniques used in measurement are not known.

1.5. SUPERSATURATION AND METASTABILITY

As we have seen in the previous section, solubility provides the concentration at which the solid solute and the liquid solution are at equilibrium. This is important because it allows calculation of the maximum yield of product crystals accompanying a change of state from one set of concentration to another in which crystals form. For example, if we look at Figure 1.15, which gives us the solubility diagram for KCl, if we start with 1000 kg of a solution at 100°C and a concentration of 567 g/kg water and cool it to 10°C at equilibrium, we will have 836 kg of solution with a KCl concentration of 310 g/kg water and 164 kg of solid KCl. While this mass balance is an important part of crystallization process design, development, and experimentation, it tells us nothing about the rate at which the crystals form and the time required to obtain this amount of solid. That is because thermodynamics tells us about equilibrium states but not about rates. Crystallization is a rate process, this means that the time required for the crystallization depends on some driving force. In the case of crystallization the driving force is called the *supersaturation*.

Supersaturation can be easily understood by referring to Figure 1.15. If we start at point A and cool the solution of KCl to a temperature of 40°C, the solution is saturated. If we continue to cool a small amount past this point to B, the solution is likely to remain homogeneous. If we allow the solution to sit for a period of time or stir this solution, it will eventually crystallize. A solution in which the solute concentration exceeds the equilibrium (saturation) solute concentration at a given temperature is known as a supersaturated solution. Supersaturated solutions are metastable. We can see what that means by looking at Figure 1.16. A stable solution is represented by Figure 1.16a and appears as a minimum. A large disturbance is needed to change the state in this instance. An unstable solution is represented by Figure 1.16b and is just the

opposite, with the solution being represented by a sharp maximum so that a differential change will result in a change in the state of the system. A metastable solution is represented by Figure 1.16c as an inflection point where a small change is needed to change the state of the system, but one which is finite. Metastability is an important concept that we will discuss in greater detail in Section 1.5.2.

1.5.1. UNITS

Supersaturation is the fundamental driving force for crystallization and can be expressed in dimensionless form as

$$\frac{\mu - \mu^*}{RT} = \ln \frac{a}{a^*} = \ln \frac{\gamma c}{\gamma^* c^*} \quad (1.54)$$

where μ is the chemical potential, c is the concentration, a is the activity, γ is the activity coefficient, and $*$ represents the property at saturation. In most situations, the activity coefficients are not known and the dimensionless chemical potential difference is approximated by a dimensionless concentration difference

$$\sigma = c - \frac{c^*}{c^*} \quad (1.55)$$

This substitution is only accurate when $\gamma/\gamma^* = 1$ or $\sigma \ll 1$ so that $\ln(\sigma + 1) = \sigma$. It has been shown that this is generally a poor approximation at $\sigma > 0.1$ (Kim and Myerson 1996), but it is still normally used because the needed thermodynamic data are usually unavailable. Supersaturation is also often expressed as a concentration difference

$$\Delta c = c - c^* \quad (1.56)$$

and as a ratio of concentrations

$$S = \frac{c}{c^*} \quad (1.57)$$

It is important to note that these definitions of supersaturation assume an ideal solution with an activity coefficient of 1. It is common practice to ignore activity coefficients in most cases and employ concentrations in expressions of supersaturation, however, in very nonideal solutions and in precise studies of crystal growth and nucleation, activity coefficients are often used.

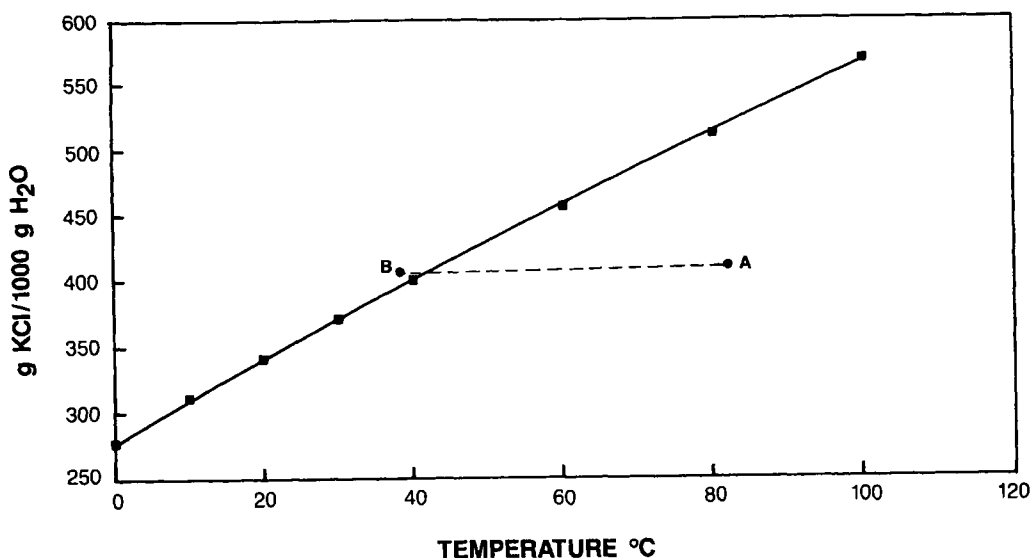


Figure 1.15 Solubility of KCl in aqueous solution. (Data from Linke and Seidell 1958, 1965.)

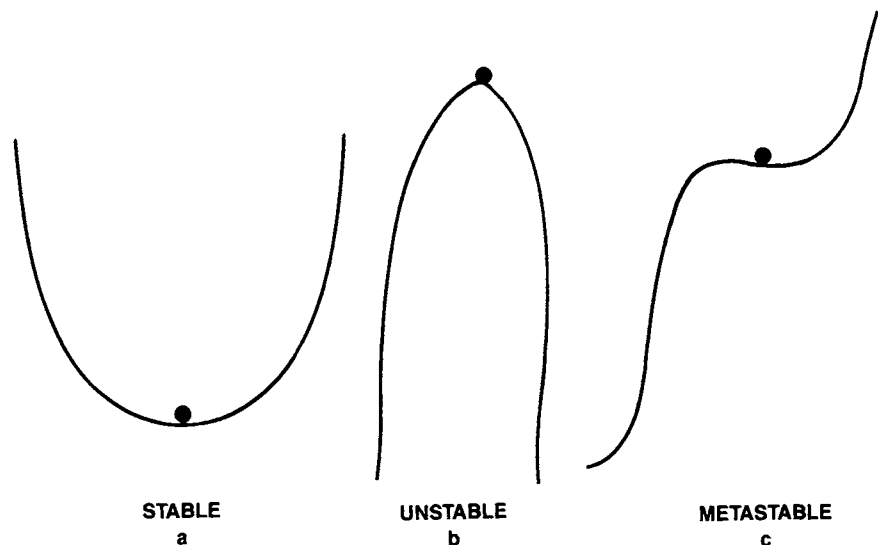


Figure 1.16 Stability states.

Another practice is to refer to supersaturation in terms of degrees. This refers to the difference between the temperature of the solution and the saturation temperature of the solution at the existing concentration. A simpler way to explain this is that the degrees of supersaturation are simply the number of degrees a saturated solution of the appropriate concentration was cooled to reach its current temperature. This is generally not a good unit to use, however, it is often mentioned in the literature.

1.5.2. METASTABILITY AND THE METASTABLE LIMIT

As we have seen previously, supersaturated solutions are metastable. This means that supersaturating a solution some amount will not necessarily result in crystallization. Referring to the solubility diagram shown in Figure 1.17, if we were to start with a solution at point A and cool to point B just below saturation, the solution would be supersaturated. If we allowed that solution to sit, it might take days before crystals formed. If we took another sample, cooled it to point C, and let it sit, this might crystallize in a matter of hours; eventually we will get to a point where the solution crystallized rapidly and no longer appears to be stable. As we can see from this experiment, the metastability of a solution decreases as the supersaturation increases. It is important to note however that we are referring to homogeneous solutions only. If crystals of the solute are placed in any supersaturated solution, they will grow, and the solution will eventually reach equilibrium. The obvious question that comes to mind is why are supersaturated solutions metastable. It seems reasonable to think that if the solubility is exceeded in a solution, crystals should form. To understand why they do not, we will have to discuss something called nucleation. *Nucleation* is the start of the crystallization process and involves the birth of a new crystal. Nucleation theory tells us that when the solubility of a solution is exceeded and it is supersaturated, the molecules start to associate and form aggregates (clusters), or concentration fluctuations. If we assume that these aggregates are spherical, we can write an equation for the Gibbs free energy change required to form a cluster of a given size

$$\Delta G = 4\pi r^2 \sigma - \left(\frac{4\pi r^3}{3V_m} \right) RT \ln(1 + S) \quad (1.58)$$

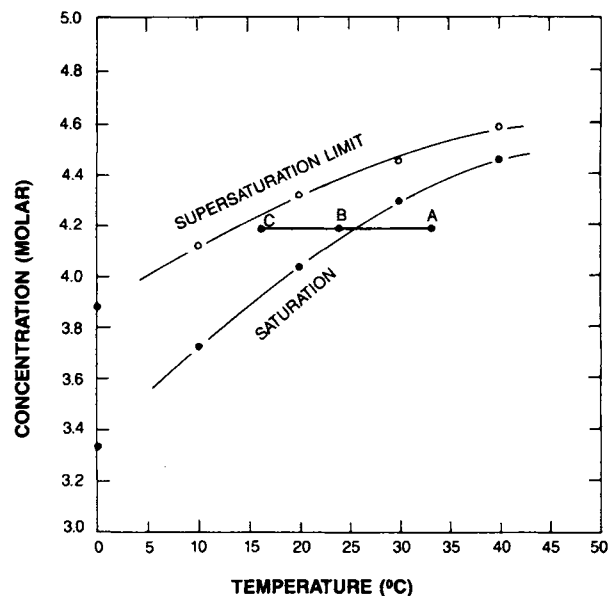


Figure 1.17 Metastable zone width for KCl-water system. (Data from Chang 1984.)

where r is the cluster radius, σ is the solid-liquid interfacial tension, and V_m is the specific volume of a solute molecule.

The first term is the Gibbs free energy change for forming the surface, and the second term is for the volume. For small numbers of molecules the total Gibbs free energy change is positive. This means that the clusters are unstable and will dissolve. A plot of ΔG as a function of cluster size (Figure 1.18) shows that as the cluster size increases, we reach a point where the Gibbs free energy change is negative and the cluster would grow spontaneously. When this happens, nucleation will occur. The reason that supersaturated solutions are metastable is, therefore, because of the need for a critical sized cluster to form. From Eq. (1.58) we can derive an expression for the critical size by setting the derivative $d\Delta G/dr = 0$ (the minimum in Figure 1.18) yields

$$r_c = 2V_m\sigma/RT \ln(1 + S) \quad (1.59)$$

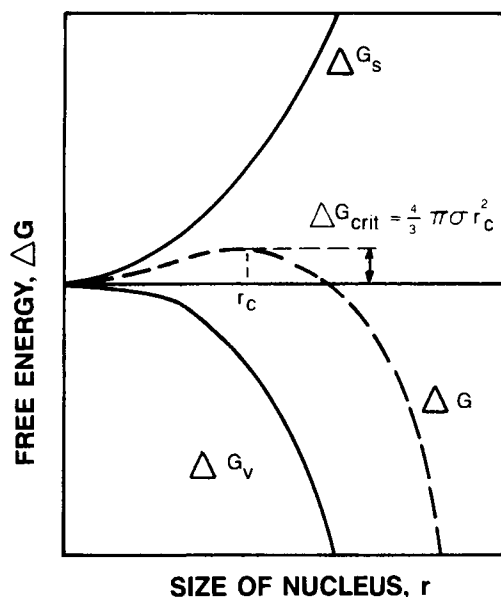


Figure 1.18 Free energy versus cluster radius. (Reproduced with permission from Mullin 1972.)

We can see from this equation that as the supersaturation increases, the critical size decreases. That is why solutions become less and less stable as the supersaturation is increased. Unfortunately, Eqs. (1.58) and (1.59) are not useful for practical calculations because one of the parameters, σ = the cluster interfacial tension, is not available or measurable and has a very significant effect on the calculation.

Every solution has a maximum amount that it can be supersaturated before it becomes unstable. The zone between the saturation curve and this unstable boundary is called the *metastable zone* and is where all crystallization operations occur. The boundary between the unstable and metastable zones has a thermodynamic definition and is called the *spinodal curve*. The spinodal is the absolute limit of the metastable region where phase separation must occur immediately. In practice, however, the practical limits of the metastable zone are much smaller and vary as a function of conditions for a given substance. This is because the presence of dust and dirt, the cooling rate employed and/or solution history, and the use of agitation can all aid in the formation of nuclei and decrease the metastable zone. Figure 1.17 gives an estimated metastable zone width for KCl in water.

Measurement of the metastable zone width and values for the metastable zone width obtained by a variety of methods for inorganic materials can be found in the work of Nývlt et al. (1985). In general there are two types of methods for the measurement of the metastable limit. In the first method, solutions are cooled to a given temperature rapidly and the time required for crystallization is measured. When this time becomes short then the effective metastable limit has been approached. A second method is to cool a solution at some rate and observe the temperature where the first crystals form. The temperature at which crystals are first observed will vary with the cooling rate used. Measured metastable limits for a number of materials are given in Table 1.10.

Data on the effective metastable limit at the conditions you are interested in (composition, cooling rate, and stirring) are important because you normally wish to operate a crystallizer away from the edge of the effective metastable zone. As we will see in later chapters, formation of small crystals, which are known as *fines*, is a common problem. Fines cause filtration problems and

TABLE 1.10 Metastable Zone Width

Substance	Equilibrium Temperature (°C)	Maximum Undercooling Before Nucleation		
		Cooling Rate		
		2°C/h	5°C/h	20°C/h
Ba(NO ₃) ₂	30.8	1.65	2.17	3.27
CuSO ₄ · 5H ₂ O	33.6	5.37	6.82	9.77
FeSO ₄ · 7H ₂ O	60.4	0.93	1.30	2.16
	30.0	0.89	1.21	1.93
KBr	40.6	0.57	0.83	1.46
	30.3	1.62	2.33	4.03
KCl	61.0	1.69	2.41	4.11
	29.8	1.62	1.86	2.30
MgSO ₄ · 7H ₂ O	59.8	1.02	1.18	1.48
	32	1.95	2.63	4.15
NH ₄ Al(SO ₄) ₂ · 12H ₂ O	30.2	0.81	1.34	2.88
	63	1.19	1.95	4.13
NaBr · 2H ₂ O	30.6	4.6	6.97	13.08

(Data from Nývlt et al. 1985.)

often are not wanted for various reasons in the final product. When a crystallization occurs at a high supersaturation (near the metastable limit) this usually means small crystals. The effective metastable zone width is an important process development and experimental design tool, and is worth the time to estimate.

1.5.3. METHODS TO CREATE SUPERSATURATION

In our discussions of supersaturation and metastability, we have always focused on situations where supersaturation is created by temperature change (cooling). While this is a very common method to generate supersaturation and induce crystallization, it is not the only method available.

There are four main methods to generate supersaturation that follow:

1. Temperature change.
2. Evaporation of solvent.
3. Chemical reaction.
4. Changing the solvent composition.

As we have discussed previously, the solubility of most materials declines with declining temperature so that cooling is often used to generate supersaturation. In many cases however, the solubility of a material remains high even at low temperatures or the solubility changes very little over the temperature range of interest. In these cases, other methods for the creation of supersaturation must be considered.

After cooling, evaporation is the most commonly used method for creating supersaturation. This is especially true when the solvent is nonaqueous and has a relatively high vapor pressure. The principle of using evaporation to create supersaturation is quite simple. Solvent is being removed from the system, thereby increasing the system concentration. If this is done at a constant temperature, eventually the system will become saturated and then supersaturated. After some maximum supersaturation is reached, the system will begin to crystallize.

There are a number of common methods used to evaporate solvents and crystallize materials based on the materials properties and solubility. One very common method for a material that has a solubility that decreases with decreasing temperature is to cool the system by evaporating solvent. Evaporation causes cooling in any system because of the energy of vaporization. If a system is put under a vacuum at a given temperature, the solvent will evaporate

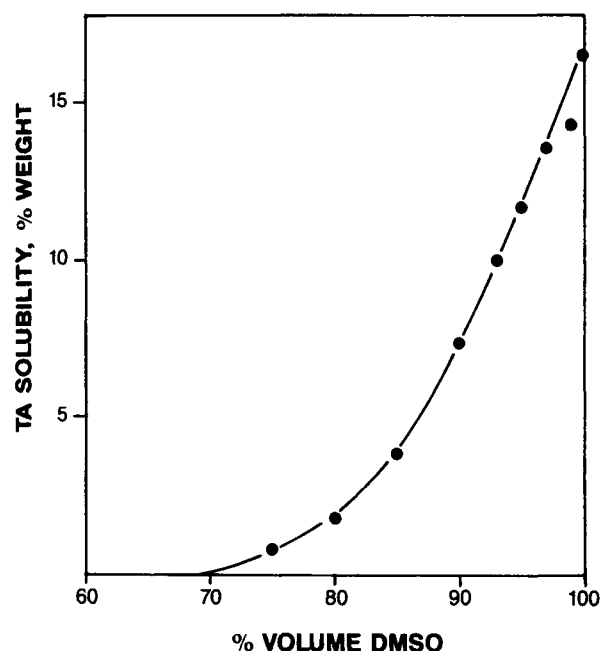


Figure 1.19 Solubility of terephthalic acid in DMSO-water mixtures at 25 °C. (Data from Saska 1984.)

and the solution will cool. In this case the concentration of the system increases while the temperature of the system decreases. In some cases, the cooling effect of the evaporation slows the evaporation rate by decreasing the system vapor pressure; in these cases, heat is added to the system to maintain the temperature and thereby the evaporation rate. Virtually all evaporations are done under vacuum.

As we saw in our discussion of solubility, the mixing of solvents can result in a large change in the solubility of the solute in the solution. This can be used to design a solvent system with specific properties and can also be used as a method to create supersaturation. If we took, for example, a solution of terephthalic acid (TPA) in the solvent dimethylsulfoxide (DMSO) at 25 °C, the solubility of the TPA at this temperature is 16.5 wt%. A cooling-

crystallization starting from some temperature above this to 23 °C (about room temperature) would leave far too much product in solution.

Imagine that evaporation cannot be used because of the lack of reasonable equipment, or because the solvent is not volatile enough and the product is heat sensitive. The third option is to add another solvent to the system to create a mixed solvent system in which the solubility of the solute is greatly decreased. If we were to add water to the TPA-DMSO system, the solubility changes rapidly from 16.5 wt% to essentially zero wt% with the addition of 30% water (by volume on the solute-free basis). This is shown in Figure 1.19. By controlling the rate of the addition, we can control the rate of supersaturation just as we can by cooling or by evaporation. In this case however, good mixing conditions are important so that we do not have local regions of high supersaturation and other regions of undersaturation.

This method of creating supersaturation is often called *drowning out* or adding a miscible nonsolvent. Normally you can find an appropriate solvent to add by looking for a material in which the solute is not soluble, that is miscible with the solute-solvent system. This can be done experimentally or screening can be done using solubility calculations prior to experimental tests. This is a particularly valuable technique with organic materials.

The last method of generating supersaturation is through chemical reaction. This is commonly called precipitation and will be discussed in detail in Chapter 6. In this case, two soluble materials are added together in solution that react to form a product with a low solubility. Since the solubility of the product is soon exceeded, the solution becomes supersaturated and the material crystallizes. This technique is commonly used in the production of inorganic materials. An example of a precipitation is the reaction of Na_2SO_4 and CaCl_2 to form NaCl and CaSO_4 (the insoluble product).

The solubility of the reactants and products are shown in Figure 1.20. Again in this type of process mixing is crucial in obtaining a homogenous supersaturation profile. Precipitation is important in the manufacture of a variety of materials. TPA, which is an organic commodity chemical used in the manufacture of polymers, is made from the oxidation of *p*-xylene in an acetic acid water mixture. The product has a very low solubility in the solvent system and rapidly precipitates out. Control of the supersaturation in a precipitation process is difficult because it involves control of the mixing of the reactants and or the reaction rate.

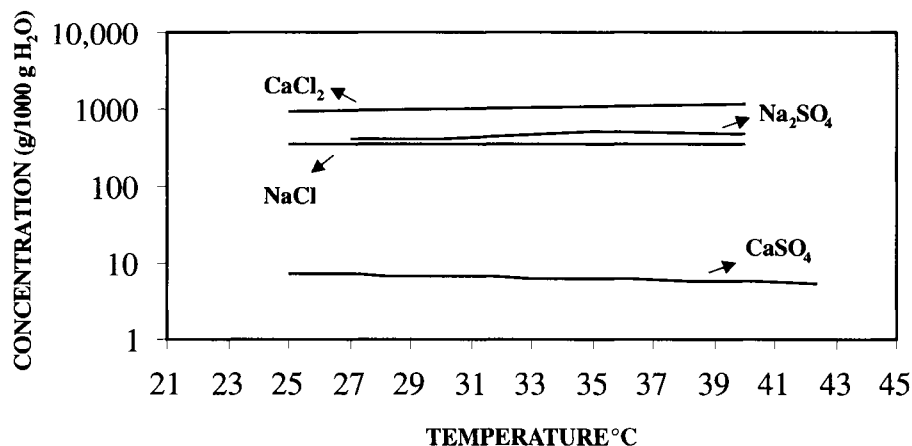


Figure 1.20 Solubility of NaCl , Na_2SO_4 , CaSO_4 , and CaCl_2 in water. (Data from Linke and Seidell 1958, 1965.)

TABLE 1.11 Density and Viscosity of Common Solvents

Substance	Density at 20°C (g/cm ³)	Viscosity at 20°C (cP)
Water	0.999	1.00
Acetone	0.789	0.322
Benzene	0.879	0.654
Toluene	0.866	0.587
Carbon tetrachloride	1.595	0.975
Methanol	0.791	0.592
Ethanol	0.789	1.19
n-Propanol	0.804	2.56

(Based on data from Mulin 1972 and Weast 1975.)

In general, you usually have the choice of more than one method to generate supersaturation. You should evaluate the system equipment available, solubility versus temperature of the material, and the production rate required before choosing one of the methods we discussed.

1.6. SOLUTION PROPERTIES

1.6.1. DENSITY

The density of the solution is often needed for mass balance, flow rate, and product yield calculations. Density is also needed to convert from concentration units based on solution volume to units of concentration based on mass or moles of the solution. Density is defined as the mass per unit volume and is commonly reported in g/cm³, however, other units such as pounds mass (lbm)/ft³ and kg/m³ are often used. When dealing with solutions, density refers to a homogeneous solution (not including any crystal present). Specific volume is the volume per unit mass and is equal to $1/\rho$.

Densities of pure solvents are available in handbooks like the *Handbook of Chemistry and Physics* (Lide 1999). The densities of a number of common solvents appear in Table 1.11. The densities of solutions as a function of concentration are difficult to find except for some common solutes in aqueous solution. The density of NaCl and sucrose as a function of concentration are given in Figure 1.21.

Densities are a function of temperature and must be reported at a specific temperature. A method for reporting densities uses a ratio known as the specific gravity. *Specific gravity* is the ratio of the density of the substance of interest to that of a reference

substance (usually water) at a particular temperature. To make use of specific gravity data it is necessary to know the density of the reference material at the correct temperature and to multiply the specific gravity by the reference density.

If density data is not available for the solution of interest, the density can be estimated by using the density of the pure solvent and pure solid solute at the temperature of interest and assuming the volumes are additive

$$\frac{1}{\rho_{\text{solution}}} = \frac{w_{\text{crystal}}}{\rho_{\text{crystal}}} + \frac{w_{\text{solvent}}}{\rho_{\text{solvent}}} \quad (1.60)$$

where w is the mass fraction of crystal or solvent. Calculating the density of a saturated solution of NaCl at 25°C using Eq. (1.60) results in a value of 1.17 g/cm³ compared with the experimental value of 1.20 g/cm³. Density can be calculated with more accuracy using thermodynamic techniques described in Reid et al. (1987).

Density can be measured in the laboratory in a number of different ways depending on the need for accuracy and the number of measurements required. Solution density can be easily estimated with reasonable accuracy by weighing a known volume of solution. Very precise instruments for the measurement of density that work employing a vibrating quartz element in a tube are sold by the Mettler Company (Hightstown, New Jersey). The period of vibration of the element is proportional to the density of the material placed in the tube. With careful calibration and temperature control the accuracy of these instruments ranges from 1×10^{-3} to 1×10^{-5} g/cm³. It is possible to use these instruments for on-line solution density measurement of fluid in a crystallizer (Rush 1991).

Another term typically used to describe solid-liquid mixtures is *slurry* or *magma density*. This is usually defined in terms of the mass of solids per unit volume of solution. A 10% slurry density therefore would indicate 100 g of solids/l of solution. Slurry density is not actually a true density but is a convenient term for indicating the amount of suspended solids in the solution.

1.6.2. VISCOSITY

The design of any equipment that involves the flow or stirring of liquids requires a knowledge of the fluids viscosity. Since crystallization operations involve the stirring and movement of suspensions of particles in fluids, the viscosity of suspensions is important in crystallization design and operation. *Viscosity* is a property of a

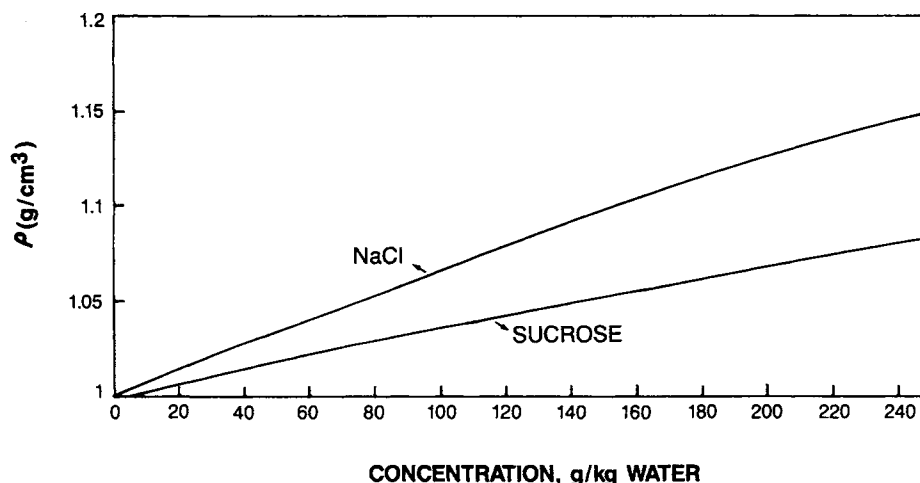


Figure 1.21 Density of sodium chloride and sucrose aqueous solutions as 20°C. (Data from Weast 1975.)

TABLE 1.12 Viscosity Units and Conversion Factors

Given a Quantity in These Units:	Multiply by Table Value to Convert to These Units: →					
	$\text{g cm}^{-1}\text{s}^{-1}$	$\text{kg m}^{-1}\text{s}^{-1}$	$\text{lb}_m \text{ft}^{-1}\text{s}^{-1}$	$\text{lb}_f \text{s}^{-1}\text{ft}^{-2}$	cP	$\text{lb}_m \text{ft}^{-1}\text{h}^{-1}$
$\text{g cm}^{-1}\text{s}^{-1}$	1	10^{-1}	6.7197×10^{-2}	2.0886×10^{-3}	10^2	2.4191×10^2
$\text{kg m}^{-1}\text{s}^{-1}$	10	1	6.7197×10^{-2}	2.0886×10^{-3}	10^3	2.4191×10^3
$\text{lb}_m \text{ft}^{-1}\text{s}^{-1}$	1.4882×10^1	1.4882	1	3.1081×10^{-2}	1.4882×10^3	3600
$\text{lb}_f \text{s}^{-1}\text{ft}^{-1}$	4.7880×10^2	4.7880×10^1	32.1740	1	4.7880×10^4	1.1583×10^5
cP	10^{-2}	10^{-3}	6.7197×10^{-4}	2.0886×10^{-5}	1	2.4191
$\text{lb}_m \text{ft}^{-1}\text{h}^{-1}$	4.1338×10^{-3}	4.1338×10^{-4}	2.7778×10^{-4}	8.6336×10^{-6}	4.1338×10^{-1}	1

(Reprinted by permission of John Wiley & Sons, Inc. from R.B. Bird, W.E. Stewart, and E.N. Lightfoot (1960), *Transport Phenomena*. © 1960 John Wiley & Sons, Inc.)

particular material defined as the ratio of the shear stress and the shear rate. Viscosity can be thought of as a measure of the resistance of a fluid to flow. When the relationship between shear stress and shear rate is linear and passes through the origin, the material is said to be Newtonian and the relationship can be represented by

$$\tau_{yx} = -\mu \frac{du_x}{dy} \quad (1.61)$$

where

τ_{yx} = shear stress

$\frac{du_x}{dy}$ = shear rate

μ = viscosity

Most common solvents are Newtonian fluids. Looking at Eq. (1.61) we can see that the units of viscosity will be given by the ratio of the shear stress and the shear rate which is mass/distance-time. Typical units used for viscosity are given in Table 1.12 along with their conversion factors. The ratio of the viscosity and the density is another commonly used term that is known as the

kinematic viscosity. The kinematic viscosity has units of length squared per unit time.

The viscosity of most common solvents is available in the literature. The values for some common solvents appear in Table 1.12. The viscosity of solutions of solids dissolved in liquids is normally not available at high concentrations except for common solutes in aqueous solution.

Viscosity increases with increasing concentration in solutions and decreases with increasing temperature. Recent work (Myerson et al. 1990; Ginde and Myerson 1991) has shown that the viscosity of supersaturated solutions increases with increasing concentration much more rapidly than in undersaturated solutions. This is demonstrated in Figures 1.22 and 1.23 for KCl and glycine in aqueous solutions. This rise in viscosity has been attributed to the formation of precritical molecular clusters in the solution. The formation of clusters in solution is a time-dependent process with the cluster size increasing with increasing time. This would indicate a possible dependence of viscosity on solution "age." In recent experiments (Ginde and Myerson 1991) this has been observed in the glycine-water system, however, the effect is quite small.

In crystallization operations, the viscosity of the slurry of solution and crystals is of importance. The viscosity of a slurry of

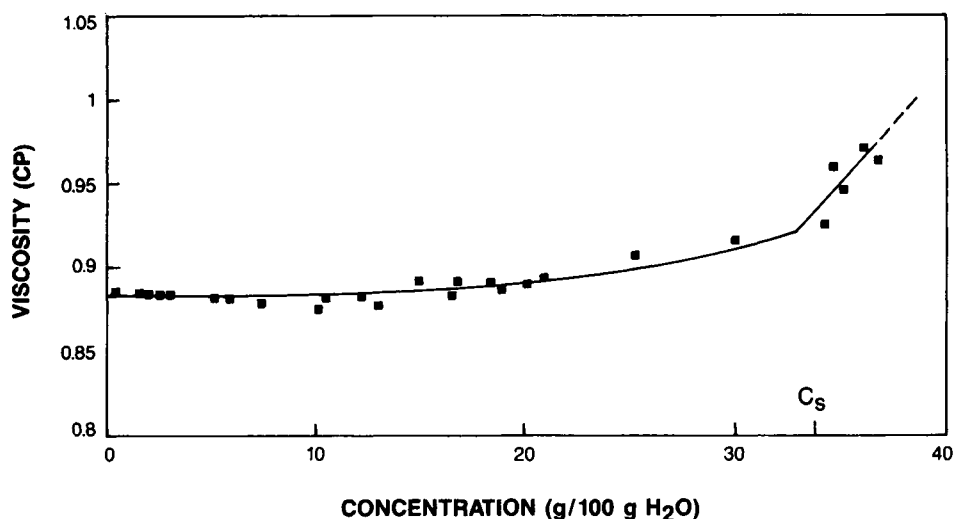


Figure 1.22 Viscosity of aqueous KCl solutions at 25°C. (Reproduced from R.M. Ginde and A.S. Myerson (1991), "Viscosity and Diffusivity in Metastable Solutions," *AIChE Symposium Series*, vol. 87, no. 284, pp. 124–129. Used by permission of the American Institute of Chemical Engineers. © 1991 AIChE.)

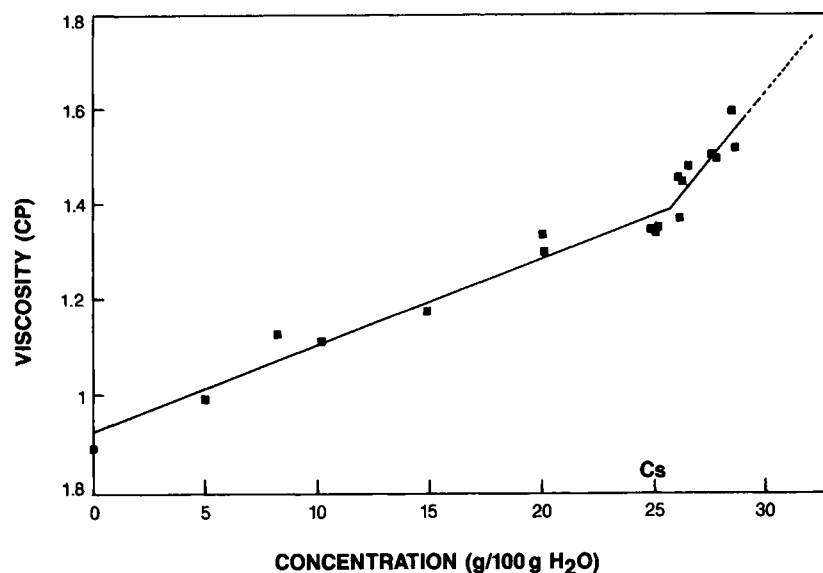


Figure 1.23 Viscosity of aqueous glycine solution at 25°C. (Reproduced from R.M. Ginde and A.S. Myerson (1991), "Viscosity and Diffusivity in Metastable Solutions," *AIChE Symposium Series*, vol. 87, no. 284, pp. 124–129. Used by permission of the American Institute of Chemical Engineers. © 1991 AIChE.)

solution and crystals usually does not obey Newton's law of viscosity but instead it follows other more complex empirical relations that must be obtained from experimental data. Systems, which do not obey Newton's law of viscosity, are called *non-Newtonian fluids*. A discussion of a number of non-Newtonian fluid models can be found in Bird et al. (1960). A commonly used non-Newtonian viscosity model used is the Power law, which can be written as

$$\tau_{yx} = -m \left| \frac{du_x}{dy} \right|^{n-1} \frac{du_x}{dy} \quad (1.62)$$

when $n = 1$, the Power law model reduces to Newton's law with $m = \mu$. Power law parameters for several different suspensions of particles in a fluid are given in Table 1.13.

The viscosity of slurries is a function of the solution and solid involved, as well as the slurry density. The viscosity can also be significantly affected by the particle size, size distribution, and particle shape. As a general rule, as particle shape varies from spheres to needles, the viscosity moves further from Newtonian behavior. A detailed discussion of factors affecting the viscosity of suspensions can be found in Sherman (1970).

TABLE 1.13 Power Law Model Parameters

Fluid Composition (wt%)	m (lb _f s ^{n} ft ⁻²)	n (dimensionless)
23.3% Illinois yellow clay in water	0.116	0.229
0.67% CMC in water	0.00634	0.716
1.5% CMC in water	0.0653	0.554
3.0% CMC in water	0.194	0.566
33% lime in water	0.150	0.171
10% napalm in kerosene	0.0893	0.520
4% paper pulp in water	0.418	0.575
54.3% cement rock in water	0.0524	0.153

(Reprinted by permission of John Wiley & Sons, Inc. from R.B. Bird, W.E. Stewart, and E.N. Lightfoot (1960), *Transport Phenomena*. © 1960 John Wiley & Sons, Inc.)

Instruments used to measure viscosity are called *viscometers*. A number of techniques and configurations are available for viscosity measurement. In rotational viscometers, some part of the viscometer is rotated imparting movement to the fluid that is transferred through the fluid to a measuring device. In capillary viscometers, the fluid flows through a capillary under the force of gravity and the time required for the fluid to flow through the capillary is measured. Some of the more common viscometers are summarized in Table 1.14.

TABLE 1.14 Viscometers

Type	Operation
Rotational	
Stormer	Stationary center cup, inner rotor
Haake Rotovisko	Fixed outer cup and inner rotor
Epprech Rheomat	Fixed outer cup and inner rotation bob
Brookfield	Measure viscous traction on spindle rotating in sample
Cone plate	Rotating small angle cone and stationary lower flat plate
Weissenberg Rheogoniometer	Cone rigidly fixed while lower flat plate rotates
Capillary	
Ostwald U-tube	Reservoir bulb from which fixed volume of sample flows through capillary to receiver in other arm of U-tube
Common-tensile	Reservoir and receiving bulbs in same vertical axis
Bingham	U-tube viscometer with third arm
	Sample extruded through capillary by air pressure

(Data from Sherman 1970.)

1.6.3. DIFFUSIVITY

If we were to prepare a solution made up of a solute in a solvent at two different concentrations and place them in contact with each

other, eventually they would achieve the same concentration through the process of diffusion. The solute molecules would diffuse from the region of high concentration to the region of lower concentration, and the solvent molecules would diffuse in the opposite direction (from higher to lower concentration of water). This process is described by Fick's first law of diffusion, which is written below

$$J_A = -D_{AB} \frac{dC_A}{dx} \quad (1.63)$$

where

J_A = molar diffusive flux

C_A = the concentration

D_{AB} = the diffusivity (or diffusion coefficient)

The diffusion coefficient is a property of a given solute in a given solvent and tells us the rate in which the solute will diffuse under a concentration gradient. The units of diffusivity are length squared/time. Diffusion coefficients vary with temperature and with solute concentration. The diffusion coefficient is important to crystallization operations because it is one of the properties that determines the degree of agitation required. If insufficient agitation is used in a crystallization process, the crystal growth rate can be controlled by the rate of solute transfer from the bulk solution to the crystal-liquid interface. This is called *mass transfer controlled crystal growth*. Normally this is undesirable because the crystal growth rate obtained is usually significantly slower than the rate that would be obtained if interfacial attachment kinetics were the rate-controlling step. This will be discussed in more detail in Chapter 2, however, the important point is that the diffusion coefficient is a property that must be taken into account in looking at mass transfer, mixing, and agitation in crystallization processes.

Data on the diffusion coefficients of solid solutes in liquid solvents are difficult to find and, if available, are usually found at low concentrations (or infinite dilution) at only one temperature. The concentration and temperature dependence of diffusion coef-

ficients in the glycine-water system is illustrated in Figure 1.24. The behavior shown in Figure 1.24 is typical nonelectrolyte behavior, with the diffusivity declining from a maximum value at infinite dilution in an approximately linear fashion. A comparison of the curves at different temperatures shows that the diffusion coefficient increases with increasing temperature. The data displayed in Figure 1.24 was for an undersaturated solution only. The diffusivity of glycine in supersaturated solutions is shown in Figure 1.25. The diffusivity declines rapidly with increasing concentration in the supersaturated region. In addition, Figure 1.25 shows that the diffusivity is a function of solution "age," decreasing as the solution age increases.

The diffusivity of KCl in aqueous solutions is shown in Figure 1.26. In electrolytes, the diffusivity initially decreases with increasing concentration, reaches a minimum, and then increases until saturation. The diffusivity then rapidly declines with increasing concentration in the supersaturated region.

The behavior of the diffusion coefficient in supersaturated solutions can be explained in two different ways, one based on thermodynamics, and the second based on metastable solution structure and nucleation theory. If we think of this thermodynamically, it is useful to look at equations used to predict concentration-dependent diffusion coefficients. Two examples are listed below

$$D = D^0 \left(1 + \frac{\partial \ln \gamma_2}{\partial \ln x_2} \right) \frac{\mu_1}{\mu_s} \quad (\text{Gordon}) \quad (1.64)$$

$$D = D^0 \left(\frac{\partial \ln a_2}{\partial \ln x_2} \right) \quad (\text{Stokes-Einstein}) \quad (1.65)$$

where

D^0 = diffusivity at infinite dilution

μ_1 = viscosity of the solvent

μ_s = viscosity of the solution

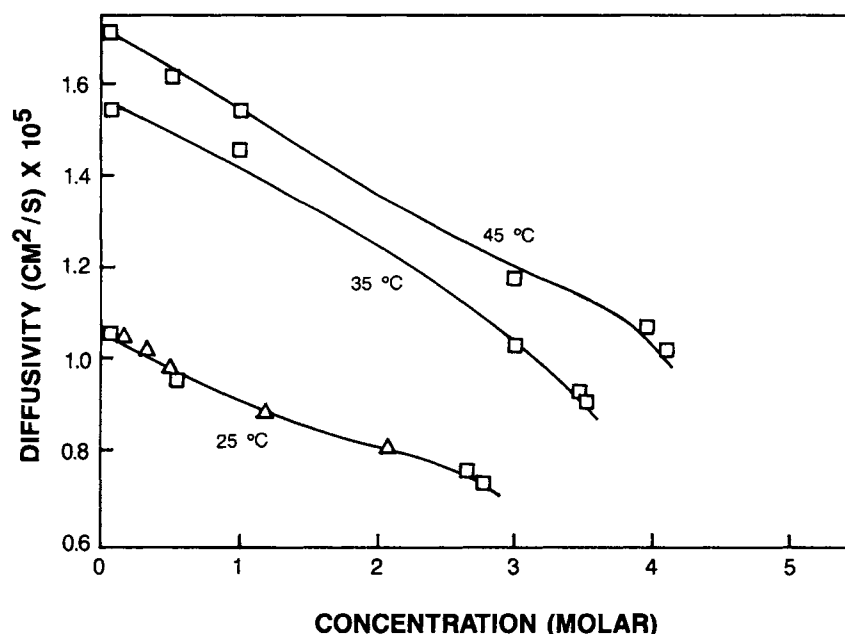


Figure 1.24 Diffusion coefficients of aqueous glycine solutions at 25, 35, and 45 °C. (Data from Chang 1984.)

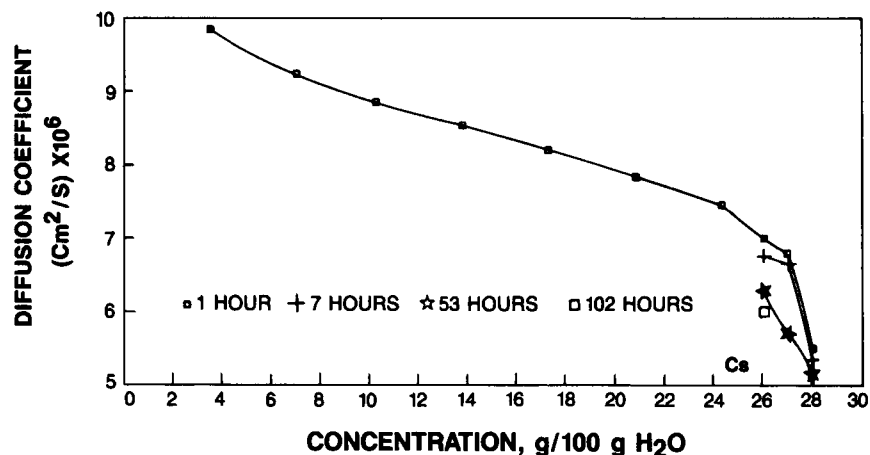


Figure 1.25 Diffusion coefficients in aqueous glycine solutions at 25°C as a function of concentration and solution "age." (Reproduced with permission from Myerson and Lo 1991.)

These, and all other equations for concentration-dependent diffusion, consist of an infinite dilution diffusivity and a thermodynamic correction term. The thermodynamic correction term in all cases is equivalent to the derivative $\partial G_2 / \partial x_2^2$. The definition of the thermodynamic metastable limit (the spinodal curve) is the locus of points where $\partial G_2 / \partial x_2^2 = 0$. This means that concentration-dependent diffusion theory predicts a diffusivity of zero at the spinodal. Thermodynamics tells us that the diffusivity goes from some finite value at saturation to zero at the spinodal. Unfortunately, it does not tell us how the diffusion coefficient declines. In addition, lack of thermodynamic data makes prediction of the spinodal difficult. We are, therefore, left with only the fact that as the concentration is increased in the supersaturated region, the diffusivity should decline towards zero; but we do not know at what concentration the diffusivity becomes zero.

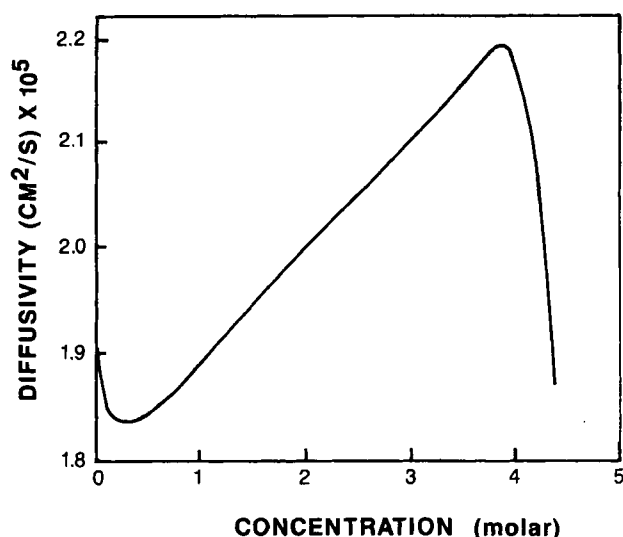


Figure 1.26 Diffusion coefficients in aqueous KCl solutions at 25°C (solution age = 24 h) in the metastable region, (Reproduced from Y.C. Chang and A.S. Myerson (1985), "The Diffusivity of Potassium Chloride and Sodium Chloride in Concentrated, Saturated, and Supersaturated Aqueous Solutions," *AIChE J.* 31, pp. 890-894. Used by permission of the American Institute of Chemical Engineers. © 1985 AIChE.)

If we look at nucleation theory, we know that as time goes on in a supersaturated solution, the cluster size in solution will increase. As the size of an entity increases, its diffusivity decreases so that nucleation theory tells us that because of cluster formation in supersaturated solutions the diffusivity should decline. Again, however, it is difficult to predict cluster size and evolution due to lack of one or more important parameters. An estimation of number average cluster size for glycine in water calculated from supersaturated diffusivity and viscosity data, and from recent theoretical work (Ginde and Myerson 1991) is shown in Table 1.15. These results and other recent studies (Myerson et al. 1990; Ginde and Myerson 1992) indicate that the number average cluster size can range from 2 to 100 molecules and is very dependent on the system, supersaturation, age, and history of the solution. In most crystallizing systems that operate at relatively low levels of supersaturation, it is likely that many of the clusters are small (dimers and trimers).

The almost total absence of diffusivity data in concentrated, saturated, and supersaturated solutions makes the estimation of diffusivity difficult in many cases. In order to estimate the diffusivity at the desired conditions, the first step is to find out if any experimental data exists (even at infinite dilution) for the diffusivity of the solute in the solvent of interest.

If you are fortunate to find diffusivity data over the entire concentration range (up to saturation) at the temperature of interest, you need to use this data to estimate the diffusivity in the supersaturated solution at the desired concentration. One simple estimation technique is to use the effective metastable limit concentration (obtained experimentally) and assume the diffusivity is zero at that concentration and that the diffusivity declines linearly from the value at saturation to zero at the estimated metastable limit concentration. This will give you a reasonable (but probably low) estimate of the supersaturated diffusivity. More complicated methods of estimating the diffusivity in metastable solutions can be found in the literature (Lo and Myerson 1990).

It is rare to find diffusivity data of most species at any concentration near saturation. It is, therefore, necessary to first estimate the diffusivity at saturation after which the diffusivity in the supersaturated solution can be estimated. To estimate the diffusivity at saturation from low concentration data requires the use of an equation for concentration-dependent diffusion coefficients that can be used with solid solutes dissolved in liquid solvents. One such equation that can be used for nonelectrolytes is the

TABLE 1.15 Cluster Size Evolution from Experimental Data for Glycine-Water

Concentration (g/100 g solvent)	Solution Age (h)	Viscosity (cP)	Cluster Size ($g_{visc} = (\frac{\eta}{\eta_s})^3$)	Diffusivity ($\times 10^6 \text{ cm}^2/\text{s}$)	Cluster Size ($g_{diff} = \frac{D_s}{D}$) ^{1.5}	Cluster Size Calculated (Lo and Myerson 1990)
25.0	—	1.508	1.0	7.07	1.0	1.0
26.0	0	1.545	1.08	6.98	1.02	1.05
	3	1.581	1.15	6.92	1.03	1.11
	9.5	1.605	1.21	6.79	1.06	1.17
	21.5	1.606	1.21	6.57	1.12	1.24
	0	1.613	1.22	6.87	1.04	1.08
	3.5	1.616	1.23	6.81	1.06	1.22
	19.0	1.642	1.29	6.43	1.16	1.35
	45.0	1.652	1.31	6.09	1.25	1.52

(Reproduced from R.M. Ginde and A.S. Myerson (1991), "Viscosity and Diffusivity in Metastable Solutions," *AIChE Symposium Series*, vol. 87, no. 284, pp. 124–129. Used by permission of the American Institute of Chemical Engineers. © 1991 AIChE.)

Hartley-Crank (Hartley and Crank 1949) equation that appears below

$$D = \left(\frac{d \ln a_2}{d \ln \gamma_2} \right) (x_1 D_{12}^0 + x_2 D_1^*) \frac{\mu_s}{\mu_1} \quad (1.66)$$

where

- D_{12}^0 = infinite dilution diffusivity
- D_1^* = self-diffusion coefficient of the solvent
- μ_s = viscosity of the solution
- μ_1 = viscosity of the solvent

The activity data required can be obtained experimentally or through thermodynamic calculations of activity coefficients similar to those described in the solubility sections. A comparison of calculated and experimental diffusion coefficients for the glycine-water system employing the Hartley-Crank equation appear in Figure 1.27.

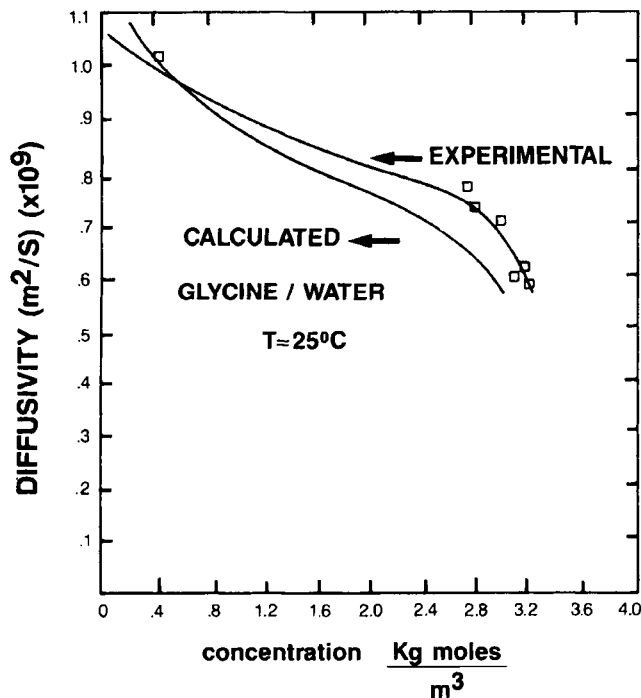


Figure 1.27 Comparison of experimental and calculated diffusivities in the glycine-water system (calculated values from the Hartley-Crank equation). (Data from Chang 1984.)

If no diffusivity data is available at any concentration, estimation can still be used. First, the infinite dilution diffusivity is estimated using one of several methods available (Reid et al. 1987) such as the Wilke-Chang (Wilke and Chang 1955) method

$$D_{21}^0 = 7.4 \times 10^{-8} \frac{(\phi M_1)^{1/2} T}{\mu_1 V_2^{0.6}} \quad (1.67)$$

where

- D_{21}^0 = infinite dilution diffusivity of the solute (2) in the solvent (1) in cm^2/s
- M_1 = molecular weight of the solvent
- T = temperature in K
- μ_1 = viscosity of the solvent in cP
- V_2 = molal volume of the solute at its normal boiling point in $\text{cm}^3/\text{g mol}$
- ϕ = association factor

The value of ϕ is 2.6 when water is the solvent, 1.9 for methanol, 1.5 for ethanol, and 1.0 for other unassociated solvents. The value of V_2 can be estimated by the Le Bas method if not known (see Reid et al. 1987).

Once a value of the infinite dilution diffusivity is estimated using Eq. (1.67), the diffusivity at saturation can be estimated using Eq. (1.66), followed by estimation of the supersaturated diffusivity using the method previously described.

The above procedure, while rather tedious, will result in a reasonable estimate of the supersaturated solution diffusivity that is quite useful in crystallization process design and development.

1.7. THERMAL PROPERTIES

A fundamental aspect in the development and design of any process involves the performance of an energy balance. Crystallization operations involve the transfer of energy in and out of the system. In addition, since phase changes are involved, through the formation of the product and through changes to the solvent system (if evaporation or change in solvent composition are used) data on the thermal properties of the solute-solvent system are important.

In a simple cooling crystallizer for example, it is obvious that a calculation must be done to determine the amount of energy to be removed from the system to cool the solution to the final temperature desired. The calculation could be seriously in error, however, if the heat effects due to the crystallization (heat of crystallization) are ignored. In crystallizations that involve evaporations, mixed solvents, or reactions, the heat effects that accompany each of

these phenomena must be known. In addition, any operation involving the dilution of a concentrated solution or the dissolution of a solid into a liquid is accompanied by heat effects that must be taken into account in any energy balance calculation.

1.7.1. HEAT CAPACITY

Imagine that you have a pure liquid and you wish to calculate how much energy is required to heat that liquid from one temperature to another. This calculation is simple, providing you know a property of the material known as the heat capacity (or specific heat). There are two types of heat capacities that can be defined.

The heat capacity at constant temperature (C_p) and the heat capacity at constant volume (C_v), which are defined as follows

$$C_p(T) = \frac{d\bar{H}}{dT} \quad (1.68)$$

$$C_v(T) = \frac{d\bar{U}}{dT} \quad (1.69)$$

where \bar{H} and \bar{U} are the enthalpy and internal energy per mole, respectively. The two heat capacities are related to each other as follows

HEAT CAPACITY: (Btu) / (lb_m) (°F) or (cal) / (g) (°C)

No.	Liquid	Range (°C)
29	Acetic Acid 100%	0 - 80
32	Acetone	20 - 50
52	Ammonia	-70 - 50
37	Amyl Alcohol	-50 - 25
26	Amyl Acetate	0 - 100
30	Aniline	0 - 130
23	Benzene	10 - 80
27	Benzyl Alcohol	-20 - 30
10	Benzyl Chloride	-30 - 30
49	Brine, 25% CaCl ₂	-40 - 20
51	Brine, 25% NaCl	-40 - 20
44	Butyl Alcohol	0 - 100
2	Carbon Disulfide	-100 - 25
3	Carbon Tetrachloride	10 - 60
8	Chlorobenzene	0 - 100
4	Chloroform	0 - 50
21	Decane	-80 - 25
6A	Dichloroethane	-30 - 80
5	Dichloroethane	-40 - 50
15	Diphenyl	80 - 120
22	Diphenylmethane	30 - 100
16	Diphenyl Oxide	0 - 200
16	Dowtherm A	0 - 200
24	Ethyl Acetate	-50 - 25
42	Ethyl Alcohol 100%	30 - 80
48	Ethyl Alcohol 80%	20 - 80
50	Ethyl Alcohol 50%	20 - 80
25	Ethyl Benzene	0 - 100
1	Ethyl Bromide	5 - 25
13	Ethyl Chloride	-30 - 40
36	Ethyl Ether	-100 - 25
7	Ethyl Iodide	0 - 100
39	Ethylene Glycol	-40 - 200

No.	Liquid	Range (°C)
2A	Freon - 11(CCl ₃ F)	-20 - 70
6	Freon - 12(CClF ₂)	400 - 15
4A	Freon - 21(CHCl ₂ F)	-20 - 70
7A	Freon - 22(CHClF ₂)	-20 - 80
3A	Freon - 113(CCl ₂ F-CClF ₂)	-20 - 70
38	Glycerol	-40 - 20
28	Heptane	0 - 60
35	Hexane	-80 - 20
46	Hydrochloric Acid, 30%	20 - 100
41	Isoamyl Alcohol	10 - 100
43	Isobutyl Alcohol	0 - 100
47	Isopropyl Alcohol	-20 - 50
31	Isopropyl Ether	-80 - 20
40	Methyl Alcohol	-40 - 20
13A	Methyl Chloride	-80 - 20
14	Naphthalene	90 - 200
12	Nitrobenzene	0 - 100
34	Nonane	-50 - 25
33	Octane	-50 - 25
3	Perchloroethylene	-30 - 140
45	Propyl Alcohol	-20 - 100
20	Pyridine	-50 - 25
9	Sulfuric Acid 98%	10 - 45
11	Sulfur Dioxide	-20 - 100
23	Toluene	0 - 60
53	Water	10 - 200
19	Xylene Ortho	0 - 100
16	Xylene Meta	0 - 100
17	Xylene Para	0 - 100

TEMPERATURE (°C) (°F)

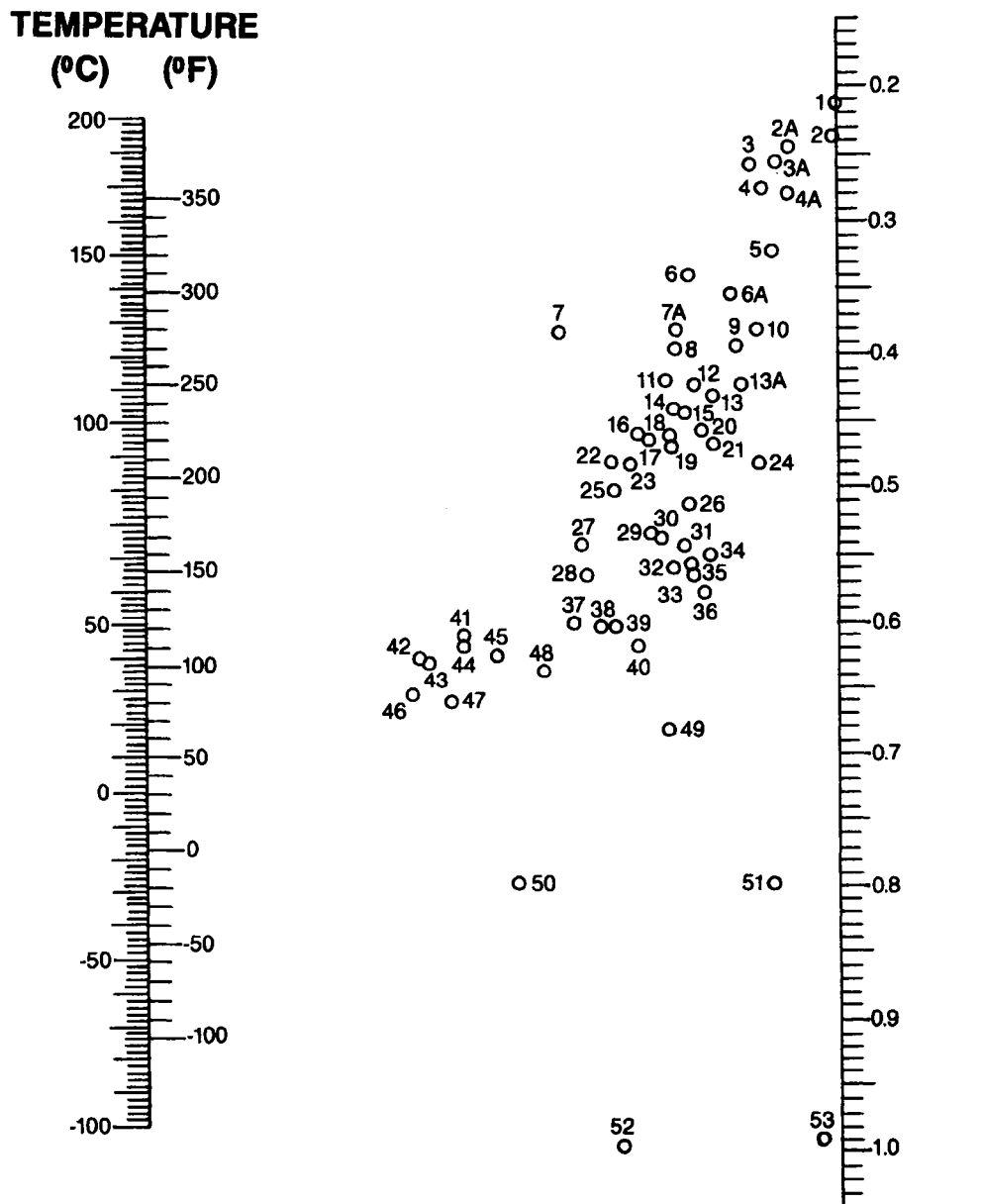


Figure 1.28 Heat capacities of liquids: (Btu) (lb_m) (°F) or (cal)/(g)(°C). Reproduced with permission of McGraw-Hill, Inc., from J.M. Smith and H.C. Van Ness, *Introduction to Chemical Engineering Thermodynamics*, 3rd ed. © 1975, McGraw-Hill, Inc., New York, p. 115.)

$$\text{Ideal gases: } C_p = C_v + R \quad (1.70)$$

$$\text{Liquids and solids: } C_p \approx C_v \quad (1.71)$$

Heat capacities are given in units of energy per mole (or mass) per unit temperature interval. Typical units used and conversion factors appear in Table 1.12.

Specific heat is another term used when heat capacity is expressed on a per mass basis. Heat capacities are a function of temperature and are usually expressed as a polynomial such as

$$C_p(T) = a + bT + cT^2 + dT^3 \quad (1.72)$$

Tables of heat capacities for a variety of pure substances can be found in the *Chemical Engineers Handbook* (Perry and Green 1997). The heat capacity of a number of liquids is given in Figure 1.28.

Heat capacity data is available for most liquids and gases, and for many solids. If not available, estimation techniques have been

developed and are summarized in Reid et al. (1987). Heat capacities of liquid mixtures can be estimated by calculating an average heat capacity from the heat capacities of the components using the relation

$$C_{Pavg}(T) = \sum x_i C_{pi}(T) \quad (1.73)$$

The heat capacity of solutions of solids dissolved in liquids is usually not available. If the solution is dilute, the usual practice is to neglect the solute and to use the solvent heat capacity. For a concentrated solution, neglecting the solute can lead to inaccuracies so that the use of enthalpy data is suggested.

1.7.2. LATENT HEAT

When a pure material undergoes a phase change, the process takes place at a constant temperature and pressure. Even though the temperature remains the same, there is an enthalpy change associated

TABLE 1.16 Enthalpy of Fusion and Melting Temperature of Some Organics

Compound	T_m (°C)	Molecular Weight	ΔH_m	
			(cal/g)	(cal/g mol)
Methane	-182.5	16.04	14.03	225
Ethane	-183.3	30.07	22.73	683
Propane	-187.7	44.09	19.10	842
<i>n</i> -Butane	-138.4	58.12	19.17	1114
Isobutane	-159.6	58.12	18.67	1085
<i>n</i> -Pentane	-129.7	72.13	27.81	2006
Isopentane	-159.9	72.13	17.06	1231
Neopentane	-16.6	72.13	10.79	779
<i>n</i> -Hexane	-95.4	86.17	36.14	3114
2-Methylpentane	-153.7	86.17	17.41	1500
2,2-Dimethylbutane	-99.9	86.17	1.61	139
2,3-Dimethylbutane	-128.5	86.17	2.25	194
<i>n</i> -Heptane	-90.6	100.2	33.47	3350
2-Methylhexane	-118.3	100.2	21.91	2195
3-Ethylpentane	-118.6	100.2	22.78	2283
2,2-Dimethylpentane	-123.8	100.2	13.89	1392
2,4-Dimethylpentane	-119.2	100.2	16.32	1635
3,3-Dimethylpentane	-134.5	100.2	16.86	1689
2,2,3-Trimethylbutane	-24.9	100.2	5.39	540
<i>n</i> -Octane	-56.8	114.2	43.40	4956
3-Methylheptane	-120.5	114.2	23.81	2719
4-Methylheptane	-120.9	114.2	22.68	2590
<i>n</i> -Nonane	-53.5	128.2	28.83	3696
<i>n</i> -Decane	-29.6	142.3	48.24	6865
<i>n</i> -Dodecane	-9.6	170.3	51.69	8803
<i>n</i> -Octadecane	28.2	254.4	57.65	14,660
Benzene	5.5	78.1	30.09	2350
Toluene	-94.9	92.1	17.1	1575
Ethylbenzene	-94.9	106.1	20.63	2188
<i>o</i> -Xylene	-25.1	106.1	30.61	3250
<i>m</i> -Xylene	-47.9	106.1	26.04	2760
<i>p</i> -Xylene	13.3	106.1	38.5	4080
<i>n</i> -Propylbenzene	-99.5	120.1	16.97	2040
Isopropylbenzene	-96.0	120.1	14.15	1700
1,2,3-Trimethylbenzene	-25.4	120.1	16.6	1990
1,2,4-Trimethylbenzene	-43.8	120.1	25.54	3070
1,3,5-Trimethylbenzene	-44.7	120.1	19.14	2300
Cyclohexane	6.5	84.1	7.57	637
Methylcyclohexane	-126.5	98.1	16.4	1610
Ethylcyclohexane	-111.3	112.2	17.73	1930
1,1-Dimethylcyclohexane	-33.5	112.2	1.32	148
1, <i>cis</i> -2-Dimethylcyclohexane	-50.0	112.2	3.50	393
1, <i>trans</i> -2-Dimethylcyclohexane	88.1	112.2	22.34	2507

(Data from Reid et al. 1987.)

with the phase change that must be taken into account in energy balance calculations. These enthalpy changes associated with phase changes in pure materials are often referred to as latent heat. The latent heat of vaporization refers to the enthalpy change required to vaporize a given amount of a saturated liquid to saturated vapor at a constant temperature and pressure. Other latent heats commonly mentioned are fusion (melting a material) and sublimation (solid to gas). It is important to note that there are also heat effects that accompany phase changes from one solid phase to another. If a material crystallizes in one crystal form and then transforms to another crystal form, there will be an enthalpy change involved.

Latent heats vary as a function of temperature and to a smaller extent pressure. The latent heat for a phase change at 1 atm (101.29 kPa) is often called the standard heat of phase change and is available for many materials in the literature (Perry and Green 1997).

A number of techniques have been developed to estimate the latent heat of vaporization and, to a lesser extent, the latent heat of fusion and sublimation. A description of these techniques can be found in Reid et al. (1987). One very useful and commonly used method known as the Watson correlation appears below

$$\Delta \bar{H}_v(T_2) = \Delta \bar{H}_v(T_1) \left(\frac{1 - (T_2/T_c)}{1 - (T_1/T_c)} \right)^{0.38} \quad (1.74)$$

where $\Delta \bar{H}_v(T_2)$ and $\Delta \bar{H}_v(T_1)$ are the heats of vaporization at T_2 and T_1 , and T_c is the critical temperature. Eq. (1.74) allows calculation of the latent heat of vaporization at any temperature if the heat of vaporization is known at one temperature. If no heat of vaporization data are available, and the normal boiling point (boiling point at 1 atm) of the liquid is known, Chen's equation can be used to estimate the heat of vaporization at the boiling point by

$$\Delta \bar{H}_{vb} = \frac{RT_c T_{br} 3.978 T_{br} - 3.938 + 1.555 \ln P_c}{1.07 - T_{br}} \quad (1.75)$$

where

T_{br} = reduced boiling point temperature (T_b/T_c)

P_c = critical pressure

Latent heats of vaporization can be calculated from vapor pressure data employing the Clausius-Clapeyron equation.

$$\Delta \frac{\bar{H}_v}{R} = \frac{d(\ln p^*)}{d(1/T)} \quad (1.76)$$

where p^* is the vapor pressure at a particular temperature. By plotting $\ln p^*$ versus $1/T$ and obtaining the slope at the temperature of interest, Eq. (1.76) can be used to calculate the heat of vaporization.

Calculation of latent heats of fusion and sublimation are more difficult and less accurate than calculating heats of vaporization. Reid et al. (1987) summarized available methods. A crude but simple approximation for standard heats of formation is (Felder and Rousseau 1986)

$$\begin{aligned} \Delta \bar{H}_m(\text{kJ/mol}) &\approx 0.0092 T_m(\text{K}) (\text{Metallic elements}) \\ &\approx 0.025 T_m(\text{K}) (\text{Inorganic compounds}) \\ &\approx 0.050 T_m(\text{K}) (\text{Organic compounds}) \end{aligned}$$

The melting temperature and latent heats of fusion for a number of organic species appear in Table 1.16.

1.7.3. HEATS OF MIXING, SOLUTION, AND CRYSTALLIZATION

In any process where the concentration of a solution is changed, there will be an enthalpy change accompanying the concentration change. This is true when two liquids are mixed, a concentrated solution is diluted, a solid is dissolved in a liquid, or when a solute crystallizes from solution. These enthalpy changes are known as heats of mixing, solution, and crystallization, respectively, and can be very significant in energy balance calculations.

The heat of mixing refers to the enthalpy change accompanying the mixing of two or more pure substances to form a solution at a constant temperature and pressure. When one species being mixed is a gas or solid, this enthalpy change is known as the heat of solution. Heats of solution are often given in terms of the dissolution of 1 mol of solute in moles of solvent at a particular temperature. This is known as an integral heat of solution. Integral heats of solution for HCl, NaOH, and H_2SO_4 appear in Table 1.17. The table shows that for each of these substances, the heat of solution is negative, meaning that the solution process results in the evolution of heat. In addition, Table 1.17 shows that the heat of solution is a function of concentration, increasing as the solution becomes less concentrated (n , the moles of water per moles of solute increases) to a limiting maximum value. This maximum value is known as the heat of solution at infinite dilution. Data in Table 1.17 can be used to calculate the enthalpy change that would result from making a solution of desired concentration from its components. It also can be used to calculate the enthalpy change that would result from the dilution of a concentrated solution.

The substances listed in Table 1.17 all have negative heats of solution, meaning that heat is released when the materials are dissolved, or a concentrated solution is diluted. This is not generally true; many substances have positive heats of solution, indicating that heat is absorbed when they are dissolved. The heats of

TABLE 1.17 Integral Heats of Solution at 25 °C

n (mol water/mol solute)	$(\Delta \bar{H}_s)_{\text{HCl(g)}} \text{ (kJ/mol HCl)}$	$(\Delta \bar{H}_s)_{\text{NaOH(s)}} \text{ (kJ/mol NaOH)}$	$(\Delta \bar{H}_m)_{\text{H}_2\text{SO}_4} \text{ (kJ/mol H}_2\text{SO}_4)$
0.5	—	—	−15.73
1	−26.22	—	−28.07
1.5	—	—	−36.90
2	−48.82	—	−41.92
3	−56.85	−28.87	−48.99
4	−61.20	−34.43	−54.06
5	−64.05	−37.74	−58.03
10	−69.49	−42.51	−67.03
20	−71.78	−42.84	—
25	—	—	−72.30
30	−72.59	−42.72	—
40	−73.00	−42.59	—
50	−73.26	−42.51	−73.34
100	−73.85	−42.34	−73.97
200	−74.20	−42.26	—
500	−74.52	−42.38	−76.73
1000	−74.68	−42.47	−78.57
2000	−74.82	−42.55	—
5000	−74.93	−42.68	−84.43
10,000	−74.99	−42.72	−87.07
50,000	−75.08	−42.80	—
100,000	−75.10	—	−93.64
500,000	—	—	−95.31
∞	−75.14	−42.89	−96.19

(Reprinted by permission of John Wiley & Sons, Inc. from R.M. Felder and R.W. Rousseau (1986), *Elementary Principles of Chemical Processes*, 2nd ed. © 1986 John Wiley & Sons, Inc.)

TABLE 1.18 Heats of Solution in Water at Infinite Dilution of 18 °C

Substance	Formula	ΔH_s (kcal/gmol)
Ammonium chloride	NH ₄ Cl	-3.82
Ammonium nitrate	NH ₄ NO ₃	-6.47
Ammonium sulfate	(NH ₄) ₂ SO ₄	-2.75
Barium bromide	BaBr ₂	+5.3
	BaBr ₂ · H ₂ O	-0.8
	BaBr ₂ · 2H ₂ O	-3.87
Calcium chloride	CaCl ₂	+4.9
	CaCl ₂ · H ₂ O	+12.3
	CaCl ₂ · 2H ₂ O	+12.5
	CaCl ₂ · 4H ₂ O	+2.4
	CaCl ₂ · 6H ₂ O	-4.11
Lithium bromide	LiBr	+11.54
	LiBr · H ₂ O	+5.30
	LiBr · 2H ₂ O	+2.05
	LiBr · 3H ₂ O	-1.59
Magnesium sulfate	MgSO ₄	+21.1
	MgSO ₄ · H ₂ O	+14.0
	MgSO ₄ · 2H ₂ O	+11.7
	MgSO ₄ · 4H ₂ O	+4.9
	MgSO ₄ · 6H ₂ O	+0.55
	MgSO ₄ · 7H ₂ O	-3.18
Potassium sulfate	K ₂ SO ₄	-6.32
Benzoic acid	C ₇ H ₆ O ₂	-6.5
Citric acid	C ₆ H ₈ O ₇	-5.4
Dextrin	C ₁₂ H ₂₀ O ₁₀	+0.268
Hexamethylenetetramine	C ₆ H ₁₂ N ₄	+4.78
<i>m</i> -Nitrophenol	C ₆ H ₅ NO ₃	-5.2
<i>o</i> -Nitrophenol	C ₆ H ₅ NO ₃	-6.3
<i>p</i> -Nitrophenol	C ₆ H ₅ NO ₃	-4.5
Phthalic acid	C ₈ H ₆ O ₄	-4.87
Urea	CH ₄ N ₂ O	-3.61

(Data from Perry and Green 1997.)

solution of selected organic and inorganic species in water appear in Table 1.18. Additional data can be found in Perry and Green (1997).

The data in Table 1.18 illustrates two other points. The first is that for hydrated compounds, the heats of solution vary as a function of the number of waters of hydration present in the solid. Looking at magnesium sulfate, we see that the heat of solution at infinite dilution at 18 °C varies from -21.1 kcal/gmol for the anhydrous form to +3.18 kcal/gmol for MgSO₄ · 7H₂O (which is the stable form at this temperature). The second point is that organic compounds with the same chemical formula but different structures such as *para*-, *meta*-, and *ortho*-nitrophenol have differing heats of solution. In this case, they are 4.49, 5.21, and 6.3 kcal/gmol, respectively, at infinite dilution and 18 °C.

The enthalpy change that results from the crystallization of a species from solution is called the *heat of crystallization*. The heat of crystallization is normally assumed to be of the same magnitude but opposite sign as the heat of solution at a concentration near saturation. This is not exactly correct since the supersaturated solution from which the crystallization is occurring has a higher concentration than a saturated solution, however, the error should be relatively small.

For binary systems of solutes and solvents that are relatively common or have industrial importance, enthalpy concentration diagrams often exist that are quite useful in energy balance calculations involving solution, dilution, or crystallization. An example of an enthalpy concentration diagram for the NaOH-H₂O system appears in Figure 1.29. It is important to be aware of the reference state on which the diagram is based when employing this data in energy balance calculations.

NOMENCLATURE

a	Activity	Eq. (1.2)
A	Debye-Hückel constant	Eq. (1.26)
B	Constant for ion interaction	Eq. (1.26)
C	Concentration of solution	Eq. (1.54)
C_s	Saturation concentration	Eq. (1.54)
C_p	Specific heat at constant pressure	Eq. (1.68)
C_v	Specific heat at constant volume	Eq. (1.69)
D_{AB}	Diffusion coefficient	Eq. (1.63)
D^*_1	Self-diffusion coefficient of the solvent	Eq. (1.66)
D^0_{12}	Infinite dilution diffusivity	Eq. (1.66)
dC_A/dx	Concentration gradient	Eq. (1.63)
dv_x/dy	Shear rate	Eq. (1.61)
e	Magnitude of the electric charge	Eq. (1.49)
F_i	Interaction parameter	Eq. (1.32)
f_i	Fugacity, mole fraction, activity coefficient	Eqs. (1.16), (1.37)
\bar{H}	Enthalpy per mole	Eq. (1.68)
I	Ionic strength	Eq. (1.26)
i	Any ion present	Eq. (1.31)
J_A	Molar diffusive flux	Eq. (1.63)
K	Equilibrium constant	Eq. (1.2)
K_{sp}	Solubility product	Eq. (1.4)
l	Distance between two charges	Eq. (1.44)
M	Molecular weight of the solute	Eq. (1.18)
M_s	Molecular weight of the solvent	Eq. (1.17)
m	Concentration of species in solution, empirical viscosity parameter	Eqs. (1.3), (1.62)
n	Power law exponent	Eq. (1.62)
P	Pressure	Eq. (1.42)
p^*	vapor pressure	Eq. (1.76)
P_c	Critical pressure	Eq. (1.75)
P^*_2	Vapor pressure of component 2	Eq. (1.41)
R	Gas constant	Eq. (1.10)
r	Cluster radius	Eq. (1.58)
S	Supersaturation ratio	Eq. (1.57)
T	Temperature, °C	Eq. (1.10)
T_{br}	Reduced boiling point	Eq. (1.75)
T_c	Critical temperature	Eq. (1.74)
T_{tp}	Triple point temperature, °C	Eq. (1.42)
V	Molar volume	Eq. (1.52)
\bar{V}	Internal energy per mole	Eq. (1.69)
V_m	Specific volume of solute	Eq. (1.58)
V^L_2	Molar volume of subcooled liquid	Eq. (1.50)
w	Mass fraction	Eq. (1.60)
x_2	Mole fraction of the solute	Eq. (1.39)
y_i	Molar activity coefficient	Eq. (1.15)
z	Number of charges on the cation or anion	Eq. (1.27)
Δc	Supersaturation	Eq. (1.56)
ΔC_p	Difference in specific heats of the liquid or solid	Eq. (1.42)
ΔG^0_f	Gibbs free energy of formation	Eq. (1.23)
ΔH_m	Latent heat of fusion	Eq. (1.47)
ΔH_{tp}	Enthalpy change at the triple point	Eq. (1.42)
ΔH_v	Heat of vaporization	Eq. (1.74)
Δu	Enthalpy of vaporization	Eq. (1.52)
Δv	Volume change for liquid-solid transformation	Eq. (1.42)

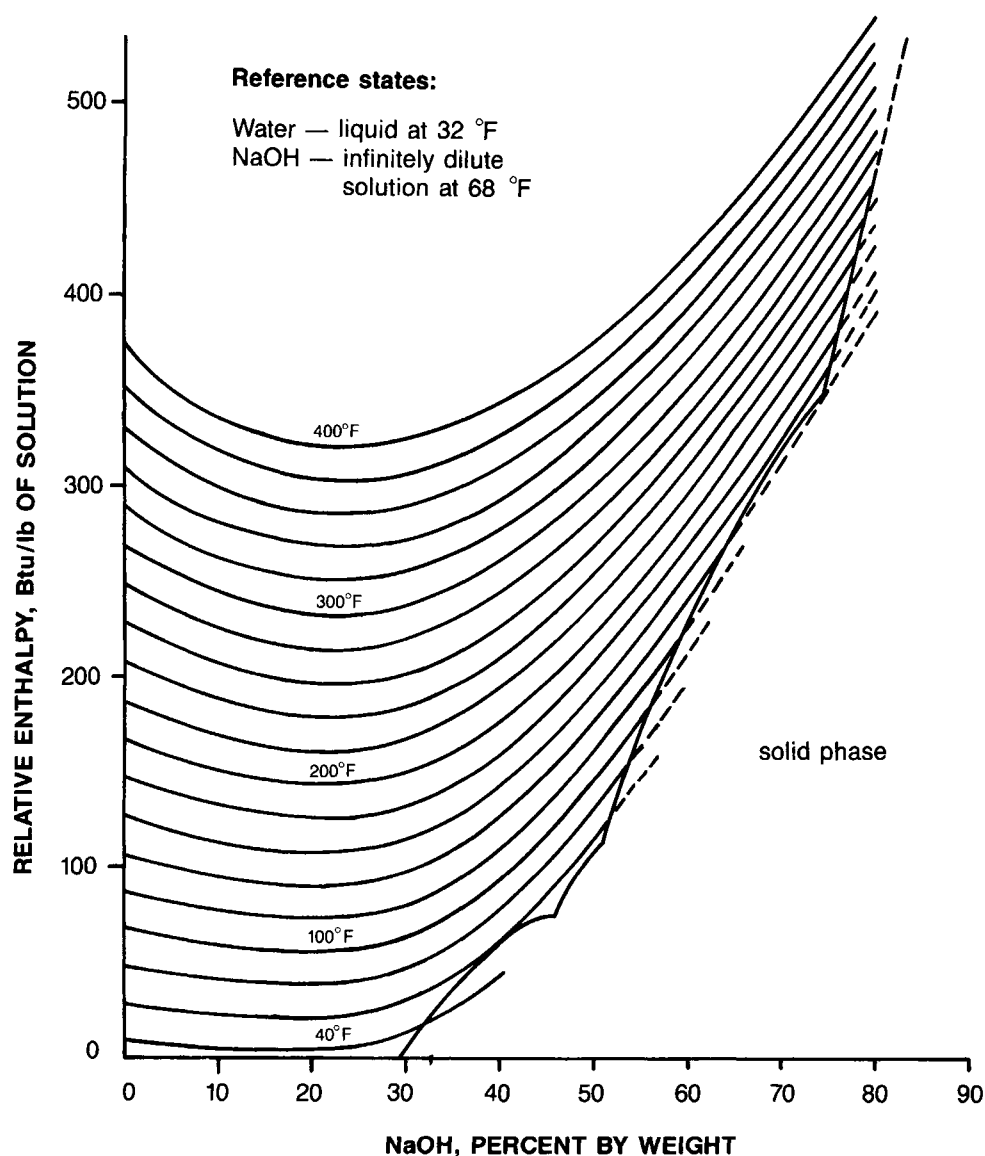


Figure 1.29 Enthalpy concentration diagram for NaOH-H₂O. (Reprinted by permission of John Wiley & Sons, Inc. from G. Brown (1950), *Unit Operations*. © 1950 John Wiley & Sons, Inc.)

Greek Letters

γ	Activity coefficient	Eq. (1.3)
μ	Chemical potential	Eq. (1.8)
ν	Stoichiometric number	Eq. (1.9)
ρ	Solution density	Eq. (1.19)
ρ_0	Solvent density	Eq. (1.19)
δ_1, δ_2	Solubility parameters of the solvent and subcooled liquid, respectively	Eq. (1.50)
ϕ	Volume fraction of the solvent	Eq. (1.50)
σ	Relative supersaturation, solid-liquid interfacial tension	Eqs. (1.55), (1.58)
τ_{yx}	Shear stress	Eq. (1.61)
μ	Viscosity	Eq. (1.61)

REFERENCES

- Bird, R.B., Stewart, W.E., and Lightfoot, E.N. (1960). *Transport Phenomena*, Wiley, New York.
- Bromley, L.A. (1972). *J. Chem. Thermo.* **4**, 669.
- Bromley, L.A. (1973). *AIChE J.* **19**, 313.
- Bromley, L.A. (1974). *AIChE J.* **20**, 336.
- Brown, G. (1950). *Unit Operations*, McGraw-Hill Book Co., New York.
- Chang, Y.C. (1984). Ph.D. dissertation, Georgia Institute of Technology, Atlanta, GA.
- Chang, Y.C., and Myerson, A.S. (1984). *AIChE J.* **31**, 890.
- Decker, S., Fan, W.P., and Myerson, A.S. (1986). *Ind. Eng. Chem. Fund.* **25**, 925.
- Felder, R.M., and Rousseau, R.W. (1996). *Elementary Principles of Chemical Processes*, 2nd ed., John Wiley & Sons, Inc., New York.
- Frank, T.C., Downey, J.R., and Gupta, S. (1999). *Chem. Eng. Prog.* **95**, 12.
- Freundslund, A., Gmehling, A.J., Micheisen, M.L., Rasmussen, P., and Prausnitz, J.M. (1977). *Ind. Eng. Chem. Process Des. Dev.* **16**, 450.

- Ginde, R.M., and Myerson, A.S. (1991). *AIChE Symposium Series*, vol. 87, **284**, 124–129.
- Ginde, R., and Myerson, A.S. (1992). *J. Cryst. Growth* **116**, 41.
- Gordon, L.J., and Scott, R.L. (1952). *J. Am. Chem. Soc.* **74**, 4138.
- Gordon, P. (1968). *Principles of Phase Diagrams in Materials Science*, McGraw-Hill Book Co., New York.
- Guggenheim, F.A. (1987). *Thermodynamics*, 5th ed., North Holland Publishing Company, Amsterdam.
- Hartley, G.S., and Crank, J. (1949). *Trans. Faraday Soc.* **45**, 80.
- Kim, S. and Myerson, A.S. (1996). *Industrial and Engineering Chemistry Research* **35**, 1078.
- Kojima, K., and Tochigi, K. (1979). *Prediction of Vapor–Liquid Equilibria by the ASOG Method*, Elsevier Science Publishing, Inc., New York.
- Linke, W.R., and Seidell, A. (1958). *Solubilities-Inorganic and Metal-Organic Compounds*, vol. 1 (vol. II, 1965), American Chemical Society, Washington, DC.
- Lide, D.R. (1999). *Handbook of Chemistry and Physics*, 79th ed., CRC Press Cleveland, OH.
- Lo, P.Y., and Myerson, A.S. (1990). *J. Cryst. Growth* **99**, 1048.
- Mullin, J.W. (1997). *Crystallization*, Butterworths, London.
- Myerson, A.S., and Lo, P.Y. (1991). *J. Cryst. Growth* **110**, 26.
- Myerson, A.S., Lo, P.Y., Kim, Y.C., and Ginde, R. (1990). In *Proceedings of the 11th Symposium on Industrial Crystallization* (Mersmann, A., ed.), p. 847, European Fed. of Chemical Engineers, Munich, Germany.
- Nývlt, J., Sohnel, O., Matuchova, M., and Brout, M. (1985). *The Kinetics of Industrial Crystallization*, Elsevier, Amsterdam.
- Perry, R.H., and Green, D.W. (1997). *Chemical Engineers Handbook*. 7th ed., McGraw-Hill Book Co., New York.
- Prausnitz, J.M., Lichenthaler, R.N., and Gomes de Azevedo, E. (1999). *Molecular Thermodynamics of Fluid-Phase Equilibria*, 3rd ed., Prentice-Hall, Inc., Englewood Cliffs, NJ.
- Reid, R.C., Prausnitz, J.M., and Poling, B.E. (1987). *The Properties of Gases and Liquids*, 4th ed., McGraw-Hill Book Co., New York.
- Robinson, R.A., and Stokes, R.H. (1970). *Electrolyte Solutions*, 2nd ed., Butterworths, London.
- Rosenberger, F. (1981). *Fundamentals of Crystal Growth*, Springer-Verlag, New York.
- Rush, S. (1991). M.S. thesis in Progress, Polytechnic University, Brooklyn, NY.
- Saska, M. (1994). Ph.D. dissertation, Georgia Institute of Technology, Atlanta, GA.
- Sherman, P. (1970). *Industrial Rheology*, Academic Press, New York.
- Smith, J.M., and Van Ness, H.C. (1975). In *Introduction to Chemical Engineering Thermodynamics*, 3rd ed., p. 115, McGraw-Hill Book Co., New York.
- Walas, S.M. (1985). *Phase Equilibria in Chemical Engineering*, Butterworths, Boston.
- Wilke, C.R., and Chang, P. (1955). *AIChE J.* **1**, 264.
- Zemaitis, J.F. Jr., Clark, D.M., Rafal, M., and Scrivner, N.C. (1986). *Handbook of Aqueous Electrolyte Thermodynamics*, American Institute of Chemical Engineers, New York.

This Page Intentionally Left Blank

CRYSTALS, CRYSTAL GROWTH, AND NUCLEATION

Allan S. Myerson and Rajiv Ginde

2.1. CRYSTALS

Crystals are solids in which the atoms are arranged in a periodic repeating pattern that extends in three dimensions. While all crystals are solids, not all solids are crystals. Materials that have short-range rather than long-range ordering, like glass, are non-crystalline solids. A noncrystalline solid is often referred to as an amorphous solid. Many materials can form solids that are crystalline or amorphous, depending on the conditions of growth. In addition, some materials can form crystals of the same composition but with differing arrangements of the atoms forming different three-dimensional structures. Other materials can have the same three-dimensional structure but appear different in shape when viewed under the microscope. To make sense of this, and to understand the nature of crystals and how they are identified requires some knowledge of crystals and their structure. The study of crystal structure is called *crystallography* and is described in a number of standard references (Bunn 1961; Cullity 1978). In this section, we will discuss the basics of crystals and their structure.

2.1.1. LATTICES AND CRYSTAL SYSTEMS

Crystals are solids in which the atoms are arranged in a three-dimensional repeating periodic structure. If we think of crystals in a purely geometric sense and forget about the actual atoms, we can use a concept known as a point lattice to represent the crystal. A point lattice is a set of points arranged so that each point has identical surroundings. In addition, we can characterize a point lattice in terms of three spatial dimensions: a , b , and c , and three angles: α , β , and γ . An example of a point lattice is given in Figure 2.1. Looking at Figure 2.1 we can see that the lattice is made up of repeating units that can be characterized by the three dimensions and three angles mentioned. We can arbitrarily choose any of these

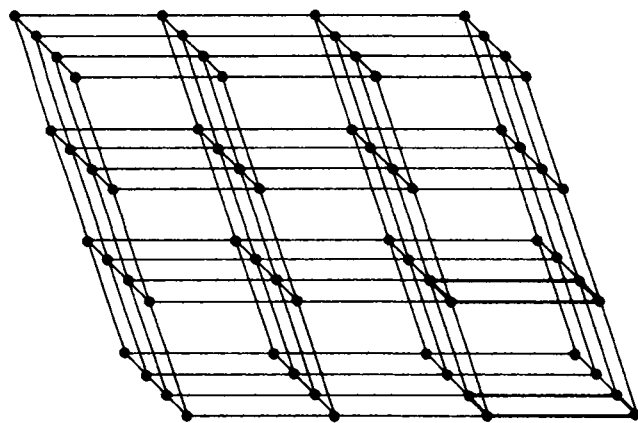


Figure 2.1 A point lattice.

units, and by making use of the spatial dimensions and angles can reproduce the lattice indefinitely. The lengths and angles mentioned are known as *lattice parameters* and a single cell constructed employing these parameters is called the *unit cell*. A unit cell is shown in Figure 2.2.

There are obviously a number of different lattice arrangements and unit cells that can be constructed. It was shown, however, in 1848 by Bravais that there are only 14 possible point lattices that can be constructed. These point lattices can be divided into seven categories (crystal systems) that are shown in Table 2.1. Figure 2.3 shows all 14 of the Bravais lattices. Looking at the crystal systems we see that they are all characterized by these lattice parameters. For example, cubic systems all must have equal lengths ($a = b = c$) and angles equal to 90° . In addition, lattices can be classified as primitive or nonprimitive. A primitive lattice has only one lattice point per unit cell while a nonprimitive unit cell has more than one. If we look at the cubic system, a simple cubic unit cell is primitive. This is because each lattice point on a corner is shared by eight other cells so that $1/8$ belongs to a single cell. Since there are eight corners, the simple cubic cell has one lattice point. Looking at a body centered cubic cell, the point on the interior is not shared with any other cell. A body centered cubic cell, therefore, has two lattice points. A face centered cubic cell has a lattice point on each face that is shared between two cells. Since there are six faces as well as the eight corners, a face centered cubic cell has four lattice points.

Another property of each crystal system that distinguishes one system from another is called symmetry. There are four types of symmetry operations: reflection, rotation, inversion, and rotation-inversion. If a lattice has one of these types of symmetry, it means that after the required operation, the lattice is superimposed upon itself. This is easy to see in the cubic system. If we define an axis normal to any face of a cube and rotate the cube about that axis, the cube will superimpose upon itself after each 90° of rotation. If we divide the degrees of rotation into 360° , this tells us that a cube has three fourfold rotational symmetry axes (on axes normal to three pairs of parallel faces). Cubes also have threefold rotational symmetry using an axis along each body diagonal (each rotation is

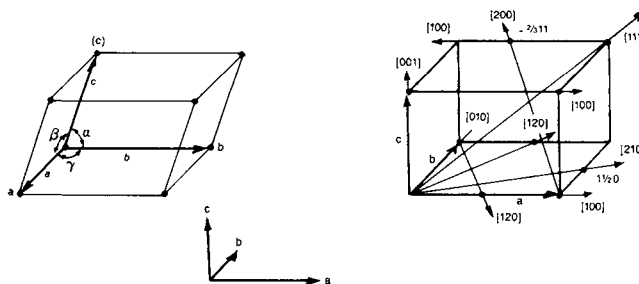


Figure 2.2 A unit cell.

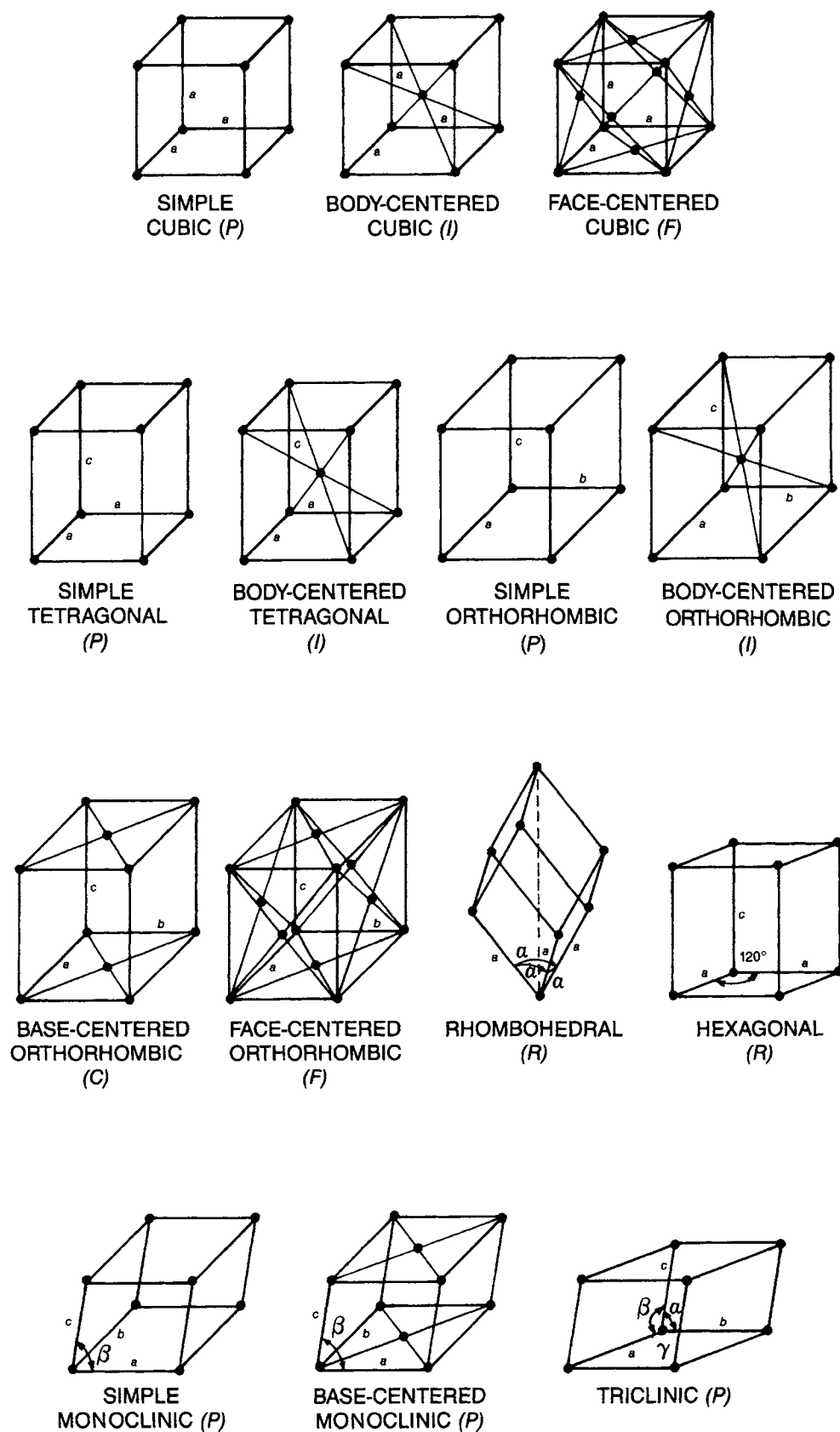


Figure 2.3 The Bravais lattices (P , R = primitive cells, F = face centered, I = body centered, and C = base centered). (From B.D. Cullity, *Elements of X-ray Diffraction*, © 1978 by Addison-Wesley Publishing Company. Reprinted with permission of the publisher.)

TABLE 2.1 Crystal Systems and Bravais Lattices

System	Axial Lengths and Angles	Bravais Lattice
Cubic	Three equal axes at right angles $a = b = c, \alpha = \beta = \gamma = 90^\circ$	Simple Body-centered Face-centered
Tetragonal	Three axes at right angles, two equal $a = b \neq c, \alpha = \beta = \gamma = 90^\circ$	Simple Body-centered
Orthorhombic	Three unequal axes at right angles $a \neq b \neq c, \alpha = \beta = \gamma = 90^\circ$	Simple Body-centered Base-centered Face-centered
Rhombohedral ¹	Three equal axes, equally inclined $a = b = c, \alpha = \beta = \gamma \neq 90^\circ$	Simple
Hexagonal	Two equal coplanar axes at 120° , third axis at right angles $a = b \neq c, \alpha = \beta = 90^\circ, \gamma = 120^\circ$	Simple
Monoclinic	Three unequal axes, one pair not at right angles $a \neq b \neq c, \alpha = \gamma = 90^\circ \neq \beta$	Simple Base-centered
Triclinic	Three unequal axes, unequally inclined and none at right angles $a \neq b \neq c, \alpha \neq \beta \neq \gamma \neq 90^\circ$	Simple

(Data adapted from Cullity 1978.)

¹Also called trigonal.**TABLE 2.2 Symmetry Elements**

System	Minimum Symmetry Elements
Cubic	Four threefold rotation axes
Tetragonal	One fourfold rotation (or rotation-inversion) axis
Rhombohedral	Three perpendicular twofold rotation (or rotation-inversion) axes
Hexagonal	One sixfold rotation (or rotation-inversion) axis
Monoclinic	One twofold rotation (or rotation-inversion) axis
Triclinic	None

(Data adapted from Cullity 1978.)

120°) and twofold rotational symmetry using the axis formed by joining the centers of opposite edges. Each lattice system can be defined in terms of the minimum symmetry elements that must be present. Table 2.2 lists the minimum symmetry elements that must be present in a given crystal system. A system can have more than the minimum but not less. A more complete discussion of lattices and symmetry can be found in Cullity (1978).

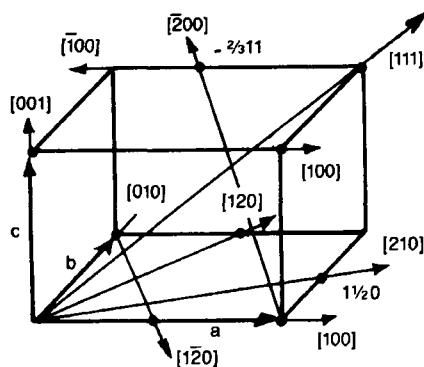


Figure 2.4 Indices of directions. (From B.D. Cullity, *Elements of X-ray Diffraction*, © 1978 by Addison-Wesley Publishing Company. Reprinted with permission of the publisher.)

2.1.2. MILLER INDICES AND LATTICE PLANES

If we take any point on a lattice and consider it the origin, we may define vectors from the origin in terms of three coordinates. If, for example, we started with a cubic cell and defined a vector going from the origin and intersecting point 1,1,1, the line would go in the positive direction along the body diagonal of the cube and would also intersect the points 2,2,2 and all multiples. This direction is represented in shorthand by $[1,1,1]$ where the numbers are called the indices of the direction. Negative numbers are indicated by putting a bar over a number so that $[\bar{1},1,1]$ means the first index is negative. We can represent a family of direction by using the symbol $\langle 1,1,1 \rangle$. This represents all the directions using both positive and negative indices in all combinations. In this case, it represents all the body diagonals of a cube. By convention, all indices are reduced to the smallest set of integers possible either by division, or by clearing fractions. An illustration of various indices and the directions they represent is shown in Figure 2.4.

The representation of planes in a lattice makes use of a convention known as Miller indices. In this convention, each plane is represented by three parameters (hkl), which are defined as the reciprocals of the intercepts the plane makes with three crystal axes. If a plane is parallel to a given axis, its Miller index is zero. Negative indices are written with bars over them. Miller indices refer not only to one plane but a whole set of planes parallel to the plane specified. If we wish to specify all planes that are equivalent, we put the indices in braces. For example, $\{100\}$ represents all the cube faces. Examples of Miller indices in the cubic system are shown in Figure 2.5.

Real crystals are often described in terms of the Miller indices of the faces (planes) present. Examples of some common crystals with their faces given in terms of Miller indices are shown in Figure 2.6.

2.1.3. CRYSTAL STRUCTURE AND BONDING

In the previous section we have developed a geometric system that can be used to represent the structure of actual crystals. In the simplest actual crystal, the atoms coincide with the points of one of the Bravais lattices. Examples include chromium, molybdenum,

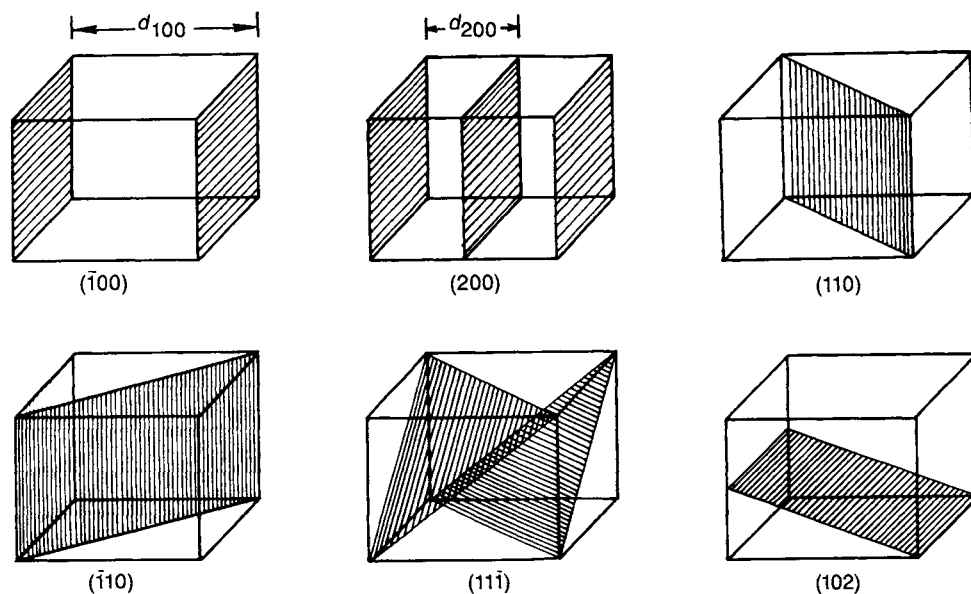


Figure 2.5 Miller indices of planes in the cubic system. The distance d is the interplanar spacing. (From B.D. Cullity, *Elements of X-ray Diffraction*, © 1978 by Addison-Wesley Publishing Company. Reprinted with permission of the publisher.)

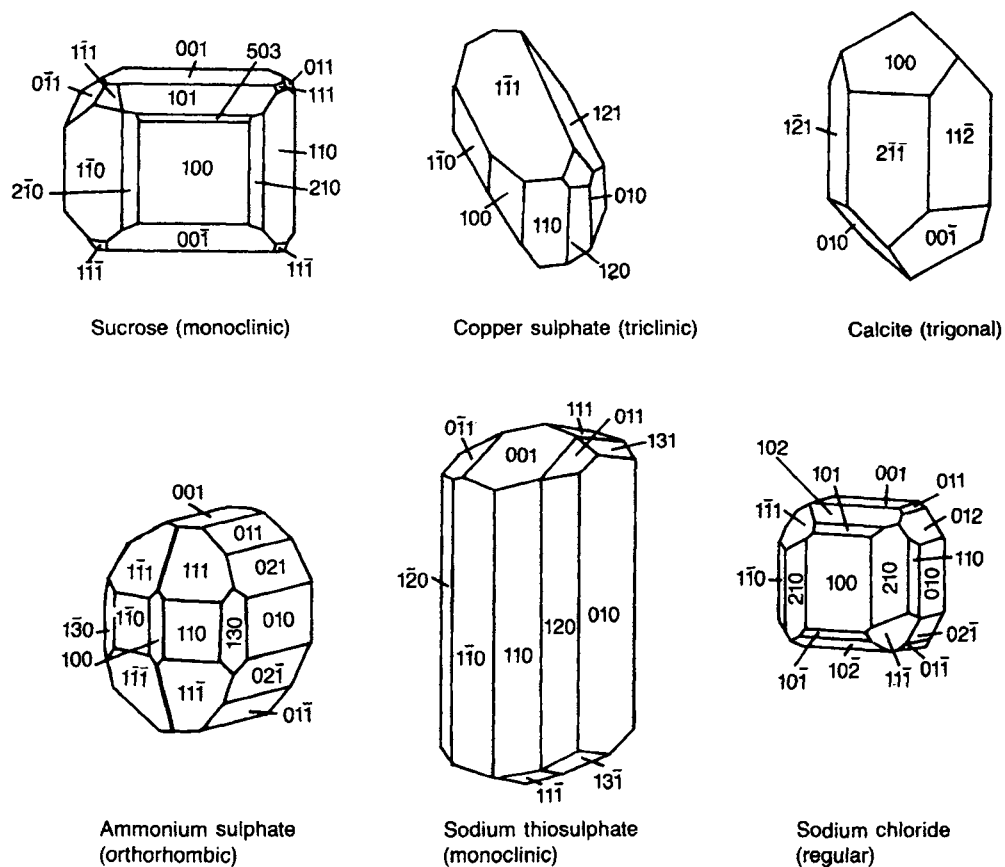


Figure 2.6 Crystal forms of some common materials with their Miller indices shown. (Reproduced with permission from Mullin 1972.)

and vanadium, which have a body centered cubic crystal structure, and copper and nickel, which are face centered cubic.

In a more complex arrangement, more than one atom of the same type can be associated with each lattice point. A structure that a number of metals have, which is an example of this, is the hexagonal close-packed structure. It is called close packed because, if the molecules are assumed to be spherical, this arrangement is one of only two possible ways spheres can be packed together to yield the greatest density yet still be in a periodic structure. The packing arrangement in crystals is another part of the information that helps to understand crystal structure. More information on packing in crystals can be found in Ruoff (1973) and Cullity (1978).

Many inorganic molecules form ionic crystals. An example of an ionic structure common to a number of molecules is that of sodium chloride, shown in Figure 2.7. Ionic crystals are made up of the individual ionized atoms that make up the species in their stoichiometric proportion. They are held in place by electronic forces. The sodium chloride structure is face centered cubic and the unit cell contains four sodium ions and four chloride ions. Because the unit cells contain two types of atoms some additional constraints on the structure exist. For example, a symmetry operation on the crystal must superimpose atoms of the same type.

Most organic species form molecular crystals in which discrete molecules are arranged in fixed positions relative to the lattice points. This of course means that the individual atoms making up the molecules are each arranged at fixed positions relative to each other, the lattice point, and the other molecules. The forces between molecules in molecular crystals are generally weak when compared with the forces within a molecule. The structure of molecular crystals is affected by both the intermolecular forces and the intramolecular forces since the shapes of the individual molecules will affect the way the molecules pack together. In addition, the properties of the individual molecule, such as the polarity, will affect the intermolecular forces. The forces between the molecules in molecular crystals include electrostatic interactions between dipoles, dispersion forces, and hydrogen bond

interactions. More information about the structure and energetics of molecular crystals can be found in the work of Kitaigorodski (1973) and in Wright (1987).

An important tool used to identify crystals and to determine crystal structure is that of x-ray diffraction. Crystals have atoms spaced in a regular three-dimensional pattern. X-rays are electromagnetic waves with wavelengths of similar size as the distance between the atoms in a crystal. When a monochromatic beam of x-rays is directed at a crystal in certain directions, the scattering of the beam will be strong and the amplitudes of the scattering will add creating a pattern of lines on photographic film. The relationship between the wavelength of the x-rays and the spacing between atoms in a crystal is known as Bragg's law, which is given below

$$\lambda = 2d \sin \theta \quad (2.1)$$

where λ is the wavelength of the incident x-rays, d is the interplanar spacing in the crystal, and θ the angle of the incident x-rays on the crystal.

Bragg's law shows us that, if x-rays of a known wavelength are used and the incident angle of the radiation is measured, determination of the interplanar spacing of a crystal is possible. This is the foundation of x-ray diffraction methods that are used to analyze or determine the structure of crystals. Several different experimental methods making use of x-ray diffraction and Bragg's law have been developed and are used depending on the type of sample that is available and the information desired.

The most powerful method that can be used to determine unknown crystal structures is the rotating crystal technique. In this method a single crystal of good quality (of at least 0.1 mm in the smallest dimension) is mounted with one of its axes normal to a monochromatic beam of x-rays and rotated about in a particular direction. The crystal is surrounded by cylindrical film with the axis of the film being the same as the axis of rotation of the crystal. By repeating this process of rotation in a number of directions, the rotating crystal method can be used to determine an unknown crystal structure.

It is unlikely that you will ever need to use the rotating crystal method to determine an unknown structure since most materials you are likely to crystallize have structures that have been determined. This will not be true for a newly developed compound, and is rarely true for proteins and other biological macromolecules.

An x-ray method more commonly used is called the *powder method* because, instead of using a single crystal, a very fine powder of the crystal is used. This is convenient since you do not have to grow a single crystal of the size and quality needed for single crystal methods. The powder method relies on the fact that the array of tiny crystals randomly arranged will present all possible lattice planes present for reflection of the incident monochromatic x-ray beam. The powder pattern of a particular substance acts as a signature for that substance so that a powder diffraction pattern can be used for identification, chemical analysis (presence of impurities), and determining if a material is crystalline or amorphous. This is made easier by the fact that a reference known as the powder diffraction file (Joint Committee on Powder Diffraction Standards 1990) is available with the powder x-ray patterns of more than 30,000 materials and is arranged in a way that makes searches based on a measured pattern quite possible. Description of powder diffraction methods and analysis can be found in Bunn (1961) and Cullity (1978). Recently (Engel et al., 1999) computer methods have been developed, which can solve crystal structures from high quality powder patterns. This is of great value when it is not possible to grow a crystal of sufficient size for single crystal structure determination.

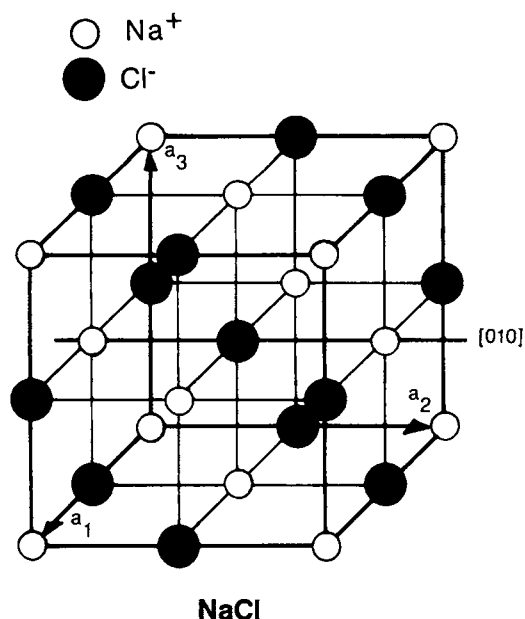


Figure 2.7 The structure of sodium chloride (NaCl).

Another method of x-ray diffraction is the Laue method, which employs a single crystal oriented at a fixed angle to the x-ray beam. The beam, however, contains the entire spectrum produced by the x-ray tube. In this method, therefore, the angle θ in Bragg's law is fixed but a variety of wavelengths are impinging on the crystal. Each set of planes that will satisfy Bragg's law with a particular wavelength will diffract and form a pattern known as a *Laue pattern*. The Laue method is used as a way to assess crystal orientation and to determine crystal quality. Other x-ray techniques are also available, making use of x-ray spectrometers and variations on the methods mentioned previously. A number of references can supply more details on any of the x-ray methods (Cullity 1978; Bunn 1961; Bertin 1975). It is important to remember that x-ray diffraction is the only unambiguous way to determine if a material is truly crystalline. In addition, as we will see in the next section, x-ray diffraction is often necessary to determine whether a material is cocrystallized or has crystallized into more than one crystal structure.

2.1.4. POLYMORPHISM

As we have seen in the previous section, crystalline materials can be characterized in terms of their crystal structures. A given chemical species, however, can have more than one possible crystal structure. The phenomena of a chemical species having more than one possible crystal form is known as *polymorphism*. The term *allotropism* is used to describe elements that can form more than one crystal form. Materials crystallize into different crystal forms as a function of the conditions of growth (temperature, pressure, impurity content, growth rate, etc.).

When a material can crystallize into a different polymorph, the chemical nature of the species remains identical, however, the physical properties of the material can be different. For example, properties such as density, heat capacity, melting point, thermal conductivity, and optical activity can vary from one polymorph to another. Table 2.3 lists common materials that exhibit polymorphism. Looking at Table 2.3 we can see that density varies significantly for the same materials when the crystal structure has changed. In addition, the change in the crystal structure often means a change in the external shape of the crystal, which is often an important parameter in industrial crystallization that has to be controlled. Many substances crystallize into structure in which the solvent is present as part of the crystal lattice. These crystals are known as *solvates* (or hydrates when the solvent is water). A substance can have multiple solvates with different crystal structures as well as a solvent free crystal form with a unique crystal structure. The solvates are often referred to as *pseudopolymorphs*. They are not true polymorphs because of the addition of the solvent molecule(s) to the crystal lattice. *Conformational polymorphism* refers to the situation where the molecular conformation of the molecules of a given substance are different in each polymorph.

Materials that exhibit polymorphism present an interesting problem. First, it is necessary to control conditions to obtain the desired polymorph. Second, once the desired polymorph is obtained, it is necessary to prevent the transformation of the material to another polymorph. Materials that form polymorphs often will transform from one form to another. This is known as a polymorphic transition. Often a simple change of temperature will cause a material to change form. In many cases, a particular polymorph is metastable, meaning that after crystallizing the material will eventually transform into a more stable state. This transformation can be relatively rapid in some systems while in others it can be infinitely slow. At room temperature, a diamond is a metastable form of carbon.

TABLE 2.3 Polymorphic Forms of Some Common Substances

Element or Compound	Chemical Composition	Known Polymorphic Forms ¹
Cesium chloride	CsCl	Cubic (CsCl type) (s), $d = 3.64$ Cubic (NaCl type) (m), $d = 3.64$
Calcium carbonate	CaCO ₃	Calcite (s), rhombohedral, uniaxial, $d = 2.71$ Aragonite (m), orthorhombic, biaxial, $d = 2.94$
Carbon	C	Diamond (m), cubic, very hard, $d = 3.5$, covalent tetrahedral binding, poor conductor Graphite (s), hexagonal, soft, $d = 2.2$ layer structure, good conductor
Iron	Fe	γ iron (m), f.c.c. α iron (s) and δ iron (m), b.c.c.
Mercuric iodide	HgI ₂	Red (s), tetragonal Yellow (m), orthorhombic
Phosphorus	P ₄	White phosphorus (m), $d = 1.8$, melts 44°C Violet phosphorus (s), $d = 2.35$; melts around 600°C
Silica	SiO ₂	Quartz (s) (α and β forms), $d = 2.655$ Tridymite (m) (α and β forms), $d = 2.27$ Cristobalite (m) (α and β forms), $d = 2.30$
Sulfur	S	α , orthorhombic (s), $d = 2.05$, melts 113°C β , monoclinic (m), $d = 1.93$, melts 120°C
Tin	Sn	White tin, tetragonal, $d = 7.286$, stable above 180°C Gray tin, cubic (diamond type), $d = 5.80$, metastable above 180°C
Zinc sulfide	ZnS	Wurtzite (m), hexagonal Sphalerite (s), cubic (diamond type)

(Data adapted from Verma and Krishna 1966.)

¹ d = density(g/km³); m = metastable and s = stable.

These transitions from one polymorph to another usually occur most rapidly when the crystals are suspended in solution, however, some materials will undergo transformation when in a dry powder form. It is possible, with some effort, to obtain a phase diagram that shows where a particular polymorph is stable and where it is unstable. When a material has multiple polymorphs and one of the polymorphs is the stable form at all temperatures the system is known as *monotropic*. If different polymorphs are stable at different temperatures the system is known as *enantiotropic*. In enantiotropic systems, the polymorph with the lowest solubility is the stable form. If the solubility is plotted versus temperature in an enantiotropic system, the transition temperature will be where the solubility curves cross. This transition temperature is independent of solvent used. It is also possible through experiment to determine which conditions of growth favors the formation of a particular polymorph. In many, if not most industrial crystallizations involving polymorphs, it is necessary to obtain the same polymorph in all cases. If the wrong polymorph is produced, the properties of the material would change, making the product unacceptable. A good example of this is in the production of precipitated calcium carbonate that is used for coating and filler in paper. Calcium

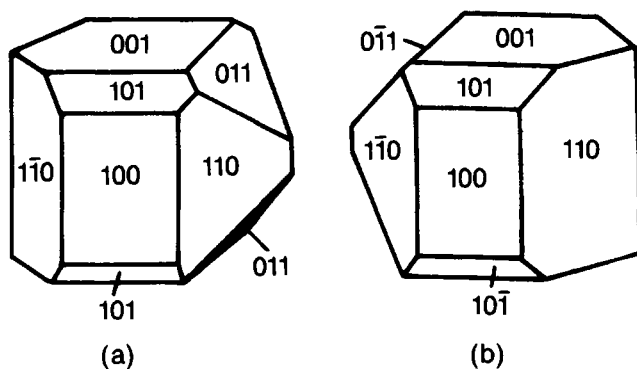


Figure 2.8 (a) D and (b) L tartaric acid. (Reproduced with permission from Mullin 1972.)

carbonate can crystallize into three forms: calcite, aragonite, and vaterite. For reasons of external crystal shape, calcite is the form needed. When aragonite is produced accidentally, which is a common occurrence, it is not usable and must be discarded and reprocessed.

In crystallization processes involving a material that displays polymorphism, it is quite common for an unstable polymorph to appear first and then transform into a stable form. This observation is summarized by Ostwald's step rule, sometimes referred to as the "Law of Successive Reactions," which says that in any process, the state which is initially obtained is not the stablest state but the least stable state that is closest in terms of free energy change, to the original state. What this means, therefore, is that a crystallization process, the initial solid phase, can be the least stable polymorph that will then transform into successively more stable forms until the stable form, at the conditions of the system, is reached. With some systems this can mean the formation of an

amorphous solid phase followed by a transformation to the least stable crystalline phase and finally transformation to the stable phase. While this is observed in a wide range of systems, it is most likely to be observed in the crystallization of organic, especially higher molecular weight materials. More information on polymorphism can be found in Gilli (1992) and Myerson (1999).

There are some materials that can crystallize into two different crystal forms that are mirror images of each other. This is given the special name of *enantiomorphism*. In general, but not always, materials that form enantiomorphs also display a property called *optical activity*. This means that the crystal will rotate the plane of polarized light that passes through it. Optically active enantiomorphs are given the designation D (for dextro) and L (for levo), which indicate the direction they rotate polarized light (to the right or left). When an optically active material crystallizes as a mixture of the D and L forms, it is known as a *racemic mixture*. The separation of racemic mixtures into the pure D or L form is an important practical industrial problem that is often attacked by using differences in properties of the two forms. There are four main techniques for the separation of racemic mixtures (Leusen 1993). Two of the methods involve the use of a chemical that interacts specifically with one racemate, either through the rate of chemical reaction (kinetic resolution) or by absorption (chromatographic separation). The two other methods involve crystallization. In direct crystallization, one racemate is selectively crystallized from a solution of the racemic mixture. This can be accomplished by seeding with the desired enantiomer or by using chiral solvents or additives that will aid the crystallization of one enantiomer (or inhibit the crystallization of the other enantiomer). Another crystallization method involves the use of an agent that will form a complex with each of the enantiomers with the complexes having different solubilities so that one complex can be selectively crystallized. This method is known as resolution by diastomeric salts. Examples of optically active enantiomorphs are tartaric acid and sodium chlorate, shown in Figures 2.8 and 2.9.

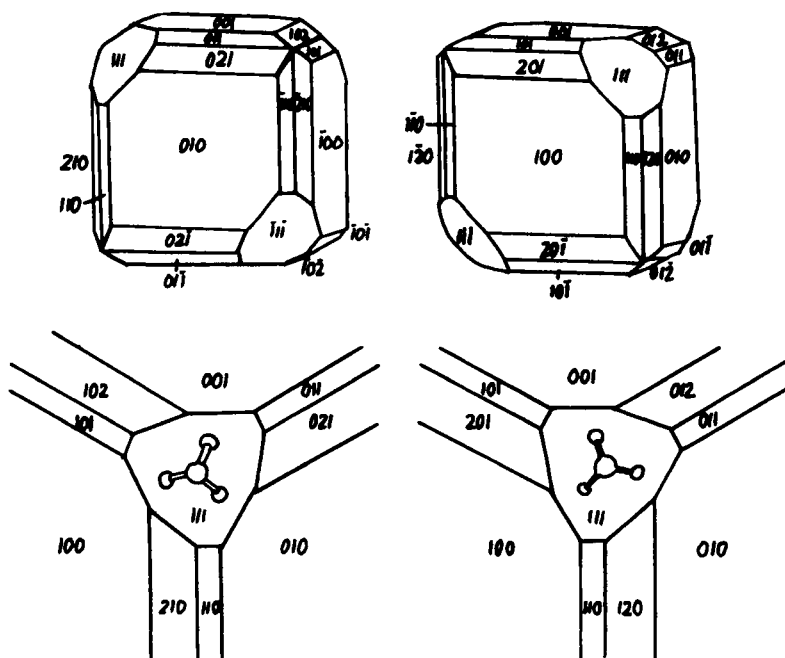


Figure 2.9 L and D sodium chlorate crystal habit (top). Orientation of ClO_3 groups on 111 faces (bottom). (Reproduced with permission from Bunn 1961.)

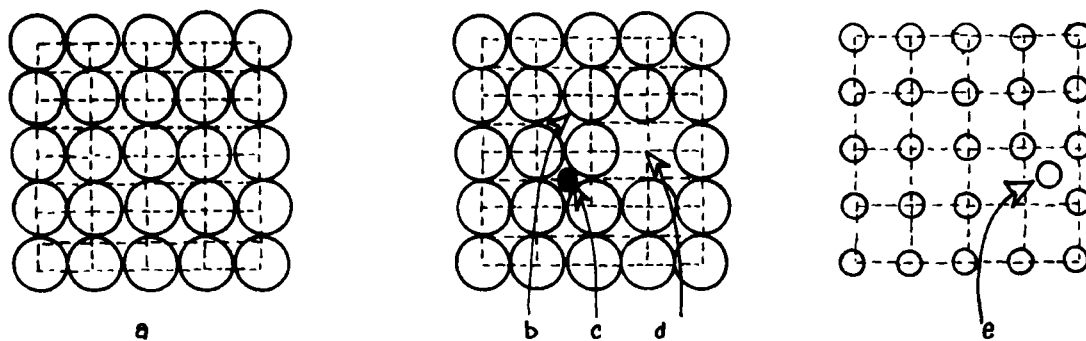


Figure 2.10 Imperfection in crystals: (a) perfect crystal; (b) substitutional impurity; (c) interstitial impurity; (d) Schottky defects; and (e) Frenkel defect. (From R.A. Laudise, *The Growth of Single Crystals*, © 1970, pp. 12–13. Reprinted by permission of Prentice-Hall, Englewood Cliffs, New Jersey.)

2.1.5. ISOMORPHISM AND SOLID SOLUTIONS

It is quite common for a number of different species to have identical atomic structures. This means that the atoms are located in the same relative positions in the lattice. We have seen this previously with the sodium chloride structure. A number of other species have this structure. Obviously, species that have the same structure have atoms present in similar stoichiometric proportion. Crystals that have the same structure are called *isostructural*.

If crystals of different species are isostructural and have the same type of bonding, they also will have very similar unit-cell dimensions and will macroscopically appear almost identical. This is known as *isomorphism*. Examples of isomorphous materials include ammonium and potassium sulfate and KH_2PO_4 and $\text{NH}_4\text{H}_2\text{PO}_4$. In each of these materials, the potassium and ammonium ions can easily substitute for each other in the lattice since they are of almost the same size. This illustrates one of the properties of isomorphous materials, that is they tend to form solid solutions, or mixed crystals. Crystallization from a solution of two isomorphous materials, therefore, can result in a solid with varying composition of each species with unit-cell dimensions intermediate between the two components. The purification of isomorphous substances can, therefore, be difficult.

Solid solutions do not all result from the substitution of isomorphous materials in the lattice sites, other types of solid solutions are possible and are described in Vainshtein (1981).

2.1.6. IMPERFECTIONS IN CRYSTALS

In our discussions of the internal structure of crystals, we have shown that each atom (or molecule) has a precise location in a repeating structure. If this structure is disrupted in some way the crystal is said to have imperfections. There are a number of different kinds of imperfections that can occur. If a foreign atom (or molecule in a molecular crystal) is present in the crystal lattice, this is known as a chemical imperfection. The foreign atom can be present at a lattice site having substituted for an atom in the structure as we saw in our brief discussion of isomorphism and solid solutions. This is called a *substitutional impurity*. The foreign atom can also be present in the crystal by fitting between the atoms in the lattice. This is called a *interstitial impurity*. Both of these types of impurities can cause the atoms in the crystal to be slightly displaced since the impurity atoms do not really fit in the perfect lattice structure. The displacement of the atoms causes a strain in the crystal.

Another type of imperfection is due to vacancies in the crystal. A vacancy is simply a lattice site in which there is no atom. A

vacancy caused by the migration of an atom to an interstitial region is called a *Frenkel defect*, while one in which a vacancy is just an empty lattice site missing an atom is called a *Schottky defect*. These types of imperfections are very important in semiconductors and microelectronics. Figure 2.10 illustrates the various types of vacancies and chemical imperfections.

The imperfections in crystals discussed so far are called *point defects* because they involve a single unit of the crystal structure, that is an atom or molecule. Another type of imperfection is known as a line defect or dislocation. There are two types of dislocations known as edge dislocations and screw dislocations.

An edge dislocation is illustrated in Figure 2.11, which is a cross section of a crystal lattice. Looking at the figure you can see half of a vertical row (the bottom half) in the middle of the lattice is missing. This row of atoms is missing in each plane of the lattice parallel to the page. The dislocation is marked at point A. If a line is drawn vertically from the book out, going through all the layers of the crystal, it would represent the edge dislocation line. Looking at the figure, we can see that the lattice points are displaced in the region of the dislocation and that this displacement gets smaller as we move away from the dislocation until the lattice returns to normal.

The dislocation is a weak point in the crystal. Again looking at Figure 2.11, if we draw a line through the crystal at the dislocation,

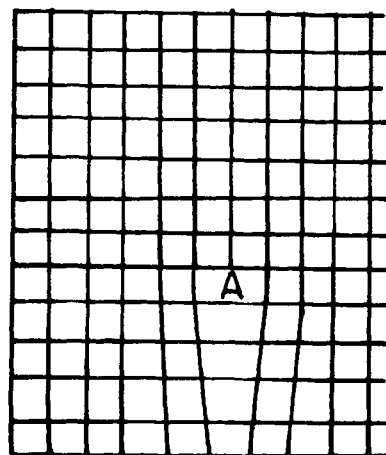


Figure 2.11 An edge dislocation shown in two dimensions. (From R.A. Laudise, *The Growth of Single Crystals*, © 1970, pp. 12–13. Reprinted by permission of Prentice-Hall, Englewood Cliffs, New Jersey.)

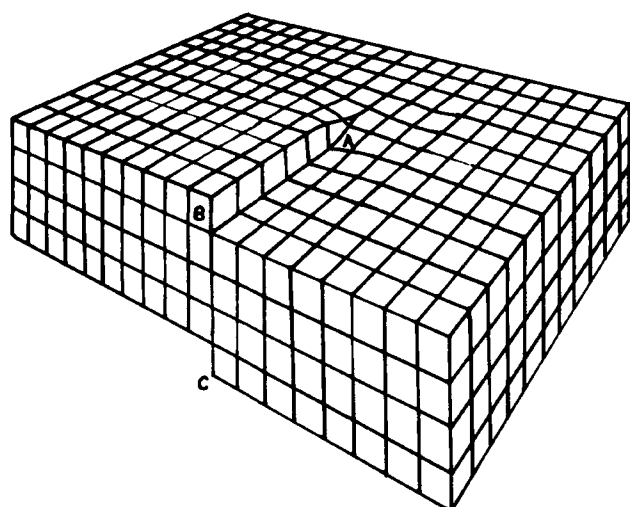


Figure 2.12 A screw dislocation in a simple cubic crystal. The screw dislocation AD is parallel to BC (D is not visible). (Reproduced with permission from Strickland-Constable 1968.)

this defines what is called a *slip plane*. If a force is exerted in the direction of the arrow on the upper half of the crystal, it will shear at this plane. A more detailed discussion of dislocations and defects can be found in several references (Laudise 1970; Strickland-Constable 1968).

The other type of line defect is called a *screw dislocation*, which is illustrated in three dimensions in Figure 2.12. Imagine that we cut the crystal along the line BC going towards point A. We then pushed up at the cut until point B was displaced one lattice unit higher at the edge along the cut. This results in a ledge running from A to B. The screw dislocation is very important in crystal growth as we will see in Section 2.3.

2.1.7. CRYSTAL HABIT

In our discussions of crystals to this point, we have been discussing the internal structure of the crystals, that is, how the atoms and molecules are arranged into their periodic lattice structure. The external appearance of the crystals is also of great importance and is referred to as the crystals habit, crystal shape, or crystal morphology. These terms are often used interchangeably, however, crystal habit is used most often.

Crystal habit refers to the external appearance of the crystal. A quantitative description of a crystal means knowing the crystal faces present, their relative areas, the lengths of the axes in the three directions, the angles between the faces, and the shape factor of the crystal. Shape factors are a convenient mathematical way of

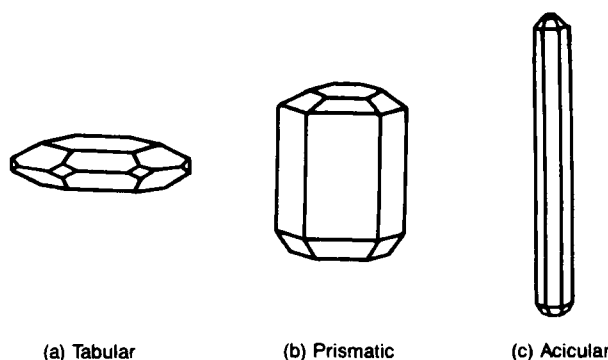


Figure 2.13 External shape of hexagonal crystal displaying the same faces. (Reproduced with permission from Mullin 1972.)

describing the geometry of a crystal. If the size of a crystal is defined in terms of a characterization dimension L , two shape factors can be defined: the volume shape factor (α) and the area shape factor (β)

$$V = \alpha L^3 \quad (2.2)$$

$$A = \beta L^2 \quad (2.3)$$

Values of shape factors for common materials and geometries are available in the literature (Mullin 1993; Nývlt *et al.* 1985). Shape factors for common geometries are given in Table 2.4.

A good question to ask at this point is whether knowledge of the internal structure of a crystal gives you knowledge of its external habit. Looking at Figure 2.13 we see three examples of external shapes of crystals. The crystals all have the same faces present and the same internal structure, however, the relative areas of the faces present are different, thus resulting in differing external habits. This is a simple example showing that the relative area of the crystal faces has a major impact on the external habit, even though the internal structure is the same. In fact, sometimes the

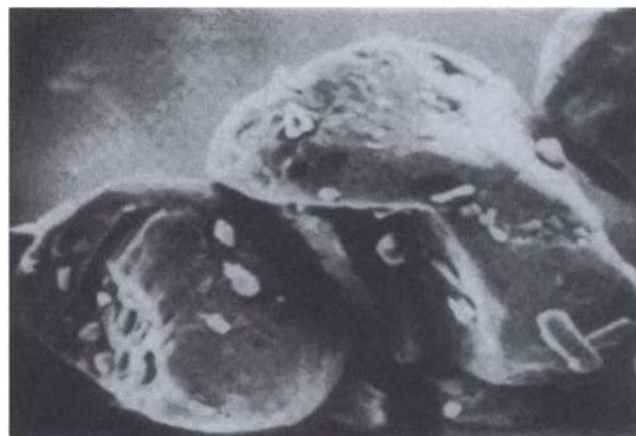


Figure 2.14 Scanning electron micrograph of terephthalic acid crystals obtained by rapid precipitation. [From M. Saska and A.S. Myerson (1987), "Crystal Aging and Crystal Habit of Terephthalic Acid," *AIChE J.* 33 (5), pp. 848–852. Used by permission of the American Institute of Chemical Engineers. © 1987 AIChE.]

TABLE 2.4 Shape Factors for Various Geometries

Body	α	β	$F = \beta/\alpha$
Sphere	0.524	3.142	6.00
Tetrahedron	0.182	2.309	12.7
Octahedron	0.471	3.464	7.35
Six-sided prism	2.60	11.20	4.31
Cube	1.00	6.00	6.00
Prism	10.00	2.00	5.00
Platelet	0.20	2.80	14.00
Needle	10.00	42.00	4.20

(Data adapted from Nývlt *et al.* 1985.)

faces present will not even be the same for two crystals of the same substance with the same internal structure. This is because the external habit of a crystal is controlled, not only by its internal structure, but by the conditions at which the crystal grows. The rate of growth, the solvent used, and the impurities present all can have a major impact on the crystal habit.

The habit of crystals obtained from an industrial crystallization process can have a major impact on a number of important properties relating to the slurry and the dry product. Crystal habit will affect the rheological properties of the suspension, the filtration or centrifugation efficiency, the bulk density of the solid, and the flow properties of the solid. The control of crystal habit (along with crystal size distribution) is, therefore, an important part of industrial crystallization processes.

Crystal habit can vary dramatically with the rate of crystal growth and nucleation. A good example of this is in reactive systems that operate with very high supersaturations with products that have very low solubilities. In the manufacture of terephthalic acid by the air oxidation of *para*-xylene, the rapid reaction and high supersaturation result in a product crystal that does not show any crystal faces and looks like a boulder. An example of such a crystal is shown in Figure 2.14. While not showing any obvious faces, this material is crystalline when examined employing x-ray analysis. Crystallization of terephthalic acid from a supersaturated solution at slower rates yields a monoclinic needle, as shown in Figure 2.15. It is only the very rapid rate that produces the boulder-like form. Very rapid crystallization processes can often produce amorphous-appearing materials (showing no faces) that are actually crystalline. This is the result of the rapidity of the growth process with all the faces growing so rapidly as to disappear. Other examples of the rate of crystal growth rate on habit are shown in Figure 2.16. In these cases, rapid growth results in fewer faces present in the grown crystal.

Changes in the solvent used or the presence of an impurity can also profoundly affect the crystal habit. Figure 2.17 shows the effect of aluminum fluoride on the habit of anhydrous calcium sulfate. The impurity transforms the needle-like habit to a cubic looking crystal. Figure 2.18 demonstrates the effect of urea on sodium chloride crystals. A large amount of qualitative information exists on the effect of impurities on crystal habit (Mullin 1993;

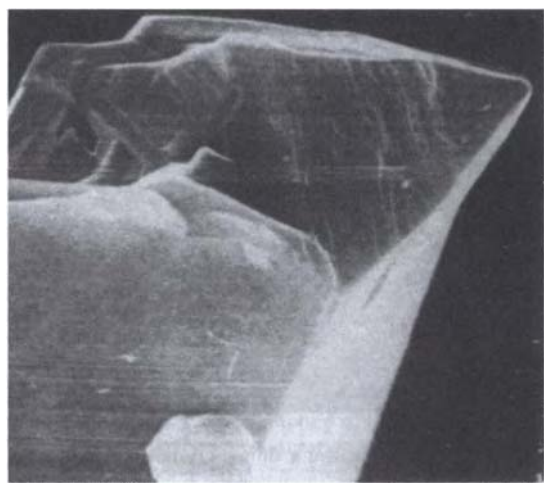


Figure 2.15 The end of terephthalic acid rod crystal (7500 \times). [From M. Saska and A.S. Myerson (1987), "Crystal Aging and Crystal Habit of Terephthalic Acid," *AIChE J.* 33(5), pp. 848–852. Used by permission of the American Institute of Chemical Engineers. © 1987 AIChE.]

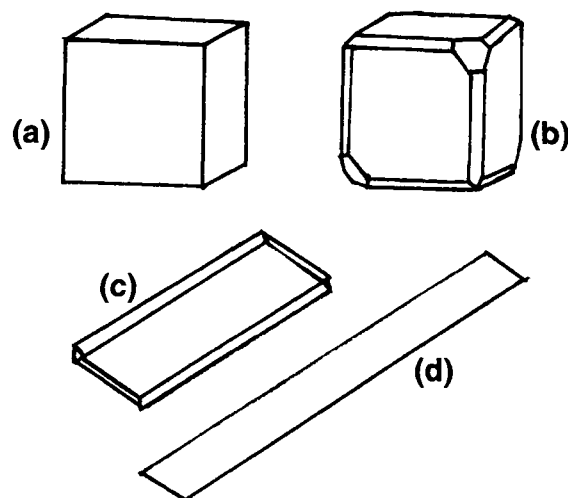


Figure 2.16 Variation of crystal shape with conditions of growth. Sodium chlorate grown (a) rapidly and (b) slowly. Gypsum grown (c) slowly and (d) rapidly. (Reproduced with permission from Bunn 1961.)

Buckley 1951), especially for inorganic systems. Known habit modifiers for inorganic materials are listed in Table 2.5. In recent years great strides have been made in developing a quantitative understanding of habit modification. More information relating to habit modification can be found in Chapter 3 of this volume, which deals with impurity crystal interactions.

2.1.8. PREDICTION OF CRYSTAL HABIT

As discussed in the previous section, crystal habit is a function of both the internal structure of the crystal and the external conditions of growth. A fundamental problem that has been of interest for many years is how to employ this information to predict the habit of crystals grown under realistic conditions.

The equilibrium shape of a crystal is that of its minimum energy. This is called the *Wulff condition* and indicates that the area of faces present will be such as to minimize the Gibbs free energy of the crystal. Unfortunately, the observed habit of crystals grown from solutions is often quite different from the prediction by the Wulff condition.

The early investigation of crystals led to interest in the relation of crystal morphology (shape) with internal structure. A simple correlation was noticed by Donnay and Harker (1937) between the interplanar spacing of a crystallographic plane, d_i , and its area on an average crystal. Since the area of a plane is roughly proportional to the inverse of its linear growth velocity, R , the Donnay–Harker law is equivalent to stating the $R_i \sim 1/d_i$. This simple relation is often useful in making a first estimate of crystal habit.

Hartman and Perdok (1955a, 1955b, 1955c) developed a theory that related crystal morphology to its internal structure on an energy basis. They concluded that the morphology of a crystal is governed by a chain of strong bonds [called periodic bond chains (PBC)], which run through the structure. The period of these strong bond chains is called the PBC vector. In addition, Hartman and Perdok divided crystal faces into three types. These types are:

1. F-faces (flat), each of which is parallel to at least two PBC vectors.
2. S-faces (stepped) parallel to at least one PBC vector.
3. K-faces (kinked) not parallel to any PBC vector.

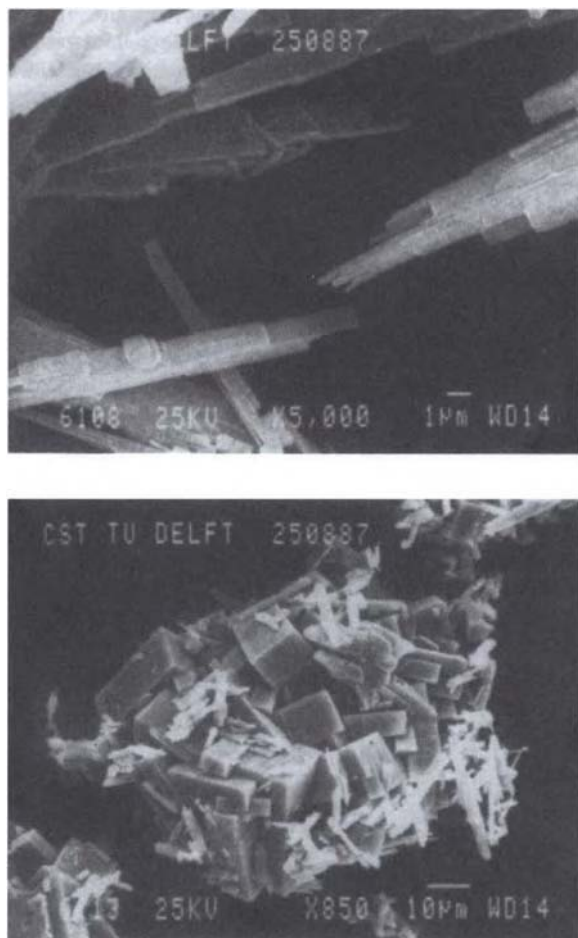


Figure 2.17 Anhydrous calcium sulfate crystals grown in pure phosphoric acid (top) and acid containing 0.8% aluminum fluoride (bottom). [Reprinted with permission from G.J. Witkamp and G.M. Van Rossmalen (1990). "Continuous Crystallization of Calcium Sulfate Phases from Phosphoric Acid Solutions," *Crystallization as a Separation Process*. A.S. Myerson and K. Toyokura (eds.), *ACS Symposium Series*, no. 438, pp. 392. © 1990 American Chemical Society.]

The attachment energy of a crystal face is the difference between the crystallization energy and the slice energy. For an F face the attachment energy can also be expressed as the bond energy of bonds belonging to the PBC's that are not parallel to the face. The attachment energy of an S face will require the formation of at least one more strong bond than an F face and a K face will require at least one more strong bond than an S face. Hartman-Perdok theory indicates that the larger the attachment energy, the faster the growth rate of a crystal. Since the largest face of a grown crystal are the faces that grow the least, Hartman-Perdok theory provides a means to predict the morphology of a grown crystal from the attachment energy of the F faces. More information on Hartman-Perdok theory can be found in Hartman (1963) and Docherty and Meenan (1999).

The use of attachment energy as a method for the calculation of crystal morphology was developed by Hartman and Bennema (1980a, b) and has since become the standard method used to calculate the morphology of organic molecular crystals. The basic method used by most investigators, as well as the method used in most software packages (CERIUS2 1999; Clydesdale, Roberts, and

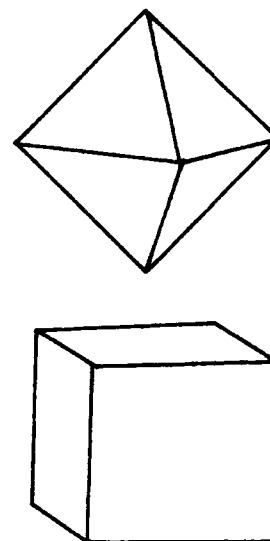


Figure 2.18 Sodium chloride crystals grown from pure solution and from a solution containing 10% urea. (Reproduced with permission from Bunn 1961.)

Docherty, 1996), first identifies the important crystallographic faces of the crystal using the Donnay-Harker method. The attachment energy of these faces is then calculated using *interatomic potential functions* (which calculate interactions between all the atoms in the face). The morphology of the crystal is then calculated by assuming the relative growth velocity of the face is directly proportional to the attachment energy. More information on methods to calculate morphology and on molecular modeling can be found in Myerson (1999).

The attachment energy and Hartman-Perdok methods for the calculation of crystal morphology has been extended to ionic crystals and is described by Strom et. al. 1999.

A major weakness in the calculations described above is that they can only be used to represent vapor grown crystals. In crystals grown from solution, the solvent can greatly influence the crystal habit as can small amounts of impurities. Several investigators (Saska and Myerson 1983; Black and Davey 1988) accounted for discrepancies between observed crystal habit and those obtained using attachment energies by assuming preferential solvent (or impurity) adsorption on crystal faces. The impurity (or solvent) can slow the growth of a face by sterically hindering the attachment of additional molecules. Additives can also be "Tailor Made" to substitute into the crystal lattice in only certain faces thus blocking growth and altering the morphology (Weissbuch, Lahav and Leiserowitz, 1999).

The prediction and control of crystal habit by the appropriate selection of solvent or addition of impurity is an area of great current interest with potential for great impact on industrial crystallization.

2.2. NUCLEATION

Crystallization from solution can be thought of as a two-step process. The first step is the phase separation, or "birth," of new crystals. The second step is the growth of these crystals to larger sizes. These two processes are known as nucleation and crystal growth, respectively. Analysis of industrial crystallization processes requires knowledge of both nucleation and crystal growth. As was discussed in Chapter 1 of this volume, a supersaturated

TABLE 2.5 Habit Modifiers and Their Effect

Substance	Normal Habit	Habit Modifier	Changed Habit
NH ₄ alum	Octahedra	Borax	Cubes
NH ₄ Cl	Dendrites	Cd ²⁺ , Ni ²⁺	Cubes
		MnCl ₂ + HCl	Granules
NH ₄ H ₂ PO ₄	Needles	Al ³⁺ , Fe ³⁺ , Cr ³⁺	Tapered prisms
NH ₄ NO ₃	Squal crystals	Acid magenta	Needles
(NH ₄) ₂ SO ₄	Prisms	FeCl ₃	Irregular crystals
H ₃ BO ₃	Needles	Gelatin, casein	Flaky crystals
CaCO ₃		Alkylaryl sulphonates	Granular precipitate
CaSO ₄ · 2H ₂ O	Needles	Sodium citrate	Prisms
		Alkylaryl sulphonates	Prisms
MgSO ₄ · 7H ₂ O	Needles	Borax	Prisms
AgNO ₃	Plates	Sodium oleate	Dendrites
K alum	Octahedra	Borax	Cubes
KBr	Cubes	Phenol	Octahedra
KCN	Cubes	Fe ³⁺	Dendrites
KCl	Cubes	Fe(CN) ₆ ⁴⁺	Dendrites
K ₂ SO ₄	Rhombic prisms	FeCl ₃	Irregular crystals
NaBr	Cubes	Fe(CN) ₆ ⁴⁺	Dendrites
NaCN	Cubes	Fe ³⁺	Dendrites
NaCl	Cubes	Fe(CN) ₆ ⁴⁺	Dendrites
		Formamide	Octahedra
		Pb ²⁺ , Cd ²⁺	Large crystals
		Polyvinyl alcohol	Needles
		Na ₆ P ₄ O ₁₃	Octahedra
Na ₂ B ₄ O ₇ · 10H ₂ O	Elongated	NaOH, Na ₂ CO ₃	Squat crystals

(Reproduced with permission from Mullin 1972.)

solution is required for crystallization to occur. A supersaturated solution is not at equilibrium. In order to relieve the supersaturation and move towards equilibrium, the solution crystallizes. Once crystallization starts, however, the supersaturation can be relieved by a combination of nucleation and crystal growth. It is the relation of the degree of nucleation to crystal growth that controls the product crystal size and size distribution, and is, therefore, a crucial aspect of industrial crystallization processes. The analysis of industrial crystallization requires some information on the kinetics of both processes. The fundamentals of nucleation and crystal growth will be discussed in this and the next section. The use of this information in the analysis of crystallizers and their size distribution of the product crystals will be discussed in Chapter 4 of this volume.

Supersaturated solutions exhibit a metastable zone in which nucleation is usually not spontaneous. When the supersaturation is increased, eventually a supersaturation will be reached at which nucleation occurs spontaneously. This is called the *metastable limit*. A precise thermodynamic definition of the metastable limit is the locus of points where $\partial^2 G / \partial x^2 = 0$. This set of points is known as the spinodal curve and marks the boundary between the metastable region (where nucleation and crystal growth are the phase separation mechanisms) and the unstable region (where phase separation is governed by a phenomena known as spinodal decomposition). In liquid solutions it is unlikely that you ever penetrate very far into the metastable region. An effective metastable zone exists for most liquid solutions that is not close to the spinodal curve. This effective metastable zone is often measured in the laboratory and used to define a working zone for industrial crystallization processes. The true metastable zone is much larger. In some melt systems, in polymer-polymer systems, and in metal systems it is possible to approach or even exceed the spinodal concentration, and spinodal decomposition is a possible phase transition mechanism. Knowledge of the width of the metastable zone is important in crystallization because it aids in understanding of nucleation behavior of each system. Unfortunately, the

width of the metastable zone is influenced by the solution history (how it was made and stored), the cooling rate employed, and the impurities present (including dust and dirt). The measurement of effective metastable limits and a tabulation of results for several inorganic species is found in Nývlt et al. (1985).

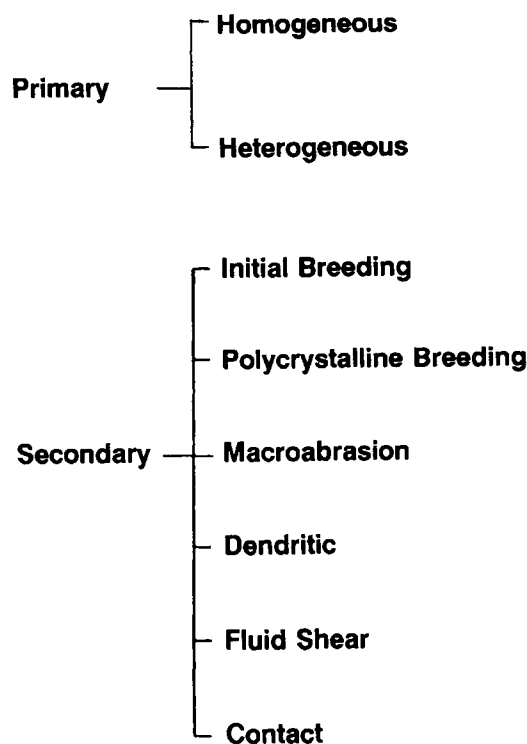


Figure 2.19 Mechanisms of nucleation.

It is desirable to classify the various mechanisms of nucleation as shown in Figure 2.19. Primary nucleation occurs in the absence of crystalline surfaces, whereas secondary nucleation involves the active participation of these surfaces. Homogeneous nucleation rarely occurs in practice, however, it forms the basis of several nucleation theories. Heterogeneous nucleation is usually induced by the presence of dissolved impurities. Secondary nucleation involves the presence of crystals and its interaction with the environment (crystallizer walls, impellers, etc.).

2.2.1. HOMOGENEOUS NUCLEATION

A supersaturated solution is not in equilibrium. In a supersaturated solution at a given temperature the mean concentration of the solution is constant. However, local concentration fluctuations give rise to ordered microregions or clusters.

The classical theory of nucleation (Volmer 1939; Nielsen 1964) assumes that clusters are formed in solution by an addition mechanism

$$\begin{aligned}
 a + a &= a_2 \\
 a_2 + a &= a_3 \\
 a_2 + a &= a_4 \\
 a_2 + a_2 &= a_4 \\
 &\dots\dots\dots \\
 &\dots\dots\dots \\
 a_{c-m} + a_m &= a_c
 \end{aligned} \tag{2.4}$$

that continues until a critical size is reached. The rate of nucleus formation by this mechanism is given by an Arrhenius type of expression

$$B_0 = A \exp\left(-\frac{\Delta G_{cr}}{kT}\right) \tag{2.5}$$

where A is the preexponential factor and has a theoretical value of 10^{30} nuclei/cm³ s.

The thermodynamic considerations for homogeneous nucleation were developed by Gibbs (1928), Volmer (1939), and others. The free energy change for the formation of this new phase is the sum of the free energy change for the formation of the nucleus surface (a positive quantity) and the free energy change for the phase transformation (a negative quantity). Thus,

$$\Delta G = \Delta G_s + \Delta G_v = \beta L^2 \sigma + \alpha L^3 \Delta G_v \tag{2.6}$$

Here, σ is the surface tension, and β and α are the area and volume shape factors (based on the characteristic length L), respectively. For a spherical nuclei, the area factor $\beta = \pi$, and the volume factor is $\alpha = \pi/6$ based on the diameter, d , of the nuclei. The shape factors are defined in Section 2.1.7. [Eqs. (2.2), (2.3)] and the values for various geometric shapes in Table 2.4. For a spherical nuclei, Eq. (2.7) becomes

$$\Delta G = 4\pi r^2 \sigma + \frac{4}{3} \pi r^3 \Delta G_v \tag{2.7}$$

The free energy changes and their sum are shown qualitatively for a spherical nuclei in Figure 2.20. It is clear from the figure that

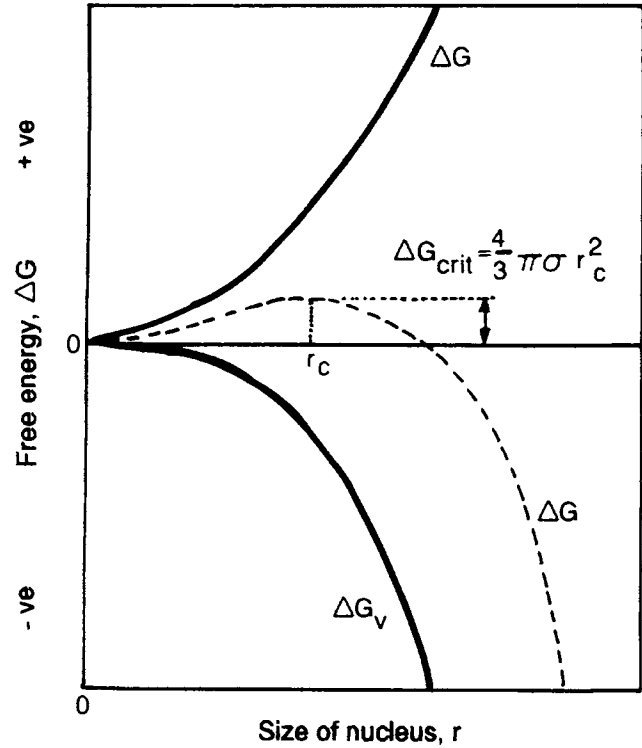


Figure 2.20 Free energy diagram showing free energy versus cluster size. (Reproduced with permission from Mullin 1972.)

clusters greater than the critical size result in a decrease in free energy and will participate in the nucleation process. The critical size can be found by minimizing the free energy function [Eq. (2.7)] with respect to the radius.

$$\frac{d(\Delta G)}{dr} = 8\pi r_c \sigma + 4\pi r_c^2 \Delta G_v = 0 \tag{2.8}$$

or

$$r_c = -\frac{2\sigma}{\Delta G_v} \tag{2.9}$$

Substituting for ΔG_v from Eq. (2.9) in Eq. (2.8) we get

$$\Delta G_{cr} = \frac{4\pi r_c^2 \sigma}{3} \tag{2.10}$$

The growth of the clusters is governed by the Gibbs-Thompson equation

$$\ln \frac{c}{c^*} = \ln S = 2\sigma v / kTr \tag{2.11}$$

where c is the concentration of clusters of size r . Thus, smaller clusters dissolve, whereas larger clusters grow until they reach a critical size r_c , and a new phase is created. Substituting for r_c in Eq. (2.10) from Eq. (2.11) we get

$$\Delta G_{cr} = \frac{16\pi \sigma^3 v^2}{3(kT \ln S)^2} \tag{2.12}$$

TABLE 2.6 Induction Time for Nucleation of Water Vapor

Supersaturation, S	Time
1.0	Infinity
2.0	10^{62} years
3.0	10^3 years
4.0	0.1 seconds
5.0	10^{-13} seconds

The nucleation rate can now be obtained from Eq. (2.5)

$$B_0 = A \exp \left[\frac{-16\pi\sigma^3 v^2}{3k^3 T^3 (\ln S)^2} \right] \quad (2.13)$$

It is clear that the nucleation rate increases with increasing supersaturation and temperature, and decreases with an increase in surface energy. The importance of the level of supersaturation is evident from the calculation of the induction time (Mullin 1960) for the formation of nuclei in supercooled water (Table 2.6). Although water would nucleate spontaneously at any supersaturation exceeding unity given enough time, instantaneous nucleation is possible only at supersaturation levels of around four.

The rate equation predicts exponential growth once a critical supersaturation is attained, however, in practice, an optimal temperature exists below which the liquid is too viscous to nucleate and above which molecular motions prevent crystal formation. This was observed by Tamman (1925) for several organic salts. He found that the optimal nucleation temperature was lower than that required for maximal crystal growth. A similar observation was made by Mullin and Leci (1969) for the spontaneous nucleation of citric acid solutions and is shown in Figure 2.21. The viscous effects can be incorporated into the rate equation by taking into account the viscous free energy (Turnbull and Fisher 1949).

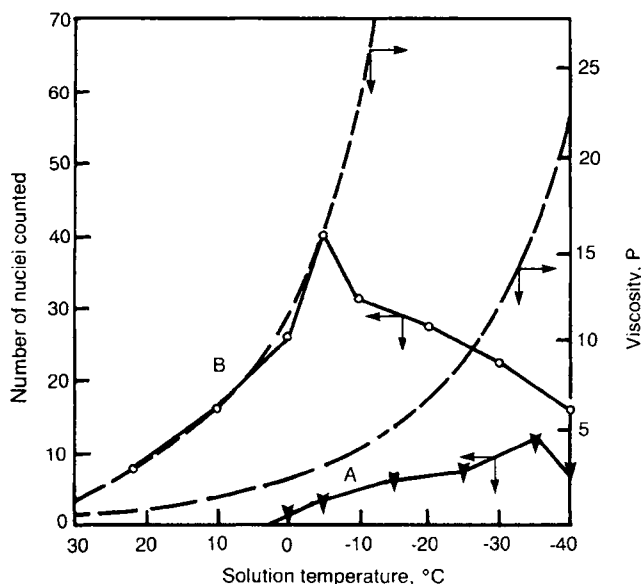


Figure 2.21 Spontaneous nucleation in supercooled citric acid solution: (A) 4.6 kg of citric acid monohydrate/kg of "free" water (temperature = 62°C) and (B) 7.0 kg/kg (temperature = 85°C). (Reproduced with permission from Nývlt 1968.)

$$B_0 = A \exp \left[-\frac{16\pi\sigma^3 v^2}{3k^3 T^3 (\ln S)^2} + \frac{\Delta G_{visc}}{kT} \right] \quad (2.14)$$

At higher supersaturation values, the first term becomes smaller, whereas the viscous energy term, ΔG_{visc} , becomes larger. Thus, the nucleation rates decline after a critical supercooling has been attained.

Homogeneous nucleation is difficult to observe in practice due to the presence of dissolved impurities and physical features such as crystallizer walls, stirrers, and baffles. Homogeneous nucleation has been studied in several inorganic systems (KNO_3 , NH_4Br , NH_4Cl) (White and Frost 1959; Melia and Moffit 1964a, 1964b) using the dispersed phase method proposed by Vonnegut (1948). All predict a preexponential factor of 10^3 – 10^5 , which is much lower than the theoretical value of 10^{30} . However, in a highly supersaturated NaCl precipitation system, a value close to the theoretical was found by using a crystalloluminescence technique (Garsten and Head 1966).

2.2.2. HETEROGENEOUS NUCLEATION

A foreign substance present in a supersaturated solution is generally known to reduce the energy required for nucleation. Nucleation in a heterogeneous system generally occurs at a lower supersaturation than a homogeneous system—the free energy barrier is lower in the case of a heterogeneous system. Volmer (1939) found that the decrease in free energy depended on the contact (or wetting) angle of the solid phase

$$\Delta G_{hom} = \phi \Delta G_{het} \quad (2.15)$$

$$\phi = \frac{1}{4} (2 + \cos \theta) (1 - \cos \theta)^2 \quad (2.16)$$

Thus, a lower supersaturation is necessary for nucleation in a heterogeneous system. Energy considerations show that spontaneous nucleation would occur for a system with zero contact angle, however, no such systems exist in practice. Partial attraction is possible in a case where the foreign substance and the crystal have almost identical atomic arrangement (see Section 2.1.5. on isomorphism). It was shown (Preckshot and Brown 1952) that the energy for nucleus formation was reduced only if the difference in isomorphism between the crystal and the foreign particle was <15%. For differences >15%, the energy requirements were similar to that for a homogeneous system. The contact angle factor ϕ is given in Table 2.7. A review of experimental work on heterogeneous nucleation is given by Turnbull and Vonnegut (1952).

2.2.3. SECONDARY NUCLEATION

Secondary nucleation results from the presence of crystals in the supersaturated solution. These parent crystals have a catalyzing effect on the nucleation phenomena, and thus, nucleation occurs at a lower supersaturation than needed for spontaneous nucleation. Although several investigations of secondary nucleation exist, the mechanisms and kinetics are poorly understood.

Several theories have been proposed to explain secondary nucleation. These theories fall into two categories—one traces the origin of the secondary nuclei to the parent crystal—that include: (1) initial or dust breeding; (2) needle breeding; and (3) collision breeding. Secondary nuclei can also originate from the solute in the liquid phase and the theories that take this into account include: (1) impurity concentration gradient nucleation and (2) nucleation due to fluid shear.

TABLE 2.7 Surface Tension Factor for Heterogeneous Nucleation

θ	ϕ
0	0
5	1.80×10^{-5}
10	1.72×10^{-4}
30	1.29×10^{-2}
45	5.81×10^{-2}
60	1.56×10^{-1}
90	0.50
120	0.84
180	1.0

(Reproduced with permission from Nývlt et al. 1985.)

In *initial breeding* or *dust breeding*, secondary nuclei originate from the seed crystals. Tiny crystallites are formed on the crystal surface during the growth of seed crystals or due to fragmentation during storage. When introduced into the solution, the crystallites act as nucleation sites (Ting and McCabe 1934; Strickland-Constable and Mason 1963). These crystallites are larger than the critical nucleus size and, as a result, the rate of nucleation is independent of the supersaturation of the solution or the stirring rate. This mechanism is important only in batch crystallization; however, it is important to minimize this effect by retreating the seed crystals with a solvent.

At high levels of supersaturation, needle-like or dendritic crystals are formed. These crystals fragment in the solution and serve as nucleation sites. This phenomena is referred to as *needle breeding*. At still higher supersaturations, irregular polycrystalline aggregates are formed. Fragmentation of the polycrystals can serve as nucleation centers. This process is called *polycrystalline breeding*. Nucleation by this mechanism is not considered very likely in industrial crystallization.

At high stirring speeds, macroabrasion of crystals results in fragments that serve as nucleation sites. As opposed to contact nucleation, which involves microabrasion of the crystals, this phenomenon results in the rounding of edges and corners of crystals. This process is referred to as *collision* or *attrition breeding*. The rate of nucleation by this mechanism is a function of the crystal hardness, the concentration of the suspension, and the retention time. Although important from an industrial point of view, this mechanism can be obscured by other mechanisms of secondary nucleation. *Contact nucleation* is probably the most important source of secondary nuclei in the crystallizer. Three types of contact can be envisioned in a crystallizer-crystal-crystal, crystal-stirrer, and crystal-crystallizer wall. Secondary nuclei are generated either by microabrasion or from the adsorbed layer of the solute that has not yet crystallized.

The *impurity concentration gradient theory* assumes that the solution is more structured in the presence of a crystal. This increases the local supersaturation of the fluid near the crystal, which is the source of crystal nuclei. Changes in the structure of the solution near the crystal surface have been observed experimentally. Dissolved impurities in the solution are known to inhibit nucleation rates. Some of the impurities are incorporated into the crystal surface. Thus, a concentration gradient is formed that enhances the probability of nucleation. Experimental evidence of the theory was presented for the nucleation of potassium chloride in the presence of lead impurities. As expected, stirring the solution causes the impurity concentration gradient to disappear and hence, lower the nucleation rates (Denk 1970).

Powers (1963) proposed *fluid shear* as a mechanism for the generation of secondary nuclei. At high supersaturation, dendritic growth occurs at the crystal surface. These crystals break, either due to the shearing flow around it (Cooke 1966; Strickland-Constable 1968) or due to a dendrite coarsening mechanism (Denk 1970; Denk and Botsaris 1971) and are the source of crystal nuclei. Another possibility assumes the boundary layer between the crystal and the solution to be the source of crystal nuclei. The solute and the solution near it are thought to be in a loosely ordered phase near the crystal surface. The shearing action of the fluid is sufficient to remove a layer of the adsorbed molecules into the solution where they grow into crystals.

Origin of Secondary Nuclei. The various theories proposed in the previous section for secondary nucleation show that secondary nuclei originate either from the seed crystal or from the boundary layer near the growing crystal.

It is generally very difficult to determine the origin of the secondary nuclei experimentally. The presence of an adsorbed layer as a source of secondary nuclei was initially proposed by Powers (1963). Several investigators (Clontz and McCabe 1971; Strickland-Constable 1972) verified this hypothesis by sliding a crystal along a solid surface, and observing the nucleation and crystallization behavior. It was found that a growing crystal was necessary for the generation of nuclei and that the nucleation rate was a function of the contact energy and degree of supersaturation.

Denk and Botsaris (1972a) devised a clever experiment in which the optical activity of the sodium chlorate crystal was used to determine the origin of the nuclei. The crystals were grown from aqueous solutions in the presence of seed crystals with and without the presence of impurities. The results for crystals grown from pure stagnant solutions are shown in Figure 2.22. If the solid phase was the source of the secondary nuclei, the resulting crystals would have the same form as the parent crystal. If the secondary nuclei originated in the liquid or transition phase, then the ratio of optically different nuclei should be similar to the ratio obtained during spontaneous nucleation. From the Figure 2.22, the change in the source of nuclei is observed around a supercooling of 3 °C. At higher supersaturations, the ratio approached to that of spontaneous nucleation. In the presence of impurity (12 ppm borax), the crystals obtained for various supersaturations showed a similar trend but the curve shifted to the right as expected. It was concluded that no single mechanism could explain secondary nucleation. The possible sources are from: (1) the parent crystals (needle breeding); (2) the boundary layer near the growing crystal (impurity concentration gradient); and (3) the solution due to reordering of water molecules near the crystal leading to local supersaturation.

Garside et al. (1979) developed an experiment in which a crystal could be contacted with a fixed energy. Their data displayed in Figure 2.23 show that the crystal size distribution (CSD) in a potassium-alum system was a function of the supersaturation of the solution. Larson and Bendig (1976) used a similar apparatus to show the dependence of nucleation on contact frequency. They found that the adsorbed layer requires time for regeneration. This regeneration time can be of the order of a few seconds and decreases with increasing undercooling or supersaturation. It was found that the nucleation rates decline by several orders of magnitude if proper regeneration times cannot be met.

Factors Affecting Secondary Nucleation. The rate of secondary nucleation is governed by three processes: (1) the generation of secondary nuclei on or near a solid phase; (2) removal of the clusters; and (3) growth to form a new solid phase. Several factors

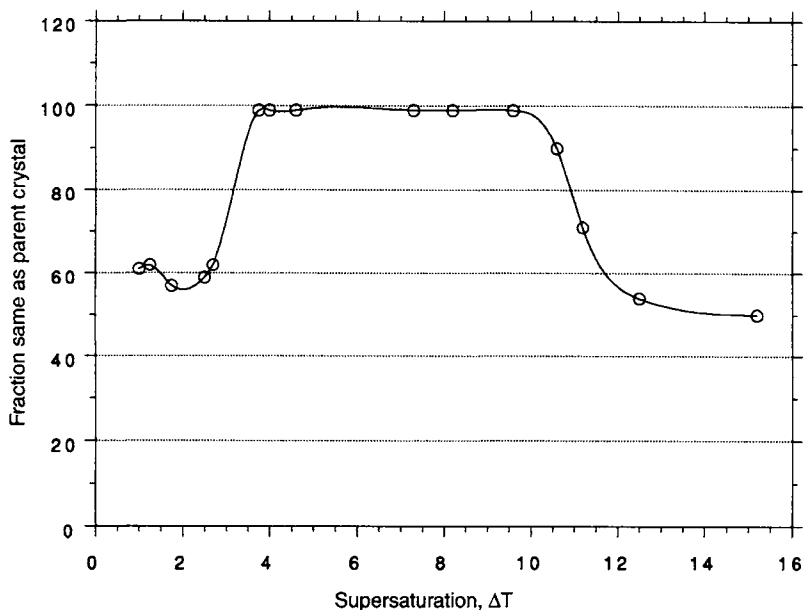


Figure 2.22 Differentiation of the secondary nucleation mechanisms using enantiomorphous crystals. The fraction of the crystals with the same modification as that of the parent crystal is denoted as percent. (Reproduced with permission from Denk and Botsaris 1972a.)

influence these processes: the supersaturation, the rate of cooling, the degree of agitation, and the presence of impurities.

The degree of supersaturation is the critical parameter controlling the rate of nucleation. The effect of supersaturation on the nucleation rate is threefold. At higher supersaturation, the absorbed layer is thicker and results in a large number of nuclei. The size of the critical nucleus decreases with increasing supersaturation. Thus, the probability of the nuclei surviving to form crystals is higher. As the supersaturation is increased, the micro-roughness of the crystal surface also increases, resulting in a larger nuclei population.

These effects have been verified by several researchers (Garabedian and Strickland-Constable 1972a, 1972b; Youngquist and Randolph 1972); in general, nucleation rates are enhanced with increasing supersaturation. However, the nucleation exponent is found to be lower than that for primary nucleation (Nývlt 1981).

The role of temperature in the production of secondary nuclei is not fully understood. For several systems, the nucleation rate declined with increasing temperature for a given supersaturation. This was attributed to the faster rate of incorporation of the absorbed layer on to the crystal surface at higher temperatures. Since the thickness of the absorbed layer was reduced, the nucleation rates also declined with increasing temperatures. A few contradictory results exist—Genck and Larson (1972) found a decrease in nucleation rate with increasing temperature for a potassium nitrate system and increasing rates with increasing temperature for a potassium chloride system. It was shown by Nývlt (1981) and others that the nucleation order is not sensitive to temperature variations.

Stirring the solution leads to a thinning of the absorbed layer and hence should lead to lower nucleation rates. However, Sikdar and Randolph (1976) found that the nucleation rate increased with the degree of agitation for smaller crystals of magnesium sulfate (8–10 μm)—the nucleation rates were independent of the degree of agitation for larger crystals. The results of Melia and Moffit

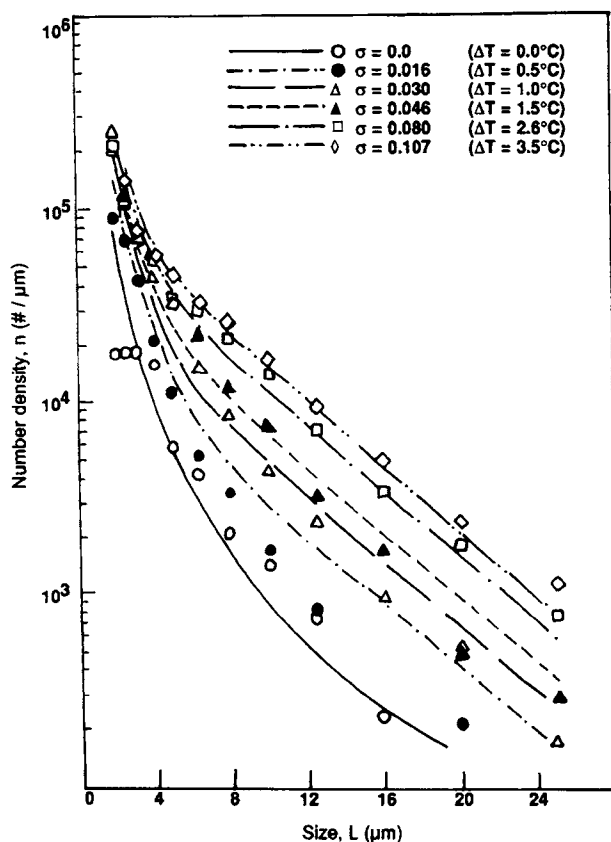


Figure 2.23 Nuclei size distribution from contact nucleation. [From J. Garside, I.T. Rusli, and M.A. Larson (1979), "Origin and Size Distribution of Secondary Nuclei," *AIChE J.* 25(1), pp. 57–64. Used by permission of the American Institute of Chemical Engineers. © 1979 AIChE.]

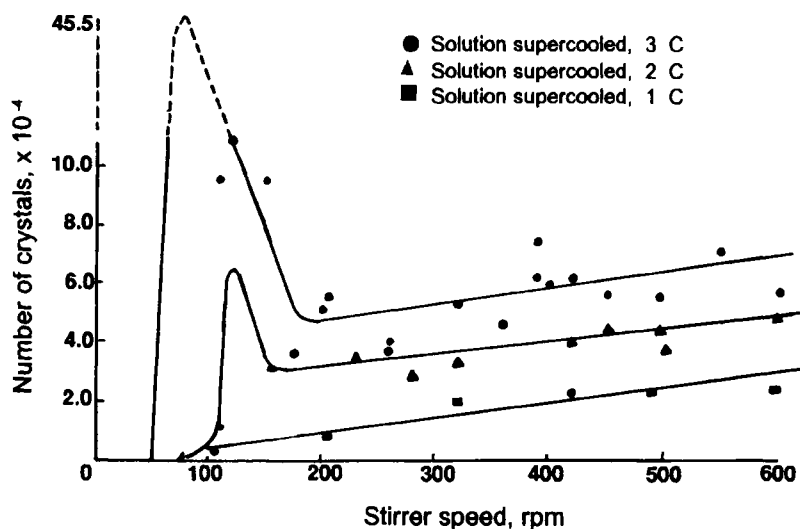


Figure 2.24 Dependence of number of secondary nuclei produced on stirrer speed and supercooling in secondary nucleation of potassium chloride. [Reprinted with permission from T.P. Melia and W.P. Moffitt (1964a), "Secondary Nucleations from Aqueous Solutions," *Ind. Eng. Chem. Fund.* 3, p. 323. © 1964 American Chemical Society.]

(1964a, 1964b) on the secondary nucleation of potassium chloride are shown in Figure 2.24. They found that the nucleation rate increases with supersaturation, and the degree of supercooling and agitation.

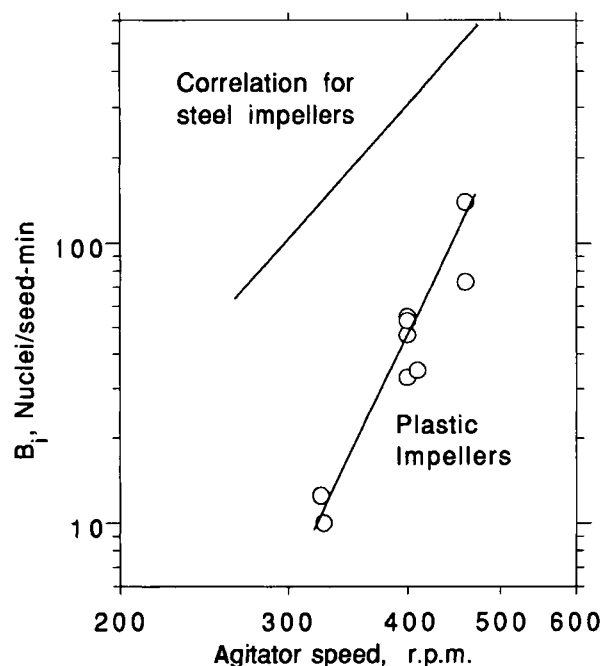


Figure 2.25 Effect of agitator speed on secondary nucleation rate for steel and plastic impellers. [From J.N. Ness and E.T. White (1976), "Collision Nucleation in an Agitated Crystallizer," *AIChE Symposium Series* 72 (153), pp. 64-73. Used by permission of the American Institute of Chemical Engineers. © 1976 AIChE.]

The effect of hardness of the contact material and the crystal hardness on the generation of secondary nuclei has been investigated by several researchers. In general, it was found that a harder material is more effective in enhancing the nucleation rates. For example, it was found that a polyethylene stirrer reduced the nucleation rates by a factor of 4-10, depending on the agitation (Figure 2.25). In situ experiments have indicated that microattrition may be an important source of nuclei in this case. Crystal hardness also affects nucleation behavior—a hard, smooth crystal is less effective. Irregular crystals with some roughness are generally more active.

It is well known that a small amount of impurity can profoundly affect the nucleation rate, however, it is impossible to predict the effect prior. The presence of additives can either enhance or inhibit the solubility of a substance. Enhanced solubilities would lead to lower supersaturations and lower growth rates. If it is postulated that the impurity adsorbs on the crystal surface, then two opposing effects come into play—the presence of an additive would lower the surface tension and lead to higher growth rates, however, the impurity adsorption blocks potential growth sites and lowers nucleation rates. Thus, the effect of impurities is complex and unpredictable.

Several experimental investigations have been undertaken to clarify the situation. For example, it was shown that Pb^{+2} acts as a nucleation agent in a NaCl system, whereas Co^{+2} inhibits nucleation in a KNO_3 solution. The effect of the presence of chromium ions on the crystallization of magnesium sulfate is shown in Figure 2.26 (Khambaty and Larson 1978). Their data show a decrease in both the nucleation and growth rate in increasing chromium concentration. Although it is difficult to generalize, certain trends can be observed from the experimental evidence. The inhibiting effect appears to increase with increasing charge of the cation, e.g., $\text{Cr}^{+3} > \text{Fe}^3 > \text{Ni}^{+2} > \text{Na}^{+1}$. The inhibiting effect also appears to decline above a certain critical impurity concentration. This can be seen in the behavior of the nucleation exponent, which is unaffected at low contaminant concentration (ppm) but changes erratically at higher concentrations (Broul 1978).

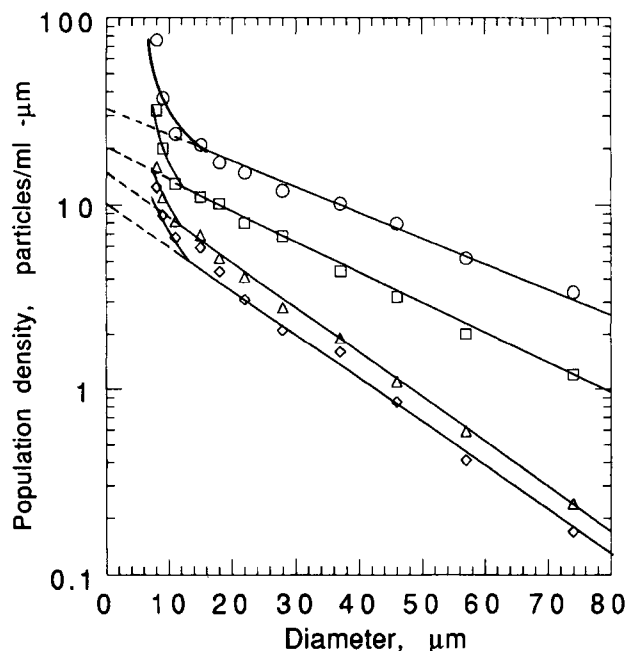


Figure 2.26 Effect of Cr^{3+} on $\text{MgSO}_4 \cdot 7\text{H}_2\text{O}$ crystallization. Chromium ion concentration $\bigcirc = 3$ ppm $\square = 8$ ppm; $\triangle = 15$ ppm; and $\diamond = 130$ ppm. [Reprinted with permission from S. Khambaty and M.A. Larson (1978), "Crystal Regeneration and Growth of Small Crystals in Contact Nucleation," *Ind. Eng. Chem. Fund.* 17, p. 160. © 1978 American Chemical Society.]

Larger seed crystals yield more secondary nuclei. Smaller crystals generally follow the path of the liquid and have a smaller probability of coming in contact with the stirrer or walls to generate secondary nuclei. The effect of several external factors such as electric and magnetic fields, x-rays, ultraviolet light, and other radiations on nucleation have been studied. The findings are summarized by Tipson (1950) and Khamskii (1969).

2.2.4. NUCLEATION KINETICS

Secondary nucleation is a complex phenomena and is not well understood. A general theory for the prediction of nucleation rates does not exist. Several correlations based on the power law model have been found to explain most of the experimental data satisfactorily. The power law (from the Becker-Doering relationship) is given by

$$B = k_N \Delta C^n \quad (2.17)$$

The nucleation rate, B , is normally given in units of $\text{no.}/\text{m}^3 \cdot \text{s}$. This form is valid if the adsorption layer mechanism described before is the source of nuclei. The nucleation rate in this case is independent of the suspension concentration.

In the industrial crystallizer, most of the nuclei are generated by contact with the crystallizer environment. The nucleation rate in this case is a function of the degree of agitation, the suspension density, and the supersaturation.

$$B = k'_N W^i M_T^j (\Delta C^n) \quad (2.18)$$

where W is the agitation rate (usually in rpm or impeller tip speed), and M_T is the suspension density (mass of crystals per volume of solution). It is important to remember that the constants k_N and k'_N have different units interchangeably. When Eq. (2.17) is used in a situation in which secondary nucleation is important, the constant k_N will actually vary with the conditions in the crystallizer (suspension density and agitation rate). In some situations an equation that does not include the effect of agitation is used

$$B = k''_N M_T^j \Delta C^n \quad (2.19)$$

In this case, k''_N may vary with the agitation rate.

Correlations are available for nucleation in flow situations. For a potassium-aluminum sulfate system, it was found that the nucleation rate was given by Toyokura et al. (1976), for a fluidized bed,

$$B = 10(\Delta C)^{3.3} Re^{2.5} \quad (2.20)$$

for a fixed bed,

$$B = 0.85(\Delta C)^{3.3} Re^{2.5} \quad (2.21)$$

where Re is the Reynolds number based on the crystal size. Several other correlations can be found in literature (Nývlt et al. 1985).

The kinetics for secondary nucleation can be measured either by measuring the width of the metastable zone, the induction time, or by counting the number of nuclei formed. One of the methods for the determination of nucleation rates is by measuring the maximum possible supercooling that can be obtained in a saturated solution when it is cooled at different rates (*metastable zone width measurement*). The polythermal experiment (proposed by Nývlt 1968) is carried out in a jacketed crystallizer cooled by a circulating water/ethylene-glycol bath accurate to $\pm 0.1^\circ\text{C}$. The temperature can be increased or decreased at a constant rate by a programmed controller. The crystallizer is fitted with an accurate thermometer $\pm 0.1^\circ\text{C}$ to read the solution temperatures. A schematic of the apparatus is shown in Figure 2.27.

Approximately 200 ml of saturated solution is placed in a crystallizer and allowed to equilibrate thermally. The solution is stirred at a constant rate and cooled slowly until a number of small crystals are formed. The temperature of the solution is then raised at a very slow rate until the last crystal disappears. This temperature is denoted as the saturation temperature, T_s . The solution is

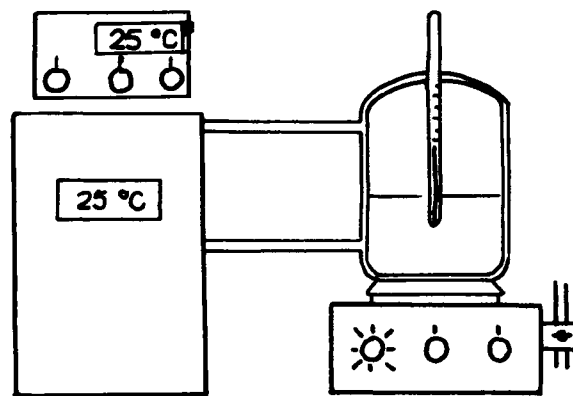


Figure 2.27 Schematic diagram of apparatus for measurement of nucleation rates.

then heated to a temperature 1° above T_s and maintained for 30 min. The solution is now cooled at a constant rate (r_1) and the temperature at which the first crystal appears is noted (T_1). The difference between this temperature and the saturation temperature is denoted as ΔT_{1max} for the cooling rate r_1 . The experiment is repeated for two different cooling rates. The measurements can also be carried out in the presence of solid phases where two to four large crystals are added to the system and the maximum supercooling is observed in a similar fashion.

The nucleation rate at the metastable limit can be approximated as

$$B = \left(\frac{dC^*}{dT} \right) r_1 \quad (2.22)$$

The maximum supersaturation is given by

$$\Delta C = \left(\frac{dC^*}{dT} \right) \Delta T_{max} \quad (2.23)$$

Combining Eqs. (2.22), (2.23), and (2.17), simplifying, and taking logarithms, yields

$$\log(-r_1) = \log k_N m \log(\Delta T_{max}) + (m-1) \log \frac{dC}{dT} \quad (2.24)$$

where m is used in place of n to signify an apparent nucleation order.

Thus, a plot of the cooling rate and the maximum possible supercooling will give the apparent order m and the rate constant k_N . If the nuclei are visible immediately after they are formed, the true order (n) and the apparent order (m) are identical. In all other cases, the true nucleation order can be found by knowing the exponent for crystal growth (g). The relationship is given by

$$n = 4m - 3g - 4 \quad (2.25)$$

The dependence of the cooling rate on the maximum attainable supercooling for a sodium chromate system (Nývlt 1968) is shown in Figure 2.28. The presence of solid phase (filled circles) decreases the maximum supercooling but the exponent remains the same. A nomograph for the estimation of the apparent nucleation order is given in Figure 2.29. The example shows that for a supercooling

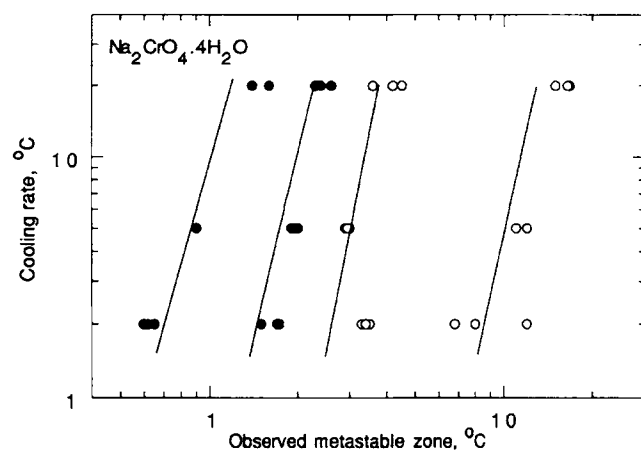


Figure 2.28 The dependence of cooling rate on the maximum attainable supercooling in aqueous sodium chromate solutions. (Reproduced with permission from Nývlt 1968.)

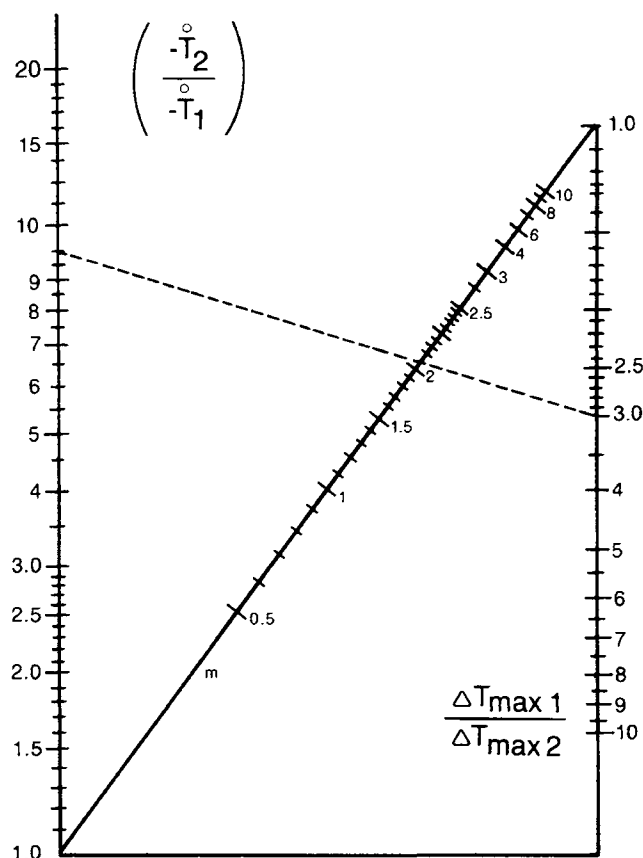


Figure 2.29 Nomograph for the estimation of the apparent nucleation order. The ratio of the cooling rates and the observed widths of the metastable zone are denoted as points on the left and right axes, respectively. The apparent nucleation order is given by the value at which the straight line joining those points intersects the diagonal. (Reproduced with permission from Nývlt et al. 1985.)

ratio of 3 and a cooling rate ratio of 9.5, the apparent order of nucleation is 2.07.

The rate of nucleation can also be determined by observing the time elapsed between the creation of supersaturation and the formation of a new phase. This time interval is defined as the *induction time* and is a function of the solution temperature and supersaturation. The formation of a new phase can be detected in several different ways—for example, by the appearance of crystals or by changes in properties (turbidity, refractive index) of the solution.

The induction time, t_{ind} , is the sum of the time needed for reaching steady-state nucleation, t_{tr} ; the nucleation time, t_n ; and the time required for the critical nucleus to grow to a detectable size, t_g . Thus,

$$t_{ind} = t_{tr} + t_n + t_g \quad (2.26)$$

It can be shown (Sohnel and Mullin 1988) that the transient period is unimportant in aqueous solutions of moderate supersaturations and viscosities. In certain special cases however, at very low supersaturations the transient period cannot be ignored (Packter 1974) and the following analysis is not applicable. Recently, Kubota et al. (1986) has suggested a method to take into account the transient period.

If the transient period can be ignored, the induction time is a function of the nucleation and growth times. Three cases emerge:

1. $t_n \gg t_g$.
2. $t_n \sim t_g$.
3. $t_n \ll t_g$.

If the nucleation time is much greater than the growth time, the induction time is inversely proportional to the steady-state nucleation rate and

$$t_{ind} = A \exp \left[\frac{F\sigma^3 V^2 \phi}{(kT)^3 \ln^2 S} \right] \quad (2.27)$$

where ϕ is the wetting angle that is 1 for homogeneous nucleation and is <1 for heterogeneous nucleation [see Eq. (2.15)], and F is the shape factor ratio (see Table 2.4).

If the nucleation and growth times are of the same order of magnitude, the induction time for nucleation followed by diffusion growth is given by (Nielsen 1969)

$$t_{ind} = \frac{v^{2/3}}{2D_s x^{1/5}} \exp \left[\frac{2Fv^2 \sigma^3}{5(kT)^3 \ln^2 S} \right] \quad (2.28)$$

where x is the solute mole fraction.

The induction time for nucleation followed by polynuclear growth is given by Sohnel and Mullin (1988). If the nucleation time is much smaller than the growth time, the induction times for various cases are given by Sohnel and Mullin (1988). For mononuclear growth, the induction time in this case is given by

$$t_{ind} = \frac{d^3}{6D_s r_c} \exp \left[\frac{F\sigma^2 v^{4/3}}{(kT)^2 \ln^2 S} \right] \quad (2.29)$$

where D_s is the surface diffusion coefficient and r_c is the critical radius of the nuclei.

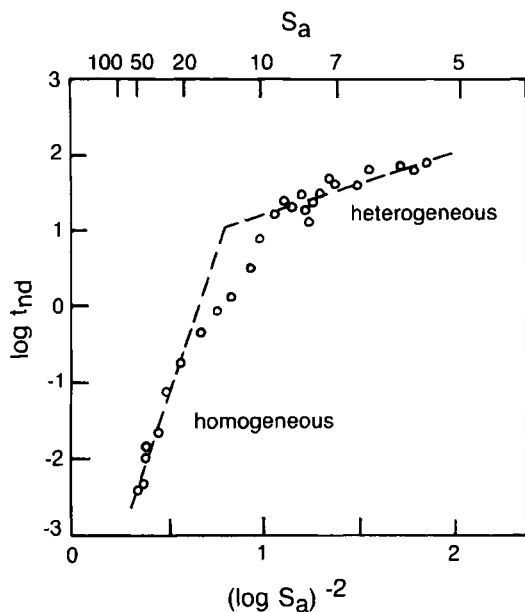


Figure 2.30 Induction period as a function of supersaturation for CaCO_3 precipitation at 25°C showing regions of homogeneous and heterogeneous nucleation. (Reproduced with permission from Sohnel and Mullin 1988.)

In general, the induction time is given by the expression

$$t_{ind} = K S_0^{-n} \quad (2.30)$$

However, Eqs. (2.26–2.29) are helpful in determining the mechanism of nucleation and growth over a wide range of supersaturations. For example, the validity of Eq. (2.27) has been verified for a number of systems from sparingly soluble, e.g., BaSO_4 , BaCrO_4 , and SrSO_4 (Nielsen 1969; Nielsen and Sohnel 1971) to readily soluble potassium and potassium aluminum phosphates (Joshi and Anthony 1979). A plot of $\log(t_{ind})$ versus $(\log S)^{-2}$ at a constant temperature is shown for CaCO_3 in Figure 2.30. From Figure 2.30 it is clear that at low supersaturations the nucleation is heterogeneous [$f(\theta) < 1$], whereas homogeneous nucleation occurs at higher supersaturations.

It is difficult to distinguish between the mechanisms proposed by Eqs. (2.27) and (2.28) by constant temperature experiments. However, experiments at different temperatures can be done to differentiate between the two mechanisms (Mullin and Osman 1973) since the surface tension, σ , is temperature dependent. Further experimental evidence can be found in Sohnel and Mullin (1988).

Nucleation kinetics are often obtained from continuous experiments employing a mixed suspension, mixed product removal (MSMPR) crystallizer and the concepts of the population balances. This technique is also used to obtain crystal growth kinetics. The details of the population balance and its uses will be discussed in Chapter 4 of this volume. A review of methods to estimate nucleation kinetics from batch and continuous experiments can be found in Tavare (1995).

In this section we have described two methods to determine the kinetics governing the nucleation process. The first method, which utilizes the width of the metastable zone, is easy to use and gives an apparent order of nucleation. The second method uses the induction time to predict the mechanism and order of nucleation processes. A third method, which employs population balance techniques and an MSMPR crystallizer, will be described in Chapter 4 of this volume.

2.2.5. APPLICATION TO INDUSTRIAL CRYSTALLIZERS

Secondary nucleation is a complex phenomena and due to the various competing mechanisms present it is difficult to predict the nucleation rates. However, general recommendations can be made to control nucleation rates and hence, the final crystal size distribution. The possible sources of secondary nuclei in an industrial crystallizer are given in Table 2.8 along with suggestions for preventing excessive nucleation (Jančić and Grootsohlten 1983).

In the industrial crystallizer, primary homogeneous nucleation is not possible due to the low levels of supersaturation employed and the presence of impurities. Primary heterogeneous nucleation is possible at places where high supersaturation is being created—for example, in heat transfer equipment. This could lead to crystal deposits on these surfaces. Undesirable nucleation can be reduced by choosing proper production rates and by allowing adequate mixing.

Secondary nucleation is the main source of crystal nuclei in an industrial crystallizer. Nuclei due to initial breeding are possible during the start-up period. Coating of seed crystals can reduce the nucleation rate due to this mechanism. Needle breeding occurs at high supersaturations and is not significant in industrial situations. Contact nucleation is the most important source of secondary nuclei. Collisions with stirrers, pumps, impellers, and crystallizer walls lead to fragmentation and generation of secondary nucleation sites. Small clearances between equipment can also lead to breakage of crystals via crystal contact. Nucleation by this

TABLE 2.8 Sources of Nuclei in Industrial Crystallization

Source of Nuclei	Type of Nucleation Process	Prevention or Remedy
Boiling zone	Primary	Reduce specific production rates, increase crystal surface area
Hot feed inlet	Primary	Enhance heat dissipation, reduce degree of superheating, carefully chosen inlet position
Inlet of direct coolant	Primary	Enhance heat dissipation, reduce temperature of coolant chosen inlet position
Heat exchangers, chillers, etc.	Primary	Reduce temperature gradients by increasing surface area, increase liquid velocities
Reaction zone	Primary	Enhance mixing and dissipation of supersaturation, increase crystal surface area
Cavitating moving parts	Primary	Adjust tip speed, suppress boiling by sufficient static head
Crystal/crystallizer contacts	Secondary	Adjust tip speed and design configuration, coat impellers with soft materials, reduce if possible magma density and mean crystal size
Collisions with moving parts (impellers, pumps etc.)		
Collisions with crystallizer walls		
Crystal/crystal contacts	Secondary, attrition	Carefully specify all clearances and hydrodynamics of two-phase flow therein
Crystal grinding in small clearance spaces (impeller/draft tube, pump stator/rotor)	breakage	
Crystal/solution interaction	Primary or secondary	Reduce jetting, get to know the effect of impurities for each particular system, prevent incrustation
Fluid shear, effect of impurities, etc.		

(Data adapted from Jančić and Grootscholten 1983.)

mechanism can be controlled by varying the frequency and energy of contact. Padded impellers and nylon or Teflon stirrers are known to reduce the nucleation rate. Allowing for adequate clearances and optimizing fluid flow conditions can also lead to lower nucleation rates.

2.3. CRYSTAL GROWTH

As we have seen in the previous section, the “birth of a new crystal,” which we have called *nucleation*, refers to the beginning of the phase separation process. The solute molecules have formed the smallest sized particles possible under the conditions present. The next stage of the crystallization process is for these nuclei to grow larger by the addition of solute molecules from the supersaturated solution. This part of the crystallization process is known as *crystal growth*.

Crystal growth, along with nucleation, controls the final particle size distribution obtained in the system. In addition, the conditions and rate of crystal growth have a significant impact on the product purity and the crystal habit. An understanding of crystal growth theory and experimental techniques for examining crystal growth from solution are important and very useful in the development of industrial crystallization processes.

2.3.1. BASIC CONCEPTS

The growth rate of a crystal can be described in a number of different ways that are often used interchangeably in the literature. It is important to understand the definition of each of these terms and their relation to each other.

The growth of a crystal is often described by the change in some dimension of the crystal with time. This is called the *linear growth rate* and has dimensions of length per unit time. It is not enough, however, to indicate that you are interested in a linear growth rate because this can mean a number of different things. As we have seen in the previous sections, crystals are made up of a

number of faces that can grow at different rates. A fundamental expression of the growth rate, therefore, is the linear growth rate of a particular face. This refers to the rate of growth of the face in the direction normal to the face.

While face growth rates are of interest in studies of the fundamentals of crystal growth, they are not normally used to describe the overall growth of a crystal. When a linear growth rate is used to describe the growth of an entire crystal it is describing the increase in some characteristic dimension of the crystal. If the crystal was a sphere, the characteristic dimension would be the diameter and we would express the crystal growth rate by the increase of the diameter with time. If the crystal is of another shape, the characteristic dimension used is usually the second longest dimension. This can be understood by thinking of what happens when you pass crystals through screens or sieves. The dimension of the crystal, which determines if it will pass through a sieve of a given size, is the second largest dimension rather than the largest dimension. This characteristic dimension can be related to the volume and surface area of the crystal through the shape factor.

Another way of measuring crystal growth rates is through the measurement of the mass change of the crystal. The increase in mass with time is often used and can be directly related to the overall linear growth velocity through the relation

$$R_G = \frac{1}{A} \frac{dm}{dt} = 3 \frac{\alpha}{\beta} \rho G = 3 \frac{\alpha}{\beta} \rho \frac{dL}{dt} \quad (2.31)$$

where

R_G = increase of mass per unit time per unit surface area

A = surface area of the crystal

α, β = volume and area shape features, respectively

ρ = crystal density

L = characteristic dimension

As we can see from Eq. (2.31), the surface and volume shape factors must be known or estimated to allow linear growth rates

to be calculated from mass growth rates. It is quite common for investigators to assume a sphere and thus calculate growth rates based on an equivalent spherical geometry. This can be a reasonable estimate or can be quite poor, depending on the crystal's actual shape.

2.3.2. THEORIES OF CRYSTAL GROWTH

Crystals and their growth and habit have long been of interest to scientists. Much early work on crystal growth centered on explaining the difference in observed crystal habits from an equilibrium or thermodynamic point of view. Of more interest to practitioners of industrial crystallization are theories that deal with the kinetics (rate) of crystal growth. Reviews of crystal growth theories can be found in the work of Ohara and Reid (1973), Strickland-Constable (1968), and Nývlt et al. (1985). Many of the theories are mathematically rather complex, however, there are certain features of these theories that are worth reviewing and are quite helpful in understanding the nature of the crystal growth process.

When discussing crystal growth it is necessary to focus on a single face or plane and examine the growth of that face. The *linear growth velocity* of a face is usually defined as the rate of growth of a face in the direction normal to the face. Crystals are thought to grow in a layer-by-layer fashion. This can be understood by looking at Figure 2.31. A molecule in solution must desolvate and absorb on the crystal surface. Looking at Figure 2.31 we can see three possible sites for the molecule to incorporate into the crystal surface. The sites A, B, and C can be distinguished by the number of bonds the molecule will form with the crystal. At site A, the molecule will be attached only to the surface of a growing layer while at site B, the molecule is attached to both the surface and to a growing step. At site C, the molecule is attached at three surfaces at what is known as a *kink site*. From an energetic point of view, C is more favorable than B, and B more favorable than A. This can be generalized by saying that molecules tend to bond at locations where they have the maximum number of nearest neighbors. These are the most energetically favorable sites. The general mechanism for incorporation of a molecule into a crystal face is its adsorption onto the surface followed by its diffusion along the surface to a step (B-type) or kink (C-type) site for incorporation. From this explanation you can see why crystals grow in a layer-by-layer fashion since it is easier for molecules to bond to an existing step that is spreading over a surface than to form a new one. The linear growth rate (G) of a face can, therefore, be written in terms of the step velocity (V_∞), the step height (h), and the step spacing (y_0)

$$G = V_\infty h / y_0 \quad (2.32)$$

Eq. (2.32) provides a simple illustration of the growth of a face, however, it does not help us with two fundamental questions.

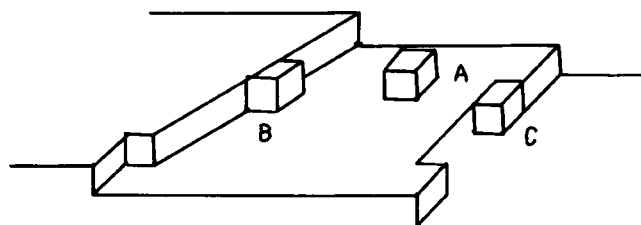


Figure 2.31 Surface structure of a growing crystal. (From M. Ohara and R.C. Reid, *Modeling Crystal Growth Rates from Solution*, © 1973, p. 3. Reprinted by permission of Prentice-Hall, Englewood Cliffs, New Jersey.)

Where do the steps come from and what is the rate controlling factor in determining the crystal growth rate? The goal of crystal growth theories is to try to answer these two questions.

Two-Dimensional Growth Theories. One way to describe the birth of a step is to use what is called *two-dimensional nucleation theory*. In our discussion of nucleation in Section 2.2., we saw that nucleation requires the formation of a critical sized cluster of molecules. When this critical size is reached, the Gibbs free energy favors the growth of the cluster, at sizes below the critical size the cluster dissolves. While our previous discussion has involved the nucleation of new particles with three dimensions, the same logic and derivation can be applied to the nucleation of a two-dimensional circular nucleus on a flat surface. Molecules will be continually absorbing on the surface diffusing and desorbing. They also will collide with each other and form two-dimensional aggregates as illustrated in Figure 2.32.

An application of nucleation theory in two dimensions yields the expression for the critical size given below

$$r_c = \sigma V_m / kT \ln S \quad (2.33)$$

where r_c is the radius of a critical size cluster, σ is the surface energy, and V_m is the volume of a molecule. As we have seen previously, Eq. (2.33) depends on knowledge of the surface energy that is difficult to obtain. Figure 2.33 gives the critical radii as a function of supersaturation at three different values of the surface energy for the KCl-water system.

Employing nucleation theory it is possible to derive an expression for the rate of formation of critical size nuclei per unit surface area per unit time. A complete derivation can be found in Ohara and Reid (1973). A simplified version of the rate expression follows.

$$I = C_1 [\ln(S)]^{1/2} \exp[-C_2/T^2 \ln(S)] \quad (2.34)$$

$$C_1 = (2/\pi)n^2 \bar{v}(V_m/h)^{1/2} \quad (2.35)$$

$$C_2 = \pi h \sigma^2 V_m / k^2 \quad (2.36)$$

where I is the two-dimensional nucleation rate, n is the equilibrium number of molecules or monomers in the solution, and \bar{v} is the speed of surface absorbed molecules. Since these values, along with the surface energy, are rarely known, C_1 and C_2 are often used as

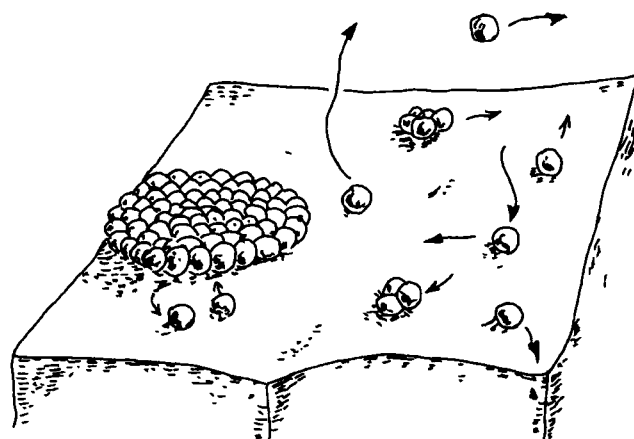


Figure 2.32 Formation of two-dimensional critical nucleus on a crystal surface. (From M. Ohara and R.C. Reid, *Modeling Crystal Growth Rates from Solution*, © 1973, p. 20. Reprinted by permission of Prentice-Hall, Englewood Cliffs, New Jersey.)

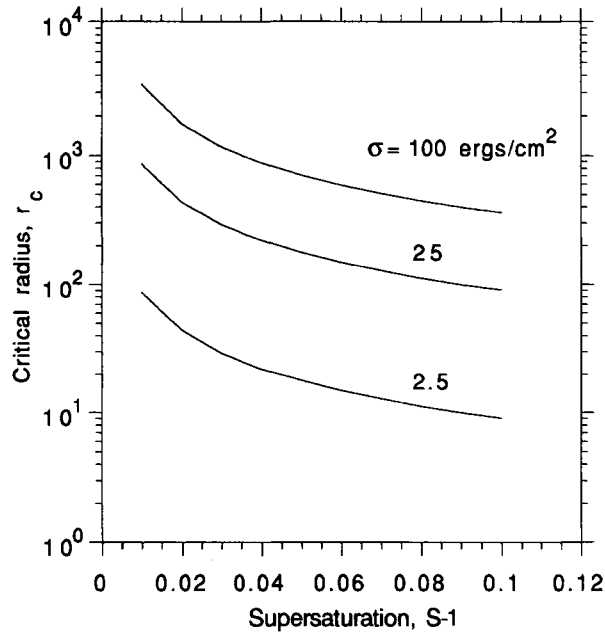


Figure 2.33 Two-dimensional critical radii estimated for KCl at 300K as a function of supersaturation. (From M. Ohara and R.C. Reid, *Modeling Crystal Growth Rates from Solution*, © 1973, p. 25. Reprinted by permission of Prentice-Hall, Englewood Cliffs, New Jersey.)

empirical parameters obtained from experimental data. As you would expect, Eq. (2.34) shows that the rate of two-dimensional nuclei formation is a strong function of temperature and supersaturation.

Once a surface nuclei is formed, the next question is how does the nuclei spread to form a complete layer. The simplest crystal growth theory assumes that when a surface nuclei is formed, it spreads across the surface at an infinite velocity. The surface must then await the formation of another surface nuclei. Since the rate-determining step in this model is the formation of a surface nuclei, the growth rate of the crystal can be expressed as

$$G = hAI \quad (2.37)$$

or substituting for I

$$G = C_1 h A [\ln(S)]^{1/2} \exp[-C_2/T^2 \ln(S)] \quad (2.38)$$

Eq. (2.38) predicts that the growth rate of a face is proportional to the area of that face. This model is known as the *mononuclear model*.

If we were to assume that the two-dimensional nucleus does not spread at all when it forms, a layer would be formed by the formation of enough two-dimensional nuclei of the critical size to cover the layer. The growth rate expression would therefore be

$$G = I\pi r_c^2 h \quad (2.39)$$

or

$$G = (C_3/T^2 [\ln(S)]^{3/2}) \exp[-C_2/T^2 \ln(S)] \quad (2.40)$$

This model is called the *polynuclear model*.

Between the extremes of the mononuclear model, in which the spreading velocity is infinite, and the polynuclear model, in which

it is zero, is a model called the *birth and spread model*. The birth and spread model allows the spreading of nuclei at a finite constant rate that is assumed to be independent of size. It also assumes that nuclei can form at any location, including incomplete layers, and that there is no intergrowth between the nuclei. A growth rate expression for this model is derived by Ohara and Reid (1973) and is

$$R = C_4 (S - 1)^{2/3} [\ln(S)]^{1/6} \exp[-C_5/T^2 \ln(S)] \quad (2.41)$$

A number of modifications of this model have been developed and reported in the literature (Bennema et al. 1973; Garside et al. 1975; Van Rosmalen and Bennema 1975).

If we examine these three models, each one makes some prediction about how crystals grow as function of supersaturation, temperature, or face area. In the case of the mononuclear model, Eq. (2.37) tells us that the crystal growth rate of a face is directly proportional to the area of that face. This would indicate that large faces grow faster than small faces, which contradicts the observation that the fastest growing faces on a crystal have the smallest areas while the slowest growing faces have the largest areas. This essentially eliminates the mononuclear model from serious consideration as a useful model.

The polynuclear model predicts [Eq. (2.40)] that the growth rate will increase with increasing nucleation rate, however, the growth rate will decline with decreasing critical nuclei size. The critical nuclei size declines as the supersaturation increases, making the growth rate a complex function of the supersaturation ratio (S). Eq. (2.40) also predicts that the growth rate should display a maximum in G at some supersaturation. This means the polynuclear model does not predict that crystal growth rate increases continuously with supersaturation, instead it predicts that at some supersaturation, growth is a maximum that will decline if the supersaturation is increased or decreased. This result seems unlikely and has not been observed.

The birth and spread model and its modifications predicts that the growth rate G increases with increasing supersaturation and increasing temperature. The dependence of growth rate on these variables is not a simple function of supersaturation and the model does not have the obvious problems of the other two models. For this reason, some semiempirical relations obtained from Eq. (2.41) are sometimes used to correlate experimental growth data and obtain the needed constants.

Another difficulty with all models that depend on two-dimensional surface nucleation is that, unless a very low value for surface energy is used in Eq. (2.34), each of the models fail at low supersaturation, predicting a much lower growth rate than is observed experimentally.

The models discussed in this section are useful in developing some understanding of possible crystal growth mechanisms and are quite illustrative in that regard. It is not recommended, however, that these models be used in any predictive sense though empirical equations obtained by reducing Eqs. (2.38), (2.40), and (2.41) are sometimes used.

Burton-Cabrera-Frank (BCF) Model. The models discussed in the previous section all require two-dimensional nucleation events for a new layer to start. These models fail to account for observed crystal growth rates at low supersaturations and are unsatisfying in the sense that they make crystal growth a noncontinuous process with the formation of a critical size two-dimensional nucleus the rate-determining step. A basis for a model in which the steps are self-perpetrating was put forward by Frank (1949). Frank's idea was that dislocations in the crystal are the source of new steps and that a type of dislocation known as a *screw dislocation* could

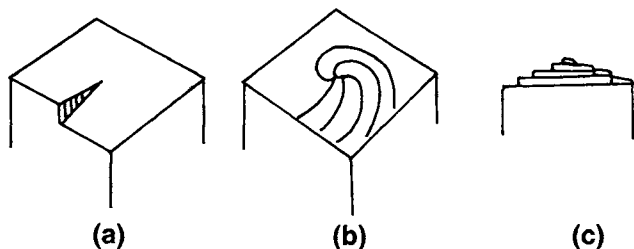


Figure 2.34 Development of a growth spiral from a screw dislocation. (Reproduced with permission from Mullin 1972.)

provide a way for the steps to grow continuously. A simple example of the growth of a screw dislocation is given in Figure 2.34. Molecules absorb on the crystal surface and diffuse to the top step of the two planes of the screw dislocation. The surface becomes a spiral staircase (which can be right- or left-handed, depending on the screw dislocation). After a layer is complete, the dislocation is still present, it is just a layer higher. The appeal of Frank's idea was that surface nucleation was not required for growth and that growth could occur at a finite rate at low supersaturations. Burton et al. (1951) formularized this concept in a growth model in which surface diffusion was assumed to be the determining rate.

Descriptions and derivations of the Burton–Cabrera–Frank (BCF) growth equation can be found in Nývlt et al. (1985), and Ohara and Reid (1973). The resulting kinetic expression is given below.

$$G = K_1 T(S - 1) \ln(S) \tan h[K_2/T \ln(S)] \quad (2.42)$$

While Eq. (2.42) has system constants (K_1 and K_2), which again are difficult to calculate or obtain from experimental data, it does provide significant information. At low supersaturations, the equation reduces to a form in which the growth is proportional to the supersaturation to the second power while at higher supersaturations, growth is linear with supersaturation. The BCF theory tells us that crystal growth rates vary from a parabolic dependence on supersaturation to a linear dependence as the supersaturation increases.

The model we have just described is called the *BCF surface diffusion model* because diffusion on the crystal surface is considered to be the rate-controlling step. While this is true in vapor growth, it is often not true in solution growth where diffusion from the bulk solution to the crystal-liquid interface can often be the limiting rate step.

Crystal growth models based on the idea of the self-perpetuating growth spiral of the BCF theory have been developed for the situation in which bulk diffusion is limiting. The most well known of these models is that of Chernov (1961). In this model, diffusion of solute molecules through a boundary layer is the rate-determining step. Details of the derivation of the model can be found in Ohara and Reid (1973), and Nývlt et al. (1985). The resulting growth equation is

$$G = \frac{V_m \xi C^* (S - 1)^2 h}{S_{cr} \delta \{1 + (\xi h/D) \ln [S_{cr} \delta / ((S - 1)h) \sin h((S - 1)/S_{cr})]\}} \quad (2.43)$$

where ξ is a coefficient that depends on kink density, δ is the boundary layer thickness, and S_{cr} is a parameter defined by

$$S_{cr} = 4V_m \sigma / kT\delta \quad (2.44)$$

S_{cr} is a dimensionless group that is sometimes called the *critical transition supersaturation* since when $(S - 1)$ is much less than S_{cr} , Eq. (2.43) reduces to the following relationship

$$G \propto (S - 1)^2 / [1 + k \ln(\delta/h)] \quad (2.45)$$

where

$$k = \xi h/D$$

Eq. (2.45) shows that at low relative supersaturations, the growth rate follows a parabolic relation with supersaturation. This is the same result as the BCF surface diffusion model. In addition, however, the growth rate, G , decreases with an increase in δ , the boundary layer thickness. This is an important result since the boundary layer thickness is directly related to hydrodynamic conditions and stirring rates. If $(S - 1)$ is much greater than S_{cr} but much < 1 , Eq. (2.44) results in a relationship in which G increases linearly with supersaturation and declines with increasing δ .

The Chernov bulk diffusion model provides an important link between crystal growth theory and the practical world of industrial crystallization where fluid flow and agitation are important. The effect of hydrodynamics on crystal growth will be discussed in the next section, *The Diffusion Layer Model*.

We have presented two models that make use of the self-perpetuating growth spiral, the BCF surface diffusion model and the bulk diffusion model of Chernov. While there are other models of this type, these two are the most well known and useful. In the surface diffusion model, the rate-limiting step is the diffusion of a molecule on the crystal surface to a step. In the bulk diffusion model, it is the diffusion of molecules from the bulk solution to the crystal-liquid interface. A more general model employing the BCF growth mechanism combines surface and bulk diffusion, and considers these effects in parallel or series on the crystal growth rate. These models are mathematically complex and are described in detail in the literature (Gilmer et al. 1971; Bennema 1969). One important result that is predicted by these types of models is that as the relative velocity between a crystal and the solution is increased, the growth will increase to a maximum value and then will remain the same. This maximum value is the value obtained when only surface diffusion limits growth. In the literature, this is known as a *growth limited by interfacial attachment kinetics*. When the crystal growth rate can be changed by changing the hydrodynamic conditions, it is known as a *mass transfer limited growth*.

The Diffusion Layer Model. The models of crystal growth discussed to this point have been mathematically complex and focused on the propagation of steps on the crystal surface either by two-dimensional nucleation or by the screw dislocation of the BCF theory. As we have seen in the bulk diffusion models of Chernov, the diffusion of the solute in the boundary layer and the boundary layer thickness can play a significant role in controlling the crystal growth rate. A simple model that focuses on the diffusion of solute through the boundary layer is known as the *diffusion layer model*. Generally, it is this model that is used in correlating data for industrial crystallization processes.

When a crystal is growing from a supersaturated solution, solute is leaving the solution at the crystal-liquid interface and becoming part of the crystal. This will deplete the solute concentration in the region of the crystal-liquid interface. Since the concentration of the solute is greater as you go away from the interface, solute will diffuse toward the crystal surface. The

concentration of the solute will continuously increase from the value at the interface to the value in the bulk solutions. The region in which the concentration is changing is called the *concentration boundary layer* (there is also a momentum and thermal boundary layer). The distance from the crystal surface to the region where the concentration is that of the bulk is called the *boundary layer thickness*. This is illustrated in Figure 2.35.

The basis of the diffusion layer model is that solute diffuses through the boundary layer and is then incorporated into the crystal. For the single one-dimensional case shown in Figure 2.35, the rate of mass increase of the crystal can be equated to the diffusion rate through the boundary layer through the expression

$$\frac{dm_c}{dt} = DA \left(\frac{dC}{dx} \right) \quad (2.46)$$

where A is the surface area of the crystal and D is the diffusion coefficient. The concentration versus position through the boundary layer can be written as

$$\frac{dC}{dx} = \frac{C - C_i}{\delta} \quad (2.47)$$

where δ is the boundary layer thickness, and C and C_i are the bulk and interfacial concentrations, respectively. Substituting Eq. (2.47) into Eq. (2.46) yields

$$\frac{dm_c}{dt} = k_d A (C - C_i) \quad (2.48)$$

where

$$k_d = D/\delta$$

The rate of solute integration into the crystal surface can be approximated by the relation

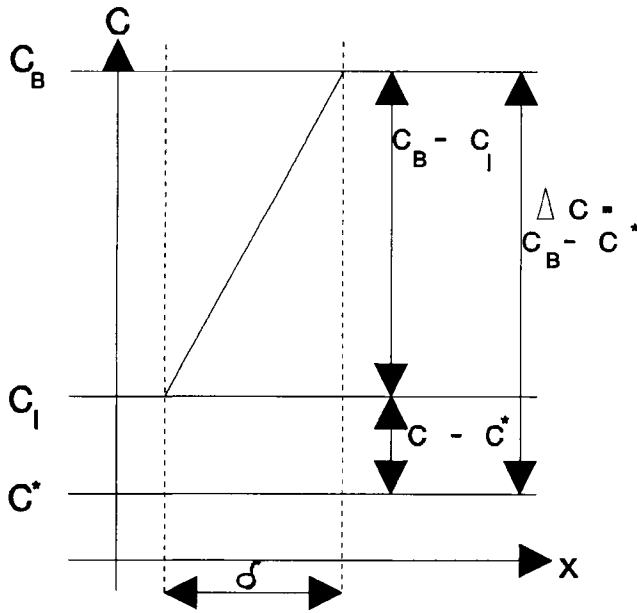


Figure 2.35 A schematic representation of the concentration profile near a growing crystal. (Reproduced with permission from Nývlt et al. 1985.)

$$\frac{dm_c}{dt} = k_i A (C_i - C)^i \quad (2.49)$$

where i is between 1 and 2, and k_i is a rate constant. If $i = 1$, then Eqs. (2.48) and (2.49) can be combined to eliminate the interfacial concentration that is difficult to obtain. This yields

$$\frac{dm_c}{dt} = K_G A \Delta C \quad (2.50)$$

where

$$\frac{1}{K_G} = \frac{1}{k_d} + \frac{1}{k_i} \quad (2.51)$$

Looking at Eqs. (2.50) and (2.51), we see that when $k_d \ll k_i$, the crystal growth rate will be diffusion controlled and $K_G = k_d$. When $k_i \ll k_d$, the crystal growth rate will be controlled by the rate of solute incorporation into the crystal.

If $i = 2$ in Eq. (2.49), combination with Eq. (2.48) yields (Nývlt et al. 1985)

$$\frac{dm_c}{dt} = A \frac{1}{2k_i/k_d^2} \left[1 + \frac{2k_i}{k_d} \Delta C - \left(\frac{4k_i}{k_d} \Delta C + 1 \right)^{1/2} \right] \quad (2.52)$$

Eq. (2.52) is a rather complex expression relating the crystal growth rate, supersaturation, and the two constants, k_d and k_i . Normally this equation is approximated by the simple relation

$$\frac{dm_c}{dt} = K_G A \Delta C^g \quad (2.53)$$

where g is between 1 and 2. When i in Eq. (2.49) is a value between 1 and 2, an explicit expression like Eqs. (2.50) or (2.52) cannot be obtained. However, Eqs. (2.50) or (2.53) are generally used in industrial crystallization processes. The constants are normally obtained from experimental data. This will be discussed in more detail in Section 2.3.3 on crystal growth kinetics.

Garside (1971) defined an effectiveness factor for crystal growth that is a measure of the relative importance of diffusion and surface integration as the rate-controlling factors. The effectiveness factor is defined by the relation

$$\eta = \frac{\text{Measured growth rate}}{\text{Rate with negligible diffusion resistance}} = \frac{R_G}{k_i \Delta C^i} \quad (2.54)$$

As $\eta \rightarrow 1$, diffusion plays a smaller and smaller role in controlling the rate. Methods for estimation η as well as other methods to determine the relative importance of diffusion and surface integration are discussed in Nývlt et al. (1985).

2.3.3. CRYSTAL GROWTH KINETICS

The development and operation of industrial crystallization processes can be made significantly easier if some data on the kinetics of crystal growth are available. This information can be incorporated in process models, can be used in process and crystallizer design, and can shed light on the observed behavior of the system.

In the previous section, we reviewed a number of different crystal growth theories. These provide a theoretical basis for the correlation of experimental crystal growth data and the determination of kinetic parameters from the data to be used in models of

industrial crystallization processes. In general, two basic expressions are used to express the relationship between supersaturation and crystal growth. These are

$$G = k_g \Delta C^g \quad (2.55)$$

and

$$R_G = K_g \Delta C^g \quad (2.56)$$

Eq. (2.55) employs a linear crystal growth velocity (length/time) with Eq. (2.56) employs a mass rate of crystal growth (mass/area time). The constants in Eqs. (2.55) and (2.56) can be related to each other through the expression

$$K_g = 3 \frac{\alpha}{\beta} \rho k_g \quad (2.57)$$

Typical units for the growth constants are

$$\frac{\text{m}}{\text{s} \left[\frac{(\text{kg solute})}{(\text{kg solvent})} \right]^g}$$

for k_g and

$$\frac{\text{kg}}{\text{sm}^2 \left[\frac{(\text{kg solute})}{(\text{kg solvent})} \right]^g}$$

for k_g . The power g in the growth equations does not depend on the form of the equation used and is normally a number between 1 and 2.

The constants k_g and K_g are temperature-dependent and are usually fit to the Arrhenius equation to obtain a general expression for growth rate as a function of temperature. The Arrhenius equation can be written as

$$k_g = A \exp(-E_G/RT) \quad (2.58)$$

where A is a constant and E_G is an activation energy. The activation energy can be used to obtain information of whether the rate-controlling step is diffusion or surface integration (Wilcox 1971; Nývlt et al. 1985). A complete crystal growth expression that includes both the effect of temperature and supersaturation on the growth rate would, therefore, be written as

$$G = A \exp(-E_G/RT) \Delta C^g \quad (2.59)$$

There are a number of experimental methods that can be used to obtain the crystal growth rate data needed to obtain kinetics. Unfortunately, unless great care is taken, these methods can provide very different results for the same system at the same supersaturation. We will first review the measurement techniques and then describe the various problems and pitfalls that may be encountered.

Measurement of Crystal Growth Rates. Techniques used to measure crystal growth rates can be divided into two main groups. The first group is comprised of methods that rely on the growth of a single crystal to obtain the needed data. The second set of methods involves the growth of a suspension of crystals. Discussion of experimental methods can be found in a number of references (Laudise 1970; Nývlt et al. 1985; Mullin 1993; Randolph and Larson 1986).

In experiments in which single crystals are grown, the goal is to allow the crystal to grow at a known supersaturation without any nucleation occurring. This implies, therefore, that the supersaturations used in these experiments must be small. In addition, seed crystals must be prepared that can be used in the experiments. A common method to prepare seed crystals is to make a saturated solution at some temperature above room temperature and then allow the solution to cool without stirring. The resulting crystals are then examined under a microscope and the one of the desired size showing discernible faces are used. In some systems this method produces very large crystals. In those cases, gentle agitation will reduce the size obtained.

As we have seen in our discussion of the diffusion layer theory of crystal growth, the rate of crystal growth is affected by the boundary layer thickness. The boundary layer thickness is, in turn, affected by the relative velocity between the crystal and the solution. In order to prevent diffusion from controlling the crystal growth rates in single crystal experiments, all methods employ some means to create a velocity between the growing crystal and the solution. A simple and commonly used experimental apparatus is shown in Figure 2.36. This apparatus consists of a round bottom flask, usually of volume of 500–1000 cm³, to which glass tubing (2.5-cm diameter) has been added to form a loop. If a stirrer is placed in the tube just below the bottom of the flask, it will push the solution down, resulting in flow in a clockwise direction. The rate of flow through the tube will increase with the speed of the impeller. The crystal is attached to a rod and placed in the path of the flow. The entire apparatus is normally placed in a constant temperature bath so that the temperature can be controlled. Since the volume of the solution is large compared to the mass of solute that will deposit on the single growing crystal, these experiments can be assumed to occur at a constant supersaturation.

The crystal is normally allowed to grow for a period of hours. The growth rate of the crystal can be measured in several ways. The simplest method is to weigh the seed crystal at the beginning of the experiment and the product crystal at the end of the experiment. The linear growth rates can also be obtained this way by measuring the crystal dimension before and after the experiment

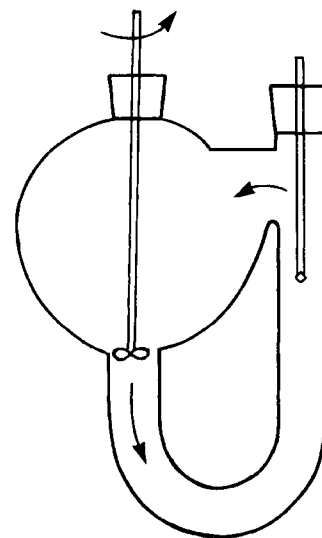


Figure 2.36 Recirculation apparatus for single crystal growth. [From P. Slaminko and A.S. Myerson (1981), "The Effect of Crystal Size on Occlusion Formation During Crystallization from Solution," *AIChE J.* 27(6), 1029–1031. Used by permission of the American Institute of Chemical Engineers. © 1981 AIChE.]

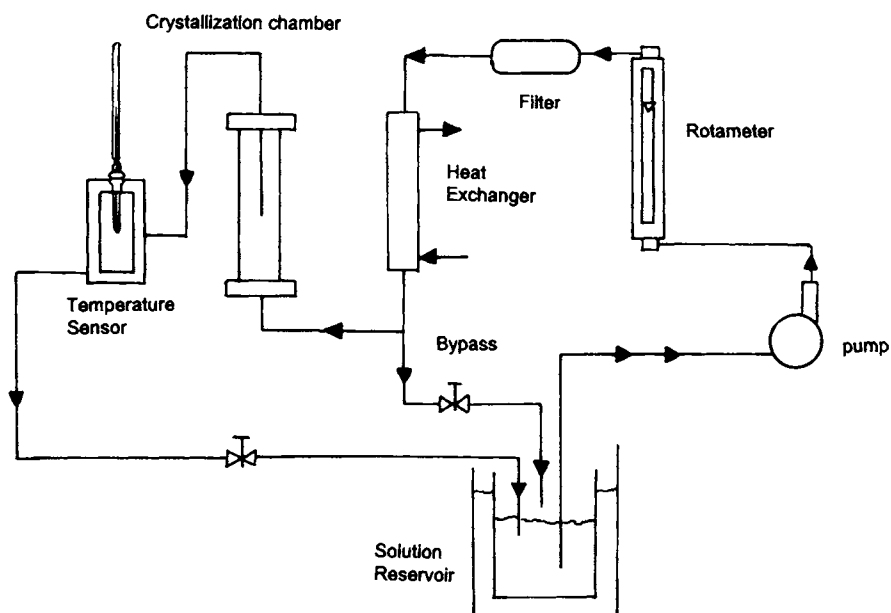


Figure 2.37 Flow apparatus for single crystal growth.

through a microscope. By use of a traveling microscope or cathetometer, the growing crystal can be observed during the experiment and the growth of a particular dimension or face can be observed. This method has been used by a number of investigators for a variety of substances (Slaminko and Myerson 1981; Clontz et al. 1972; Botsaris and Denk 1970).

One of the most difficult aspects of this method is the attachment of the seed crystal to the rod. This can be accomplished by heating a glass rod tip and attaching the crystal to the molten glass. Other methods include using a heated metal rod and inserting the heated metal directly into the crystal. The use of epoxy and silicon rubber to attach the crystal has also been reported.

An alternate method that is quite similar to the circulation method and is described in the literature (Myerson 1977; Myerson and Kirwan 1977) is shown in Figure 2.37. In this method, solution is pumped past a crystal that is suspended from a rod in a chamber. The flow rate can be directly measured by a rotameter, which is not possible in the circulation apparatus. As previously mentioned, the mass or change in dimension of the crystal can be measured at the beginning and end of the experiment or can be directly observed by using a microscope. This method is more difficult to use for several reasons. First, pumping of the solution tends to increase the chance of nucleation as does the presence of the various tubing and connections. Second, the lines must be kept at the desired temperature or material will crystallize in the lines.

A third single crystal growth method involves rotating the crystal instead of moving the liquid. The simplest way this is done is by attaching a seed crystal to a rod that is inserted into a variable speed agitator. A more complex sample preparation method known as the *rotating disk method* involves fixing the crystal in a Teflon epoxy disk with a particular face exposed. The advantages of the rotating disk are the well-defined geometry and hydrodynamics. More details on this method can be found in Nývlt et al. (1985).

Determining the crystal growth kinetics of a particular material using one of the single crystal growth methods just described involves conducting a series of experiments at different supersaturations (at a given temperature). The resulting data at each

supersaturation are used with Eqs. (2.55) or (2.56) to obtain the parameter k_g (or K_g) and g . Normally this means that the \ln of G is plotted versus the \ln of ΔC and a least squares fit is performed. The slope of this line will be g and the intercept $\ln k_g$. The entire process can then be repeated at a different temperature if desired. It is important to conduct these experiments at well-defined flow or stirring rates. Usually in measurements of this type it is desired to minimize the effect of bulk diffusion so that surface integration is the rate-controlling step. This is normally done in practice by measuring the growth rate as a function of flow rate (or stirring speed) at a given supersaturation. If mass transfer is controlling, the growth rate will increase with increasing flow rate. This is continued until a point is reached where no observable increase in growth rate is noted with increasing flow rate. A flow rate in this range is then used for all additional experiments. An example of this type of data is shown in Figure 2.38 for potassium aluminum sulfate dodecahydrate (potassium alum). Looking at Figure 2.38, we see that above a flow rate of about $2300 \text{ cm}^3/\text{min}$, the growth rate does not increase. It is important to note that in our discussion of crystal growth to this point we have assumed that the size of the crystal does not affect its growth rate. This is often known as a McCabe ΔL law (McCabe 1929). This is a good first assumption but it is not necessarily true. We will discuss size-dependent growth and related issues in Section 2.3.5 of this chapter.

The methods for measurement of crystal growth kinetics discussed to this point all involve the growth of a single seed crystal. This is clearly different from the environment in an industrial crystallizer where many crystals are growing in a suspension. A laboratory method known as a *fluidized bed crystallizer*, which attempts to measure the growth rates of a number of crystals, is shown in Figure 2.39. In this method, solution is circulated through a crystallizer in which seed crystals are suspended by the flowing fluid. The flow is such that the crystal will not settle and will not flow out of the crystallization vessel. As in single crystal growth experiments, the mass of solute depositing on the growing crystals must be small enough so that the system is considered to be at constant supersaturation. By using seed crystals of the same initial size, the final size and mass of the crystals can be used to

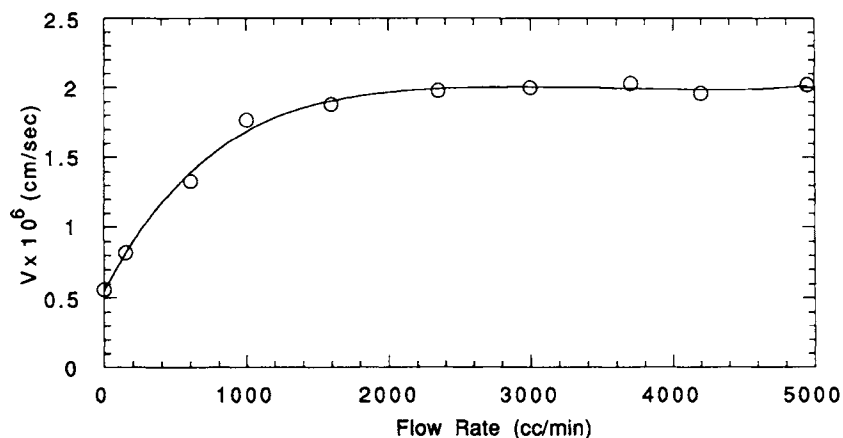


Figure 2.38 Effect of flow rate on the growth rate of single crystal of potassium aluminum sulfate to dodecahydrate.

obtain an average growth rate. More details on the method and the operation can be found in the literature (Mullin et al. 1966; Mullin and Gaska 1969).

The most common method for obtaining crystal growth kinetics involving suspensions involves the use of a mixed suspension, mixed product removal continuous crystallizer operating at steady state. By using the population balance concepts developed and described by Randolph and Larson (1986), growth rates can be obtained. The population balance method and the use of the crystal size distribution in obtaining kinetic parameters will be discussed in detail in Chapter 4 of this volume.

Estimation of Crystal Growth Kinetics. The techniques for crystal growth measurement discussed in the last section all involved direct measurement of the change in mass or size of a crystal (or crystals) at a fixed temperature and supersaturation. To obtain kinetic parameters, these experiments are repeated at a several different supersaturations at each temperature of interest and then fit to a power law model given by Eqs. (2.55) or (2.56). In the MSMR method, which will be described in detail in Chapter 4

of this volume, a continuous crystallizer must be operated at steady state to obtain the crystal size distribution and the growth rate. To obtain kinetics, this must be repeated at several different supersaturations.

All of the direct measurement techniques are time consuming and require a significant number of experiments to obtain sufficient data to obtain kinetic parameters. This has led a number of investigators (Garside et al. 1982; Tavare and Garside 1986; Qiu and Rasmussen 1990; Witkowski et al. 1990) to look at indirect methods for the estimation of both growth and nucleation kinetics. Most of the indirect methods are based on the measurement of the solution concentration versus time in a seeded isothermal batch experiment. This is often called the *desupersaturation curve* since the concentration and the solubility can be used to calculate the supersaturation of the system versus time.

The procedure using this type of experiment involves the preparation of a saturated solution of known concentration in a batch crystallizer or other vessel where the temperature can be controlled. The vessel should be equipped with stirring. With the stirrer on, the temperature of the solution is lowered several degrees, making the solution supersaturated. The solution must remain clear with no crystals present at the lower temperature. Seed crystals of the solute of known mass and size (or size distribution) are added to the solution. Since the solution is supersaturated, these crystals will grow, causing a decline in the concentration at the solution that is measured as a function of time. This is done by taking samples and using one of a number of concentration measurement techniques. Myerson (unpublished data) used density measurement to obtain desupersaturation curves on line using the apparatus shown in Figure 2.40. Solution is continuously pumped from the crystallizer to a ceramic cross-flow filter. Clear solution is obtained in a small side-stream that flows through the density meter. All solution and crystals are returned to the crystallizer. Readings from the density meter are sent directly to a computer. Typical results obtained from this system for the potassium aluminum sulfate dodecahydrate are shown in Figure 2.41.

A number of methods can be used to estimate growth kinetics from the desupersaturation curve obtained during batch-seeded isothermal experiments. The simplest of these methods was developed by Garside et al. (1982) and involves using the derivatives of the desupersaturation curve at time zero. It is assumed in this method that the concentration change is due only to crystal growth

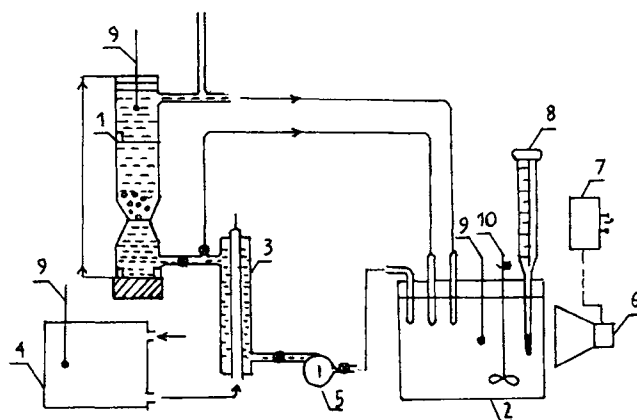


Figure 2.39 Fluidized bed crystallizer; glass tube (1), stock vessel (2), cooler (3), thermostat (4), centrifugal pump (5), infrared lamp (6), power source (7), contact thermometer (8), mercury thermometer (9), and stirrer (10). (Reproduced with permission from Nývlt et al. 1985.)

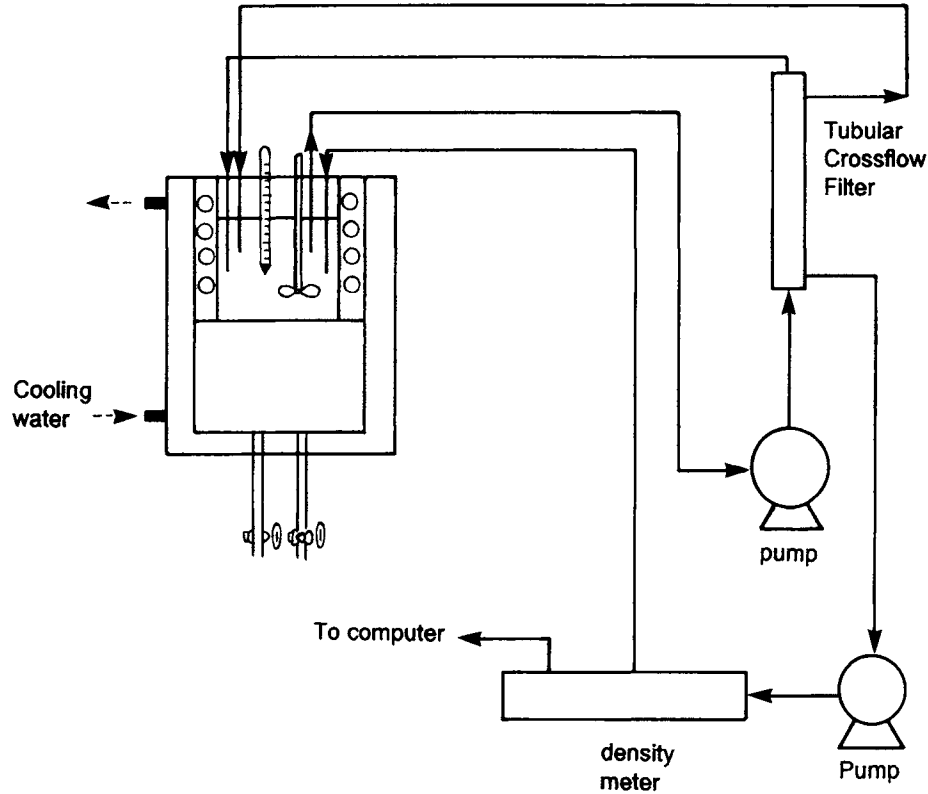


Figure 2.40 Apparatus to measure the desupersaturation curve on line.

with no nucleation occurring. Using this analysis, the power g and constant k_g of Eq. (2.56) can be obtained from the relations

$$g = \frac{2F\Delta C_0}{3\rho\bar{L}_0 A_{T0}} + \frac{\Delta C_0 \Delta \ddot{C}_0}{\Delta \dot{C}_0^2} \quad (2.60)$$

$$K_g = \frac{-\Delta \dot{C}_0}{A_{T0} \Delta C_0^g} \quad (2.61)$$

where

ΔC_0 = supersaturation at time zero
 $\Delta \dot{C}_0$ and $\Delta \ddot{C}_0$ = first and second derivatives of the desupersaturation curve at time zero, respectively
 F = shape factor ratio (β/α)
 \bar{L}_0 = average size of the seeds
 A_{T0} = surface area of the seeds at time zero

The derivatives $\Delta \dot{C}_0$ and $\Delta \ddot{C}_0$ are usually obtained by fitting the desupersaturation to a polynomial of the form

$$\Delta C = a_0 + a_1 t + a_2 t^2 \quad (2.62)$$

so that $\Delta C_0 = a_0$, $\Delta \dot{C}_0 = a_1$, and $\Delta \ddot{C}_0 = 2a_2$. While simple, results obtained from this method are quite sensitive to measurement errors since the method relies on derivatives.

More sophisticated techniques for the estimation of growth kinetics involve the use of the entire desupersaturation curve with parameter estimation techniques (Qiu and Rasmussen 1990). The combination of the desupersaturation curve and the crystal size distribution can be used to estimate both growth and nucleation

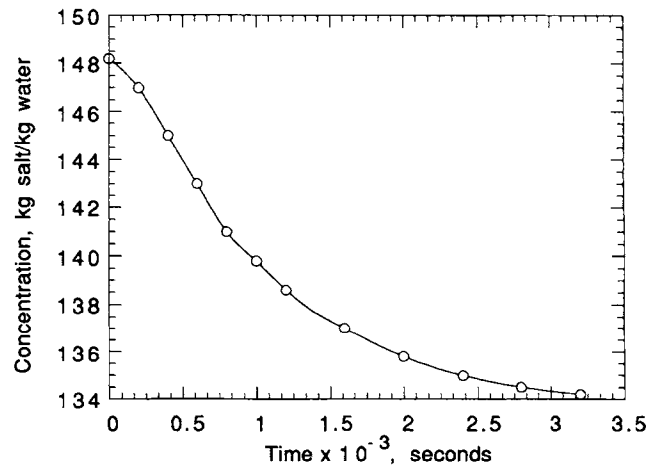


Figure 2.41 Desupersaturation curve.

kinetics (Tavare and Garside 1986; Witkowski et al. 1990; Tavare 1995). While these methods do not supply very accurate kinetic data, the experiments are fast and the data are easy to obtain, thus allowing for relatively quick estimation of kinetic parameters that can be used for process design and modeling purposes.

2.3.4. OSTWALD RIPENING

As we saw in Chapter 1 of this volume, the solubility of a solid solute in a liquid solution is an equilibrium property of the

solution. When a crystalline solid with a particular CSD is in contact with a saturated solution, however, the CSD can change with time. This is the result of the system trying to minimize its Gibbs free energy. This can be seen in looking at Eq. (2.63).

$$dG = -SdT - VdP + \sum \mu_i dn_i + \sigma_s dA \quad (2.63)$$

where μ_i is the chemical potential of species and σ_s is the specific surface energy of the solid particle. Since the system will try to minimize G , the surface area A will try to achieve a minimum. What this means in practice is that particles have different solubilities based on their size when present in a suspension of particles with a size distribution. This difference in solubility results in the small particles dissolving and depositing on the larger particles, decreasing the surface area A and moving the system towards a minimum in Gibbs free energy. It also increases the average crystal size. This process is called *Ostwald ripening*. The effect of size on particle solubility can be shown using the Gibbs-Thomson (Ostwald-Freundlich) equation

$$\ln \frac{c(r)}{c^*} = \beta V \sigma_s / rkT \quad (2.64)$$

where

- $c(r)$ = solubility of a particle of size r
- c^* = equilibrium solubility
- β = surface shape factor
- r = particle radius
- V = molecular volume

The equilibrium solubility refers to the solubility that would be obtained with very large particles (therefore, small surface areas). As in all thermodynamic calculations, activity coefficients should be used in nonideal solutions.

If the crystal growth process accompanying the aging phenomenon is diffusion-controlled, it can be shown (Nývlt et al. 1985) that the size of particle in equilibrium with the solution can be obtained from the relation

$$r(c) = \frac{\beta V \sigma_s c^*}{(c - c^*)kT} \quad (2.65)$$

Particles larger than $r(c)$ will grow and particles smaller than $r(c)$ will dissolve.

Ostwald ripening is often important in processes in which crystallization is rapid and crystal sizes are small. This is especially true in a precipitation process and will be discussed in detail in Chapter 6 of this volume. It is important to remember that the effect of Ostwald ripening is to alter the crystal size distribution with time in a suspension of crystals that is an apparent equilibrium with its saturated solution. Ostwald ripening is an important phenomena if you are concerned with obtaining fine particles or are concerned about changes in the crystal size distribution of your product prior to drying.

2.3.5. SIZE-DEPENDENT GROWTH AND GROWTH RATE DISPERSION

In our discussions of crystal growth theory and kinetics, we have assumed that the crystal growth rate is not a function of crystal size. While a good first assumption, this is not always true. As we saw in our discussion of Ostwald ripening, there is a difference in solubility between very small particles and larger particles. This differential solubility will result in a difference in supersaturation as a function of particle size. The smaller particles will be at a lower supersatura-

tion than larger particles and will, therefore, not grow as fast. This is an example of size-dependent growth, however, this mechanism is important only when the crystal size is very small (under $1 \mu\text{m}$).

For crystals of larger size, a size-dependent growth mechanism has been proposed for the situation when interfacial attachment kinetics control the crystal growth rate. This mechanism (Garside et al. 1976, 1974) is based on the idea that, as a crystal gets larger its total surface area increases, as does the probability of the occurrence of dislocations on the surface. If the crystals grow by a BCF-type mechanism, this would indicate that larger crystals will likely grow faster than smaller crystals. A mechanism has also been proposed based on bulk diffusion (Garside and Jančić 1976), which also indicates that under certain conditions larger crystals can grow faster than smaller ones. A number of investigators have developed empirical growth rate expressions that include a size dependence. This work is summarized by Randolph (1984).

While size-dependent growth does occur, work in recent years has shown that in many instances what had been attributed to size-dependent growth was due to another phenomenon, known as *growth rate dispersion*. This unexpected concept says that crystals of the same size and material exposed to identical conditions of supersaturation, temperature, and hydrodynamics do not necessarily grow at the same rate. This is not the same as size-dependent growth in which crystals of different sizes display differences in growth rate. The concept of growth rate dispersion was first used by White and Wright (1971) to explain an observed widening of the size range during the batch growth of sucrose.

Studies of growth rate dispersion have resulted in two distinctly different mechanisms being proposed. In one mechanism it is assumed that crystals have a distribution of growth rates but that each individual crystal grows at a constant rate (at a fixed set of conditions). This implies that nuclei are born with a distribution of growth rates and the observation of two nuclei in a crystallizer at steady-state conditions will reveal each nuclei growing at a constant but different rate. This type of behavior has been demonstrated experimentally for crystal fragments produced by attrition (Van't Land and Wunk 1978), for secondary nuclei (Berglund et al. 1983; Berglund and Larson 1982), and for single crystal produced by primary nucleation (Garside and Ristic 1983).

The second mechanism for growth dispersion says that while all crystals have the same time-averaged growth rate, the growth rates of individual crystals can fluctuate significantly with time. This mechanism, therefore, implies that the observation of two different crystals growing under identical conditions might be different at any time that the time-averaged growth rate over a long time period would be identical. Experimental evidence has also appeared (Human et al. 1982) that supports this mechanism.

Explanations of growth rate dispersion that have appeared in the literature employ the surface integration step of the BCF theory of crystal growth as the primary cause of the observed phenomena. The BCF theory indicates that the growth rate of a crystal is dependent on screw dislocations present on the surface. Experimental work has shown that changes in the location or density of screw dislocations can cause large changes in the crystal growth rate. Collisions of the crystals with the impeller, walls, and each other can result in damage to the dislocations and, therefore, changes in the crystal growth rate. This is especially true with secondary nuclei that could display very different dislocation densities. In addition, the imperfect nature of the crystal growth process could lead to changes in the dislocations of the crystal faces.

Both growth rate dispersion and size-dependent growth affect the crystal size distribution obtained from laboratory and industrial crystallizers. They must, therefore, be taken into account when analyzing the modeling crystallization processes. More information on this topic can be found in Chapter 4 of this volume.

NOMENCLATURE

A	Constant	Eq. (2.58)
A	Surface area of crystal, cm^2	Eq. (2.3)
A_{10}	Surface area of the seeds at time zero	Eq. (2.61)
B	Secondary nucleation rates, nuclei/ $\text{cm}^2\text{-s}$	Eq. (2.17)
B_0	Primary nucleation rate, nuclei/ $\text{cm}^2\text{-s}$	Eq. (2.5)
c	Bulk concentration	Eq. (2.47)
c	Concentration of clusters	Eq. (2.11)
c^*	Concentration of clusters at equilibrium, equilibrium solubility	Eq. (2.11), (2.64)
C_1, C_2	Empirical parameters	Eq. (2.34)
C_i	Interfacial concentration	Eq. (2.47)
d	Interplanar spacing, cm	Eq. (2.1)
D	Diffusion coefficient, cm^2/s	Eq. (2.28)
D_s	Surface diffusion coefficient, cm^2/s	Eq. (2.29)
E_G	Activation energy, ergs	Eq. (2.58)
F	Shape factor ratio	Eq. (2.27)
g	Exponent for crystal growth	
G	Linear growth rate, cm/s	Eq. (2.32)
h	Step height, cm	Eq. (2.32)
i, j	Empirical exponents	Eq. (2.18)
I	Two-dimensional nucleation rate	Eq. (2.34)
k	Boltzman's constant	Eq. (2.5)
k_N''	Empirical constant	Eq. (2.19)
k_N'	Empirical constant	Eq. (2.18)
k_d	Diffusion rate constant	Eq. (2.48)
k_i	Rate constant	Eq. (2.49)
k_N	Empirical constant	Eq. (2.17)
L	Characteristic crystal length, cm	Eq. (2.2)
m	Apparent nucleation order	Eq. (2.24)
M_T	Suspension density, g/cm^3	Eq. (2.18)
n	Equilibrium number of molecules or monomers in solution	Eq. (2.34)
n	Nucleation order	Eq. (2.17)
\bar{L}_0	Average size of the seeds	Eq. (2.60)
P	Pressure	Eq. (2.63)
r	Nucleus radius, cm	Eq. (2.7)
R	Growth rate for birth and spread model	Eq. (2.41)
r_1	Cooling rate, $^\circ\text{C}/h$	Eq. (2.22)
r_c	Critical nucleus radius, cm	Eq. (2.8)
Re	Reynolds number	Eq. (2.20)
R_G	Increase in crystal mass per unit time per unit area	Eq. (2.31)
S	Supersaturation ratio	Eq. (2.11)
S	Entropy	Eq. (2.63)
S_{cr}	Critical transition supersaturation	Eq. (2.44)
T	Solution temperature, K	Eq. (2.5)
T_1	Temperature at which the first crystal appears, $^\circ\text{C}$	

t_g	Time for nucleus to grow to a detectable size, s	Eq. (2.26)
t_{ind}	Induction time for formation of new phase, s	Eq. (2.26)
t_n	Nucleation time, s	
T_s	Saturation temperature, $^\circ\text{C}$	
t_{tr}	Time needed to reach steady-state nucleation, s	Eq. (2.26)
v	Molecular volume, cm^3/g	Eq. (2.11)
V	Volume of crystal, cm^3	Eq. (2.2)
V'	Step velocity, cm/s	Eq. (2.32)
V_m	Volume of the molecule, cm^3	Eq. (2.33)
W	Agitation rate, rpm	Eq. (2.18)
x	Solute mole fraction	Eq. (2.28)
y_0	Step spacing, cm	Eq. (2.32)
ΔC	Supersaturation	Eq. (2.17)
ΔC_0	Supersaturation at time zero	Eq. (2.60)
ΔG	Free energy change for the formation of a new phase, ergs	Eq. (2.5)
ΔG_{cr}	Critical free energy for nucleation, ergs	Eq. (2.5)
ΔG_{hom}	Free energy change for homogeneous nucleation, ergs	Eq. (2.15)
ΔG_{het}	Free energy change for heterogeneous nucleation, ergs	Eq. (2.15)
ΔG_s	Free energy change for the formation of a new surface, ergs	Eq. (2.5)
ΔG_V	Free energy change for the phase transformation, ergs	Eq. (2.5)
ΔG_{visc}	Free energy change due to viscous effects, ergs	Eq. (2.14)

Greek Letters

α	Volume shape factor	Eq. (2.2)
β	Area shape factor	Eq. (2.3)
δ	Boundary layer thickness	Eq. (2.43)
ξ	Kink density coefficient	Eq. (2.43)
η	Effectiveness factor	Eq. (2.54)
Θ	Contact angle/wetting angle of the crystal, radians	Eq. (2.16)
θ	Incident angle of x-ray, radians	Eq. (2.1)
λ	Wavelength, cm^{-1}	Eq. (2.1)
μ_i	Chemical potential of species i	Eq. (2.63)
ρ	Crystal density, g/cm^3	Eq. (2.31)
σ	Surface tension, dynes/cm	Eq. (2.6)
ϕ	Multiplication factor for heterogeneous nucleation	Eq. (2.16)
σ_s	Specific surface energy of solid particles	Eq. (2.63)
\bar{v}	Speed of surface-adsorbed molecules	Eq. (2.35)

REFERENCES

- Bennema, P. (1969). *J. Cryst. Growth* **5**, 29.
- Bennema, P., Boon, J., Van Leeuwen, L., and Gilmer, G.H. (1973). *Krist. U. Technic.* **8**, 659.
- Berglund, K.A., and Larson, M.A. (1982). *AIChE Symposium Series* **78**, 9.
- Berglund, K.A., Kaufman, E.L., and Larson M.A. (1983). *AIChE J.* **25**, 876.
- Bertin, E.P. (1975). *Principles and Practice of X-Ray Spectrometric Analysis*, Plenum Press, New York.
- Black, S.N., and Davey, R.J. (1988). *J. Cryst. Growth* **90**, 136.
- Botsaris, G.D., and Denk, E.G. (1970). *Ind. Eng. Chem. Fund.* **9**, 276.
- Broul, M. (1978). Ph.D. thesis, University of Chem. Tech., Prague.
- Buckley, H.E. (1951). *Crystal Growth*, Wiley, New York.
- Bunn, C.W. (1961). *Chemical Crystallography*, 2nd ed., Oxford University Press, London.
- Burton, W.K., Cabrera, N., and Frank, F.C. (1951). *Phil. Trans.* **A243**, 299.
- CERIUS2 Software (1999). Molecular Simulations Inc. San Diego, CA.
- Chernov, A.A. (1961). *Soviet Phys. Usp.* **4**, 116.
- Clontz, N.A., and McCabe, W.L. (1971). *Chem. Eng. Prog. Symp. Ser.* **110**, 67, 6.
- Clontz, N.A., Johnson, A.T., McCabe, W.L., and Rousseau, R.W. (1972). *Ind. Eng. Chem. Fund.* **11**, 368.

- Clydesdale, G., Roberts, K.J., and Docherty, R., (1996). In *Crystal Growth of Organic Materials* (Myerson, A.S., Green D., and Meenan, P., eds.), pp. 43–52, American Chemical Society, Washington DC.
- Cooke, E.G. (1966). *Krist. U. Technic.* **1**, 119.
- Cullity, B.D. (1978). *Elements of X-Ray Diffraction*, 2nd ed., Addison-Wesley Publishing Co., Reading, MA.
- Denk, E.G. (1970). Ph.D. thesis, Tufts University, Medford, MA.
- Denk, E.G., and Botsaris, G.D. (1971). *Fundamental Studies in Secondary Nucleation from Solution*, International Conference on Crystal Growth-3, Marseille.
- Denk, E.G., and Botsaris, G.D. (1972a). *J. Cryst. Growth* **13–14**, 493.
- Denk, E.G., and Botsaris, G.D. (1972b). *J. Cryst. Growth* **15**, 57.
- Docherty, R., and Meenan, P. In *Molecular Modeling Applications in Crystallization* (Myerson, A.S., ed.), pp. 106–165, Cambridge University Press, New York, 1999.
- Donnay, J.D.H., and Harker, D. (1937). *Am. Mineral.* **22**, 446.
- Engle, G.E., Wilke, S., Konig, O., Harris, K.D.M., and Leusen, F.J.J., (1999). *J. Appl. Cryst.* **32**, 1169–1179.
- Frank, F.C. (1949). *Symposium on Crystal Growth, Discussions of the Faraday Society*, no. 5.
- Garabedian, H., and Strickland-Constable, R.F. (1972a). *J. Cryst. Growth*, **12**, 53.
- Garabedian, H., and Strickland-Constable, R.F. (1972b). *J. Cryst. Growth*, **13–14**, 506.
- Garside, J. (1971). *Chem. Eng. Sci.* **26**, 1425.
- Garside, J., and Jančić, S. (1976). *AIChE J.* **22**, 887.
- Garside, J., and Ristic, R.I. (1983). *J. Cryst. Growth*, **61**, 215.
- Garside, J., Mullin, J.W., and Das, S.N. (1974). *Ind. Eng. Chem. Fund.* **13**, 299.
- Garside, J., Van Rosmalen, R., and Binnema, R. (1975). *J. Cryst. Growth*, **29**, 353.
- Garside, J., Phillips, V.R., and Shah, M.B. (1976). *Ind. Eng. Chem. Fund.* **15**, 230.
- Garside, J., Rusli, I.T., and Larson, M.A. (1979). *AIChE J.* **25**, 57.
- Garside, J., Gibilaro, L.G., and Tavaré, N.S. (1982). *Chem. Eng. Sci.* **37**, 1625.
- Garsten, V.A., and Head, R.B. (1966). *Phil. Mag.* **14**, 1243.
- Genck, W.J., and Larson, M.A. (1972). *AIChE Symposium Series*, **68(121)**, 57.
- Gibbs, J.W. (1928). *On the Equilibrium of Heterogeneous Substances*, Collected Works, Longmans-Green, New York.
- Gilli, G., In *Fundamentals of Crystallography*, Giacobozzo, C., (ed.) Oxford University Press, Oxford 1992.
- Gilmer, G.A., Ghez, R., and Cabrera, N. (1971). *J. Cryst. Growth*, **8**, 79.
- Hartman, P. (1980a). *J. Cryst. Growth*, **49**, 157.
- Hartman, P. (1980b). *J. Cryst. Growth*, **49**, 166.
- Hartman, P., and Binnema, P. (1980). *J. Cryst. Growth*, **49**, 145.
- Hartman, P., and Perdok, W.G. (1955a). *Acta Crystallogr.* **8**, 49.
- Hartman, P., and Perdok, W.G. (1955b). *Acta Crystallogr.* **8**, 521.
- Hartman, P., and Perdok, W.G. (1955c). *Acta Crystallogr.* **8**, 525.
- Human, H.J., Van Enckerk, W.J.A., and Binnema, P. (1982). In *Industrial Crystallization 81* (Jančić, S.J., and De Jong, E.J., eds.), p. 387, North Holland, Amsterdam.
- Jančić, S.M., and Grootsholten, P.A.M. (1983). In *Industrial Crystallization*, pp. 36–37, Delft University Press, Delft, The Netherlands.
- Joint Committee on Powder Diffraction Standards (1990). 1601 Park Lane, Swarthmore, PA.
- Joshi, M.S., and Anthony, A.V. (1979). *J. Cryst. Growth* **46**, 7.
- Khambaty, S., and Larson, M.A. (1978). *Ind. Eng. Chem. Fund.* **17**, 160.
- Khamskii, E.V. (1969). *Crystallization from Solution*, Consultants Bureau, New York.
- Kitaigorodski, A.I. (1973). *Molecular Crystals and Molecules*, Academic Press, New York.
- Kubota, N., Kawakami, T., and Tadaki, T. (1986). *J. Cryst. Growth* **74**, 259.
- Larson, M.A., and Bendig, L.L. (1976). *AIChE Symposium Series* **72(153)**, 11.
- Laudise, R.A. (1970). *The Growth of Single Crystals*, Prentice-Hall, Englewood Cliffs, NJ.
- Leusen, F.J.J. (1993). Ph.D. dissertation, Nijmegen University, Nijmegen, The Netherlands.
- McCabe, W.L. (1929). *Ind. Eng. Chem.* **21**, 112.
- Melia, T.P., and Moffitt, W.P. (1964a). *Ind. Eng. Chem. Fund.* **3**, 313.
- Melia, T.P., and Moffitt, W.P. (1964b). *Nature (London)* **201**, 1024.
- Mullin, J.W. (1993). *Crystallization*, 3rd ed., Butterworth-Heinemann, Oxford.
- Mullin, J.W. (1960). *Ind. Chemist* **36**, 272.
- Mullin, J.W. (1972). *Crystallization*, 2nd ed., Butterworths, London.
- Mullin, J.W., and Gaska, J. (1969). *Can. J. Chem. Eng.* **47**, 483.
- Mullin, J.W., and Leci, C.L. (1969). *J. Cryst. Growth* **5**, 75.
- Mullin, J.W., and Osman, M.M. (1973). *Krist. U. Technic.* **8**, 471.
- Mullin, J.W., Garside, J., and Gaska, C. (1966). *Chem. Ind.* **1966**, 704.
- Myerson, A.S. (1999). *Molecular Modeling Applications in Crystallization*, Cambridge University Press, New York.
- Myerson, A.S. (1977). Ph.D. diss., University of Virginia, Charlottesville, VA.
- Myerson, A.S., and Kirwan, D.J. (1977). *Ind. Eng. Chem. Fund.* **16**, 420.
- Ness, J.N., and White, E.T. (1976). *AIChE Symposium Series* **72**, 153.
- Nielsen, A.E. (1964). *Kinetics of Precipitation*, Pergamon Press, New York.
- Nielsen, A.E. (1969). *Krist. U. Technic.* **4**, 17.
- Nielsen, A.E., and Sohnel, O. (1971). *J. Cryst. Growth* **11**, 233.
- Nývlt, J. (1968). *J. Cryst. Growth* **3–4**, 377.
- Nývlt, J. (1972). *Collect. Czech. Chem. Commun.* **37**, 3155.
- Nývlt, J. (1976). *AIChE Symposium Series* **72(153)**, 61.
- Nývlt, J. (1981). *Cell. Czech.* **46**, 79.
- Nývlt, J., Sohnel, O., Matuchova, M., and Broul, M. (1985). *The Kinetics of Industrial Crystallization*, Elsevier, Amsterdam.
- Ohara, M., and Reid, R.C. (1973). *Modeling Crystal Growth Rates from Solution*, Prentice-Hall, Englewood Cliffs, NJ.
- Packter, A.J. (1974). *J. Cryst. Growth* **21**, 191.
- Powers, H.E.C. (1963). *Ind. Chemist.* **39**, 351.
- Preckshot, G.W., and Brown, G.G. (1952). *Ind. Eng. Chem.* **44**, 1314.
- Qiu, Y., and Rasmussen, A.C. (1990). *AIChE J.* **36**, 665.
- Randolph, A.D. (1984). *AIChE Symposium Series* **240**, (80).
- Randolph, A., and Larson, M. (1986). *Theory of Particulate Processes*, 2nd ed., Academic Press, New York.
- Ruoff, A.L. (1973). *Materials Science*, Prentice-Hall, Englewood Cliffs, NJ.
- Saska, M., and Myerson, A.S. (1983). *J. Cryst. Growth*, **61**, 546.
- Saska, M., and Myerson, A.S. (1987). *AIChE J.* **33**, 848.
- Sikdar, S.K., and Randolph, A.D. (1976). *AIChE J.* **22**, 110.
- Slaminko, P., and Myerson, A.S. (1981). *AIChE J.* **27**, 1029.
- Sohnel, O., and Mullin, J.W. (1979). *Krist. U. Technic.* **14**, 217.
- Sohnel, O., and Mullin, J.W. (1988). *J. Colloid. Interface Sci.* **123**, 43.
- Stephen, L., and Stephen, R. (1963). *Solubilities of Inorganic and Organic Compounds*, Macmillan, New York.
- Strickland-Constable, R.F. (1968). *Kinetics and Mechanism of Crystallization*, Academic Press, New York.
- Strickland-Constable, R.F. (1972). *Chem. Eng. Prog. Symposium Series* **68(121)**, 1.
- Strickland-Constable, R.F., and Mason, R.E.A. (1963). *Nature (London)* **197**, 897.
- Tamman, G. (1925). *States of Aggregation*, Van Nostrand and Co., New York.
- Tavaré, N.S., (1995). *Industrial Crystallization Process Simulation Analysis and Design*, Plenum Press, New York.
- Tavaré, N.S., and Garside, J. (1986). *Chem. Eng. Res. Des.* **64**, 109.
- Ting, H.H., and McCabe, W.L. (1934). *Ind. Eng. Chem.* **26**, 1201.
- Tipson, R.S. (1950). *Techniques of Organic Chemistry*, 3rd ed. (Weissberger, A., ed.), Interscience, New York.
- Toyokura, K., Yamazoe, K., and Mogi, J. (1976). *AIChE Symposium Series* **72(153)**, 53.
- Turnbull, D., and Fisher, J.C. (1949). *J. Chem. Phys.* **17**, 71.
- Turnbull, D., and Vonnegut, B. (1952). *Ind. Eng. Chem.* **44**, 1292.
- Vainshtein, B.K. (1981). *Modern Crystallization I*, Springer-Verlag, New York.
- Van Rosmalen, R., and Binnema, P. (1975). *J. Cryst. Growth* **29**, 342.
- Van't Land, C.M., and Wunk, B.G. (1978). *Control of Particle Size in Industrial Sodium Chloride Crystallization* (Mullin, J.W., ed.), p. 51, Plenum Press, New York.
- Verma, A.R., and Krishna, P. (1966). *Polymorphism and Polytypism in Crystals*, Wiley, New York.
- Volmer, M. (1939). *Kinetik der Phasenbildung*, Steinkoff, Dresden, Germany.
- Volmer, M., and Schultze, W. (1931). *Z. Phys. Chem.* **A156**, 1–22.
- Vonnegut, B. (1948). *J. Colloid Sci.* **3**, 563.
- Weissbuch, I., Lahav, M., and Leiserowitz, L. (1999). In *Molecular Modeling Applications in Crystallization*, Myerson, A.S., (ed.), Cambridge University Press, New York.
- White, E.T., and Wright, A.G. (1971). *Chem. Eng. Prog. Symposium Series* **110**, 67–81.
- White, M.L., and Frost, A.A. (1959). *J. Colloid Sci.* **14**, 247.

- Wilcox, W.R. (1971). *Preparation and Properties of Solid State Materials*, Lefever, New York.
- Wilson, W.R. (1986). *Preparation and Properties of Solid State Materials*, Lefever, New York.
- Witkamp, G.J., and Van Rosmallen, G.M. (1990). *American Chemical Society Symposium Series* no. 438 (Myerson, A.S., and Toyokura, K., eds.), pp. 392, American Chemical Society, Washington, DC.
- Witkowski, W.R., Miller, S.M., and Rawlings, S.B. (1990). *American Chemical Society Symposium Series* no. 438 (Myerson, A.S., and Toyokura, K., eds.), pp. 102, American Chemical Society, Washington, DC.
- Wright, J.D. (1987). *Molecular Crystals*, Cambridge University Press, New York.
- Youngquist, G.R., and Randolph, A.D. (1972). *AIChE J.* **18**, 421.

This Page Intentionally Left Blank

THE INFLUENCE OF IMPURITIES AND SOLVENTS ON CRYSTALLIZATION

Paul A. Meenan, Stephen R. Anderson, and Diana L. Klug

3.1. INTRODUCTION

In many instances, small amounts of impurities have dramatic effects on crystal growth, morphology, and nucleation. In industrial crystallization operations in particular, the presence of impurities, synthesis by-products, and corrosion products can influence the crystallization process, negating improvements that can be made using normal operating parameters such as temperature, supersaturation, and residence time. Until rather recently, a largely empirical approach was used to quantify the effect of impurities and solvents on these processes. The advent of sophisticated molecular modeling tools coupled with the increasingly accurate means of determining crystal structure has now led to a greater understanding of crystal surfaces and consequently crystal surface-impurity/crystal surface-solvent interactions.

As crystallization is essentially a molecular recognition process occurring on a grand scale; impurity and solvent influences can be rationalized in terms of intermolecular interactions. This chapter reviews the fundamentals of impurity incorporation, solvent interaction, and solution thermodynamics. Since the interactions of solvent and impurity at the interface play a central role in all aspects of crystallization, emphasis is placed on describing the structure and environment at the interface, and explaining its impact on crystal size, shape, and purity. These concepts are first explored conceptually and then more quantitatively to allow application to the design and improvement of industrial crystallization processes. In particular, emphasis is placed on utilizing theories of crystal growth and adsorption to understand how impurities and solvents affect the growth process and the resulting quality of crystalline materials obtained from industrial processes.

Because of the requirement of high-purity crystalline products, an understanding of the effects of solvents on purification is also necessary. As shown in this chapter, the solvent can influence the separation efficiency through its effect on crystallization kinetics, solution thermodynamics, and crystal interface structure. A poor initial choice of solvent can thermodynamically and kinetically limit the effectiveness of the separation, irrespective of all other factors, including crystallizer design and cost. There is also the question of the solvent directly incorporating into the lattice of the crystallizing host. This phenomena leads to the formation of solvates, which can prove critical in the organic specialty crystallization arena.

As a starting point for considering the effect of impurity and solvent on crystallization, the growth and interaction process is examined in the framework of the fundamental solid-state, interfacial, and liquid phase (solute-solvent-impurity) chemistry. The solid-state chemistry is specific to a given crystalline material and the nature of the bonds (e.g., ionic, covalent, van der Waals, etc.) that hold the crystal structure together. A complete description of the solid-state aspects of crystal growth is beyond the scope of this

chapter and will only be reviewed in the context of its role in solvent and impurity effects. More detailed information can be found in Chapter 1 of this volume, or elsewhere (Ladd 1979; Byrn 1999).

Lastly, the mass transport processes at the crystal-liquid interface play a central role in crystallization. The influence of solvent and impurities on the structure and growth rates of faces is considered in this chapter along with its effect on the incorporation of impurities. The solvent-solute-impurities interactions in solution will also be shown to interact in subtle, but important, ways with the interface during the crystallization process. With appropriate thermodynamic analysis it is shown how these interactions ultimately affect crystallization as a purification process.

3.2. FACTORS DETERMINING CRYSTAL SHAPE

The shape of a crystal is determined by the relative growth rates of individual faces of a crystal, and can be strongly influenced during crystallization by the presence of impurities, and even the solvent itself. A two-dimensional representation of the effect of face growth rates on the evolution of crystal shape is shown in Figure 3.1. During crystallization, fast growing faces normally grow out of existence, leaving the crystal bounded by the slowest growing faces. Impurities or solvents that adsorb or interact with the crystal face in such a way to slow the grow rate can further increase its relative area.

Under conditions of very slow growth, the ultimate crystal shape is determined strictly by thermodynamics. Under such conditions, the faces appearing on the crystal correspond to the smallest convex polyhedron having minimum surface free energy. Gibbs

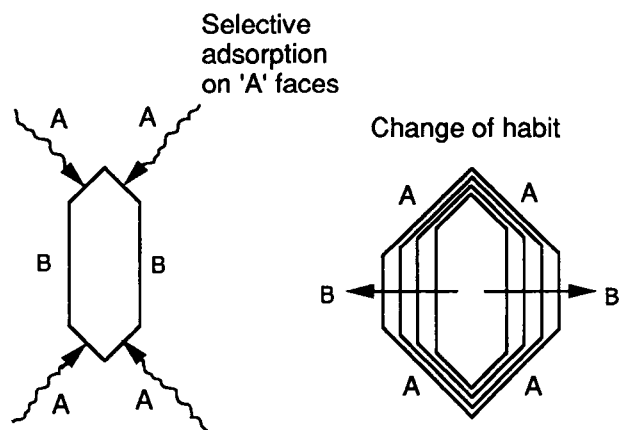


Figure 3.1 Effect of impurities on crystal growth habit. (Reproduced with permission from Addadi et al. 1985.)

(1878) showed that, in the case of a crystal in equilibrium with its environment, the condition $\sum_i(\sigma_i A_i)$ is a minimum (where σ_i is the surface free energy of the face and A_i is its corresponding area). The Gibbs condition, however, is not normally realized in practice as crystal growth in crystallizers is significantly removed from the equilibrium state.

Under most conditions, the shape (i.e., the habit) of a crystal is determined by kinetics rather than thermodynamics and the resulting habit is termed the "growth," as opposed to the "equilibrium," habit. The kinetics of each crystal face can be influenced by such external factors as supersaturation, temperature, and mixing. However, the complexity of crystallization operations arises from the fact that the mass transfer processes at the crystal interface, as opposed to the "bulk," are often rate-determining. Thus, without consideration of the role of the interface during crystallization it is impossible to predict the influence of impurities or solvents on crystallization, or explain such diverse processes as secondary nucleation and inclusion formation.

3.2.1. THE ROLE OF THE SOLID STATE IN SHAPE DEVELOPMENT

A crystal can be defined as a material consisting of an ordered solid array (lattice) of atoms or molecules exhibiting long-range order in three dimensions. In the early developments of crystallography, attempts were made to relate crystal shape to some aspect of lattice structure, independent of considerations of chemical or bonding interactions; indeed the field of morphological crystallography was initiated by showing that by stacking cubes, various crystal shapes could be obtained. This "cube" or primary building block was considered the minimum repeating unit to build a crystal. Thus, only the structural and not the bonding aspects of the solid state were considered in these early studies. Upon the development and application of X-ray diffraction tools, it became apparent that the structural aspects could be redefined in terms of molecular and bonding aspects. The primary building block was redefined as the unit cell. The unit cell contains all the molecular information required to generate a crystal structure, e.g., molecular conformation, symmetry and intra-/inter-molecular bonding aspects. The development of crystallography techniques led to the recognition that the different crystal faces of a material may exhibit different chemical properties, arising from the inherent crystal chemistry within the lattice and the molecular functional groups exposed at each crystal face. Consequently, crystalline faces exhibit specific structural and chemical attributes that determine, among other things, their interaction with impurities and solvents. For example, crystal faces can vary considerably in polarity (and therefore relative hydrophobicity) depending on the atoms that emerge at the surface [where, for instance, carbon and sulfur are relatively nonpolar, and nitrogen and oxygen are polar (Richards 1977)].

The variation of polarity among the primary faces of succinic acid crystals illustrates this point. As illustrated in Figure 3.2, the polar portion of the succinic acid molecule (the hydrocarboxylic groups) emerge at the $\{001\}$ face, while the less polar portion (hydrocarbon backbone) appears predominantly at the $\{100\}$ and $\{010\}$ faces (Berkovitch-Yellin 1985). The resulting crystal is bounded with faces that vary in polarity and relative hydrophobicity. As a result, certain solvents and impurities have drastically different affinities for the different faces of succinic acid crystals. As emphasized throughout this chapter, it is precisely this chemical and structural heterogeneity of the crystal surfaces that is often responsible for morphological and growth rate modifications in the presence of solvents and impurities.

As the next step in understanding the factors influencing crystal shape, and the effect of solvents and impurities, models

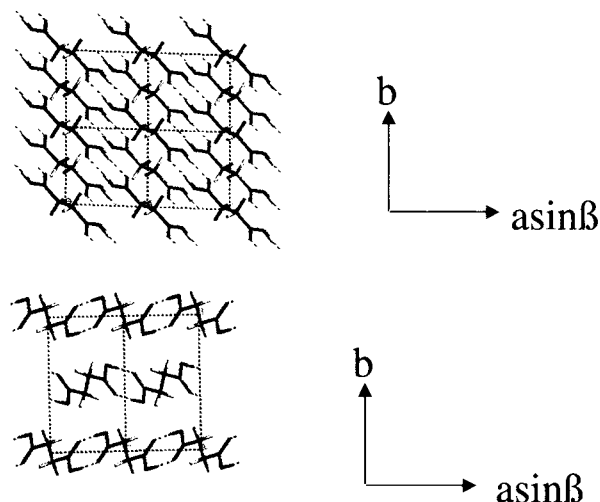


Figure 3.2 Crystal lattice structure of succinic acid.

of various complexities will be discussed. The simplest models are based only on atomic arrangement and spacing (so-called structure-based models) and neglect all interatomic bonding considerations. However, they do provide background in illustrating the central role of crystal lattice structure on the growth of crystals and their interactions with solvents and impurities.

The earliest advances in structure/morphology relationships came from Hauy, which stated that the crystal faces with the simplest indices will predominate on the crystal surface. Gibbs (1906) related the crystal morphology to energetic considerations

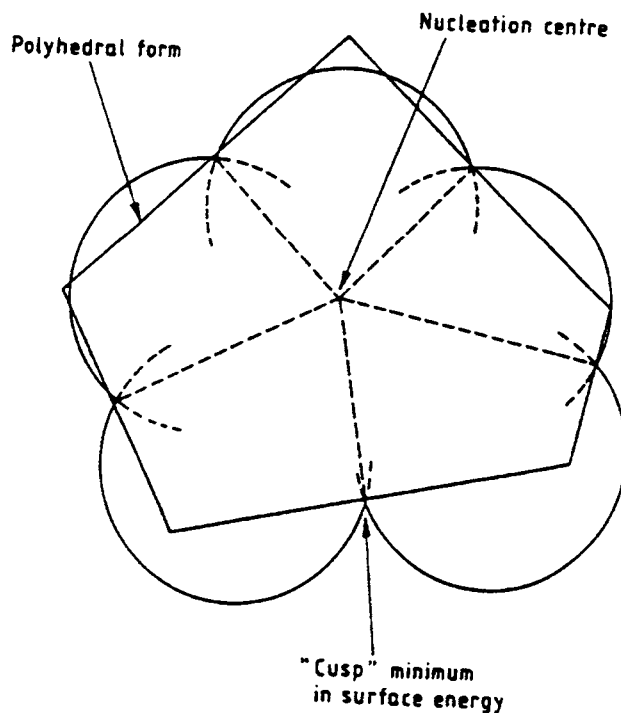


Figure 3.3 Wulff plot for the derivation of equilibrium form. (From *Powder Technology*, 65, "Understanding and Controlling the Crystal Morphology of Some Ionic Crystals," 219–225. Used by permission of Elsevier Science, © 1991.)

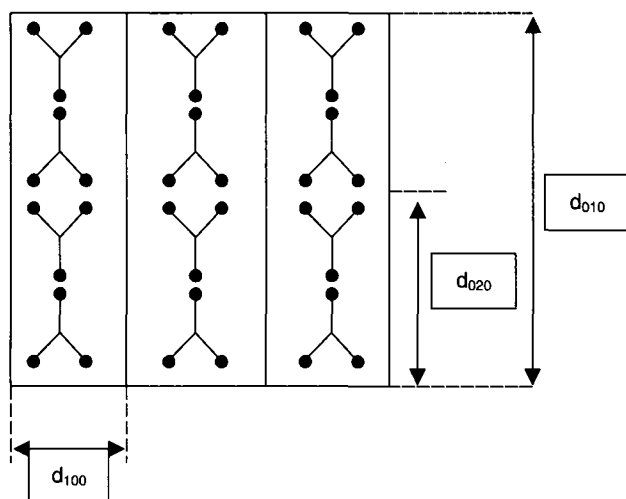


Figure 3.4 Representation of interplanar spacings (d_{hkl}).

stating that the equilibrium crystal morphology was one in which the total free energy was minimised. Wulff (1901) further defined the relationship between surface energy and equilibrium morphology. A Wulff plot is a 3-D polar representation of the surface energy, which reveals (see Figure 3.3) several well-defined minima, which correspond to the expected low surface energy directions for crystal growth. Constructing planes tangent to the cusp minimum for each growth vector results in a regular polyhedron typical for a freely grown crystal.

Later key developments came from morphological simulations based on the geometry of the crystal lattice, developed by a number of workers (Bravais 1866; Friedel 1907; Donnay and Harker 1937); developments commonly now quoted collectively as the BFDH law. The basis of these laws can be qualitatively illustrated with the use of the two-dimensional representation of a crystal lattice in Figure 3.4. It can be noted that the minimum repeat distance varies from face to face. The BFDH law can be summarized as:

“Taking into account submultiples of the interplanar spacing d_{hkl} due to space group symmetry, the most important (MI) crystallographic forms (hkl) will have the greatest interplanar spacings. Hence, if there are two forms

$$(h_1, k_1, l_1) \text{ and } (h_2, k_2, l_2)$$

and

$$d(h_1, k_1, l_1) > d(h_2, k_2, l_2)$$

then

$$MI(h_1, k_1, l_1) > MI(h_2, k_2, l_2)."$$

Using the BFDH law a morphological index can be defined as the reciprocal of the interplanar spacing ($1/d_{hkl}$) and employed as an alternative to surface energy in the Wulff plot. This model can rapidly provide morphological data, however the level of accuracy of the prediction is subject to the degree of anisotropy in the intermolecular bonding within the crystal structure. Typically, a prediction based on energetic considerations would be considered to be a better simulation of the crystal morphology (Docherty and Roberts 1988).

The BFDH model was further refined (Hartman and Perdok 1955) by taking into account bonding within the crystal structure and at the crystalline interface. They laid the foundation for predicting crystal shape based on qualitative considerations of bond energies at growing crystalline interfaces. In general, a strong bond (e.g., the ionic bonding in sodium chloride or the hydrogen bonds between succinic acid molecules) release a relatively large amount of

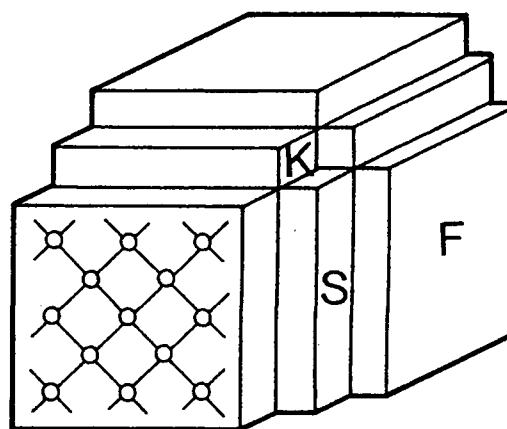


Figure 3.5 Schematic highlighting of “F,” “K,” and “S” faces. (Reproduced with permission from Davey and Garside (2000), from *Molecules to Crystallizers: An Introduction to Crystallization*, 1st ed., OUP, Oxford © University Press, Inc., New York.)

energy when formed and correspond to fast directions of growth. Hartman and Perdok identified chains of bonds within the crystal structure known as Periodic Bond Chains (PBC's). The weakest bond within these PBC's is the rate-determining step and governs the rate of growth along the direction of the chain. Depending on the geometry of the PBC chains, three categories of crystal faces could be defined.

A flat (F) face contains two or more PBC's in a layer d_{hkl} , a stepped (S) face contains one PBC in a layer d_{hkl} and a kinked (K) face contains no PBC's within a layer d_{hkl} . These faces grow by different mechanisms: F faces grow according to a layer mechanism, are slow growing and hence are important faces on a morphology. S faces grow according to one dimensional nucleation, whereas K faces need no nucleation, grow fast and are not normally found on crystals (Figure 3.5). A further development of this theory was the definitions of slice and attachment energies. The slice energy (E_{sl}) is defined as the energy released upon the formation of a slice of thickness d_{hkl} . The attachment energy (E_{att}) can be defined as the fraction of the lattice energy released upon attachment of a slice of thickness d_{hkl} to a crystal surface. This can be visualized pictorially in Figure 3.6. The combination of the slice and attachment energies is known as the lattice energy (E_{latt}).

$$E_{latt} = E_{sl} + E_{att} \quad (3.1)$$

The lattice energy E_{latt} often referred to as the crystal binding or cohesive energy is obtained by summing all the interactions between a central molecule and all the surrounding molecules,

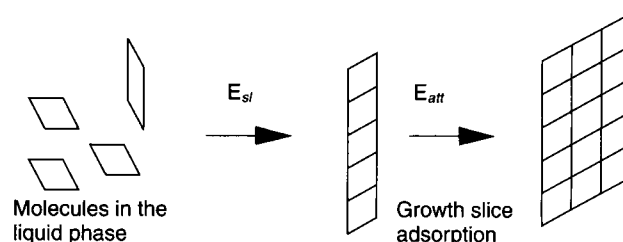


Figure 3.6 Representation of the attachment of host molecules into a slice d_{hkl} releasing energy E_{slice} and consequent attachment of the slice onto a growing surface of a crystal, releasing energy E_{att} . (Reproduced with permission from Walker, 1997.)

including both coulombic and nonbonded van der Waals type interactions.

It was proposed (Hartman and Bennema 1980) that the attachment energy is proportional to the growth rate; the larger the attachment energy (E_{att}) the faster the growth rate and hence the less important the corresponding form within the morphology. This assumption has been shown to be valid for a number of growth theories and has formed the basis for a variety of successful morphology simulations (e.g., Docherty et al. 1991; Black et al. 1990; Telfer et al. 1997; Givand et al. 1998; Grimbergen et al. 1998) and has formed the basis for a number of morphology simulation packages (Clydesdale et al. 1996; Grimbergen et al. 1996; Winn et al. 2000).

It can be seen that the crystal habit of organic systems can be predicted using a variety of models. A more detailed treatment of the aforementioned theories and models can be found elsewhere (Docherty and Meenan 1999). Care must be taken in the choice of the intermolecular potential chosen to simulate the intermolecular interactions and the method of calculating the partial charge associated with each atom. A variety of intermolecular potentials are readily available for the calculation of the interactions required for derivation of a lattice energy and subsequent slice/attachment energies. For inorganic systems however, there are a lack of suitable intermolecular potentials for molecular ions such as phosphates, carbonates, and sulfates, and their interaction, often, with water of crystallization. The means that these potentials often have to be derived before any calculation of morphology can be undertaken. This, in conjunction with the predominance of long range forces, which are not as important in organic systems, hinders such calculations. However, there has been some success in this arena, using both a PBC/attachment energy approach (e.g., Jackson et al. 1995; Clydesdale et al. 1998) and also surface energy considerations (e.g., Fleming et al. 2000; Gay et al. 1995; Sayle et al. 1996).

The preceding models serve to illustrate that crystal faces may form at different rates, depending on factors related to the underlying crystal chemistry and the experimental conditions under which the growth morphology was obtained. In industrial crystallization processes, the influence of solvents and impurities on crystal growth must also be included, as clearly such factors can have a dramatic effect on crystal growth rates and morphologies.

Typically, crystal habits predicted based on crystal chemistry alone are best compared with crystals grown from sublimation processes, or to solution-based systems where the solvent/impurity interactions are negligible. In fact, significant deviations from structure-based predictions are often best explained by such solvent and impurity interactions (Davey et al. 1992; Winn et al. 2000). There are significant efforts underway to understand such phenomena at the molecular level and to consequently predict the influences of solvent and impurities on crystal growth rates. This will be further highlighted in subsequent sections.

3.3. INFLUENCE OF SOLVENTS ON VOLUME AND SURFACE DIFFUSION STEPS

Crystal growth proceeds on a molecular level by the sequential addition of growth units (single solute molecules, ions, or atoms, or possibly clusters of these) to the crystal lattice. In solution growth, these growth units are typically solvated, i.e., closely surrounded by a number of solute molecules that must be rejected at the growing crystal interface. Growth proceeds by volume and surface diffusion steps in series, as indicated in Figure 3.7.

Close to the interface, transport is restricted to molecular diffusion through a diffusion boundary layer, irrespective of the convective conditions outside this region (Rosenberger 1986). The width of the boundary layer, in which transport by molecular diffusion dominates, is a function of the diffusivity of the diffusing

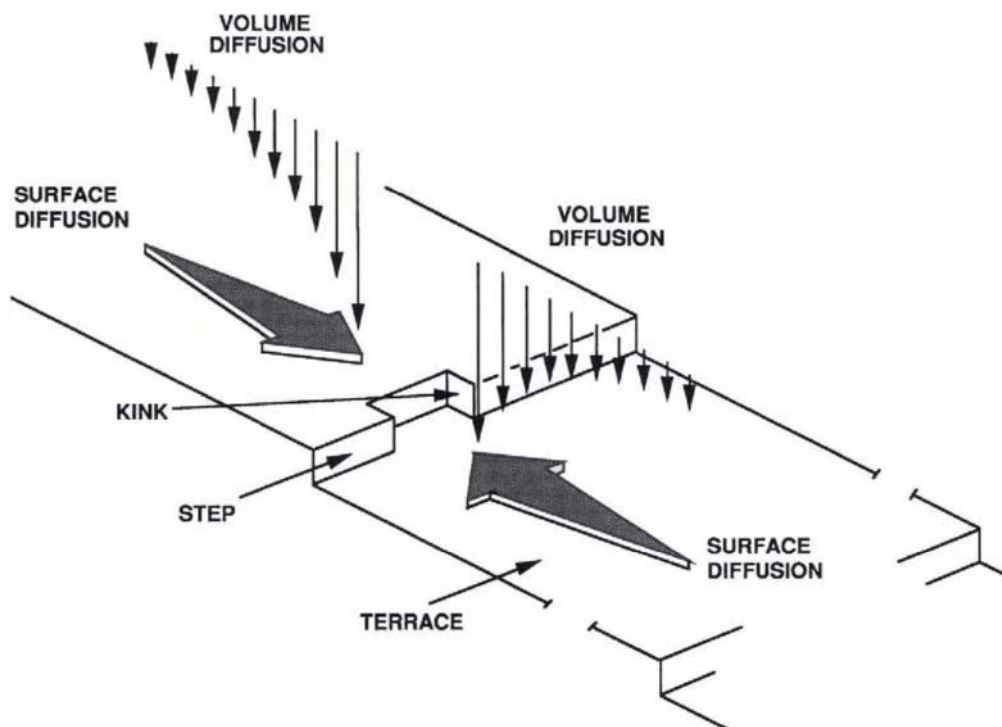


Figure 3.7 Important diffusional processes (volume and surface) affecting crystal growth. (Reproduced with permission from Rosenberger 1986.)

species as well as hydrodynamics near the interface. Consequently, the solvent may influence crystal growth through its effect on viscosity, molecular density, diffusivity, and other heat and mass transport-related properties.

The structural nature of the interface of a growing crystal is still not completely understood, but is perhaps best considered as a narrow region that is, structurally, between the condensed (crystalline) and liquid states. Kinetic studies of the crystal solution interface of ammonium dihydrogen phosphate crystals using synchrotron radiation reveals that this interfacial region is, in fact, highly labile (Cunningham et al. 1990). There has also been a variety of other techniques applied to probe the crystal-solution interface, including grazing angle incidence diffraction and crystal truncation-rod techniques (Robinson 1986; Feidenhans'l 1989; Gidalevitz et al. 1997; De Vries et al. 1998). It should be noted that although the semioordered interfacial region is probably only 10 to 100 Å in thickness, it plays a central role in crystal growth as well as secondary nucleation processes (Mullin 1972).

After the solute molecules diffuse from the bulk liquid phase to the interfacial region, they adsorb on the surface, and under some circumstances, diffuse two-dimensionally on the surface before being integrated into the crystal lattice. During the surface diffusion step, bonds between the solute and solvent molecules are broken, freeing the solute to form bonds with the surface molecules, thus completing its integration into the crystal lattice. This step is referred to as desolvation in general, and dehydration for the specific case of solvated water molecules.

The solvent can directly affect crystal growth through its influence on the desolvation process. Depending on the relative ease and speed in which desolvation occurs, this step can be rate-determining to crystal growth, as in the case of growth of potassium hydrogen phthalate (KAP) crystals from aqueous solution. Crystals of KAP grow by the successive addition of two strongly hydrated ions, potassium (K^+) and phthalate (HP^-), to the crystal lattice (Hottenhuis and Lucasius 1989). The rate-determining step in the growth process is the incorporation of potassium ions due to its relatively slow desolvation rate as compared to the counter ion phthalate.

Another example of dominant solvation effects is observed in the growth kinetics of the {100} faces of KI, KBr, and KCl crystals grown from aqueous solution. The desolvation energies of the anionic species of the potassium halide crystals increase in the order $Cl^- > Br^- > I^-$. Consequently, crystals composed of easily desolvated species are expected to grow fastest. In accordance with this hypothesis, the growth rates of the {100} faces of potassium halide crystals are found to decrease in the order $KI > KBr > KCl$ (Bliznakov et al. 1971).

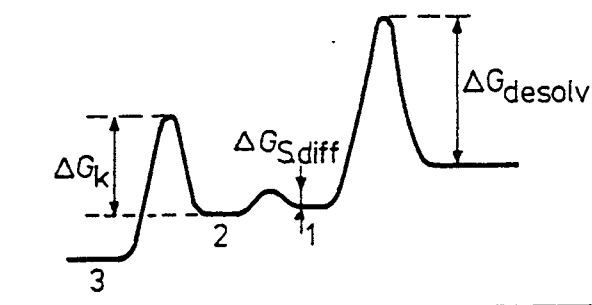


Figure 3.8 Free energy barriers to be overcome during crystal growth. (Reproduced with permission from Davey and Garside (2000), from *Molecules to Crystallizers: An Introduction to Crystallization*, 1st ed., OUP, Oxford © University Press, Inc., New York.)

The relative importance of bulk diffusion, desolvation, and integration depends on the solid-state properties and solution properties. These processes are analogous to a reaction pathway, similar to a homogeneous chemical reaction pathway (Bennema 1969). Pictorially this is represented in Figure 3.8. (Davey et al. 2000). Although the volume diffusion step may be analyzed in a classical manner, the quantification of the surface diffusion steps requires consideration of the structure of the interface as well as the physical and chemical nature of the adsorption and diffusion process. The impact of the strength of adsorption on the surface diffusion process is discussed in Section 3.6.

3.4. STRUCTURE OF THE CRYSTALLINE INTERFACE

To explain the large effect of some impurities at the part per million level on the growth and nucleation of crystals, the presence of key growth sites on the surface that dominate the growth process must be invoked (Davey 1976). Kossel (1934) was one of the first investigators to recognize the importance of atomic inhomogeneities of crystalline surfaces and its relevance to growth processes. Accordingly, some review of this model is useful for illustrating the effect of impurities and solvents on crystal growth.

As illustrated in Figure 3.9, the Kossel model divides the crystal interface into regions having unique structural attributes:

1. Flat surfaces, or terraces, which are atomically smooth.
2. Steps, which separate terraces.
3. Kink sites formed from incomplete regions on steps.

Kossel hypothesized that kink sites present the most probable position for solute integration due to the higher bonding energy

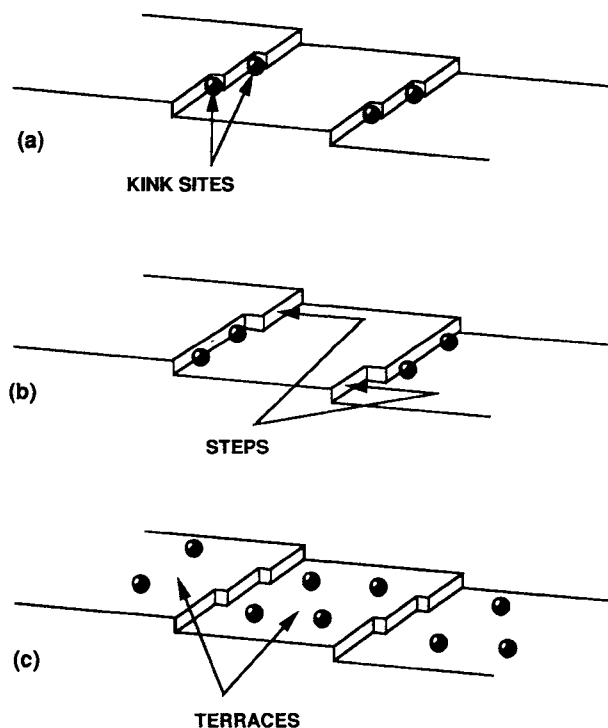


Figure 3.9 Key surface structures on an idealized crystal face: (a) kinks; (b) steps; and (c) terraces. Adsorbed impurities at each of these sites are illustrated. (Reproduced with permission from Mullin 1993.)

associated with integration there. Steps correspond to intermediate binding energy and terraces the lowest, and as a result are energetically less probable sites for incorporation. Since the growth process consists of surface diffusion of solute, diffusion along the step to a kink, and incorporation into the lattice at the kink site, the concentration of kinks and steps become a fundamental quantity in the growth process (Cabrera and Coleman 1963). This in fact is observed; crystal faces that are atomically smooth grow by attachment of solute molecules to step edges either by spiral growth or two-dimensional nucleation growth mechanisms. Faster growth rates are observed on faces that are atomically "rough," i.e., contain numerous kink sites.

Boistelle et al. (1974) confirmed experimentally that three types of adsorption sites do indeed exist on some crystals. In impurity adsorption studies on NaCl crystals, high-energy binding sites, postulated to be kinks on the crystal surface, are almost immediately occupied by a divalent metal additive Cd^{2+} . The other two types of sites, corresponding to steps and ledges, are of lower energy and are occupied less frequently. For example, Brecevic et al. (2000) have indicated that the probability of having a sparingly soluble low molecular weight electrolyte in a step position is in the range (0.7–0.8)% and the probability of having it on the surface is between $(2 \times 10^{-7} - 0.004)\%$. This has been shown by calculations based on the increase of surface free energy caused by the addition of growth units to nonkink positions (Nielsen et al. 1982). Other studies independently confirm the presence of kinks, steps, and ledges on crystal surfaces. The advent of Atomic Force Microscopy (AFM) now allows researchers to be able to visualize crystal growth mechanisms at submicron length scales. This has led to the visualization of the kinks, steps, and ledges previously mentioned and their influence on crystal growth (e.g., Bonafede et al. 1995). Protein crystallization has provided an excellent example of such visualizations. Due to the size of these molecules, it is possible via AFM to monitor crystal growth processes and watch the adsorption onto a growing surface and the consequent migration and incorporation of these growth units into the growing crystal (e.g., Bottomeley et al. 1996). Interestingly, calculations carried out by W.K. Burton et al. (1951) suggest that concentration of kink sites on some faces can be extremely high: perhaps as many as one kink site for every five molecules. However Chernov (1998) has indicated that at a high kink energy/ kT ratio, the density of kinks may be very low compared to the lattice sites, leading to the formation of straight steps.

It has been observed that crystals grow at exceedingly small supersaturation, leading to the conclusion that sources of steps are nearly always present on the crystal surface. The problem of the creation of steps was solved by W.K. Burton et al. (1951), who postulated the existence of crystal dislocations, capable of providing a continuous source of steps on the surface. The resulting layer growth model considers two simultaneous processes at the interface: (1) the continuous creation of steps at a source somewhere on the growing crystal face; and (2) motion of steps away from the source (Cabrera and Coleman 1963). Based on the layer growth model, it follows that impurity adsorption, even at low concentrations but still high enough to poison kinks, can have a dramatic influence on supersaturation (e.g., Sangwal et al. 2000; Kubota et al. 1997; Kubota et al. 1995) and resultant growth kinetics. Qualitatively, this explains the ability of adsorbed impurities at the part per million level to dramatically influence the growth of crystals (Davey 1976). However, the adsorption of an impurity species onto a growing crystal surface can result in conflicting effects (Davey 1979), since the resultant fall in interfacial tension will cause an increased density of steps, while the reduction in surface flux and blocking of kink sites by the impurities will decrease the step advance rate, as discussed by Davey (1976). The action of

impurities at ledges, steps, and kink sites will be considered further in Section 3.6. For a more detailed view of the current view of crystal growth theories, growth kinetics and the surface morphology of crystals, the reader is referred to a number of detailed reviews (Sangwal 1998; Chernov 1998; McPherson et al. 1996).

3.5. FACTORS AFFECTING IMPURITY INCORPORATION

3.5.1. EQUILIBRIUM SEPARATION

Crystallization is frequently used to affect a separation. The ability to achieve purification of materials that are free of impurities at the parts per million level is due to the ordered lattice of a crystal, and more precisely, the energetic penalties for disrupting this order. In order for an impurity to enter the lattice substitutionally (Figure 3.10), impurity molecules must replace host molecules at lattice sites. If the two species are significantly different in size, shape, or chemical composition, this replacement can only be achieved at the expense of distorting the crystal lattice. Distortions, in general, cost a great deal of energy, and thus are energetically unfavorable, i.e., the total energy of the solid solution is greater than the energy of the two pure solids, each in an undistorted crystalline state (Sandler 1977). For this reason, true solid solutions in organic systems are rare and are only expected where the host and impurity are similar in size and shape (isomorphous) (Hildebrand and Scott 1950). Important exceptions do occur, as in the case of the isomorphous pair of organic molecules caproic acid and adipic acid, which separate poorly by crystallization (Narang and Sherwood 1978; Walker 1997; Klug et al. 1994). Moreover, many types of semiconductors are constituted by incorporating small amounts of foreign atoms in the lattice in this manner (Strickland-Constable 1968).

The relative amount of impurity incorporated in the crystalline phase is related in a quantitative way to the energy change upon binding of the impurity molecule relative to the binding change with incorporation of the normal solute molecule (Berkovitch-Yellin 1985). This concept of binding energy is central to calculation of both the influences of additives (e.g., Clydesdale et al. 1996) and solvent (Walker 1997) on crystal morphology. Binding energy calculations have also been shown to correlate with metastable zonewidth (Myerson et al. 1995). An example is the incorporation of carboxylic acids in amide crystals where the degree of incorporation was found limited to 1–2 wt% due to large energy loss in the amide-amide hydrogen bonding relative to

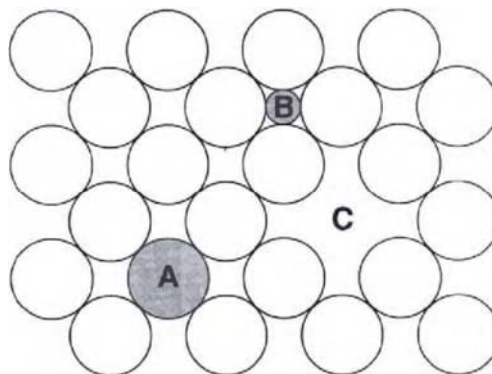


Figure 3.10 Point defects in crystalline lattice: (A) substitutional; (B) interstitial; and (C) vacancy. (Reprinted with permission from J.W. Mullin (1993), *Crystallization*, 3rd ed., CRC Press. © CRC Press Inc., Boca Raton, Florida.)

amide-carboxyl bonding (Wang et al. 1985). Similarly, the incorporation of cinnamic acid into cinnamide crystals does not exceed 0.5% due to the fact that acid/amide hydrogen bonds are less stable than amide/amide bonds and a hydrogen bond is disrupted (Vaida et al. 1989). Aspartic acid, on the other hand, can incorporate up to 20 wt% in crystals of asparagine due to a number of other hydrogen bonds that are formed upon incorporation that offset energy losses from normal bonding modes (Addadi et al. 1982). This inter-relationship between impurity uptake and the impact on crystal structure has also been studied by other authors (e.g., Hendriksen et al. 1998).

It is interesting to note that when small mismatches in size occur, the solubility of small molecules in a host lattice of larger ones is more probable than the solubility of a large molecule in a lattice of smaller ones (Hildebrand and Scott 1950). A striking example of this behavior is found in a comparison of impurity incorporation in L-glutamic acid crystals where incorporation decreases with increasing molecular volume of impurity (Harano and Yamamoto 1982). A similar result is found for the incorporation of cationic species in ionic crystals where the uptake is found directly related to the charge on the species and its molecular size (van der Sluis et al. 1986).

When similarly shaped compounds incorporate at small levels, it is possible to estimate the segregation of impurities in the interfacial region on the basis of thermodynamics, given a number of thermochemical properties of the host and impurity components (Rosenberger 1979). The incorporation can be characterized by a segregation coefficient, K , numerically equal to the ratio of impurity concentration in the solid phase, x_{sol} , to that in the liquid phase, x_{liq} , assuming both phases are at equilibrium at a given temperature. Thus, when crystallization occurs very slowly, the crystal has impurity concentration $x_{sol} = Kx_{liq}$ (Burton, J.A., et al. 1953). For values of K less than unity, purification is achieved, whereas for values greater than unity, the crystalline phase becomes enriched in the impurity. For $K = 1$, no impurity segregation occurs. For example, Chernov (1984) highlights Ruff's rule—for mutually isomorphic inorganic salts that co-crystallize from solution, the lower the impurity solubility in a given liquid solvent as compared to the macrocomponent, the more impurity is incorporated into the crystalline material.

A number of studies have examined the segregation of an impurity between a liquid phase and crystalline phase at equilibrium (Ratner 1933; Hall 1953; Thurmond and Struthers 1953; Burton, J.A., et al. 1953; Weiser 1958; Rosenberger and Riveros 1974; Sloan and McGhie 1988; Woensdregt et al. 1993; Sangwal et al. 2000; Thomas et al. 2000). The simplest case to consider theoretically is that of a dilute binary mixture of B in a nearly pure component A . If both liquid phase and solid phases are assumed ideal, then at equilibrium at temperature T the distribution across both phases is given by

$$\ln K_B = \ln \frac{x_{B,sol}}{x_{B,liq}} = \frac{\Delta H_B^{fus}}{R} \left(\frac{1}{T} - \frac{1}{T_B} \right) \quad (3.2)$$

where $x_{B,sol}$ and $x_{B,liq}$ (expressed in weight or mole fraction) represents the concentration of impurity in solid and liquid phases, respectively. ΔH_B^{fus} is the heat of fusion of the impurity B , and T_B is its freezing point. With the use of Eq. (3.2), only the freezing point and heat of fusion of an impurity is needed to compute its segregation between the liquid and crystalline phase. However, the relative steric and chemical complementarity of the impurity and solute in the solid phase is not taken into consideration, and as a result, only a few systems conform to this elementary relationship.

In a more realistic case, both the solid and liquid phases are assumed to behave regularly (the underpinning assumptions of regular solution theory are discussed in Section 3.9.2) (Rosenberger and Riveros 1974)

$$\ln K_B = \frac{\Delta H_{B,liq}^{dis}}{RT} - \frac{\Delta H_{B,sol}^{dis}}{RT} + \frac{\Delta H_B^{fus}}{R} \left(\frac{1}{T} - \frac{1}{T_B} \right) \quad (3.3)$$

where $\Delta H_{B,sol}^{dis}$ is the heat of mixing in the solid state and $\Delta H_{B,liq}^{dis}$ is the heat of mixing in the liquid state. From Eq. (3.3), it can be seen, qualitatively, that the incorporation of an impurity in the crystalline phase is decreased as the heat of mixing in the solid phase increases. More precisely, depending on the relative values of the heat of mixing terms, the impurity accumulates in the phase (solution or crystalline) in which its presence causes less energy increase (Rosenberger and Riveros 1974).

Plotted in Figure 3.11 is the distribution coefficient of copper in solid silicon. As predicted by Eqs. (3.2) and (3.3), the logarithm of the distribution coefficient is linear with the inverse of absolute temperature. From the slope of this graph, and the known heat of fusion of copper (3100 cal/g), the heat of mixing copper in solid silicon is established to be approximately 55,400 cal/g.

Other models for the segregation coefficient have been developed specifically for the case of solution crystal growth and with less restrictive assumptions that allow for nonidealities in both the liquid and solid phases. For such a development, the interfacial segregation coefficient is redefined in the following manner

$$K_I = \frac{x_{l,sol}/x_{H,sol}}{x_{l,liq}/x_{H,liq}} \approx \frac{x_{l,sol}x_{H,liq}}{x_{l,liq}x_{H,sol}} \quad (3.4)$$

where

$x_{l,sol}$ = mole fraction of impurity in the solid phase

$x_{l,liq}$ = mole fraction of impurity in the liquid phase

$x_{H,sol}$ = mole fraction of host (solute) in the solid phase

(approximately equal to unity under most conditions)

$x_{H,liq}$ = mole fraction of solute dissolved in the liquid phase

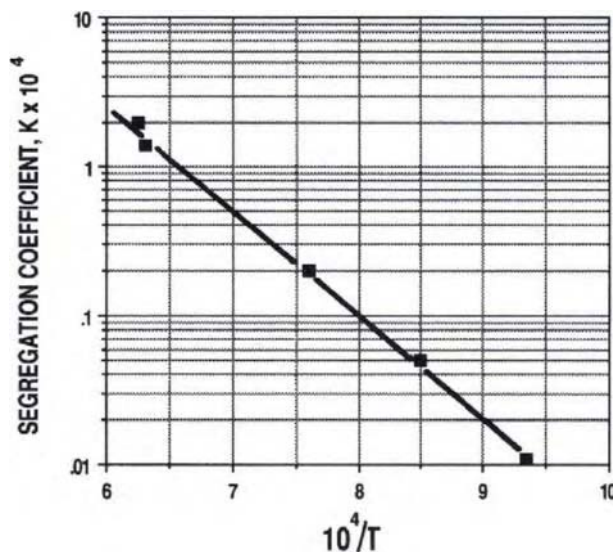


Figure 3.11 Logarithm of the segregation coefficient versus $1/T$ for copper in silicon crystals. (Reprinted with permission from C.D. Thurmond and J.D. Struthers (1953), *J. Phys. Chem.* 57, pp. 831–835. © 1953 American Chemical Society.)

Based on the thermodynamics of solid and liquid solutions, a fairly general expression has been derived by Rosenberger and Riveros (1974) for determining impurity segregation in crystals grown from solution

$$K_I = \left(\frac{\gamma_{I,liq}}{\gamma_{I,liq}^{sat}} \right) \left(\frac{x_{H,liq}^{sat}}{x_{I,liq}^{sat}} \right) \exp \left(\frac{-\Delta H_{I,sol}^{dis} + T \Delta S_{I,sol}^{vib}}{RT} \right) \quad (3.5)$$

Substituting Eq. (3.3) yields

$$x_{I,sol} = \left(\frac{\gamma_{I,liq}}{\gamma_{I,liq}^{sat}} \right) \left(\frac{x_{H,liq}^{sat}}{x_{I,liq}^{sat}} \right) \left(\frac{x_{I,liq}}{x_{H,liq}} \right) \exp \left(\frac{-\Delta H_{I,sol}^{dis} + T \Delta S_{I,sol}^{vib}}{RT} \right) \quad (3.6)$$

where $\gamma_{I,liq}^{sat}$ and $\gamma_{I,liq}$ represent, respectively, the activity coefficient of the impurity at its equilibrium (i.e., solubility) and actual values in solution; $x_{H,liq}^{sat}$ and $x_{I,liq}^{sat}$ represent the solubility ratio of the solute and impurity in solution. The entropy term, $\Delta S_{I,sol}^{vib}$, represents the change in vibrational entropy in transferring the impurity from the solution to the crystalline phase. As before, the heat of solution of the impurity in the solid phase ($\Delta H_{I,sol}^{dis}$) appears in the numerator. Weiser (1958) presents analytical methods for computing $\Delta H_{I,sol}^{dis}$, which are applicable to crystals with simple lattice structures.

Although the activity coefficients of the impurity in solution in the saturated and unsaturated states ($\gamma_{I,liq}$ and $\gamma_{I,liq}^{sat}$) may be different from unity, they are likely to be of the same order of magnitude, hence the ratio $\gamma_{I,liq}/\gamma_{I,liq}^{sat}$ can be considered essentially unity. Weiser (1958) has also shown that in many cases the change in vibrational energy is negligible as compared with the enthalpy change. With these two simplifying assumptions, Eq. (3.6) can be written as

$$x_{I,sol} = \left(\frac{x_{I,liq}}{x_{H,liq}} \right) \left(\frac{x_{H,liq}^{sat}}{x_{I,liq}^{sat}} \right) \exp \left(\frac{-\Delta H_{I,sol}^{dis}}{RT} \right) \quad (3.7)$$

The thermodynamic analyses described provide an important quantitative understanding of impurity incorporation from solution, namely, the factors affecting the separation can be broken into two parts related to: (1) the relative liquid phase behavior of solute and impurities; and (2) the relative solid-state host-guest complementarity. This can be more generally stated, as

$$\begin{aligned} &\text{Impurity distribution coefficient} \\ &= \text{function (solution thermodynamics)} \\ &\times \text{(solid-state thermodynamics)} \end{aligned} \quad (3.8)$$

Considering first the solid-state thermodynamics, the separation from solution is determined by the chemical dissimilarities between the impurity and host (i.e., mismatches in molecular volume, ionic radii, or unfavorable steric interactions). As in the case of crystal growth from the melt, those mismatches have a tendency to increase the energy and entropy of incorporation and correspond to a reduced probability for incorporation in the crystal lattice. For a given impurity-solute system, little can be done to affect changes in the solid-state thermodynamics except through changes in temperature. For melt systems, the solubility of an impurity in the crystal often is a function of temperature, as shown for the case of antimony in solid germanium and copper in solid silicon (Thurmond and Struthers 1953). However, in solution crystallization, the temperature dependence of the solubility of both impurity and

solute in the solution phase may be an even more important factor in the quality of separation. Namely, product purity is improved by crystallization from solvents in which the impurities have high solubility relative to the product material over the likely range of crystallization temperature (i.e., the solvent maximizes the ratio $x_{I,liq}^{sat}/x_{H,liq}^{sat}$). In other words, the highest levels of purification are achieved from those solvents in which impurities are freely soluble. This commonly holds true in industrial crystallization, and explains the strong influence of temperature on some separations through its direct effect on component (solute and impurity) solubilities.

Two other important concentration effects are also worth noting: (1) impurity uptake is proportional to the concentration of impurities in the crystallizer, $x_{I,liq}$, thus efforts should be made to minimize their formation or introduction into the crystallization stage; and (2) the segregation is predicted to improve with increasing solute concentration, $x_{H,liq}$. Thus, a few key thermodynamic considerations can be used to tailor solvents and processing conditions to greatly improve the purification of crystalline materials.

3.5.2. NONEQUILIBRIUM SEPARATION

In industrial crystallizers, the amount of impurities incorporated in the crystalline phase normally significantly exceeds the amount predicted by thermodynamics. This arises from a number of factors, all related to nonequilibrium growth processes (such as inclusion and defect formation) that commonly occur in crystals grown from commercial-scale crystallizers. In such processes, the degree of defects and the level of impurity incorporated is often strongly related to the kinetics of crystallization. In a very general sense, the tendency for defects and impurities to increase with growth rate arises from the fact that arriving molecules (or atoms, or ions) at the growing crystal interface need a certain finite time to settle into their equilibrium positions, thereby avoiding the formations of voids and defects. Because intermolecular forces in crystals are generally weak, molecules arriving at the growing interface are subject to only weak orienting effects. For this reason, rapid growth raises the likelihood of mis-orientations in the lattice with resulting higher impurity capture. In fact, optimum growth rates for molecular crystals (i.e., crystals composed of molecules as opposed to atoms or ions), where the intermolecular forces are relatively small, are a factor of 10 slower than those of ionic crystals where the aligning forces are much stronger (Wright 1987).

Many industrial crystallization processes, by necessity, push crystal growth rates into a regime where defect formation becomes unavoidable and the routes for impurity incorporation are numerous. Since dislocations, inclusions, and other crystal lattice imperfections enhance the uptake of impurities during crystallization, achieving high purity crystals requires elimination of impurity incorporation and "carry-over" by both thermodynamic and non-thermodynamic mechanisms. Very generally, the impurity content in crystals can be considered as the sum of all of these contributions

$$C_{tot} = C_{sub} + C_{ads} + C_{inc} + C_{def} + C_{ml} \quad (3.9)$$

where C_{tot} is the total concentration of impurities found in the crystalline phase under growth conditions. The other terms represent substitutional impurities (C_{sub}) (e.g., impurities distributed monomolecularly throughout the lattice), adsorbed impurities on the crystal surface (C_{ads}), impurities trapped in inclusions (C_{inc}), impurities incorporated at dislocation planes and other defect sites (C_{def}), and impurities left in mother liquid adhering to the crystal surface (C_{ml}).

In industrial practice, the major cause of impurities in the product is frequently incomplete separation and washing of crystals that leaves significant amounts of impure mother liquid with the crystalline phase (C_{ml}). This appears especially true in crude or first-step separations. The mechanical separation of crystalline materials from the liquid phase is beyond the scope of this chapter, but the optimization of this step should not be overlooked in these cases. As the purity of the crystals increase (to over 99.9%), other mechanisms actually become more dominant, and the emphasis shifts to the challenge of minimizing the other modes described by Eq. (3.9), as discussed in the following sections.

Effect of Crystallization Rate on Impurity Incorporation. The thermodynamic analysis given in Section 3.5.1 considered the case of a perfect crystal lattice and the effect of distorting that lattice by the replacement of a host lattice molecule with an impurity molecule. This type of substitutional incorporation can be strongly influenced by the rate of crystal growth, as many published examples show (Hall 1953; Holmes and Kamath 1982; Narang and Sherwood 1978; Rosenberger 1986). The incorporation of lead and tin in potassium chloride crystals, for instance, exhibits a growth-rate-dependent segregation coefficient at all but the lowest growth rates (Malicko 1970). Similar behavior is evident in the data of Figure 3.12, where the effect of crystal growth rate and agitation on the incorporation of antimony in germanium crystals is shown (Burton, J.A., et al. 1953). Industrially, such behavior is frequently observed as the crystallization rate is increased through decreased residence time or increased feed concentration.

The mechanism by which the impurity incorporation increases with growth rate was first thoroughly investigated by J.A. Burton et al. (1953), and later by Wilson (1978a) and Rosenberger (1986). These workers postulated that partial rejection of impurities at the crystal-solution interface (i.e., $K < 1$) cause the concentration of impurities in the interfacial region to increase above its value in bulk solution. Thus with increasing growth rates, impurities can be rejected at a rate faster than they can diffuse into the bulk solution,

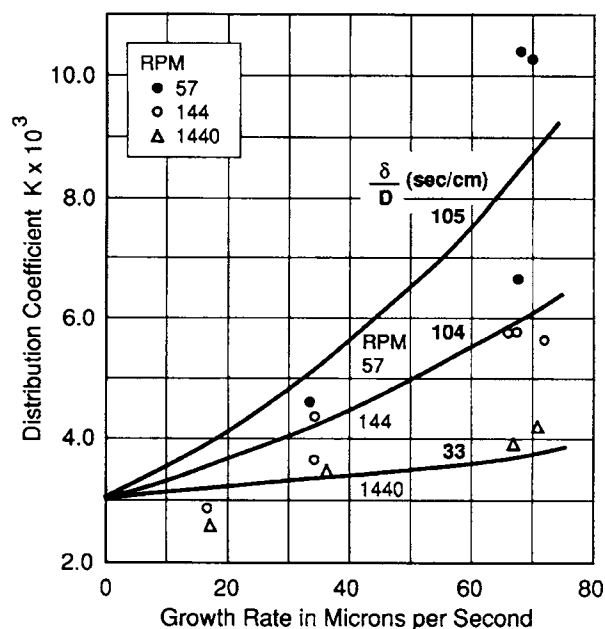


Figure 3.12 Effect of growth rate and agitation on the distribution coefficient of antimony in germanium crystals. (Reproduced with permission from Burton et al. 1953.)

resulting in their accumulation in the interfacial region, as illustrated in Figure 3.13.

The accumulation of impurities in the interfacial region causes an effective increase in incorporation in the crystalline phase relative to that predicted by Eq. (3.5) alone. J.A. Burton et al. developed an expression that quantitatively relates the effective impurity distribution coefficient, K_{eff} , to the equilibrium distribution coefficient, K

$$K_{eff} = \frac{K}{K + (1 - K) \exp\left(-\frac{\delta G}{D}\right)} \quad (3.10)$$

where G is the crystal growth rate, D is the molecular diffusivity of impurity in solution, and δ is a parameter related to the diffusion boundary layer thickness. Various definitions for δ have been proposed, as discussed by Buckley (1951), Wilson (1978b), and Favier and Wilson (1982). Irrespective of its precise value, the diffusion layer is strongly related to the hydrodynamics at the crystal interface, and decreases in thickness with increasing agitation.

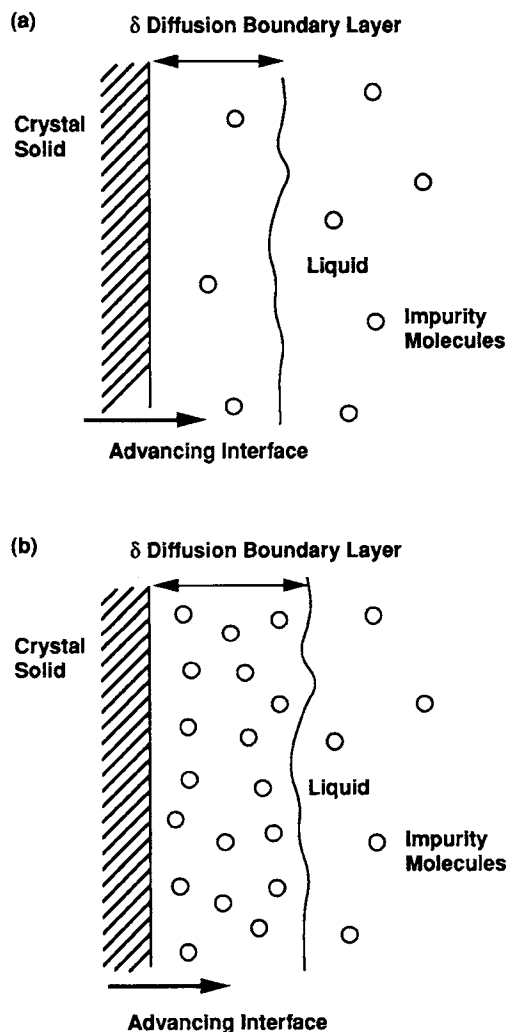


Figure 3.13 (a) Uniform distribution of impurities in solution and boundary layer. (b) Accumulation of impurities in the boundary layer of a growing crystal.

For values of the equilibrium distribution coefficient K much less than unity (i.e., good separation), and low growth rates, the approximate behavior of Eq. (3.10) is given by (Hall 1953)

$$K_{eff} = K \exp(\delta G/D) \quad (3.11)$$

With the use of the Burton-Slichter-Prim model, the influence of crystallizer operating conditions on the amount of substitutional impurity uptake can be assessed. Namely, for values of K less than unity, the quality of separation tends to improve with lower growth rate, increasing diffusivity of the impurity, and decreasing diffusion film thickness. Thus, stronger convection (which reduces the boundary layer thickness δ) is expected to improve separation in these cases (Rosenberger 1986).

As evidenced in the data of Figure 3.12 the separation of germanium crystals from antimony is improved as the stirring rate is increased. In accordance with Eqs. (3.10) and (3.11), the data also show that the separation worsens as the growth rate is increased. However, the sensitivity of the separation to growth rate becomes significantly reduced at the highest agitation levels. Thus, the obvious implications of this model for industrial crystallization includes design for good mass transfer (mixing) in all regions of the vessel, and minimization of crystallization rate (and normally, growth rate) by increased residence time or lowered feed concentration.

Impurity Incorporation at Defect Sites. As explained in Section 3.5.1, the amount of impurity retained by substitutional mechanism is a function of the relative impurity-host chemical and structural complementarity. Interestingly, the degree of complementarity affects nonequilibrium incorporation mechanisms as well. In fact, as Cabrera and Vermilyea (1958) hypothesized, the "molecular fit" of an impurity in the crystal determines whether impurities will primarily reside as adsorbed species (C_{ads}) on the crystal surface, or be incorporated in the lattice (in the crystal bulk) at the moving step fronts (C_{sub}) during growth.

The chemical and structural similarity of impurities to the crystal also influences the spatial distribution of impurities in the lattice. It is known, for example, that certain impurities tend to enter the lattice substitutionally (e.g., monomolecularly), whereas others are found segregated along defects in the lattice, or even aggregated in inhomogeneous distributions. Morantz and Mathur (1972) determined that impurities of similar molecular size and chemistry tend to be distributed monomolecularly at defects in the lattice. By contrast, molecules of greater molecular dimensions, which are less compatible with the host, had a tendency to preferentially aggregate in "macrosegregation" regions of up to a micrometer in size.

The amount of impurities that are found segregated at defect sites, C_{def} , is determined by the type and extent of defects appearing in the crystal lattice (Morantz and Mathur 1971). Since defects form readily from stresses induced by temperature, supersaturation, and mechanical action, large numbers of defects occur in crystals grown in industrial crystallizers. It has, in fact, been estimated that the total number of dislocations in such crystals normally average $10^4/\text{cm}^2$ and can rise as high as $10^{10}/\text{cm}^2$ in "bad" crystals (Strickland-Constable 1968). Hence, it is extremely difficult to grow crystals from industrial crystallizers that are even moderately free of defects.

It is interesting to note that not all defects in product crystals arise from the crystallization process itself. Thermal stresses induced in crystals are sometimes greater during the cooling and drying than during the crystallization period, and can be so large as to crack the crystalline material. These thermal stresses, which can produce defect concentrations on the order of 10^4 – $10^5/\text{cm}^2$,

normally increase as the thermal conductivity of the material decreases (Tiller 1963). The details on this and the numerous other causes of defect formation can be found in several reviews of the subject (Washburn 1958; Tiller 1963; Strickland-Constable 1968; Mullin 1993).

The mechanism by which defects concentrate impurities is a subject of research that has important bearing on crystal growth, especially related to formation of crystalline materials for use in the electronics industry. Besides imperfections associated with isolated impurities (i.e., point defects), the other major types of structural defects are line defects (both edge and screw), planar defects, grain boundaries, and structural disorder (Wright 1989). The connection between defect formation and impurity uptake is evident in two of these defects in particular: the edge defect and point defect.

The edge dislocation is a common position of impurity uptake in crystals mainly due to its unique structure. In edge dislocations the crystal lattice is compressed by the insertion of an extra lattice plane creating numerous sites on the surface that can preferentially concentrate impurities. As indicated in Figure 3.14, the compressed region just above the slip plane can serve as sites for impurities occupying a smaller molecular volume than the host. Conversely, the region below the slip plane presents sites for impurities having larger molecular volumes. As a result, impurities are often found concentrated at dislocation regions compared with more perfect regions of the crystal lattice (Wright 1989).

As illustrated in Figure 3.10, impurities can also reside at "point defects" in the crystal lattice, as occurs when they replace a lattice molecule or occupy a position in the interstices between lattice molecules (termed *interstitial impurity*) (Mullin 1993). In interstitial substitution, the insertion of a foreign species between lattice molecules results in distortion of the lattice since the neighboring molecules are displaced outwards from their normal position (Strickland-Constable 1968). In the case of vacancies, a lattice molecule is simply missing from a lattice site. Depending on the crystalline material, the concentration of vacancies can be large, and can be computed from the expression $n_v = n_o(-E_v/kT)$, where E_v is the energy to form a vacancy, and n_o is typically on the order of $1 \times 10^{15} \text{ cm}^{-2}$ (Cabrera and Coleman 1963). Since E_v is often

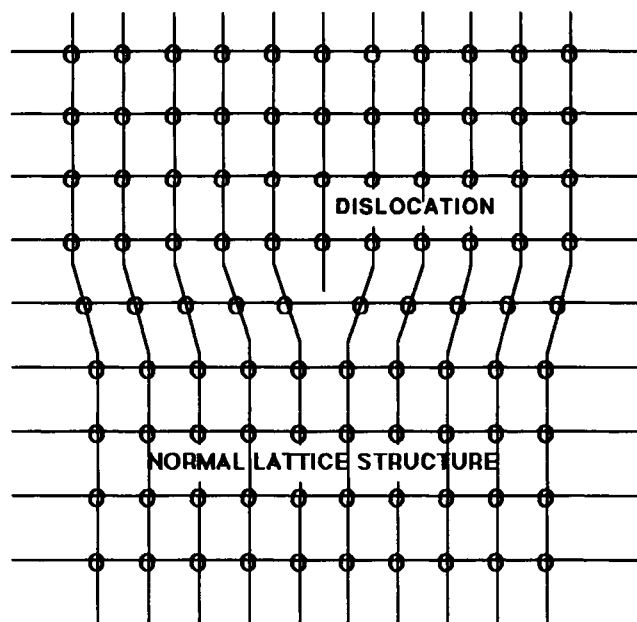


Figure 3.14 Edge dislocation in a crystal lattice.

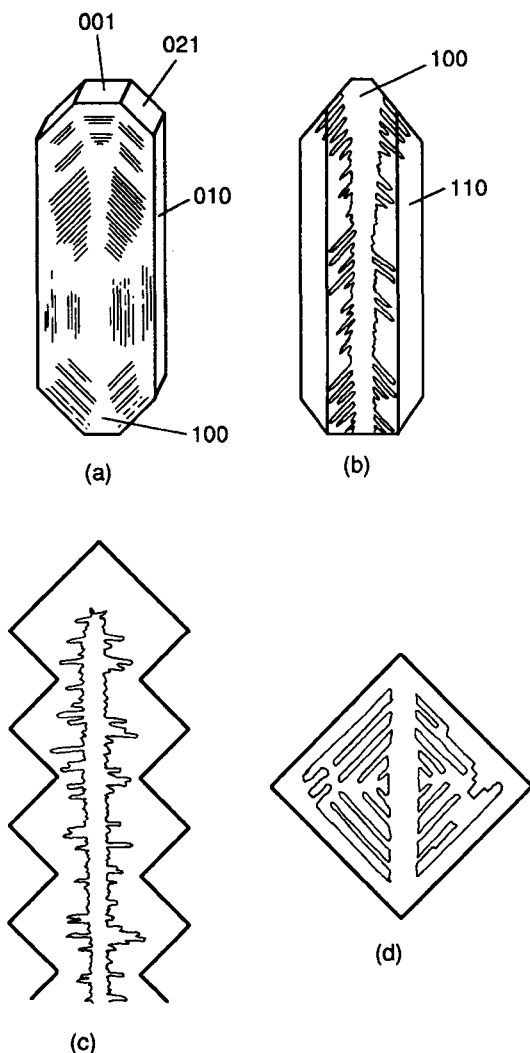


Figure 3.15 Different types of inclusion patterns observed in crystals. (After Buckley 1951.)

comparable to the enthalpy of sublimation of the pure material, vacancies are uncommon in molecular crystals (e.g., crystals composed of molecules) but common in ionic ones (Wright 1989).

Inclusion Formation. Impurities present in macroscopic pockets (C_{inc}), termed *inclusions*, are often a major source of impurity incorporation during industrial crystallization. Their presence in crystals grown from melts and solutions has been widely reported in the literature (Denbigh and White 1966; MacKintosh and White 1976; Wilcox 1968; Janssen-Van Rosmalen and Bennema 1977; Slaminko and Myerson 1981; Myerson and Saska 1984; Smet et al. 1988; Halasz et al. 1993; Zhang et al. 1999). However, there may exist instances where impurity incorporation is erroneously assumed to be by inclusion formation. A recent study by Zhang et al. (1999) however suggested that for eight guest/host systems, the mechanism of guest incorporation was not by inclusion formation, but by solid solution formation. This was based on calculations of the guest/solvent mole ratio in the crystallizing medium and in the putative inclusions. Since crystals grown from aqueous solution can contain as much as 1–2% by weight included liquid, the effect of inclusions on purification can be significant. It has

also been suggested that liquid inclusions contribute to caking problems by seepage of solvent out of the crystals upon storage (Mullin 1993) and can also influence the mechanical properties of the crystals (Law 1994).

Inclusions are generally distributed in a random array in the crystalline matrix, but also may appear in regular patterns, as illustrated in Figure 3.15. A striking example of the latter behavior is reported in hexamethylene tetramine (HMT) crystals where, in almost every product of crystals grown from a batch crystallizer, the crystals exhibited a symmetrical pattern of 12 inclusions (Denbigh and White 1966). Another symmetrical phenomena is the formation of “hourglass” inclusions. For example, acid fuschine dye will be included in growing potassium sulfate (Kahr et al. 1994), forming a distinct hourglass motif (Figure 3.16). A detailed review of the many inclusion types and modes of formation can be found in Buckley (1951), Wilcox (1968), Mantovani et al. (1985) and Mullin (1993).

In order for an inclusion to form, the crystal-liquid interface must break up and grow in an unstable manner (Slaminko and Myerson 1981). Instability of the interface can be related to a number of factors including growth rate, mixing, supersaturation, and presence of certain impurities. In the latter case, impurities have been found, in different instances, to both promote and suppress inclusion formation (Senol and Myerson 1982), hence impurities in the crystallizer are often, but not always, responsible for this undesirable growth behavior.

Most commonly, factors such as rapid crystal growth and uneven levels of supersaturation across the crystal interface are related to the formation of inclusions. The formation of inclusions in the crystals of ammonium dihydrogen phosphate ($\text{NH}_4\text{H}_2\text{PO}_4$) and sodium chlorate (NaClO_3) crystals have, for example, been correlated with sudden step changes in supersaturation (Brooks et al. 1968). Thus, it appears likely that nonuniform concentration and temperature in industrial crystallizers can also promote the formation of inclusions.

The tendency to form inclusions also appears fundamentally related to certain crystal/solution parameters affecting heat and mass transfer to the growing crystal. In particular, inclusions can be influenced by the heat of fusion of the crystalline material, viscosity and thermal conductivity of the solution, and anisotropy of crystal shape (Buckley 1951). Thus, careful control of operating conditions and the choice of a solvent itself may be used to improve purity through a reduced number of liquid inclusions. The latter is true in HMT crystals that readily form inclusions

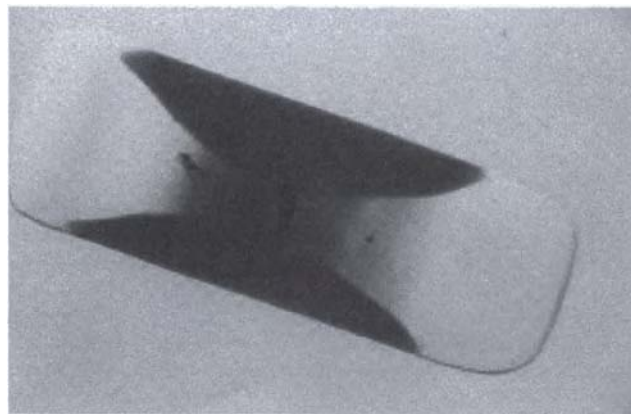


Figure 3.16 Hourglass inclusion of acid fuschine dye in potassium sulfate (Kahr et al. 1993). (Reproduced with permission from Division of Chemical Education, Inc., American Chemical Society.)

from aqueous solutions under most conditions, but rarely when crystallized from methanol or ethanol (Denbigh and White 1966). In this same manner, inclusions can sometimes also be reduced by increasing the viscosity of the solvent (Mullin 1993). Hence, solvent choice should not be overlooked in efforts to improve product purity through reduction of inclusions. There have been other, more exotic means proposed to reduce inclusions. For example, it has been stated that application of ultrasonic energy during crystallization can successfully reduce inclusion content (Anderson et al. 1995). Although not stated by the authors, the ultrasonic energy may be influencing the heat and mass transfer parameters that govern crystal growth.

In addition to the aforementioned factors, inclusions have an interesting tendency to occur more frequently as crystal size increases (Slaminko and Myerson 1981). A mechanistic explanation is given by Brice and Bruton (1974), who conclude that the growth process itself provides a stabilizing effect that decreases as the crystal grows larger. In accordance with this theory, HMT crystals have been found to grow free of inclusions until they reached a critical size of approximately $65\mu\text{m}$ at which point cavities, and eventually inclusions, formed (Denbigh and White 1966). Slaminko and Myerson (1981) also report a critical size for both potassium aluminum sulfate dodecahydrate crystals and sodium chloride crystals. In batch crystallization studies, Denbigh and White (1966) demonstrate that inclusion formation among a batch of crystals decrease with higher stirring rate. In this case, it was postulated that higher stirring speeds resulted in smaller particles, thereby reducing the amount of included liquid through this critical particle size effect. In contrast to this point, it has been suggested that damage to growing crystal surfaces can actually lead to inclusion formation (Garside et al. 1979; Noboru et al. 1999). It was proposed by examination of topographic pictures in the latter publication that inclusion formation could be related to macrostep formation, bunching and the relationship between macrosteps. Thus, damage to crystals could also lead to inclusion formation. Equations have been developed allowing the theoretical prediction of the critical size below which no inclusions are expected to form (Brice and Bruton 1974; Slaminko and Myerson 1981).

3.5.3. EXPERIMENTAL APPROACHES TO DISTINGUISHING IMPURITY RETENTION MECHANISM

Improving product quality by limiting impurity incorporation requires an understanding of all major incorporation mechanisms as well as their root causes. In determining the primary causes of impurity retention, it is necessary to identify the location and type of impurities in the crystalline phase: surface trapped, surface adsorbed, bulk phase, or lattice substituted. A few useful experimental techniques for making these determinations are mentioned below.

Selective Crystal Dissolution. An effective method for distinguishing bulk (lattice trapped) versus surface impurities involves the selective dissolution of a crystal sample while testing the liquid and/or crystalline phases for relative purity. In this technique, a small sample of crystals of a narrow size fraction is washed with successive small amounts of clean solvent until most of the crystalline phase is dissolved. The filtrate and/or crystalline phase are analyzed after each washing to discern whether impurities reside predominantly at the surface, or are more evenly distributed throughout the crystalline phase. The general approach is described by Narang and Sherwood (1978) for quantifying caproic acid incorporation in adipic crystals, and by Addadi et al. (1982) for amino acid separations.

Optical Microscopy. Optical microscopy is an underutilized tool for examining a broad range of crystal imperfections ranging from gross external damage (such as cracks stemming from thermal gradients) to more subtle forms of nonideal growth, as discussed in the previous sections. It is known that when a crystal is rotated on the microscope stage between cross polarizers, departures from uniform extinction will indicate structural defects in the lattice, such as inclusions, twinning, or grain boundaries. Hence, these defects may be counted using microscopy and correlated with operating or run conditions. Reflection type differential microscopy has even been successfully applied to growing crystals from aqueous solution (Tsukamoto and Sunagawa 1985).

The shape and number of inclusions can, in particular, be identified using optical microscopy. Since the shape of inclusions have been linked to formation mechanism (Wilcox 1968), microscopy may give clues for reducing their concentration. For instance, strings of inclusions along the edge of crystals seem to be formed by rapid growth of a crystal previously rounded by dissolution. Temperature increases have been found to correlate with faceted inclusions, i.e., "negative crystals." Veils, or thin sheets of small inclusions, may be caused by cracking and subsequent rehealing. Small or oval inclusions in KNO_3 crystals were found unrelated to growth rate, whereas funnel-shaped inclusions correlated with fast or suddenly increased growth rate.

Optical microscopy is used extensively in the pharmaceutical industry to identify phases (crystalline or amorphous), crystal twinning, epitaxial growth, refractive index, shape analysis, and particle size distribution. As a consequence of the crystal symmetry and space group, most drug substances exhibit anisotropic behavior. The birefringence of plane polarized light is an example of such an anisotropic property and is used to quickly identify the presence of a crystalline phase. Crystallization development studies can be aided by the rapid visual analysis of samples taken during a crystallization reaction to determine the fate of seeds or to monitor particles for possible phase transformations, fracture through mechanical attrition, desolvation, or nucleation mechanism (primary, secondary or epitaxial growth on seeds). Hot stage optical microscopy with cross polars is helpful when interpreting thermal analysis data from a Differential Scanning Calorimeter (DSC) or from Thermalgravimetric analysis (TGA).

Optical microscopy can also be used to determine whether inclusions are liquid or gaseous. The determination may be made by observing a crystal immersed in saturated solution. Upon slow heating, a bubble rising through the liquid from the inclusion is evidence of its gaseous nature. Conversely, if the inclusion is liquid, concentration streamlines will be observed as the liquid from the inclusion mixes with the surrounding saturated solution (Mullin 1993).

The nature of a desolvation endotherm observed in a DSC trace can be assessed by observing whether bubbles appear at regular intervals from a crystallographic face. This may be indicative of a channel structure (Byrn 1999). Alternatively the crystals may catastrophically fracture upon desolvation potentially leading to lattice collapse and no true primary phase transition (melt). Undoubtedly the most common use of crossed polarized light in optical microscopy is to determine a sample's relative crystallinity or not and any gross morphology differences from process to process or habit changes from batch to batch.

The identification of various types of defects in crystals using optical techniques can be greatly extended by etching the crystal surface before examination (Wright 1989). In the presence of an etching solvent, molecules occupying sites at or near defects dissolve more rapidly than molecules in normal lattice positions, leaving pits that can be located and counted. Typical etching agents for this purpose include concentrated sulfuric acid, methanol,

acetone, cyclohexanone, and acetone/water mixtures. Details of these methods can be found in Buckley (1951) and Wright (1989).

Size Versus Impurity Relationship. In investigating the cause of unacceptably high impurities in crystal product, it is informative to divide a representative crystal sample into several different size fractions and analyze each fraction for relative purity. The detection of a size-purity correlation can give insight into the mechanism of impurity retention. In general, impurity content is not expected to be a function of size unless there are significant size-dependent defects among the product crystals (such as sometimes occurs with inclusions), or surface area-dependent adsorption or liquid entrainment. In the second instance, a size-dependent effect is observed due to the fact that small crystals have significantly greater surface area than do larger particles, and as a result, carry over more impurities per unit mass of product by adsorption and adhering liquor. Thus, a high impurity content in the smallest size fraction usually indicates that appreciable amounts of impurities are adsorbed on the crystal surface or retained in adhering liquid. The amount of impurities retained adsorbed on the surface will, in general, follow an adsorption isotherm, as described in Section 3.6.2. When impurities are adsorbed or trapped on the surface, a reduction in the amount of fines in the product by either recycling or destruction can improve purity.

If the size versus impurity analysis shows that relatively greater amounts of impurity reside in the largest crystal size fraction, this can indicate the presence of inclusions, or other crystal size-dependent defects. In such a case, a complimentary technique, such as optical microscopy, can be applied to confirm the type and distribution of defects in the crystalline phase.

The ability to impact product purity through tailoring product size distribution is illustrated in quality improvements achieved in the Union Carbide (South Charleston, West Virginia) process for crystallizing high purity bisphenol A (Moyers 1986). Improving crystal quality from operating levels of 99.5% (original levels) to 99.9% (goal level) required the identification of the mechanisms by which trace impurities were carried with the product. In this case, carryover occurred mainly from adhering mother liquor on crystal surfaces. Accordingly, the quality index for the product (in this case, color) was found to improve as the amount of fine crystals in the product was reduced.

Based on these findings, quality improvements to 99.8% were obtained by increasing particle size through a combination of fines destruction and temperature staging. The remaining traces of impurities in the crystalline product were trapped inside the crystalline phase. A recrystallization process to remove residual impurities in the lattice resulted in product quality of up to 99.99% bisphenol A. Thus, the successful upgrading of this process resulted from investigative work to discover both the source and carry-over mechanisms of impurities during crystallization.

Surface Analyses. There are an increasing variety of characterization tools that now can be applied to characterize crystal surfaces and the distribution and nature of defects in crystals. A review of many of these techniques is given by Brune et al. (1997). Kelly (1987) has provided an informative review of many of these techniques. The specific application of these techniques to defect recognition in crystals is covered in Wright (1989) or in optical crystallography texts (e.g.). X-ray techniques (including laboratory and synchrotron sources) have become standard within the crystallization arena. Imaging tools now include Scanning Electron Microscopy (SEM), Scanning Tunneling Microscopy (STM) and Atomic Force Microscopy (AFM), in addition to

standard optical microscopy. Frequently, these techniques are being applied to *in-situ* experiments, allowing real-time data to be gathered. There are numerous articles that can be found on the applications of X-ray radiation to crystallization. X-rays allow us to probe the internal structure of crystals and is the primary tool for elucidating the presence of lattice defects and the position of impurities within the lattice (e.g., Authier et al. 1991). Synchrotron X-ray radiation experiments have become increasingly more common, as synchrotron radiation can have many advantages over conventional laboratory sources for crystallization. These advantages provide the ability to discriminate between species containing different atoms due to the wide spectral range of uniform intensity, and also the high photon flux and intensity, allowing rapid experimentation and the ability to penetrate the growth environment for *in-situ* studies of the growth processes. An excellent review by Roberts (1993) outlines a variety of applications of synchrotron radiation to crystallization. There are a variety of X-ray techniques that can be utilized in crystallization experiments. For example, X-ray transmission topography is still one of the most commonly applied techniques for assessing crystal quality (Wright 1989; Klapper 1996). Crystal defects, e.g., dislocations and defects induced by impurities are identified by regions of contrast in the reflecting beam. This technique is particularly useful in the characterization of nonlinear optical materials, where the presence and distribution of crystal defects dictate the crystal properties. An example of this type of study example of this is given by Halfpenny et al. (1997). Powder X-ray diffraction has traditionally been used for phase identification and quantification, although there are a number of studies where *in-situ* X-ray diffraction has been used to determine when crystallization has occurred and whether the correct polymorph has been obtained (e.g., MacCalman et al. 1995; Craig et al. 1999; Norby et al. 1999). Grazing incidence X-ray diffraction (Weissbuch et al. 2000) studies have been used to study two dimensional chiral separations. The nature of impurity incorporation during crystallization and the local environment of impurities within the crystal lattice can be probed using extended X-ray fine structure (EXAFS) (e.g., Cunningham et al. 1995).

Scanning electron microscopy (SEM) is a useful method for examining internal and external morphology as well as gross defect structure of crystals. It is well suited for the identification of inclusions in crystals, as illustrated in the SEM of an adipic acid crystal in Figure 3.17. To obtain this cross-sectional sample, the crystal (originally 700 μm in size) was cleaved with a scalpel. Smaller crystals can be cooled with dry ice or liquid nitrogen and fractured. As evident from this figure, the number and size of cavities in the crystalline phase can be clearly and unambiguously determined. Higher magnification images of areas can also be obtained. A related technology, transmission electron microscopy, can also be employed for examining the detailed defect structure in crystals. However, crystal samples of $<0.5\text{-}\mu\text{m}$ thick are needed, hence chemical thinning of the samples (with the use of jet polisher, for example) is normally necessary. Contrast arising from defects shows up in final images in an analogous way to X-ray topography (e.g., Wright 1989).

In the unusual instances where impurities are incorporated at extremely high concentration in the crystalline phase ($>5\text{ wt}\%$). X-ray diffraction has been successfully used to determine the precise atomic positions of the impurity in the host crystal (Wang et al. 1985). Secondary ion mass spectroscopy has also been used to map the distribution of impurities in inorganic crystals. Other techniques, such as scanning tunneling microscopy, have been applied to crystallization (Wichman et al. 1990) and offer potential to observe surface features and atomic arrangements on the order of fractions of a nanometer.

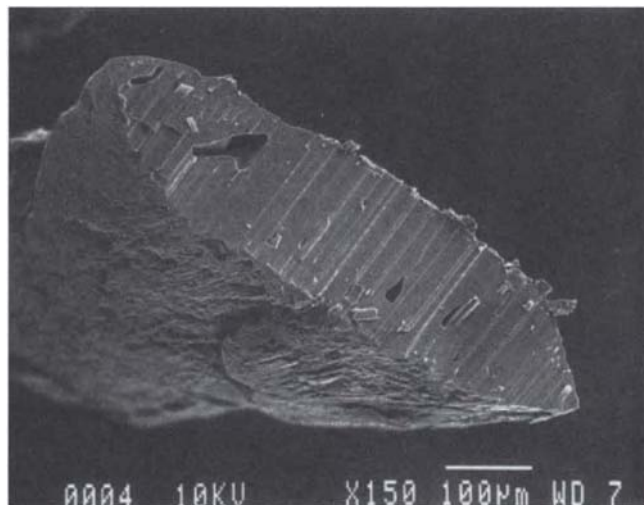


Figure 3.17 An inclusion in an adipic acid crystal examined with scanning electron microscopy.

It is necessary to gain a fundamental and “real world” understanding of the nature of crystal growth before one can attempt to apply “crystal engineering” techniques to enhance a material’s desirable characteristic or minimize the effect of a material weakness. Recent inroads in the field of Atomic Force Microscopy (AFM) have allowed researchers to observe crystallization processes in real time (Mao 1997; Konnert 1994). The past decade has seen a tremendous surge in structural surface chemistry research (Bottomley 1996; Jandt 1998). Scanning Probe Microscopy (SPM) has played a leading role because it has the capability to resolve at the atomic scale and relative cost to electron microscopy. Techniques such as SXM (where the X signifies the numerous chemical properties measured), Energy Dispersive X-ray Analysis (EDAX), and X-ray Emission (EXAFS) allow the experimentalist to “watch” crystals evolve and decay and thus provide evidence to quantitatively describe surface chemistry mechanisms. In addition, the characteristics of the growth unit and the mechanism by which incorporated into high energy sites, requires non-destructive *in-situ* techniques such as laser interferometry (Smol’skii 1985) and electronic speckle interferometry (Piano 2000).

Mechanisms of crystal growth, morphological changes, kinetics, defect structure, and surface lattice parameters have been reported on numerous organic (Overney 1991; Mao 1997; Last 1998), inorganic (Ott 1994; Hillner 1994; Bosbach 1995; Marinkovic 1996), and macromolecular (Konnert 1994; Nakada 1999; Malkin 1999; Braun 2000; Yip 2000) systems.

AFM takes advantage of the complementary bulk surface characteristics such as elasticity, adhesion, and cohesion utilizing electrostatic and van der Waals forces to provide a detailed map of the crystal surface at the 10–100 nm² area.

It is now routine to incorporate methods such as Energy Dispersive X-ray Analysis (EDAX) and Atomic Force Microscopy (AFM) into the battery of tests used to characterize surface chemistry. In addition, EDAX and AFM, Scanning Tunneling Microscopy (STM) offer similar advantages over the traditional long established techniques, X-ray diffraction and neutron scattering. Bulk characterization techniques such as X-ray diffraction and neutron scattering average over large volumes of the sample obscuring the critical differences in surface chemistry that distinguish materials in solid state reactions. STM and AFM allow the

experimentalist to image atom relationships on a surface (Frommer 1992).

To obtain a reproducible image with an STM, the surface molecules must be immobile and oriented. Small changes in atom positions relative to the bulk are distinguishable. For example, smectic *d*-spacings of 4-*n*-alkyl-cyanobiphenyl for a series of alkyl chain lengths (*n* = 6, 8, 10, 12) were analyzed using STM (Smith 1989). A correlation of average *d*-spacings from STM surface analysis and X-ray diffraction studies of single crystals demonstrates the difference between bulk structure and surface structure. The *d*-spacings for alkyl chain lengths of 8, 10, and 12 are on average 1.2 times greater from STM images than those measured from X-ray structure data (Smith 1989; Brownsey 1980; Leadbetter 1979). This type of lattice relaxation at the crystal surface may result from interfacial forces and slight changes in molecular conformation that may lead to unexpected surface effects such as impurity incorporation or solvent induced growth changes. It would be prudent not to extrapolate bulk inter- and intra-molecular relationships to explain surface chemistry without investigating the structure of the surface with an appropriate technique.

In-situ crystal growth kinetics for normal growth (or dissolution) rate and the surface tangential velocity (step velocity) data can be obtained using laser interferometry (Shekunov 1997a). This technique presents a topographical map of the growing crystal face and allows the study of various crystallization parameters (i.e., degrees of supersaturation) on liquid inclusion formation, dislocation site and defect formation mechanisms (Shekunov 1997b). The same technique has been used to identify the mechanism of crystal dissolution in slightly undersaturated solutions. Laser interferometry and X-ray transmission topography have been used to enhance our understanding of the role dislocation sites play in impurity incorporation and associated adsorption mechanisms (Chernov 1988; Ristic 1997; Shekunov 1995).

In lieu of structural information from X-ray diffraction studies to determine the chemical moieties resident on morphologically important crystal faces EDAX can be employed to identify the different atoms present on a given surface. (Joseph 1997; Goldstein 1997).

Extensive lattice relaxation such that the surface is theorized to be highly disordered is the basis for explaining various physical chemical phenomena for organic small molecules. Water vapor sorption to crystal hydration or potentially to the point of deliquescence, physical instability, chemical reactivity, changes in solubility, and interparticle bonding during compaction (Kontny 1995; Nyström 1996; Hancock 1997; Buckton 1999) are all dependent on the physical chemical characteristics of the morphologically important crystal surfaces.

3.6. EFFECT OF IMPURITIES ON CRYSTAL GROWTH RATE

3.6.1. EFFECT ON THE MOVEMENT OF STEPS

The adsorption of impurities and their specific effect on growth processes can be explored within the framework of the Kossel model described in Section 3.4. As a starting point, the chemical bonds that form between the impurity, solvent, and crystal determine whether the impurity will ultimately adsorb on terraces, steps, or ledges. To a large degree, the process of impurity adsorption, diffusion, and integration is analogous to the growth process by solute transport and integration at the interface. Accordingly, the relative “mobility” of the impurity on the crystal surface, and its tendency to incorporate in the crystal lattice, depends on a number of factors that are influenced by temperature, concentration, and supersaturation. As a general rule, the “efficacy,” or

degree of adsorption, of an impurity (or additive), diminishes with increasing growth rate and temperature (Buckley 1951). Other important factors determining efficacy relate directly to the structure and chemistry of the crystal interface, i.e., the atomic roughness and the atom types that appear. The thermodynamic parameters that affect the degree to which these adsorbed impurities incorporate into the lattice are discussed in Section 3.5.1. The adsorption process, and its effect on crystal growth, will be covered in this section.

Surface adsorbed impurities can reduce the measured growth rate of crystals by reducing or hindering the movement of steps on the crystal surface. Depending on the amount and strength of adsorption, the effect on crystal growth can be extreme or hardly noticeable. These two limiting extremes can be qualitatively related to limiting adsorption mechanisms: (1) completely "immobile" impurities that adsorb and remain fixed at the site where they first reach the crystal surface; and (2) completely "mobile" impurities that adsorb and then diffuse "two-dimensionally" on the surface. The strength of bonds between the lattice molecules and impurity determines the relative mobility of the impurity. In this section it will be shown that the relative mobility of an impurity relates to its effect on crystal growth rate, surface structure, and morphology. In Section 3.7, the specific chemical interactions that determine the relative strength of adsorption are explored.

Cabrera-Vermilyea Model. Cabrera and Vermilyea (1958) hypothesized that strongly absorbing, "immobile," impurities can adsorb on terraces of crystal surfaces and "pin" steps, thus drastically impeding the step movement relative to that expected without impurities present. Figure 3.18 is a schematic picture showing the qualitative effect of immobile impurities on step movement. Cabrera and Vermilyea suggested that step movement, and hence, growth rate, would be halted altogether when the distance between impurities on the surface was $<2\rho_c$ apart, where ρ_c was postulated to be the medium radius curvature of a step. For spacings greater than this, the step may squeeze past the adsorbed impurities, but in doing so lose its characteristic shape and be reduced in velocity.

Although the Cabrera-Vermilyea model represents an idealized picture of the growth and interaction process, experimental observations of the features and movement of the steps on crystal faces validate the model (van der Eerden and Müller-Krumbhaar 1986). A striking example is the effect of Al^{3+} adsorption on the

{010} faces of KAP crystals, which causes normally polygonized growth spirals to become almost round with a smaller step velocity (Hottenhuis and Lucasius 1986). The addition of a strongly adsorbing impurity (Cr^{3+}) to KAP crystals has also been shown to completely block the growth (i.e., velocity of step, $v = 0$) at concentrations as low as 16 ppm, in accordance with the prediction of Cabrera and Vermilyea.

With the assumption that the source of new steps on the crystal surface is a spiral defect, Cabrera and Vermilyea developed an approximate expression for the reduction in step velocity in the presence of immobile impurities.

$$v_l = v_p \sqrt{1 - 2\rho_c d^{1/2}} \quad (3.12)$$

where $d^{1/2}$ is assumed to be the average density of impurities on the ledge ahead of the step (number of impurities/area), and v_l and v_p represent the step velocity with and without impurities present, respectively. Eq. (3.12) indicates that the velocity of steps in the presence of impurities is reduced by an amount proportional to the concentration of adsorbed impurities on the terraces. When the concentration of impurities becomes so high that the distance between them becomes less than the critical radius, then step movement is blocked and, by definition, $v_l = 0$. If the concentration of impurity on the surface is assumed to be in equilibrium with the concentration of impurity in solution, then the average density of adsorbed impurities can be correlated with the use of an adsorption isotherm (Cabrera and Vermilyea 1958; Black et al. 1986; Black and Davey 1988), allowing the reduced growth velocity, v_l , to be determined. Additional details are given in Section 3.6.3.

The hypothesis that impurities can significantly retard crystal growth is verified in industrial practice, especially in highly impure systems such as found in the first ("crude") steps of crystallization. A large growth rate reduction by impurities can manifest itself in an industrial crystallizer by the production of ultrafine particles, or in some cases, agglomeration of small ones. Under some circumstances, exceedingly slow growth rates from strongly adsorbing impurities may contribute to a slow approach to equilibrium, (i.e., a "Class I" separation) where the mass of crystals produced is less than that predicted based solely on solubility data.

The Cabrera-Vermilyea model also implies the existence of a critical supersaturation below which no growth would take place in the presence of impurities. Mathematically, this is given by the condition $d^{1/2} < 2\rho_c$, indicating that the density of impurities has reached the point where step movement by two-dimensional nucleation is prohibited. The size of the critical two-dimensional nucleus is related to supersaturation through the expression (Cabrera and Vermilyea 1958; Black et al. 1986)

$$2\rho_c = \frac{2a\gamma_{\text{surface}}}{kT\sigma} \quad (3.13)$$

where a is a lattice constant, γ_{surface} is the interfacial tension, k is the Boltzman constant, and σ is the supersaturation. Equation (3.13) indicates that the size of the critical two-dimensional nucleus varies inversely with the supersaturation driving force. Since the size of $2\rho_c$ relative to the impurity spacing on the surface determines whether steps can advance or not, Eq. (3.13) indicates a critical supersaturation for growth. Specifically, as supersaturation levels are lowered, more significant impurity effects (such as extremely reduced growth rate) are expected to result. At the other extreme, where the density of adsorbed impurities molecules is small, or the supersaturation levels are very high (i.e., $d^{1/2} \gg 2\rho_c$), the movement of steps depends on the concentration of unaffected kink sites in the classical manner.

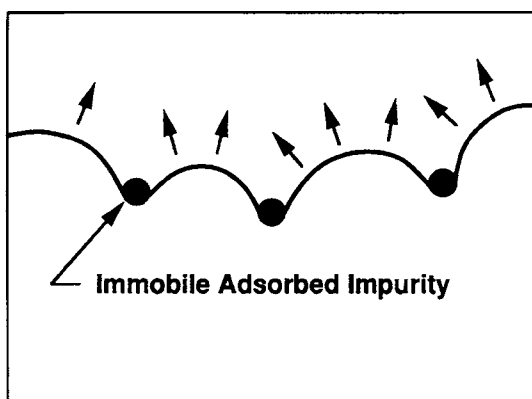


Figure 3.18 Pinning of an advancing step by immobile adsorbed impurities. (Reprinted with permission from *Electrochimica Acta*, vol. 31, no. 8, J.P. van der Eerden and H. Müller-Krumbhaar, "Formation of Macrosteps Due to Time Dependent Impurity Adsorption," © 1986, Pergamon Press, Ltd.)

An intriguing class of compounds that exhibits many of the theoretical attributes of immobile impurities are the so-called "tailor-made" additives. These are compounds that are "designed" (i.e., synthesized) to have certain structural and chemical characteristics of the "host" (crystalline) phase. As a result of the relative host-impurity complementarity, these impurities have a tendency to strongly adsorb and, in some cases, incorporate into the bulk at concentrations as high as 20 wt%. Consequently, the application of the Cabrera-Vermilyea model is particularly appropriate, and has been successfully used to model certain tailor-made additive systems (Black and Davey 1988).

Figure 3.19 shows kinetic data for crystal growth in the presence of several tailor-made additives that illustrates one of the most important predictions of the Cabrera-Vermilyea model, namely, the growth rate approaches zero as the adsorbed impurity concentration increases. This model explains, in a general way, why impurities in industrial processes that are structurally similar to the product often have an extreme effect on product crystal size and shape. More details are given in Sections 3.6.2 and 3.6.3 on adsorption-based growth models and tailor-made additives.

The differences between immobile and mobile impurities on crystal step movement can be summarized. Immobile impurities impede the movement of steps and may become incorporated as steps move around and past them, whereas mobile impurities are normally swept away from each advancing step. In general, strongly adsorbing impurities are expected to have a much greater effect on the growth rate of crystals than impurities that tend to be less strongly bound. In industrial crystallization processes, strongly bound impurities are also expected to be found in greater concentrations in the product crystals than more loosely bound impurities.

Conversely, the main effect of mobile impurities on the rate of advance of steps is probably through adsorption at kink sites rather than adsorption on ledges as for the case of immobile impurities. Since the rate of advance of steps is directly related to the density of kink sites on the steps, large reductions in crystal growth rate may still occur if these sites are selectively "poisoned" by adsorbed impurities. For instance, it was found that only 4.5% surface coverage of the additive nitrilotri(methylenephosphonic acid) on barium sulfate crystals is needed to completely inhibit crystal growth (Leung and Nancollas 1978). This supports the conclusion that many additives, including loosely bound ones, may effectively slow growth by adsorbing at a relatively small number of key growth sites on the crystal surface (Davey 1982a).

3.6.2. IMPURITY ADSORPTION ISOTHERMS

Since the adsorption of impurities at the crystalline interface affects growth rates, it is useful to have quantitative measures of the amount of adsorption occurring. Hence, the focus of this section is on the description of quantitative, macroscopic methods of measurement, and mathematical modeling of impurity adsorption on crystal faces. In this regard, it should be pointed out that the *direct* measurement of adsorption is experimentally challenging, and has only been reported for a few specific systems. In one such case, measurements of the adsorption of impurities on barium sulfate crystals were accomplished using C^{14} -labeled additives (Leung and Nancollas 1978). In similarly exacting experiments, Curreri et al. (1981) have used both radioisotopic as well as electrophoresis experiments to measure the adsorption of citrate ions on calcium oxalate monohydrate. These methods and other types

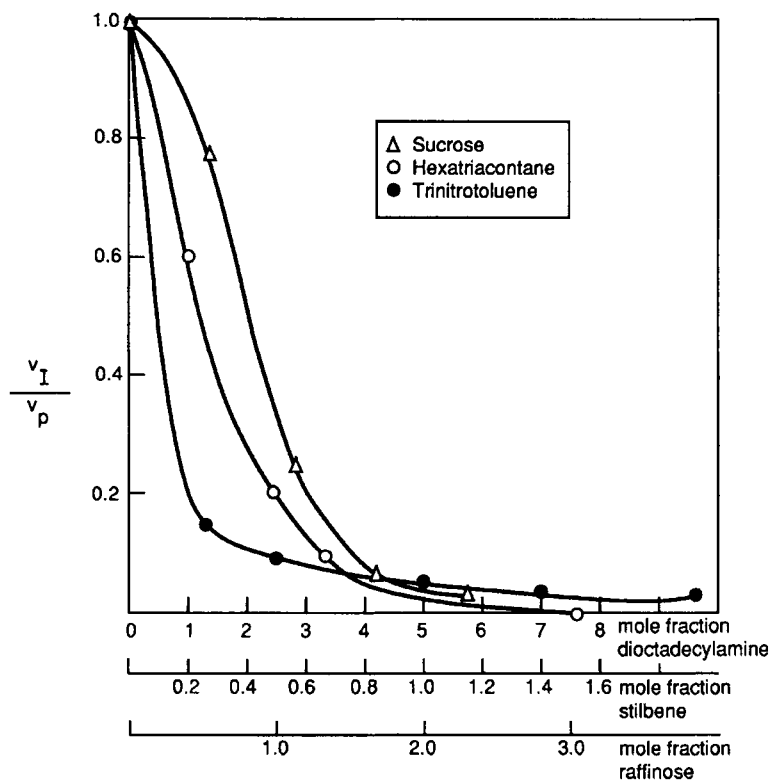


Figure 3.19 Growth rate of crystals grown in the presence of "tailor-made" additives. (Reproduced with permission from Black et al. 1986.)

of experiments for direct adsorption measurements are reviewed by Davey (1982b).

Macroscopic models of adsorption are probably more useful for elucidating information about the nature of adsorption sites and valuable in developing models that can relate the concentration of adsorbed impurity to its concentration in the solution phase. There are several ways to mathematically model adsorption, but the most common method is with the use of an adsorption isotherm that relates the amount of impurity adsorbed per unit mass of crystals (or per unit area of crystal) at a fixed temperature to the concentration of impurity in solution. A type of adsorption isotherm commonly observed experimentally is the Langmuir isotherm (Langmuir 1918) of the general form

$$q_l^{ads} = q_l^{mono} \left(\frac{K \cdot x_{l,liq}}{1 + K \cdot x_{l,liq}} \right) \quad (3.14)$$

where q_l^{mono} (mol/cm²) is the surface concentration of adsorbed impurities at monolayer coverage, $x_{l,liq}$ is the mole fraction of impurity in the liquid phase, and q_l^{ads} (mol/cm²) is the concentration of adsorbed impurities. The parameter K is termed the *Langmuir constant* and is defined by the expression $K = \exp(-\Delta G/RT)$, where ΔG is the free energy of adsorption.

The surface concentration of adsorbed impurity may be determined experimentally using the following expression (Rosen 1989)

$$q_l^{ads} = \frac{\Delta C_{l,liq} \cdot V}{a_s \cdot m} \quad (3.15)$$

where $\Delta C_{l,liq} = C_{l,liq}^0 - C_{l,liq}$; $C_{l,liq}^0$ (mol/l) and $C_{l,liq}$ (mol/l) are the molar concentration of impurities in solution before and after adsorption; V (l) is the volume of the liquid phase; m (g) is the mass of crystals; and a_s (cm²/g) is the surface area per unit mass of crystals.

Rearranging Eq. (3.14) yields a useful linear form

$$1/q_l^{ads} = 1/(x_{l,liq} \cdot K \cdot q_l^{mono}) + 1/q_l^{mono} \quad (3.16)$$

where a plot of $1/q_l^{ads}$ versus $1/x_{l,liq}$ gives a straight line of slope $1/K \cdot q_l^{mono}$ and intercept $1/q_l^{mono}$.

The specific surface area of the crystalline phase, a_s , can be computed using adsorbates of a known cross-sectional area. Some of the criteria for carrying out this determination are discussed by Kipling (1965), Gregg and Sing (1982). Solutes for this determination include steric acid from benzene solution (Daniel 1951; Kipling and Wright 1962) and *p*-nitrophenol from aqueous or xylene solution (Giles and Nakha 1962). When the specific surface area of the crystalline phase is unknown and cannot be directly measured by these methods, an alternative adsorption relationship can be used

$$n_l^{ads} = n_l^{mono} \left(\frac{K \cdot x_{l,liq}}{1 + K \cdot x_{l,liq}} \right) \quad (3.17)$$

where n_l^{ads} is the amount of impurity adsorbed per unit mass of crystals (in mol/g) and n_l^{mono} is the corresponding amount adsorbed at monolayer coverage (in mol/g). The linearized form of Eq. (3.17) is

$$1/n_l^{ads} = 1/(x_{l,liq} \cdot K \cdot n_l^{mono}) + 1/n_l^{mono} \quad (3.18)$$

where a plot of $1/n_l^{ads}$ versus $1/x_{l,liq}$ yields a straight line of slope $1/K \cdot n_l^{mono}$ and intercept $1/n_l^{mono}$.

The amount adsorbed on the surface, per unit mass of crystals, can be determined experimentally with the use of the expression

$$n_l^{ads} = \Delta C_{l,liq} \cdot V/m \quad (3.19)$$

Although Eqs. (3.17–3.19) contain parameters that are easily found by experiment, their disadvantage is that adsorption studies must be carefully limited to crystals of fixed particle size distribution so that surface area per unit mass does not vary considerably. With this consideration, Eqs. (3.17–3.19) provide a simple means to correlate impurity incorporation as a function of solution concentration that may especially have value in investigations where, because of time or resources, more detailed studies cannot be carried out.

3.6.3. GROWTH MODELS BASED ON ADSORPTION ISOTHERMS

Numerous studies have shown a direct relationship between the growth kinetics of crystals and the surface concentration of adsorbed impurities (Davey and Mullin 1974; Davey 1975, 1976; Rousseau et al. 1976; Leung and Nancollas 1978; Nancollas 1979; Black and Davey 1988; Zhmurova et al. 1970a, 1970b; Hottenhuis et al. 1988a; Hottenhuis et al. 1988b; de Vreugd et al. 1994; Mielniczek-Brzoska et al. 2000). Modeling growth rate as a function of impurity adsorption is a method for correlating data of crystals grown from impure solutions, and in many instances, yields insight into the impurity interactions. In this regard, several different growth rate models based on impurity adsorption have been proposed (Cabrera and Vermilyea 1958; Sears 1958; Albon and Dunning 1962; Davey and Mullin 1974; Rousseau et al. 1976; Black and Davey 1988). (E.g., Kubota et al. 1995; Kubota et al. 1997; Mielniczek-Brzoska et al. 2000).

Depending on the action of the impurity at the interface, different growth behaviors can result. Thus, in selecting an adsorption model, it is useful to examine kinetic data in the presence of impurities for one of two types of limiting behavior. In the first case, the growth rate of crystals tends to zero at high impurity concentrations, indicative of strong impurity interaction. Such behavior is physically consistent with the Cabrera-Vermilyea model, which predicts no crystal growth above a critical impurity concentration (models for this type of crystal growth are discussed in *Limiting, Zero-Growth Rate Behavior*, in this section. The second class of systems, described in the following section, show non-zero asymptotic growth rate at high additive concentration and total surface coverage. These extremes are contrasted in comparing the effect of L-glutamic acid on two different faces of L-asparagine monohydrate crystals (Figures 3.20 and 3.21). Growth laws for both types of behavior are discussed in the following sections.

Limiting, Non-Zero Growth Rate Behavior. One of the most generally applicable growth rate expressions, developed for either kink, step, or ledge adsorption, is given as (Bliznakov 1959, 1965)

$$v_l = v_p - (v_p - v_{mono})\Theta \quad (3.20)$$

where Θ is the fractional surface coverage of adsorbed impurity equal to x_l^{ads}/x_l^{mono} , v_l is the step velocity in the presence of impurities, v_p is the step velocity in pure solution, and v_{mono} is the limiting step velocity at monolayer impurity adsorption. Thus, at monolayer coverage, $\Theta = 1$, Eq. (3.19) predicts a limiting growth rate of $v_l = v_{mono}$. Assuming Langmuir adsorption, Eq. (3.20) can be expressed as (Davey 1976)

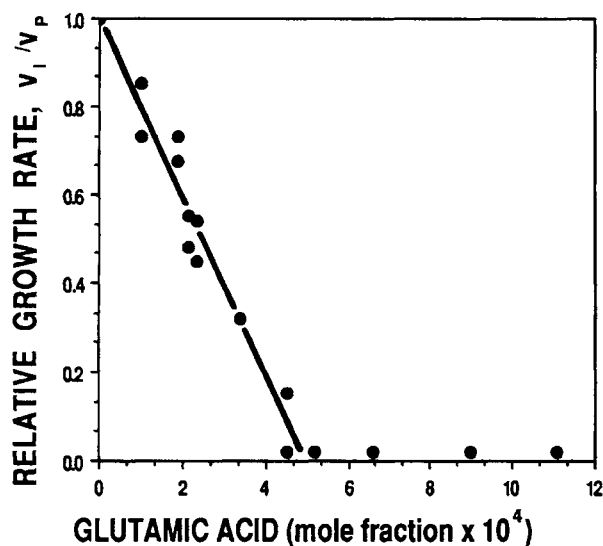


Figure 3.20 Effect of L-glutamic acid on the growth rate of {101} faces of L-asparagine monohydrate crystals. (Reproduced with permission from Black et al. 1986.)

$$\frac{v_{mono} - v_p}{v_l - v_p} = 1 + 1/(K \cdot x_{l.liq}) \quad (3.21)$$

where K is the Langmuir constant given by $K = \exp(-\Delta G/RT)$, ΔG is the free energy of adsorption of the impurity on the crystal surface, and $x_{l.liq}$ is the mole fraction of dissolved impurity. Thus, a plot of the left-hand side of Eq. (3.21) versus $1/x_{l.liq}$ gives directly the Langmuir adsorption constant K , from which ΔG can be computed.

Listed in Table 3.1 are values of the adsorption energies ΔG determined for several different crystalline systems. In general, adsorption energies of impurities at ledge sites are found to be on

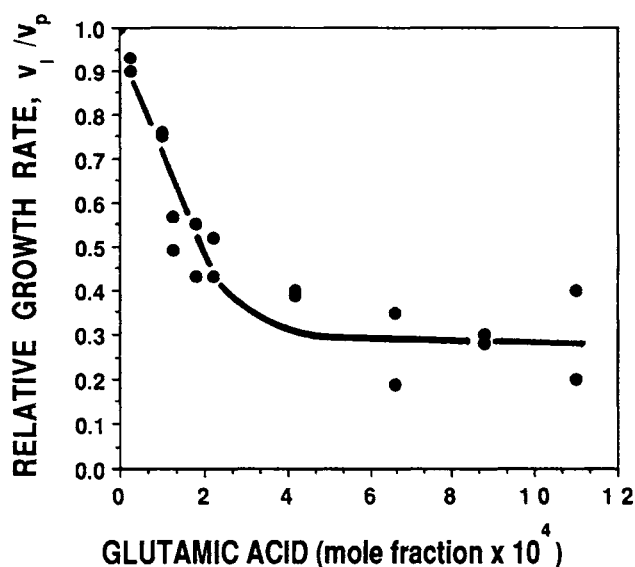


Figure 3.21 Effect of L-glutamic acid on the growth rate of the {012} faces of L-asparagine monohydrate crystals. (Reproduced with permission from Black et al. 1986.)

TABLE 3.1 Estimated Values of Adsorption-Free Energies

Material	Impurity	Temperature (°C)	ΔG (kcal/mol)
NH ₄ H ₂ PO ₄	FeCl ₃	24	-3.8
	AlCl ₃		-3.7
KBr	Phenol	26	-2.6
KClO ₃	Ponceau 3R	20	-3.6
KBr	HCOOH	19	-2.8
	CH ₃ COOH		-3.4
	C ₂ H ₅ COOH		-3.8
	C ₃ H ₇ COOH		-4.1
NaClO ₃	Na ₂ SO ₄	17	-3.2

(Reproduced with permission from Davey 1976.)

the order of 3 kcal/mol. Kink site adsorption energies are considerably higher, as reported by Davey (1976) for Cd²⁺ and Pb²⁺ adsorption on the {111} faces of NaCl and KCl (where ΔG is -11.2 and -9.9 kcal/mol, respectively).

Limiting, Zero-Growth Rate Behavior. One of the most useful models for correlating crystal growth in the presence of strongly adsorbed impurities is the Cabrera-Vermilyea model for immobile impurities described in Section 3.6.1. Based on the underlying assumptions of the model, it appears especially suited to describing systems containing tailor-made additives or otherwise chemically similar impurities that strongly interact with the product during crystallization. Such impurities characteristically contain functional groups that bear strong structural and chemically resemblance to the host crystalline phase, resulting in strong surface adsorption, high levels of incorporation, and completely blocked growth rate at high concentration.

Based on the Cabrera and Vermilyea adsorption model, Black and Davey (1988) developed the following growth rate expression

$$[1 - v_l^2/v_p^2]^2 = 2 \cdot \rho_c^2/d^{1/2} \cdot \Theta \quad (3.22)$$

Black and Davey used Eq. (3.22) to study the effect of the tailor-made additive L-glutamic acid on L-asparagine monohydrate crystals. With the use of a linear adsorption isotherm, Eq. (3.22) fit the crystal growth rate data. Consistent with a structural model in which impurities are embedded in the growing crystal surface, the growth rate of the crystals tended to zero at a high L-glutamic level.

Other simpler models that predict limiting, zero-growth rate behavior have been developed. Davey and Mullin (1974), and Davey (1976) derived an expression specifically related to ledge adsorption, assuming that adsorbed impurities reduce the surface flux of growth units to steps

$$v_l = v_p(1 - \Theta) \quad (3.23)$$

Note that v_l approaches zero as the fractional surface coverage Θ approaches unity, and that this equation is equivalent to Eq. (3.20) with v_{mono} set equal to zero. Assuming that the impurity adsorption obeys the Langmuir isotherm, Eq. (3.22) becomes

$$v_p/(v_p - v_l) = 1 + 1/K \cdot x_{l.liq} \quad (3.24)$$

The use of Eq. (3.24) is illustrated in Figure 3.22, where the measured face growth rates of ammonium dihydrogen phosphate crystals are plotted against the inverse of the concentration of impurities (AlCl₃ and FeCl₃). Both sets of data are consistent with Eq. (3.24), which predicts $v_l = 0$ at high impurity concentration

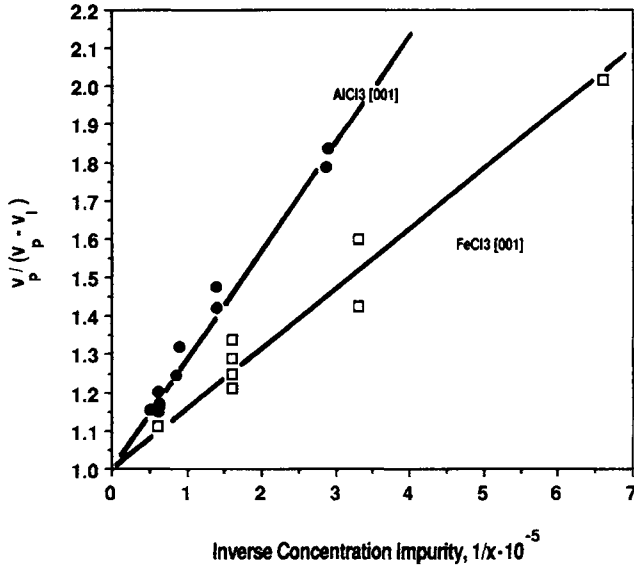


Figure 3.22 Growth rate of $\text{NH}_4\text{H}_2\text{PO}_4$ crystals grown in the presence of FeCl_3 and AlCl_3 impurities. (Reproduced with permission from Davey 1976.)

and a limiting value of unity for the ratio $v_p/(v_p - v_l)$. However, as Mullin et al. (1995) indicated, the growth suppression characteristics of an impurity on crystal growth should also include an effectiveness factor (α) as well as the adsorption factor (Θ).

$$V_l/V_p = 1 - \alpha\Theta \quad (3.25)$$

When $\alpha > 1$, the step velocity approaches zero at $\Theta < 1$ (incomplete fractional surface coverage). When $\alpha = 1$, eq. (3.23) is

obtained and when $\alpha < 1$, the velocity does not approach zero, even at $\Theta = 1$. This effectiveness factor can be related to the relative supersaturation " σ " (Mullin et al. 1995) to give

$$\alpha = \gamma a / k T \sigma L \quad (3.26)$$

where " γ " is the edge free energy, " a " the surface area occupied by one crystallizing molecule and " L " the separation of active sites available for impurity incorporation. Thus, the effectiveness factor α decreases as the supersaturation σ increases. This model has been used effectively to describe literature reports of growth rate modification due to the presence of impurities on the growing surface (e.g., Kubota et al. 1997). For example, the face growth rate of a paraffin ($\text{C}_{36}\text{H}_{74}$) crystal in the presence of the impurity dioctadecylamine ($(\text{C}_{18}\text{H}_{37})_2\text{NH}$) is shown in Figure 3.23. The solid lines are those obtained from the aforementioned model; the excellent agreement is evident. Expressions have also been developed (Sangwal et al. 2000) to relate the effective segregation coefficient K_{eff} to the relative supersaturation " σ ." Based on an analysis of published data, it has been proposed that the relationship between these two factors is associated with the accumulation and depletion of solute molecules at kink steps on the F faces of a crystal. In the same vein, Mielniczek et al. (2000) have highlighted that there is a relationship between growth kinetics and the impurity segregation coefficient via the absorption of impurities on the growing surfaces.

The adsorption free energies of AlCl_3 and FeCl_3 can be found from the slopes of the lines in Figure 3.22. Assuming that the adsorbing species consist of both positive and negative ions, the values of ΔG obtained are -3.8 kcal/mol (FeCl_3) and -3.7 kcal/mol (AlCl_3). These data are in the range of other reported values for ledge site adsorption. For example, the adsorption free energy for phenol on the ledges of $\{100\}$ faces of KBr crystals is -2.6 kcal/g mol (Davey 1976), which is in good agreement with the value of -2.7 kcal/g mol found by an independent method (Bliznakov et al. 1965).

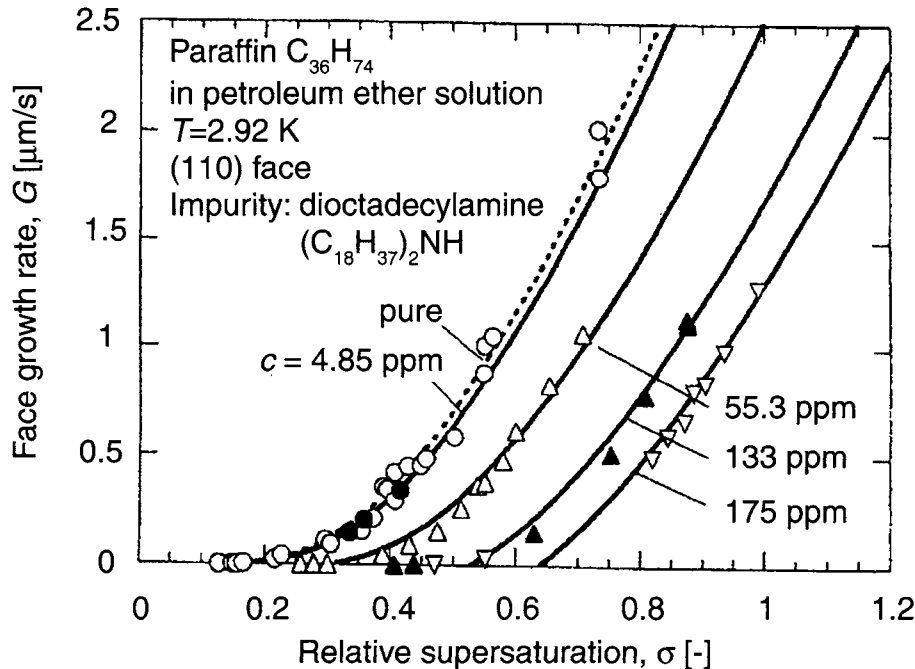


Figure 3.23 Illustration of the variation of the face growth rate of a paraffin ($\text{C}_{36}\text{H}_{74}$) crystal in the presence of the impurity dioctadecylamine ($(\text{C}_{18}\text{H}_{37})_2\text{NH}$). (From "Supersaturation Dependence of Crystal Growth in the Presence of Impurity", *J. Cryst. Growth* **182**, pp. 86–94. Used by permission of Elsevier Science, © 1997.)

3.7. SOME CHEMICAL ASPECTS OF SOLVENT AND IMPURITY INTERACTIONS

The effect of impurities and solvents on crystal growth is ultimately related to the strength of intermolecular bonds that form during the adsorption process. Cabrera and Vermilyea qualitatively addressed this point with the development of the concept of mobile and immobile impurities. The immobile impurities are recognized as forming strong bonds on the surface that effectively disrupt the movement of steps, hence the growth rate. Conversely, completely mobile impurities, forming relatively weak bonds, are swept away in the advance of steps and have a much smaller effect on the reduction in growth rate. Thus, a basic tenet drawn from this model is that strongly adsorbing solvents and impurities are more likely to cause noticeable changes in the crystallization behavior than weakly interacting ones.

A determination of the effect of solvents and impurities on the crystallization requires a fairly detailed understanding of the chemical interactions at the interface. Molecular modeling is increasingly being used to help elucidate such interactions. Investigators are increasingly using this approach to select and design "tailor made" additives, which chemically interact at selected crystal faces (e.g., Vaida et al. 1989; Weisenger-Lewin et al. 1989; Lewtas et al. 1991; Black et al. 1991; Karfunkel et al. 1993; Clydesdale et al. 1996; Weissbuch et al. 1995; Coveney et al. 1996; Erk et al. 1997; Borchadt et al. 1998). Since this method requires the understanding of chemical interaction at the interface, a brief review of some of the common chemical interactions will be made. It should be understood, however, that most interactions are complex, and often are a composite of several modes of chemical and steric interaction, as discussed in detail in the cited literature.

Chemical interactions that commonly occur at the crystalline interface during adsorption include van der Waals, ionic, and hydrogen bonding (a specific type of van der Waal interaction). Adsorption of impurities leading to the formation of covalent bonds is not likely to occur in most crystallization processes, and are thus not discussed here.

Adsorption by van der Waals interaction is important, not only as an independent mechanism, but also as a supplementary mechanism in all other types of adsorption (Rosen 1989). It accounts, in part, for the pronounced ability of long-chain ionic surfactant molecules to displace similarly charged simple inorganic ions from solid substrates. A number of crystalline systems are affected by the action of surfactants, often by van der Waals adsorption of the hydrocarbon portion ("tail-end") of surfactants onto the crystal surface.

As a general rule, adsorption by van der Waals forces increases with the molecular weight of the adsorbate since the adsorption energy also increases with molecular weight. The retarding effect of aliphatic solvents such as pentane, heptane, and decane on the crystal growth of *n*-alkanes (such as *n*-C₃₆H₇₄) is a case in point (Boistelle 1980). As illustrated in Figure 3.24, these aliphatic solvents can selectively adsorb on the {110} faces of *n*-C₃₆H₇₄ crystals. The adsorption at the interface decreases the growth rate by as much as a factor of five as the chain length of the solvent is increased, even though the solubility of *n*-C₃₆H₇₄ is roughly the same in each solvent.

The relative strength of van der Waals to ionic interactions is apparent when comparing the action of additives on the growth of potassium hydrogen phosphate crystals (KAP: C₆H₄ · COOH · COOK). KAP is a particularly interesting model compound for this purpose because it is partially organic and partially inorganic. Chromium ions (Cr³⁺) have a large effect on the spiral growth of the {010} faces of the KAP crystals, and at a level as low as 16 ppm, movement of steps is observed to be totally blocked. However, the addition of benzoic acid to KAP solutions has a less pronounced effect on crystal growth, and only after the addition of 750 ppm can inhibiting action be observed. The difference is related to the mechanism of additive interaction; in the case of Cr³⁺, strong electrostatic interactions occur, while in the case of benzoic acid, weaker van der Waals interactions dominate (Hottenhuis and Lucasius 1986). Consequently, growth in the presence of the cationic impurities is retarded to the degree that polygonized growth steps become rounded, as predicted by the Cabrera-Vermilyea model. The less strongly adsorbed benzoic acid molecules do not show the same effect and, as a consequence, the steps remain more or less straight, although slowed in velocity.

Hydrogen bonding frequently plays a primary role in the action of impurities and solvents on the growth of both organic and inorganic crystals. In addition to a covalent bond, hydrogen is capable of forming a second strong bond, most notably with oxygen, nitrogen, or fluorine atoms, thus enhancing the strength of the normal intermolecular interactions with these atoms (Ladd 1979). Some examples of hydrogen bonded interactions at interfaces are shown schematically in Figure 3.25. In general, there have been a number of key works in this area (e.g., Etter et al. 1990; Desiraju 1995) that illustrate the development of rules dictating the strengths and types of hydrogen bonding in organic solids.

In particular, these forces are known to have a major influence on the lattice packing and growth of so-called "molecular" crys-

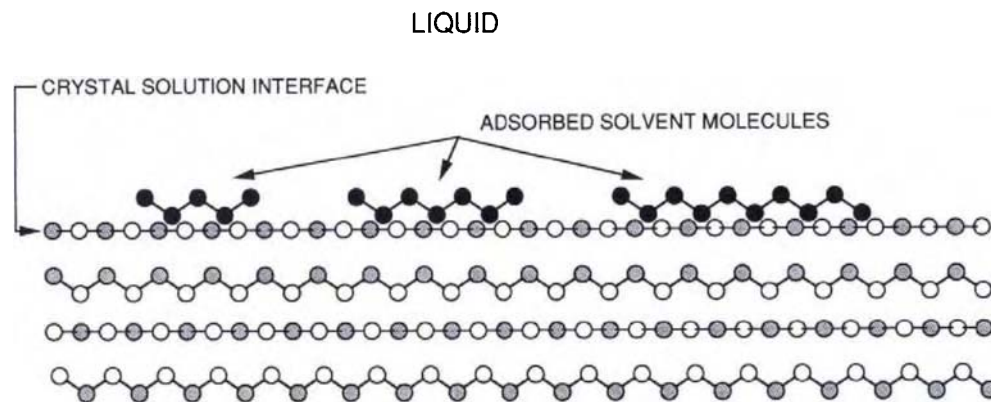


Figure 3.24 Adsorption of short-chain aliphatic solvent molecules on the faces of *n*-alkane crystal (*n*-C₃₆H₇₄). (Reproduced with permission from Davey 1986.)

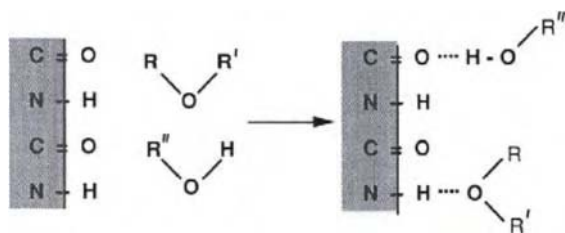


Figure 3.25 Hydrogen bonding of molecules at a crystalline interface. (After Rosen 1989.)

tals, i.e., those crystals consisting of discrete molecules (for example, crystals of benzoic acid, naphthalene, adipic acid, etc.) as opposed to ions or atoms.

Because hydrogen bonding is stronger than other van der Waals type interactions, and in most instances, directionally more specific, the action of hydrogen bonding impurities can be quite selective to certain crystal faces. A number of examples where hydrogen bonding plays a key role in impurity-host relationships have been explored by a number of workers (Vaida et al. 1989; Weisinger et al. 1989; Walker 1997; Hendricksen et al. 1998)

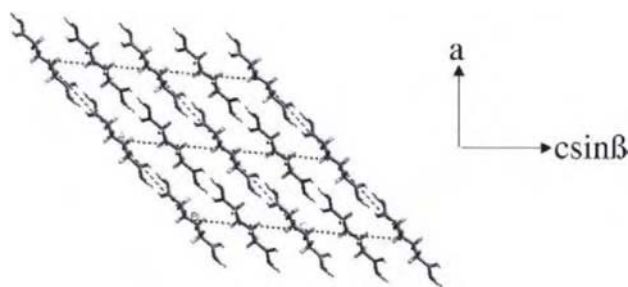


Figure 3.26 Crystal structure of adipic acid.

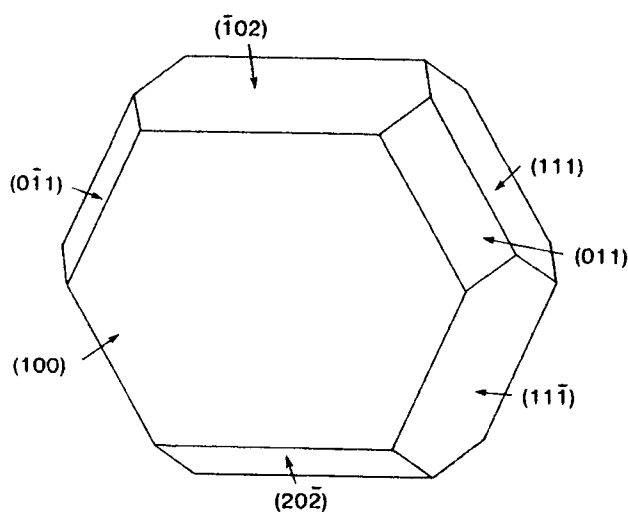


Figure 3.27 Bravais Friedel Donnay Harker (BFDH) simulation of adipic acid. (R.J. Davey, S.N. Black, D. Logan, S.J. Maginn, J.E. Fairbrother, and D.J.W. Grant (1992), *J. Chem. Soc. Faraday Trans.* 88(23), 3461–3466. Reproduced by permission of the Royal Society of Chemistry.)

Especially illustrative of the importance of these interactions is the action of polar and nonpolar solvents on the growth of succinic acid. The succinic acid crystal lattice is composed of “ribbons” or succinic acid molecules hydrogen bonded end-to-end. Carboxylic acid groups project normal to the $\{011\}$ and $\{100\}$ faces of the succinic acid crystals, rendering these faces relatively polar. On the $\{010\}$ face, there are both hydrophobic sites, where CH groups project normal, as well as hydrophilic sites at which carboxyl oxygen atoms are exposed. Correspondingly, the overall order of polarity for the various faces of succinic acid decrease in polarity in the following order (Berkovitch-Yellin 1985)

$$\{011\} > \{100\} > \{111\} > \{110\} > \{010\}.$$

Based on the preceding ranking of face polarity, polar solvents that hydrogen bond with polar faces (i.e., those with emergent carboxyl groups) would be expected to reduce that face's relative growth velocity, thus increasing its relative area. Succinic acid crystals grown from polar solvents, such as water, ethanol, and 2-propanol, do, in fact, show precisely this behavior. Conversely, crystals grown from nonpolar solvents, such as benzene, appear as long fragile needles, exposing mostly nonpolar faces. Ibuprofen is another example following the same trend. In the presence of a nonpolar solvent such as hexane, long needles will grow, whereas in the presence of a polar solvent such as a hexane/methanol mix, equidimensional prismatic crystals are obtained (Bunyan et al. 1991). The paper by Davey et al. (1992) is also a clear indication of this phenomena. In this paper, the authors have studied adipic acid. Adipic acid exhibits essentially the same packing motif as succinic acid, characterized by infinite chains of hydrogen bonds essentially in the “a” direction (Figure 3.26). A study obtained morphology predictions both by geometrical and energetic considerations. The $\{100\}$ faces that were predominant in the BFDH simulation (Figure 3.27) and also the growth morphology (Figure 3.28) (obtained from aqueous media), were much less significant in the attachment energy model (Figure 3.29). This face contains the acid end groups and consequently would be expected to grow fast, due to the attachment of the incoming acid groups by hydrogen bonding, versus weaker van der Waals faces that would predominate in other faces. Consequently one would expect this face to have a higher growth rate therefore a lower morphologically importance. The authors have postulated that since the crystals have been obtained from an aqueous media, the polar solvent has hydrogen bonded to the growing $\{100\}$ surface more-so than the other faces. The competing acts of desorption of the water

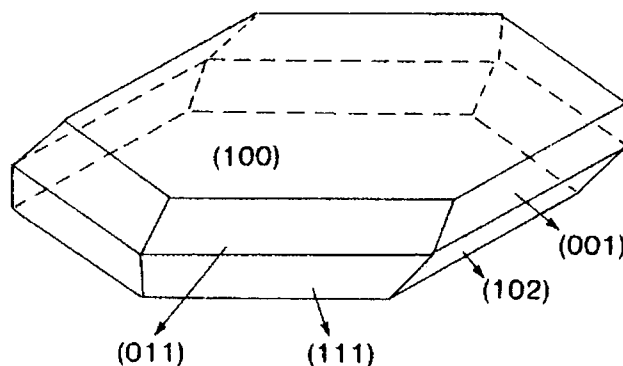


Figure 3.28 Growth morphology of adipic acid. (R.J. Davey, S.N. Black, D. Logan, S.J. Maginn, J.E. Fairbrother, and D.J.W. Grant (1992), *J. Chem. Soc. Faraday Trans.* 88(23), 3461–3466. Reproduced by permission of the Royal Society of Chemistry.)

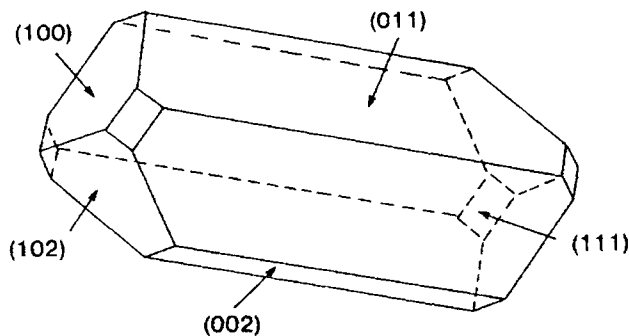


Figure 3.29 Attachment energy simulation of adic acid. (R.J. Davey, S.N. Black, D. Logan, S.J. Maginn, J.E. Fairbrother, and D.J.W. Grant (1992), *J. Chem. Soc. Faraday Trans.* 88(23), 3461–3466. Reproduced by permission of the Royal Society of Chemistry.)

molecules and absorption of the adic acid molecules reduces the growth rate of this face thus leading to the habit modification and the increased morphological importance of this face.

Several broad conclusions can be drawn from this and other studies on the effects of solvents. Namely, large solvent effects are expected in crystalline systems that have faces of significantly different polarity (Berkovitch-Yellin 1985). This general rule may, in fact, be one of the best indicators of the ability to change crystal morphology by the use of an alternative solvent. Effort is being placed on developing quantitative methods to quantify the relative polarity of crystal faces by electrostatic potential mapping (Addadi et al. 1985; Berkovitch-Yellin 1985). This determination can often be made with molecular modeling tools (D.L. Klug, unpublished data) or by simple inspection of the atom types at the surface [for example, carbon and sulfur atoms are considered nonpolar; nitrogen and oxygen are considered polar (Richards 1977)]. Studies on succinic acid as well as many other systems further indicate that crystals grown from polar solvents have a tendency to exhibit predominantly polar faces, while those grown from nonpolar solvents exhibit nonpolar faces. Accordingly, crystals obtained from solvents of intermediate polarity contain a mix of polar and nonpolar faces (Berkovitch-Yellin 1985).

Based on these considerations, modifying the crystal habit by tailoring solvent polarity should be a primary consideration during process development. Determining whether a solvent change will improve crystallization can be accomplished by testing (in a small-scale apparatus) the effect of solvents of widely different polarities to allow the possible extremes of crystal shapes to be explored. A solvent system for this purpose is the binary solvent mixture acetone/toluene, which is miscible at all concentrations. Since toluene is nonpolar, and acetone is polar and capable of hydrogen bonding with many crystal surfaces, the relative polarity of this solvent mixture can be continuously tailored by varying the relative amounts of toluene and acetone. Small-scale crystallizations from mixtures of various compositions of toluene/acetone do, in some cases, show dramatic morphological changes (D.L. Klug, unpublished data). There are other instances where a mixed solvent system can be beneficial to the mechanical properties of the crystallizing system. Liquid inclusions do form in adic acid crystals (as shown in Figure 3.17) during crystallization. A mixed solvent system comprising acetone/water has the propensity to reduce such inclusions (Grant et al. 1995). However, the propensity of a crystallizing system to form a solvate, should not be underestimated (e.g., Byrn et al. 1999).

Ionic interactions are of considerable importance in crystallization, most notably in aqueous systems. Highly polarizable ions, for instance, constitute a very important group of additives for ionic crystals. As evident from the listing in Table 3.2, commonly occurring ionic impurities, such as Cr^{3+} , Al^{3+} , and Fe^{3+} , are frequently observed to have a pronounced effect on the growth of simple inorganic salts from aqueous solution (Mullin and Gar-side 1974). Table 3.2 also clearly illustrates through certain examples, the wide variety of organic systems whose crystallization characteristics have been influenced by additives of varying complexity. So-called “multifunctional” additives such as phosphonic acids, polycarboxylic acids, and polysulfonic acids, as well as high molecular weight copolymers with various acidic groups are another important class of ionic compounds under recent investigation (van Rosmalen et al. 1989). These additives are capable of forming bonds with cationic species at crystal-liquid interfaces. Illustrated in Figure 3.30 are ionic species from solution adsorbing onto oppositely charged sites on a solid surface.

The use of long chain additives to modify crystallization behaviour has been well documented. Canselier (1993) has provided an excellent extensive review of this area, including organic and inorganic crystallizations. Control of primary particle morphology (Wilson et al. 1994), degree of agglomeration, size distribution (Dugua et al. 1978; Sarig et al. 1980) level of caking (Chen et al. 1993) and metastable zonewidth (Myerson et al. 1995) have all been reported. Molecular modeling tools have been employed to gain some insight into these phenomena. The study by Myerson et al. (1995) is one such example. The influences of alkanolic acids on the crystallization of adic acid was examined, via the calculation of a binding energy of the additive with various crystal faces and the metastable zonewidth determined when the additive is present during the adic acid crystallization. It was found that the binding energy of alkanolic acids with adic acid were much stronger than that of the growth solvent and indeed the adic acid molecules themselves, indicating that the alkanolic acids were potential growth inhibitors. There was also a trend in the degree of binding of these additives (depending on the chain length), which mirrored the experimental metastable zonewidth data obtained.

Frequently additives are considered where a particle morphology may be deleterious for further processing, e.g., dendrites in solid/liquid separation and drying. However, there are surprising instances where a desirable morphology (from a particle processing point of view) is altered to a form more suitable for the products application. For instance, burkeite ($\text{Na}_2\text{CO}_3 \cdot (\text{Na}_2\text{SO}_4)_2$) typically crystallizes with a prismatic habit. This material is extensively used within the detergent industry as a highly porous, high surface area powder. This can only be achieved by altering the morphology of this material from a prismatic habit to a needle

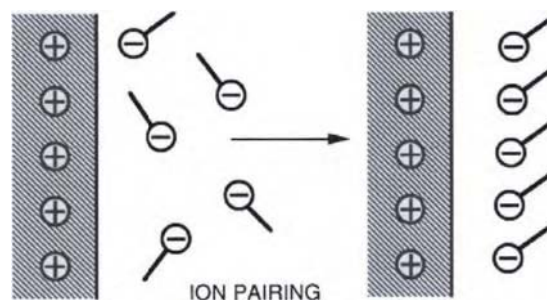


Figure 3.30 Ion pairing of charged species at a charged crystalline interface. (After Rosen 1989.)

TABLE 3.2 Additives Affecting the Growth of Crystals

Crystallizing material	Additive
Acetaminophen	Acetanilide, methyl <i>p</i> -hydroxybenzoate, <i>p</i> -acetoamidobenzoic acid, <i>o</i> -acetamidophenol, <i>m</i> -acetamidophenol ¹ , <i>p</i> -acetoxyacetanilide ³⁴
KH ₂ PO ₄ , K(D _x H _{1-x})PO ₄	Ethyl alcohol, glycol, glyceryl alcohol ²
Perylene red	Perylene-3, 4dicarboxylic acid imides ³
benzamide	Benzoic acid, <i>o</i> -toluamide, <i>p</i> -toluamide ⁴
sucrose	Monosaccharides, oligosaccharides ⁵
NaBrO ₃	Acetic acid ⁶
Paraffins	Polyacrylates ⁷
L-alanine	L-leucine, L-phenylalanine, L-valine ⁸
BaSO ₄	Homo- and copolymers of maleic acid and acrylamide ⁹
Na ₂ CO ₃ · H ₂ O	Polyacrylates ¹⁰
Adipic acid	<i>n</i> -alkanoic acids ¹¹
BaSO ₄	Diphosphonates ¹² , Phosphonates ¹³
NaClO ₃	S ₂ O ₆ ²⁻ ¹⁴
Ca ₂ SO ₄ · 2H ₂ O	La ³⁺ , Ce ³⁺ ¹⁵
KDP	Cr ³⁺ , Fe ³⁺ , Al ³⁺ ¹⁶
KAP	Ce ³⁺ , Fe ³⁺ , Al ³⁺ , Cr ³⁺ , Rh ³⁺ ^{17,18}
a-glycine	a-amino acids ^{19,20}
L-asparagine monohydrate	L-glutamic acid ²¹
N-(2-acetamido-4-nitrophenyl) pyrrolidene (PAN)	Polyelectrolytes ²²
Glycylglycine	glycyl-(S)-alanine, glycyl-(RS)-alanine, glycyl-(S)-leucine, glycyl-(R)-leucine, glycyl-(RS)-leucine ²³
Benzamide, phenol, glycine,	Triphenylphosphine Oxide ²⁴
Succinic Acid	alkanoic acids ²⁵
Caprolactam	benzoic acid, 2-chlorobenzoic acid, acetic acid ²⁷
Sodium perborate tetrahydrate	Silica ²⁸
InP	Ge ²⁹
<i>n</i> -hexadecane	sucrose polyester – palmitic acid (P-170) ³⁰
Hen and turkey egg-white lysozyme, thaumatin,	carbohydrates and derivatives, alcohols, amino acids and derivatives, polyamines, surfactants ³¹
aspartyl-tRNA synthetase	solvents, surfactants, dyes, tailor made additives, amino acids, inorganic salts ^{32,33}
Methyltrexate	

¹Hendricksen et al. (1998).²Jianzhong et al. (1997).³Erk et al. (1997).⁴Weissbuch et al. (1995).⁵Sgualdino et al. (2000).⁶Inoue et al.⁷Kern, R. and Dassonville, R. (1996).⁸Lechuga, Ballesteros et al. (1993).⁹Benton et al. (1993).¹⁰Atkinson et al. (1987).¹¹Davey et al. (1992).¹²Rohl et al. (1996).¹³Black et al. (1991).¹⁴Ristic et al. (1994).¹⁵Van Rosmalen et al. (1990).¹⁶Veintemillas-Verdaguer et al. (1987).¹⁷Hottenhuis et al. (1986).¹⁸Hottenhuis et al. (1988).¹⁹Weissbuch et al. (1983).²⁰Weissbuch et al. (1984).²¹Black et al. (1986).²²Staab et al. (1990).²³Weissbuch et al. (1985).²⁴Etter et al. (1988).²⁵Jang et al. (1998).²⁷Niehorster et al. (1996).²⁸Yuksel et al. (1996).²⁹Miyazaki et al. (1999).³⁰Kaneko et al. (1999).³¹Sauter et al. (1999).³²Chan et al. (1989).³³Chan et al. (1991).³⁴Chow et al. (1985).

habit that will ultimately agglomerate to form the high surface area powder. This habit modification is obtained by using surfactant systems that contained at least three carboxylate groups, such as polyacrylates (Atkinson et al. 1987).

A further examination of this habit modification (Meenan et al. 1991) showed that the carboxylate groups in the polyacrylate would be coulombically attracted to cation rich crystal surfaces, rather than a more homogeneous charged environment. This attraction, when occurring along two crystal axis, will alter the morphology from a prismatic habit to the desired needle-like habit. Pictorially, Figure 3.31 shows the cation rich {020} forms and the more homogeneous {011} (Figure 3.32). The segregated cation structure of the {020} surfaces will allow adsorption of the modifier onto these faces in contrast to the homogeneous {011} faces, where coulombic repulsion and steric hindrance effects would preclude adsorption of the modifier on or close to anionic lattice sites.

The relationship between the chemical structure of the ionic additive and the structural characteristics at the crystal-liquid interface is known to be of importance in determining the relative efficacy of many of these additives (Davey 1982b). An approximately equal spacing between crystal surface cations and ionizable

groups in the additive is often observed to enhance the relative activity of the additive. For instance, the effect of carboxylic acids on the growth of gypsum crystals shows that the separation of ionizable groups in the most effective additives closely correspond to the separation of Ca²⁺ ions at the surface (Tadros and Mayes 1979).

Many solvents, most notably water, alter the habit of ionic crystals through the degree of hydration on charged faces, or by their specific interaction with the additive. This occurs in crystals of ammonium dihydrogen phosphate (NH₄H₂PO₄ or ADP) crystals grown in the presence of Cr³⁺ where the Cr³⁺ salts undergo hydrolysis to yield [Cr(H₂O)₄(OH)]⁺. The growth of ADP crystals is believed to be retarded by the complexation of hydrolyzed Cr³⁺ ions in solution to H₂PO₄⁻ sites on the crystal surface (Mullin 1980).

Surface hydration effects stemming from differences in charge density among faces of ionic crystals can also affect growth kinetics. This behavior is seen in silver halide crystallization from aqueous solutions because the electrical charge density varies among the primary faces of silver halide crystals (Claes et al. 1973). The charge density differences, which are ordered $F_{111} \gg F_{110} > F_{100}$, lead to the relative hydration energy $H_{111} \gg H_{110} > H_{100}$.

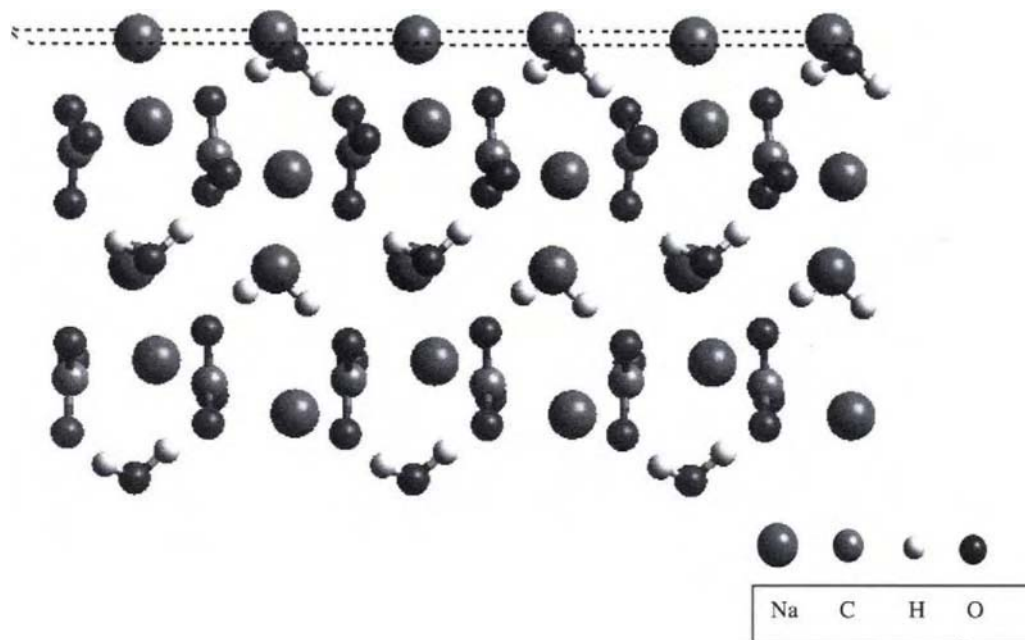


Figure 3.31 Visualization of the (020) crystal surface of $\text{Na}_2\text{CO}_3 \cdot \text{H}_2\text{O}$. (Reproduced with permission from Cambridge International Science Publishing.)

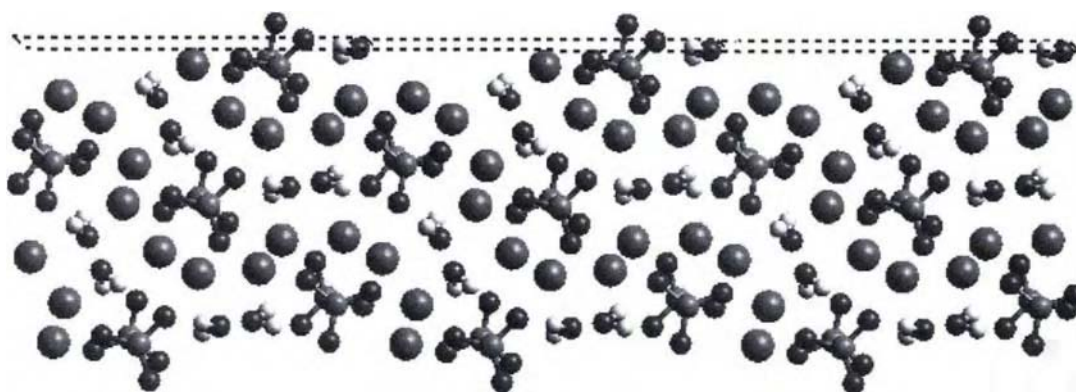


Figure 3.32 Visualization of the (011) crystal surface of $\text{Na}_2\text{CO}_3 \cdot \text{H}_2\text{O}$. (Reproduced with permission from Cambridge International Science Publishing.)

at each face. Consequently, the growth of $\{111\}$ faces is slowed by a relatively higher degree of adsorption of water molecules, resulting in an octahedral $\{111\}$ crystal habit (Figure 3.33).

3.8. TAILOR-MADE ADDITIVES

An important class of additives are the so-called, “tailor-made” additives, which are designed to interact in very specific ways with selected faces of crystalline materials. These compounds are designed to contain a portion (e.g., chemical groups or moieties) that mimic the solute molecule and are thus readily adsorbed at growth sites on the crystal surface. The additives are designed to expose a “reverse” side, which chemically or structurally differs from the host molecule, thereby disrupting subsequent growth

processes at the affected faces. In some cases this effect is achieved by tailoring the additive to introduce steric hindrance, for example, by substituting methyl or chlorine substituents for hydrogen atoms in the host molecule or by replacing planar molecules with twisted ones (Berkovitch-Yellin et al. 1985). Chemical differences (as opposed to structural ones) may be built in, as in the case of using carboxylic acid derivatives ($\text{R}-\text{CO}_2\text{H}$) to act on the corresponding amide molecules ($\text{R}-\text{CONH}_2$) (Weisinger-Lewin et al. 1989).

The specificity of tailor-made additives for certain faces arises from the fact that the additive is adsorbed only at those faces in which the reverse, i.e., modified side emerges from the crystal surface. The effect of these additives on crystallization is significant growth reduction and enlargement of the affected faces.

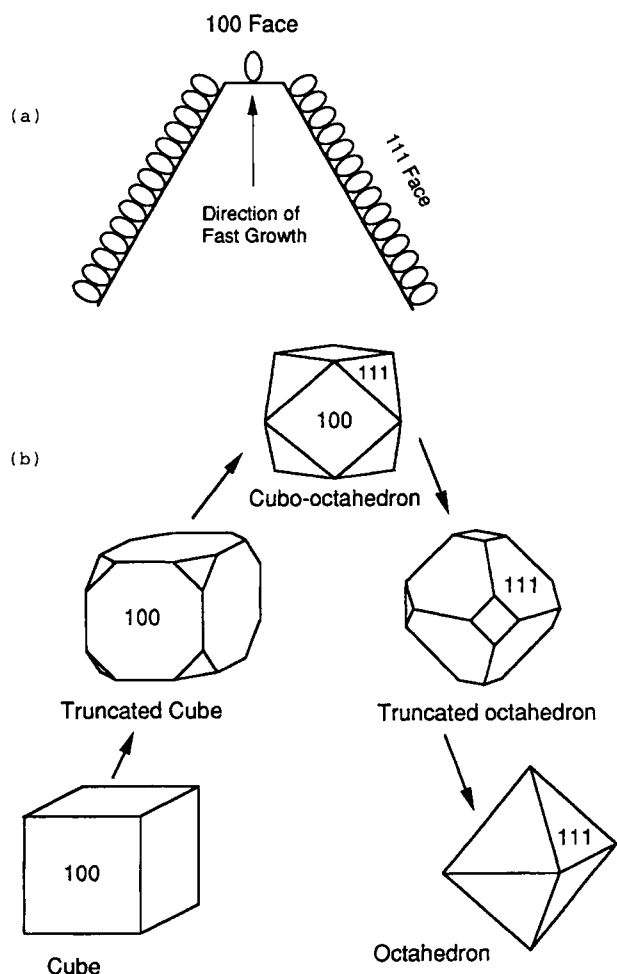


Figure 3.33 (a) Preferential adsorption of water molecules at the $\{111\}$ faces of silver halide crystal. (b) Transformation of crystal habit from cubic $\{100\}$ to octahedron $\{111\}$ due to solvent adsorption. (Reprinted with permission from J.W. Mullin (1993), *Crystallization*, 3rd ed., CRC Press. © CRC Press Inc., Boca Raton, Florida.)

Based on this approach, it is possible to systematically modify the morphology of crystals by tailoring additives to bind at preselected faces, thus changing growth rate in a predictable manner (Addadi et al. 1985). There are a number of excellent studies highlighting this area (e.g., He et al. 1994; Weissbuch et al. 1986; Weissbuch et al. 1995).

An illustration of the tailor-made additive action is given in Figure 3.34. It can be seen that there can be two modes of action. Molecules do not contain the required functionality (*disrupter* molecule) will interrupt the crystal packing, upsetting the conventional intermolecular bonding pattern adopted by the host. Another mode is having a structurally similar molecule that is slightly similar (*blocker* molecule), which uses the structural similarity to incorporate itself into selected surface sites. Due to steric hindrances, it physically inhibits the path of incoming host molecules to the growth surface. Using the concepts of attachment energy outlined in Section 3.2.1, modified attachment energies $E_{att'}$ and E_{att} can be modeled, thus allowing the prediction of morphology in the presence of tailor-made additives (Clydesdale et al. 1996).

The effects of tailor-made additives can be illustrated by the influence of benzoic acid on crystallizing benzamide. In the absence of benzoic acid, benzamide crystallizes in a flat plate like morphology dominated by $\{001\}$ faces with $\{100\}$ and $\{011\}$ facets (Figure 3.35). As can be seen in Figure 3.36, the predicted morphology (based on attachment energy considerations) is in excellent agreement with experiment. Calculations of the binding energies for benzoic acid for each of the crystal faces indicate that preferential incorporation occurs in the $\{011\}$ surfaces, however this binding energy is very similar to that calculated for a benzamide molecule. Calculated attachment energies show a reduction in the growth rate along the b -axis, agreeing well with experimental data (Figure 3.37).

Figure 3.38 shows the crystal packing, with benzamide molecules hydrogen bonding ($C=O \cdots HN$) along the b -axis. Benzoic acid is directly incorporated into the crystal lattice forming the same hydrogen bonding pattern. However, continuation of the same hydrogen bonding pattern by consequent benzamide molecules is disrupted by the repulsive $C=O \cdots O=C$ interactions between the incoming benzamide molecules and the adsorbed benzoic acid molecule. The addition of benzoic acid thus inhibits growth in the b -direction, yielding benzamide crystals elongated along the a -direction.

Perhaps the most significant implication of this work is the understanding it sheds on the separation of chemically similar by-products derived from industrial processes. In many instances, chemical syntheses yield a series of homologous compounds, many of which naturally possess the structural and chemical attributes of the tailor-made additives just described. The result is often significant reduction in crystal growth rate with accompanying changes in crystal habit. In this manner, inadvertent tailor-made impurities are produced that must be separated at high efficiency from the desired product. Because of their chemical similarity, these impurities have the tendency to strongly adsorb in a mechanism corresponding to the Cabrera-Vermilyea model, thus strongly reducing growth rate, and in many instances, particle size. Recalling from Section 3.5.1 that the relative complementarity between

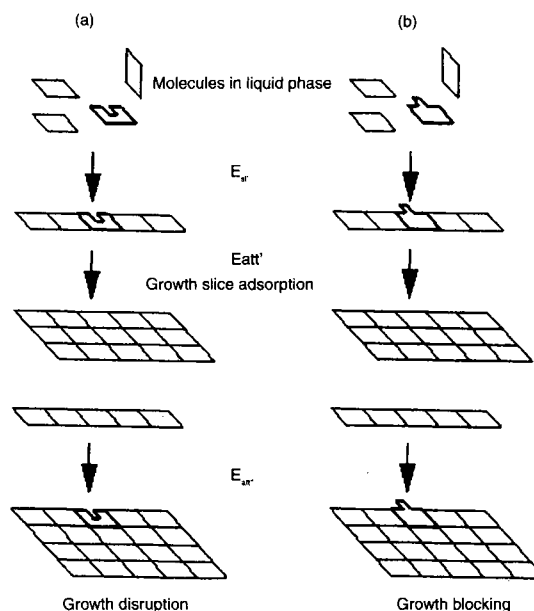


Figure 3.34 Representation of the attachment of (a) disrupter and (b) blocker additive molecules to a growing crystal surface. (Reproduced with permission from Walker, 1997.)

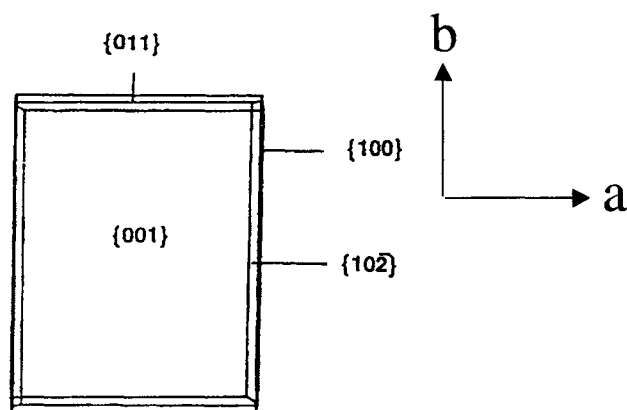


Figure 3.35 Observed morphology for benzamide. (Reproduced with permission from A.S. Myerson (1999), *Molecular Modeling Applications in Crystallization*, 1st ed., © Cambridge University Press.)

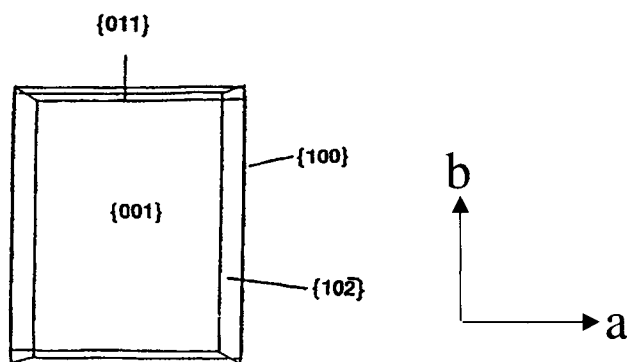


Figure 3.36 Predicted morphology (based on attachment energy considerations) for benzamide. (Reproduced with permission from A.S. Myerson (1999), *Molecular Modeling Applications in Crystallization*, 1st ed., © Cambridge University Press.)

host guest determines the degree to which impurities will substitute, some tailor-made impurities may be thermodynamically difficult to separate due to their relative compatibility with the crystal lattice.

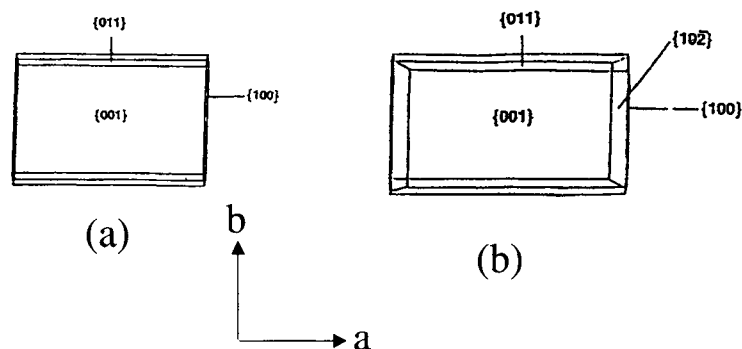


Figure 3.37 Illustration of the calculated (a) and observed (b) morphologies of benzamide, doped with benzoic acid. (Reproduced with permission from A.S. Myerson (1999), *Molecular Modeling Applications in Crystallization*, 1st ed., © Cambridge University Press.)

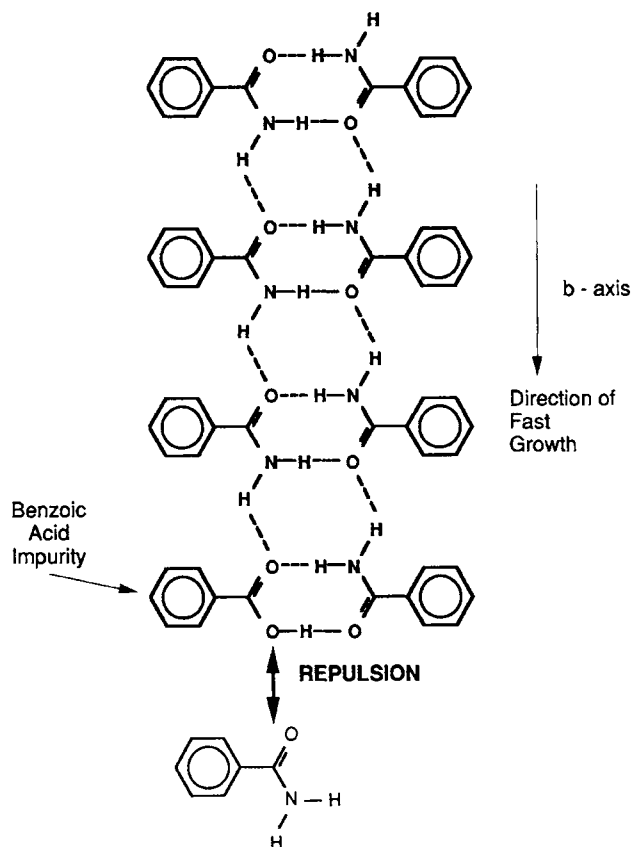


Figure 3.38 Disruption of crystal growth process by the incorporation of tailor-made additive benzoic acid at the interface of a growing benzamide crystal. (After Wright 1987.)

Although a significant amount of work on industrial crystallization processes is unpublished, a study by Davey et al. (1986) illustrates some general features of the separation of chemically similar compounds and the analogy to tailor-made additives. In the high-pressure reaction of ammonia and carbon dioxide to form urea, the dimer decomposition product biuret is formed. The biuret has a beneficial effect on the crystallization of urea from aqueous solution by reducing the aspect ratio (length-to-width ratio), thus improving the filtration and handling. Mechanistically, the biuret impurity replaces two adjacent urea molecules at the

{001} faces. Subsequent growth is impeded due to the modified surface and its relative deficiency of NH_2 groups for hydrogen bonding. The biuret molecule has little specificity for the other major faces of urea due to loss of hydrogen bonding possibilities upon incorporation. Kinetic data also confirm that at high enough concentrations (approximately 0.5% at the lowest supersaturation and 6% at the highest supersaturations measured), the growth rate is completely blocked, as predicted by the immobile adsorption model of Cabrera and Vermilyea.

Adipic acid is also an excellent example. During the adipic acid synthesis, a number of byproducts are generated that have enough structural similarity that they can be incorporated into kink sites and consequently the crystal structure and thus can be viewed as "tailor-made additives." These byproducts include succinic acid, glutaric acid, and caproic acid. The face specific nature of these interactions has been studied (Klug et al. 1994) who showed that caproic acid adsorbs primarily on the {001} faces, whereas the glutaric and succinic acids adsorb primarily on the {100} and {011} faces. A consequent study (Walker 1997) further investigated this adsorption using molecular modeling tools. Figure 3.26 illustrates the crystal packing of adipic acid, highlighting the infinite chain of molecules linked through hydrogen bonding. Figure 3.39 shows the incorporation of succinic, glutaric, and caproic acids incorporating into the crystal structure respectively.

The three impurities will all incorporate into the crystal structure, using the same hydrogen bonding recognition as an incoming adipic acid molecule. The next incoming adipic acid molecule cannot complete the requisite hydrogen bonding scheme and thus alterations of growth rate and consequently, habit occur. For example, glutaric acid is a C5 di-acid and not a C6 diacid, consequently there is a shift in the orientation of the carboxylate groups,

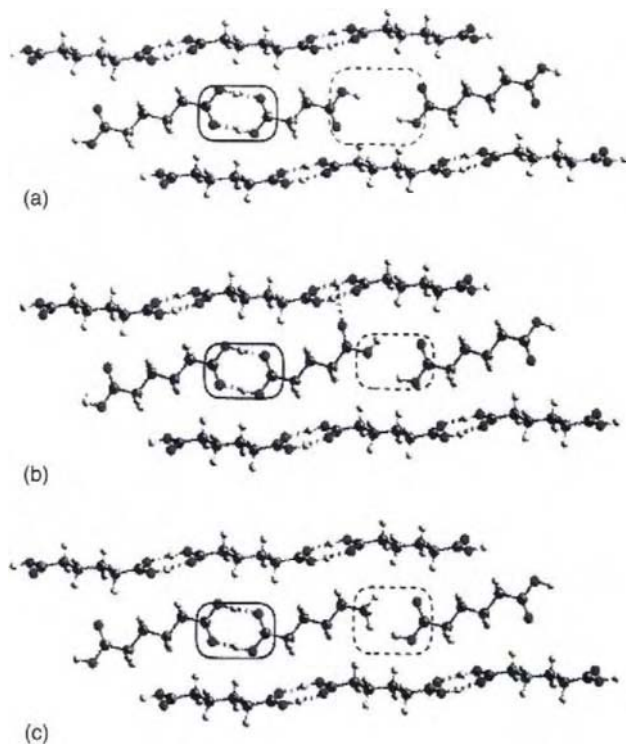


Figure 3.39 Schematic illustrating the incorporation of (a) succinic, (b) glutaric and (c) caproic acids into the crystal structure of adipic acid. (Reproduced with permission from Walker, 1997.)

which leads to coulombic repulsion effects and disruption to the lattice occurs. Caproic acid is a C6 monoacid by the same hydrogen bonding scheme. Due to the fact that it is a monoacid (and consequently the terminal end is a methyl group), an incoming adipic acid molecule will not be able to complete the same hydrogen bonding scheme; this, coupled with the steric hindrances introduced by the methyl group leads to disruption of the crystal growth kinetics.

Another example of the crystallization of chemically related compounds is found in the commercial separation of fructose from the impurity difructose dianhydride (Chu et al. 1989). Fructose undergoes irreversible dehydration during the crystallization process to yield several forms of difructose dianhydride impurities. Since the difructose dianhydride molecule consists of two fructose moieties, it exhibits some of the chemical and structural features of the host fructose molecule. In an analogous fashion to a tailor-made additive, the difructose dianhydride impurities appear to incorporate into the crystal (at <1 wt% level), thus inhibiting the subsequent adsorption and growth of fructose molecules. The resulting fructose crystal growth rates are so low that the crystallization time in fructose manufacture is often on the order of days.

3.9. EFFECT OF SOLVENTS ON CRYSTAL GROWTH

The impact of solvent on product quality should be given early consideration in process development efforts since it can have a significant effect on crystal size, morphology, and purity. A poor initial choice of solvent may thermodynamically limit the effectiveness of the separation, irrespective of all other factors, including crystallizer design and cost. In Section 3.5.1, the thermodynamic considerations for minimizing impurity incorporation are outlined based on solvent selection.

The other factors in selecting a solvent include product characteristics (e.g., impurity level, crystal size, morphology, and product yield), health and safety (e.g., solvent toxicity, inflammability, chemical reactivity, and environmental impact), and economics (e.g., solvent cost, recycling, and disposal). An example of where the aforementioned factors are considered has been given by Frank et al. (1999). In many instances, attention is given to the last two important items without consideration of product quality and downstream separations. With the development and refinement of new theories, it is now possible to optimize product characteristics by selecting the solvent on the basis of fundamental properties of the crystalline material and solution thermodynamics. There have been a number of recent advances in the calculation of solubility data, based on thermodynamic considerations (e.g., Dyer 1997; Dyer et al. 1998). This is yet limited to inorganic systems but it is anticipated that the required data will be developed for organic systems in the near future. A particular challenge will be to model the solubilities of mixed solvent systems, a situation typical in the organic specialty arena.

3.9.1. ROLE OF THE SOLVENT

Fundamentally, the solvent can influence crystal structure, crystal size, morphology, and purity by modifying solution properties (i.e., density, viscosity, and component diffusivities), solute solubility, as well as the structure of the crystal-liquid interface. The influence of the solvent on the first three factors are well known especially morphology (e.g., Srinivasan et al. 2000; Maruyama et al. 2000; Wang et al. 1999; Walker 1997; Khoshkhoo et al. 1996; Blagden et al. 1998; Roberts et al. 1994; Geertman et al. 1992; Docherty et al. 1991; Shimon et al. 1990; van der Voort et al. 1990). The solvent properties affecting heat and mass transport

are readily accounted for in standard transport analyses. The degree of solute solubility in the solvent determines the mass (i.e., yield) of crystals obtained during processing. Depending on the process, there are many ways of recovering material left dissolved in the solvent, including recycling, or secondary treatment such as adsorption, distillation, and ion exchange. An excellent review of these considerations is given in Mullin (1972).

The effect of solvent on interface structure and fundamental growth mechanism has become an active area of research that has yielded insight into the importance of the solvent on crystallization. In Section 3.4, the ideal nature of interfaces was outlined as consisting of regions of terraces, steps, and kink sites. Numerous studies now link the appearance of such sites, not only to the solid-state chemistry of the crystallizing solute, but also to the nature of solute-solvent interactions occurring at the interface (van der Voort et al. 1990; Liu et al. 1995). Since the presence of steps and kinks correlate with the rate of movement of steps, the influence of solvents on these structures plays a key role in determining measured growth rates.

The effect of solvent on crystallization can first be explained in a qualitative manner. From Section 3.4, it is recalled that a rough interface is characterized by the presence of numerous step and kink sites. In this case, growth on these faces is fast and "continuous," i.e., every solute molecule arriving at the interface immediately finds an integration site (Davey 1982a). Conversely, a smooth interface is characterized by large spacings between steps and kink sites, and exhibits slower kinetics due to the necessary surface diffusion step (Jetten et al. 1984). Since the fundamental growth mechanism depends on the interface structure, it follows that solvents which modify interface structure can also alter growth kinetics.

3.9.2. JACKSON α -FACTOR

One of the most important results of theoretical investigations of crystal growth has been the quantification of the effect of solvents on crystal interface structure. In particular, a key parameter, called the α -factor, has been developed from fundamental theories that allows identification of likely growth mechanisms based only on solute and solution properties.

Interfacial structures of crystals were first related to thermodynamics by Jackson (1958) for melt growth, and more recently by Davey (1982a), Davey et al. (1982, 1988), and Bourne (1980) for solution growth. Jackson recognized that the number of extra molecules on a planar face (i.e., its relative roughness) could be related to the free energy of the face and developed the following expression relating the change in interfacial free energy to the fraction of sites occupied

$$\frac{\gamma_{tension}}{nKT} = \alpha = (1 - \Theta)\Theta + \Theta \ln \Theta + (1 - \Theta) \ln (1 - \Theta) \quad (3.27)$$

where

$$\alpha = (\Delta H^{fus}/RT)\Psi \quad (3.28)$$

The "surface entropy factor," α , can be considered a relative measure of the degree of smoothness of a crystal face on the atomic level. In Section 3.9.3 it is shown how α correlates the effect of solvents on both growth rate and growth mechanism.

The parameter, Ψ , can be physically interpreted as the fraction of the total binding energy that binds a molecule to other molecules at the solid-liquid interface. It can be calculated with the approximate relationship, $\Psi = n_s/n_b$, where n_s and n_b are the number of nearest neighbors on the surface and in the bulk, respec-

tively. For most low index planes, Ψ has values between 0.5 and 1 (Sloan and McGhie 1988).

For melt systems, the value of α can be determined with the use of Eq. (3.25) for any plane of the crystal based solely on the latent heat of fusion, the melting point of the material, and knowledge of the crystal structure (for calculating Ψ). It has been found that α is <2 for most metals, acids and bases, silica, and a number of other glass-forming materials. For a number of semimetals and semiconductors it is between 2.2 and 3.2, while it is >3.5 for most organic materials, silicates, borates, and other inorganic compounds (Jackson 1958; Sloan and McGhie 1988).

For growth from solution, the analysis becomes somewhat more complex because solute-solvent interactions play a role in the growth process. For growth from solution, the molar heat of fusion is replaced by the enthalpy of dissolution, ΔH_{liq}^{dis} , and the corresponding equation for calculation of α -factor for growth from solution becomes (Jetten et al. 1984; Davey et al. 1982; Davey 1986)

$$\alpha = \Psi \frac{\Delta H_{liq}^{dis}}{RT} \quad (3.29)$$

where ΔH_{liq}^{dis} represents the enthalpy change upon dissolving the crystals in solution (Bourne and Davey 1976; Jetten et al. 1984). Note, however, that this equation fails when the heat of solution is exothermic (i.e., $\Delta H_{liq}^{dis} < 0$).

If it is assumed that the process of dissolution is thermodynamically equivalent to a process of melting followed by mixing of the melt with the saturated solution, then the following expression holds (Jetten et al. 1984)

$$\alpha = \Psi(\Delta H^{fus} + \Delta H^{mix})/RT \quad (3.30)$$

In ideal solutions, the pure solute and solvent mix with no heat of mixing, $\Delta H^{mix} = 0$, and the heat of dissolution is numerically equal to the heat of fusion. However, only a limited number of systems form ideal solutions. A less restrictive assumption is that the solution is represented by a regular solution model. This model assumes the heat of mixing is nonzero, but independent of solution composition and temperature (i.e., $\Delta H^{mix} = \text{constant}$) (Hildebrand and Scott 1950). For a regular solution the differential entropy of mixing is also assumed ideal (i.e., $\Delta S = -R \cdot \ln x$).

Assuming the regular solution model holds, the following expression for the α -factor has been derived by Jetten et al. (1984)

$$\alpha = \Psi \left[\frac{\Delta H^{fus}}{RT_m} - \ln x_{H.liq}^{sat} + \frac{1}{R} \int_T^{T_m} \frac{\Delta C_p}{T} dt \right] \quad (3.31)$$

where $x_{H.liq}^{sat}$ is the solubility of the crystalline material in the solvent at operating temperature T , ΔH^{fus} is the heat of fusion evaluated at the melting point T_m , and ΔC_p (equal to $C_{p.sol} - C_{p.liq}$) is the difference in heat capacity of the solid and liquid phases. In many instances the heat capacity term is negligible, resulting in the following useful approximation for α

$$\alpha = \Psi \left[\frac{\Delta H^{fus}}{RT_m} - \ln x_{H.liq}^{sat} \right] \quad (3.32)$$

It should be noted that the regular solution theory, upon which Eqs. (3.31) and (3.32) are based, is valid only for solute-solvent systems that are free of strong associative behavior, such as hydrogen bonding, solvation, or complex formation (Modell and Reid 1983). As such, Eq. (3.32) is correctly applied to ideal systems or nonideal systems that exhibit positive, as opposed to negative,

deviations from ideal behavior (Sandler 1977). Even under such restrictions, Eq. (3.32) has been found acceptable in many cases (Elwenspoek et al. 1987; Davey et al. 1988).

From the foregoing analysis, several key insights into the role of solvents on the growth process can be made. If the solute strongly interacts with the solvent, the solution is said to deviate negatively from ideal behavior and the solubility is greater than predicted from ideal solution theory. In such cases, the corresponding heat of mixing is negative. Examining Eq. (3.30), it can be seen that such behavior results in a reduced value of α , and according to theory, faster growth rate. Conversely, systems in which the solute has a tendency to self-associate yield positive deviations from ideal behavior, positive heats of mixing, and therefore, lower solubilities and higher values of α .

The same general conclusions can be drawn from Eq. (3.32), which indicates that as the solute solubility increases, the value of α decreases, leading to faster growth. Hence, at a given level of supersaturation, the fastest growth rates are expected from solvents in which the solute has a high solubility.

The relative behavior of the solution system can be experimentally determined by comparing measured solubilities to the ideal solubility, as calculated by the following expression (Hildebrand and Scott 1950)

$$\ln x_{H,liq}^{sat} = \frac{\Delta H_{fus}}{R} \left(\frac{1}{T} - \frac{1}{T_m} \right) \quad (3.33)$$

If the solution is ideal, a plot of $\ln x_{H,liq}^{sat}$ versus $1/T$ will yield a straight line with slope equal to $-\Delta H_{fus}/R$. Solubilities greater than predicted by Eq. (3.33) show negative (and those smaller, positive) deviations from ideal solution behavior.

3.9.3. EFFECT OF α -FACTOR ON GROWTH MECHANISM

In computer simulations (Gilmer and Bennema 1972) and experimental studies (Bourne and Davey 1976), the value of α -factor has been linked to the controlling growth mechanism. Depending on the value of α , three distinct growth regimes have been identified (Davey 1982a).

1. Fast Growth Regime ($\alpha < 3$). Fast, linear growth rate on atomically rough surface prevails. The growth rate is linearly proportional to supersaturation, $G = k'\sigma$.

2. Intermediate Growth Regime ($3 < \alpha < 5$). Creation of steps is limiting; growth follows birth and spread type mechanism, $G = k''\sigma \exp(-B/\sigma)$.

3. Slow Growth Regime ($\alpha < 5$). The surface is atomically smooth and growth is controlled by the movement of steps emerging from dislocations. Slow growth kinetics and parabolic dependence on supersaturation results, and growth behavior is as predicted by the Burton-Cabrera-Frank (Burton, W.K., et al. 1951) model

$$G = C \frac{\sigma^2}{\sigma_1} \tan h \left(\frac{\sigma_1}{\sigma} \right) \quad (3.34)$$

where C and σ_1 are temperature-dependent constants. For small values of supersaturation, σ becomes proportional to the square of the supersaturation

$$G = (C/\sigma_1)\sigma^2 \quad (3.35)$$

The different growth regimes just described are qualitatively evident in Figure 3.40, where computed values of growth rate are plotted against supersaturation for various values of α .

It can be concluded that where mass transfer resistance is negligible, the relative growth rate and growth mechanism of a substance can be predicted with the use of the α -factor. Moreover, this approach provides a thermodynamically based method to correlate the effects of solvents that can eventually lead to methods for choosing optimal solvents. A specific example illustrating these concepts and calculations is given in the next section.

Growth of Hexamethylene Tetramine (HMT) from Various Solvents. Detailed studies of the effect of solvents on crystal growth have been conducted using the crystalline material HMT (Bourne and Davey 1976; Bourne 1980; Davey 1986). An analysis of HMT solubility data through the use of Eq. (3.33) indicates that HMT forms an approximately ideal solution with ethanol. By contrast, large negative deviations from ideal behavior are observed in water.

The calculation of α -factor involves two steps: (1) calculation of Ψ , which varies depending on crystal face; and (2) calculation of thermodynamic properties [using ΔH_{fus} and solubility with Eq. (3.32), or ΔH_{liq}^{dis} with Eq. (3.29)]. From the unit cell, the number of nearest neighbors of the HMT body centered cubic lattice is known to be 8. Since the number of nearest neighbors on the {110} face is 4, the value of Ψ for this face is $\Psi = n_s/n_b = 0.5$ (Davey 1986).

Using Eq. (3.32), the value of α is computed to be 2.7 for water and 3.7 for ethanolic solution (Davey 1986). As shown in Figure 3.41, the growth of HMT from water is considerably faster than from ethanol. In accordance with the theory, the observed growth behavior out of aqueous solution is approximately linear, while it is quadratic from ethanol (Bourne 1980). The measured and calculated values are summarized in Table 3.3.

Although no studies to date have attempted to relate impurity retention specifically to the α -factor of the solvent, it is interesting to note that HMT grows inclusion-free from ethanol (high α) at nearly all conditions, but grows with inclusions from water (low α) (Denbigh and White 1966). This is consistent with the previously

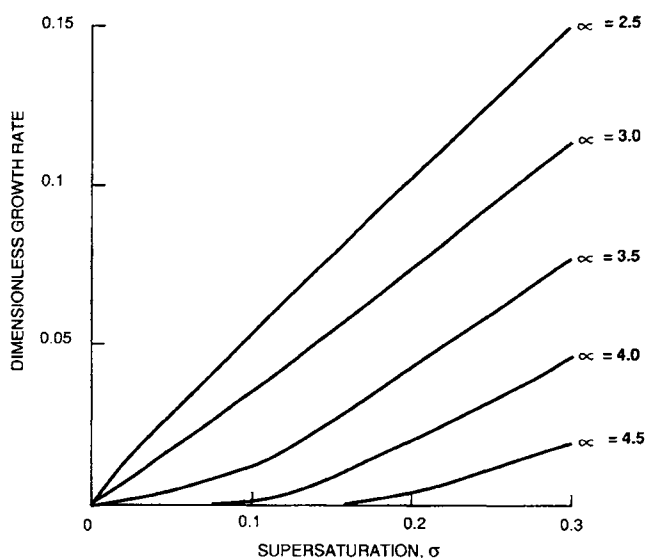


Figure 3.40 Influence of supersaturation on growth rate with the α -factor as a parameter. (Reproduced with permission from Davey 1982a.)

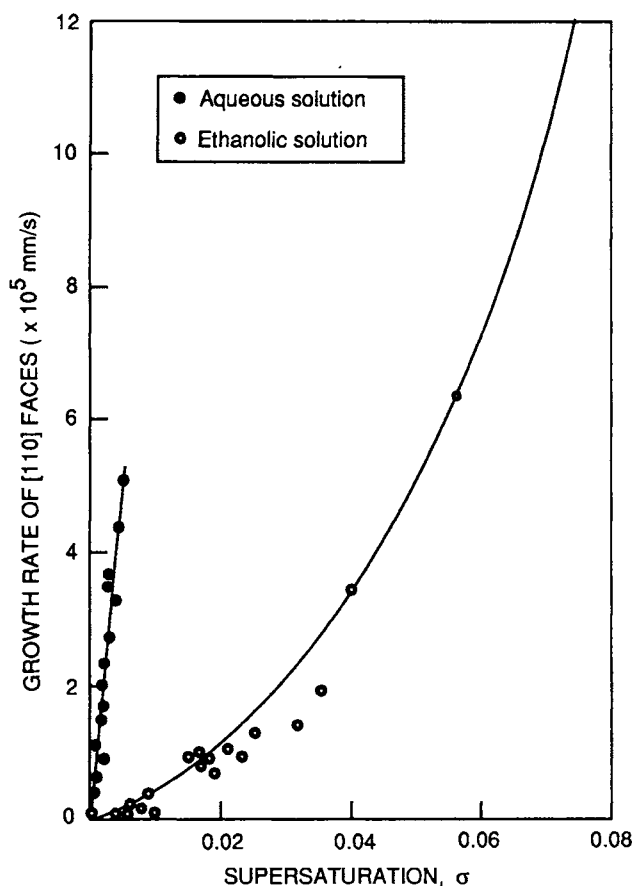


Figure 3.41 Comparison of the growth rate of hexamethylene tetramine (HMT) crystals from water and ethanol solutions. (Reproduced with permission from Davey 1982a.)

mentioned observations that fast growth rates are often linked to inclusion formation.

3.10. SUMMARY

As shown in this chapter, the solvent can influence crystal product quality through its effect on crystallization kinetics, solution thermodynamics, and crystal interface structure. However, in many instances, the presence of impurities, reaction by-products, or corrosion products in the commercial system can override the solvent-induced behavior, yielding results different from those obtained in pure solvent. The strong influence of impurities at the parts per million level stems from the unique ability of certain impurities to adsorb at key growth sites on the crystal growth surface, as discussed in detail in Section 3.6.

TABLE 3.3 Growth of Hexamethylene Tetramine (HMT) from Ethanol and Water Solvents

Property	Water	Ethanol
Heat of solution (kcal/mol)	-5.00	3.90
γ_{HMT}	0.27	2.60
Solubility (mol%)	10.00	1.10
α -Factor	2.70	3.70
Observed growth law	Fast, linear	Slow, quadratic

(Reproduced with permission from Davey 1986.)

Depending on their structure, some impurities are readily incorporated into the bulk of the crystal, and their concentration can be predicted on the basis of thermodynamics alone (Section 3.5.1). However, the concentration of impurities in crystals grown industrially is often greater than that predicted thermodynamically, and normally correlates directly with production rate (i.e., growth rate). As discussed in Section 3.5.2, *Effect of Crystallization Rate on Impurity Incorporation*, simple, powerful models can be employed to explain this behavior and to relate crystal growth kinetics to impurity incorporation.

Many other nonequilibrium modes of impurity incorporation occur, primarily through segregation of impurities at defect and inclusion sites. As discussed throughout this chapter, these impurities can be systematically reduced from the final product through optimization of crystallization and separation steps. In particular, the thermodynamic approach outlined in Section 3.5.1 can be effectively used commercially to select solvents and optimize processing conditions to greatly improve the purification of crystalline materials.

Based on the current lack of accurate methods for predicting nonequilibrium impurity uptake (through, for instance, defects and inclusions), it is recommended to conduct screening experiments with as many known impurities as possible, and with several different solvents chosen on the basis of methods described in Sections 3.5.1, 3.7.2, and 3.9. These tests can be conducted using test tubes, microscopic hot stages, or batch crystallizers, and can be used to examine crystals for evidence of inclusions, twinning, agglomeration, dendritic growth, and other nonideal behavior. At this time, checks can also be made to ensure that the desired polymorph is crystallized. This is critical in the pharmaceutical industry, where polymorphic form can potentially influence dissolution rate and consequent bioavailability. For completeness, the final steps before commercialization should include prototypic lab-scale crystallization in which the effect of temperature, supersaturation, and mixing are also examined. These studies are described in detail in Chapters 1 and 2 in this book.

As crystallization is essentially a molecular recognition process occurring on a grand scale, molecular modeling techniques are playing an increasingly important role in understanding the role of impurities on crystal growth rates and consequent crystal habit development. Such techniques, however do require that a crystal structure of the material in question be available. This is not always the case and significant effort must be made to grow single crystals of sufficient size and quality for a X-ray structural analysis. Indeed, certain impurities present may inhibit nucleation occurring, leading to the buildup of excessive supersaturation. The resultant crystals formed typically are too small for conventional X-ray structural analysis. Consequently there is significant effort devoted to elucidating the crystal structure using molecular modeling tools. There have been a variety of efforts underway to predict the crystal structure from *ab-initio* means (Verwer et al. 1998) and methods based on calculating the crystal structure from knowledge derived from powder diffraction data (David et al. 1998; Engel et al. 1999; Le Bail et al 2000; Hammond et al. 1999; Harris et al. 1998).

Once a crystal structure has been obtained, the choice of force-field and partial atomic charges can significantly influence the quality of the morphology simulation. Depending on the molecular complexity of the system in question, a generic force field may be used (e.g., Clydesdale et al. 1996), or for molecular inorganic species, intermolecular force fields must initially be derived for the system in question, before any morphology simulation may be made (e.g., Telfer et al. 1998).

As stated previously, the simulated morphology obtained from PBC methods, attachment energy methods and surface energy

methods essentially do not include the influences of solvent/impurities directly. Typically these influences have to be understood and calculated after the initial calculation has been made. There have been recent advances in calculation of the influences of solvent on crystal habit (e.g., Winn et al. 2000; Walker 1997) and in the calculation of the influence of impurities on crystal habit (e.g., Clydesdale et al. 1996). However, there does not currently exist reliable methods to simultaneously quantify the influences of solvent and impurities on the growing crystal morphology. Although a daunting task, it is to be hoped that there will be advances in the future in this area and it is further hoped that this chapter has illustrated that this may be a daunting, but not impossible task.

REFERENCES

- Addadi, L., Berkovitch-Yellin, Z., Domb, N., et al. (1982). *Nature (London)* **296**, 21–26.
- Addadi, L., Berkovitch-Yellin, Z., Weissbuch, I., et al. (1985). *Angewandte Chemie Int. (in English)* **24**, 466–485.
- Addadi, L., Weinstein, S., Gati, E., Weissbuch, I., and Lahav, M. (1982). *J. Am. Chem. Soc.* **104**, 4610–4617.
- Albon, N., and Dunning, W.J. (1962). *Acta Cryst.* **15**, 474–476.
- Anderson, H.W., Carberry, J.B., Staunton, H.F., and Sutradhar, B.C. (1995). U.S. Patent no. 5,471,001.
- Atkinson, C., Heybourne, M.J.H., Iley, W.J., Russell, P.C., Taylor, T., and Jones, D.P. (1987). European Patent EP221776A.
- Authier, A., Lagomarsino, S., and Tanner, B.K. (1997). *X-Ray and Neutron Dynamical Diffraction, Theory and Applications*, vol. 357, Plenum Publishing Corporation.
- Bennema, P. (1969). *J. Cryst. Growth* **5**, 29–43.
- Benton, W.J., Collins, I.R., Grimsey, I.A., Parkinson, G.M., and Rodger, S.A. (1993). *Faraday Discuss.* **95**, 281–297.
- Berkovitch-Yellin, Z. (1985). *J. Am. Chem. Soc.* **107**, 8239–8250.
- Berkovitch-Yellin, Z., Addadi, L., Idelson, M., Leiserowitz, L., and Lahav, M. (1982). *Nature (London)* **296**, 27–34.
- Berkovitch-Yellin, Z., van Mil, J., Idelson, M., Lahav, M., and Leiserowitz, L. (1985). *J. Am. Chem. Soc.* **107**, 3111–3122.
- Black, S.N., and Davey, R.J. (1988). *J. Cryst. Growth* **90**, 136–144.
- Black, S.N., Bromley, L.A., Cottier, D., Davey, R.J., Dobbs, B., and Rout, J.E., (1991). *J. Chem. Soc. Faraday Trans.* **87(20)**, 3409–3414.
- Black, S.N., Davey, R.J., and Halcrow, M. (1986). *J. Cryst. Growth* **79**, 765–774.
- Black, S.N., Davey, R.J., and McLean, T.D. (1988). *Mol. Cryst. Liquid Cryst. Including Nonlinear Optics* **161**, 283–290.
- Black, S.N., Williams, L.J., Davey, R.J., Moffat, F., McEwan, D.M., Sadler, D.E., Docherty, R., and Williams, D.J. (1990). *J. Phys. Chem.* **94**, 3223–3226.
- Blagden, N., Davey, R.J., Lieberman, H.F., Williams, L., Payne, R., Roberts, R., Rowe, R., and Docherty, R. (1998). *J. Chem. Soc. Far. Trans.* **94(8)**, 1035–1044.
- Bliznakov, G. (1959). *Fortschr. Mineral* **36**, 149–191.
- Bliznakov, G. (1965). In *Adsorption et Croissance Cristalline*, p. 291, CNRS, Paris.
- Bliznakov, G., Kirkova, E., and Nilolaeva, R. (1965). *Z. Physik. Chem.* **228**, 23–32.
- Bliznakov, G., Kirkova, E., and Nikolaeva, R. (1971). *Krist. Tech.* **6(1)**, 33–38.
- Boistelle, R. (1980). In *Current Topics in Materials Science*, vol. 4 (Kaldis, E., ed.), pp. 413–480, North-Holland Publishing Co., Amsterdam.
- Boistelle, R., Mathieu, M., and Simon, B. (1974). *Surface Sci.* **42**, 373–388.
- Bonafede, S., and Ward, M.D. (1995). *J. Am. Chem. Soc.* **117**, 7853–7861.
- Borchardt, T.B., Stowell, J.G., and Byrn, S.R. (1998). *Mol. Cryst. Liq. Cryst.* **313**, 271–276.
- Bosbach, D., Jordan, G., and Rammansee, W. (1995). *Eur. J. Mineral* **7**, 267–276.
- Bourne, J.R. (1980). *AIChE Symposium Series* **76(193)**, 59–64.
- Bourne, J.R., and Davey, R.J. (1976). In *Industrial Crystallization* (Mullin, J.W., ed.), pp. 223–237, Plenum, New York.
- Braun, N., Tack, J., Fischer, M., Bacher, A., Bachmann, L., and Weinkauff, S. (2000). *J. Cryst. Growth* **212**, 270–282.
- Bravais, A. (1913). *Etudes Crystallographiques*, Paris.
- Brechevic, L., and Kralj, D. (2000). *Surfactant Sci. Ser.* **88**, 435–474.
- Brice, J.C., and Bruton, T.M. (1974). *J. Cryst. Growth* **26**, 59–60.
- Brooks, R., Horton, A.T., and Torgesen, J.L. (1968). *J. Cryst. Growth* **2**, 279–283.
- Brownsey, G., and Leadbetter, A. (1980). *Phys. Rev. Lett.* **44**, 1608.
- Brune, D., Hellborg, R., Hunderi, O., and Whitlow, H.J. (1997). *Surface Characterization: A User's Sourcebook*, John Wiley & Sons, Inc.
- Buckley, H.E. (1951). In *Crystal Growth*, pp. 147–224, John Wiley and Sons, New York.
- Buckton, G., and Darcy, P. (1999). *Int. J. Pharm.* **179**, 141–158.
- Bunyan, J.M.E., Shankland, N., and Sheen, D.B. (1991). *AIChE Symp. Ser.* **284(87)**, 44–57.
- Burton, W.K., Cabrera, N., and Frank, F.C. (1951). *Phil. Trans. Roy. Soc. London* **243**, 299–358.
- Burton, J.A., Prim, R.C., and Slichter, W.P. (1953). *J. Chem. Phys.* **21(11)**, 1987–1996.
- Byrn, S., Pfeiffer, R., and Stowell, J. (1999). *Solid State Chemistry of Drugs*, 2nd ed., SSCI Inc., West Lafayette, IN.
- Cabrera, N., and Coleman, R.V. (1963). In *The Art and Science of Growth Crystals*, pp. 3–28, John Wiley & Sons, New York.
- Cabrera, N., and Vermilyea, D. (1958). In *Growth and Perfection of Crystals*, (Doremus, R.H., Roberts, B.W., and Turnbull, D., eds.), pp. 393–410, Wiley, New York.
- Canselier, J.P. (1994). *J. Disp. Sci. and Techn.* **14(6)**, 625–644.
- Chan, H.-K., and Gonda, I. (1989). *J. Cryst. Growth* **94**, 488–498.
- Chan, H.-K., and Gonda, I. (1991). *Int. J. Pharm.* **68**, 179–190.
- Chen, Y.L., and Chou, J.Y. (1993). *Powder Technology* **77**, 1–6.
- Chernov, A.A. (1984). *Modern Crystallography III*, Crystal Growth Springer Series on Solid State, **36**, Springer, Berlin, p. 179.
- Chernov, A.A. (1998). *Acta Cryst. Sect. A* **A54**, 859–872.
- Chernov, A.A., and Malkin, A.I. (1988). *J. Cryst. Growth* **92**, 432–444.
- Chow, A.H.L., Chow, P.K.K., Zhongshan, W., and Grant, D.J.W. (1985). *Int. J. Pharm.* **24**, 239–258.
- Chu, Y.D., Shiau, L.D., and Berglund, K.A. (1989). *J. Cryst. Growth* **97**, 689–696.
- Claes, F.H., Libeer, J., and Vanassche, W. (1973). *J. Photographic Sci.* **21**, 39–50.
- Clydesdale, G., Docherty, R., and Roberts, K.J. (1996). *HABIT95, Quantum Chemistry Program Exchange (QCPE)*, Bloomington, IN, 47405, Program Number 670, QCPE **16**, 1.
- Clydesdale, G., Roberts, K.J., and R. Docherty, R. (1996). *J. Cryst. Growth* **166(4)**, 78–83.
- Clydesdale, G., Roberts, K.J., and R. Docherty, R. (1991). *Comp. Phys. Comm.* **64**, 311–328.
- Clydesdale, G., Roberts, K.J., Telfer, G.B., Saunders, V.R., Pugh, D., Jackson, R.A., and Meenan, P. (1998). *J. Phys. Chem.* **102**, 7044–7049.
- Coveney, P.V., and Humphries, W.J. (1996). *Chem. Soc., Faraday Trans.* **92(5)**, 831–841.
- Craig and Sing (1982).
- Craig, S.R., Hastie, G.P., Roberts, K.J., Sherwood, J.N., Tack, R.D., and Cernik, R.J. (1999). *J. Mat. Chem.* **9**, 2385–2392.
- Cunningham, D., Davey, R.J., Roberts, K.J., Sherwood, J.N., and Shripathi, T. (1990). *J. Cryst. Growth* **99**, 1065–1069.
- Cunningham, D.A.H., Hammond, R.B., Lai, X., and Roberts, K.J. (1995). *Chem. Mater.* **7**, 1690–1695.
- Curreri, P.A., Onoda, G., and Finlayson, B. (1981). *J. Cryst. Growth* **53**, 209–214.
- Daniel, S.G. (1951). *Trans. Faraday Soc.* **47**, 1345–1359.
- Davey, R.J. (1975). *J. Cryst. Growth* **29**, 212–214.
- Davey, R.J. (1976). *J. Cryst. Growth* **34**, 109–119.
- Davey, R.J. (1979). *Industrial Crystallization '78* (De Jong, E.J., and Jančić, S.J. eds.), pp. 169–185, North-Holland Publishing Co., Amsterdam.
- Davey, R.J. (1982a). In *Current Topics in Materials Science*, vol. 8 (Kaldis, E., ed.), pp. 431–479, North-Holland Publishing Co., Amsterdam.
- Davey, R.J. (1982b). In *Industrial Crystallization 81* (Jančić, S.J. and deJong, E.J., eds.), pp. 123–135, North-Holland Publishing Co., Amsterdam.
- Davey, R.J. (1986). *J. Cryst. Growth* **76**, 637–644.

- Davey, R.J., Black, S.N., Logan, D., Maginn, S.J., Fairbrother, J.E., and Grant, D.J.W. (1992). *J. Chem. Soc. Faraday Trans.* **88**(23), 3461–3466.
- Davey, R.J., and Mullin, J.W. (1974). *J. Cryst. Growth* **26**, 45–51.
- Davey, R.J., and Dobbs, B. (1987). *Chem. Eng. Sci.* **42**(4), 631–637.
- Davey, R., and Garside, J. (2000). *From Molecules to Crystallizers: An Introduction to Crystallization*, Oxford University Press.
- Davey, R.J., Mullin, J.W., and Whiting, M.J.L. (1982). *J. Cryst. Growth* **58**, 304–312.
- Davey, R., Fila, W., and Garside, J. (1986). *J. Cryst. Growth* **79**, 607–613.
- Davey, R.J., Milisavljevic, B., and Bourne, J.R. (1988). *J. Phys. Chem.* **92**, 2032–2036.
- David, W.I.F., Shankland, K., and Shankland, N. (1998). *Chem. Comm.* **8**, 931–932.
- Davies, R.D., Schurr, G.A., Meehan, P., Nelson, R.D., Bergna, H.E., and Martin, C.J. (1998). *Adv. Mat.* **10**, 1264–1270.
- De Vreugd, C.H., Witkamp, G.J., and van Rosmalen, G.M. (1994). *J. Cryst. Growth* **144**, 70–78.
- De Vries, S.A., Goedtkind, P., Bennett, S.L., Huisman, W.J., Zwanenburg, M.J., Smilgies, D.M., De Yoreo, J.J., van Enkevort, W.J.P., Bennema, P., and Vlieg, E. (1998). *Phys. Rev. Lett.* **80**, 227–231.
- Denbigh, K.G., and White, E.T. (1966). *Chem. Eng. Sci.* **21**, 734–753.
- Desiraju, G.R. (1995). *Ange. Chem. Int. Ed. Eng.* **34**, 2311–2327.
- Docherty, R., and Roberts, K.J. (1988). *J. Cryst. Growth* **88**, 159–168.
- Docherty, R., Clydesdale, G., Roberts, K.J., and Bennema, P. (1991). *J. Phys. D. App. Phys.* **24**, 89–99.
- Donnay, J.D.H., and Harker, D. (1937). *Am. Mineral.* **22**, 446–467.
- Dowty, E. (1980). *Am. Mineral.* **65**, 465–471.
- Dugua, J., and Simon, B. (1978). *J. Cryst. Growth* **44**, 265–279.
- Dyer, J.A. (1997). *MSc. Thesis*, University of Delaware.
- Dyer, J.A., Scrivner, N.C., and Dentel, S.K. (1998). *Env. Progr.* **17**(1), 1–8.
- Elwenspoek, M., Bennema, P., and van der Eerden, J.P. (1987). *J. Cryst. Growth* **83**, 297–305.
- Engel, G.E., Wilke, S., König, O., Harris K.D.M., and Leusen, F.J.J. (1999). *J. Appl. Cryst.* **32**, 1169–1179.
- Erk, P., Hetzenegger, J., and Böhm, A. (1997). *European Coating Journal*, 906–910.
- Etter, M., and Baures, P.W. (1988). *J.A.C.S.* **110**, 639–640.
- Etter, M.C., Urbanczyk-Lipowska, Z., Zia-Ebrahimi, M., and Panunto, T.W. (1990). *J.A.C.S.* **112**, 8415–8426.
- Favier, J.-J., and Wilson, L.O. (1982). *J. Cryst. Growth* **58**, 103–110.
- Feidenhans'l, R. (1989). *Surf. Sci. Rep.* **10**, 105–188.
- Fleming, S.D., Rohl, A.L., Lee, M.-Y., Gale J.D., and Parkinson, G.M. (2000). *J. Cryst. Growth* **209**, 159–166.
- Frank, T.C., Downey, J.R., and Gupta, S.K. (1999). *Chem. Eng. Prog.* **95**(12), 41–61.
- Frommer, J. (1992). *Angew. Chem. Int. Ed. Engl.* **31**, 1298–1328.
- Garside, J., Rusli, I.T., and Larson, M.A. (1979). *AIChE J.* **25**, 57–64.
- Gay, D.H., and Rohl, A.L. (1995). *J. Chem. Soc., Far. Trans.* **91**, 925–936.
- Geertman, R.M., and van der Heijden, A.E.D.M. (1992). *J. Cryst. Growth* **125**, 363–372.
- Gibbs, J.W. (1878). *On Equilibrium of Heterogeneous Substances*. The Collected Works of J. Willard Gibbs, Longmans, Green and Co., New York.
- Gibbs, J.W. (1906). *Collected Works*, Longmans Green, New York.
- Gidalevitz, D., Feidenhans'l, R., Smilgies, D.M., and Leiserowitz, L. (1997). *Surf. Sci. Lett.* **4**, 721–934.
- Giles, C.H., and Nakhwa, S.N. (1962). *J. Appl. Chem.* **12**, 266–273.
- Gilmer, G.H., and Bennema, P. (1972). *J. Cryst. Growth* **13/14**, 148–153.
- Givand, J.C., Rosseau, R.W., and Ludovice, P.J. (1998). *J. Cryst. Growth* **194**, 228–238.
- Goldstein, J.I., Newbury, J.L., Goldstein, R., and Fiori, L. (1997). *Scanning Electron Microscopy and X-ray Microanalysis*, Kluwer Academic Publishers.
- Grant, D.J.W. et al. (1995). private communication.
- Gregg, S.J., and Sing, K.S.W. (1982). In *Adsorption, Surface Area, and Porosity*, 3rd ed., pp. 277–307, Academic Press, London.
- Grimbergen, R.F.P., and Bennema, P. (1996). *Proceedings of the Third International Workshop of the Crystal Growth of Organic Materials (CGOM-3)*, (Myerson, A.S., Green, D.A., and Meenan, P. eds.)
- Grimbergen, R.F.P., Meekes, H., Bennema, P., Strom, C.S., and Vogels, L.J.P. (1998). *Acta Cryst.* **A54**, 491–500.
- Halasz, S., and Bodor, B. (1993). *J. Cryst. Growth* **128**, 1212–1217.
- Halfpenny, P.J., Sherwood, J.N., and Simpson, G.S. (1997). *Nuovo Cimento Soc. Ital. Fis. D.* **19D**(2–4), 123–135.
- Hall, R.N. (1953). *J. Phys. Chem.* **57**, 836–839.
- Hammond, R.B., Roberts, K.J., Smith, E.D.L., and Docherty, R. (1999). *J. Phys. Chem.* **103**(37), 7762–7770.
- Hancock, B., and Zografi, G. (1997). *J. Pharm. Sci.* **86**, 1–12.
- Harano, Y., and Yamamoto, H. (1982). In *Industrial Crystallization 81* (Jančić, S.J., and deJong, E.J., eds.), pp. 137–145, North-Holland Publishing, Co., Amsterdam.
- Harris, K.D., Johnson, R.L., and Kariuki, B.M. (1998). *Acta Crystallogr. Sect. A* **A54**(5), 632–645.
- Hartman, P., and Bennema, P. (1980). *J. Cryst. Growth* **49**, 145–156, 157–165, 166–170.
- Hartman, P., and Perdok, W.G. (1955). *Acta Cryst.* **8**, 49–52, 521–524, 525–529.
- Hartshorn, N.H., and Stuart, A. (1964). *Practical Optical Crystallography*, Arnold, London.
- He, S., Oddo, J.E., and Tomson, M.B. (1994). *J. Coll. Int. Sci.* **162**, 297–303.
- Hildebrand, J.H., and Scott, R.L. (1950). In *The Solubility of Nonelectrolytes*, 3rd ed., pp. 300–319, Reinhold, New York.
- Hillner, P.E., Manne, S.H., Ansmä, P.K., and Gratz, A.J. (1993). *Faraday Discuss* **95**, 191–197.
- Holmes, D.E., and Kamath, G.S. (1982). *J. Cryst. Growth* **57**, 607–609.
- Hottenhuis, M.H.J., and Lucasius, C.B. (1986). *J. Cryst. Growth* **78**, 379–388.
- Hottenhuis, M.H.J., and Lucasius, C.B. (1988a) *J. Cryst. Growth* **91**, 623–631.
- Hottenhuis, M.H.J., and Oudenampsen, A. (1988b) *J. Cryst. Growth* **92**, 513–529.
- Hottenhuis, M.H.J., and Lucasius, C.B. (1989). *J. Cryst. Growth* **94**, 708–720.
- Inoue, T., and Nishioka, K. (2000). *J. Cryst. Growth* **212**, 507–511.
- Jackson, K.A. (1958). In *Growth and Perfection of Crystals* (Doremus, R.H., Roberts, B.W., and Turnbull, D., eds.), pp. 319–324, John Wiley & Sons, New York.
- Jackson, R.A., Meenan, P., Roberts, K.J., Telfer G.B., and Wilde, P.J. (1995). *J. Chem. Soc.: Far. Trans.* **91**(22), 4133–4128.
- Jang, S.-M., and Myerson, A. (1996). *Proceedings of the Third International Workshop of the Crystal Growth of Organic Materials (CGOM-3)* (Myerson, A.S., Green, D.A., and Meenan, P. eds.)
- Janssen-Van Rosmalen, R., and Bennema, P. (1977). *J. Cryst. Growth* **42**, 224–227.
- Jetten, L.A.M.J., Human, H.J., Bennema, P., and van der Eerden, J.P. (1984). *J. Cryst. Growth* **68**, 503–516.
- Jianzhong, C., Sukun, L., Fengtu, Y., Jiahe, W., and Jianming, L. (1997). *J. Cryst. Growth* **179**, 226–230.
- Joseph, C., Ittyachenm, M.A., and Raju, K.A. (1997). *Bull. Mater. Sci.* **20**, 37–48.
- Kahr, B., Chow, J., and Peterson, M. (1994) *J. Chem. Edu.* **71**(7), 584–586.
- Kaneko, N., Horie, T., Ueno, S., Yano, J., Katsuragi, T., and Sato, K. (1999). *J. Cryst. Growth* **197**, 263–270.
- Karfunkel, H.R., Rohde, B., Leusen, F.J.J., Gdanitz, R.J., and Rihs, G. (1993). *J. Comp. Chem.* **14**, 1125–1135.
- Kelly, M.J. (1987). *Chemtech*, **18**, 30–33.
- Kern, R., and Dassonville, R. (1996). *J. Cryst. Growth* **116**, 191–203.
- Khoshkhoo, S., and Anwar, J. (1996). *J. Chem. Soc. Far. Trans.* **92**, 1023–1025.
- Kipling, J.J. (1965). In *Adsorption from Solutions of Non-Electrolytes*, pp. 288–298, Academic Press, New York.
- Kipling, J.J., and Wright, E.H.M. (1962). *J. Chem. Soc.* **1962**, 855–860.
- Klapper, H. (1996). *NATO ASI Ser.* **B357**, 167–176.
- Klug, D.L., and van Mil, J.H. (1994) U.S. Patent no. 5,296,639.
- Konnert, J., D'Antonio, P., and Ward, K. (1994). *Acta Cryst.* **D50**, 603–613.
- Kontny, M., and Zografi, G. (1995). In *Physical Characterization of Pharmaceutical Solids* (Brittain, H.G., ed.), **70**, 387–418, Marcel Dekker, New York.
- Kossel, W. (1934). *Ann. Physik.* **21**, 457–480.
- Kubota, N., and Mullin, J.W. (1995). *J. Cryst. Growth* **152**, 203–208.
- Kubota, N., Yokota, M., and Mullin, J.W. (1997). *J. Cryst. Growth* **182**, 86–94.

- Ladd, M.F.C. (1979). *Structure and Bonding in Solid State Chemistry*, Horwood Ltd., West Sussex, England.
- Lahav, M., and Leiserowitz, L. (1986). *Pure and Appl. Chem.* **58**, 947–954.
- Lahav, M., Berkovitch-Yellin, Z., van Mil, J., Addadi, L., Idelson, M., and Leiserowitz, L. (1985). *Israel J. Chem.* **25**, 353–361.
- Langmuir, I. (1918). *J. Am. Chem. Soc.* **40**, 1361–1402.
- Last, J.A., Hillier, A., Hooks, D.E., Maxson, J.B., and Ward, M.D. (1998). *Chem. Mater.* **10**, 422–437.
- Law, D. (1997). *Ph.D. Thesis* University of Minnesota.
- Le Bail, A. (2000). <http://sdpd.univ-lemans.fr/sdpd/espoir/epdic-7.html>.
- Leadbetter, A., Frost, J., Gaughan, J., and Gray, G. (1979). *J. Phys (Paris)*, **40**, 375.
- Lechuga-Ballesteros, D., and Rodriguez-Hornedo, N. (1993). *Pharm. Res.* **10**(7), 1008–1014.
- Leung, W.H., and Nancollas, G.H. (1978). *J. Cryst. Growth* **44**, 163–167.
- Lewtas, K., Tack, R.D., Beiny, D.H.M., and Mullin, J.W. (1991). *Advances in Industrial Crystallization*, p. 166, Butterworth-Heinemann.
- Liu, X.Y., Boek, E.S., Briels, W.J., and Binnema, P. (1995). *Nature* **374**, 342–345.
- MacCalman, M.L., Roberts, K.J., Kerr, C., and Hendriksen, B. (1995). *J. App. Cryst.* **28**, 620–623.
- MacKintosh, D.L., and White, E.T. (1976). *AIChE Symposium Series* **72**(153), 11–20.
- Malicksco, L. (1970). *J. Cryst. Growth* **7**, 13–19.
- Malkin, A.J., Kuznetsov, Y.G., and McPherson, A. (1999). *J. Cryst. Growth* **196**, 471–488.
- Mantovani, G., Vaccari, G., Squallino, G., Aquilano, D., and Rubbo, M. (1985). *L'Industria Saccifera Italiana* **78**, 7–14, 79–86.
- Mao, G., Lobo, L., Scaringe, R., and Ward, M. (1997). *Chem. Mater.* **9**, 773–783.
- Marinković, V. (1996). *C.C.A.C.A.A.* **69**, 1039–1052.
- Maruyama, S., and Ooshima, H. (2000). *J. Cryst. Growth* **212**, 239–245.
- Matsuoka, M., Garside, J., Rout, J.E., Black, S.N., and Davey, R.J. (1990). *J. Cryst. Growth* **99**, 1138–1141.
- McPherson, A., Malkin, A.J., Kuznetsov, Y.G., and Koszelak, S. (1996). *J. Cryst. Growth* **168**, 74–92.
- Meenan, P., Roberts, K.J., Sherwood, J.N., and Yuregir, K.R. (1991). *Powder Technology*, **65**, 219–225.
- Mielniczek-Brzoska, E., Gielzak-Kocwin, K., and Sangwal, K. (2000). *J. Cryst. Growth* **212**, 532–542.
- Miyazaki, N., and Kuroda, Y. (1999). *J. Cryst. Growth* **196**, 62–66.
- Modell, M., and Reid, R.C. (1983). *Thermodynamics and Its Applications*, 2nd ed., Prentice-Hall, Englewood Cliffs, NJ.
- Morantz, D.J., and Mathur, K.K. (1971). *J. Cryst. Growth* **11**, 1–5.
- Morantz, D.J., and Mathur, K.K. (1972). *J. Cryst. Growth* **16**, 147–158.
- Moyers, C.G. (1986). *Chem. Eng. Progress* **82**(5), 42–46.
- Mullin, J.W. (1972). *Crystallization*, 2nd ed., CRC Press, Boca Raton, FL.
- Mullin, J.W. (1980). *Chem. Ind.* **3**, 372–377.
- Mullin, J.W. (1993). *Crystallization*, 3rd ed., Butterworth-Heinemann, Oxford.
- Mullin, J.W., and Garside, J. (1974). *Chem. Eng.* **286**, 402–404.
- Myerson, A.S., and Jang, S.M. (1995). *J. Cryst. Growth* **156**, 459–466.
- Myerson, A.S., and Saska, M. (1984). *AIChE J.* **30**(5), 865–867.
- Nakada, T., Sasaki, G., Miyashita, S., Durbin, S.D., and Komatsu, H. (1999). *J. Cryst. Growth* **196**, 503–510.
- Nancollas, G.H. (1979). *Adv. Colloid Interface Sci.* **10**, 215–252.
- Narang, R.S., and Sherwood, J.N. (1978). *AIChE Symposium Series* **54**, 267–277.
- Niehorster, S., Hennig, S., and Ulrich, J. (1996). *Proceedings of the Third International Workshop of the Crystal Growth of Organic Materials (CGOM-3)* (Myerson, A.S., Green, D.A., and Meenan, P., eds.)
- Nielsen, A.E., and Christoffersen, J. (1982). *Biological Mineralization and Demineralization* (Nancollas, G.H. ed.) Springer Verlag, Berlin.
- Noboru, S., Masaaki, Y., Akira, S., and Noriaki, K. (1999). *AIChE J.* **45**(7), 1153–1156.
- Norby, P., Christensen, A.N., and Hanson, J.C. (1999). *Inorg. Chem.* **38**, 1216–122.
- Nyström, C., and Karehill, P. (1996). In *Pharmaceutical Powder Compaction Technology* (Alderborn, G., and Nyström, C., eds.), pp. 17–54, Marcel Dekker, New York.
- Nývlt, J. (1978). In *Industrial Crystallization*, pp. 26–31, Verlag Chemie Publishers, New York.
- Ott, M., and Mizes, H. (1994). *Colloids Surfaces*, **87**, 245–256.
- Overney, R.M., Howald, L., Frommer, J., Meyer, E., and Güntherodt, H.-J. (1991). *J. Chem. Phys.* **94**, 8441–8443.
- Piano, E., Dall'Aglio, G.A., Crivello, S., Chittofrati, R., and Puppo, F. (2000). *Mater. Chem. Phys.* **66**, 266–269.
- Ratner, A.P. (1933). *J. Chem. Phys.* **1**, 789–794.
- Richards, F.M. (1977). *Ann. Rev. Biophys. Bioeng.* **6**, 151–176.
- Ristic, R., Shekunov, B.Yu., and Sherwood, J.N. (1994). *J. Cryst. Growth* **139**, 336–343.
- Ristic, R.I., Shekunov, B.Y., and Sherwood, J.N. (1997). *J. Cryst. Growth* **179**, 205–212.
- Roberts, K.J. (1993). *J. Cryst. Growth* **130**, 657–681.
- Roberts, K.J., Sherwood, J.N., Yoon, C.S., and Docherty, R. (1994). *Chem. Mater.* **6**, 1099–1102.
- Robinson, I.K. (1986). *Phys. Rev.* **B33**, 3380–3386.
- Rohl, A.L., Gay, D.H., Davey, R.J., and Catlow, C.R.A. (1996). *J.A.C.S.* **118**, 642–648.
- Rosen, M.J. (1989). In *Surfactants and Interfacial Phenomena*, 2nd ed., pp. 39–67, John Wiley & Sons, New York.
- Rosenberger, F. (1979). In *Fundamentals of Crystal Growth I*, pp. 395–493, Springer-Verlag, Berlin.
- Rosenberger, F. (1986). *J. Cryst. Growth* **76**, 618–636.
- Rosenberger, F., and Riveros, H.G. (1974). *J. Chem. Phys.* **60**(2), 668–670.
- Rousseau, R.W., Tai, C.Y., and McCabe, W.L. (1976). *J. Cryst. Growth* **32**, 73–76.
- Sandler, S.I. (1977). In *Chemical and Engineering Thermodynamics*, pp. 333–402, John Wiley & Sons, New York.
- Sangwal, K. (1998). *Prog. Cryst. Growth Charact. Mater.* **36**(3), 163–248.
- Sangwal, K., and Palczynska, T. (2000). *J. Cryst. Growth* **212**, 522–531.
- Sarig, S., and Mullin, J.W. (1980). *Ind. Eng. Chem. Proc. Des. Dev.* **19**, 490–494.
- Saska, M., and Myerson, A.S. (1983). *J. Cryst. Growth* **61**, 546–555.
- Sauter, C., Ng, J.D., Lerber, B., Keith, G., Brion, P., Hosseini, M.W., Lehn, J.-M., and Giege, R. (1999). *J. Cryst. Growth* **196**, 365–376.
- Sayle, D.C., Gay, D.H., Rohl, A.L., Catlow, C.R.A., Harding, J.H., Perrin, M.A., and Nortier, P. (1996). *J. Mater. Chem.* **6**, 653–650.
- Sears, G.W. (1958). *J. Chem. Phys.* **29**, 1045–1048.
- Senol, D., and Myerson, A.J. (1982). In *Effect of Impurities on Occlusion Formation during Crystallization from Solution*, *AIChE Symposium Series* **78**(215), 37–41.
- Squallino, G., Aquilano, D., Tamburini, E., Vaccari, G., and Mantovani, G. (2000). *J. Cryst. Growth* **66**, 316–322.
- Shekunov, B., and Grant, D.J.W. (1997b). *J. Phys. Chem.* **101**, 3973–3979.
- Shekunov, B., Grant, D.J.W., Latham, R., and Sherwood, J.N. (1997a). *J. Phys. Chem.* **101**, 9107–9112.
- Shekunov, B., Sheperd, E.E.A., Sherwood, J.N., and Simpson, G.S. (1995). *J. Phys. Chem.* **99**, 7130–7136.
- Shimon, L.J.W., Vaida, M., Addadi, L., Lahav, M., and Leiserowitz, L. (1990). *J.A.C.S.* **112**, 6215–6220.
- Shimon, L.J.W., Wireko, F.C., Wolt, J., et al. (1986). *Mol. Cryst. Liquid Cryst.* **137**, 67–86.
- Slaminko, P., and Myerson, A.S. (1981). *AIChE J.* **27**(6), 1029–1031.
- Sloan, G.J., and McGhie, A.R. (1988). In *Techniques of Melt Crystallization*, vol. 19, pp. 422–447, John Wiley & Sons, New York.
- Smet, F.M., and van Enckevort, W.J.P. (1988). *J. Cryst. Growth* **88**, 169–179.
- Smith, D., Hober, H., Gerber, C., and Binnig, G. (1989). *Science* **245**, 43–45.
- Smol'skii, I.L., Malkin, A.I., and Kuznetsov, Y.G. (1985). *Soviet Phys. Cryst.* **30**, 331–338.
- Srinivasan, K., Sankaranarayanan, K., Thangavelu, S., and Ramasamy, P. (2000). *J. Cryst. Growth* **212**, 246–254.
- Staab, E., Addadi, L., Leiserowitz, L., and Lahav, M. (1990). *Adv. Mat.* **2**, 40–43.
- Strickland-Constable, R.F. (1968). In *Kinetics and Mechanism of Crystallization*, pp. 130–145, Academic Press, New York.
- Strom, C.S. (1979). *J. Cryst. Growth* **46**, 185–188.
- Tadros, M.E., and Mayes, I. (1979). *J. Colloid Interface Sci.* **72**, 245–254.
- Telfer, G.B., Clydesdale, G., Roberts, K.J., and Grant, D.J.W. (1997). *J. Pharm. Sci.* **86**, 135–141.
- Thomas, B.R., Chernov, A.A., Vekilov, P.G., and Carter, D.C. (2000). *J. Cryst. Growth* **211**, 149–156.
- Thurmond, C.D., and Struthers, J.D. (1953). *J. Phys. Chem.* **57**, 831–835.

- Tiller, W.A. (1963). In *Art and Science of Growing Crystals* (Gilman, J.J., ed.), pp. 277–312, John Wiley & Sons, New York.
- Tsukamoto, K., and Sunagawa, I. (1985). *J. Cryst. Growth* **71**, 183–190.
- Vaida, M., Shimon, J.W., van Mil, J., et al. (1989). *J. Am. Chem. Soc.* **111**, 1029–1034.
- van der Eerden, J.P., and Müller-Krumbhaar, H. (1986). *Electrochimica Acta* **31**(8), 1007–1012.
- van der Sluis, S., Witkamp, G.J., and van Rosmalen, G.M. (1986). *J. Cryst. Growth* **70**, 620–629.
- van der Voort, E., and Hartman, P. (1990). *J. Cryst. Growth* **104**, 450–456.
- van Rosmalen, G.M., and Bennema, P. (1990). *J. Cryst. Growth* **99**, 1053–1060.
- van Rosmalen, G.M., Witkamp, G.J., and de Vreugd, C.H. (1989). In *Industrial Crystallization*, vol. 87, pp. 15–20, Elsevier Publisher, New York.
- Veintemillas-Verdaguer, Rodriguez-Clemente, R., and Sangwal, K. (1987). *J. Cryst. Growth* **83**, 367–375.
- Verwer, P., and Leusen, F.J.J. (1998). *Rev. Comput. Chem.* **12**, 327–365.
- Walker, E. (1997). *Ph.D. Thesis* University of Strathclyde.
- Wang, J.L., Berkovitch-Yellin, Z., and Leiserowitz, L. (1985). *Acta Cryst.* **B41**(5), 341–348.
- Wang, W.S., Aggarwal, M.D., Choi, J., Gebre, T., Shields, A.D., Penn, B.G., and Frazier, D.O. (1999). *J. Cryst. Growth* **198/199**, 578–582.
- Washburn, J. (1958). In *Growth and Perfection of Crystals*, pp. 342–349, John Wiley & Sons, New York.
- Weiser, K. (1958). *J. Phys. Chem. Solids* **7**, 118–126.
- Weisinger-Lewin, Y., Frolov, F., McMullan, R.K., et al. (1989). *J. Am. Chem. Soc.* **111**, 1035–1040.
- Weissbuch, I., Addadi, L., Berkovitch-Yellin, Z., Gati, E., Weinstein, S., Lahav, M., and Leiserowitz, L. (1983). *J.A.C.S.* **105**, 6613–6621.
- Weissbuch, I., Addadi, L., Berkovitch-Yellin, Z., Gati, E., Weinstein, S., Lahav, M., and Leiserowitz, L. (1984). *Nature (London)* **310**, 1161–1164.
- Weissbuch, I., Berkovitch-Yellin, Z., Leiserowitz, L., and Lahav, M. (1985). *J. Isr. Chem.* **25**, 362–372.
- Weissbuch, I., Kuzmenko, I., Berfeld, M., Leiserowitz, L., and Lahav, M. (2000). *J. Phys. Organ. Chem.* **13**(7), 426–434.
- Weissbuch, I., Shimon, L.J.W., Landau, E.M., Popovitz-Biro, R., Addadi, L., Weissbuch, I., Popovitz-Biro, R., Berkovitch-Yellin, Z., Lahav, M., and Leiserowitz, L. (1995). *Acta Cryst.* **B51**, 115–148.
- Wichman, B., van der Eerden, J.P., and Gerritsen, J.W. (1990). *J. Cryst. Growth* **99**, 1333–1338.
- Wilcox, R.W. (1968). *Ind. Eng. Chem.* **60**, 13–23.
- Wilson, O.C., and Riman, R.E. (1994). *J. Coll. Int. Sci.* **167**, 358–370.
- Wilson, L.O. (1978a). *J. Cryst. Growth* **44**, 371–376.
- Wilson, L.O. (1978b). *J. Cryst. Growth* **44**, 247–250.
- Winn, D., and Doherty, M.F. (2000). *AIChE J.* **46**(7), 1348–1367.
- Woensdregt, C.F. (1993). *Farad. Discuss.* **95**, 97–107.
- Wright, J.D. (1987). *Molecular Crystals*, Cambridge University Press, Cambridge.
- Wulff, G. (1901). *Z. Krist. Min.* **34**, 499–530.
- Yip, C., Brader, M., Frank, B., DeFelippis, M.R., and Ward, M.D. (2000). *Biophys. J.* **78**, 466–473.
- Yuksel, G.Y., Sayan, P., Titiz, S., and Bulutcu, A.N. (1996). *J. Cryst. Growth* **160**, 370–374.
- Zhang, G.G.Z., and Grant, D.J.W. (1999). *J. Cryst. Growth* **181**, 61–70.
- Zhmurova, Z.I., and Khaimov-Mal'kov, V.Ya. (1970a). *Kristallografiya.* **15**, 136–141.
- Zhmurova, Z.I., and Khaimov-Mal'kov, V.Ya. (1970b). *Kristallografiya.* **15**, 142–148.

ANALYSIS AND MEASUREMENT OF CRYSTALLIZATION UTILIZING THE POPULATION BALANCE

K.A. Berglund

4.1. PARTICLE SIZE AND DISTRIBUTION

The size and shape of particles in a particulate product are important for several reasons. The efficiency of any process for production of a particulate material relies on the size, shape, and size distribution. A very small mean size product is difficult to centrifuge, wash, and package. Many products must be dissolved for subsequent use and a broad size range leads to variation in time necessary for dissolution among product crystals. Shape can also be important in applications such as pharmaceuticals wherein different crystal faces have different dissolution rates, leading to variation in bioavailability for crystals of different shapes. Therefore, any comprehensive discussion of crystallization must include the genesis of size and size distribution, as well as its possible measurement and control.

The population balance approach to analysis of crystallizers was formalized and presented by Randolph and Larson (1971, 1988). The technique parallels other balance approaches such as material and energy balances, which are familiar to process engineers. The population balance is used to account for both the size (an attribute to be described later in this section) and number of particles. Therefore, before a discussion of the development and application of the population balance can be enjoined, it is necessary to consider size and size distributions of particles.

The concept of particle size and its measurement is both very simple and complex. We all know what we mean by size, but it is difficult to quantify in many instances. In the specific case of size definition for crystallization, we generally resort to a single linear dimension to establish size. This dimension, which we will denote the characteristic dimension, will be determined by the method of measurement to be discussed later in this section.

Crystals do not occur in single sizes, but have distributions. Two types of crystal size distributions are normally considered, the density distribution and the cumulative distribution. The density distribution is defined as

$$\int_0^{\infty} f(L)dL = 1 \quad (4.1)$$

where $f(L)dL$ denotes the fraction of particles in the size range between L and $L + dL$. Eq. (4.1) is written in normalized form, which results in the integral being equal to one. The second type of size distribution is the cumulative distribution defined as

$$F(L) = \int_0^L f(L)dL \quad (4.2)$$

The density distribution has arbitrary units of no./size \times volume while the cumulative distribution has arbitrary units of no./volume.

The relative importance of the two distributions becomes more apparent when one considers the type of data usually

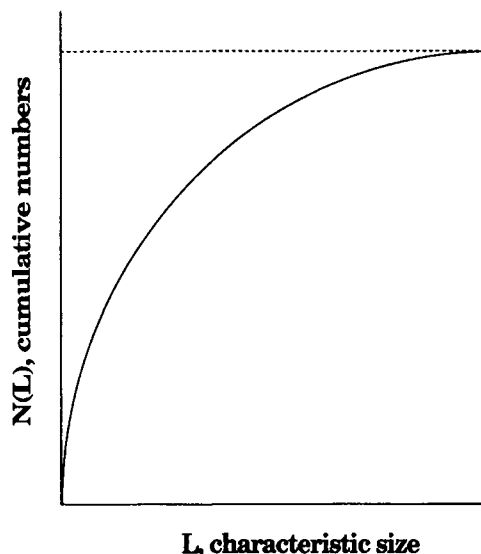


Figure 4.1 A typical cumulative numbers oversize plot.

encountered in the analysis of crystallizers. A typical cumulative oversize plot is shown in Figure 4.1. Such a plot would be constructed by summing the number of particles greater than zero. In this instance we are assuming that we can use a single characteristic dimension to describe each particle. This will be determined by the method of size measurement. The transformation from the numbers data, N , to population density, n , is then defined by

$$n = \left. \frac{dN}{dL} \right|_L \quad (4.3)$$

A population density distribution plot is shown in Figure 4.2. Typical units for n and N are no./m³ · m and no./m³, respectively.

The relationship between the number distribution, $N(L)$, and the number density distribution, $n(L)$, can be thought of as a transform. Specifically, Eq. (4.3) can be used to transform in one direction while Eq. (4.4) can be used for the reverse transformation.

$$N(L) = \int_0^L n(L)dL \quad (4.4)$$

This is very important in a practical sense because we measure distribution in the integral domain, i.e., $N(L)$. We do not directly measure $n(L)$, but calculate it. The conventional approach to use of the population balance utilizes $n(L)$; therefore, we almost always deal with transformed experimental data.

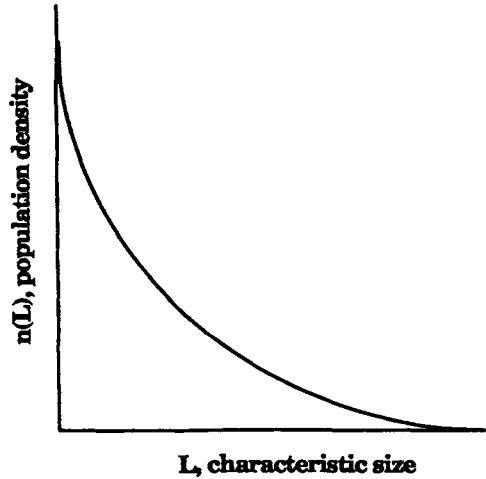


Figure 4.2 A typical population density versus size plot.

Many important properties of the crystal size distribution (CSD) can be calculated utilizing the population density. The total number of particles per unit volume, N_T , is

$$N_T = \int_0^{\infty} n(L) dL \quad (4.5)$$

In a similar fashion, the total area of the size distribution per unit volume, A_T , is

$$A_T = \int_0^{\infty} k_a L^2 n(L) dL \quad (4.6)$$

where k_a is the area shape factor that relates the area of a particle to the square of the characteristic dimension. A third property is the total mass per unit volume, M_T , which is also referred to as the suspension density. M_T is calculated

$$M_T = \rho k_v \int_0^{\infty} L^3 n(L) dL \quad (4.7)$$

Here, ρ is the density of the solid and k_v is the volumetric shape factor that relates the volume of a particle to its characteristic dimension cubed.

Eqs. (4.5), (4.6), and (4.7) can be used in a different manner upon changing the limits of integration. If the upper limit of integration is changed to L instead of ∞ , we obtain the number [shown in Eq. (4.4)], area, and mass distributions, $n(L)$, $A(L)$, and $M(L)$, respectively. The latter distribution is very important in that we often have specifications based on mass distribution. Furthermore,

we can use this relationship to convert from $M(L)$ to $n(L)$ when working with sieves.

Mean size can also be defined through use of the population density. For example, if it is desired to calculate the number based mean size, it can be found from

$$\bar{L}_{1.0} = \int_0^{\infty} L n(L) dL / \int_0^{\infty} n(L) dL = \int_0^{\infty} L n(L) dL / N_T \quad (4.8)$$

A more common mean size is that based on mass which is

$$\bar{L}_{4.3} = \int_0^{\infty} L^4 n(L) dL / \int_0^{\infty} L^3 n(L) dL \quad (4.9)$$

In fact, any weighting of mean size can be used in addition to Eqs. (4.8) and (4.9) through use of the recursion

$$\bar{L}_{i+1, i} = m_{i+1} / m_i \quad (4.10)$$

where m_i is the i th moment of the size distribution defined as

$$m_i = \int_0^{\infty} L^i n(L) dL \quad (4.11)$$

In a subsequent discussion of the population balance we will utilize the concept of moments in more detail. A comparison of the different mean sizes will be given for the distribution resulting from a continuous crystallizer.

4.2. MEASUREMENT OF SIZE DISTRIBUTION

There are two major classes of sizing techniques commonly used in practice: mass-based and number-based. The mass-based techniques include classical sieving procedures. Sieves are used by measuring the mass retained on a series of screens of progressively smaller size when moving from the top to the bottom of the stack. The mean size calculated on the basis of these weight measurements is the mass mean size, $\bar{L}_{4.3}$. If one wishes to convert sieve data to population density data, the following equation should be used

$$n = \frac{\Delta m}{k_v \rho \bar{L}^3 (\Delta L)} \quad (4.12)$$

where Δm is the weight retained on a sieve, k_v is the volumetric shape factor defined earlier, ρ is the particle mass density, \bar{L} is the mean size of the sieve on which the particles are retained and the sieve above it in the stack, and ΔL is the size difference between the two sieves just discussed. Example 4.1 shows data reduction reproduced from Randolph and Larson (1988).

EXAMPLE 4.1 Reduction of Sieve Data to Population Density Data

A known volume of mother liquor containing crystals is sampled from a crystallizer. They are filtered, washed with an appropriate washing solution to avoid agglomeration, dried, and weighed. Using the weight of crystals obtained and the volume of mother liquor sampled, the slurry density, M_T , is calculated to be 0.1 g/cm^3 of solids-free liquor (i.e., filtrate). The crystals are then sieved and the mass size range is 0.1. The crystal density and volumetric shape factor are known to be 2.0 g/cm^3 and 0.6, respectively. Determine the population density at $110 \mu\text{m}$ (the average size of the 100- to $120 \mu\text{m}$ size range).

Using Eq. (4.12) for the average size, which in this case is $110 \mu\text{m}$, is

$$n = \frac{\Delta m}{k_v \rho \bar{L}^3 (\Delta L)}$$

using $\Delta m = \Delta w M_T$, where Δw is the weight fraction in the size range.

$$\begin{aligned} n &= \frac{(0.1)(0.1 \text{ g/cm}^3)(10^{12} \mu\text{m}^3/\text{cm}^3)}{(0.6)(2.0 \text{ g/cm}^3)(110 \mu\text{m})^3(120 - 100 \mu\text{m})} \\ &= 313 \text{ no./cm}^3 \cdot \mu\text{m} \end{aligned}$$

Other techniques also based on mass are sedimentation and light scattering/diffraction. The most popular technique offered by several companies is Fraunhofer diffraction. In each case, including sieves, there will be some difficulty in measuring small particles in the presence of larger particles. This will manifest itself in poor estimation of the small size population density, a shortcoming that will become more obvious when nucleation rates are determined from crystal size distribution measurements.

A second class of measurement techniques, based on particle number, overcomes some of the problems associated with mass-based techniques. Electronic zone sensing, sometimes referred to as the "Coulter" principle, permits simultaneous particle size and number measurement. Particles are sized by suspending them in an electrolyte and drawing them through an aperture tube across

which a current is passed. As particles pass through the aperture, a change in conductivity occurs and an electrical pulse is created, the magnitude of which is proportional to the volume of the particles. Typically, the size reported is the equivalent spherical diameter, the diameter of a sphere with the same volume as the particle measured.

The electronic zone-sensing technique has been widely used as both a research and quality control tool. The major shortcoming of the technique is the requirement of an electrolyte solution in which to suspend the particles without causing dissolution. Other problems such as electrical noise and coincidence (two particles passing through the aperture at the same time) can usually be overcome by choice of appropriate experimental conditions. Example 4.2 shows data reduction using the Coulter-type data.

EXAMPLE 4.2 Reduction of Electronic Zone Sensing Data to Population Density Data

A set of typical electronic zone-sensing data are given in Table 4.1. The sample volume from the crystallizer was 1 ml and it was diluted into 100 ml of electrolyte. A sample of 0.1 ml was drawn through the aperture to record the particle numbers given in Table 4.2. Therefore, the basis for the particles is

$$\begin{aligned} \text{no./volume} &= \left(\frac{100 \text{ ml of electrolyte}}{1 \text{ ml of sample of magma}} \right) \frac{1}{(0.1 \text{ ml of electrolyte})} \\ &= \text{no./ml sample of magma} \times 1000 \end{aligned}$$

Therefore, the particle numbers appearing in Table 4.1 should be multiplied by 1000 to get them on the basis of milliliters of crystallizer magma.

To calculate the population density, where i denotes the channel number,

$$n_i = \frac{\Delta N_i}{L/\text{upper end} - L/\text{lower end}} = \frac{\Delta N_i}{\Delta L_i}$$

Using the data from Table 4.1, Table 4.2 can be constructed. A comparison of the numbers, $N(L)$, and population density, $n(L)$, plots are shown in Figures 4.3 and 4.4. It is important to note how similar the two plots can look, depending on the data under consideration.

TABLE 4.1 Example of Raw Data Obtained in a Coulter-Type Size Measurement Device

Channel	Size at Edge of Channel (μm)	Average Size of Channel (μm)	Particle No. in Channel
1	10	12.0	1000
2	14.0	17.0	2000
3	20.0	24.2	3000
	28.3		

TABLE 4.2 Coulter-Type Data Reduced to Population Density

Channel	$L_i (\mu\text{m})$	$\Delta N_i (\text{No./ml})$	$\Delta L_i (\mu\text{m})$	$n_i (\text{No./ml} \cdot \mu\text{m})$
1	12.0	1,000,000	4.0	250,000
2	17.0	2,000,000	6.0	333,000
3	24.2	3,000,000	8.3	361,000

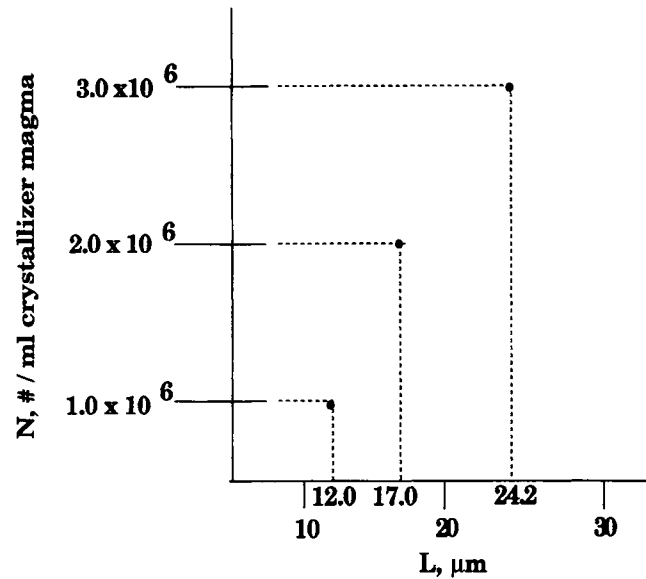


Figure 4.3 Numbers distribution data from text Example 4.2.

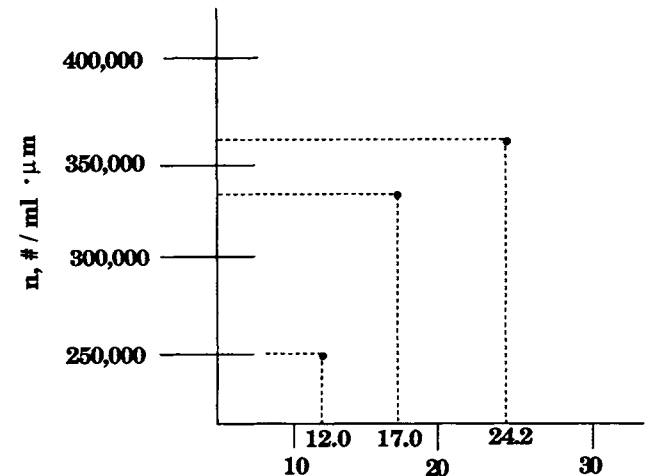


Figure 4.4 Population density distribution from text Example 4.2.

More recently, there have been in-process techniques developed. Focused Beam Reflectance Measurement (FBRN®) uses an immersion probe and is capable of in situ measurement of particle chord length. Obscuration measurement can also be used as an in line size measurement. Acoustic size measurement is also emerging as in-process technique that permits use in heavy slurries that are difficult to measure using optical techniques.

Microscopy can also be employed as a number-based sizing technique. The major shortcoming is the requirement of counting individual particles. Even with use of image analysis techniques, this shortcoming makes it difficult to acquire sufficient counts so as to be statistically significant. Another shortcoming is the two-dimensional nature of the sizing technique. While the third dimension can sometimes be inferred by shadowing techniques, only two dimensions are directly measured. The main considerations in choosing a sizing technique are usually cost and convenience. Irrespective of the technique chosen, it is imperative that the practitioner is aware of the technique's strengths and shortcomings.

4.3. THE MIXED SUSPENSION, MIXED PRODUCT REMOVAL (MSMPR) FORMALISM FOR THE POPULATION BALANCE

The power of the population balance for analysis of crystallizers is demonstrated by its application to a continuous crystallizer. It is desired to predict the product CSD from a continuous, stirred tank reactor (CSTR). Such a continuous crystallizer is called a mixed suspension, mixed product removal (MSMPR) crystallizer (Randolph and Larson 1988). Several assumptions are involved in this formalism. First, it is assumed that the product CSD is the same as that found within the crystallizer, i.e., no classification of the particles in the crystallizer takes place. This is the standard assumption used in reaction engineering to define a well-mixed reaction vessel. Second, it is assumed that particles are formed only by nucleation and increase in size only through growth. The processes of breakage, attrition, and agglomeration are negligible. Finally, the shape factors for particles are not a function of size. This permits the use of a single characteristic size to be used as the dimension to describe the entire size range.

Using the same approach as is used to write material and energy balances, a population balance can also be constructed. Consider an arbitrary size within the crystallizer (Figure 4.5), for the size range L_1 to L_2 with population densities n_1 and n_2 , respectively, the balance is

$$\text{No. in} = \text{no. out} \quad (4.13)$$

Particles may enter or leave the size range via either growth or flow. If G is denoted as the growth rate of the characteristic dimension, V is the crystallizer volume, and Q is the volumetric flow rate, the four terms to be considered are

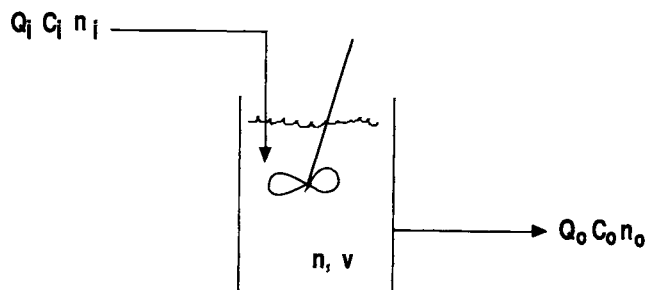


Figure 4.5 Schematic diagram of an MSMPR crystallizer.

1. Number of particles entering size range by growth— Vn_1G_1 .
2. Number of particles leaving the size range by growth— Vn_2G_2 .
3. Number of particles entering the size range by flow— $Q_i\bar{n}_i\Delta L$, where \bar{n}_i = average in L_1 to L_2 and $\Delta L = L_2 - L_1$.
4. Number of particles leaving the size range by flow— $Q\bar{n}\Delta L$.

Equating the terms in Eq. (4.13), yields,

$$Vn_1G_1 + Q_i\bar{n}_i\Delta L = Vn_2G_2 + Q\bar{n}\Delta L \quad (4.14)$$

Upon arrangement, Eq. (4.14) becomes

$$V \left[\frac{n_2G_2 - n_1G_1}{\Delta L} \right] = Q_i\bar{n}_i - Q\bar{n} \quad (4.15)$$

Taking the limit as ΔL approaches zero permits the mean values to be replaced by single values and results in

$$V \frac{d(Gn)}{dL} = Q_i n_i - Qn \quad (4.16)$$

Upon observing that $V/Q = \tau$, mean retention time, and assuming no particles are in the feed stream, i.e., $n_i = 0$, Eq. (4.16) reduces to

$$\tau \frac{d(Gn)}{dL} + n = 0 \quad (4.17)$$

If the system under consideration follows McCabe's ΔL law, $G \neq G(L)$, the result becomes

$$\frac{dn}{dL} = -\frac{n}{G\tau} \quad (4.18)$$

Eq. (4.18) is an ordinary differential equation that can be separated and integrated. If the boundary condition of n^0 representing zero-sized particles is employed, i.e., $n(0) = n^0$, the final result is

$$n = n^0 \exp\left(-\frac{L}{G\tau}\right) \quad (4.19)$$

Therefore, the growth rate, G , can be determined from the slope of the CSD.

The second kinetic parameter that can be deduced from the CSD is the nucleation rate. If the nucleation rate, B^0 , is the rate of appearance of near zero-sized particles, an expression can be derived, thus

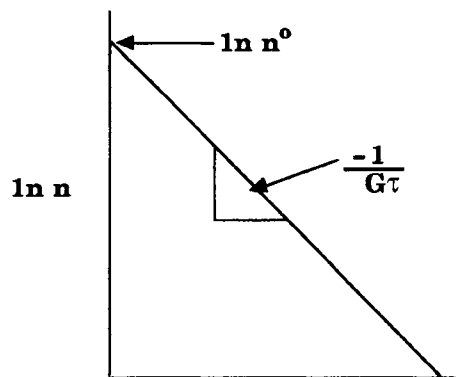


Figure 4.6 Semilogarithmic population density versus size plot predicted by application of the MSMPR crystallizer formalism.

$$B^o = \frac{dN}{dt} \Big|_{L=0} = \left[\frac{dN}{dL} \cdot \frac{dL}{dt} \right]_{L=0} = n^o G \quad (4.20)$$

Therefore, a semilogarithmic plot of the population density versus size yields n^o from the intercept and G from the slope (Figure 4.6).

EXAMPLE 4.3
Sieve Analysis for an MSMPR Crystallizer. (Adapted from Belter et al. 1988.)

An MSMPR crystallizer was used to produce sucrose. At steady-state, a sieve analysis was performed to determine the size distribution. The percentage retention on the respective sieves was measured and is presented in Table 4.3.

The suspension density was measured as 335 g/l and the retention time was fixed at 2.5 h. We would like to perform an MSMPR analysis on these data to determine the crystal nucleation and growth rates.

First, the data must be converted from cumulative percentages to population density. This is done by first determining what the mean size will be for each size range. Since the crystals retained on a given sieve must be larger than the sieve size and smaller than the sieve size above it in the stack, we will use the arithmetic mean to represent the size. So, for example, the crystals average size retained on the 20 mesh in our example is

$$\bar{L}_{20} = \frac{1.199 + 0.841}{2} = 1.02 \text{ mm}$$

The cumulative sieve data are reduced to population density by using Eq. (4.12). We will assume $k_v = 1$ and $\rho = 1588 \text{ g/cm}^3$. For the 28-mesh crystals

$$\begin{aligned} n &= \frac{\Delta m}{k_v \rho \bar{L}^3 \cdot \Delta L} \\ &= \frac{(0.14 - 0.03)335 \text{ g/l}}{(1)(1.588 \text{ g/cm}^3)} \\ &\quad \times (1 \text{ cm}^3/1000 \text{ mm}^3)(0.718 \text{ mm/no.crystals})^3(0.246 \text{ mm}) \\ &= 255,000 \frac{\text{no.crystals}}{\text{mm} \cdot \text{l}} \end{aligned}$$

TABLE 4.3 Mass Retained in Sieve Analysis of Example 4.3

Sieve (Mesh)	Size of Mesh (mm)	Cumulative Percent Retained
14	1.199	—
20	0.841	3
28	0.595	14
35	0.420	38
48	0.297	76
65	0.149	92

TABLE 4.4 Population Density Distribution Data Obtained from Sieve Analysis in Example 4.3

Sieve (Mesh)	Average Size Retained (mm)	Difference, ΔL (mm)	ln (Population Density)
20	1.02	0.358	9.80
28	0.72	0.246	12.5
35	0.51	0.175	14.6
48	0.36	0.123	16.5
65	0.25	0.148	17.0

Since τ is fixed by the choice of experimental conditions, nucleation and growth rates can be determined simultaneously by a single measurement of the CSD at steady-state. Example 4.3 shows the use of the population balance in determination of nucleation and growth kinetics.

The remaining values are given in Table 4.4.

Upon constructing the semilogarithmic population density versus size plot, Figure 4.7 results. The growth rate is calculated

$$\begin{aligned} G &= \frac{1}{\text{slope}} \left(\frac{1}{\tau} \right) \\ &= - \frac{1}{9.9(2.5 \text{ h})} \\ &= 0.040 \text{ mm/h} \end{aligned}$$

Since the intercept is $n^o = 3.25 \times 10^8 (\text{no./mm} \cdot \text{l})$, the nucleation rate is

$$\begin{aligned} B^o &= n^o G \\ &= \left(3.25 \times 10^8 \frac{\text{no.}}{\text{mm} \cdot \text{l}} \right) (0.40 \text{ mm/l} \cdot \text{h}) \\ &= 1.3 \times 10^7 \frac{\text{no.}}{\text{l} \cdot \text{h}} \end{aligned}$$

An alternate approach (one that should be used with caution!) is to plot the cumulative numbers directly. Since

$$N(L) = \int_L^\infty n dL$$

where $N(L)$ is cumulative oversize, we can insert the MSMPR crystallizer result from Eq. (4.18) and upon integrating obtain

$$N(L) = B^o \tau \exp(-L/G\tau)$$

So we see that cumulative oversize plots can also yield exponentials only with a different intercept. This feature is often responsible for novices' confusion on whether they are plotting n or N ! Caveat emptor!

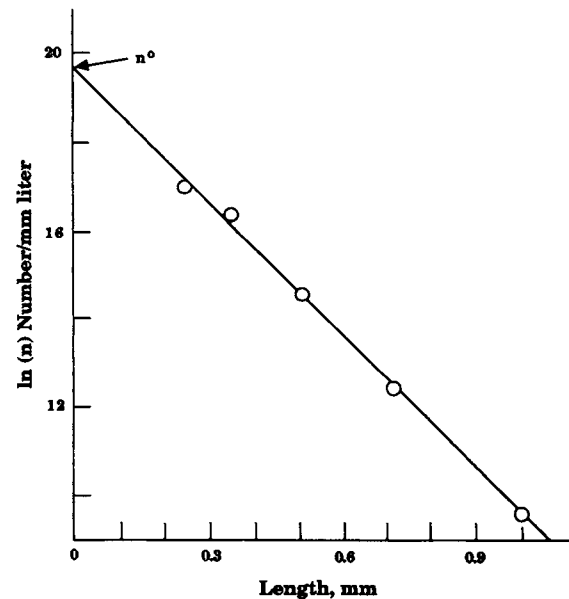


Figure 4.7 Semilogarithmic population density versus size plot obtained by MSMPR analysis of data in Example 4.3. (Data from Belter et al. 1988.)

The exponential distribution given in Eq. (4.19) has a convenient analogy to reaction engineering. An exponential residence time distribution is obtained from a CSTR. Therefore, since an MSMR crystallizer has an exponential residence time distribution, it should come as no surprise that the CSD has that form because it is caused by kinetic events, namely nucleation and growth.

In addition to its physical significance, the exponential size distribution is convenient for calculation of several quantities relative to the CSD. For example, from Eq. (4.5) the total number of particles, N_T , can be determined

$$\begin{aligned} N_T &= \int_0^\infty n(L) dL \\ &= \int_0^\infty n^0 \exp\left(-\frac{L}{G\tau}\right) dL = m_0 = n^0 G\tau \end{aligned} \quad (4.21)$$

Similarly, the area, A_T , and suspension density, M_T , can be determined from Eqs. (4.5) and (4.6), respectively.

$$A_T = k_a m_2 = 2k_a n^0 (G\tau)^3 \quad (4.22)$$

$$M_T = \rho k_v m_3 = 6k_v \rho n^0 (G\tau)^4 \quad (4.23)$$

Finally, using Eq. (4.10) the various mean sizes can be calculated

$$\bar{L}_{1,0} = G\tau \quad (4.24a)$$

$$\bar{L}_{2,1} = 2G\tau \quad (4.24b)$$

$$\bar{L}_{3,2} = 3G\tau \quad (4.24c)$$

$$\bar{L}_{4,3} = 4G\tau \quad (4.24d)$$

4.3.1. MASS BALANCE

From the preceding discussion, it is clear that irrespective of the crystallization system under consideration the size distribution will

have the same form. However, the mass balance must also be satisfied.

The mass balance for a crystallization system is written for the phase change. That is, the rate at which solute is lost from the solution phase must be equal to the rate at which mass is gained by the solid phase. In the absence of seeding, $n_i = 0$, the mass balance can be written

$$Q_i C_i - Q_0 C_0 = Q_0 M_T \quad (4.25)$$

Since the mass rate of deposition due to nucleation is usually negligible relative to that of crystal growth, $Q_0 M_T$ can be equated to the growth on the particle surface

$$Q_i C_i - Q_0 C_0 = Q_0 M_T = \frac{1}{2} G A_T \rho V \quad (4.26)$$

where the 1/2 is necessary to account for face growth and L refers to a diameter rather than a radius. If $\delta C = (Q_i/Q_0)(C_i - C_0)$ and Eq. (4.21) is used for A_T , then Eq. (4.26) can be rearranged

$$G = \frac{2(\delta C)}{\rho k_a \tau \int_0^\infty n L^2 dL} \quad (4.27)$$

Growth rate is a function of supersaturation. If a linear relation is assumed (a nonlinear relation can also be assumed)

$$G = k_1 (C - C_{eq}) = k_1 s \quad (4.28)$$

where C_{eq} is the saturation concentration and supersaturation is defined thus, $s = C - C_{eq}$. Upon equating Eqs. (4.27) and (4.28) and rearranging, the following result is obtained

$$s = \frac{k(\delta C)}{\tau \left[\int_0^\infty n L^2 dL \right]} \quad (4.29)$$

Previously, it has been shown that both growth and nucleation are functions of supersaturation, i.e., $B^0 = B^0(s)$ and $G = G(s)$.

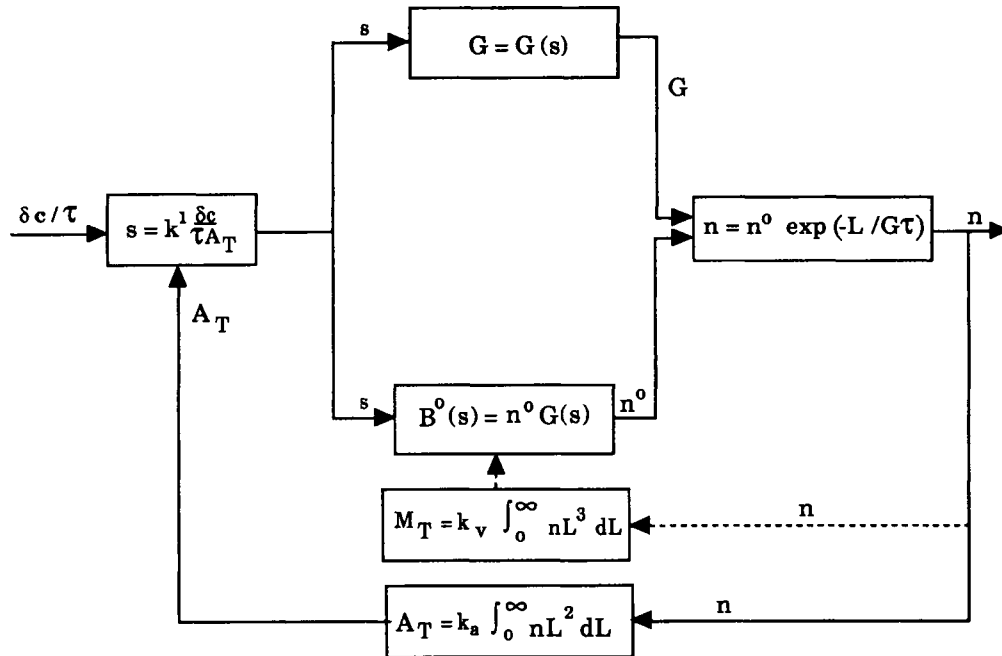


Figure 4.8 Information feedback diagram illustrating the interaction between size distribution and kinetics resulting from the constraint of the mass balance.

The interaction among the kinetic expressions and the mass balance can be conveniently expressed in the form of an information feedback loop as shown in Figure 4.8. Here it is shown how the size distribution, which dictates the area and mass of the distribution, impacts on the kinetics by altering the supersaturation, s . It is this information feedback of the system that makes control of crystallizers a challenging problem in that overshoot is easily caused.

4.4. GENERALIZED POPULATION BALANCE

As is the case for all balance equations, we can generalize the population balance. The details of the derivation are presented elsewhere (Randolph and Larson 1988).

The basis of the derivation is the concept of particle phase space, of a system, i.e., the least number of independent coordinates that allows a complete description. These coordinates are either internal, which describe properties independent of position, or external, which describe spatial distribution.

EXAMPLE 4.4 Reduction of the Macro-Distributed Population Balance for an MSMR Crystallizer

At steady state, all time derivatives are zero so

$$\frac{\delta n}{\delta t} + \frac{d(\log V)}{dt} = 0$$

No breakage or agglomeration occurs in an MSMR crystallizer so $B = D = 0$. The internal coordinate of interest is particle length so, $v_i = G = dL/dt$. Furthermore,

$$\nabla \cdot v_i n = \frac{d(Gn)}{dL} = G \frac{dn}{dL}$$

if $G \neq G(L)$. The only flow rate of particles occurs in the exit stream

A Lagrangian viewpoint results in the form

$$\frac{\delta n}{\delta t} + \nabla \cdot (v_e n) + \nabla \cdot (v_i n) = B - D \quad (4.30)$$

where n is the population density; t is time; v_e is the velocity along an external coordinate, i.e., particle velocity; v_i is the velocity along an internal coordinate, e.g., $G = dL/dt$; B is a birth function; and D is a death function. This form is also known as the micro-distributed population balance.

An Eulerian viewpoint results in the form

$$\frac{\delta n}{\delta t} + \nabla \cdot v_i n + n \frac{d(\log V)}{dt} = B - D - \sum_k \frac{Q_k n_k}{V} \quad (4.31)$$

where all items are the same as before with the addition of the system volume, V , and the flow rates across the system boundary, Q_k . This expression is also known as the macro-distributed population balance and is the most useful form for crystallizers. Example 4.4 shows reduction of the expression.

(if we assume no seeding) so

$$\frac{Q_k n_k}{V} = \frac{Q}{V} n = \frac{n}{\tau}$$

Collecting all terms we obtain

$$G \frac{dn}{dL} + \frac{n}{\tau} = 0$$

or

$$\frac{dn}{dL} + \frac{n}{G\tau} = 0$$

which is the same result obtained previously for an MSMR crystallizer.

The macro-distributed population balance also permits us to analyze the performance of a continuous crystallizer, which is not at steady state. The population balance reduces to

$$\frac{\delta n}{\delta t} + G \frac{dn}{dL} + \frac{n}{\tau} = 0$$

for an unsteady state MSMR crystallizer.

4.5. EXTENSION AND VIOLATIONS OF THE MSMR MODEL

Unfortunately, in many cases the semilogarithmic population density size plot shown in Figure 4.6 is not obtained. A common occurrence when analyzing data at smaller sizes, e.g., $< 100 \mu\text{m}$, is to obtain a strong upward curvature. The following discussion gives possible reasons and approaches to analyzing such data.

4.5.1. SIZE-DEPENDENT CRYSTAL GROWTH

A possible interpretation is size-dependent growth, wherein smaller crystals grow slower than larger ones. In order to model this

situation it is necessary to return to the differential equation derived from the population balance

$$\frac{d(Gn)}{dL} + \frac{n}{\tau} = 0 \quad (4.32)$$

At this point, instead of assuming $G \neq G(L)$, an empirical relation is assumed for $G(L)$. The most widely used one is the ASL model (Abegg et al. 1968)

$$G = G_0(1 + \gamma L)^b, \quad b < 1 \quad (4.33)$$

Upon substitution into the population balance and solutions, the following result is obtained for the population balance

$$n(L) = K n^0 (1 + \gamma L)^{-b} \exp[-(1 + \gamma L)^{1-b} / G_0 \tau \gamma (1 - b)]. \quad (4.34)$$

where $K = \exp[1/G_0 \tau \gamma (1 - b)]$ and $b < 1$. The equation can be fit to experimental data to determine the constants G_0 , b , and γ . An example of a plot resulting from the results in Eq. (4.34) is shown in Figure 4.9.

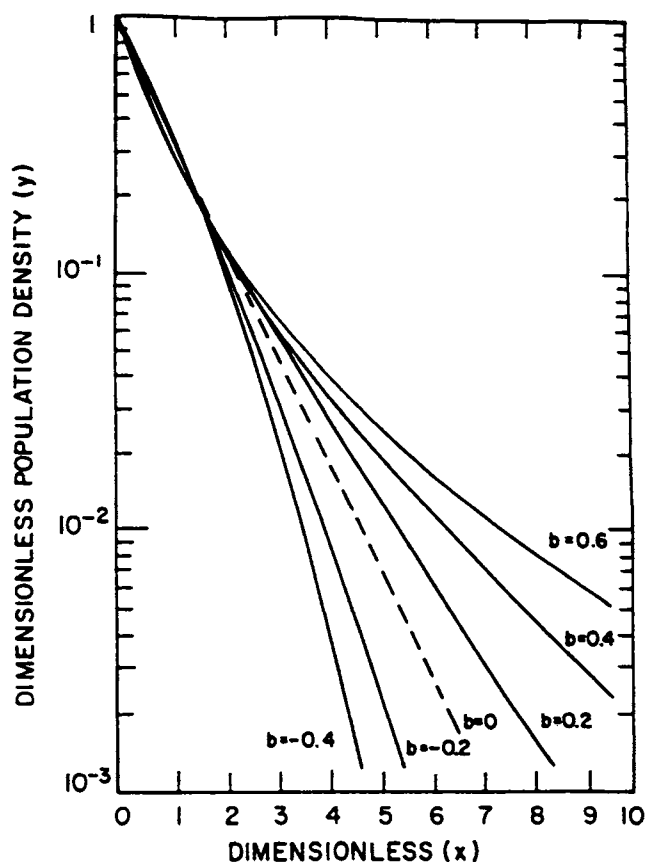


Figure 4.9 Dimensionless CSD from Eq. (4.34). [From "Crystal Size Distributions in Continuous Crystallizers when Growth Rate is Size Dependent," C.F. Abegg, J.D. Stevens, and M.A. Larson (1968), *AIChE J.*, 14(1), pp. 118–122. Reproduced by permission of the American Institute of Chemical Engineers © 1968 AIChE.]

4.5.2. GROWTH RATE DISPERSION

A second set of phenomena that should be included in CSD modeling is growth rate dispersion. Two possible mechanisms have been modeled and observed experimentally.

Random Fluctuation Model (Randolph and White 1977). In this case the growth of crystals fluctuates during the course of time. It is possible to write the overall population balance as

$$\frac{\partial n}{\partial t} + \nabla \cdot \mathbf{N} = \text{sum of sources and sinks} \quad (4.35)$$

In this form the flux vector \mathbf{N} is

$$\mathbf{N} = (\nu_z n) \delta_z + (Gn) \delta_L \quad (4.36)$$

where, as before, there is the external term, $\nu_z n$, and an internal term, Gn .

In the Random Fluctuation Model, it is proposed that both flow and velocity fluctuations occur, requiring two more diffusivity terms

$$\mathbf{N} = \left(\nu_z n + D_a \frac{\partial n}{\partial z} \right) \delta_z + \left(Gn + D_G \frac{\partial n}{\partial L} \right) \delta_L \quad (4.37)$$

where

D_a = axial diffusivity

D_G = growth rate diffusivity

Substituting into the general population balance equation yields for the micro-distributed case

$$\frac{\partial n}{\partial t} + \nu_z \frac{\partial n}{\partial z} + \frac{\partial(Gn)}{\partial L} = B - D + D_a \frac{\partial^2 n}{\partial z^2} + D_G \frac{\partial^2 n}{\partial L^2} \quad (4.38)$$

and the macro-distributed case

$$\frac{\partial n}{\partial t} + \frac{\partial(Gn)}{\partial L} + n \frac{\partial(\log V)}{\partial t} = \sum_j \frac{Q_j n_j}{V} + B - D + D_G \frac{\partial^2 n}{\partial L^2} \quad (4.39)$$

An interesting consequence of this model is its solution for an MSMPR crystallizer. The net result is to produce a linear semilogarithmic population density size plot with a larger mean size than would be predicted from the growth rate. Therefore, the standard MSMPR analysis can be used.

Constant Crystal Growth Model. In this instance, crystals have an inherent constant growth rate, but the rate from crystal-to-crystal varies. The modeling of this phenomenon must be accomplished by use of probability transform techniques due to the presence of a growth rate distribution. The complete solution for the population density yields a semilogarithmic population density plot that is concave upwards similar to size-dependent growth (Berglund and Larson 1984). Since it is relatively difficult to handle, a moment approximation was developed for an MSMPR crystallizer (Larson et al. 1985).

$$m_L(j) = j! \tau^j m_G(j) \quad (4.40)$$

where

$m_L(j)$ = j th moment of the CSD

$m_G(j)$ = j th moment of the growth rate distribution

Determination of which of the preceding phenomena is operative is not always an easy matter. One approach is to study the growth of individual crystals. If one can satisfactorily accomplish this, the different phenomena can be separated. Figure 4.10 depicts the type of results one would expect from the various phenomena.

4.5.3. METHODS TO TREAT EXPERIMENTAL DATA

Effective Nucleation Rates. A simple approach to handling the problem of upward curvature of the semilogarithmic size plot at small size is to use linear extrapolation. Figure 4.11 shows an example of such data for the sucrose-water system. Previously, we saw data for sucrose crystallization in Figure 4.7. These data obeyed the MSMPR formalism since small-size population densities were not measured. The data shown in Figure 4.11, also for the sucrose-water system, were measured using a Coulter counter, which allowed the smaller sizes to be determined. Since the linear portion of the plot represents the product sized crystals, a linear extrapolation to zero size yields an "effective" zero-size population density. Therefore, an "effective" nucleation rate can also be determined. This approach does not require knowledge of the cause of the curvature.

Sum of Growth Rate Distributions. Berglund and de Jong (1990) devised a method of data treatment that allows use of the entire size distribution. It was previously shown that the moments of the growth rate distribution can be related to the moments of the size distribution, thus,

$$m_L(j) = j! \tau^j m_G(j) \quad (4.41)$$

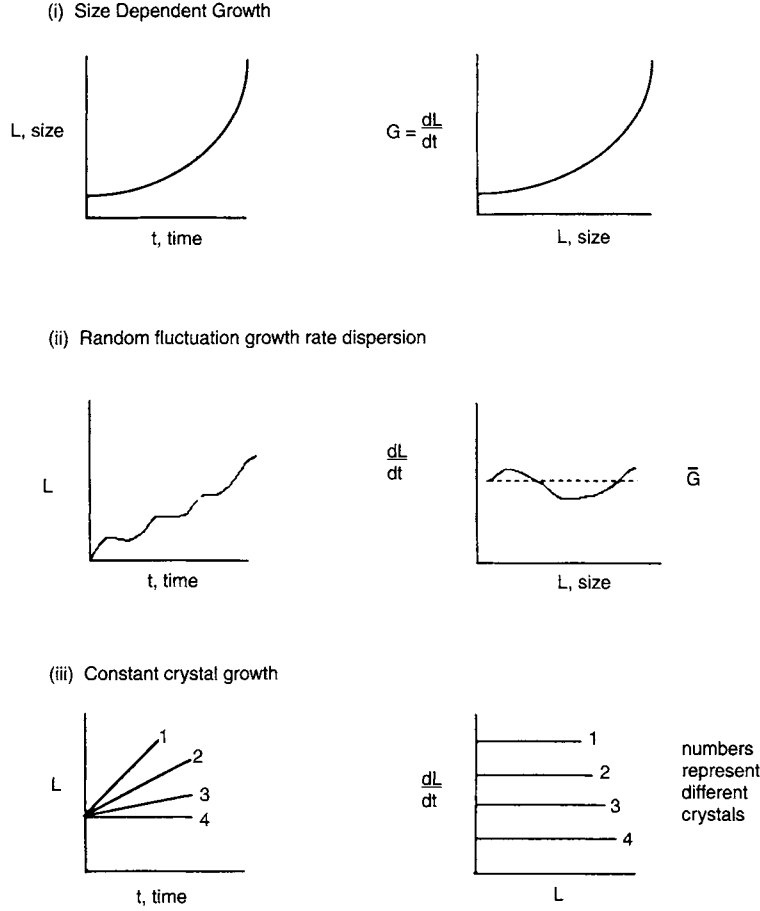


Figure 4.10 Comparison of the consequences of size-dependent growth and growth rate dispersion. Consider an experiment wherein several crystals can be monitored independently in time.

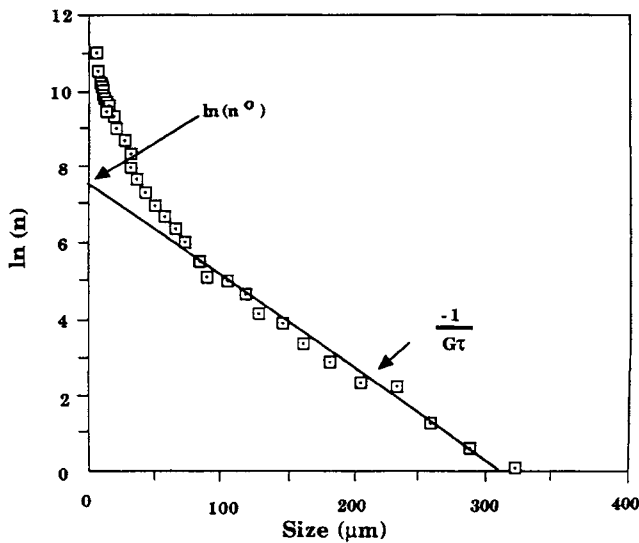


Figure 4.11 Semilogarithmic population density size plot depicting use of linear extrapolation to determine “effective” zero-size population density. Data are for the sucrose-water system. (Liang and Hartel 1991.)

Using the definition of mean sizes

$$\bar{L}_{j+1,j} = \frac{m_L(j+1)}{m_L(j)} \quad (4.42)$$

we can rewrite this as

$$\bar{L}_{j+1,j} = (j+1)\tau \frac{m_G(j+1)}{m_G(j)} \quad (4.43)$$

From this relation the growth rate distribution that causes curvature can be determined by guessing different forms and checking against the mean sizes.

Upon successful fit of data the nucleation and growth kinetics can be determined.

Since

$$m_T = \rho k_v B^0 \tau m_L(3) \quad (4.44)$$

and

$$m_L(j) = j! \tau^j m_G(j), \text{ then} \quad (4.45)$$

$$m_T = 6 \rho k_v B^0 \tau^4 m_G(3) \quad (4.46)$$

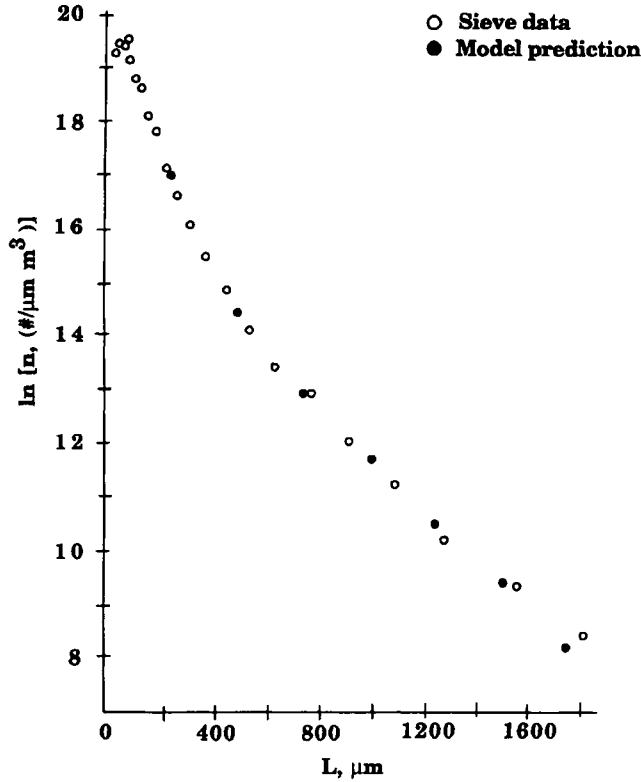


Figure 4.12 Semilogarithmic population density size plot for the sucrose-water system depicting the quality of fit when using a sum of two exponentials for the data. (Berghlund and de Jong 1990.)

and upon rearranging

$$B^0 = 6\rho k_v \tau^4 m_G(3) \quad (4.47)$$

using the parameters of the growth rate distribution

$$\bar{G} = m_G(1) \quad (4.48)$$

$$\sigma_G^2 = m_G(2) - m_G(1)^2 \quad (4.49)$$

A typical semilogarithmic population density size plot obtained from a 1400-l pilot scale sucrose crystallizer is shown in Figure 4.12. It was found that a single growth rate distribution is insufficient to the data. Surprisingly, a combination of two growth rates was all that was necessary, i.e., the sum of two exponentials reproduced the experimental data. This is particularly useful since it now permits the use of effective rates that can be determined unambiguously.

4.5.4. AGGLOMERATION

In many systems, particularly precipitating systems such as proteins, agglomeration is an important factor and cannot be overlooked. Unlike the simple case of crystal growth, it is necessary to write the population balance in volume coordinates (Hartel and Randolph 1986).

$$\frac{\partial n}{\partial t} + \partial \left(\frac{nG_v}{\partial v} \right) + \frac{n - n_i}{\tau} = B_a - D_a + B_d - D_d + \int_0^\infty \delta(v - v_a) B_a dV \quad (4.50)$$

where

$$B_a - D_a = \text{net formation by aggregation}$$

$$B_d - D_d = \text{net formation by disruption}$$

The last term corresponds to growth and aggregation into the lowest measurable size range v_a . The aggregation of two particles of size u and $v - u$ into a particle of size v can be written

$$B_a = \frac{1}{2} \int_0^v K(u, v-u) n(u, t) n(v-u, t) du \quad (4.51)$$

and

$$D_a = n(v, t) \int_0^\infty K(u, v) n(u, t) du \quad (4.52)$$

where the aggregation kernel, $K(u, v)$, is chosen to correspond to the mechanism of aggregation. Several possible aggregation kernels are listed in Table 4.5.

Several possible forms exist for the disruption terms, B_d and D_d . The most tractable form is the two-body equation volume function. It is assumed that one particle breaks into two smaller equal volume particles

$$B_d(v) = 2D_d(2v) \quad (4.53)$$

In the case where D_d is proportional to volume and population density

$$D_d = K_d v n(v) \quad (4.54)$$

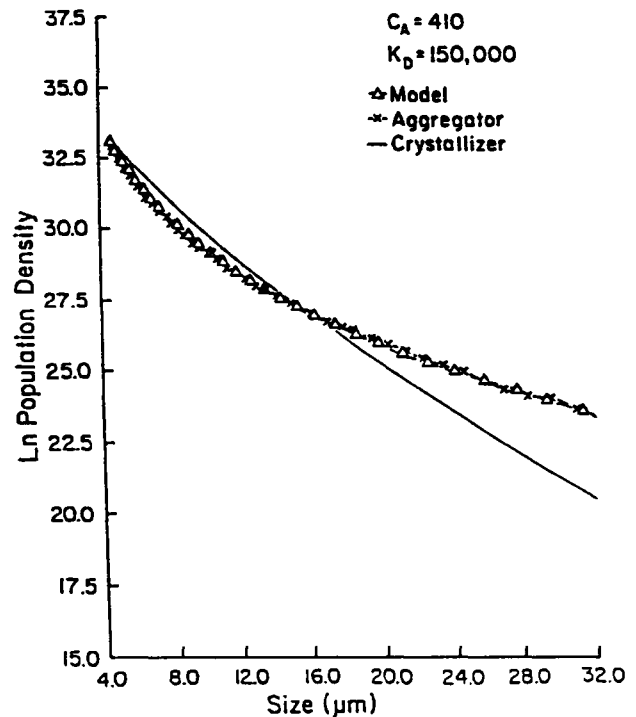


Figure 4.13 Curvature in a semilogarithmic population density size plot caused by agglomeration. [From "Mechanisms and Kinetic Modeling of Calcium Oxalate Crystal Aggregation in a Urinelike Liquor," R.W. Hartel, B.E. Gottung, A.D. Randolph, and G.W. Drach (1986), *AIChEJ.* 32(7), pp. 1176-1185. Reproduced by permission of the American Institute of Chemical Engineers. © 1986 AIChE.]

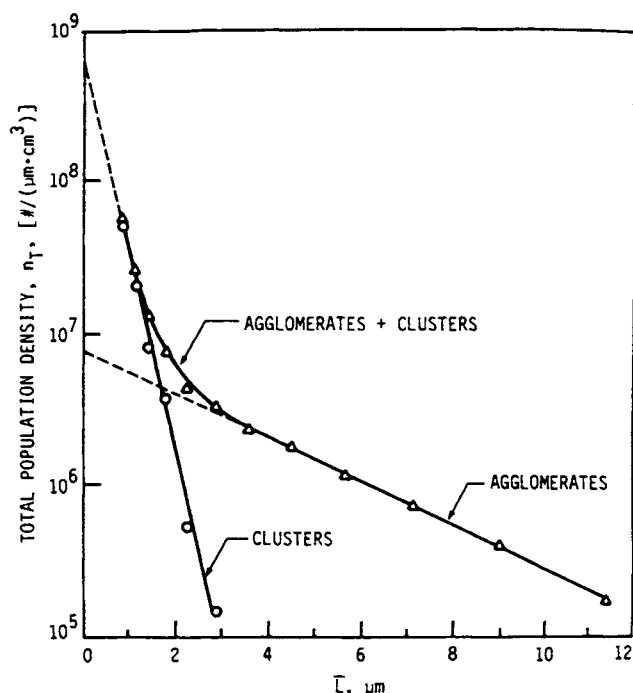


Figure 4.14 CSD of ammonium polyuranate showing clusters and agglomerates. NH_3 : Uranium mole ratio = 2.20; pH = 7.10; $\tau = 13\text{min}$; $T = 25^\circ\text{C}$. (Data from Hoyt 1978.)

and

$$B_d = 4K_D v n(2v) \quad (4.55)$$

Clearly, solutions to the population balance in the presence of agglomeration are difficult. However, many important industrial systems exhibit this behavior making it a very active area of research.

An example of aggregation and its modeling can be seen in Figure 4.13, taken from Hartel and Randolph (1986). Clearly, aggregation can result in similar semilogarithmic population density size plots to those found in size-dependent growth and growth rate dispersion.

Other examples of agglomeration have appeared in the literature. In the first case, Hoyt (1978) showed that a curved population density size plot resulted from agglomeration during the precipitation of ammonium polyuranate. An example of such data are shown in Figure 4.14. Glatz et al. (1987) showed

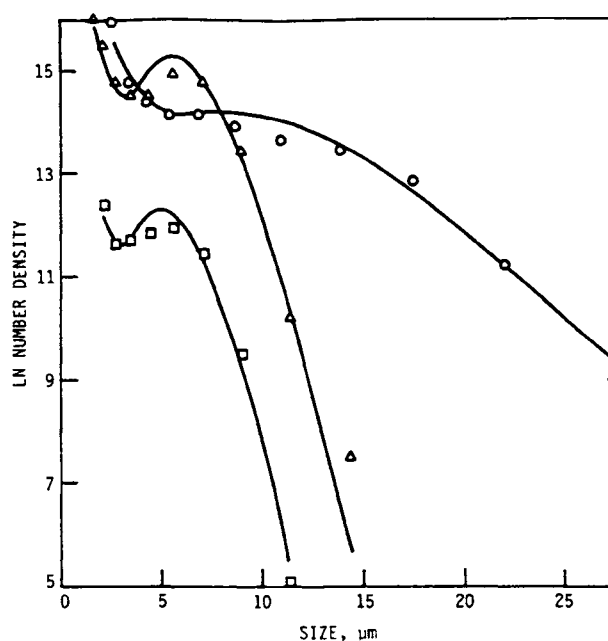


Figure 4.15 Particle size distribution of protein aggregate in a continuous stirred-tank reactor: comparison of model with experimental data. 0.15 kg/m^3 ; Δ , 300 kg/m^3 ; \circ , 25.00 kg/m^3 . [From "The Formation and Growth of Protein Precipitates in a Continuous Stirred-Tank Reactor," C.E. Glatz, M. Hoare, and J. Landa-Vertiz (1987), *AIChE J.* 32(7), pp. 1196–1204. Reproduced by permission of the American Institute of Chemical Engineers. © 1987 AIChE.]

that agglomeration and breakup could result in the appearance of a local maxima in a population density plot as shown in Figure 4.15.

4.5.5. ALTERATION OF RESIDENCE TIME DISTRIBUTION TO CONTROL CSD

A possible method for changing a CSD from an MSMPR crystallizer is the use of fines destruction or classified product removal. In the case of fines destruction, it is assumed that small crystals in the size range from 0 to L_F are withdrawn at a flow rate $(R - 1)Q_0$, while crystals in the range L_F to ∞ are withdrawn at Q_0 .

R is the ratio of product to fines drawdown times and

$$\begin{aligned} \tau_F &= V/RQ_0 & L < L_F \\ \tau_p &= V/Q_0 & L > L_F \end{aligned}$$

The population density plot for this case is shown in Figure 4.16, so it can be seen that larger average size can be obtained at the expense of a wider distribution.

TABLE 4.5 Aggregation Kernels

Brownian motion	$K(u, v) = \frac{2kT}{3\mu} [u^{1/3} + v^{1/3}] [u^{-1/3} + v^{-1/3}]$
Laminar shear	$K(u, v) = \frac{4}{3} Sh [u^{1/3} + v^{1/3}]^3$
Turbulent diffusion	$K(u, v) = k_1 U [u^{1/3} + v^{1/3}]^3$
Turbulent inertia	$K(u, v) = 0.2 \frac{\rho^{3/4}}{\rho_0^{3/4} \nu^{3/4}} E_i [u^{1/3} + v^{1/3}]^2 (u^{2/3} - v^{2/3})$
Gravitational settling ($L < 50\text{ }\mu\text{m}$)	$K(u, v) = C_A E_i (u^{1/3} + v^{1/3})^2 u^{2/3} - v^{2/3} $
Gravitational settling ($L > 50\text{ }\mu\text{m}$)	$K(u, v) = C_A E_i (u^{1/3} + v^{1/3})^2 u^{1/3} - v^{1/3} $
Semiempirical formulation	$K(u, v) = C_A E_i (u - v)^2 / (u + v)$

(Data from Hartel and Randolph 1986.)

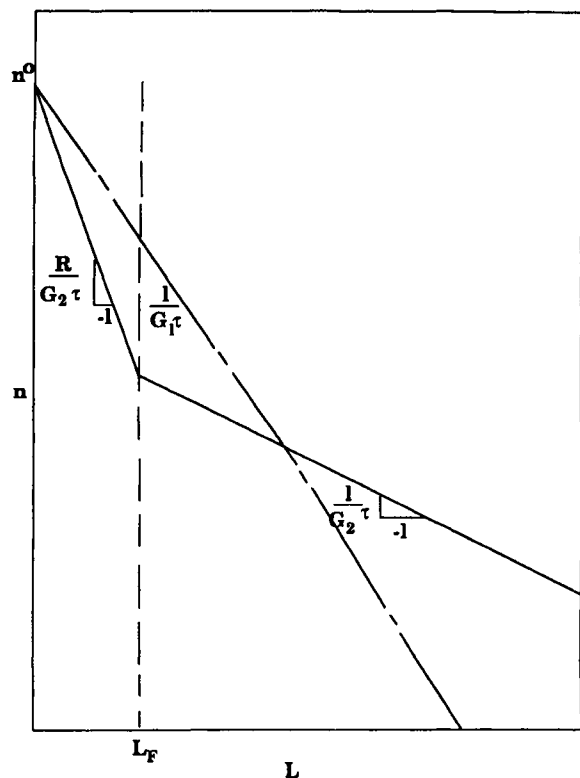


Figure 4.16 Hypothetical population density plot without (---) and with (—) fines removal. (Data from Larson and Randolph 1969.)

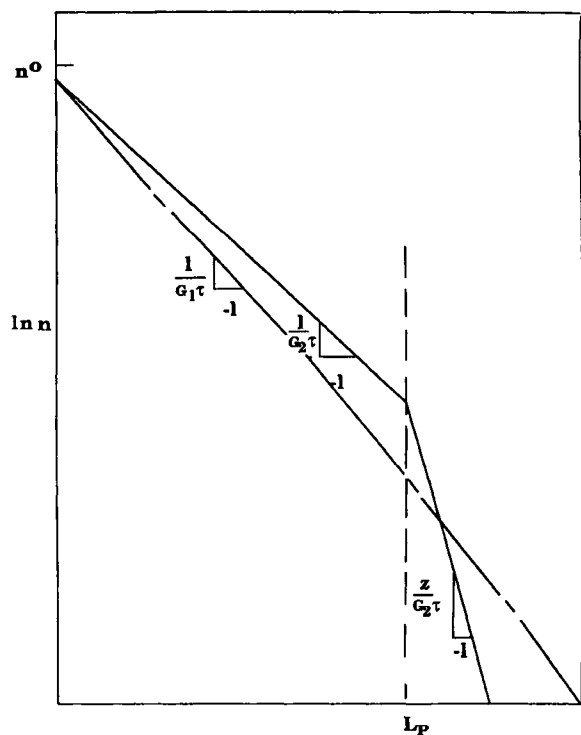


Figure 4.17 Hypothetical population density plot without (---) and with (—) classified product removal. (Data from Larson and Randolph 1969.)

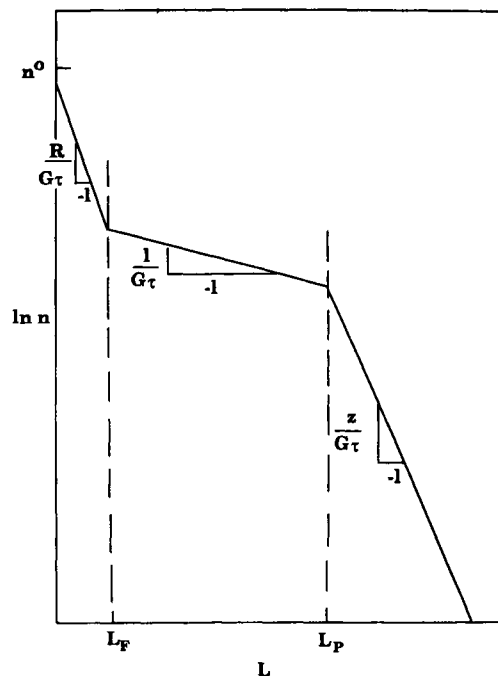


Figure 4.18 Hypothetical population density plot with classified product removal and fines destruction. (Data from Larson and Randolph 1969.)

A second alternative is classified product removal. Figure 4.17 shows the

$$\tau_u + V/Q_0 = \tau \quad L < L_p$$

$$\tau_p + V/zQ_0 = \tau/z \quad L > L_p$$

of this possibility to the general MSMPR case.

TABLE 4.6 Summary of Types of Semilogarithmic Population Density Plots and Potential Causes

Type	Appearance	Cause
linear		MSMPR formalism is obeyed
concave upward		(i) size dependent growth rate (ii) growth rate dispersion (iii) agglomeration (iv) classification
local maxima		(i) agglomeration with breakup (ii) classification

Finally, a combination of fines destruction and classified product removal is shown in Figure 4.18.

4.6. SUMMARY

The population balance approach to analysis of crystallizers has been presented. Table 4.6 summarizes the various outcomes discussed for continuous crystallizers.

NOMENCLATURE

$f(L)$	Normalized size density distribution function	τ	Mean retention time defined by V/Q
$F(L)$	Normalized cumulative size distribution function	n^0	Zero size population density
L	Characteristic size of a particle	B^0	Nucleation rate
$n, n(L)$	Population density distribution	C	Concentration of a solution
$N, N(L)$	Number distribution	k_i	Rate constant from Eq. (4.28)
\mathbf{N}	Number distribution vector in Eq. (4.35)	\mathbf{v}_e	Velocity along an external coordinate
N_T	Total number of particles per unit volume	\mathbf{v}_i	Velocity along an internal coordinate
A_T	Total surface area of particles per unit volume	t	Time
M_T	Total mass of particles per unit volume	B	Birth function for particles
k_a	Area shape factor	D	Death function for particles
k_v	Volume shape factor	G_0	Zero constant in ASL model in Eq. (4.33)
ρ	Density of particles	γ	Constant in ASL model in Eq. (4.33)
$A(L)$	Distribution of particle area as a function of size	b	Constant in ASL model in Eq. (4.33)
$M(L)$	Distribution of particle mass as a function of size	D_a	Axial diffusivity
m_i	i th moment of the population density distribution as defined by Eq. (4.11)	D_G	Growth rate diffusivity
$\bar{L}_{i+1,i}$	Mean size as defined by Eq. (4.10)	v_z	Velocity in the z -direction
Δm	Mass retained as a given sieve	δ_z, δ_L	Unit vector
V	Volume	$m_L(j)$	j th moment of the size distribution
G	Growth rate based on a characteristic dimension	$m_G(j)$	j th moment of the growth rate distribution
Q	Volumetric flow rate	K	Aggregation kernels
		ϵ	Rate of energy dissipation per unit mass
		ν	Kinematic viscosity
		u	Particle volume
		v	Particle volume
		E_i	Collection efficiency in aggregation kernel
		C_A	Aggregation parameter
		μ	Absolute viscosity
		$K(u, v)$	Aggregation kernel
		U	Velocity gradient
		ρ	Particle density
		ρ_o	Fluid density
		sh	Shear rate

REFERENCES

- Abegg, C.F., Stevens, J.D., and Larson, M.A. (1968). *AIChE J.* **14**, 118.
- Belter, P.A., Cussler, E.L., and Hu, W.-S. (1988). *Bioseparations*, Wiley-Interscience, New York.
- Berglund, K.A., and de Jong, E.J. (1990). *Separations Technology* **1**, 1.
- Berglund, K.A., and Larson, M.A. (1984). *AIChE J.* **30**, 280.
- Glatz, C.E., Hoare, M., and Landa-Vertz, J. (1987). *AIChE J.* **32**, 1196.
- Hartel, R.W., and Randolph, A.D. (1986). *AIChE J.* **32**, 1136.
- Hoyt, R.C. (1978). Ph.D. dissertation, Iowa State University, Ames, IA.
- Larson, M.A., and Randolph, A.D. (1969). *Chem. Eng. Progr. Symp. Ser.* **95(65)**, 1.
- Larson, M.A., White, E.T., Ramanarayanan, K.A., and Berglund, K.A. (1985). *AIChE J.* **31**, 90.
- Liang, B., and Hartel, R.W. (1991). *J. Cryst. Growth* **108**, 129.
- Randolph, A.D., and Larson, M.A. (1971). *Theory of Particulate Processes*. Academic Press, New York.
- Randolph, A.D., and Larson, M.A. (1988). *Theory of Particulate Processes*. 2nd ed., Academic Press, San Diego, CA.
- Randolph, A.D., and White, E.T. (1977). *Chem. Eng. Sci.* **32**, 1067.

This Page Intentionally Left Blank

CRYSTALLIZER SELECTION AND DESIGN

Richard C. Bennett

Crystallization is a very old technology and information regarding the crystallization of both salt and sugar goes back to the beginning of civilization. Naturally, many kinds of crystallizers have been developed during such a long historical period, and as science and technology have progressed, changes in equipment design have occurred that are a continuing process even today. Calandria pans for the crystallization of salt were developed in the last century and some of this equipment is still in operation.

Within the last 30 years, the technical means to measure nucleation in operating equipment have been developed that have given a new insight into the design of crystallization equipment, with the result that modern crystallization designs are far more flexible in terms of their ability to control crystal product size and size distribution than earlier equipment. Within the last few years, electronic instruments have been developed that make possible the continuous on-line measurement of particle size distribution and other operating variables required for the control of industrial crystallizers.

In approaching any new or existing crystallizer installation, it is important to evaluate how the unique properties of the crystal product and its mother liquor impact on the crystallizer design selection. It is also necessary for anyone involved in selecting and designing crystallization equipment to know the characteristics of at least the major crystallizer designs in use today and how to apply these to specific industrial problems.

5.1. FUNDAMENTALS

5.1.1. DEFINITION

Crystals may be defined as solids composed of atoms arranged in an orderly repetitive array. The interatomic distances in a crystal of any definite material are constant and are characteristic of that material. Thus, for each chemical compound there are unique physical properties that differentiate that material from others, therefore, it is not unexpected that the formation of the crystalline material from its solution or mother liquor is accompanied by unique growth and nucleation characteristics.

One of the important advantages of crystallization compared with other means of separation is that it is capable of producing very high purity products from impure solutions with very low energy input. Often these separations can be performed in one step, yielding a product not only of high purity but of good appearance with high bulk density and good handling characteristics, and the drying requirements are minimal due to the low moisture content of the cake leaving the filter or centrifuge.

In terms of energy requirements, crystallization requires much less energy for separation than do distillation or other commonly used methods of purification. It may be carried on at relatively high or low temperatures on a scale that varies from a few kilograms up to thousands of tons per day.

While crystallization is a unit operation embracing well-known concepts of heat and mass transfer, it nevertheless is

strongly influenced by the individual characteristics of each material processed. Therefore, each crystallization plant requires many unique features and must be evaluated on an individual basis in order to achieve optimum results.

Crystallization has long been considered an art rather than a science, although recent theoretical discoveries and new analytical techniques have produced a change in this historic position. It is also true that the mechanical design of the crystallizer has a significant influence on the nucleation rate due to contact nucleation, which is that caused by contact of the crystals with each other or with the pump impeller or propeller when suspended in a supersaturated solution. This phenomenon yields varying rates of nucleation on scaleup and differences in nucleation rate when the same piece of equipment is used to crystallize different materials.

5.1.2. HEAT EFFECTS IN A CRYSTALLIZATION PROCESS

Accompanying the separation of a crystalline material from saturated solution are heat effects that are most commonly calculated from the heat of crystallization and the sensible heat of the solution from which the crystalline material separates. Where there is sufficient data available, an enthalpy balance can be made. For most materials having normal solubility the separation of a crystalline phase is accompanied by the release of heat. In evaporative crystallizers this release of heat is part of that supplied to vaporize the solvent (commonly water) and the crystallizing material may itself contain a significant amount of water in the form of water of hydration. A starting point, therefore, for the design of any crystallizer is a preparation of the heat and material balance that accounts for the net changes brought about by this unit operation.

With compounds whose solubility increases with increasing temperature (normal solubility), there is usually an absorption of heat when the compound dissolves, which is called the *heat of solution*. In compounds with decreasing solubility, as the temperature increases, there is an evolution of heat when solution occurs. When there is no change in solubility with temperature, there is no heat effect. The solubility curve will be continuous as long as the solid substance of a given phase is in contact with the solution. Any sudden change in the slope of the curve will be accompanied by change in the heat of solution and a change in the solid phase in contact with the saturated solution. Heats of solution are generally reported as the change in enthalpy associated with the dissolution of a quantity of solute in an excess of pure solvent.

At equilibrium the heat of crystallization is equal and opposite in sign to the heat of solution. Using the heat of solution at infinite dilution as equal but opposite in sign to the heat of crystallization is the equivalent, however, of neglecting the heat of dilution. With many chemicals the heat of dilution is small in comparison with the heat of crystallization and the approximation is justified. However, there are some exceptions.

Relatively large heat effects are usually found in the crystallization of hydrated salts, such as Glauber's salt or epsom salt. In

such cases, the total heat released on crystallization may be a substantial portion of the total heat removed in a cooling-type crystallization. In evaporative-type crystallizers, the heat of crystallization is usually negligible when compared with the heat required for vaporizing the solvent.

The heat effects in a crystallization process can be computed by two methods:

1. A heat balance can be made wherein the individual heat effects, such as the sensible heat required for heating or cooling the solution, the heat of crystallization of the product formed, and the latent heat of vaporization for liquid vaporized can be combined into an equation for the total heat effects.
2. An enthalpy balance can be made in which the total enthalpy of all leaving streams minus the total enthalpy of all entering streams is equal to the heat absorbed from external sources by the process.

The advantage of the enthalpy-concentration diagram method is that both heat and mass effects are taken into account simultaneously. This method has only limited use, however, because of the difficulty in obtaining enthalpy-concentration data that have been published for only a few systems. In using either method, however, it is necessary to make a corresponding mass balance since the heat effects in a crystallization process are related to the quantities of solids produced through the heat of crystallization.

5.1.3. YIELD OF A CRYSTALLIZATION PROCESS

In most cases, the process of crystallization is slow and the final mother liquor is in contact with a sufficiently large crystal surface so that the concentration of the mother liquor is substantially that of a saturated solution at the final temperature in the process. In such cases, it is normal to calculate the yield from the initial solution composition and the solubility of the material at the final temperature. Some solutions, such as sucrose and water, supersaturate easily and do not attain equilibrium with respect to the final mother liquor temperature. In such cases, an assumption must be made as to the mother liquor composition at the end temperature.

If evaporative crystallization is involved, the solvent removed must be taken into account in determining the final crystal yield. If the crystals removed from solution are hydrated, then the water of crystallization in the crystals must be taken into account in making the final calculation since this water is not available for retaining solute in the solution. The crystal yield is also influenced in many plants by the removal of some mother liquor with the crystals being separated in the centrifuge or on the filter. Typically the product separated on the centrifuge or filter carries with it adhering mother liquor that is in the range of 2–10% of the weight of the crystals.

The actual yield is computed from a knowledge of the solubility of the system at various temperatures under consideration and may be calculated by algebraic equations or trial and error calculations. When the calculations are made by hand, it is generally preferable to use the trial and error system since it permits easy adjustments for relatively small deviations found in practice, such as the addition of wash water, instrument and purge water, or liquid purges from the system. While the calculation of yield for an anhydrous salt formed by cooling a saturated solution can be calculated quite simply, the calculation of yield for systems crystallizing hydrated salts by evaporation is considerably more complex and often requires use of a solubility curve for the hydrated salt plotted in terms of solubility per pound of "free" water. If calculations are to be made with a digital computer, the formula method can be used; however, calculation via the spread sheet method

offers significant advantages and permits modifications and recalculation quite easily. The following equation is based on a material balance (Perry 1973) and may be used for direct yield calculations.

$$C = R \frac{100W_o - S(H_o - E)}{100 - S(R - 1)} \quad (5.1)$$

where

- C = weight of crystals in final magma, kg
 R = $\frac{\text{mole weight of hydrated crystal}}{\text{mole weight of anhydrous crystal}}$
 S = solubility at the final mother liquor temperature (anhydrous basis) in kg/100 kg solvent
 W_o = weight of anhydrous solute in the original batch
 H_o = total weight of solvent at the beginning of the batch, kg
 E = evaporation, kg

5.1.4. FRACTIONAL CRYSTALLIZATION

When two or more solutes are dissolved in the solvent, it is sometimes possible to separate these into pure components or separate one and leave the other in solution. Whether or not this can be done depends upon the solubility and phase relations of the system under consideration. How to plot and use this data is explained by Fitch (1970), and Campbell and Smith (1951). It is helpful if one of the components has a much more rapid change in solubility with temperature than does the other. A typical example, which is practiced on a large scale, is the separation of KCl and NaCl from water solution. A simplified phase diagram for this system is shown in Figure 5.1. In this case, the solubility of NaCl is plotted on the Y-axis as parts per 100 parts of solvent, and the solubility of the KCl is plotted on the X-axis in the same units. The isotherms show a marked decrease in solubility for each component as the other component is increased. This example is typical for many inorganic salts.

The line marked CE in Figure 5.1 is the mixed salt line and corresponds to compositions of the solution where both solid phases are in equilibrium. To make a separation of the two solutes, it is necessary to operate on one side of this line or the other. When crystallizing solid-phase NaCl, the solution compositions lie above the line CE. When crystallizing KCl only, the solution composition lie below the line. Practically, it is possible to approach the line very closely (within a few percent) and still precipitate the solid phase indicated without coprecipitation of the other material. On this curve, evaporation from a solution of any specific composition is represented by movement away from the origin, and dilution of the system is represented by movement from the composition in question towards the origin.

A typical separation could be represented as follows. Starting at E with a saturated brine at 100°C, a small amount of water is added to dissolve any traces of solid-phase NaCl that might be present so as to be sure the solids precipitated initially are KCl. This dilution is represented by the line E-H. Evaporative cooling along line H-G represents the precipitation of KCl. During this evaporative cooling, part of the water evaporated must be added back to the crystallizer to prevent coprecipitation of NaCl. The final composition at G can be calculated by the NaCl/KCl/water ratios and the known amount of NaCl in the incoming solution at point E. The solution at point G may be concentrated by evaporation at 100°C. During this process the solution will increase in concentration with respect to both components until point I is reached. At this point, NaCl will precipitate and the solution will become more concentrated with KCl, as indicated by the line I-E, until the original point E is reached. If concentration is carried on beyond point E, a mixture of NaCl and KCl will precipitate.

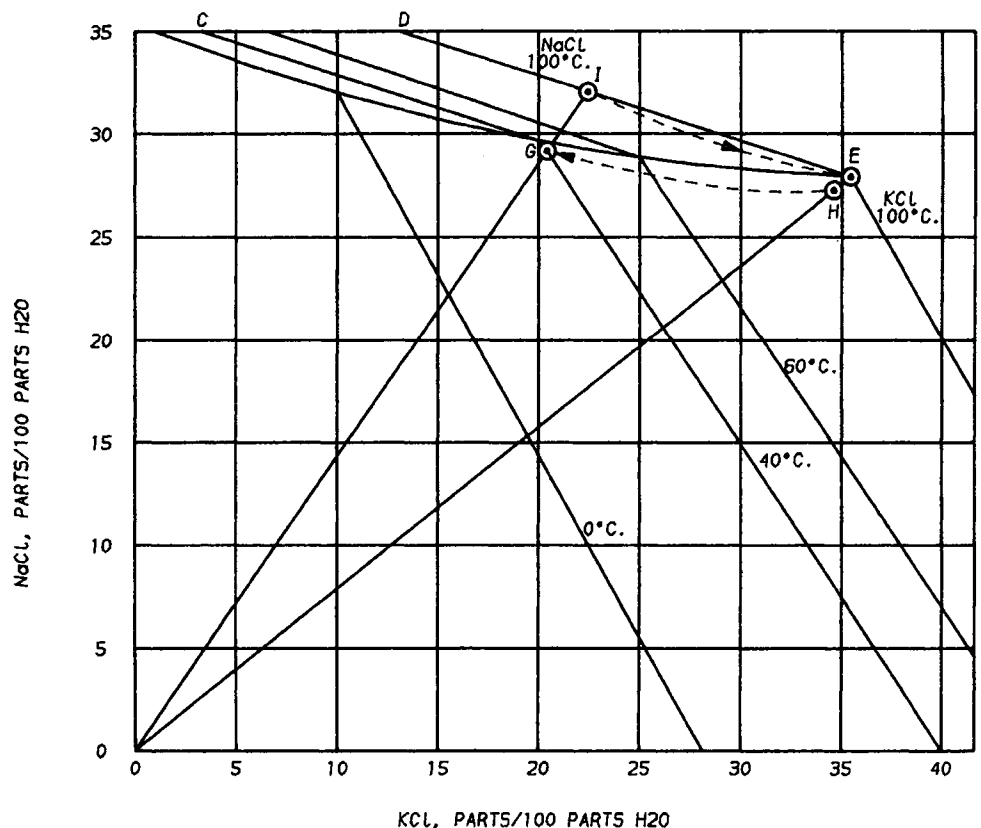


Figure 5.1 Mutual solubility of KCl and NaCl in water.

5.1.5. NUCLEATION

In all crystallization phenomena, the crystals must first form and then grow. The formation of a new solid phase may occur on either an inert particle surface or in the solution itself, and is called *nucleation*. The increase in size of the nucleus by layer-upon-layer addition of solute is called *growth*. Both nucleation and crystal growth have *supersaturation* as a common driving force. If the solution remains (only) saturated, the crystals will not grow. If it becomes unsaturated, the crystal phase present will gradually disappear.

Most early work on crystallization and nucleation was done with extremely pure solutions. There are numerous literature references in the high degree of supersaturation created and the energies associated with the formation of nuclei under such conditions; this work is summarized in Chapter 2 of this volume. Within the last few years there has been a substantial rethinking of this aspect of crystallization. Most modern students of the subject agree that there are at least four identifiable sources of nucleation that must be considered in industrial crystallization:

1. Homogeneous nucleation.
2. Heterogeneous nucleation.
3. Attrition.
4. Contact nucleation (secondary nucleation).

In addition to these, one must consider intentional and accidental *seeding* as a surrogate form of nucleation, which is so often encountered industrially that it is convenient to consider it with other types of nucleation.

Homogeneous and Heterogeneous Nucleation. Homogeneous and heterogeneous nucleation occur at very high levels of supersaturation, either in the solution, or in the case of heterogeneous nucleation, on other inert particles that are present in the form of crystals or as amorphous solid material. Most industrial crystallizers of the types in commercial use operate at levels of supersaturation far below those at which these types of seeding are expected, except under startup conditions.

Attrition. Attrition causes small particles of crystalline material that have already been formed to be broken from identifiable crystals, and thereby, to be added to the body of solids that are present as individual or discrete particles. Their presence increases as the level of mechanical energy input in the system increases. They can be formed by contact of the crystals with a pump impeller or due to impact of the slurry on tube sheets, piping, or vessel walls. In some crystallizer designs, the attrition is sufficiently large so that if the crystallization rate is reduced to a very low value, the product size progressively decreases as particles separate from the existing solids and become new particles. Attrition can occur whether or not supersaturation is present.

Contact or Secondary Nucleation. Contact or secondary nucleation is another significant source of crystallizer seed. It occurs when crystals touch each other, some metal object, such as a pump impeller, vessel walls, or piping while the crystals are growing. The amount of nucleation caused is proportional to the energy expended when striking the crystal and the degree of supersaturation. It is a significant source of nucleation in most industrial crystallization equipment and was first quantified by Clotz and McCabe (1971). The effects have been described by Ottens and

deJong (1972) and Bennett et al. (1973). In recent years, this phenomenon has been investigated by a number of authors, including Rusli et al. (1980), Grootsholten et al. (1984), Shaw et al. (1973), and Ness and White (1976).

This phenomenon differs from attrition in that it is proportional to and dependent upon supersaturation.

5.1.6. POPULATION DENSITY BALANCE

Modern industrial crystallization theory dates essentially from the work of Randolph and Larson (1962), who developed the concept of *population density* insofar as it applies to mixed suspension, mixed product removal crystallization equipment. A detailed treatment of the development of these concepts is given in Chapter 4 of this volume. The population density concept is useful because it allows the user to take the data developed from a crystal screen analysis along with knowledge of the operating parameters of the crystallizer, such as the retention (drawdown) time, slurry density,

and active volume, to calculate the growth rate and nucleation rate. From multiple sets of data it is possible to determine the kinetics of the system and thereby have sufficient data to predictably model the effect of other changes and modifications in the system. Although these equations are limited to fully mixed suspensions such as the forced circulation and draft tube baffle (DTB) crystallizers described in Section 5.3.3 and 5.3.4 (and do not apply to agitated trough crystallizers, static tanks, etc.), they are important because this type of equipment accounts for the vast bulk of the important commercial applications. At the present time, mathematical analogs for other types of crystallizers are either lacking or not as well developed.

5.1.7. CRYSTAL SIZE DISTRIBUTION

As developed in Chapter 4 of this volume, if a crystallizer (such as shown in Figure 5.2) is operating at steady-state, is thoroughly mixed, is discharging a representative sample of the suspended

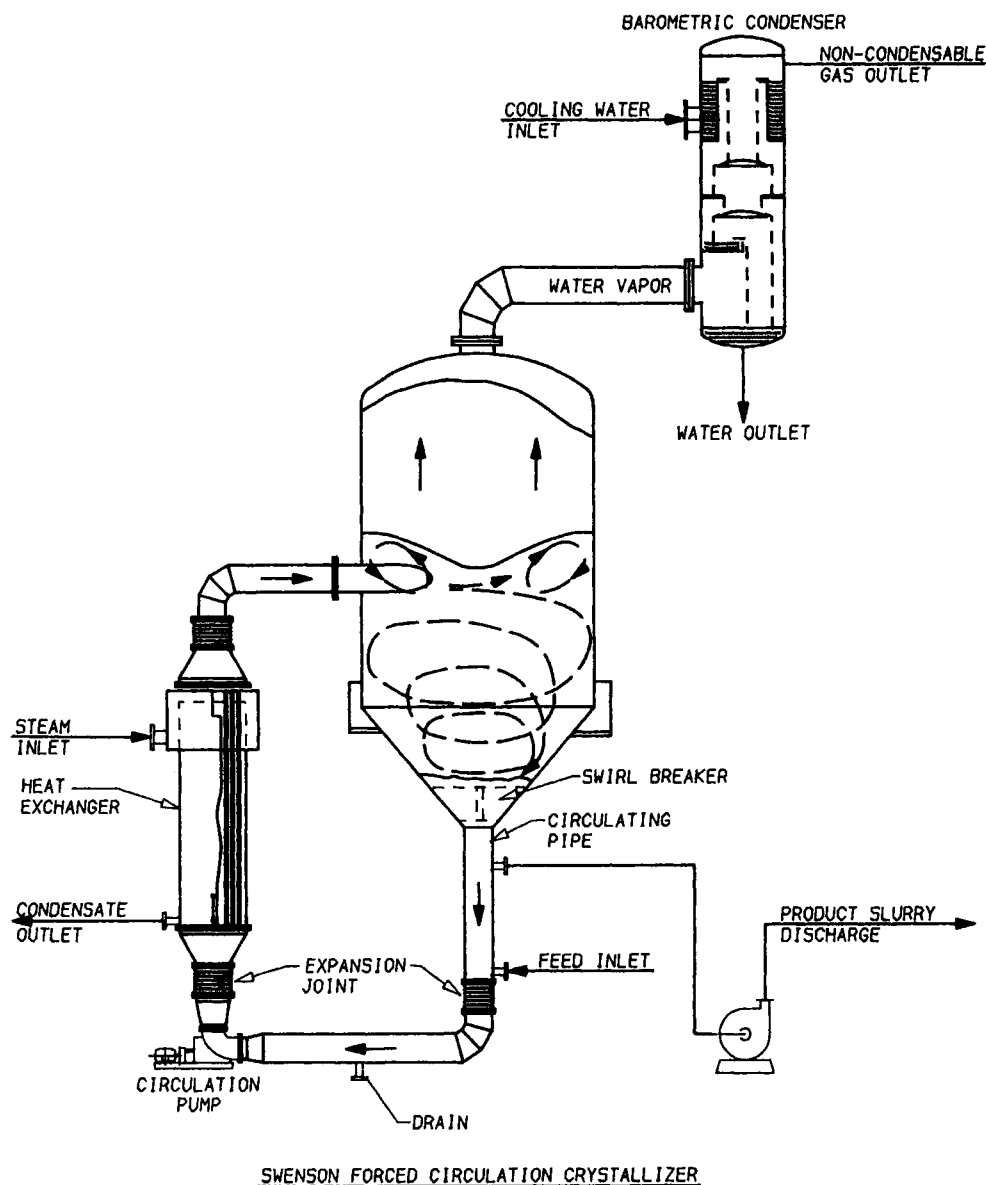


Figure 5.2 Swenson forced-circulation crystallizer.

magma, and if McCabe's ΔL law is applicable, a straight line plot of $\ln n$ versus L will result. The intercept of this straight line with the size corresponding to $L = 0$ is the nuclei population density and the slope of this straight line is equal to $(-1/Gt)$. The growth rate (G) so calculated is the diametral growth rate, which is twice the facial growth rate. The retention time (t) used in these calculations is sometimes referred to as the drawdown time and is the slurry containing (active) volume of the crystallizer divided by the slurry discharge rate. The population density in the crystallizer under these conditions is shown in Eq. (5.2).

$$n = n^0 \exp(-L/Gt) \quad (5.2)$$

By definition, therefore, the nucleation rate, which is the birth of crystals at size $L = 0$ is shown in Eq. (5.3). As will be shown later, B^0 is also a function of other properties of the system and the crystallizer.

$$B^0 = n^0 G \quad \text{no./h/volume} \quad (5.3)$$

The total number of crystals, the total area of the crystals, and the mass of the crystals in the sample are shown in equations below.

$$\text{Total no. of crystals: } N = \int_0^\infty n^0 \exp(-L/Gt) dL = n^0 (Gt) \quad (5.4)$$

$$\begin{aligned} \text{Total area of crystals: } A &= \int_0^\infty KL^2 n^0 \exp(-L/Gt) dL \\ &= 2Kn^0 (Gt)^3 \end{aligned} \quad (5.5)$$

$$\begin{aligned} \text{Total mass of crystals: } M &= \int_0^\infty k_v L^3 n^0 \exp(-L/Gt) dL \\ &= 6pk_v n^0 (Gt)^4 \end{aligned} \quad (5.6)$$

Since nucleation is also a function of supersaturation, it is frequently expressed as a power law model similar to that shown in Eq. (5.7) when the crystallizer design effects on the nucleation rate can be neglected.

$$B^0 = k_n M^j G^i \quad (5.7)$$

This power law model contains an expression for slurry density and, as will be shown later, there are other considerations that could have been added that have a demonstrated influence on nucleation rate. In order to satisfy any given condition, the mass of crystals per unit volume of the crystallizer, as shown in Eq. (5.7), must be consistent insofar as the nuclei population density and growth rate are concerned with that shown in Eq. (5.2).

Growth rate, therefore, is a constrained variable and the correct solution to any new set of conditions involves a simultaneous knowledge of both the nucleation rate and the growth rate.

5.1.8. CRYSTAL WEIGHT DISTRIBUTION

Once the growth rate at any given retention time is known and if the plot of $\ln n$ versus L is a straight line, then the crystal weight distribution may be computed by the following equations.

$$X = L/Gt \quad (\text{Dimensionless size}) \quad (5.8)$$

$$\begin{aligned} \text{Weight fraction: } W_X &= \frac{M_X}{M} \\ &\equiv \frac{\text{Mass to size } X}{\text{Total sample mass or mass at } L = \infty} \\ W_X &= 1 - \exp^{-X} \left(1 + X + \frac{X^2}{2} + \frac{X^3}{6} \right) \end{aligned} \quad (5.9)$$

This equation can be easily solved for many different L values to give the crystal size distribution. The solution to this equation is also given in table form in Appendix A of the book *Theory of Particulate Processes* (Randolph and Larson 1971). The generalized solution to Eq. (5.9) for certain specific properties, such as the dominant particle, is given in Eq. (5.10).

$$\text{Dominant particle (area wt avg): } L_D = 3Gt \quad (5.10)$$

The average particle by weight may be computed from Eq. (5.11). This is a very useful equation for quick estimates of size versus growth rate and vice versa.

$$\text{Average particle by weight: } L_{av} = 3.67Gt \quad (5.11)$$

The techniques for evaluating growth and nucleation rates have been widely used in the analysis of forced-circulation crystallizers and other systems that are being operated continuously, are thoroughly mixed, and where growth follows the ΔL law. There is good agreement between field measurements and results predicted by the theory. The nucleation sensitivity parameter (i) shown in Eq. (5.7) is believed to be characteristic of many systems and is often the same in large-scale and in laboratory tests.

Nonlinearity of the plot of $\ln n$ versus L is frequently encountered for a variety of reasons. In a thoroughly mixed suspension, a straight line plot of $\ln n$ versus L will generally not occur until 6–10 retention periods have passed following start-up or serious perturbations in operating conditions. Since the suspension is thoroughly mixed, larger particles present must have time to grow, and frequently the coarsest fractions have a retention period many times the average. Until these larger crystals are present at equilibrium, the straight line will show a downward curve at the larger-crystal fractions. An illustration of the curved plots and the ideal plot is shown in Figure 5.3.

Also, during start-up conditions with systems that nucleate heavily or with systems that exhibit cycling behavior with regard to crystal size, it will be found that lower-than-equilibrium values of the finer crystal sizes will be present for a time during the growth cycle.

Many crystallizers employ classification of the product discharge either intentionally through the use of elutriation legs or hydrocyclones on the discharge stream, or unintentionally because of inappropriate locations for the slurry discharge connection. The use of an elutriation leg or cyclone to remove the coarsest solids in the system will cause a concave curve in the larger crystal sizes, representing a decrease in the population density of the coarsest fractions. Randolph et al. (1968) generalized on the degree of crystal size distribution narrowing that could be obtained using a combination of classified product removal and vessel staging.

If growth of the crystals does not follow McCabe's ΔL law, then an underlining assumption of the derivation of the population distribution shown in Eq. (5.2) is not fulfilled. A generalized treatment of the curvature that can exist in the plot of $\ln n$ versus L under such conditions is given by Abegg et al. (1968).

Multiple staging of crystallizers where nucleation per stage is small will result in a significant narrowing of the crystal size distribution. At least one large-scale continuous sugar crystallization system works in this manner and a theoretical treatment of the subject is given by Abegg and Balakrishnan (1971).

Concave curvature upwards in the small crystal sizes has been noted by many experimenters (Sikdar and Randolph 1976), and the size-dependent growth rate theory proposed by Bujak (1976) appears to have a solid basis. Recent work by Berglund and Larson (1992), Human et al. (1982), Randolph and White (1977), and Zumstern and Rousseau (1986) make useful comments on this theory.

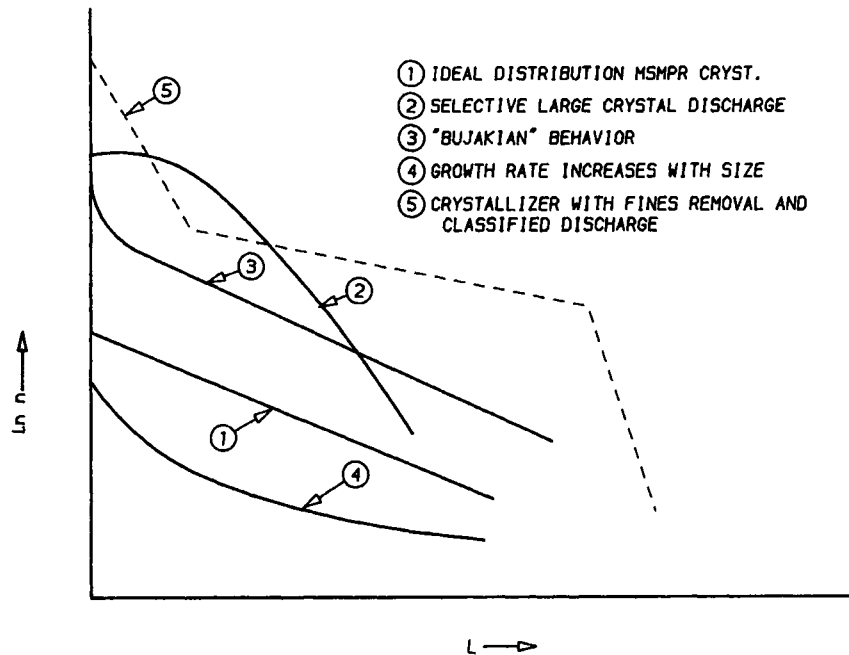


Figure 5.3 Typical plots of the population density (n) versus length (L).

5.1.9. CONTACT NUCLEATION

As mentioned earlier, the nucleation rate is actually not a simple power law model of growth rate and slurry density, but should contain terms dependent upon contact nucleation effects caused by the pump or propeller circulator and the motion of crystals striking each other within the crystallizer suspension. This is shown algebraically in Eq. (5.12).

$$B^0 = K_n M^j G^i + B_e^0 \quad (5.12)$$

where

B^0 = nucleation rate (total)

B_e^0 = contact nucleation

G = growth rate mm/h

M = slurry density g/l

i, j, K_n = experimentally determined constants

Work has been done by Bennett et al. (1973) to indicate the correlation between mechanical nucleation and crystallizer physical parameters as shown in Eq. (5.13).

$$B_e^0 = K_{ep} \left[\frac{TIPS^2}{TO} \right] G \int_0^\infty L^4 n dL \quad (5.13)$$

where

$TIPS$ = tip speed of pump or impeller

$TO = \frac{\text{active volume}}{\text{circulation rate}} = \text{time/turnover}$

The nucleation term B_e^0 used in Eq. (5.13) includes terms containing specific design perimeters from the crystallizer. If a straight-line plot of $\ln n$ versus L is obtained, Eq. (5.13) can be solved as shown below.

$$B_e^0 = K_{ep} n^0 G \left[\frac{TIPS^2}{TO} \right] L_D^5 \quad (5.14)$$

As shown in Eq. (5.14), small changes in the dominant particle size have a fifth-order influence on contact nucleation, other factors being equal, thereby explaining the historical character of most forced-circulation type systems to operate stably with a particle size distribution (for a given pump speed) that is changed very little by changes in slurry density or retention time.

Another mechanism that must be mentioned in connection with nucleation in real crystallization equipment is attrition. In a classic paper by Randolph (1969), this subject is reviewed. Randolph demonstrated that crystal breakage, classified product removal, and decrease in linear growth rate with crystal size all skew the crystal size distribution, producing a narrower size range of crystals than would be expected in a mixed suspension, mixed product removal system. This skewing results in a curve of the plot of $\ln n$ versus L .

There probably exists no good way to separate the influence of attrition or breakage from contact nucleation at the present time other than by observation of the product crystals and measurements of the crystal size distribution or coefficient of variation. With ammonium sulfate, there is relatively little observable distortion of the crystal habit by attrition. In the earlier work by Bennett et al. (1973), there was significant rounding of the salt particles in the largest size range and at the highest pump speeds.

Whether the increased nucleation mechanism is due to the McCabe-type contact nucleation, attrition, or the action of high liquid turbulence of the Estrin type, the final result will be a smaller particle size and probably a narrowing of the size distribution as the pump speed increases.

5.1.10. CRYSTALLIZERS WITH FINES REMOVAL

Crystallizers of the draft tube baffle type that employ fines removal and destruction devices can also be analyzed by the techniques described previously, as shown in Perry (1973) and by Larson (1978).

$$M = K_v \rho \int_0^\infty [n^0 \exp(-L_F/Gt_F)] (\exp(-L/Gt)) L^3 dL \quad (5.15)$$

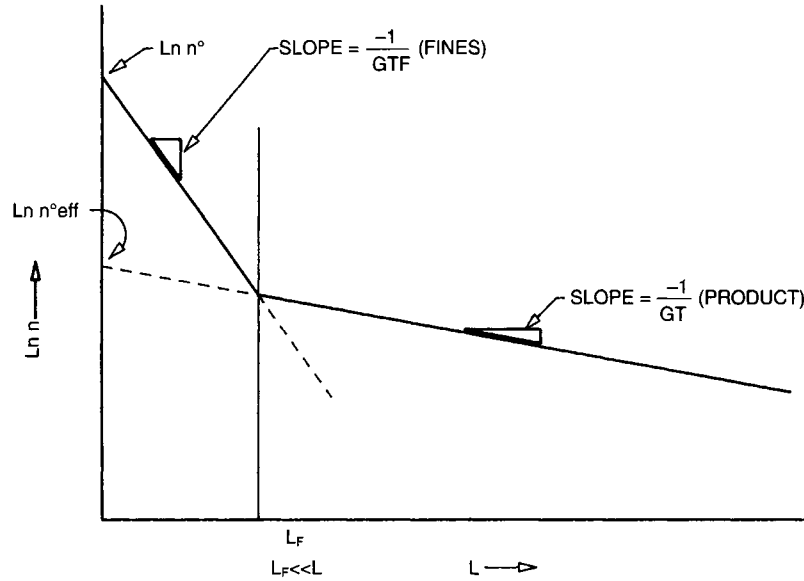


Figure 5.4 Plot of $\ln n$ versus L for a crystallizer with fines destruction.

As shown in the above Figure 5.4, the size removed by the baffle (crystals up to L_F) determines the effective nucleation rate and growth rate, whereas the size of the product crystals is represented by a straight line of lower slope, but at a longer retention. An extension of this line defines the effective nucleation rate, $\ln n^0_{\text{eff}}$. As long as the particle size removed by the baffle is relatively small compared with the product size crystals, the overall distribution can be represented by Eq. (5.15).

The weight size fraction from a crystallizer of the DTB type for particles up to size X is

$$W_X = \frac{6k_v \rho n^0 e^{(-L_F/GT_F)(Gt)^4} \left[1 - \exp^{-X} \left(1 + X + \frac{X^2}{2} + \frac{X^3}{6} \right) \right]}{M} \quad (5.16)$$

where

M = slurry density, g/l

$X = L/Gt$ (dimensionless size)

Figure 5.5 shows the calculated and experimental data for an ammonium sulfate crystallizer operating at a retention time of 5.4 h. The calculated size distribution for various L_F sizes at constant

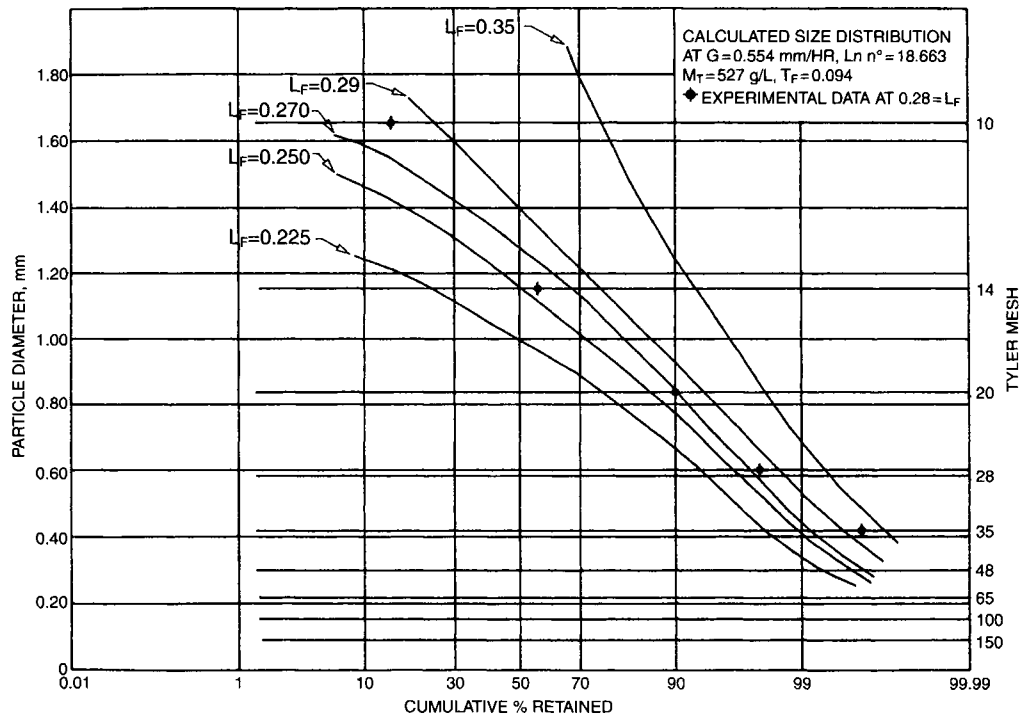


Figure 5.5 Calculated size distribution of $(\text{NH}_4)_2\text{SO}_4$ in a DTB crystallizer as a function of L_F .

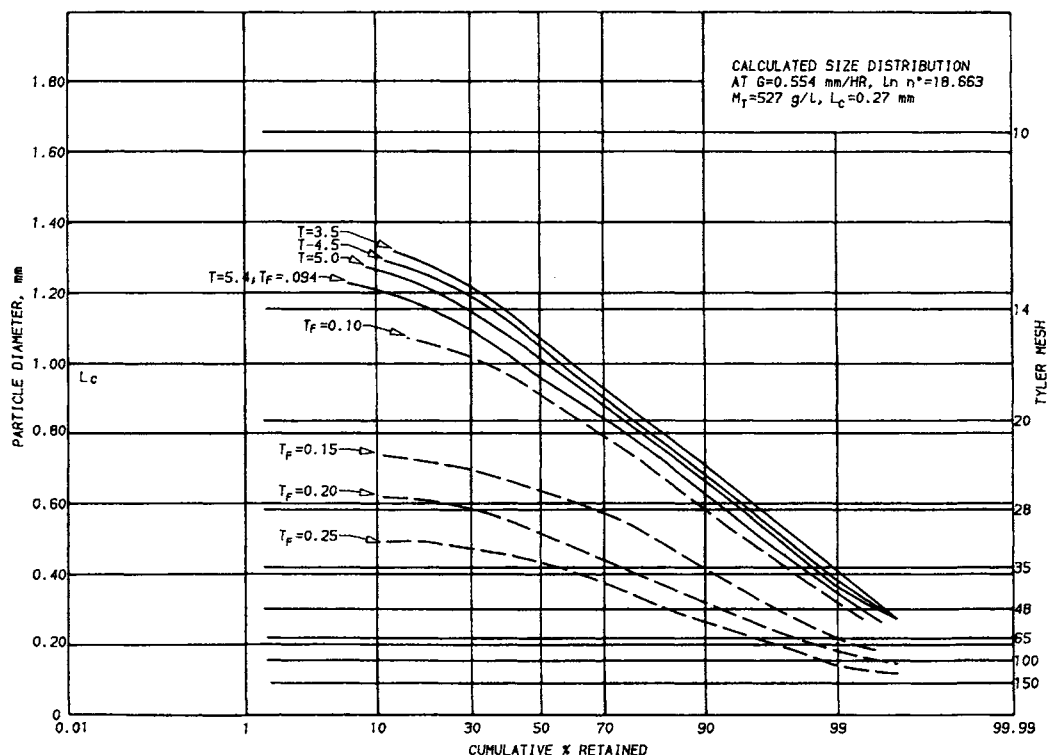


Figure 5.6 Calculated size distribution of $(\text{NH}_4)_2\text{SO}_4$ in a DTB crystallizer as a function of T_F .

mother liquor retention times of $t_F = 0.094$ h (5.64 min) is shown. The influence of this change is very great—much greater than that of either t_F or t , which are shown in Figure 5.6.

5.1.11. CYCLIC BEHAVIOR

With control techniques such as fines destruction, the particle size distribution within a crystallizer body may be varied through relatively wide ranges by changing the velocity behind the baffle and hence, the diameter of the particle withdrawn. The quantity of liquor removed with the particle separated and its residence time within the crystallizer body is another important variable. Experience has shown that such systems, when pushed beyond their capacity, can produce cyclic crystal size behavior due to homogeneous nucleation that occurs as the supersaturation rises beyond the metastable limit.

Numerous attempts have been made by operators and designers to stabilize such systems; the normal technique for doing this is by an appropriate selection of the maximum particle size separated by the baffle (L_F) and the flow through the fines destruction system. A pioneering paper by Randolph et al. (1973) developed the mathematical basis for instability in systems of this type, and predicted instability in such systems as a function of the fines dissolving parameter and the nucleation sensitivity parameter. Experimental verification of these concepts was demonstrated by Randolph and Beckman (1977) for a KCl crystallizer.

To control a crystallizer of this type in such a way that cycling can be avoided is extremely difficult and for the most part has only been conducted with limited success. The retention time required to grow large KCl or $(\text{NH}_4)_2\text{SO}_4$ crystals in industrial equipment is in the order of 4–6 h. The time required for overnucleation when the system exceeds the metastable zone is a matter of minutes. The kind of operator attention required to make adjustments in the

fines destruction system that would be effective in this kind of a crystallizer requires greater operator attention than can be normally expected. In addition, the presence of excess fines in the fines destruction system is difficult to detect visually until the particles are 200 mesh or larger in size.

In the last few years, laser particle size measuring equipment capable of being used for on-line measurements in the fines destruction system of crystallizers has become available. Such systems can respond to particle diameters down to a few microns in size even when the solution is not clear. These systems have been demonstrated as effective tools in on-line control in crystallization equipment by Rovang and Randolph (1980), Randolph et al. (1977), Randolph and Low (1982), and Bennett and Randolph (1983).

Figure 5.7 shows a cooling KCl crystallizer of the DTB type, including a fines destruction system with variable velocity and flow control. The baffle is divided by vertical baffles into several areas and the recycle flow can be changed, thus giving independent control over t_F (fines destruction retention) and the separation velocity behind the baffle.

Figure 5.8 shows an on-line particle size counter installed in the fines destruction system of such a crystallizer, and arranged for continuous monitoring of the nuclei population density and a feedback control system for regulating the fines destruction system. The use of an in-line laser particle counting system is surprisingly insensitive to the presence of small amounts of foreign material; the characteristics of the feed required for such a system are compatible with the liquid delivered by the fines separation baffle of a DTB-type crystallizer. With sampling times of around 3–6 min, this equipment is capable of generating the basic data required for continuous evaluation of the nuclei population density. Coupled with a modern highspeed distributed computer control system, calculations may be readily made and the control

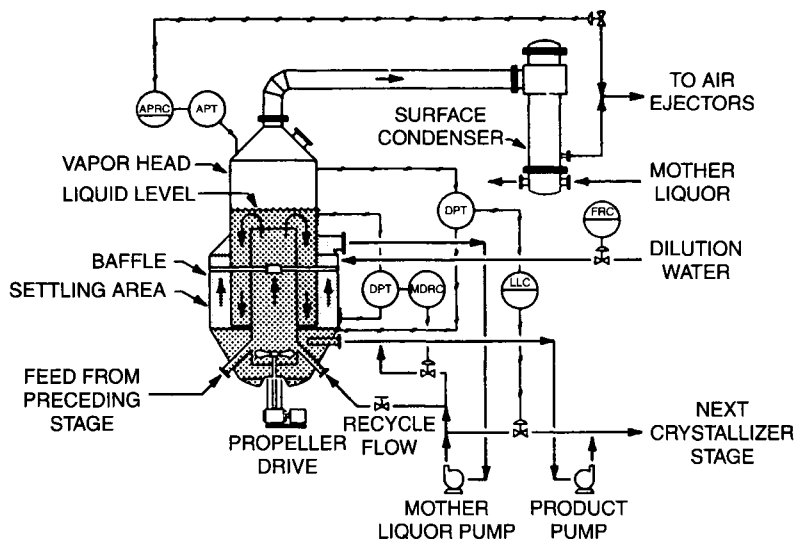


Figure 5.7 Flows and instrumentation on a typical DTB crystallizer.

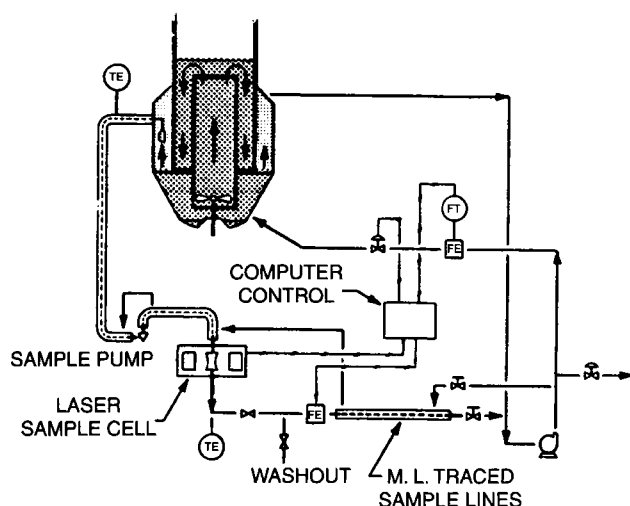


Figure 5.8 Particle size measurement and control of a DTB crystallizer.

algorithm may be updated as required to achieve the best control characteristics. Use of this system is an outstanding example of the application of complex mathematical modeling to practical industrial equipment to achieve optimum results.

5.2. SELECTION OF A CRYSTALLIZER

A crystallizer is an apparatus in which an environment can be created suitable for the formation and growth of crystalline materials. Paramount in the design of such equipment is the means that are chosen to create supersaturation at a temperature level that produces a desired or proper hydrate or composition of the product crystals.

5.2.1. INFORMATION REQUIRED FOR EVALUATION

Before a potential crystallizer application can be properly evaluated, it is necessary to have certain basic information regarding the

material to be crystallized and its mother liquor. Typical solubility curves are shown in Figure 5.9. Is the material a hydrated or anhydrous material? What is the solubility of the compound in water or any other solvents under consideration and how does this change with temperature and pH? Are there other compounds in the solution that coprecipitate or remain in solution, if so, how does their presence affect the solubility of the main component? What will be the influence of the impurities on the crystal habit and the growth and nucleation rate? What are the physical properties of the solution and the crystal? What vapor pressure of water exists over the saturated solution and crystals as a function of temperature? What is the heat of crystallization? What is the production rate and on what basis is this production rate computed? What materials of construction can be used in contact with the solutions at various temperatures? What utilities will be used at the crystallizer location and what are the costs associated with these utilities? Is the final product to be blended or mixed with other crystalline materials or solids? What size of product crystal is required and how can this material be separated from the mother liquor and dried? How can these solids or mixtures be handled and stored without undue breakage or caking?

5.2.2. SOLUBILITY

In working with materials of very *steep solubility*, such as Glauber's salt or other hydrated salts, it is common to use cooling-type crystallizers since they permit very high overall yields and reduce the overall energy requirements of the separation process. With materials whose solubility curves have a normal but moderate slope, many choices are available including evaporative cooling, surface cooling, or constant temperature evaporation. With materials having *flat or inverted solubility*, it is necessary to use evaporative crystallization. This can be done by causing water to be evaporated from the solution at a wide variety of temperatures, depending on the economics, the crystal phase desired, and the materials of construction available. Evaporative crystallization is generally done at constant temperature but can also be performed at relatively low temperatures in solar ponds.

In general, cost considerations dictate that cooling crystallization be used in cases where the precipitated salts are highly

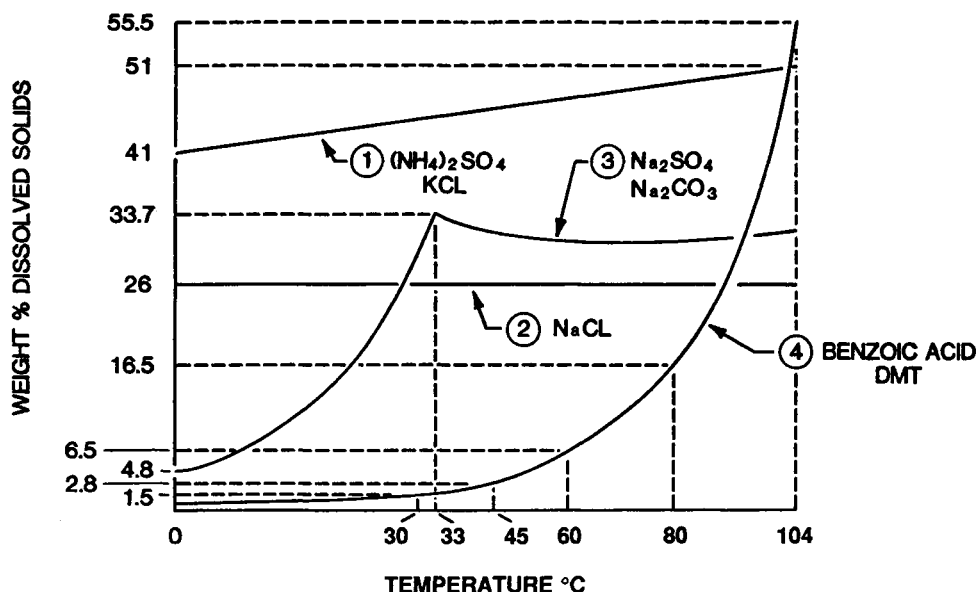


Figure 5.9 Solubility versus temperature for various compounds.

hydrated or where the solubility curve is relatively steep. The reason for this is that to produce solids by cooling only requires removal of the heat of crystallization and the sensible heat of cooling the mother liquor. In general, these effects are quite small, typically 0.7 cal/gm°C for cooling the solution and from 18–55 kcal/kg of product crystallized. To produce a pound of crystals by evaporation requires vaporization of water that is a function of the solubility, but typically might represent 1100 kcal/kg of product crystallized for a material whose solubility is 33%. Obviously there are other factors that are highly specific to each case under consideration, but typically, surface cooling requires somewhat higher investment than does evaporative cooling. In addition, the operating cycles of surface-cooled equipment tend to be shorter than those of evaporative crystallizers.

5.2.3. SCALE OF OPERATION

The *scale of operation* often has an overriding importance on the selection of the equipment because of the means used for heat transfer. For very small-scale crystallization work it is common to use radiation. The capacity of such equipment varies from a few liters up to several hundreds of liters per day (of solution cooled). For operation on scales up to several thousand liters per day, it is possible to use tanks with water-cooled coils and an agitator. For large-scale applications where the quantity of solution is thousands of liters per day, it is almost universal practice to use vacuum evaporation to remove the solvent; this is true whether the solution is cooled by adiabatic evaporation or in equipment where crystallization occurs because of isothermal evaporation.

5.2.4. BATCH OR CONTINUOUS OPERATION

Another consideration is whether the crystallization should be carried out on a *batch* or *continuous* basis. The present tendency in most processing plants is to use continuous equipment wherever possible. Continuous equipment permits adjusting the operating conditions to a relatively fine degree to get the best results in terms of overall energy usage and product characteristics. It permits the use of a smaller operating labor force and results in a continuous

utility demand that minimizes the size of boilers, cooling towers, and power generation facilities. It also minimizes the capital investment not only in the crystallizer but in the feed storage and product liquor storage facilities. Continuous separating devices for the product crystals have been developed to the point where they can operate reliably for long periods of time and the drying of crystalline products is also generally done on a continuous basis.

Batch handling of wet or semidry crystalline materials presents considerable difficulties as compared with the storing and handling of dried crystalline materials. On the other hand, a train of continuous processing equipment, such as just described, has economic application only on relatively large production rates from approximately 50 tons of product per day and upward.

Batch crystallization still has some range of application where production rates are very small, where very expensive materials are being handled and losses must be kept to an absolute minimum, or where a careful inventory of materials is required. Wall deposits in batch crystallizers are generally removed by each new charge of unsaturated feed. Batch operation also has useful application where the cooling range is very wide, such as in handling material whose initial feed concentration corresponds to relatively high pressure and whose final mother liquor temperature corresponds to room temperatures or values significantly below it. In such systems the use of batch crystallization avoids the shock introduced to the system by mixing high-temperature feed solutions with relatively low-temperature mother liquor in continuous equipment.

Another area of application is when the final liquor temperature is so low that it requires the use of extensive vapor compression equipment. In such systems, the use of batch equipment is frequently more economical than anything else, other than a relatively large number of multiple-stage series crystallizers.

5.2.5. MULTISTAGE CRYSTALLIZERS

The use of *multistage crystallization equipment*, while not analogous to multistage evaporation equipment, nevertheless permits certain economics in operation. It is normally employed when a

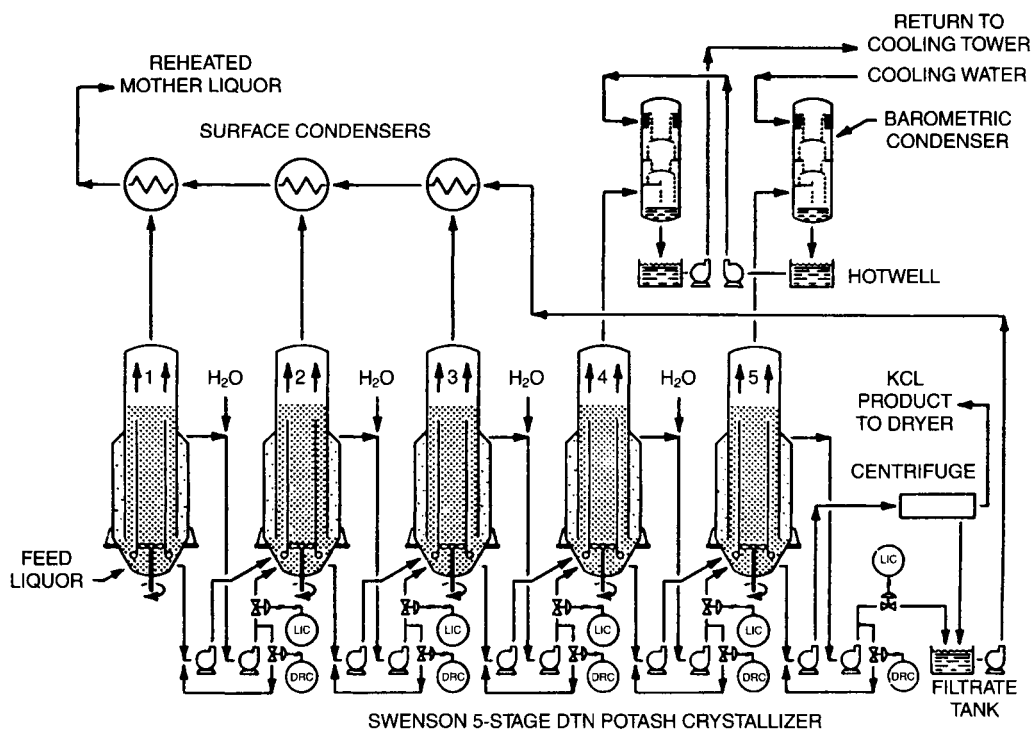


Figure 5.10 Swenson five-stage DTB potash crystallizer.

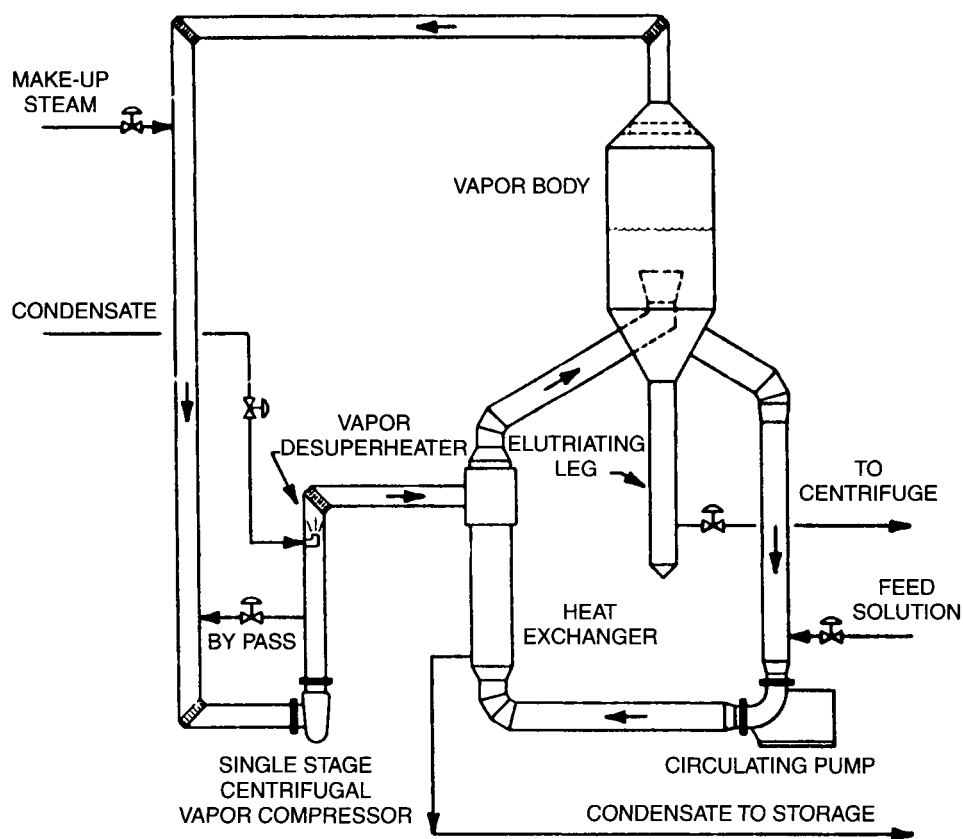


Figure 5.11 Swenson single-effect recompression crystallizer.

large flow at a high temperature and concentration is cooled to produce crystals and the mother liquors are returned to a dissolving or leaching station for reconcentration. In such systems, it is possible to use multistage cooling so that the mother liquor from the final crystallizer can be heated by crystallizers in the first one or several stages of the process. This heating can be done in either barometric heaters or in tube and shell-type exchangers. The use of this type of system not only reduces the steam required to raise the leach solution to its operating temperature, but also reduces the cooling water required on the last one or two stages of crystallization. Shown in Figure 5.10 is a five-stage potash cooling crystallizer with three stages of mother liquor reheating. Systems employing more than 12 stages of cooling have been built and successfully operated.

5.2.6. MECHANICAL VAPOR RECOMPRESSION

As the cost of energy has increased in recent years, attention is again being directed to *mechanical vapor recompression*, which by its nature, permits substitution of electrical energy for evaporation and crystallization rather than requiring heat energy (steam). A typical recompression crystallizer flow sheet is shown in Figure 5.11. In a single-stage evaporative crystallizer operating at approximately atmospheric pressure, the amount of heat energy necessary to remove a kilogram of water to produce the equivalent in crystal product is approximately 555 kcal. If the water evaporated is compressed by a mechanical compressor of high efficiency to a pressure where it can be condensed in the heat exchanger so as to supply the energy needed to sustain the process, then the equivalent power for this compression is about 6.3 kcal (Bennett 1978).

Although this technique is limited to those materials having relatively low boiling point elevation and to those cases wherein a

significant amount of heat input is required to produce the evaporation required for a given crystallization step, it nevertheless offers an attractive technique for reducing the use of heat energy and substituting mechanical energy (or electrical energy) in those cases where there is a cost advantage in doing so. This technique finds many applications in the crystallization of sodium sulfate, NaCl, and sodium carbonate monohydrate.

As shown in Figure 5.12, the amount of vapor compressed per horse-power decreases rapidly with increasing ΔT . Normal design considerations, therefore, dictate that recompression evaporators have a relatively large amount of heat transfer surface so as to minimize the power cost. In order to maintain adequate tube velocity for heat transfer and suspension of crystals, this increased surface requires a larger amount of internal recirculation within the crystallizer body, which results in a lower supersaturation of the fluid pumped through the tubes. One beneficial consequence is that with low temperature differences between the liquid temperature and the steam temperature, as indicated in Figure 5.13, the supersaturation created at the tube wall with materials of inverse solubility tends to be small. This effect is enhanced by operation where the solubility curve is as flat as possible. For instance, increasing the liquid temperature from 71 to 100°C would significantly reduce the supersaturation of the solution in Figure 5.13. Such design parameters tend to increase the operating cycle of the equipment when handling solutions of inverted solubility that can frequently be troublesome if higher ΔT s are used, as is often the case in normal evaporative crystallizers.

5.2.7. REACTIVE CRYSTALLIZERS

When a solid-phase crystalline material results from the reaction of two components, it is often advantageous to perform this reaction in a *reactive crystallizer* rather than in a separate reactor. This is commonly done, for example, in the case of ammonium sulfate where liquid or gaseous ammonia and concentrated sulfuric acid are reacted in the crystallizer to produce ammonium sulfate crystals, as shown in Figure 5.14. The reaction is carried on in a liquid suspension of growing crystals and the heat of reaction is removed by vaporizing water that is condensed and recycled to maintain the liquid balance. Other examples are the production of $(\text{NH}_4)_2\text{HPO}_4$ from NH_3 and H_3PO_4 the oxidation of calcium sulfite by oxygen (air), and the neutralization of waste acid by lime.

The reactants can be mixed in the circulation piping of a forced-circulation-type crystallizer, or "Oslo" crystallizer (Figure

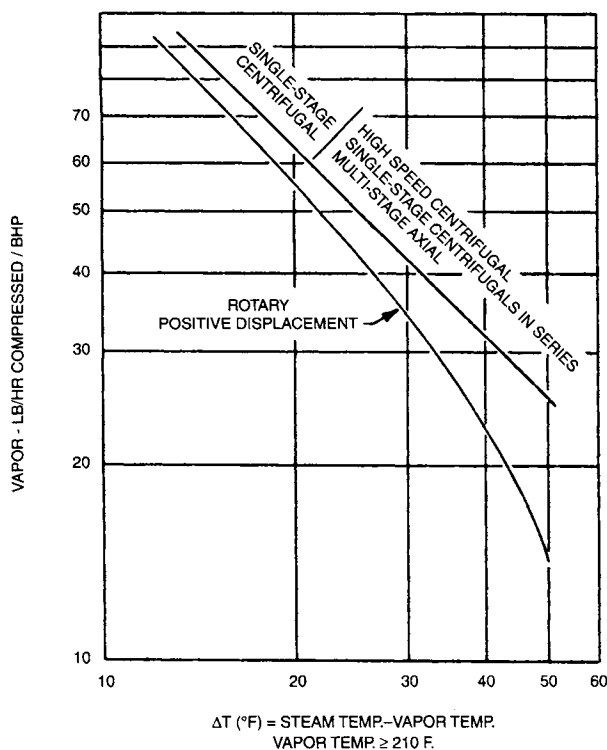


Figure 5.12 Pounds per hour of vapor compressed per BHP versus temperature difference.

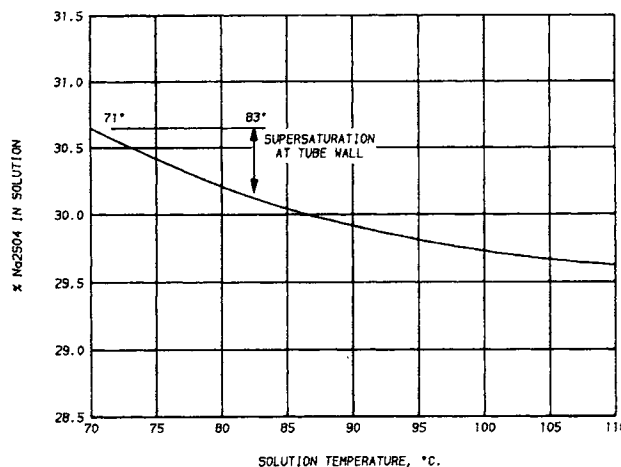


Figure 5.13 Maximum supersaturation at 12°C. GTD.

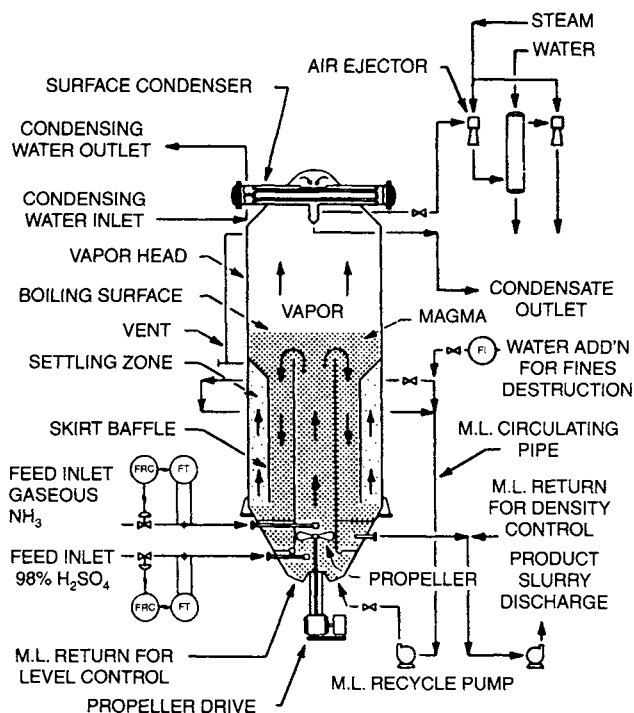


Figure 5.14 Swenson reaction-type DTB crystallizer.

5.17) or in the draft tube of a DTB-type crystallizer (Figure 5.14), where a large volume of slurry is mixed continuously with the reactants so as to minimize the driving force (supersaturation created by the reaction). Removal of heat is conveniently done by vaporizing water or other solvents as in a conventional evaporative-type crystallizer.

The reaction need not be limited to liquids and gases as shown in Figure 5.14. In Figure 5.15, for example, an ore is dissolved (decomposed) in mother liquor with the resultant supersaturation and crystallization of another crystalline material. Examples are the decomposition of schonite to form K_2SO_4 , the decomposition of carnallite to form KCl , and the conversion of Na_2CO_3 to form $Na_2CO_3 \cdot H_2O$.

5.3. EQUIPMENT TYPES

5.3.1. BATCH CRYSTALLIZERS

For applications involving relatively small amounts of material or when the material being processed must be handled on other than a continuous basis, it is often convenient to use a batch vacuum crystallizer similar to that shown in Figure 5.16.

Typically, the cycle on batch equipment of this type ranges from 2–8 h. At the conclusion of the cycle, the material is dumped to an agitated tank from which it is removed on either a batch or continuous basis for separation and drying. The time required for filling the crystallizer and dumping the crystallizer must be added to the time actually used for processing the material within the crystallizer to calculate the batch cycle time.

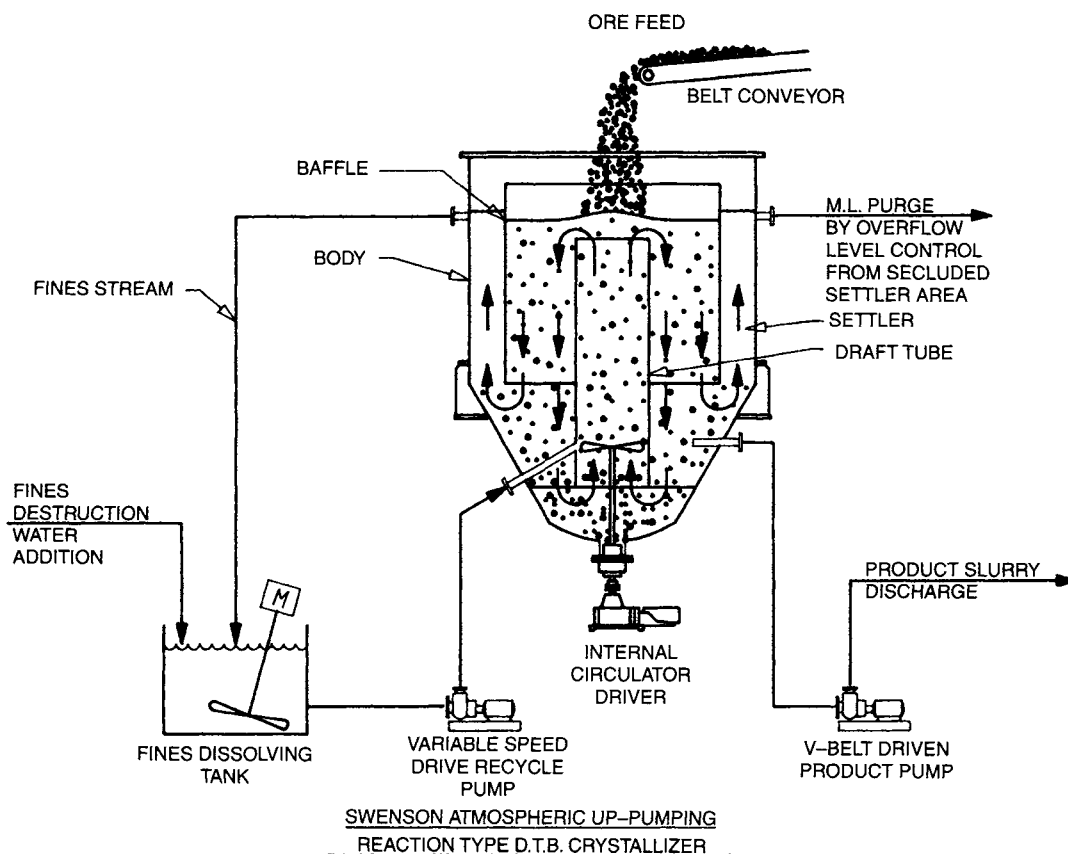
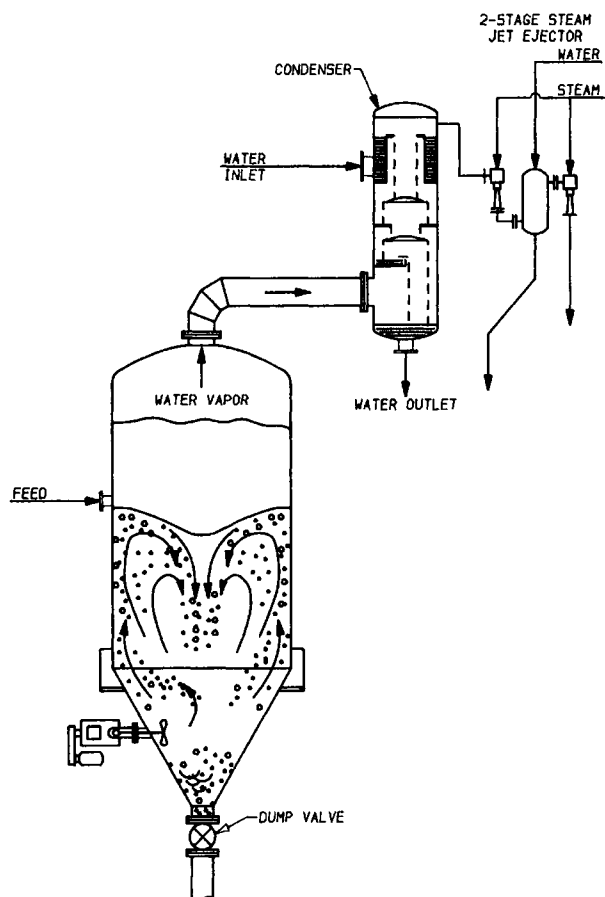


Figure 5.15 Swenson atmospheric up-pumping reaction-type DTB crystallizer.



SWENSON BATCH VACUUM CRYSTALLIZER WITHOUT BOOSTER

Figure 5.16 Swenson batch vacuum crystallizer without booster.

Other applications that are best handled in batch vacuum crystallizers are those wherein the material is cooled through a very wide range and/or to a final temperature that requires very high vacuum. In these cases, a large ejector or booster is utilized during part of the cooling to compress the vapor from the end conditions to a pressure high enough so it can be condensed with available cooling water. In such cases, the batch vacuum crystallizer economies of steam usage are approached only by going to multiple-stage continuous equipment of five or more stages.

The entire cycle for such equipment may be automated; however, in most small processing plants, this expense is not justified. There is some variation in the product size made in batch equipment since the quantity of initial nuclei is difficult to control from one batch to the next. With those materials that are very prone to grow on the walls of the crystallization equipment in continuous equipment, a possible solution is the batch crystallizer that is inherently self-cleaning.

5.3.2. FLUIDIZED SUSPENSION CRYSTALLIZER

Shown in Figure 5.17 is a fluidized suspension crystallizer, or Oslo crystallizer as it is sometimes known. This design was one of the earliest available for the crystallization of coarse materials and operates by mixing a hot concentrated feed solution with a circulated stream of liquid pumped to the vaporizer where solvent is evaporated adiabatically. Liquid that is supersaturated at this point leaves the vaporizer through the downcomer and enters the suspension chamber at the lowest portion. Here the incoming fluid agitates the largest crystals present in the suspension chamber and maintains them in a fluidized condition in the incoming stream of supersaturated solution. A portion of the coarsest crystals can be removed continuously as shown by pumping the slurry directly from the lower portion of the suspension chamber. In the upper portion of the suspension chamber, the product crystals separate from the mother liquor leaving only a small quantity of fines to

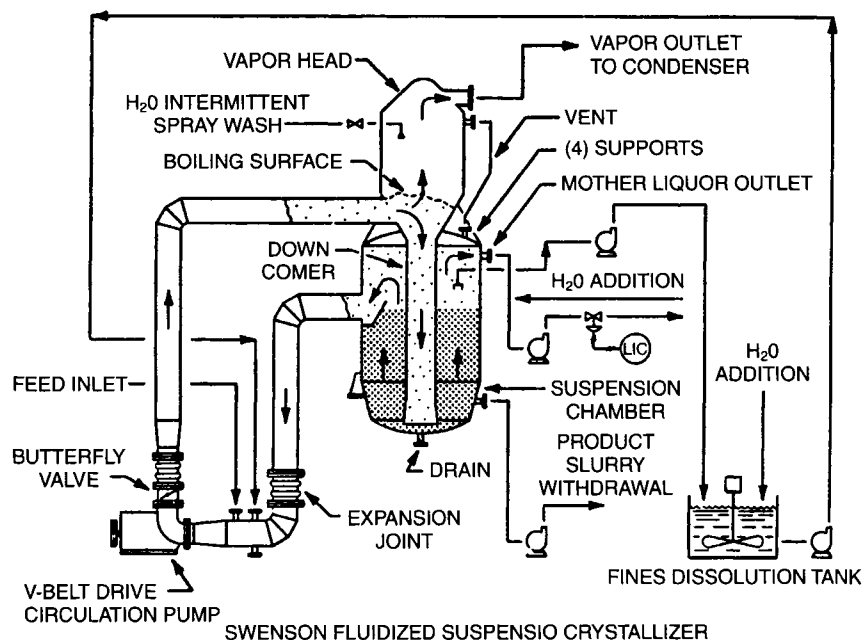


Figure 5.17 Swenson fluidized suspension crystallizer.

recirculate with the incoming feed solution. Unwanted fine crystals are dissolved by mixing with water and returned to the crystallizer where the water must be evaporated.

Although close clearances between the downcomer and the bottom of the suspension chamber can lead to difficulties with plugging by crystalline growth, this design has been widely used for the production of some coarse materials such as ammonium sulfate. Its best field of application is for crystals of very high settling rate such as nickel sulfate.

5.3.3. FORCED-CIRCULATION CRYSTALLIZER

This crystallizer, shown in Figure 5.2, is also known as forced-circulation (FC) crystallizer, or the mixed suspension, mixed product removal (MSMPR) crystallizer. The crystallizer consists of a body that is sized for vapor release with a liquid level high enough so as to enclose a volume sufficient for retention of the growing crystals. The circulation rate must be large enough to maintain suspension of the crystals present. Suction from the lower portion of the body passes through a circulation pump, through a heat exchanger back to the body through a tangent inlet or a vertical inlet. The heat exchanger is omitted in those cases where adiabatic cooling is sufficient to produce a yield of crystals.

The most common use of this crystallizer is as an evaporative crystallizer with materials having relatively flat solubility or

inverted solubility. It is also useful for evaporation from solutions where there are scaling components.

When the heat exchanger is used, it normally is one pass or two pass, and is designed for relatively low temperature rises of the solution pumped through the exchanger. This limits the supersaturation when heating materials of inverted solubility. In most applications, the steam-liquid ΔT is also limited so as to prevent mass boiling of the solution pumped through the tubes or vaporization at the tube wall.

This type of crystallization equipment is probably the most widely used of any and is found in sizes ranging from 0.6m for laboratory equipment up to over 12m in diameter. Per pound of product produced, it is normally the least expensive type of equipment available, particularly when substantial amounts of evaporation are required.

The FC crystallizer is recommended for the crystallization of a wide range of organic and inorganic compounds, such as NaCl, sodium sulfate, sodium carbonate monohydrate, citric acid, urea, sugar, etc.

5.3.4. DRAFT TUBE BAFFLE (DTB) CRYSTALLIZER

The DTB crystallizer shown in Figure 5.18 consists of a body in which growing crystals are circulated from the lower portion to the boiling surface by means of a large, slow-moving propeller circulator. Surrounding the suspended magma of growing crystals is an

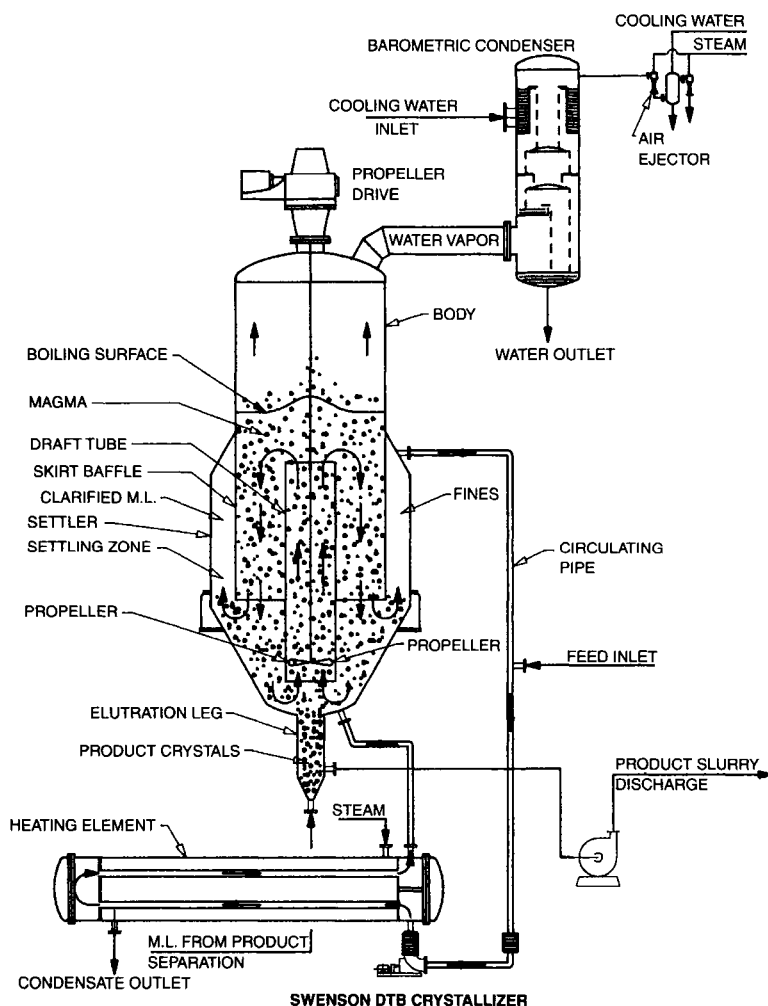


Figure 5.18 Swenson DTB crystallizer.

annular settling zone from which a stream of mother liquor can be removed bearing fine crystals. The fine crystals separate from the growing suspension of crystals by gravitational settling in the annular baffle zone.

Fine crystals in the mother liquor leaving the baffle zone are sent to a following stage, settler, or heat exchanger in the case of an evaporative-DTB crystallizer. The mother liquor is returned to the suction of the propeller circulator after the fines have been destroyed by heating, mixing with dilute feed, or water, depending on the flow sheet. Incoming feed is also mixed at the eye of the propeller, and in the case of adiabatic cooling crystallizers or evaporative crystallizers, the temperature rise in the circulated magma caused by the mixing of the feed or heated mother liquor is in the order of 1°C . This low temperature rise can be achieved at very low power consumption because of the small head loss in the circulated liquid-solid circulation path.

The amount of temperature change as this slurry is pumped past the boiling surface limits the amount of supersaturation created per pass to about 1°C and thereby limits the nucleation rate to very low values. The boiling action is concentrated mostly in the center of the vessel and is well distributed across the surface by the vertical inlet. Typically, crystallizers of this type operate with a suspension of solids that is 25–50% apparent settled volume. The low temperature drop at the boiling surface and the uniform distribution of boiling created by the circulation pattern and the uniform distribution of boiling created by the circulation pattern minimizes crystallization buildup on the walls of the crystallizer and extends the operating cycle. There are no close clearances where the buildup of solids can produce a large reduction in the rate of circulation such as can occur in other crystallizer designs.

Control of the population of fine particles by the mother liquor pumped from the baffle zone permits crystallization of products such as ammonium sulfate, KCl, and $(\text{NH}_4)_2\text{HPO}_4$ in the range of 6–20 mesh.

This type of equipment is especially useful in multiple-stage cooling crystallizer applications where the cooling of the feed solu-

tion in each stage limits the natural slurry density to a few percent. By means of the baffle zone, the operating slurry density within the crystallizer can be raised to any convenient value by regulating the slurry underflow rate and removing mother liquor from the baffle section.

When a solid-phase crystallized material results from the reaction of two components, it is often advantageous to perform this reaction in a *reactive crystallizer* rather than in a separate reactor. This is commonly done, for example, in the case of $(\text{NH}_4)_2\text{SO}_4$ where liquid or gaseous NH_3 and concentrated H_2SO_4 are reacted in the crystallizer to produce $(\text{NH}_4)_2\text{SO}_4$ crystals, as shown in Figure 5.14. The reaction is carried on in a liquid suspension of growing crystals and the heat of reaction is removed by vaporizing water that is condensed and recycled to maintain the liquid balance. Other examples are the oxidation of CaSO_3 by oxygen (air) or the neutralization of $\text{Ca}(\text{OH})_2$ by waste acid.

The reactants can be mixed in the circulation piping of an FC-type crystallizer or in the draft tube of a DTB-type crystallizer where a large volume of slurry is mixed continuously with the reactants so as to minimize the driving force (supersaturation created by the reaction). Removal of heat is conveniently done by vaporizing water or other solvents as in a conventional evaporative-type crystallizer.

The reaction need not be limited to liquid and gases, as shown in Figure 5.14. In Figure 5.15, for example, an ore is dissolved (decomposed) in mother liquor with the resultant supersaturation and crystallization of another crystalline material. Materials may also be precipitated by common-ion effect or by "salting out" through the addition of solutions or other solids. These techniques are important because they frequently reduce energy consumption.

5.3.5. SURFACE-COOLED CRYSTALLIZERS

Figure 5.19 shows a surface-cooled, FC crystallizer. The equipment consists of a tube and shell heat exchanger through the tubes

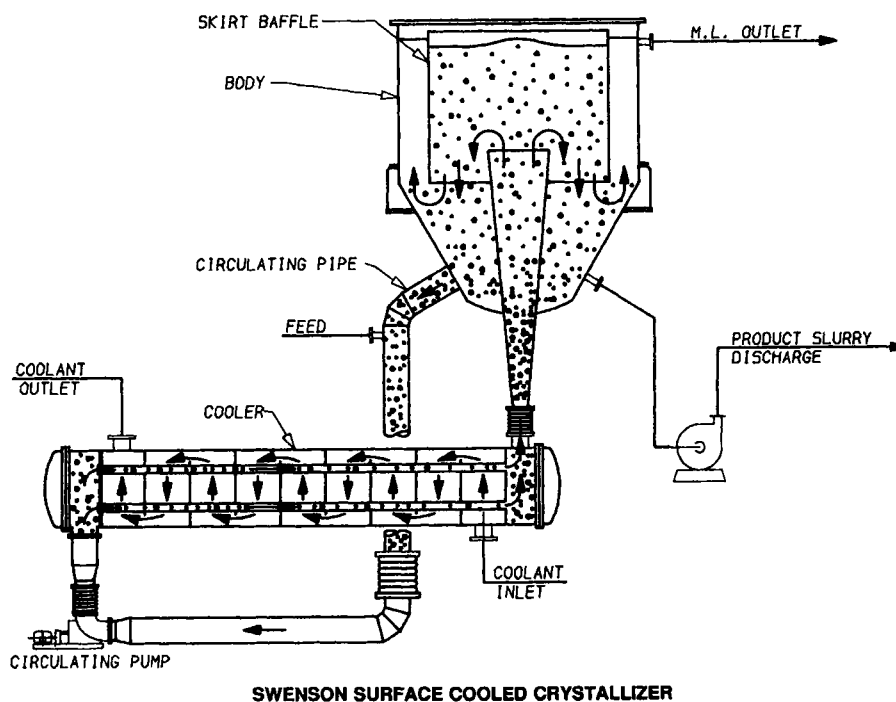


Figure 5.19 Swenson surface-cooled crystallizer.

of which is pumped the slurry of growing crystals, a crystallizer body to provide retention time, and a recirculation pump and piping. Internally, within the crystallizer body is a baffle so that fine particles may be separated from the growing magma of crystals for size control and slurry density control.

The circulation rate through the heat exchanger tubes is normally large enough so the temperature drop is in the range of 1–2°C. Surrounding the tubes is the cooling media that may be either tempered with water circulated through segmental baffles or a refrigerant that is vaporized by heat removed through the tubes. Since the tube wall is the coldest part of the crystallizing system, it is important that the difference in temperature between this tube wall and the slurry pumped through the tube be as small as practical. Practical values depend on the operating cycle and with many materials, ΔT s in the range of 5–10°C are required so as to achieve reasonable operating cycles.

This type of equipment is often used where the boiling point elevation of the solution is extremely high, as in the case of caustic solutions or when the temperature level is so low that there is no real possibility of using vacuum evaporation.

Typical applications are the crystallization of NaCl from caustic solutions, sodium carbonate from waste solutions, and sodium chlorate from solutions saturated with NaCl.

5.3.6. DIRECT-CONTACT REFRIGERATION CRYSTALLIZERS

Either the draft tube baffle, as shown in Figure 5.20, or the FC crystallizer may be used as a direct-contact refrigeration crystallizer in those cases where crystallization occurs at such a low temperature that it is impractical to use surface cooling or when the rapid crystallization of solids on the tube walls would foul a conventional surface-cooled crystallizer.

In direct-contact refrigeration crystallizers, the refrigerant is mixed with the magma circulated within the crystallizer body where it absorbs heat and is vaporized. Refrigerant vapor leaves the surface of the crystallizer similar to water vapor in a conventional evaporative crystallizer. The refrigerant vapor must be compressed, condensed, and then recirculated to the crystallizer to maintain the continuous operating conditions. Refrigerants chosen must be relatively insoluble in the solutions processed and have the necessary thermodynamic characteristics to minimize compressor horsepower.

Examples of this are the crystallization of caustic dihydrate with Freon or propane, and the crystallization of paraxylene with liquid propane refrigerant.

5.3.7. TEFLON TUBE CRYSTALLIZER

Figure 5.21 shows a surface-cooled crystallizer that utilizes Teflon tubes as the heat exchanger media. The Teflon tubes

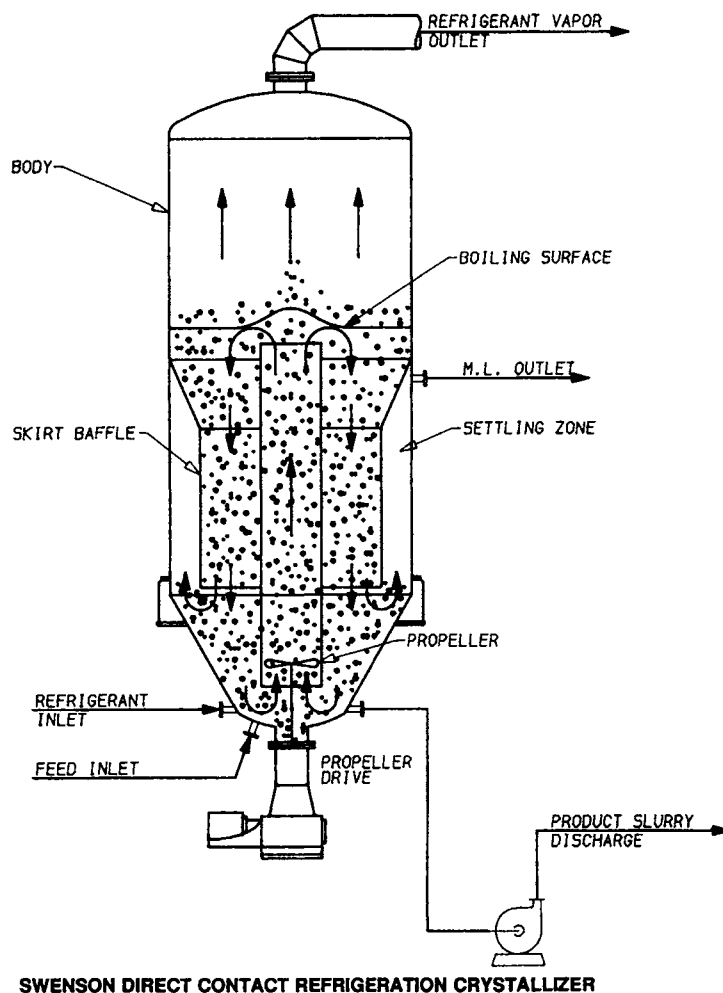


Figure 5.20 Swenson direct-contact refrigeration crystallizer.

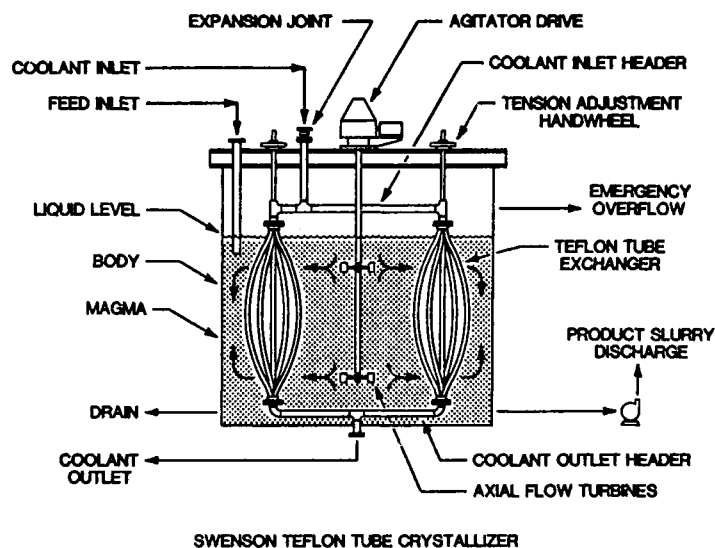


Figure 5.21 Swenson Teflon tube crystallizer.

are suspended within the magma in a relaxed or flexible position so that they move during agitation from the turbines or propeller. Crystal deposits that would normally build up on the surface being cooled do not adhere to the Teflon tubes as readily as they would to metal tubes. The gentle movement of the Teflon tubes is also instrumental in preventing buildup of solids, which is essential to long operating cycles. Using this technique, both longer operating cycles and greater differential tem-

peratures between the coolant and the magma may be employed, for example, the crystallization from Glauber's salt from waste brines.

5.3.8. SPRAY CRYSTALLIZATION

For applications where waste heat at very low temperature is available and where the product will not be contaminated by atmospheric

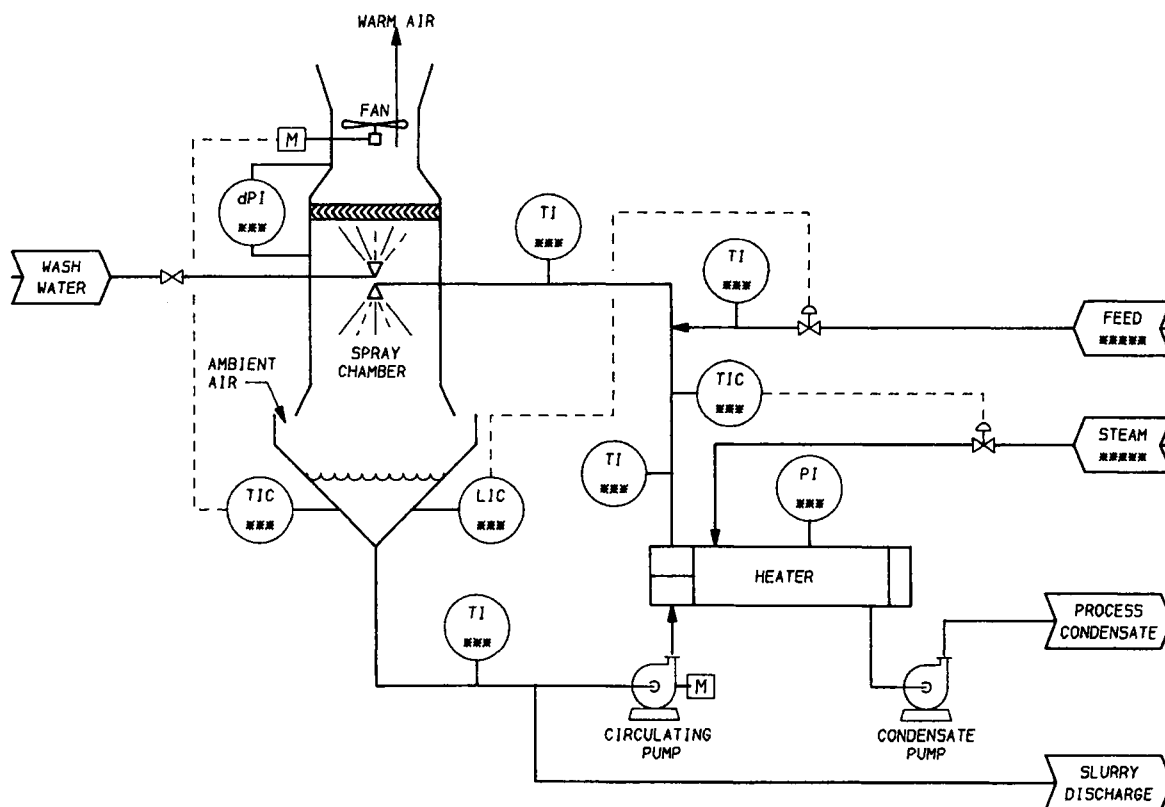


Figure 5.22 Typical flow sheet spray evaporator crystallizer.

air nor contaminate the air itself, it is possible to use spray crystallization. A cross-section of a typical unit is shown in Figure 5.22. In this type of equipment, the slurry to be crystallized is sprayed into a stream of air where cooling takes place, thereby supersaturating the solution circulating with the suspended crystals. In other respects, the slurry cycle on the crystallizer is similar to a forced circulation crystallizer in that heat input through a heat exchanger or by adiabatic cooling can be used to supply the heat for vaporization of the solvent. Systems of this type can operate during the winter months and produce end temperatures that are lower than 0°C, and can condense the heat from a multiple-effect evaporator, thereby adding one additional crystallizing stage and eliminating the need for a source of cooling water or a cooling tower. Although such equipment is relatively new, its use is increasing and it shows great potential, particularly for applications where crystal size and final liquid temperature are not critical, such as in the recovery of KCl, Na₂CO₃ · 10H₂O, and Glauber's salt from purge brines.

5.3.9. GENERAL CHARACTERISTICS

As a general guide, the data shown in Table 5.1 give the approximate crystal size made for various designs when crystallizing the indicated products.

5.4. CRYSTALLIZER DESIGN PROCEDURE

The following steps are outlined for the design of a crystallizer of the FC type. Although these calculations are limited to

that style, the procedure has general application to other types of equipment.

1. Choose the type of crystallizer that best meets the requirements for (a) product size, (b) product quality, (c) process economics, and (d) scale of operation. See Table 5.1 for a list of the general characteristics of crystallization equipment.
2. It is convenient to make a listing of the temperatures and physical properties required for the calculations, which is called a *temperature frame*, as shown below. As the calculation procedure proceeds, the table can be filled out and serves as a summary of the calculated values.
3. Make a material balance, heat balance, and flow sheet.
4. Decide what retention time is required to make the required product, (a) by experience, and (b) from growth and nucleation rate data.
5. Size the body on the basis of the controlling volume required for crystal retention with due consideration for the minimum cross-section required for vapor (evaporation) release.
6. Size the heat-transfer surface (for evaporative types) and the recirculation rate.
7. Size the condenser and vapor pipe, and entrainment separators (for evaporative types).
8. Select the vacuum equipment (for vacuum types).
9. Select the circulating pump or agitator.
10. Select the slurry, feed, condensate, and related pumps.
11. Specify the mechanical requirements and construction codes (such as ASME, UPV Section VIII) required.

TABLE 5.1 General Characteristics

Equipment Type	Crystal Size (Tyler Mesh)	Solubility Type	Typical Products	Remarks
Forced-circulation (Figure 5.2)	30–150	Normal, flat, or inverted	NaCl, Na ₂ SO ₄ , citric acid, Na ₂ CO ₃ · 1H ₂ O, lactose	Large or small capacity. Very stable operation. Little wall salting. Long or short retention.
Fluidized suspension (Figure 5.16)	6–65	Normal, flat	KCl, NH ₄ SO ₄ , Na ₂ B ₄ O ₇ · 1H ₂ O	Wall salting is a problem. Can operate above natural slurry density.
Draft tube baffle (Figure 5.17)	6–48	Normal, flat	KCl, (NH ₄) ₂ SO ₄ , H ₃ BO ₃ , (NH ₄) ₂ HPO ₄ , (NH ₄) ₂ HPO ₄	Low wall salting. Can operate above the natural magma. Good fines destruction system.
Reactive type (Figure 5.13)	6–100	All	(NH ₄) ₂ SO ₄ , (NH ₄) ₂ HPO ₄ , (NH ₄) ₂ HPO ₄	Can be DTB or DT type. Good fines destruction ability.
Surface-cooled (Figure 5.18)	20–150	Normal	Na ₂ ClO ₃ , KCl Na ₂ SO ₄ · 10H ₂ O	Can operate above natural slurry density. Medium washout cycles. Good for low temperatures.
Direct contact refrigeration (Figure 5.19)	6–48	Normal	Paraxylene, NaOH · 2H ₂ O	Little wall salting. Can operate at very low temperature. Avoids problems with surface cooling.
Batch type (Figure 5.15)	20–100	Normal, steep	Na ₂ SO ₄ · 10H ₂ O, FeSO ₄ · 7H ₂ O, Tri-P.E.	Simple-little instrumentation. Small capacity. Self-cleaning.
Teflon tube (Figure 5.20)	14–65	Normal	Na ₂ SO ₄ · 10H ₂ O	Generally used for low-temperature cooling applications at natural density.
Air-cooled (Figure 5.21)	30–200	Normal	Na ₂ CO ₃ · 10H ₂ O, H ₃ BO ₃ , Na ₂ SO ₄ · 10H ₂ O	Lowest energy consumption. Operation at ambient temperature condition.

EXAMPLE 5.1

Design a urea crystallizer given the following:

1. Production rate; 75 metric tons/day (3125 kg/h)
2. Feed concentration; 75% urea, 0.3% biuret, 0.35% NH₃ and 0.22% CO₂ (balance water) at a temperature of 93°C
3. Boiling point elevation; 13°C
4. Crystal size required; 90% plus 65 Tyler mesh

5. Mother liquor composition; 65.73% urea, 4.5% biuret at 54°C
6. Wash water added on the centrifuge; 0.12 kg/kg of product crystals
7. Cooling water for the condenser; 30°C.

Make the following assumptions:

1. The volatile NH₃ and CO₂ flash off and need not be considered in the material balance for the liquids and product crystals.

2. A forced-circulation crystallizer operating at 3.38 h retention will make this sized product (Bennett and Van Buren 1969).
3. Slurry density approximately 450 g/l.
4. Heat transfer coefficient; 4088 kJ/m² h °C (200 Btu/h ft² °F).

Refer to the figure on page 135 for the flow sheet of this process.

Temperature Frame

Steam temperature	ST	100 °C
Greatest terminal difference	GTD	46 °C
Least terminal difference	LTD	44 °C
Liquid temperature	LT	54 °C
Boiling point elevation	BPE	13 °C
Vapor temperature	VT	41 °C
Vapor pressure, mm Hg	VP	57 mmHg
Specific volume, m ³ /kg	SPV	18.48 m ³ /kg
Heat of vaporization	LHV	2402.76 kJ/kg
Evaporation, kg/h	Evap	1380 kg/h
Maximum vapor velocity	V_{max}	3.84 m/s
Minimum vapor release area	CSA	1.84 m ²
Crystal production	Yield	3125 kg/h
Minimum active volume	AV	23.47 m ³
Crystallizer body diameter	Dia	2.75 m
Crystallizer liquid level	LL	3.20 m
Heat transfer coefficient	U	4088 kJ/m ² h °C
Heating surface	HS	11.48 m ²
Circulation rate	Circ	465 m ³ /h
Temperature rise	T_R	1.5 °C
Tube velocity	u_t	2.158 m/s

Material Balance

(kg/h)	Total	Urea	Biuret	Miscellaneous	Water
Feed	100	75.00	0.30	0.57	24.13
Evaporation	22.68	—	—	0.57	22.11
Crystals	70.55	70.55	—	—	—
Purge	6.77	4.45 ²	0.3 ¹	—	2.02

¹Purge stream assuming no biuret formation in the crystallizer and a final concentration in the purge of 4.5% biuret and a loss of miscellaneous CO₂ and NH₃ by evaporation.

²65.73% urea in purge per given data.

For 75 metric tons per day (3125 kg/h) production by ratio.

Feed = (100/70.55)(3125 kg/h)	= 4430 kg/h
Purge = (6.77/100)(4430)	= 300 kg/h
Evaporation = (22.68/100)(4430)	= 1005 kg/h
Wash water = 0.12 kg/kg (3125 kg/h)	= 375 kg/h
Design evaporation = 1005 + 375	= 1380 kg/h

Heat Balance

(Basis: Liquid temperature of 54 °C)

		kJ/h
Heat in vapor (1380 kg/h)(2402.8 kJ/kg)	=	-3,315,864
Sensible heat (4430)(93 - 54)(2.59 kJ/kg °C)	= +	447,474
Heat of crystallization (3125)(242 kJ/kg)	= +	756,250
(Heat required from steam)		-2,112,140

$$\text{Steam flow} = \frac{2,112,140 \text{ kJ/h}}{2257 \frac{\text{kJ}}{\text{kg}} (0.95)} = 985 \text{ kg/h}$$

*Latent heat of vaporization of steam at atmospheric pressure.

Sizing of Crystallizer Body

Volume Required.

$$\frac{(3125 \text{ kg/h})(3.38 \text{ h})}{(0.450 \text{ kg/l})(1000 \text{ l/m}^3)} = 23.47 \text{ m}^3$$

Maximum Vapor Velocity. The maximum velocity of the vapor leaving a free-liquid surface from which liquid particles may be entrained by force balance has been investigated by Sanders and Brown (1934) in connection with distillation columns and by York and Popele (1963) in connection with mesh separators.

$$V_{max} = C_v \left(\frac{Dl - Dg}{Dg} \right)^{1/2} \quad (5.17)$$

The constant, C_v , depends on loading, pressure, and allowable entrainment. For vapor heads, a conservative value of 0.0244 m/s (0.08 ft/s) is recommended. For mesh separators, this value may be increased to the range 0.0305–0.0610 m/s (0.10–0.2 ft/s).

Since $Dg = 1/\text{sp vol.}$ and Dg is negligible compared with the Dl for the liquid

$$\begin{aligned} V_{max} &= 0.0244(Dl \times \text{sp vol.})^{1/2} \\ V_{max} &= 0.0244[(1.34)(1000)(18.48 \text{ m}^3/\text{kg})]^{1/2} \\ &= 3.84 \text{ m/s (12.6 ft/s)} \end{aligned}$$

Minimum Cross-Sectional Area Required.

$$\frac{(1380 \text{ kg/h})(18.48 \text{ m}^3/\text{kg})}{(3600 \text{ s/h})(3.84 \text{ m/s})} = 1.84 \text{ m}^2 \text{ (19.8 ft}^2\text{) or 5.02 dia}$$

(This value is not controlling.)

Crystallizer Volume. Say 2.75-m diameter with a 3.2-m liquid level.

$$\text{Cone volume} = 0.2267(2.75)^3 = 4.71 \text{ m}^3$$

$$\text{Straight side} = \frac{\pi}{4}(2.75)^2(3.2) = 19.01 \text{ m}^3$$

$$\text{Total volume} = 23.72 \text{ m}^3$$

Heat Transfer Area Required

Design the heat exchanger by assuming a coefficient of 4088 kJ/(m² h °C)(200 Btu/h ft² °F) for sizing the heat exchanger and then check the inside and outside tube coefficients to be sure the values can be achieved in the design selected.

$$\begin{aligned} \text{Heating surface} &= \frac{2,112,140 \text{ kJ/h}}{(4088 \text{ kJ/m}^2 \text{ h } ^\circ\text{C})(45 ^\circ\text{C})} \\ &= 11.48 \text{ m}^2 \text{ (123.58 ft}^2\text{)} \end{aligned}$$

Circulation Rate. Assuming a maximum temperature increase through the heater 1.5 °C (2.7 °F) corresponding to a reasonable peak supersaturation developed in the flow path, the circulation rate is

$$\begin{aligned} \text{Circulation} &= \frac{2,112,140 \text{ kJ/h}}{1.5 ^\circ\text{C}(2.59 \text{ kJ/kg } ^\circ\text{C})1170 \text{ kg/m}^3} \\ &= 465 \text{ m}^3/\text{h (2044 gal/min)} \end{aligned}$$

Assume $1\frac{3}{4}$ -inch 16-gauge tubes 2 m long (based on inside surface).

(41.15-mm i.d., $0.129\text{ m}^2/\text{m}$ surface area)

Cross section = 1330 mm^2 each

No. of tubes required = $11.48\text{ m}^2/0.129\text{ m}^2/\text{m}$ (2 m)

No. required = 45 tubes

$$\text{Tube velocity} = \frac{465\text{ m}^3/\text{h}}{(45)(0.001330\text{ m}^2\text{ each})(3600\text{ s/h})}$$

$$= 2.158\text{ m/s (7.08 ft/s)}$$

For the temperatures, tube velocity, and heat flux, the sizing above must now be checked for outside and inside film coefficients by typical heat transfer techniques, as outlined in the *Chemical Engineers Handbook* (Perry 1973).

Vapor Pipe and Condenser Design

Assume a vapor pipe velocity of 46 m/s (150 ft/s) for a pressure drop at this vacuum of under 1°C .

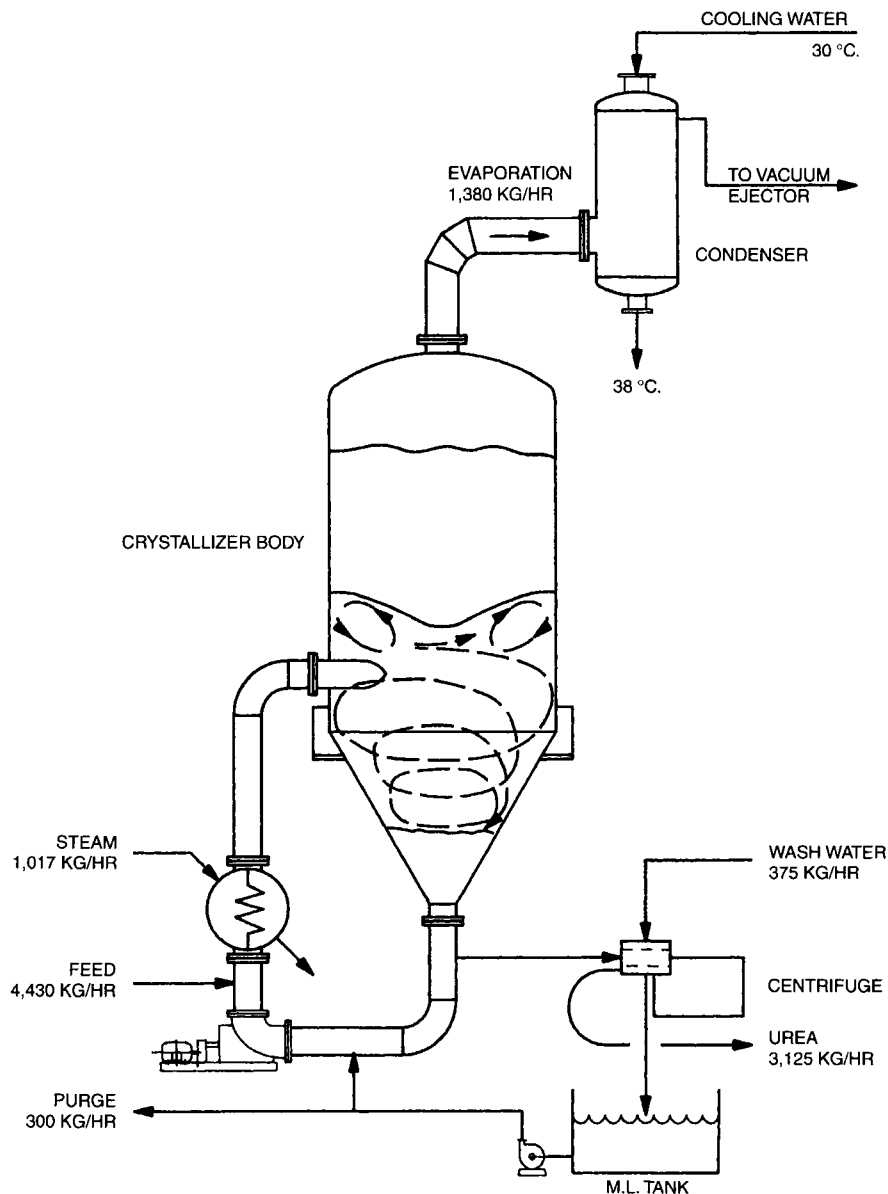
$$\text{Area required} = \frac{1380\text{ kg/h (18.48 m}^3/\text{kg)}}{3600\text{ s/h (46 m/s)}} = 0.15\text{ m (1.66 ft)}$$

$$\text{Diameter} = \sqrt{\frac{0.15(4)}{\pi}} = 0.44\text{ m (17-inch dia)}$$

$$\text{Condenser water flow} = \frac{1380\text{ kg/h (2402 kJ/kg)}}{(100)(2.59\text{ kJ/kg}^\circ\text{C})(8^\circ\text{C})}$$

$$= 160\text{ m}^3/\text{h (705 gal/min)}$$

The condenser can be purchased by specifying a water flow of 700 gal/min and an operating pressure of $57\text{ mm of Hg absolute}$.



Flow sheet for Example 5.1

Selection of the Vacuum Equipment. The sources of all non-condensable gas entering the system must be accounted for and an estimate made of the air leakage.

1. Noncondensable CO₂ and NH₃.

$$\text{NH}_3 = 0.35\%(4430) = 15.51 \text{ kg/h}$$

$$\text{CO}_2 = 0.22\%(4430) = 9.75$$

$$\text{Air} = 0.05\%(4430) = 2.22$$

2. Air in the steam vented to the condenser from the heater. Estimated at 2 kg/h.
3. Air in the barometric condenser water. Estimated at 3 kg/h.
4. Gas liberated by reaction (breakdown of the urea to CO₂, NH₃). Estimated at 10 kg/h (6NH₃, 4CO₂).
5. Estimated air leakage 5 kg/h (air).

$$\text{Totals : Air} = 12.2 \text{ kg/h}$$

$$\text{NH}_3 = 21.5 \text{ kg/h}$$

$$\text{CO}_2 = 13.75 \text{ kg/h}$$

Most of the NH₃ will dissolve in the condenser water and much of the air and CO₂ will be entrained in the tail water from the barometric condenser. The sizing should be for 10 kg/h air and 6 kg/h CO₂.

The head for the circulating pump and the slurry pumps can be calculated from information in the *Chemical Engineers Handbook* (Perry 1973). The mechanical design should be in accordance with the information in the American Society of Mechanical Engineers Code for Unfired Pressure Vessels, Section VIII, for the current year. There is a section devoted to the design of vessels under external pressure.

5.5. INSTRUMENTATION AND CONTROL

Crystal growth is a layer-by-layer process that occurs in a relatively long period of time. Crystallizers frequently have a suspension of growing crystals that represent 2–6 h of production. The mixed suspension of crystals that exist within the crystallizer is a combination of growing particles having a wide range of retentions. The small particles may have been in the crystallizer far less than the nominal retention time, whereas large particles frequently have a retention within the crystallizer that is three or four times the nominal retention time. Nucleation, on the other hand, is a phenomenon that can occur almost instantaneously as a result of a severe upset in operating conditions, such as a rapid drop in crystallizer temperature with materials of normal solubility. Control of liquid level and absolute pressure are variables, which must be maintained by the instruments on a minute-by-minute basis. The design of the control system for a crystallizer, therefore, must simultaneously accommodate these various needs in order to maintain the conditions required for the growth of the product crystals.

Changing the production rate from one value to another normally results in an increase in the boiling rate and therefore, an increase in temperature rise in the heat exchanger or in the draft tube circulation system. This increase in temperature represents a higher level of supersaturation as the liquid flashes to equilibrium at the liquid surface; the influence of this higher level of supersaturation is normally a greater nucleation rate as well as a greater growth rate.

The effects of perturbation of this type can be seen in the crystal size distribution for a period of 6 to 10 times the nominal retention period. For an ammonium sulfate crystallizer, for instance, operating at a retention time of 4 h, the effects of an upset would not be fully dissipated until a period of 1–2 days had passed. Because of this fundamental characteristic, it is necessary that the control system of a crystallizer and the flow sheet be arranged in such a way that stable operations can be maintained for extended periods of time. Only small changes in production rate should be made within any operating shift. The following controls are typical of those required for most continuous crystallizers similar to that shown in Figure 5.16, however, no list of this type can be all inclusive.

5.5.1. LIQUID LEVEL CONTROL

Most vacuum crystallizers operate at constant liquid level and this requires liquid level controls capable of maintaining the level within about 6 inches (15 cm) of any predetermined point. This

level sets the relation of the inlet to the boiling surface in the vessel. This determines the character of the boiling within the vessel, which influences the entrainment and the wall salting that often occurs in vacuum crystallizers. With vertical inlet designs such as a draft tube baffle crystallizer, the distance between the inlet and the liquid surface controls the exposure of the solids to the highest levels of supersaturation created at the boiling surface, and also affects the head on the circulation system. Since the shutoff head of the internal circulators is relatively low, small changes in the liquid level can have an adverse effect on the operation. A liquid level controller of the differential pressure type vented to the upper portion of the vapor head is normally used for this service. The side connected to the upper portion of the vapor head should be purged with water to prevent condensation from causing a change in set point. The differential pressure cell can be of the flush type or connected to the vessel through impulse lines that are purged. The purge solution should be colder than the temperature equivalent to the vapor pressure in the vessel. It should also be at a temperature below ambient temperature to prevent upsets due to boiling in the impulse lines. The liquid level controller need not be a recording type, but should contain reset and proportional control. Normally, this level controller would control the feed to the system, however, in some cases it controls a recycle stream of mother liquor.

5.5.2. ABSOLUTE PRESSURE CONTROL

The temperature in a vacuum crystallizer is normally controlled by an absolute pressure recorder controller that purges air into the vacuum system or bleeds off vent gas from a condenser if the vessel is operated above atmospheric pressure. It should be capable of maintaining the temperature in the vessel to within 1/2 °C of the set point. Typically, this is done through an absolute differential pressure cell mounted on top of the vessel so that drainage can be back into the vapor space and the control signal is transmitted to a remote recorder controller.

5.5.3. MAGMA (SLURRY) DENSITY RECORDER CONTROLLER

The slurry density in a crystallizer whose fluidization is maintained by a propeller or external circulating pump can be determined by a differential pressure measurement between two points in the suspension located far enough apart so that suitable differential reading can be obtained. With crystals of relatively high specific gravity, these two points of measurement can be in the range of 6–10 ft (2–3 m) apart. Normally, they would be mounted at two points on

the body beneath the liquid surface; however, in some cases, such measurements have been successfully made by measuring taps installed on the circulation system. The liquid turbulence causes considerable noise on the input signal and this must be removed by variable restrictors on air impulse lines or suitable electrical damping. The calibration on such instruments tends to shift slightly with time since the instruments must be relatively sensitive to give a control value. The most important use of such instruments is to determine the trend in the slurry density so that adjustments can be made in the discharge rate to maintain a constant body density.

5.5.4. STEAM FLOW RECORDER CONTROLLER

It is desirable to set the heat flux in an evaporative crystallizer because, in essence, this sets the maximum supersaturation level within the equipment. While at any one condition, this can be done by controlling either pressure or steam flow, experience shows the best technique is to control the steam flow. (Not shown in Figure 5.7.) For most evaporative units, the steam flow is directly proportional to the production rate and to the temperature rise in the recirculation system and the ΔT in the heat exchanger. Both of these values have an important influence on the scaling rate in cases where materials of inverted solubility are being handled or where there are scale-forming components within the system. In systems where this value is critical, the ΔT can be monitored and used to reset the steam rate. An interlock should be provided that will cut off the steam flow to the system if the circulating pump or propeller circulator in a draft tube baffle unit is off due to motor overload or power failure.

5.5.5. FEED-FLOW RECORDING CONTROLLER

The preferred type of instrument for this control is the magnetic type. In cooling crystallizers, the feed flow determines the heat flux and, therefore, the peak supersaturation level within the crystallizer. (Not shown in Figure 5.7.) In addition, it is directly proportional to the production rate and, therefore, this control serves an important function. In multistage crystallizers, the feed is discharged mother liquor from the preceding stage and the rate is subject to control changes in that stage. Maintaining stable control is, therefore, more critical in multistage units.

5.5.6. DISCHARGE CONTROL

Many continuous crystallizers are supplied with a throttling valve on the slurry discharge line to regulate the discharge rate. For most applications, this is not satisfactory since such valves tend to plug. Plugging can be reduced somewhat by having a timer fully open the valve once every 1 or 2 min in order to remove blockage that may accumulate in the throttled condition. Pinch-type valves or Saunders-type valves are frequently used for this service. The tendency to plug varies considerably with the crystal size. In general, the throttling technique can only be used with relatively fine products. An alternative is to use a variable speed pump that can be operated by a liquid level control or a remote manual operator. The limitation in this technique is that only about a 2 to 1 flow variation can be accommodated while still staying above the critical line velocity. A more common technique in modern equipment, as shown in Figure 5.7, is to operate the discharge system at constant flow rate and return a stream of mother liquor to the discharge line at the point where it leaves the body. By regulating the flow in this line, the quantity of slurry removed from the body may be varied through a wide range. The disadvantage of this technique is that the slurry being discharged must pass through a settler or thickener

in order to increase its density to a point where it is suitable for handling in a filter or centrifuge.

5.5.7. MISCELLANEOUS

Temperature recorders should be included at all feed, discharge, and cooling water streams in the system. It is also desirable to monitor the differential temperature across the heat exchanger in FC or draft tube evaporative units. The amperage on the main circulators should be monitored and, in some cases, the slurry pump as well. Purge water should be supplied to the glands of all pumps through small purge rotameters, and the pressure at the seal connected to a pressure switch and alarm system so that if water pressure fails, the operator is notified.

5.5.8. DISTRIBUTED CONTROL SYSTEMS

Use of the instruments mentioned previously, in connection with temperature indicators, provides sufficient information so that the operator can troubleshoot the equipment and set it so as to maintain the steady conditions of operation that are required to achieve the optimum results and particle size. The information available from these instruments, however, is capable of being combined through the use of a distributed control system or computer in such a way as to yield far more information about the process than is available by monitoring the instruments required for maintaining stable operation. Through the use of known physical laws and the known physical properties of the solution, it is possible to calculate the production rate and the heat transfer coefficient. By trending this data, projections can be made regarding the heat-transfer data, expected operating cycle, and production rate.

5.5.9. DISCHARGING

The discharge line from a crystallizer should be taken from a point that is well away from the boiling surface and away from the point where feed is admitted to the system. The sample from a well-mixed suspension should be representative and the velocity in the sampling line should be close to the line velocity at the point where the sample is separated. In some cases, it is necessary to incline the discharge line to the direction of flow in order to achieve a good sample without segregation. This is particularly true when the crystals are large or have relatively high settling rates.

5.5.10. SAMPLING

Normally, the product made in a crystallizer is for customer use and, therefore, the product size must be carefully monitored in order to stay within the prescribed limits. Typically, the product from a crystallizer will be sampled every 1–2 h during conditions when the operation is monitored to make adjustments in product size or characteristics. Ideally, the best place to sample the product is before it enters the slurry discharge pump and preferably from the slurry discharge line.

The disadvantage of this technique is that a sample of slurry is taken that must be filtered or centrifuged without causing appreciable precipitation of solids from the mother liquor. With materials of high solubility and relatively high temperature, this problem can be a difficult one to solve. In some cases, it is necessary to use the centrifuge cake sample in order to monitor the product size, but if this is done, it is necessary to get a representative sample from the centrifuge; this may involve stopping the centrifuge basket and taking a section sample. Typically for operator control checks, the centrifuge sample or dryer discharge sample is used and the

screening is reduced to one or two screen fractions. Such samples only show trends, however, and are not suitable for use by the calculation techniques described in Section 5.1.7. The reason for this is that breakage of the product crystals occurs in both the centrifuge and the dryer. Typically, this may be 10–20% at the mean particle size.

Samples removed on an hourly or bihourly basis for screen analysis should be taken through sample lines that can be readily back flushed and are running at a discharge rate equivalent to 3 ft/s (1 m/s) so that no segregation of solids occurs during the sampling process. It is best to take approximately 0.5 l or 1 l of slurry and centrifuge or filter this sample and screen all of the solids present to avoid segregation in the sampling process. Care must be taken so that hot liquids do not flash or splatter and injure the operator. Often such sample lines are brought to a common point where a header is provided for back flushing the lines with hot water or condensate.

Samples of the product should be dried and screened, and it is usually convenient to wash the sample during the centrifugation or filtration process with alcohol or other suitable volatile solvent so that the samples can be dried in 15–20 min. Screening can be done by a number of techniques, but the use of the rototap screen shaker is almost universal.

The data from a screen analysis is normally presented on arithmetic probability paper, similar to that shown in the example in Figure 5.23. The coefficient of variation of the product can be

computed from the size intercepts at 16 and 84% providing the plot results in a straight line between these two points.

In the example in Figure 5.23 this is not quite true, however, the intercept values selected are those corresponding to the points indicated in the formula. An FC crystallizer or any design that results in a thoroughly mixed suspension and whose characteristics are similar to those described in Section 5.1.7 for Eq. (5.2) will have a coefficient of variation of 50% when operating steadily. Substantial deviations from this characteristic coefficient of variation indicate lack of equilibrium or classification of the product.

5.6. CRYSTALLIZER COSTS

As outlined in the aforementioned pages, each crystallizer design depends upon some unique features that are dependent upon the product being crystallized as well as the impurities present in the solution from which it is crystallized. It is difficult to generalize about equipment costs for this reason; however, some industrial operations are carried on so widely and at such a large scale, that generalized information can be presented.

Figure 5.24 shows a graph indicating the equipment costs as a function of capacity for sodium sulfate crystallizers and ammonium sulfate crystallizers of the FC and the DTB type.

The costs shown are plotted versus capacity, and cover the cost of the crystallizer and its ancillary equipment, including circulating pumps, circulating piping, vacuum equipment, con-

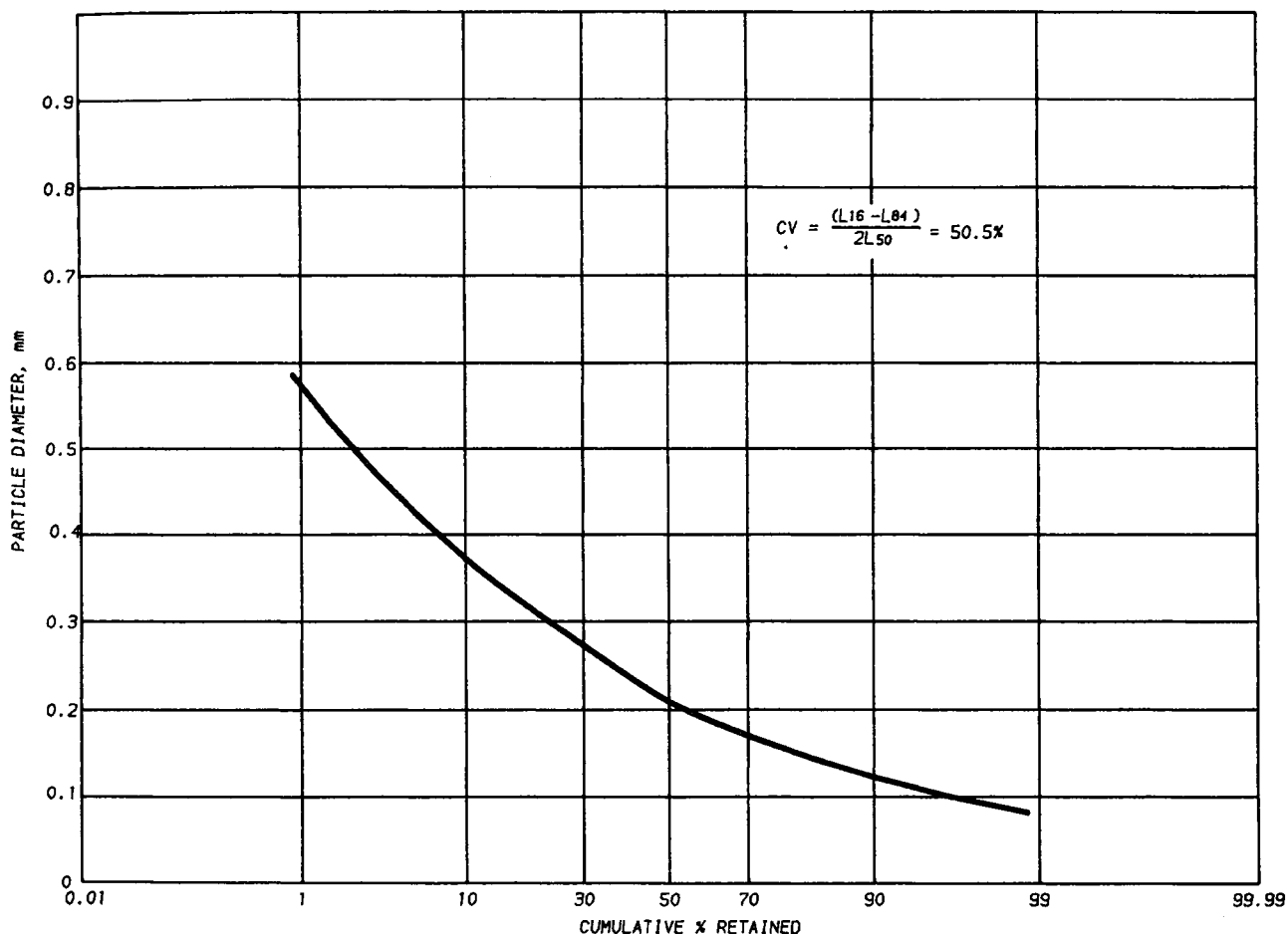


Figure 5.23 Crystal size distribution and coefficient of variation (CV) calculation.

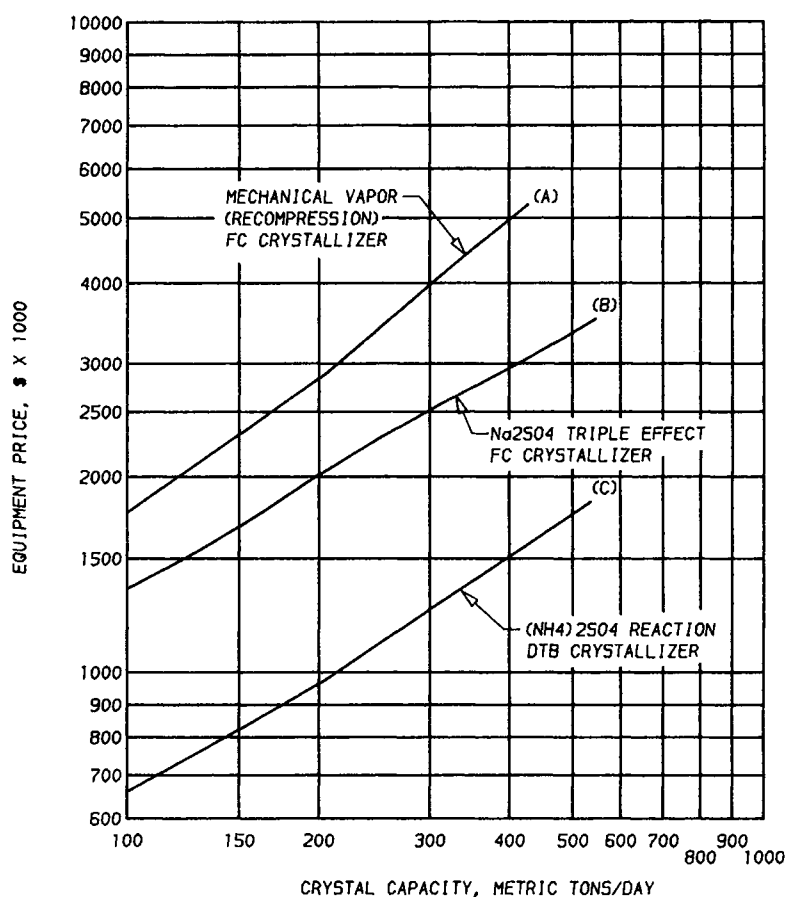


Figure 5.24 Plot of cost versus capacity for typical crystallizers. (A), (B) Na₂SO₄ production from Glauber's salt, melting tank included; and (C) reaction of NH₃ + H₂SO₄ to make (NH₄)₂SO₄.

denser, vapor piping, and, where applicable, the mechanical vapor recompressor and driver. Not included are instrumentation, structural steel, electrical interconnection, control room, or buildings.

Typically, the cost of supporting structural steel, erection, interconnecting piping, and electrical interconnections would be from 40–100% of the cost of the equipment itself. Costs vary so much from one application to another and from one location to another that checking for each specific application is required.

NOMENCLATURE

<i>A</i>	Area, m ²
<i>B</i>	Nucleation rate, no./h
<i>C</i>	Weight of crystal phase in the magma in Eq. (5.1)
<i>C_v</i>	Constant in Eq. (5.17)
<i>D_g</i>	Gas density, kg/l
<i>D_l</i>	Liquid density, kg/l
<i>E</i>	Evaporation, kg
<i>G</i>	Growth rate, mm/h
<i>H₀</i>	Total weight of solvent
<i>i</i>	Exponent of <i>G</i> in Eq. (5.7)
<i>J</i>	Exponent of <i>M</i> in Eq. (5.7)
<i>K_e</i>	Experimentally determined constant, Eq. (5.13)

<i>K_n</i>	Experimentally determined coefficient, Eq. (5.7)
<i>K_v</i>	Coefficient, relates volume of a crystal to the characteristic length, <i>L</i> , where <i>L</i> ³ = 1 for a cube
<i>L</i>	Length or characteristic length, mm
<i>L_{av}</i>	Average particle by weight, Eq. (5.11)
<i>L_d</i>	Dominant particle, Eq. (5.10)
<i>L_F</i>	Largest size removed in fines destruction baffle, mm
<i>M</i>	Magma density, or mass of crystals per unit volume, g/l
<i>N</i>	Total number of crystals per liter of crystallizer volume
<i>n</i>	Population density, no./mm, per liter of crystallizer volume
<i>ρ</i>	Specific gravity, gm/ml
<i>Q_d</i>	Discharge rate, m ³ /h
<i>R</i>	Ratio of mole weights in Eq. (5.1)
<i>S</i>	Solubility in kg solute/100 kg solvent
<i>t</i>	Characteristic time, h, or volume/discharge rate, <i>V</i> / <i>Q_d</i>
<i>t_F</i>	Retention time in the fines destruction system, h
<i>TIPS</i>	Tip speed of the pump or impeller, m/min
<i>TO</i>	Time to turn over the crystallizer volume, volume/circulation rate, min
<i>U</i>	Heat transfer coefficient, kJ/(m ² h °C)
<i>V</i>	Active volume of the crystallizer, m ³
<i>W₀</i>	Weight of anhydrous solute in original batch
<i>W_X</i>	Weight fraction to size <i>X</i> , in Eq. (5.9)
<i>X</i>	Dimensionless length, <i>L</i> / <i>Gt</i>

REFERENCES

- Abegg, C.F., and Balakrishnan, N.S. (1971). *The Tanks-in-Series Concept a Model for Imperfectly Mixed Crystallizers*, American Institute of Chemical Engineers Symposium Series, vol. 67, p. 110, American Institute of Chemical Engineers, New York.
- Abegg, C.F., Stevens, J.D., and Larson, M.A. (1968). *AIChE J.* **14**, 118.
- Bennett, R.C. (1978). *Chem. Eng. Progress* **1978**, 67–70.
- Bennett, R.C., and Randolph, A.D. (1983). *Application of On-Line CSD Control to Industrial KCl Crystallizers*, presented at the International Conference on Potash Technology, Saskatoon, October 1983.
- Bennett, R.C., and Van Buren, M. (1969). *Chem. Eng. Progress, Symposium Series* **65(95)**, 46.
- Bennett, R.C., Fiedelman, H., and Randolph, A.D. (1973). *Chem. Eng. Progress* **69**, 7.
- Berglund, K.A., and Larson, M.A. (1992). *AIChE J.* (in press).
- Bujac, P.D.B. (1976). *Industrial Crystallization* (Mullen, J., ed.), Plenum, New York.
- Campbell, A.N., and Smith, N.O. (1951). *Phase Chemistry*, Dover Publications.
- Clotz, N.A., and McCabe, W.L. (1971). *Chem. Eng. Progress Symposium Series* **110(67)**, 6.
- Fitch, B. (1970). "How to Design Fractional Crystallization Processes," *Industrial Eng. Chem.* **62(12)**, 6–33.
- Grootscholten, P.A.M., Brekel, L.D.M., and deJong, E.J. (1984). *Chem. Eng. Res. Des.* **62**.
- Human, H.J., Enckerork, W.J.P., and Bennema, P. (1982). In *Industrial Crystallization 81* (Jančić, S.J., and de Jong, E.J., eds.), p. 387, North-Holland Publishing Co., Amsterdam.
- Larson, M.A. (1978). *Chem. Eng.* February 13, 1978.
- Mullen, J. (1961). *Crystallization*, Butterworth, London.
- Ness, N.J., and White, E.T. (1976). *AIChE Symposium* **72(195)**, 64.
- Ottens, E., and deJong, E.J. (1972). In *5th Symposium Industrial Crystallization*, UST and Labem, Yugoslavia.
- Perry, R. (1973). *Chemical Engineers Handbook*, 5th ed., McGraw-Hill Book Co., New York.
- Randolph, A.D. (1969). *Industrial Eng. Chem. Fund* **8(1)**, 58–63.
- Randolph, A.D., and Beckman, J.R. (1977). *AIChE J.* **23(4)**, 500–520.
- Randolph, A.D., and Larson, M.A. (1962). *AIChE J.* **8(5)**, 639.
- Randolph, A.D., and Larson, M.A. (1971). *Theory of Particulate Processes*, Academic Press, New York.
- Randolph, A.D., and Low, C.C. (1982). *Industrial Crystallization 81* (Jančić, S.J., and deJong, E.J., eds.), North-Holland Publishing Co., Amsterdam.
- Randolph, A.D., and White, E.T. (1977). *Chem. Eng. Sci.* **32**, 1067.
- Randolph, A.D., Beer, G.L., and Keener, J.P. (1973). *AIChE J.* **19(6)**, 1140.
- Randolph, A.D., Deepak, C., and Iskandar, M. (1968). *AIChE J.* **14**, 827.
- Randolph, A.D., White, E.T., and Low, C.C. (1981). *Ind. Eng. Chem. Process Des. Dev.* **1981**, 496–503.
- Rovang, R., and Randolph, A.D. (1980). *Chem. Eng. Progress Symposium Series* **193(76)**, 18.
- Rusli, M.A., Larsen, M.A., and Garside, J. (1980). *AIChE Symposium Series* **193(76)**.
- Sanders and Brown (1934). *I&EC*, **26**, 98.
- Shaw, B.C., McCabe, W.L., and Rousseau, R.W. (1973). *AIChE J.* **19(1)**, 194.
- Sikdar, S., and Randolph, A.D. (1976). *AIChE J.* **22**, 110.
- York, O.H., and Popele, E.W. (1963). *CEP* **59**, 45.
- Zumstern, R.C., and Rousseau, R.W. (1986). *AIChE J.*

PRECIPITATION PROCESSES

P.H. Karpinski and J.S. Wey

6.1. INTRODUCTION

Precipitation generally refers to a relatively rapid formation of a sparingly soluble solid phase from a liquid solution phase. Precipitation is rather poorly understood when compared with crystallization of more soluble materials. It generally involves the simultaneous and rapid occurrence of nucleation, crystal growth, and other processes, such as Ostwald ripening and agglomeration. All these processes are difficult to separate and independently investigate both mechanistically and experimentally.

Precipitation has several important characteristics. First, the “precipitates” are usually sparingly soluble and their formation occurs under relatively high supersaturation conditions. Typically, rapidly occurring precipitation is not affected by the presence of solute crystalline material and thus does not involve secondary nucleation. Rather, it results from homogeneous or heterogeneous nucleation processes. Second, because of the presence of high supersaturation, nucleation plays a major role in the precipitation processes. As a result, a large number of crystals with relatively small sizes are produced. The particle concentration is usually between 10^{11} and 10^{16} particles per cm^3 , and the crystal size is typically between 0.1 and $10\ \mu\text{m}$. Third, because of the high particle concentration and small crystal size, a number of secondary processes—such as Ostwald ripening and aggregation—may occur and greatly affect the properties of the resulting precipitates. Thus, the development of colloidal systems must be considered in order to manage these secondary processes to achieve the desirable precipitate quality. Fourth, the supersaturation necessary for prompting precipitation frequently results from a chemical reaction; indeed, precipitation is sometimes referred to as reactive crystallization. The chemical reactions may involve rapid mixing of concentrated chemical reactants and are generally very fast. Thus, the role of both macro- and micromixing is frequently important in precipitation processes. Many of these key precipitation characteristics will be discussed further in later sections.

Precipitation processes are of great importance in the chemical and process industries. The increasing emphasis on high added value specialty chemicals (e.g., pharmaceuticals, dyes, pigments, paints, printing inks) has also highlighted the important role of precipitation. Many consumer products are produced via precipitation processes. Perhaps the two most common examples are magnetic recording media, which contain ferric or chromic oxides, and photographic materials where the specific properties of the photosensitive silver halide crystals are determined by the precipitation process. In addition, precipitation has also played an important role in wastewater treatment (e.g., removal of calcium salts) and in reducing emissions to the environment.

In most practical applications, the properties of the precipitated particles are of key importance and great attention must be paid to “particle design” or “crystal engineering.” Many crucial properties of precipitates are physical in nature. The crystal size

distribution and crystal habit or morphology can have a major impact on the post-precipitation processing, such as filtration, drying, etc. Other key particle properties are chemical in nature. Chemical composition as represented by the chemical purity and impurity levels must be controlled. Many precipitated products can form a range of polymorphs. In most cases, only one specific polymorphic modification is acceptable and thus precipitation conditions must be controlled in order to obtain the desired product. In addition to particle design, one needs to ensure reproducibility of particle properties from batch to batch. This is of particular importance if the product is subject to statutory or regulatory requirements, as is the case of pharmaceuticals. In all industrial applications, significant challenges still exist in scaling up the precipitation processes that involve fast chemical reaction of concentrated reactants. Some of these practical aspects of precipitation will be discussed further in later sections.

Despite its practical importance, precipitation still remains a relatively underdeveloped field. This is reflected in the small number of books on precipitation available. Two specific books were published in the 1960's—one by A.E. Nielsen (*Kinetics of Precipitation*, Pergamon 1964) and the other by A.G. Walton (*The Formation and Properties of Precipitates*, Interscience, 1967). Walton's book tends to focus on the materials science aspects of precipitation and precipitates, whereas Nielsen's focus is mechanistic and more process oriented. Nielsen also covers some of the mass transport aspects of mechanical mixing of reactive solutions. Much of these books' contents are now outdated but still serve as useful introductions to the topics covered. A more recent addition to the literature of precipitation is the book by O. Söhnel and J. Garside (*Precipitation*, Butterworth/Heinemann 1992). It places considerable emphasis on developing a rigorous theoretical background to the kinetics of precipitation as well as on attempting to show how this might be applied to industrial operations.

6.2. PHYSICAL AND THERMODYNAMIC PROPERTIES

6.2.1. SUPERSATURATION DRIVING FORCE AND SOLUBILITY

Supersaturation is the key variable in any precipitation system, and the level of supersaturation in the precipitating solution governs the rates of component processes, such as nucleation, growth, and Ostwald ripening. For sparingly soluble precipitates, precipitation is generally achieved by mixing solutions of reacting components. The solubility of the precipitating component must be known in order to determine the driving force for the reaction. When a precipitate coexists in equilibrium with the solution, the appropriate equilibrium constant representing interphase equilibrium is the solubility product, K_{sp} . For an electrolyte $A_{\nu+}B_{\nu-}$, the supersaturation ratio S can be defined as the ratio of the

activity-based product, $\pi = a_A a_B$, to the activity-based solubility product $K_{sp} = a_{Aeq} a_{Beq}$

$$S = \frac{\pi}{K_{sp}} = \frac{a_A a_B}{K_{sp}} \quad (6.1)$$

where a is the activity of the ionic species and the solubility product represents the value of the activity product at equilibrium. The subscript “eq” designates that such indexed activities necessitate equilibrium with large solid entities of the solute $A_{\nu^+} B_{\nu^-}$. The ionic product involves activities that actually exist in the solution under consideration.

Other definitions of the supersaturation ratio can be found in the literature (Nielsen 1983; Söhnel and Garside 1992). These include the two most common expressions

$$S = \left(\frac{\pi}{K_{sp}} \right)^{1/\nu} = \left(\frac{a_A^{\nu^+} a_B^{\nu^-}}{K_{sp}} \right)^{1/\nu}, \quad \nu = \nu^+ + \nu^- \quad (6.2)$$

where ν denotes the number of moles of ions formed from one mole of electrolyte; or alternatively, using concentrations

$$S = \frac{C}{C_{eq}} \quad (6.3)$$

where “ C_{eq} ” is the equilibrium concentration at solubility. We opted to use S to designate supersaturation ratio in a “generic sense,” i.e., independent of which definition is used. The supersaturation driving force is also frequently expressed as the concentration difference

$$\Delta C = C - C_{eq} \quad (6.4)$$

Both S and ΔC will be used in this chapter to quantify supersaturation.

6.2.2. THE GIBBS-THOMSON EQUATION AND SURFACE ENERGY

The Gibbs-Thomson equation links crystal size with the equilibrium solubility. For crystal-solution equilibrium, the solubility $C_{eq}(r)$ of spherical crystals of radius r is related to the solubility $C_{eq}(\infty)$ of crystals of very large sizes by the equation (Enustun and Turkevich 1960):

$$\ln \frac{C_{eq}(r)}{C_{eq}(\infty)} = \frac{2\sigma V_m}{RT r} \quad (6.5)$$

where σ is the surface energy of the solid phase, V_m is the molar volume, R is the universal gas constant, and T is the absolute temperature. According to Eq. (6.5), the solubility of a substance increases with decreasing crystal size. Principally, the surface tension forces between the crystal and the solution cause this larger solubility of small crystals. For example, the solubility of 0.05- μm crystals of AgBr is about 15% higher than that of large crystals (Berry 1976). In general, a significant increase of solubility is only apparent for crystals smaller than about 1 μm .

The concept of surface energy of a solid phase is somewhat controversial. The experimental methods, which have been suggested for determination of σ are frequently ambiguous. Söhnel and Garside (1992) gave a summary of the energy parameters of the surface under consideration. They also showed the values of experimentally determined surface energy as a function of equilibrium solubility for many solid substances that covered a solubility range of approximately eight orders of magnitude.

The consequences of the Gibbs-Thomson equation and surface energy can be important for the sparingly soluble substances. For example upon Ostwald ripening, very small crystals (which are more soluble than the larger ones) dissolve preferentially and the dissolved material (which forms a supersaturated solution with reference to the coarse crystals) precipitates on them. Thus, the large crystals grow at the expense of the small ones. The Ostwald ripening process will be discussed further later.

6.2.3. PRECIPITATION DIAGRAMS

A practically important information on the type of precipitate that results from given reaction conditions can be found from “precipitation diagrams.” The precipitation diagram of a sparingly soluble solid depicts the regions of concentration, pH, temperature or other property, where exists solid phase of a uniform composition, morphology, color or crystal habit (Söhnel 1991). For example, Figure 6.1a shows an idealized precipitation diagram in $p[\text{Me}^+] = -\log[\text{Me}^+]$ versus $p[\text{X}^-] = -\log[\text{X}^-]$ coordinates, where $[\text{Me}^+]$ and $[\text{X}^-]$ are the cation and anion concentrations. A straight line bisecting the diagram, a so-called equivalence line, represents stoichiometric compositions for the compound MeX , i.e., $[\text{Me}^+] = [\text{X}^-]$. Equations for a constant ionic product: $[\text{Me}^+][\text{X}^-] = \text{constant}$ or $p[\text{Me}^+] + p[\text{X}^-] = \text{constant}$ are satisfied along any line, perpendicular to the equivalence line. However, the ratio $[\text{Me}^+]/[\text{X}^-]$ changes along the former. Thus, line (a) represents the equilibrium solubility, line (b) solubility, and (c) boundary of the metastable zone. Line (d) divides the heterogeneous nucleation region into zones: (3),

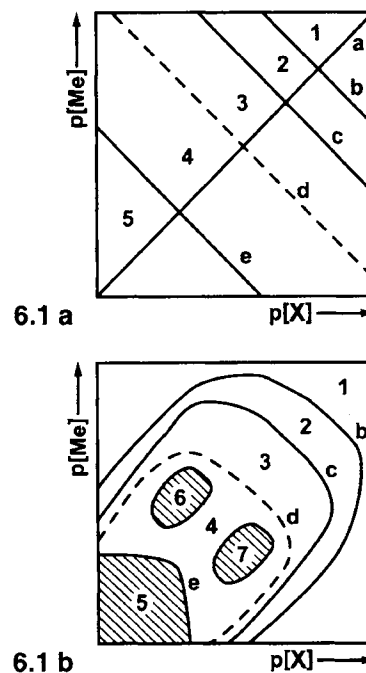


Figure 6.1. (a) Idealized precipitation diagram (after Söhnel 1991). Zones: (1) undersaturated solution, (2) metastable supersaturated solution, (3) and (4) heterogeneous nucleation, (5) homogeneous nucleation. Lines: (a) equivalence line (stoichiometric composition), (b) solubility line, (c) metastable zone boundary, (d) and (e) zone boundaries separating zones (3), (4), and (5). (b) Precipitation diagram with nonlinear boundaries separating the regions delineated in Figure 6.1a. Zones: (5) transient precursor formation, (6) positively charged colloids, (7) negatively charged colloids.

where compact shapes of crystals are formed, and (4), where dendrite formation is favored. Finally, line (e) separates zone (4) from homogeneous nucleation zone (5).

In many cases, precipitation does not follow a simple stoichiometric reaction, such as



but proceeds through formation of polymeric species that transform to one another with various rates. If the ion complexation occurs, i.e., the total analytical concentration of the anion is expressed by

$$[\text{X}] = [\text{X}^-] + [\text{MeX}] + [\text{MeX}_2] + \dots \quad (6.7)$$

the boundaries separating the regions take on the form of curves, as schematically shown in Figure 6.1b. The actual solid phase composition is then time dependent and changes during the initial part or even the entire system lifetime. The lifetime of evolving polymeric and complexation species may be as short as milliseconds (Tanaka and Iwasaki 1983, 1985). The area (5) may then represent the region of a transient precursor formation, while islands (6) and (7) may represent the regions of stable negatively and positively charged colloidal suspensions. The regions (5), (6), and (7) may not appear in the precipitation diagram of a specific compound.

6.2.4. SURFACE CHEMISTRY AND COLLOID STABILITY

Because of the high particle concentration and small particle sizes involved in the precipitation systems, the surface chemistry and colloidal stability of the resulting dispersed systems are of particular importance. In general, particle aggregation, and thus the stability of the system, is determined by the prevailing forces between the solid particles in the dispersion. These forces between particles can be repulsive or attractive (Hunter 1987).

The attractive forces are of the nature of van der Waals forces between the atoms in two approaching colloidal particles. The magnitude of this effect is inversely proportional to the second power of the separation distance between the two particles.

The repulsive forces arise from the electromagnetic interactions of the charged layer surrounding the particles, the so-called electrical double layer. On the surface of the particles, a charged layer may be formed due to selective adsorption of ions. This part of the double layer is immobile and consists of tightly adsorbed ions in direct contact with the particle surface. In the solution adjacent to the particle, a second layer, in which the ions are more diffusely distributed, penetrates into the liquid. This part of the double layer is termed the diffusion layer. The extent of this diffusion layer depends on the electrolyte concentration: increasing electrolyte concentration causes this diffuse double layer to shrink closer in to the particle, so that the electrostatic potential falls off more quickly with distance. The process by which the particles are stabilized by the repulsive forces of the electrical double layers is known as electrostatic stabilization.

The well-known DLVO theory (Derjaguin and Landau 1941; Verwey and Overbeek 1948) predicts quantitatively the rate of coagulation of colloidal sols by electrolytes from the height of the potential barrier to be surmounted before two particles can come into contact. The height of this barrier is controlled by van der Waals attraction and electrostatic repulsion of the double layers of each particle contributing to the effective energy barrier. This theory accounts for the increase in the rates of aggregation with reduction in the electrical repulsion by successive additions of electrolyte, as a consequence of the decrease of the electrical double layer of each particle.

Polymeric or macromolecular adsorbents can also be used to affect colloidal stability. For example, gelatin has been used to stabilize silver halide and other dispersions for over 100 years (James 1977). Adsorbed polymers tend to form loops and chains that protrude into the solution from the particle surfaces and prevent their close approach. Such a process is known as steric stabilization. Although at high surface concentrations a given polymer may stabilize a dispersion, destabilization is often observed at very low polymer levels at which segments from the same molecules may be adsorbed to various particles and thus, by bridging, hold them together. The effects of particle aggregation in the precipitation process will be discussed later.

6.3. NUCLEATION KINETICS

A progressive buildup of supersaturation in a solid-free solution results in the formation of a new solid phase, i.e., nucleation. This phenomenon may proceed by two mechanisms: primary nucleation, occurring in the absence of the crystallizing material, or secondary nucleation, which is brought about by the very presence of the crystallizing material. Primary nucleation is termed homogeneous or spontaneous if the new solid phase formation is not caused by the presence of any solid phase. If the new solid phase formation is induced by the presence of the foreign solid phase, the process is said to be heterogeneous primary nucleation. In precipitation, unless the concentration of both or one of the reactants is very low, nucleation proceeds at a very high rate, and the size of detectable nuclei is on the order of 10–100 nm. The terminology introduced by Nielsen (1964) will be used to distinguish between an embryo, i.e., a subcritical-size solid phase particle, and a nucleus that exists above the critical size.

6.3.1. KINETICS OF PRIMARY NUCLEATION

Homogeneous Nucleation. The classical theory of nucleation developed for homogeneous nucleation from the gaseous and liquid phases is assumed to be applicable also for nucleation from a supersaturated solution. The free Gibbs energy change, ΔG , to form a crystal from homogeneous supersaturated solution is given by (Nielsen 1964)

$$\Delta G = -N\Phi + A\sigma \quad (6.8)$$

where N is the number of molecules or ions in the crystal, Φ is the reaction affinity, A is the surface area of the crystal ($A \sim N^{2/3}$), and σ is surface tension. A general expression for the affinity Φ is given by

$$\Phi = kT \ln(a/a^*) \quad (6.9)$$

where k is Boltzmann's constant, T is temperature, a is the activity of the solute in solution, and a^* is the activity of the pure solute in a macroscopic crystal. By assuming the activity coefficients to be unity,

$$(a/a^*) = (C/C^*) = S \quad (6.10)$$

where S is the supersaturation ratio, and thus

$$\Phi = kT \ln S \quad (6.11)$$

The first term on the right-hand side of Eq. (6.8) is always negative, and both terms increase as N increases due to the attachment of subsequent molecules or ions. As shown in Figure 6.2., $\Delta G > 0$ for small N , then reaches a maximum, $\Delta G = \Delta G^*$, for $N = N^*$,

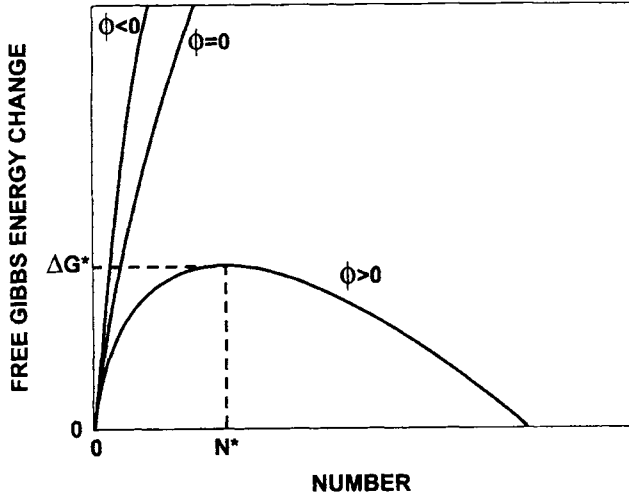


Figure 6.2 The free Gibbs energy change, ΔG , as a function of number of ions or molecules forming a crystal. (Nielsen 1964).

and eventually, $\Delta G < 0$ as the first term outweighs the second. The increase in N corresponds to an increase in embryo or nucleus size. Of particular importance is critical embryo-nucleus formed by N^* molecules or ions. It can be shown, that for the spherical critical embryo-nucleus

$$\Delta G^* = \frac{16\pi\sigma^3 v^2}{3k^2 T^2 (\ln S)^2} \quad (6.12)$$

where the quantity v represents the number of moles of ions formed from one mole of electrolyte. For a non-electrolyte $v = 1$.

Nielsen (1964), developed an expression for the homogeneous nucleation rate:

$$J = \frac{D}{d_m^5 N^*} \left(\frac{4\Delta G^*}{3\pi k T} \right)^{\frac{1}{2}} \exp\left(\frac{-\Delta G^*}{k T}\right) = \Omega \exp\left(\frac{-\Delta G^*}{k T}\right) \quad (6.13)$$

where D is the diffusion coefficient of the solute, d_m is the molecular diameter, and Ω is a pre-coefficient (pre-exponential frequency factor) defined as shown above. The dependence of the nucleation rate on supersaturation ratio is obtained by substituting Eq.(6.12) into Eq. (6.13):

$$J = \Omega \exp\left[\frac{-16\pi\sigma^3 v^2}{3k^3 T^3 (\ln S)^2}\right] = \Omega \exp\left[\frac{-B}{(\ln S)^2}\right] \quad (6.14)$$

where B is a constant defined as

$$B = \frac{16\pi\sigma^3 v^2}{3k^3 T^3} \quad (6.15)$$

As discussed by Nielsen (1964), Nývlt (1971), and Söhnel and Garside (1992), over limited ranges of supersaturation, Eq. (6.14) may be simplified to

$$J = k_N S^n \quad (6.16)$$

where k_N is the nucleation rate constant and n is the kinetic "order" of nucleation. Although k_N and n have no physical significance, the kinetic power law equation, Eq. (6.16), is very often used in the technical literature.

The values of the pre-exponential term, Ω , for sparingly soluble substances range widely from 10^{25} to $10^{56} \text{ s}^{-1} \text{ m}^{-3}$ (Nielsen 1969; Nielsen and Söhnel 1971). Values from 1 to 10 were reported for the kinetic order of nucleation, n (Nývlt 1971; Tanaka and Iwasaki 1985). The activation energy for nucleation, E_N , determined from the Arrhenius-type of the temperature dependence

$$\frac{d \ln k_N}{dT} = \frac{-E_N}{RT^2} \quad (6.17)$$

is believed to be of the same order of magnitude as the activation energy of viscosity or diffusion (Nývlt 1971).

Heterogeneous nucleation. Particulate contaminants of foreign substances are always present in a solution and may act as "catalysts" of nucleation. Even liquid from which physical impurities have been removed, may contain from 10^{13} to 10^{23} such particulate contaminants per 1 m^3 (Söhnel and Garside 1992). This catalytic effect is due to the decrease in the energy barrier to nucleation thanks to the reduction of σ in Eq. (6.12), and therefore $\Delta G^*_{het} < \Delta G^*_{hom}$. The wettability of the surface of a foreign solid phase seems also to play a role. For solutions wetting the surface of a foreign solid phase, $\Delta G^*_{het} < \Delta G^*_{hom}$. Turnbull and Vonnegut (1952) proposed to evaluate the rate of heterogeneous nucleation by an equation whose form corresponds to that of Eq. (6.13) for homogeneous nucleation

$$J_{het} = \Omega_{het} \exp\left(\frac{-\Delta G^*_{het}}{k T}\right) \quad (6.18)$$

where $\Omega_{het} < \Omega$.

The above kinetic equations, developed based on the thermodynamic approach of Gibbs (1928), Volmer and Weber (1926), and Becker and Döring (1935), belong to the so-called classical nucleation theories. They have been criticized for the use of surface energy (interfacial tension), σ , which is probably of little physical significance when applied to small molecular assemblies of the size of critical nucleus.

6.3.2. INVESTIGATIONS OF NUCLEATION KINETICS

Onset of Nucleation. Investigations of initial moments of nucleation using a stopped flow technique revealed that the nuclei formation may be preceded by the formation of complexes of the reacting species as precursors of nuclei (Tanaka and Iwasaki 1983, 1985). The lifetime of precursors depends on the concentration ratio of the reacting species, and is on the order of 60–500 ms for AgBr. Even for simple 1–1 electrolytes, the reaction of particle formation may involve two or more stages.

Following the approach proposed by Nielsen (1964), Tanaka and Iwasaki (1985) used Eqs. (6.14) and (6.15) to estimate the nucleation kinetic order, n , at the onset of nucleation. For the initial precipitation conditions characterized by the supersaturation ratio, S_0 , they obtained

$$n = \frac{d \ln J_0}{d \ln S_0} = \frac{B}{(\ln S_0)^3} \quad (6.19)$$

Nielsen (1964) documented that the curves $\ln J$ versus $\ln S$ are almost straight lines over several decades of J , so that approximations—Eqs. (6.16) and (6.19)—are justified.

Although σ is not well defined for nanocrystalline particles, Eq. (6.19) can be used to estimate n . The range of the values of n calculated by Tanaka and Iwasaki (1985) were from 3.6 ($S_0 = 71$) to 10.4 ($S_0 = 20$) for AgBr, and from 3.7 ($S_0 = 273$) to 9.7 ($S_0 = 58$) for AgCl.

Induction Period. By a common definition, the time elapsed between mixing two reacting solution and the appearance of first crystals of precipitate is termed an induction period. In diluted or slowly reacting systems precipitation starts slowly, then accelerates, and eventually slows down. This initial part is well characterized by an induction period. The induction period t_{ind} has become an experimental basis to determine the nucleation rate J , using a simple relationship.

$$J = K/t_{ind} \quad (6.20)$$

where K is a constant. By combining Eq. (6.16) and (6.20) one obtains

$$t_{ind} = (K/k_N)S^{-n} \quad (6.21)$$

The above equation has been used to characterize the mechanism of nucleation. Indeed, certain precipitating systems exhibit different slope of the empirical dependence $\log t_{ind}$ versus $\log S$. Figure 6.3 illustrates such a dependence with three distinctive regions: Region I for low supersaturation, characteristic of heterogeneous nucleation mechanism; Region III for high supersaturation where homogeneous nucleation mechanism dominates, and an intermediate Region II, in which both mechanisms may coexist. With an increasing stirring intensity at constant supersaturation, t_{ind} decreases up to a certain critical stirring speed, beyond which it remains unchanged.

In the case of a rapid chemical reaction and elevated reactants concentration or a diffusion-controlled precipitation, the induction period is too short to be measured effectively. When the induction period is shorter than the mixing period, as frequently occurs in very fast reactions, mixing becomes a process-controlling factor.

Stable Nuclei. In the opening of this section, a distinction has been made between nuclei and embryos (subcritical nuclei). Now, another distinction will be introduced to differentiate between transient and stable nuclei.

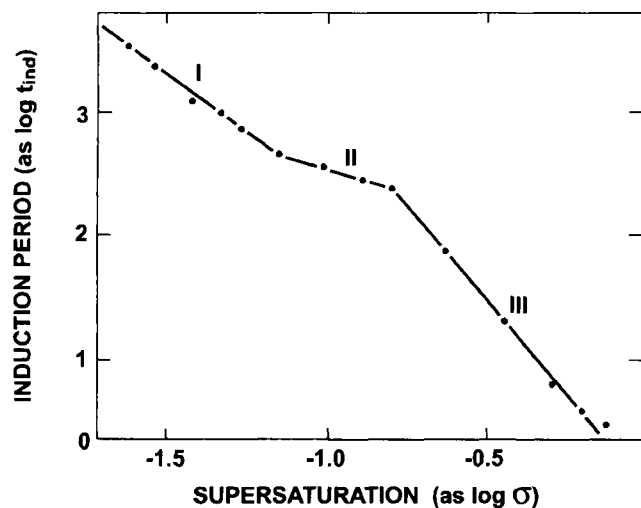


Figure 6.3 Empirical dependence of induction period of $\text{Ni}(\text{NH}_4)_2(\text{SO}_4)_2 \cdot 6\text{H}_2\text{O}$ at 25°C on relative supersaturation in logarithmic coordinates (after Söhnel and Mullin 1979): Region I—predominant heterogeneous nucleation mechanism; Region III—predominant homogeneous nucleation mechanism, and Region II—possible coexistence of both nucleation mechanisms.

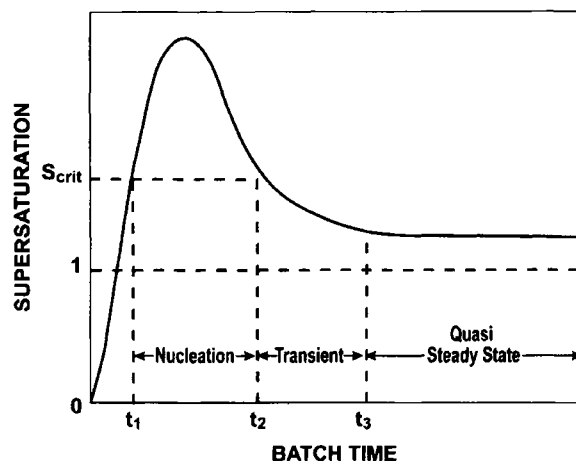


Figure 6.4 The course of the supersaturation ratio (S) during precipitation of sparingly soluble materials.

As soon as nuclei are formed, a part of them grow under local supersaturation conditions. At the same time, the other part may gradually dissolve via the Ostwald ripening mechanism creating supersaturation and thus becoming a source of solute for the growth of surviving nuclei (Berry 1976). As a result, in the first minutes of precipitation, a population of stable (surviving, effective) nuclei, establishes itself. In some applications, additional measures, such as: a temporary stoppage of the reactant delivery, an increase of temperature, excess of one of the reactants, addition of a ripening agent, or solvent addition may be employed to accelerate the nuclei stabilization process. Once such a stable population of nuclei has been established, the subsequent addition of reactants during a double-jet precipitation results in the growth of the stable nuclei, without any significant addition of new crystals to this population, Figure 6.4. According to Leubner et al. (1980), the number of stable nuclei increased with increasing reactant addition rate and decreased with increasing solubility.

Secondary Nucleation. In many crystallization processes, the width of the metastable zone decreases in the presence of crystals of the crystallizing material. Such crystals, in the form of seeds, are sometimes intentionally added to the precipitator to induce nucleation of highly supersaturated but not yet crystallizing systems. New nuclei are then formed via a secondary nucleation mechanism. On the other hand, for systems with a very short induction period (e.g., precipitation via ionic reactions), primary nucleation mechanism is overwhelming.

Contact secondary nucleation, important in variety of crystallization operations producing millimeter-range crystals, is seldom of concern for precipitation processes. Very small crystals of typical precipitate follow the streamlines within the turbulence eddies and rarely come into collisions with the mixer, baffles and walls of the precipitator, or other crystals. Due to the sub- and micron- size range of precipitate, only low-impact energy collisions take place. Such collisions do not produce contact secondary nuclei. Although contact secondary nucleation is not an important mechanism of nuclei formation in a typical precipitation process, there are cases in which nuclei are also generated via this mechanism. Those cases include rapid agglomeration of dendritic or needle-shaped crystals, or final stages of precipitation occurring at very low supersaturation. The resultant agglomerates in the former and non-agglomerated grown crystals in the latter case may reach the size range of 0.1 mm to 1.0 mm. Such a size range assures a sufficiently

high impact energy for the crystal-crystal, and crystal-equipment collisions, which is a prerequisite for the formation of contact nuclei.

In some industrial applications involving rapid chemical reactions—notably in the silver halide precipitation technology—protective colloids are used to subdue the agglomeration propensity of nuclei. In the pharmaceutical industry, surfactants are used to the same goal. Such colloids or surfactants adsorb onto and modify the electric charge of nuclei or provide steric stabilization. Under properly selected conditions, agglomeration can be nearly completely eliminated and contact secondary nucleation does not occur even under vigorous mixing conditions.

6.4. CRYSTAL GROWTH KINETICS

As soon as nuclei are formed in a supersaturated solution, they begin to grow into crystals. Several theories have been proposed to describe the mechanism and rate of crystal growth. Reviews by Ohara and Reid (1973) and Söhnel and Garside (1992) detail advances in the kinetics of crystal growth from solution. Generally, two main processes occur sequentially during the growth of crystals from solution: the mass transport of growth units from the bulk supersaturated solution to the crystal-solution interface by bulk diffusion and the incorporation of growth units into the crystal lattice through the surface integration process (sometimes also referred to as the surface reaction process). If the mass transport to the crystal has a much higher rate than that of the subsequent surface integration step, the surface integration process controls the overall rate of growth. In the opposite case, when the surface integration has a much higher rate than that of the mass transport, the overall rate of growth is determined by the rate of mass transport from the solution to the crystal.

6.4.1. GROWTH CONTROLLED BY MASS TRANSPORT

The simplest model of mass transport is the bulk diffusion of growth units through a stagnant diffusion layer adjacent to the crystal surface with complete mixing beyond. For a diffusion layer of thickness δ , the linear growth rate G can be derived by integrating Fick's law as

$$G = \frac{4D}{\rho_c} \left(\frac{1}{L} + \frac{1}{2\delta} \right) (C - C_i) \quad (6.22)$$

where D is diffusion coefficient, ρ_c is crystal density, L is the crystal size (edge length or diameter), C is the bulk solute concentration, and C_i is the solute concentration at the crystal-solution interface. Although Eq. (6.22) was derived primarily for a spherical crystal, it may also, to the first approximation, be applied to other crystal shapes such as cubic, octahedral, etc. When the diffusion layer thickness is small compared to the crystal size ($2\delta \ll L$), Eq. (6.22) can be reduced to

$$G = \frac{2D}{\rho_c \delta} (C - C_i) \quad (6.23)$$

Equation (6.23) suggests that G is inversely proportional to δ and is independent of L . However, hypothetically, when the diffusion layer thickness is large compared to the crystal size ($2\delta \gg L$), Eq. (6.22) becomes

$$G = \frac{4D}{\rho_c L} (C - C_i) \quad (6.24)$$

Here, G is independent of δ but is inversely proportional to L . Eq. (6.24) also represents molecular diffusion in an infinite unstirred solution.

To avoid the uncertainty in determining the stagnant diffusion layer thickness δ , the following semi-empirical engineering model is often used

$$G = \frac{2k_d}{\rho_c} (C - C_i) \quad (6.25)$$

where k_d is the mass transfer coefficient (Bird et al. 1960) which accounts for the fluid dynamics and the physical properties important to the process. For mass transport associated with suspended crystals in an agitated solution, bulk diffusion often involves molecular diffusion and convective transport. For spheres and other simple geometric shapes, k_d can be correlated by the Frossling equation (Frossling 1938)

$$Sh = 2 + 1.10 Re^{1/2} Sc^{1/3} \quad (6.26)$$

where $Sh = k_d L / D$ is the Sherwood number, $Re = u_s L \rho / \mu$ is the Reynolds number, u_s is the particle "slip" velocity, ρ is the solution density, μ is the solution viscosity, and $Sc = \mu / \rho D$ is the Schmidt number.

The first term on the right-hand side of Eq. (6.26) represents the contribution of molecular diffusion, and the second term is related to the contribution of convective transport. For the very small particle sizes (e.g., 0.1 to 10 μm) associated with the sparingly soluble precipitates, the suspended phase tends to move with no slip along with the circulating fluid (i.e., $u_s = 0$). In this case, the effect of convective transport is negligible and bulk diffusion occurs mainly by molecular diffusion. Thus,

$$Sh = k_d L / D = 2 \quad (6.27)$$

Substitution of Eq. (6.27) into Eq. (6.25) gives Eq. (6.24), which describes diffusion-controlled growth in an infinite diffusion field. Such a relationship is appropriate to describe growth of very small crystals such as those produced during precipitation processes. It should be emphasized that Eq. (6.24) is applicable only if the diffusion fields around separate crystals do not influence each other and may be taken to be infinite in extent. This will be case if the distance between the crystals is greater than about 20 particle diameters. When the distance between the crystals is less than about 20 particle diameters, the diffusion fields around the individual crystals begin to influence one another. The effect of particle "crowding" on diffusion-controlled growth will be discussed later.

6.4.2. GROWTH CONTROLLED BY SURFACE INTEGRATION

Surface integration is the process by which the growth units of the crystallizing material are incorporated into the crystal lattice after they have been transported to the crystal surface. Two main mechanisms controlling surface integration are described here.

Two-Dimensional Nucleation Mechanisms. According to the two-dimensional nucleation growth concept, planar crystal faces are energetically unfavorable for the formation of new growth layers. To initiate crystal growth on a perfectly flat surface, a two-dimensional nucleus must be generated to provide incorporation sites (steps) for the growth units. Several models have been proposed for two-dimensional nucleation growth. They differ in the assumptions of the rate at which the growth units spread across the crystal surface compared with the time taken to form a new nucleus for a new layer (Ohara and Reid 1973).

In the mononuclear model, the limiting step is the formation of a nucleus. Once one is formed, the subsequent growth spreading across the crystal surface is infinitely rapid. For the polynuclear model, the spreading velocity is taken as zero and the crystal surface can only be covered by the accumulation of a sufficient number of nuclei. These two growth models represent two extreme cases. A third model, known as the “birth-and-spread” model, allows for formation of nuclei and their subsequent growth at a finite rate. In this case, new nuclei can form on top of uncompleted layers.

Different linear growth rate expressions for the above three cases were given by Ohara and Reid (1973) and Söhnel and Garside (1992) and will not be repeated here. In general, these growth rate expressions represent a somewhat complex function of supersaturation and other crystal physical properties. In the mononuclear model, the growth rate is also proportional to the crystal surface area. These two-dimensional nucleation models are sometimes unsatisfactory in predicting or correlating crystal growth rates. For example, at low supersaturation levels, the predicted growth rates are often much less than those observed experimentally.

Screw Dislocation Mechanisms. In order to explain the discrepancy between experimental observations and the two-dimensional nucleation models, Frank (1949) proposed a growth model based on dislocation theory. A screw dislocation can give rise to a spiral step, which does not disappear during growth. Hence, the formation of a two-dimensional nucleus at the crystal surface is not required to sustain growth. Burton et al. (1951) considered growth of the spiral to be limited by diffusion of adsorbed growth units across the crystal surface—the BCF theory—and developed a growth equation of the form

$$G \propto \frac{\sigma^2}{\sigma_c} \tanh\left(\frac{\sigma}{\sigma_c}\right) \quad (6.28)$$

where σ is the supersaturation parameter defined by $(C_i - C_{eq})/C_{eq}$, and σ_c is a complex temperature-dependent constant which includes parameters depending on step spacing. At low supersaturations, the BCF equation approximates to $G \propto \sigma^2$, and at high supersaturations to $G \propto \sigma$.

A simple power-law equation of the form

$$G = k_i(C_i - C_{eq})^m \quad (6.29)$$

has been used frequently to represent the surface integration process. This clearly represents the two limiting cases of the BCF equation and is a good approximation to the two-dimensional nucleation models over a limited range of supersaturation. Note that the surface integration constant k_i is independent of crystal size except for the mononuclear growth model where $k_i \propto L^2$. The parameter m is usually referred to as the “order” of the surface integration process.

6.4.3. GROWTH CONTROLLED BY COMBINED MECHANISMS

Both the bulk diffusion process and the surface integration process generally influence crystal growth. For very small crystals, such as those produced during precipitation, the bulk diffusion growth process can be adequately described by the molecular diffusion of growth units in an infinite diffusion field, Eq. (6.24). Equations (6.24) and (6.29) can be combined to eliminate the interface solute concentration, C_i . If the surface integration process is first-order (i.e., $m = 1$), which is a reasonable assumption for high super-

saturation (Liu et al. 1971), a growth rate expression, which involves both bulk diffusion and surface integration can be given by

$$G = \frac{g}{1 + \xi L} \quad (6.30)$$

where

$$g = K_i(C - C_{eq}) \quad (6.31)$$

and

$$\xi = \rho K_i / 4D \quad (6.32)$$

The parameter g in Eq. (6.31) represents a size-independent growth rate when surface integration is dominating. The parameter ξ represents the ratio of the relative “resistance” of bulk diffusion to surface integration so that when $\xi L \ll 1$, growth is controlled by surface integration, and when $\xi L \gg 1$, by bulk diffusion. Söhnel and Garside (1992), Nývlt a Karpinski (1977), and Karpinski (1981) provided a more general treatment of the crystal growth controlled by combined mechanisms. The application of Eqs. (6.30)–(6.32) to study the growth mechanism of AgBr crystals in aqueous gelatin solution will be discussed later.

6.4.4. CRITICAL GROWTH RATE

Most precipitation systems exhibit a metastable supersaturation zone where supersaturation is too low for nucleation to take place. As the supersaturation is increased, the point at which nucleation just begins to occur corresponds to the maximum metastable (critical) supersaturation allowable without nucleation. If crystals are present at this moment in the precipitation vessel, they grow at a maximum (critical) growth rate.

Unfortunately, the supersaturation generally cannot be measured accurately in most precipitation systems so that determination of the maximum metastable supersaturation and the corresponding critical growth rate becomes more difficult. Wey and Strong (1977a) presented an experimental technique, which involved initial seeding, to examine the critical growth rate of AgBr crystals. Their approach involves a balanced double-jet precipitation in which aqueous silver nitrate and sodium bromide solutions are added simultaneously to an agitated aqueous gelatin solution. For each experiment, the precipitation vessel is charged initially with monodisperse AgBr seed crystals. When the number of seed crystals is decreased or the reactant addition rate is increased from one experiment to the next, nucleation eventually occurs (as detected by the presence of small crystals in the samples taken from the experiments) at the point where solution reaches the maximum metastable supersaturation. The corresponding critical growth rate is determined from a simple mass balance. This technique is applicable to the high-yield (Class II) precipitation systems. A more detailed description of the experimental technique will follow.

Wey and Strong (1977a) followed this approach for each of five different monodisperse AgBr seed sizes ranging from 0.047 to 0.64 microns. The temperature and the bromide ion concentration in suspension were maintained constant for all the experiments. Since the critical growth rates of different seed sizes were obtained at the same maximum metastable supersaturation condition, the effect of supersaturation can be eliminated from the correlation between growth rate and crystal size. Furthermore, the maximum metastable supersaturation can be estimated when comparing the experimental results with growth models.

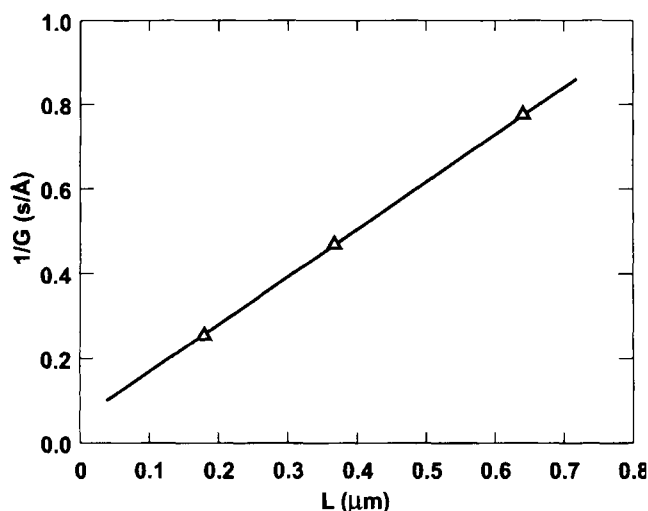


Figure 6.5 Dependence of critical growth rates on crystal size for AgBr octahedra. (Wey and Strong 1977a.)

The experimental data of Wey and Strong (1977a) are shown in the plot of $1/G$ versus L in Figure 6.5. The data correlate very well with a straight line in such a plot predicted from Eq. (6.30). From the slope and intercept of this plot, the values of ξ and g parameters can be estimated. An ξ value of about $16 \mu\text{m}^{-1}$ was obtained for AgBr growth at 70°C and $p\text{Br } 3.3$ (Wey and Strong 1977a). Since ξ represents the ratio of the "resistance" of bulk diffusion to surface integration, the results suggest that bulk diffusion is important in most conventional AgBr precipitations. Furthermore, from the values of ξ and g , the supersaturation ratio (C/C_{eq}) at this maximum metastable condition was estimated to be about 1.5 (Wey and Strong 1977a). It is worth mentioning that this experimental approach was also successfully applied to the AgCl system (Strong and Wey 1979).

6.4.5. OTHER FACTORS AFFECTING CRYSTAL GROWTH

In addition to the bulk diffusion and surface integration processes, several other factors may affect the growth of the sparingly soluble precipitates.

Gibbs-Thomson Effect. As discussed earlier, the solubility of a crystal may increase with decreasing crystal size as predicted from the Gibbs-Thomson equation, Eq. (6.5). That is, the equilibrium concentration associated with small crystals is higher than that of large crystals. Thus, in a common growth environment, the "effective" supersaturation for the growth of small crystals would be lower than that for large crystals, leading to a lower growth rate for small crystals. This effect (sometimes referred to as the Gibbs-Thomson effect) becomes more pronounced for submicron crystals of sparingly soluble precipitates.

To describe the various AgBr growth behaviors observed under different double-jet precipitation conditions, Wey and Strong (1977b) developed a growth model that includes the Gibbs-Thomson effect in addition to bulk diffusion. The relative importance of these two mechanisms is influenced by the precipitation conditions. According to this growth model, at high supersaturation ratios, the growth of AgBr is dominated by bulk diffusion so that small crystals grow at a higher rate than the large ones. Conversely, at low supersaturation ratios, the dominant influence on crystal growth is the Gibbs-Thomson effect, which

causes a substantial reduction in the growth rate of the small crystals relative to the large ones. Therefore, the small AgBr crystals grow at a lower rate than the large ones. Between these two extremes, there are conditions that exhibit balanced influences of bulk diffusion and the Gibbs-Thomson effect. Due to the opposite effect of these two mechanisms on the growth behavior, size-independent growth can occur. Wey and Strong (1977b) used this growth model to qualitatively explain several contrasting observations of AgBr growth behavior reported in the literature.

Particle "Crowding" Effect. The growth of a crystal in a suspension can be influenced by the presence of other crystals when the crystal number concentration (number/volume) exceeds a certain level so that the interparticle distance becomes smaller than 20 particle diameters. For most precipitation systems, the crystal number concentration is typically higher than 10^{11} per cm^3 , and the interparticle distances are normally less than 15 times the crystal size. In such a "crowded" system, the diffusion fields around the individual crystals begin to influence one another and one may expect some interparticle effects on crystal growth.

Jagannathan and Wey (1981) developed a theoretical model for the diffusion-controlled growth of crystals in a crowded open system where new solute materials are continuously introduced. The interparticle effect can be represented by a "crowding factor," η , which depends on the crystal size, diffusion layer thickness, and interparticle distance. The value of η is equal to one for a non-crowded system. However, when the interparticle distance is smaller than or comparable to the finite diffusion layer thickness, η is greater than one. The model shows that, for a given supersaturation, the crowded system exhibits a higher solute concentration gradient within the diffusion layer and hence a higher crystal growth rate than the noncrowded system. The theoretical concepts were used to explain the effect of interparticle distance on the growth rates of AgBr crystals in double-jet precipitations (Jagannathan and Wey 1982).

6.5. OTHER PROCESS ATTRIBUTES IN PRECIPITATION

In addition to nucleation and crystal growth, several other processes (e.g., Ostwald ripening, agglomeration, and mixing) may have a profound effect on the final precipitates. These important processes will be briefly discussed here.

6.5.1. OSTWALD RIPENING

A heterogeneous system, with a solid phase in a dispersed state, is unstable thermodynamically until its free energy has reached a minimum. This is because the large interfacial area contributes to the free energy, that may be reduced by decreasing this area. Ostwald (1901) provided the first description of this process, which therefore was later called "Ostwald ripening." Its driving force is the difference in solubility between the particles of the solid phase, as given by the well-known Gibbs-Thomson equation, Eq. (6.5). This solubility difference establishes a concentration gradient that leads to the transport of solute material through the solution phase from the smaller crystals to the larger ones. The rate of this ripening process is determined by the crystal size distribution, the growth and dissolution kinetics, and the transport properties of the solution phase (Bogg et al. 1976; Wey 1981; Wey and Schad 1986). In general, Ostwald ripening reduces the number of crystals present in the system, increases the average size of crystals, and increases the width of the crystal size distribution, Figure 6.6 (Enustun and Turkevich 1960).

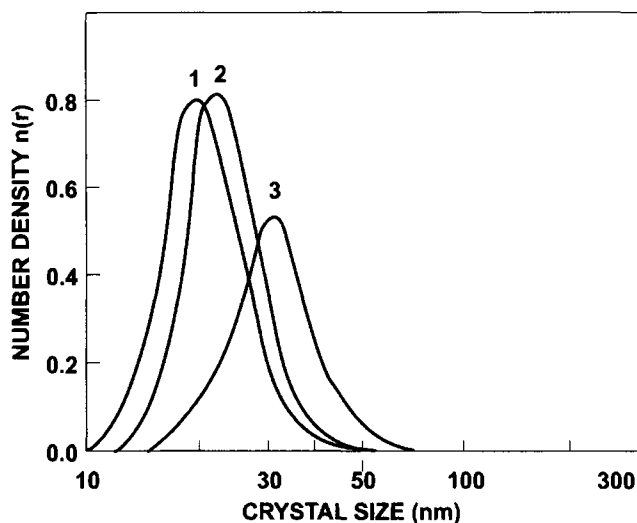


Figure 6.6 Illustration of the Ostwald ripening effect for SrSO_4 precipitation (after Enustun and Turkevich, 1960). The initial CSD (1) in contact with a saturated solution changed to (2) after 60 days but transformed to (3) in just 45 minutes upon dilution with water.

Experiments designed to investigate Ostwald ripening are usually done with a suspension of crystals under quasi-equilibrium conditions (e.g., without the addition of reactant solutions). The mechanism of Ostwald ripening was normally inferred either from the relationship between the average crystal volume and the time of ripening or from the values of the apparent activation energy for Ostwald ripening. For example, diffusion was considered to be the rate-determining step if the average crystal volume was linearly proportional to the time of ripening (Wagner 1961) or if the activation energy was about 3.5–5 kcal/mole. However, these results, in general, do not provide mechanistic information for the dissolution of the smaller crystals or the growth of the larger crystals in the polydisperse crystal population.

Another technique to study Ostwald ripening is to use a mixture of two monodisperse populations of crystals with widely different sizes. Two general approaches were used to elucidate the mechanisms associated with the dissolution of the small crystals and the growth of the large crystals. In the first approach, an excessively large amount of the small crystals is used so that the rate-limiting step of Ostwald is the deposition of solute material onto the large crystals. In this case, the growth rate of the large crystals can be obtained from the initial change of their average volume or size. Sugimoto (1983) used this approach to study the growth mechanism AgBr cubic and octahedral crystals for $1.0 < \text{pBr} < 2.5$ in the presence of 0.5 M ammonia. In the second approach to study Ostwald ripening of a mixture of two monodisperse populations of crystals, the “ripening time” (the time for the small crystals in the mixture to dissolve completely) is measured. The amount of the small crystals is normally kept relatively low so that the size increase of the large crystals is relatively small. In this case, both the dissolution of the small crystals and the growth of the large crystals can influence the ripening process. Bogg et al. (1976) used this approach to study the growth and dissolution kinetics of AgBr crystals under different Ostwald ripening conditions. Wey and Schad (1986) also used this technique to conduct a systematic study of the effects of pBr and crystal habit on the growth and dissolution kinetics of AgBr crystals in the absence of ammonia.

6.5.2. AGGREGATION

As discussed earlier, colloid stability and particle aggregation can play an important role because of the high particle concentration and small particle sizes involved in the precipitation systems. To avoid the confusion of terminology given in the literature, the terms “aggregation” and “agglomeration” are used generically, whereas the terms “flocculation” and “coalescence” are used to designate special phenomena (Antoniades and Wey 1993, 1998). *Flocculation* refers to loosely held aggregates of noncontacting colloidal particles. In this case, the attraction forces are almost counterbalanced by the repulsion forces, thus preventing particle contact. *Coalescence* refers to the event by which two or more single crystalline particles combine to form a new, larger crystalline particle. Both electrostatic stabilization (via repulsive forces of the electrical double layers) and steric stabilization (via polymeric or macromolecular adsorbents to impart colloid stability) are considered.

Outcome of the precipitation processes, particularly the particle numbers and size distribution, can be influenced significantly by the occurrence of aggregation. In the case of CMSMPR crystallizers, aggregation will be important if the half-life of aggregation (defined as the time in which the initial particle number falls by half) is smaller than the suspension residence time in the crystallizer (Lamey and Ring 1986). Antoniadis and Wey (1993, 1998) studied the effects of aggregation on the double-jet precipitation of AgBr crystals in which the silver nitrate and sodium bromide solutions were added simultaneously to an agitated aqueous gelatin solution. In these applications, AgBr crystals are peptized by gelatin, which through surface adsorption provides steric stabilization. At high gelatin concentrations, the stable number of crystals formed during the initial stage of the double-jet precipitation increases with increasing reactant addition rate, as predicted by a model developed by Leubner et al. (1980). However, if the amount of gelatin is progressively reduced, deviations from this model are exhibited. The controlling parameter is the relative amount of gelatin available to the precipitating AgBr at the silver reactant introduction point, expressed by the gelatin-to-AgBr ratio, and is dependent on the silver reactant addition rate, the gelatin concentration in the bulk suspension, and the dilution rate of the silver reactant stream. When the gelatin-to-AgBr ratio is decreased below a critical level (50 g/mol at 40°C), coalescence occurs, and the number of stable crystals decreases as the reactant addition rate increases. At intermediate gelatin-to-AgBr ratios (50–150 g/mol) flocculation occurs. Unlike coalescence, flocculation is reversible and does not interfere with the nucleation and growth of AgBr crystals (Antoniades and Wey 1993).

Bramsley et al. (1997) observed a well-pronounced dependence of the aggregation rate constant of calcium oxalate monohydrate (COM) on supersaturation. They proposed a mathematical model, according to which a successful aggregation event is a two-stage process. First, crystals must collide and then are “cemented” together. The model suggests that the rate of aggregation of COM crystals is limited by diffusion of solute ions to a cementing site.

Antoniades and Wey (1995) studied the relationship between coalescence and the formation of twinned AgBr nuclei that are suitable for growth into tabular crystals. Their experimental results showed that the formation of high populations of tabular AgBr crystals correlated very well with the presence of flocculation during nucleation, as detected by turbidimetry. This correlation, along with their observation that flocculation always precedes coalescence, suggests that twinning is a result of coalescence of colloidal nuclei.

6.5.3. MIXING

It is a well-known fact that the crystallization kinetics of soluble substances is greatly influenced by the hydrodynamic conditions. Similarly, there is a large body of experimental evidence that the size of crystals obtained by precipitation—and frequently, the morphology of precipitate—are greatly affected by hydrodynamic conditions. The size distribution of precipitate depends also on the manner and the spatial position of the reactant introduction to the precipitator. In industrial practice, there is always a stirrer or other device or provision in place that assures a certain level of mixedness via usually rather vigorous, turbulent mixing. The process of turbulent mixing in precipitation is very complex. By analogy with the description of the mixing phenomena in chemical reactors, this complex process can be conveniently divided into three simpler stages, as shown in Table 6.1.

In the turbulent mixing process sequence that proceeds from macro- to meso- to micromixing the latter is the fastest of the three. Its prominent importance in precipitation arises from the fact that most of the subprocesses of precipitation are very fast. In a typical precipitation process, the generation of supersaturation and its temporal and spatial distribution in the precipitator are affected by micromixing. It is also micromixing that enables circulating crystals to reach the regions of high supersaturation. It needs to be emphasized that it is macromixing occurring in the precipitator that sets a general environment for micromixing and indirectly influences the distribution of supersaturation.

The three component-processes of precipitation: chemical reaction, nucleation, and growth are molecular level processes. Therefore, the effect of mixing on these processes must be also considered on the appropriately small, molecular scale. Although micromixing takes place by unsteady molecular diffusion within energy dissipation vortices, micromixing models incorporate chemical reaction, nucleation, and growth kinetics by reducing the scale of observation to the level where homogeneity can be assumed.

According to Baldyga and Bourne (1986), vortex tubes of stable scale δ_ω incorporate fluid from the environment via the convective process termed by them an engulfment, Figure 6.7. The engulfment leads to the growth of volume spots, V_i , of substance i at the expense of the environment

$$\frac{dV_i}{dt} = EV_i \quad (6.33)$$

where the engulfment parameter, E , and the characteristic time of engulfment (which is roughly equal to E^{-1} and can be considered as a characteristic time for micromixing), τ_ω , are defined as follows:

$$E \cong 0.058(\varepsilon/\nu)^{1/2} \quad (6.34)$$

$$\tau_\omega \cong 12(\nu/\varepsilon)^{1/2} \quad (6.35)$$

where ε denotes the rate of energy dissipation per unit mass and ν is the kinematic viscosity.

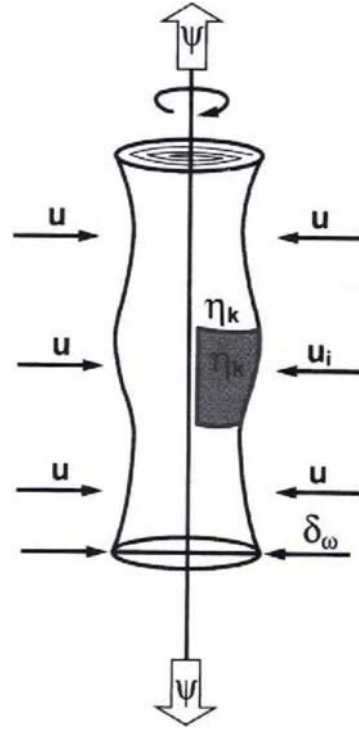


Figure 6.7 Engulfment of fluid from environment caused by vortex stretching. (After Baldyga and Bourne 1995.)

The engulfment of elements of the same fluid (self-engulfment) slows the growth of the mixing zone (reaction zone) and is ineffective for mixing

$$\frac{dV_i}{dt} = EV_i(1 - Y_i) \quad (6.36)$$

where Y_i is the volume fraction of substance i .

The concentration profile of substance i in this zone is described by

$$\frac{dC_i}{dt} = E(1 - Y_i)(\hat{C}_i - C_i) + R - Q \quad (6.37)$$

where terms R and Q represent creation and consumption of substance i , respectively.

A complete description of micromixing is included in the engulfment-deformation-diffusion model (EDD), Baldyga and Bourne (1986).

Micromixing and Precipitation. In order to assess the importance of micromixing in precipitation one can compare character-

TABLE 6.1 Mixing Stages in Precipitation

	Macromixing	Mesomixing	Micromixing
Scale	whole precipitator	diameter of the feed pipe	molecular
Phenomena	bulk fluid movement and blending determine environment concentrations	coarse scale turbulent exchange between the fresh feed and its surroundings; inertial-convective disintegration of large eddies	viscous-convective deformation of fluid elements followed by molecular diffusion
Characteristic Time	$const \frac{V_t}{sD^3}$	$\frac{V_t}{uD_t}$	$\cong 12(\nu/\varepsilon)^{1/2}$

istic time constants for these processes. A characteristic time for the micromixing process was defined by Eq. (6.35), and precipitation characteristic times may be approximated by the characteristic time constant for chemical reaction.

$$\tau_R = \frac{1}{k\bar{C}_{A0}^{n-1}} \quad (6.38)$$

or—for primary nucleation—by the induction period. Based on these characteristic times, Bourne (1985) delineated three regimes.

1. $\tau_\omega \ll \tau_R$: *slow regime*, the reaction or nucleation kinetics controls the process, the precipitator is homogenous, and the reaction takes place throughout the precipitator.
2. $\tau_\omega \approx \tau_R$: *fast regime*, the kinetics is influenced by both physical and chemical properties and the reaction is localized to a zone on either side of the diffusion plane.
3. $\tau_\omega \gg \tau_R$: *instantaneous regime*, the process is limited by the molecular-scale mixing and the reaction takes place in the diffusion plane.

Another useful criterion was proposed by Baldyga and Bourne (22) who found that engulfment controls mixing for not too elevated Schmidt numbers, i.e., for $Sc \ll 4000$.

Mixing-Precipitation Model for Double-Jet Semi-batch Precipitation. The process under consideration involves homogeneous instantaneous irreversible chemical reaction $A + B \Rightarrow C$. Two liquid ionic solutions A and B are added to a precipitator by a double jet (double feed). The reaction between A and B generates supersaturation, which triggers nucleation and subsequent growth of precipitate crystals. Chemical reaction is a molecular level process and in the case of an instantaneous reaction, the generation of supersaturation is controlled by micromixing. Mixing also affects redistribution of supersaturation via dilution and convection and brings the precipitate crystals into the contact with regions of high supersaturation. Kinetics of nucleation and growth that determine product quality depend on supersaturation, which is influenced by the reactant addition mode, initial concentrations, and the configuration of feed. Therefore, micromixing influences all four stages involved.

An analysis of this nonintuitive and complex process was proposed by Baldyga et al. (1995) with the use of “mixing-precipitation” model. The model assumes interactions among three distinctive scales of mixing from the slowest to the fastest in the turbulent mixing sequence: macro-, meso-, and microscale.

Macromixing—as a process of mixing on the scale of the whole precipitator—is considered in the model as a plug flow through the circulation loop. Macromixing determines environment concentration \bar{C}_i for meso- and micromixing and conveys fluids through environments characterized by different rates of energy dissipation. For a sufficiently slow feed addition, a uniform composition of the bulk can be assumed.

Mesomixing is regarded as an inertial-convective disintegration of large eddies that in turn forms a direct environment for micromixing. The mechanism of mixing in this subrange is very complex. Large, passive scalar eddies are created by the active, energy containing eddies. Moving randomly, these eddies produce a segregation of large scale and transfer the local mixture properties to the new environment. Baldyga (1989) and Baldyga et al. (1994) describe the inertial-convective mixing in detail. Its practical importance can be summarized as follows. For a high feed rate and large feed tube radius, the initial volume fraction of liquid i in large eddies, $Y_i^c = 1$. On the other hand, if the feed tube radius is much smaller than the scale of turbulence, $Y_i^c(0)$ value can be estimated

as the volume fraction of liquid “injected” into large eddies of the size of turbulence macroscale. The mixture can be interpreted as a swarm of blobs of the scale proportional to the integral scale of turbulence. The blobs move randomly and lose their identity due to inertial-convective mesomixing. The micromixing process is occurring within the blobs in the environment determined by mesomixing. The volume fraction of i -rich region, Y_i , which is initially equal to unity, decreases due to mesomixing and increases due to micromixing. The profiles $Y_i(t)$ and $\bar{C}_i(t)$ are resultants of this competition between the two mechanisms.

Micromixing is realized by an unsteady molecular diffusion within deforming slabs or laminar structures, which are embedded within energy dissipating vortices (Baldyga and Bourne 1986), and it is assumed to be controlled by the fluid engulfment.

The fresh reactants are added into large, inertial-convective eddies that also contain bulk liquid. These large eddies constitute an environment for micromixing. The initial volume fraction of fresh feed in such eddies depends on the feed tube radius, the discharge velocity, the velocity of surrounding fluid, and the lateral integral length scale. The inertial-convective mixing process is responsible for the disintegration of the large eddies that affect the fresh feed fraction.

The process of precipitation from ionic solutions is usually so fast that the characteristic time for micromixing defined by Eq. (6.35) is of the same order of magnitude as the characteristic times for precipitation or larger. For example, a double-jet precipitation of $BaSO_4$, when the low concentration (4.5 mmol/dm^3) reagents were fed above an impeller revolving at the highest speed (8 s^{-1}), the time constant for micromixing, τ_ω , was nine orders of magnitude larger than the characteristic time constant for nucleation, τ_N . The physical meaning of the inequality, $\tau_\omega \gg \tau_N$, is that the concentration of nuclei in the feed zone is larger than the concentration of crystals in the bulk, which also means that the nucleation process is localized very close to the feed point. An immediate consequence for the precipitation modeling is that since micromixing strongly affects or even controls the precipitation process, one must include micromixing in the general model of precipitation. Such models were formulated and published (Baldyga et al. 1995; Nývlt and Žáček 1986). According to Nývlt and Žáček (1986), who employed a simplified micromixing model, an increase of micromixing intensity always causes a decrease of the size of precipitate.

Baldyga et al. (1995) introduced a general mixing-precipitation model that coupled interactions between macro-, meso-, and micromixing with the population balance. The model was verified experimentally for a double-jet (double feed) precipitation of $BaSO_4$ carried out in a low-yield, laboratory stirred tank precipitator with a Rushton turbine mixer. Two different feed configurations, shown in Figure 6.8, were used. An equimolar, constant flow rate of both reactants was employed in each experiment. The effect of operating variables assessed by both model simulations and experimental results indicated the same trends. For the feed configuration I and larger reactant concentrations, the mean crystal size increased with the batch time, stirrer speed, and reactant flow rate. At small reactant concentrations, these operating conditions had practically no influence on the mean crystal size. The coefficient of variation, CV, increased with an increase of the reactant concentration.

The feed configuration II gave similar trends but smaller crystals were produced and the mean crystal size was in this configuration much more sensitive to the operating conditions even at low concentrations. It is important to emphasize that either feed configuration employed resulted in different supersaturation profile, as depicted in Figure 6.9.

It is interesting to realize how meso- and macromixing influence the driving force for micromixing and thus affect the outcome

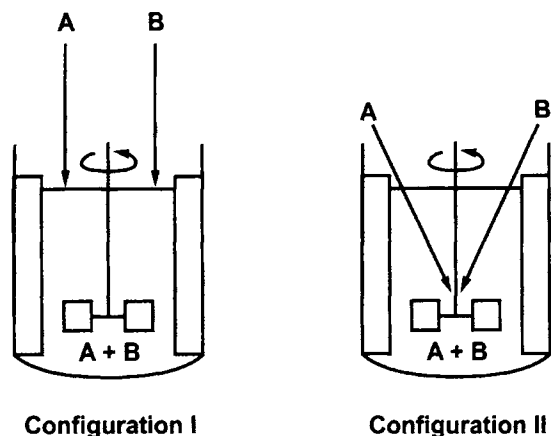


Figure 6.8 Double-jet (two feed) reactant addition configurations investigated by Baldyga et al. (1995). I—surface addition, II—subsurface axial addition near the impeller shaft.

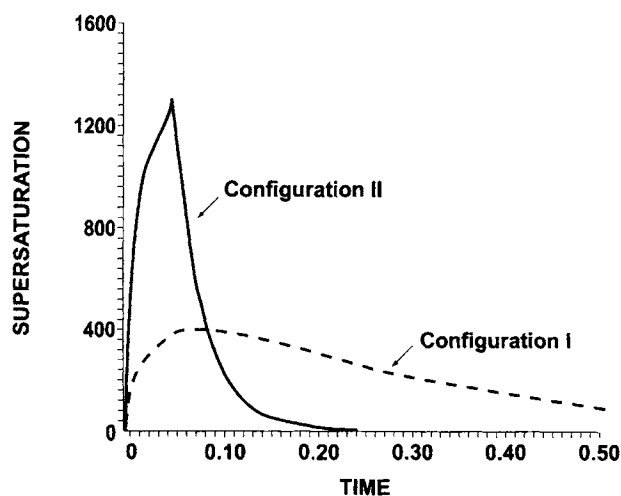


Figure 6.9 Effect of feed configuration—see Figure 6.8—on supersaturation profile in semi-batch precipitation of BaSO_4 (after Baldyga et al. 1995). Configuration I—after 1/3 feed added; configuration II—for initial period of feeding.

of precipitation. As the batch time for a constant reactant flow rate is extended, the local average concentration of reactants in the large, inertial-convective eddies decreases and so do the environment concentrations, $\bar{C}_i(t)$. As a result, the driving force for micro-mixing is increased, the local supersaturation is suppressed, and the nucleation rate is slower, producing less crystals whose final size is larger.

Similarly, higher stirrer speeds decrease the initial local environment concentration causing the improvement of micromixing, slower nucleation rate, and larger mean crystal size of precipitate.

6.6. EXPERIMENTAL TECHNIQUES

Experimental techniques used in the assessment of kinetics of precipitation and sizing of precipitate must address the specificity of this process. In particular, they need to be concerned with rapid chemical reactions, high initial supersaturation, high-order nucleation kinetics, very short time-scale of concurrently occurring component-phenomena, and small size of the crystals.

6.6.1. SUPERSATURATION MEASUREMENTS

In cooling crystallization of readily soluble substances it is possible to utilize the local slope of the solubility versus temperature curve to determine supersaturation based on accurate and precise temperature measurements. In precipitation, supersaturation is generated by chemical reaction and one must measure the activity or concentration of the reactants in order to determine supersaturation based on definitions, Eqs. (6.2) or (6.3). Accurate measurement of the momentary ionic activities in a precipitating system is theoretically complex, experimentally tedious, and time consuming. Publications that address this problem explicitly are scarce. First, expressions for the ionic conductivity of the solution that correlate the activity (or concentration and activity coefficient) with the molar conductivity of the reactants and the reaction conversion ratio, along with the method of their solution need to be set up. In a rigorous approach, the dependence of the electric potential on the ionic strength of the solution, the temperature, pH, electrophoretic mobility of the ionic species, and the adsorption of ions and precipitate on electrodes must be addressed. Second, reliable ion-specific electrodes must be selected (or built) and experimental procedures that involve some calibration experiments developed and tested. Marcant (1992) gave an example of such an organized research approach, for calcium oxalate.

In general, it is very difficult to measure directly the activity or concentration of reactive species independently one from another. Unless a sufficiently sensitive, quick dynamic response, species-specific probe-electrode can be applied for each of the reactants, the direct measurement of such a fundamental precipitation property as momentary supersaturation is rarely possible. Therefore, often the ratio of concentration of one of the reagents whose concentration can be monitored independently, to its solubility, is used as a measure of supersaturation. As a further simplification, a ratio between the concentration of the influx reagent stream and the solubility, i.e., an initial supersaturation ratio, can be used to characterize supersaturation at the onset of nucleation, Tanaka and Iwasaki (1985).

6.6.2. CONSTANT COMPOSITION METHOD

As described above, the dynamic measurements of supersaturation in precipitation could be a formidable task. For fundamental research purposes, it is possible to investigate precipitation kinetics by fixing, and carefully maintaining and monitoring, the supersaturation level throughout the test. Such an experimental technique introduced by Thomson and Nancollas (1978) and known as a constant composition method (CC), has been employed to investigate nucleation, growth, and dissolution kinetics of sparingly soluble salts. In the CC method, maintenance of solution composition is made possible by the use of suitable techniques such as conductometry or potentiometry involving ion selective electrodes. These are not required to measure ion activities as a function of time but only indicate a departure from a set value of potential, even slowly responding probe-electrodes may be employed.

In a typical CC growth kinetics experiment, carefully prepared and well-characterized seed crystals are introduced to a thermostated crystallization cell containing solution at a preset supersaturation. The reactant solutions are prepared with appropriate stoichiometry matching that of the precipitating phase. To maintain the composition of the supersaturated solution at a constant value, both reactants (titrant solutions) are added at the rate sufficient to replace reactant ions that precipitated, and to bring the supersaturation of the resultant total volume to the value of the initial supersaturated solution.

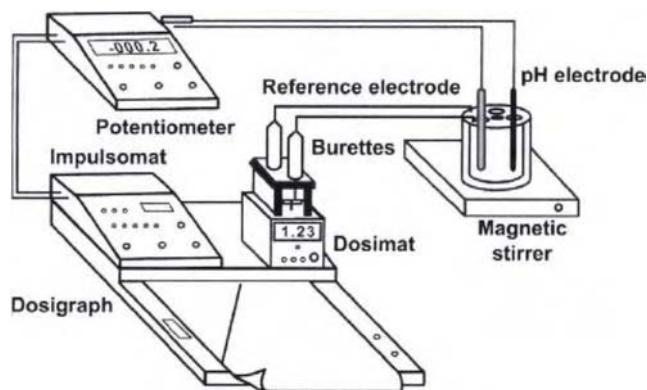


Figure 6.10 Schematic of constant composition method (CC) experimental setup. (After Thomson and Nancollas 1978.)

The reagent addition rate is controlled by the emf of the glass electrode, Figure 6.10. The titrants of the same molarity contain the respective reagent ions at a concentration that accounts for dilution due to the volume increase. In addition, neutral electrolyte is added to all solutions to maintain the ionic strength at the desired value. The growth rate of the crystals is calculated from the volume of titrant solutions added. Good precision and reproducibility characterize the method. Low solubility and necessarily limited amount of the crystals whose kinetics are examined require that very diluted reagents (titrants) are used.

The technique was found particularly useful in growth and dissolution kinetics measurements for pure and impurity-contaminated systems, and for the investigation of simultaneous precipitation of two or more phases.

6.6.3. CRITICAL GROWTH RATE MEASUREMENTS

As the solubility decreases, the induction period becomes too short to be a practical tool in kinetic investigations of precipitation. Furthermore, economical considerations require that practical precipitation processes be characterized by a high yield. The only way to achieve the latter is the use of concentrated reactants, whose concentration is measured in moles rather than millimoles. Even if a species-specific electrode can be used to measure supersaturation of ionic species, the sensitivity of such an electrode is typically limited to the region of rather low concentrations.

The concept of a maximum (critical) growth rate that enables one to probe the boundary of the supersaturation metastable zone without the actual measurement of the supersaturation, can be explained as follows. The seed crystals in the previously outlined CC method have a finite value of the growth rate. If the addition rate of the titrants is gradually increased in a step-wise fashion, there will be a certain addition rate at which new nuclei—in addition to the seeds unable anymore to consume all the incoming reagents for growth—will appear, relieving the excess supersaturation. The presence of these new nuclei can be detected either by a suitable in line technique or by sampling and an off line sample evaluation, such as optical or electron microscope observations. At the same time, the reagent addition rate employed just before the one causing renucleation, allowed the seeds to growth at a very high rate without causing the system to produce new nuclei. If the reagent addition increments are sufficiently small, such a maximum allowable growth rate can be experimentally determined for a given set of growth conditions with good accuracy and precision.

The critical growth rate method enables one to delineate the region of allowable growth rates for a given precipitating closed

system, which ensure an efficient growth of precipitate without adding new crystals to the growing crystals population. As shown by Wey and Strong (1977a), the critical growth rates are size-dependent, see Figure 6.5. Therefore, different growth rates may be employed at different stages of the growth of precipitate.

The knowledge of the critical growth rate for a given system characterized by a set of growth conditions, allows one to maximize the yield of the precipitation operation without the danger of generating new nuclei and causing a bimodal size distribution of the product crystals. Operating at the conditions slightly below the critical growth rate may also have other advantages. For example, a narrower size distribution can be obtained by reducing Ostwald ripening, characteristic of low supersaturation growth conditions.

6.6.4. 'INSTANTANEOUS' MIXING DEVICES

The time necessary for complete homogenization of the reacting solutions becomes critical for the systems with the induction period $t_{ind} < 1$ s. There are devices, such as Roughton chamber (Nielsen 1969) or rapid mixing device (Regenfuss et al. 1969) that ensure very rapid solution mixing and the reduction of mixing time to milliseconds or even microseconds. These devices may operate in a flow mode or in stopped-flow mode.

In the flow method, the reacting solutions are introduced continuously, rapidly mixed, and discharged through a sufficiently long outlet tube. After reaching steady state, the change of a certain measurable property is followed at a specific distance from the mixing point. This distance together with the flow rate determines the induction period.

In the stopped flow method, the property change is followed from the moment of the injection of the reacting solutions to the mixing device to determine the induction period.

In either method, the time-resolution characteristics of the instruments employed must be sufficient to detect and follow the property change. Examples of physical properties measured in such applications include intensity of transmitted, scattered, or absorbed light (Tanaka et al. 1979; La Mer and Dinegar 1951), solution conductivity (Söhnel and Mullin 1978), heat released (Nývlt and Pekárek 1980), light emission (Garten and Head 1963), and chemical composition of the solution (Packter 1974; Koutsoukos and Kontoyannis 1984).

The above outlined measurements of the solution property change to determine the induction period may be complemented by the count of the number of nuclei formed within unit solution volume to assess nucleation rates. The simplest but somewhat tedious method of nuclei count is that via a hematocytometer (Burker cell) (Nielsen and Söhnel 1971). Sampling, sample handling, and sample quenching are critical in order to obtain a reliable count. A particle counter with a well-defined optical volume (sensing zone) can also be used. A less accurate procedure is based on determination of the number of nuclei from the mean size of a known mass of precipitate. In such experiments, size can be determined either from optical or electron photomicrographs or measured by an appropriate particle sizer.

6.6.5. SIZING OF PRECIPITATES

Particle size measurement has evolved from a time-consuming sizing of each individual particle under the microscope to the automatic counting and sizing of a number of particles by a variety of instruments. Reliable sizing of precipitates is a rather challenging task. The crystals of interest remain in concentrated suspensions, their sizes extend from submicron to micron range, they have a tendency to agglomerate due to their surface chemistry,

and may continue to change sizes due to Ostwald ripening. Therefore, an on-line sizing is preferable. Alternatively, careful sample collection, preparation, and handling are necessary for off-line size measurements. The quest for fast, sensitive, and reliable particle sizing methods frequently requires the use of increasingly sophisticated and costly instrumentation.

Measurement methods for particle suspensions can be categorized into two groups:

1. Single-particle techniques (require dilution)
 - narrow aperture (light obscuration and resistive pore)
 - light scattering.
2. "Ensemble" techniques that process information produced simultaneously by many particles and require the use of complex mathematical algorithms to invert the data
 - sedimentation (gravitational and centrifugal)
 - Fraunhofer diffraction
 - dynamic light scattering.

Electrical Sensing Zone Method. This class of instruments, suitable for low concentration suspensions, determines the number and size of particles suspended in a conductive liquid, such as an electrolyte. The suspension is forced to flow through a small orifice on either side of which electrodes are located. The crystals passing through the aperture displace their own volume of electrolyte, which is sensed by a momentary change in electrical impedance, producing a voltage pulse proportional to the particle volume. The instrument needs to be calibrated against monodisperse spheres. An average analysis time is ≈ 30 min. The dynamic range is from 0.3 to 500 μm .

Static or Elastic Light Scattering. Static light scattering is a sensitive, noninvasive technique that can be used to study particles in suspension. The absolute intensity of scattered light is directly related to the size (or mass) of the scatterers in suspension and the contrast between the particles in the medium (the difference between either the refractive indices or scattering length densities of the particles and the medium). The angular dependence of the scattered intensity is related to other details of the geometry of the particle. The scattered intensity also depends on the geometry of the apparatus and scattering cell and the concentration of scattering particles.

Disc Centrifuge Photosedimentometer. The suspension is injected on top of spinfluid. White light is extinguished due to scattering and/or absorption by particles passing through the light beam near the bottom of the disc cavity. The transmitted light, detected by photodiode, is recorded as a function of time (run time is ≈ 30 min). Time values are converted to particle size using Stokes law of sedimentation, whereas the transmitted light data are converted to the number, surface, or weight distribution using Mie theory.

Sedimentation Field Flow Fractionator. The chromatography-related principle of this particle size and size distribution analyzer is based upon the interaction of the particle suspension under centrifugal field motion in a thin channel. The elution time of the particles is a function of particle size, particle density, flow rate of mobile phase, density of mobile phase, and the centrifugal force applied. After the size separation has occurred, the particles are detected in the mobile phase using a turbidity detection system. The dynamic range of the instrument is dependent on particle density and operating conditions and is typically within 0.03 μm –1 μm range.

Dielectric Sedimentation Method. The measurement relies upon the sensing of changes in the dielectric constant of medium between a pair of capacitance sensing plates placed around the sedimentation tube.

Laser Diffraction Methods. The operating principle is based on the complex interactions of laser light with particle that involves diffraction, reflection, absorption, and refraction. For particles larger than the wavelength of light, these interactions result in scattering of light in forward direction with only a small change in angle. This is known as Fraunhofer diffraction. The diffracted light is condensed with a lens and a light intensity pattern is produced on a multi-element photosensitive detector. The diameter and the intensity distribution of this pattern are dependent on the particle size distribution. For smaller particles—near the size of the wavelength of the light source—the Mie light scattering theory is used, which requires that the refractive index and the light absorptency of the particles are known.

Photon Correlation Spectroscopy (Quasi-Elastic Light Scattering). This method determines the velocity distribution of particle movement by measuring dynamic fluctuations of intensity of scattered light. The particle suspension undergoes Brownian motion, which causes the fluctuation of local concentration of the particles, resulting in local perturbances of the refractive index. This in turn brings about fluctuations of intensity of the scattered light. Information about the light scattering spectrum can be obtained from the autocorrelation function of the light scattering intensity. For the simplest case of monodisperse noninteracting spheres in a dust-free liquid, the characteristic decay of the correlation function is inversely proportional to the linewidth of the spectrum. The dynamic range of the method is from 0.005 to 1 μm , and the analysis time is ≈ 30 min.

Ultrasonic Spectrometry. Acoustic attenuation spectroscopy has many similarities with conventional light scattering techniques but—as the name suggests—uses ultrasound rather than light to examine the sample. The major practical advantage is sizing of opaque samples in suspensions at concentrations up to 50-vol.%. In the measurement step, a transducer directs sound waves of different frequencies through the sample. Suspended particles scatter, diffract, and absorb the ultrasound, and the second transducer detects the attenuated portion of the original signal. The attenuation of the sound waves as a function of frequency is measured over a wide frequency range. In the mathematical modeling step, the attenuation spectrum associated with any particle size and size distribution, and the concentration of the dispersed phase is predicted. Finally, the data inversion step utilizes algorithms that invert modeling equations to derive particle size distribution and concentration from the measured attenuation spectra.

6.7. MODELING AND CONTROL OF CRYSTAL SIZE AND CSD

6.7.1. MODELING OF CRYSTAL SIZE DISTRIBUTION

Continuous MSMPR Precipitator. The population balance, which was put forward by Randolph and Larson (1962) and Hulbert and Katz (1964), provides the basis for modeling the crystal size distribution (CSD) in precipitation processes. For a continuous mixed-suspension, mixed-product-removal (CMSMPR) precipitator with no suspended solids in the feed streams, the population balance equation (PBE) can be written as (Randolph and Larson 1988)

$$\frac{\partial n}{\partial t} + \frac{\partial(Gn)}{\partial L} + n \frac{d(\log V)}{dt} + \frac{nQ}{V} = B - D \quad (6.39)$$

where $n(L, t)$ is the population density per suspension volume (V), Q is the total volumetric flow rate, and B and D represent the net birth and death density functions, respectively, accounting for particle aggregation and breakage in the suspension. Under the conditions of constant suspension volume and negligible particle aggregation and breakage, Eq. (6.39) can be simplified to

$$\frac{\partial n}{\partial t} + \frac{\partial(Gn)}{\partial L} + \frac{n}{\tau} = 0 \quad (6.40)$$

where $\tau = V/Q$ is the mean residence time in the precipitator. Equation (6.40) requires a boundary condition and an initial condition. The initial condition is

$$n(L, 0) = 0 \quad (6.41)$$

and the boundary condition $n(0, t)$ is the nuclei population density (n^0 which can be related to the nucleation rate (\bar{B}) by

$$n(0, t) = n^0 = \bar{B}^0/G \quad (6.42)$$

In addition, a dynamic mass balance on solute being precipitated is required. Namely,

$$\frac{dC}{dt} = \frac{Q_i C_i}{V} - \frac{QC}{V} - \frac{\rho k_a G}{2} \int_0^\infty n L^2 dL \quad (6.43)$$

where Q_i and C_i are the volumetric flow rate and solute concentration of the input stream. The population balance, Eq. (6.40), together with the nucleation and growth kinetic expressions and the dynamic mass balance, Eq. (6.43), usually result in integro-differential equations that are difficult to solve, even numerically. One solution method involves the moments of the CSD and is discussed in some detail by Randolph and Larson (1988) and Tavare (1995). Under steady state condition, the population balance, Eq. (6.40), may be solved analytically. For example, the following well-known expression can be obtained under size-independent growth (i.e., McCabe's ΔL law) condition

$$n = n^0 \exp(-L/G\tau) \quad (6.44)$$

The population balance approach has been successfully applied to many precipitation processes. Morales et al. (1996) developed a population balance model to predict the crystal size distribution of calcium carbonate crystals in a CMSMPR precipitator operating under steady-state conditions. Their model was used to derive the size and supersaturation dependent growth kinetics for calcite. Wey et al. (1980) applied the population balance technique to the analysis of AgBr precipitation in a CMSMPR precipitators operating under steady-state conditions. Both McCabe's ΔL law and a size-dependent growth model based on bulk diffusion and surface integration were examined. Their obtained nucleation kinetic expression indicates that nucleation rate depends on supersaturation to the fourth power and is insensitive to the level of agitation and AgBr suspension density. Their results gave no indication that a contact secondary nucleation mechanism is involved in AgBr precipitation.

The population balance technique was also successfully applied to the run-seed, triple-jet precipitation of silver halide crystals (Wey 1990). In addition to silver nitrate and halide salt solutions, a third solution containing stable silver halide seed crystals was simultaneously introduced into the precipitation vessel. For a seed-crystal solution that contains monodisperse seed

crystals with an average size of L_s and number concentration of N_s , the PBE can be written as

$$\frac{\partial n}{\partial t} + \frac{\partial(Gn)}{\partial L} = Q_s N_s \delta(L - L_s) \quad (6.45)$$

where Q_s is the volumetric flow rate of the seed crystal solution, and δ is the Dirac delta function. For size-independent growth [i.e., $G \neq G(L)$], Eq. (6.44), together with a mass balance equation, can be solved by the moment technique. In the special case where Q_s is a linear function of t , Eq. (6.44) can be solved analytically. Figure 6.2 shows the theoretical crystal size distributions and the corresponding results of three experimental runs. Good agreement between the theoretical prediction and experimental results was obtained under several AgBr precipitation conditions (Wey 1990). The results indicate the highly predictable nature of the run-seed, triple-jet technique.

Hostomsky and Jones (1991) studied the effects of agglomeration (or aggregation) on the precipitation of calcium carbonate crystals in a CMSMPR precipitator operating under steady state conditions. An agglomeration expression was incorporated in the PBE, which was subsequently solved by a numerical technique. Their results show that the population balance model can be used to estimate nucleation, growth and agglomeration kinetic parameters simultaneously. Neglecting agglomeration in the analysis can lead to an overestimation of crystal growth rate.

Continuous Tubular Precipitator. At steady state, the PBE for a continuous tubular precipitator (Randolph and Larson 1988; Raphael and Rohani 1999) is given by

$$D_z \frac{\partial^2 n}{\partial z^2} - u_z \frac{\partial n}{\partial z} - \frac{\partial(Gn)}{\partial L} - B + D + B_0^0 \delta(L - L_0) = 0 \quad (6.46)$$

where the population density is a function of particle size and position (z) along the tubular precipitator, $n = n(L, z)$. D_z is the axial dispersion coefficient, u_z is the mean flow velocity, and B_0^0 is the (contact) secondary nucleation rate of particles of size L_0 . Equation (6.46) assumes no radial dispersion and has the initial condition

$$n(0, z) = J/G \quad (6.47)$$

In the above equation, J is the primary nucleation rate that is assumed to be the dominant nucleation mechanism. The boundary condition at the entrance is

$$u_z n(L, 0) - D_z \frac{dn(L, 0)}{dz} = 0 \quad (6.48)$$

i.e., there is no seeding or solids at the entrance. At the exit of the precipitator, the boundary condition is $dn/dz = 0$. Raphael and Rohani (1999) applied Eq. (6.46) to isoelectric precipitation of sunflower protein. By introducing the aggregation and breakage terms, they obtained a nonlinear integro-differential equation with initial and boundary conditions, subsequently solved using orthogonal collocation and nonlinear multiple shooting method.

Semi-Batch Precipitator. Assuming constant feed rate and no outflow, in addition to the assumptions made for the MSMPR precipitator, the PBE for a semi-batch precipitator is as follows (Kim and Tarbell 1991)

$$\frac{\partial n}{\partial t} + G \frac{\partial n}{\partial L} + \frac{n}{\tau_0 + t} = 0 \quad (6.49)$$

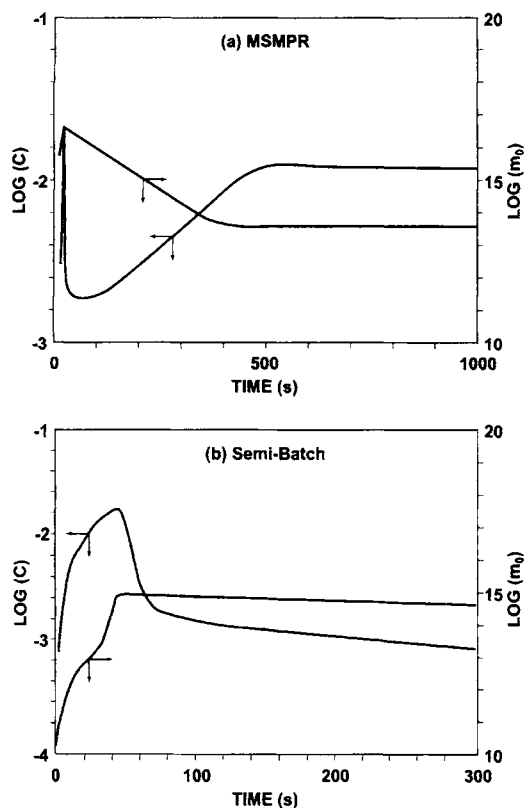


Figure 6.11 Dynamics of solute concentration (C) and particle number per unit volume (m_0), after Kim and Tarbell (1991). $C_0 = 0.15 \text{ kmol/m}^3$, $k_d = 0.023 \text{ kg} \cdot \text{m/kmol} \cdot \text{s}$. (a) MSMPR precipitator, $\tau = 50 \text{ s}$; (b) semi-batch crystallizer, $\tau_0 = 300 \text{ s}$.

The initial and the boundary conditions, Eqs. (6.41) and (6.42), apply and $\tau_0 = V_0/Q$, where V_0 is the initial volume of semi-batch crystallizer, is the initial holding time.

Numerical simulation results of the dynamics of the solute concentration (C) and the 0th moment (m_0) (i.e., the particle number per unit volume) in a MSMPR precipitator initially filled with crystal free solvent and in a semi-batch crystallizer filled with crystal free solvent to 50% of its final volume, are shown in Figure 6.11. In the initial stage of a MSMPR precipitator operation, both the solute concentration and the particle number per unit volume increase rapidly. However, due to the rapid growth of these initial nuclei a subsequent rapid desupersaturation occurs. A steady state is established after about 10 mean residence times. On the other hand, in a semi-batch crystallizer, the particle number per unit volume quickly reaches a constant value while the solute concentration continues to decline steadily throughout the feed period as the precipitate growth proceeds.

Mixing-Precipitation Models. Much more involved models, the so-called mixing-precipitation models, for double jet (Baldyga et al. 1995) and single jet (Phillips et al. 1999) semi-batch precipitation, in which the PBE's are coupled with mixing models, have recently been developed and successfully applied to elucidate barium sulfate precipitation. In Section 6.5.3., we briefly reviewed ramifications of such a model applied to the double jet precipitation (Baldyga et al. 1995). A detailed presentation of the mixing-precipitation models could not be given here due to the limitations of this handbook's volume.

6.7.2. SIZE CONTROL

A large part of high-added value, sparingly soluble crystalline materials are produced via batch precipitation. The properties of such materials are frequently determined by the precipitate particle design. In view of the complexity and difficult control of rapidly occurring nucleation in precipitation, Karpinski (1996) proposed the following approach for the precipitate size control. The stable (effective) nuclei formation stage should be evaluated experimentally, and an acceptable nucleation process and conditions adopted as a result of such evaluation. An average size and the total number of stable nuclei should be then used as the entry data for a now precisely controlled growth stage that ultimately shapes the crystal surface and final properties of the precipitated crystals.

Various supersaturation and growth control strategies have been investigated for batch crystallization processes. In cooling crystallization, such control may be achieved by cooling rate manipulations; in evaporative crystallization, a manipulation of the evaporation rate has been suggested; e.g., Mullin and Nývlt (1971), Larson and Garside (1973), Karpinski et al. (1980). For a chemical reaction-driven process, such as batch precipitation of sparingly soluble materials, the tools of the crystal size and morphology control suggested in the literature for batch cooling or evaporative crystallization are not directly applicable.

Based on the approaches proposed for batch crystallization—which employed cooling/evaporation rates to control supersaturation, and on the specifics of the batch precipitation process—the reactant addition rate was chosen as the controlling variable.

Development of the Growth Ramp Equation. It is a well-known fact that during the course of batch precipitation, the entire nuclei population is established and stabilized in the first minutes of the process, and that the supersaturation driving force during the subsequent growth stage does not change significantly with the precipitation time, Nývlt (1974), Leubner et al. (1980); see also Figure 6.4. Therefore, in the development of the reactant flow rate versus time equation, or growth ramp equation, it seems safe to assume a constant supersaturation level for the entire growth domain of precipitation. The strategy adopted, which aims at a constant supersaturation level, may be found particularly useful for those precipitations in which a specific morphology of the precipitate needs to be obtained. It is conceivable that the changes in the supersaturation level that are characteristic of arbitrary growth ramps, may introduce supersaturation conditions that allow for or promote the growth of undesirable morphological facets.

The relation between the growth rate G and supersaturation ratio S may be conveniently expressed by means of the power-law equation, similar to Eq. (6.29)

$$G = \frac{dL}{dt} = k_G S^g \quad (6.50)$$

where k_G is the growth rate constant and g is the growth order. Assuming the validity of the above kinetic equation, one may argue that for an isothermal process, by fixing and maintaining the driving force at a constant level, a constant growth rate is assured as well, i.e., $G = \text{const}$. Naturally, the assumed growth rate must not exceed the critical (maximum) value for the largest crystals throughout the growth process. This requirement is a consequence of the fact that the critical growth rates for AgBr were found to be inversely proportional to the grain size (Wey and Strong 1977), Figure 6.5. If the assumed value $G > G_{\text{crit}}$, then renucleation is inevitable, the population of crystals may increase

even by orders of magnitude during the course of the growth stage due to renucleation, and a bimodal CSD results.

The simplified overall (total, integral) material balance of the batch precipitation states that the mass increase due to the growth of precipitate crystals of the molecular weight M from the initial size L_0 to an arbitrary size L , in an arbitrary time t , is equal to the mass of the solute of volume V delivered by the equimolar double-jet whose molar concentration is C_R

$$N\alpha\rho(L^3 - L_0^3) = VMC_R \quad (6.51)$$

where α is the volumetric shape factor, constant for a given morphology, and ρ is the crystal density. The number of individual crystals N , fixed in or shortly after the nucleation stage, remains constant throughout the growth of the precipitate. The material balance equation, Eq. (6.51), may be differentiated with respect to time to give

$$3N\alpha\rho GL^2 = QMC_R \quad (6.52)$$

where $Q = dV/dt$ denotes the equimolar volumetric flow rate of reactants. One can proceed with the differentiation of Eq. (6.52) until all the quantities but $Q = Q(t)$ become constant. After the two subsequent differentiations

$$\frac{d^2Q}{dt^2} - \frac{6N\alpha\rho G^3}{MC_R} = 0 \quad (6.53)$$

Equation (6.53), whose second term on the left side is now constant, is a second-order ordinary differential equation (ODE). In order to solve this ODE for $Q(t)$, two initial conditions are necessary. They come in naturally, by realizing that at time $t = 0$, the size of crystals is $L = L_0$ (seeds or stable nuclei size). The first initial condition is obtained from Eq. (6.52) as

$$Q(0) = Q_0 = \frac{3N\alpha\rho GL_0^2}{MC_R} \quad (6.54)$$

and the second initial condition is as follows

$$\frac{dQ(0)}{dt} = \frac{6N\alpha\rho L_0 G^2}{MC_R} \quad (6.55)$$

The solution to the ODE, Eq. (6.53), subject to the initial conditions (6.54) and (6.55), yields the sought-after growth ramp equation

$$Q = \frac{3N\alpha\rho}{MC_R}(L_0^2 G + 2L_0 G^2 t + G^3 t^2) \quad (6.56)$$

Equation (6.56) is parabolic in t . For a nonzero initial size it does not reduce to $Q = 0$ at $t = 0$. This is quite understandable, since the initial crystals whose size is L_0 are able to accept the growth material, incoming at the volumetric rate equal to that given by Eq. (6.54). The latter equation determines the magnitude of the allowable initial reactant addition rate for the first moment of the growth stage of batch precipitation.

The significance of Eq. (6.56) lies in the fact that it prescribes the reactant flow rate at any moment of the growth of precipitate crystals, provided that the number and size of the seeds used are known or alternatively, that the number and size of stable nuclei population at the beginning of the growth stage of precipitation are known from the previous experiments. In the latter case, by knowing the size of the final precipitate and the number of moles

precipitated, one can determine the number of individual crystals that were formed as a result of the particular nucleation procedure employed in the process.

Equation (6.56) may be rearranged to the form (one may find it to be more convenient to use)

$$Q = \frac{n_n}{C_R} \left(\frac{G}{L_0} + \frac{2G^2 t}{L_0^2} + \frac{G^3 t^2}{L_0^3} \right) \quad (6.57)$$

where n_n denotes the number of moles of solute used in the nucleation stage. In order to use Eq. (6.57) in programming Q versus t , it is necessary to substitute the moles of solute used in the nucleation stage n_n and the size of grains after nucleation, $L_0 = L_n$. The former is known for a given formulation, and the latter can be measured by an on-line or off-line particle-sizer.

The manipulative variables in Eqs. (6.56) and (6.57) are the growth rate G , the reactants concentration C_R , the total growth time t_f , and the final size of the precipitate grains, L_f . There are always limiting values for these variables. The maximum reactant concentration is limited by the solubility of the least soluble reactant. In addition, the total growth time t_f and the minimum value for C_R should, for practical reasons, be such that the product cycle time is minimized. G , t_f , and L_f are related as follows: $G = (L_f - L_0)/t_f < G_{crit}$. This relationship and the preceding discussion impose certain limitations on the achievable final precipitate size L_f . If the dependence of the crystal size on G_{crit} is known, the growth time may be further optimized (shortened) by the use of two or more growth segments, each having its own constant growth rate $G_i < G_{crit, i}$.

Example of Application of the Growth Ramp. The experimental verification of the growth ramp equation, Eq. (6.56), was carried out by Karpinski (1996), for octahedral and cubic AgBr submicron crystals in a 6.0-l batch reactor-precipitator. In the preliminary experiments, the number and size of the effective (stable) nuclei were determined. To this end, trial precipitations were performed with samples for sizing taken just prior to the growth stage and at the end of precipitation. The size was measured by a disc centrifuge-sizer, and the number of crystals was determined from the material balance.

A very good agreement between measured and calculated final size of precipitate was obtained. The author concluded that the proposed growth ramp equation, Eq. (6.56), which assumes a constant growth rate throughout the segment of a growth stage or the entire growth stage, provided a successful growth strategy for the precipitation of AgX ($X = \text{Cl, Br, I}$) photosensitive materials.

The constant growth rate strategy presented above allows one to predictably (i.e., quantitatively) manipulate the final size of the precipitate by adjusting the growth rate and/or the batch time of the batch precipitation process, for which known data exist regarding its nucleation stage. By setting the growth rate—and thus the supersaturation—at a constant level, an additional means of controlling crystal morphology and/or properties of the crystal surface may be achieved. The use of any growth rate that does not exceed the critical (maximum) one assures a renucleation-free process and a narrow CSD with limited fines contribution.

6.8. PRECIPITATION IN PRACTICE

Requirements regarding the morphology, purity, yield, size range, and CSD of precipitate are case specific. Therefore, only brief, qualitative discussion will be devoted to the practical aspects of the precipitation process. Precipitation as much as crystallization, is seen now not just as a separation and purification operation but

rather as a process capable of delivering a range of value added materials that meet certain specifications. Furthermore, the circumstances of the competitive global economy add factors outside of the specification, such as speed in developing new materials or meeting specific customer needs. Very frequently, the manner by which the precipitation process is carried out predetermines the final properties of the material manufactured.

6.8.1. CONTINUOUS PRECIPITATION

A basic criterion used to select a continuous precipitation process is the amount or the mass rate of product to be manufactured. Bulk inorganic chemical, catalyst, fertilizer, and food processing industries are typical examples of such high-capacity precipitation operations.

CMSMPR Precipitator. In the continuous precipitation technique, continuous streams of reactants are fed to a stirred vessel while product is simultaneously removed to maintain a constant reaction volume. Following a transient period, a steady state is reached, during which the CSD and morphology of crystals removed from the precipitator remain unchanged. Uniform morphology and rather polydisperse precipitate crystals are typically obtained. Such a continuous operation may exhibit more or less pronounced oscillations.

The results of the application of the CMSMPR precipitator to an inorganic material, such as AgBr, were summarized earlier, in Section 6.7 (Wey et al. 1980). Raphael et al. (1997), reported that the application of the CMSMPR precipitator to protein precipitation may result in unimodal or bimodal CSD depending on the precipitation conditions and the tendency of the material to aggregate. They found that low protein feed concentration the growth process is dominant leading to the bimodal CSD at longer mean residence times. At high-protein feed concentrations smaller particles with unimodal CSD were obtained after longer mean residence times.

Tubular Precipitator. This type of continuous operation may be employed to reduce polydispersity of precipitates (Raphael et al. 1997; Raphael and Rohani 1999). The tubular precipitator may operate either under the turbulent flow or laminar flow regime. The reactants are added into the inlet section equipped with static mixers and may also enter as a multi-port feed along the length of the tubular precipitator. If the reactant feeding streams are too concentrated or if too excessive formation of precipitate occurs in the inlet section of the precipitator, a third stream of solvent is also fed to dilute the flowing suspension. The latter may contain a protective colloid or surfactant that prevent agglomeration of precipitate.

6.8.2. BATCH PRECIPITATION

Batch (Semi-batch) Precipitator. This is the most commonly used precipitator. The batch volume may range from 100 L to 12,000 L (Rusli 1991). There are two basic types of batch (semi-batch) precipitation operations: single-jet (single-feed) and double jet (double-feed). In a single-jet operation, one of the reactant is placed in an agitated vessel and the other is fed throughout the batch time. In a double-jet operation, as that schematically shown in Figure 6.8., the reactants are fed to the vessel, which initially contains a certain amount of a solvent at preset conditions. The addition rate of reactant may proceed at a constant rate or may be accelerated with time (Karpinski 1996). In a double-jet operation, the reactant concentration usually reflects the stoichiometry of the compound being precipitated, and so do the reactant flow rates. One of the feeds may be controlled in order to maintain a certain

property, found to be important for the successful operation, at a constant level. An excess concentration of one or more ionic species above the stoichiometric value may be employed (and controlled) in order to assure formation of a specific morphology of precipitate. It has been well documented in literature (Söhnle and Garside 1992; Marcant and David 1993; Baldyga et al. 1995) that feed position in double-jet precipitation can significantly influence the properties, such as the size and the CSD of the product.

Marcant and David (1993) studied precipitation of calcium oxalate using several precipitator configurations. They observed that in a single-jet precipitation, the largest average size of precipitate was obtained with a feed point next to the tip of the impeller, followed by the feed point above the impeller and close to the impeller shaft. The smallest average size was obtained when the feed point was located near the liquid surface. Baldyga et al. (1995), obtained qualitatively similar results for barium sulfate. Double-jet precipitation gave a much larger average size of precipitate, and appeared to be very sensitive to the impeller stirring speed (Marcant and David 1993; Baldyga et al. 1995).

In any batch precipitation scheme, a selection must be made between a high-yield, high-supersaturation (without exceeding the critical supersaturation), short operation, and a longer batch time, low-supersaturation one. Such a decision must weigh both the product properties desired and the cost factor associated with the implementation of either scheme. Often, additional considerations may need to be taken into account. For example, as reported by Yokoyama and Toyokura (1993), different polymorphic forms of precipitate can be obtained by controlling the supersaturation level in a double jet-precipitation.

6.9. SUMMARY

Precipitation or reactive crystallization is very common in industrial applications and laboratory practice. A large number of high-value added product and intermediate materials are produced via precipitation. The precipitation process is very complex and the properties of precipitate strongly depend on the kinetics of the component subprocesses and their conditions. All these factors, and also the fact that the typical size of precipitate is in the submicron to 100 μm range, make the precipitation process very unique. Frequently, different theoretical and experimental approaches than those used for typical crystallization are required.

In the entire chapter, a strong emphasis has been put on sparingly soluble, rapid kinetics crystalline materials because the authors felt that this domain of the reactive crystallization spectrum is the most representative for precipitation as well as distinct from other crystallization processes.

In addition to considering a typical crystallization sequence: generation of supersaturation, nucleation, and crystal growth, one may be additionally concerned with the chemistry of precursors, colloidal properties, micromixing, Ostwald ripening, renucleation leading to bimodal distribution, aggregation, and ageing of precipitate. All these phenomena and their underlying principles are briefly discussed.

Also discussed are precipitation specific experimental techniques, such as: supersaturation measurements, constant composition (CC) method, instantaneous mixing devices, maximum (critical) growth rate experiments, and sizing. Due to the intrinsic difficulties with the direct supersaturation measurements and the microsecond characteristic time scale of precipitation reaction and nucleation, the CC method is used to study the precipitation kinetics. For the same reasons, the critical growth experiments are used to delineate the domain of the reactant feed rate that assures a renucleation-free process and a unimodal CSD.

The importance of mixing in precipitation is generally appreciated but not well understood due to its complexity. The concepts of macro-, meso-, and micromixing are presented, with a particular attention devoted to micromixing.

In spite of the intricacy of precipitation, the population balance modeling tools for the CMSMPR and semi-batch crystallizers, along with the mixing-precipitation model have been proposed and adopted to predict the CSD of precipitates. These modeling approaches are very briefly outlined. An unprecedented progress in both the computational power of personal computers and the development of software codes have set the stage for a rapid progress in the area of modeling of the precipitation process.

Once prenucleation, nucleation, and post-nucleation processes have resulted in a stable nuclei population—or if seeding material is available—the final size of the precipitate from a batch precipitation process can be controlled via manipulation of the reactant feed rate versus time profile. This concept is described in details and illustrated with an example for submicron crystals of AgBr.

Finally, we touch upon selected practical aspects of typical precipitation operations, using continuous MSMPR and tubular precipitators, and a semi-batch precipitator as illustrative examples.

NOMENCLATURE

a	activity of ionic species
A	surface area of crystal
B	constant defined by Eq. (6.15); birth density function in population balance
\tilde{B}	nucleation rate
C	bulk concentration
C_{eq}	equilibrium concentration at solubility
C_i	concentration of reagent i ; concentration at crystal-solution interface
\hat{C}_i	concentration of reagent i in environment
C_R	molar concentration of reactants
ΔC	supersaturation driving force
d	impeller diameter
d_m	molecular diameter
D	molecular diffusivity of the solute; death density function in population balance
D_t	turbulent diffusivity
E	engulfment parameter
E_N	activation energy for nucleation
g	growth order
G	linear growth rate
G_{crit}	critical (maximum) linear growth rate
ΔG	free Gibbs energy change
ΔG^*	maximum free Gibbs energy change
J	nucleation rate
J_0	nucleation rate
k	Boltzmann constant, rate constant
k_a	surface shape factor
k_d	mass transfer coefficient
k_G	growth rate constant
k_i	surface integration rate constant
k_N	nucleation rate constant
K	constant
K_{sp}	solubility product
L	crystal size as equivalent diameter or edge length
L_0	initial size
L_f	final size
L_s	seed crystal size
m	surface integration order, order of chemical reaction
M	molecular weight

n	nucleation order; population density per suspension volume
n^0	nuclei population density
n_n	moles precipitated in the nucleation stage
N	number of molecules, ions, or crystals
Q	volumetric flow rate; consumption function
r	crystal radius
R	universal gas constant; creation function
Re	Reynolds number
S	supersaturation ratio
S_0	initial supersaturation ratio
Sc	Schmidt number
Sh	Sherwood number
t	time
t_f	batch time
t_{ind}	induction period
T	absolute temperature
u	local fluid velocity
\bar{u}	local average fluid velocity
u_s	particle slip velocity
V	volume of reactant solution added; suspension volume
V_0	initial volume of semi-batch precipitator
V_i	volume spot of substance i
\dot{V}_i	volumetric rate of growth of volume spots of substance i
V_m	molar volume
V_t	volume of precipitator
Y_i	volume fraction of substance i

Greek Letters

α	volumetric shape factor
δ	thickness of diffusion layer rate of energy dissipation per unit mass reaction affinity
η_k	Kolmogorov microscale
μ	viscosity
ν	number of moles of ions formed from one mole of electrolyte, kinematic viscosity
π	activity product
ρ	crystal density
σ	surface energy; relative supersaturation in BCF theory
σ_c	the BCF model's constant
σ_w	characteristic dimension of vortices
τ	mean residence time
τ_N	characteristic time constant for nucleation
τ_R	characteristic time constant for chemical reaction
τ_w	characteristic time of engulfment pre-coefficient (pre-exponential frequency factor) ratio defined by Eq. (6.32)
ψ	deformation parameter

Subscripts

A	cation of an electrolyte
B	anion of an electrolyte
c	crystal
eq	value at equilibrium
het	heterogeneous
i	value at solid-liquid interface, input value ind induction period
0	initial value at time = 0

REFERENCES

- Antoniades, M.G., and Wey, J.S. (1993). *J. Imaging Sci. Technol.* **37**, 272.
 Antoniades, M.G., and Wey, J.S. (1995). *J. Imaging Sci. Technol.* **39**, 323.
 Antoniades, M.G., and Wey, J.S. (1998). *J. Imaging Sci. Technol.* **42**, 393.
 Baldyga, J., (1989). *Chem. Eng. Sci.* **44**, 1175.

- Baldyga, J., and Bourne, J.R. (1984). *Chem. Eng. Comm.* **28**, 243.
- Baldyga, J., and Bourne, J.R. (1986). In *Encyclopedia of Fluid Mechanics*, p. 145, Gulf Publishing, Houston.
- Baldyga, J., and Bourne, J.R. (1989). *Chem. Eng. J.* **42**, 83.
- Baldyga, J., Bourne, J.R., and Zimmermann, B. (1994). *Chem. Eng. Sci.* **44**, 1937.
- Baldyga, J., Podgorska, W., and Pohorecki, R. (1995). *Chem. Eng. Sci.* **50**, 1281.
- Becker, R.R., and Döring, W. (1935). *Ann. Physik.* **24**, 719.
- Berry, C.R. (1976). *Photogr. Sci. Engng.* **20**, 1.
- Bird, R.B., Stewart, W.E., and Lightfoot, E.N. (1960). *Transport Phenomena*, Wiley, New York.
- Bogg, T.G., Harding, M.J., and Skinner, D.N. (1976). *J. Photogr. Sci.* **24**, 81.
- Bramley, A.S., Hounslow, M.J., Newman, R., Paterson, W.R., and Pogessi, C. (1997). *Trans IchemE*, **75A**, 119.
- Burton, W.K., Cabrera, N., and Frank, F.C. (1951). *Philos. Trans. Roy. Soc. (London)* **243**, 299.
- Enustun, B.V., and Turkevich, J. (1960). *J. Am. Chem. Soc.* **82**, 4502.
- Frank, F.C. (1949). *Discuss. Faraday Soc.* **5**, 48.
- Frossling, N. (1938). *Gerlands Beitr. Geophys.* **52**, 170.
- Garten, V.A., and Head, R.B. (1963). *Phil. Mag.* **8**, 1793.
- Gibbs, J.W. (1928). *Collected Works*, Longmans, London, England.
- Hostomsky, J., and Jones, A.G. (1991). *J. Phys. D: Appl. Phys.* **24**, 165.
- Hulbert, H.M., and Katz, S. (1964). *Chem. Eng. Sci.* **19**, 555.
- Hunter, R.J. (1987). *Foundations of Colloid Science*, vol. 1, Clarendon Press, Oxford, England.
- Jagannathan, R., and Wey, J.S. (1981). *J. Crystal Growth* **51**, 601.
- Jagannathan, R., and Wey, J.S. (1982). *Photogr. Sci. Eng.* **26**, 61.
- James, T.H. (1977). *The Theory of the Photographic Process*, 4th ed., Macmillan, New York.
- Karpinski, P. (1981). *Mass Crystallization in a Fluidized Bed*, Wroclaw Univ. of Technology, Wroclaw, Poland.
- Karpinski, P.H., (1996). In *13th Symposium on Industrial Crystallization Proceedings*, vol. 2, p. 727, PROGEP, Toulouse, France.
- Karpinski, P., Budz, J., and Naruc, Z. (1980). In *Scientific Papers of Wroclaw University of Technology*, vol. 38, no. 5, p. 163, Wroclaw, Poland.
- Kim, W.-S., and Tarbell, J.M. (1991). *Chem. Eng. Comm.* **101**, 115.
- Koutsoukos, P.G., and Kontoyannis, Ch.G. (1984). *J. Chem. Soc., Faraday Trans. I*, **80**, 1181.
- La Mer, V.K., and Dinegar, R.H. (1951). *J. Am. Chem. Soc.* **73**, 380.
- Lamey, M.D., and Ring, T.A. (1986). *Chem. Eng. Sci.* **41**, 1213.
- Larson, M.A., and Garside, J. (1973). *The Chemical Engineer*, 318 (June).
- Leubner, I.H., Jagannathan, R., and Wey, J.S. (1980). *Photogr. Sci. Eng.* **24**, 268.
- Liu, C.Y., Tsuei, H.S., and Youngquist, G.R. (1971). *Chem. Eng. Progr. Symp. Ser.* **67(110)**, 43.
- Morales, J.G., Clemente, R.R., Lopez, A.H., Macipe, L., and Raskopf, G. (1996). In *13th Symposium on Industrial Crystallization Proceedings*, vol. 2, p. 713, PROGEP, Toulouse, France.
- Mullin, J.W., and Nývlt, J. (1971). *Chem. Eng. Sci.* **26**, 369.
- Nielsen, A.E. (1964). *Kinetics of Precipitation*, Pergamon Press, Oxford, England.
- Nielsen, A.E. (1969). *Krist. Technik* **4**, 17.
- Nielsen, A.E. (1983). In *Treatise on Analytical Chemistry*, vol. 3, 2nd ed. (Kolthoff, I.M., and Elving, P.J., eds.), pp. 269–347, John Wiley & Sons, New York.
- Nielsen, A.E., and Söhnel, O. (1971). *J. Crystal Growth* **11**, 233.
- Nývlt, J. (1971). *Industrial Crystallisation from Solutions*, Butterworths, London, England.
- Nývlt, J. (1974). *Coll. Czech. Chem. Commun.* **39**, 3463.
- Nývlt, J., and Karpinski, P. (1977). *Krist. Technik* **12**, 1233.
- Nývlt, J., and Pekárek, V. (1980). *Z. physik. Chem., Neue Folge* **122**, 199.
- Nývlt, J., and Žáček, S. (1986). *Colln. Czech. Chem. Commun.* **51**, 1609.
- Ohara, M., and Reid, R.C. (1973). *Modeling Crystal Growth Rates from Solution*, Prentice-Hall, Englewood Cliffs, New Jersey.
- Ostwald, W. (1901). *Analytische Chemie*, 3rd ed., Engelmann, Leipzig.
- Packter, A. (1974). *Krist. Technik* **9**, 249.
- Regenfuss, P., Clegg, R.M., Fulwyler, M.J., Barrantes, F.J., and Jovin, T.M. (1985). *Rev. Sci. Instru.* **56**, 283.
- Rusli, I.T. (1991). In *Opportunities and Challenges in Crystallization Research*, p. 241, Ames, IA.
- Randolph, A.D., and Larson, M.A. (1962). *AIChE J.* **8**, 639.
- Randolph, A.D., and Larson, M.A. (1988). *Theory of Particulate Processes*, 2nd ed., Academic Press, New York.
- Raphael, M., and Rohani, S. (1999). *Can. J. Chem. Eng.* **77**, 540.
- Rohani, M., Rohani, S., and Sosulski, F. (1997). In *Separation and Purification by Crystallization*, (Botsaris, G.D., and Toyokura, K., eds.), p. 188, ACS Symposium Series 667, Washington, DC.
- Söhnel, O. (1991). In *Advances in Industrial Crystallization* (Garside, J., Davey, R.J., and Jones, A.G., eds.) p. 63, Butterworth-Heinemann, Oxford, England.
- Söhnel, O., and Garside, J. (1992). *Precipitation*, Butterworth-Heinemann, Oxford, England.
- Söhnel, O., and Mullin, J.W. (1978). *J. Crystal Growth* **44**, 377.
- Söhnel, O., and Mullin, J.W. (1979). *Krist. Technik* **14**, 217.
- Strong, R.W., and Wey, J.S. (1979). *Photogr. Sci. Eng.* **23**, 344.
- Sugimoto, T. (1983). *J. Colloid Interface Sci.* **91**, 51.
- Tanaka, T., Matsubara, T., Saeki, N., and Hada, H. (1976). *Photogr. Sci. Eng.*, **20**, 213.
- Tanaka, T., and Iwasaki, M. (1983). *J. Photogr. Sci.* **31**, 13.
- Tanaka, T., and Iwasaki, M. (1985). *J. Imaging Science* **29**, 86.
- Thomson, M.B., and Nancollas, G.H. (1978). *Science* **200**, 1059.
- Tavare, N.S. (1995). *Industrial Crystallization*, Plenum Press, New York.
- Turnbull, D., and Vonnegut, B. (1952). *I&EC* **44**, 1292.
- Volmer, M., and Weber, A. (1926). *Z. physik. Chem.* **119**, 277.
- Wey, J.S. (1981). In *Preparation and Properties of Solid State Materials*, vol. 6, chap. 2 (Wilcox, W.R., ed.), Marcel Dekker, New York.
- Wey, J.S. (1990). *J. Imaging Sci.* **34**, 202.
- Wey, J.S., and Schad, M.J. (1986). *J. Imaging Sci.* **30**, 193.
- Wey, J.S., and Strong, R.W. (1977a). *Photogr. Sci. Eng.* **21**, 14.
- Wey, J.S., and Strong, R.W. (1977b). *Photogr. Sci. Eng.* **21**, 248.
- Wey, J.S., Terwilliger, J.P., and Gingello, A.D. (1980). *AIChE Symposium Series* **193(76)**, 34.
- Wagner, C. (1961). *Z. Elektrochem.* **65**, 581.
- Walton, A.G. (1967). *The Formation and Properties of Precipitates*, Interscience Publishers, New York.

MELT CRYSTALLIZATION

J. Ulrich and H.C. Bülow

7.1. DEFINITIONS

In crystallization processes, two expressions are often used, crystallization from solution and crystallization from melts. A *solution* is a homogeneous mixture of more than one species. A *melt* most correctly refers to a pure molten solid such as molten silicon. Unfortunately, the term melt is used in a more general way to describe solutions of materials that are usually solid at room temperature.

The phase diagrams, as seen in Figure 7.1, give the melting point curve for the full range of concentrations possible for a binary system. The solubility diagrams are usually plotted with exchanged axis and give only a limited section of concentrations. (For a diagram see Chapters 1 and 3 of this volume.) In the case of a two-component system, there is no difference between a solution and a melt when looking at the phase diagram.

How can you differentiate between the two expressions melt and solution as they are used today?

It was suggested by Ulrich et al. (1988) that whenever the expression "solution" is used the mass transfer effects should dominate a process, and whenever the heat transfer is dominating a process of liquid solid phase change it should be called "melt" crystallization. An additional explanation could be found in the different growth rates that have their origin in the rate domination effect.

Crystal growth rates within crystallization processes from solutions in most cases are in the range 10^{-7} – 10^{-9} m/s. Growth rates in melt crystallization are quite often in the range of about 10^{-6} m/s and in extreme cases in some solid layer processes as high as 10^{-4} m/s.

Another expression that needs a definition is "fractional crystallization." *Fractional crystallization* is a repetition of a crystallization process performed in order to receive a further purified

product. A fractional crystallization can therefore be conducted from the melt as well as from the solution but does not differentiate between the two.

7.2. BENEFITS OF MELT CRYSTALLIZATION

Melt crystallization as a unit operation in chemical engineering takes advantage of the fact that in a different state of aggregation of a substance its equilibrium composition is different. This will be discussed in more detail in the next chapter. Good background information can be found in Zief and Wilcox (1967), Matz (1969), Mullin (1972, 1993), Atwood (1976), Matsuoka (1991), Jansens and van Rosmalen (1994), Ulrich and Kallies (1994), Arkenbout (1995), Toyokura et al. (1995), Ulrich (1995), and Ulrich and Bierwirth (1995). One major advantage of melt crystallization as a separation technology becomes obvious when comparing the energy required for the phase change for melt crystallization (solid/liquid) to distillation (liquid/vapor). Another advantage is reflected in investment and running costs. Tiedtke (1997), e.g., compared these two types of costs for a melt suspension crystallization and a high-pressure extraction process applied in the fractionation of milk fats. For the same capacity, the extraction plant has investment costs three times higher than those of the crystallization process and running costs exceeding those of the crystallization process by a factor of even eleven.

The much *lower level of temperature* and the much *smaller difference in latent heats* are the benefits. In the case of the temperature level, little explanation is necessary when heat sensible substances such as, e.g., polymers or food as described in Tiedtke et al. (1995) are processed. In the case of materials like waste waters from heat-treating processes, a temperature above a certain level can lead to chemical reactions and accelerated corrosion so that a treatment with crystallization instead of distillation would be sensible. A third point in this context is that most known organic chemicals have melting points in a range where low-level waste heat from other processes can be used. This last point becomes clearer after looking at the graph (Figure 7.2) from Matsuoka et al. (1986). His analysis was based on the data available in the *CRC Handbook* (1984). The number of substances are plotted over their melting points. More than 71% of the examined substances have melting points between 0°C and 200°C and more than 86% between 0°C and 300°C.

The just-mentioned advantage of the melt crystallization processes concerning temperature level of the product component do not exist if the comparison is made to the crystallization from solutions (see Chapter 1 in this volume) since the product is crystallized in solution at temperatures lower than its melting point. However, the solvent has to be evaporated, usually in larger amounts, and this fact makes up for the disadvantages in many cases.

A very important point is that crystallization processes are *highly selective* and can lead to a 100% pure product within one separation step—at least in theory—if the mixture to be separated

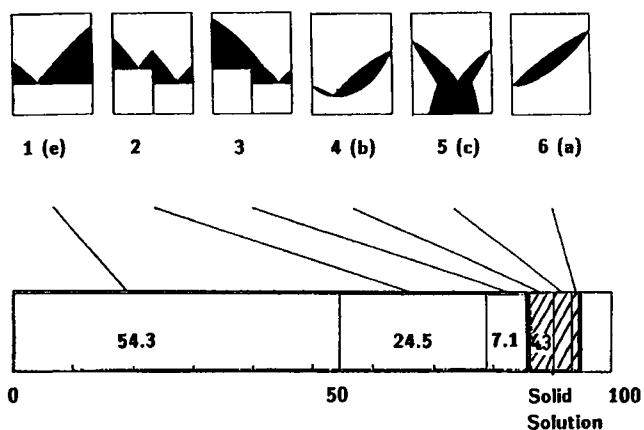


Figure 7.1 Typical phase diagrams: Types of binary organic systems according to Matsuoka (1977) and data from ICT.

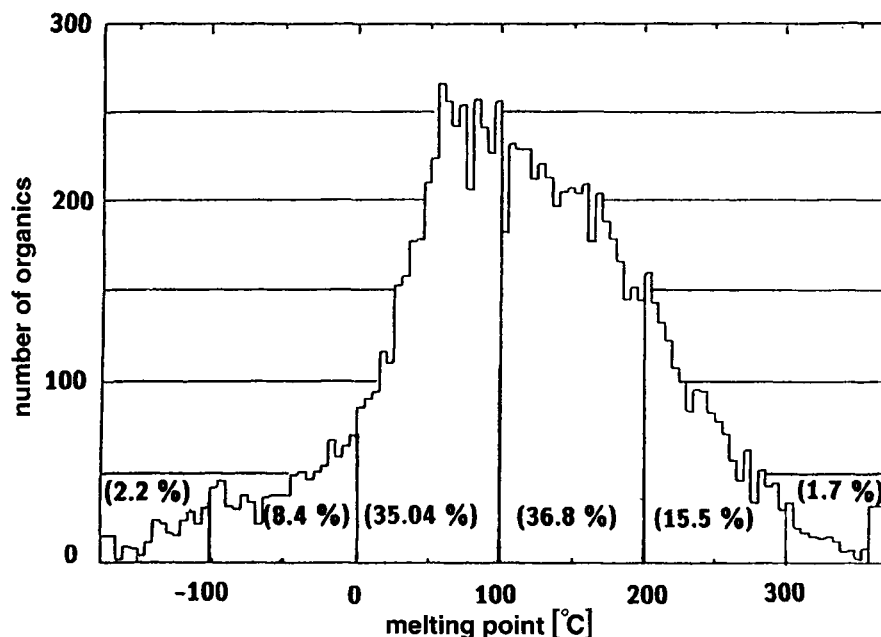


Figure 7.2 Distribution of melting points according to Matsuoka and Fukushima (1986).

is an eutectic one. If a system is eutectic, then product recovery is limited although product purity is not. Here again, it can be shown with a diagram (Figure 7.1) from Matsuoka (1977) that 54.3% of all organic mixtures for which phase diagrams can be found (there are 1,486 in International Critical Tables 1927–1930) are eutectic. Further, 31.6% belong to the group of molecular-forming compounds and systems with peritectic and eutectic points. Only 14.1% of all the investigated substances belong to the group of solid solution-forming substances (over a part or the total range of composition).

In solid solutions, the separation has to be done step by step, as in distillation processes. The number of steps is determined by the phase diagram and the required purity of the product. As a result, complete product recovery is possible, although the number of stages required increases rapidly as recovery approaches unity.

Known solid solution forming systems include: naphthalene–naphthalene; thiophene–benzene; hexadecane–octadecane; and *m*-chloronitrobenzene–*m*-fluoronitrobenzene. Further advantages of melt crystallization are the *smaller volume* of the liquid phase compared to the vapor phase of a substance. A smaller volume leads towards less space or less construction work, which means less capital costs. These advantages are sometimes lost if the process of crystallization and remelting is very slow; therefore, the retention time in the apparatus is high.

The nonexistence of a vapor phase, however, also leads to better control of leakages. *Totally closed equipment* leads to high environmental safety.

Melt crystallization does not need any additional substances, therefore, *no waste water* will be produced and *no other chemicals* (solvents) have to be reprocessed. Solvent recovery capital and energy cost can represent a major portion of a product isolation process utilizing solution crystallization.

7.3. PHASE DIAGRAMS

7.3.1. WHAT TO LEARN FROM PHASE DIAGRAMS

Phase diagrams provide fundamental information about the physico-chemical interaction between the substances in a mixture to

be separated by the crystallization process. The knowledge of the phase diagram gives the information about the temperature level on which the process must be operated as well as the change of composition. This is important in order to ascertain other physical properties, such as density, viscosity, and diffusion coefficient, etc. at the right temperature for the mixture. These physical properties are not only important for the separation process itself but also for the calculation of the flow regime (laminar or turbulent), which is important for the pump design, etc.

The most important information from phase diagrams is the knowledge of the fundamental type of the mixture to be separated. The diagram (Figure 7.1) according to Matsuoka (1977) shows the fundamental types of possible diagrams.

Eutectic forming mixtures provide a theoretical opportunity to achieve one component by crystallization that has 100% purity. This is of course only possible if, on the one hand, the crystal growth rates are so extremely slow that perfect crystals are created and, on the other hand, the necessary solid–liquid separation after the growth process is also perfect.

Solid solutions, which represent the other extreme in the phase diagrams, show that only an enrichment of one component is possible. Therefore, a number of steps would be necessary to achieve the desired purity.

In chemical engineering practice, however, no separation process yields a perfect separation. Therefore, the effectiveness of the process has to be considered. This means more steps are necessary than indicated by the equilibrium phase diagram.

If the melting points of the components are too close, the separation will be difficult for solid solutions. If the feed composition of an eutectic forming mixture is at or near the eutectic point, then no or little product can be recovered. This is true for solution crystallization as well unless the solvent–solute interaction is far from ideal, resulting in different activity coefficients for the components. In such cases other separation technologies should be used.

All that has been said thus far applies only to constant pressure. However, the phase diagrams are affected by change of pressure if the pressure is as high as 10 to 100 MPa. This is demonstrated for *p*- and *m*-cresol, in the work of Moritoki and

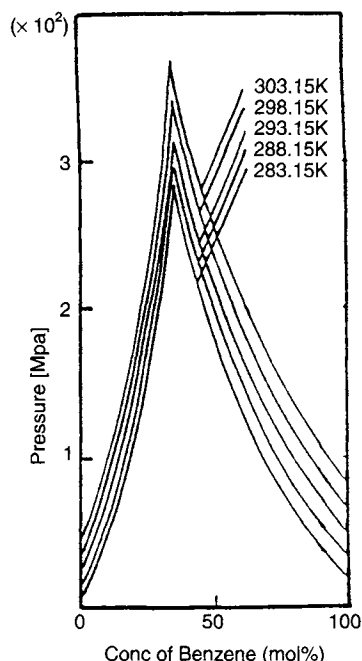


Figure 7.3 Phase diagram of benzene-cyclohexane according to Moritoki et al. (1989)

Fujikawa (1984) and for benzene-cyclohexane, in the work of Moritoki et al. (1989), as shown in Figure 7.3. The dependence of the phase diagram on the pressure can be exploited to improve both, crystallization and post purification steps as is demonstrated for sweating by Freund, König, and Steiner (1997).

One problem is that there are hardly any phase diagrams available giving the pressure dependence, except those published in the works of Moritoki et al. (1979, 1989). In addition to the above mentioned substances this is *p*- and *m*-xylene and benzene from benzene-cyclohexane mixtures.

7.3.2. HOW TO OBTAIN PHASE DIAGRAMS

The method for obtaining phase diagrams is to find the required data in books on physical properties. Some examples are: *International Critical Tables* (1924); *Beilsteins Handbook of Organic Chemistry* (1960); *CRC Handbook* (1984); *D'Ans, Lax Handbuch* (1967); *Ullmann's Encyclopedia of Industrial Chemistry* (1988); *Kirk-Othmer's Encyclopedia of Chemical Technology* (1979); and *VDI-Wärmeatlas* (1988).

If the data required to construct a phase diagram are not available in the literature for the mixture of interest, the data will have to be obtained experimentally. In this case, the determination of the melting points of known compositions of the mixture has to be carried out. Several experimental techniques are described in detail by Sloan and McGhie 1988.

Melting points can be measured with commercially available melting point measuring devices or with highly sensitive temperature measuring instruments. The systems work by detecting the temperature (the melting temperature) at that moment when the optical appearance of the material is changing due to melting. This optical method can be conducted by the human eye or by the change of the light absorption for which laser light is usually used.

Another method is to record the temperature curve as a function of time while the temperature increases with a constant tem-

perature gradient. There will be an inflection in the temperature time curve at the melting temperature, since energy supplied will be used for the phase change, particularly before the sample can continue its temperature increase. A differential scanning calorimeter is quite useful for these measurements.

Many mixtures, however, have a melting zone rather than a melting point. This is due to a number of reasons. One is the error in the detection, another the quality of the specimen. This second point can be caused by an unrepresentative specimen or because of a less than ideal mixture within the specimen.

If an experiment is performed in which the temperature is recorded to detect the point where crystallization begins, one is more likely to find a zone instead of a point. This is due to the different nucleation conditions in each measurement, which is dependent strongly on the statistical distribution of nucleation incidents (metastable zone). Thus, a different supercooling will occur in each measurement before nucleation starts, which will then control the crystal growth. This leads, of course, to differently detected crystallization temperatures (hence a zone and not a point).

The melting point can also be used to specify the purity of a product. This means also that the purification effect achieved by a crystallization process can be evaluated by comparing melting points.

In addition to melting point measurements, there are other methods to evaluate or prove the achieved progress in purification. These are gas chromatography, density measurements, or the different types of color tests.

The achieved purity is quite often plotted in diagrams as an effective distribution coefficient. The *effective distribution coefficient* has been defined by Burton et al. (1953) and Wintermantel (1986) as the ratio of the impurity content in the crystals to the impurity content in the feed melt. Impurities can be incorporated in crystals or crystal layers as a result of a kinetic process.

In the ideal case, very slow, indefinitely slow, crystal growth leads to perfect crystals, which also means perfect purity of the crystals. However, the indefinite slow growth is not possible in industrial applications. Faster growth leads from the perfect, flat, planar crystals to a more rough interface between melt and crystal or melt and crystal layers.

An even faster growth rate, achieved by higher driving forces and expressed by higher temperature gradients, will lead to dendritic type of growth. The dendrites, which look like christmas trees, are still pure crystals but a lot of melt will be entrapped between the dendrites. This melt is, of course, highly contaminated with the not wanted impurities. Due to the fast growth, only a local separation of the compounds occurs. This means the pure compound has formed the dendrite and the impurity is enriched in the remaining, entrapped, melt.

7.4. CRYSTALLIZATION KINETICS

7.4.1. IMPORTANCE OF THE CRYSTALLIZATION KINETICS TO MELT CRYSTALLIZATION

Kinetics in crystallization means nucleation and crystal growth. Both effects are important in melt crystallization but not as important as in crystallization from solutions. In melt crystallization, the process is mainly controlled by the rate of heat transfer and not by mass transfer as it is in solution crystallization.

All crystallization processes need a nucleation step. Nuclei are the smallest solid units to survive and are able to grow as the crystalline substance. The nucleation could be heterogeneous, meaning that particles other than the crystallizing substance itself, e.g., dust or roughnesses of walls, are the nuclei. The nuclei could also be homogeneous, which need considerably higher driving forces to be created. The most common way to start and maintain

crystallization, however, is to have a seeding procedure or a secondary nucleation effect. Secondary nuclei are nuclei of material from the crystalline substance that already exist within the crystallizer apparatus.

The nature of the nuclei and the place where they form inside the crystallizer both influence the following growth process. The nucleation process should therefore be controlled in order to ensure reproducibility. The nucleation details depend strongly on the process and the equipment.

The growth of crystals from the melt is influenced by at least four steps.

1. Transport of crystallizing material from the bulk of the melt to the vicinity of the crystal surface.
2. A surface integration process, which means an integration of molecules into the crystal lattice.
3. A transport of the noncrystallizing substance (impurity) from the vicinity of the crystal surface into the bulk of the melt.
4. A transport of the dissipated heat resulting from the solidification process.

The mass transfer can be influenced by convection, while surface integration cannot. Surface integration is affected by the impurity content. Both effects depend on the temperature level since physical properties such as diffusion coefficient and viscosity are temperature dependent.

Melt crystallization processes are dominated by heat transfer. In the case of melt crystallization in suspension processes, the crystals are surrounded by melt and the system is almost isothermal at the crystallization temperature. The heat of the solidification process is only transported away through the melt. Such a system is often called *adiabatic grown*, which results in moderate growth rates with rather pure crystals.

The so-called solid layer processes (see Section 7.5.), where the crystals are formed on a cooled surface, show nonadiabatic conditions. The heat resulting from the phase change is directly transferred through the crystals themselves and the cooled surface to the outside of the system. Unlike suspension processes, the supercooling at the solid/liquid interface is not limited by the requirement to avoid encrustations at the heat exchanger surfaces since the encrustation is the desired product. Consequently, high supercoolings and, hence, rather fast growth rates are possible. Unfortunately, these are in most cases accompanied by increased impurity concentrations of the crystallized material as will be discussed in detail in the following section.

7.4.2. THEORETICAL APPROACH TO CRYSTALLIZATION KINETICS

For the design and optimization of melt crystallization processes it is vital to have a complete understanding of the process. To this, a detailed knowledge about the crystallization kinetics is essential. Nevertheless, there is only little theory available to describe melt crystallization processes mathematically or to predict their separation efficiency. This is mainly a consequence of the complex heat and mass transfer processes prevailing in the crystallizers which lead to a non-linear system of differential equations for the transfer processes. These equations can only be solved numerically and even then require a considerable number of simplifying assumptions and boundary conditions.

The first important part of every crystallization operation, namely the nucleation step, reveals the same mechanisms underlying the kinetics in the fields of melt and solution crystallization. Therefore, it is here referred to Section 2.2 of this book which gives a detailed introduction into the corresponding theoretical background.

The crystal growth kinetics on the other hand differ in that the heat transfer is the dominant mechanism controlling the process in case of melt crystallization whereas in solution crystallization it is the mass transfer. This, of course is also reflected in the equations describing the process.

In both, layer and suspension crystallization solid material forms from the melt starting with a nucleus through which a solid/liquid interface is created. As crystallization proceeds the mass of solidified substance steadily increases which causes the interface to move. The impurity components remaining in the melt thereby enrich in front of the solid/liquid interface, forming a concentration boundary layer. The concentration profile in this boundary layer changes as the interface advances which is in literature referred to as "moving boundary problem."

Among the first ones to present a complete theoretical approach are Burton, Prim, and Slitcher (1953). The authors developed a mathematical formulation of the problem for metallic systems with partial solid solubility crystallized from the melt in a suspension process. Their theory is based on a boundary layer model and does not account for the mutual dependence of heat and mass transfer but regards the influence of heat transfer as negligible.

Cheng et al. (1967) empirically extended this model to the crystallization of organic, eutectic forming mixtures the crystalline layers of which contain liquid inclusions. However, their model does not consider the influence of the growth rate on the amount of liquid inclusion incorporated in the layer and therefore even contradicts own experimental findings of the authors. Based on these publications Wintermantel and Kast (1973) developed the "v/k-criterion" which enables the prediction of the maximum allowable growth rate v at which the layers still grow essentially pure i.e., without incorporating liquid inclusions as a function of the mass transfer coefficient k . In a later publication Wintermantel (1986) introduces an equation which is founded on the v/k criterion and describes the relationship between physical properties of the substance, parameters of the process, and the separation efficiency more successfully for the case of eutectic forming, aqueous and organic mixtures:

$$k_{eff} = 1 - \frac{c_i - c_\infty}{c_\infty \cdot \left(e^{\frac{v_{cr}}{k} \cdot \frac{\rho_s}{\rho_l}} - 1 \right)} \quad (7.1)$$

with

$$k_{eff} = \frac{c_{cr}}{c_\infty}$$

where k_{eff} is the effective distribution coefficient, c_i is the concentration at the solid/liquid interface, c_{cr} is the average concentration in the layer, c_∞ is the concentration in the bulk, v_{cr} the velocity of the interface normal to the crystal surface, k is the mass transfer coefficient, ρ_s is the solid density, and ρ_l is the liquid density.

Unfortunately, the concentration at the solid/liquid interface c_i changes with time and usually is unknown which makes a calculation of the effective distribution coefficient impossible. However, Wintermantel (1986) was able to show that equation (7.1) provides a valuable means to uniformly describe the relationship between the effective distribution coefficient and the process parameters if it can be shown experimentally that c_i is only a function of v_{cr} , k , ρ_l , and ρ_s . The applicability of this approach could be successfully shown by a number of authors in the meantime (e.g., Kehm (1990) and özoguz (1992)). Its advantage is that the user does not have to worry about the special process and its operating conditions since these parameters are not contained in

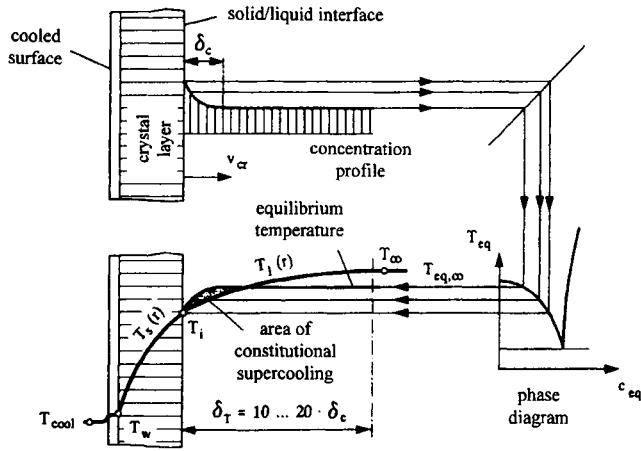


Figure 7.4 The impose temperature profile ($T_L(x)$; $T_S(x)$) and the equilibrium temperature profile (T_{eq}) encircle the area of constitutional supercooled melt (shaded area).

the equation. As mentioned above, however, the approach also neglects the coupling of heat and mass transfer in crystallization processes. For this reason, the prediction potential of the approach is limited to systems which exhibit a rather weak dependence between heat and mass transfer.

A second kind of approach avoids this disadvantage by taking the mutual dependence of heat and mass transfer into account. These approaches were introduced by Rutter and Chalmers (1953) and are referred to as the “gradient criterion.” Their theory is based on the conditions shown in Figure 7.4. As can be seen in the diagram, the solidification of material onto the growing solid layer leads to the rejection of impurities which in turn are enriched in front of the solid/liquid interface. These impurities form a concentration boundary layer since the diffusion of the impurities back into the mother liquor usually is slower than the actual crystallization. To this concentration profile, a profile of equilibrium temperatures corresponds resulting from the phase diagram. Depending on the specific process conditions the real temperature can locally be lower than the equilibrium temperature leading to an additional supercooling in front of the solid/liquid interface. This effect is called “constitutional supercooling” (see shaded area in diagram) and leads to dendritic growth of the layer, which in turn causes the incorporation of impurities into the crystalline layer, thus resulting in an impure product. To quantify the conditions at which no constitutional supercooling occurs, i.e., pure layers are produced, Rutter and Chalmers demand the gradient of the real temperature at the solid/liquid interface to be greater than or equal to that of the equilibrium temperature:

$$\frac{\partial T_{eq}}{\partial x} \leq \frac{\partial T}{\partial x} \quad (7.2)$$

with

$$\frac{\partial T_{eq}}{\partial x} = -m \cdot \frac{v_{cr}}{D} \cdot \frac{\rho_s}{\rho_l} \cdot e^{\left(\frac{v_{cr} \cdot \rho_s}{k \cdot \rho_l}\right)} \quad \text{and} \quad \frac{\partial T}{\partial x} = \frac{\alpha}{\lambda} \cdot (T_i - T_\infty)$$

where T_{eq} is the equilibrium temperature, T is the actual temperature, T_i is the temperature at the solid/liquid interface, x is the distance from the cooled surface, m is the linear gradient in the phase diagram, D is the diffusion coefficient, α is the heat transfer coefficient, and λ the heat conductivity.

The strictness of this criterion could be reduced by subsequent investigations as e.g., Wintermantel (1972) and Scholz (1993). The experiments revealed that the growth of pure layers is also possible under constitutional supercooling conditions as long as a certain maximum level of supercooling is not exceeded. However, even applying this weaker criterion often leads to uneconomical growth rates in the industrial process. For this reason, the optimum between an economical growth rate and a still acceptable product purity has to be searched for every process and substance mixture.

A modified version of this criterion was developed by Mullins and Sekerka (1964). The authors attribute the incorporation of impurities essentially to the nonplanar growth of the crystalline layer and analytically describe this by superposing a planar layer with a sinusoidal disturbance. Afterwards, they determine the conditions under which this disturbance is damped and derive a criterion which generally guarantees such conditions during the process. The applicability of this stability criterion was proven for a variety of metallic and organic compounds.

The disadvantages of the approaches described above, namely the v/k approach and the gradient criterion, are that they both do not provide an analytical relationship between the separation efficiency and the process parameters, i.e., they still rely on experiments. Furthermore, they assume a planar growth of the crystalline layer which often contradicts reality. This nonplanar growth of the crystalline layer has liquid inclusion of impure mother liquor as a consequence and hence leads to an impure layer. However, these inclusion do not necessarily remain in the layer since the temperature gradient always present in the layer causes a migration of the inclusion towards the warm side of the layer. The migration rate of these inclusion is of special interest because it determines the time necessary to remove the inclusions from the layer. For this reason, researchers in the field developed correlations to predict the migration rate as a function of process parameters. Assuming, that diffusion in the inclusion is the determining factor in the migration of liquid inclusions and that the influence of convection is negligible Wilcox (1968) gives the following relationship for the influencing parameters

$$D \cdot \frac{\partial^2 c}{\partial x^2} + v_{mig} \cdot \frac{\rho_s}{\rho_l} \cdot \frac{\partial c}{\partial x} = 0 \quad (7.3)$$

where v_{mig} is the migration rate.

By integrating Eq. (3) twice with the corresponding boundary conditions and further introducing the experimentally found restriction, that all inclusions are smaller than $100 \mu\text{m}$, Scholz (1993) finally derived the following correlation for the migration rate

$$v_{mig} = \left(\frac{\rho_l}{\rho_s} \cdot \frac{D}{m \cdot c_{cry}} \right) \cdot \frac{dT}{dx} \quad (7.4)$$

where c_{cry} is the concentration at the crystallizing side of the inclusion.

Equation (4) is based on experiments with different water/sodium-chloride mixtures and yields good agreement between experiment and calculations. Henning and Ulrich (1997) and Henning et al. (1995), however, conducted detailed experiments regarding the migration of liquid inclusions for various caprolactam/water mixtures and did not only find, that the inclusions can be considerably larger than $100 \mu\text{m}$ but also that they grow and change their shape during migration. The authors, therefore, indicate a growing demand for a correlation which accounts for these factors.

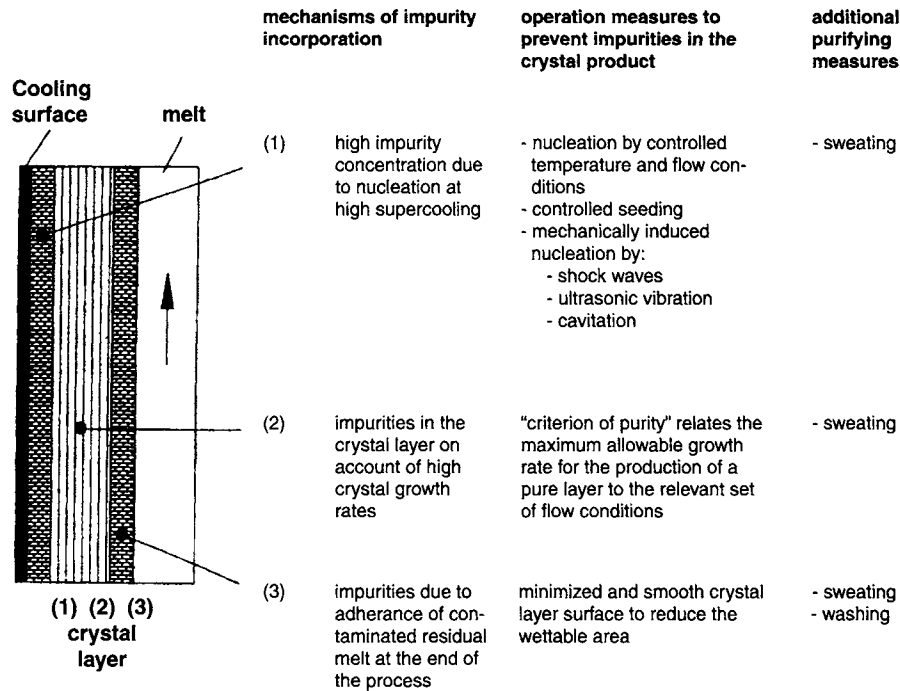


Figure 7.5 Mechanisms of impurity incorporation, measures to prevent it, and additional purification steps.

The effect of the migration of liquid inclusions theoretically enables the creation of completely pure crystalline layers, namely if the migration rate is in the same order of magnitude as the crystal growth rate.

If the migration rate of the inclusions is considerably lower than the crystal growth rate, the crystallization will yield a layer still containing inclusions. In order to remove them, additional purification steps such as sweating and washing will be necessary (see section 7.8 and 7.9). Figure 7.5 shows the different possible origins of inclusions in the layer as well as measures to reduce or even prevent them. Along with this information the potential of the post purification steps to partially or fully remove the inclusions is listed.

7.5. SOLID LAYER CRYSTALLIZATION

A solid layer type of crystallization from the melt is often called *progressive freezing* (see, e.g., Jančić 1989), or *directed crystallization* (Ulrich 1988), and *directed solidification* (Smith 1988). All expressions describe a crystal layer growing perpendicular to a cooled wall and use the phase change as the basis for the separation of the feed mixture. This is possible due to different equilibrium concentrations of the solid and liquid phase of a mixture (see Section 7.3.).

7.5.1. ADVANTAGES

The main advantages of the solid layer crystallization techniques are as follows:

- No incrustations problems since the incrustations are the solid layers, which are the product, and formation and removal is controlled by equipment operating strategy.
- Good controllable crystal growth rates (layer growth rates) due to a good controllable driving force (the temperature difference through the cooled wall).

- Hardly any solid-liquid separation problems due to draining by gravity and separately discharging the liquid residue and the remolten solid layer, hence, the product.
- Easy possibilities for post crystallization treatments of the crystal layer on the cooled surface. Treatments such as "sweating" and "washing" should lead to a further purification of the product (see Sections 7.8. and 7.9.). The amount of impure liquid entrapped in the layer or sticking on the surface of the crystal coat should be reduced by these treatments.
- Easy to operate equipment due to no slurry handling in the equipment. That means that other than pumps, there are no *moving parts* in the process.
- Easy staging opportunities, since the product leaving the process needs no treatment in order to be ready for the next production step.

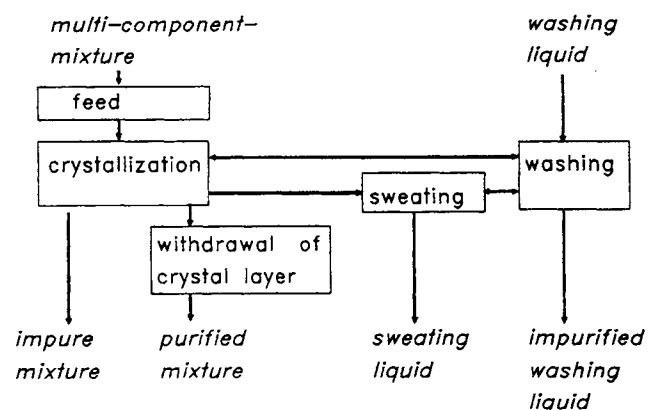


Figure 7.6 Flow diagram of possible process steps in solid layer crystallization.

Figure 7.6 is a flow diagram showing all liquid streams and all operational steps in a solid-layer process.

7.5.2. LIMITATIONS

Limitations are to be found mainly in four points. First, the limited surface area of the cooled surface and thereafter the surface area of the solid layer, since the surface area is a limiting factor for mass transfer processes. This is a weak point in solid layer processes compared to suspension processes.

Second, solid layer formation by the product on the heat transfer surface requires either an increase in temperature driving force to maintain the same growth rate (therefore production rate) or leads to a reduction in capacity with increasing thickness.

Third, it is a limiting point that the product sticks like an encrustation on the cooled surfaces of the apparatus and has to be remolten in order to be discharged. This requires not only additional energy for melting the crystal coat but also a partial heating up of the whole apparatus. On the other hand, this remelting makes it necessary to have batch processes.

Finally, in some cases it can also be a disadvantage for the product to leave the apparatus in liquid form and to be solidified again. The last point as well as the third, could well be avoided someday if it becomes possible to build continuously operating processes in one plant for solid layer melt crystallization processes.

7.6. SUSPENSION CRYSTALLIZATION

7.6.1. ADVANTAGES

Mass transfer processes are governed by the driving force difference in the chemical potentials, the physical proportions (mass transfer coefficient) of the substance, and the surface area (the interface between the phases to be separated). This is known from the basic transport equations of heat and mass transfer. A large surface area, therefore, favors separation processes. A suspension with a distribution of mainly small particles would feature a high interface area. There is, however, a limitation to the size of the disperse solid phase. This is due to the necessary liquid-solid separation at the end of the process, on the one hand, and the necessity of the disperse phase to move in different directions as the main flow direction of the continuous phase so that a maximum of the driving potential between the two phases can be maintained, on the other hand.

A second advantage of suspension processes is that remelting the solid phase in order to clear the apparatus as necessary in progressive freezing processes is *not* necessary here. This saves energy and also the potential process step of resolidification in pastilles or other forms as requested by customers.

The third major advantage is that due to more moderate crystal growth rates and the large surface area, very high pure crystals are created. The crystals exist as crystalline particulate solids as the final product.

7.6.2. LIMITATIONS

Limitations are found in the field of the apparatus mainly in the slurry handling, in dealing with moving parts of the apparatus, and with encrustation problems. All the just-mentioned limitations are connected in one way or another with each other. In other words, special pumps to handle the suspensions, stirrers to avoid sedimentation, and discharge units are necessary and might lead to problems.

The second set of problems occurs when preparing the final product. The very pure crystals must be separated from the

remaining, highly contaminated liquid. This requires unit operations such as filtration, centrifugation, and washing by either a solvent or the melt which is in most cases purified product or feed material. Afterwards a "drying" step is required during which the remaining impure melt or the washing liquid, respectively, evaporates or solidifies on the surface of the pure crystals. During this last step, caking is often a problem needing attention. The additional operations are costly, need energy, contaminate already purified products, or reduce the production capacity from reflux of pure product as wash.

Only moderate growth rates can be achieved as compared to the very high rates in solid layer crystallization. This is due to the isothermal growth, whereas in the layer technique, high thermal gradients can be forced on the crystals within the layer.

Finally, but *very importantly*, are the limitations in many of the suspension techniques due to high viscosities of the melts and to very small differences in densities between the melt and the crystals. These difficulties always occur when the process depends on natural settling velocities of the solids within the melts.

7.7. CONCEPTS OF EXISTING PLANTS

Concepts of plants and/or existing and commercially available equipment can be divided according to different aspects (see Figure 7.7, Özoguz 1992). One possibility is to split suspension techniques and solid layer techniques, another possibility is to split up continuous and batch type equipment. One other point to distinguish is the question of whether the melt is moving (flowing) or stagnant.

Continuously operated plants will be discussed in Section 7.10. Most suspension crystallizers for melt crystallization require crystals to be in the feed stream. In most cases, these crystals originate from scraped crystallizers, which are based on a solid layer created at the wall of a crystallizer vessel and then scraped off, in most cases, by a rotating steel blade. Such equipment is commercially available for various purposes (cf. Ruemekorf 1993) from, e.g., Gresco, a subsidiary of Niro Process Technology, B.V. which in turn belongs to GEA Process Technology (1997).

7.7.1. SOLID LAYER PROCESSES

The first group to be discussed is the batch type of solid layer techniques with stagnant melts. Here, for instance, the Proabd Refiner (GB-PS 1958; GB-PS 1959; DE-AS 1976; FR-PS 1980; FR-PS 1981) and the Hoechst AG process (see Rittner and Steiner 1985) have to be named. Both processes feature cold surfaces, usually in the form of tubes in which in the stagnant melt is located inside or outside. The melt feedstock is progressively crystallized. As the crystallization proceeds, the remaining melt becomes more and more impure. The crystallization process needs about 2–30 h. The remaining residual melt is allowed to drain after the crystallization is stopped by an opening at the bottom of the apparatus. The product is achieved by melting the crystal coat and collecting it in a different tank than the residue. A film of highly contaminated melt of residue composition will be held back on the crystal coat. This film, or at least most of it, can be removed by some post-crystallization treatment. This treatment can be a washing or a partial melting, which is called a *sweating step* (see Sections 7.8 and 7.9). The two apparatus can be seen in Figures 7.8 and 7.9 respectively. A production cycle can be 15–20 h according to Proabd patent (FR-PS 1981), and even up to 50 h according to Erdmann (1975) for Proabd types of equipment.

According to Rittner and Steiner (1985), plants of the Proabd type for the refining of, e.g., *p*-nitro-chlorobenzene, *p*-diclorobenzene,

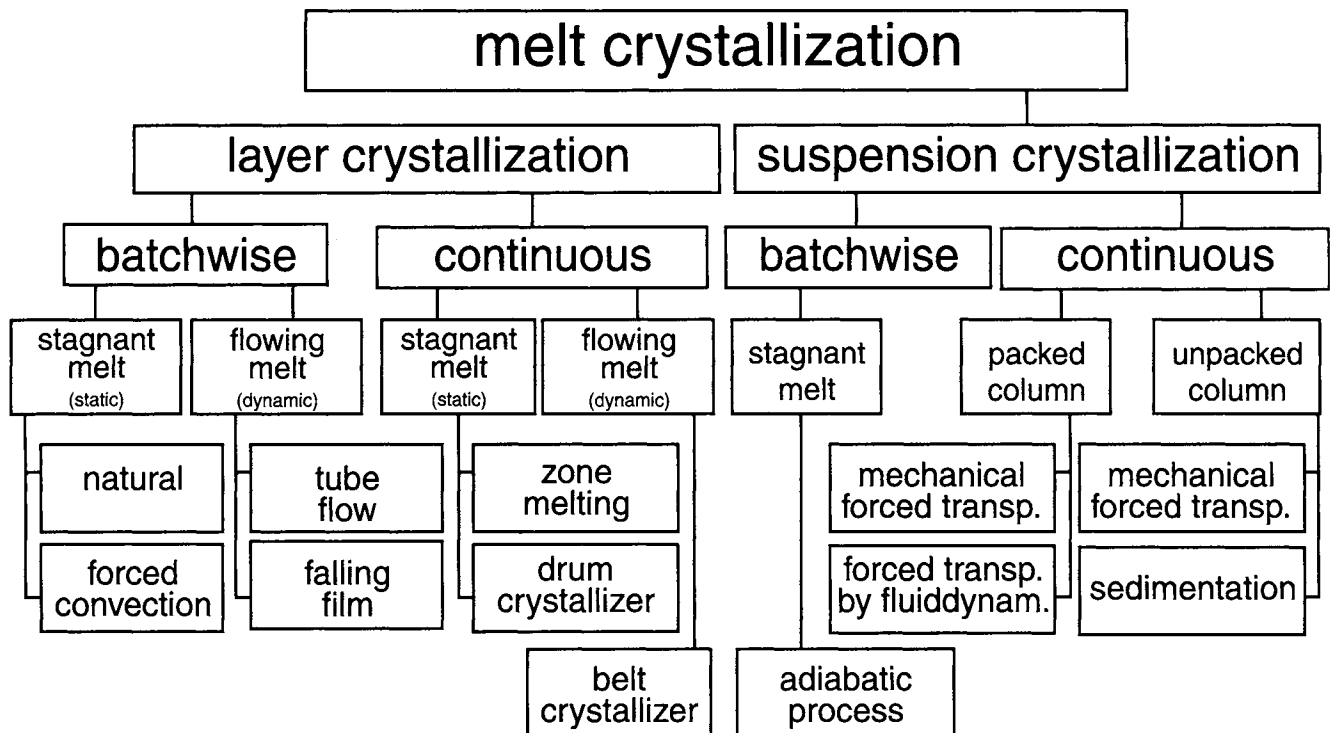


Figure 7.7 Melt crystallization, a structure of different aspects to subdivide.

dichloronitrobenzene, monochloroacetic acid, naphthalene, phenol, and anthracene, have been built in western Europe.

Sulzer Brothers, Inc. (1988), offer a type of equipment that functions on the same principle, using cooled plates instead of tubes.

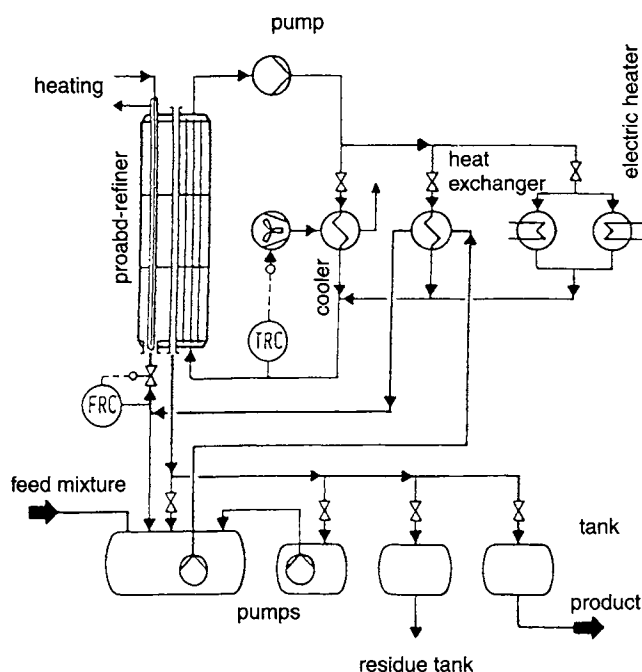


Figure 7.8 The Proabd process. (Reproduced with permission of Rittner and Steiner 1985.)

The second group of the batch type of solid layer techniques are those with moving melts. Here again, three processes must be named: the MWB-Sulzer, nowadays called Sulzer falling film (CH-PS 1967; U.S. 1985), the ICI-process (GB-PS 1964), and the BASF-process (DE-PS 1976), which is now distributed by the Kvaerner company. In all processes, the crystallization takes place on the inside of tubes, which are cooled from the outside. The melt coming from a feed tank is continuously circulated through the tubes until the crystal coat at the walls is thick enough, i.e., until

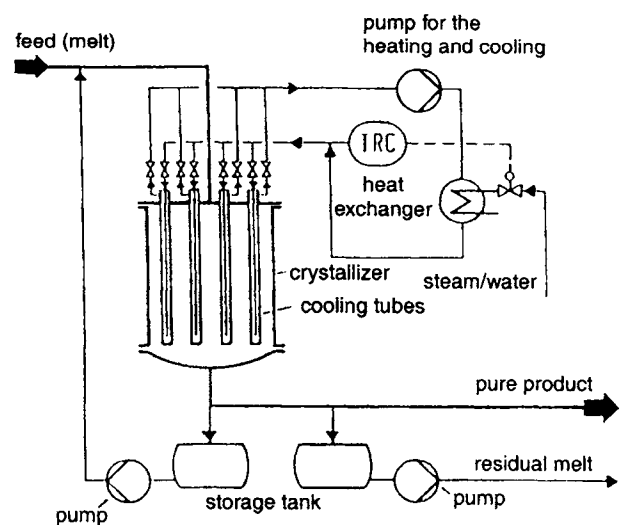


Figure 7.9 A tube bundle crystallization plant of the Hoechst Company. (Reproduced with permission from Rittner and Steiner 1985.)

the desired percentage of product from the amount of feed is reached. In all cases, crystal clear post-treatments like sweating and washing can be and are conducted.

All three processes can easily be used for multistaging if extremely high purities are needed. Each stage after another can be conducted in the same crystallizer just by storing the products of the different purities in different tanks. All processes have, aside from pumps no moving parts and produce a product in liquid form.

The important difference is that the Sulzer falling film process, as indicated by its name, features a falling film on the inside for the product and on the outside for cooling fluid. The ICI as well as BASF processes have spaces completely filled by themelt inside the tubes and on the outside by the cooling fluid. The last two processes function with standard tube bundle heat exchangers with a length up to 10 m. A modified version of the Sulzer falling film process (see EP 0 811 410 A1 (1997)) does not realize the cooling as a falling film but condensates the refrigerant on the outside of the tubes instead, thus enabling a constant temperature along the length of the tubes. This in turn leads to more homogeneous thickness of the crystalline layer and, consequently improves the efficiency of post purification steps.

The BASF process is recommended, e.g., for acrylic acid, adipic acid nitril, and β -naphthol. According to Ritner and Steiner (1985), this process has not been used on a commercial scale.

The Sulzer falling film process, however, is built throughout the world for a variety of products. The equipment has 12-m high tubes as the standard, and scale up is achieved by adding tubes or a new apparatus of tubes. The largest equipment so far has 1100 tubes, which means it is 4 m in diameter, and produces with two apparatus of that size 100,000 tons per year of a product with a purity in the parts per million range. The picture depicted in Figure 7.10 shows a crystallizer that is in production at the Sulzer Brothers Company, Winterthur, Switzerland. Figure 7.11 shows a plant in Brazil for producing *p*-dichlorobenzene, which has tube bundles of 250 tubes that are 12 m height. To show the size of the

equipment, compare the size of the distillation columns on the right. (These having nothing to do with Sulzer falling film).

More materials are purified by the Sulzer falling film processes (Sulzer Brothers, Inc. 1988), some of which are included in the following list:

- Bisphenol
- Acrylic acid
- Benzoic acid
- Fatty acids
- Pharmaceutical intermediates
- Nitrated aromatics
- Caprolactam
- Naphtalene
- Monochloroacetic acid
- Palm oil
- Dichlorobenzene
- Tetrachlorobenzene
- Chloro-Nitrobenzene
- Hexachlorophenylene
- Mono-, di-, trinitrotoluene
- Isocyanates
- Alpha-/Beta-Naphthol
- Diphenylphenol
- Xylenole
- p*-Xylene
- Aqueous solutions
- Chlorinated aromatics
- p*-Cresole
- p*-Phenylene-diamine
- Phenol
- Anthracene

The third group we will discuss are the patents of the Ruttgers Company (DE-OS 1982; EP-OS 1982) and the patent application of the Sulzer Brothers Company (CH-V 1990) that improves the mass transfer by mixing without circulating the melt.

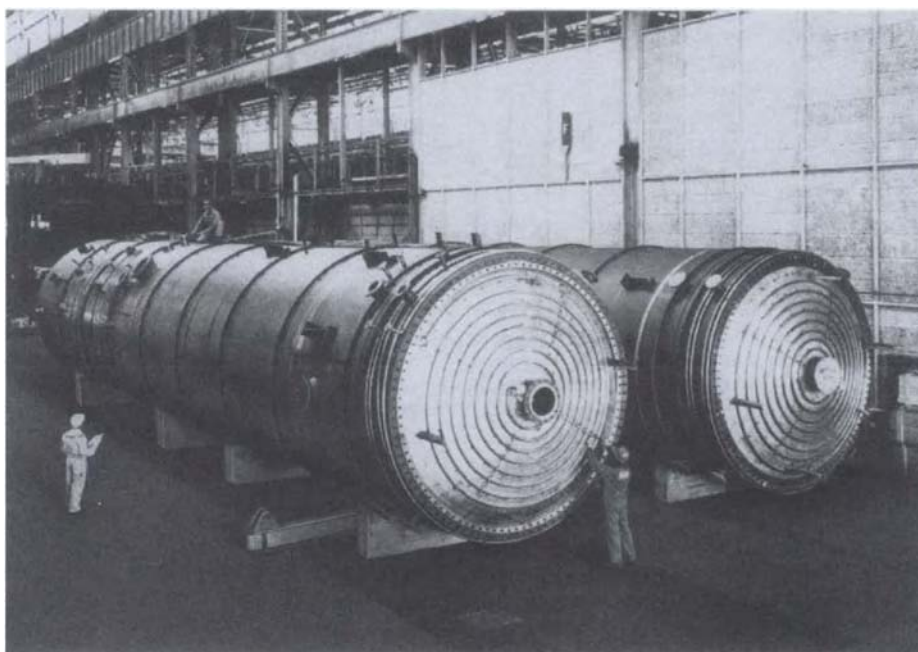


Figure 7.10 Two Sulzer falling film crystallizers with 1000 tubes each and a 12 m tube height under construction. (Courtesy of Sulzer Brothers, Inc.)



Figure 7.11 Crystallization plant of the Nitro Chlor Company, Brazil, built by Sulzer Brothers. (Courtesy of Sulzer Brothers, Inc.)

The aim of mixing in front of the boundary layer of the crystallization front to reduce the concentration gradients is achieved by the Ruttger process with bubbles of inert gases. The bubbles rise from the bottom of the vertical tube that serves as crystallizer. The crystallizer tube is cooled from the outside and the solid layer crystallization takes place on the inside wall. The inert gas is introduced through a thin central tube within the crystallizer coming from the top, which has its outlet at the bottom of the crystallizer. The gas bubbles form a plug and mix the melt when they rise through the crystallizer. This process has been built as a pilot plant. It is shown schematically in Figure 7.12.

The Sulzer process uses a pulsation of the melt in a static-tube type of melt crystallizer. The pulsation of the bubbles in the Ruttgers process should serve the purpose of mixing in order to reduce the boundary layer thickness.

In the papers of Ulrich et al. (1990) and Kuszil (1990), it was shown that when diffusion coefficients are low, viscosities are high; therefore natural convection is low. This means that the boundary layers are thick and only poor separation effects can be achieved. This is especially true in cases of rapid crystallization rates. In these cases, however, a mixed process, e.g., by pulsation, can reduce the impurity by as much as threefold compared to a process with a stagnant melt (see Kehm (1990)). The apparatus is shown in Figure 7.13.

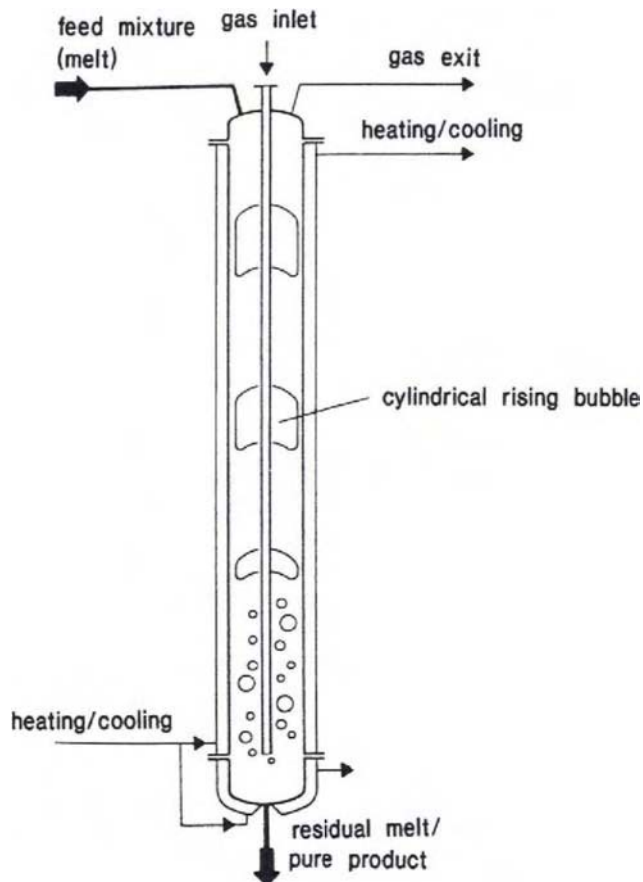


Figure 7.12 Bubble column crystallizer according to the Ruttgers patent. [Reproduced with permission from Rittner and Steiner (1985).]

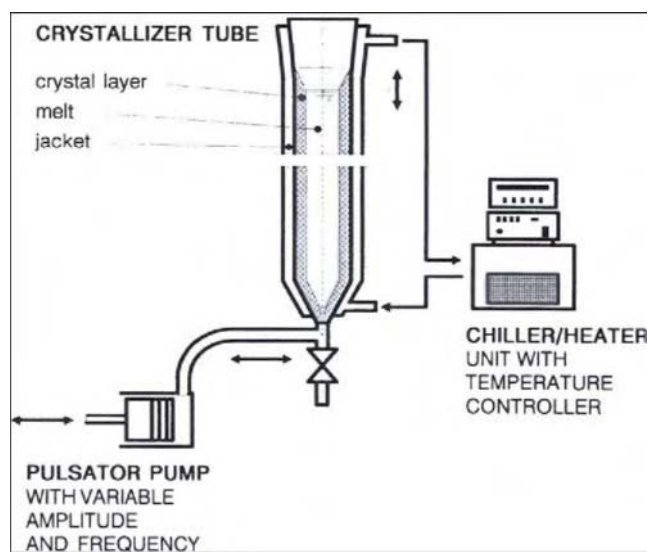


Figure 7.13 Pulsed crystallizer according to the Sulzer Brothers patent.

As an example, for the purification of caprolactum, it has been shown that the effectiveness of such a pulsation of the melt is especially helpful in cases of a low impurity content. It is rather easy to add a pulsation pump to an existing static crystallization unit, which makes it more efficient. In many cases the pulsation should be applied only in the final stage when impurity content in the feed is lowest, because the pulsation unit is most effective at that time, and additional costs and additional energy input in the crystallizer can be avoided in the earlier stages.

In order to set the design procedure for batch-type layer crystallization processes on a somewhat more theoretical basis rather than on empiricism, several authors as, e.g., Neumann (1996), Guardani and Belline (1997), and Bierwirth (1998) developed approaches to predict the separation efficiency of a process as a function of the properties of the mixture and the considered plant principle. However, all approaches still require experimental data *keff* as the basis for the calculation, even if the total necessary number of tests could be considerably reduced.

7.7.2. SUSPENSION PROCESS CONCEPTS

In the group of suspension processes, there are the jacket cooled and the directly (e.g., by inert gases) cooled processes. The Amoco process, on the one hand, and the Maruzen or Chevron process, on the other hand, are, according to Ransley (1984), representatives for such processes. Other developments are scrapes crystallizers according to the Humble-Oil, the Krupp-Harpen (see Ritzler 1973), or the Hoechst AG (DE-PS 1969) process which are used for the production of *p*-nitrochlorobenzene. These scraped surface crystallizers are in fact solid layer processes, but in the handling of the products—crystals in suspension—they have to be treated like suspension processes. A number of processes that feature a combination of a scraped crystallizer and suspension techniques will be discussed.

Before discussing the above-mentioned equipment crystallizers with rotating discs, which provide smooth mixing of the suspension, should be introduced. This is a process unit that has different chambers in which crystals are created by nucleation and grown while moving from one chamber to the next. Such equipment is built by Goudsche Maschinefabriek B.V. (1984) and provides quite a number of products, such as *p*-dichlorobenzene, *p*-chlorotoluene, and fatty acids. The solid-liquid separation is the primary disadvantage of the apparatus; however, the simple construction and operation features application of the apparatus for smaller product quantities. Also, crystallizers with direct immixable coolant should be mentioned, wherein the crystals are taken out by centrifugation and the coolant is recycled (Newton-Chambers Process, Molinari 1967). The advantage of the direct coolant is the energy efficiency. The disadvantages are problems with separating the coolant gas completely from the crystals, and that the gas bubbles hamper the growth of the crystals by occupying the crystal surface. Plants were built in 1964 for the purification of benzene, according to Molinari (1967).

One type of suspension processes using a scraped crystallizer to create the feed suspension is the Phillips process (see McKay 1967). The crystallizer consists of a vessel with filters in the wall of the upper section. There is a heater at the bottom to remelt the crystals. Some of the melt is taken as product, some is used as reflux. The reflux serves mainly as washing liquid for the crystals which are forced downward by a reciprocating piston, or with pulses from a pulsator pump. The Phillips crystallizer column is shown in Figure 7.14.

The pumping helps to wash away the highly contaminated liquid sticking to the crystals. The contaminated reflux melt, which worked

its way through the crystal bed, leaves the crystallizer through the wall filter. Details about mass flow rates, equipment size, and purified substances other than paraxylene are discussed by Walas (1988).

The TNO crystal purifier (Arkenbout et al. 1976) is a column with a number of sieve trays fixed to a central shaft that oscillates vertically. The trays have bouncing balls caused by the oscillation. The balls break up some of the crystals through collisions. Small crystals melt quickly because they have greater solubility than larger ones, thereby enriching the melt with pure product. The large crystals in the slurry feed, which are introduced in the middle of the column, move down and become remolten. Some of the remolten liquid is removed as product, some is used as reflux. The small crystals move up with the reflux and will be molten. The highly contaminated reflux is removed from the column at the top. A pilot plant column with 19 trays has been built and is expected to have a capacity of 300 tons per year.

According to Arkenbout (1978), the first compound to be purified was naphthalene. This was achieved after successful results with laboratory scale in the purification of *p*-xylene from an eutectic system and benzene-based system as a solid solution system. There is no published data on industrial experience for this process.

A third process, the Kureha Double Screw Purifier (Yamada et al. 1982), also called the KCP column, works with a crystal slurry introduced at the bottom of a column. The crystal is transported to the top by a double screw conveyor. There is a melter at the top of the column. The molten crystals are the product and some part is used as reflux. The reflux washes the crystals while moving in a counter current direction. Some residue is taken out at the bottom.

A commercial unit is used to produce 7000 tons of *p*-dichlorobenzene per year. The process is described in more detail by Rittner and Steiner (1985) and can be seen in Figure 7.15.

A fourth process is the Brennan-Koppers crystal purifier (Brennan 1982). The apparatus has wall filters like the Phillips column and a melter at the top like the Kureha process. The crystals move up due to the movement of the liquid. The crystal bed is held compact with a rotating top plate, which is called a harvester. Some crystals at the top of the bed are collected (scraped off) and some openings thereafter permit these crystals to enter the melting zone at an adjustable rate. Some of the remolten liquid flows back through the harvester and washes the crystals in the bed. The residue leaves the apparatus by the filters. Details are given in the patent cited above.

The so-called TNO-Thijssen crystallization process (Thijssen and Arkenbout 1983; Arkenbout et al. 1984) is again a combination of a countercurrent flow-through cascade of scrape crystallizers and a washing column with countercurrent movement of melt and crystals. The crystallizer has a special design. The slurry enters at the top, flows into the washing column and forms a rather dense bed due to the discharge of the melt by filters in the walls of tubes inside the column. Crystals then move through a rather diluted section and become remolten. Some of the product of the remolten crystals is used as reflux. The equipment has been successfully applied in aquarius concentration processes and for paraxylene.

The concepts introduced here are not all available on the market. However, this is only intended to provide information about possible designs and process varieties. All the described equipment and processes have their strong and weak points, and no general principles for the selection are available. The selections have to be based on the substances to be purified and the required purities to be achieved.

The postcrystallization treatments discussed in the following sections should also be carefully taken into account before a decision is made.

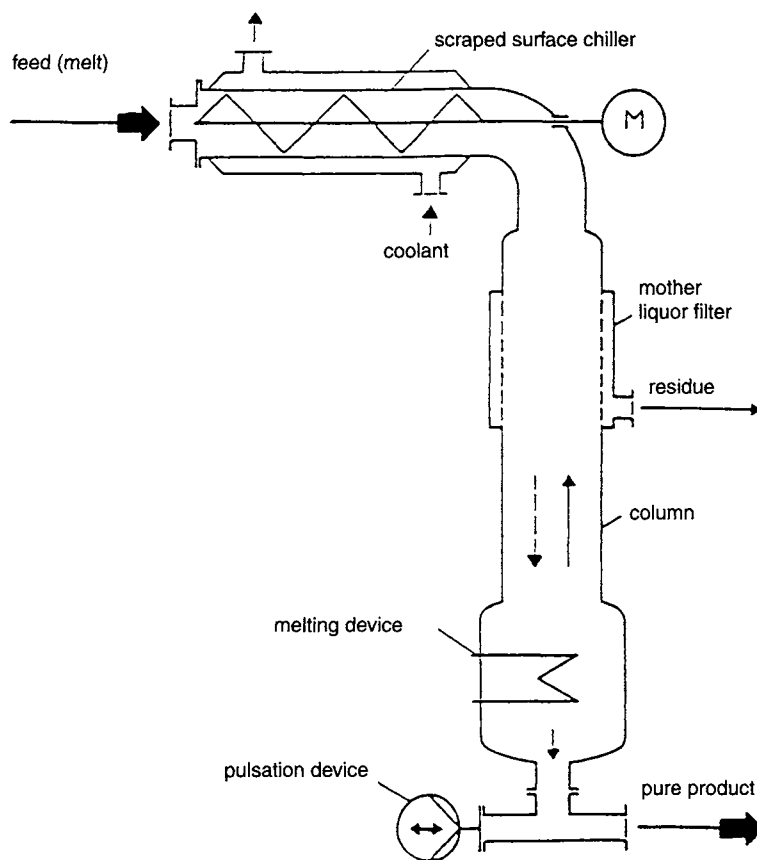


Figure 7.14 Phillips crystallizer column. (Reproduced with permission of Rittner and Steiner 1985.)

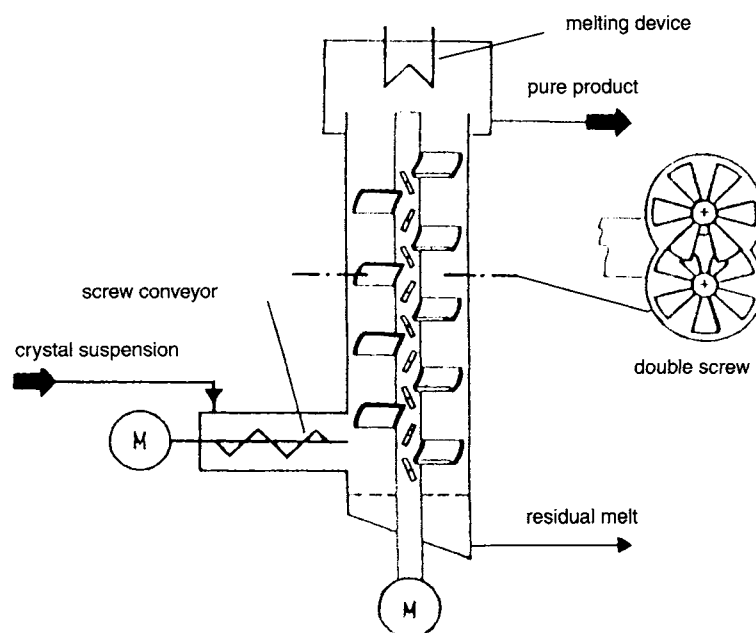


Figure 7.15 The double screw KCP column. (Reproduced with permission from Rittner and Steiner 1985.)

A brief reference should be made to the high-pressure crystallization presented in many papers by Moritoki et al. (1984b) (Kobe Steel Company). The pressure applied is up to 300 MPa under adiabatic conditions. The high-pressure equipment works batchwise in cycles of about 20 min. The pressure is increased in steps of 20 MPa. At a specific time, about 10 out of a total of 20 min, the pressure is slightly released.

The period of released pressure is used as sweating time (see the following section). After discharge of the created crystals the remaining highly contaminated melt must be separated before receiving the pure product. The equipment is used industrially, e.g., for the purification of *p*-cresol from *p*-/*m*-cresol mixtures. Successfully executed experiments on the laboratory level are described by Moritoki et al. (1989) for the purification of benzene from benzene-cyclohexane mixtures.

7.8. THE SWEATING STEP

Sweating is defined in, e.g., Ulrich and Bierwirth (1995) as a temperature induced purification step based on a partial melting of crystals or crystal layers by means of a warm gas or heating of the cooled surface closely up to the melting point of the pure component. As a consequence, the impurities adhering to the crystal surface and those contained in pores of the crystalline material remelt, partially dilute with pure material and then drain under the influence of gravity. The temperature rise going along with the sweating simultaneously reduces the viscosity of the impurities and thus further eases the draining off.

A process step of this kind is used with the knowledge that it leads to less product. However, the liquid film sticking on the crystal surface or crystal layer surface on the one hand and the liquid inclusions on the other hand are highly contaminated and

therefore reduce the overall purity of the product considerably. Therefore, from an economical point of view it is worthwhile to reduce the amount of product by the sweating step and raise the purity at the same time. It is not always recommended to conduct a sweating operation in the fastest possible way, according to Ulrich and Özoguz (1990). The sweating step remains, however, much faster than a crystallization step. Furthermore, it does not require another phase transformation as does the latter and hence saves the corresponding amount of energy, especially if layer processes are considered where a final heating up is necessary in any case in order to remove the crystal layer from the cooled surfaces.

According to Jančić (1989), the product lost in a sweating step is about 10%. The sweating times are also rather different with respect to the processes. Between 10 min in the dynamic Sulzer falling film process (see Jančić 1989) and 30 h in case of the static Hoechst process (see Rittner and Steiner 1985) are example sweating times for the purification of monochlorous acetic acid.

In addition to the advantage of draining off the attached liquid film, the important part of the purification effect is that the liquid inclusions have a lower melting temperature. At temperatures where the product compound is still solid, the impurity is already liquid or becomes liquid and will therefore drain out of the crystals and crystal coats. According to Matsuoka et al. (1986), sweating is also possible with single crystals. The purification effect is, however, much stronger in the case of solid layer crystallization. According to Ulrich and Özoguz (1989) and Delannoy (1993) it can even reach the same extent as the purification by a crystallization step as shown in Figure 7.16.

In summary the possible advantages are:

1. An additional purification in the same range as a crystallization step.
2. A much shorter retention time of the process (about one-third of a crystallization step), which means less energy consumption.
3. A product loss of about 10% of the crystal coat, but which should be compared to a yield of a crystallization step that in many cases is about 80%.

The importance of the sweating step is discussed in detail by Jančić (1989) and Saxer (1993), the former of which also gives examples of overall product recovery and temperature curves for a multi-compound mixture of impurities for the purification of benzoic acid.

A theoretical treatment of the sweating process is presented in Wangnick (1994) for layer melt processes. The author derives a correlation for predicting the additional purification that can be achieved by sweating. The equation accounts for the physical properties of the substance mixture under consideration as well as for the history of the layer and reads as follows

$$\Delta k_{eff, sw} = 0,028 - 0,277 \cdot \Pi_{sw} + 1,235 \cdot \Pi_{sw}^2 \quad (7.5)$$

with

$$\Delta k_{eff} = k_{eff, before} - k_{eff, after} \quad \text{and} \quad \Pi_{sw} = k_{eff, before} \cdot \frac{T_{sw}}{T_{eq}}$$

where Δk_{eff} is the difference of the effective distribution coefficients before and after sweating, Π_{sw} is the characteristic dimensionless number of sweating, $k_{eff, before}$ is the effective distribution coefficient before sweating corresponding to the effective distribution coefficient of the preceding crystallization step, $k_{eff, after}$ is the effective distribution coefficient after sweating, T_{sw} is the sweating temperature, and T_{eq} is the equilibrium temperature.

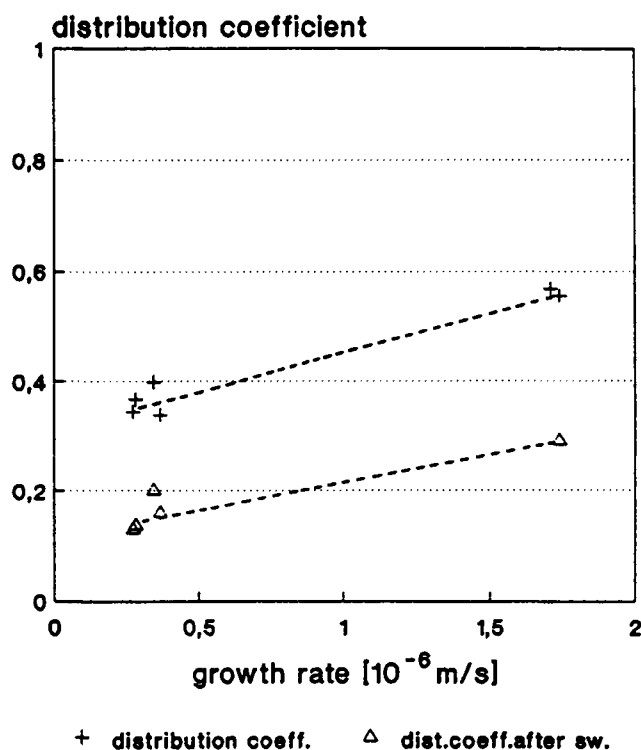


Figure 7.16 The purification of sweating. (Delannoy et al. 1993.)

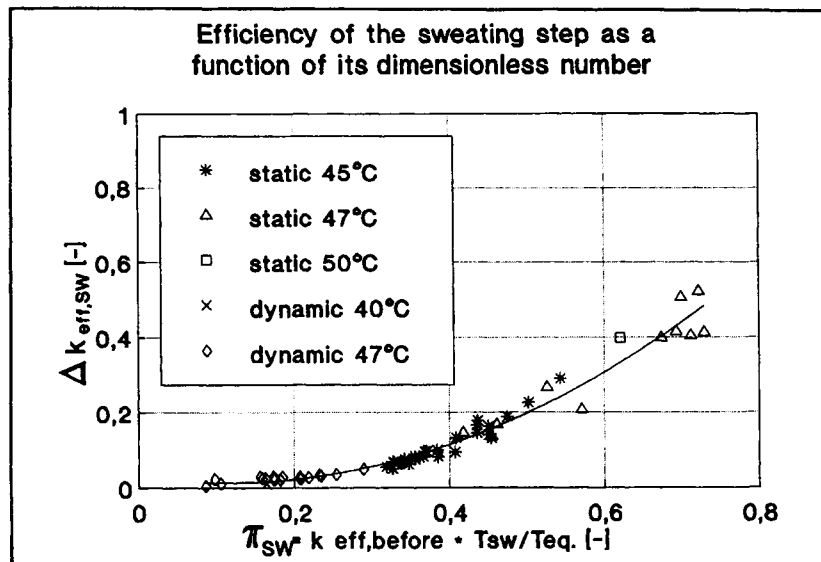


Figure 7.17 Prediction of the sweating result. (Wangnick 1994.)

The application of this equation to data gained from experiments with *p*-*o*-dichlorobenzene in different plant types (static, dynamic) and at different sweating temperatures leads to a uniform representation for all setups. Some exemplary results are shown in Figure 7.17 and demonstrate the usefulness of this approach using a dimensionless number which is based on the physical background of the sweating process.

7.9. THE WASHING STEP

As is defined in, e.g., Ulrich and Bierwirth (1995) one distinguishes between two different processes when talking about washing. The first one is *rinsing*, where the highly contaminated melt that is attached to the crystal or crystal layer surface is *substituted* with a film of the purer rinsing liquid. As mentioned before, rinsing typically requires residence times in the range of only seconds whereas the second washing process, the diffusion washing, effectively operates at residence times longer than 15 min. Here, the washing liquid causes a liquid-liquid diffusion of impurities from the pores of the crystalline material into the washing liquid. To prevent solidification of pure material onto the crystals or the crystal layer the washing liquid must be superheated. For this reason diffusion washing is always, at least to some extent, accompanied by sweating which further increases the purification effect. The efficiency of these process steps becomes obvious if one considers the equipment installed all over the globe which contain washing columns of various types as part of the process. In the case of crystal suspensions, which have much higher surface areas than the solid layer processes, the importance of such a washing step is easy to understand. In cases of solid layer processes, washing is also an important step for increasing purity. By means of experiments Poschmann (1996) and Poschmann and Ulrich (1996) were even able to show quantitatively that the post purification processes are as efficient for suspension crystallization as they are in case of layer processes. This is also expressed by the BASF (DE 1987) patent dealing exclusively with the washing step.

Parameters to consider are the purity, the temperature, the amount, and the flow regime of the washing liquid. An optimization of all these parameters is a current research project in the author's laboratory (cf. e.g., Poschmann and Ulrich 1993; Wang-

nick 1994; Wangnick and Ulrich 1994; Poschmann 1996; Neumann 1996; Neumann and Ulrich 1997; Bierwirth 1998).

The efficiency of a washing operation depends, of course, on the quality, which means purity as well as smoothness, of the crystal layer.

Finally, it should be stated that improvements in product purity are achieved by a contamination of the washing liquid. In most cases the washing liquid is purified melt which contaminates through the washing step and has to be purified again afterwards.

In order to enable the prediction of the purification effect of the rinsing step, Wangnick (1994) introduces a characteristic dimensionless number won from a dimension analysis of all influencing parameters

$$\Delta k_{eff,ri} = 0,012 + 6,17 \cdot 10^{-6} \cdot \Pi_{ri} - 3,979 \cdot 10^{-11} \cdot \Pi_{ri}^2 \quad (7.6)$$

with

$$\Pi_{ri} = \frac{A}{s^2} \cdot \frac{c_{ml}}{c_{\infty}}$$

where Π_{ri} is the characteristic dimensionless number of rinsing, A is the surface area of the crystalline layer, s is the thickness of the crystalline layer, c_{ml} is the concentration of the adhering mother liquor, and c_{∞} is the initial concentration of the melt.

Based on Eq. (7.6) the rinsing result can be predicted independently of the plant geometry, the conditions of the preceding crystallization step, and the substance mixture used as can be seen from Figure 7.18.

The same procedure as in case of sweating and rinsing was chosen by Wangnick (1994) to predict the efficiency of a diffusion washing step following the crystallization. Considering the influencing parameters of diffusion washing a dimension analysis yields the characteristic dimensionless number of diffusion washing for which an approximation to the experimental data for different substance mixtures (*p*-*o*-dichlorobenzene, caprolactam/cyclohexanone) and different operation modes (static, dynamic) leads to the following correlation

$$\Delta k_{eff,diff} = 0,03 + 0,0121 \cdot \sqrt{1,083 \cdot \Pi_{diff}} \quad (7.7)$$

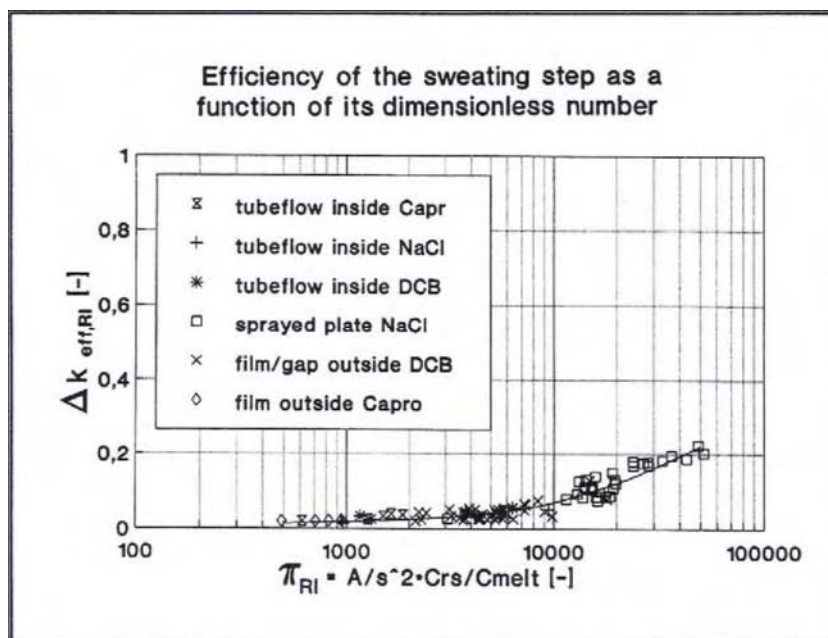


Figure 7.18 Prediction of the rinsing results. (Wangnick 1994.)

with

$$\Pi_{diff} = \frac{D \cdot t}{s^2} \cdot \frac{(c_{inc,0} - c_{wl})}{c_{\infty}} \cdot k_{eff,before} \cdot Sc$$

where Π_{diff} is the characteristic dimensionless number of diffusion washing, t is the diffusion time, s is the thickness of the crystalline layer, $c_{inc,0}$ is the concentration in the liquid inclusions, c_{wl} is the concentration of the washing liquid, c_{∞} is the initial concentration of the melt, $k_{eff,before}$ is the effective distribution coefficient before diffusion washing, i.e., the one of the crystallization step, and Sc is the Schmidt number.

A comparison between the experimental results and the correlation is given in Figure 7.19. As can be seen, theory and experiment fit very well.

Wellinghoff et al. (1995) derived a correlation directly from a pore diffusion model based on Fick's law and obtained an equation which predicts the effective distribution coefficient of diffusion washing as a function of four dimensionless numbers. The apparent differences between the two approaches vanish upon closer examination. Namely, when neglecting the factors that cannot be arbitrarily influenced due to process inherent restrictions the two approaches are essentially alike. They only differ in that Wellinghoff et al. (1995) additionally consider a dimensionless area which corresponds to the ratio of the pore surface to the surface of the crystal layer. This factor can only be determined experimentally yet which is fairly complicated and thus limits the applicability of the approach.

In order to predict the separation potential of a crystallization step followed by one or more of the aforementioned post purification processes, Wangnick proposes to superpose the corresponding equations using the v/k -criterion to model the crystallization step.

Neumann (1996) compares the approach of Wangnick to his experimental results from mixtures of naphthalene/diphenyl and caprolactam/cyclohexanone and finds in all cases that the correlations cited above overestimate the experimental values. He attributes this to the fact that Wangnick, due to the special setup of her apparatus, was not able to completely exclude the effect of sweat-

ing from the results which caused an additional purification that is not contained in the results of Neumann.

7.10. CONTINUOUS PLANTS

7.10.1. ADVANTAGES

The goal in chemical engineering is to aim for continuous plants in order to save the deadtime of charging and discharging the apparatus and to save the energy required to heat and cool the apparatus for each production cycle. Another goal is to unite various stages within one apparatus. This last advantage would feature a countercurrent flow of melt and crystals.

7.10.2. PROCESS CONCEPTS

The simplest approach is a drum cooler, which is used in many cases as a solidification unit (e.g., a drum flaker). Steel belts are used for the same purpose, an example is the equipment of the Sandvik Company (1987) together with the Rotoformer (see Gehrmann 1988).

Many scraped coolers also serve the purpose of creating solids; however, these solids are often processed in suspension processes (see Section 7.6.).

Drum coolers are often introduced in cascades to serve as continuous countercurrent purification process. See, for example Chaty and O'Hern (1964) and Gelperin et al. (1972) for naphthalene, and Graham (1949) for benzene. Commercialized units are, however, not known.

The idea of a column was followed by Schildknecht (see, e.g., Maas and Schildknecht 1963) in many papers. The column was fed in the center and used a spiral conveyor to transport the crystals upward countercurrently to melt through the purification zone.

The bottom has a freezing unit and the top has a heating unit, or melter. Crystals are primarily formed at the bottom, but some are nucleated at the walls of the columns and are removed by the scraping conveyor. The column is operated with a reflux.

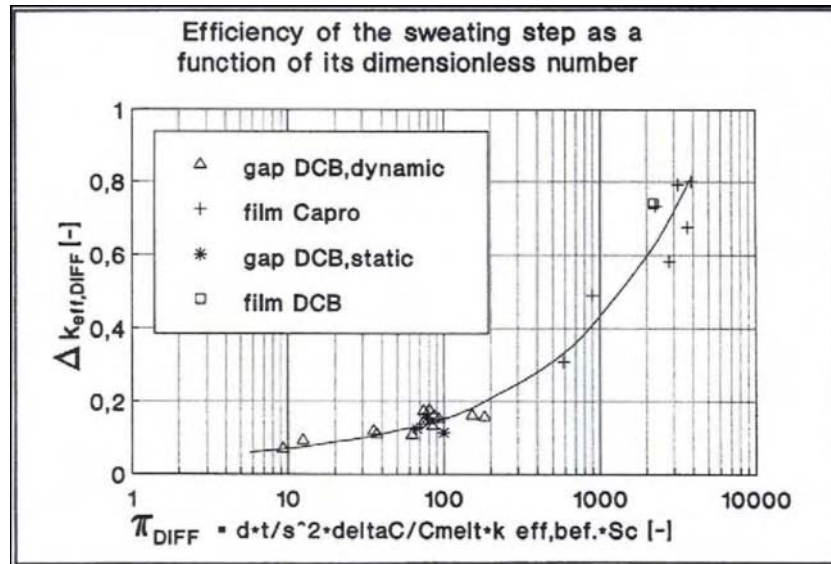


Figure 7.19 Prediction of result of diffusion washing. (Wangnick 1994.)

Basically the same idea was used by Brodie (1971) to create the Brodie Purifier of Union Carbide Corp. (GB-PS 1968), which features a horizontally scraped surface crystallizer with a vertical purification section. The performance of the apparatus depends strongly on the size of the crystals entering the purification section. Walas (1988) reports that as much as 24 h residence time is needed to create the correct crystal size. He also presents data about *p*-dichlorobenzene purification. Mullin (1988) reports that in addition to the *p*-dichlorobenzene, large-scale production has also been installed for naphthalene. Figure 7.20 shows a diagram of the Purifier.

The Tsukishima Kikai (TSK) countercurrent cooling crystallization process introduced by Takegami et al. (1984) and Morita et al. (1986) is also called the four C process. TSK is a development resulting from the Brodie process. The feed moves through three cooling crystallizers (scraped ones). The crystals move in the opposite flow direction within the sequence of the stages and end in a Brodie type purification column. A melter is at the bottom of the column. The product is also discharged at the bottom but some amount is used as reflux to wash the descending crystals.

Finally, the back mixing column (BMC) of Nippon Steel Chemical Co., introduced by Sakuma and Ikeda (1984) has to be

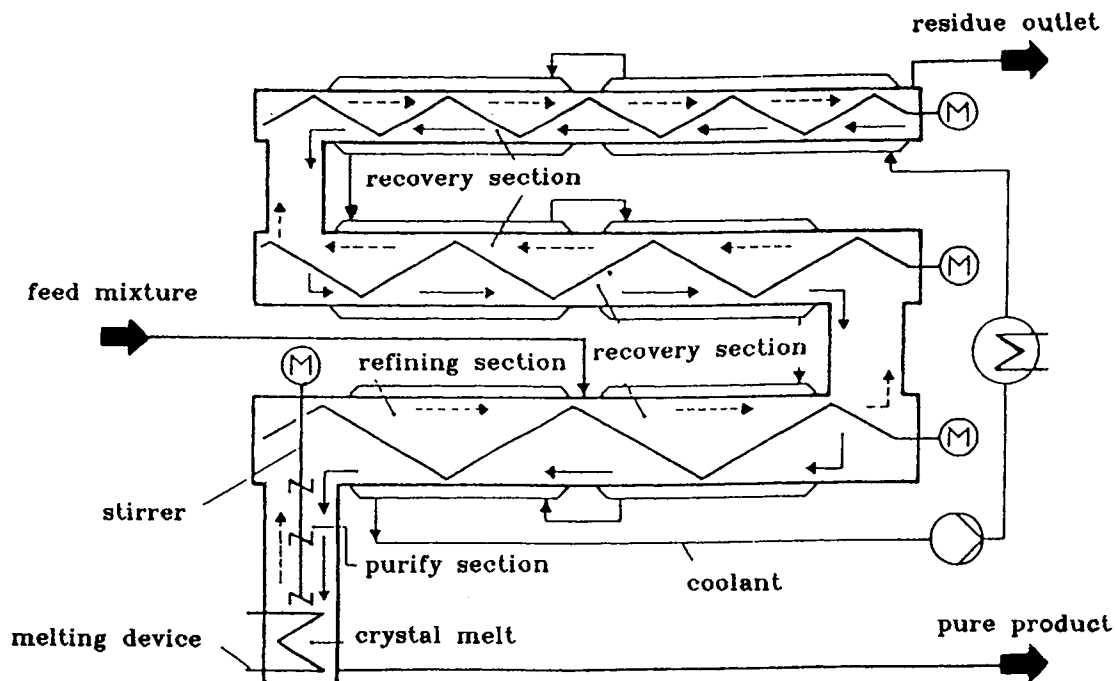


Figure 7.20 Brodie purifier. (Reproduced with permission from Rittner and Steiner 1985.)

mentioned. A cooling section at the top of the column has scraper blades. The crystals move down from the top to the purification section and further down to the melting section. The crystals are in countercurrent flow to a reflux of melt since not all remolten crystals are removed as product. At the top of the column some residue is taken out. The process has an agitator in the purification section. Nippon Steel is operating a BMC-type commercial plant for the recovery of naphthalene.

7.10.3. PROBLEMS

Drum cascades are not found in large scale. Schildknecht columns never did work when they were too large (larger than laboratory scale), due to problems with axial back mixing and scaling. Since the Brodie purifiers only worked in a few special cases, the TSK process was created. At first glance, the TSK process appears to be continuous, but it is, in fact, a cascade of crystallizers with a purification column. The Kureha purifier and the Nippon Steel BMC work within their companies for special cases or products.

Back mixing, slurry transport, moving parts in the equipment, and scaling problems are the biggest difficulties in continuously running plants. Therefore, a truly ideal continuous countercurrent melt crystallizer that is flexible enough to handle a variety of substances with high efficiency is not, unfortunately, found to date. Due to problems, the semibatch-type of processes dominates in most of the recently built plants.

7.10.4. SUMMARY AND A VIEW TO THE FUTURE

Melt crystallization, with all the mentioned advantages, has not found the place it deserves among the unit operations in chemical engineering today. Research efforts conducted by industry during the last few years, however, are a good beginning in the efforts to change this.

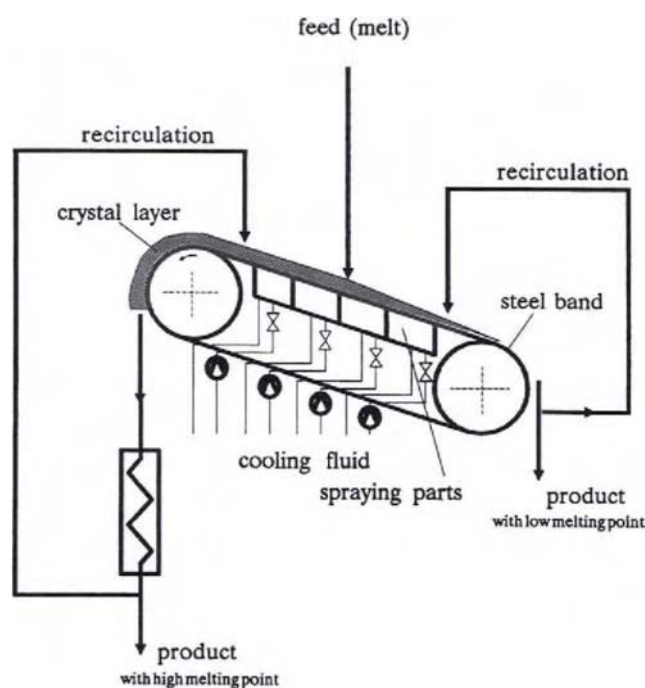


Figure 7.21 Bremband-process, continuous solid layer process.

Missing knowledge about heat and mass transfer in melt crystallization on the one hand and problems of handling the solid transport and solid-liquid separation on the other hand are being worked on. Even the dream of having a continuous countercurrent solid layer crystallization process with integrated sweating and washing processes seems possible.

The patent application by Ulrich et al. (1990) (see Figure 7.21) uses a Sandvik-type conveyer positioned at an angle and is cooled from the bottom. The crystallized material is transported to the upper end of the steel belt while the residue flows—as in the Sulzer falling film equipment—down over the already crystallized product. By using different cooling or heating zones on the bottom side of the belt and different positioning of the recirculations of the product, sweating and washing operations are possible in the one apparatus, as is shown in Ulrich et al. (1992) and Hünken (1993).

A second, new approach uses the aforementioned Sandvik conveyer to produce pastilles from an impure melt by a drop formation process which are then fed to a wash column thus improving the fluid dynamical behavior of the plant (DE 1995). Inside the wash column the impurities are removed from the pastilles. The dependence of the pastille properties on the production parameters and their influence on the purification potential of the pastilles was intensively investigated and is described in Bülau (1997).

An optimization of all three purification steps is needed for all types of melt crystallization processes in order to make melt crystallization more economically competitive. For such an optimization, a mathematical description of the phenomena is necessary. When such a description becomes reality, a great deal of progress for the unit operation melt crystallization will be made. Research in the field continues, therefore this technique is likely to have a bright future.

REFERENCES

- Arkenbout, G.J. (1978). *Separation and Purification Methods* 7(1), 99–134.
- Arkenbout, G.J. (1995). *Melt Crystallization Technology*, TECHNOMIC Publishing Company, Inc., Lancaster, U.S.A.
- Arkenbout, G.J., van Kujik, A., and Smit, W.M. (1976). In *Industrial Crystallization* (Mullin, J.W., ed.), pp. 431–435, Plenum Press, New York.
- Arkenbout, G.J., van Kujik, A., and Schneiders, H.J.M. (1984). In *Industrial Crystallization* (Jančić, S.J., and de Jong, E.J., eds.), pp. 137–142, Elsevier Publishing Co., Amsterdam.
- Atwood, G.R. (1976). In *Recent Developments in Separation Science*, vol. I (Li, N.I., ed.), pp. 1–33, CRC Press, Inc., New York.
- Beilstein (1987). *Beilsteins Handbook of Organic Chemistry*, Springer-Verlag, Berlin, Germany.
- Bierwirth, J. (1998). Ph.D. dissertation, University of Bremen, Bremen, Germany.
- Brennan, E.D. (Koppers Co.) (1982). U.S. Patent no. 4309878.
- Brodie, J.A. (1971). *Mech. Chem. Trans. Inst. Eng. Australia* 7(1), 37–44.
- Bülau, H.C., and Ulrich, J. (1997). In *Crystal Growth of Organic Materials*, vol. 4, (Ulrich, J., ed.), pp. 123–130, Shaker Verlag, Aachen, Germany.
- Burton, J.A., Prim, R.C., and Slichter, W.P. (1953). *J. Chem. Phys.* 21(11), 1987–1991.
- Chaty, I.C., and O'Hern, H.A. (1964). *AIChE J.* 10, 74–78.
- Cheng, C., Irvin, D., and Kyle, B. (1967). *AIChE Journal* 13(4), 739–744.
- CH-PS 501 421 (1967). Metallwerke AG, Buchs, Switzerland.
- CH-V 4890 (1990). Sulzer Brothers, Winterthur, Switzerland.
- CRC Press (1984). *CRC Handbook of Chemistry and Physics*, CRC Press, Inc., New York.
- D'Ans-Lax (1983). *Taschenbuch für Chemiker und Physiker*, vol. 4. Aufl., Springer-Verlag, Berlin, Germany.
- Delannoy, C., Ulrich, J., and Fauconet, M. (1993). *Symposium on Industrial Crystallization*, vol. 1 (Rojkowski, Z.H., ed.), pp. 49–54, 21–23 Sept., Warsaw, Poland.
- DE 3708709 (1987). BASF AG, Ludwigshafen, Germany.
- DE 44 15 845 C1 (1995). Santrade Ltd., Luzern, Switzerland.
- DE-AS 1793 345 (1971). Proabd, S.A., Nancy, France.

- DE-OS 3203818 (1982). Rüttgers Werke AG, Germany.
- DE-PS 1958 461 (1969). Hoechst AG, Germany.
- DE-PS 2606 364 (1976). BASF AG, Germany.
- EP 0 811 410 A1 (1997). Bischof, R., Switzerland.
- EP-OS 85791 (1982). Rüttgers Werke AG, Germany.
- Erdmann, H.H. (1975). Ph.D. dissertation, University of Dortmund, Germany.
- Freund, H., König, A., and Steiner, R. (1997). In *Crystal Growth of Organic Materials*, vol. 4, (Ulrich, J., ed.), pp. 1114–122, Shaker Verlag, Aachen, Germany.
- FR-PS 8023 769 (1980). BEFS Engineering, Mulhouse, France.
- FR-PS 8108 509 (1981). BEFS Engineering, Mulhouse, France.
- GB-PS 1275 798 (1968). Union Carbide Corp., Australia.
- GB-PS 837295 (1958). Proabd S.A., Nancy, France.
- GB-PS 899799 (1959). Proabd S.A., Nancy, France.
- GB-PS 1083850 (1964). ICI, England.
- GEA Process Technology (1997). Brochure, 's-Hertogenbosch, The Netherlands.
- Gehrmann, S. (1988). *Verfahrenstechnik* **8**, 54–55.
- Gelperin, N.I., Nosov, G.A., and Makotkin, A.W. (1972). *Tr. MITChT Im. M.W. Lomonosova* **2**(1), 16–34.
- Goudsche Machinefabriek, B.V. (1984). P.O. Box 125, 2800 AC Gouda, The Netherlands.
- Graham, B.L. (1949). US-PS 2651922. Phillips Petroleum Co., Bartlesville, OK.
- Guardani, R. and Belline, A. (1997). *Chem. Eng. Technol.* **20**, 495–501.
- Henning, S. and Ulrich, J. (1997). *Trans IChemE* **75** (A), 232–236.
- Henning, S., Ulrich, J., and Niehörster, S. (1995). In *Crystal Growth of Organic Materials*, vol. 3, (Myerson, A.S., Green, D.A., and Meenan, P., eds.), pp. 137–144, American Chemical Society, Washington, DC.
- Hünken, I., Ulrich, J., Fischer, O., and König, A. (1993). In *Symposium on Industrial Crystallization*, vol. 1 (Rojkowski, Z.H., ed.), pp. 55–60, 21–23 Sept., Warsaw, Poland.
- International Critical Tables (1927–1930). McGraw-Hill, New York.
- Jančić, S.J. (1987). In *Industrial Crystallization*, vol. 87 (Nývlt, J., and Zacek, S., eds.), pp. 57–70, Elsevier Science Publishers, Amsterdam.
- Jansens, P.J., and van Rosmalen, G.M. (1994). In *Handbook of Crystal Growth*, vol. 2 (Hurle, D.T.J., ed.), Elsevier Science B.V., Amsterdam, The Netherlands.
- Kehm, D. (1990). Ph.D. dissertation, University of Dortmund, Germany.
- Kirk-Othmer (1979). Kirk-Othmer Encyclopedia of Chemical Technology, vol. 7, pp. 243–285, John Wiley and Sons, New York.
- Kuszlik, A. (1990). Ph.D. dissertation, University of Bremen, Bremen, Germany.
- Maas, K., and Schildknecht, H. (1963). *Wärme* **69**, 121–127.
- Matsuoka, M. (1977). *Bunri Gijutsu (Separation Process Engineering)* **7**, 245–249.
- Matsuoka, M. (1991). In *Advances in Industrial Crystallization* (Garside, J., Davey, R.J., and Jones, A.G., eds.), Butterworth-Heinemann, Oxford.
- Matsuoka, M., and Fukushima, H. (1986). *Bunri Gijutsu (Separation Process Engineering)* **16**, 4–10.
- Matsuoka, M., Ohishi, M., Sumitani, A., and Otori, K. (1986). In *World Congress III of Chemical Engineers*, Tokyo, 21–25 Sept. 1986, pp. 980–983.
- Matz, G. (1969). *Kristallisation*, 2. Aufl., Springer Verlag, Berlin, Germany.
- McKay, D.L. (1967). In *Fractional Solidification* (Zief, M., and Wilcox, W.R., eds.), pp. 427–439, Marcel Dekker, New York.
- Molinari, J.G.D. (1967). In *Fractional Solidification* (Zief, M., and Wilcox, W.R., eds.), pp. 393–400, Marcel Dekker, New York.
- Morita, M., Nakamura, K., and Takegami, K. (1986). In *World Congress III of Chemical Engineers*, Tokyo, 21–25 Sept. 1986, pp. 1072–1075.
- Moritoki, M., and Fujikawa, T. (1984a). In *Industrial Crystallization* **84**, (Jancic, S.J., and de Jong, E.J., eds.), pp. 369–372, Elsevier Science Publishers, Amsterdam.
- Moritoki, M., Ito, M., Sawada, T., et al. (1989). In *Industrial Crystallization*, vol. 87, (Nývlt, J., and Zacek, S., eds.), pp. 485–488, Elsevier Science Publishers, Amsterdam.
- Moritoki, M., Kitagawa, K., Onoe, K., Kaneko, K. (1984b). In *Industrial Crystallization*, vol. 84, (Jancic, S.J., and de Jong, E.J., eds.), pp. 377–380, Elsevier, Amsterdam.
- Moritoki, M., Wakabayashi, M., and Fujikawa, T. (1979). In *Industrial Crystallization* **78**, (de Jong, E.J., and Jancic, S.J., eds.), pp. 583–584, North Holland Company, Amsterdam.
- Mullin, J.W. (1972). *Crystallization*, Butterworths, 2nd ed., London.
- Mullin, J.W. (1993). *Crystallization*, Butterworths, 3rd ed., London.
- Mullin, J.W. (1988). In *Ullmann's Encyclopedia of Industrial Chemistry*, VCH Verlagsgesellschaft, Weinheim, Germany.
- Mullins, W.W. and Sekerka, R.F. (1964). *J. Appl. Phys.* **35**(2), 444–451.
- Neumann, M. (1996). *Vergleich statischer und dynamischer Schichtkristallisation und das Reinigungspotential der Diffusionswäsche*, Papierflieger, Clausthal-Zellerfeld, Germany.
- Neumann, M., and Ulrich, J. (1997). *Journal of Thermal Analysis* **48**, 527–533.
- Özoguz, Y. (1992). *VDI-Fortschritts-Berichte*, no. 271, VDI-Verlag, Düsseldorf, Germany.
- Poschmann, M. (1996). *Zur Suspensionskristallisation organischer Schmelzen und Nachbehandlung der Kristalle durch Schwitzen und Waschen*, Shaker Verlag, Aachen, Germany.
- Poschmann, M., and Ulrich, J. (1993). *Symposium on Industrial Crystallization*, vol. 1 (Rojkowski, Z.H., ed.), pp. 67–72, 21–23 Sept., Warsaw, Poland.
- Poschman, M., and Ulrich, J. (1996). *Journal of Crystal Growth* **167**, 248–252.
- Ransley, D.L. (1984). In *Kirk-Othmer: Encyclopedia of Chemical Technology*, John Wiley and Sons, New York.
- Rittner, S., and Steiner, R. (1985). *Chem.-Ing.-Techn.* **57**(2), 91–102.
- Ritzner, H. (1973). *Erdöl, Kohle, Erdgas, Petrochem.* **26**, 327–331.
- Ruemekorf, R. (1993). In *Process Engineering for Pollution Control and Waste Minimization*, (Wise, D.L., and Trantolo, D.J., eds.), pp. 513–524, Marcel Dekker, Inc., New York.
- Rutter, J.W. and Chalmers, B. (1953). *Can. J. Phys.* **31**, 15–39.
- Sandvik Company (1987). Brochure, Fellbach, Germany.
- Sakuma, K., and Ikeda, J. (1984). In *Industrial Crystallization*, vol. 84, (Jancic, S.J., and de Jong, E.J., eds.), pp. 147–152, Elsevier, Amsterdam.
- Saxer, K., Stadler, R., and Ignjatovic, M. (1993). *Symposium on Industrial Crystallization*, vol. 1 (Rojkowski, Z.H., ed.), pp. 13–18, 21–23 Sept., Warsaw, Poland.
- Scholz, R. (1993). *VDI-Fortschritts-Berichte*, no. 347, VDI-Verlag, Düsseldorf, Germany.
- Scholz, R., Genthner, K., and Ulrich, J. (1990a). *Chem.-Ing.-Tech.* **62**(10), 850–852.
- Scholz, R., Genthner, K., and Ulrich, J. (1990b). In *BIWIC 1990* (Ulrich, J., ed.), pp. 26–33, Verlag Mainz, Aachen, Germany.
- Sloan, G.J., and McGhie, K. (1988). *Techniques of Melt Crystallization; Techniques of Chemistry*, vol. XIX, John Wiley and Sons, New York.
- Smith, M.F. (1988). *J. Fluid Mech.* **1988**, 547–570.
- Sulzer Brothers, Inc. (1988). Brochure, Buchs, Switzerland.
- Takegami, K., Nakamura, N., and Morita, M. (1984). In *Industrial Crystallization*, vol. 84, (Jancic, S.J., and de Jong, E.J., eds.), pp. 143–146, Elsevier, Amsterdam.
- Thijssen, H.A.C., and Arkenbout, G.J. (1983). U.S. Application no. 456,988, Zeist, The Netherlands.
- Tiedtke, M., Ulrich, J., and Hartel R.W. (1995). In *Crystal Growth of Organic Materials*, vol. 3, (Myerson, A.S., Green, D.A., and Meenan, P., eds.), pp. 137–144, American Chemical Society, Washington, D.C.
- Toyokura, K., Wintermantel, K., Hirasawa, I., and Wellinghoff, G. (1995). In *Crystallization Technology Handbook* (Mersmann, A., ed.), pp. 459–538, Marcel Dekker, Inc., New York.
- Ullmann's Encyclopedia of Industrial Chemistry (1988). VCH Verlagsgesellschaft mbH, New York.
- Ulrich, J. (1995). In *Crystal Growth of Organic Materials*, vol. 3, (Myerson, A.S., Green, D.A., and Meenan, P., eds.), pp. 112–115, American Chemical Society, Washington, D.C.
- Ulrich, J. (1988). *Chem. Eng. Symp. Ser. Jpn.* **18**, 172–175.
- Ulrich, J., and Bierwirth, J. (1995). In *Science and Technology of Crystal Growth*, (von der Erden, J.P., and Bruinsma, O.S.L., eds.), pp. 245–258, Kluwer Academic Pub., Dordrecht, The Netherlands.
- Ulrich, J., Hünken, I., Fischer, O., and König, A. (1992). *Chem.-Ing.-Tech.* **64**, 842–844.
- Ulrich, J., Jancic, S.J., and Kuszlik, A. (1990). *Symposium on Industrial Crystallization*, (Mersmann, A., ed.), pp. 815–820, 18–20 Sept., Garmisch, Germany.
- Ulrich, J., and Kallies, B. (1994). In *Current Topics in Crystal Growth Research*, vol. 1, Research Trends, Trivandrum, India.
- Ulrich, J., and Özoguz, Y. (1989). *Chem.-Ing.-Tech.* **61**, 76–77.

- Ulrich, J., Özoguz, Y., and Stepanski, M. (1988). *Chem.-Ing.-Tech.* **60(6)**, 481–483.
- Ulrich, J., and Özoguz, Y. (1990). *J. Crystal Growth* **99**, 1134–1137.
- Ulrich, J., Stepanski, M., and Özoguz, Y. (1990). Swiss Patent no. 03750/90–0.
- U.S. Patent 4552572 (1985). Sulzer Brothers, Buchs, Switzerland.
- VDI-Wärmeatlas, (1988). VDI-Verlag, Düsseldorf, Germany.
- Walas, S.M. (1988). *Chemical Process Equipment*, Butterworths Publ., Stoneham, England.
- Wangnick, K. (1994). *VDI-Fortschritts-Berichte*, no. 355, VDI-Verlag, Düsseldorf, Germany.
- Wangnick, K., and Ulrich, J. (1994). *Crystal Research and Technology* **29(3)**, 349–356.
- Wellinghoff, G., Holzknicht, B., and Kind, M. (1995). *Chem.-Ing.-Tech.* **67(3)**, 333–337.
- Wintermantel, K. (1972). Ph.D. dissertation, TH Darmstadt, Germany.
- Wintermantel, K. (1986). *Chem.-Ing.-Tech.* **58**, 498–499.
- Wintermantel, K. and Kast, W. (1973). *Chem.-Ing.-Tech.* **45(10a)**, 728–731.
- Yamada, J., Shimizu, C., and Saitoh, S. (1982). In *Industrial Crystallization*, vol. 89, (Jancic, S.J., de Jong, E.J., eds.), pp. 265–270, North Holland, Amsterdam.
- Zief, M., and Wilcox, W.R. (1967). *Fractional Solidification*, Marcel Dekker, Inc., New York.

This Page Intentionally Left Blank

CRYSTALLIZER MIXING: UNDERSTANDING AND MODELING CRYSTALLIZER MIXING AND SUSPENSION FLOW

Daniel Green

8.1. INTRODUCTION

Mixing determines the environment in which crystals nucleate and grow and is therefore central to industrial crystallization. Individual nucleating and growing crystals respond to their microenvironment and not in a simple way to the macroenvironment, often thought of as the bulk or average environment. Since a growing crystal removes solute from solution and a dissolving crystal releases it, the solute concentration and therefore the supersaturation is in general different at the crystal surface than in the bulk. Crystals grow when the microenvironment is supersaturated, stop when it is just saturated, and dissolve when it is undersaturated. In the majority of cases, impurities are rejected by growing crystals; therefore, each growing crystal face creates a zone of locally higher impurity concentration just ahead of it. The growth rate and amount of impurity taken up by the growing crystal is a function of the impurity concentration where growth is occurring—at the crystal face itself. Mixing is the family of processes that link this local microenvironment to the macroscopic scale of the crystallizer by affecting the mass transfer between crystal and the larger environment and the dynamics of crystal suspension in the crystallizer. Mixing, therefore, to a large extent creates the micro crystal environments. Furthermore, it determines the homogeneity of the macroenvironment, both temporally and spatially. Inhomogeneity in the macroenvironment affects microenvironments, causing temporal variations as the crystals circulate from one zone to another inside the crystallizer. This is particularly important because local values of key variables such as supersaturation and solids concentration are often much more important in crystallization than the bulk or global averages of these quantities, as is discussed below.

For example, in practice it is often found that the feed location plays a large role in determining particle size distribution and other crystal characteristics. This is because the local environment in the vicinity of the feed point is strongly affected by position relative to the agitation system and the rest of the vessel. This is where the feed solution begins the transition from the conditions in the feed line, typically under or just saturated, to the supersaturated conditions in the vessel. Therefore, here is where nucleation frequently first occurs.

The intent of this chapter is to make the reader aware of mixing and related phenomena as encountered in typical industrial crystallization processes. The effect of mixing on crystal characteristics will be stressed. The fundamentals of the flow of suspension crystallizers will be presented. The information presented here should enable the practitioner to troubleshoot simple mixing problems in his or her processes. The principles of vessel and agitator design, from the standpoint of providing adequate mixing (and not mechanical design), will be discussed. The issues and difficulties of scaling up are discussed from the perspective of suspension mixing. Finally, methods of investigation are presented, including both experimental and mathematical modeling.

8.2. CRYSTALLIZER FLOWS

Crystallizers are typically, although not exclusively, agitated tanks. In many respects, they are similar to vessels used as chemical reactors and mixing vessels in many other processes. Mechanical energy is usually used to physically mix the contents. Feed streams are incorporated into the bulk by the turbulence created by large turbines or impellers. Relatively large flows sweep the vessel from top to bottom and from center to outside in an effort to homogenize the contents. One key difference, of course, is that crystallizers need to suspend and distribute the crystals that are being formed within them.

It is important then to recognize that the flow in crystallizers is of a *suspension* and not a single-phase fluid. There are obvious differences. The effective viscosity of the suspension is larger than that of the solution by itself. The flow velocities everywhere must be large enough so that the particles do not settle appreciably. Then, there are more subtle differences. The presence of particles blunts velocity profiles and affects turbulence. The particles are not in general uniformly suspended, but are distributed in unexpected ways. The particle size distribution is also not uniform throughout the vessel. The net result is that transport properties and the variables that affect crystallization most, such as supersaturation, are affected.

Because crystallizer flows are in general turbulent, we must first distinguish between the instantaneous and time averaged flows in our descriptions. Consider the flow in a simple crystallizer: a baffled tank with a single axial flow impeller. If we were to sketch the streamlines associated with this configuration, as in Figure 8.1, we would implicitly be drawing the time averaged or bulk flow. Superimposed on this time-averaged flow are turbulent fluctuations, largely aperiodic velocity fluctuations associated with swirling eddies of various sizes and strengths. Although we tend to understand the flow in a vessel in terms of the time-average flow, it is important to keep in mind the nature of the turbulence because it has a great effect on the mixing and therefore on the crystallization process itself.

Let's consider several characteristics of turbulence. Turbulent fluctuations are associated with eddies of various length scales. In fact, turbulent eddies are characterized by a cascade of length scales. In the case of an agitated crystallizer, turbulence is generated largely by the agitator impeller, which creates large-scale turbulent eddies on the order of the vessel dimensions, say impeller blade height, in size. These eddies in turn create smaller eddies. Each eddy length scale breeds smaller eddies. Energy input into turbulence by the agitator at the largest turbulent length scales flows down the length scale cascade until a limit is reached the Kolmogorov length scale (Deen 1998). Turbulence is a high Reynolds number phenomenon, meaning that the ratio of inertial to viscous forces in the flow is very large and inertial forces dominate. However, as the length scale of the turbulent structures decreases, a limit is

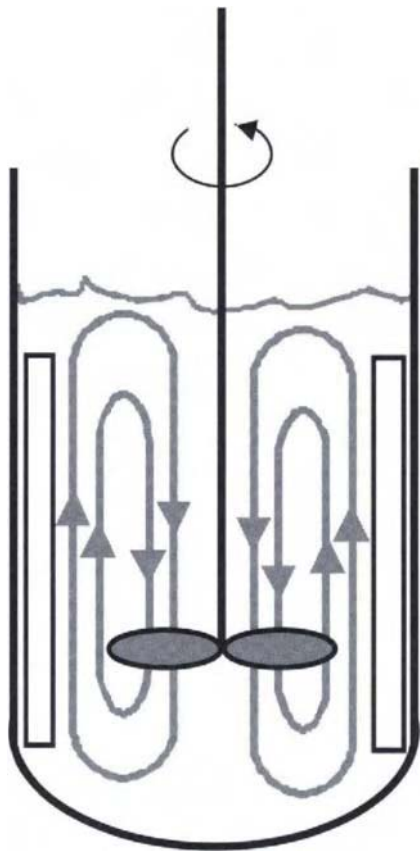


Figure 8.1 Simplified schematic of streamlines associated with a single axial flow impeller in a baffled tank.

reached at which viscous forces become important and finally dominate.* At this point, viscosity dissipates the turbulent energy. The Kolmogorov scale for a typical crystallizer, is $o(10\ \mu\text{m})$. Therefore, the cascade of turbulent length scales is huge, say from $o(1)$ to $o(10^{-5})\text{m}$. The importance of this range of length scales will become obvious below, when mixing mechanisms are discussed.

8.3. DISTRIBUTION OF KEY VARIABLES IN CRYSTALLIZERS

Depending on the means of generating supersaturation (see e.g., Chapter 5), the details of how mixing determines the distribution of process variables change. For example, in reacting systems, where two reactants mix to generate a product present above saturation, it is the mixing of the two reactants, coupled with their reaction rate, that determines the distribution of the product concentration, and subsequently the supersaturation. In cooling crystallization, mixing determines both the dispersion of the hot feed stream into the cooler bulk of the crystallizer and the heat transfer to the heat transfer surfaces. In evaporative crystallizers, the boiling zone, with higher supersaturation because of both cooling and solvent removal, must be mixed into the bulk.

Mixing determines the distribution of both solute and suspended solids. In addition, it determines the temperature profile

in the vessel. These three quantities are coupled and the net result is the distribution of supersaturation. Supersaturation will be highest where solute concentration is highest, and solids concentration and temperature lowest. The dependence on solute concentration is clear. High solids concentration means a large specific crystal area for precipitation that decreases solute concentration. Low temperature means that the saturation concentration is lower, which of course raises supersaturation.

Other variables with potentially significant impact on crystallization are affected by mixing: the distribution of impurities and of reactants in chemically reacting systems, for example.

The distributions of these key variables that control crystallization variables are determined by a number of factors, including:

- Flow field in the vessel, $\mathbf{v}(\mathbf{r})$
- Distribution of the turbulent kinetic energy and dissipation in the vessel, $k(\mathbf{r})$, $\varepsilon(\mathbf{r})$
- Location of the feed point, and
- Location of product withdrawal point.

Here \mathbf{r} is the position vector. \mathbf{v} is the velocity vector, and k and ε are the local turbulence kinetic energy and rate of dissipation, respectively.

The flow and dissipation fields are determined in turn by the agitator(s), its (their) placement and rotational speed(s), the placement and dimensions of baffles and draft tubes, and geometry of the vessel.

It turns out that the distributions of a crystallizer's key variables are often not uniform. While it is often possible to achieve uniformity or near uniformity at the laboratory scale, it is almost never achieved at the industrial scale. Therefore, the effect of inhomogeneity in crystallizers can not be underestimated. Let us now consider the effects of nonuniform distribution of supersaturation.

Nucleation is a strong function of supersaturation and this dependence is frequently modeled as

$$B \propto \sigma^n$$

where B is the nucleation or "birth" rate of crystals and σ is the dimensionless supersaturation (Randolph and Larson 1988), defined $\sigma = (c - c_{sat})/c_{sat}$. Here c is the solute concentration and c_{sat} is the concentration at saturation. n is determined by data correlation, and typically falls in the range: $1 \leq n \leq 3$ for secondary nucleation, and is often ≥ 2 . (For primary nucleation, which is encountered much less frequently in industrial crystallization, n is typically much higher.)

Because of this relatively strong dependence on supersaturation, local regions of sustained supersaturation higher than the vessel average can dominate the nucleation rate of the entire vessel. In these cases, these local supersaturation maxima, and NOT the vessel average may control the nucleation rate of the entire process. Regions of locally higher supersaturation will result, for example, where a concentrated feed is injected into a poorly mixed region or if the evaporation zone of an evaporative crystallizer is poorly mixed into the bulk.

The growth rate of crystals also depends strongly on supersaturation. This dependence is frequently modeled as

$$G \propto \sigma^m$$

where G is the growth rate and $1 \leq m \leq n$ (Randolph and Larson 1988). Then, similar to nucleation, growth of individual crystals

*In the Navier-Stokes equations, viscous dissipation is represented by a term proportional to $\mu \nabla^2 \mathbf{v}$, where μ is viscosity, \mathbf{v} the fluid velocity vector, and ∇^2 the operator $\frac{\partial^2}{\partial x^2} + \frac{\partial^2}{\partial y^2} + \frac{\partial^2}{\partial z^2}$. At the smallest length scales, the partial derivatives of the velocity become very large; therefore, this viscous dissipation term, negligible at the larger length scales, becomes dominant.

may be nonuniform, growing more rapidly in regions of high supersaturation. This may alter crystal morphology and possibly induce defects and strain.

Controlling the effect of locally higher supersaturation may be particularly important in cases where the goal is to minimize fines generation. Efforts to decrease the average supersaturation in the vessel may fail to reduce the number of fines produced. Often the key is rather to eliminate or moderate the local maximum supersaturation, say in the vicinity of a feed point or in the boiling zone of an evaporative vessel.

Inhomogeneity in supersaturation has a similar effect on encrustation, also a strong function of supersaturation. Small high supersaturation zones may be the trigger to initiate encrustation, which then may spread to cover a much broader area of the crystallizer wall. In this case, a local cold spot on a wall or at the entrance of a heat transfer coil may be where the supersaturation becomes higher locally.

It must be noted that while it is almost always beneficial to have a homogeneous suspension, this is not always true. In some cases, there are benefits to having a nonhomogeneous suspension. This is the case when there is an advantage to separating nucleation and growth phenomena, for example: when polycrystalline particles are formed by nucleating new crystallites on existing particles in a zone of very high supersaturation; then circulating these particles through a lower supersaturation zone in which growth of the crystallites occurs without additional nucleation (Green et al. 1995).

Similar to the dependence of nucleation and growth on supersaturation, the mechanisms of attrition and aggregation are sensitive functions of particle collision rate. Since particle collision rate scales with solids concentration to the second power (Smoluchowski 1916), these processes are exceptionally sensitive to locally higher particle concentration. Therefore, if particles are not suspended uniformly, much of the attrition and/or aggregation in the system can occur in a relatively small zone of higher particle concentration. Again, the solution to an excessive attrition condition may be to make the solids suspension more uniform, minimizing or moderating the concentration in the small zone, rather than decreasing the average solids concentration for the entire vessel. Therefore,

we should strive to achieve uniformity in solids suspension; not the "just suspended" condition (Nienow 1997) often used as a criterion for solids suspension.

Let us now examine what determines the uniformity of these fields. First let us consider solute concentration in a simple cooling crystallizer fed at a single point. Mixing occurs at all length scales. Many people speak of mixing occurring at small length scales as "micromixing," and that at larger length scales as "macromixing" (Bourne 1997).

Micromixing is the intimate mixing that occurs at molecular and near molecular length scales. It is a diffusional process. Macromixing is the overall blending that occurs by convection. It is associated with length scales that are roughly equivalent to vessel dimensions. The term mesomixing describes mixing occurring at intermediate length scales, say of the order of the envelope of the feed zone in size (Baldyga and Bourne 1992). Mesomixing is associated with the turbulent diffusion of the feed into the surrounding fluid and occurs at length scales above that of micromixing, but still quite small relative to vessel dimensions.

Mixing in a crystallizer occurs by all these mechanisms. In the immediate vicinity of the feed point, mixing of the concentrated feed into the fluid streaming by is by meso- and then micromixing. Turbulent eddies capture packets of the feed solution and mix it with the bulk fluid. Molecular diffusion take over below the Kolmogorov scale. Convection carries the fluid in the vicinity of the feed point away and into the rest of the vessel. Mixing at all length scales is important in the crystallizer. In the absence of macromixing, the concentration would build around the feed location and not be blended with the rest of the vessel. Micromixing is required for the final homogenization of the solution.

The distribution of solids depends on the velocity field. There is also a feed back effect, because the solids themselves affect the flow, altering velocity profiles and affecting the turbulence.

The spatial distribution of the solids can be quite surprising. Figure 8.2 shows data from Shamlou and Koutsakos 1989, for solids suspended in a baffled tank agitated with an axial flow impeller. The distribution is unexpected and complicated. Note several features: Generally, the particle concentration is higher lower in the tank. The particles are concentrated immediately

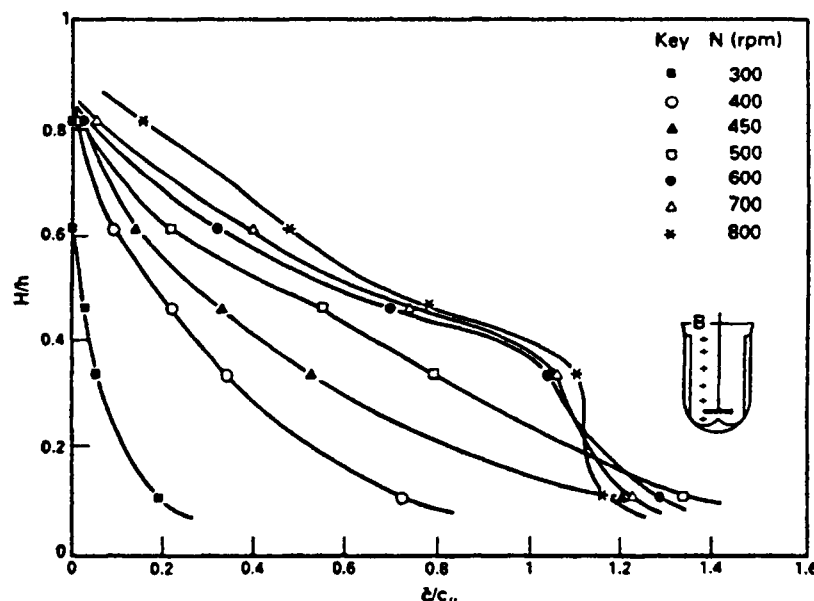


Figure 8.2 Particle concentration as a function of height in a tank mixed with an axial flow impeller according to Shamlou and Koutsakos (1989).

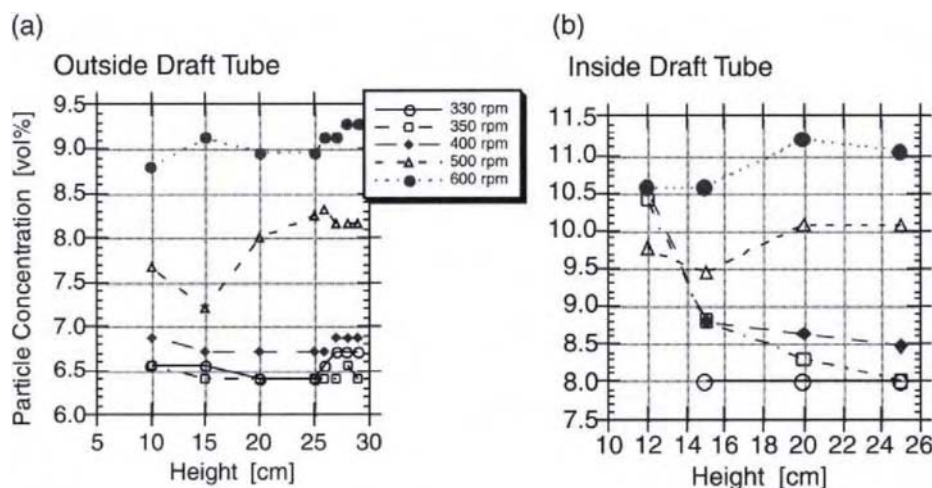


Figure 8.3 Particle concentration as a function of height (a) inside and (b) outside the draft tube of a laboratory scale DTB model crystallizer.

above the impeller. The profiles depend rather strongly on rpm. Since this configuration would commonly be found in a batch crystallizer, these data indicate a range of behavior possible in actual crystallizers.

Continuous crystallizers frequently employ draft tubes to enforce mixing up and down the vertical axis. Even with draft tubes, however, the solids will not be uniformly distributed in general. Figure 8.3 shows solids distribution in a laboratory model of a draft tube crystallizer (Green and Robertson 1993). Notice that there are variations with vertical position inside the crystallizer. In addition, the average concentration inside the draft tube is different from that outside because the net particle velocity and therefore particle hold-up is different where the particle settling velocity is opposite the net flow, i.e., in up flow; than where they settle in the net direction of the flow, i.e., down flow. This is discussed in more detail in Mullin (1994), Jones and Mullin (1973), and the experimental modeling section below.

Temperature also varies spatially in crystallizers, being higher near feed points where hot feed is added, exothermic reactions are preferentially occurring, and near any heating surfaces. Even zones where crystallization is happening more rapidly could conceivably have higher temperatures since crystallization is normally exothermic. Temperatures will be lower near cooling surfaces and in and near the boiling zone of an evaporative crystallizer. Since temperature is easier in general to measure than either solute or solids concentration, one would expect more data on temperature distribution in crystallizers than seems to exist. Chiampo et al. (1996) measured the temperature in a draft tube baffled crystallizer (DTB) (see Chapter 5) at 5 points. They found significant temperature variations, particularly at low agitation rates. Warmer temperatures, varying with time because of the formation of eddies, were found near the feed point. Temperatures near the solid surface heat transfer surfaces were lower than the bulk, but not greatly so. The temperature just under the surface of the suspension was found to be low in most cases studied. They found good thermal homogeneity when the ratio of agitator pumping flow rate to the feed flow rate is ≥ 450 for upward pumping and ≥ 700 for downward pumping agitators.

Of course, the combined effect of the distributions of the above three variables: solute concentration, solid concentration, and temperature; is to determine the spatial distribution of supersaturation, the dominant variable in determining crystal nucleation and growth rates. To reiterate, it is likely that supersaturation is higher in zones such as the vicinity of feed points and in and near

the boiling zone in evaporative crystallizers. Supersaturation can be expected to be lower in the bulk of the crystallizer and where the temperature is higher.

It should be noted that the situation could be more complicated when a hot undersaturated feed is introduced into a crystallizer. Let's assume that there is a plume associated with the feed point. The center of the plume may well be hot and undersaturated, indeed similar to the conditions in the feed stream itself. Surrounding this zone, however, will be a zone where the temperature has begun to fall, yet the concentration may still be high enough to create significant supersaturation. Therefore, the picture is of a plume with an undersaturated core surrounded by a shell in which the supersaturation will be higher, perhaps significantly higher, than that in the bulk of the crystallizer. The degree to which this happens and the spatial extent of such a plume of course depend strongly on the local mixing conditions in the vicinity of the feed location and on the diameter and velocity of the feed tube or nozzle.

8.4. CRYSTALLIZERS

The following section discusses crystallizer design from the perspective of mixing and solids suspension. See Chapter [5], "Crystallizer Selection and Design" for more information.

8.4.1. AGITATED SUSPENSION

Let us consider the agitated tank used as a crystallizer. Most agitated tanks are employed for liquid-liquid mixing; however, when used as a crystallizer, there are many other considerations. The goal, recall, is generally to achieve as nearly a homogeneous system as possible. Solids must be suspended. (For this discussion, we will assume that the crystals settle.) Feed streams must be rapidly mixed into the bulk of the suspension. The same is true for any other zones where the solution is concentrated or cooled, such as evaporation or heat transfer zones. Sufficient heat transfer surface and flow must be provided for efficient heat transfer. Finally, all of this must be accomplished in such a way that the shear imposed by the agitation system does not cause undue damage to the growing crystals or cause too much secondary nucleation.

Draft tubes are often used in crystallizers as they are particularly effective and efficient at imparting a good degree of vertical mixing. They are discussed in detail below. However, they are

usually employed only for continuous crystallizers because they do not operate well with the suspension level below the top of the draft tube, except as noted below.

Let us first focus on crystallizer geometries suitable for batch crystallization. Since these usually do not use draft tubes, other arrangements must be made to suspend particles over the entire height of the vessel. A low crystallizer height to diameter ratio can be used so that a single agitator will keep the solids in the entire tank suspended, or multiple impellers on a single shaft can be used in various combinations. Common arrangements include either two (or more) axial flow impellers, or a radial flow impeller near the bottom of the tank and one or more axial flow impellers above. The radial flow impeller is used to keep solids moving along the bottom of the vessel; perhaps also to provide a high shear region in the vicinity of an injection point for efficient mixing of the feed into the bulk. Ideally, all the impellers in the vessel need to act in concert. The flow from one impeller needs to feed smoothly into the zone of the next to keep the suspension smoothly flowing vertically in the vessel. Therefore, the spacing between impellers is crucial. Spaced too widely apart, the effect is to create individual mixing zones around each impeller, with relatively poor mixing between zones. Figure 8.4 shows the two situations schematically.

The use of baffles to provide adequate mixing and suspension is nearly a requirement. Impellers impart axial, radial and tangential (swirl) flow to the suspension. Baffles convert much of the tangential flow from the impeller to axial flow. Since axial flow is needed both for crystal suspension and macromixing, baffles are generally required for efficient mixing and suspension. Nonbaffled tanks are occasionally found in crystallizer service, perhaps in glass-lined or other specialty configurations, but upon closer examination, one will usually find significant mixing deficiencies associated with the absence of baffles.

Draft tubes function very much like multiple axial flow impellers in an open tank. They force a very efficient vertical mixing because the average flow has no choice but to go up and over the draft tube. This, plus the fact that there are no multiple impellers, each with its own potentially particle damaging high shear zone, means that draft tubes are generally the geometry of choice for crystallizers where the suspension level can be maintained within a somewhat limited range. Continuous crystallizers obviously usually fit this description, as well as some batch crystallizers, say when cooling begins only after the vessel is fully filled or when an anti-solvent or salting out component is a small fraction of the overall volume. In other cases, the advantages of the draft tube can still be used by cutting "windows" in the draft tube, thereby allowing the suspension to "short circuit" through the windows when the vessel is not full. Much of the benefit is retained (with some losses due to "short circuiting") when the suspension level is over the top of the tube.

The reason that draft tubes work only for a limited range of suspension heights is first that there is no flow over the top of the draft tube when the suspension height is much lower than the top of the draft tube. When this is the case, the suspension is higher in the region of up flow because the impeller imparts a pressure differential. The hydrostatic pressure difference created by the difference in heights outside and inside the draft tube equals the pressure difference produced by the agitator. When the height of the suspension in the up flow region is less than the height of the draft tube, there is no flow up and over the top and therefore no net circulation through the draft tube. Second, when the suspension height is greater than some critical height over the top of the draft tube, a clarified solution layer forms that is very poorly mixed into the rest of the vessel. This effect is dramatic and is shown in Figure 8.5 for a 20-liter laboratory crystallizer. The critical height depends in part

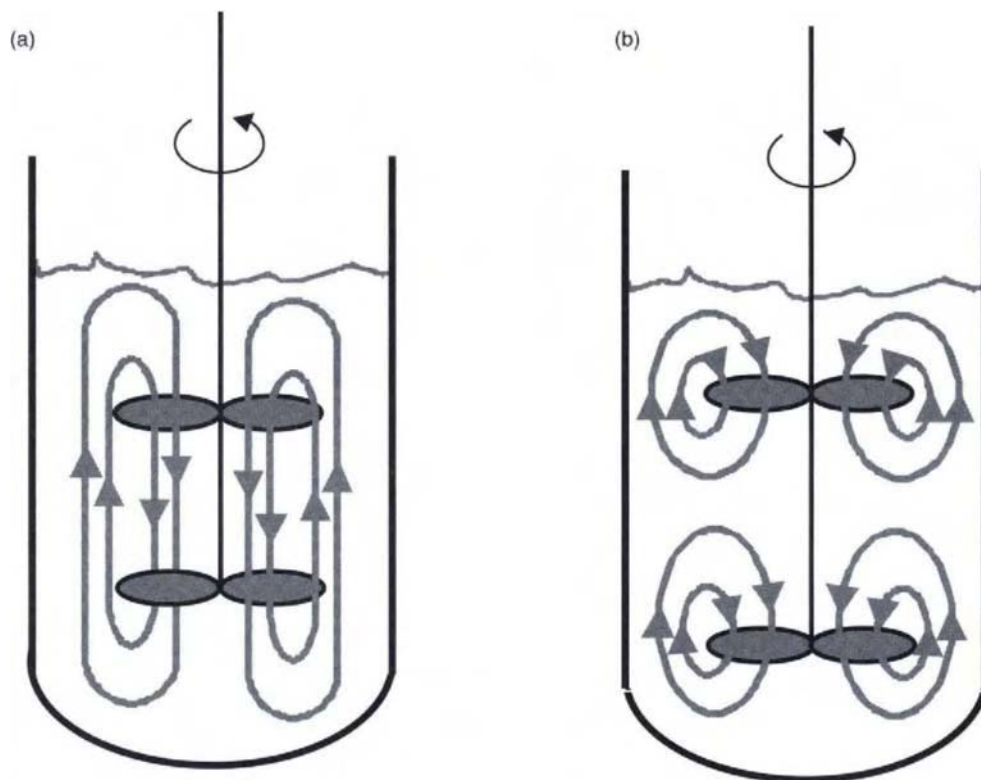


Figure 8.4 Placement of multiple axial flow impellers, (a) good and (b) bad.



Figure 8.5 Photograph showing clarified liquid well above the draft tube in a 20-liter laboratory crystallizer.

on the up flow velocity and the vessel geometry. Therefore, it is vital to maintain the suspension level in the crystallizer within these limits.

A related phenomenon is sometimes encountered when starting the flow in a draft tube vessel after the solids have slumped to the bottom. An initial flow rate large enough to disperse the particles and carry them over the top of the draft tube is needed to initiate complete suspension. This flow rate may be considerably higher than the steady state value needed once flow has been established. If the initial flow rate is insufficient, a situation can develop where liquid flows through the bed of particles which are now fluidized (see below) in the up flow region, but not conveyed over the top of the draft tube. Sufficient additional flow must be provided to expand the fluidized bed until the height of the bed is barely above the height of the draft tube. At this point, the solids

spill over into the down flow region and the suspension quickly disperses throughout the vessel.

There are two schools of thought as to draft tube diameter. To minimize damage to particles by minimizing the energy and velocities created by the agitation, the first school maintains that since a velocity significantly higher than the particle settling velocity is necessary only in upward flow, it makes sense to have a higher velocity in upward flow. This is created by choosing a draft tube diameter so that the cross sectional area of the up flow region is smaller than the down flow region. The second school of thought is that because of the dependence of the hindered particle settling velocity on particle size distribution, particle concentration, and fluid properties (Mullin 1994) any attempt to optimize the choice of draft tube diameter is futile since these values change frequently. Therefore, one may just as well choose that the cross sectional areas inside and outside the draft tube be approximately equal, meaning of course that the average velocities will also be equal in each zone. A draft tube diameter approximately $0.7 D_t$ creates these equal cross sectional areas. D_t is the tank diameter of the crystallizer.

It should be noted here that the choice of draft tube diameter affects mainly the ratio of the *average* suspension velocities inside and outside the draft tube. The velocity profiles in both regions often show marked deviation from uniform velocity profiles near the average value. Large recirculating zones are common, particularly next to the draft tube and associated with the turn the suspension makes around the top or bottom of the tube. The result is that there will be a higher speed flow adjacent to a low speed or recirculating zone. The velocity maximum may be *several times* the average velocity. Therefore, the average velocity may have little importance on the overall performance. A very simple computational fluid dynamics model illustrates this point. Figure 8.6 shows the prediction of flow around the top of a draft tube. A uniform up flow in the annulus of a $0.7 D_t$ draft tube is assumed. A large low-speed region forms inside and adjacent to the draft tube when the flow turns over the top of the tube, while a high speed down flow travels down the center. The velocity of this high-speed core is

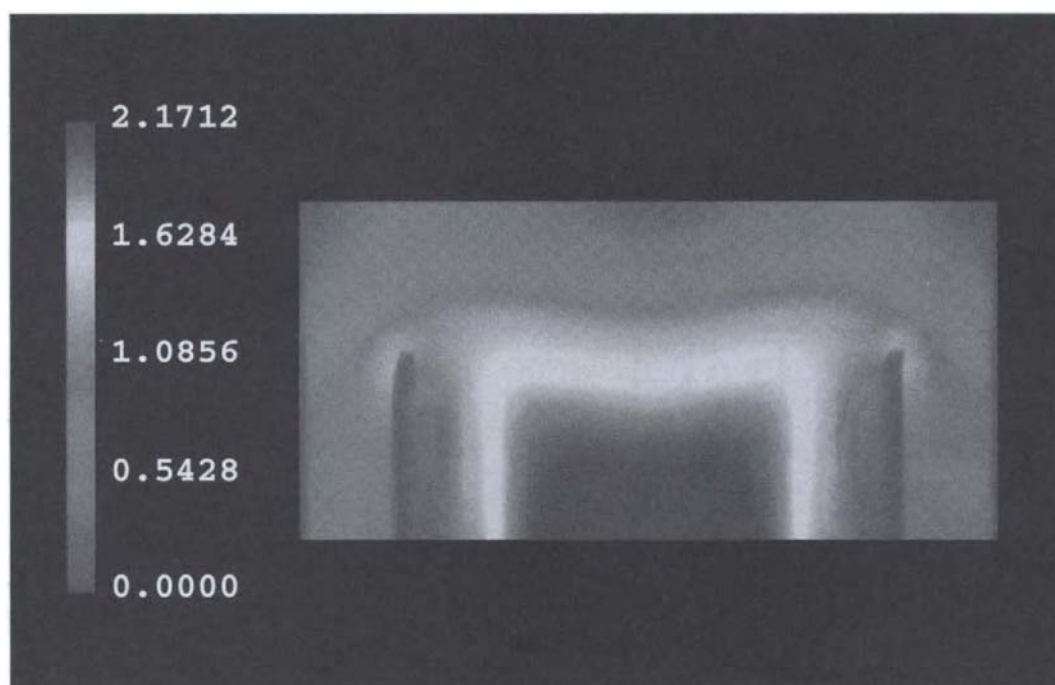


Figure 8.6 Results of CFD model of flow around top of draft tube, magnitude of velocity.

approximately twice that of the assumed uniform up-flow. Empirically, a tracer study in a 50,000 gallon industrial crystallizer found that the tracer velocity was approximately twice the computed average circulation velocity (Kendall, private communication).

The most well known example of the higher up flow velocity school is the "draft-tube baffled" or DTB design. In addition to a $0.5 D_i$ draft tube with up flow inside, an annular zone outside the main body of the crystallizer is provided to serve as a nearly quiescent fines settling zone to disengage mother liquor and fines from the rest of the suspension. The fines are separated for separate treatment such as fines destruction or clear liquor advance (also known as clear liquid overflow) (Mullin 1994). The use of this annular zone is possible because the flow outside the draft tube is downward and the relatively small flow of mother liquor and fines removed from the annulus must be upward to effect crystal segregation based on differing settling velocities. An axial flow impeller, now shrouded by the draft tube, provides up flow inside the draft tube. This impeller is placed at such a height inside the draft tube that in the event of an interruption to agitation and subsequent settling of the entire charge, the impeller will be above the sedimented particles in clear fluid, and therefore better able to reinitiate flow upon restarting.

One drawback of this design is the tendency of particles to sediment to the bottom of the vessel and remain. Aeschbach and Bourne studied vessel bottom configurations of model draft tube crystallizers to improve particle suspension (Aeschbach and Bourne 1972). They found that a shaped bottom can significantly improve the uniformity of particle suspension. The design found to be best has rounded tank "corners" and a center peak under the agitator. The rounding of the corners means there is less settling caused by low velocities associated with sharp corners and the center peak virtually eliminates the stagnation point that would otherwise be present (in the time averaged flow) at the bottom center of the tank under the agitator. Several features can easily be added to combat this tendency in DTB (or similar) crystallizers (Swenson Process Equipment, Inc., Harvey, Illinois). The bottom of the vessel can be made conical and the bottom of the draft tube slightly flared to constrict the clearance between the end of the draft tube and the lower part of the tank, thereby accelerating the flow for better crystal suspension. An upward pointing conical section in the very center of the bottom of the vessel is there for the same reason, and also to fill a region particularly subject to sedimentation because of the stagnation point in the center of the vessel bottom. See Figure 8.7. These additions approximate the slightly more complicated geometry recommended by Aeschbach and Bourne.

Accepted designs using equal cross sectional areas include crystallizers manufactured by Tsukishima Kikai (TSK) Co., Ltd., Tsukishima, Tokyo, Japan, and a proprietary design by DuPont (Randolph et al. 1990). The former uses a proprietary "double propeller" impeller that penetrates the draft tube and imparts momentum to the suspension both inside and outside the draft tube. The latter uses a radial flow impeller at the bottom of the draft tube, just above the vessel bottom. The principle advantage of these designs is that the impeller can be made large diameter and therefore turned relatively slowly. Circulation velocity nominally scales with the tip velocity of the impeller, while specific power input, the agitator power divided by either the swept volume of the agitator or the total suspension volume, scales with the rotational velocity cubed. This creates relatively high circulation velocities in the suspension with relatively low specific power inputs. Minimizing the rotational velocity of the impeller and therefore the specific power input for a given circulation velocity is often desired, particularly when crystallizing fragile materials, because particle damage generally increases with increasing specific power input: increasing strongly with impeller tip speed and decreasing with increasing agitator diameter (Offermann and Ulrich 1982).

Not all crystallizers are agitated with impellers in the vessel itself in agitated tank configuration. A common arrangement is to use a pump (or an axial flow impeller in an external pipe) to generate flow in a loop external to, but drawing from, and discharging to the main vessel. Such crystallizers are known as "forced circulation" crystallizers. These are widely used, for example, in sodium chloride crystallization (see Chapter 5, section 5.3.3.). These can be quite effective. Advantages are that the crystallizer feed can be introduced into the side stream, perhaps immediately upstream of the pump so that local turbulence can be very high, leading to very effective feed mixing. A conventional heat exchanger can be used on the side stream to add or remove heat from the crystallizer. It may be less expensive to use such a heat exchanger rather than a jacketed vessel and/or an internal vessel coil, or it can be used to supplement other heat transfer equipment. Also, product crystal suspension can be removed from the circulation loop, eliminating the need for a separate pumping system. A significant disadvantage is that the pump impeller or in-tube axial flow impeller is necessarily of a much smaller diameter compared to one rotating in the tank itself; therefore, as discussed above, the specific power input for forced circulation crystallizers is *much* larger than for properly designed conventional crystallizers. This, of course, means that they are generally a poor choice for the crystallization of fragile materials.

Crystallizers need not be mechanically agitated at all. Air injection inside a draft tube drives the circulation in the older Pachuca (Oldschue 1983) design. Because of the cost of compressing air, this design is no longer widely used. A modern variation, however, has been developed (Proxair, Inc., Tarrytown, New York). A cryogenic liquid is introduced into the bottom of a crystallizer, either with or without a draft tube. The liquid then boils, cooling the crystallizer and simultaneously driving the circulation of suspension with the resulting vapor stream.

8.4.2. FLUIDIZED BED

There is a class of crystallizers that are not agitated tanks, rather a bed of growing crystals is fluidized by a recirculating stream of

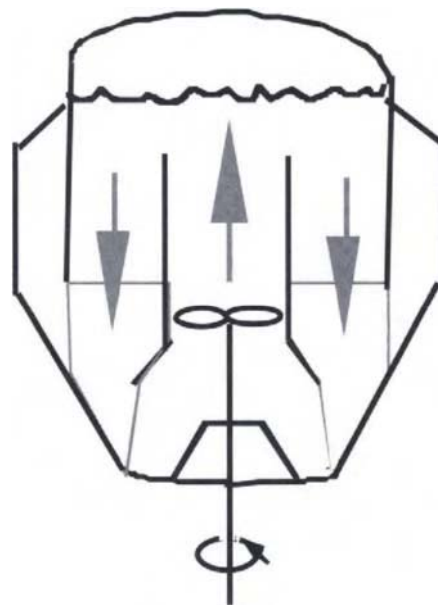


Figure 8.7 Features commonly used to combat settling of particles for DTB crystallizers.

mother liquor. Fluidization is the state where the drag force on a bed of particles exerted by upward flowing fluid equals or exceeds their weight. The bed expands and takes on fluid-like properties: it can be stirred; if a hole is punched in the side of the bed, the solids pour out, etc (Kunii and Levenspiel 1969). Fluidized beds are good solid/fluid contacting devices; hence their use as crystallizers where the fluid transports solute to the bed of growing crystals. One can envision a stable state of fluidization, with a nearly rectilinear vertical flow of fluid upward through a bed of largely motionless particles. However, at nearly all fluid flows above the minimum necessary to just fluidize the solids, the flow is unstable (Anderson and Jackson 1968). The instability produces voidage fluctuations in the dispersed solid phase. The usual state is that the bed is “bubbling”, that is particle-lean fluid-filled voids very similar in appearance to bubbles in a gas-liquid system propagate upward through the bed. These “bubbles” drag a particulate wake behind them as they rise through the bed and very efficiently backmix the solids. Therefore, the composition of the solid phase tends to be well mixed.

In fluidized bed crystallizers, the larger particles remain in the bed and are not circulated with the mother liquor (and smaller crystals). Therefore, they undergo considerably less attrition and breakage than in circulating suspension crystallizers. This type crystallizer is then particularly well suited for the crystallization of large crystals (Mersmann and Rennie 1995). In the typical fluidized bed crystallizer design, supersaturation is generated separately from the bed of particles; therefore, the supersaturation can become higher than it would be otherwise. Consequently, these designs are subject to fouling for systems with narrow metastable zones.

8.4.3. MELT CRYSTALLIZERS

The principle intent of this chapter is to review mixing in suspension crystallizers, most of which involve crystallizing a solute from solution, but we will consider the mixing of melt crystallizers briefly. (Chapter 7 provides a more complete review of mixing considerations and equipment options for melt crystallization.) Some melt crystallization processes involve mixing suspensions although the considerations are slightly different. Other melt crystallization processes feature the growth of a stagnant crystal layer. In melt crystallization, the liquid is entirely or predominantly a melt of the substance being crystallized. Mass transfer of the substance to the growing crystals is therefore not the rate limiting step as it can be in crystallization from solution. Instead, it is frequently the rate of heat transfer from crystals growing from the melt that sets the average crystal growth rate. Also of crucial importance (as it is also for solution crystallization) is the mass transfer of impurity away from the growing crystals where it is usually at least partially rejected. For these reasons, adequate mixing of the crystallizing suspension is also very important and many of the same considerations, except perhaps for the concern about distributing the crystallizer feed, apply.

Because melt crystallization is heat transfer limited, the formation of a layer of crystals on the heat transfer surface is commonly employed. For processes that employ the formation of a crystalline layer, agitation may be provided both to improve the local heat transfer coefficient between the melt and the heat transfer surfaces and also to reduce the accumulation of impurity adjacent to growing crystal surfaces. When a suspension is involved, it may be produced by scraping crystals from the heat transfer surfaces. Agitation may be provided to keep the resulting crystals suspended, provide improved heat transfer through a now subcooled melt to the growing crystals, and improve the mass transfer of rejected impurities away from the growing crystals.

8.4.4. FEED STRATEGIES

The location and arrangement of the crystallizer feed determines, to a large extent, how well the feed will mix into the bulk. As discussed above, this will have a great impact on the overall nucleation and growth rates, and on the uniformity of crystal growth of the entire process. Therefore, it behooves us to choose feed configurations with care!

To generalize, the feed stream should be introduced below the surface of the crystallizer, generally into a highly turbulent region to maximize micromixing. The region should also be subject to strong bulk flow to convect the newly mixed solution away into the bulk of the vessel to avoid concentrating the micromixing region (i.e., create good macromixing).

Often in the laboratory and in batch crystallization, the feed is dribbled onto the top suspension surface of the crystallizer. Usually this is a poor way to feed because the top surface is often not very well mixed into the bulk. The result is that the feed solution pools on the surface and a high supersaturation envelope forms around it, leading to high nucleation and encrustation rates. As a general rule, it is usually far preferable to introduce the feed well beneath the top surface of the suspension.

To satisfy the micro and macromixing requirements, it is usually preferred to introduce the feed near the agitator, just above or below an axial flow agitator or just to the outside of a radial flow agitator. The reasons for this are that the region adjacent to the agitator has generally the highest turbulence and therefore the best micromixing region to be had in the vessel. Adding just above or below an axial flow impeller insures a good flow through the micromixing region; therefore good macromixing. Similarly, feeding just to the outside of a radial flow impeller, where the flow is leaving the impeller accomplishes the same thing.

To enhance the turbulence at the very point of injection, it is often helpful to narrow the stream into a jet. This has two positive effects. Additional turbulence is generated by the jet action that enhances mixing. Also, the increased momentum of the jet carries the feed farther into the bulk, enlarging the feed mixing zone; therefore, decreasing the local maximum supersaturation occurring there.

Another often fruitful approach to dispersing crystallizer feeds is simply to distribute them. Instead of feeding the vessel at a single point, use multiple injection points. This can be done with discrete feed pipes, or a ring can be used with multiple orifices. It must be recognized, however, that the performance of such a system can be significantly degraded if one or more of the feed points becomes clogged or encrusted or if a distributor ring corrodes so that the feed preferentially flows through fewer orifices. Instrumentation to detect this possibility is helpful.

The above discussion of feed strategies has been concerned only with the feed of one component. This is typical of many crystallization process configurations, such as cooling or antisolvent addition crystallizations, but not all. In these others, such as reaction precipitation in which two reactant feed streams are fed, there are two separate feed streams or one reactant can be fed in semibatch fashion to another reactant already present in the vessel. The strategy of feeding the streams is important, particularly for fast reactions. See, for example, Tosun (Tosun 1988). Here the position of each of the streams has a strong influence on the particle size distribution and even on the morphology of the product. To generalize, it is best to separate the streams and to feed them into high shear regions as in the single feed stream case.

8.4.5. AGITATORS

There is always much discussion as to what particular type of agitator is best for crystallization. There are many considerations.

First, one must decide whether a radial or axial flow impeller, or some combination, is needed.

Radial flow impellers produce a high shear/high turbulence region. They do a good job producing flow in the vicinity of the impeller. They are normally placed near the bottom of the vessel so that the strong radial and not the weaker axial flow suspends particles. They must be placed nearer the center of the tank because typically they do not produce nearly as much vertical mixing as axial flow impellers (oriented to produce vertical flow). One shortcoming, particularly for radial flow impellers such as the Rushton turbine, which have a radial disk as part of their construction, is that they divide the tank into upper and lower sections, with less mixing *between* the regions. (This feature, however, may be beneficial in certain specialized cases, such as the precipitation of the product of two reactants, one fed above the impeller and one below.)

Axial flow impellers produce less radial flow, and much more axial flow for similar power input (as the name suggests). They therefore produce much more vertical mixing when so oriented. They also do a much better job mixing between the region above and below the impeller.

Since radial flow impellers generally produce a higher turbulence zone and axial flow impellers produce more vertical vessel flow, a good combination in applications where two or more impellers are used is to use a radial flow impeller near the bottom where the feed is introduced, and one or more axial flow impellers on the same shaft above it to provide vertical mixing and induce flow through the otherwise partially segregated region under the radial flow impeller.

Much work in recent years has gone into designing more efficient axial flow impellers. By efficient, it is meant that they produce more axial flow for the same power input. These are the so-called "fluid-foil" designs. They use airfoil-like blade cross sections to produce more axial flow and less blade drag and turbulence at the blade. Often they also use "winglets" at the tips of the blades. These reduce the blade tip vortices that form because fluid rushes from the high to the low pressure side of the blade, creating a vortical flow trailing from the blade tip. This flow serves little useful purpose, so to increase efficiency, it is damped with these additions. It should be noted that these highly developed designs will suffer from changes to their shape caused by encrustation and erosion much more than simpler but more robust designs.

It should be noted, however, all the energy input to an impeller or system of impellers is dissipated by the flow in the vessel, regardless of the type of impeller(s). What does change with the type impeller(s), of course, is the overall flow field in the vessel and the spatial dissipation of the energy dissipation. Turbulent energy is dissipated, as noted above, by the smallest scales of turbulence, so of course the spatial distribution of dissipation and turbulence intensity are closely related.

8.5. SCALE-UP

Industrial crystallization has the (at least partially deserved) reputation of being difficult to scale-up. If one considers that, as stated at the outset of this chapter, individual crystals respond only to their micro-environment and that mixing determines how the micro- and macroenvironments in the crystallizer interact as well as their spatial and temporal homogeneity, it is clearly mixing that determines the ease or difficulty of scaling this process.

A rapid examination of dimensional analysis is sufficient to convince us that, under most circumstances, the detailed dynamic behavior of a full scale crystallizer can not be captured with a geometrically similar laboratory scale experimental model. It is well known that it is impossible to achieve dynamic similarity between model and full scale of even liquid only mixing tanks and still use liquids of similar viscosity and density (Bird et al.

1960). In crystallizing systems, of course, we are not free in general to change the solvent and solute, so we must use the same crystallizing system in both lab and full scale. Complicating the situation is the fact that the particle size itself does not scale with the vessel dimensions. Neither of course do the transport properties associated with the particles and the suspension. Therefore, the settling velocity of the particles and consequently the necessary suspension velocities to suspend the particles also do not scale.

The crux of the scale-up problem is really that it is usually easy to achieve homogeneity at the bench scale, but almost always difficult or impossible to achieve at large scale. It is obviously easier to mix a smaller vessel. Length scales are smaller and circulation times are therefore less. The lab unit geometry is inevitably simpler than the full scale unit's.

We expect overall mass transfer in the system associated with liquid-liquid mixing, that is the mass transfer between solution in the macro- and microenvironments, to scale with the turbulent energy dissipation rate (Nienow et al. 1997). Therefore, let's assume that the mass transfer scales with the specific power intensity input to the crystallizers, which should roughly equal the turbulent dissipation rate. (Specific power intensity P is frequently defined as the power input by the vessel agitator divided by the volume of the suspension (Oldschue 1983). Another choice that is often preferred because the influence of the turbulent energy may be localized around the agitator is to divide the power input by the swept volume of the impeller.) While it is tempting to simply scale-up by keeping the specific power intensity equal between scales, this is usually impractical and often undesirable. The amount of power required is often simply too large. Also, if such power can be applied, it will often cause unacceptable damage to the growing crystals and unwanted secondary nucleation.

The ramification of the difference in suspension homogeneity between small and large scale is that mixing related problems are often encountered upon scale-up. Conversely, experimentally modeling full scale equipment in the laboratory often does not capture mixing related phenomena observed at the larger scale.

The unavoidable compromise of scaling crystallizer mixing is that high specific power input improves mixing and crystallizer homogeneity, which leads to the choice of high agitator speeds. On the other hand, particle damage and the control of secondary-nucleation (which are strong functions of agitator shear rate) argue for the use of low agitator speeds. Therefore, the appropriate trade-offs must be made to achieve sufficiently good mixing while minimizing particle damage and managing secondary crystal nucleation.

Many "rules" for scaling-up mixing in crystallizers (and/or suspending particles in tanks) have been proposed (Zwietering 1958, Rieger and Dittl 1982, Voit and Mersmann 1986, Kneule and Weinspach 1967, Zlokarnik and Judat 1988, Hemrajani et al. 1988, Buurman et al. 1985, Rieger et al. 1988, Davies 1986, Herndl 1982, Molerus and Latzel 1987, Chohey and Hicks 1984, Gates et al. 1976, Eienkel and Mersmann 1977, Nienow 1968, Baldi et al. 1978, Müller and Todtenhaupt 1972, Zehner 1986, Todtenhaupt et al. 1986, and Niesmak 1982). Geisler et al. compiled this list and reviewed the many options suggested for scaling the power input to vessels containing suspensions (Geisler et al. 1993). The range of the ratio of specific power intensity from lab to full scale is presented as a function of the scale-up ratio expressed as the ratio of vessel diameters in Figure 8.8. Remarkably, previous workers have suggested a range of specific power input scalings: $(D_{t,lab}/D_{t,fs})^{0.5} \leq P_{lab}/P_{fs} \leq (D_{t,lab}/D_{t,fs})^{-1}$.

To more fully appreciate the inherent conflicts in mixing scale-up, let us consider solids suspension, fluid mixing, and crystal damage separately.

First, we'll consider solids suspension. Zwietering found empirically that the angular velocity necessary to just suspend

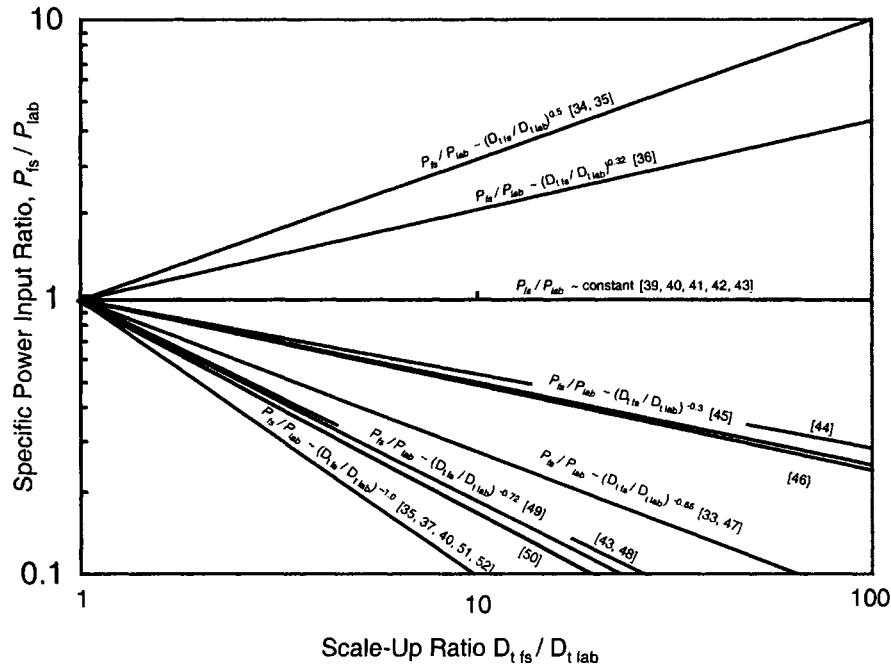


Figure 8.8 Scale-up rules. (Figure 1 in Geisler et al. 1993)

(but not *uniformly* suspend) similar particles in agitated tanks scales as $\omega D_a^\kappa = \text{constant}$, where ω is the angular velocity, D_a is the diameter of the agitator and κ is an empirically determined exponent (Zwietering 1958). The criterion of “just suspended” means that all particles are in motion, but implies nothing about the state of the suspension. Therefore, this correlation should generally be regarded as the absolute minimum requirement for solids suspension; not the desired operating point for processes sensitive to particle distribution, particularly crystallization.

To suspend particles, the linear velocity developed in the fluid by the impeller must exceed the settling velocity of the particles, $V > V_s$, where V is the linear velocity produced in the fluid by the impeller, and V_s is the settling velocity of the particles. To first approximation, V scales with the agitator tip speed, ωD_a , that is $V \sim \omega D_a$. Assuming that the settling velocity of the particles doesn't change with the scale of the apparatus, and that $V = o(V_s)$, $(\omega D_a)_{\text{model}} \sim (\omega D_a)_{fs}$. Therefore, $\frac{\omega_{\text{model}}}{\omega_{fs}} \approx \frac{D_{a,fs}}{D_{a,model}}$. This is equivalent to keeping the tip velocity of the impeller constant, as proposed by the more complete analysis of Nienow et al. (1996). (The linear velocity generated by the impeller is related to the tip velocity of the agitator by the “flow number,” N_Q (Oldschue 1983). For an axial flow impeller, the average velocity $\langle V \rangle \approx 4Q/\pi D_a^2$, where Q is the volumetric flow rate discharged by the agitator. Since $Q = N_Q \omega D_a^3$, $\langle V \rangle \approx 4N_Q \omega D_a/\pi$. Therefore, the tip velocity equals $\langle V \rangle$ when $N_Q \approx \pi/4$.)

Let us now consider the requirements. Typically, the first attempt at scale-up involves keeping the specific power input constant between scales (Oldschue 1983). The specific power input scales with the cube of the angular velocity, ω^3 . Therefore, while the ratio of angular velocities is proportional to the inverse of the ratio of the radii, the specific power intensity is proportional to the inverse *cube* of the ratio of the radii. Consequently, we can not maintain both the tip velocity and the specific power input constant upon scale-up. Either the tip velocity of the full scale agitator must be very much greater than in the laboratory if specific power intensity is kept constant, or the specific power

intensity of laboratory models is very much greater than that found in the full scale vessel if the tip velocities are kept constant.

Particle damage is a function of the shear produced by the agitator, which is nominally proportional to the agitator tip velocity (at least in the vicinity of the agitator). Particle damage is evidenced in different ways such as collision induced defects and crystal attrition. Crystal attrition fragments become additional growing crystals, effectively new nuclei. Additional secondary nuclei are produced by crystal collisions via mechanisms, which are still not fully understood, but thought to be either the disruption of the boundary layer around the crystals or dislodging microscopic surface nuclei (see Chapter 2, section 2.2.3.). At any rate, the result is a clear increase in the rate of nuclei produced with increasing agitator induced shear. Offermann and Ulrich showed that the number of crystal nuclei produced by an impeller is linearly related to the impeller tip velocity (Offermann and Ulrich 1982). A commonly used model of the nucleation rate includes $B \sim \omega^l$, where the exponent l is determined experimentally (Randolph and Larson 1988).

This suggests that we minimize tip velocity when possible upon scale-up (while keeping it large enough to uniformly suspend particles). This is why one should never use a small diameter impeller in a large crystallizer: the tip velocity to produce both the required flow to suspend particles and the specific power intensity to mix would be far higher than necessary and would probably cause excessive crystal damage and secondary nucleation. Also, the typical particle path for a complete circuit of the vessel will be much longer for the full scale vessel. Therefore, if the average linear velocities are comparable, the particles in the laboratory scale vessel pass through the high shear region of the agitator much more frequently than they do in the large scale vessel. For these reasons, it is often possible to *reduce* particle damage upon scale-up.

So, the various mixing considerations put conflicting requirements on the parameters involved in scale-up and there is no clear choice of scale-up rule. Geisler et al. (1993) argue that “there is no constant scale-up rule possible...scale-up prediction always

depends on the particle and fluid properties, as well as on the diameter ratios.” The appropriate choice of scale-up variables may also depend on both the nature of the material being crystallized and the equipment configuration. A fragile, damage prone compound may well have a greater dependence on agitator shear than a more robust crystal. A system with a well designed crystallizer feed, taking advantage of a highly turbulent high shear zone near an agitator, may reduce the sensitivity to specific power input. The individual merits of the system being crystallized and the chosen equipment must be carefully evaluated and tested to determine suitability. Certainly, practical measures to enable mixing conditions to be varied at full scale, such as variable speed agitator drives, should be considered, since the scale-up can not be reliably predicted.

8.6. MODELING

By now, you should be convinced that good mixing and the ability to achieve it at full scale are absolutely vital to crystallization. You should also have an understanding of some of the considerations, as well as the overall complexity, of the problem. Compounding these concerns are the nearly myriad possible configurations possible for a proposed process, or even the more constrained, but still very broad choice of conditions and configurations available to one trying to improve an existing process. A means of investigating and predicting the effects proposed changes in mixing conditions and configurations have is necessary. For these reasons, we turn to modeling.

Since, as discussed above, it is impossible to achieve dynamic similarity between laboratory and full scale, the predictive capability of empirical modeling of crystallization is limited. Mathematical modeling also has its shortcomings. Suspension flows in crystallizers are turbulent, two and perhaps even three phase (for boiling crystallizers), the particle size is distributed, and the geometry is complicated with perhaps multiple moving parts (impellers). This is of course beyond the possibility of analytical solution of the equations of motion, so we must turn to computational fluid dynamics (CFD). However, even CFD is not capable of successfully dealing with all of these features. Successful computational models of crystallizers to date are limited to very specific limited problems.

Is modeling then still worthwhile? Yes. It must, however, be applied to answer very specific questions, not the global prediction

of crystallizer operation. Some of the results must be recognized as being qualitative and not quantitative. Nevertheless, even such limited information can be very enlightening. The knowledge accumulated from model results, perhaps both experimental and computational, combined with knowledge and experience of what occurs in the actual process, frequently allows the crystallization practitioner to piece together a reasonable picture of the entire crystallization process, at least to the extent that specific problems can be solved or avoided.

8.6.1. EXPERIMENTAL MODELING

Recognizing that dynamic similarity can not be achieved, general quantitative predictions from laboratory models are not possible. It has often been found, however, that laboratory modeling is still valuable. The qualitative results obtained are often quite instructive. Additionally, many of the techniques applied in the laboratory can be adapted and applied to full scale mixing tests in actual industrial equipment.

By far the simplest approach is single phase (liquid only) experimentation in a laboratory model crystallizer. It is of very great value to use a transparent scale model so that the flow can be seen and photographed. Single phase experiments can be quite valuable, as long as their very great limitations are understood, primarily the scaling problems discussed above and the fact that the very important effect of particles on the flow is not included. Nonetheless, one can get a qualitative sense of overall flow patterns, areas of recirculation, and often identify poor mixing zones with these experiments. Standard techniques of flow visualization can be used, e.g., dye slowly injected at a point or following the progress of a few tracer particles. One method particularly valuable for studying mixing, which can also be applied when particles are present, is to put an indicator in the vessel, which is made either slightly acidic or basic; followed by the addition of the opposite, either base or acid, mixed with the feed stream at the usual feed point. Either a pulse or a continuous feed can be used. Mixing can then be evaluated by following the plume of indicator and noting its position and duration—how long until the plume either dissipates or the entire vessel turns color. Recently, we have been successful using phenolphthalein in a slightly acidic model crystallizer and adding a pulse of concentrated base to a continuous feed (Jacobs 1996). See Figure 8.9.

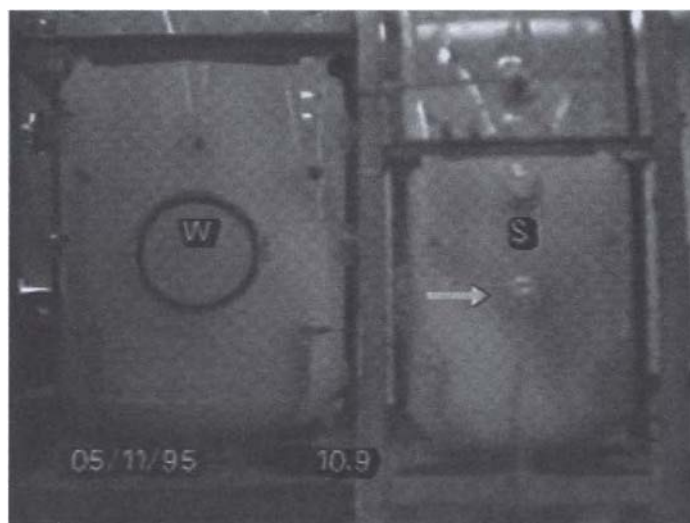


Figure 8.9 Photo of mixing experiments with phenolphthalein.

Thimol blue, which shows up better in video photography, is another good choice of indicator.

These experiments show how fast tracer mixes with the bulk. On the other hand, we are primarily interested in the steady state spatial distribution of solute concentration. In experiments with a 1 m diameter model crystallizer with a 0.7 m draft tube (Jacobs 1996), some regions receive tracer almost immediately, while others do not receive the tracer for several seconds or more. This indicates that when there is a continuous flow of solute containing feed into a crystallizer with growing crystals in suspension there will be spatial variation of the solute concentration (i.e., supersaturation). This is because nucleating and growing crystals are a solute "sink," relieving supersaturation everywhere in the suspension. Therefore, areas that receive feed/tracer more slowly will have lower supersaturation than regions that receive it sooner because the longer it takes for feed solute to reach a region, the more time is available for solute removal from solution by crystallization.

To fully convert the temporal information from tracer experiments to the spatial distribution of continuous feed injection requires a knowledge of the entire flow field in the vessel. Of course, we do not now have this information in general. It is necessary then to either measure or model the flow field before these results can be fully interpreted. In the interim, tracer experiments are useful in developing mathematical models, model verification, and also in estimating model adjustable parameters.

To determine how segregated the feed to a crystallizer is, a technique involving consecutive fast chemical reactions pioneered by Bourne can be used (Bourne et al. 1981). Sequential reactions $A + B \rightarrow R$ and $R + B \rightarrow S$ are run in the mixing tank or crystallizer, with A injected into the tank and B already present. In the version proposed by Bourne, A is 1-naphthol and B is diazotized sulfanilic acid in dilute alkaline solution. B is the limiting reagent. By examining the ratio of the intermediate and final products, R and S , we can determine whether the reaction occurs uniformly throughout the vessel, in a relatively small zone near the injection point, or some intermediate case. To clarify, let's examine the limiting cases. First, the concentration ratio X , the fraction of B which is finally present as S , is defined: $X = 2[S]/([R] + [S])$. (Square brackets indicate the concentration of the enclosed species.) Given the stoichiometry and the fact that B is the limiting reagent, $[B_0] = [B] + [R] + 2[S]$, where $[B_0]$ is the initial concentration of B in the vessel. $[B_0] = [R] + 2[S]$, assuming the reactions go to completion. Therefore, $X = 2[S]/[B_0]$.

Conveniently, the final reaction product composition can be determined simply by spectrophotometry since both R and S are dyes. If the mixing is slow compared to the reaction rate, the reaction occurs in a thin layer at the envelope of the feed plume, as shown schematically in Figure 8.10a. The rate of reaction is controlled by the rate of diffusion of A across the envelope boundary. In this case, all A is immediately consumed by B and only R results. X in this case, therefore, equals 1. If, on the other hand, the vessel is completely well mixed, the reaction occurs throughout the

vessel volume, as shown schematically in Figure 8.10c, as B has equal access to both A and the intermediate product R . Now, both R and S are produced. The value of X obtained is determined by the kinetics of the individual reactions, but is the minimum value for this system. X is therefore bounded, $1 \leq X \leq X_{min}$. The intermediate case, where the reaction is neither fully diffusion nor kinetically controlled is shown in Figure 8.10b. The reactions proposed by Bourne are fast enough to probe most mixing applications, but may not be fast enough to probe very rapid mixing devices such as impinging jets or grid mixers. Mahajan and Kirwan have developed an alternate pair of reactions with much lower time scales to probe these situations (Mahajan and Kirwan 1996).

The above technique can of course be applied quite easily to characterize mixing conditions in laboratory scale equipment, but can also in principle be applied to characterize the mixing performance of full scale equipment.

The capabilities of laser Doppler anemometry (Durst et al. 1981) (LDA) are continually improving. Advances such as the use of fiber optics and the ability to coordinate measurements with agitator passage make it much more accessible. It has been applied to crystallizer geometries and to mixing tank and agitator geometries similar to crystallizers (Stoots and Calabrese 1995), and has greatly advanced our understanding of these flows. LDA can be used to simultaneously measure all three spatial components of velocity by using and resolving three colors of laser light simultaneously. LDA is inherently a point-wise measurement. Mapping out an entire flow field is very cumbersome and the resolution is necessarily coarse. Particle image velocimetry (PIV), in which images of particles taken a short, known interval apart are cross correlated region by region to determine the particle velocity as a function of position in the image plane, measures the velocity over a two-dimensional slice of the flow field. Both LDA and PIV actually measure particle velocities and not fluid velocities directly. To measure fluid velocity, a fairly low concentration of particles is dispersed in the flow. These particles are chosen so that they very closely follow the fluid, i.e., they are small and with a small density difference relative to the fluid. Both techniques can in principle be used to directly measure crystal velocities, but in general crystal concentrations are too high to allow the necessary optical access for either of these techniques to operate, except in limited cases with low particle concentration (Yu and Rasmuson 1999).

For a more complete understanding, it is necessary to include the effect of prototypic particle concentrations on the flow. For experimental flow modeling, it is generally best to employ a non-crystallizing, attrition resistant solid in a convenient liquid. Otherwise, the particle size distribution (PSD) and potentially the morphology of the particles will constantly change over the course of the experiments. Various such solids have been used, such as glass or plastic spheres, sand, and polymer resin pellets. Some thought should be given to the density difference between the solid and liquid, as well as the PSD. It usually makes sense to select a system with a settling velocity approximately equal to that found in the actual process.

There are several approaches to obtaining information about the flow patterns and mixing. Dye injection and acid/base/indicator neutralization experiments used for single phase experiments have some value, but less than for single phase, because the particles obstruct the view and one can only see typically one to a few centimeters into the flow. Often, however, enough information can be extracted to make this a useful exercise. In particular, it is valuable to follow single phase experiments with selected two-phase experiments used as verification of the single phase results.

We have used a simple fiber optic reflectometer (MTI Photonic reflectometer, Mechanical Technologies, Inc., Latham, New York) (Figure 8.11) to measure local particle concentration. For

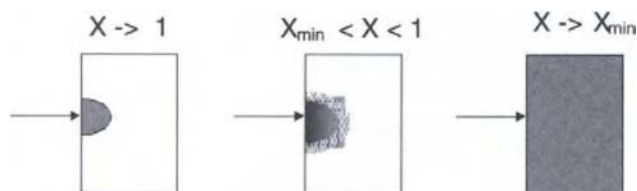


Figure 8.10 Schematic of limiting cases with Bourne reactions.

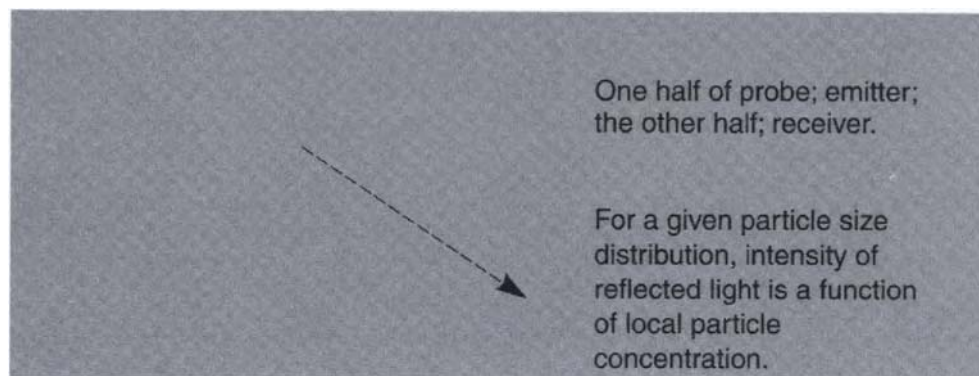


Figure 8.11 Schematic of a simple fiber optic reflectometer used to measure particle concentration in a model crystallizer.

suspensions of particles with a narrow size distribution, this device can be calibrated to give particle concentration. By traversing the probe around the vessel, the spatial uniformity of the particle concentration can be estimated. For suspensions of glass spheres in water in a laboratory model of a DTB crystallizer (average particle concentration 10 volume %; 128 μm average diameter), we find particle concentration gradients vertically that are complicated functions of the agitation rate (Figures 8.3a and b). There is also a clear difference between the average concentration inside and outside the draft tube (comparing the average particle concentrations of Figures 8.3a and b) caused by the different particle residence times in each zone resulting from the difference in net particle velocities, the vector sum of the particle settling velocity and the local average fluid velocity. This can be crudely modeled by considering hindered settling. The Richardson-Zaki correlation (1954) can be used along with an estimate of the fluid velocity in each region: the pumping rate of the agitator divided by the cross sectional area. The predicted particle concentrations are 13 and 9.1 volume %, inside and outside the draft tube respectively, significantly overpredicting the actual difference of approximately 2 volume %.

The residence time distribution of both solution and crystals can be measured, although this information typically shows only gross differences in mixing quality. We have injected spikes of sodium chloride into an 8 liter laboratory DTB crystallizer model filled with a suspension of water and glass spheres (Green and Robertson 1993). Water was continuously fed and solution with-

drawn through a screen so that particles were retained in the vessel. A spike of sodium chloride solution was added to the feed and the chloride ion concentration of the withdrawal stream monitored as a function of time. As can be seen in Figure 8.12, there is a considerable difference between feed injected on the centerline above the agitator and that injected at the side of the vessel for a low rpm with incomplete suspension. On the other hand, the difference for higher rpm and complete suspension is much less. The residence time distribution for the crystals can be characterized as outlined by Nienow (1997). Bourne and Zabelka (1980) used this technique to characterize the average residence time of crystals in a laboratory crystallizer as a function of crystal size.

Process tomography has recently made dramatic advances and is a very good candidate for application to crystallizers. McKee has made measurements of particle concentration in an agitated tank (1994), clearly showing gradients in particle concentration. To my knowledge, the technique has not yet been applied to draft tube vessels, but in principle this could be easily done by dividing the vessel into two zones, inside and outside the draft tube, each with its own array of sensors. This is a particularly promising technique because it can be applied to large process vessels.

For full flow visualization, a transparent slurry must be obtained. Transparent particles, such as clear plastic or glass, are used with a liquid formulated to match the index of refraction of the solids (Karnis et al. 1966). The problem encountered is that liquids with high enough index of refraction tend to be either very

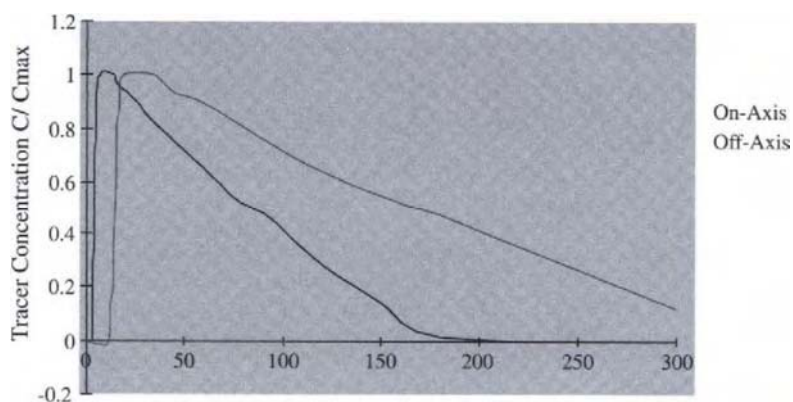


Figure 8.12 Residence time distribution in a laboratory-scale model DTB crystallizer.

viscous, toxic, flammable, or likely to dissolve plastics. Abbott et al. report using polymethylmethacrylate (PMMA) spheres in a solution of tetrabromomethane and a polyalkylene glycol (1993). We have used glass spheres in xylene with a small amount of diiodomethane, but this is only partially satisfactory. Although suspension transparency increased dramatically over the same spheres in water, it was never fully transparent. We suspect that there is some dispersion of the index of refraction of the glass. Merzkirch (1987) has tabulated data from Donnely (1981) on liquids having refractive indices close to PMMA. Tracer particles are used to follow the flow. The particle flow is tracked by marked particles similar in size, shape, and density to the transparent particles, while the fluid flow can be resolved by tracking very small ($o(1\ \mu\text{m})$) (Bachalo 1994) marked particles.

Once the model suspension has been rendered transparent, a whole range of techniques that rely on optical access to the flow field becomes available. LDA, for example, can measure the velocity at a particular point. Sheets of laser light can illuminate slices of the flow and PIV can in principle be applied (Liu and Adrian 1993). Generally, these techniques require specialized equipment, but practitioners should be encouraged to investigate crystallizer flows.

Although instrumentation capabilities are continually improving, the limitation of experimental modeling that dynamic similarity can not be obtained is absolute, imposed by the physics of the system. However, computational modeling is continually improving and is indeed the great hope for future comprehensive crystallizer mixing models.

8.6.2. COMPUTATIONAL MODELING

The majority of applications of crystal population balance modeling have assumed that the solution and suspension in the crystallizer are homogeneous, i.e., the Mixed-Suspension Mixed-Product Removal (MSMPR) approximation (Randolph and Larson 1988). (This is simply the analog of the Continuous Stirred Tank (CSTR) (Levenspiel 1972) approximation for systems containing particles. It means that the system is well mixed from the standpoint of the solute concentration and the particle concentration and PSD. In addition, the effluent is assumed to have the same solute concentration, particle concentration, and PSD as the tank.) This approximation is clearly not justified when there is significant inhomogeneity in the crystallizer solution and suspension properties. For example, it is well known that nucleation kinetics measured at laboratory scale do not scale well to full scale. It is very likely that the reason they do not is because MSMPR models used to define the kinetic parameters may apply fairly well to relatively uniform laboratory crystallizers, but do considerably worse for full scale, relatively nonhomogeneous crystallizers.

In cases where significant inhomogeneity exists, a distributed parameter model is needed that allows for and predicts the spatial distribution of key process parameters. The ultimate goal is a comprehensive model that predicts characteristics of the crystals produced, taking into account, e.g., flow fields, mass transfer, dynamic particle population balance, and crystal growth. Of course, developing and solving such a model is vastly more difficult. This comprehensive model remains significantly beyond reach for the general case of crystallization. Let's examine some of the difficulties.

Realistic treatment of most crystallizers requires modeling turbulent high concentration two phase flow, which is at the cutting edge of CFD development. Recent advances both in constitutive relations and computer processor speed have advanced this field, but there are still significant limitations. New developments in user interfaces and the general decrease in cost of computational

power are making this type CFD modeling available to more and more crystallization practitioners.

Modeling the feed zone, with its attendant micromixing, is difficult because the small length scales of the micromixing ($o(\text{Kolmogorov scale})$) are below the grid size of the computational mesh. The mesh can not be made fine enough to model these scales because the number of computations necessary will overwhelm even today's fastest computers. Therefore, micromixing models for the subgrid scales are necessary and discussed below.

Examining some of the successful CFD work on crystallization that has been reported, each model has significant limitations to its applicability. For example, several workers have modeled precipitation, using the assumption that since the particles are present at a small size and low concentration, they do not significantly affect the fluid flow, for example the work of Wei and Garside (1997) and van Leeuwen et al. (1996). Others have had a more limited initial goal, such as predicting only the flow field (Ten Cate et al., accepted, and Derksen and Kontomaris, in preparation), or the flow fields and the distribution of solids (Green et al. 1998), as discussed in more detail below. Still others have used greatly simplified hydrodynamic models to examine the effect on other aspects of the process, such as using Poiseuille flow and examining the effect on aggregation (Mumtaz and Hounslow, in press).

There is another more pragmatic approach to crystallizer modeling. By dividing the crystallizer into individual zones or "compartments," which are then generally treated as individual MSMPRs, spatial variation in the actual crystallizer can be modeled by allowing the parameters to vary between the individual compartments (Neumann et al. 1999). The relative simplicity of this approach, while still capturing some of the effects of the spatial distribution of variables in the vessel is encouraging. There are of course drawbacks: Deciding how to divide the crystallizer into compartments is vital to the success of the approach. Typical choices of compartments are one for the feed zone; the evaporation zone, if there is one; and several for the bulk of the crystallizer, say at least one inside and one outside of a draft tube. The exchange flow rates between compartments must be specified. Since these are not known in general, they are often treated as adjustable parameters. Alternately, CFD flow modeling can be used to determine appropriate values for these exchange velocities (Zauner and Jones 1999).

The logical extension of this approach is to divide the crystallizer into many compartments. This is known as the "network of zones" approach and has been used successfully by Mann (1993). Here, the exchange flows between compartments are not modeled but applied separately, either from a knowledge of the overall flow pattern achieved from experimental measurements or from a CFD flow model. Additionally, rules are applied which describe the turbulent transport of particles and species between zones.

Coupling CFD with one of the much simpler zone models is potentially particularly valuable. It is difficult and time consuming to add the additional complexity of mixing, heat and mass transfer, and dynamic population balance modeling to the CFD model, plus it makes the CFD model very slow. Sufficient accuracy may be achievable for many applications from applying the population balance modeling to the simpler zone models, although accuracy will be limited because the effects of the particle concentration, distribution and PSD will not be fed back to the transport models. Alternately, comprehensive CFD models can be used to understand the flow and its variation for a limited number of conditions, but simpler zone models may be used for application of the model where speed and convenience are important and detailed accuracy is not, e.g., process control.

Let us now take a closer look at some of the detailed considerations of modeling crystallizer flows.

8.6.3. IMPELLER TREATMENT

The standard method of CFD is to set up a geometrical grid on which to perform the finite difference/finite element analysis of the equations of motion. This mesh is fixed to the boundaries of the problem and the fluid moves through it. For a tank with an agitator, i.e., the configuration of most crystallizers, the agitator impeller represents a portion of the boundary that moves relative to the rest of the boundary, i.e., the tank and baffles. This is a complicated problem to treat rigorously. Of course, the agitator can not be treated explicitly with a fixed grid, except as noted below. There are several different options to treat the impeller problem, each offers a particular combination of fidelity to the problem and computational complexity.

The simplest approach is to not attempt to model the detailed impeller dynamics, but rather to apply a specified momentum source at or near the impeller location. A series of mesh points are selected where a momentum source condition is applied. For example, the fluid velocity can be specified at a plane just above the impeller. Since the impeller is the primary source of turbulent energy in the system, a turbulence source should be specified as well. This approach is the only choice for 2 dimensional models, and can be used for 3 dimensional models as well.

The advantages of the momentum source approach are that it is simple and computationally efficient. The other treatments that will be discussed all require additional computation. One disadvantage is that the momentum source must be specified. Frequently experimental data obtained at the desired conditions are the basis of the values chosen, but for a nonstandard agitator or a standard agitator working under nonstandard conditions, an experimental program to measure the velocities in the vicinity of the agitator under process conditions is necessary. An alternate approach may be to perform one of the more detailed calculations discussed below for a single case; then use this information, perhaps scaled appropriately, to specify the momentum and turbulence sources for production calculations. Another disadvantage is that none of the dynamics of the rotating impeller are captured. In cases where it is important to capture these dynamic interactions, this approach will be inadequate.

The next more complicated treatment is the use of "multiple reference frames" (Ranade 1997). Here, a mesh is generated that is stationary with respect to the vessel. Inside this mesh, meeting it in a cylindrical boundary, is another mesh which is stationary with respect to the impeller, in other words it is "attached" to the impeller and moving with respect to the tank and the other mesh. A quasisteady state flow problem is then solved in each mesh, with the two solutions being matched where the two mesh boundaries meet. The problem, as you might imagine, is in making the solutions match at the interface. For this reason, this approach is limited to problems where the inner and outer flows are not strongly coupled. This approach has been applied with good success for single phase modeling of agitated, baffled tanks. The advantage is, for an approach that is slightly more computationally intensive, the impeller itself is actually modeled, which may be important for those cases where impeller/fluid or impeller/solids interactions are important. Its disadvantages include that it does require more computational time, and the limitation to problems with weakly interacting inner and outer flows.

The third "standard" for modeling rotating impellers is the "sliding mesh" approach (Rai 1985). Here, a grid is attached to the impeller that does not extend much beyond the outer radius of the impeller. This is the most computationally intensive of the three standard techniques, but also the most accurate. In principle, it fully captures the effect of the agitator on the flow.

As in many other areas of CFD, advances in impeller treatment are occurring rapidly, both in developing new treatments and in making the established treatments more accurate and more efficient computationally. For example, Derksen and Van den Akker (1999) have applied an adaptive force field technique in a model of Rushton turbine flow. VanderHeyden et al. (private communication) at Los Alamos have developed a technique of switching a momentum source term at certain mesh node points on and off in a pattern that simulates the effect of a rotating impeller. These and other approaches promise increased fidelity with greater computational efficiency.

8.6.4. TREATMENT OF TURBULENCE

Modeling turbulence is difficult because it is impossible to use a mesh fine enough to capture the fine scales of the turbulence for realistically sized vessels. This poses a significant problem for modeling. To rigorously capture turbulent behavior computationally, our numerical grid must resolve the smallest length scales and still be large enough to fit the entire vessel. In practice, in all but some very specific cases, the necessary number of grid points is too large. Even with the fastest modern computers, the computational load is too high. Therefore, several approaches have been taken. One, Direct Numerical Simulation (DNS) resolves the smallest turbulence scales, but attempts to model only a very small volume of the flow domain. Boundary conditions are necessarily highly idealized. Since the volume is often too small to allow realistic representations of turbulence generating elements, a spatially uniform source of turbulent energy is frequently used (Moin and Mahesh 1998). Despite the obvious limitations, we rely on this type modeling to investigate features of the turbulence that we can then incorporate into other, less rigorous, but more realistic models.

To model turbulence in realistic geometries, such as process vessels, another approximation must be employed. Since the computational grid can not be made fine enough to capture the fine scales of the turbulence, the turbulence itself is modeled. These models are called "closure models" One family of approximations is called Reynolds Averaged Navier Stokes (RANS) models, including the familiar $k-\epsilon$ model (Hinze 1975). There are significant limitations, chief among them that the turbulence is assumed to be isotropic.

Models of turbulent flow continue to evolve. A very promising technique is Large Eddy Simulation (LES) (Galperin and Orzag 1993). Clearly, the larger scales of turbulence, created as they are by inherently anisotropic vessel elements and highly influenced by the vessel envelope, are not isotropic. LES then models the large scale turbulent structures realistically, relying on a closure model, which assumes isotropic properties, to capture only the subgrid scales. Since there is a very much greater chance that the *subgrid* scales are approximately isotropic, this is potentially a much more accurate approach. Techniques, such as the Lattice-Boltzmann method, have also been developed that significantly speed the computations. This in turn allows the use of finer computational grids and therefore more accurate rendering of a broader spectrum of turbulence length scales.

Most often, simpler turbulence models are chosen for crystallizer flow modeling because of the complexity of the rest of the model system. Some variant of the $k-\epsilon$ model is typically used for the liquid phase.

8.6.5. MODELING MULTIPHASE FLOW

Modeling dense multiphase flows is difficult. Consider some of the complexities of the problem. A full solution to the equations of

motion for a solid/liquid suspension flow would require that the flow field around each individual particle be determined, as well as all the interactions among the particles, including their effect on the liquid. The complexity of this for suspensions of anything much over a few volume % solids is daunting and has not been successful. Therefore, we need to approximate. Two fundamental approaches are taken: First LaGrangian particle tracking, where computationally we predict the trajectories of a finite number of particles in a flow field; then use this information to extrapolate and infer some properties of more concentrated suspensions. The second approach is to view the particles as their own “continuous” phase. This requires resolving the flow on a large enough length scale that the flow and motion of individual particles are not resolved, rather the flow of the overall solids phase is. (This seems surprising at first, but in fact is analogous to using the continuum approximation for the description of the flow of discrete fluid molecules.) There are then two continuous phases modeled that interpenetrate each other and exchange momentum: the liquid and the solid, hence the name for this technique: the interpenetrating continua (IC) model, also known as the “two-fluid” model.

The principle drawback of LaGrangian particle tracking is that to model dense suspensions, just too many particles have to be tracked. Since the computational time is at least proportional to the number of particles, the time required for computation increases very quickly with particle number. There are different degrees of realism possible with this approach. Particle collisions may or may not be allowed, as may the interparticle effects associated with perturbations to the liquid flow field. Of course, each level of additional complexity requires more computation. Part of the method’s strength is that, since particles are essentially treated individually, accounting for particle size distribution among particles is straightforward. Particle growth, breakage, and agglomeration can all be modeled.

The underpinning of the IC approach is volume averaging of the equations of motion (Drew 1983, and Anderson and Jackson 1967). In this approach, the equations of motion are averaged over volumes sufficiently small so as to be small relative to the domain being studied, but large relative to the individual particle diameter. (The same equations can also be derived from mixture theory (Homsy et al. 1980))

The IC model has particle concentration as a parameter, but higher particle concentrations do not automatically require more computations, so it becomes more efficient for dense suspensions. Some of the drawbacks of this technique, however, lie in the empiricism necessary to close the model. Treating the particles as a continuous phase, while of considerable merit, is obviously not completely accurate. Terms arise in the model that have a somewhat unclear meaning and whose values, although estimable, can not be rigorously measured. One of these is the “viscosity” of the dispersed solid phase. This arises because momentum is clearly dissipated by the solids as the suspension is sheared. Think of the flow around each individual particle: each creates shear and has a wake, dissipating momentum. The way in which this is captured in the model is to include a term in which the solids phase is assigned a viscosity. Momentum exchange between the fluid and solids continua also clearly occurs and is included in the model, but can not be rigorously measured. The values for these terms are inferred from measured suspension properties and other relationships, such as drag laws.

The treatment of particle size distribution, particularly time varying particle size distribution is problematic. Particle size distribution figures in the model only in the choice of empirical parameters chosen to represent the solids phase. These would be averaged quantities for a given particle size distribution and set of particles. In crystallization, of course, this particle size distribution is in general evolving with time. As there are no satisfactory models to

predict the dependence of all of the empirical parameters on the details of the particle size distribution, it is not now possible to capture an evolving particle size distribution with a simple liquid/solids IC model. One possible approach, although prohibitive in computational cost for all but very limited cases, would be to divide the particle size distribution into a number of size ranges (of number n); then to define each as its own “continuum” and incorporate into the interpenetrating continuum model. Of course, another drawback would be all the exchange of momentum terms needed to express momentum exchange between what is then $n + 1$ continua. Although limited, this approach would be valuable when the PSD can be divided into a very small number of ranges (say fine and large particles). In fluidization, Sinclair is working on incorporating the effects of bimodal PSDs into IC models (VanWachem 2000).

Another approach being developed that shows great promise is to use the modes of the size distribution to account for the effect of particle size distribution on flow. Brown et al. (1995) have shown that this modal approach can be applied to polydisperse aerosol particles in air flow. Here, moments of the PSD are used to couple the evolving PSD with the IC model. The additional computational load imposed is relatively low.

Although less well defined than turbulence of the continuous phase, the dispersed, particle phase also experiences turbulence. Turbulence in the solids is usually either treated with a simple RANS model, such as $k-\epsilon$, or ignored. There are other considerations, such as the influence turbulence in one phase has on turbulence in the other phase. These effects are not captured in the momentum transfer terms contained in the time averaged equations and must be separately included.

Recently, we applied IC modeling to monodisperse suspension flows in crystallizers with mixed success. Specifically, we modeled an experimental model crystallizer in which we had measured the spatial distribution of glass spheres in suspension (Green and Robertson 1993). Glass spheres being denser than typical crystals, we thought this would be an interesting, although perhaps overly difficult case, to model. The availability of experimental measurements on the laboratory scale gives us the ability to evaluate the quality of the computational predictions. The geometry, a modified DTB geometry without external fines settling zone, is shown in Figure 8.13.

We were able to capture some details of the distribution of particles with the computational model, but not all. The experi-

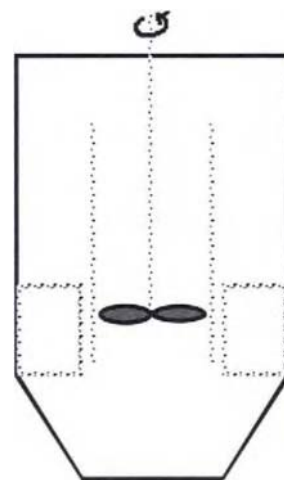


Figure 8.13 Geometry of laboratory DTB crystallizer; data are in figures 3 and 14.

mental data were introduced above and shown in Figure 8.3. There was significant temporal variation of the signal; therefore, the reported values are time-averaged. Readings were taken at a number of agitator rotational speeds from 330 to 600 rpm. We estimate the accuracy of the measurement to be about ± 0.5 volume %. Outside the draft tube, there is only a slight variation with vertical position. Inside the draft tube, however, there is a significant variation with vertical position; furthermore, there is a dependence on the angular velocity of the agitator. For lower rotational speeds, there is clearly a zone of higher particle concentration just above the agitator; while for higher angular velocity, the situation is much more uniform; perhaps even reversed: higher concentration at the top of the draft tube than just above the agitator. (Because of the presence of the agitator, the lowest measurable position is just above the agitator inside the draft tube.)

The predicted spatial distribution of the solids concentration is shown in Figure 8.14 for several agitator speeds. The resolution of these plots is adjusted to 0.5 volume %, about the same as the expected experimental accuracy. The results successfully capture the dependence of the solids concentration inside the draft tube on vertical position. The predicted solids concentration is more uniform outside the draft tube, as in the experimental observations. However, the magnitude of the variation in the solids concentration is underpredicted. Also, the CFD model does not successfully capture the difference in average particle concentration inside and outside the draft tube. The model evidently over represents the dispersion of the particles.

8.6.6. MIXING MODELS

Similar to turbulence itself, mixing occurs over a range of length scales. The treatment of macromixing is straightforward, coupling mass transfer with the equations of motion. However, in regions such as the feed point where micromixing is important, a closure model is needed because the length scales of micromixing are below the scale of the computational grid. This is analogous to the need of a closure model for the smallest turbulent length scales. One example of such a model is the engulfment model proposed by Baldyga and Bourne (1989).

The capabilities of mixing models are improving. It is now possible to predict blend times, the time needed for a mixing tank to reach a nearly homogeneous state after the injection of a pulse of tracer. Efficient LaGrangian methods are making it possible to follow both fluid elements and particles to determine fates and develop probability density functions for phenomena in mixing.

8.6.7. COMPREHENSIVE MODELS

The difficulty of obtaining a comprehensive model becomes apparent when we consider that mixing models alone are insufficient. The CFD flow model predicts the flow fields for both solution and crystals, as well as the spatial crystal distribution (as a function of time, in general). The mixing model and coupled mass transport modeling can then predict the solute concentration as a function of position and time. The energy equation must be coupled so that the temperature distribution can be predicted. Once the concentration and temperature fields are solved, the supersaturation can be predicted given knowledge of the saturation of the solute as a function of temperature. Then, the dynamic population balance must be applied. Supersaturation is the dominant variable, but a complete representation of the flow opens the possibility of using more realistic models of the fundamental crystallization mechanisms. For example, the dependence of crystal nucleation on local shear rate and particle concentration could be included. The particle population properties: particle concentration and PSD must then be fed back into the transport models because of the coupling of the particle field with supersaturation and transport properties. Each step in this process is significant, creating great computational demands. When coupled, the ability to achieve this envisioned comprehensive model remains elusive. The computational demands are simply too great.

Even though this comprehensive model for the general case of high solids loading industrial crystallization remains unachieved, the success of modeling the limited cases of low concentration precipitation (to which I've previously referred) suggests that this approach should be quite successful when advances in computing power and model efficiency make the extension to conventional crystallization possible.

8.7. SUMMARY

Understanding mixing is vital to understanding and controlling the basic phenomena associated with industrial crystallization. Our limited understanding and ability to predict the effects of mixing has caused many of the problems encountered in controlling and scaling-up industrial crystallization.

Our hope is that this situation can be improved, particularly as our ability to characterize and predict crystallizer mixing improves. While we do not yet have complete predictive capability applicable to the vast majority of industrial crystallization processes, our predictive ability is steadily improving. Computational modeling is advancing. Special cases, such as precipitation can now be treated

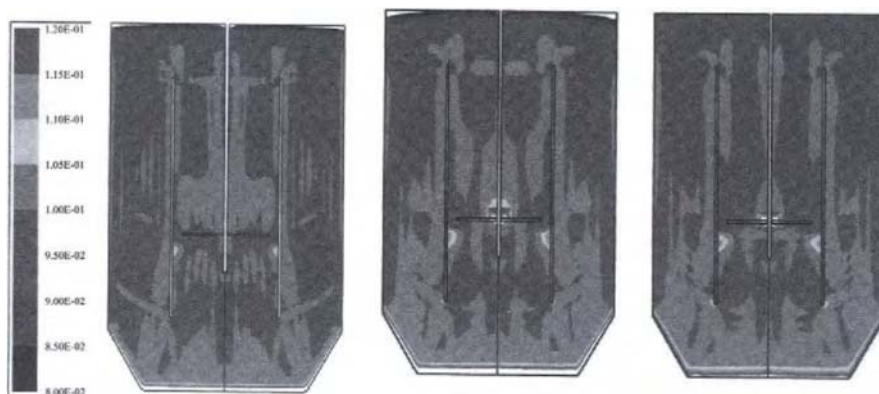


Figure 8.14 CFD prediction of solids distribution of a laboratory model DTB crystallizer.

that would have been impossible only a few years ago. The fidelity of our models and the range of applicability will steadily improve as both constitutive models and computational power increase.

We also have many tools to characterize mixing both in the laboratory and to a more limited extent at full scale. While we must constantly remember that experimental modeling is in general limited to a qualitative understanding, we should gather whatever information is possible and utilize it to synthesize a much better understanding of our crystallization processes. We should employ modern characterization techniques to full scale crystallizers as often as possible. First, by doing so we will obtain unambiguous data on full scale crystallizer mixing. Second, it will only be with such data that we will be able to verify the predictions of our computational and laboratory models. In fact, recently the progress in obtaining such data has not kept pace with the advances being made in modeling, so that there is now a paucity of data with which to compare developing computational models.

Even though quantitative predictions are not in general available for crystallizers, the importance of good qualitative understanding of the mixing phenomena occurring in operating crystallizers should not be underestimated. Both laboratory and computational modeling can now give us qualitative insight into the mixing processes. There are also tools available to investigate specific details of our processes, which is a great help in designing, operating, and troubleshooting. The level of understanding our improving capabilities now provide allows us to intelligently design crystallization vessels and anticipate many of the problems that will be encountered in many, if not all, cases.

ACKNOWLEDGMENT

I gratefully acknowledge the input, assistance, and encouragement provided by colleagues Ross Kendall, Kostas Kontomaris, Richard Grenville, and Art Etchells.

REFERENCES

- Abbott, J., Mondy, L.A., Graham, A.L., and Brenner, H. (1993). "Techniques for Analyzing the Behavior of Concentrated Suspensions," In *Particulate Two-Phase Flow* (Rocco, M.C., ed.), Butterworth-Heinemann, Boston.
- Aeschbach, S., and Bourne, J.R. (1972). "The Attainment of Homogeneous Suspension in a Continuous Stirred Tank," *Chem. Eng. J.* **4**, 234–242.
- Anderson, T.B., and Jackson, R. (1967). "A Fluid Mechanical Description of Fluidized Beds; Equations of Motion," *I&EC Fund.* **6**(4), November, pp. 527–539.
- Anderson, T.B., and Jackson, R. (1968). "Fluid Mechanical Description of Fluidized Beds; Stability of the State of Uniform Fluidization," *I&EC Fund.* **7**, pp. 12–21, February.
- Bachalo, W.D. (1994). "Experimental Methods in Multiphase Flows," *Int. J. Multiphase Flow* **20**, pp. 261–295.
- Baldi, G., Conti, R., and Alaria, E. (1978). "Complete Suspension of Particles in Mechanically Agitated Vessels," *ChemESci.* **33**, pp. 21–25.
- Baldyga, J., and Bourne, J.R. (1989). "Simplification of Micromixing Calculations. I. Derivation and Application of New Model," *Chem. Engr. J.* **42**, pp. 83–92.
- Baldyga, J., and Bourne, J.R. (1992). "Interactions Between Mixing on Various Scales in Stirred Tank Reactors," *ChemESci.* **47**(8), pp. 1839–1848.
- Bird, R.B., Stewart, W.E., Lightfoot, E.N. (1960). *Transport Phenomena*, pp. 108–111, John Wiley & Sons, New York.
- Bourne, J.R. (1997). "Mixing in Single-Phase Chemical Reactors," In *Mixing in the Process Industries*, 2nd ed. (Harnby, N., Edwards, M.F., and Nienow, A.W., eds.), pp. 184–199, Butterworth-Heinemann, Oxford.
- Bourne, J.R., and Zabelka, M. (1980). "The Influence of Gradual Classification on Continuous Crystallization," *ChemESci.* **35**, pp. 533–542.
- Bourne, J.R., Kozicki, F., and Rys, P. (1981). "Mixing and Fast Chemical Reaction—I: Test Reactions to Determine Segregation," *ChemESci.* **36**(10), pp. 1643–1648.
- Brown, D.P., Rubin, S.G., and Biswas, P. (1995). "Development and Demonstration of a Two/Three Dimensional Coupled Flow and Aerosol Model," In *Proceedings of the 13th AIAA Applied Aerodynamics Conference*, American Institute of Aeronautics and Astronautics.
- Buurman, C., Resoort, G., and Plaschkes, A. (1985). "Scaling-Up Rules for Solids Suspension in Stirred Vessels," *Proceedings of the 5th European Conference on Mixing*, BHRA Fluid Engineering, Cranfield, UK.
- Chiampo, F., Camanni, G., and Conti, R. (1996). "Thermal Characterization of a Crystallizer," In *Proceedings of the 5th International Conference: Multiphase Flow in Industrial Plants*, September, Amalfi, pp. 269–279.
- Chopey, N.P., and Hicks, T.G. (1984). *Handbook of Chemical Engineering Calculations*, McGraw-Hill, New York.
- Davies, J.T. (1986). "Particle Suspension and Mass Transfer Rates in Agitated Vessels," *Chem. Eng. Process* **20**(4), pp. 175–181.
- Deen, W.M. (1998). *Analysis of Transport Phenomena*, pp. 518–519, Oxford University Press, Oxford.
- Derkens, J., and Kontomaris, K. "Numerical Simulation of Turbulence Dynamics in an Industrial Agitated Tank," in preparation.
- Derkens, J., and Van den Akker, H.E.A. (1999). "Large Eddy Simulations on the Flow Driven by a Rushton Turbine," *AIChEJ* **45**(2), pp. 209–221.
- Donnelly, R.J. (1981). "Fluid Dynamics" In *AIP 50th Anniversary Physics Vade Mecum* (Anderson, H.L., ed.), Am. Inst. Phys., New York.
- Drew, D. (1983). "Mathematical Modeling of Two-Phase Flow," *Ann. Rev. Fluid Mech.* **15**, pp. 261–291.
- Durst, F., Whitelaw, J.H., and Melling, A. (1981). *Principles and Practice of Laser-Doppler Anemometry*, 2nd ed., Academic, New York.
- Einenkel, W.D., and Mersmann, A. (1977). "Erforderliche Drezahl zum Suspendieren in Rührwerken," *Verfahrenstechnik (Mainz)*, **11**(2), pp. 90–94.
- Galperin, B., and Orzag, S.A., eds. (1993). *Large Eddy Simulation of Complex Engineering and Geophysical Flows*, Cambridge University Press, Cambridge, UK.
- Gates, L.E., Morton, J.R., and Fondy, P.L. (1976). "Selecting Agitator Systems to Suspend Solids in Liquids," *Chem. Eng.* **83**, pp. 144–150.
- Geisler, R.K., Buurman, C., and Mersmann, A.B. (1993). "Scale-Up of the Necessary Power Input in Stirred Vessels with Suspensions," *Chem. Engr. J.* **51**, pp. 29–39.
- Green, D. A., Rogers, J.M., Robertson, D.C., and Tolbert, L.F. (1995). "Formation of Attrition- and Breakage-Resistant Polycrystalline Sodium Perborate Tetrahydrate Particles," In *Proceedings of the 1995 Topical Conference "Recent Developments and Future Opportunities in Separations Technology"*, AIChE, New York.
- Green, D.A., and Robertson, D.C. (1993). "Suspension Dynamics and Mixing in Draft Tube Crystallizers," In *Proceedings of the 12th Symposium on Industrial Crystallization*, vol. 2, (Rojkowski, Z.H., ed.), Politechnika Warszawska, Warsaw.
- Green, D.A., Kontomaris, K., and Kendall, R.E. (1988). "Computational Fluid Dynamics as a Tool for Understanding Industrial Crystallization," presented at AIChE Annual Meeting, November 1998.
- Hemrajani, R.R., Smith, D.L., Koros, R.M., and Tarmy, B.L. (1988). "Suspending Floating Solids in Stirred Tanks—Mixer Design, Scale-Up and Optimization," *Proceedings of the 6th European Conference on Mixing*, Associazione Italiana di Ingegneria Chimica, Milan.
- Herndl, G.T. (1982). *Stoffübergang in gerührten Suspensionen*, Ph.D. thesis, Technical University of Munich.
- Hinze, J.O. (1975). *Turbulence*, 2nd ed., pp. 197–202, McGraw-Hill, New York.
- Homsy, G.M., El-Kaissy, M.M., and Didwania, A. (1980). "Instability Waves and the Origin of Bubbles in Fluidized Beds—II: Comparison with Theory," *Int. J. Multiphase Flow* **6**, pp. 305–318.
- Jacobs, G. (1986). "DuPont HARDTAC Crystallizer Feed Point Mixing," Ingenieurs Titel degree thesis, Technical University of Delft, The Netherlands.
- Jones, A.G., and Mullin, J.W. (1973). "The Design of a Draft-Tube Agitated Vessel," *Chemistry and Industry* **21**, pp. 387–388, April.
- Karnis, A., Goldsmith, H.I., and Mason, S.G. (1966). "The Kinetics of Flowing Dispersions; 1. Concentrated Suspensions of Rigid Particles," *J. Colloid and Interface Science* **22**, 531–553.

- Kendall, R.E., private communication.
- Kneule, F., and Weinspach, P.M. (1967). "Suspendieren von Feststoffpartikeln im Rührgefäß," *Verfahrenstechnik*, (Mainz), **1**(12), pp. 531–540.
- Kunii, D., and Levenspiel, O. (1969). *Fluidization Engineering*, pp. 3–5, John Wiley and Sons, New York.
- Levenspiel, O. (1972). *Chemical Reaction Engineering*, 2nd ed., pp. 97–98, Wiley, New York. (Levenspiel uses the abbreviation CFSTR for "continuous flow stirred tank reactor," which is synonymous.)
- Liu, Z.C., and Adrian, R. (1993). "Simultaneous Imaging of the Velocity Fields of Two Phases," In *Particulate Two Phase Flow* (Rocco, M.C., ed.), Butterworth-Heinemann, Boston.
- Mahajan, A., and Kirwan, D.J. (1996). "Micromixing Effects in Two Impinging Jets Precipitator," *AIChEJ.* **42**, pp. 1801–1814.
- Mann, R. (1993). "Computational Fluid Dynamics (CFD) of Mixing in Batch Stirred Vessels Used as Crystallizers," In *Proceedings of the 12th Symposium on Industrial Crystallization*, vol. 2. (Rojkowski, Z.H., ed.), Politechnika Warszawska, Warsaw.
- McKee, S. (1994). *Tomographic Measurements of Solid Liquid Mixing*, Ph.D. dissertation, University of Manchester Institute of Science and Technology, Manchester, UK.
- Mersmann, A., and Rennie, F.W. (1995). "Design of Crystallizers and Crystallization Processes," In *Crystallization Technology Handbook*, (Mersmann, A., ed.), Marcel Dekker, New York.
- Merzkirch, W. (1987). *Flow Visualization*, 2nd ed., Academic Press, Orlando.
- Moin, P., and Mahesh, K. (1998). "Direct Numerical Simulation: A Tool in Turbulence Research," *An. Rev. Fluid Mechanics* **30**, pp. 539–78.
- Molerus, O., and Latzel, W. (1987). "Suspension of Solid Particles in Agitated Vessels, Part I and II," *ChemESci.* **42**(6), pp. 1423–1437.
- Müller, W., and Todtenhaupt, E.K. (1972). "Grossrührwerke in der Grundstoffindustrie," *Aufbereit. Tech.*, **1**, pp. 38–42.
- Mullin, J.W. (1994). *Crystallization*, 3rd ed., pp. 384–386 and 410–411, Butterworth-Heinemann, Oxford.
- Mumtaz, H.S., and Hounslow, M.J. "Aggregation During Precipitation from Solution: an Experimental Investigation Using Poiseuille Flow," *ChemESci.* **55**, in press.
- Neumann, A.M., Bermingham, S.K., Kramer, H.J.M., and van Rosmalen, G.M. (1999). "Modeling Industrial Crystallizers of Different Scale and Type," *Industrial Crystallization 1999; Proceedings of the 14th International Symposium on Industrial Crystallization*, IChemE, Rugby, UK.
- Nienow, A.W. (1997). "The Suspension of Solid Particles," In *Mixing in the Process Industries*, 2nd ed., (Harnby, N., Edwards, M.F., and Nienow, A.W., eds.), pp. 364–393, Butterworth-Heinemann, Oxford.
- Nienow, A.W. (1996). "The Effect of Agitation and Scale-Up on Crystal Growth Rates and on Secondary Nucleation," *TransIChemE.* **54**, pp. 205–207.
- Nienow, A.W. (1968). "Suspension of Solid Particles in Turbine-Agitated Baffled Vessels," *ChemESci.* **23**, pp. 1453–1459.
- Nienow, A.W., Harnby, N., and Edwards, M.F. (1997). "Introduction to Mixing Problems," In *Mixing in the Process Industries*, 2nd ed. (Harnby, N., Edwards, M.F., and Nienow, A.W., eds.), p. 10, Butterworth-Heinemann, Oxford.
- Niesmak, G. (1982). *Feststoffverteilung und Leistungsbedarf gerührter Suspensionen*, Ph.D. thesis, Technical University of Braunschweig.
- Offermann, H., and Ulrich, J. (1982). "On the Mechanical Attrition of Crystals," *Industrial Crystallization*, vol. 81, (Jancic, S.J., and de Jong, E.J., eds.), pp. 313–314, North Holland Publishing Co.
- Oldschue, J.Y. (1983). *Fluid Mixing Technology*, Chemical Engineering, pp. 155, 198, 200 and 469–470, McGraw-Hill, New York.
- Rai, M.M. (1985). "Navier-Stokes Simulations of Rotor-Stator Interaction Using Patched and Overlaid Grids," AIAA-85-1519, American Institute of Aeronautics and Astronautics.
- Ranade, V.V. (1997). "An Efficient Computational Model for Simulating Flow in Stirred Vessels: a Case of Rushton Turbine," *ChemESci.* **53**(24), pp. 4473–4484.
- Randolph, A.D., and Larson, M.A. (1988). *Theory of Particulate Processes: Analysis and Techniques of Continuous Crystallization*, 2nd ed., pp. 80–94 and 125–126, Academic Press, San Diego.
- Randolph, A.D., Mukhopadhyay, S., Sutradhar, B.C., and Kendall, R. (1990). "Double Draw-Off Crystallizer; Major Player in the Acid Rain Game?" In *Crystallization as a Separations Process*, (Myerson, A.S., and Toyokura, K., eds.) ACS Symposium Series No. 438, American Chemical Society, Washington.
- Richardson, J. F., and Zaki, W.N. (1954). "Sedimentation and Fluidization: Part I," *TransIChemE.* **32**, pp. 35–53.
- Rieger, F., and Dittl, P. (1982). "Suspension of Solid Particles in Agitated Vessels," In *Proceedings of the 4th European Conference on Mixing*, BHRA Fluid Engineering, Cranfield, UK.
- Rieger, F., Dittl, P., and Havelkova, O. (1988). "Suspension of Solid Particles—Concentration Profiles and Particle Layer on the Vessel Bottom," In *Proceedings of the 6th European Conference on Mixing*, Associazione Italiana di Ingegneria Chimica, Milan.
- Shamlou, P.A., and Koutsakos, E. (1989). "Solids Suspension and Distribution in Liquids Under Turbulent Agitation," *ChemESci.* **44**(3), pp. 529–542.
- Smoluchowski, M.V. (1916). "Versuch einer mathematischen Theorie der Koagulationskinetik kolloider Lösungen," *Zeitschrift f. physik. Chemie.* **92**, pp. 129–168.
- Stoots, C.M., and Calabrese, R.V. (1995). "Mean Velocity Field Relative to a Rushton Turbine Blade," *AIChEJ.* **41**(1), January, pp. 1–11.
- Ten Cate, A., Derksen, J.J., Kramer, H.J.M., van Rosmalen, G.M., van den Akker, H.E.A. "The Microscopic Modeling of Hydrodynamics in Industrial Crystallizers," *ChemESci.*, accepted.
- Todtenhaupt, P., Forschner, P., Grimsley, D., and Lases, A.B.M. (1986). "Design of Agitators for the ERGO Carbon-in-Leach Plant," In *Proceedings of the International Conference on Gold*, South African Institute of Mining and Metallurgy Symposium series, **58**(2), pp. 195–207.
- Tosun, G. (1988). "An Experimental Study of the Effect of Mixing on the Particle Size Distribution in BaSO₄ Precipitation Reaction," *Proceedings of the Sixth European Conference on Mixing*, May, BHRA, Cranfield, UK.
- van Leeuwen, M.L.J., Bruinsma, O.S.L., and van Rosmalen, G.M. (1996). "Influence of Mixing on the Product Quality in Precipitation," *ChemESci.* **51**(11), pp. 2595–2600.
- VanderHeyden, B., Los Alamos National Laboratory, private communication.
- VanWachem, B., Schouten, J., Krishna, R., van den Bleek, C., and Sinclair, J. (2000). "CFD Modeling of Gas-Fluidized Beds with Bimodal Particle Distribution," *AIChEJ.* (in press).
- Voit, H., and Mersmann, A. (1986). "General Statement for the Minimum Stirrer Speed During Suspension," *Ger. Chem. Eng.* **9**, pp. 101–106.
- Wei, H.Y., and Garside, J. (1997). "Application of CFD Modelling to Precipitation Systems," *TransIChemE.* **75**(A), pp. 217–227.
- Yu, Z., and Rasmuson, Å. (1999). "Hydrodynamics Generated by a Pitched-Blade Turbine in a Stirred Suspension," In *Industrial Crystallization 1999; Proceedings of the 14th International Symposium on Industrial Crystallization*, IChemE, Rugby, UK.
- Zauner, R., and Jones, A.G. (1999). "A Hybrid CFD-Mixing Approach for Scale-Up of Reactive Precipitation—Experimental and Modelling Results," *Industrial Crystallization 1999; Proceedings of the 14th International Symposium on Industrial Crystallization*, IChemE, Rugby, UK.
- Zehner, P. (1986). "Fluidodynamik beim Suspendieren im Rührbehälter," *Chem-ing.-Tech.* **58**(10), pp. 830–831.
- Zlokarnik, M., and Judat, H. (1988). "Stirring," In *Ullmann's Encyclopedia of Industrial Chemistry*, vol. B3, Verlag Chemie, Weinheim, Germany.
- Zwietering, T.N. (1958). "Suspending of Solid Particles in Liquid Agitators," *ChemESci.* **8**, pp. 244–253.

This Page Intentionally Left Blank

CONTROL OF CRYSTALLIZATION PROCESSES

J.B. Rawlings, C.W. Sink, and S.M. Miller

9.1. INTRODUCTION

9.1.1. OVERVIEW

In this chapter we take a fairly broad look at industrial crystallizer control. Since the people working on these problems may come from an instrumentation and control background or a crystallization process background, we begin with a review of the basics of crystallizer design and operation as well as a discussion of some of the measurements and manipulated variables available for use in the simple control schemes outlined in Section 9.2. Section 9.3 presents the state of the art in practiced crystallizer control. As such, this section is probably of primary importance to the audience responsible for actual crystallizer design, instrumentation, and operation. Finally, Sections 9.4 and 9.5 review the progress being made in improving crystal quality control for both continuous and batch crystallizers. It is hoped that this article will serve as a useful reference for industrial practitioners as well as pointing out fruitful opportunities for academic researchers.

The operation of an industrial crystallizer, whether batch or continuous, must satisfy the customer's requirements for product purity and crystal size distribution (CSD), and the manufacturer's requirements for economic and trouble-free production. The generated CSD also affects other customer acceptance criteria such as dusting, ability to flow, and dissolution rate. From the manufacturer's point of view, the production cost is influenced by the effects of the CSD on the efficiency of downstream product recovery processes such as thickening, solid-liquid separation, and drying. To meet these diverse production objectives, all the variables affecting the crystallization process must be controlled within an acceptable range that is dictated by the chemical nature of the product, solvent, and impurities present. The linchpin between the process definition and an economical and reliable production capability is a strategy for controlling these variables.

The effectiveness of the control strategy is not determined by the computational power of the control system, or the user-friendliness of the operator interface, but by the ability to achieve and maintain the conditions in the process that meet the process objectives. Some of the process variables must be controlled by the configuration of the equipment, an important consideration during the mechanical design. Others must be controlled during operation through manipulation of the equipment to effect process condition changes during batch crystallization, or to compensate for disturbances and changes in the system to maintain constant conditions for continuous crystallization.

The principal variables that must be controlled in crystallization are the solution supersaturation, the crystal surface area available for growth, and the nucleation rate. These are affected by multiple interacting secondary variables, which may be divided into two categories—equipment design variables and dynamic variables affecting the crystallization. It is the secondary dynamic variables, such as those listed in Table 9.1, to which automatic process control is applied in a typical crystallizer; for these vari-

ables, proven measurement techniques are available, and a direct response is obtained by manipulating some final control element. As delineated in Tables 9.2 and 9.3, it is the equipment design variables that determine many of the dynamic variables' interactions and the range over which these variables may be manipulated.

Three additional considerations are required to successfully control a crystallization process. Local conditions rather than bulk, and instantaneous rates of change rather than mean values control the relative rates of nucleation and crystal growth. Further, the response of the system to control changes is history dependent. Spontaneous nucleation that accompanies an excursion beyond the supersaturation metastable limit dramatically affects the surface area available for crystal growth and influences the product CSD of a continuous process for several residence times or the final CSD of a batch process.

Griffiths (1925) provides a discussion of some of the first attempts to move the design and determination of operating policies for crystallizers to the scientific arena from the realm of intuition and experience. This chapter will discuss some of the successful, currently practiced industrial control strategies and

TABLE 9.1 Process Variables Dynamically Controlled

Continuous Process	Batch Process
Operating temperature	Rate of temperature change
Absolute pressure	Rate of pressure change
Agitator or pump speed	Agitator or pump speed
Residence time of product	Batch time
Crystal by size (via fines destruction or classified product withdrawal)	
Level	Rate of addition of nonsolvent
Feed rate	
Feed temperature	
Feed concentration	
Slurry density (via mother liquor advance or evaporation)	

TABLE 9.2 Process Variable Constraints Imposed by Equipment Design Variables

Design Variable	Constraint
Feed entrance depth	Maximum temperature of feed in evaporative crystallizer
Vacuum source and size	Minimum operating temperature in evaporative crystallizer
Condenser size or vessel diameter	Maximum evaporation rate based on heat transfer area or liquid droplet entrainment limitation
Volume	Maximum residence time at design capacity

TABLE 9.3 Process Variables Interactions Determined by Equipment Design Variables

Design Variable	Determines Relationship Between		
Heat transfer area	Heat removal rate	and	Maximum local supersaturation
Agitator or pump type and size	Volumetric turnover	and	Shear (energy input)
Baffle cross-sectional area	Fines cut-off size	and	Removal rate (flow)
Volume	Residence time	and	Feed rate
Agitation and geometry	Rate of generation of supersaturation	and	Distribution of supersaturation
Number of stages	Temperature, supersaturation,	and	Yield

review the current understanding of relating process control technology to the requirements of automating crystallization processes.

9.1.2. TYPICAL CRYSTALLIZER DESIGN

There are many means by which crystallization from solution is carried out, including evaporative and cooling crystallization and crystallization in which the supersaturation is produced by salting out or by reaction crystallization. The method employed depends on the characteristics of the material being crystallized. For example, materials with relatively flat temperature-solubility curves are usually crystallized by evaporative methods, while materials with a large sensitivity of solubility to temperature are crystallized by cooling (Larson 1978). Even after the type of crystallization is selected, there are several possible permutations: in a cooling crystallizer, the cooling can be obtained by either vacuum evaporation or by surface cooling; a fines destruction loop may be used. For a continuous crystallizer, classified product removal may be employed. Larson (1978) discusses the relationship between the CSD and various design parameters and gives several examples of industrial crystallizer configurations.

Obviously, there are many different configurations of batch and continuous crystallizers. The design used for a particular chemical system must be selected in light of the nature of the material being crystallized and the desired properties of the product, such as purity, habit, and CSD. For simplicity, the discussion

of feedback controllers given in Section 9.2 is illustrated with cooling crystallizers; however, the concepts presented are applicable to other types of crystallizers.

Figure 9.1 is a schematic of a continuous cooling crystallizer equipped with the measurement devices and manipulated variables that will be discussed subsequently.

9.1.3. MEASUREMENTS

For any process, the lack of accurate process measurements limits the successful implementation of model identification and control. Crystallizers are dispersed-phase systems, and the shortcomings of on-line measurement techniques for these types of systems are particularly evident.

An accurate measurement of the concentration of the solute in the continuous phase can be obtained by sampling and evaporating to dryness, but this is, of course, prohibitively time-consuming for control purposes. There are several methods for the rapid measurement of continuous-phase concentration. The measurement of refractive index has been shown to provide quick and accurate concentration determination (Helt and Larson 1977; Mullin and Leci 1972; Sikdar and Randolph 1976). Garside and Mullin (1966) suggested the use of an on-line densitometer to determine solution concentration, and Witkowski (1990) successfully used densitometry for concentration measurements to estimate the kinetic parameters of an isothermal crystallizer. It should

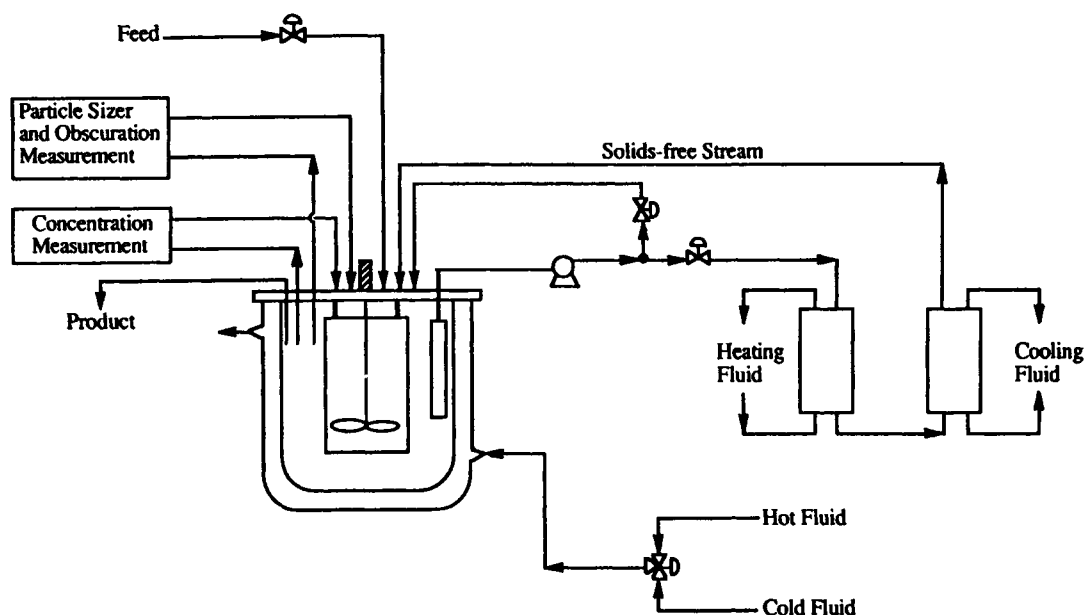


Figure 9.1 Schematic of a continuous cooling crystallizer.

be noted that the results from both of these on-line methods are temperature dependent, and precautions should be taken during nonisothermal crystallizer operation.

The limitations of methods for the on-line measurement of solid-phase properties have restricted development and implementation of model identification and control algorithms. While sieve analysis can provide CSD measurements that are suitably accurate for most purposes, this technique is labor intensive and the results are obtained with delays that are undesirable for crystallizer control.

There are now instruments that yield on-line crystal size information. A Coulter Counter provides an accurate measurement of the volume of particles flowing through a sensing zone. The limitations of the Coulter Counter are that a zone pore chosen for a given use is acceptable for a relatively narrow size range, thus, only part of the CSD can be determined. Also, pore plugging is a common occurrence. Light scattering has emerged as an attractive measurement technique because it is on line and free of many of the operational difficulties of other techniques. While determination of the CSD by light scattering methods is quick and convenient, it is important to note that the translation of the directly measured scattered light pattern into a CSD is an ill-conditioned and hence difficult operation. The ill-conditioning means that small changes in the measurement, the light energy, lead to large changes in the inferred CSD. Methods have been developed to overcome this problem, but one must exercise appropriate caution to avoid erroneous results.

One of the central limitations of this measurement technology is the assumption that the particles scattering the light are spherical. Care must be taken in using the CSDs obtained from methods based on light scattering theory for spheres. In a study by Brown and Felton (1985), particle shape corrections were made by using the theorem proved by Cauchy and, more simply, by van de Hulst (1981), that the average geometrical cross section of a convex particle with random orientation is one-fourth its surface area. The light-scattering-theory particle sizer produced by Malvern Instruments gives the weight percent in 16 size classes of spheres with the same cross-sectional area as the projected area of the actual particles. Jones et al. (1986) used the above theorem to correct the Malvern particle size to correspond to the characteristic length of potassium sulfate crystals, which are approximately parallelepipeds. They found that after this correction, the results from the Malvern agreed reasonably well with the CSD determined by standard sieve analysis. While in many instances this correction method may be adequate, it can be demonstrated via simulation and experiment that, even after correction, significant errors result when sizing particles of large aspect ratio such as needles and platelets (Miller 1993).

Obscuration is the fraction of light that is obscured by the crystals in a flow cell; thus, obscuration is defined as $1 - I/I_0$ where I is the intensity of undiffracted light that passes through the suspension of crystals and I_0 is the intensity of the incident light. The obscuration can be accurately measured, and the Beer-Lambert law provides a means by which it can be modelled for comparison with experimental data. As discussed by Witkowski et al. (1990), the obscuration provides a measure of the second moment of the CSD. Preliminary experimental tests indicate that the theorem discussed above relating geometrical cross section to surface area may be helpful in extending the use of obscuration measurement to cases with nonspherical particles.

Another limitation of light scattering techniques is that it must be assumed that the concentration of crystals is sufficiently low so that there is no significant multiple scattering. To extend the use of these techniques to the case of high slurry concentration, an automatic dilution unit has been developed for fast and representative dilution of samples (Jager et al. 1987).

Rohani and Paine (1987) proposed a sampling/suspension density measuring device that is based on the temperature change required to dissolve the crystals in a small sample cell. This method has the advantage of being insensitive to the presence of foreign particles and entrained air bubbles. While this method does not conveniently yield an absolute measure of the fines suspension density and the sampling delay is at least 1 min, it has been shown that the resulting temperature difference measurement can be used successfully in a feedback control scheme (Rohani et al. 1990).

9.1.4. MANIPULATED VARIABLES

The final CSD can be dramatically influenced by the temperature at which a continuous crystallizer is operated or by the temperature profile followed over a batch run, because the crystallizer temperature affects the degree of supersaturation and the growth and nucleation rates. Therefore, the manipulation of variables controlling the cooling rate (e.g., crystallizer jacket temperature, evaporation rate) can be used to influence the CSD. The adjustment of the feed rate to a continuous crystallizer has also been suggested as a means of affecting the CSD (Myerson et al. 1987; Han 1969).

The manipulation of the flow rate to a fines dissolution loop provides another means to control the CSD. The effect of the selective segregation and dissolution of fines in continuous crystallization has been studied extensively and a thorough discussion of its effect on the CSD is given by Randolph and Larson (1988). Fines destruction is commonly used in industry and there have been several investigations of its use as a manipulated variable to alter the product CSD and to reduce oscillations in continuous crystallizers (Lei et al. 1971a, 1971b; Beckman and Randolph 1977; Randolph and Low 1981; Randolph et al. 1986). The fines are usually classified using gravity settling in a quiescent zone. An appropriate volumetric flow rate can be determined for a desired cut size using Stokes' law. Using this method to segregate fines, the manipulation of the flow rate to the fines dissolution system, would obviously lead to disturbances in the fines trap and, subsequently, the cut size of the fines being removed. In a study of the use of fines dissolving for the control of a continuous crystallizer, Randolph et al. (1987) manipulated the fraction of the flow actually sent to the dissolver while keeping the flow rate from the fines trap constant. The advantage of this approach is that the cut size remains constant with changes to the flow rate to the dissolver, resulting in a simple linear relationship between the fines dissolution rate and the manipulated variable. It should be noted that the application of this technology to batch crystallization was not investigated until 1984 (Jones et al. 1984), and there have been few studies of its use as a manipulated variable in batch crystallization (Rohani et al. 1990; Rohani and Bourne 1990).

9.1.5. CONTROL ALGORITHM

The control algorithm is the part of the control system that uses the available measurements and level of process understanding to determine the best means to influence the process with the available manipulated variables to achieve the designer's performance objectives. In the discussion of control algorithms in this chapter, standard control notation is used. This notation is explained below in reference to crystallizer control:

- y is a measurable output or controlled variable. Examples include crystallizer temperature, slurry density, solute concentration, and obscuration.
- u is a manipulated variable. Examples are the coolant temperature and the flow rate to the fines dissolution loop.

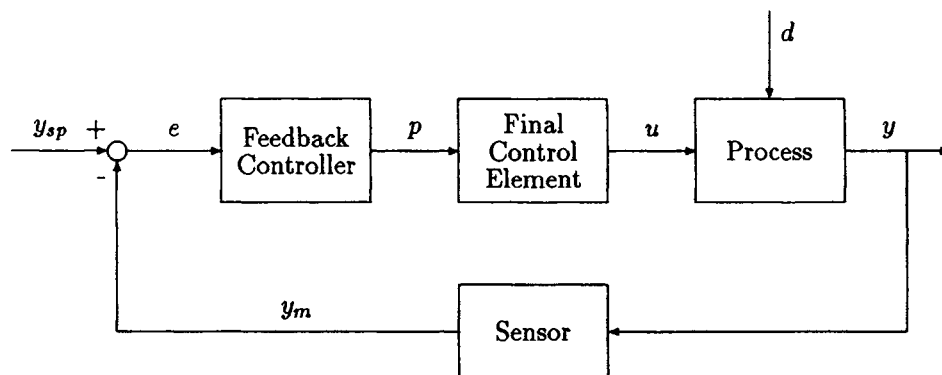


Figure 9.2 Block diagram for feedback control structure.

- d is a disturbance that affects the states of the system. Possible disturbances include fluctuations in the coolant temperature or fines destruction rate, changes in the cut size for the fines dissolution system, and changes in the heat transfer to the surroundings.
- e is the error between the measured output variable, y_m , and the set point for the output variable, y_{sp} . Differences between y and y_m are due to sensor error and noise.

For multiple-input-multiple-output (MIMO) control algorithms, these variables are written in bold type to denote that they are vectors of variables (e.g., \mathbf{u} is a vector of manipulated variables).

9.2. FEEDBACK CONTROLLERS

The material in this section is a brief overview of process control. The reader familiar with the contents of any recent undergraduate control textbook such as Seborg et al. (1988), Smith and Corripio (1985), or Stephanopoulos (1984) is encouraged to proceed directly to Section 9.3.

Feedback control is a fundamental concept that is employed in most control algorithms. Figure 9.2 shows a block diagram for a feedback control system. In feedback control the controlled variable is measured and compared to the set point, resulting in an error signal that is used by the controller to calculate the appropriate corrective action by the manipulated variable. The manipulated variable influences the controlled variable through the dynamic process.

The advantage of feedback control is that corrective action is taken regardless of the source of the disturbance. Its chief drawback is that no corrective action is taken until after the controlled variable deviates from the set point. Feedback control may also result in undesirable oscillations in the controlled variable if the controller is not tuned properly; that is, if the adjustable controller parameters are not set at appropriate values. Although trial-and-error tuning can achieve satisfactory performance in some cases, the tuning of the controller can be aided by using a mathematical model of the dynamic process.

9.2.1. THREE MODE (PID) CONTROLLERS

In many process control applications, the control algorithm consists of three modes: proportional (P), integral (I), and derivative (D). The ideal PID controller equation is

$$p(t) = \bar{p} + K_c \left[e(t) + \frac{1}{\tau_I} \int_0^t e(t) dt + \tau_D \frac{de}{dt} \right] \quad (9.1)$$

where p is the controller output, e is the controlled variable's error, and \bar{p} is the bias, which is set at the desired controller output when the error signal is zero. The PID controller's input and output signals are continuous signals, which are either pneumatic or electrical. The standard range for pneumatic signals (psig) is 3–15 psig, while several ranges are available for electronic controllers including 4–20 mA and 1–5 V. Thus, the controllers are designed to be compatible with conventional transmitters and actuators. If the PID controller is implemented as part of a digital control system, the discrete form of the PID equation is used

$$p_n = \bar{p} + K_c \left[e_n + \frac{\Delta t}{\tau_I} \sum_{k=0}^n e_k + \frac{\tau_D}{\Delta t} (e_n - e_{n-1}) \right] \quad (9.2)$$

where Δt is the sampling period for the control calculations and n denotes the current sampling time.

The controller gain K_c can be varied and is usually tuned after the controller has been installed. Large values of K_c cause a large change in controller output for a small change in error signal. A small value of K_c is a more conservative choice since it causes a smaller change in controller output. More information on selecting controller tuning parameters (K_c , τ_I , and τ_D) to achieve desirable performance is given subsequently. The actual behavior of a proportional pneumatic controller is shown in Figure 9.3. Note that the controller output “saturates” when the limits of 3 or 15 psig are reached (Seborg et al. 1988).

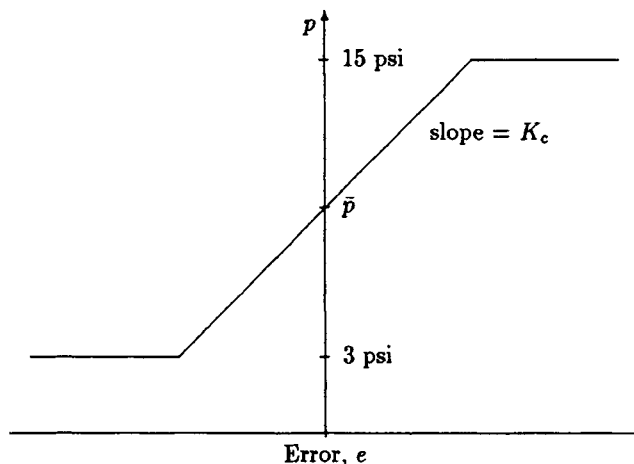


Figure 9.3 Output signal of a proportional controller based on the error. The horizontal lines represent controller saturation limits.

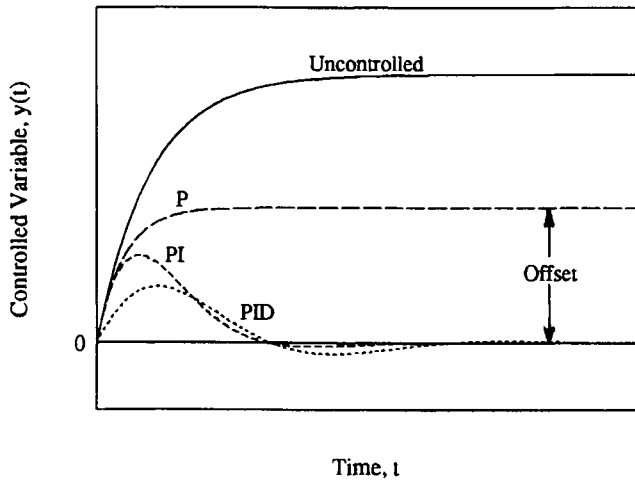


Figure 9.4 Response for a step change in disturbance with tuned P, PI, and PID controllers and with no control.

Integral action in the controller brings the controlled variable back to the set point in the presence of a sustained upset or disturbance. Since the elimination of offset (steady-state error) is an important control objective, integral action is normally employed. A potential difficulty associated with integral action is a phenomenon known as “reset windup.” If a sustained error occurs, then the integral term in Eq. (9.1) becomes quite large and the controller output eventually saturates. After saturation of the actuator, the integral term continues to grow, leading to large overshoots due to the delay of response in the saturated control action when the error is eventually reduced. Reset wind-up commonly occurs during the start-up of a process, after a large set-point change, or as a consequence of a large sustained load disturbance that is beyond the range of the manipulated variable. Fortunately, many commercial controllers provide “anti-reset wind-up” by disabling the integral mode when the controller output is at a saturation limit.

Derivative control action is also referred to as rate action, pre-act, or anticipatory control. Its function is to anticipate the future behavior of the error signal by considering its rate of change. Derivative action is never used alone, but in conjunction with proportional and integral control. Derivative control is used to

improve the dynamic response of the controlled variable by decreasing the process response time, but it is seldom employed when the process measurement is noisy, because it amplifies the noise unless the measurement is filtered.

To illustrate the influence of each control mode, consider the control system responses shown in Figure 9.4. These curves illustrate the typical response of a controlled process for different types of feedback control after the process experiences a sustained disturbance. Without control the process slowly reaches a new steady state that differs from the desired steady state. The effect of proportional control is to speed up the process response and reduce the offset. The addition of integral control eliminates offset but tends to make the response more oscillatory. Adding derivative action reduces the degree of oscillation and the “response time,” i.e., the time it takes the process to reach steady state. While there are exceptions to Figure 9.4, the responses shown are typical of what occurs in practice.

9.2.2. STABILITY CONSIDERATIONS

An important consequence of feedback control is that it can cause oscillations in closed-loop systems. If the oscillations damp out quickly, then the control system performance is generally considered to be acceptable. However, in some situations the oscillations may persist or their amplitudes may increase with time. In the latter situation, the closed-loop system is said to be unstable. An unstable or excessively oscillatory closed-loop response can usually be eliminated by proper adjustment of the PID controller constants, K_c , τ_I , and τ_D . Consider the closed-loop response to a unit step change in set point for various values of controller gain, K_c . For small values of K_c , say K_{c1} and K_{c2} , typical closed-loop responses are shown in Figure 9.5. If the controller gain is increased to a value of K_{c3} , the sustained oscillation of Figure 9.6 results; a larger gain, K_{c4} , produces the unstable response shown in Figure 9.6. Note that the amplitude of the unstable oscillation does not continue to grow indefinitely since a physical limit will eventually be reached, as previously noted. In general as the controller gain increases, the closed-loop response typically becomes more oscillatory and, for large values of K_c , can become unstable. The conditions under which a feedback control system becomes unstable can be determined using a number of different techniques (Seborg et al. 1988; Stephanopoulos 1984).

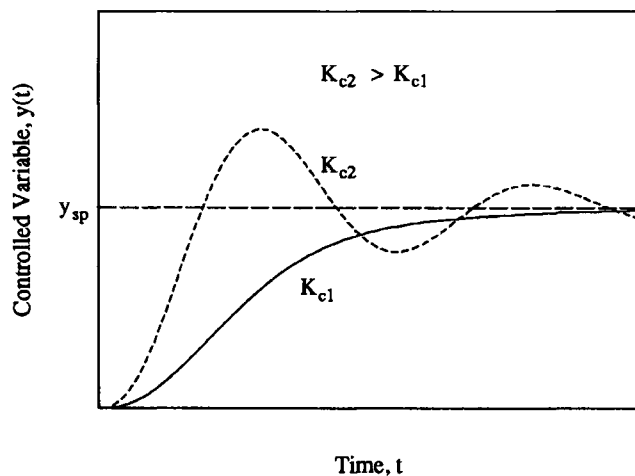


Figure 9.5 Closed-loop response for different values of the controller gain.

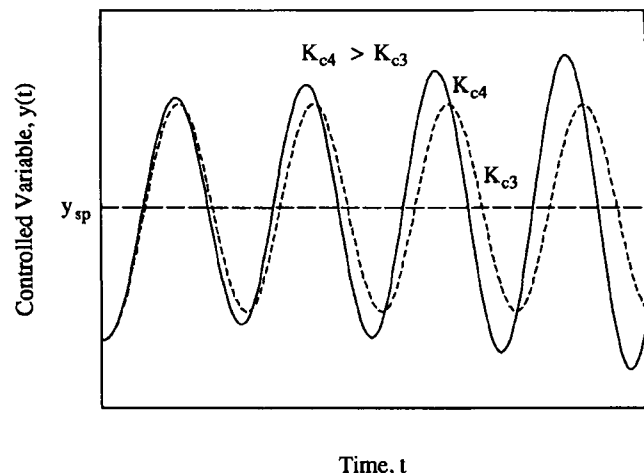


Figure 9.6 Transition to instability as controller gain increases.

9.2.3. AUTOMATIC/MANUAL CONTROL MODES

In certain situations the plant operator may wish to override the automatic mode and adjust the controller output manually. In this case there is no feedback loop. This manual mode of operation is very useful during a plant start-up, shut-down, or emergency situation. Testing of a process to obtain a mathematical model is also sometimes carried out in the manual mode. Commercial controllers have a manual/automatic switch for transferring from the automatic mode to the manual mode or vice versa. Bumpless transfers that do not upset the process can be achieved with commercial controllers.

9.2.4. TUNING OF PID CONTROLLERS

There are several approaches that can be used to tune PID controllers, including model-based correlations, response specifications, and frequency response (Smith and Corripio 1985; Stephanopoulos 1984). An approach that has received much attention recently is model-based controller design. Model-based control requires a dynamic model of the process; the dynamic model can be empirical, such as the popular first-order plus time delay model, or it can be a physical model. The selection of the controller parameters (K_c , τ_I , τ_D) is based on optimizing the dynamic performance of the system while maintaining closed-loop stability.

Figure 9.7 shows a set-point change for a tuned controller. The following characteristics are identified in the figure: rise time, overshoot ratio, decay ratio, and period of oscillation. Tuning correlations developed by instrument manufacturers in the 1940s and 1950s sought to achieve a decay ratio of 1/4. The well-known process reaction curve (PRC) method utilizes this performance criterion, although the PRC method also embraces the notion of model-based design. In the PRC technique, the actual process is operated under manual control and a step change in the controller output (Δp) is applied. For many processes, the response of the system (change in the measured value of the controlled variable) follows the curve shown in Figure 9.8. This type of response is called first order plus time delay and is described by three parameters: the process gain, K ; the time delay, θ ; and the dominant time constant, τ .

One representation of the dynamic model employs Laplace transforms and is called the transfer function, $G(s)$ (Stephanopoulos 1984).

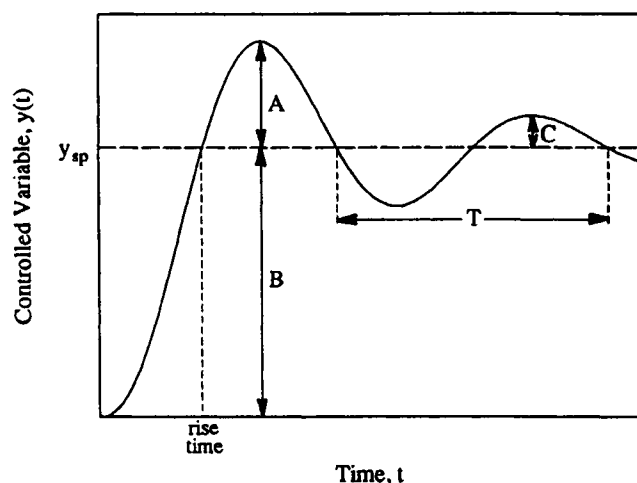


Figure 9.7 Common performance criteria for PID tuning techniques. The peak overshoot is the ratio A/B , C/A is the decay ratio, and T is the period of oscillation.

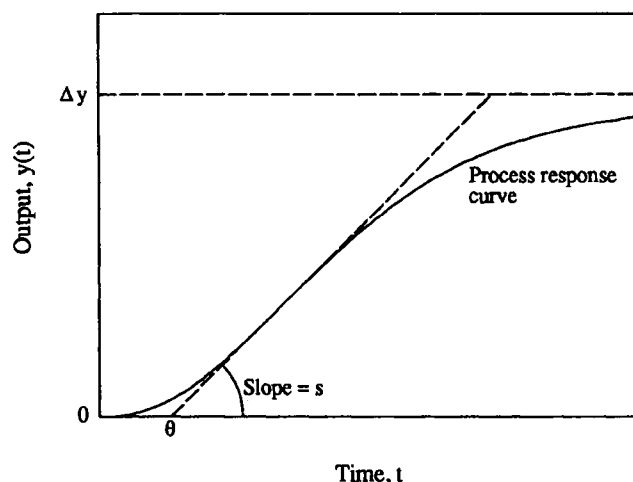


Figure 9.8 Process reaction curve for Cohen-Coon tuning technique. $K = \Delta y / \Delta p$, $\tau = \Delta y / s$.

$$G(s) = \frac{Ke^{-\theta s}}{\tau s + 1} \quad (9.3)$$

The process gain is a steady-state characteristic of the process and is simply the ratio, $\Delta y / \Delta p$. The time delay, θ , is the time elapsed before Δy deviates from zero. The time constant is indicative of the speed of response; the time to reach 63% of the final response is equal to $\theta + \tau$. Graphical analysis of the step response can be employed to compute good estimates of θ and τ when the response deviates from the simplified model. Table 9.4 lists one popular correlation of P, PI, and PID controllers (Stephanopoulos 1984), based on the 1953 work of Cohen and Coon using the 1/4 decay ratio.

TABLE 9.4 Cohen-Coon PID Tuning Rules

Controller	K_c	τ_I	τ_D
P	$\frac{\tau}{K\theta} \left(1.0 + \frac{\theta}{3\tau} \right)$	—	—
PI	$\frac{\tau}{K\theta} \left(0.9 + \frac{\theta}{12\tau} \right)$	$\theta \frac{30 + 3\theta/\tau}{9 + 20\theta/\tau}$	—
PID	$\frac{\tau}{K\theta} \left(\frac{4.0}{3.0} + \frac{\theta}{4\tau} \right)$	$\theta \frac{32 + 6\theta/\tau}{13 + 8\theta/\tau}$	$\frac{4\theta}{11 + 20\theta/\tau}$

TABLE 9.5 Tuning Relations for PID Controller Based on ITAE Performance Criterion

Type of Input	Type of Controller	Mode	A	B
Load	PI	P	0.859	−0.977
Load	PI	I	0.674	−0.680
Load	PID	P	1.357	−0.947
Load	PID	I	0.842	−0.738
Load	PID	D	0.381	0.995
Set point	PI	P	0.586	−0.916
Set point	PI	I	1.030*	−0.165*
Set point	PID	P	0.965	−0.850
Set point	PID	I	0.796*	−0.1465*
Set point	PID	D	0.308	0.929

$Y = KK_c$ for proportional mode, τ/τ_I for integral mode, and τ_D/τ for derivative mode. θ , τ are the time delay and time constant based on the process reaction curve, respectively.

*For set-point changes, the tuning relation for the integral mode is $\tau/\tau_I = A + B(\theta/\tau)$.

Seborg et al. (1988) have tabulated power law correlations for PID controller settings for a range of first-order model parameters. The best tuning parameters have been fitted using a general equation, $Y = A(\theta/\tau)^B$, where Y depends on the particular controller mode to be evaluated. Table 9.5 presents correlations to minimize the time-weighted, integral of the absolute error (ITAE) for both set-point and load changes.

There are several general features of the correlation of Tables 9.4 and 9.5 that should be noted:

1. The controller gain is inversely proportional to the process gain for constant θ and τ .
2. The allowable controller gain is higher when the ratio of dead time to time constant becomes smaller. This is because dead time has a destabilizing effect on the control system, limiting the controller gain, while a larger time constant generally demands a higher controller gain.
3. As (θ/τ) increases, more derivative action and less integral action should be used.

A recent addition to the model-based tuning correlations is that based on *Internal Model Control* (Rivera et al. 1986), which offers some advantages over the other methods described here. However, the form of the correlations are similar to those discussed previously.

On-Line Tuning. The model-based tuning of PID controllers presumes that the model is accurate; thus these settings are only a first estimate of the best parameters for an actual operating process. Minor on-line adjustments of K_c , τ_I , and τ_D are usually required. However, often it is necessary to completely retune the controller after it is put into service, using a trial and error approach. A typical procedure recommended by instrument manufacturers is as follows:

1. Eliminate the integral and derivative action by setting τ_D at its minimum value and τ_I at its maximum value.
2. Set K_c at a low value (e.g., 0.5) and put the controller on automatic.
3. Increase the controller gain, K_c , by small increments until continuous cycling (see Figure 9.6) occurs after a small set-point or load change.
4. Reduce K_c by a factor of two.

5. Decrease τ_I in small increments until continuous cycling occurs again. Set τ_I equal to three times this value.
6. Increase τ_D until continuous cycling occurs. Set τ_D equal to one-third of the final value.

This trial and error tuning procedure has a number of disadvantages. It is obvious that it may be quite burdensome if a large number of trial settings are required and the process dynamics are quite slow. Furthermore, continuous cycling of a process may be objectionable since the closed-loop system is at a stability limit. Thus external disturbances or a change in the process could result in unstable operation.

9.2.5. FURTHER FEEDBACK CONTROL TECHNIQUES

While the single-loop PID controller is satisfactory in many process applications, it does not perform well for processes with slow dynamics, frequent disturbances, or multivariable interactions. We discuss several advanced control methods below that can be implemented via computer control.

Cascade Control. One of the disadvantages of using conventional feedback control for processes with large time lags or delays is that disturbances are not recognized until after the controlled variable deviates from its set point. In these processes, correction by feedback control is generally slow and results in long-term deviation from set point. Cascade control can improve the dynamic response to load changes by using a secondary measurement and controller to recognize upsets and adjust the manipulated variable before the primary controlled variable is affected.

To illustrate the cascade control approach, consider the control of the temperature of a jacketed crystallizer by manipulating the ratio of the flows to the crystallizer jacket from a heating stream and a cooling stream. The crystallizer temperature can be influenced by disturbances in the temperature of the heating and cooling streams and the heat transfer to the surroundings. Obviously, the crystallizer temperature could be measured and used in a feedback control scheme as shown in Figure 9.9; however, the manifestation of the disturbances would be slow, and the corrective action taken by the controller would be delayed.

In the cascade control scheme shown in Figure 9.10, there are two controllers. The primary or master controller is the crystallizer

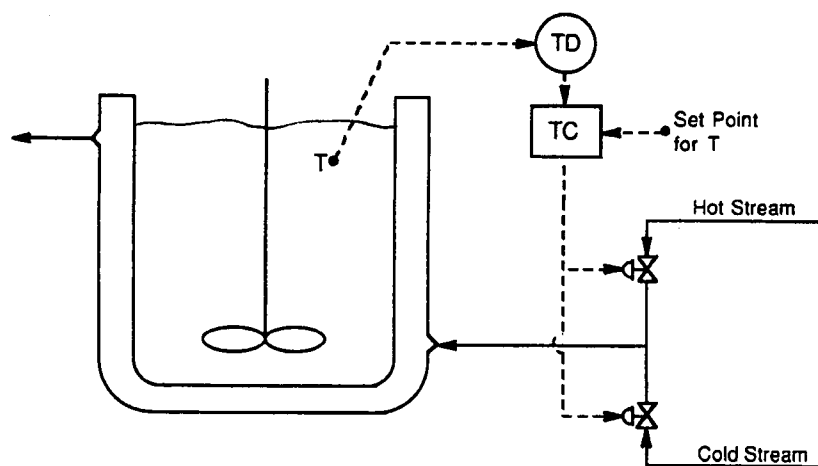


Figure 9.9 Control of crystallizer temperature using standard feedback control. TD, temperature detector; TC, temperature controller.

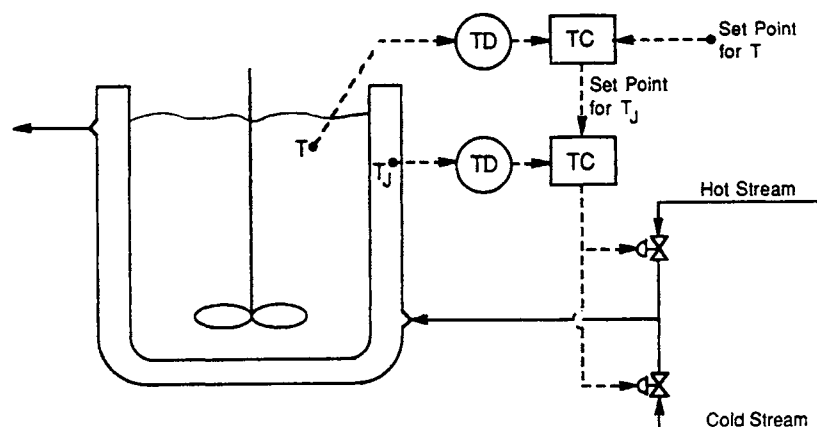


Figure 9.10 Control of crystallizer temperature using a cascade configuration. TD, temperature detector; TC, temperature controller.

temperature controller. It compares the crystallizer temperature measurement to the specified set point and computes the set point for the jacket-temperature controller. This secondary or slave controller compares the jacket-temperature set point to the measurement and adjusts the valves that determine the flow ratio. The principal advantage of cascade control is that a secondary measurement (jacket temperature) is located closer to a potential disturbance in order to improve the closed-loop response.

In tuning a cascade control system, the slave controller is tuned first with the master controller in manual. Often only a proportional controller is needed for the slave loop, since offset in that loop can be treated by using proportional plus integral action in the master loop. When the slave controller is transferred to automatic, it can be tuned using the techniques described earlier in this section. Seborg et al. (1988) and Stephanopoulos (1984) provide further analysis of cascade control systems.

Time-Delay Compensation. Time delays are a common occurrence in the process industries because of the presence of recycle loops, fluid-flow transport lags, and “dead time” in composition analysis. In crystallization processes, certain techniques for CSD analysis and concentration measurement involve significant time delays. The presence of a time delay (θ) in a process severely limits the performance of a conventional PID control system, reducing the stability margin of the closed-loop control system. Consequently, the controller gain must be reduced below that used for a process without delay. Thus, the response of the closed-loop system will be sluggish compared to that of the system with no time delay.

In order to improve the performance of time-delay systems, special control algorithms have been developed to provide time-delay compensation. The Smith predictor technique is the best known algorithm; a related method is called the analytical predictor. Various investigators have found that based on integral squared error, the performance of the Smith predictor can be as much as 30% better than a conventional controller (Donoghue 1977; Schleck and Hanesian 1978).

The Smith predictor is a model-based control strategy that involves a more complicated block diagram than that for a conventional feedback controller, while a PID controller is still one component of the control strategy (Seborg et al. 1988). The key concept is based on better coordination of the timing of manipulated variable action. The loop configuration takes into account the fact that the current controlled variable measurement is not a

result of the current manipulated variable action, but the value of u taken θ time units earlier. Correct selection of time-delay compensation blocks can yield excellent performance; however, if the process model parameters change (especially the time delay), the Smith predictor performance deteriorates. If the time delay is highly variable, it becomes necessary to use an adaptive controller for satisfactory performance (Seborg et al. 1988).

Feedforward/Feedback Control. If the process exhibits slow dynamic response and disturbances are frequent, then the use of feedforward control with feedback control may be advantageous. Feedforward control differs from feedback control in that the primary disturbance is measured via a sensor and the manipulated variable is adjusted so that, ideally, the controlled variable does not change. As shown in Figure 9.11, the controller calculates the manipulated variable, u , needed to counteract the system upset introduced through the disturbance, d . By taking control action based on measured disturbances, rather than controlled variable error, the controller can reject disturbances before they affect the controlled variable, y .

Feedforward control requires the development of models that capture the effects of the manipulated variable and disturbance on the controlled variable. The performance of the feedforward controller depends on the accuracy of these models. If the models are exact and the manipulated variables do not reach constraints, then the predictive nature of the feedforward control offers the potential of perfect control. However, since models are only approximate and not all disturbances are measurable, it is standard practice to utilize feedforward control in conjunction with feed-

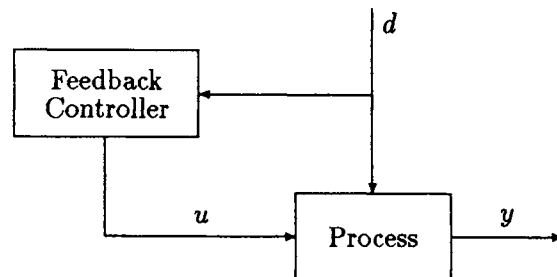


Figure 9.11 Block diagram for feedforward control configuration.

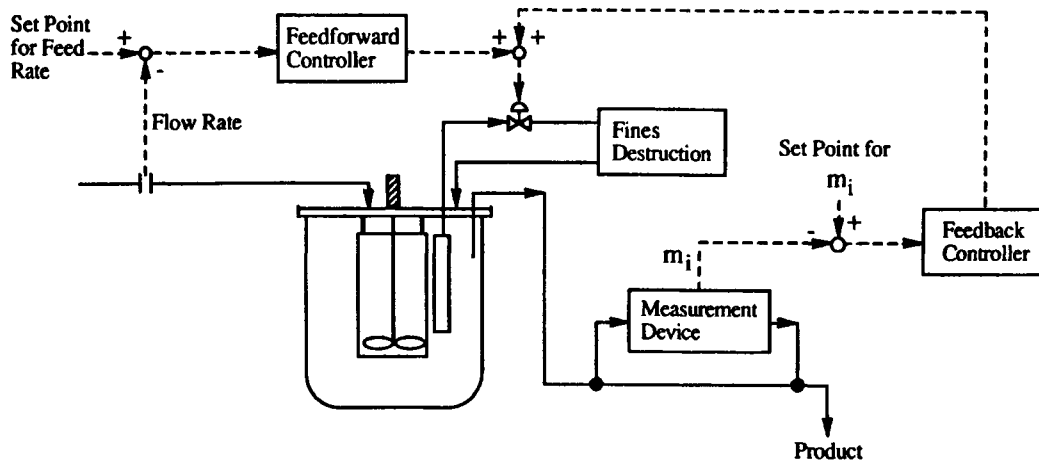


Figure 9.12 Schematic diagram of feedforward/feedback control of a continuous crystallizer. $m_i = i^{th}$ moment of CSD.

back control. By combining the two control methods, the strengths of both schemes can be utilized (Stephanopoulos 1984).

Figure 9.12 shows a schematic diagram of a feedforward/feedback control configuration for a continuous crystallizer similar to that suggested by Gupta and Timm (1971). Suppose the feed rate changes with time and the resulting fluctuation affects the product CSD. The feed rate can be measured easily, and with a model relating the feed rate to a specified moment of the CSD, the flow rate to the fines destruction system can be adjusted to compensate for the disturbance. To alleviate error due to an inaccurate model, a feedback loop that acts on the deviation between a measured CSD moment and its set point is used to augment the feedforward-loop control signal. The tuning of the controller in the feedback loop can be performed independent of the feedforward loop; i.e., the feedforward loop does not introduce instability in the closed-loop response. For more information on feedforward/feedback control and the design of such controllers, refer to Stephanopoulos (1984) and Shinskey (1979).

Feedback Control of Multivariable Systems. Many processes contain several manipulated variables and controlled variables; this type of process is called multivariable. A multivariable process can also be represented in a block diagram, as shown in Figure 9.13. In many applications we can treat a multivariable process with a set of single-loop controllers by pairing inputs and outputs in the most favorable way. This method employs the relative gain array (McAvoy 1983), which provides guidelines on which variable pairings should be selected as well as a measure of the potential quality of control for such a multiloop configuration.

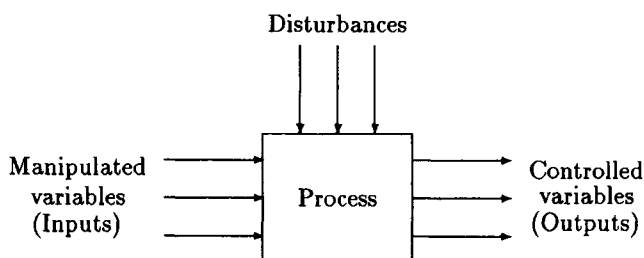


Figure 9.13 Block diagram for a multivariable process.

If the loop interactions are not severe, then each single-loop controller can be designed using the techniques described earlier in this section. However, the presence of strong interactions requires that the controllers be detuned to reduce oscillations. There are multivariable control techniques, such as optimal control, that provide frameworks in which to handle the interactions between various inputs and outputs. Optimal control methods also allow one to deal directly with nonlinear system dynamics, rather than the linear model approximation required for the techniques discussed in this section. A thorough presentation of optimal control theory is given by Bryson and Ho (1975). Optimal control is discussed further in Section 9.5.

9.3. INDUSTRIAL CRYSTALLIZER CONTROL

9.3.1. CRYSTALLIZER CONTROL OBJECTIVES

The objectives of an industrial crystallization process are to produce crystals of consistent product size and purity at the minimal production cost. Consistent quality requires process control to compensate for disturbances and variations in the crystallizer feed and utilities. A successful control strategy must contain both design features and process variable control features operating in concert to achieve and maintain the desired crystallization conditions. The economic objective includes equipment cost, utility cost, equipment maintenance cost, and capacity loss during downtime for equipment cleaning. To achieve an overall minimum cost for a crystal production process that includes solid-liquid separation and drying, additional expense may be justified at the crystallization stage to increase the mean size or reduce the spread of the CSD. This permits substitution of a lower capital cost separator such as a rotary filter for a centrifuge or lower steam consumption in a dryer due to less adhering moisture in the filtered cake. Controlling the CSD or minimizing the energy consumption by heat integration necessitates additional control capabilities for the additional process streams that must be handled to accomplish the goal. The level of control implemented varies with the mode of operation (batch or continuous), the requirements of product specifications, and the degree of overall process optimization attempted. Various control strategies practiced in industry to achieve these process goals will be discussed using specific examples in relation to the mode of operation and method of

crystallization. The examples are illustrative only since different combinations of equipment and control methods are also in use.

9.3.2. CONTINUOUS CRYSTALLIZATION CONTROL

Continuous crystallization processes employ dedicated equipment intended to create and maintain constant growing conditions for the crystal product. Although general estimates for the minimum production rate justifying continuous crystallization vary from 1 ton/day (Nývlt 1978) to 50 tons/day (Bennett 1988), the scale of the equipment unavoidably creates nonhomogeneous regions of temperature, product concentration, and slurry density within the crystallizer at locations such as the heat exchanger or boiling surface, feed entrance, and in areas of lower mixing intensity or within baffled regions. The design intent is achieved if the vessel operation is controlled in a manner such that the vessel locations of these regions are time invariant and the process variables within the regions do not violate desired bounds. Operation outside these bounds generally results in fouling, deviations in crystal size, and lowered product purity. Additionally, the rate of change of the variables within acceptable bounds must be moderated to the extent that a higher supersaturation, or driving force, is not created than can be relieved by crystal growth and secondary nucleation. Such rapid changes would trigger spontaneous nucleation, producing a cyclic swing of smaller crystals for the downstream product recovery equipment to handle.

The supersaturation, crystal attrition, and residence time of the crystals are manipulated through a combination of equipment design features and secondary variable control. For batch crystallization, the secondary variables include temperature, pressure, and agitation (including volumetric turn over and shear). Continuous operation requires the control of additional secondary variables such as feed-to-bulk mixing ratio, and level or operation volume. Continuous operation also affords the option to independently control the residence time of the different size ranges of crystals, the concentration of crystals within the vessel, and the concentration of the product in the feed. All these options have been implemented by various schemes in industrial practice (for example, achieved through fines destruction, classified product removal, and double draw-off configurations). Increasing the variety of process control strategies is the number of vessel types to which the control is applied. In the following sections, different control implementations will be illustrated using popular crystallizer designs, recognizing that several of the illustrated techniques are not unique to that vessel type.

Draft Tube Baffle Crystallizer. A draft tube baffle (DTB) crystallizer design as illustrated in Figure 9.14 is designed to grow larger crystals by segregating the smallest crystals through gravity settling in a baffled region and dissolving them in an external heat exchanger. With the addition of an elutriation leg to fluidize the fines while the larger crystals are withdrawn, control of both ends of the CSD is achieved. The principle method of heat transfer in continuous crystallizers is by solvent evaporation because of the propensity to foul surface-cooling heat exchangers. Here, adiabatic evaporative cooling has been implemented using a steam ejector as the vacuum source. A wash ring, used to remove solid crystals from the wall above the boiling liquid surface, is also shown.

The feed is introduced into the external circulating fines destruction stream to provide sufficient liquid head to suppress flashing, which would spawn nuclei and sabotage the fines reducing effort. The feed is controlled by an independent flow control loop from an upstream surge tank. The surge tank prevents upstream flow variations from forcing oscillations in the residence time of the crystallizer. A second and more critical reason for

choosing this control strategy is to maintain the mixing ratio in this external loop within the enthalpy-concentration bounds to prevent the solution from exceeding its supersaturation limit and generating fines during mixing (Toussaint and Donders 1974).

The flow from the baffled section through the fines destruction heat exchanger is commonly maintained at a set rate by employing a control valve that responds to the flow measurement. This control device is acceptable because the potential for valve plugging is minimized by the low concentration of solids in the clarified stream, and crystal attrition in the high shear of the valve is inconsequential because the solids are intended for dissolution. In industry, the flow rate of the fines destruction stream is controlled without feedback of the amount of fines in the stream, because of the poor reliability of devices that measure crystal size population. Nevertheless, recent success has been claimed for using a turbidity sensor (Anonymous 1986). Although crystal size and concentration information are convoluted in the turbidity measurement, turbidity is indicative of the dissolving duty required.

It is desirable to maintain a constant cut size while manipulating the flow rate to the fines destruction system. As discussed in Section 9.1.4, it has been demonstrated on a laboratory scale that this can be accomplished by maintaining a constant flow rate through the settling or baffled region while varying the fines destruction rate by bypassing a portion of the flow. With the control configuration shown in Figure 9.14, increasing the flow through the heat exchanger increases the cut size. This effect can be moderated if the baffled region is partitioned and the number of participating partitions is increased with increasing external flow rate.

The product classification in the elutriation leg is operated under flow rate control without automatic feedback from the product CSD. The rate of slurry discharge is set by the level control loop, responding to the differential pressure generated by the varying slurry-gas interface. A progressive cavity pump is the final control element to achieve the level control while providing minimal degradation of the crystals in the product slurry.

The rate of heat removed from the vessel is varied by manipulating the rate of solvent evaporated. The pressure and, thus, the evaporation rate are manipulated by varying the recycle rate of the stream exhausted from the steam ejector. A control loop that links the recycle valve position directly to the operating temperature would not permit compensation for short cycle variations in the steam supply pressure, permitting rapid swings in pressure and surface-solution temperature that could result in spontaneous nucleation. Therefore, a cascade configuration that uses the temperature measurement in a master loop and a pressure measurement in a slave loop is employed.

The solvent condensed to achieve the cooling may be returned directly to the crystallizer, but in the crystallizer illustrated here, it is sent to a solvent tank to feed an intermittent wash ring. Continuous return would not provide sufficient volume or pressure to effectively clean the walls. Frequent flushings, each a few seconds, through a wash ring in the vapor space have been proven to keep deposits down (Wohlk 1981). To prevent the solvent supply from being constrained by the evaporation rate, a high-low acting level controller opens a solenoid to return the tank level from a low limit to the set point. The controller will also open a solenoid valve to lower the level from a high limit to the set point. Under constant operating conditions, only one of the valves would be operated, and the choice would depend on the relative supply and consumption. Wash consumption would be set based on experience. Wash duration, delivery rate, and idle time are variable. A flow indicator on this stream has been recommended to indicate proper operation and to permit determination of a mass balance about the crystallizer (Wohlk 1981).

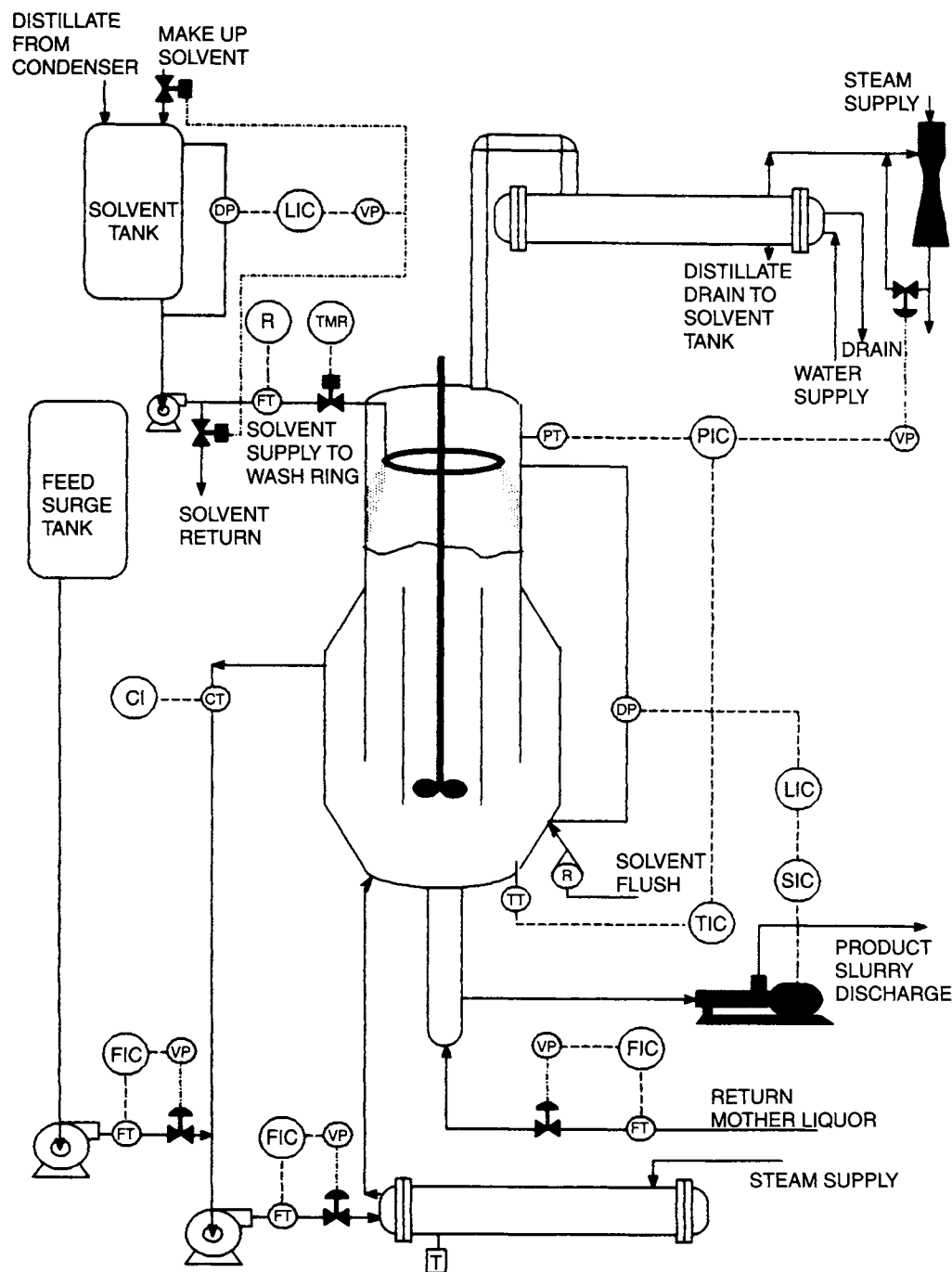


Figure 9.14 Schematic of a draft tube baffle crystallizer.

Growth Type Crystallizer. The growth type crystallizer illustrated in Figure 9.15, like the DTB, is designed to grow larger crystals. Both purposefully segregate the larger from the smaller crystals and both reduce the population of fines such that the remaining crystals will grow larger. But the DTB uses the addition of heat energy to destroy fines that are generated from pumping the larger crystals, and the growth type crystallizer reduces the number of fines generated by reducing the mechanical energy applied to the larger crystals. This is accomplished by fluidizing the crystal slurry in a growth chamber from which a baffled stream

containing up to 5 weight percent entrained crystal mass, representing the smallest crystals, is pumped to an evaporating chamber where supersaturation is generated. The pump controls the level of entrained crystals. The thin slurry returns to the growth chamber through a downcomer and its supersaturation is relieved as it fluidizes the major crystal mass.

Although not under feedback control, manual control may be required to balance the production and product size objectives. The production rate is controlled by the heat removal rate through adiabatic evaporation. The evaporation rate is controlled by the

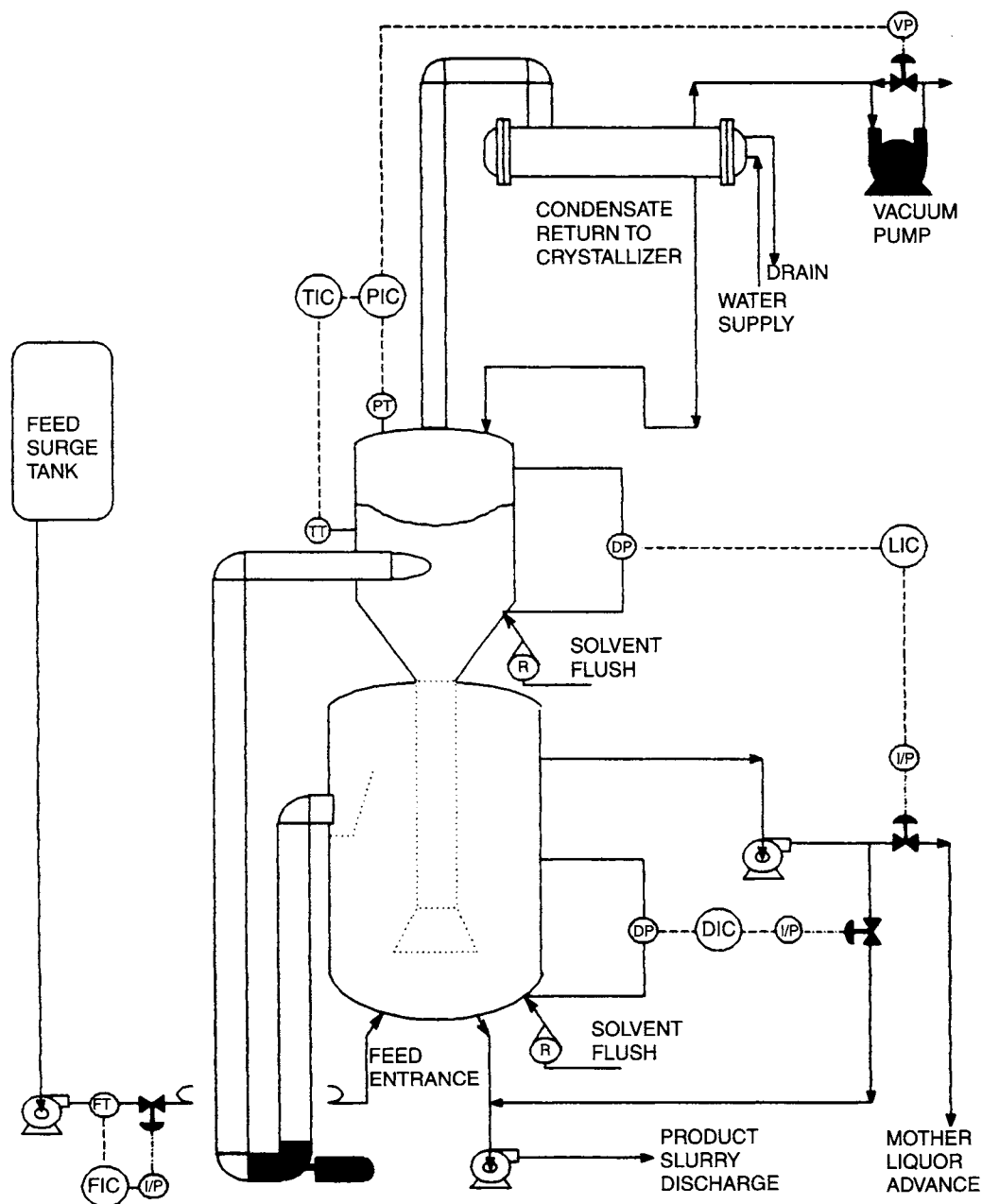


Figure 9.15 Schematic of a growth-type crystallizer.

operating pressure loop to cool the incoming solution to the target exit temperature. Reducing the pump rate by reducing secondary nucleation due to crystal-impeller collisions favors growth of existing crystals. However, as lower pumping rates reduce the crystal surface area in the evaporating chamber, and high production rates increase the solute concentration rise from solvent removal at the boiling surface, excessive local supersaturation can lead to spontaneous nucleation and subsequent fouling that requires an early shutdown. Conversely, increasing the pumping rate can disrupt the classified crystal bed, leading to operation in the same mode as a forced circulation crystallizer and degradation of the mean crystal size.

Means by which to obtain large retention times include using a large vessel volume and using slurry density control that permits

independent crystal residence time control in conjunction with crystal mass control. With a constant feed rate and volume, the crystal residence time is varied by controlling two exit streams. The stream pumped from the stagnant top contains few crystals and advances the mother liquor in response to the need to control the level in the upper chamber for optimum mixing and evaporating. The stream from the bottom of the growth chamber withdraws from the crystal slurry based on a target slurry density. In the configuration illustrated, a centrifugal pump operating at constant speed maintains a constant pump discharge. The withdrawal of slurry from the crystallizer is varied by controlling the volume of mother liquor from the top of the growth chamber that is fed to the slurry pump suction. This dilutes the slurry for transport and simplifies the pump hardware and control.

This mode of extending the crystal residence time, commonly referred to as double draw off or mother liquor advance, will produce a larger mean size at the expense of a bimodal distribution resulting from the population of fines with a lower residence time entrained in the advanced mother liquor. For a given vessel and production rate, the size and mass of fines entrained increases with the flow rate of mother liquor. As a consequence, increasing the crystal residence time to obtain a larger mean size by increasing the mother liquor advance, also increases the mass of fines in the product stream when these two are combined. Filtration rates are severely hampered by bimodal distributions as the fines tend to fill the interstitial spaces between the larger crystals to reduce the filtration flux (Jones et al. 1987). An optimum does exist, and the control strategy is suited to maintain the correct conditions. Feedback from the downstream process to automatically control this characteristic is not industrially practiced, but the time constant for changing the distribution is long enough that off-line measurements and manual set point changes in the slurry density loop are sufficient for control.

In the adiabatic evaporative growth type crystallizer shown, the pressure is controlled by recirculating exhausted noncondensables to a vacuum pump suction, and the condensate is returned to the crystallizer body. Returning the condensate maintains a dilution of the impurities in the feed and provides a means of controlling the product purity by preventing crystallization of the impurities. It also lowers the concentration of impurities in the mother liquor adhering to the crystal mass in downstream separation operations.

Multi-stage Forced-Circulation Crystallizers. Forced-circulation crystallizers are the workhorse of the inorganic crystallization industry. As such, they are often incorporated into multivessel configurations to maximize operating economy for large-volume commodity chemical production. The evaporating capacity of steam fed to the heat exchanger of one crystallizer can be enhanced by using the vapor removed from that vessel as the steam source for a heat exchanger (effect) of another crystallizer operated at a lower pressure and, hence, solution boiling temperature. Multiple effects of two to eight crystallizers are in operation. As the discussion of the controllability of multi-effect crystallizers will reveal, staging in this manner is suitable for solutions with little or no temperature sensitivity of solubility.

Although series heat flow offers the greatest economy, the choice of flow pattern for the process stream is determined by the control objective. If maximum product purity is desired, the process stream may be routed through the series of crystallizers. Impurities concentrate in the mother liquor as product is crystallized by solvent evaporation; therefore, the minimum mother liquor impurity concentration is in the first-stage evaporative crystallizer. A counterflow of solids to the liquor progressing through the series can be achieved using an external cyclone to separate a mother liquor stream from the slurry. By this mode, the product slurry can be withdrawn from the first stage with the least impurities adhering to the crystal surface, and the residue mother liquor discharged at the end of the train.

If maximum product size is desired, the process stream flow is parallel, with a fresh feed and slurry discharge to product recovery equipment from each crystallizer. Cascaded product flow is avoided because flow through a series of tanks narrows the residence time distribution and the CSD and reduces the mass mean size by reducing the number of larger crystals in the distribution tail. This tail represents the major mass-weighted fraction. Population models have been solved to verify this effect, assuming an equal nucleation rate in each stage (Randolph and Larson 1988). The actual mean in industrial practice is lower because transfer of

the slurry between stages increases crystal attrition, which provides an additional source of nuclei to compete for the remaining solute.

The parallel product flow configuration for a two-effect evaporative forced-circulation crystallizer is illustrated in Figure 9.16. The feed rate is maintained at a constant rate by feedback flow control. The level is controlled by varying the mother liquor return from downstream solid-liquid separation to the suction of a centrifugal pump.

Regardless of the number of crystallizers in the series, there is only one steam flow rate and one pressure control loop. Steam flow rate to the heat exchanger on the first crystallizer is set to control the evaporation rate in that vessel. The heat exchanger on the second crystallizer serves as the condenser for the first crystallizer. In this example, the evaporation rate in the second vessel is determined by the pressure maintained by throttling steam to an ejector. Note that the evaporation rate in these units are coupled. The lower the pressure in the second vessel, the more is evaporated, and the lower the slurry temperature. The lower slurry temperature increases the condensing capacity of the heat exchanger, and the evaporation rate increases while the operating temperature of the first crystallizer decreases. Multiple effects are likewise coupled so that neither the temperature nor pressure of intermediate vessels can be independently set. For an acceptable yield from each stage, this interaction limits this mode of control to solutes with solubilities of little or no sensitivity to temperature.

Since the evaporation rate varies between stages, the feed rate needs to be adjusted to allow sufficient concentration to achieve the target yield. One method to accomplish this is to set the feed rate directly proportional to the solvent removal rate, which is determined by monitoring the condensate flow rate from the subsequent effect. The gain on the condensate controller output will determine the concentration of the mother liquor, leaving the crystallizer and control product yield. Product purity is likewise controlled if the saturation limits of other components in the feed are being approached.

A second reason for staging continuous crystallizers is to control the process stream concentration-temperature profile for products with a steep solubility curve (i.e., exponential increase in solubility with temperature). Even though the volumetric flow rates would permit a single crystallizer of reasonable size, staged temperature for adiabatic cooling crystallization requires multiple vessels to prevent the local concentration at the hot concentrated feed entrance from exceeding its supersaturation limit when it is diluted and mixed with the circulating bulk.

A multi-stage crystallizer configuration sufficient to crystallize temperature-sensitive products is illustrated in Figure 9.17. Here, precise temperature control is obtained via adiabatic evaporation by controlling the operating pressure independently in each stage. A separate condenser and vacuum source for each stage are required. The vacuum sources are kept separate to prevent disturbances in one from affecting the other and to permit the use of different utilities or grades of steam since the various crystallizer temperatures will require different condenser temperatures and operating pressures.

If the operating temperature of the first stage, dictated by the shape of the solubility curve, does not crystallize much product, the resulting low slurry density could lead to fouling due to the lack of sufficient crystal surface area to moderate the supersaturation at the boiling surface. Short operating cycles between cleanouts would increase the production cost. To control the cost, the slurry density could be artificially increased using a low-pressure-drop hydrocyclone to create a clarified mother liquor that could be advanced to the next stage under level control. The crystal mass can then be removed to the next stage independently based on slurry density measurement. The slurry density loop should be

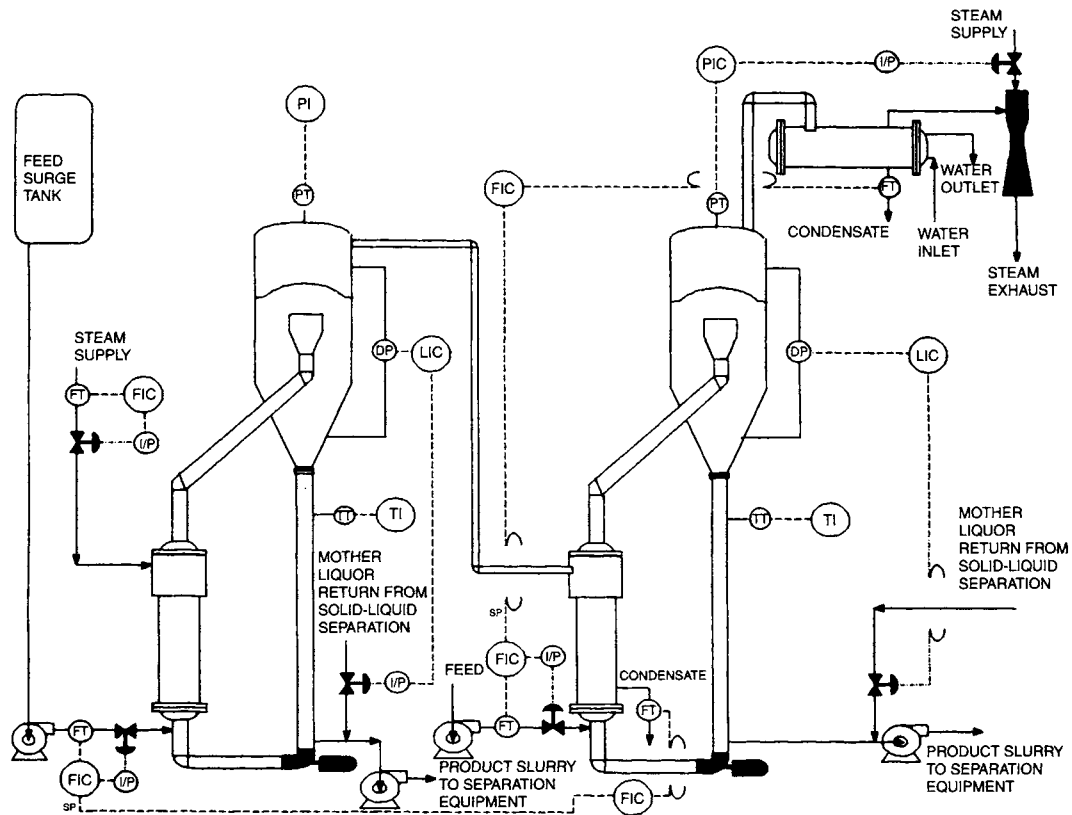


Figure 9.16 Schematic of a multi-effect forced-circulation crystallizer with parallel product flow.

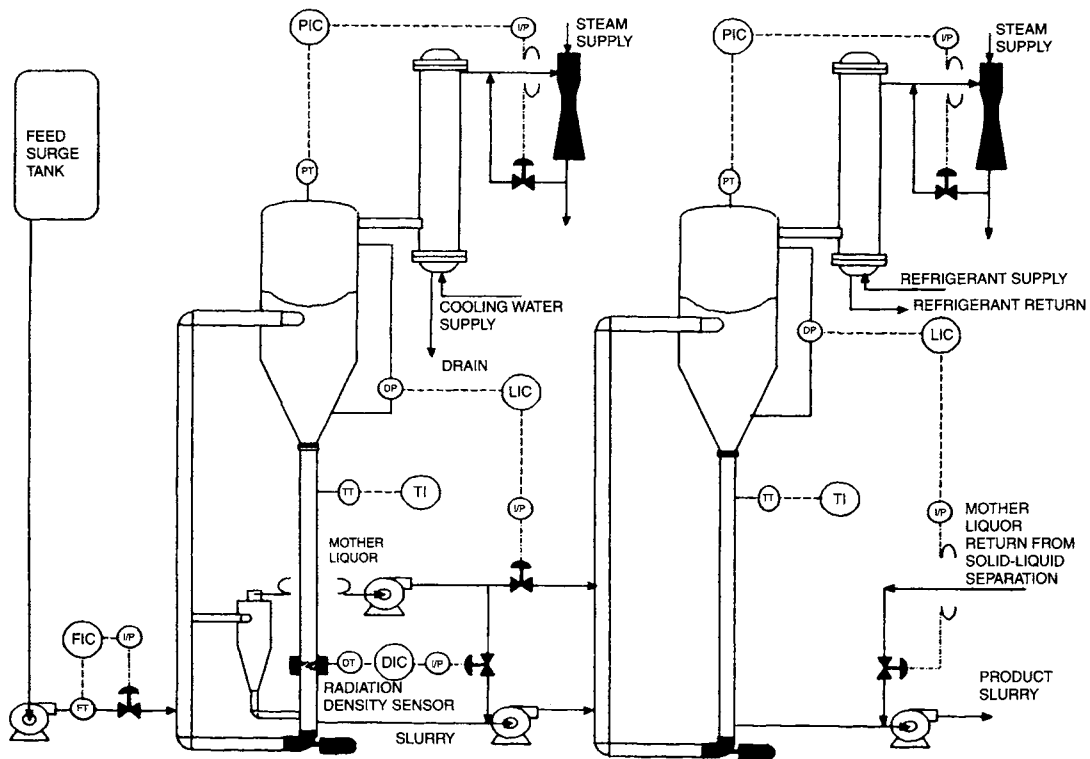


Figure 9.17 Schematic of a multi-stage forced-circulation crystallizer.

operated to minimize the fouling instead of maximizing the inter-stage crystal size, because the seeding effect at higher mother liquor advance rates will more than offset any CSD gains in the first stage. It should be noted that the clarified stream does entrain fines to seed the downstream crystallizer, in addition to the main slurry delivered.

The control strategy for the growth-type crystallizer would be the same as shown for the forced circulation crystallizers, but the hardware implementation for classification would differ. This hardware and control scheme could also satisfy the counterflow crystallization duty described above.

9.3.3. BATCH CRYSTALLIZATION CONTROL

Batch crystallization employs time-varying control targets such that the process operating conditions are constantly changing. The ability of the control system to shift the process conditions to the changing target, while preventing excursions outside the process variable bounds, determine the suitability of the control strategy and hardware implementation. Typically, batch operation is employed for products of small volume and/or where the crystallizing vessel may be used for more than one product. Also, a batch crystallization vessel is commonly used for more than one processing step, including reaction, distillation, and batch extraction with decanting. The utilities and control system must accommodate all operations and sometimes represent a compromise for crystallization control. Sometimes crystallization control requirements are not considered when specifying a multifunction batch vessel and utilities, leading to disappointing results.

A common vessel used in the batch production of fine chemicals and pharmaceutical is the jacketed glass-lined reactor-still as shown in Figure 9.18. It is available in 5 to 4,000 gallon capacities and is usually fitted with a retreat curve agitator and single baffle or thermowell/baffle assembly cantilevered from the vessel lid, a distillation column, and a condenser. The same temperature sensor

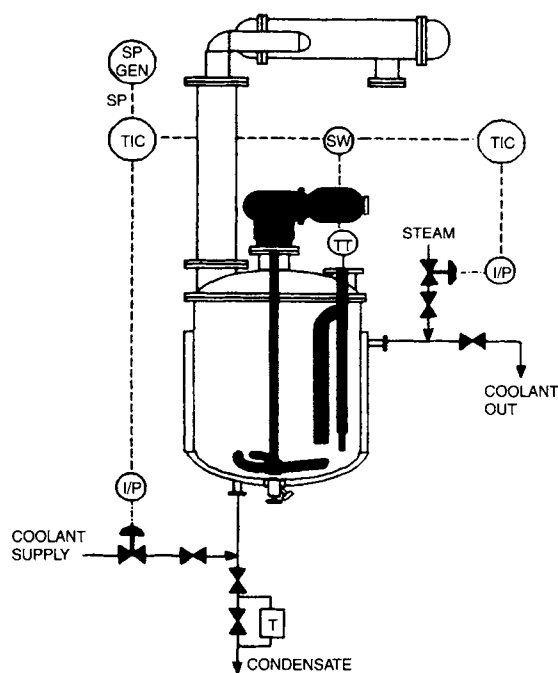


Figure 9.18 General purpose glass-lined batch reactor/crystallizer.

would be utilized for all indications of the contents temperature because of the limited number of access ports in the vessel head. The agitator drive may be single, dual, or variable speed.

A critical control aspect common to all batch crystallization is controlling the initial population of crystals. Control action intended to produce large crystals may be insufficient to compensate for the massive generation of nuclei that results from spontaneous nucleation. Industrial experience supports the copious academic documentation that seeding with a defined mass and size range of crystals permits the growth of larger crystals with a narrower size distribution.

The introduction of seed crystals to a solution that is saturated or within the lower portion of the metastable zone prevents spontaneous nucleation (Karpinski et al. 1980). In most industrial cases, seeding is a manual operation. The indication of when to seed is derived from an indication of the process temperature, typically provided by the control system, and knowledge of the product solubility and current solution concentration, whether measured on-line, off-line, or calculated from charge amounts. Obviously, accurately calibrated temperature sensors in the laboratory, where the solubility relationship was established, as well as in the crystallizer, where the solubility relationship will be utilized, are necessary.

In addition to seeding, the CSD is controlled by influencing the supersaturation by manipulating temperature, pressure, the distribution of solids within the vessel, and the rate of introduction and dispersion of nonsolvents during the batch crystallization. Implementation of techniques and strategies based on the manipulation of these variables is illustrated with the following examples.

Unbalanced Batch Temperature Control. The simplest and least expensive control configuration employs trapped steam heating for reaction and distillation with the steam flow rate moderated to maintain either the vessel contents temperature or a pressure drop across the column. Cooling can be accomplished by blocking the steam and controlling the flow of a coolant (water, brine, or glycol) to achieve the desired bulk temperature. Water is commonly used to reduce the crystallizing slurry temperature to 20–25°C.

This strategy is effective for cooling the vessel contents to near the coolant media temperature. A varying rate cooling profile could be implemented with this strategy using a cam or sequence program to feed a varying set point to the controller, but basic design deficiencies would severely limit product size improvements realized. Supplying only a coolant, the control system is not balanced; upon a temperature undershoot, the controller would saturate at zero output until the set point dropped below this temperature. Since control stability is poor within the bottom or top 10% of control valves, an oscillating temperature response is likely. These oscillations may cause the instantaneous cooling rate to far exceed the varying target rate and excessive nucleation may occur from temporarily high supersaturation.

Additionally, during the initial cooling phase, the temperature difference is high between the coolant and the bulk solution. Approximately two-thirds of the temperature drop is obtained through the wall of glass-lined vessels, leaving one-third between the inside wall and the bulk solution (Bondy and Lipka 1983). This significantly lower temperature at the vessel wall can lead to local supersaturation levels above the metastable limit, causing excessive nucleation rates in the solution and fouling on the vessel wall. Small mean crystal size and a large spread in the distribution will result from continued nucleation. Product loss, increased cycle time required for cleaning, and variable initial solution concentration (if carry-over product is acceptable in the subsequent batch) will be caused by the wall fouling.

Once-Through Balanced Temperature Control. Improved cooling control can be obtained through a steam/water mix for the jacket heat transfer media, as depicted in Figure 9.19. The injection of steam into a jacket water feed can provide a temperature range from the water temperature to 5°C below the vapor pressure of the water in the jacket (95°C unless backpressure control is applied to the drain). This strategy provides a balanced control to move the process temperature to the target from either side. The steam flow could be controlled directly in response to the vessel contents temperature, the steam/water mix temperature, or the steam flow. Controlling the steam flow to a flow rate target is usually advantageous because a flow sensor responds faster than a temperature sensor due to its thermal mass. Flow control should also be provided for the water supply to compensate for water line pressure fluctuations. This will also provide a constant flow of water to maintain sufficient velocity in the jacket to permit a reasonable outside heat transfer coefficient and full utilization of the jacket area for heat transfer. As illustrated in Figure 9.19, a cascade control strategy can be employed that uses measurements of the temperatures of the mixed stream and the vessel contents in a master loop that provides a set point for the steam flow loop. This allows the temperature difference between the jacket and the vessel contents to be limited to prevent fouling.

The disadvantage of this strategy lies in the high steam usage near the maximum operating temperature and the loss of condensate from the boiler, which frequently contains expensive anti-corrosive additives. Water consumption is also high. The temperature range may be insufficient for multi-function use.

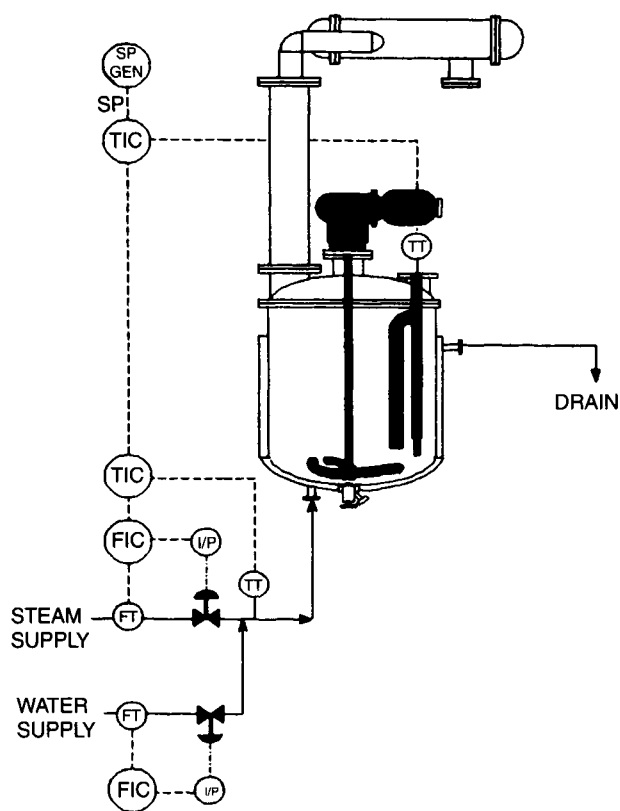


Figure 9.19 Batch crystallizer with once-through balanced temperature control.

Recirculating Temperature Control with Injection Heat Transfer. Figure 9.20 illustrates a strategy to reduce utility consumption by implementing a recirculating water system into which steam and water are injected as needed for balanced temperature control (Hafeez and Baumer 1980). The fastest jacket temperature response rate can be achieved by minimizing the volume in the recirculating pump head tank. Level control in the head tank is required; a mechanical float valve would serve as effectively as the electronic control loop shown. Since water is employed in both the above strategies, temperatures below 0°C are not possible.

Recirculating Temperature Control with Indirect Heat Transfer. To extend the operating temperature range, a heat transfer oil may be substituted for water in the recirculating system. Indirect heat transfer is required to contain the oil, and an oil surge tank is supplied to compensate for density changes in the oil over the operating temperature range. Heat may be supplied through a heat exchanger using trapped steam or by an electric heater. Cooling of the circulating oil would be provided by a refrigerant-supplied heat exchanger. The temperature range is dependent on the limit of the utilities and the range of the heat transfer oil. The only limit to the temperature driving force in the external heater or heat exchangers is preventing wall temperatures that will cause degradation of the heat transfer oil. For this reason, if an electrical heater is employed, an additional temperature control loop is required to limit the oil temperature inside the heater when the oil flow is restricted or stopped.

Control valves with opposing action are fitted to the heat and cooling exchangers and require equal proportion valve trims such that the total flow rate to the vessel jacket is maintained whether heating or cooling. Additionally, the flow rates through each unit should provide the same heat transfer capacity (Btu/hour) such that the same controller tuning parameters will apply whether heating or cooling. Without this constraint, oscillation about the set point would occur.

To reduce the cooling burden on the refrigeration system, the majority of the cooling duty would be met by a water-supplied heat exchanger. A temperature switch would circulate the oil through the water exchanger whenever a sufficient temperature difference is available for efficient heat transfer. The flow of refrigerant or water is blocked to reduce utility requirements whenever it is not in use. The schematic of a system for such a strategy to manipulate crystallizer temperature is given in Figure 9.21.

Batch Adiabatic Evaporative Crystallization. Figure 9.22 depicts a control strategy for performing cooling crystallization by removing heat from a vessel via adiabatic evaporation. Here the heat is removed from the crystallizing solution by evaporating some of the solvent. The controlling heat transfer rate is vapor condensation, which is much greater than conductive heat transfer through vessel walls. The solvent may be returned to the vessel to maintain the total volume or removed to effect a higher yield by reducing the solution volume at the final temperature. Additional concentration may be achieved by adding additional heat through the vessel wall. This is most often performed by condensing trapped steam. The temperature range depends on the jacket steam supply pressure, vacuum system limitation, and the vapor pressure-temperature profile of the solvent. The vacuum source may be a steam ejector, vacuum pump, or combination.

Temperature control by this strategy is not balanced for adiabatic cooling to allow recovery if the target temperature is undershot; however, it does permit higher heat transfer rates without wall fouling encountered from jacket cooling. An additional caution is required for vessels with retreat curve impellers. These have adequate pumping capacity for solids suspension but seldom

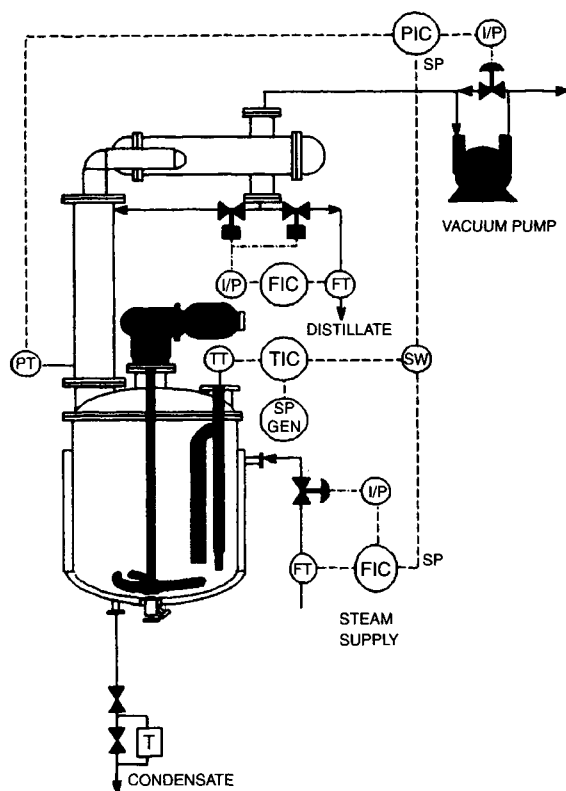


Figure 9.22 Batch adiabatic evaporative crystallizer.

achieve a uniform solids distribution within the vessel unless the density difference between the crystal and solution is small. As a result, the minimum crystal surface area is present at the solution surface where the maximum supersaturation is being generated by the solvent evaporation. A higher nucleation rate will occur under these circumstances, and the CSD will have a smaller mean size and a broader distribution from continued nucleation.

The pressure of the vessel is controlled by a bypass valve that recirculates exhausted gas to the suction side of the vacuum source, giving the fast response that is required of the pressure loop to compensate for the varying vapor load to the condenser. Nevertheless, the contents temperature responds more slowly to pressure changes due to the time required to mix the surface with the vessel contents and the capacitance of the vessel. To decrease the response time, the contents temperature can be controlled by cascading the temperature to the pressure loop. The master temperature loop will then adjust the pressure set point at a rate commensurate with the temperature process response while maintaining the solution at the surface within the metastable zone; the slave pressure loop will react to the pressure fluctuations during boiling.

For the same vacuum level, a crystallizing slurry will have a higher temperature than predicted for the pure solvent because the vapor pressure of the solvent is reduced by the presence of the solute (boiling point elevation). For adiabatic crystallization with the contents temperature as the input to the master control loop, the same temperature profile appropriate for crystallization by jacket cooling would apply here. However, the capability of the vacuum source and the line pressure drop should be considered in conjunction with the boiling point elevation to ensure that the desired final temperature can be met. If this is not satisfied, the desired yield may be achieved by removing some of the distillate, provided the saturation of an impurity is not reached. For most

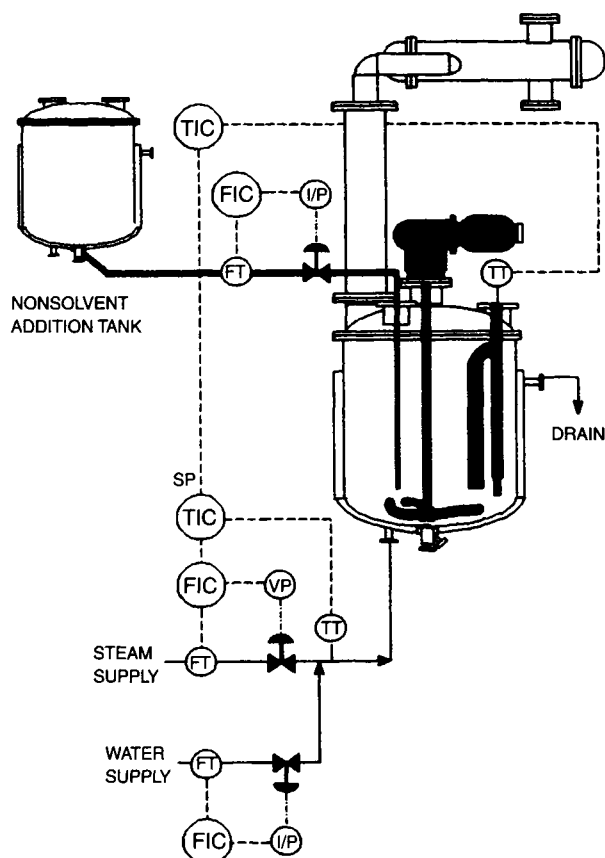


Figure 9.23 Batch crystallization by nonsolvent dilution (drown-out crystallization).

products to which cooling crystallization would be applied to recover the product, the solubility decreases exponentially with decreasing temperature. Evaporating solvent at an elevated temperature, therefore, often provides a less sensitive method for generating supersaturation than attempting to reduce the contents temperature, in which case temperature oscillations can make the instantaneous supersaturation unacceptably high. To implement this strategy, the distillate rate would need to be controlled while maintaining a constant temperature of the vessel contents. Figure 9.22 shows how this may be accomplished by controlling the reflux ratio to achieve a target distillate flow rate.

Batch Crystallization by Nonsolvent Dilution. Batch crystallization rates may also be controlled by varying the characteristics of the solvent from which the solute is crystallizing. Any two miscible solvents in which the product has different solubilities at the same temperature are possible solvent pairs. Crystallization of the solute from the solvent with the highest solubility is accomplished by dilution with the poorer solvent. The larger the solubility difference, the less poor solvent is required, and the higher the yield. A schematic of a crystallizer based on this strategy is given in Figure 9.23. Provided that the vessel is of sufficient size to hold the volume generated at the end, the poorer solvent is usually metered into the crystallizer and incorporated by the agitation. A time-varying flow rate is required to maintain a constant level of supersaturation in the bulk. To minimize local areas of high supersaturation, the poorer solvent should be introduced at the point of highest turbulence for rapid dispersion. The reduction of primary nucleation that accompanies improved mixing of the solv-

ents by using a higher agitator speed or a higher sheer impeller may produce larger crystals, despite the potential for higher secondary nucleation. The volumetric turnover (bulk mixing) and the uniformity of solids suspension will vary with the increasing volume of the slurry. Increasing agitation rate may be required because the initial agitation rate, constrained to prevent vortexing at the lower solution volume, may be inadequate at the final volume. Control of the agitator speed may be automated by supplying a remote set point to an inverter powering the agitator.

If the poorer solvent is less volatile than the initial solvent, distillation may be combined with nonsolvent addition to accomplish solvent exchange or at least minimize the volume change on addition. Since the relative volatilities change with composition in the crystallizing solution, reflux ratio and distillate take-off rate must be controlled separately to follow the desired time-solubility profile. If the solubility of the solute has a suitable sensitivity to temperature, jacket cooling may be combined with the nonsolvent addition. The temperature of the nonsolvent should also be considered, and adequate control provided to prevent operation outside the expected temperature-dependent metastable zone.

All three modes of generating supersaturation can be incorporated if the temperature reduction is accomplished by vacuum distillation. Solubility as a function of temperature and solvent ratio, as well as vapor-liquid equilibrium data, must be employed to design the time-varying control targets. For maximum controllability, the path that maintains the minimum slope to the final target on the three-dimensional solubility surface should be followed. This is the most complex batch crystallization control problem, because the objective is to control solubility, which is seldom measurable within the time frame in which control action is required. If implemented using single loop controllers for the three variables, each can only take compensating action for the property it measures and cannot accommodate interactions from the combined errors of all the controllers. A model-based optimal control strategy employing MIMO control should be considered for this case.

Fines Destruction for Batch Crystallization. Selective classification and destruction of fines from the slurry during a batch crystallization has been implemented in industrial practice, although no specific results have been published to date. Fines destruction has been employed for two applications. As an alternative to seeding, a batch may be cooled until spontaneous nucleation occurs. At this point, the vessel temperature is maintained, while a stream from a classifying baffle is circulated through an external heat exchanger to reduce the number of nuclei generated to an acceptable level. One robust and inexpensive indication of nucleation and concentration of fines can be provided by a turbidity sensor. To prevent color variation in successive batches from being interpreted as varying levels of fines, the measured value just before rapid change at nucleation should be the reference point for inferring fines concentration during the remainder of the batch. Also, operation of the fines destruction loop has been continued throughout the batch in either an open-loop mode at a set flow rate or in response to the concentration of fines present. Although not yet commonly practiced in industry, it offers a significant opportunity because it is the only control strategy that enables a reduction in the number of crystals present in a batch to provide some compensating action for process condition excursions that cause spontaneous nucleation.

9.3.4. SENSOR AND CONTROL ELEMENT CONSIDERATIONS

A correctly selected and sized crystallizer and a control strategy incorporating the best understanding of crystallization kinetics

and process dynamics do not ensure a successful crystallizer operation. Proper selection and installation of the process measurement sensors and the final control elements are also required to complete the control system. An accurate description of the current process from the sensors is required by the control algorithms to translate knowledge about the process into the correct directions for the control devices. A discussion of selecting and installing sensors and control devices, practical considerations of implementing a control strategy, is given below.

General Problem of Incrustation. Incrustations are hard masses of crystals adhering to and growing on internal surfaces of an operating crystallizer. These deposits are a frequent cause for deteriorating performance of control systems. Incrustations can interfere with sensor and control element operation to effect fundamental changes in the characteristics of the process (e.g., time constant) and the controller response (e.g., process gain). Solids deposition over temperature sensors causes a lag in the measurement response to temperature changes and increases the process time constant as the growing deposit thickens. Without alteration of tuning parameters for the temperature control loop, performance degrades and instability could result from control actions tuned for process dynamics that no longer exist. Incrustation over pressure sensors can isolate the sensor from the conditions in the vessel, causing erroneous measurements of vapor pressure or liquid level. Incrustation at valves used for flow control changes their C_v , or flow delivered at the same valve opening, changing the process gain of the flow control loop (Jančić and Grootsholten 1984).

Attention to installation details can alleviate many of the causes for incrustation at sensors and control elements. Sensors installed below the liquid surface should be mounted to the body using a flanged pad instead of a stub end, which would typically extend 4 to 5 inches, to allow the flange bolts to clear the insulation. The extension creates a reservoir for accumulating crystals from the slurry and a cold spot for fouling deposition by radiating heat from the large metal mass. If the flanged extension ports already exist on a vessel, a sensor insert that fills the extension cavity or a solvent flush to maintain a clear opening may be used. The flange should have additional insulation and possibly heat tracing to prevent heat loss from the extended surface. Whether a flanged pad or flanged extension, connecting welds should be ground smooth to prevent entrapment of crystals from the slurry. Once lodged, they will continue to grow and form interfering incrustations.

Sensor Selection and Installation.

Temperature. The location and choice of process sensors used to control a crystallizer affect the accuracy of the measurement and its sensitivity to operating condition changes. The glassed steel baffle-thermowell combination common to multipurpose batch vessels leads to considerable thermal lag in the temperature measurement during crystallization. Additionally, temperature inhomogeneity can result from cooling by either jacket or vacuum when the vessel is full. A separate sensor measuring the property creating the cooling driving force (jacket temperature or pressure) should be used for rapid feedback control in a slave loop to provide stability, while a controller using the vessel temperature adjusts the set point for the slave loop. The rate at which this set point should be changed is limited by the dynamics of the temperature measurement.

In continuous adiabatic evaporative crystallizers, the temperature distribution in the vessel is a function of the operating level. (The pumping rate also affects the distribution but is not subject to change during normal operation.) The surface temperature is set

by the pressure. The temperature in the body will increase relative to the surface temperature at a rate that is dependent upon the level, which increases to allow slurry flow to bypass the boiling surface. However, the vapor temperature, offset by the boiling point elevation of the solution, will accurately follow the liquid surface temperature. The generation of supersaturation at the surface can be decoupled from level disturbances by using the vapor temperature instead of the body temperature to determine the pressure set point.

Pressure. The location of pressure sensors in evaporative crystallizers also affect their reliability. If the operating pressure measurement is made in the vacuum line or condenser, it will be affected by the evaporation rate of the solvent and pressure drop changes due to any incrustation in the lines or mist eliminator. Measurement of the pressure in the vessel headspace circumvents this interaction. The sensor should be equipped with a solvent flush line to ensure that incrustation does not distort the measurement.

Level. Level sensors that depend on a pressure difference between two points, one submerged and one in the vapor, are subject to the same installation considerations described for pressure measurement. The inferred level measurement is more accurate when determined by a differential pressure transducer using remote diaphragms than when calculated from the difference between two absolute pressure transducers due to errors from calibration and transducer drift. In either case, the measurement is affected by changes in the weight percent solids in the solution; an increase in the liquid density would be interpreted as an increase in the level. Ultrasonic level sensors are not affected by the slurry density but are sensitive to fouling.

Slurry Density. The same differential pressure measurement employed for liquid level measurement is suitable for determining the weight percent solids in the slurry by submerging both diaphragms. The measurement should be made where the slurry is uniformly mixed over the distance between the taps and representative of the slurry density in the active volume. Differential pressure measurements in an evaporator body with a swirling vortex will reflect the tangential force of agitation. Measurements over an extended length in the growth chamber of a growth type crystallizer will confound changes in the bed depth with the maximum slurry density in the bottom. Pressure fluctuations from turbulent flow in circulation pipes will provide a noisy but reliable measurement. Radiation sensors provide a high resolution measurement with the above considerations, except vortex depth rather than tangential force should be considered for evaporator chamber installation.

Flow. Nonintrusive sensors that can be maintained at the process temperature are ideally suited to measure the flow rate of feed and product streams. Magnetic flow meters are suitable and inexpensive choice for aqueous streams. Organic streams with low dielectric constants require a vibrating tube mass flow meter to satisfy these criteria. Although commonly installed, flow meters that operate by inducing a pressure drop proportional to the flow rate present restrictions for solids accumulation that may alter the calibration. An alternative approach is to monitor the rotational speed of a positive displacement pump. Accuracy of this method is subject to wear and tolerances in the pump.

Fines Volume or Size Distribution. Increased industrial automation for the fines destruction loop is the subject of several academic research programs. Several measurement techniques for

feedback control of this loop employ optical techniques, such as the light scattering method discussed in Section 9.1.3, to infer the relevant states from the analysis of the size distribution and/or volume of fines in a clarified stream. The sensor location is constrained to the fines loop to provide sufficient dilution for measurement. Also, since the nucleation rate is often of interest for control purposes, installing the sensor in this loop automatically provides the classification necessary for resolution of the nuclei population.

Implications of long-term operation require consideration in installing and maintaining such sensors. Fouling within the classifying devices will shift the volume and velocity of liquor through the device and will shift the apparent number density and distribution of fines due to changing the cut size. Increases in colored impurity concentration reduce the light transmittance and increase the apparent concentration. Finally, fouling or etching of the glass in an optical sample cell will distort and reduce the light signal with technique-specific complications.

Final Control Element Selection and Implementation. Several industrially practiced options for final control element implementation were identified in the control strategy examples. The particular device chosen to control the manipulated variables will affect the process flexibility and responsiveness and impact the product quality.

Temperature. The process temperature of an evaporative crystallizer may be controlled by the absolute pressure in the vessel. Direct flow control of steam to an ejector, while economizing on steam utilization, is subject to pressure fluctuations due to disturbances in the steam supply pressure. Applying cascaded flow control would decrease the response time of the control loop. Flow control of a bleed gas or exhausted gas into the suction of the vacuum source is the most responsive and precise control option. Critically damped tuning of the pressure control loop should be implemented to prevent rapid temperature changes and high supersaturation generation from fast swings in pressure.

Process temperature control for cooling by surface heat exchange is only practiced when the vapor pressure of the solvent is too low for economical vacuum and condenser operation. Cooling through the crystallizer wall is only practical for small volume vessels where sufficient surface area to volume is available to maintain the temperature driving force within the metastable zone width. For volumes typical of continuous vessels, external heat exchangers are required and are normally operated with a 0.5–2 °C temperature difference between the process stream and cooling media. The media supply temperature is controlled by blending coolant from a refrigeration source with recirculating coolant. By this method, a constant and high heat transfer rate is maintained with a constant flow rate through the exchanger, and the blending technique removes the lags of the refrigeration source and surge tank from the control loop response.

Temperature control requiring additional heat input is normally controlled by regulating the flow rate of steam to the process heat exchanger. A desuperheater should be installed to prevent steam quality variation from causing heat exchanger fouling due to temperature spikes at constant flow.

Level. Level control using a control valve to throttle the exit flow rate presents a potential for plugging at the constricting point. Attrition of the crystals from the shear in the valve will generate additional nuclei, especially if the crystallizer head is insufficient to supply slurry to the downstream process and a centrifugal pump is required upstream of the valve. If the slurry is sent to solid-liquid separation equipment, the nuclei are inconsequential because they

have negligible mass and do not have time to grow to practically affect the product CSD. However, the additional nuclei in the feed of a second crystallizer would reduce the mean of the product CSD.

A variable speed positive displacement pump can minimize crystal attrition. The speed range must satisfy the flow requirements during start up and transients. Below a critical speed, crystals will settle out of the slurry. The minimum pump operating speed should be clamped above this rate for normal operation, and a line flush interlocked to stopping the pump for emergency shut-down.

Level control by moderating mother liquor flow to a slurry transfer pump suction, as illustrated for the multistage forced-circulation crystallizers, maintains a safe slurry line velocity by varying the weight percent solids transported. Slurry density control can also be implemented by this arrangement. The constant-speed slurry pump may be either centrifugal or positive displacement if the crystals are fragile. Fragile crystals require an internal baffle in the crystallizer body rather than a hydrocyclone to prevent attrition at the source of the mother liquor. If the natural make of the first crystallizer is high, slurry concentration would not be advised, and returned mother liquor from the solid-liquid separation source would be substituted. Care must be taken to ensure that no fines exist in the returned stream to seed the second crystallizer and reduce the mean product size.

Flow. All the options for controlling the level have been actually accomplished by flow control. An important consideration is that all streams, slurry, and clarified mother liquor removed from a continuous crystallizer and those removed immediately at the end of a batch crystallization are supersaturated. Crystals carried by these streams that become lodged in internal cavities of valves therefore continue to grow even if heat loss is eliminated by tracing and insulation. Only valve designs having no cavities, such as pinch type or rotating plug, are suitable. The potential for plugging due to solids accumulation in the throttled valve can be reduced by installing a timer-driven solenoid to periodically fully open the valve (Bennett 1983). This technique is not suitable if the valve is controlling the feed to a second crystallizer since the metastable limit may be exceeded at the mixing point, spawning undesired nuclei.

9.4. ADVANCED CONTINUOUS CRYSTALLIZER CONTROL

Having discussed many of the practical issues of operating and controlling continuous and batch industrial crystallizers in Section 9.3, this section and the next focus on the largely unsolved problems of crystal quality control. By crystal quality, one usually means crystal size, purity, and habit (morphology). Of these three, advances in crystal size and CSD control have been the most marked. As on-line CSD measurement continues to improve and implementable strategies for nonlinear, distributed parameter process control become better developed (Eaton and Rawlings 1990; Rawlings et al. 1992), the technology may soon be in hand to reduce CSD control to common industrial practice. It is crucial to bear in mind, however, that none of these advanced CSD control strategies will have any chance of success unless the basic design and instrumentation problems discussed in Section 9.3 have been addressed.

A considerable amount of academic research in the area of advanced crystallizer dynamics followed the development of the population balance crystallizer model (Randolph and Larson 1962; Hulbert and Katz 1964). Much of this work was primarily motivated by the occurrence of limit-cycle behavior in continuous

crystallizers. Partially due to the limitations of on-line measurement devices and also because of the inherent difficulties in distributed parameter system control, there have been considerably fewer studies of CSD control. This section includes a discussion of model identification methods, summarizes stability considerations and the work related to stabilizing open-loop unstable systems, and summarizes investigations of the CSD control problem.

9.4.1. MODEL IDENTIFICATION

Advanced control strategies require a model that accurately represents the behavior of the process. Model identification involves determining an appropriate model structure, performing experiments, collecting data that allow identification of model parameters, and estimating the parameters. There are several ways to model crystallization processes, but a review of parameter estimation is beyond the scope of this chapter. A discussion of the most relevant methods of model identification for continuous crystallizers is given below.

Model Formulation. Modelling in chemical engineering usually involves using material, energy, and momentum balances to develop equations that, along with constitutive models of material behavior, yield average properties of the system as functions of spatial coordinates and time. The population balance approach (Hulbert and Katz 1964; Randolph and Larson 1988) provides an appropriate modelling framework for dispersed-phase systems, allowing specification of particle quality (i.e., size, age, purity, etc.) in addition to location. If one linear dimension is adequate for crystal characterization, the population balance for a continuous cooling crystallizer with a solids-free feed and constant volume gives:

$$V \frac{\partial n(L, t)}{\partial t} + V \frac{\partial [G(L, t)n(L, t)]}{\partial L} + \dot{V}_f(t)h_f(L)n(L, t) + \dot{V}_p(t)h_p(L)n(L, t) = 0 \quad (9.4)$$

where $n(L, t)$ is the population density function at time t on a per volume suspension basis; V is the suspension volume; $\dot{V}_f(t)$ and $\dot{V}_p(t)$ are volumetric flow rates to the fines destruction system and of the product, respectively; and h_f and h_p are classification functions; idealized examples are

$$h_f = \begin{cases} 1 & L \leq L_f \\ 0 & L > L_f \end{cases}$$

$$h_p = \begin{cases} 0 & L < L_p \\ 1 & L \geq L_p \end{cases}$$

Note that $h_f = 0$ and $h_p = 1$ for all L correspond to a mixed suspension, mixed product removal (MSMPR) crystallizer.

When the growth rate is size independent and secondary nucleation is predominantly responsible for new crystal formation, the following semiempirical constitutive models are commonly used

$$G = k_g e^{-E_g/RT} \left(\frac{C - C_s}{C_s} \right)^g \quad (9.5)$$

$$B = k_b e^{-E_b/RT} \left(\frac{C - C_s}{C_s} \right)^b m_3^j \quad (9.6)$$

where m_3 is the third moment of the distribution. The mass balance on the solute being crystallized gives

$$\epsilon(t)V \frac{dC}{dt} = \dot{V}_i(t)C_i(t) + \dot{V}_r(t)C_r(t) - \dot{V}_p(t)C(t) - \dot{V}_f(t)C(t) - 3[\rho_c - C(t)]k_v \int_0^x G(L, t)n(L, t)L^2 dL \quad (9.7)$$

where ϵ is the void fraction (i.e., $\epsilon(t) = 1 - k_v m_3$).

The energy balance yields

$$V \frac{d(\rho c_p T)}{dt} = \dot{V}_i \rho_i c_{pi} T_i + \dot{V}_r \rho_r c_{pr} T_r - \dot{V}_f \rho_f c_{pf} T - \dot{V}_p \rho_p c_p T + \dot{Q}_{mix} + \dot{Q}_c - \dot{Q}_{ext} - \dot{Q}_{surr} \quad (9.8)$$

where c_p is the suspension specific heat; the subscripts i , r , and f refer to the inlet, recycle, and fines removal streams, respectively; \dot{Q}_{mix} is the rate of heat added by physical mixing, \dot{Q}_c is the rate of heat evolved by crystallization; \dot{Q}_{ext} is the rate of heat removed by the external cooling system; and \dot{Q}_{surr} is the rate of heat loss to the surroundings. The necessary initial and boundary conditions are

$$\begin{aligned} n(L, t = 0) &= n_0(L) \\ n(L = 0, t) &= B/G \\ C(t = 0) &= C_0 \\ T(t = 0) &= T_0 \end{aligned} \quad (9.9)$$

Parameter Estimation. The kinetic parameters of the model given above that must be estimated for model identification include k_g , g , E_g , k_b , b , E_b , j . Parameter estimation for this type of model is quite difficult because the parameters appear nonlinearly, the nucleation rate parameters enter only in the boundary condition, and availability of accurate data is limited. Certainly a model that describes the behavior of a nonisothermally operated crystallizer is needed if the temperature is to be manipulated, but there have been only a few studies of the effect of temperature on crystallization processes (Helt and Larson 1977; Randolph and Cise 1972; Rousseau and Woo 1980). For isothermal crystallization, the terms involving E_g and E_b are absorbed into k_g and k_b , and only k_g , g , k_b , b , and j need to be estimated.

Because of the simplicity of the analysis of the data from steady-state MSMPR crystallizers, the MSMPR configuration has been popular for kinetic parameter estimation studies. For size-independent growth, the steady-state CSD for a MSMPR crystallizer is given by

$$n = n^0 \exp\left(-\frac{L}{G\tau}\right)$$

Since the mean residence time, τ , is known for a particular set of operating conditions, the growth rate, G , can be determined from the slope of the semilog plot of the CSD, and the nucleation rate, B , can be obtained from the intercept, n^0 (recall $B = n^0 G$).

Tavare (1986) proposed a method using population density information from MSMPRs to provide a check on the reliability of kinetic parameter estimates and possibly to be used as a means of parameter estimation. Garside and Shah (1980) provide a review of the published MSMPR parameter estimation studies. They demonstrate the disagreement in parameters obtained by different investigators for the same chemical systems. They also point out that the range over which most kinetic studies are made is too small and suggest conditions under which future laboratory studies should be made.

An approach to the model identification problem is taken by de Wolf et al. (1989) that involves determining an input-output, black-box model that has a state-space structure. The advantage of this approach over a physical-principles model is that no model assumptions are required. The disadvantages are that the estimated parameters have no physical meaning, and parameter estimation may need to be frequently repeated as operating conditions vary.

9.4.2. STABILITY CONSIDERATIONS

The need for large-tonnage fertilizers created the demand for continuous crystallizers that could produce large and uniform crystals and operate stably for long periods of time (Bennett 1984). Sustained oscillations in continuous crystallizers have been observed in academic investigations with bench-scale crystallizers (Song and Douglas 1975; Randolph et al. 1977), and are an important industrial problem that can lead to off-specification products, overload of dewatering equipment, and increased equipment fouling.

As discussed in Section 9.2.2., the introduction of feedback can lead to oscillations in a system. As pointed out by Randolph and Larson (1988) and as illustrated in Figure 9.24, a crystallizer has an inherent feedback structure because of the interrelationship between the growth rate, the nucleation rate, and the CSD. This feedback is responsible for observed instabilities of an open-loop crystallizer (i.e., a crystallizer that is not externally controlled).

The stability of the open-loop, continuous crystallizer has received considerable attention (Anshus and Ruckenstein 1973; Epstein and Sowul 1980; Ishii and Randolph 1980; Jerauld et al. 1983; Randolph et al. 1973; Randolph and Larson 1988; Rawlings and Chan 1988; Sherwin et al. 1967; Witkowski and Rawlings 1987). As summarized by Randolph (1980), the two explanations that have been developed for CSD instability have been termed *high-order cycling* and *low-order cycling*. High-order cycling corresponds to a high-order kinetic relationship between the nucleation rate and the supersaturation. Low-order cycling is due to nonrepresentative product removal (i.e., h_p not constant for all L). For an MSMPR, the value of b required to cause cycling is much higher than has been estimated for most chemical systems. Therefore, low-order cycling is the more likely explanation for the commonly observed CSD instabilities.

9.4.3. FEEDBACK CONTROLLER DESIGN

Numerous investigators have addressed the problem of stabilizing an oscillating crystallizer using feedback control. Many of the early studies proposed measuring some moment of the CSD on-line and adjusting the flowrate of the fines destruction system (Gupta and Timm 1971; Lei et al. 1971a, 1971b). Beckman and Randolph (1977) demonstrated via simulation that limit-cycle instability could be eliminated by manipulating the flow rate to a fines dissolution loop in proportion to deviations of the nuclei density from its steady-state value. The corresponding proportional control law is given below

$$\frac{\dot{V}_f - \bar{V}_f}{\bar{V}_f} = K_c \frac{n_0 - \bar{n}^0}{\bar{n}^0} \quad (9.10)$$

They determined the controller gain, K_c , theoretically required to eliminate instability.

Rovang and Randolph (1980) suggested and experimentally tested the use of extrapolation of the data from a Coulter Counter to determine the nuclei density in the fines dissolution loop. Randolph and Low (1981) demonstrated the similar use of a light scattering instrument to infer the fines-loop nuclei density. The use of this

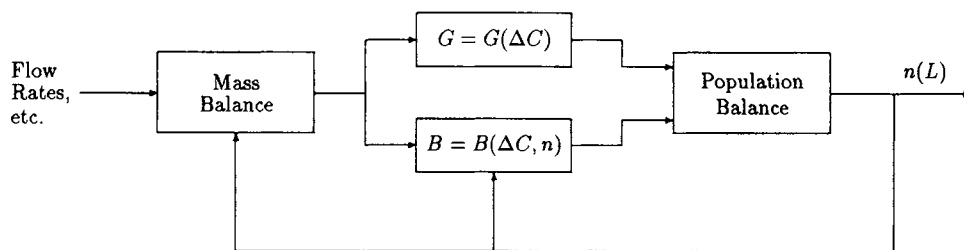


Figure 9.24 Inherent feedback structure of crystallizers.

measurement of the nuclei density in the control law given by Eq. (9.10) has been shown experimentally to stabilize a crystallizer and reduce the effect of external disturbances (Randolph and Low 1981). Rohani (1986) suggested the substitution of the slurry density measurement in the fines loop, readily obtained from a turbidimeter, for the nuclei density.

The use of the supersaturation as the measured variable for a control algorithm was first suggested by Han (1969). Rousseau and Howell (1982) used simulations to demonstrate that the substitution of the supersaturation for n^0 in Eq. (9.10) could stabilize a cycling crystallizer. While the on-line supersaturation measurement is in general more easily obtained than the determination of properties of the CSD, it is pointed out that the scheme based on supersaturation measurement is more sensitive to measurement noise.

One of the primary motivations for feedback is to overcome model uncertainty. For the controller to work well in practice, it should be tuned to be robustly stabilizing. That is, the controller should not only stabilize the nominal model, but also all models within some uncertainty region that reflects how well the system has been identified. The areas of robust stability and robust performance are current topics of control research. To date, essentially none of this research has been applied to crystallization.

There have been relatively few studies of multi-variable controllers for continuous crystallizers. Most studies of MIMO control algorithms are based on linear state-space models of the form

$$\dot{\mathbf{x}} = \mathbf{A}(t)\mathbf{x}(t) + \mathbf{B}(t)\mathbf{u}(t) \quad (9.11a)$$

$$\mathbf{y} = \mathbf{C}(t)\mathbf{x}(t) + \mathbf{D}(t)\mathbf{u}(t) \quad (9.11b)$$

in which \mathbf{x} is a vector of state variables, and $\dot{\mathbf{x}} = d\mathbf{x}/dt$. The state variables completely specify the state of the crystallizer and include the measurable states such as temperature, slurry density, etc.

Nevertheless, as discussed previously, the physical model for a crystallizer is an integro-partial differential equation. A common method for converting the population balance model to a state-space representation is the method of moments; however, since the moment equations close only for a MSMPR crystallizer with growth rate no more than linearly dependent on size, the usefulness of this method is limited. The method of lines has also been used to cast the population balance in state-space form (Tsuruoka and Randolph 1987), and as mentioned in Section 9.4.1, the "black-box" model used by de Wolf et al. (1989) has a state-space structure.

Hashemi and Epstein (1982) linearized the set of ordinary differential equations (ODEs) resulting from the application of the method of moments on an MSMPR crystallizer model and used singular value decomposition to define controllability and observability indices. These indices aid in selecting measurements and manipulated and control variables. Myerson et al. (1987) suggested the manipulation of the feed flow rate and the crystallizer temperature according to a nonlinear optimal stochastic control scheme with a nonlinear Kalman filter for state estimation.

On-line densitometry was proposed as a means of measuring the third moment of the CSD.

9.5. ADVANCED BATCH CRYSTALLIZER CONTROL

Despite the activity in continuous crystallizer control studies, there have been relatively few studies on the development of control algorithms for batch crystallizers. Uncontrolled or natural cooling of a seeded batch crystallizer usually leads to undesirable CSDs because the supersaturation often exceeds the metastable limit; operation above the metastable limit results in the production of a large number of nuclei, competing with seed growth and reducing the rate of subsequent solid-liquid separation. Griffiths (1925) suggested maintaining the supersaturation in the metastable region to improve the product CSD; he termed this "controlled cooling." Certainly such simple strategies as isothermal operation and linear cooling fall into the category of controlled cooling, and experimental studies of such approaches have been performed (Garside et al. 1972).

Jones and Mullin (1974) demonstrated the model-based computation of a cooling policy that attempts to maintain a constant nucleation rate. It was demonstrated experimentally that this constant-nucleation-rate cooling policy leads to a product CSD superior to that obtained by natural cooling.

The determination of an optimal operating policy for crystallization was considered by Ajinkya and Ray (1974). They suggested that an optimal policy for batch crystallizers would be one that maximizes mean particle size and minimizes CSD variance in minimum time. While the satisfaction of such an objective would be economically beneficial, especially in light of recent experimental work on the relationship between CSD and filterability (Jones et al. 1987), the problem actually addressed was the maximization of the seed particle size subject to a simplified crystallizer model (assumptions included monodispersed seeds and negligible nucleation). Morari (1980) extended this work by determining the analytic solution of the problem and testing the algorithm using computer simulation. These studies provide insight for optimal batch crystallizer operation, but they are based on unrealistically simple models and lack experimental verification.

Jones (1974) used the moment transformation of the population balance model to obtain a lumped parameter system representation of a batch crystallizer. This transformation facilitates the application of the continuous maximum principle to determine the cooling profile that maximizes the terminal size of the seed crystals. It was experimentally demonstrated that this strategy results in terminal seed size larger than that obtained using natural cooling or controlled cooling at constant nucleation rate. This method is limited in the sense that the objective function is restricted to some combination of the CSD moments. In addition, the moment equations do not close for cases in which the growth rate is more than linearly dependent on the crystal size or when fines destruction is

employed; thus, it cannot be used for these types of crystallization systems.

Chang and Epstein (1987) also took the approach of applying optimal control theory to the set of ODEs resulting from the moment transformation of the population balance equation. The optimal control problem was solved using control vector iteration for objective functions formed from various combinations of the CSD moments. The study performed by Chang and Epstein is the only attempt in the literature to introduce feedback to an optimal control strategy for batch crystallizers. This approach was tested using simulation, but no experimental verification was performed. Note that neither the method proposed by Jones nor the one suggested by Chang and Epstein allows for convenient incorporation of manipulated variable constraints such as cooling rate limitations.

In this section, a discussion of model identification for batch crystallizers is given and a model-based control strategy is illustrated that conveniently handles input, output, and final-time constraints and is applicable to cases in which fines destruction is used and the growth rate is size dependent. This control scheme permits flexibility in objective function formulation and allows consideration of objective functions that take into account solid-liquid separation in subsequent processing steps.

9.5.1. MODEL IDENTIFICATION

Model Formulation. The population balance equation for a batch crystallizer with a fines dissolving system is

$$\frac{\partial[M(t)n(L, t)]}{\partial t} + M(t)\frac{\partial[G(L, t)n(L, t)]}{\partial L} + \dot{M}_{fi}(t)h_f(L, t)n(L, t) = 0 \quad (9.12)$$

where $n(L, t)$ is the population density function at time t on a per mass of solvent basis (this is often a convenient basis for batch crystallizers), M is the mass of solvent in the crystallizer, and $\dot{M}_{fi}(t)$ is the solvent mass flow rate into the fines dissolution system.

Mass balances on the solute being crystallized and on the solvent in the crystallizer give

$$\frac{dC}{dt} = \frac{\dot{M}_{fo}}{M}(C_{fo} - C) - 3\rho_c k_v \int_0^x G(L, t)n(L, t)L^2 dL \quad (9.13)$$

where \dot{M}_{fo} and C_{fo} are the mass flow rate of solvent and solute concentration, respectively, in the stream from the dissolution system, k_v is the crystal area shape factor, and ρ_c is the crystal density.

The energy balance for a jacketed crystallizer yields

$$\begin{aligned} M_s \frac{d(c_p T)}{dt} &= \dot{M}_{fo} c_{pfo}(T_{fo} - T_{ref}) - \dot{M}_{fi} c_p (T - T_{ref}) \\ &\quad - \Delta H_c \left[3M \rho_c k_v \int_0^x G(L, t)n(L, t)L^2 dL \right] \\ &\quad - UA(T - T_j) + \dot{Q}_{mix} \end{aligned} \quad (9.14)$$

where M_s is the mass of the suspension, c_p is the suspension specific heat, c_{pfo} is the specific heat of the solution returning from the dissolution system, T_{ref} is a reference temperature, ΔH_c is the heat of crystallization, U is the overall heat-transfer coefficient, A is the total area of heat-transfer surface, and T_j is the temperature of the jacket fluid.

The kinetic expressions for growth and nucleation such as those given by Eqs. (9.5) and (9.6), and the initial and boundary conditions given by Eq. (9.9) complete the model formulation.

Parameter Estimation. As discussed in Section 9.4.1., model identification requires the determination of the parameters k_g , g , E_g , k_b , b , E_b , and j for a particular chemical system and batch crystallizer configuration using the available measurements. Garside et al. (1982) proposed a method using the initial first and second derivatives of the transient desupersaturation curve to calculate the growth rate parameters k_g and g . The disadvantages of this method are that it is limited to cases in which the nucleation rate can be assumed to be negligible, and since numerical differentiation of experimental data is required, it is sensitive to measurement noise.

Halfon and Kaliaguine (1976) measured transient CSD, yield, and concentration over the batch run, and used a least-squares approach to estimate the kinetic parameters. Tavaré and Garside (1986) obtained parameter estimates by using transient CSD measurements from a Coulter Counter in a procedure based on a linear least squares technique in the Laplace transform domain. Witkowski and Rawlings (1990) and Rawlings et al. (1989) discussed the weaknesses of some commonly used parameter estimation techniques; these shortcomings include inflexibility with respect to model formulation and no assessment of parameter uncertainty. They proposed simultaneously deducing growth and nucleation kinetic parameters by determining the parameters that minimize an objective function that represents the error between the model predicted and experimental states (e.g., sum of the squares of the errors). For a batch crystallizer with fines dissolution this technique comprises solving the nonlinear optimization problem

$$\min_{\theta^T} \Phi[y(t), \hat{y}(t); \theta]$$

subject to Eqs. (9.5), (9.6), (9.9), and (9.12) through (9.14)

where θ is the vector of parameters to be estimated. Discussions of nonlinear programming are given by Edgar and Himmelblau (1988) and Gill et al. (1981), and there are several computer codes available for the solution of the nonlinear programming problem.

Witkowski and Rawlings (1990) point out that for the estimation technique outlined above, methods exist for the calculation of approximate confidence intervals of the estimated parameters (Bard 1974; Caracotsios 1986). These confidence intervals provide a means by which to assess the parameter uncertainties. Obtaining parameter estimates with small confidence intervals indicates that the available measurements contain enough information for parameter estimation. It has been shown that concentration and obscuration measurements are sufficient for estimating the four kinetic parameters corresponding to an isothermal batch crystallizer (Witkowski et al. 1990). A number of parameter estimation methods for batch crystallization are summarized by Tavaré (1995).

9.5.2. OPTIMAL OPEN-LOOP CONTROL

After the identification of a model, the open-loop optimal control policy for the nominal plant can be determined by solving the following optimization problem.

$$\min_{u(t)} \Phi[u(t), x(t); \theta] \quad (9.15)$$

subject to Eqs. (9.5), (9.6), (9.9), (9.12) through (9.14) and

$$\mathbf{h}[\mathbf{u}(t), \mathbf{x}(t); \theta] = 0$$

$$\mathbf{g}[\mathbf{u}(t), \mathbf{x}(t); \theta] \geq 0$$

This approach enables the incorporation of input, output, and final-time constraints and is flexible with respect to the crystallizer configuration, the objective function definition, and the choice of manipulated variables. Examples of the use of nonlinear programming to solve this problem are given subsequently.

The population and mass balances for batch crystallization without fines destruction and with size-independent growth are as follows:

$$\frac{\partial n(L, t)}{\partial t} + G(t) \frac{\partial n(L, t)}{\partial L} = 0 \quad (9.16)$$

$$\frac{dC}{dt} = -3\rho k_v G m_2 \quad (9.17)$$

It should be emphasized that the expressions for growth rate and nucleation rate given above are valid for operation in the metastable zone only (i.e., operation in which the concentration is maintained between the saturation concentration and the metastable limit, the concentration above which homogeneous nucleation occurs).

The determination of the temperature profile that is optimal in some sense can be formulated as a nonlinear programming problem as follows:

$$\min_{\mathbf{T}} \Phi[\mathbf{T}, \mathbf{x}(t)]$$

subject to Eqs. (9.5), (9.6), (9.9), (9.16), (9.17) and

$$\mathbf{b}_u \geq \begin{Bmatrix} \mathbf{T} \\ \mathbf{AT} \end{Bmatrix} \geq \mathbf{b}_l$$

$$\mathbf{g}(\mathbf{T}) \geq 0$$

where $\mathbf{x}(t)$ is a vector of system states, \mathbf{A} is a constant matrix, $\mathbf{g}(\mathbf{T})$ is a vector of smooth nonlinear constraints, and \mathbf{T} is a vector of temperature values at n points equally spaced in time between $t = 0$ and $t = t_f$ that, with linear interpolation, define the temperature profile.

There are various methods for solving this problem, including reducing the model constraints to a set of algebraic equations and

using simultaneous optimization and model solution (Eaton and Rawlings 1990). For the example presented here, orthogonal collocation in space was used to reduce Eq. (9.16) to a set of ODEs. The resulting set of ODEs were integrated in time using the differential algebraic solver DASSL (Petzold 1983). This solution technique was used in conjunction with the successive quadratic programming code NPSOL (Gill et al. 1986) to solve the optimal control problem.

The model parameters used in the following examples are summarized below.

$$k_g = 8.64 \times 10^9 \mu\text{m/min}$$

$$E_g/R = 4859 \text{ K}$$

$$g = 1.5$$

$$k_b = 1.71 \times 10^{16} 1/(\text{min cm}^3)$$

$$E_b/R = 7517 \text{ K}$$

$$b = 2.25$$

$$j = 1$$

$$\rho = 2.66 \text{ g/cm}^3$$

$$k_v = 1.5$$

$$M = 3000 \text{ g}$$

$$m_{s0} = 16.60$$

$$C_0 = 0.1742 \text{ g solute per grams of solvent}$$

$$t_f = 30 \text{ min}$$

The following expressions for the saturation and metastable concentrations of potassium sulfate were used (Jones and Mullin 1974).

$$C_s = 6.29 \times 10^{-2} + 2.46 \times 10^{-3} T - 7.14 \times 10^{-6} T^2$$

$$C_m = 7.76 \times 10^{-2} + 2.46 \times 10^{-3} T - 8.10 \times 10^{-6} T^2$$

The initial seed distribution was assumed to be a parabolic distribution from 250 to 300 μm .

EXAMPLE 9.1

Using constant-rate cooling while maintaining the concentration in the metastable zone is a simple operating policy for a batch crystallizer that results in a greater yield than isothermal operation and a smaller terminal mass of small crystals than natural cooling. The simulated results corresponding to cooling at a constant rate from 50 to 30°C are given in Figures 9.25 and 9.26. Growth and nucleation are competing phenomena for the deposition of solute, and both are driven by supersaturation. The relatively high supersaturation over the batch run leads to substantial nucleation rates and subsequent growth of the nuclei, reducing the deposition of solute on the seed crystals.

Jones (1974) used control vector iteration on the lumped parameter system resulting from the moment transformation of the population balance to determine the cooling policy that maximizes the terminal size of the seed crystals subject to $T(t) \in [T_0, T_f]$ for all $t \in [0, t_f]$. This problem, along with the additional constraint

that the concentration must be maintained in the metastable zone, can be cast in the form of the nonlinear programming problem given above by defining the following objective function and constraints

$$\Phi = - \int_0^{t_f} G(t) dt$$

$$T_0 \geq T_i \geq T_f \quad i = 1, 2, \dots, n$$

$$C_m(t_i) - C(t_i) \geq 0 \quad i = 1, 2, \dots, n$$

For $T_0 = 50^\circ\text{C}$ and $T_f = 30^\circ\text{C}$, the resulting optimal temperature profile is given in Figure 9.27, and the corresponding concentration profile and CSD are given in Figures 9.28 and 9.29, respectively. The supersaturation is kept as small as possible at first, resulting in small nucleation and growth rates. The supersaturation

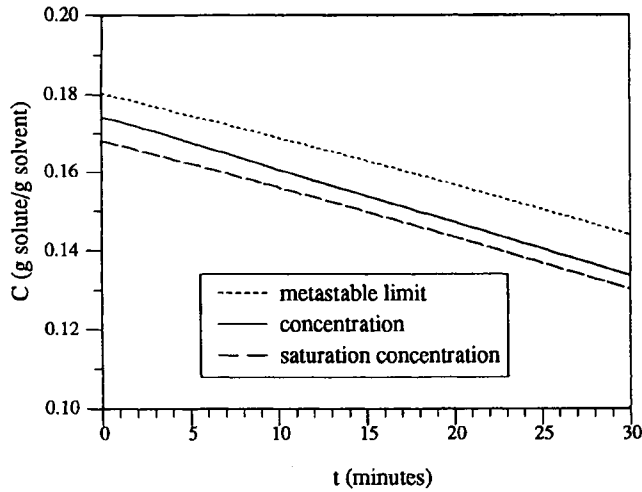


Figure 9.25 Concentration profile due to constant-rate cooling from 50–30 °C.

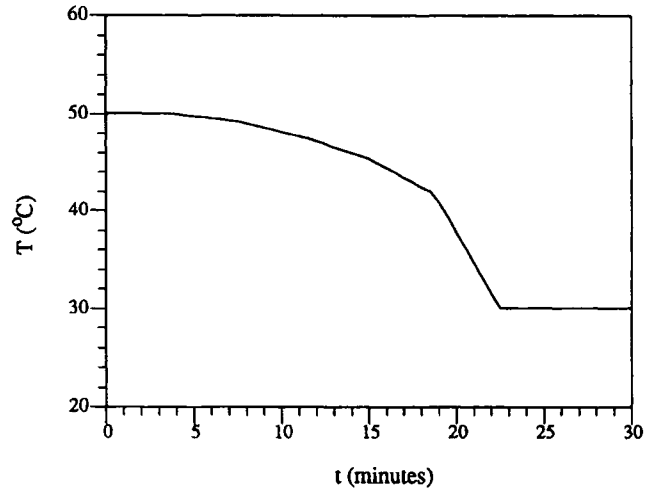


Figure 9.27 Temperature profile for maximizing terminal size of the seed crystals.

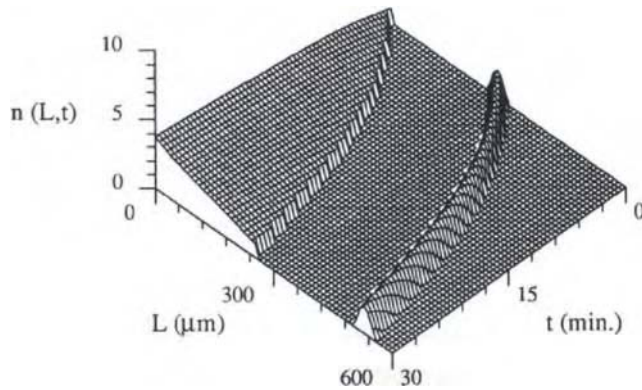


Figure 9.26 CSD due to constant-rate cooling from 50–30 °C.

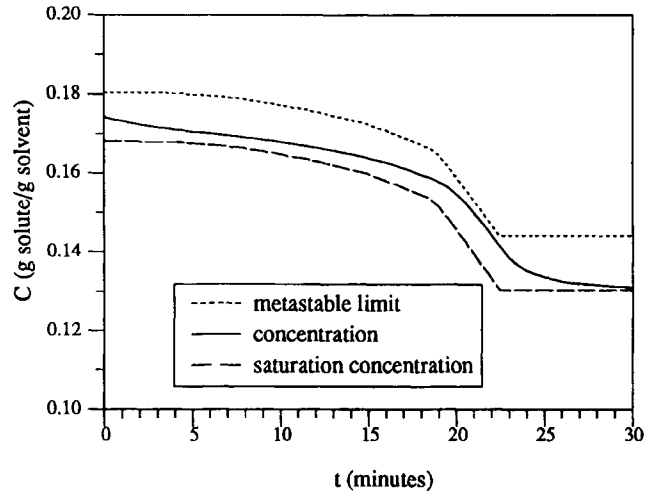


Figure 9.28 Concentration profile corresponding to the cooling policy for maximizing terminal size of seed crystals.

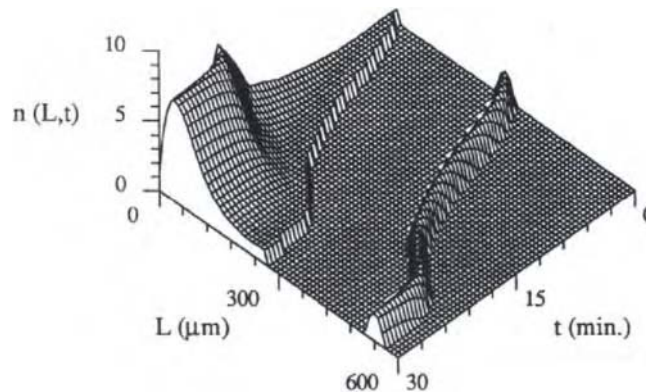


Figure 9.29 CSD due to cooling policy for maximizing terminal size of seed crystals.

is then slowly increased by decreases in the temperature. The temperature rapidly drops to the lower bound, producing a large growth rate at the cost of a large production of nuclei. After the

temperature reaches the lower bound, the nucleation rate quickly decreases due to the lower temperature and a decrease in the supersaturation.

EXAMPLE 9.2

There are indications that the permeability of the precipitates is diminished due to the bimodal nature of the CSD of a seeded crystallizer. Thus, the minimization of the final mass of nucleation-formed crystals, $m_n(t_f)$, would be expected to favorably affect the rate of subsequent filtration. The corresponding optimal control problem involves the solution of the nonlinear programming problem with the following objective function and constraints:

$$\Phi = m_n(t_f)$$

$$C_m(t_i) - C(t_i) \geq 0 \quad i = 1, 2, \dots, n$$

$$C^* - C(t_f) \geq 0$$

The last constraint represents the requirement of a minimum acceptable yield. For this problem, C^* was selected to be the final concentration for the constant-cooling-rate operating policy. The resulting optimal temperature profile is given in Figure 9.30, and the corresponding concentration profile and CSD are given in Figures 9.31 and 9.32, respectively. A small nucleation rate is maintained until the end of the run, at which point the supersaturation is substantially increased to drive large growth and nucleation rates to satisfy the yield constraint. While there is a burst of nucleation, the crystals formed are not given the opportunity for significant growth. As shown in Table 9.6, this operating policy leads to the same yield as the operation at a constant cooling rate, while reducing $m_n(t_f)$ by 24%.

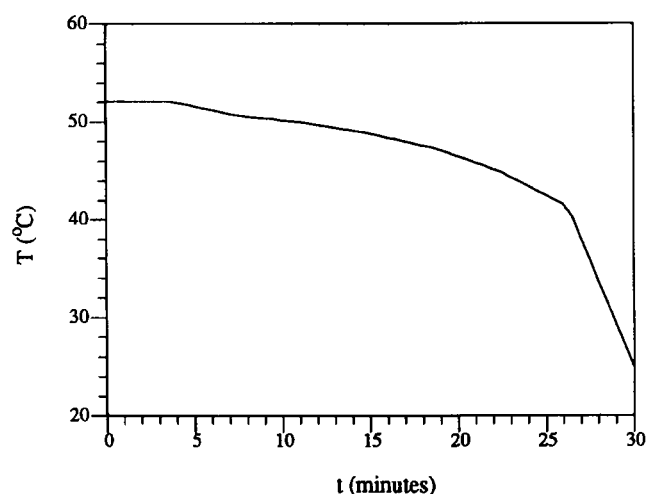


Figure 9.30 Temperature profile for cooling controlled to minimize $m_n(t_f)$.

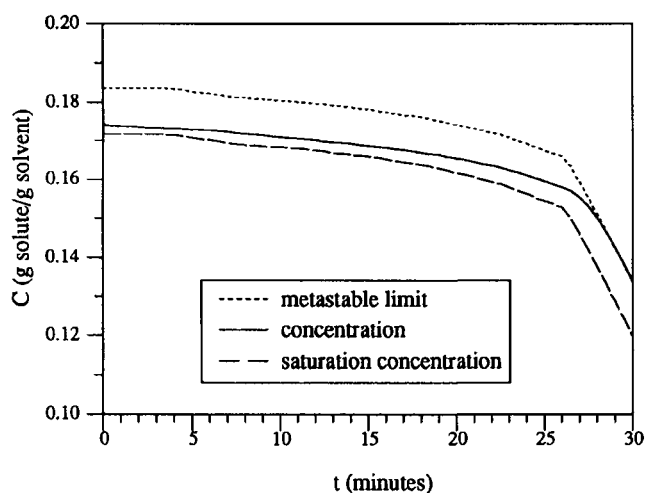


Figure 9.31 Concentration profile for cooling controlled to minimize $m_n(t_f)$.

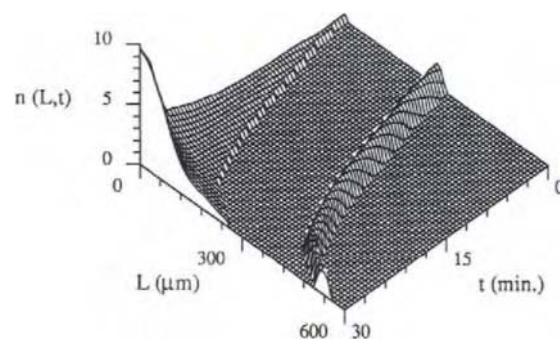


Figure 9.32 CSD for cooling controlled to minimize $m_n(t_f)$.

TABLE 9.6 Effect of Operating Policies on States of Interest

Operating Policy	Size of Largest Seed Crystal at t_f	Final Mass of Crystals Formed by Nucleation, $m_n(t_f)$	$C(t_f)$ g solute/g solvent
Constant cooling rate	254	20.6	0.1337
Maximize seed size at t_f	266	19.4	0.1311
Minimize $m_n(t_f)$	261	15.7	0.1337

The flexible formulation of the optimal control problem stated in Eq. (9.15) allows the inclusion of the fines destruction rate as a manipulated variable. Intuition suggests that for most objective functions of interest, the optimal policy for the fines destruction system is to operate at maximum dissolution rate. Nevertheless, this may not be the case due to the following:

1. Since some crystals are dissolved, crystallization must be performed at a higher rate to maintain a desired production rate. The correspondingly higher supersaturation results in a higher nucleation rate. Depending on several factors, such as the cut size and the crystallization kinetics, the net nuclei density may or may not be decreased by operation at the maximum dissolution rate.
2. The possible benefits of maximum fines dissolution may be outweighed by the increased energy costs of dissolving the fines and then recrystallizing.

9.5.3. FEEDBACK CONTROLLER DESIGN

An open-loop control policy is effective only if the model can accurately predict the behavior of the plant and if there are no large external disturbances. The introduction of feedback would allow compensation for plant/model mismatch and perturbations from the nominal control profile. Nevertheless, there have been only a few attempts to use feedback in a control algorithm for batch crystallizers; these are briefly outlined below.

A strategy suggested by Chang (1982) is based on the assumption that the perturbed trajectory is in the vicinity of the nominal trajectory and uses one-step iteration in a gradient search technique to improve the perturbed performance index. This approach assumes that the moments of the CSD (the states of the lumped model resulting from the method of moments) can be measured or estimated.

Rohani et al. (1990) postulated that it may be desirable to maintain the fines slurry density at some constant value over a batch run. They experimentally realized an improvement of the final CSD (larger mean size and smaller coefficient of variation) by using a conventional PI controller that manipulated the fines destruction rate to maintain a set point for the fines slurry density. Rohani and Bourne (1990) used simulations to demonstrate a self-tuning regulator to be more effective in set-point tracking and disturbance rejection than the PI controller.

An obvious approach to add feedback to the optimal control algorithm previously discussed is to solve the optimization problem periodically using a new set of measured or estimated initial conditions (possibly after re-estimating parameters); however, preliminary work has shown that this may not be presently practical in real time. An approach that is currently being studied comprises periodically determining and following "improved" trajectories instead of new "optimal" trajectories. This approach could be compared to state estimation with a standard linear quadratic (LQ) optimal controller design for the model resulting from lumping via collocation in space and linearizing about the nominal trajectory. References for LQ design include Kwakernaak and Sivan (1972) and Bryson and Ho (1975). It should be noted that even the implementation of given temperature and fines destruction rate profiles is not a trivial task, and the inability to do so is one of the expected disturbances of the system.

NOMENCLATURE

A	Total area of heat-transfer surface (m^2)
B	Nucleation rate [number/($\text{cm}^3 \cdot \text{min}$) or number/($\text{g solvent} \cdot \text{min}$)]
b	Exponent relating nucleation rate to supersaturation
C	Solute concentration (g solute/ cm^3 or g solute/g solvent)

C_0	Initial concentration (g solute/ cm^3 or g solute/g solvent)
C_s	Saturation concentration (g solute/ cm^3 or g solute/g solvent)
C_m	Metastable limit (g solute/ cm^3 or g solute/g solvent)
C_{fo}	Solute concentration of stream from dissolution system (g solute/ cm^3 or g solute/g solvent)
c_p	Suspension specific heat [J/($\text{g} \cdot \text{K}$)]
c_{pfo}	Specific heat of the solution in stream from dissolution system [J/($\text{g} \cdot \text{K}$)]
d	Disturbance that affects the states of the system
E_b	Nucleation activation energy [J/(mole $\cdot \text{K}$)]
E_g	Growth activation energy [J/(mole $\cdot \text{K}$)]
e	$y_{sp} - y_m$
G	Crystal growth rate ($\mu\text{m}/\text{min}$)
g	Exponent relating growth rate to supersaturation
h_f	Fines classification function
h_p	Product classification function
ΔH_c	Heat of crystallization (J/g)
j	Exponent relating nucleation rate to slurry density
K_c	Controller gain
k_b	Nucleation rate constant (units depend on value of j)
k_g	Growth rate constant ($\mu\text{m}/\text{min}$)
k_v	Volumetric shape factor (cm^3/μ^3)
L	Characteristic length of crystal (μm)
M	Mass of solvent in the crystallizer (g)
M_{fi}	Solvent mass flow rate into fines dissolution system (g/min)
M_{fo}	Solvent mass flow rate from fines dissolution system (g/min)
m_i	i^{th} moment of distribution
m_s	Mass of seed crystals (g)
m_n	Mass of crystals formed by nucleation (g)
n	Crystal size distribution [number/($\mu\text{m} \cdot \text{cm}^3$) or number/($\mu\text{m} \cdot \text{g solvent}$)]
p	Controller output
\dot{Q}_c	Rate of heat evolved by crystallization (J/min)
\dot{Q}_{mix}	Rate of heat added by physical mixing (J/min)
\dot{Q}_{ext}	Rate of heat removed by the external cooling system (J/min)
\dot{Q}_{surr}	Rate of heat loss to the surroundings (J/min)
t	Time (min)
t_f	Final time (min)
Δt	Sampling period (min)
T	Crystallizer temperature ($^{\circ}\text{C}$)
T_0	Initial crystallizer temperature ($^{\circ}\text{C}$)
T_{ref}	Reference temperature ($^{\circ}\text{C}$)
T_J	Crystallizer jacket temperature ($^{\circ}\text{C}$)
\mathbf{T}	Vector of temperature values at n points equally spaced in time between $t = 0$ and $t = t_f$
U	Overall heat-transfer coefficient [J/($\text{m}^2 \cdot \text{min} \cdot \text{K}$)]
V	Suspension volume (m^3)
\dot{V}	Volumetric flow rate (m^3/min)
u	Manipulated variable
\mathbf{x}	Vector of state variables
y	Measurable output or controlled variable
y_m	Measured output variable (includes sensor error and noise)
y_{sp}	Set point for the controlled variable

Greek Letters

ϵ	Void fraction
ρ	Density of crystals (g/cm^3)
Φ	Objective function for parameter estimation or optimal control problem
τ_I	Integral time constant
τ_D	Derivative time constant
θ	Parameter vector

REFERENCES

- Ajinkya, M.B., and Ray, W.H. (1974). *Chem. Eng. Commun.* **1**, 181–186.
- Anonymous. (1986). *Chem. Eng.* **93(22)**, 11.
- Anshus, B.E., and Ruckenstein, E. (1973). *Chem. Eng. Sci.* **28**, 501–513.
- Bard, Y. (1974). *Nonlinear Parameter Estimation*, Academic Press, New York.
- Beckman, J.R., and Randolph, A.D. (1977). *AIChE J.* **23(4)**, 510–520.
- Bennett, R.C. (1983). In *Process Equipment Series*, (Bhatia, M.V. ed.), vol. 5, pp. 210–246, Technomic Publishing Company, Lancaster, PA.
- Bennett, R.C. (1984). *Chem. Eng. Prog.*, March, 89–95.
- Bennett, R.C. (1988). *Chem. Eng.* **95(8)**, 118–127.
- Bondy, F., and Lipka, S. (1983). *Chem. Eng.* **90(7)**, 62–71.
- Brown, D.J., and Felton, P.G. (1985). *Chem. Eng. Res. Des.* **63**, 125–132.
- Bryson, A.E., and Ho, Y.-C. (1975). *Linear Optimal Control Systems*, Hemisphere Publishing Corporation, New York.
- Caracotsios, M. (1986). Ph.D. dissertation, University of Wisconsin, Madison.
- Chang, C.-T. (1982). Ph.D. dissertation, Columbia University, New York.
- Chang, C.-T., and Epstein, M.A.F. (1987). *AIChE Symp. Ser.* **83(253)**, 110–119.
- de Wolf, S., Jager, J., Kramer, H.J.M., et al. (1989). *IFAC Symposium on Dynamics and Control of Chemical Reactors, Distillation Columns and Batch Processes*, August 21–23, 1989, Maastricht, The Netherlands, pp. 107–114.
- Donoghue, J.F. (1977). *ISA Trans.* **16(2)**, 27–34.
- Eaton, J.W., and Rawlings, J.B. (1990). *Comput. Chem. Eng.* **14(4/5)**, 469–479.
- Edgar, T.F., and Himmelblau, D.M. (1988). *Optimization of Chemical Processes*, McGraw-Hill Book Company, New York.
- Epstein, M.A.F., and Sowul, L. (1980). *AIChE Symp. Ser.* **76(193)**, 6–17.
- Garside, J., Gaska, C., and Mullin, J.W. (1972). *J. Cryst. Growth* **13/14**, 510–516.
- Garside, J., Gibilaro, L.G., and Tavares, N.S. (1982). *Chem. Eng. Sci.* **37**, 1625–1628.
- Garside, J., and Mullin, J.W. (1966). *Chem. Ind.* November, 2007–2008.
- Garside, J., and Shah, M.B. (1980). *Ind. Eng. Chem. Proc. Des. Dev.* **19**, 509–514.
- Gill, P.E., Murray, W., Saunders, M.A., and Wright, M.H. (1986). *User's Guide for NPSOL (Version 4.0): A Fortran Package For Nonlinear Programming*, Technical Report, Systems Optimization Laboratory, Department of Operations Research, Stanford University, Stanford, CA.
- Gill, P.E., Murray, W., and Wright, M.H. (1981). *Practical Optimization*, Academic Press, London.
- Griffiths, H. (1925). *J. Soc. Chem. Ind. Trans.* **44**, 7T–18T.
- Gupta, G., and Timm, D.C. (1971). *Chem. Eng. Progr. Symp. Ser.* **67(110)**, 121–128.
- Hafeez, M.A., and Baumer, A.R. (1980). *Chem. Eng.* **87(4)**, 81–87.
- Halfon, A., and Kaliaguine, S. (1976). *Can. J. Chem. Eng.* **54**, 160–167.
- Han, C.D. (1969). *Ind. Eng. Chem. Proc. Des. Dev.* **8(2)**, 150–158.
- Hashemi, R., and Epstein, M.A.F. (1982). *AIChE Symp. Ser.* **78(215)**, 81–90.
- Helt, J.E., and Larson, M.A. (1977). *AIChE J.* **23(6)**, 822–830.
- Hulbert, H.M., and Katz, S. (1964). *Chem. Eng. Sci.* **19**, 555–574.
- Ishii, T., and Randolph, A.D. (1980). *AIChE J.* **26**, 507–510.
- Jager, J., de Wolf, S., Klapwijk, W., and de Jong, E.J. (1987). *Industrial Crystallization 87* (Nývlt, J., and Žáček, S., eds.), pp. 415–418. Elsevier Science Publishers, Amsterdam.
- Jančić, S.J., and Grootscholten, P.A.M. (1984). *Industrial Crystallization*, Delft University Press, Dordrecht, The Netherlands.
- Jerauld, G.R., Vasatis, Y., and Doherty, M.F. (1983). *Chem. Eng. Sci.* **38**, 1673–1681.
- Jones, A.G. (1974). *Chem. Eng. Sci.* **29**, 1075–1087.
- Jones, A.G., Budz, J., and Mullin, J.W. (1986). *AIChE J.* **32(12)**, 2002–2008.
- Jones, A.G., Budz, J., and Mullin, J.W. (1987). *Chem. Eng. Sci.* **42(4)**, 619–629.
- Jones, A.G., Chianese, A., and Mullin, J.W. (1984). In *Industrial Crystallization 84*, (Jančić, S.J., and de Jong, E.J., eds.), pp. 191–195. Elsevier Science Publishers, Amsterdam.
- Jones, A.G., and Mullin, J.W. (1974). *Chem. Eng. Sci.* **29**, 105–118.
- Karpinski, P., Budz, J., and Naruc, Z. (1980). In *Science Papers of the Institute of Chemical Engineering and Heat Systems* (Danuta Belina, ed.), no. 38, symposium no. 5, pp. 172–179, March 21–25, 1980, Wrocław, Poland, Technical University of Wrocław, Wrocław.
- Kwakernaak, H., and Sivan, R. (1972). *Linear Optimal Control Systems*, Wiley-Interscience, New York.
- Larson, M.A. (1978). *Chem. Eng.* **85(4)**, 90–102.
- Lei, S.J., Shinnar, R., and Katz, S. (1971a). *Chem. Eng. Progr. Symp. Ser.* **67(110)**, 129–144.
- Lei, S.J., Shinnar, R., and Katz, S. (1971b). *AIChE J.* **17(6)**, 1459–1470.
- McAvoy, T.J. (1983). *Interaction Analysis*, Instrument Society of America, Research Triangle Park, NC.
- Miller, S.M. (1993). *Optimal Quality Control of Batch Crystallizers*, Ph.D. dissertation, The University of Texas, Austin.
- Morari, M. (1980). *Chem. Eng. Commun.* **4**, 167–171.
- Mullin, J.W., and Leci, C.J. (1972). *AIChE Symp. Ser.* **68(121)**, 8–20.
- Myerson, A.S., Rush, S., Schork, F.J., and Johnson, J.L. (1987). In *Industrial Crystallization 87* (Nývlt, J., and Žáček, S., eds.), pp. 407–410. Elsevier Science Publishers, Amsterdam.
- Nývlt, J. (1978). *Industrial Crystallization: The Present State of the Art*, Verlag Chemie, Weinheim, West Germany.
- Petzold, L.R. (1983). In *Scientific Computing* (Stepleman, R.S., ed.), pp. 65–68, North-Holland Company, Amsterdam.
- Randolph, A.D. (1980). *AIChE Symp. Ser.* **76(193)**, 1–5.
- Randolph, A.D., Beer, G.L., and Keener, J.P. (1973). *AIChE J.* **19(6)**, 1140–1148.
- Randolph, A.D., Beckman, J.R., and Kraljević, Z.I. (1977). *AIChE J.* **23**, 500–509.
- Randolph, A.D., Chen, L., and Tavana, A. (1986). “Feedback control of CSD in a KCl crystallizer with fines dissolving,” *AIChE 1986 Spring Annual Meeting*, New Orleans, LA, April 1986.
- Randolph, A.D., and Cise, M.D. (1972). *AIChE J.* **18(4)**, 798–807.
- Randolph, A.D., and Larson, M.A. (1962). *AIChE J.* **8**, 639–645.
- Randolph, A.D., and Larson, M.A. (1988). *Theory of Particulate Processes*, 2nd ed., Academic Press, San Diego, CA.
- Randolph, A.D., and Low, C.C.D. (1981). In *Industrial Crystallization 81* (Jančić, S.J., and de Jong, E.J., eds.), pp. 29–34, North-Holland Publishing Company, Amsterdam.
- Rawlings, J.B., and Chan, W.M. (1988). “Stability and bifurcation of population balance models,” *Annual AIChE Meeting*, Washington, DC, November 1988.
- Rawlings, J.B., Witkowski, W.R., and Eaton, J.W. (1989). In *Proceedings of the 1989 American Control Conference*, June 21–23, Pittsburgh, PA, pp. 677–682.
- Rawlings, J.B., Witkowski, W.R., and Eaton, J.W. (1992). *Powder Technology* **69**, 3–9.
- Rivera, D.E., Morari, M., and Skogestad, S. (1986). *Ind. Eng. Chem. Proc. Des. Dev.* **25**, 252–265.
- Rohani, S. (1986). *Can. J. Chem. Eng.* **64**, 112–116.
- Rohani, S., and Bourne, J.R. (1990). *Chem. Eng. Sci.* **45(12)**, 3457–3466.
- Rohani, S., and Paine, K. (1987). *Can. J. Chem. Eng.* **65**, 163–165.
- Rohani, S., Tavares, N.S., and Garside, J. (1990). *Can. J. Chem. Eng.* **68**, 260–267.
- Rousseau, R.W., and Howell, T.R. (1982). *Ind. Eng. Chem. Proc. Des. Dev.* **21**, 606–610.
- Rousseau, R.W., and Woo, R. (1980). *AIChE Symp. Ser.* **76(193)**, 27–33.
- Rovang, R.D., and Randolph, A.D. (1980). *AIChE Symp. Ser.* **76(193)**, 798–807.
- Schleck, J.R., and Hanesian, D. (1978). *ISA Trans.* **17(4)**, 39–46.
- Seborg, D.E., Edgar, T.F., and Mellichamp, D.A. (1988). *Process Dynamics and Control*, John Wiley and Sons, New York.
- Sherwin, M.B., Shinnar, R., and Katz, S. (1967). *AIChE J.* **13**, 1141–1153.
- Sikdar, S.K., and Randolph, A.D. (1976). *AIChE J.* **22(1)**, 110–117.
- Shinskey, F.G. (1979). *Process Control Systems*, 2nd ed., McGraw-Hill Book Company, New York.
- Song, Y.H., and Douglas, J.M. (1975). *AIChE J.* **21**, 924–930.
- Smith, C.A., and Corripio, A.B. (1985). *Principles and Practice of Automatic Process Control*, John Wiley and Sons, New York.

- Stephanopoulos, G. (1984). *Chemical Process Control*, Prentice-Hall Inc., Englewood Cliffs, NJ.
- Tavare, N.S. (1986). *Can. J. Chem. Eng.* **64**, 752–758.
- Tavare, N.S. (1995). "Industrial Crystallization: Process Simulation Analysis and Design," Plenum, New York.
- Tavare, N.S., and Garside, J. (1986). *Chem. Eng. Res. Des.* **64**, 109–118.
- Toussaint, A.G., and Donders, A.J. (1974). *Chem. Eng. Sci.* **29**, 237–245.
- Tsuruoka, S., and Randolph, A.D. (1987). *AIChE Symp. Ser.* **83(253)**, 104–109.
- van de Hulst, H.C. (1981). *Light Scattering by Small Particles*, Dover, New York.
- Witkowski, W.R. (1990). Ph.D. dissertation, The University of Texas, Austin.
- Witkowski, W.R., Miller, S.M., and Rawlings, J.B. (1990). In *Crystallization as a Separations Process* (Myerson, A.S., and K. Toyokura, eds.), *American Chemical Society Symposium Series 438*, pp. 102–114, American Chemical Society, Washington, DC.
- Witkowski, W.R., and Rawlings, J.B. (1987). In *Proceedings of the American Control Conference*, June 10–12, Minneapolis, MN, pp. 1400–1405.
- Witkowski, W.R., and Rawlings, J.B. (1990). In *Proceedings of Second World Congress on Particle Technology*, Sept. 19–22, 1990, Kyoto, Japan, pp. 486–493.
- Wohlk, W. (1981). In *Industrial Crystallization 81* (Jančić, S.J., and de Jong, E.J., eds.), pp. 227–235, North-Holland Publishing Company, Amsterdam.

BATCH CRYSTALLIZATION

J.S. Wey and P.H. Karpinski

10.1. INTRODUCTION

Batch crystallization is different from continuous crystallization in that the withdrawal of crystal product for the batch system is made only once at the end of the batch run. Batch crystallization may also include the semibatch system in which one or more feed solutions are continuously added to the crystallizer.

Batch crystallization is commonly used in the chemical, pharmaceutical, photographic, and many other industries as a manufacturing process to prepare a wide variety of crystalline products. There are several desirable features associated with batch crystallization. The equipment is relatively simple and flexible, and requires a relatively low level of maintenance. Batch crystallization is particularly applicable to chemical systems difficult to process, that is, owing to toxic or highly viscous properties. Also, batch crystallization experiments can be used to examine a large number of operational variables in a short time. Systems that are difficult to operate continuously may conveniently be investigated in a batchwise manner with relatively minimum development time and investment. Furthermore, if the crystals are growing very slowly, a batch process can be controlled more easily in order to produce larger crystals than in a continuous process. In addition, batch crystallizers can produce a narrower crystal size distribution (CSD) than the continuous well-mixed crystallizers (Wey 1981; Moyers and Rousseau 1987; Randolph and Larson 1988). Thus, if monodisperse crystals are needed, batch crystallization can offer significant advantages in meeting the product requirement.

10.2. BATCH CRYSTALLIZERS

The types of batch crystallizers are basically the same as those for continuous crystallizers. There are, in general, four types of batch crystallizers classified by the way in which supersaturation is generated (Larson 1979). Cooling crystallizers usually operate by direct or indirect heat exchange between a hot solution containing the solute to be crystallized and a colder fluid, which may be a gas or a liquid. Systems exhibiting steep solubility curves are preferably crystallized by such cooling techniques. Evaporative crystallizers depend on the evaporation of solvent to generate supersaturation by heating and usually operate under vacuum. Systems exhibiting flat solubility curves, such as sodium chloride, are preferably crystallized in this manner. Reaction crystallizers are those in which supersaturation is generated by carrying on a chemical reaction, the product of which is only sparingly soluble. Salting-out crystallizers function by the addition of an antisolvent or "precipitant" that reduces the solubility of the solute in the solvent. In the pharmaceutical industry, for example, water is often used as the precipitant to induce the crystallization of organic substances from water-miscible organic solvents. Both reaction crystallizers and salting-out crystallizers are usually operated under the semibatch mode in which one or more feed solutions are continuously added to the crystallizer.

10.2.1. LABORATORY BATCH CRYSTALLIZERS

Laboratory batch crystallizers have been used successfully to develop crystallization kinetic expressions and to measure the effects of process conditions on the kinetics in realistic crystallization environments approximating those in industrial practice. Laboratory data are needed to help decide what mode of crystallization to use and to determine the features of design that will produce to the greatest degree the crystal properties and yield desired.

Probably the simplest laboratory batch crystallizer was described by Misra and White (1971). Kinetics of the crystallization of aluminum trihydroxide from caustic aluminate solutions were studied in a 5-l round-bottomed flask equipped with a stirrer, thermometer, and a sampling tube (Figure 10.1). The crystallizer was immersed in a constant-temperature bath.

A batch evaporative crystallizer (Figure 10.2) was used by Baliga (1970) to study the crystallization kinetics of potassium sulfate crystals. The crystallizer was equipped with a reflux condenser and a controlled distillate splitter so that the net solvent removal rate could be controlled closely. Heating of the crystallizer

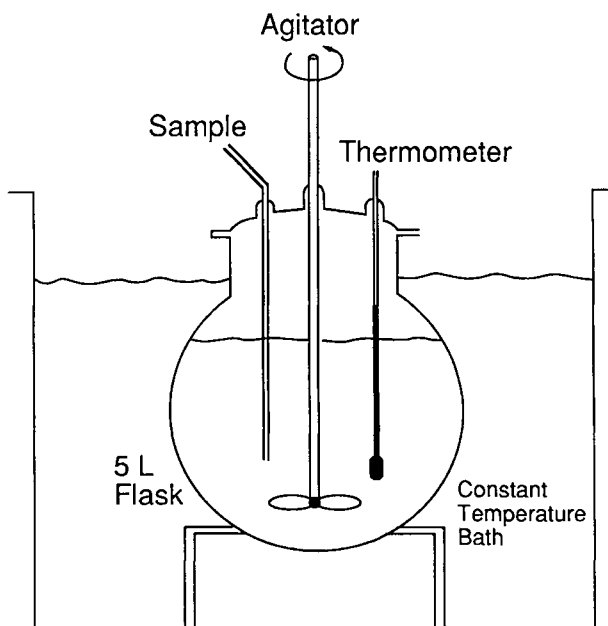


Figure 10.1 Laboratory batch crystallizer. (Reproduced by permission of the American Institute of Chemical Engineers © 1971 AIChE from "Kinetics of Crystallization of Aluminum Trihydroxide from Seeded Caustic Aluminate Solutions," Misra, C., and White, E.T., *CEP Symposium Series*, vol. 67, no. 110, pp. 53–65 (1971).)

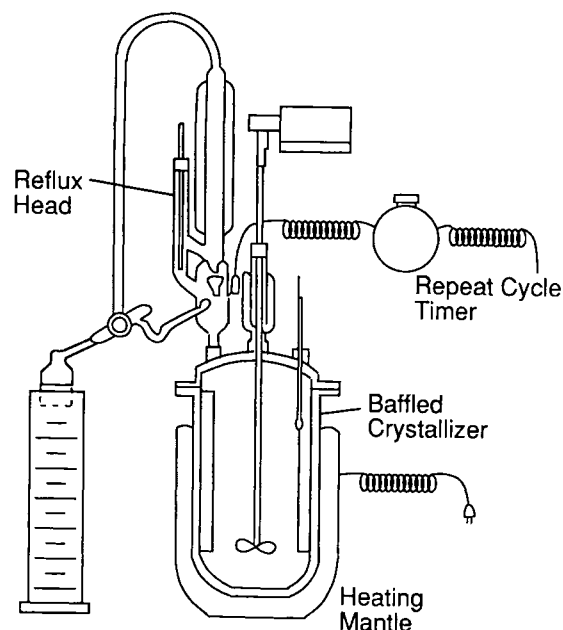


Figure 10.2 Laboratory batch evaporative crystallizer equipment. (Reproduced with permission from Baliga 1970.)

was provided by a heating mantle. Good mixing of the crystallizer volume was maintained by a mixer and a baffle system. Provision was made for sampling during a run so that the CSD could be monitored as it changed with time. During operation, the volume in the crystallizer decreased with time while the suspension density increased.

A batch cooling crystallizer (Figure 10.3) was employed by Mullin and Nývlt (1971) to study the effect of programmed cooling on the CSD of potassium sulfate and ammonium sulfate crystals. The crystallizer was a cylindrical glass vessel (4 or 30 l) with a round bottom provided with a discharge outlet. It was fitted with

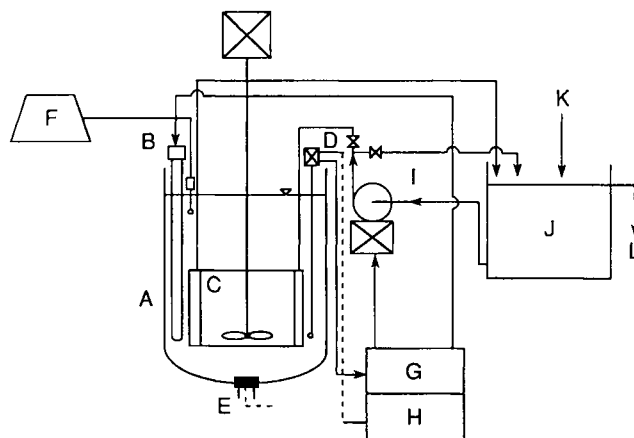


Figure 10.3 Scheme of a laboratory batch cooling crystallizer. A, crystallizer; B, control heater; C, control cooler (jacket forming the agitated draft tube); D, contact thermometer; E, drain plug; F, recorder; G, relay; H, controller; I, cooling water pump; J, cooling water bath; K, water inflow; and L, water outflow. [Reprinted with permission from J.W. Mullin and J. Nývlt (1971), *Chemical Engineering Science*, vol. 26, p. 373, Pergamon Press, Inc.]

an internal cooler, electric heater, propeller stirrer, and contact thermometer. The temperature was controlled by the contact thermometer connected to a relay that switched on either the heater or the cooling water pump. The magnet of the contact thermometer was turned by a motor that received impulses from a controller. The programming of the nonlinear cooling curves was provided by the controller.

A batch fluidized bed crystallizer is frequently used for precise measurements of the crystal growth kinetics (Karpinski 1981). The technique is particularly suitable for systems with the density of crystals exceeding that of the solution by more than 10%, and for seed crystals in the $1 \times 10^{-4} - 1 \times 10^{-3}$ m size range. Most inorganic salts fall into that category. An example of an experimental

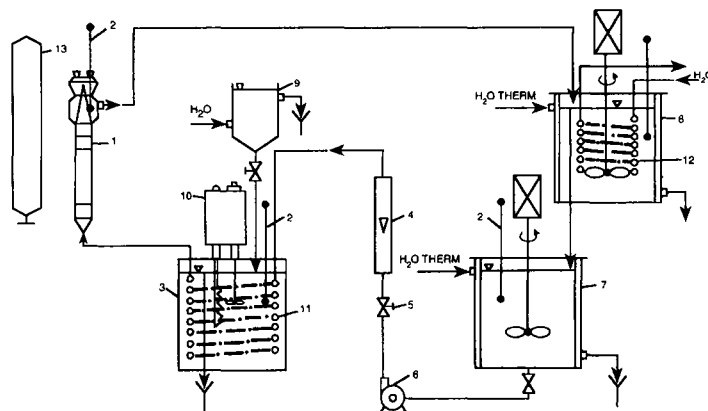


Figure 10.4(a) Experimental setup for investigation of crystal growth and dissolution kinetics in a laboratory-scale batch fluidized bed crystallizer. (1) Crystallizer; (2) Thermometer; (3) Cooling tank; (4) Rotameter; (5) Flow control valve; (6) Feed pump; (7) Feed tank; (8) Dissolution tank; (9) Cooling water head tank; (10) Thermostat; (11) Cooling coil; (12) Heating coil; (13) Heater. (Reproduced by permission of the American Institute of Chemical Engineers © 1985 AIChE from "Effect of Temperature on Crystallization and Dissolution Process in a Fluidized Bed," J. Budz, P.H. Karpinski and Z. Naruc, *AIChE Journal*, vol. 31, no. 2, pp. 259–268 (1985).)

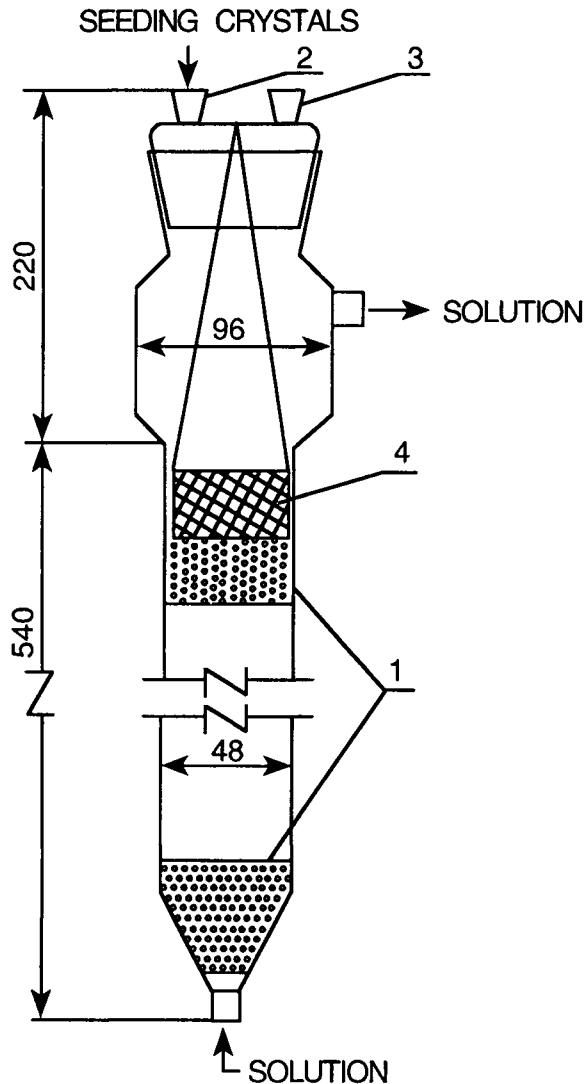


Figure 10.4(b) Fluidized bed crystallizer (dimensions in mm). (1) Packing of glass beads; (2) and (3) Stub pipes; (4) Removable cylindrical basket. (Reproduced by permission of the American Institute of Chemical Engineers © 1984 AIChE from "Influence of Hydrodynamics on Crystal Growth and Dissolution in a Fluidized Bed," Budz, J., Karpinski P.H., and Z. Naruc, *AIChE Journal*, vol. 30, no. 5, pp. 710–717 (1984).)

setup with such a laboratory-scale fluidized bed crystallizer is shown in Figures 10.4a and 10.4b (Budz et al. 1984, 1985). The glass crystallizer with a diameter of 48 mm has two sections of glass bead packing, which flatten the velocity profile. A fluidized bed crystal growing zone is situated just above the upper packing, which is held in place by means of a tight-fit, fine-mesh, removable cylindrical basket. The cross-sectional area of the upper part of the crystallizer is four times larger than that of the growth zone in order to prevent the crystals from escaping from the bed. A known number of pre-weighed, uniformly sized seed crystals are introduced to the top and, after a suitable growth time, discharged from the crystallizer using the removable mesh-basket. Elaborate temperature and flow control systems assure that the growth takes place at a constant solution flow rate and at a precisely maintained constant temperature, which is lower than the saturation temperature of the solute.

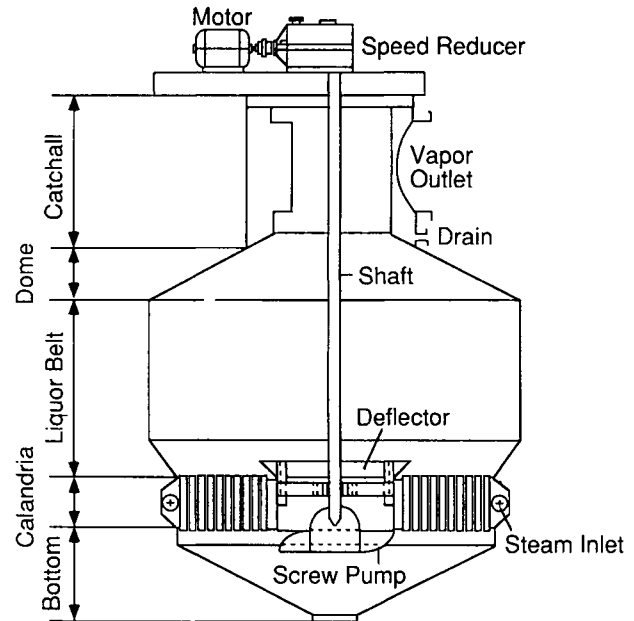


Figure 10.5 Industrial calandria batch evaporative crystallizer. (Reproduced by permission of the American Institute of Chemical Engineers © 1984 AIChE from "Advances in Industrial Crystallization Techniques," Bennett, R.C. *AIChE Symposium Series*, vol. 80, no. 240, pp. 45–54 (1984).)

A semibatch reaction crystallizer with a profiled bottom and/or a draft tube was used by Stavek et al. (1988) to study the influence of hydrodynamic conditions on the controlled double-jet precipitation of silver chloride microcrystals. The crystallizer is a cylindrical vessel (14 cm in diameter) equipped with four radial baffles and a six-pitched-blade impeller to provide good mixing. Silver nitrate and potassium chloride solutions were added at a constant rate to the crystallizer, which contained aqueous gelatin solution. The temperature and silver ion concentration in the crystallizer were controlled during the run.

10.2.2. INDUSTRIAL BATCH CRYSTALLIZERS

Although most of the industrial crystallizers described in the literature (e.g., Bamforth 1965; Bennett 1984; Moyers and Rousseau 1987) are continuous crystallizers, they often can be operated in a batch mode. For capacity requirements less than 500 kg/h, batch crystallization is usually more economically advantageous. Furthermore, if the product requires a relatively narrow CSD, a batch crystallizer clearly has the advantage. Several industrial batch crystallizers are described here.

A calandria batch evaporative crystallizer (Bennett 1984) commonly used from the late 1890s to the present day is shown in Figure 10.5. It has been used frequently for the crystallization of sodium chloride and sugar. The calandria consists of a heat exchanger with a large central downtake to permit natural recirculation up the tubes and down the central downtake. The hydrostatic head required for circulation is developed by boiling within the tubes themselves. The natural circulation in the crystallizer is gentle, and crystal attrition is relatively low. To augment capacity, an extended downcomer is sometimes employed to improve the circulation path within the bottom liquor chamber. Because of the relatively low velocity beneath the bottom tubesheet, the product from such a crystallizer is classified, resulting in a relatively narrow CSD.

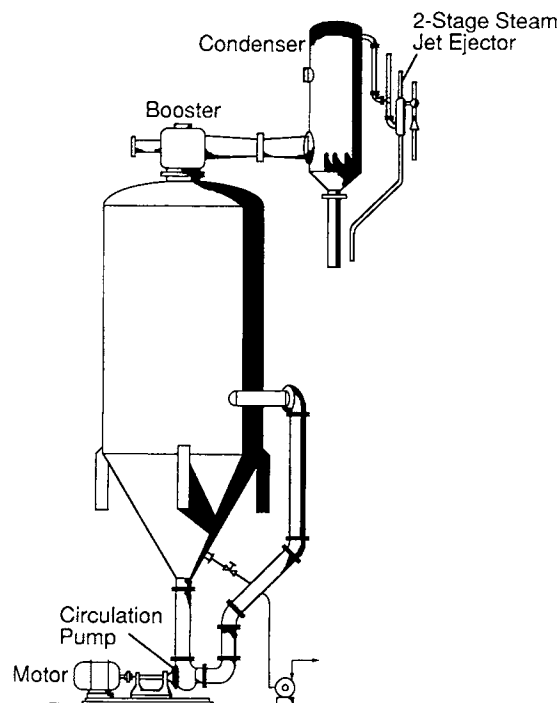


Figure 10.6 Industrial batch vacuum crystallizer with forced circulation. (Reproduced with permission from Bamforth 1965.)

A batch vacuum crystallizer with forced circulation (Bamforth 1965) is illustrated in Figure 10.6. The crystallizer is a simple cylindrical vessel with a conical base fitted with side agitator(s). Agitation provided by the agitator(s) and/or the forced circulation loop is needed to bring all parts of the crystal suspension to the liquid surface periodically. A "booster" is interposed between the crystallizer and condenser to compress the lower temperature vapors to maintain a constant temperature in the condenser. A two-stage steam jet ejector is used to extract noncondensable gases and to maintain the vacuum. This type of crystallizer has been used for many applications throughout the world. A typical application is the recovery of Glauber's salt from spin bath liquor.

A Buflovak draft tube batch crystallizer (Bamforth 1965) is shown in Figure 10.7. It consists of a vertical cylindrical vessel with an internal draft tube baffle. Vapor is boosted by means of a steam jet thermocompressor and delivered to a barometric condenser. The lower part of the crystallizer body is coned and fitted with an underdriven agitator that pushes the solution up the draft tube to the evaporating surface. The circulation induced by the agitator keeps the crystals in suspension and helps to maintain an even temperature distribution throughout the crystal suspension. Some crystal deposition may take place at the liquor surface, but this can be redissolved at each fresh charge. Such a batch draft tube vacuum crystallizer can be applied to a wide range of chemical products, both organic and inorganic.

10.3. BATCH CRYSTALLIZATION ANALYSIS

The analysis of batch crystallization processes is generally more difficult than that of continuous crystallization processes. This is mainly due to the complexity of problems encountered in the batch systems: the mass and surface area of the crystals increase during the run, and the supersaturation varies in a complex way as a function of time. Thus, in the development of a descriptive model, one needs to consider the time-dependent batch conservation

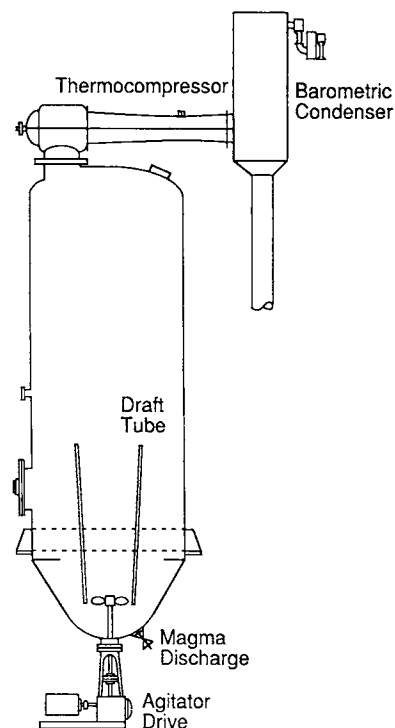


Figure 10.7 Buflovak draft tube batch crystallizer. (Reproduced with permission from Bamforth 1965.)

equations that include the population, mass, and energy balances (Wey and Estrin 1973; Hulbert 1976; Wey 1985; Tavare 1987).

10.3.1. BATCH CONSERVATION EQUATIONS

The population balance, which was put forward by Randolph and Larson (1962) and Hulbert and Katz (1964), serves as the basis for characterizing the CSD in suspension crystallization systems. For a batch crystallizer or a semibatch crystallizer with no net inflow or outflow of crystals, the population balance can be written as (Randolph and Larson 1988)

$$\frac{\partial(nV)}{\partial t} + \frac{\partial(GnV)}{\partial L} = 0 \quad (10.1)$$

where n is the population density per unit suspension volume, V is the total suspension volume, G is the linear growth rate, L is the crystal size, and t is the time. Because the working volume of a batch or semibatch system may vary with time, it is convenient to redefine the population density and other volume-sensitive quantities on the basis of the total operating volume of the crystallizer; thus

$$\tilde{n} = nV \quad (10.2)$$

With this substitution, Eq. (10.1) becomes

$$\frac{\partial \tilde{n}}{\partial t} + \frac{\partial(G\tilde{n})}{\partial L} = 0 \quad (10.3)$$

Equation (10.3) requires a boundary condition and an initial condition. The boundary condition $\tilde{n}(0, t)$ is the nuclei population density (\tilde{n}_0), which can be related to the nucleation rate (\tilde{B}_0) by

$$\tilde{n}(0, t) = \tilde{n}_0(t) = \tilde{B}_0(t)/G(0, t) \quad (10.4)$$

The initial population density $\tilde{n}(L, 0)$ for a batch crystallizer is not well defined. For a crystallizer seeded externally, $\tilde{n}(L, 0)$ may be denoted by an initial seed distribution function $\tilde{n}_s(L)$. However, in an unseeded system, initial nucleation can occur by several mechanisms, and one cannot realistically use a zero initial condition for the size distribution. To overcome this difficulty, Baliga (1970) suggested the use of the size distribution of crystals in suspension at the time of the first appearance of crystals as the initial population density.

In addition to the population balance equation, appropriate kinetic equations are needed for evaluation of the nucleation rate (\tilde{B}_0) and the growth rate (G). Empirical power-law expressions are frequently used to correlate G and \tilde{B}_0 (Randolph and Larson 1988). For the growth rate,

$$G = k_G \Delta c^g \quad (10.5)$$

where Δc is the supersaturation, equal to the difference between the bulk solute concentration (c) and the equilibrium solute concentration (c^*). The growth kinetic order (g) is usually 1–2 (Karpinski 1980, 1981). The growth rate constant (k_G), which may be influenced by temperature and degree of agitation, is a function of size if crystal growth is affected by bulk diffusion or the Gibbs-Thomson effect (Wey and Strong 1977b). The nucleation rate may be represented by

$$\tilde{B}_0 = k_N \Delta c^b m_T^j \quad (10.6)$$

where m_T is the crystal suspension density. The nucleation kinetic order (b) is usually 0.5–2.5 for secondary nucleation and higher for primary nucleation. The exponent of m_T , (j), may be taken as unity if secondary nucleation is the predominant nucleation mechanism. The nucleation rate constant (k_N) is likely to depend on temperature and degree of agitation.

The bulk solute concentration (c) can be determined from the mass balance for batch system (Baliga 1970)

$$\frac{d}{dt}(V - m_T/\rho_c)c + \frac{dm_T}{dt} = 0 \quad (10.7)$$

where ρ_c is the crystal density. In general, the volume occupied by the crystals is much smaller than the volume of the mother liquor ($m_T/\rho_c \ll V$). Under this assumption, Eq. (10.7) reduces to

$$\frac{d(Vc)}{dt} + \frac{dm_T}{dt} = 0 \quad (10.8)$$

The mass balance for a semibatch system would contain an additional term in Eq. (10.8) for solute input. The crystal suspension density (m_T) can be related to \tilde{n} by

$$m_T = \alpha \rho_c \int_0^\infty \tilde{n} L^3 dL \quad (10.9)$$

where α is the crystal volume shape factor.

The equilibrium solute concentration (c^*) is usually influenced by the suspension temperature (T) through the solubility-temperature relationship. In a nonisothermal batch crystallizer (e.g., batch cooling crystallizer or when the heat of crystallization is significant), the suspension temperature may change with time. In this case, an energy balance is needed to determine the suspension temperature (and the associated c^*) as a function of time.

The energy balance can be obtained by applying the first law of thermodynamics to the batch crystallizer. The expression of this energy balance, however, varies according to the specific configuration of the batch crystallization system.

The structure and interrelationship of the batch conservation equations (population, mass, and energy balances) and the nucleation and growth kinetic equations are illustrated in an information flow diagram shown in Figure 10.8. To determine the CSD in a batch crystallizer, all of the above equations must be solved simultaneously. The batch conservation equations are difficult to solve even numerically. The population balance, Eq. (10.3), is a nonlinear first-order partial differential equation, and the nucleation and growth kinetic expressions are included in Eq. (10.3) as well as in the boundary conditions. One solution method involves the introduction of moments of the CSD as defined by

$$m_i = \int_0^\infty \tilde{n} L^i dL; \quad i = 0, 1, 2, 3 \quad (10.10)$$

The population balance can be multiplied through by L^i and integrated to yield equations in terms of moments (m_i) of \tilde{n}

$$\frac{dm_i}{dt} + \int_0^\infty L^i \frac{\partial}{\partial L} (G \tilde{n}) dL = 0 \quad (10.11)$$

For size-independent growth [i.e., $k_G \neq k_G(L)$], Eq. (10.11) can be simplified to the following moment equations

$$\frac{dm_0}{dt} = \tilde{n} G = \tilde{B}_0 \quad (10.12)$$

$$\frac{dm_1}{dt} = m_0 G \quad (10.13)$$

$$\frac{dm_2}{dt} = 2m_1 G \quad (10.14)$$

$$\frac{dm_3}{dt} = 3m_2 G \quad (10.15)$$

The mass balance, Eq. (10.8), can also be expressed in terms of m_3

$$\frac{d(Vc)}{dt} + \alpha \rho_c \frac{dm_3}{dt} = 0 \quad (10.16)$$

The initial conditions of the moment equations are derived directly from the initial population density $\tilde{n}(L, 0)$. Equations (10.12) through (10.16), together with the nucleation and growth kinetic expressions [Eqs. (10.5) and (10.6)], can be solved numerically to give the moments of the CSD for a batch or semibatch system as a function of time. The CSD can be reconstructed from its moments by the methods described by Hulbert and Katz (1964) and Randolph and Larson (1988).

For size-dependent growth [i.e., $k_G = k_G(L)$], the mathematical treatment of Eq. (10.11) becomes more complicated. One solution method, which included the use of moments and an orthogonal polynomial to simulate the population density function, was discussed by Wey (1985). Tavare et al. (1980) developed a

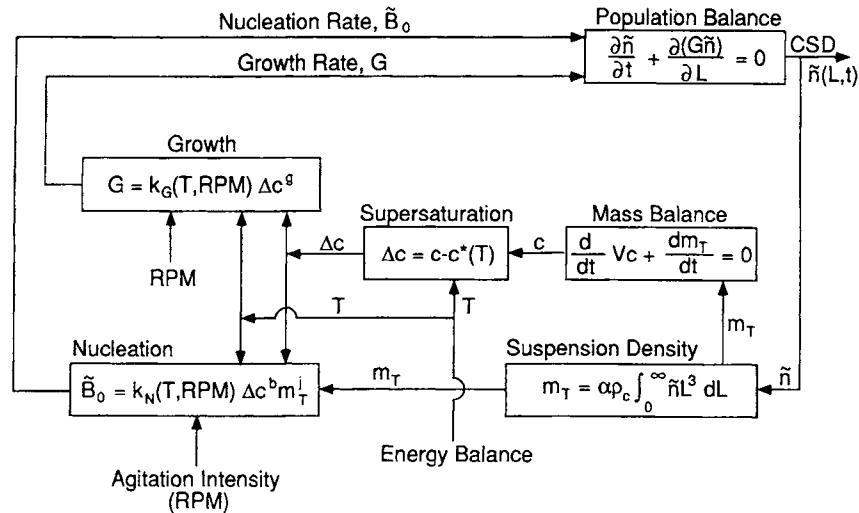


Figure 10.8 Information flow diagram showing interrelationships of batch conservation equations, nucleation and growth kinetic equations, and the resulting CSD in batch suspension crystallizers. (Reproduced by permission of Gordon and Breach Science Publishers S.A. from Wey 1985.)

transformation technique in which the time domain (t) was reduced into the size domain (y) as given by

$$y = \int_0^t G dt \quad (10.17)$$

The population balance, Eq. (10.3), was then expressed in terms of the new variable y and the crystal size, L . Analytical solutions of the population balance equation were obtained for both the size-independent growth and the linear size-dependent growth. This technique was applied to the analyses of CSDs in different types of batch crystallizers (Tavare et al. 1980). Other solution methods for the population balance equation were discussed by Tavare (1987).

As discussed earlier, the analytical solutions for the CSD for a batch or semibatch crystallizer are difficult to obtain unless both the initial condition for the CSD and appropriate kinetic models for nucleation and growth are known. An example of such an analytical solution—simple yet not overly restrictive—was given by Nývlt (1991). It is assumed that the process, in which both external seeding and nucleation take place, occurs at constant supersaturation ($G = \text{constant}$, $\tilde{B}_0 = \text{constant}$) in an ideally mixed crystallizer. An additional assumption of size-independent growth allows one to rewrite the time-dependent moments, Eqs. (10.12)–(10.15), in terms of the physical properties such as the total number (\tilde{N}), length (\tilde{L}), surface area (\tilde{A}), and mass of crystals (\tilde{m}) as follows

$$d\tilde{N}/dt = \tilde{B}_0 \quad (10.18)$$

$$d\tilde{L}/dt = \tilde{N}G \quad (10.19)$$

$$d\tilde{A}/dt = 2\beta\tilde{L}G \quad (10.20)$$

$$d\tilde{m}/dt = 3\alpha\rho_c\tilde{A}G/\beta \quad (10.21)$$

where β is the crystal surface area shape factor. All the above time-dependent physical properties of crystals are defined on the basis of the total operating volume of the crystallizer.

At time $t = 0$, the total number of seeds introduced per unit of the total operating volume of the crystallizer is given as

$$\tilde{N}(0) = \tilde{N}_s \quad (10.22)$$

For most practical batch crystallization processes, the total length, surface area, and mass of seeds are negligible as compared with the corresponding quantities characterizing the final product. Thus

$$\tilde{L}(0) = 0 \quad (10.23)$$

$$\tilde{A}(0) = 0 \quad (10.24)$$

$$\tilde{m}(0) = 0 \quad (10.25)$$

Integrating the moment equations Eqs. (10.18)–(10.21) with the initial conditions Eqs. (10.22)–(10.25) from $t = 0$ to t , gives

$$\tilde{m} = \alpha\rho_c G^3 (\tilde{B}_0 t^4/4 + \tilde{N}_s t^3) \quad (10.26)$$

The total suspension density in the batch crystallizer increases rapidly with time according to the biquadratic function, Eq. (10.26). This equation is applicable to cooling crystallization or evaporative crystallization, and illustrates a generalization of more restrictive approaches employed to derive cooling and evaporation profiles in sections 10.5.1. and 10.5.2.

10.3.2. CSD ANALYSIS AND KINETIC STUDIES

Several experimental techniques and data analysis methods can be employed to study the nucleation/growth kinetics and CSD in batch crystallizers.

Thermal Response Technique. Thermal response is a convenient method for studying a crystallization process in which the heat of crystallization is significant enough to cause a temperature change following the onset of nucleation. Omran and King

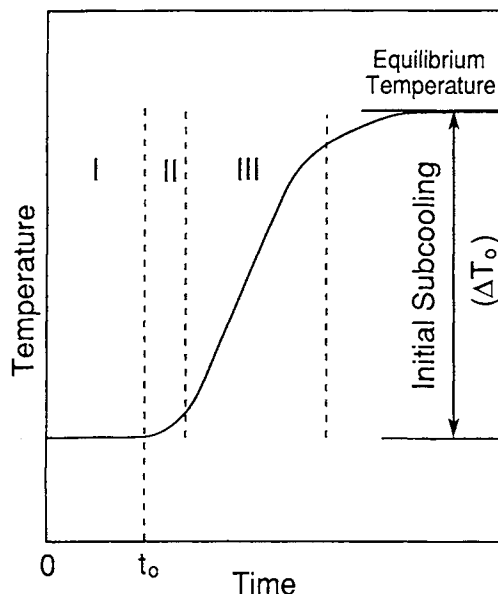


Figure 10.9 Temperature-time response curve. (Reproduced by permission of Gordon and Breach Science Publishers S.A. from Omran and King 1974.)

(1974) applied the thermal response technique to follow ice crystallization in a batch cooling crystallizer in which solution subcooling was closely controlled. Figure 10.9 shows a typical temperature-time curve for an experimental run in which the solution subcooling is held constant before crystallization is started. After the introduction of a seed crystal at $t = 0$, the temperature of the solution remained constant for a period of time until $t = t_0$. During this period some nuclei became visible and others were being formed in the solution. This was followed by a rise in the temperature of the solution (end of Stage I). After the early rise (Stage II), the temperature rises in a monotonic fashion (Stage III) until the equilibrium temperature of the solution is reached.

Omran and King (1974) considered mass and energy balances for this system and derived an equation to relate the change of subcooling in the crystallizer to the nucleation and growth kinetics. For a specified, small temperature change at the end of Stage I, the nucleation kinetic order (b) can be determined from the slope of a logarithmic plot of t_0 versus initial subcooling (ΔT_0). For the crystallization of ice from sugar solutions, the values of b were about 1.25 and independent of the sugar concentration (Omran and King 1974). Stocking and King (1976) improved the experimental technique by using quartz thermometry to achieve the high-resolution measurement of initial thermal response. Kane et al. (1974) also used the thermal response method to determine the crystallization kinetics of ice crystals from saline, emphasizing a later portion of the response curve.

Desupersaturation Curve Technique. Two different modes of experiment under the condition of negligible solute consumption by nucleation have often been used to determine crystal growth kinetics. In the differential mode, a small quantity of crystals with relatively uniform size is allowed to grow for a given period of time. In this type of operation, the change in solution supersaturation is relatively small and the crystals grow at essentially constant supersaturation. Direct measurement of the changes in crystal weight enables the determination of the overall growth rate. In the integral mode, however, a relatively large seed loading of closely sized crystals is charged to the crystallizer. The growth

process consumes appreciable solute, thus resulting in a decay in supersaturation during the experiment. In this case, the growth rate is a time-varying quantity so that the analysis of the growth kinetics is somewhat complicated.

Garside et al. (1982) developed an elegant technique to evaluate crystal growth kinetics from an integral mode of batch experiments. For size-independent growth, the crystal mass deposition rate (R_G) can be given by

$$R_G = k_G \rho_c \Delta c^g \quad (10.27)$$

The kinetic parameters (k_G and g) in Eq. (10.27) can be related to the mean size (\bar{L}) and total surface area (A_T) of the seed crystals and zero-time values of the supersaturation (Δc_0) and its time derivatives (Δc_{01} and Δc_{02})

$$g = \frac{2\beta\Delta c_0}{3\alpha\rho_c\bar{L}A_T} + \frac{\Delta c_0\Delta c_{02}}{(\Delta c_{01})^2} \quad (10.28)$$

$$k_G = -\frac{\Delta c_{01}}{\rho_c A_T (\Delta c_0)^g} \quad (10.29)$$

If the initial portion of a measured desupersaturation curve is approximated by a second-order polynomial

$$\Delta c(t) = a_0 + a_1 t + a_2 t^2 \quad (10.30)$$

then the zero-time derivatives are given by

$$\Delta c_0 = a_0, \quad \Delta c_{01} = a_1, \quad \Delta c_{02} = 2a_2 \quad (10.31)$$

Garside et al. (1982) used the above technique to study the growth kinetics of potassium sulfate crystals in a seeded batch crystallizer. The first few Δc values of the experimental desupersaturation curve were fitted to the second-order polynomial [Eq. (10.30)], from which the values of Δc_0 , Δc_{01} , and Δc_{02} were determined according to Eq. (10.31). The values of the growth kinetic parameters g and k_G were then calculated from Eqs. (10.28) and (10.29), respectively. Tavare (1985) extended the above technique to the growth kinetic study of ammonium sulfate crystals in a batch cooling crystallizer. The initial derivatives of supersaturation and temperature profiles obtained in a series of integral batch experiments were used to directly evaluate the kinetic parameters in crystal growth correlations.

Cumulative CSD Method. Misra and White (1971) used a cumulative CSD method to study the crystallization kinetics of aluminum trihydroxide from a seeded batch crystallizer. The population balance equation corresponding to Eq. (10.3) can be written as

$$\frac{\partial(NF)}{\partial t} + NG \frac{\partial F}{\partial L} = 0 \quad (10.32)$$

where N is the total number of crystals and F is the cumulative size distribution on a crystal number basis. The growth rate (G) represents the rate of change of crystal size at a constant value of F and is given by

$$G = \left(\frac{\partial L}{\partial t} \right)_F \approx \left(\frac{\Delta L}{\Delta t} \right)_F \quad (10.33)$$

The sizing methods for the cumulative CSDs are unfortunately limited to a minimum crystal size below which accurate counts

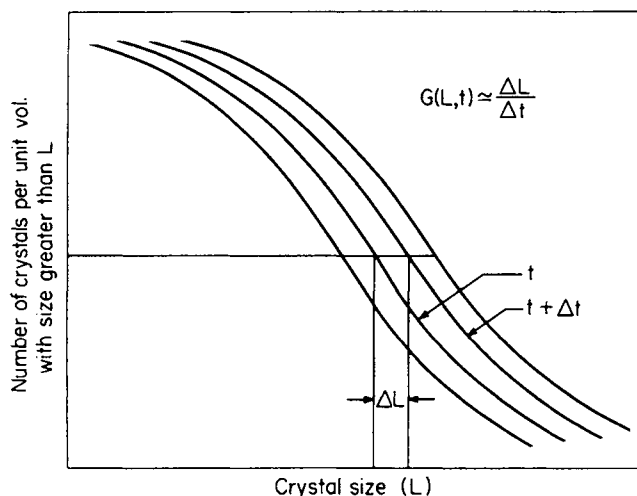


Figure 10.10 Determination of growth rate from cumulative size distributions. (Reproduced by permission of Gordon and Breach Science Publishers S.A. from Misra and White 1971.)

cannot be made. Thus, the total number of crystals (N) and the number of crystals smaller than a particular size (NF) are unknown. However, the experimental data can give $N(1-F)$, the number of crystals with size greater than any prescribed size L . Since a constant value of F corresponds to a constant value of $N(1-F)$ for the chosen conditions, the concept given by Eq. (10.33) is still valid and is illustrated in Figure 10.10. Misra and White (1971) obtained substantially parallel cumulative size distributions of aluminum trihydroxide from caustic aluminate solutions. Their results suggest a size-independent growth behavior because the smaller crystals increased in size by the same amount as the larger ones. Garside and Jančić (1976) applied the same method to study the growth and dissolution of potash alum crystals in the subsieve size range and obtained a strongly size-dependent behavior.

Misra and White (1971) also developed a procedure to determine the nucleation rate based on the cumulative size distribution data.

Characterization of CSD Maximum. The changes in the magnitude and location of the CSD maximum with time are useful in revealing the growth mechanism involved in batch crystallization and can be given by (Wey and Estrin 1973)

$$\frac{d\bar{n}}{dt} = -\left(\bar{n} \frac{\partial G}{\partial L}\right)_{L_p} \quad (10.34)$$

$$\frac{dL_p}{dt} = (G)_{L_p} + \left(\bar{n} \frac{\partial^2 G / \partial L^2}{\partial^2 \bar{n} / \partial L^2}\right)_{L_p} \quad (10.35)$$

where L_p is the size at which the peak is located. Equation (10.34) reveals how the magnitude of \bar{n} at L_p changes with time. For size-independent growth, the peak will remain unchanged in value. For size-dependent growth, the magnitude of the peak will increase with time if $\partial G / \partial L < 0$ and decrease with time if $\partial G / \partial L > 0$. (The same is true for the minimum of the distribution.) Thus, if one can follow the values of the CSD maximum (or minimum) during a batch crystallization experiment, growth characteristics of the crystals may be inferred. Figure 10.11 shows some short-time CSD data obtained from a Couette-flow batch crystallizer for the

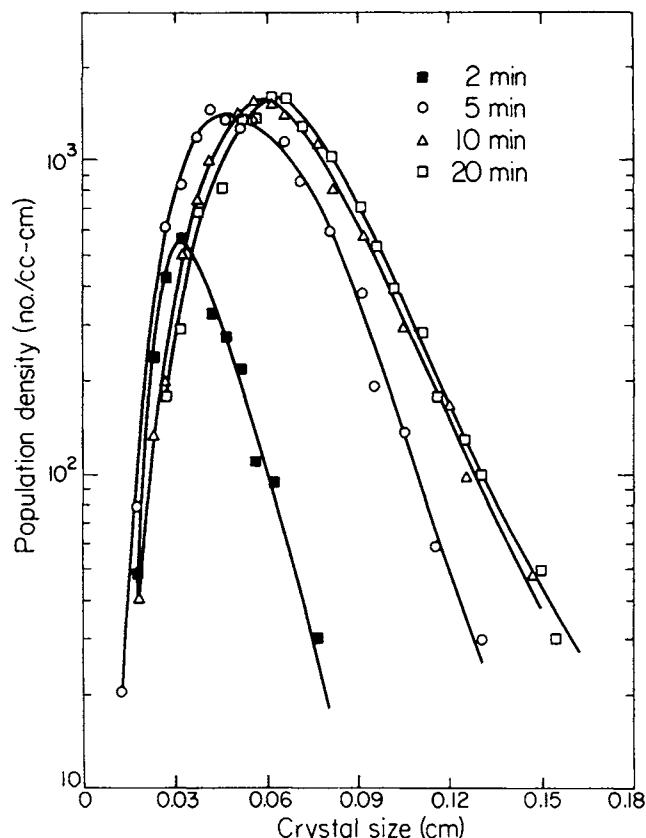


Figure 10.11 Short-time CSD data obtained from a batch crystallizer for the ice-brine system. (Reproduced by permission of Gordon and Breach Science Publishers S.A. from Wey and Estrin 1974.)

ice-brine system (Wey and Estrin 1973, 1974). The experimental data qualitatively show that $d\bar{n}/dt > 0$ for $L_p < 0.06$ cm and $d\bar{n}/dt \approx 0$ for $L_p > 0.06$ cm. The results suggest that $\partial G / \partial L < 0$ for $L_p < 0.06$ cm and $\partial G / \partial L \approx 0$ for $L_p > 0.06$ cm. This growth behavior is qualitatively consistent with a size-dependent growth model based on a heat and mass diffusion mechanism (Wey and Estrin 1973).

Equation (10.35) reveals how the location of the peak changes with time. For size-independent growth the peak remains distinct and moves toward larger sizes at a velocity equal to G . For the growth function of ice crystals, the second term on the right is negative and the minimum moves to the right more rapidly than the maximum. This may be demonstrated by the skewness of the CSD data shown in Figure 10.11.

10.4. FACTORS AFFECTING BATCH CRYSTALLIZATION

The quality, productivity, and batch-to-batch consistency of the final crystal product can be affected by the conditions of the batch crystallizer. Several factors considered here include batch cycle time, supersaturation profile, external seeding, fouling control, CSD control, growth rate dispersions, and mixing.

10.4.1. BATCH CYCLE TIME

In the operation of a batch crystallizer, several steps need to be performed in succession to complete a batch cycle (Nývlt 1978).

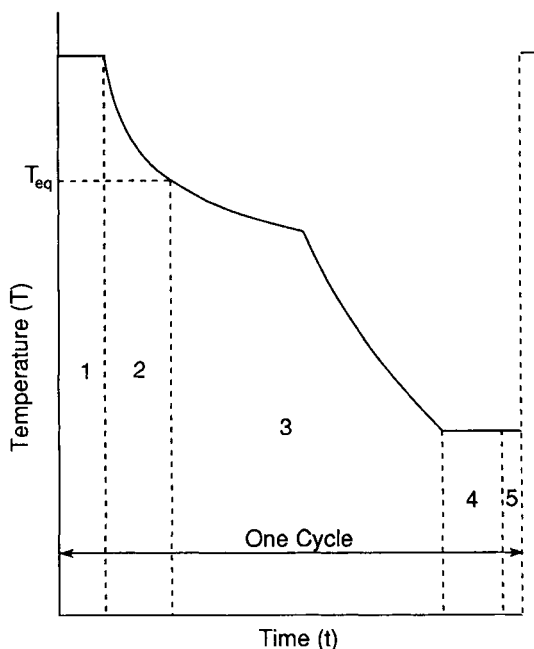


Figure 10.12 Schematic description of a batch cycle. (Reprinted by permission of VCH Publishers, Inc., 220 East 23rd St., New York, NY 10010, from Figure 8, p. 41, J. Nývlt, *Industrial Crystallization*, 1978.)

For a cooling crystallizer, the various periods of a batch cycle are shown in a plot of temperature versus time (Figure 10.12). These periods include: (1) filling the crystallizer; (2) cooling to saturation temperature (T^*); (3) crystallization period; (4) removing the suspension; and (5) cleaning the crystallizer.

The time needed to complete a period is determined by the attainable rate of the rate-limiting process associated with each period. For example, the time needed for Period 2 is determined by the attainable heat transfer rate for cooling. In Period 3, however, the heat transfer rate may need to be restricted in order to control the nucleation and growth rates or to minimize fouling of the cooling surfaces. The time required for Period 4 may be determined by the capacity of the filter if filtration is needed during the transfer of the crystallizer suspension to a storage vessel. The required total batch cycle time can be calculated if all times required to complete the individual periods are known. Since the size of the crystallizer may affect the duration of all the stages of a batch cycle, the batch cycle time is expected to be a function of the crystallizer volume. Thus, the batch cycle time information can be used to determine the crystallizer volume required for meeting a production rate specification.

10.4.2. SUPERSATURATION PROFILE

The supersaturation profile in a batch crystallizer has a profound effect on the nucleation and growth processes and the resulting CSD. It can also affect other factors (e.g., batch cycle time) related to the batch crystallization operation. Figure 10.13 shows schematically a supersaturation profile in a batch crystallization experiment (Nývlt et al. 1985). At $t = 0$, the batch crystallizer is filled with a just-saturated solution that contains crystals with a negligible surface area. The solution begins to be supersaturated at a constant rate, and the supersaturation increases until it reaches the limit of the metastable zone (Δc_{max}). At this point, nucleation

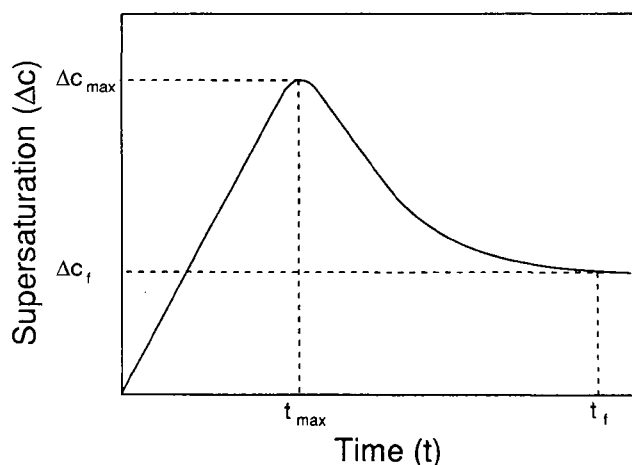


Figure 10.13 Schematic supersaturation profile in a batch crystallization experiment. (Reproduced with permission from Nývlt et al. 1985.)

starts and crystals with a certain surface area begin to form. The increase in total crystal surface area due to nucleation and crystal growth would remove more and more of this supersaturation until, at the end of the batch ($t = t_f$), the supersaturation decreases to value Δc_f .

The supersaturation profile shown in Figure 10.13 represents a special case in which the supersaturation is increased at a constant rate. In practice, the supersaturation profile in a batch crystallizer may deviate from this profile. For example, if a constant cooling rate is imposed throughout the batch cooling crystallization operation, significantly high supersaturation will be generated at the beginning of the run, and very low supersaturation will be generated near the end of the run. As a consequence, excessive nucleation will occur at the beginning and low growth rates will be obtained near the end. Both results will contribute to the production of smaller crystals and lengthen the batch cycle time required to achieve the desired crystal size.

Significant improvement in CSD and operation can be achieved by controlling the supersaturation levels during the batch crystallization process. Mullin and Nývlt (1971) and Larson and Garside (1973) showed how programmed cooling or programmed evaporation could be designed so that the optimum rate of supersaturation generation could be achieved at all stages of the batch run. Their results demonstrated that supersaturation control during a batch run was beneficial for increasing crystal size and reducing the batch cycle time. Jones and Mullin (1974) showed that programmed cooling also markedly narrowed the CSD obtained from batch potassium sulfate crystallization. Programmed cooling will be addressed further in section 10.5.1.

10.4.3. EXTERNAL SEEDING

One of the main challenges in batch crystallization is to control the supersaturation and nucleation during the initial stage of the batch run. During this period, very little crystal suspension is present on which solute can crystallize, so that high supersaturation and excessive nucleation often occur. Another difficulty associated with batch crystallization is the determination of the initial condition for the population density function. In an unseeded batch crystallizer, initial nucleation can occur by several mechanisms and usually occurs as an initial shower followed by a reduced nucleation rate. Thus, an initial size distribution exists and one

cannot realistically use the zero initial condition for the size distribution.

One method for overcoming the above mentioned difficulties is the use of external seeds so that initial nucleation can be controlled or minimized. Most crystallization systems exhibit a metastable supersaturation zone where crystal growth continues but the supersaturation is too low for nucleation to take place. Thus, if the supersaturation can be maintained below the metastable zone upper limit after seeding, then only growth on the seed crystals will occur. In this case, the initial condition for the population density will be the initial seed distribution.

The external seeding technique can also be used to determine the maximum allowable growth rate without nucleation at the limit of the metastable zone. Larson and Garside (1973) suggested an experimental technique to determine this maximum growth rate for the low-yield (Class I) crystallization system in which the supersaturation can be measured. Seed crystals, which are closely sized between two adjacent sieve sizes, are placed in a supersaturated solution of known concentration and allowed to grow until they have about doubled in weight. The final solution concentration is measured and the crystal product is dried. From the final mass of crystals (m_f), the growth rate (G) can be calculated from the following equation

$$G = \frac{L_s}{t_f} [(m_f/m_s)^{1/3} - 1] \quad (10.36)$$

where L_s and m_s are the size and mass of the seed crystals, respectively. Results at different supersaturations may be correlated by the growth kinetic equation [Eq. (10.5)]. As the supersaturation is increased, the point at which nucleation just begins to occur is noted. This corresponds to the maximum metastable supersaturation (or the maximum growth rate) allowable without nucleation in the crystallizer. This technique will serve to give a maximum allowable growth rate that is accurate to within about 50%.

For the high-yield (Class II) crystallization system where the supersaturation generally cannot be measured accurately, determination of the maximum metastable supersaturation and the corresponding maximum growth rate becomes more difficult. Wey and Strong (1977a) presented an experimental technique, which involved external seeding, to examine the maximum growth rate of AgBr crystals (Class II system). Their approach involves a balanced double-jet precipitation in which aqueous silver nitrate and sodium bromide solutions are added simultaneously to an agitated aqueous gelatin solution. For each experiment, the reaction vessel is charged initially with monodisperse AgBr seed crystals. When the number of seed crystals is decreased or the reactant addition rate is increased from one experiment to the next, nucleation eventually occurs at the point where solution reaches the maximum metastable supersaturation. The corresponding maximum growth rate is determined from a simple mass balance for the Class II system. Wey and Strong (1977a) followed this approach for each of five different monodisperse AgBr seed sizes ranging from 0.047 to 0.64 micrometers. The temperature and bromide ion concentration in suspension were maintained constant for all the experiments. Since the maximum growth rates of different seed sizes were obtained at the same maximum metastable supersaturation condition, the effect of supersaturation can be eliminated from the correlation between growth rate and crystal size. Furthermore, the maximum metastable supersaturation can be estimated when comparing the experimental results with growth models. The maximum growth rate of AgBr crystals obtained from this study shows a strong size-dependent behavior that can be explained by a growth model based on bulk diffusion and surface integration

mechanisms. The supersaturation ratio (c/c^*) at this maximum metastable condition was estimated to be about 1.5.

As mentioned before, in an ideal case, the supersaturation level during the externally seeded batch growth process stays below the critical (maximum) supersaturation so that the number of uniformly sized seeds introduced at the onset of the batch crystallization remains unchanged throughout the growth. As a result, a fines-free product of uniform size can be obtained.

Aside from special cases (e.g., high-value product), the preparation of the uniformly sized seeds is considered to be non-economical and troublesome. Therefore, a common industrial practice is the use of a narrowly sized fraction of the seeds, usually taken from the fines fraction of the product from the preceding batches. Typically, no particular attention is paid to assure that no primary nucleation (renucleation) occurs during the course of the seeded process. The equipment employed is either not capable or not set to maintain a desirable constant, subcritical supersaturation throughout the run. Nonetheless, it has been a common belief that even bad seeding is better than no seeding at all for it allows one to harness a massive spontaneous nucleation in the initial part of the run and to prevent excessive supersaturation excursions along the course of the batch crystallization process. The benefits of external seeding are less dramatic for solutions with a narrow width of the metastable zone and for those crystalline materials that are prone to secondary nucleation.

The most frequently studied effect for externally seeded batch crystallization is that of the number or amount of seeds and its effect on the CSD. In theory, the number of seeds introduced into a well-mixed and well-controlled batch crystallizer should be equal to that of the product. In practice, inadequate seeds population, nonuniform mixing, and excessive cooling or evaporation rates may contribute to the occurrence of spontaneous nucleation in spite of the presence of seeds. Furthermore, unavoidable secondary nucleation may be an additional—and often rather significant—source of nuclei. As a result, only a part of the product crystals originates from the seeds. Nevertheless, the benefits of seeding for subsiding the primary nucleation and for coarsening of the mean product size are apparent. Figure 10.14 shows an example of computer simulations investigating the influence of the number of seeds on the course of the primary nucleation rate during batch crystallization (Bohlin and Rasmuson 1992a). As expected, the nucleation rate decreased very significantly with a

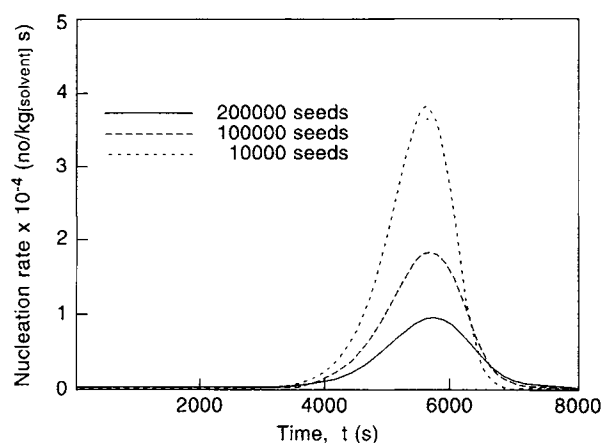


Figure 10.14 Effect of the number of seeds on primary nucleation rate in a controlled cooling batch crystallization. Computer simulation results for citric acid, as reported by Bohlin and Rasmuson (1992a).

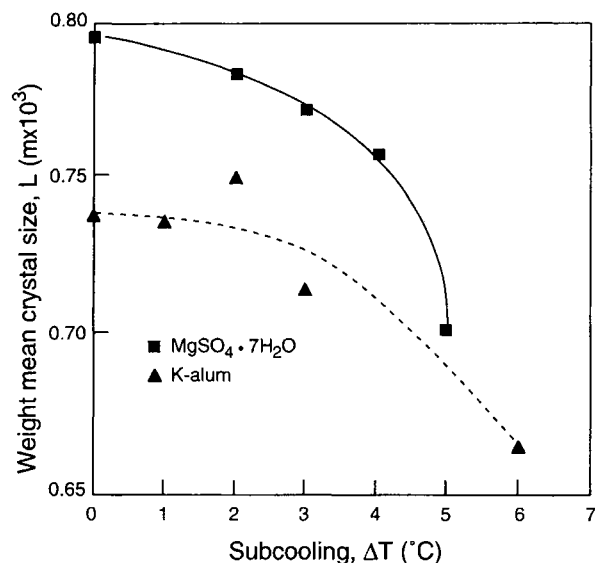


Figure 10.15 Effect of “point of seeding” within the metastable zone on the weight mean size of product crystals, as reported by Karpinski et al. (1980a). Mean seed size $L_s = 0.4075$ mm, linear cooling rate = 7.5 K/h. The saturation temperature and maximum subcooling were: $T^* = 298$ K and $\Delta T_{max} = 6$ K, for $\text{MgSO}_4 \cdot 7\text{H}_2\text{O}$; and $T^* = 293$ K and $\Delta T_{max} = 7$ K, for K-alum.

larger number of seeds introduced. In experimental studies, the amount of seeds ranging from a fraction of 1.0 wt% to 10 wt% of the theoretical yield (e.g., Karpinski et al. 1980a; Johnson et al. 1997) have successfully been used in order to improve the CSD of the product crystals over an unseeded batch crystallization.

It is generally recommended that the seeding should take place at the moment when the initially undersaturated solution is brought to the saturation condition (i.e., when the solubility concentration is achieved). An excessive buildup of supersaturation prior to the seeding should be avoided because it may lead to either spontaneous or seeds-induced nucleation, which would undermine the benefits of seeding. Karpinski et al. (1980a) investigated the effect of the “point of seeding” within the subcooling metastable zone on the CSD in cooling crystallization. Two inorganic salts with a wide width of the metastable zone: $\text{MgSO}_4 \cdot 7\text{H}_2\text{O}$ and K-alum were studied. Figure 10.15 shows the effect of the point of seeding—measured by the subcooling below the supersaturation temperature, ΔT —on the average size of the product. The authors concluded, that seeding at any point up to 40% of the maximum subcooling metastable zone width, ΔT_{max} , had little effect on the product size. However, progressively more and more fines were observed in the product as a result of “late” seeding points, at the temperatures corresponding to the subcooling within the range 40–100% ΔT_{max} .

10.4.4. FOULING CONTROL

One of the major operational problems in batch (or continuous) crystallization is the fouling (or incrustation) of crystals on the heat transfer surfaces. This is because the supersaturation is normally highest near these surfaces. Once the deposition of crystals takes place on these surfaces, the accumulation of crystal deposits can increase rapidly, resulting in a severe fouling problem of the heat transfer equipment. To minimize this fouling problem, one needs to maintain sufficient agitation and a low-temperature gradient on the heat transfer surface. For batch crystallization, the

external seeding technique mentioned earlier can also be used to suppress nucleation and fouling during the initial period of the batch run (Randolph and Larson 1988).

Other techniques may be used to reduce the fouling problem. For example, dual cooling elements may be operated alternately in a batch cooling crystallizer (Bamforth 1965). When fouling of the first cooling element occurs, the cooling fluid is then directed to the second cooling element, while the first is heated to remove the fouling deposits. Later, fouling may occur on the second cooling element and the cycle is repeated. Also, heat transfer equipment with some type of scraper mechanism may be used to prevent excessive buildup of deposits (Bamforth 1965). In addition, fouling can be completely eliminated by using a direct-contact refrigeration technique. In this case, the refrigerant is directly mixed with the crystal suspension where it absorbs heat and is vaporized. Refrigerant vapor leaves the surface of the crystallizer and is compressed, condensed, and recirculated to the crystallizer. Margolis et al. (1971) successfully used liquid isobutylene as a direct-contact refrigerant to perform ice crystallization from brine solutions.

10.4.5. CSD CONTROL

CSD control in batch crystallization can provide a significant improvement in product quality and features and in downstream processing efficiency and economics. Two important technologies considered here include fines destruction and preparation of narrow CSD.

Fines Destruction. In the operation of industrial crystallizers, one would usually want to avoid the fines (i.e., small crystals) since they may cause difficulties in downstream processing equipment (e.g., filtration) and affect both product quality and process economics. Excessive fines may also require a relatively long batch run time to achieve the desired final size of the product crystals. Karpinski (1981) proposed a controlled dissolution of secondary nuclei in order to improve CSD from fluidized bed crystallizers. Jones et al. (1984) first described the application of fines destruction in batch crystallization of potassium sulfate solutions. Their study demonstrated the experimental feasibility of this technology to dramatically reduce the amount of fines in the final product CSD. Their theoretical predictions, obtained from population balance models, agreed with the experimental results.

Zipp and Randolph (1989) studied the crystallization of pentaerythritol with and without fines removal and dissolution in a batch cooling crystallizer. The fines segregation device used a tube tapered at the top through which fines flow was removed. The maximum fines size removed was determined by Stoke's law of settling by the upward velocity through the tube. Larger crystals settled back into the agitated bulk suspension. Fines were pumped from the crystallizer via the fines segregation device, passed through a coil immersed in a hot water bath, and returned to the crystallizer. Figure 10.16 shows the experimental cumulative number distributions of the initial and final samples obtained with and without fines destruction. The results show that fines destruction causes a decrease in the number of small crystals and an increase in the number of large crystals. Fines destruction also gives a larger average crystal size and a smaller coefficient of variation in CSD. Thus, selective fines destruction is a viable technology for batch-operated crystallizers that could allow significant manipulation of the CSD.

Preparation of Narrow CSD. In batch crystallization, the withdrawal of crystal product is made only at the end of the batch

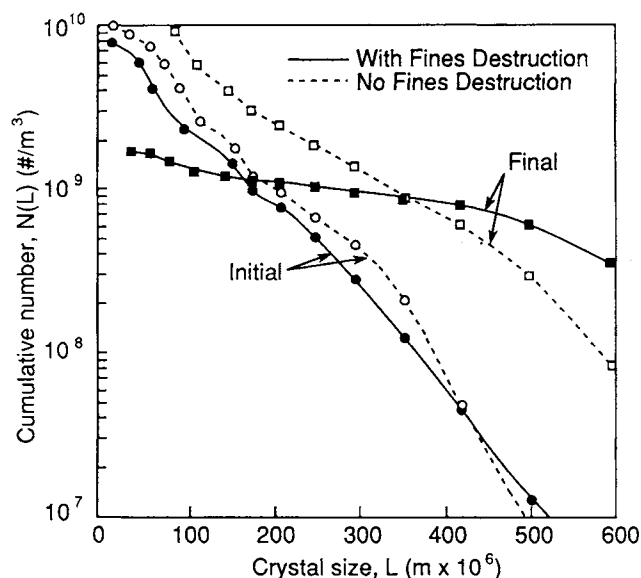


Figure 10.16 Effect of fines destruction on cumulative number distribution in a batch crystallizer. (Reprinted with permission from Zipp G.L., and Randolph A.D. (1989), *Industrial Engineering and Chemical Research*, vol. 28, p. 1447. © 1989 American Chemical Society.)

run so that there is no residence time distribution of individual crystals associated with the product withdrawal. This is different from continuous crystallization, in which the product is continuously withdrawn from the crystallizer and there is a residence time distribution associated with the individual crystals being withdrawn. Thus, batch crystallizers are inherently more capable of making products with a narrow CSD than continuous crystallizers due to this difference in the product withdrawal.

An effective strategy to achieve a narrow CSD in batch crystallization is to separate nucleation and growth. That is, nucleation is controlled so that nuclei are generated only at the very early stage of the batch run. After the initial nucleation, the supersaturation is maintained within the metastable zone where the growth of these nuclei will take place without the formation of additional nuclei. A population-balance analysis may be used to derive cooling or evaporation programs to accomplish this (Randolph and Larson 1988). The external seeding technique mentioned earlier can also be used to control or eliminate the initial nucleation step. For some batch crystallization systems, some fines may still be formed due to nucleation occurring even at low levels of supersaturation. In this case, the above fines destruction technique can be used to help achieve a narrow CSD.

The strategy of separating nucleation and growth was successfully applied to the preparation of monodisperse AgBr crystals by a double-jet precipitation technique (i.e., a semibatch system) as discussed by Leubner et al. (1980). In the double-jet technique in which silver and halide ion solutions are simultaneously added to an agitated aqueous gelatin solution, observable nucleation occurs only at the very early stage of precipitation (within 1 min). The number of stable nuclei quickly reaches a constant value, and further addition of reactants causes only growth of these stable nuclei. Thus, relatively monodisperse AgBr crystals can be obtained by this method. Sugimoto (1987) gave a comprehensive review on the requirements and general conditions for obtaining monodisperse particles from many typical colloidal systems.

10.4.6. GROWTH RATE DISPERSIONS

The phenomenon of growth rate dispersion (GRD) refers to the fact that individual crystals in suspension, even having the same size and subjected to identical growth conditions, may grow at different rates. The usual consequence of GRD in batch crystallization is widening of the CSD as the process progresses. This is mainly due to the accumulation of small slow-growing crystals, which may account for as much as 85–90% of the total number of product crystals in the case of highly soluble materials (Randolph and Larson 1988).

By analogy to the one-dimensional axial dispersion plug flow model, Randolph and White (1977) proposed the random fluctuation (RF) model, in which growth rate fluctuations were represented by the growth rate diffusivity, D_G , which interacts with the average linear growth rate G as follows

$$\frac{\partial n}{\partial t} + G \frac{\partial n}{\partial L} = D_G \frac{\partial^2 n}{\partial L^2} \quad (10.37)$$

Tavare and Garside (1982) used the solution of the above equation to derive its parameters in terms of the differences in initial and final mean size, $\Delta L = L_f - L_0$, and variance, $\Delta \sigma_L^2$

$$G = \Delta L / t_f \quad (10.38)$$

$$D_G = \frac{\Delta \sigma_L^2}{2t_f} \quad (10.39)$$

The RF model was found applicable to sugar and Al_2O_3 systems (Randolph and White 1977) and some slow-growing systems (Garside 1985).

Another concept of GRD, a constant crystal growth (CCG) model, was introduced by Ramanarayanan et al. (1985). They assumed that individual crystals have inherent, constant growth rates, but different crystals have different inherent growth rates. The CCG model was found applicable to the citric acid monohydrate system and to a number of systems for periods of a few hours (Garside 1985; Shiau and Berglund 1990). A detailed treatment of the available experimental data based on the CCG model that accounts for primary and secondary nucleation and unseeded and seeded processes was given by Bohlin and Rasmussen (1992b). They concluded that even moderate growth rate dispersions can significantly influence CSDs in a batch cooling crystallization.

Zumstein and Rousseau (1987) introduced a dual-mechanism model and demonstrated that both RF and CCG mechanisms may be present during batch crystallization and can contribute to the increase in variance of the CSD during growth.

According to Lacmann et al. (1996), the growth rate of each individual crystal may be a consequence of the following factors: the amount of the lattice strain, the macro- and microsurface structure of the growing crystal surface, the adsorption of foreign ionic and molecular species, and the stress introduced by the incorporation of foreign molecules.

In order to account for GRD, the population balance needs to be modified, and its solution becomes a very difficult task, in particular for batch crystallization. Recently, Butler et al. (1997) concluded that because different batches of seeds of the same material have different growth rates, it is impossible to assign a "growth rate dispersion" property for a given material. Instead, they advocated a common history (CH) seed concept. As the name suggests, CH seed comprises crystals of a common history. Furthermore, CH seed has the following properties

1. the size of the crystals is directly related to the growth rate and the time of growth,
2. the CSD reflects the distribution of growth rates inherent in the crystals.

For such characterized CH seed, the authors were able to obtain a simple solution to the batch crystallization population balance, and offered a relatively simple technique to model the behavior of a batch crystallizer.

10.4.7. MIXING

Mixing is an important factor affecting batch crystallization. On one hand, sufficient mixing is required to maintain crystals in suspension, to assure an adequate rate of energy transfer, and to achieve uniformity of suspension properties throughout the crystallizer. On the other hand, the effect of mixing on batch crystallization is largely system-dependent.

In a somewhat idealized case, when crystals do not agglomerate and are not prone to contact secondary nucleation, the use of the general diffusion mass transfer correlation of the form

$$Sh = 0.29 Re^{0.6} Sc^{0.33} \quad (10.40)$$

has been proposed (Karpinski and Koch 1979). In the above correlation, the applicable definitions of the dimensionless groups are as follows

$$Sh = \frac{k_d L}{\rho_{sol} D} \quad (10.41)$$

the Sherwood number

$$Sc = \frac{\mu}{\rho_{sol} D} \quad (10.42)$$

the Schmidt number

$$Re = \frac{L^{4/3} \rho_{sol} E_m^{1/3}}{\mu} \quad (10.43)$$

the particle Reynolds number for stirred vessels, and

$$Re = \frac{u L \rho_{sol}}{\varepsilon \mu} \quad (10.44)$$

the particle Reynolds number for a fluidized bed.

The problem becomes complicated and essentially escapes a rigorous theoretical description when the crystals in a stirred suspension are susceptible to secondary nucleation or grow via an agglomeration mechanism. In order to suppress the formation of contact secondary nuclei, the impeller may be covered with a plastic coating, and its speed reduced to the lowest acceptable level. Sometimes a fines destruction loop is the only possibility in order to control an excessive secondary nucleation (Karpinski 1981).

Figure 10.17a compares experimental R_G versus Δc data for the growth of potassium hydrogen tartrate (KHT) occurring in a fluidized bed and in a stirred vessel (Ratsimba and Laguerie 1991). Because the mixing intensity of the fluidized bed is relatively low as limited by the maximum upward solution velocity, the growth rates are much slower than those occurring in the stirred vessel. The mixing intensity for the stirred vessel experiments was suffi-

ciently high so that the diffusional resistance—significant in the case of the fluidized bed—was no longer important. An example for the case of the crystal growth occurring via an agglomeration mechanism is illustrated in Figure 10.17b where the mean crystal size dramatically decreases with an increase in the mixer speed (Mullin et al. 1990). Needless to say, there are many examples where the mean crystal size initially increases with the intensity of mixing due to an improved convective mass transfer and then decreases as vigorous mixing produces more and more contact

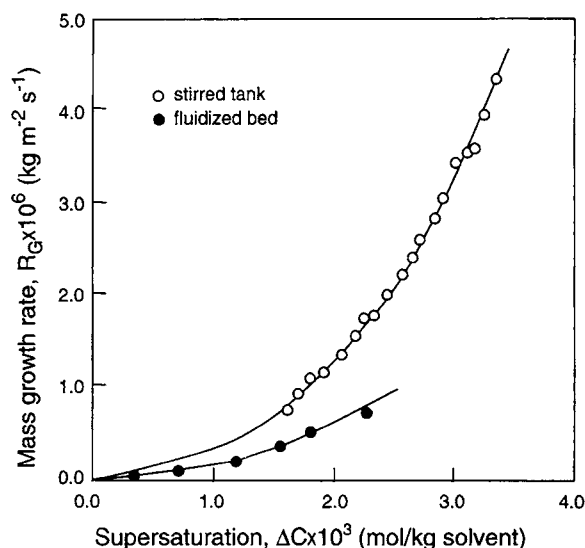


Figure 10.17(a) Comparison of the growth rates of potassium hydrogen tartrate (KHT) occurring in a fluidized bed and in a stirred vessel, as reported by Ratsimba and Laguerie (1991). Initial crystal mean size $L_s = 1.125 \times 10^{-4}$ m, ethanol content = 10% volume, crystallization temperature $T = 273$ K.

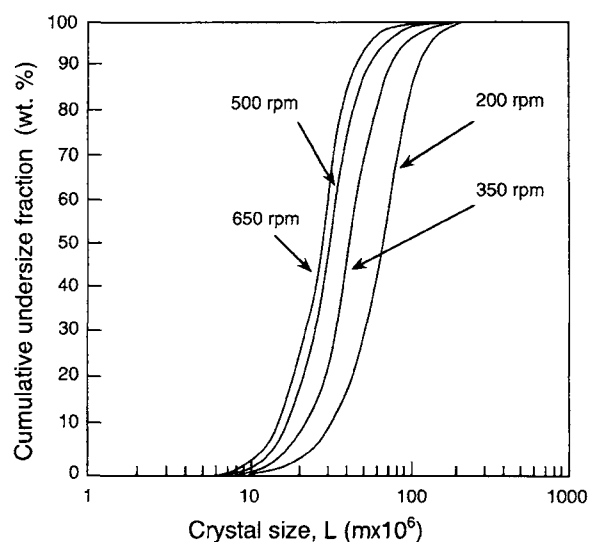


Figure 10.17(b) Cumulative undersize CSD in a suspension containing $SrMoO_4$ after 1-h stirring time as a function of mixer revolutions, as reported by Mullin et al. (1990). Growth occurred via an agglomeration mechanism.

secondary nuclei and the breakage phenomena may become significant.

The inherent scale-dependency of mixing and liquid-solid suspension dynamics can cause significant differences between laboratory, pilot, and industrial manufacturing scales (Green et al. 1996). In fact, scale-up usually amplifies inhomogeneity resulting from inadequate mixing. Single-phase flow theoretical models are of limited value because the complicated flows of mother liquor and crystals in a crystallizer significantly affect viscous dissipation and alter turbulence. Physical models of mixing and suspension flow via application of specialized techniques for flow pattern visualization (dye, tracer particles) and characterization have been more successful. Nevertheless, the results of physical modeling are usually qualitative because of the nearly impossible scaling of the results from one vessel size to another.

Significant progress is being made in fundamental approaches. The current powerful computational fluid dynamics (CFD) tools (e.g., FLUENT and CFX software)—based on the solution of differential mass and momentum balances—have made it possible to allow simulations of the flow patterns within the crystallizer. Both physical and mathematical modeling add to our knowledge and understanding of the nature of high-concentration suspension flows.

The remarks made so far were mainly concerned with the bulk or macromixing. For batch precipitation, one also needs to consider micromixing in order to properly describe the rapid chemical reaction at a molecular level.

10.5. BATCH CRYSTALLIZATION OPERATIONS

Classification of batch crystallizers and batch crystallization operations according to the means by which supersaturation is created is still a widely accepted method. Therefore, the discussion of such operations may include cooling crystallization, evaporative crystallization, vacuum crystallization, antisolvent crystallization, reaction (reactive) crystallization, etc. The vacuum crystallization operation can be considered as a combination of the evaporative and cooling crystallization and thus will not be discussed separately. Reaction crystallization (precipitation) is discussed in detail in Chapter 6.

10.5.1. COOLING CRYSTALLIZATION

Cooling is probably the most common way of creating supersaturation. It is applicable to those aqueous and nonaqueous systems, in which the solute solubility sharply increases with temperature. Batch cooling crystallization is undoubtedly one of the most frequent methods of crystallization. Its yield and economy depend on the temperature and concentration of the feed solution to be crystallized, and on whether cooling water or another cooling agent is employed. Typically, a high temperature, concentrated solution is delivered into a jacketed crystallizer equipped with a stirrer and often also a cooling coil to increase the cooling surface area. The solution is stirred, and cold water or cooling agent is pumped through the jacket and—if so equipped—the cooling coil. Such a “natural” cooling is continued until the temperature of the solution in the crystallizer is near that of the cooling medium. As shown in Figure 10.9, at the beginning of the above described process, the temperature difference between the cooling surface and the solution is at a maximum. This huge subcooling quickly brings the solution to the maximum (critical) supersaturation level. Moreover, the excessive subcooling persists for a significant portion of the batch operation. As a result, massive nucleation of the solute can occur more than once (renucleation). On the other hand, nuclei subjected to the maximum

supersaturation conditions grow at a high rate that may cause dendritic growth and occlusions. Furthermore, the cooling surfaces become quickly covered with layers of crystallizing solute (fouling, scaling, incrustation). This phenomenon is detrimental to the heat transfer efficiency and may bring about a decrease in the rate change of supersaturation. Also, as the process progresses, a large surface area of the crystal population created thus far is able to harness the excessive supersaturation level, so no further nuclei are formed spontaneously. The crystals that originate from the spontaneous nucleation and those secondary nuclei that are formed due to the contact secondary nucleation may grow now at a somewhat slower rate. As the temperature in the bulk approaches that of the cooling medium, the growth of the crystal population becomes much slower in rate.

There are two basic practical approaches that can help control CSD in batch cooling crystallization. The first is concerned with the use of seed crystals (external seeding), and the second is concerned with limiting the occurrence of spontaneous nucleation only to the initial stage of the process. Both require the control of the cooling rate via the control of the solution temperature in the crystallizer and the manipulations of the flow rate of cooling agent.

The mass m of uniform, three-dimensional crystals of an average size L can be expressed as

$$m = N\alpha\rho_c L^3 \quad (10.45)$$

If secondary nucleation does not occur and the concentration of solution C (expressed as mass of solute per mass of solvent) is higher than the solubility, the mass rate of the depletion of solute from solution caused by cooling is equal to the sum of the mass rates due to spontaneous nucleation and due to growth

$$-m_{sol} \frac{dC}{dt} = \frac{dm_N}{dt} + \frac{dm_G}{dt} \quad (10.46)$$

where m_{sol} is the mass of the solvent part of the solution in the crystallizer.

Seeded Cooling Crystallization. It is assumed that a certain number N of seed crystals of a uniform size L_s are introduced to the crystallizer at the saturation temperature T^* . No nuclei are formed spontaneously and the seeds are allowed to grow, at a constant growth rate G , until the final size L_f has been reached after the batch time t_f . In the absence of spontaneous nucleation, Eq. (10.46) becomes simplified to

$$m_{sol} \frac{dC}{dt} + \frac{dm_G}{dt} = 0 \quad (10.47)$$

By denoting the linear growth rate as $G = dL/dt = \text{constant}$, one can obtain the following ODE, from Eqs. (10.45) and (10.47)

$$m_{sol} \frac{d^3 C}{dt^3} + 6N\alpha\rho_c G^3 = 0 \quad (10.48)$$

with three initial conditions

$$C(0) = C^* \quad (10.49)$$

$$\frac{dC(0)}{dt} = \frac{-3N\alpha\rho_c L_s^2 G}{m_{sol}} \quad (10.50)$$

$$\frac{d^2 C(0)}{dt^2} = \frac{-6N\alpha\rho_c L_s G^2}{m_{sol}} \quad (10.51)$$

Integration of the above ODE, Eq. (10.48), subject to the initial conditions, Eqs. (10.49)–(10.51), yields

$$\frac{m_{sol}}{3m_s}(C^* - C) = \frac{G^3 t^3}{3L_s^3} + \frac{G^2 t^2}{L_s^2} + \frac{Gt}{L_s} \quad (10.52)$$

a concentration profile that is cubic in time.

In order to obtain a cooling profile, $T(t)$, it is necessary to utilize the appropriate expression for the dependence of concentration on temperature. In a simple case, the concentration may be expressed as a linear function of T

$$C = aT + q \quad (10.53)$$

where a and q are constants. From Eqs. (10.52) and (10.53), one can obtain the cooling profile as follows

$$T = T^* - \frac{3m_s}{am_{sol}} \left(\frac{G^3 t^3}{3L_s^3} + \frac{G^2 t^2}{L_s^2} + \frac{Gt}{L_s} \right) \quad (10.54)$$

Because the above cooling profile is cubic in time, the cooling rate

$$\frac{dT}{dt} = -\frac{3m_s}{am_{sol}} \left(\frac{G^3 t^2}{L_s^3} + \frac{2G^2 t}{L_s^2} + \frac{G}{L_s} \right) \quad (10.55)$$

is parabolic in time. Therefore, as the growth of the crystals progresses, higher and higher cooling rates are required to maintain the assumed constant growth rate (and supersaturation).

As it will be shown for evaporative crystallization, a population balance approach subject to the same assumptions will yield similar results as far as the mathematical form of the solution is concerned.

Unseeded Cooling Crystallization. In a similar fashion, a cooling profile can be derived for the unseeded case in which spontaneous nucleation and growth are allowed to occur at constant rates. The actual solutions to the resultant third-order differential equations found in the literature differ due to the different sets of the four initial conditions used by various authors (Karpinski et al. 1980b; Nývlt 1991; Randolph and Larson 1988). Understandably, all of them result in a cooling profile of the general form

$$T = T^* - f(t, G, \bar{B}_0, L_N, a) \quad (10.56)$$

which is biquadratic in time; and the cooling rate profile of the general form

$$\frac{dT}{dt} = \varphi(t, G, \bar{B}_0, L_N, a) \quad (10.57)$$

which is cubic in time.

Karpinski et al. (1980b) investigated the effect of different cooling profiles on the CSD for batch cooling crystallization of $\text{MgSO}_4 \cdot 7\text{H}_2\text{O}$. The four cooling profiles studied are shown in Figure 10.18. Curves (1) and (2) represent the cooling profiles calculated from Eqs. (10.54) and (10.56), respectively. A good agreement between the theoretical and the actual product size, and a narrow CSD was obtained for these two profiles. The arbitrary linear cooling profile (3) resulted in a product of a

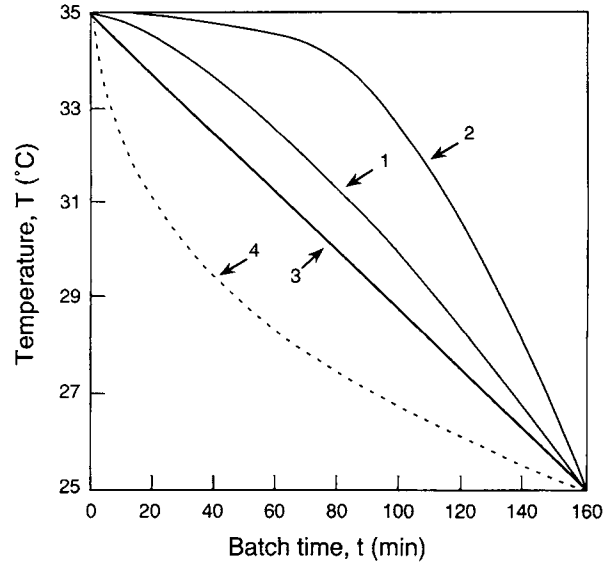


Figure 10.18 Cooling profiles for crystallization of $\text{MgSO}_4 \cdot 7\text{H}_2\text{O}$ in a 21-L batch cooling crystallizer, as reported by Karpinski et al. (1980b). Saturation temperature $T^* = 35^\circ\text{C}$. Seeded crystallization: (1) Cooling profile calculated from Eq. (10.54), mean seed size $L_s = 0.4075$ mm. Unseeded crystallization: (2) Cooling profile calculated from Eq. (10.56), (3) Linear cooling profile, (4) Natural cooling profile.

smaller mean size and much wider CSD. The application of the natural cooling profile (4) produced a very polydisperse product. It is worth noticing that the shape of the natural cooling profile is “opposite” to that resulting from Eqs. (10.54) and (10.56).

Based on the two cases discussed so far, one can consider yet another case of interest, in which nucleation is allowed to proceed at a constant rate from $t = 0$ until a certain time t_1 , after which no new nuclei are generated. For such a cooling crystallization, a biquadratic cooling profile applies until $t = t_1$, and Eq. (10.54) for the time $t > t_1$. This is the preferred method of practical unseeded batch cooling crystallization.

In order to calculate the above cooling profiles, one needs to know the values of the growth rate G , the nuclei size L_N , and the nucleation rate \bar{B}_0 . For the seeded run, the value of the growth rate G must be lower than the critical growth rate, which can be determined experimentally in growth kinetics experiments (Karpinski 1981)

$$G = (L_f - L_s)/t_f < G_{crit} \quad (10.58)$$

The critical growth rate is a maximum growth rate attainable without the occurrence of spontaneous nucleation. The average size of effective nuclei L_N can be determined from the microscopic observations, screening, or any applicable instrumental sizing techniques. If the cooling strategy allows for spontaneous nucleation, the magnitude of the nucleation rate \bar{B}_0 must be estimated, which usually requires a population balance approach (Randolph and Larson 1988). Once the value of the parameter n^0 is determined from the semilog plot of population density n versus size L via the continuous crystallization experiments, the nucleation rate can be calculated as

$$\bar{B}_0 = n^0 VG \quad (10.59)$$

10.5.2. EVAPORATIVE CRYSTALLIZATION

For substances whose solubility is weakly dependent on temperature (e.g., NaCl) or for those with an "inverse" dependence of the solubility on temperature (e.g., Na₂SO₄), a method of choice to create supersaturation is evaporation of the solvent. In practice, evaporative crystallizers usually operate at constant temperature and reduced pressure.

Larson (1978) considered the operation of a batch, externally seeded evaporative crystallizer with a constant growth rate, G , in which no spontaneous nucleation was allowed. Applying the population balance Eq. (10.1) to this system gave the following equations for the solvent profile

$$\frac{C_V}{3m_s}(V_{sol,0} - V_{sol}) = \frac{G^3 t^3}{3L_s^3} + \frac{G^2 t^2}{L_s^2} + \frac{Gt}{L_s} \quad (10.60)$$

and for the solvent evaporation rate

$$\frac{dV_{sol}}{dt} = -\frac{3m_s}{C_V} \left(\frac{G^3 t^2}{L_s^3} + \frac{2G^2 t}{L_s^2} + \frac{G}{L_s} \right) \quad (10.61)$$

It is important to recognize the similarity of the mathematical form of Eqs. (10.54) and (10.60), and Eqs. (10.55) and (10.61). One may conclude that all batch crystallization processes may be controlled by a properly designed time-profile of the supersaturation-inducing quantity (e.g., the cooling or evaporation rate, in the cases discussed in this chapter; and the reagent addition rate, in Chapter 6 on precipitation).

The type and area of the energy-exchange surface as well as the process control must be adequate to accommodate both low evaporation rates at the beginning of the batch evaporation and elevated evaporation rates in the final stage of the run. These rates may differ by two orders of magnitude.

10.5.3. ANTISOLVENT CRYSTALLIZATION (SALTING-OUT)

In this type of batch crystallization, a solute is crystallized from a primary solvent by the addition of a second solvent (anti-solvent) in which the solute is relatively insoluble. The anti-solvent is miscible with the primary solvent and brings about a solubility decrease of the solute in the resulting binary solvent mixture.

If an organic solvent is added to an aqueous solution containing the substance to be crystallized (typically an inorganic salt), the process is termed salting-out. The inverse procedure, common in pharmaceutical and organic chemicals technology, when water is added to the organic solvent in order to crystallize a dissolved organic substance, is known as drowning-out. The fundamental principle is the same in both cases.

The major advantage of the anti-solvent crystallization is that the process can be carried out at the ambient temperature, which—aside from the convenience and economical aspects—is of a paramount importance for heat-sensitive substances. The disadvantage of this process is that the binary solvent mixture must be subsequently separated in order to recover and recycle one or both solvents. Frequently, however, the added cost of the separation operation is fully absorbed by the valuable and expensive products, such as pharmaceuticals.

Using an analogy with the programmed cooling crystallization, Karpinski and Nývlt (1983) suggested that the quality of the

product obtained by means of salting-out can be improved by a programmed addition rate of the anti-solvent, proportional to the instantaneous crystal surface area. Typical operational parameters affecting batch anti-solvent crystallization are as follows (Budž et al. 1986; Johnson et al. 1997): the solubility and actual concentration of a solute in both primary solvent and the binary mixture (primary solvent-anti-solvent), the anti-solvent addition rate, the use of seeds, the form of seeds (dried versus slurry), the amount and properties of seed crystals, intensity of mixing, the crystallization temperature, and the batch time.

Quite often, the addition of anti-solvent even at low addition rates, may still create extremely high supersaturation levels leading to an excessive amount of fines in the final product and subsequent problems in the downstream processes. One way of avoiding this problem, suggested by Karpinski and Nývlt (1983), is a dilution of the anti-solvent with the primary solvent, or the use of a diluted solute-primary solvent solution, as advocated by Budž et al. (1986). Such measures help with the CSD control but due to the operating volume increase also have an adverse effect on the yield of the process. An interesting approach to maintain a high yield and to operate within a reasonable supersaturation range was proposed by Mydlarz and Budž (1986). Namely, a low-volatility anti-solvent can be introduced to the concentrated primary solvent solution in the form of a gaseous mixture, such as a carrier gas-anti-solvent vapor mixture, rather than as a liquid. The supersaturation level can be controlled by the ratio between the carrier gas (e.g., air, nitrogen) and the anti-solvent vapor. The volume increase due to the anti-solvent vapor condensation is rather small and, therefore, the attainable yield may be significantly increased.

10.6. SUMMARY

Batch crystallization has several desirable features and advantages in laboratory and industrial applications. Industrial batch crystallizers are commonly used to manufacture a wide variety of crystalline materials with desirable product features and quality. Laboratory batch crystallizers are often used to characterize crystallization kinetics and CSDs and to determine the effects of process conditions on these kinetics and CSDs.

The analysis of batch crystallizers normally requires the consideration of the time-dependent, batch conservation equations (e.g., population, mass, and energy balances), together with appropriate nucleation and growth kinetic equations. The solution of these nonlinear partial differential equations is relatively difficult. Under certain conditions, these batch conservation equations can be solved numerically by a moment technique. Several simple and useful techniques to study crystallization kinetics and CSDs are discussed. These include the thermal response technique, the desupersaturation curve technique, the cumulative CSD method, and the characterization of CSD maximum.

Several factors affecting batch crystallization are also discussed. These include batch cycle time, supersaturation profile, external seeding, fouling control, CSD control, growth rate dispersions, and mixing. The batch cycle time information is needed to determine the crystallizer volume required for meeting the production rate requirement. The supersaturation profile has a profound effect on the nucleation and growth processes, and the resulting CSD. Supersaturation control during a batch run is beneficial in increasing crystal size and in reducing the batch cycle time. The external seeding technique can be used to control the supersaturation and nucleation during the initial stage of the batch run. External seeding can also be used to determine the maximum metastable supersaturation (or the maximum growth rate) allow-

able without nucleation in the batch crystallization process. Several techniques are used to minimize the fouling of crystals on the heat transfer surfaces during the batch run. Fines destruction and a strategy to separate nucleation and growth during the batch crystallization operation can be used to prepare crystal products with a narrow CSD. Growth rate dispersions resulting from inherently different growth rates of individual crystals, may significantly influence the CSD in batch crystallization. Several growth rate dispersion models were proposed to explain the widening of the CSD during the course of batch crystallization. Good mixing is required in a crystallizer not only to maintain crystals in suspension, but also to assure adequate rates of mass and energy transfer. Crystallization-specific phenomena, such as secondary nucleation and agglomeration, are also strongly affected by mixing. The inherent scale-dependency of mixing and liquid-solid suspension dynamics further complicates rigorous description of the mixing effect on batch crystallization.

The control of supersaturation must be employed in batch crystallization in order to obtain a desired CSD of the product. In the three common batch crystallization operations (cooling crystallization, evaporative crystallization, and anti-solvent crystallization), such a control may be realized by employing appropriate time-profiles for cooling rate, evaporation rate, and anti-solvent addition rate, respectively. When an external seeding is used and the crystal growth occurs at a constant rate, mathematically similar expressions for cooling and evaporation rate profiles can be derived. For an unseeded operation, the knowledge of growth and nucleation rates and the nuclei size distribution are necessary in order to obtain the time-profiles via a population balance approach.

NOMENCLATURE

A_T	Total crystal surface area
\bar{A}	Total crystal surface area based on total operating volume of the crystallizer
b	Nucleation kinetic order
\bar{B}_0	Nucleation rate based on total operating volume of the crystallizer
c	Bulk solute concentration, volume basis
c^*	Equilibrium solute concentration
C	Bulk solute concentration per unit mass of solvent
C^*	Equilibrium solute concentration per unit mass of solvent
C_V	Bulk solute concentration per unit solvent volume
Δc	Supersaturation
Δc_0	Initial supersaturation
Δc_{01}	First derivative of Δc_0
Δc_{02}	Second derivative of Δc_0
Δc_f	Final supersaturation
Δc_{max}	Supersaturation at the limit of the metastable zone
D	Kinematic diffusion coefficient
D_G	Growth diffusivity
E_m	Energy dissipated in a stirred vessel per unit mass of suspension
F	Cumulative mass distribution
g	Growth kinetic order
G	Linear growth rate, average linear growth rate
G_{crit}	Critical (maximum) linear growth rate
j	Exponent of suspension density in Eq. (10.6)
k_d	Mass transfer coefficient for the diffusion step of crystal growth

k_G	Overall growth rate constant
k_N	Nucleation rate constant
L	Crystal size
L_0	Initial crystal size
L_f	Final crystal size
L_N	Nucleus size
L_p	Crystal size at which CSD maximum is located
L_s	Size of seed crystals
L_t	Size of crystals at time t
\bar{L}	Mean crystal size
\bar{L}	Total length of crystals based on total operating volume of the crystallizer
m	Crystal mass
m_f	Final mass of crystals
m_i	i^{th} moment of population density distribution
m_s	Mass of seed crystals
m_t	Mass of crystals at time t
m_T	Crystal suspension density
\bar{m}	Total mass of crystals based on total operating volume of the crystallizer
n	Population density per unit suspension volume
n^0	Nucleation parameter: the intercept from the semilog population density plot
\bar{n}	Population density based on total operating volume of the crystallizer
\bar{n}_0	Nuclei population density based on total operating volume of the crystallizer
\bar{n}_s	Initial seed distribution based on total operating volume of the crystallizer
N	Total number of crystals
\bar{N}	Total number of crystals based on total operating volume of the crystallizer
\bar{N}_s	Total number of seeds based on total operating volume of the crystallizer
q	Constant in Eq. (53)
R_G	Crystal mass growth rate
Re	Reynolds number
Sc	Schmidt number
Sh	Sherwood number
t	Time
t_f	Batch time
t_{max}	Time at which Δc_{max} occurs
t_0	Duration of the constant subcooling stage of the batch run
T	Temperature
T^*	Saturation temperature
ΔT_0	Initial subcooling
ΔT_{max}	Maximum allowable subcooling
u	Superficial velocity of solution in a fluidized bed
V	Total operating volume of the crystallizer
$V_{sol,0}$	Initial total volume of solvent in evaporative crystallizer
V_{sol}	Total volume of solvent in evaporative crystallizer

Greek Letters

α	Crystal volume shape factor
β	Crystal surface area shape factor
ϵ	Void fraction in a fluidized bed
μ	Dynamic viscosity of solution
ρ_c	Crystal density
ρ_{sol}	Solution density
$\Delta \sigma_L^2$	Difference between final and mean variance of CSD

REFERENCES

- Baliga, J.B. (1970). Ph.D. dissertation, Iowa State University, Ames, IA.
- Bamforth, A.W. (1965). *Industrial Crystallization*, Leonard Hill, London.
- Bennett, R.C. (1984). *AIChE Symp. Ser.* **80**(240), 45.
- Bohlin, M., and Rasmuson, A.C. (1992a). *Can. J. ChE.* **70**, 120.
- Bohlin, M., and Rasmuson, A.C. (1992b). *AIChE J.* **38**, 1853.
- Budz, J., Karpinski, P.H., and Naruc, Z. (1984). *AIChE J.* **30**, 710.
- Budz, J., Karpinski, P.H., and Naruc, Z. (1985). *AIChE J.* **31**, 259.
- Budz, J., Karpinski, P.H., Mydlarz, J., and Nývlt, J. (1986). *I&EC Prod. R&D.* **25**, 657.
- Butler, B.K., Zhang, H., Johns, M.R., Mackintosh, D.L., and White, E.T. (1997). Paper 38b, presented at AIChE Meeting, Los Angeles, CA.
- Garside, J. (1985). *Chem. Eng. Sci.* **40**, 3.
- Garside, J., Gibilaro, L.G., and Tavare, N.S. (1982). *Chem. Eng. Sci.* **37**, 1625.
- Garside, J., and Jančić, S.J. (1976). *AIChE J.* **22**, 887.
- Green, D.A., Kontomaris, K., Grenville, R.K., Etchells, A.W., Kendall, R.E., and Jacobs, G. (1996). In *13th Symposium on Industrial Crystallization Proceedings*, pp. 515, PROGEP, Toulouse (France).
- Hulburt, H.M. (1976). In *Industrial Crystallization* (Mullin, J.W., ed.), pp. 343, Plenum Press, New York.
- Hulburt, H.M., and Katz, S. (1964). *Chem. Eng. Sci.* **19**, 555.
- Johnson, B.K., Szeto, C., Davidson, O., and Andrews, A. (1997). Paper 16a, presented at AIChE Meeting, Los Angeles, CA.
- Jones, A.G., and Mullin, J.W. (1974). *Chem. Eng. Sci.* **29**, 105.
- Jones, A.G., Chianese, A., and Mullin, J.W. (1984). In *Industrial Crystallization*, vol. 84 (Jančić, S.J., and de Jong, E.J., eds.), pp. 191, Elsevier, Amsterdam.
- Kane, S.G., Evans, T.W., Brian, P.L.T., and Sarofim, A.F. (1974). *AIChE J.* **20**, 855.
- Karpinski, P. (1981). *Mass Crystallization in a Fluidized Bed*, Wrocław University of Technology Press, Wrocław (Poland).
- Karpinski, P.H. (1980). *Chem. Eng. Sci.* **35**, 2321.
- Karpinski, P., Budz, J., and Naruc, Z. (1980a). In *Scientific Papers of Wrocław University of Technology*, vol. 38, no. 5 p. 172, Wrocław, Poland.
- Karpinski, P., Budz, J., and Naruc, Z. (1980b). *Ibidem*, pp. 163.
- Karpinski, P.H., and Koch, R. (1979). In *Industrial Crystallization*, vol. 78 (de Jong, E.J., and Jančić, S.J., eds.), pp. 205, North Holland, Amsterdam.
- Karpinski, P.H., and Nývlt, J. (1983). *Cryst. Res. Technol.* **18**(7), 959.
- Lacmann, R., Herden, A., Tanneberger, U., Klapper, H., Schmiemann, D., Mersmann, A., and Zacher, U. (1996). In *13th Symposium on Industrial Crystallization Proceedings*, p. 515, PROGEP, Toulouse (France).
- Larson, M.A. (1978). *Chem. Eng. (N.Y.)* **85**(4), 90.
- Larson, M.A. (1979). In *Industrial Crystallization*, vol. 78 (de Jong, E.J., and Jančić, S.J., eds.), p. 310, North Holland, Amsterdam.
- Larson, M.A., and Garside, J. (1973). *Chem. Eng. (London)* **274**, 318.
- Leubner, I.H., Jagannathan, R., and Wey, J.S. (1980). *Photogr. Sci. Eng.* **24**, 268.
- Margolis, G., Brian, P.L.T., and Sarofim, A.F. (1971). *Ind. Eng. Chem. Fundam.* **10**, 439.
- Misra, C., and White, E.T. (1971). *Chem. Eng. Prog. Symp. Ser.*, vol. 67, no. 10 (Larson, M.A., ed.), p. 53, American Institute of Chemical Engineers, New York.
- Moyers, Jr., C.G., and Rousseau, R.W. (1987). In *Handbook of Separation Process Technology* (Rousseau, R.W., ed.), p. 587, Wiley-Interscience, New York.
- Mullin, J.W., and Nývlt, J. (1971). *Chem. Eng. Sci.* **26**, 369.
- Mullin, J.W., Söhnel, O., and Jones, A.G. (1990). *Proceedings of the 11th Symposium on Industrial Crystallization'90*, Garmisch-Partenkirchen, Germany, p. 214.
- Mydlarz, J., and Budz, J. (1986). *Scientific Papers of Poznan University of Technology*, **18**, p. 28, Poznan, Poland (in Polish).
- Nývlt, J. (1978). *Industrial Crystallization*, p. 40, Verlag Chemie, Weinheim, West Germany.
- Nývlt, J. (1991). In *Advances in Industrial Crystallization* (Garside, J., Davey, R.J., and Jones, A.G., eds.), p. 197, Butterworth-Heinemann Ltd, Oxford.
- Nývlt, J., Söhnel, O., Matuchová, M., and Broul, M. (1985). *The Kinetics of Industrial Crystallization*, p. 261, Elsevier Science Publishers, New York.
- Omran, A.M., and King, C.J. (1974). *AIChE J.* **20**, 795.
- Ramanarayanan, K.A., Berglund, K.A., and Larson, M.A. (1985). *Chem. Eng. Sci.* **40**, 1604.
- Randolph, A.D., and Larson, M.A. (1962). *AIChE J.* **8**, 639.
- Randolph, A.D., and Larson, M.A. (1988). *Theory of Particulate Processes*, 2nd ed., Academic Press, New York.
- Randolph, A.D., and White, E.T. (1977). *Chem. Eng. Sci.* **32**, 1067.
- Ratsimba, B., and Laguerie, C. (1991). *Fourth World Congress of Chemical Engineering. Strategies 2000. Preprints IV: Sessions 10.1–13.4*, pp. 10.7–28, Karlsruhe, Germany.
- Shiau, L.D., and Berglund, K.A. (1990). *AIChE J.* **36**, 1669.
- Stavek, J., Fort, I., Nývlt, J., and Sipek, M. (1988). *Proceedings of the Sixth European Conference on Mixing*, p. 171, Pavia, Italy.
- Stocking, J.H., and King, C.J. (1976). *AIChE J.* **22**, 131.
- Sugimoto, T. (1987). *Adv. Colloid Interface Sci.* **28**, 65.
- Tavare, N.S. (1985). *AIChE J.* **31**, 1733.
- Tavare, N.S. (1987). *Chem. Eng. Commun.* **61**, 259.
- Tavare, N.S., Garside, J., and Chivate, M.R. (1980). *Ind. Eng. Chem. Process Des. Dev.* **19**, 653.
- Tavare, N.S., and Garside, J. (1982). In *Industrial Crystallization*, vol. 81 (Jančić, S.J., and de Jong, E.J., eds.), p. 21, North Holland, Amsterdam.
- Wey, J.S. (1981). In *Preparation and Properties of Solid State Materials*, vol. 6 (Wilcox, W.R., ed.), p. 67, Marcel Dekker, New York.
- Wey, J.S. (1985). *Chem. Eng. Commun.* **35**, 231.
- Wey, J.S., and Estrin, J. (1973). *Ind. Eng. Chem. Process Des. Dev.* **12**, 237.
- Wey, J.S., and Estrin, J. (1974). *Desalination* **14**, 103.
- Wey, J.S., and Strong, R.W. (1977a). *Photogr. Sci. Eng.* **21**, 14.
- Wey, J.S., and Strong, R.W. (1977b). *Photogr. Sci. Eng.* **21**, 248.
- Zipp, G.L., and Randolph, A.D. (1989). *Ind. Eng. Chem. Res.* **28**, 1446.
- Zumstein, R.C., and Rousseau, R.W. (1987). *AIChE J.* **33**, 1921.

CRYSTALLIZATION IN THE PHARMACEUTICAL AND BIOPROCESSING INDUSTRIES

D.J. Kirwan and C.J. Orella

11.1. THE ROLE OF CRYSTALLIZATION IN BIOPROCESSES

The application of crystallization in the pharmaceutical industry directly parallels crystallization in other industries. There is a need to control particle size distribution through control of crystal growth versus nucleation and to control the purification achieved through crystallization. The latter requirement often requires different approaches and operating conditions than those for optimizing yield. Precipitation is commonly used in the pharmaceutical industry. [In this chapter, we shall use the term precipitation to mean the creation of a solid phase (crystalline or not) by the addition of an agent. Precipitation historically often referred to reactions resulting in the formation of a solid phase.] What is unique in the pharmaceutical industry is the chemical complexity of the entities that are crystallized. This complexity and chemical diversity impacts the thermodynamics (solubility and crystal structure) as well as the kinetics of crystallization. Several examples of the chemical diversity of products crystallized in the pharmaceutical industry are shown in Figure 11.1. In this chapter we will focus on low molecular weight pharmaceutical compounds while protein crystallization is discussed in Chapter 12.

The majority of these pharmaceutical compounds are between 100 and 1000 daltons, and exhibit a great diversity of functional groups ranging from ionic moieties to very lipophilic or hydrophobic groups. Thus, their interactions with one another, with solvents or anti-solvents, and with co-solutes and impurities in solution are very diverse. The solid phases (including polymorphs and various solvates) formed by such molecules are very poorly understood. The transformation rate between such solid phases may be kinetically limited. Therefore, solids of differing characteristics or even immiscible liquid phases, "oiling out," might be obtained from different modes of crystallization. This complexity is compounded by the limited experimental studies on such compounds from which generalizations can be made.

Owing to the final use of such compounds, strict control is required on their purity, crystal form and morphology, and particle size distribution (PSD). All of these characteristics are governed by the crystallization process. Obviously, control of purity is of great importance for products intended for human medicinal use in order to minimize exposure to anything other than the intended therapeutic agent. But, equally important is the PSD, which can dramatically impact the in-vivo dissolution of a drug, especially one that is hydrophobic and has limited solubility in aqueous solutions. This "bioavailability" can be strongly hindered if many larger particles are present, and is enhanced by the presence of predominantly smaller particles. Less obvious is that a change in crystal morphology (shape) or crystal structure can impact the bioavailability. In addition, these same properties of the crystals can play a dramatic role in the stability of the product; and, therefore, its purity at time of use. Whereas small particle size is generally good for bioavailability, it is a disadvantage to crystals

subject to oxidation during processing or storage because of the greater surface area per crystal mass.

Crystallization also is employed as an intermediate purification step in many processes because of good separation factors per stage and its effectiveness at low temperatures for thermally labile compounds. Particle size and habit are important in these steps as well because of their effect on filtration or centrifugation rates. The influence of crystallization conditions on morphology and PSD, and, therefore, on the "de-liquoring" characteristics is often overlooked when laboratory work is conducted. However, this becomes much more important in pilot- or full-scale manufacturing where slow "de-liquoring" can result in low productivity and reduced stability.

There are several common problems encountered in the use of crystallization in the pharmaceutical industry; (1) the control of supersaturation (and PSD) in a batch crystallizer; (2) the effective use of seed; (3) efficient measurement of solubilities in multiple solvent systems to maximize purification and yield; and (4) identification and retention of the most stable polymorphic form.

As stated above, control of the crystallization or precipitation process is essential to obtain crystals of biochemical compounds having appropriate properties. The phenomena, techniques, and analysis discussed in many of the previous chapters: solubility and supersaturation, nucleation and growth kinetics, population balance methods, batch and continuous crystallizers, and factors governing crystal purity, habit and morphology are all relevant to the discussion of the crystallization of pharmaceuticals. We shall analyze the crystallization/precipitation of biomolecules in terms of these concepts.

11.2. SOLUBILITY AND THE CREATION OF SUPERSATURATION

Crystallization obviously requires the creation of a condition where the equilibrium solubility value is below that of the concentration of solute in the solution. Both growth and nucleation rates are dependent upon the departure of the solution conditions from equilibrium values. Further, the single-step yield achieved in a given crystallization is directly related to the equilibrium amount of solute remaining in solution, after nucleation and growth have relieved supersaturation. Crystallization can be accomplished by reducing the temperature as in a cooling crystallizer, by removing solvent as in an evaporative crystallizer, or by altering the composition of the solution by the addition of acid, base, miscible anti-solvents, or salts as in a precipitating crystallizer. These techniques also can be used in concert to accomplish the desired solubility reduction. While solubility is a thermodynamic variable not influenced by the mode of crystallizing; in precipitation crystallization, the mode of addition in a batch crystallizer can be used to create very different transient conditions of solubility and supersaturation.

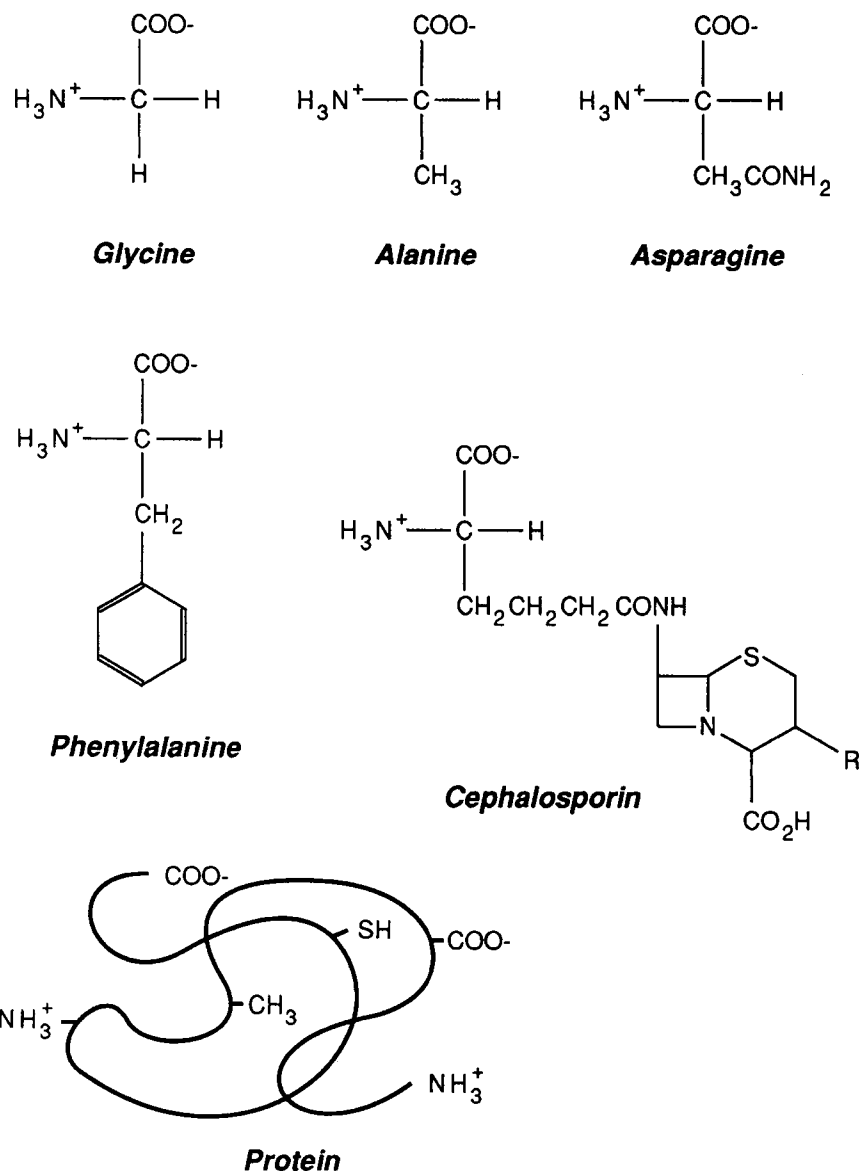


Figure 11.1 Molecular structures of various biochemicals.

That is, adding nonsolvent to the solute in solution is very different from the “reverse addition” of solution to nonsolvent and both are different from a rapid in-line blending to the final proportions.

11.2.1. TEMPERATURE EFFECTS ON SOLUBILITY

Most solutes, whether biological in nature or not, exhibit increasing solubility with increasing temperature. For example, Figure 11.2 shows the solubilities of citric acid and glutamic acid in water as a function of temperature. There can be complicating factors in the solubility behavior related to the actual form of the solute in the crystal phase and in solution as evidenced by the various forms of glutamic acid. For the case of citric acid a monohydrate exists below about 37 °C and the anhydrous form at higher temperatures. Although it can be useful to raise the temperature to increase the amount of material in solution for low molecular weight solutes prior to a crystallization step, such a practice may not be acceptable for temperature sensitive materials subject to thermal degrad-

ation. The operational temperature range is limited, therefore, by the freezing point of the solvent (solution) at low temperatures and by thermal degradation of the solute at higher temperatures. Low temperatures generally minimize solubility and favor stability but slow kinetics. As with citric acid anhydrous forms can only exist above some temperature. The particular form may greatly affect kinetics as well as solid stability and morphology.

11.2.2. pH EFFECTS ON SOLUBILITY

The acidic and basic salts of glutamic acid exhibit very different solubility behavior as can be seen in Figure 11.2b. The solubility of amphoteric compounds such as amino acids or antibiotics are strongly pH dependent because the predominant form existing in solution changes with the hydrogen ion concentration. Acid/base solution equilibria for a compound having one acidic and one basic group could be represented as

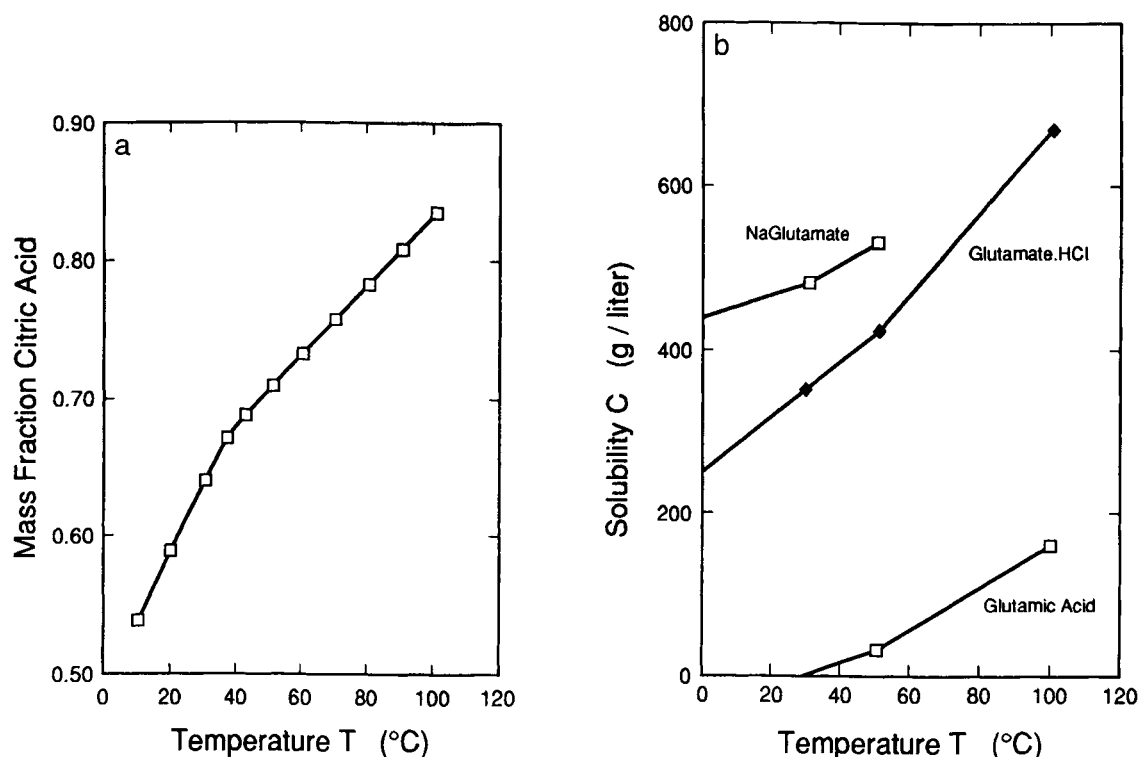
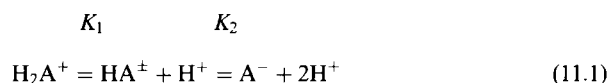


Figure 11.2 Temperature dependence of the aqueous solubility of (a) citric acid; and (b) glutamic acid. (Data from Samejima 1972.)



The crystal-solution equilibrium relates to that between a particular form of the solute in solution and the same form in the crystalline phase. The isoelectric (zwitterionic) form usually exists in the crystalline phase over most of the pH range. Such compounds usually exhibit the lowest *apparent* solubility at their isoelectric pH since at other pH's some fraction of the solute exists in solution in the acid or base form. However, at very high acid or base concentrations, a salt, e.g., $H_2A^+Cl^-$, could be the crystalline form.

Figure 11.3 shows the solubilities (defined as total solute dissolved) of some β -lactam antibiotics as a function of pH. All of these compounds exhibit a minimum in their solubility, C^*_0 , at the isoelectric point of the compound. At a pH significantly removed from the isoelectric point, the total (apparent) solubility is increased. The U-shape of the apparent solubility versus pH curve can be described by taking into account the acid-base equilibria of the antibiotic solute and assuming that the solute in the crystal is in the zwitterionic (isoelectric) form.

$$C^* = C^*_0 \left(1 + \frac{k_1}{a_{H^+}} + \frac{a_{H^+}}{K_2} \right) \quad (11.2)$$

In Eq. (11.2) a_{H^+} is the hydrogen ion activity.

Further complications arise when the concentrations of salts formed at low or high pH exceed their solubility limit. Such an instance is shown in Figure 11.4 for *L*-isoleucine. At pH values above 2, the zwitterion is the dominant species in solution and in

the crystalline phase. Upon addition of acid the solubility reaches a maximum at pH = 1 corresponding to the formation of the chloride salt. When the chloride ion is further increased whether from HCl or a chloride salt, precipitation of the chloride salt of leucine occurs (common ion effect.)

11.2.3. REDUCTION OF SOLUBILITY WITH ANTI-SOLVENTS

The use of miscible anti-solvent liquids to precipitate low molecular weight compounds is quite common in pharmaceutical processing as it often can rapidly create higher supersaturations as compared to cooling or evaporation. For example, aliphatic alcohols such as isopropanol can be added to aqueous solutions of amino acids to reduce their solubility by orders-of-magnitude. Of course, this results in dilution of the stream. For compounds soluble in organic liquids, water or an alkane (heptane) may be the precipitating agent. The precipitating agent usually can be recovered by distillation for re-use in these processes.

In Figure 11.5 are shown the solubilities of various amino acids at their isoelectric point as a function of isopropanol concentration (Orella and Kirwan 1989). Simple theories suggest that the effect of the alcohol is to reduce the dielectric constant and thereby reduce solubility (Kirkwood 1936). In fact, the solubility behavior is much more complex and significantly influenced by the nature of the amino acid side chain. For example, compare the behavior of phenylalanine (hydrophobic side chain) and asparagine (hydrophilic side chain) in Figure 11.5. Both hydrophobic and polar interactions between the mixed solvent and the various groups present on the molecule can occur. Correlation of the solubility behavior in these solutions using Margules, NRTL, or Wilson activity coefficient equations can be successful (Orella and

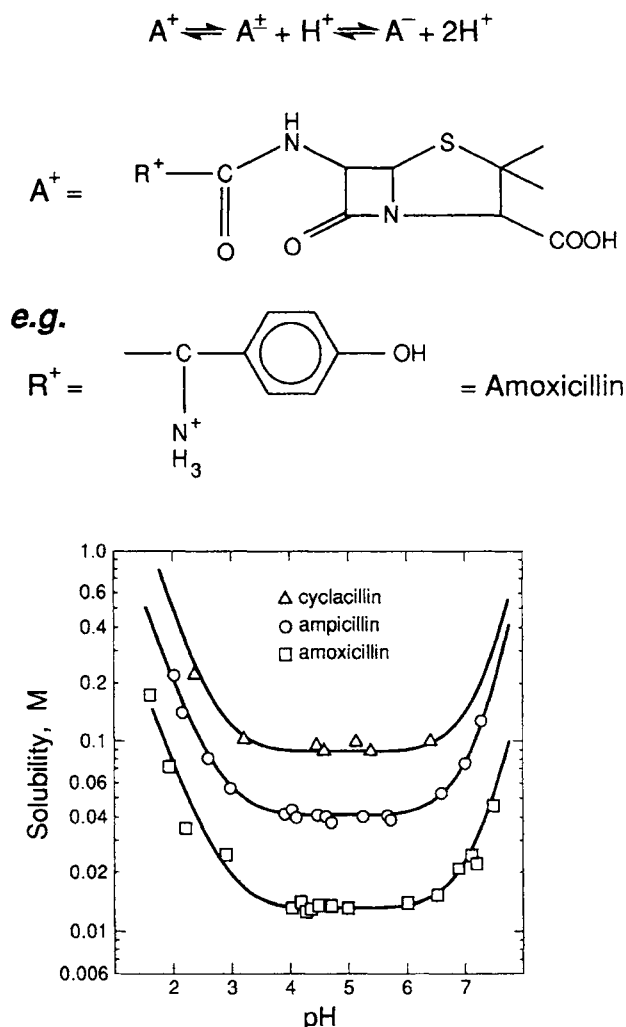


Figure 11.3 Aqueous solubility of some antibiotics as a function of pH. (Data from Tsujima et al. 1978.)

Kirwan 1991); however predictive models await a more fundamental understanding of the solution thermodynamics of complex organic/charged species in mixed organic-aqueous solvents.

11.2.4. EFFECTS OF SALTS ON SOLUBILITY

Since many biological molecules have groups capable of ionization, they may exist as singly- or multiply-charged species or as neutral molecules with strong dipoles. As such, they are particularly susceptible to other ions in solution through effects on ionic strength as well as to specific interactions with counter-ions. As one example, the solubility of glutamic acid in the presence of different anions is shown in Figure 11.6. These data show that the pH and the counter-ion both can have a significant impact on the solubility of the glutamate salt. In addition, the presence of an inorganic sodium salt such as sodium chloride will also impact the solubility. This type of behavior is most simply characterized by the recognition of ionic equilibria involving the solute and common ions. This leads to an equation for the equilibrium constant, known for a product with limited solubility as the “solubility

product” (Chapter 1). In ideal solutions, where activities can be represented by concentrations, the solubility product is

$$K_{sp} = [Na^+][Glu^-] \quad (11.3)$$

Thus, adding sodium chloride to a solution of sodium glutamate drives sodium glutamate out of solution, provided the added salt remains in solution. However, as noted in Chapter 1 more complex behavior may be observed, where adding a common ion may either increase or decrease the solubility.

The solubility of low molecular weight biological solutes depends on a variety of thermodynamic variables, which can be manipulated for an effective precipitation or crystallization process. Hence, solubility relationships should be understood for effective design and optimization of a recovery process. For example, a typical crystallization step might involve adjustment of pH to near the isoelectric point, the lowering of temperature to reduce solubility and minimize degradation, and the use of anti-solvents, specific ions, or evaporation to effect precipitation or crystallization. It should be apparent from the above discussion that many unanswered questions remain on the relationship of the solubility of a biological molecule to the relevant thermodynamic variables necessitating an experimental investigation during process research and development.

Given the limited data base from which solubility correlations can be drawn, it is essential to measure the solubility directly for the system of interest during process development. Since process conditions often favor operation with high concentrations of solute, such systems are often thermodynamically nonideal. It is necessary to measure the solubility in the solvent system(s) of interest in order to optimize the yield and the purity. To accomplish the latter relies upon the ability to measure the solubility of the *key impurities* as well as the product of interest. This requires the availability of both the key impurities and product; however, the impurities often are not available as isolated solids. In that case, the solubility of impurities must be deduced from the purity profile of mother liquors taken from crystallizations of the actual process stream. It is often simplest and always fastest to measure the solubility and carry out crystallizations in a single-solvent system. However, working in multiple-solvent systems increases the likelihood of improving the yield, the separation factor, and the prospects of observing more of the possible crystal forms that may exist.

Once the solubility is sufficiently defined, then the different operating modes should be considered. As mentioned earlier, there are three customary modes of carrying out a batch crystallization that uses a precipitating agent. The first mode is a “normal” addition of the crystallizing agent to the solution. The second is a “reverse” addition in which the solution is added to the precipitating agent. The third is a semi-continuous addition to blend a constant ratio of the solute solution and the crystallizing agent into a separate tank. These three modes define very different environments at which the crystallization occurs. In the normal mode, the concentration of solute is high throughout much of the crystallization, and the ratio of agent to solution is steadily increased to the final ratio. In the reverse mode, the concentration of solute is much lower, and the ratio of agent to solution is steadily decreased to the final ratio. Finally, the third mode is represented by a single ratio of agent to solution, and the concentration of solute drops from the concentration achieved by simply blending along a vertical line to the solubility at the constant ratio of agent to solution. This last mode is often referred to as “semi-continuous” crystallization. The different solvent environments can have an influence on the crystal morphology (Section 11.3.2), and the difference in solute concentration can be important if competing processes consume the solute (e.g., degradation).

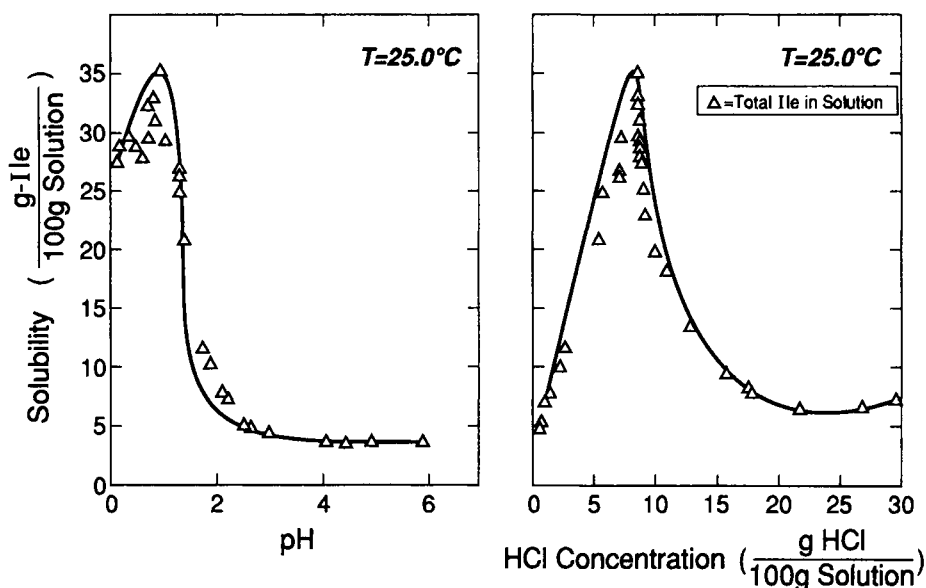


Figure 11.4 The Solubility of *L*-isoleucine as function of pH or HCl concentration. (Reprinted with permission from Zumstein, R.C., and Rousseau, R.W., *Ind. Eng. Chem. Res.*, 28, 1989, pp. 1226–1231. © 1989, American Chemical Society.)

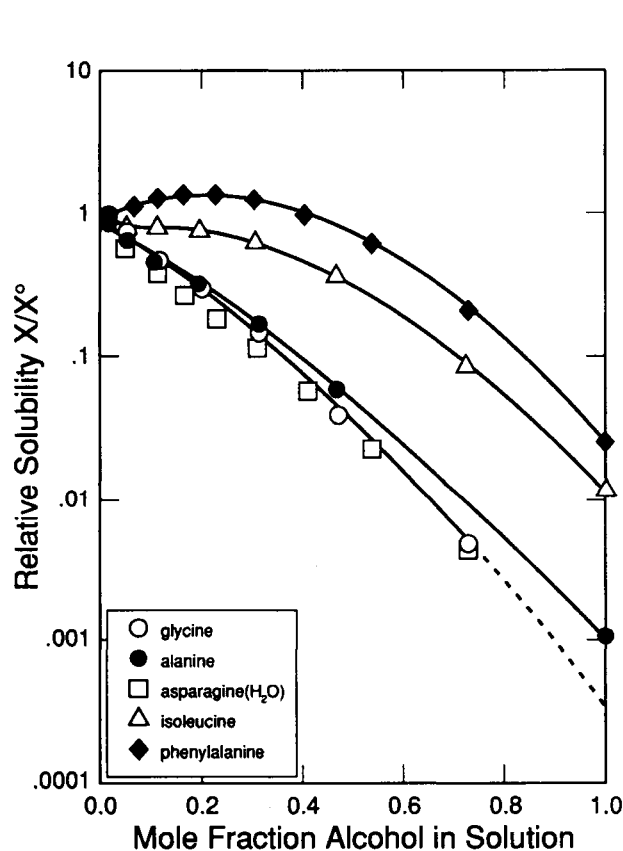


Figure 11.5 The solubility of various amino acids in aqueous *L*-propanol solutions. (Reprinted with permission of the American Institute of Chemical Engineers from Orella, C.J., and Kirwan, D.J., *Biotech. Progress* 5, pp. 89–93 (1989). © 1989. All rights reserved.)

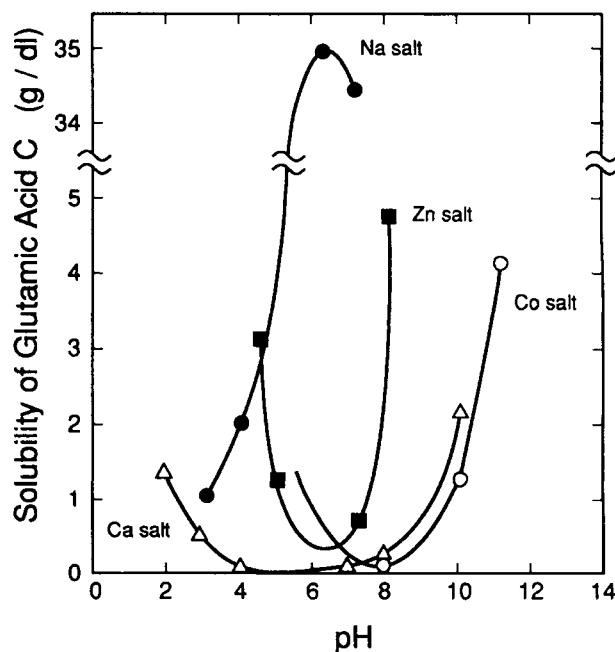


Figure 11.6 Solubilities of various metallic salts of *L*-glutamic acid. (Reprinted with permission of the publisher from Yamada, K. et al., *Microbial Production of Amino Acids*, J. Wiley, New York, 1972, p. 234.)

11.3. CONTROL OF PARTICLE SIZE AND MORPHOLOGY

Pharmaceutical products are usually subject to quite restrictive particle size and shape specifications. For final products, small (micron-size) particles with a narrow size distribution are desirable because of their short and uniform dissolution time and consequent good bio-availability. Similarly, particle shape influences

bio-availability as well as breakage and flow characteristics of the powder. Usually the simplest and preferred means of characterizing the particle size distribution is with a particle size analyzer (See Chapter 4) supplemented by microscopic examination. However, particle size is sometimes simply characterized by an adsorption area per gram measurement without a direct measurement of particle size and habit. Image analysis can be used to more fully characterize a distribution of particles. It has been common in the pharmaceutical industry to mill powders to a final desired size. This has a number of disadvantages: excessive local temperatures may degrade bio-active material and effective containment of fine powders of highly potent drugs can be costly to implement. For these reasons crystallization processes that can directly produce fine crystals of controlled small sizes are an area of active research and development. (See Section 11.5.2.)

As noted earlier, when crystallization is employed as a crude fractionation step earlier in the purification train, larger particles are desired to facilitate centrifugation or filtration of the slurries. Control of particle size during these crystallizations, therefore, is of great importance due to its influence on subsequent handling steps.

The basic principles of particle size control for the crystallization of pharmaceuticals are generally the same as those discussed in earlier chapters, that is, control of nucleation and growth rates with attention paid to agglomeration and breakage effects. The population balance approach permits incorporation of all of these factors. Our discussion here, therefore, focuses on these phenomena for biological solutes. Some complicating factors in crystallizing pharmaceutical molecules are: (1) the complexity of the molecules involved; (2) the need for very fine particles (high supersaturation conditions); and (3) the common use of batch crystallizers. The use of batch processes inherently results in crystallization under time-varying conditions and often under high (initial) supersaturations. The vessels may have poor mixing as well which causes spatial variations in supersaturation resulting in broader size distributions and variable quality.

11.3.1. CRYSTAL GROWTH KINETICS

Single-crystal and multi-particle intrinsic growth rates for biochemical compounds have only been measured in a relatively few instances. In general, similar techniques are used as are employed for inorganic compounds: observation of the change of size of single crystals growing under a microscope, measurement of the change in mass of single crystals over time; measurement of the PSD in an MSMPR crystallizer, or measurement of the de-supersaturation rate or PSD time evolution during batch crystallization. Of course, the influence of solution mass transfer on the rate must be experimentally eliminated or taken into account in interpreting the results.

Growth kinetics from solution often are represented by a power law model in supersaturation.

$$G = k_1[C - C^*]^p \quad (11.4)$$

For intrinsic growth kinetics C is the interfacial solution concentration of solute. The rate law may be expressed in terms of relative supersaturation, σ .

$$G = k_2\sigma^p \quad (11.5)$$

The relative supersaturation, $\sigma = (C - C^*)/C^*$, is proportional to the difference of the solute chemical potential between solution and crystal, $RT \ln(C/C^*)$, for small values of $(C - C^*)/C^*$ under the assumption of an ideal solution. For large supersaturation

ranges, as commonly occur in precipitation, the chemical potential difference is more appropriately used as the driving force.

$$G = k_3[RT \ln(C/C^*)]^p \quad (11.6)$$

For nonideal solutions, the concentration ratio in Eq. 11.6 is replaced with the ratio of thermodynamic activities. Since, for biological compounds, the equilibrium solubility, C^* , is affected by a number of thermodynamic factors (e.g., anti-solvent concentration, ionic strength, pH) studies of their effect on growth rate can be used to test the relative usefulness of Eq. 11.4 versus Eq. 11.5 or 11.6.

Orella (1990) made single crystal intrinsic growth rate measurements for a number of amino acids at their isoelectric points growing in aqueous and aqueous-propanol mixtures. Figure 11.7 presents some of his results showing power law model kinetics for *L*-asparagine growth from water and from 1- and 2-propanol aqueous mixtures. The high apparent kinetic order of nearly 3 for these systems suggests that the mechanism may involve two-dimensional nucleation (see Chapter 2). Comparison of Figures 11.7a-b illustrates the advantage of using the relative supersaturation as the driving force in the rate expression. The presence of alcohol reduces C^* by well over an order-of-magnitude in these cases. The use of relative supersaturation appears to provide a means of properly distinguishing the effect of variables on the kinetic coefficient and on the driving force. For this case, the alcohols appear to have little effect on the kinetic coefficient (Figure 11.7a). If the data were treated as in Figure 11.7b, one might (incorrectly) conclude that growth kinetics in alcohol mixtures are more rapid than in water. This formulation using $\square\square r$ the chemical potential expression at large supersaturations) should be useful in growth rate modeling of biological compounds where many thermodynamic variables may affect the equilibrium solubility and growth rate.

There have been a number studies of the growth kinetics of biochemicals in suspension crystallization. Rodriguez-Horneda et al. (1986) used an MSMPR crystallizer to obtain the growth rate kinetics for the drug, phenytoin, as a function of pH. They found the kinetics to be size-independent and to increase at lower pH. An MSMPR crystallizer study by Harano and Yamamoto (1982) determined the growth rate of glutamic acid from the measured size distribution.

A series of studies by Orella (1990), Mahajan et al. (1991), Mahajan and Kirwan (1994), and Deshpande (1998) compared the growth kinetics of asparagine monohydrate in mixed propanol-water solutions as measured for single crystals, in batch and MSMPR crystallizers, and with the use of a rapid (grid) mixer at very high supersaturations. Figure 11.8 demonstrates good agreement among these measurements considering that they were made by different investigators; that the suspension crystallizer environment was quite different from that for single crystal growth, i.e., the presence of collisions; and that the crystal sizes were different in each of these systems. Single crystals were 1.5–3 mm, crystals in the MSMPR crystallizer were 20–300 μm , crystals in the batch vessel were 20–80 μm and those from the rapid mixing device were 3–20 μm . The results suggest a slight size dependence of the growth kinetics.

A primary conclusion from the above results is that the standard methods for determining intrinsic crystal growth rates are well-suited for biochemical compounds. At present there are limited data on which to generalize with respect to growth mechanisms and the effects of various thermodynamic variables. Indeed, the large number of variables that may affect solubility and kinetics in these systems suggests that extensive and careful laboratory studies

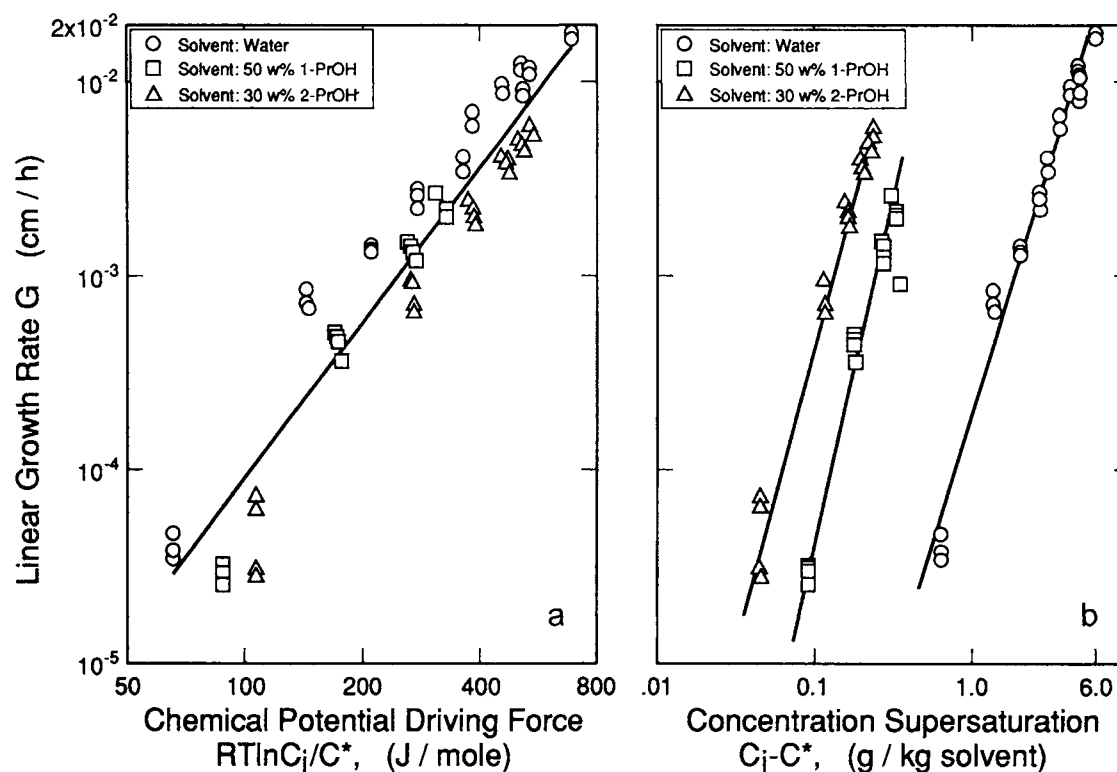


Figure 11.7 Single-crystal growth kinetics of *L*-asparagine in aqueous and aqueous-propanol solvents at 25°C (Data from Orella, 1990.)

should be conducted to understand and predict larger scale performance.

11.3.2. EFFECTS OF ADDITIVES, SOLVENTS, AND IMPURITIES

Chapter 3 of this text describes in detail the mechanisms and effects of various components of a solution on the resulting crystal size, morphology (habit), growth rate, and purity. Here we simply

relate some observations made on biochemical crystals. We consider the effects both of low concentrations of additives or impurities, particularly similar compounds commonly found in the process stream of a particular product, and of solvent (anti-solvent) present at relatively high concentrations.

Additives. Black et al. (1986) reported that small amounts of glutamic acid (mole fraction $<10^{-3}$) reduced the growth rate of asparagine from aqueous solution by a factor of 10. Harano and Yamamoto (1982) observed that small amounts of four other amino acids reduced the growth rate of glutamic acid in an MSMR crystallizer as well as having marked effects on crystal morphology. Differential kinetics (adsorption) on different crystallographic faces may explain the effect of additives or impurities on crystal habit or morphology. Since biochemical molecules contain a variety of chemical groups (Figure 11.1); it is clear that different chemical groups will exist on different crystal faces and will provide, therefore, a variety of possible interactions with solution components.

There has been a series of systematic studies of the effect of impurities and tailor-made additives on the shape of crystals grown from solution (Addadi et al. 1982; Berkovitch-Yellin 1985; Weissbuch et al. 1999.) They used amino acids and amino acid derivatives as model solutes. By combining habit observations with crystal structure and molecular orientation, they were able to rationalize a number of effects, including resolution of stereoisomers. Hopefully, further studies in this area will provide a rational basis for the many impurity and additive effects found during crystallization of biochemicals.

Solvent Effects. Changes of solvent, as in the use of alcohols as anti-solvents for precipitation from aqueous solution, may also influence particle shape through altering growth kinetics on

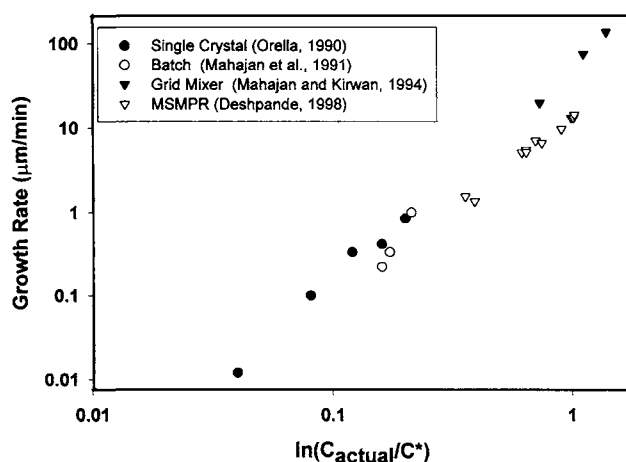


Figure 11.8 Comparison of growth kinetics of *L*-asparagine as single crystals, in batch and MSMR crystallizers and from a rapid mixing device. (Adapted from the data of Orella (1990), Mahajan et al. (1991), Mahajan and Kirwan (1994) and Deshpande (1998).)

different crystal faces. Solvent effects on a number of organic compounds, such as resorcinol, hexamethylene diamine and succinic acid, grown from solution were interpreted in terms of either a surface roughness effect or specific solvent adsorption on particular faces (Davey 1986; Bourne and Davey 1976; Davey et al. 1982).

Orella (1990) and Mahajan et al. (1991) did not observe any effect of solvent composition on the growth rate and habit of asparagine crystals grown from aqueous propanol solutions of varying composition. However, Orella (1990) found significant effects on alanine crystal growth and habit (see Figure 11.9.) As the propanol concentration increased from 0 to 35% by weight, the aspect ratio of the crystals changed from approximately 1 to well over 50! In fact, the growth rates in 35% propanol as compared to water were reduced in both directions but by a factor of about 10 in the axial direction and by a factor of 100 in the transverse direction.

A number of studies on prediction and control of crystal habit for pharmaceutical applications were presented in an AIChE Symposium Series (Ramanarayanan et al. 1991) and in the Proceedings of the 3rd International Workshop on Crystal Growth of Organic Materials (Myerson et al. 1996). Molecular modeling (computational chemistry) approaches are now quite extensively used to predict the effects of solvent and impurities on crystal morphology, often making use of the CERIUSTM programs. See, for example, the review papers by Docherty (1996) and Clydesdale et al. (1996), the papers by Green and Meehan (1996) on acetaminophen, and Jang and Myerson on succinic acid (1996) as well as the recent text edited by Myerson (1999).

11.3.3. NUCLEATION AND SEEDING

As described in Chapter 2, new crystals may be formed by primary nucleation (homogeneous and heterogeneous), secondary nucle-

ation in the presence of particles, or by the addition of seed crystals.

Nucleation. There is relatively little information available on nucleation rates of biochemicals from solution, yet the control of nucleation rates controls the number of particles produced and has a direct bearing on crystal size for a given yield of crystallizing product. Uncontrolled nucleation either heterogeneously from contaminants or as secondary particles produced from existing crystals can greatly affect the desired size distributions. The general principles of nucleation theory as discussed in Chapter 2 apply to biochemical systems.

Primary homogeneous nucleation is a particularly important mechanism when anti-solvent addition is used to produce high supersaturations in order to produce fine particles. Such systems often encounter mixing problems that influence the resulting size distributions. At the process scale, impinging jet mixing is being explored to overcome this (see Section 11.5.2.) At the laboratory scale, homogeneous nucleation rates or nucleation induction times (time after mixing before measurable particles can be observed) can be measured by employing a rapid mixing device, such as a grid mixer, to produce a uniform environment very quickly (milliseconds) before nucleation has occurred (Mahajan and Kirwan 1994). Figure 11.10 gives an example of such results. The nucleation induction time for lovastatin when precipitated from methanol by water is shown as a function of supersaturation. The graph is plotted according to the expected theoretical dependence of nucleation rate on supersaturation as discussed in Chapter 2, i.e., $\ln B$ versus $1/S^2$. The results obey the classical theory very well. The steeper slope at higher supersaturations corresponds to homogeneous nucleation and the lower slope to a heterogeneous nucleation mechanism. This same grid mixing device can be used to measure growth kinetics by following the time evolution of the

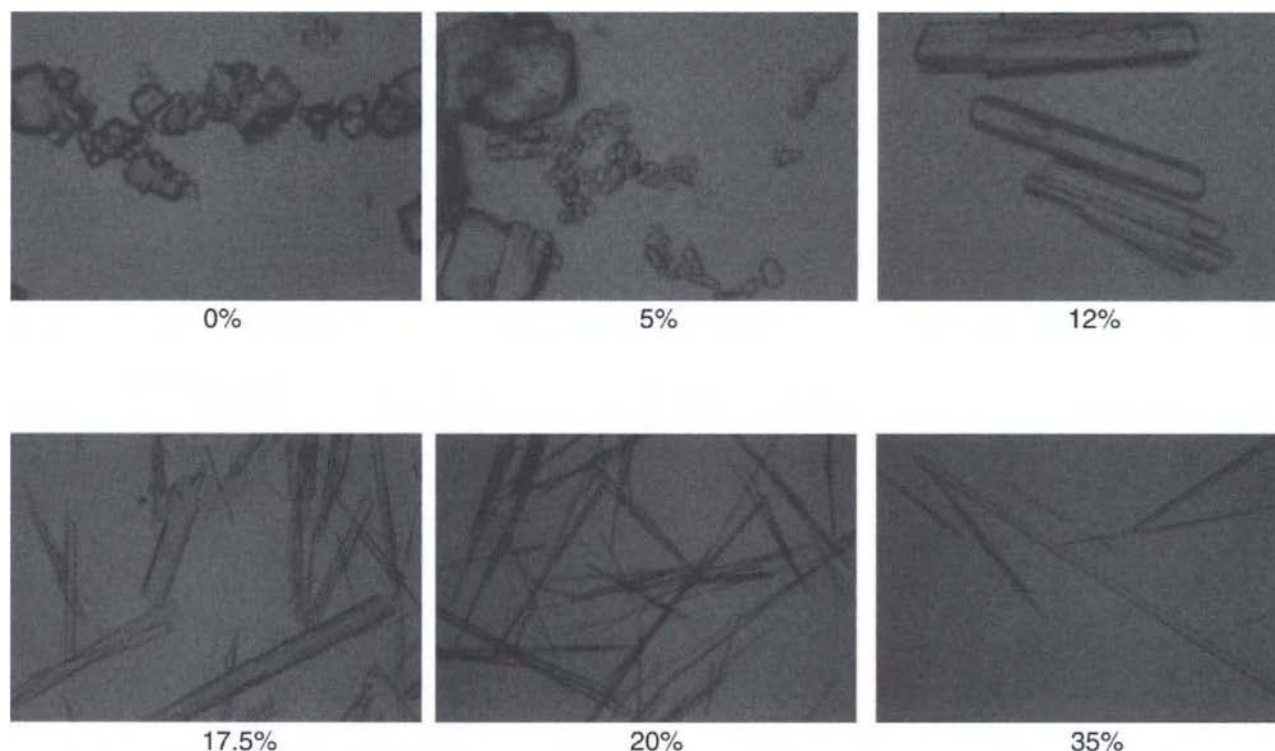


Figure 11.9 Effect of isopropanol concentration on the habit of *L*-alanine crystals. (Data from Orella 1990.)

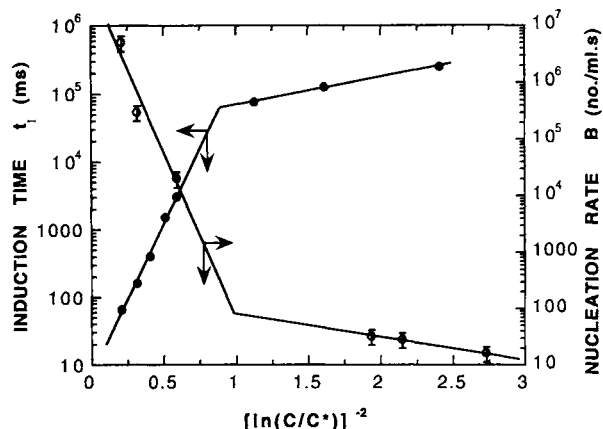


Figure 11.10 Rate and induction time for the nucleation of lovastatin from methanol at 25°C plotted according to Classical Nucleation Theory. (Reprinted from Mahajan, A.J., and Kirwan, D.J., *J. Crystal Growth* **144**, pp. 281–286. © 1994 with permission from Elsevier Science.)

crystal size distribution in an observation tube after mixing (Mahajan and Kirwan 1994).

A study of the primary and secondary nucleation of *L*-glutamic acid including the effects of agitation and additives such as aspartic acid was conducted by Black and Davey (1988). Mahajan et al. (1991) in their study of the batch precipitation of *L*-asparagine with propanol were able to obtain nucleation rates from observed size distributions such as that shown in Figure 11.11. The flattening of the distributions at longer times is due to agglomeration—another complicating factor in suspension crystallization. As long as the agglomeration was not extensive (as was true at shorter times), nucleation rates could be extracted from the data. The nucleation rates were proportional to the suspension density in the crystallizer and to a high power of the supersaturation suggesting that secondary nucleation was of importance (Figure 11.12). Further, the results in Figure 11.12 suggest that use of a

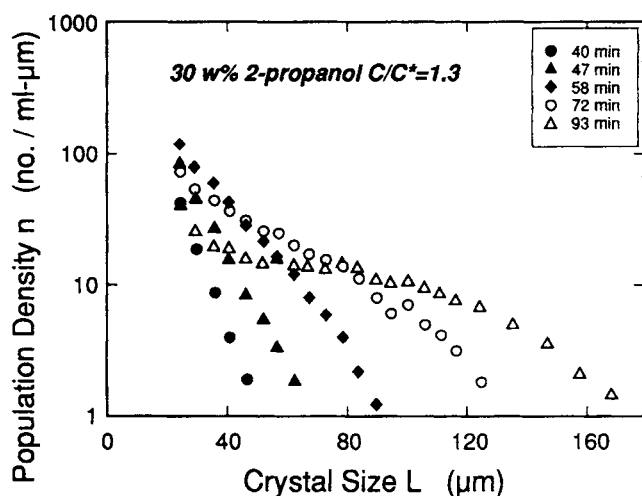


Figure 11.11 Population density plot for the batch precipitation of *L*-asparagine with isopropanol. (Reprinted with permission of the American Institute of Chemical Engineers from Mahajan et al., *AIChE Symp. Ser.* **87**, (284), pp. 143–153 (1991). © 1991. All rights reserved.)

driving force proportional to chemical potential difference can bring together nucleation rates of a given solute in different solvent systems. As in the case of growth kinetics only limited data are available in support of this hypothesis.

Very little work has been done on nucleation rate expressions under high supersaturations, on the nature of the solids formed during rapid nucleation (which may be nonequilibrium and/or amorphous phases), or on the relative nucleation rates of polymorphs or optical isomers. Devices to achieve high supersaturations such as jet mixers or supercritical fluid precipitators must be designed properly to achieve rapid mixing and uniform crystallization conditions. Research in these areas will facilitate production of fine particles of desired crystallinity and morphology.

Seeding. Seeding is a common practice in many batch crystallizations in an attempt to control particle size uniformity. However, it is limited by the ability to produce seeds of the proper crystal structure having an appropriately narrow size distribution

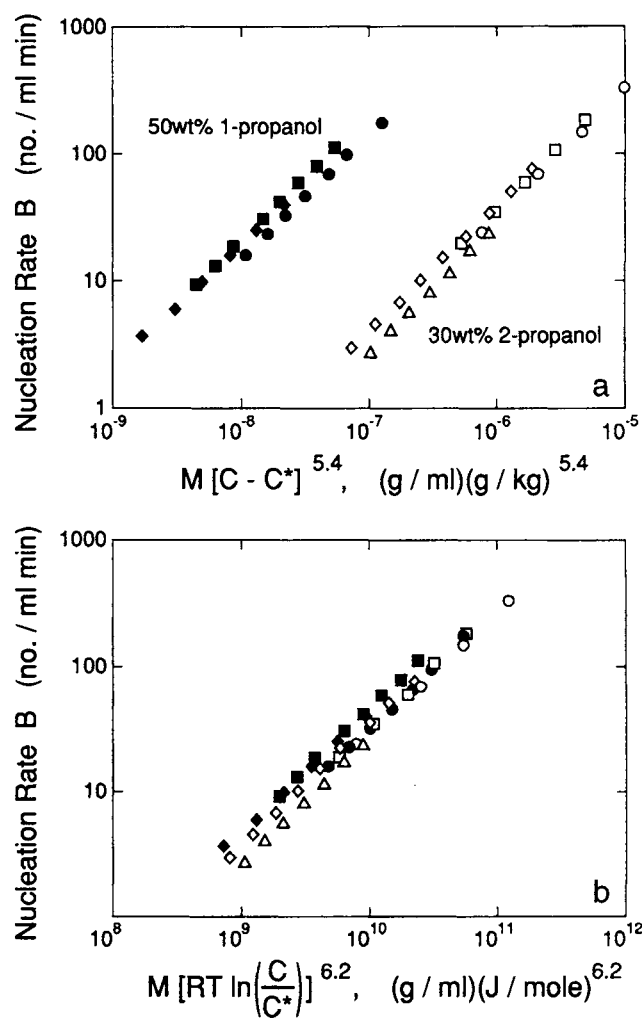


Figure 11.12 Nucleation rates of *L*-asparagine in 1- and 2-propanol as a function of slurry density and (a) supersaturation or (b) chemical potential. (Reprinted with permission of the American Institute of Chemical Engineers from Mahajan et al., *AIChE Symp. Ser.* **87**, (284), pp. 143–153 (1991). © 1991. All rights reserved.)

in the proper size range. This can be especially difficult if very small sizes are required.

If seeds with a particular size distribution (number distribution) are introduced, at time zero, into a batch crystallizer (without crystals initially present), then the PSD at later times is described using the population balance equation (Randolph and Larsen 1988, or Chapter 4 of this book) where it has been assumed no breakage or agglomeration occurs.

$$\frac{\partial n}{\partial t} + \frac{\partial}{\partial L}[Gn] = 0 \quad (11.7)$$

The initial distribution $n(0, L)$ is simply that of the seeds. If conditions are such that no further nucleation occurs, then the particle size distribution is well-defined provided the growth rate, G , is known as a function of supersaturation and that the loss of supersaturation by crystallization is taken into account. In a batch crystallization using cooling and/or the addition of precipitating agents, Eq. 11.7 would be solved simultaneously with an energy balance, material balances for dissolved solute and anti-solvent, and appropriate rate expressions as described in Chapters 4 and 10. If the supersaturation and mixing conditions are such that additional nucleation occurs or, if there is size dependent growth, then broadening of the distribution will occur.

The practical benefit to evaluating the number of seed particles charged is very important. The simplest assumption is that little nucleation takes place during the crystallization. If true, then to achieve a PSD with a narrow distribution around a size L , it is best to always charge seed with a narrow PSD. The amount of seed desired should be such that it provides the appropriate number of particles so that, when grown, they will represent the proper mass and average size of product crystals. For example, to crystallize 1 kg of solid mass onto cubic particles of average size 1 mm with density 1000 kg/m³, a million seed particles would be required.

$$\begin{aligned} N_p &= \frac{M_c}{\rho d_p^3} \\ &= \frac{1 \text{ kg}}{(1000 \text{ kg/m}^3)(0.001 \text{ m})^3} \\ &= 1,000,000 \end{aligned}$$

If the seed's mean particle size is known and the distribution is narrow, the required mass of seed is readily calculated. In this example, 1 g of seed would be required if the seed size were 0.1 mm, or 0.125 g if the average seed size were 0.05 mm. Note that the surface area available for growth is different in each of these cases, since the area is proportional to the square of the seed size or second moment of the number distribution. For the case of seed of 0.1 mm size, the total surface area of seed charged is 0.06 m² assuming that there are six faces on the cubic crystals. For the case of the 0.05 mm seed, the total surface area of the seed charged is 0.015 m². Thus, the rate of crystallization will be different for these two cases. The use of the smaller seed will give the desired number of particles, but if the supersaturation were increased too rapidly, the smaller growth area will result in hindered growth and slower relief of supersaturation. This in turn may lead to nucleation. This very simple case demonstrates that the size and mass of seed charged should be expected to influence both the ultimate particle size and the rate of crystallization. This latter factor is often overlooked, but it can have a profound impact on the growth rate when a seed charge with insufficient surface area is used.

Because small final crystal sizes are often desired for pharmaceuticals, seeds must be very small (microns) and often are pro-

duced by milling. The resulting crystals may generate very fine secondary nuclei or fragments resulting in a broader (and bimodal) distribution than anticipated. The desire to avoid some of these difficulties has prompted the investigation of continuous anti-solvent, impinging jet precipitation and supercritical precipitation which operate at very high supersaturations.

A particularly interesting use of seeds is in the resolution of the isomers of methy l-dopa as practiced by Merck & Co., Inc. In this process two fluidized beds operate in tandem, each of which is seeded with one of the optical isomers. Supersaturation is controlled to minimize nucleation so that growth of each isomer occurs on the existing crystals in their respective beds (see Section 11.5.1.)

11.4. THE PURITY OF BIOCHEMICALS PRODUCED BY CRYSTALLIZATION

As has been discussed throughout this book, crystallization can generally result in very large purification factors as well as being useful as a concentration step that removes most of the solvent from the desired solute. Impurities within crystals that limit purification efficiency arise from:

1. Occluded solution (solvent and dissolved solutes).
2. Direct incorporation into the lattice structure (solid-solution formation) and surface adsorption.
3. Co-precipitates (intimately mixed-physical mixtures).

Quantitative and even qualitative information on impurity incorporation in pharmaceutical crystals is quite limited in the open literature, but the general trends are expected to follow the behaviors described in Chapter 3. Given that the molecular size of most biological compounds are larger than inorganic substances the resulting crystal structures are rather more open and better able to accommodate "interstitial" impurities including solvent.

11.4.1. SOLVENT OCCLUSION

Occlusion of solution in crystals is generally thought to arise from growth conditions leading to unstable crystal faces and dendritic growth resulting in solvent entrapment (Edie and Kirwan 1973; Myerson and Kirwan 1977a,b; Slaminko and Myerson 1981). As such, it is generally found to increase with increased crystal growth rates, poorer solution transport, and increased crystal size. Solvent occlusion results in increased drying costs and difficulties in crystal handling. Further, when organic nonsolvents that have some toxicity are used to precipitate pharmaceuticals then entrapment of solvent in the crystal has serious implications for the final product acceptability. For example, care must be taken that when amino acids for intravenous fluids use are recovered by alcohol precipitation they do not contain traces of alcohol. It also should be realized that it is the solution, with its dissolved impurities, that is entrapped rather than just solvent. Although solvent can be removed by drying, nonvolatile impurities will remain.

Unpublished studies at the University of Virginia, using the precipitation of *L*-proline (a very hydrophilic amino acid) from aqueous solutions by 2-propanol, yielded some interesting results. Microscopic examinations of crystals obtained by batch precipitation clearly showed regular, conical-shaped occlusions in the crystals (Figure 11.13). Generally the crystals were found to contain a few percent solvent with a higher ratio of water to isopropanol than in was in the mother liquor. This "enrichment" may be due to the fact that proline is very hygroscopic. In a related study, we examined the effect of the isopropanol addition mode during semi-batch crystallization on the degree of solvent occlusion. We com-

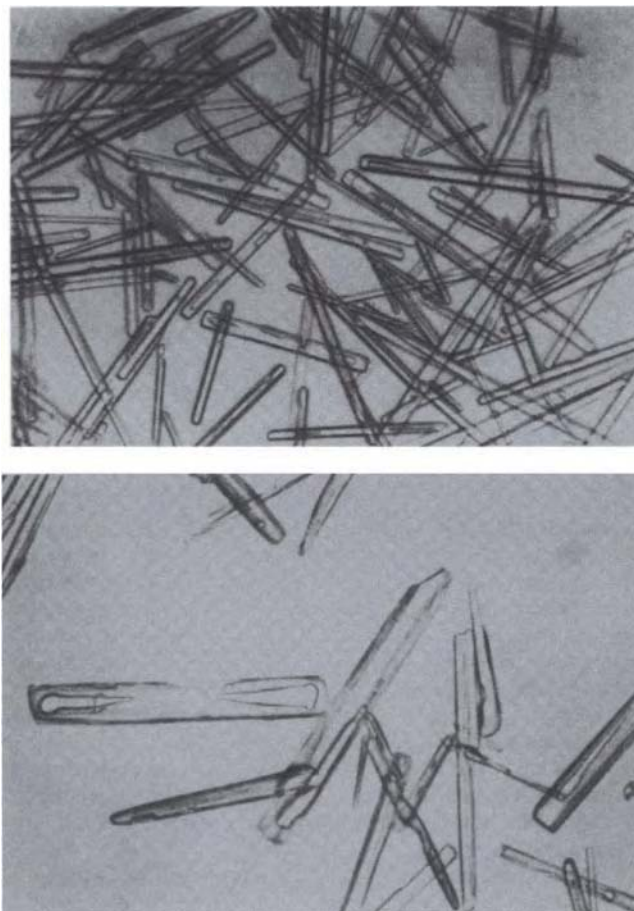


Figure 11.13 Occlusions in proline crystals precipitated from aqueous solution with isopropanol.

pared the effects of the addition of alcohol to a nearly saturated aqueous proline solution to that of the addition of the saturated aqueous solution to isopropanol. For both addition modes it was found that similar amounts of solvent were entrapped. This was a somewhat surprising result in that a more rapid crystallization would be expected with solution addition to propanol with correspondingly greater solvent occlusion.

Charmolue and Rousseau (1990) studied solvent entrapment during batch precipitation of the amino acid, *L*-serine, by methanol addition. In their study, residual methanol was measured in the crystals after drying. Presumably, this would also be a measure of occluded solvent. The protocol involved cooling a batch at a fixed rate and at a particular agitation speed and then adding methanol at a particular rate when the temperature reached 10°C. They examined the effect of these three variables on the methanol content of the dried crystals. Methanol levels ranged from 700 to 1400 ppm and were minimized at an intermediate agitation rate, which the authors associated with minimum crystal agglomeration and crystal breakage. Higher cooling rates or higher methanol addition rates only slightly increased impurity content. They also found that an intermediate crystal size seemed to correlate with minimum solvent levels in the crystals. Figure 11.14 reproduced from their paper summarizes the interacting effects of some of these variables. These authors also observed that higher supersaturations produced by large ratios of methanol to solution resulted in needle-like crystals. This observation is similar to that

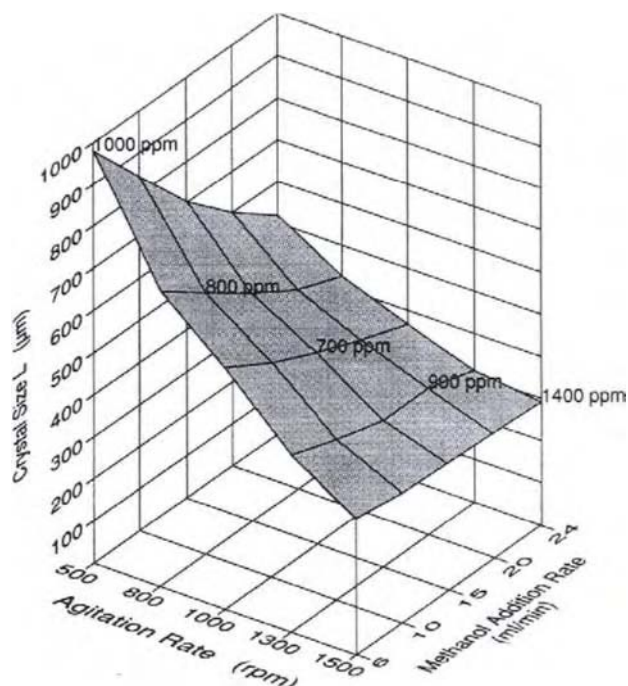


Figure 11.14 Effect of operating variables on impurities in serine precipitated by methanol. (Reprinted with permission from the American Institute of Chemical Engineers from Charmolue, H. and Rousseau, R.W., *AIChE J.* 37, pp. 1121–1128 (1991). © 1991. All rights reserved.)

shown in Figure 11.9 for alanine crystallization with isopropanol. In this case, however, the change in morphology was due to a change from a monohydrate to an anhydrous crystal. The needle-like crystals entrapped much more solvent and had a detrimental effect on the ability to remove solvent from crystals in processing.

Additional work on the fundamental mechanisms of occlusion formation under various crystallization conditions is needed. The interactions of mixing and addition rates with rates of nucleation and growth, and with interfacial stability need further elucidation.

11.4.2. INCORPORATION OF SOLUTE IMPURITIES

The earlier discussion on the effects of additives or impurities on crystal growth (Section 11.3.2) suggests that impurity incorporation is often surface specific. Black and Davey (1988) have reviewed much of the available information on the crystallization of amino acids. Amino acids are interesting model systems because of their common zwitterion group coupled with a variety of side chains, which may be present on a particular crystal face. *L*-asparagine can accommodate some 15% of *L*-aspartic acid as a mixed crystal (solid solution). From the effects of aspartic acid on the habit of asparagine crystals it is believed that aspartic acid primarily is incorporated at the 010 face whose growth rate is considerably reduced.

The fact that impurities can be incorporated by growth on a particular face is exploited in doping of organic materials for electronic use. For example, triglycine sulfate crystals are doped throughout the lattice with alanine by growth only on the 010 face held in a crystal holder (White et al. 1976). A number of amino acids (*L*-aspartic, *L*-valine, *L*-leucine and *L*-phenylalanine) have been observed to be incorporated into the lattice of glutamic acid

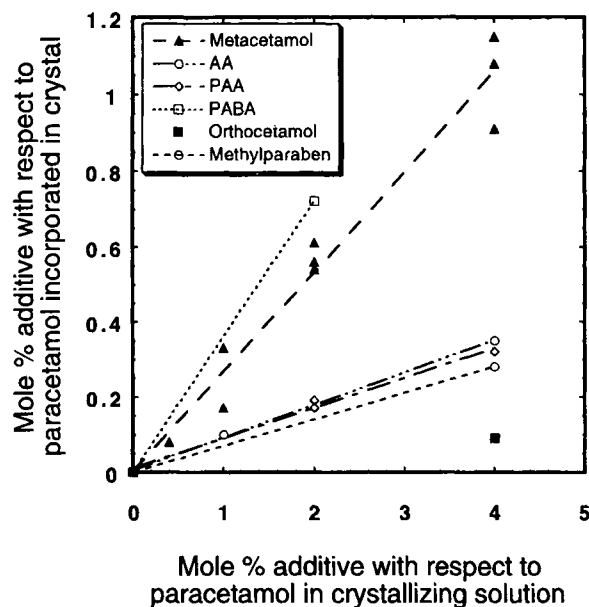


Figure 11.15 Uptake of impurities by paracetamol crystals. (Reprinted with permission from Hendricksen, B.A., Grant, D.J. W., Meehan, P., and Green, D.A., In *Crystal Growth of Organic Materials*, ACS Conf. Proc. Series, Myerson, A.S., Green, D.A., Meehan, P. eds., pp. 95–104 (1996). © 1996. American Chemical Society.)

crystals growing in an agitated crystallizer to concentration levels of up to 1% (Harano and Yamamoto 1982). The impurity distribution coefficient between crystal and solution was about 0.1. The impurities typically dramatically inhibited growth and altered habit. In a single crystal study of the effect of glutamic acid on *L*-asparagine growth, it was found that about 3% glutamic acid was incorporated into the crystal from a solution containing about 0.1% glutamic acid (distribution coefficient >10). Glutamic acid reduced growth on the 101 face of asparagine to zero and reduced 012 face growth by about 70% (Black et al. 1986).

Hendrickson et al. (1996) examined the effect of structurally-related substances on the nucleation and growth of paracetamol (acetaminophen) and the incorporation of such substances into the crystal. Each impurity had a constant segregation coefficient over the composition ranges studied (Figure 11.15). They used molecular modeling of the various crystal faces of paracetamol to account for differences in growth inhibition, habit modification, and the segregation coefficients of various impurities. Some impurities were taken up by the crystal without affecting habit and growth, e.g., methylparaben, while others were taken up and inhibited growth (e.g., metacetamol).

These few examples indicate the importance of understanding the molecular and crystal structure of a given system to understand impurity incorporation and habit modification in the crystallization of these complex molecules.

11.4.3. CO-CRYSTALLIZATION OF SOLUTES AND POLYMORPHS

When a mixture of solutes exists in a solution under supersaturation conditions (as depicted in Figure 11.16), then the solid product formed may be a physical mixture of more than one species if operation occurs in region B of the diagram. In addition to process impurities, such a situation can arise when one has a mixture of optical isomers in solution, a mixture of different solvates or

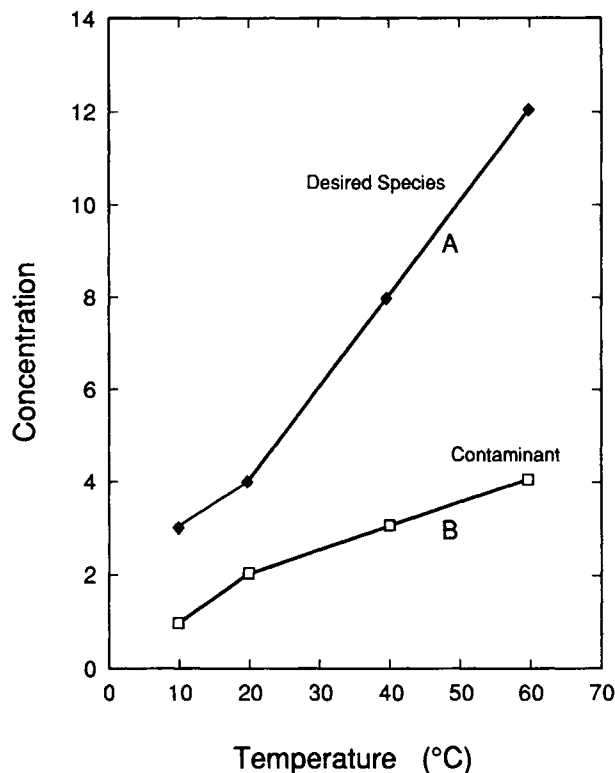


Figure 11.16 Co-crystallization can occur when a number of species exist under supersaturated conditions (Region B of diagram).

hydrates, or multiple polymorphic forms (different crystal structures of the identical molecule).

Polymorphs are a particularly important class of problems in pharmaceutical processing not only from a purity standpoint, but also from the standpoint of producing a well-defined product approved by regulatory agencies. Different polymorphs will have different thermodynamic properties including solubility; and, therefore, they represent different final products. In a supersaturated solution, often a less stable polymorph will first crystallize. Later it may (slowly) transform into the more stable form, that is, the processes are often kinetically rather than thermodynamically controlled. Both solution-mediated and solid phase transformations are known (Cardewa and Davey 1985; Kitamura 1989; Sata et al. 1984, 1985). Thus, the designer needs a knowledge of solubility relations and the possible crystalline forms (hydrates, solvates and polymorphs) to choose appropriate operating conditions for the crystallization operation. Given that the presence of other solutes or anti-solvents, the pH and other crystallization conditions can greatly alter solubility, nucleation and growth rates, and crystal habit (Kitamura et al. 1996, Kagara et al. 1996); it is a complex challenge to understand and control crystallization in these systems.

11.4.4. IMPROVING PURITY BY CHANGE OF CRYSTAL FORM

We have seen in previous sections that complex organic molecules have a tendency to form polymorphs. In addition, the solubility behavior is dependent on the counter-ion of a salt and on the solvent composition when anti-solvent is used to drive the crystallization. Changes in these variables, therefore, have the potential

to cause different purification behavior because they alter the crystal form. As a result, it is often advantageous to investigate the phase behavior even if a crystallization procedure is already available. For example, it was noted in Section 11.2 that citric acid forms either a monohydrate or anhydrous crystalline phase depending upon temperature. This is common for many low molecular weight pharmaceuticals that form solvates and anhydrous forms. Such changes in crystals can have dramatic effects on chemical stability and handling characteristics. For example, the effect of solvent on the morphology of alanine crystals (Figure 11.9) would significantly change the filtration rates of the crystals. There is no best method to examine the solution chemistry of a new crystallization system. However, alternative solvents and anti-solvents and temperature should be examined for possible advantageous exploitation. Investigation of different solvent systems is more likely to lead to crystallization of more of the system's possible crystal forms.

When crystallization is carried out in an aqueous system, it is sometimes possible to crystallize various salts of the compound with a change in ion content. This may result in very significant changes in solubility although, at present, there is no way to predict these effects. The impact of various cationic counter-ions on glutamic acid solubility was noted in Section 11.2. Leugo (1985) reported similar behavior for penicillin recovery. The addition of ammonium sulfate to solution or to filtered fermentation broth would cause the precipitation of the ammonium salt of penicillin G, V, K or F; but 6-aminopenicillanic, a related compound typically difficult to separate, was not crystallized. Similarly, Glaxo (Wall 1988) patented a method for purifying vancomycins by complexing the antibiotic with imidazole. The complex then precipitates, but complexation and precipitation greatly improve selectivity.

These principles also apply to special cases of purification including chiral separations, particularly important in the pharmaceutical industry (see Section 11.5.) Phan (1999) has recently patented an improvement for the purification of certain, profen class of carboxylic acids including naproxin, an analgesic (pain reliever) and a nonsteroidal anti-inflammatory drug. The general structure of naproxin is $R_1R_2R_3\text{CCOOH}$. He found that recrystallization of alkali or amine salts of naproxin with mineral acids such as sulfuric acid will reproducibly increase the purity of the S-enantiomer. By a process of extraction of naproxin solutions with a base such as sodium hydroxide to form a starting solution for the crystallization, Phan claims purification to better than 99% S-enantiomer when starting from solutions of at least 82% purity. Although not presented in the patent, the phase behavior of the salt form of the carboxylic acid must have a much lower eutectic composition than does the acid, making purity enhancement favorable at lower purities. (Section 11.5.)

11.5. APPLICATIONS OF CRYSTALLIZATION IN THE PHARMACEUTICAL INDUSTRY

The implementation of crystallization in the pharmaceutical industry has traditionally been as a batch operation. In most cases, these batch operations can be successfully used to provide economic and consistent purification. Generally, successful scaling involves maintaining the same supersaturation history at small and large scales. Owing in part to the impact of constraints by regulatory agencies, it is necessary to maintain a high degree of consistency and control of each manufacturing step as explained in greater detail by Paul and Rosas (1990). While batch is still the most common crystallization mode, semi-continuous and continuous crystallizers can provide more easily achievable consistent perform-

ance throughout scale-up. This easier scale comes at the expense of greater equipment requirements and costs.

Control of crystallization operations in pharmaceutical manufacturing requires good control of purity, PSD, and morphology. In this it mirrors discussions in earlier chapters. First, it relies on sufficient knowledge of the solubility. Second, it requires good control of supersaturation through seeding and equipment designed with proper mixing to ensure the desired ratio of nucleation to growth. This control helps to avoid problems discussed earlier such as inclusion of impurities, the co-crystallization of similar substances, or the tendency of organic molecules to "oil out" (appear as a liquid phase) from a supersaturated solution. In the remainder of this section, several examples will be described to illustrate recurring problems and their solutions in the use of crystallization in the pharmaceutical industry.

11.5.1. THE SEPARATION OF OPTICAL ISOMERS

One problem with a special emphasis in the pharmaceutical industry involves the isolation of stereoisomers (optical isomers). An organic molecule with no asymmetric carbon atoms is denoted as achiral, but if it contains one or more asymmetric carbon atoms, it would be denoted as a stereoisomer. If a single asymmetric carbon exists, there will be two enantiomers, while with two asymmetric carbon atoms the molecule forms four diastereomers. A reader not familiar with the general concept of stereochemistry should refer to a introductory organic chemistry text. Biological systems are inherently based on enantiomeric or stereoisomeric biochemistry. Thus, there has been a trend toward selecting a single stereoisomer as a new chemical entity for pharmaceuticals (Collins et al. 1997; Stinson 1999).

In practice, there are multiple methods for creating and isolating a stereoisomer, which may apply to the system of interest. It may be possible to synthesize the molecule with chiral chemistry or to use chiral-inducing enzymatic chemistry. It is often possible to separate stereoisomers by chromatography, and it is sometimes possible to crystallize stereoisomers.

The history of the crystallization of stereoisomers is fascinating. Pasteur noted the visible difference in morphology between crystals of the isomers of ammonium sodium tartrate in 1848. This turned out to be a fortuitous circumstance as ammonium sodium tartrate happens to crystallize as "conglomerate crystals," that is, a eutectic mixture containing crystals of the two pure isomers. Such behavior has since been found to be infrequent, although it has proved industrially important. Pasteur separated the crystals manually to achieve the first documented isomeric separation!

The second important observation on stereoisomer separation also involved ammonium sodium tartrate. Thirty-four years after Pasteur's observation, Jungfleisch (1882) observed that carefully introducing crystals of the individual isomers into different areas of a supersaturated solution of ammonium sodium tartrate resulted in the growth of isomerically pure crystals. These two observations form the basis for most industrial scale crystallizations for the purification of enantiomers or diastereoisomers. However, it is more common for a solute to crystallize with the thermodynamically stable crystal form being a compound of the two isomers. This is typically denoted as a racemic compound. Secor (1963) made the first systematic review of optical isomer separation by crystallization, based upon phase behavior. Collet, Brienne, and Jacques (1980) applied systematic thermodynamics to the phase behavior, and developed straightforward methods for correlating the solubilities of isomers.

Before proceeding, we first review the thermodynamics that apply to stereoisomers. The isomers have the same chemical

formula, differing only in their absolute configuration which impacts the way that such molecules rotate light. The rotation of light originally formed the basis for discriminating among different isomers, giving rise to both a naming convention and a method of quantifying the observation. The naming convention, based on the rotation of light being positive (+) or negative (−), led to the *l*- and *d*-notation system. That has since been replaced by nomenclature based on the absolute configuration at the atomic level, known as the *R*- and *S*-system. Since the isomers are chemically equivalent in all ways but configuration, they have identical physical properties: heats of reaction, specific heats, boiling points, melting points, etc. Since the isomers have identical melting points and heats of fusion, they exhibit solubility behavior that mimics that of the isomeric opposite. In other words, the phase diagram for such a pair will be symmetric. Figure 11.17 illustrates this for the simplest case of two enantiomers crystallizing from the binary melt. Figure 11.17a represents the typical phase behavior of a conglomerate with a eutectic point at E. In Figure 11.17a the point at which the two melting curves intersect at the eutectic represents the lowest melting point in the system. Since the solubility curves of the two isomers must be symmetric, the eutectic occurs at an equimolar composition of the *R* and *S* isomers. In chiral chemistry, this also corresponds to the “racemic” composition. Crystals of the pure isomers will be thermodynamically stable, and crystallization from

any solution composition should yield improved purity of one of the enantiomeric solids.

In Figure 11.17b the melting point curves have a temperature maximum corresponding to the two enantiomers forming a racemic compound. Due to the two enantiomers sharing the same physical properties of melting temperature and heat of fusion, the compound will occur at an equimolar composition. The compositions of the two eutectics between the pure isomers and the compound will be symmetrical. For example, the eutectics might occur at ratios of *R*:*S* of 10:90 and 90:10. For crystallizations carried out with solution compositions between the two eutectics compositions, the racemic compound will be the solid phase formed. Outside of this region equilibrium occurs between crystals of one of the pure isomers and a solution. In these regions, purification of the respective isomers can be achieved, but the extent of purification depends very strongly on the composition of the eutectic. An illustration of this dependence will be given later. If crystallization is continued, the solution composition approaches that of the eutectic at which point the solid will contain a mixture of crystals of the compound and pure isomer.

In most practical situations the isomers will be dissolved in at least one solvent, meaning that analysis of a ternary system is required. The concepts are similar to those discussed above for binary systems. Jacques et al. (1994) provides an excellent description of ternary cases, and review much of the published literature on chiral separations.

Practical separation methods fall into two categories. First, when the phase behavior is as shown in Figure 11.17a, crystallization is usually carried out at low supersaturation in a method known historically as the “method of resolution.” In less common cases, a single isomer can be crystallized without crystallization of the second isomer despite reaching high supersaturation of the second. For cases where the phase diagram is not favorable for the formation of pure enantiomers (Figure 11.17b), then chemical treatment or an alternate separation approach is required unless starting with a feedstock that is already quite high in purity (e.g., purer than the eutectic composition). Chemical treatments include enzymatic treatment or chiral-inducing chemistry. Alternate separations include chromatography, and diastereomeric separation, wherein a salt is formed using a chiral auxiliary.

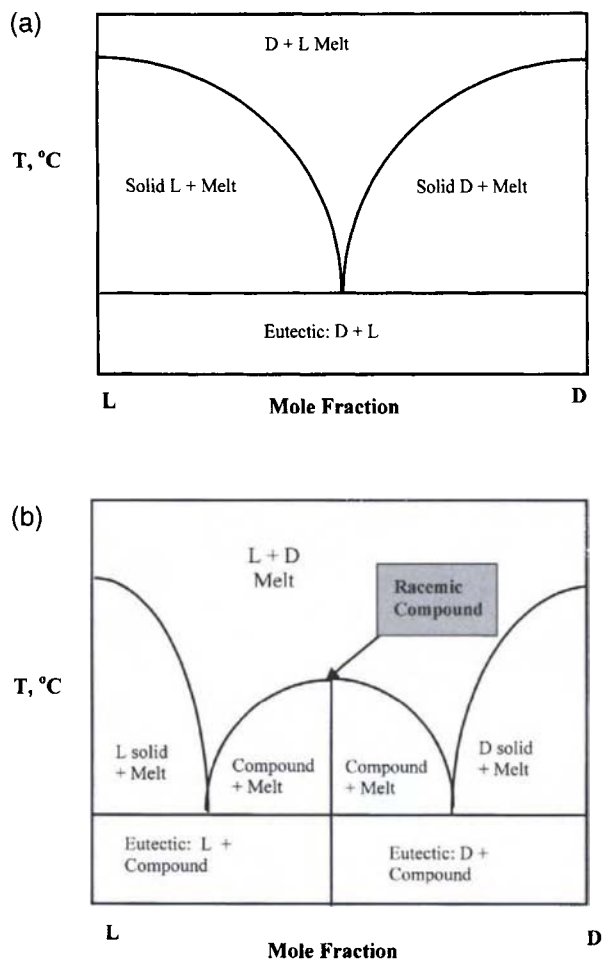


Figure 11.17 Phase diagrams for optical isomers that form (a) eutectic or (b) racemic compounds.

Methyldopa. An example of a mixture with favorable solubility behavior is found in the crystallization of *l*-methyldopa. Methyldopa is used as an antihypertensive agent, although only the *levo* rotary enantiomer is active biologically. Thus, in developing a manufacturing process to produce enantiomerically pure *l*-methyldopa, crystallization emerged as a practical step for the separation of the *l*- and *d*-enantiomers. The selective crystallization of the *l*-enantiomer can be accomplished by seeding a supersaturated racemic mixture (i.e., both *l*- and *d*-enantiomers present and supersaturated) with crystals of pure *l*-methyldopa. Due to steric differences, the *d*-enantiomer remains in solution while the *l*-methyldopa crystallizes on the existing seed bed; that is, the *d*-isomer does not nucleate either homogeneously or heterogeneously on the *l*- seeds. The crystallization of the compound is carried out in an aqueous system using buffer to increase the solubility and achieve a more productive process (Krieger et al. 1968; Chilton 1965). Later, a continuous crystallization system (Midler 1970, 1975, 1976) was developed that employed two fluidized bed crystallizers (FBC) that were operated at very low supersaturation to prevent nucleation. A schematic representation of the crystallization operation is presented in Figure 11.18.

The design has several unique features that make it well suited to resolution of optical isomers. First, as already mentioned, the system is operated with an established seedbed at low supersaturation,

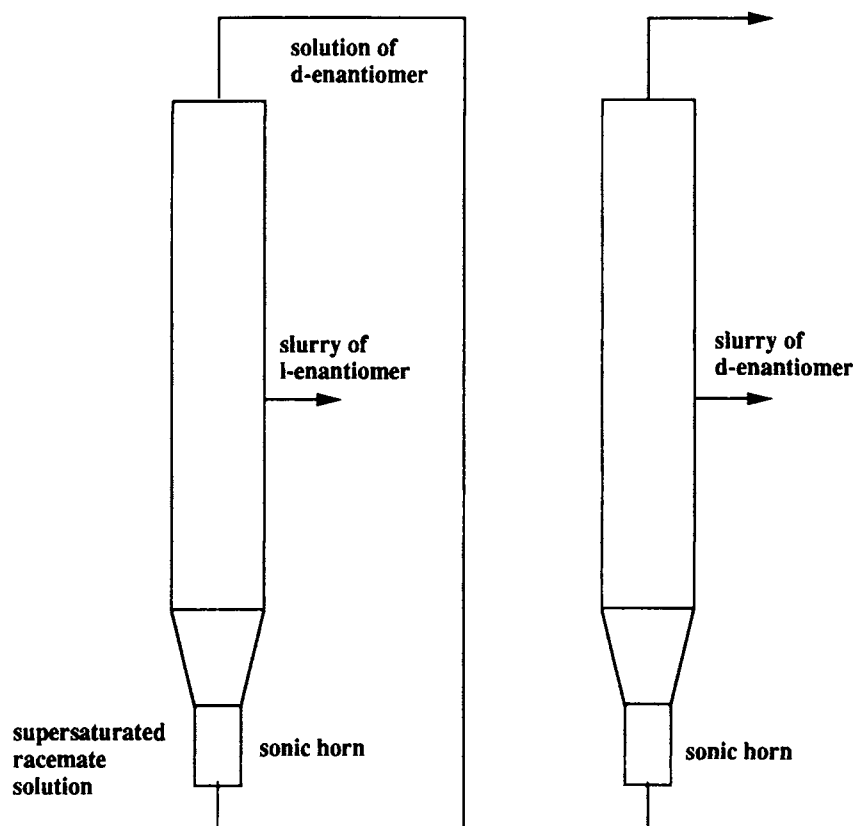


Figure 11.18 Schematic of two-fluid bed crystallizer for isomer separation.

which eliminates nucleation of any new particles, and minimizes the occlusion of solution that could entrap the undesired enantiomer. Second, a seed generating system that employs an ultrasonic generates enantiomerically pure seed *in-situ* in each of the two beds. In order to produce seed, the column is designed with a taper at the bottom, such that the fluid velocity at the inlet to the bed is higher than the superficial velocity throughout the rest of the bed. As a result, the bottom zone accumulates the largest particles. At the bottom of the bed, there is a chamber that houses the ultrasonic horn. The large particles that settle to the bottom zone eventually reach the seed chamber and are fractured by sonication. Klink et al. (1971) showed that the seed generated in this manner resulted from the fracture of the oversize particles from the fluidized bed crystallizer. Fracture along cleavage planes was observed as the oversized crystals underwent crystal-crystal or crystal-horn contacts in the sonication chamber.

A supersaturated solution containing both enantiomers is fed to the first FBC, where crystallization of the *l*-enantiomer takes place by growth on the established seedbed. At periodic intervals, slurry is removed via a port on the side of the column. The solids-free overflow from this stream serves as the feed to the second column, where the *d*-enantiomer crystallizes on a seedbed of pure *d*-methyldopa. Successful operation of the crystallization in this configuration hinges upon the methyldopa system forming conglomerate *l*- and *d*-crystals. In addition, it's essential that the supersaturation of *d*-methyldopa in the first FBC be maintained below a critical level in order to avoid nucleation of *d*-crystals in this FBC. This crystallization system maintains a low supersaturation, yet still affords a fairly high productivity. The latter comes from the large seedbed employed which provides a very large

surface area for crystal growth resulting in a high mass accumulation of solids even at low supersaturation. The use of two crystallizers allows the crystallization of the *d*-isomer, so that it does not reach high supersaturation.

Ibuprofen. An example of switching salt forms to improve the solubility characteristics of an enantiometric system is found in the isolation of ibuprofen. Ibuprofen is the active ingredient in several marketed analgesics (painkillers), and has historically been marketed as a racemic mixture, although there have been recent attempts to market the *S*-isomer.

The use of crystallization to isolate *S*-ibuprofen is not practical, since ibuprofen acid forms a racemic compound with eutectics that are reported by Manamartin et al. (1993) to be at 90 and 10%. (Phase diagram similar to Figure 11.17b.) However, they also report that the sodium salt of ibuprofen, while still forming a racemic compound, has eutectic compositions at about 60 and 40%. Thus, syntheses which produce sodium ibuprofenate (*S*-isomer) in purity greater than 60% can be crystallized to yield salts of high purity. In this case, isolating the sodium form rather than the acid accommodates a wider array of chemistry performance. The unwanted isomer from the sodium salt will initially be lost or unusable. However, complete conversion to the required form could be accomplished using chemical or enzymic racemization (Larsen and Reider 1990) to convert the *R*-isomer to *S*-isomer.

Tung et al. (1991) devised another approach to the problem of isolating *S*-ibuprofen. They determined that the formation of a diastereomeric salt yielded favorable solubility characteristics. They reacted *S*-lysine with racemic ibuprofen to form the (*S*, *S*) and (*R*, *S*) salts. This afforded a 50–50 mixture of the two salts, from

which they could crystallize the (*S,S*) salt without co-current crystallization of the (*R,S*) salt. While this is highly desirable, and similar behavior to that of the ammonium tartaric acid system, it is typically only observed in 10–20% of chiral crystallizations. The use of crystallization by resolution, as discussed earlier for methyldopa, in which both enantiomers are crystallized in order to avoid nucleation of the undesired enantiomer, is much more common.

11.5.2. RAPID MIXING AND RAPID PRECIPITATION WITH AN IMPINGING JET MIXER

Rapid precipitation under high supersaturation conditions favors nucleation over growth and results in particles of small average size as are often needed for final pharmaceutical products. Very high supersaturation conditions can be achieved by supercritical precipitation (e.g., Larson and King 1986; Tavana and Randolph 1992), but high-pressure equipment appears to not be favored in the pharmaceutical industry. Anti-solvent or reactive precipitation also can effect high supersaturation, but it requires the achievement of uniform conditions for the process, i.e., rapid macro- and micro-mixing. Careful design of the feed location in a conventional agitated vessel to ensure high-energy dissipation in this location can accomplish this. However, workers at Merck (Midler et al. 1989; Midler et al. 1994) have developed a low volume, high throughput continuous precipitator to accomplish this based upon two-impinging jet (TIJ) technology. Due to the dissipation of the kinetic energy of the jets in a small volume, high energy dissipation rates can result in micro-mixing times of a few milliseconds or less (Mahajan and Kirwan 1996). This rapid mixing permits a uniform supersaturation environment to exist before nucleation takes place resulting in greater uniformity in the crystal size distribution. Midler et al. (1989) report the production of a narrow distribution of small particles (ca. 10 microns). Such mixers can be used either submerged in a tank or in-line where subsequent nucleation and growth occurs in a plug flow configuration in the exit line from the mixer.

To examine the performance of a two impinging jet mixing device, Mahajan and Kirwan (1994) independently measured the nucleation induction times (for example, Figure 11.10) and growth kinetics of model compounds under high supersaturation conditions using the grid mixing device described earlier. They then employed a modification of the Bourne reaction system to measure the micromixing times in a jet mixer as a function of jet geometry and hydrodynamics (Mahajan and Kirwan 1996). Finally, they conducted precipitation experiments in a two impinging jet mixer under conditions where the micromixing time was either less than or greater than the nucleation induction time. Some results are shown in Figure 11.19 for the precipitation of lovastatin from methanol using water as the precipitant. When the micromixing time was shorter than the nucleation induction time, the supersaturation environment was uniform and the crystal size distribution was independent of hydrodynamics when sampled at the same residence time. For a poorly micro-mixed system the PSD varies with the hydrodynamics in the precipitator. Understanding both the mixing characteristics of a precipitator and the kinetics of the crystallizing system permits the design and control of the supersaturation environment to achieve the desired size distribution. The jet precipitator is an interesting device because it provides independent control of a nucleation environment, which can then be followed by a growth stage.

The impinging jet device has also been reported to be useful for other problems in pharmaceutical crystallization. As noted earlier some solutes precipitate as a liquid phase (“oiling out”), with subsequent transformation to a solid. In a conventional agitated vessel, these oils have a tendency to accumulate on the walls

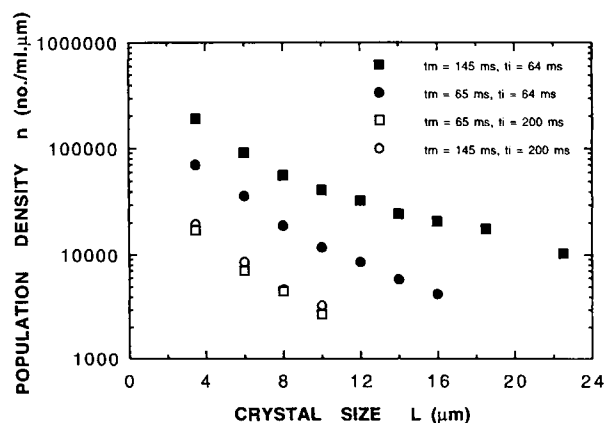


Figure 11.19 Effect of relative values of nucleation induction time (t_i) and micromixing time (t_M) on PSD in a TIJ precipitator. (Reprinted with permission of the American Institute of Chemical Engineers from Mahajan, A.J., and Kirwan, D.J., *AIChE J.* 42, pp. 1801–1814 (1996). © 1996. All rights reserved.)

of the vessel or on the agitator, which inhibits the later transformation to a solid. Midler et al. (1989) reported that the use of the impinging jet device for such a compound provides an emulsion leaving the device in which the liquid droplets readily transformed. They have also reported that, despite the rapid crystallization at high supersaturations, small particles produced from the jet crystallizer had a lower impurity level than crystals formed in other ways.

11.5.3. ETHANOL FRACTIONATION OF PLASMA PROTEINS

The problems involved in the use of crystallization to fractionate a number of similar solutes in solution can be illustrated by the current approaches to the fractionation of plasma proteins. Chapter 12 in this book discusses the fundamentals of crystallization of proteins. Here our purpose is to demonstrate how the manipulation of relevant process variables can effect the fractionation of mixtures of pharmaceutical-like compounds.

In the late 1940s, a method was developed (Cohn et al. 1946) for the fractionation of proteins from blood plasma by means of ethanol (an anti-solvent) addition to aqueous solutions at specified conditions of temperature, pH, and ionic strength. Briefly, a series of five successive batch ethanol precipitations were used to prepare fractions of fibrinogens, globulins, and albumin. The conditions used in each step are in Table 11.1 along with the major protein(s) precipitated at each step. More recently, a method employing a series of MSMPR precipitators has been reported (Chang 1988).

This system provides an excellent illustration of many of the most common problems encountered in optimizing and scaling up crystallizations for pharmaceuticals and biologicals. First, there are multiple solutes with similar solution behavior. In this case, there are five protein fractions that precipitate between 0 and 40% (v/v) ethanol. In addition to control of the ethanol concentration, the optimum pH is different for the five precipitation steps. As the alcohol concentration is increased at each precipitation stage, the operating temperature also decreases slightly, although not at every stage. In the batch system, ethanol or aqueous ethanol solutions are added via subsurface line. Typically such a line is designed to produce a high fluid velocity for the anti-solvent exiting the line in order to promote mixing and minimize the potential

TABLE 11.1 Conditions for Ethanol Fractionation of Plasma Proteins

Stage	Buffer	pH	Ethanol (%)	Precipitate
1	Sodium acetate/acetic acid	7.2	8	Fibrinogen
2	Sodium acetate/acetic acid	6.9	25	Globulins
3	Sodium acetate/acetic acid	5.2	18	Globulins/lipids
4	Sodium acetate/sodium carbonate	5.8	40	Globulins/albumin
5	Sodium acetate/acetic acid	4.8	40	Albumin

(Adapted from Cohn et al. (1946).)

for local regions of high supersaturation, and to avoid backmixing of crystallizer fluid into the subsurface line. This line typically ejects fluid into the region of the agitator to aid mixing. Poor mixing can result in local regions of high ethanol concentration that creates a high supersaturation region. Indeed, Chang reported that when carried out in a 0.1 m^3 batch crystallizer, albumin precipitated in the fourth precipitation stage at ethanol concentrations below that which was expected, leading to a loss of albumin yield.

Just as this case illustrates some of the commonly encountered difficulties in the crystallization of pharmaceuticals, the continuous fractionation system described by Chang (1988) illustrates some of the solutions that are often employed to minimize these difficulties. Figure 11.20 shows one stage of the continuous pre-

cipitation train. In the continuous system, both alcohol and buffer for pH control were added by spraying (misting) a dispersion of fine droplets above the surface of the suspension in the MSMPR precipitator. Gradients in density and surface tension that exist between the droplets and the continuous solution phase would hinder dispersing the ethanol, in particular, since the upper regions of the tank are typically the least well-mixed. Chang reported that additional mechanical agitation of the tank as well as the small droplet size hastened mixing. A more common solution to the blending of the anti-solvent would be by a sub-surface line or by blending with the aid of a static mixer and external recycle line. A recycle line with an in-line static mixer was used to promote mixing of the protein solution as it was added. The solid-free protein solution is mixed into the recirculating suspension from the tank by continuously injecting it just upstream of the static mixer so that it was rapidly diluted into the stream recycling from the MSMPR. The flow rate of the recycle stream was about 10 times that of injected feed so a significant dilution is achieved in the recycle line.

By employing a well designed system and using on-line pH control for the addition of buffers, several improvements were achieved beyond the standard batch process. First, yield and purity of albumin from the final fractionation step increased. Second, larger particles were formed which eased recovery by centrifugation. Finally, the time cycle was reduced significantly since long ages were required for the batch process. Presumably, the use of a continuous system allowed operation at low supersaturation that minimized nucleation and co-precipitation. This favorably impacted both purity and yield, since co-precipitation of albumin in stage four would result in yield loss. Further, co-precipitation of fibrinogen or globulins in the final precipitation stage when recovering albumin would lead to a loss of purity in albumin.

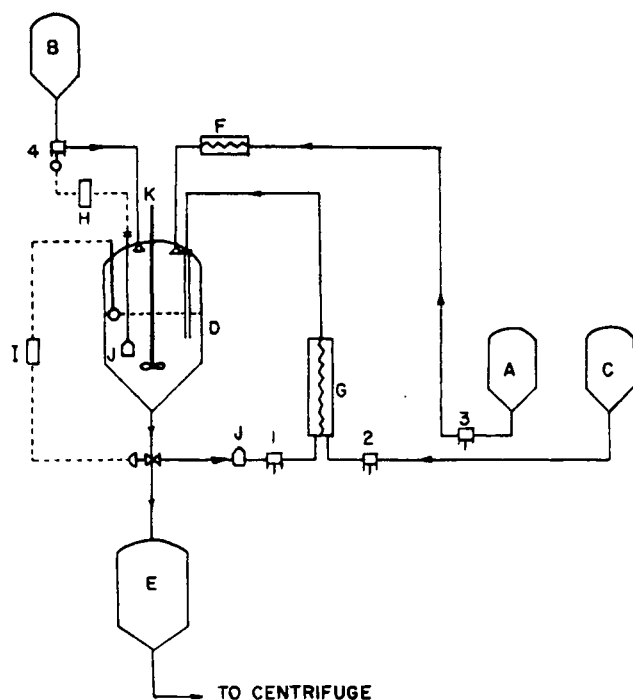


Figure 11.20 Precipitation stage in continuous plasma fractionation system: (A) alcohol tank; (B) buffer tank; (C) plasma tank; (D) suspension tank; (E) product receiving tank; (F) tubular cooler; (G) in-line static mixer; (H) pH analyzer/recorder; (I) level controller; (J) pH probes; (K) agitator. (1) Metering pump for suspension recirculation; (2) metering pump for feed; (3) metering pump for alcohol; (4) metering pump and controller for buffer. (Reprinted with permission of J. Wiley & Sons, Inc. from Chang, C.E., *Biotech. Bioeng.* 31, pp. 841–847. © J. Wiley & Sons, Inc., 1988.)

NOMENCLATURE

a_i	Activity of component i	kmol m^{-3}
C	Concentration	kmol m^{-3}
C_o	Reference concentration	kmol m^{-3}
C^*	Concentration of saturated solution	kmol m^{-3}
G	Crystal growth rate	ms^{-1}
L	Particle size	m
M	Suspension density	kg m^{-3}
n	Population density per unit volume	m^{-4}
p	Order of crystallization rate	
R	Gas constant	$\text{J mol}^{-1} \text{K}^{-1}$
t	Time	s
t_1	Nucleation induction time	s
t_M	Micromixing time	s
T	Temperature	K
X_i	Mole fraction of species i	

Greek Letters

σ relative supersaturation

ACKNOWLEDGMENT

Some material in this chapter is based upon work supported by the National Science Foundation under Grant No. 9510171. Any opinions, findings, and conclusions, or recommendations expressed in this material are those of the authors and do not necessarily reflect the views of the National Science Foundation.

REFERENCES

- Addadi, L., Berkovitch-Yellin, Z., Domb, N., Gati, E., Lahav, M., and Leiserowitz, L. (1982). *Nature* **296**, 21.
- Berkovitch-Yellin, Z. (1985). *J. Am. Chem. Soc.*, **107**, 3111–3122.
- Black, S.N., and Davey, R.J. (1988). *J. Crystal Growth* **90**, 136–144.
- Black, S.N., Davey, R.J., and Halcrow, M. (1986). *J. Cryst. Growth* **79**, 765–774.
- Bourne, J.R., and Davey, R.J. (1976). *J. Cryst. Growth* **36**, 278–286.
- Cardew, P.T., and Davey, R.J. (1985). *Proc. Roy. Soc. (London)* **A398**, 415–428.
- Chang, C.E. (1988). *Biotech. Bioeng.* **31**, 841–843.
- Charmolue, H., and Rousseau, R.W. (1991). *AIChE J.* **37**, 1121–1128.
- Chilton, C. (ed.) (1965). *Chem. Eng. Mag.* November 7, 235.
- Clydesdale, G., Roberts, K.J., and Docherty (1990). In *Crystal Growth of Organic Materials*, ACS Conf. Proceedings Ser. (Myerson, A.S., Green, D.A., and Meehan, P., eds.) 43–52.
- Cohn, E.J., Leutscher, J.M., and Ondey, J.L. (1940). *J.A.C.S.* **62**, 3396–3402.
- Collet, A., Brienne, M., and Jacques, J. (1980). *Chem. Rev.* **80**, 215–230.
- Collins, A.N., Sheldrake, G.N., and Crosby, J. (eds.) (1997). *Chirality in Industry I & II*. J. Wiley & Sons.
- Davey, R.J. (1986). *J. Cryst. Growth* **76**, 637–644.
- Davey, R.J., Mullin, J.W., and Whiting, M.J.L. (1982). *J. Cryst. Growth* **58**, 304–312.
- Deshpande, S. (1998). “Effect of Mixing on Crystallization in a Continuously Agitated Crystallizer,” M.S. Thesis, U. Virginia.
- Docherty, R. (1996). In *Crystal Growth of Organic Materials*, ACS Conf. Proceedings Ser., (Myerson, A.S., Green, D.A., and Meehan, P. eds.), pp. 2–13.
- Edie, D.D., and Kirwan, D.J. (1973). *Ind. Eng. Chem. Fundam.* **12**, 100–106.
- Green, D.A., and Meehan, P. (1996). In *Crystal Growth of Organic Materials*, ACS Conf. Proceedings Ser. (Myerson, A.S., Green, D.A., and Meehan, P. eds.), pp. 78–84.
- Harano, Y., and Yamamoto, H. (1982). “Impurity Effect of Amino Acids on Formation and Growth of L-Glutamic Acid”, *Industrial Crystallization*, vol. 81 (Jančić, S.J., and de Jong, E.J., eds.), pp. 137–145, North Holland Publ. Co.
- Hendricksen, B.A., Grant, D.J.W., Meehan, P., and Green, D.A. (1996). In *Crystal Growth of Organic Materials*, ACS Conf. Proceedings Series (Myerson, A.S., Green, D.A., and Meehan, P., eds.), pp. 95–104.
- Jang, S., and Myerson, A.S. (1996). In *Crystal Growth of Organic Materials*, ACS Conf. Proceedings Ser. (Myerson, A.S., Green, D.A., and Meehan, P., eds.), pp. 53–58.
- Jacques, J., Collet, A., and Wilen, S. (1994). *Enantiomers, Racemates, and Resolutions*, Krieger Publishing, Malabar, Florida.
- Jungfleisch, M.E. (1882). *J. Pharm. Chim.* **5**, 346.
- Kagara, K., Machiya, K., Takasuka, and Kawai, N. (1996). *Proceed. 13th Symposium on Ind. Crystallization*, Toulouse, France, September 1996, pp. 13–18.
- Kirkwood, J.G. (1934). *J. Chem. Phys.* **2**, 351–356.
- Kitamura, M. (1989). *J. Cryst. Growth* **96**, 541–546.
- Kitamura, M., and Yamanani, T. (1996). *Proceed. 13th Symposium on Ind. Crystallization*, Toulouse, France, September, pp. 55–60.
- Klink, A., Midler, M., and Allegretti, J. (1971). *AIChE Symp. Ser.* no. 109, 67, 77–78.
- Krieger, K.H., Lago, J. and Wantuck, J.A. (1968). U.S. patent 3,405,159.
- Larson, K.A., and King, M.L. (1986). “Evaluation of Supercritical Fluid Extraction in the Pharmaceutical Industry,” *Biotech. Prog.* **2**, 73–76.
- Larsen, R., and Reider, P. (1990). U.S. patent 4,946,997.
- Luengo, J.M. (1985). *Anal. Biochem.* **149**, 466.
- Mahajan, A., Orella, C.J., and Kirwan, D.J. (1991). *AIChE Symp. Ser.* no. 87, **284**, 143–153.
- Mahajan, A.J., and Kirwan, D.J. (1994). *J. Crystal Growth* **144**, 281–286.
- Mahajan, A.J., and Kirwan, D.J. (1996). *AIChE J.* **42**, 1801–1814.
- Manamarin et al. (1993). *Tetrahedron Asymmetry* **4**, 1949.
- Midler, M. (1970). U.S. patent 3,510,266.
- Midler, M. (1975). U.S. patent 3,892,539.
- Midler, M. (1976). U.S. patent 3,996,018.
- Midler, M., Paul, E.L., and Whittington, E.F. (1989). “Production of High Purity, High Surface Area Crystalline Solids by Turbulent Contacting and Controlled Secondary Nucleation,” Paper Presented at 12th Biennial Engineering Foundation Conference on Mixing, August 1989.
- Midler et al. (1994). U.S. patent 5,314,506.
- Myerson, A.S. (ed.) (1999). *Molecular Modeling Applications in Crystallization*, Cambridge, University Press, Cambridge, UK.
- Myerson, A.S., Green, D.A., and Meehan, P. (eds.) (1996). *Crystal Growth of Organic Materials*, ACS Conf. Proceedings Ser.
- Myerson, A.S., and Kirwan, D.J. (1977a). *Ind. Eng. Chem. Fundam.* **16**, 414–419.
- Myerson, A.S., and Kirwan, D.J. (1977b). *Ind. Eng. Chem. Fundam.* **16**, 420–425.
- Orella, C.J. (1990). “Crystallization of Amino Acids,” Ph.D. Dissertation, U. of Virginia, May 1990.
- Orella, C.J., and Kirwan, D.J. (1989). *Biotech. Prog.* **5**, 89–93.
- Orella, C.J., and Kirwan, D.J. (1991). *Ind. Eng. Chem. Res.* **29**, 1040–1045.
- Paul, E.L., and Rosas, C.B. (1990). *Chem. Eng. Prog.* **86**, 17–25.
- Phan, H.V. (1999). U.S. patent 5,936,118.
- Randolph, A.D., and Larson, M.A. (1988). *Theory of Particulate Processes*, 2nd ed., Academic Press, New York.
- Ramanarayan, K.A., Kern, W., Larson, M.A., and Sikdar, S. (1991). “Particle Design by Crystallization”, *AIChE Symp. Ser.* No. 284 **29**.
- Rodriguez-Hornedo, N., Yang, L.Y., and Randolph, A.D. (1986). “Effect of pH on the Crystallization Kinetics of Phenytoin,” *AIChE Annual Meeting*, Miami, November 1986.
- Samejima, H. (1972). In *Microbial Production of Amino Acids* (Yamada, K., Kinoshita, S., Tsunoda, T., Aide, K., eds.), 227–259. John Wiley, New York.
- Sato, K., and Boistelle, R. (1984). *J. Crystal Growth* **66**, 441–450.
- Sato, K., Suzuki, K., and Okada, K. (1985). *J. Crystal Growth* **72**, 699–704.
- Secor, R.M. (1963). *Chem. Rev.* **63**, 297.
- Slaminko, P., and Myerson, A.S. (1981). *Amer. Inst. Chem. Eng. J.* **27**, 1029–1031.
- Stinson, S.C. (1999). *Chem. and Engr. News* **77(41)**, 101–120.
- Tavana, A., and Randolph, A.D. (1989). *AIChE J.* **35**, 1625–1630.
- Tsujima, A., Nakashima, E., Hamano, S., and Yamana, T. (1978). *J. Pharm. Sci.* **67**, 1059–1066.
- Tung, H., Waterson, S., and Reynolds, S.D. (1991). U.S. patent 4,994,604.
- Wall, W.F. (1988). European patent application 88307339.7.
- Weissbuch, I., Lahav, M., and Leiserowitz, L. (1999). “Towards an Understanding and Control of Nucleation, Growth, Habit and Structure of Crystals Using Tailor-Made Auxiliaries.” In *Molecular Modeling Approaches in Crystallization* (Myerson, A.S., ed.), Chapter 4, Cambridge University Press, Cambridge, UK.
- White, E.A.D., Wood, J.D.C., and Wood, V.M. (1976). *J. Cryst. Growth* **32**, 149.
- Yamada, K., Kinoshita, S., Tsunoda, T., and Aide, K. (eds.) (1972). *Production of Amino Acids*, J. Wiley, NY.
- Zumstein, P.C., and Rousseau, R.W. (1989). *Ind. Eng. Chem. Res.* **28**, 1226–1231.

CRYSTALLIZATION OF PROTEINS

John Wiencek

12.1. INTRODUCTION

Much of this handbook is concerned with the how and why of crystallization and crystallizer design. This chapter will focus on the crystallization of one particular class of chemical compounds, namely the proteins. In the timeline of crystallization, protein crystallization is a newcomer. The first mention of protein crystal formation, roughly 150 years ago, involved crystallizing hemoglobin from the blood of various species (Lehman 1853; Reichert and Brown 1909; Debru 1983; McPherson 1991). This work was followed by the crystallization of a variety of proteins from plants to egg white (Sumner 1926). These early studies were pivotal in establishing that enzymes are proteins (Dounce and Allen 1988). The use of protein crystallization in purification and classification of biological chemicals resulted in the Nobel Prize for Chemistry being awarded to Sumner, Nothrop, and Stanley in 1946.

Protein crystallization has since become a critical scientific tool. Crystallization is a simple yet effective means of purifying one protein from a mixture and has found some industrial applications. In addition, crystallization of proteins within living organisms seems to be linked to a variety of diseases. However, the most prevalent use for protein crystallization today is the production of single, high-quality crystals for use in the determination of atomic structure via X-ray diffraction.

After the crystallization of pepsin and urease by Nothrop and Sumner, X-ray crystallographers attempted to collect diffraction data of mounted crystals. Unfortunately, the protein crystals were treated in a fashion typically utilized for inorganic crystals, which required removing the crystal from its mother liquor and drying it. The absence of a sharp diffraction pattern confirmed the belief of many scientists of the time that proteins were not distinct molecules, but rather a colloid lacking a definite structure. Bernal and Crowfoot (1934) decided to conduct an X-ray diffraction experiment on a pepsin crystal suspended in the mother liquor. A sharp diffraction pattern was discovered with lattice spacings that correspond to atomic distances. The determination of the atomic structure was still beyond the capabilities of crystallographers, with the phase problem looming as the major stumbling block. Perutz, after 16 years of working on the phase problem, postulated the now commonly employed multiple isomorphous replacement (MIR) technique in 1954 (Green et al. 1954). The first atomic structures of myoglobin (Kendrew et al. 1958) and hemoglobin (Perutz et al. 1960) soon followed.

The knowledge of the native structure of a given protein is essential for both practical applications such as drug discovery as well as for fundamental studies such as enzymology. Structure-based drug design relies on molecular-level structural knowledge of a disease-associated receptor or ligand. Such targets are usually proteins, allowing the living organism to take advantage of the cascade effect inherent in many enzymatic processes. After the protein target is identified and its structure determined, a chemical is specifically designed to bind this target irreversibly and thus negate its

activity. Such a structure-based drug design minimizes the extensive screening, which is typically employed to identify an appropriate drug. Captopril, a drug used to relieve hypertension, was developed using structure-based design and more drugs are in development (Bugg et al. 1993). Additionally, understanding the relationship between the structure of a protein and its function in vivo leads to a better fundamental understanding of cellular mechanisms.

Two methods are now commonly employed to determine the atomic structural models for proteins. Nuclear magnetic resonance (NMR) can provide such structural models. Although this method allows the direct, noninvasive determination of protein structure, it is hampered by low sensitivity and is limited to proteins less than approximately 30,000 molecular weight (Branden and Tooze 1991). X-ray crystallography is not limited in these respects but does require the formation of a single, highly ordered three-dimensional crystal. The crystal used for X-ray diffraction experiments has a significant influence on the utility of the method. The generation of a crystal of sufficient size (typically at least 0.1 mm in all dimensions) is usually a time-consuming task that relies heavily on empirical screening studies. In addition, large crystals must be of high internal order. Measurement of order in protein crystals is not trivial, but the most important measure is the resolution limit of the collected data. High-resolution data (i.e., diffracting to Bragg spacings of 2.0 Å or less) is required to distinguish individual atoms within the large protein structure. Although large, high-quality crystals are essential for structural determination, there are no hard and fast rules for success of their growth. In fact, protein crystal growth is an area of quite active research and will likely see major advances in the near future.

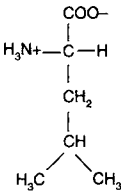
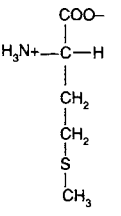
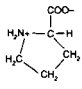
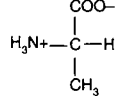
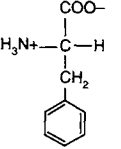
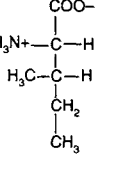
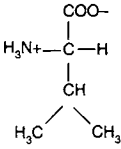
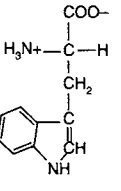
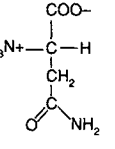
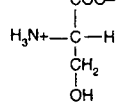
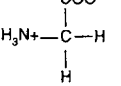
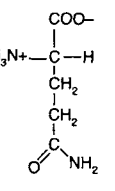
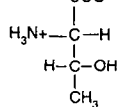
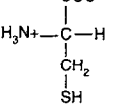
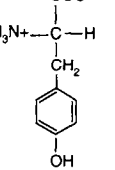
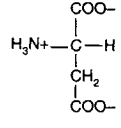
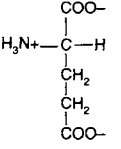
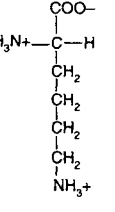
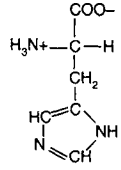
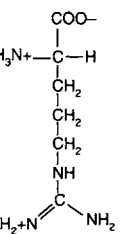
Protein crystallization does play an important role in industry. For example, the development of small molecule drugs is often accelerated by the structure-based design methods that result from X-ray diffraction studies of single protein crystals. But protein crystallization is also an important purification and packaging step for bulk industrial enzymes. Important industrial enzymes include a variety of stable proteases as well as the key enzymes utilized to convert starch to sweeteners, amyloglucosidase, and glucose isomerase. These enzymes are often sold in a purified form for use in immobilized enzyme reactors. The key purification technique is selective precipitation or crystallization. Thus, the ability to crystallize proteins has industrial relevance. In the pharmaceutical area, proteins have already carved a niche. For example, human insulin is now produced from recombinant *E. Coli* and precipitation/crystallization is a major unit operation required for its downstream processing (Datar and Rosen 1991). Indeed, with the advent of recombinant DNA technology, many of the next generation pharmaceuticals will likely be large proteins requiring purification via crystallization.

The scale up and optimization of protein crystallization is no different than for any other chemical system. The only notable differences for protein crystallization systems is the requirement of

very high supersaturation to induce nucleation and subsequent growth (relative supersaturations of 100–500% are not uncommon) as well as the high solvent content of the crystals that renders them fragile objects. Thus, this chapter will focus on basic protein chemistry, variables affecting solubility, growth rate mechanisms,

and the typical means of screening crystallization conditions. Once the solution conditions that produce the desired crystals are identified and necessary solubility and growth relationships quantified, the crystallizer design and scale-up can follow the well-established procedures outlined earlier in this handbook.

TABLE 12.1 Structures of Amino Acids

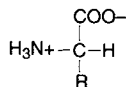
Leucine (Leu, L) <i>nonpolar</i>		Methionine (Met, M) <i>nonpolar</i>		Proline (Pro, P) <i>nonpolar</i>	
Alanine (Ala, A) <i>nonpolar</i>		Phenylalanine (Phe, F) <i>nonpolar</i>		Isoleucine (Ile, I) <i>nonpolar</i>	
Valine (Val, V) <i>nonpolar</i>		Tryptophan (Trp, W) <i>nonpolar</i>		Asparagine (Asn, N) <i>polar</i>	
Serine (Ser, S) <i>polar</i>		Glycine (Gly, G) <i>polar</i>		Glutamine (Gln, Q) <i>polar</i>	
Threonine (Thr, T) <i>polar</i>		Cysteine (Cys, C) <i>polar</i>		Tyrosine (Tyr, Y) <i>polar</i>	
Aspartic acid (Asp, D) <i>acidic</i>		Glutamic acid (Glu, E) <i>acidic</i>		Lysine (Lys, K) <i>basic</i>	
Histidine (His, H) <i>basic</i>		Arginine (Arg, R) <i>basic</i>			

The backbone structure of the 20 naturally occurring amino acids. Common abbreviations (three-letter and one-letter) are shown in parentheses. The general chemical character of the side chain (nonpolar, polar, acidic, basic) is shown in italics.

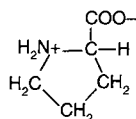
12.2. PROTEIN CHEMISTRY

12.2.1. AMINO ACIDS AND THE PEPTIDE BOND

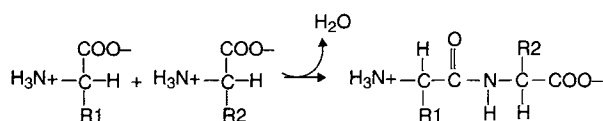
Proteins are condensation reaction polymers of the 20 naturally occurring amino acids. With the exception of proline, the amino acids have the generic chemical form of:



where the R group is defined for the various amino acids in Table 12.1. Proline has its side chain (R group) attached to the nitrogen as well, producing the imino acid:



With the exception of glycine, the amino acids have chiral central carbon atoms. The naturally occurring amino acids are of the L isomer form. These 20 amino acids are linked into a polymeric structure via peptide bonds formed by the condensation of the carboxyl and amino groups of adjacent amino acids:



The resulting peptide bond is very rigid and stable. Proteins typically have molecular weights in excess of 10,000 and display distinctive structural features such as alpha helices or beta sheets. Smaller, less structured, polymers of amino acids are typically referred to as polypeptides or polyamino acids. The fundamental hypothesis of biophysical chemistry is that the ordering of amino acids in the protein polymer (referred to as the primary structure) dictates all other properties of the protein. Thus, the side chain groups listed in Table 12.1 possess certain physical properties, which are the driving force for any protein's equilibrium conformation, folding pathway and biological function. Table 12.1 nominally lists the amino acids as polar, nonpolar, and charged. Although one may conjecture that charged groups will always be exposed to the high dielectric media of water, some of these sidechains also contain a strong hydrophobic character (e.g., lysine) and it is not obvious how these sidechains will arrange themselves in the final protein structure. Biochemists have recognized the complexity of the structure of such large molecules and have studied the varying levels of structural detail, which together form the entire protein molecule.

12.2.2. LEVELS OF STRUCTURE: PRIMARY, SECONDARY, TERTIARY, QUATERNARY

When speaking of protein structure, the ideas of levels of structure have proven useful. As mentioned earlier, the primary structure is the amino acid sequence and indicates the covalent bonds, which exist between adjacent amino acids. However, these amino acids contain functional groups, which can interact through noncovalent bonds or forces such as hydrogen bonding or electrostatic interactions (i.e., salt bridges). Secondary structure refers to local structures of a segment of the protein, such as an alpha helix or a beta sheet. Placing such secondary elements in a sequence and then

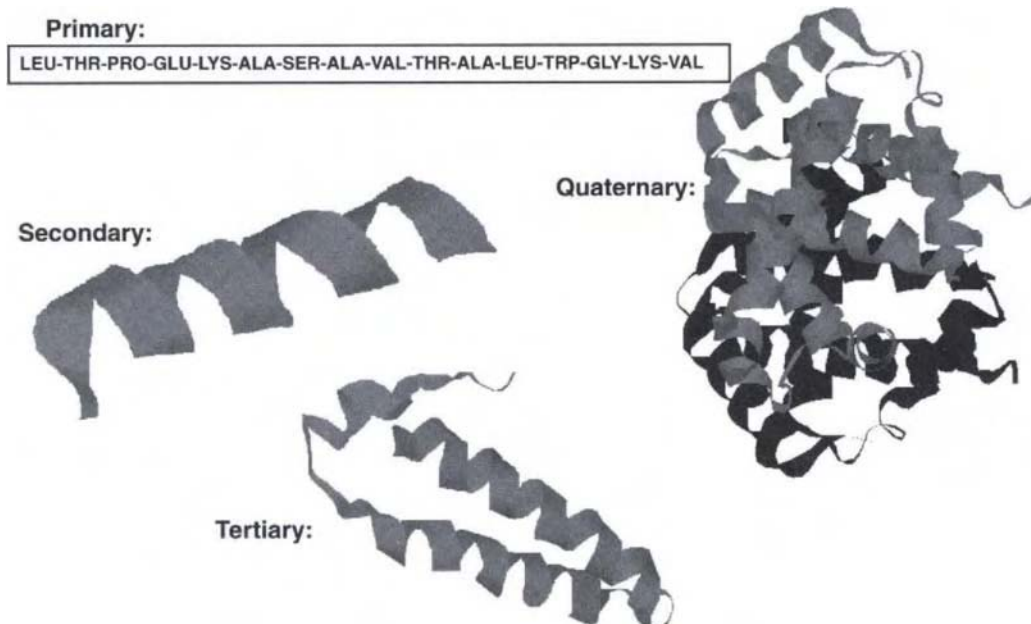


Figure 12.1 The levels of structural detail in a typical protein using the ribbon depiction. The primary structure gives the ordering of the peptide bonds between adjacent amino acids in a protein. In three dimensions, short segments of the primary sequence will fold into distinctive shapes such as the alpha helix structure of the backbone. Such short range three-dimensional structures are referred to as secondary structure. Putting successive secondary structural elements together over the entire length of a given primary sequence will yield a polypeptide's tertiary structure. Finally, such single polypeptide chains can associate to form a larger protein complex. The geometry of such an association is referred to as the quaternary structure.

arranging them in three-dimensional space is referred to as tertiary structure. Finally, a given polypeptide may bind with other separate polypeptides to form a larger complex protein. The arrangement of these separate subunit proteins into a complex protein is referred to as the quaternary structure of a protein. Figure 12.1 displays schematically the various levels of protein structure using the popular ribbon method to indicate the nature of the protein's backbone structure. Typically the whole protein is fairly compact in structure indicating that the weak noncovalent forces act in a cooperative fashion to stabilize the overall structure. The physicochemical explanations for such cooperativity is the subject of several excellent textbooks on proteins, with the book by Creighton being an excellent starting point (Creighton 1993). It is beyond the scope of this chapter to review all of the noncovalent forces stabilizing protein structures. However, a few of these interactions are actually adjusted or tuned to produce the protein crystalline state. Forces that promote protein crystal formation and packing are relatively weak and few in number compared to small molecules. The crystal stabilizing forces include salt bridges, hydrogen bonds, van der Waals, and dipole-dipole interactions (Bergdoll and Moras 1988; Salemne et al. 1988; Wang and Teng 1988).

12.2.3. IONIZABLE SIDECHAINS AND PROTEIN NET CHARGE

As outlined in Table 12.2, there are a variety of sidechains that can become charged at appropriate pH. Thus, each protein will possess a unique titration curve, comprised of a variety of ionization reactions taking place on the surface of the molecule. Near pH of 7.0, most proteins will possess several positive charges as well as several negative charges. The net charge of the protein can be calculated by summing these positive and negative charges. The point of zero net charge is referred to as the isoelectric point of the protein (or pI). Under these conditions, the protein will not migrate in the presence of an electric field. However, it is important to note that the point of zero net charge does not imply that the

protein is uncharged. Rather, at the isoelectric point, the protein contains as many positively charged groups as negatively charged groups. Salt bridges between protein molecules can be fine tuned by adjustments of pH away from the pI. In fact, a common strategy in protein crystallization is to attempt to crystallize at a pH near the isoelectric point of the protein, since solubility is usually minimal at this pH.

12.2.4. DISULFIDE BONDS AS CROSSLINKERS WITHIN PROTEINS

Two of the naturally occurring amino acids contain sulfur atoms, methionine and cysteine. The sulfur atom in both of these amino acids is susceptible to oxidation by air and the resulting sulfoxide and sulfone can alter the protein conformation and general solution chemistry. The cysteine amino acid can react with other cysteine amino acids within a given protein to yield a disulfide bond, which is a crosslinker in the polypeptide. Such bonds are referred to as disulfide or cystine bonds. Disulfide bonds are generally present to stabilize the protein structure with a more durable covalent bond. Disulfide bonds can be broken by reacting with a large excess of a thiol reagent such as mercaptoethanol or dithiothreitol. Maintaining the proper crosslinking is an important chemical consideration when crystallizing proteins. The mechanism of disulfide bond formation within the cell is believed to involve a thiol-disulfide exchange between the protein-bond cysteine and glutathione. With proteins containing more than two cysteine amino acids, there are multiple pairs of possible disulfide bonds. Only one configuration is the "preferred" arrangement and shuffling between the various disulfide bond configurations can be the rate-limiting step in protein folding pathways. In view of the apparent role of glutathione in maintaining the proper disulfide bonds in proteins within the cell, many biochemists insist on maintaining physiological levels of glutathione in the crystallization mother broth, typically 1–10 mM.

12.2.5. CHEMICAL MODIFICATIONS OF PROTEINS—GLYCOSYLATION, LIPIDATION, PHOSPHORYLATION

The crystallization of a protein, or any molecule, requires that sufficient molecules of a chemically homogenous form be present in the solution. Thus, the purity of the sample is an important variable impacting the formation of large, highly ordered protein crystals. The source of protein is the living organism, and ultimately a cell. Within the cell, there are discrete compartments responsible for producing the polypeptide and folding it into its native form. The active form of the protein is often a chemically modified form of the nascent polypeptide sequence. Such chemical modifications are commonly referred to as post-translational modifications. Translation within the cell refers to the conversion of information stored in the gene of the cell to the polypeptide sequence. After the cell generates the polypeptide, it undergoes further processing, including the addition of other chemical moieties such as sugar groups, lipids, and phosphorus.

The function of these additional chemical groups is not well understood. In some cases, they serve as molecular switches, activating the protein only when it is needed. Glycosylation is the most prevalent modification in eukaryotic cells, and it appears to increase the protein's solubility and decrease its susceptibility to proteolytic attack. Lipid attachment to proteins is usually seen when the protein's function requires its presence near a membrane surface within the cell. The polar portion of the lipid is attached covalently to the protein while the hydrophobic tail of the lipid is imbedded in the membrane. The lipid group thus serves as an anchor for the soluble protein. Finally, many of the enzymes

TABLE 12.2 The Ionization Constants (pKa) of each of the 20 Natural Amino Acids

Acid	α -COOH	α -NH ₃	R group
Gly	2.34	9.60	
Ala	2.34	9.69	
Val	2.32	9.62	
Leu	2.36	9.68	
Ile	2.36	9.68	
Ser	2.21	9.15	
Thr	2.63	10.43	
Met	2.28	9.21	
Phe	1.83	9.13	
Trp	2.38	9.39	
Asn	2.02	8.8	
Gln	2.17	9.13	
Pro	1.99	10.60	
Asp	2.09	9.82	3.86
Glu	2.19	9.67	4.25
His	1.82	9.17	6.0
Cys	1.71	10.78	8.33
Tyr	2.20	9.11	10.07
Lys	2.18	8.95	10.53
Arg	2.17	9.04	12.48

The first two columns are for terminal carboxyl or amino groups; whereas, the third column applies only to those amino acids with an ionizable (charged) side group. (After Lehninger 1975.)

involved in energy conversion within the cell are, at least transiently, phosphorylated. This phosphorylation allows the conversion of ATP to ADP, with the concomitant release of chemical energy. Phosphorylation is not always important to the protein's function; for example, milk protein casein is phosphorylated, apparently for no other reason than as a nutritional supplement. There are varieties of other, less common, post-translational modifications (e.g., sulfation, hydroxylation and acetylation), which occur in the cell. The modifications usually pose a serious challenge to protein crystallization, since heterogeneous protein mixtures generally yield poor or no crystals. The usual strategies include purification by chromatography or homogenization by chemically cleaving pendant groups. However, these strategies are not always successful and the crystallization of modified proteins remains a challenging problem.

12.2.6. EFFECTORS

One of standard tenets of protein crystallization is that the protein is more likely to crystallize if it has a globular, rigid structure. Flexibility is often exhibited in enzymes near their active site. Such flexibility is an advantage for making contact and binding the substrate during an enzymatic reaction. Unfortunately, such flexibility introduces a dynamic heterogeneity in the system and may inhibit crystallization, or result in crystals of poor diffraction quality. Effectors are any chemical moiety, which can bind to such flexible sites and rigidify such sites. Effectors include small divalent ions such as calcium, enzyme cofactors such as NAD, or enzyme inhibitors. It is common practice to screen with such additives if the native protein crystallization screens are not successful.

12.2.7. DETERMINING PROTEIN CONCENTRATION

Protein concentration can be determined by many different analytical techniques including a variety of spectroscopic methods. However, the most commonly used techniques are fluorescence and ultraviolet (UV) absorption spectroscopy. The optically active portion of the protein in both cases is the amino acid residues containing aromatic ring structures. Phenylalanine, tyrosine, and tryptophan are the residues contributing most significantly to both fluorescence and UV absorption in proteins. Disulfide linkages within a protein are also UV active, although to a much lesser extent at the wavelength typically utilized (280 nm). In view of its ease and nondestructive nature, UV absorption is typically employed to measure protein concentrations in aqueous solutions typically at a wavelength of 280 nm.

Ultimately, the protein concentration is measured by invoking the Beer-Lambert law:

$$A(\lambda) = \epsilon_{\lambda} b C \quad (12.1)$$

where A is the optical absorbance as measured at a particular wavelength, λ (typically 280 nm); ϵ_{λ} is the molar absorption coefficient ($M^{-1}cm^{-1}$) at the wavelength of the measurement; b is the optical pathlength (cm); and C is the protein concentration (M). ϵ_{λ} is the important "calibration constant," which allows one to translate the measured absorbance into the protein concentration. One alternative is to generate a suitable calibration solution and accurately determine its optical absorbance at the desired wavelength. The molar absorption constant can be calculated after the protein concentration in such a solution is determined by other techniques such as dry weight analysis (Hunter 1966; Kupke and Dorrier 1978; Nozaki 1986), Kjeldahl nitrogen determination (Jaenicke 1974), colorimetric techniques (Bradford 1976; Lowery et al. 1951), or amino acid analysis (Benson et al. 1975). Unfortunately,

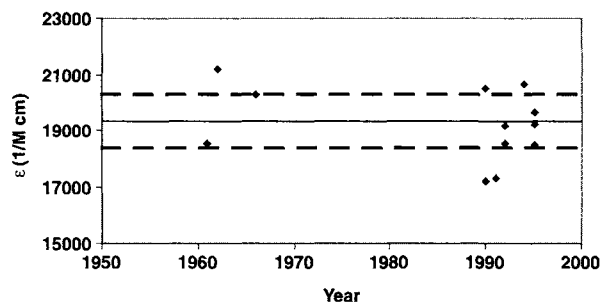


Figure 12.2 The molar absorptivity of RNase T1 as measured through the years. The $\pm 5\%$ error range is shown with the dashed lines.

such calibration procedures destroy significant amounts of the protein, which is usually not available. In addition, the accuracy of the molar absorption constant is usually limited by the secondary method. Indeed, the molar absorption constant can be quite variable based on who measures it and what secondary method is used. Figure 12.2 shows the measured value of the molar absorption constant for RNase T1 as measured through the years. At best, an error of 5% is expected based on experiences with a variety of proteins.

Most proteins that are of enough interest to purify and crystallize are also sequenced at the DNA level and, thus, the amino acid sequence is well known. Gill and von Hippel (1989) have shown that such information is sufficient to accurately (within 5% relative error) estimate the molar absorption constant at 280 nm. The spectra of the aromatic amino acids are shown in Figure 12.3. The unfolded protein is found to display an absorption spectra, which is the molecular average of the constituent amino acids; thus, these model compound spectra can be used to predict the protein absorption properties, provided the primary sequence is known. Further, Gill and von Hippel (1989) experimentally measured the difference between the molar absorption constant in both native and unfolded conformations of the protein and found the deviations were, on average, 3.8%, and thus negligible. This methodology is a simple extension of the Edelhoch method and was further refined by Pace et al. (1995). They arrive at the following empirical correlation for the molar absorption constant ($M^{-1}cm^{-1}$) for proteins at 280 nm:

$$\epsilon_{280} = 5,500 (\#Trp) + 1,490 (\#Tyr) + 125 (\#Disulfide) \quad (12.2)$$

where $\#Trp$ is the number of tryptophan amino acids in the protein, $\#Tyr$ is the number of tyrosine amino acids in the protein

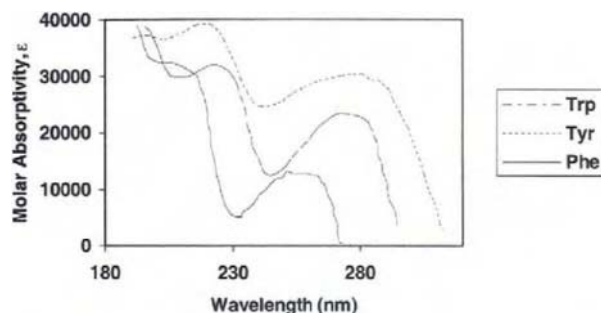


Figure 12.3 The UV absorption spectra of tryptophan (Trp), tyrosine (Tyr) and phenylalanine (Phe) amino acids. (From Creighton 1993.)

and #Disulfide is the number of disulfide bonds in the protein. It is interesting to note that phenylalanine is not included in this correlation. This observation is consistent with the weak absorbance of phenylalanine at 280 nm as seen in Figure 12.3.

The above procedures are applicable to pure proteins, not to mixtures. It is often desirable to quantify the total mass of protein per volume of a given protein mixture. In such cases, the colorimetric techniques (Bradford 1976; Lowery et al. 1951) are preferred. An ideal colorimetric protein assay procedure would give an identical response for all proteins and thus reflect accurately the total protein mass in solution. For example, an assay of just peptide bonds would produce such an ideal response. However, most procedures show variable response from one protein to another. Thus, standards typically utilized with such colorimetric procedures should reflect a related protein in terms of amino acid composition and molecular weight. The chemistry of such colorimetric techniques, although not thoroughly understood, is described by Creighton (1993). Such colorimetric techniques are commonly employed by practicing biochemists and molecular biologists and are readily available from a variety of chemical vendors (Sigma, Biorad, Pierce).

12.2.8. PROTEIN PURITY AND HOMOGENEITY

Production of high quality crystals demands very pure and homogeneous protein solutions. Recent work by Rosenburger and coworkers (Vekilov et al. 1996) has clearly linked trace impurities, usually other proteins or aggregated protein, to poor crystal quality. Analytical methods to measure protein purity and homogeneity are well established and must be routinely used when attempting to identify solution conditions suitable for generating high quality protein crystals. Some techniques are more specialized such as electron microscopy and nuclear magnetic resonance and, thus,

are not used on a routine basis. There exists a family of fairly inexpensive, yet exacting, tools to measure protein purity. Routine protein analysis should include electrophoretic and chromatographic evaluation. In addition, some simple particle sizing analysis can go a long way towards assuring successful protein crystallization screens.

The most common method for evaluating protein purity is electrophoresis. The protein is subjected to an electric field and due to its net charge tends to migrate, either to the cathode (if positively charged) or anode (if negatively charged). Due to the electrical resistance of the buffer, the apparatus tends to heat slightly during the separation, which can lead to undesirable mixing due to natural convection. To prevent this effect, the electrophoretic separation is typically conducted in a gel phase (typically polyacrylamide), which stabilizes the slow migrating band of protein against the mixing effects of natural convection. More recently, the same stabilizing effect has been realized by conducting the electrophoresis within small diameter capillary tubing (i.e., capillary electrophoresis). There are many chemistries that can be utilized to verify the protein purity in an electrophoresis experiment but the most commonly employed techniques are separations based on (1) molecular weight (SDS-PAGE) and (2) isoelectric pH of the protein (isoelectric focusing or IEF).

Electrophoretic separation of proteins based on their molecular weights is a common assay. The protein is denatured by boiling it in the presence of the detergent, sodium dodecyl sulfate (SDS). The SDS adsorbs strongly to the protein molecule and the charge of the SDS far exceeds the inherent charge of the protein. Thus, the charge to mass ratio of the all proteins is essentially constant and the proteins migrate in the presence of the electric field at velocities inversely proportional to their molecular weights. By utilizing molecular weight standards, one can verify the purity of a given protein as well as the molecular weight of its subunits. Care must

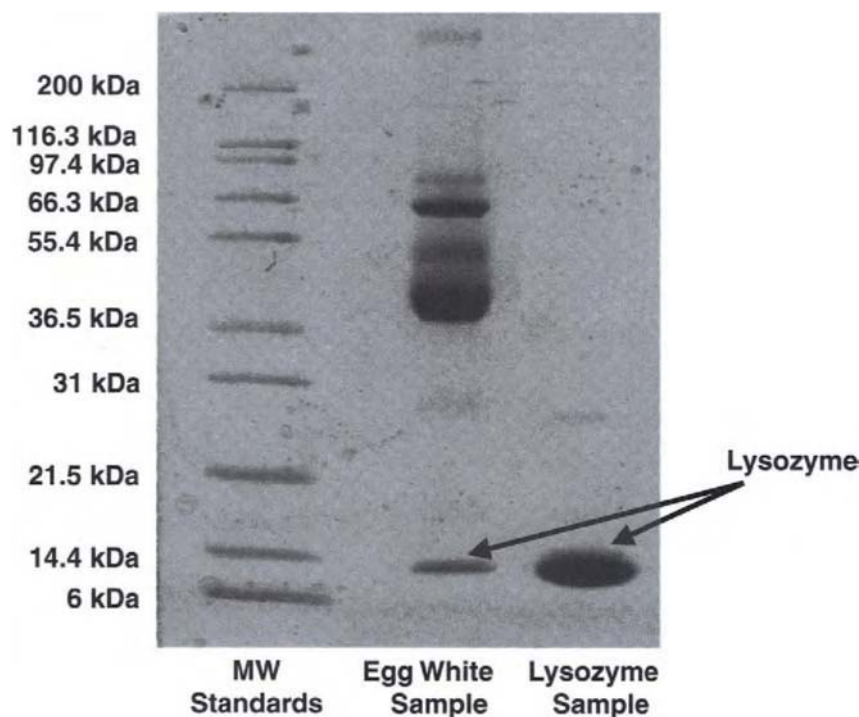


Figure 12.4 A typical SDS-PAGE evaluation of a protein. Notice the lysozyme is essentially pure as compared to the source egg white. Other significant bands in the egg white sample include ovalbumin (42 kDa) and conalbumin (78 kDa).

be exercised when interpreting the results of such an analysis. Two distinct bands in a SDS-PAGE may be due to two separate proteins or it may be that the protein of interest is composed of subunits, which have two distinct molecular weights. However, SDS-PAGE is an effective means for screening for protein impurities. For example, Figure 12.4 shows a SDS-PAGE experiment of lysozyme purchased from a vendor and chicken hen egg white versus a series of molecular weight standards. The various bands can be assigned molecular weights, which can then be related to known contaminants, which are not adequately removed during protein purification. Of course, a similar experiment can be run without denaturing the protein (typically referred to as a native PAGE experiment); however, the results cannot be correlated to molecular weight or net charge on the protein since both of these effects simultaneously impact the net migration through the electrophoresis gel.

The other common electrophoresis experiment is the isoelectric focusing or IEF experiment. This experiment relies on the protein migrating to its equilibrium position in a gel possessing a pH gradient. Carrier ampholytes are carefully layered throughout the gel to generate an equilibrium pH gradient. Figure 12.5 depicts the chemistry in an IEF gel. At one end of the gel the local pH is held at a relatively low value, say $\text{pH} = 4$; whereas, at the opposite end of the gel the pH is relatively high, say $\text{pH} = 10$. As the protein migrates through the gel, its side chains are ionized or neutralized depending on the local pH. If the protein is in the gel at a pH exceeding its isoelectric point (or pI), it will possess a net negative charge and tend to move towards the anode. Conversely, if the protein is in the gel at a pH less than its pI , it will possess a net positive charge and move towards the cathode. By placing the low pH end of the gel near the anode and the high pH end of the gel near the cathode, the protein will migrate to an equilibrium position in the gel, which is determined by its pI . Figure 12.6 depicts an IEF gel for the egg white sample shown in Figure 12.4. Once again, appropriate standards help identify the pI of the various bands. For small pH gradient IEF gels, one can separate proteins with pI s that differ by as little as 0.01 pH units. Generally, IEF gels are available in the pH range of 3–10. Due to reaction with the gel, the high end of the pH gradient tends to degrade over the course of the IEF experiment. This phenomenon, known as cathodic drift, tends to limit IEF separation to proteins with pI between 3 and 8.5. Fortunately, this range of pI 's covers most common proteins.

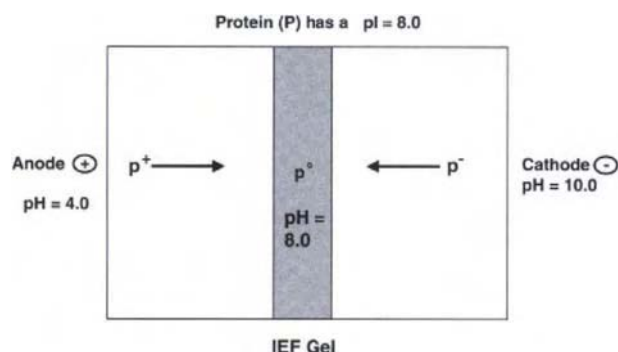


Figure 12.5 Mechanism of isoelectric focusing (IEF). A electrophoresis gel containing a stabilized pH gradient is arranged as shown in the figure. This configuration causes the protein to migrate to a single band in the gel where the local pH is equivalent to the protein's isoelectric point (pI). Since the protein has a net zero charge at this pH, it no longer migrates. Thus, the equilibrium location of the protein on an IEF gel indicates its pI .

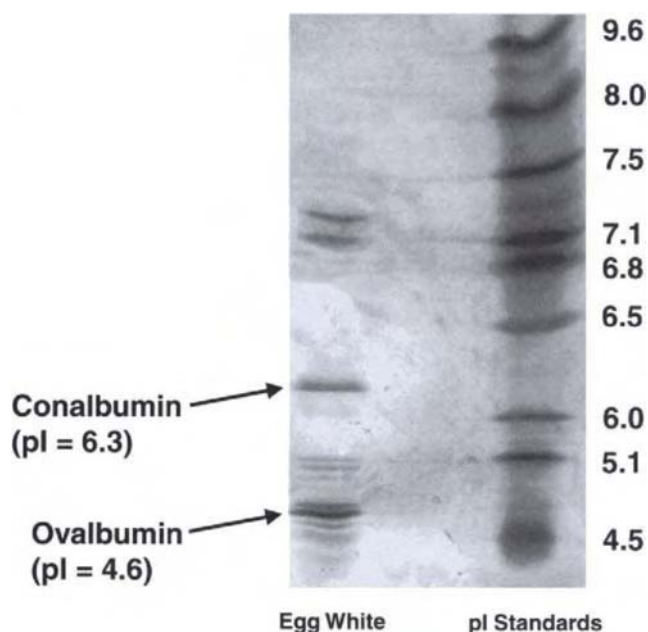


Figure 12.6 A typical IEF evaluation of a protein. In this case, lysozyme is not visible because it runs off the end of the gel since its pI (11.0) is larger than the highest pH within the gel. The egg white shows distinct pI bands at 6.3 (conalbumin) and 4.6 (ovalbumin) as well as some other minor bands near 5.0 and 7.0.

There are many other variations of electrophoresis experiments, which can be utilized to assay a protein for purity. For example, a protein may be subjected to an IEF separation. If there are multiple proteins within a given pI band, it is unlikely that they will have the same molecular weight. By conducting the IEF experiment in one dimension (the x-direction in Figure 12.7), followed by an SDS denaturation of the bands and SDS-PAGE in the other dimension (y-direction), a 2D electrophoresis experiment can provide even higher resolving power. However, such added effort is not usually profitable. Typically, one must run the IEF and SDS-PAGE experiments. If the IEF gel yields one band and the SDS yields one or a few distinct bands, then your protein is considered chemically pure.

A second analytical measurement of protein purity, which should be conducted, is HPLC analysis. Various chromatography columns can be utilized to verify the purity of the protein. The most commonly employed methods are ion exchange chromatography, molecular sieve chromatography (also known as gel permeation chromatography), and hydrophobic interaction chromatography (HIC). Each of these techniques probe a different chemical aspect of the protein and provide excellent independent check of purity and homogeneity.

Ion exchange chromatography is the most commonly employed chromatographic separation for proteins. The separation relies on electrostatic attraction between the protein and an oppositely charged stationary phase. The pH of the eluent is adjusted to assure the protein maintains a net charge, which is opposite to the stationary phase charge. The protein is injected onto the column under conditions of relatively low ionic strength. The protein immediately sticks to the stationary phase. The column is then subjected to a gradient of increasing ionic strength (while maintaining the same pH). Eventually, the protein is displaced from the column as the ionic strength increases due to Debye screening. Impurity proteins with a net charge less than

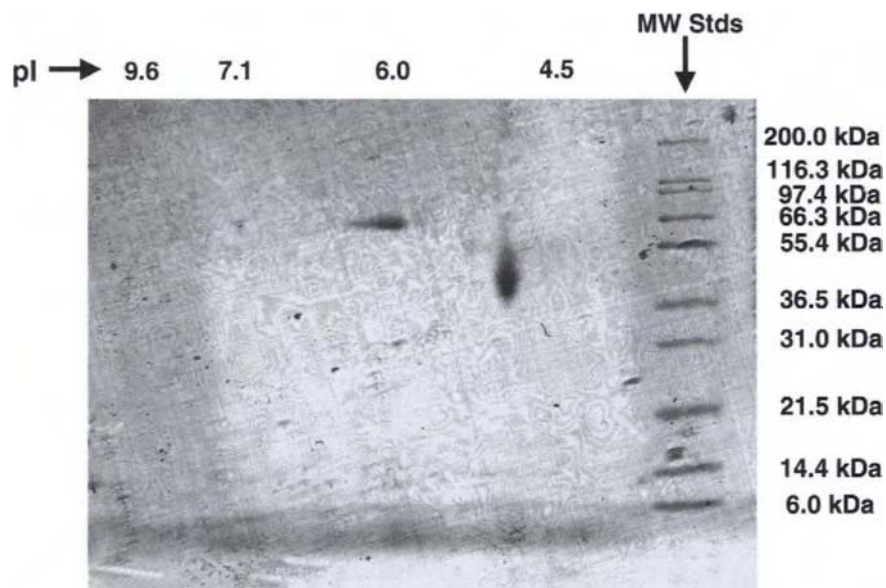


Figure 12.7 A two-dimensional gel of egg white proteins. The IEF gel is run first, shown in x -direction on the top of the figure, followed by the SDS-PAGE in the vertical direction. Each resulting spot is a unique pI/MW combination and is a more discriminating method to positively identify a protein as well as proving purity. In this case, the two major proteins in egg white are identified: conalbumin with pI = 6.3/MW = 78 kDa; and ovalbumin with pI = 4.6/MW = 42 kDa.

the desired protein will elute at lower ionic strengths and conversely impurities with a net charge larger than the desired protein will elute at higher ionic strengths. Thus, ion exchange chromatography is an excellent analytical tool for guaranteeing charge homogeneity in the protein mixture. In a like fashion, molecular sieve chromatography can be used to assure uniform molecular weight and shape of the protein and HIC assures a uniform hydrophobicity. If a given protein shows only one major peak by each of these chromatographic assays, one can be fairly confident of the purity of the system.

One last tool is finding increased use among protein crystal growers. The protein can exist as a fairly uniform and chemically homogeneous solution as assayed by the electrophoretic and chromatographic techniques described above. However, the screening conditions used to induce crystallization can dramatically alter the physical state of the protein, leading to aggregates of protein, which are very polydisperse. In general, there is now a consensus among protein crystal growers that proteins that exist as monodisperse solutions in a single aggregation state are likely to crystallize (Ferre-D'Amare and Burley 1997). Conversely, polydispersed aggregation states consistently fail to yield useful crystals. The use of dynamic light scattering for quickly assaying protein crystallization solution conditions has gained favor in recent years. Using very small volumes (approximately 10 μ l), the protein crystal grower can mix the protein in a potential growth solution at very low concentration and then assay for monodispersity. Only those solutions yielding monodisperse aggregates should be further optimized.

12.3. VARIABLES AFFECTING PROTEIN SOLUBILITY

As in any crystallization, the production of protein crystals requires bringing the protein into a supersaturated liquid state. The degree of supersaturation determines the rate of nucleation as well as crystal growth rate. Each of these phenomena are

important players in the crystal's diffraction quality and morphology. The degree of supersaturation is defined by the equilibrium solubility of the protein. Whatever variable affects the solubility of the protein can also be utilized to control supersaturation in the system and, thus, indirectly, the rates of nucleation and growth. The thermodynamic variables of temperature, pressure, and composition are typically utilized to alter the solubility of proteins. Biochemists have tended to focus on changes in composition to bring about supersaturation, but temperature and pressure have also been recently shown to be effective means of controlling supersaturation.

12.3.1. THE EFFECT OF pH ON PROTEIN SOLUBILITY

The effect of pH on protein solubility is significant and is one of the common variables in early screening trials. Generally, the solubility will change dramatically as pH is altered by roughly 0.5 pH units; however, some systems are sensitive to pH changes as small as 0.1 pH units (Zeppenauer 1971). The protein of interest will often dictate acceptable pH ranges for crystallization. Only pH values, which maintain the folded structure of the protein, are acceptable conditions for protein crystal growth. Unfolded structures will not crystallize and will tend to form an amorphous precipitate.

Usually the protein solubility is minimal at the protein's isoelectric point (Ries-Kautt and Ducruix 1992), where its net charge is zero. Such behavior is predicted by a naive application of the Debye-Huckel theory for ionic solutions (Edsall 1952):

$$\ln\left(\frac{S}{S_0}\right) = \frac{Z^2 \epsilon^2 N \kappa}{2 D R T (1 + \kappa a)} \quad (12.3)$$

where S is the protein solubility when the electrolyte is present in the solution; S_0 is the protein solubility in the absence of the electrolyte; and Z is the net charge on the protein (other symbols

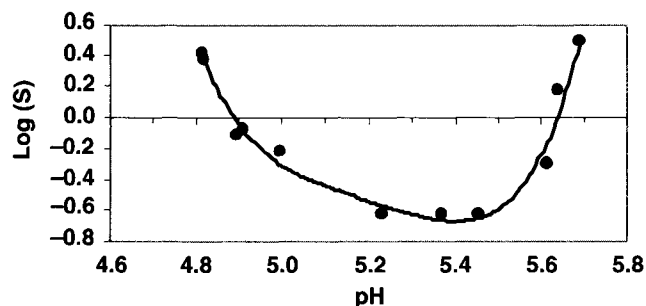


Figure 12.8 The effect of pH on solubility (S) of β -lactoglobulin. The pI of this protein is 5.2. (Data from Gronwell 1942.)

are defined in the nomenclature section). Thus, at the isoelectric point, $Z = 0$ and the protein solubility is at its minimum. Further, if one assumes that the protein charge is a linear function of the pH near the isoelectric point, one expects a parabolic dependence of the natural log of solubility ($\ln(S)$) near the pI. Indeed, such a parabolic dependence is observed for some systems (Figure 12.8) but is not the general rule. Far from the protein's pI, pH becomes a less significant variable affecting protein solubility as shown in Figure 12.9 for lysozyme. Many proteins are not stable near their pI and require crystallization at pH values far from the pI and, thus, pH may not be a significant screening variable in these cases. However, knowledge of the pI from the isoelectric focusing electrophoresis analysis (described in Section 12.2.8) provides valuable information. Knowing the suitable pH region over which the protein is stable and the pI defines the useful pH range for initial screening studies.

One additional concern when exploring the effect of pH on protein solubility is the nature of the buffer solution. Screening a wide variety of pH values usually means changing the buffer type, which prevents a true one-to-one comparison. Buffers are generally soft acids or bases and may bind to the protein, leading to anomalous behavior. In addition to affecting the equilibrium solubility of protein, changes in pH and buffer type can dramatically affect the crystal habit and the unit cell. This alteration can often lead to crystals more amenable to downstream processing (e.g., filtration) or X-ray diffraction analysis. In general, crystals possessing needle or plate geometries are less desirable than more block-like crystals.

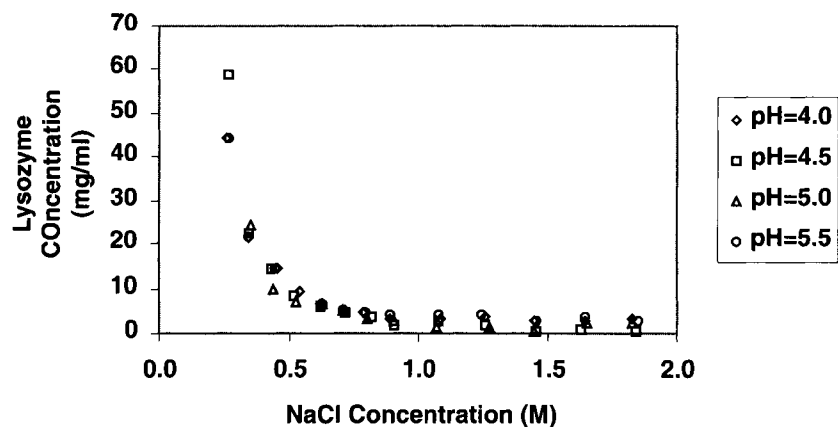


Figure 12.9 The effect of pH on lysozyme solubility. Note that these solubility measurements are at pH values far from lysozyme's pI of 11, which accounts for the insensitivity to pH. (Data from Howard et al. 1988.)

12.3.2. THE EFFECT OF ELECTROLYTE ON PROTEIN SOLUBILITY

Protein purification has long relied on precipitation via "salting out." The basic idea is that "salting" the solution (adding electrolyte) causes the protein to come "out" as separate solid phase. The effect of the electrolyte on protein solubility is usually described as "salting out" or "salting in." Salting-in implies an increase in the protein solubility as the electrolyte is added to the solution. Depending on the type of electrolyte employed either or both of these phenomena are observed. Hofmeister ranked the efficiency of a variety of electrolyte types to salt-in or salt-out egg white proteins in 1887 (Hofmeister 1887); yet, the physical rationale for such a ranking still remains debatable.

Just as the Debye-Huckel theory can be used to explain the solubility minimum at a $\text{pH} = \text{pI}$, it also explains the role of electrolyte concentration. Referring to Eq. (12.3), the electrolyte concentration affects the value of κ , the inverse Debye length, as shown below:

$$\kappa = \sqrt{\frac{8\pi N \epsilon^2 I}{1000 D k T}} \quad (12.4)$$

Increasing the electrolyte concentration causes an increase in the ionic strength (I), increasing κ and, thus, protein solubility. Therefore, the Debye-Huckel theory predicts salting-in of the protein. Indeed, this effect is evident for a number of proteins at low ionic strength as shown in Figure 12.10. However, at moderate to high electrolyte concentrations, the Debye-Huckel theory fails to predict the commonly observed salting-out behavior of proteins. In fact, some proteins such as lysozyme display salting-out but not salting-in behavior.

Salting-out is not well understood. One popular explanation for this effect relies on the relative hydration of the protein versus bulk electrolyte. In this model, the electrolyte is assumed to bind bulk water as water of hydration near the ion's surface. Likewise, the protein needs to be hydrated with water. As the bulk electrolyte and the protein compete for bulk water to hydrate their respective surfaces, the protein become partially dehydrated and prefers to fill such exposed surface (dehydrated surface) with other protein molecules; thus, facilitating crystal contacts. Thus, the solubility of the protein is reduced as the electrolyte is added to the protein solution. The effectiveness of ions (cations and anions) to cause phase separation (or lower solubility) has been documented by

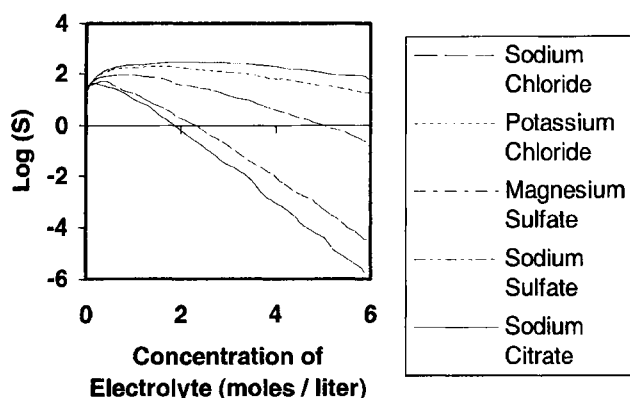


Figure 12.10 Various electrolyte types can salt-out (sodium citrate), salt-in (sodium chloride) or both salt-out and salt-in (magnesium sulfate) horse carboxyhemoglobin. (Data from Green 1931.)

many investigators and is named the Hofmeister (or lyotropic) series. Such lists exist for both anions and cations, and are often reported differently by different authors. An abbreviated list follows from three different sources:

1. From Shaw (1992):
Cations: Cs (least effective) -Rb-NH₄-K-Na-Li-Ba-Sr-Ca-Mg (most effective)
Anions: SCN (least effective) -I-NO₃-Cl-SO₄-citrate (most effective)
2. From Hunter (1993):
Cations: Cs (least effective) -Rb-K-Na-Li (most effective)
Anions: SCN (least effective) -I-Br-Cl-F-NO₃-chlorate (most effective)
3. From von Hippel and Schleich (1969):
Cations: Li (least effective) -Na-K-NH₄-Mg (most effective)
Anions: SO₄ (least effective) -PO₄-COO-citrate- tartrate-bicarbonate-chromate-Cl-NO₃-chlorate-SCN (most effective)

Thus, the general ordering of ions shows some consistency, but there is not a clear agreement as to the proper order of ions for effectiveness in causing crystallization. Cohn (1925) empirically modeled the salting out effect using the following equation:

$$\ln(S) = \beta - k_s C_s \quad (12.5)$$

where β and k_s (the salting-out constant) are experimentally determined parameters. This equation tends to work well at moderate to high electrolyte concentration, but fails at low electrolyte concentrations for systems which show mixed (i.e., both salting-in and salting-out) behavior (see Figure 12.11). The β parameter is often modeled separately as a function of pH and temperature (Sorenson 1933; Green 1931; Czok and Bucher 1961).

There have been a number of recent studies of the effect of electrolyte on the solubility of both acidic ($pI < 7$) and basic ($pI > 7$) proteins. The acidic protein, α -amylase ($pI = 5.9$), follows the trends predicted by the Hofmeister series for anions (Veesler et al. 1996). This study was complimented with work on another acidic protein, collagenase ($pI = 4.1$), which was also found to obey the Hofmeister series (Lecroisey et al. 1979; Carbonnaux et al. 1995). On the other hand, lysozyme ($pI = 11$) tends to follow a trend exactly opposite than that predicted by the Hofmeister series for anions (Guilloteau et al. 1992). This surprising result was also seen for Erabutoxin b ($pI = 9.2$) (Low et al. 1976) and

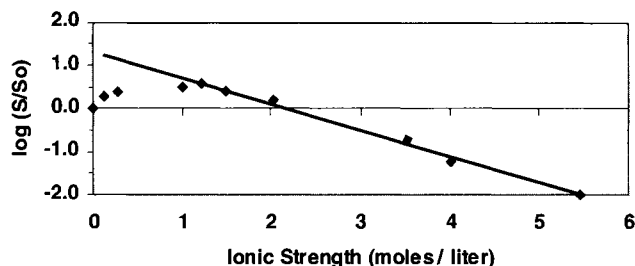


Figure 12.11 Cohn's salting-out equation is accurate at moderate to high concentrations but can display significant errors at low electrolyte concentrations where salting-in predominates. (Data from Green 1931.)

for BPTI ($pI = 10.1$) (Lafont et al. 1997). These results indicate a clear trend in the effect of electrolyte type on protein solubility, depending on the pI of the protein. Acidic proteins follow the Hofmeister series for anions, while basic proteins follow the reverse of the Hofmeister series for anions. These studies also consistently found that the anion dominates the effect of the electrolyte on the protein solubility. Collins (1997) predicts that anion should have a much larger effect based on the anion's ability to more significantly alter the structure of water than cations. In addition, anions are more strongly hydrated than cations for a given charge density.

12.3.3. THE EFFECT OF ANTI-SOLVENTS ON PROTEIN SOLUBILITY

Another common chemical additive utilized to reduce protein solubility is small, polar organic molecules such as methanol, ethanol, and acetone. Such water-miscible solvents are often called anti-solvents. The most widely known separation utilizing such solvents is the Cohn method of blood fractionation, which utilizes ethanol for the recovery of a variety of proteins from blood (Cohn et al. 1940). Such separations are usually carried out near the isoelectric point in order to bring the protein to a point of minimal solubility and minimize the amount of anti-solvent required to achieve the precipitation or crystallization.

Anti-solvent addition has multiple effects on the protein. First, these water-miscible solvents tend to act in a manner similar to electrolytes, competing with the protein for water of hydration and "solventing-out" the protein. Second, the solvent tends to lower the dielectric constant of the water, thereby enhancing electrostatic interactions between protein molecules and reducing their solubility. The lower dielectric constant also tends to solubilize the hydrophobic core of the protein molecule, which can lead to protein unfolding or denaturation. Thus, anti-solvents are generally added while the protein is kept cold, typically at or below the freezing point of water. Even when carefully cooled, proteins will denature at some critical anti-solvent concentration and great care must be exercised to assure that crystallization is conducted below this critical concentration. Empirical models analogous to the salting-out equation have been proposed to account for the effect of the anti-solvent on protein solubility. One reasonable model proposed by Hoare and coworkers (Hoare et al. 1983) semi-empirically relates the solubility of the protein to the mixture dielectric constant (D_m):

$$\ln\left(\frac{S}{S_o}\right) = k\left(\frac{1}{D_w^2} - \frac{1}{D_m^2}\right) \quad (12.6)$$

Although a reasonable model, the real source of reduced solubility is more complicated than a simple dielectric constant reduction as

discussed by Orella and Kirwan (1989, 1991) in their studies of model compounds (amino acids).

12.3.4. THE EFFECT OF SOLUBLE SYNTHETIC POLYMERS ON PROTEIN SOLUBILITY

The use of polyethylene glycol (PEG) as a chemical additive to induce protein crystallization has found widespread use in the past two decades. PEG is the water-soluble polymer of choice for protein crystallization; however, there is no reason to suspect that other water-soluble polymers would be any less effective. The role of PEG in promoting protein crystallization is not clear. PEG, like small water-miscible organic solvents, will hydrate as well as alter the dielectric constant of the solvent. So, in some respects, PEG will act as an anti-solvent. However, the volume exclusion effect must account for its effectiveness, especially for the high molecular weight PEGs. Polyethylene glycol is available in a wide range of molecular weights ranging from oily liquids (molecular weights of a few hundred) to waxy solids or powders having molecular weights as high as 20,000. All of these PEGs have proven effective in a variety of protein systems but each protein system needs to be optimized with respect to the molecular weight. PEGs of molecular weight 4000 or 6000 seem to be very effective for most protein systems. In general, the higher the molecular weight, the more effective the PEG is at reducing the protein solubility. Most proteins will crystallize in a fairly narrow concentration range of PEG, typically between 4 and 18% w/w. The exact concentration is not needed to produce crystals, so rather crude grids can be screened to identify efficacy of PEG for protein crystallization. Systematic studies of the effect of PEG on protein solubility are lacking; thus, only the above trends are discussed in the literature.

12.3.5. THE EFFECT OF PRESSURE ON PROTEIN SOLUBILITY

In 1990, Visuri and coworkers (Visuri et al. 1990) reported that glucose isomerase crystallized rather rapidly at elevated pressures (100 MPa or higher pressure). This initial exciting result motivated a body of work which studied the effect of pressure on lysozyme solubility and growth kinetics (Gross and Jaenicke 1993; Schall et al. 1994; Suzuki et al. 1994; Saikumar et al. 1995; Lorber et al. 1996; Takano et al. 1997). Although this field continues to advance at rapid rate, it has come to some definite conclusions for lysozyme. First, Schall et al. (1994) clearly demonstrated that the rates of growth are dramatically depressed for lysozyme at high pressures, which is in sharp contrast to the results of Visuri et al. (1990) on glucose isomerase. Subsequent studies (Saikumar et al. 1995; Takano et al. 1997) provided further quantitative support of this conclusion. The reduced growth is primarily attributed to the increased solubility of lysozyme under high pressures as shown by Takano et al. (1997). The discrepancy between the results for lysozyme and glucose isomerase suggests that pressure can have a variable effect on protein solubility and growth. Nevertheless, the effect of pressure is evident only at extremes of pressure and, for most practical applications, the effect is negligible.

12.3.6. THE EFFECT OF TEMPERATURE ON PROTEIN SOLUBILITY

Proteins have been documented to crystallize at a wide variety of temperatures, yet most proteins are crystallized at room temperature (25°C) or in a refrigerator (4°C). This observation is a reflection of experimental tradition in the protein crystallography field. Accessibility to cold rooms operating at 4°C and fear of protein losses due to microbial attack prompts crystallographers to inves-

tigate this temperature as an alternative to more typical room temperature screening. Most proteins will denature at temperatures above 40°C, so temperature can only be varied over a limited region (i.e., 0–40°C). Further, the protein crystal can undergo a phase transition within this narrow accessible temperature range.

For example, lysozyme is documented to undergo a crystalline phase transition from tetragonal (low temperature form) to orthorhombic (high temperature form) at approximately 25°C (Pusey and Gernert 1988). Protein solubility can increase, decrease or remain constant as the temperature of the system increases. All three effects have been observed on real protein systems.

Classical thermodynamics describes the effect of temperature on the solubility of a molecule in solution. If the heat of crystallization, ΔH_{cry} , and solubility, C_1^* , at one temperature (T_1) are known, the solubility as a function of temperature can be determined via the van't Hoff equation:

$$\ln\left(\frac{C^*}{C_1^*}\right) = \left(\frac{\Delta H_{cry}}{R}\right)\left(\frac{1}{T} - \frac{1}{T_1}\right) \quad (12.7)$$

where C^* is the solubility of the protein in the liquid phase at temperature, T , and R is the gas constant. At least for lysozyme, this model is in excellent agreement with the data. Calorimetric measurement of the heat signal upon crystallization under isothermal conditions (Darcy and Wiencek 1998) shows excellent agreement between the solubility predicted by the direct measurement of ΔH_{cry} (see Figure 12.12) and the experimental data (Ewing et al. 1994).

For those systems that do display a temperature-dependent solubility, a common observation is that the protein solubility is more sensitive to temperature variations at low ionic strengths. McPherson (1989) explicitly states, "the use of temperature [as a means to induce crystallization] is usually of value when the protein solution is at low ionic strength." Ries-Kautt and Ducruix (1992) have come to the same general conclusion; "protein solubility is more sensitive to temperature variations at low salt concentrations." To further emphasize the veracity of this statement, Figure 12.13 shows the temperature-sensitivity (as measured by the magnitude of ΔH_{cry}) of lysozyme as a function of salt concentration. Large magnitudes for ΔH_{cry} imply a very temperature-sensitive system. In all cases, the supposition that low ionic strength systems display enhanced sensitivity to temperature is shown to be correct for lysozyme. The sensitivity of low ionic strength solutions to temperature is physicochemically intuitive. Within a crystal lattice, the protein molecules will be in closer proximity than they normally are in solution. At low ionic strength, the charged side chains of the protein molecule are not effectively screened. Thus, the enthalpic effects are expected to be more significant in the absence of a screening electrolyte.

Temperature is a particularly attractive tool for easily controlling the relative rates of nucleation and crystal growth. However, the solubility of the protein must change dramatically with temperature if such a control strategy is to be effective. Thus, generating solution conditions which produce protein crystals at low ionic strength should increase the temperature-sensitivity of a given protein system. It is well known that crystals can be produced by dialysis against low ionic strength buffers (McPherson 1989). This method will not always be successful, forcing the researcher to rely on salt or PEG addition to induce the crystallization. The choice of electrolyte used for salting-out has traditionally been limited to common electrolytes such as ammonium salts or sodium chloride. Recently, systematic studies of the effect of electrolyte type on protein solubility are yielding information that is fundamental enough to be generalized. The works of Ries-Kautt and Ducruix (1989, 1991, 1992) are particularly noteworthy. They have shown

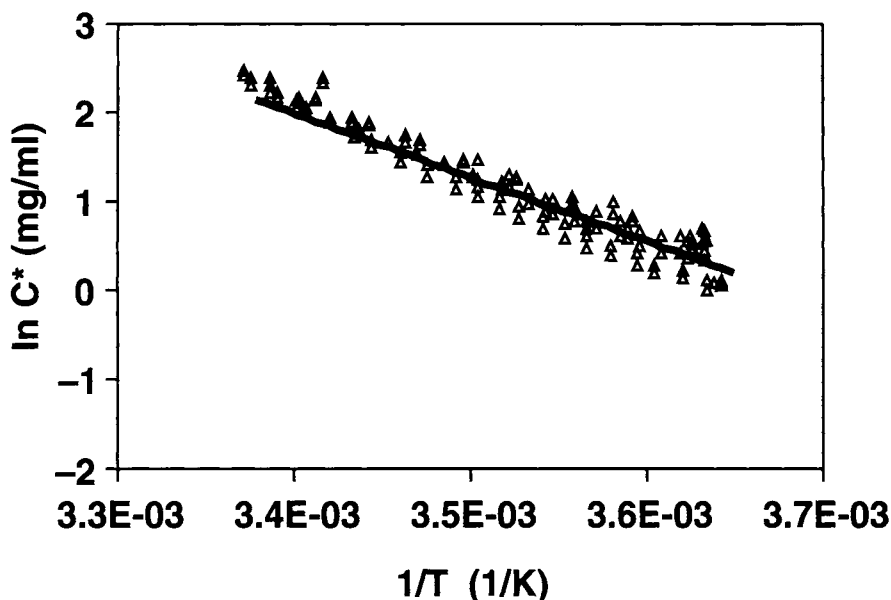


Figure 12.12 Van't Hoff plot of experimentally determined lysozyme solubility as a function of temperature (triangles) compared to solubilities calculated directly from the ΔH_{cry} and the van't Hoff equation (Eq. (12.7)). (Data from Ewing et al. 1994.)

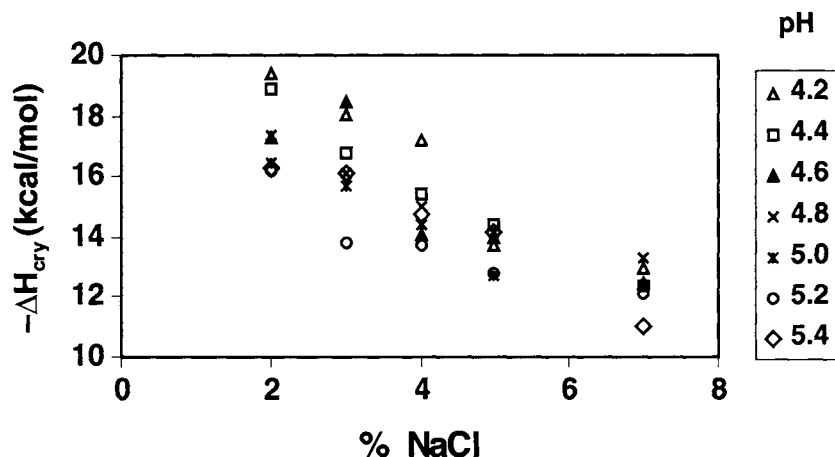


Figure 12.13 The role of electrolyte on the temperature sensitivity of solubility for lysozyme. The temperature sensitivity is directly measured by ΔH_{cry} , with large magnitudes indicating high sensitivity. At a variety of pH values, lysozyme's solubility is most sensitive to temperature at low electrolyte concentration (NaCl in this case). (Data from Ewing et al. 1994.)

in a convincing fashion that the effect of a given anion or cation on a protein's solubility is directly related to the position of the anion or cation in the Hofmeister series. Thus, the desired level of salting-out can potentially be attained at the low ionic strengths (0.5 M or less). Indeed, recent work (Wienczek and Darcy 1997) confirms that lysozyme can be effectively crystallized at low ionic strengths while increasing its temperature sensitivity (see Figure 12.14) as measured by ΔH_{cry} .

12.3.7. CASE STUDIES IN LYSOZYME AND THE GENERIC PROTEIN PHASE DIAGRAM

Lysozyme is the most common subject of protein crystallization studies. Lysozyme is relatively inexpensive to purchase in a pure

form and the abundant physicochemical data tends to catalyze its continued study. In addition, lysozyme displays many of the features that are commonly seen in small molecule crystal growth. Most protein crystallographers will view lysozyme as a trivial system, which does not display the typical problems encountered with most protein crystal growth experiments. However, the study of lysozyme does have tremendous value and can explain many of the undesirable outcomes of protein crystallization trials.

Traditionally, those who grow crystals have viewed the role of temperature in terms of the Miers diagram (Figure 12.15). The Miers diagram is divided into three regions: (1) the stable zone where the protein concentration is below the solubility concentration; (2) the metastable zone where the concentration of protein in solution is greater than the solubility concentration and growth

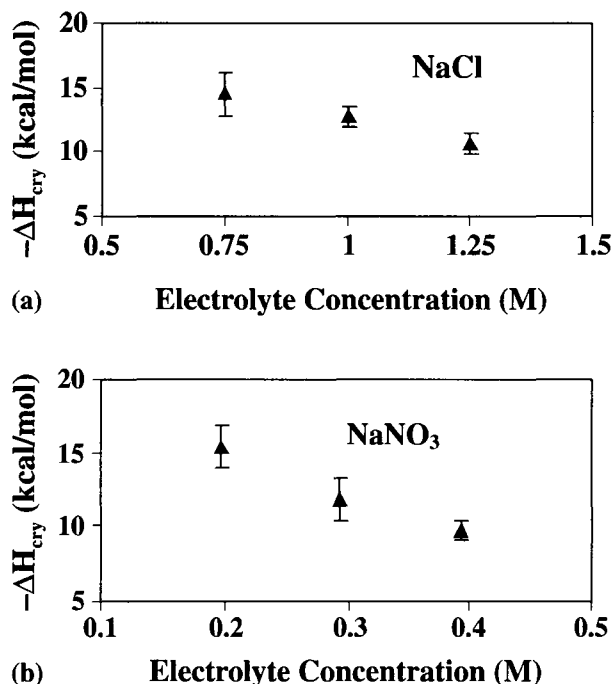


Figure 12.14 The electrolyte type can affect the relative temperature sensitivity of solubility. (a) Lysozyme crystallization typically requires 1.0–1.25 M NaCl with a concomitant value of $\Delta H_{\text{cry}} = -10$ kcal/mol. (b) Only 0.2 M NaNO₃ is required to attain similar quality crystals with increased sensitivity of $\Delta H_{\text{cry}} = -15$ kcal/mol.

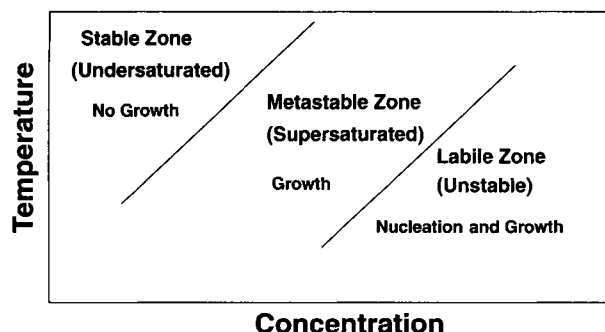


Figure 12.15 The Miers phase diagram for crystallization and nucleation as a function of temperature. The three zones of the phase diagram include: (1) the stable zone where the solution is undersaturated and no solid phase can exist at equilibrium; (2) the metastable zone where the solution is moderately supersaturated and growth of existing crystals continues until the solution reaches the solubility line, but no new nucleation can occur; and (3) the labile zone where the solution is highly supersaturated and both crystal growth and nucleation occur simultaneously.

of existing crystals occurs but no new crystals are nucleated; and (3) the labile zone where the concentration of protein in solution is much greater than the solubility concentration and spontaneous nucleation as well as crystal growth occur. To obtain large crystals with minimal nucleation, one temperature control strategy would be to reduce the protein solution temperature and enter the labile zone to allow for nucleation. After a short time, the temperature

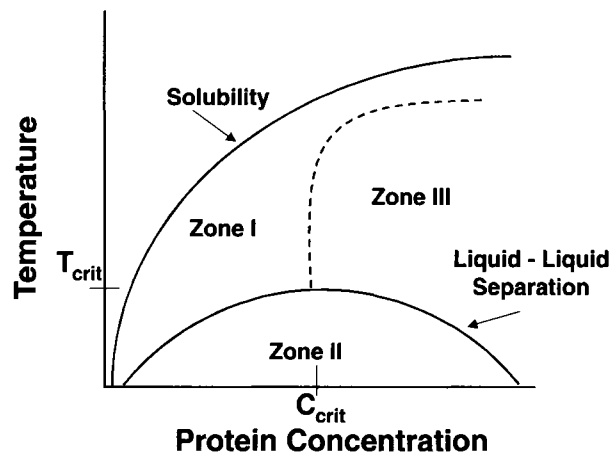


Figure 12.16 The generic protein phase diagram as presented by Muschol and Rosenberger (1997). Zone I depicts the region of supersaturation where well formed lysozyme crystals form. Zone II is a region where lysozyme undergoes a rapid liquid-liquid phase separation, with the resulting concentrated lysozyme phase quickly transforming to the more stable crystalline form. Crystals formed in Zone II are of poor quality. Zone III depicts a region characterized by gel formation, unsuitable for crystal growth.

would be elevated and the solution placed into the metastable zone to halt the nucleation and allow subsequent crystal growth.

Recently, Muschol and Rosenberger (1997) have discussed the “generic” protein phase diagram, which is summarized in Figure 12.16. This phase diagram is significantly more complex than phase diagrams of the type shown in Figure 12.15. The phase envelope indicates a solid-liquid equilibria (crystallization) as well as a meta-stable liquid-liquid equilibria. Zone I encompasses the traditional concepts of supersaturated liquid solutions that should produce a crystal, provided a seed crystal is present or the labile zone (not plotted) is penetrated. Zone II encompasses the liquid-liquid phase separation where the protein will spontaneously separate into two liquid phases, one phase having extremely high concentrations of protein in the liquid phase (several hundred mg/ml).

Zone III is at unrealistically high protein concentrations (>200 mg/ml) and is composed of a highly viscous gel phase of the protein. Crystals grown while limiting solution conditions to Zone I are of acceptable to high quality. Although the nucleation rate in Zone II is dramatically accelerated due to the segregated high concentrations of protein, the resulting growth centers located within protein-rich droplets tend to grow as clumps with facets of faster growth rates extending out into the second protein phase (also supersaturated) resulting in a “sea urchin” crystal morphology which is unacceptable. Thus, nucleation by penetrating into Zone II, even for very short times, will not result in diffraction-quality crystals. Indeed, one of the features that protein crystallographers believed to be absent from the model lysozyme system was “oiling out” or phase separation of the protein as a separate liquid. As these results show, lysozyme does possess this feature although not under the conditions that are typically employed to grow lysozyme crystals. Thus, years of study on lysozyme have tuned the growth conditions of this protein so that many of the nonideal effects seen in more typical protein crystallization experiments are not observed with lysozyme. By extending the studies on lysozyme to include extremes in composition, the generic nature of protein crystallization is starting to emerge.

12.4. NUCLEATION AND GROWTH MECHANISMS

The fundamentals of nucleation and growth of protein crystals have not been of interest to the general protein crystallography community until the last decade or so. Protein crystallographers, in general, have only been interested in obtaining one good crystal of their particular favorite protein. In fact, the methods typically used to grow a few crystals of X-ray diffraction quality are not suited for fundamental investigations on protein crystal nucleation and growth. These methods, which are described in more detail below, are ideal for screening experiments since a wide variety of precipitants are utilized in a manner such that supersaturation is increased during the course of the experiment in order to induce nucleation. Unfortunately, once the experiment starts, there is no simple way to track the relative protein and precipitant concentrations let alone measure the supersaturation of the system. Thus, fundamental information on the nucleation rate and the growth rate of protein crystals is impossible to extract from such screening experiments.

Within the last decade, there has been a rapid increase in the number of investigations focused on the fundamentals of protein crystallization. Classical studies of crystal growth (experimental methods described below) have shown that many of the well-developed models for protein crystal growth (as described in Chapter 2) apply. More recent studies of protein crystal growth have allowed for the direct visualization, at the atomic level, of the growing crystal face (Malkin et al. 1995) using atomic force microscopy (AFM). Growth steps are clearly seen in such images, all with their dynamics. The presence of two-dimensional nucleation as well as screw dislocations is directly visualized and validates the mechanisms postulated based on macroscopic measurement of crystal face growth rates (Malkin et al. 1996).

Nucleation of protein crystals typically requires extremely high supersaturation levels. Studies of protein nucleation are limited, with most efforts focused on light scattering as a tool to detect nucleation. Feher and Kam's work set the tone for much of the work that followed (Feher and Kam 1985). They model nucleation in a classical fashion, as a cooperative step-by-step addition of monomers to a cluster. Light scattering is utilized to follow the cluster size distribution as a function of time and solution variables, which yield estimates for the relative forward (cluster growth) and reverse (cluster dissolution) rates of monomer addition. Certainly, the protein crystal nucleation is an area that deserves additional study.

12.5. PHYSICOCHEMICAL MEASUREMENTS

12.5.1. SOLUBILITY DETERMINATION

Solubility curves have traditionally been determined by either crystallization of a supersaturated solution or by dissolution of crystals in an undersaturated solution. Suitable solution conditions, which produce crystals, must be known in advance for both methods. Protein solubility can be determined as a function of many parameters including temperature, salt concentration, salt type, buffer and pH. For the crystallization method, a grid is made of samples of two or three different initial protein concentrations and at least four different values of a given variable (e.g., three protein concentrations at four different temperatures = 12 samples). Aliquots are removed periodically for concentration determination for up to 6–12 weeks after crystals appear. In the case of dissolution experiments, a batch of crystals previously grown in the appropriate buffer is needed. Crystals are placed in undersaturated solutions and allowed to dissolve. Again, for six to

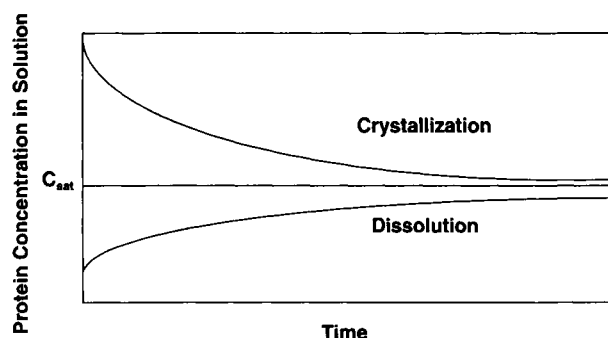


Figure 12.17 Proper solubility measurement requires monitoring the liquid phase concentration of protein in both crystallizing as well as dissolving systems.

twelve weeks, aliquots are periodically removed for concentration determination.

As shown in Figure 12.17, both methods should converge to the same solubility for each value of the parameter being measured (Ries-Kautt and Ducruix, 1992). The main disadvantages of these methods for solubility determination are the amount of protein (typically gram quantities), and time (6–12 weeks) required. The protein may be recovered at the end of the experiment if contamination has not occurred. Cacioppo et al. (1991) developed a micro-method technique for protein solubility determinations. This method requires less protein, about 200 mg of protein or less, to determine key regions of a protein's solubility diagram. Broide and coworkers (Broide et al. 1996; Berland et al. 1992) measure solid-liquid phase boundaries for protein solutions by alternate heating and cooling of a crystal. The dissolving temperature is the minimum temperature at which the sharp edges of the crystal are rounded. In a similar fashion, AFM has been utilized to detect the cessation of step formation to detect the solid-liquid phase boundary (Malkin et al. 1996). As mentioned earlier, the effect of temperature on solubility can be detected by directly measuring the enthalpy of crystallization (Darcy and Wiencek, 1998).

12.5.2. GROWTH RATE DETERMINATION

Crystal growth rates are typically measured via video microscopy. A standard setup consists of a light microscope with some form of temperature controlled stage where the crystals are observed. A video camera and time-lapse recorder are often used to obtain images of the crystals over a period of time (Durbin and Feher 1986). A computer can also capture images in a time-dependent manner for analysis using image analysis software. Pusey has developed a computer-controlled apparatus able to simultaneously follow the growth rate of up to 40 crystals (Pusey 1994). Typical experiments may require a week or more for growth rate analysis at a fixed solution condition and temperature.

AFM is now utilized to relate microscopic measurement of step velocity to macroscopic face growth rates (Malkin et al. 1996). Such data can be collected at a very rapid rate but does require some familiarity with the technique and access to a research caliber AFM. Likewise, microcalorimetry may be utilized to extract crystal growth rates at a very rapid rate, provided the protein's heat of crystallization is sufficient to yield a measurable signal (Darcy and Wiencek, 1998). Both of these techniques can provide growth rates over a wide range of conditions within days, as opposed to months by more traditional video microscopy techniques.

12.6. TRADITIONAL SCREENING TOOLS

Protein crystallographers have dominated the field of protein crystallization through the years and will likely continue to do so. The crystallographer is primarily concerned with identifying one magical solution condition or “gizmo,” which will give a relatively large (at least 0.1 mm in all dimensions) crystal that diffracts to high resolution. After collecting the X-ray diffraction data on the native crystal and a few heavy atom derivatives, the crystallization is no longer a concern to the crystallographer. Rarely, if ever, are fundamental studies of solubility, nucleation, and growth kinetics conducted to aid in the process of generating high-quality protein crystals. This lack of a fundamental approach is driven by the lack of material (usually only a few milligrams of protein are available) as well as tremendous pressure to get a crystal, get an X-ray data set, get a structure, and get a publication.

For these reasons, protein crystallization has and will continue to rely on screening techniques, which utilize micromethods. Typical methods allow one to screen over 100 solution conditions with just a few milligrams of protein. The choice of which solution conditions to screen has been greatly simplified through the years. Early crystallographers had to rely on totally random screening to identify suitable solution conditions for protein crystallization. As more data accumulated, it became obvious to Gilliland and coworkers (1994) that a database of crystallization conditions would be extremely helpful. Thus, one first surveys the Biological Macromolecular Crystallization Database (BMCD) for related proteins and conditions that worked well with such proteins. The BMCD is now available at no cost via an Internet interface (<http://www.bmcd.nist.gov:8080/bmcd/bmcd.html>). Concurrently, Jancarik and Kim (1991) proposed that most protein crystals are produced by a relatively limited number of precipitants and developed a sparse sampling matrix, which efficiently sampled these precipitants under a variety of combinations and pH. Screening kits based on this sparse matrix approach, as well as a variety of other useful solution conditions, can be purchased in ready-to-use form (for example, see <http://www.hamptonresearch.com>). Such pre-formulated precipitant solutions are typically tested in a variety of crystallization experiments, which are described below. In general, these techniques require minimal volumes (1–2 μ l volumes are not unusual). The protein is normally available in a fairly concentrated form (5–50 mg/ml) in a stabilizing buffer. The designs described below attempt to modify the nucleation and growth kinetics of the system by slowly increasing supersaturation in the system.

For each experiment described below, there is an “ideal” trajectory that the experiment needs to traverse in the phase diagram of the protein. Typically, the protein concentration as well as the precipitant concentration is varied simultaneously to move around the phase diagram. Unfortunately, screening experiments typically sample just one or a few starting conditions for a given precipitant and may yield poor or no crystals even though the precipitant may, indeed, be ideal for the protein at hand. For each of the crystallization experiments described below only the ideal trajectory will be presented, but the reader must remember that screening is usually far from the optimal solution conditions. Typically, once screening is completed, further optimization is required and such optimization is amenable to tried-and-true statistical treatments (Carter 1997).

12.6.1. VAPOR DIFFUSION EXPERIMENTS

Vapor diffusion experiments rely on water (and other volatile species) evaporation from a small droplet containing the protein and precipitant to slowly increase both the protein concentration

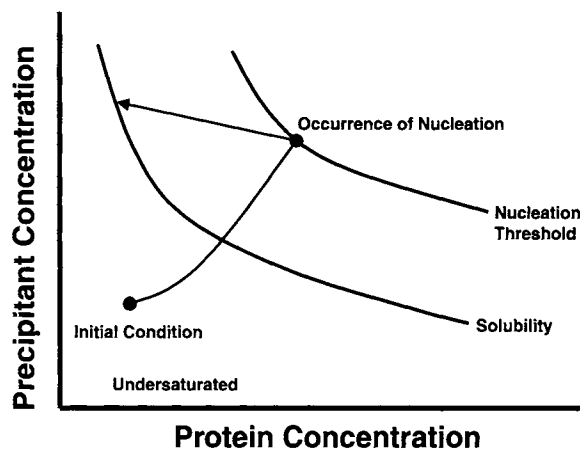


Figure 12.18 The ideal trajectory of a vapor diffusion experiment. The arrow indicates the composition changes that might take place in the evaporating droplet with a simultaneous protein nucleation and growth.

and precipitant concentration within the droplet. Although the least controlled method that one can employ, vapor diffusion has proven to be the most popular technique for growing protein crystals. As shown in the phase diagram of Figure 12.18, this method allows one to simultaneously increase the protein concentration, while also decreasing the protein solubility due to the increased precipitant concentration. In vapor diffusion, the initial conditions are usually undersaturated. The most commonly employed technique is the hanging drop method, although the same effect is achieved with sitting drops. A small drop (1–10 μ l) of a solution containing the protein is typically mixed with an equal volume of the precipitant solution and placed on a microscope cover slip. The cover slip is inverted over a reservoir of precipitant solution as shown in Figure 12.19. The reservoir solu-

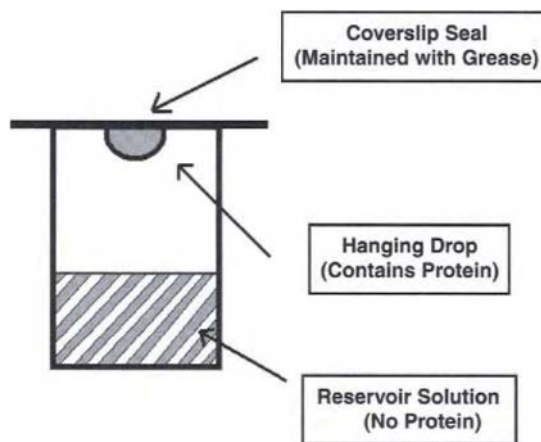


Figure 12.19 The vapor diffusion experiment (hanging drop device shown) relies on water evaporating from the protein-containing droplet and diffusing away to the reservoir solution. Along with the protein, the droplet contains some crystallizing agent such as salt or PEG. The water evaporates until the droplet reaches chemical equilibrium with the reservoir solution. This evaporation simultaneously increases the protein and crystallization agent concentration that will, in the ideal case, cause nucleation and growth of a few protein crystals.

tion is protein free and typically at twice the precipitant concentration of the drop. The supersaturation of the protein solution changes over time as the water in the hanging drop equilibrates with the water in the reservoir solution. Thus, the protein concentration and the precipitant concentration in the drop increase causing nucleation and crystallization.

12.6.2. FREE INTERFACE DIFFUSION

This technique has a strong analogy to the vapor diffusion technique. First employed by Salemne (1972), the technique relies on carefully layering the precipitant solution on top of the concentrated protein solution in a capillary (see Figure 12.20). The narrow diameter of the capillary minimizes mixing due to natural convection in the system. Thus, the precipitant and protein slowly inter-diffuse. As time proceeds, there is a sampling of solution conditions along the axis of the capillary ranging from very low precipitant and high-protein concentrations to the converse. In essence, many combinations of protein and precipitant concentration pairs are sampled locally within one capillary. Thus, many trajectories are sampled simultaneously on the phase diagram. If we focus on one local slice, which yields excellent crystals, the trajectory outlined in Figure 12.21 is expected. The protein is initially at a high concentration and is slowly diluted by the faster moving (small molecule) precipitant. The precipitant concentration increases to the point where nucleation occurs and the crystals start growing and consuming local supplies of protein.

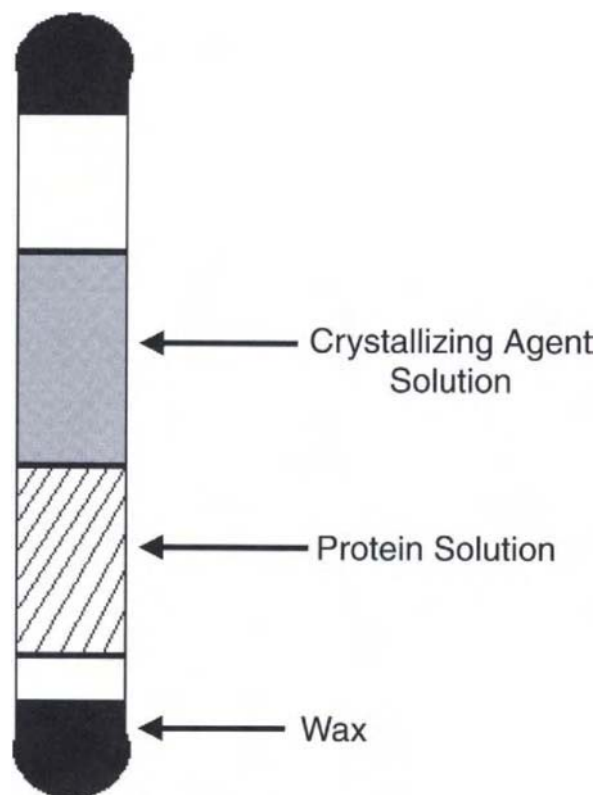


Figure 12.20 The free interface diffusion method utilizes a capillary to minimize convective mixing between the protein solution and the second layer of solution containing the crystallization agent (e.g., salt or PEG). The capillary is sealed at both ends with an appropriate adhesive or wax to prevent evaporation of the solution.

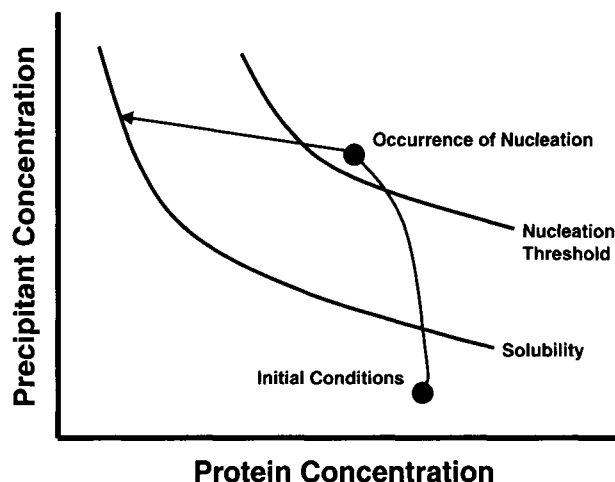


Figure 12.21 The ideal trajectory of a free interface diffusion experiment. Each location within the tube undergoes a different trajectory. At one particular location within the capillary, the ideal trajectory will be sampled as depicted above. Note that this ideal trajectory is very similar to Figure 12.19.

12.6.3. DIALYSIS

Dialysis and batch crystallization methods are the most controlled experiments but also the least commonly employed technique for growing protein crystals. Microdialysis chambers are manufactured from plastic cores to accommodate volumes ranging from 10 to 100 μ l. The dialysis membrane is fastened over this dialysis button with a rubber O-ring of suitable diameter. The button is placed in the precipitant solution. Provided the precipitant is a small molecule like a salt or alcohol, it can easily penetrate the dialysis tubing and the protein is slowly brought into equilibrium with the precipitant solution. The trajectory on the phase diagram (Figure 12.22) is a direct vertical rise as the precipitant concentration is increased at a constant protein concentration until the labile zone is penetrated and nucleation commences to consume the protein. If the precipitant has a large molecular weight, like PEG 6000, then the precipitant must be placed in the button along

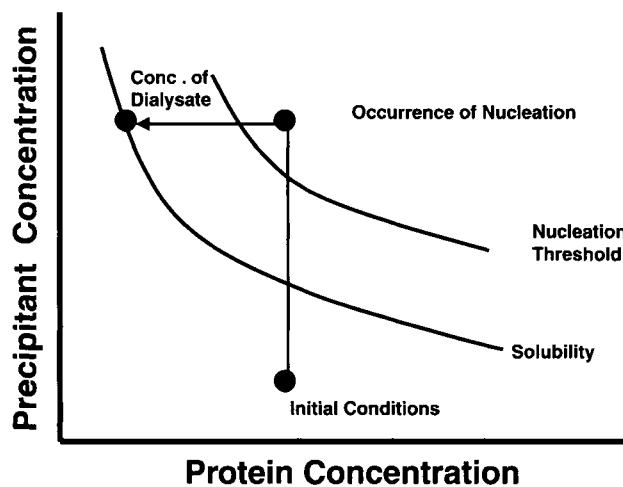


Figure 12.22 The ideal trajectory of a dialysis experiment. The arrow indicates the composition changes that might take place in the dialysis chamber.

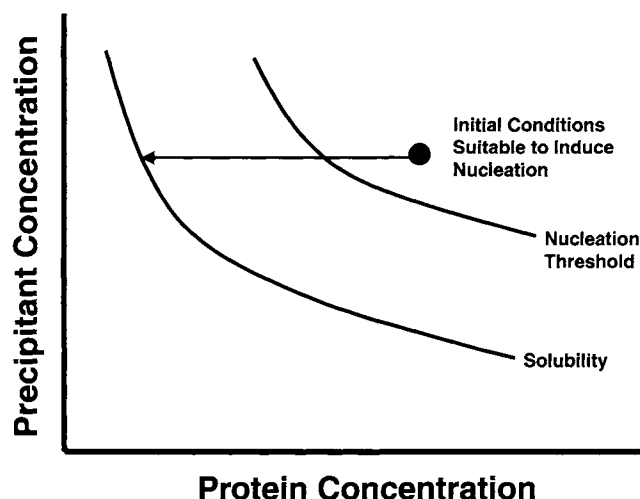


Figure 12.23 The ideal trajectory of a batch experiment. The arrow indicates the composition changes that might take place in the batch container. Note that this experiment requires that the experiment be initiated in the labile zone or that a seed crystal be placed in the original setup.

with the protein. Water will transfer through the dialysis membrane until the PEG activity is equalized on both sides of the membrane.

12.6.4. BATCH GROWTH

Batch techniques require mixing the precipitant and the protein at the onset of the experiment. In order to minimize evaporation of the small droplets, the mixture is typically overlaid with water immiscible oil such as mineral oil (Cheyan 1992). For protein crystal growth by batch techniques, the initial solution must be in the labile zone at a given temperature for nucleation to occur. Thus, the trajectory for batch experiments must start in the labile zone if crystals are to be generated, with the system relaxing to the solubility curve at an essentially constant precipitant concentration (see Figure 12.23). The batch method has become a popular technique for implementing temperature controlled protein crystallization (Schall et al. 1996).

12.6.5. SEEDING TECHNIQUES

In cases where protein microcrystals are available, seeding techniques can be utilized to increase the size of the crystal to a range acceptable for X-ray diffraction studies. An excellent review of seeding techniques typically employed for protein crystals is presented by Stura and Wilson (1992).

The main difficulty with manipulating protein crystals (as required for seeding) is their extremely fragile nature. Typically containing 50% water, the crystals tend to easily fracture when transported from one solution to another. The movement of a single macroscopic (i.e., easily seen under a microscope) crystal from one solution to a new growth solution is referred to as macroseeding. The new growth solution should be at a relatively low supersaturation so that growth of the seed crystal is preferred to nucleation of new crystals. Due to the fragile nature of the protein crystals, such direct transfer often generates small crystalline fragments, which slough off into the new growth solution. In an attempt to minimize such fragmentation, the crystal can be transferred to an intermediate solution, which contains no protein and thus promotes dissolution of the crystal. Crystalline fragments are usually very small and difficult to see, even under a microscope. If the original crystal is allowed to dissolve to roughly one

half of its original size, it is very likely that the small fragments will have totally dissolved.

Microseeding attempts to avoid the issue of secondary nucleation via fragmentation. In this case, the seed crystal is crushed into many microcrystals on purpose. A set of serial dilutions is conducted until the number of seeds is one or a few within a given aliquot (typically a few microliters). The desirable level of dilution requires some judgement and some screening, but the technique can reproducibly generate a few crystals within a given drop without concern for secondary nucleation.

A final technique, streak seeding, is also utilized to transplant microseeds from an original solution to a new growth solution. In this case, a fine glass fiber is drawn across the top of an existing crystal. Small crystal fragments are dislodged by the fiber and tend to stick to its surface. If the fiber is quickly transported to another growth solution, the microcrystals will dislodge and grow in that new solution. Due to the fairly gentle removal process, only a few crystals tend to move with the fiber.

12.7. SUMMARY

This chapter is by no means a comprehensive review of the protein crystallization area. Other excellent reviews may be found in the book of McPherson (1989), the monograph edited by Ducruix and Giege (1992), and Volumes 114 and 276 of *Methods in Enzymology*. The application of the basic principles of crystallization to proteins is not different than other small molecule applications. This chapter has attempted to highlight these similarities, while pointing out the important physicochemical properties of proteins. Ultimately, the crystallization of proteins is going to remain primarily a lab-scale process; however, new pharmaceuticals based on proteins are entering the marketplace and will ultimately require scale up to, most likely, large batch operations. The principles of design outlined in earlier chapters will equally apply to proteins. The highly compressible and fragile nature of the crystals must be explicitly factored into any design of protein crystallization equipment. As with any chemical system, the key challenges for protein crystallization will be identifying suitable solution conditions to generate crystals of the desired size, shape, and density as well as measuring the solubility, nucleation rates and growth rates as function of such solution variables.

NOMENCLATURE

A	Optical absorbance
a	Radius of an ion (from Debye-Huckel theory)
b	Optical pathlength
C	Protein concentration
C^*	Solubility of the protein in the liquid phase
D	Dielectric constant
D_m	Mixture dielectric constant
D_w	Water dielectric constant
ΔH_{cry}	Heat of crystallization
I	Ionic strength
k	Empirical constant in Eq. (12.6)
k_s	Salting-out constant
N	Avogadro's number
R	Gas constant
S	Protein solubility
S_o	Protein solubility in the absence of electrolyte
T	Temperature
Z	Net charge on the protein
#Disulfide	Number of disulfide bonds in a protein
#Trp	Number of Tryptophan amino acids in a protein
#Tyr	Number of Tyrosine amino acids in a protein

Greek Letters

β	Empirical salting-out intercept
ϵ	Charge on an electron
ϵ_λ	Molar absorption coefficient
κ	Inverse Debye length
λ	Wavelength of light

ACKNOWLEDGMENT

The author would like to acknowledge the following: Robert Salach for his assistance in preparing figures; his graduate students for their hard work in the laboratory (Connie Schall, Jill Bonita, Patricia Darcy, Wayne Jones, Charlie Hitscherich, Lokesh Gakhar and Jin Li); and NASA and The Whitaker Foundation for their generous financial support of our work. Finally, the invitation from Alan Myerson to be part of this Handbook is gratefully acknowledged.

REFERENCES

- Benson, A.M., Suruda, A.J., and Talalay, P. (1975). *J. Biol. Chem.* **250**, 276.
- Bergdoll, M., and Moras, D. (1988). *J. Crystal Growth* **90**, 283.
- Berland, C.R., Thurston, G.M., Kondo, M., Broide, M.L., Pande, J., Ogun, O., and Benedek, G.B. (1992). *Proc. Natl. Acad. Sci.* **89**, 1214.
- Bernal, J.D., and Crowfoot, D. (1934). *Nature (London)* **133**, 794.
- Bradford, M.M. (1976). *Anal. Biochem.* **72**, 248.
- Branden, C., and Tooze, J. (1991). *Introduction to Protein Structure*, Garland Publishing, New York.
- Broide, M.L., Tomine, T.M., and Saxowsky, M.D. (1996). *Phys. Rev. E* **53**, 6325.
- Bugg, C.E., Carson, W.M., and Montgomery, J.A. (1993). *Scientific American* **269**, 92.
- Cacioppo, E., and Pusey, M.L. (1991). *J. Crystal Growth* **114**, 286.
- Cacioppo, E., Munson, S., and Pusey, M.L. (1991). *J. Crystal Growth* **110**, 66.
- Carbonnaux, C., Ries-Kautt, M., and Ducruix, A. (1992). *J. Crystal Growth* **122**, 223.
- Carter, C.W. (1997). *Methods Enzymol.* **276**, 74.
- Cheyan, N.E. (1992). *J. Crystal Growth* **122**, 176.
- Cohn, E.J. (1925). *Physiol. Rev.* **5**, 349.
- Cohn, E.J., Leutscher, J.A., and Oncley, J.L. (1940). *J. Am. Chem. Soc.* **62**, 3396.
- Collins, K. (1997). *Biophys. J.* **72**, 65.
- Creighton, T.E. (1993). *Proteins: Structure and Molecular Properties*, 2nd ed., W.H. Freeman and Co., New York.
- Czok, R., and Bucher, Th. (1961). *Adv. Protein Chem.* **15**, 315.
- Darcy, P.A., and Wienczek, J.M. (1998). *Acta Cryst.* **D54**, 1387.
- Datar, R., and Rosen, C.G. (1990). In *Separation Processes in Biotechnology* (Asenjo, ed.), Chapter 20, Marcel Dekker, New York.
- Debru, C. (1983). *L'esprit des protéines: histoire et philosophie biochimiques*. Herman, Paris.
- Dounce, A.L., and Allen, P.Z. (1988). *Trends in Biochem. Sci.* **13**, 317.
- Ducruix, A., and Giege, R. (eds.) (1992). *Crystallization of Nucleic Acids and Proteins*, Oxford University Press, New York.
- Durbin, S.D., and Feher, G. (1986). *J. Crystal Growth* **76**, 583.
- Edsall, J.T. (1952). *Adv. Protein Chem.* **3**, 383.
- Ewing, F., Forsythe, E., and Pusey, M.L. (1994). *Acta Cryst.* **D50**, 424.
- Feher, G., and Kam, Z. *Methods Enzymol.* **114**, 77.
- Ferre-D'Amare, A., and Burley, S.K. (1997). *Methods Enzymol.* **276**, 157.
- Gill, S.C., and von Hippel, P.H. (1989). *Anal. Biochem.* **182**, 319.
- Gilliland, G.L., Tung, M., Blakeslee, D.M., and Ladner, J. (1994). *Acta Cryst.* **D50**, 408.
- Green, A.A. (1931). *J. Biol. Chem.* **93**, 495.
- Green, D.W., Ingram, V.M., and Perutz, M.F. (1954). *Proc. R. Soc. London, Ser. A* **225**, 287.
- Gronwall, A. (1942). *Compt. Redn. Trav. Lab Carlsberg* **24**, 8.
- Gross, M., and Jaenicke, R. (1993). *Biophys. Chem.* **45**, 245.
- Guilloteau, J., Ries-Kautt, M., and Ducruix, A. (1992). *J. Crystal Growth* **122**, 223.
- Hoare, M., Bell, D.J., and Dunnill, P. (1983). *Adv. Biochem. Eng. Biotechnol.* **26**, 1.
- Hofmeister, T. (1887). *Arch. Exptl. Pathol. Pharmacol. Naunyn-Schiedeborg's* **24**, 274.
- Howard, S.B., Twigg, P.J., Baird, J.K., and Meehan, E.J. (1988). *J. Crystal Growth* **90**, 94.
- Hunter, M.J. (1966). *J. Phys. Chem.* **70**, 3285–3292.
- Hunter, R.J. (1993). *Introduction to Modern Colloid Science*, Oxford, New York.
- Jaenicke, L. (1974). *Anal. Biochem.* **61**, 623.
- Jancarik, J., and Kim, S.H. (1991). *J. Appl. Cryst.* **24**, 409.
- Kendrew, J.C., Bodo, G., Dintzis, H.M., Parrish, R.G., and Wyckoff, H. (1958). *Nature (London)* **181**, 662.
- Kupke, D.W., and Dorrier, T.E. (1978). *Methods Enzymol.* **48**, 155.
- Lafont, S., Veesler, S., Astier, J., and Boistelle, R. (1997). *J. Crystal Growth* **173**, 132.
- Lecroisey, A., Boulard, C., and Keil, B.C. (1979). *Eur. J. Biochem.* **101**, 385.
- Lehman, C.G. (1853). *Lehrbuch der physiologische Chemie*. Leipzig.
- Lehninger, A.L. (1975). *Biochemistry*, 2nd ed., Worth Publishers, New York.
- Lorber, B., Jenner, G., and Giege, R. (1996). *J. Crystal Growth* **158**, 103.
- Low, B., Preston, H., Sato, A., Rosen, L., Searl, J., Rudko, A., and Richardson, J. (1976). *Proc. Natl. Acad. Sci.* **73**, 2991.
- Lowry, O.H., Rosebrough, N.J., Farr, A.L., and Randall, R.J. (1951). *J. Biol. Chem.* **193**, 265.
- Malkin, A.J., Kuznetsov, Y.G., Glantz, W., and McPherson, A. (1996). *J. Phys. Chem.* **100**, 11736.
- Malkin, A.J., Kuznetsov, Y.G., Land, T.A., DeYoreo, J.J., and McPherson, A. (1995). *Nature Structural Biology* **2**, 956.
- McPherson, A. (1989). *Preparation and Analysis of Protein Crystals*, Kreiger Publishing Co., Malabar, Florida.
- McPherson, A. (1991). *J. Crystal Growth* **110**, 1.
- Muschol, M., and Rosenberger, F. (1997). *J. Chem. Phys.* **107**, 1953.
- Nozaki, Y. (1986). *Arch. Biochem. Biophys.* **249**, 437.
- Orella, C.J., and Kirwan, D.J. (1989). *Biotechnol. Prog.* **5**, 89.
- Pace, E.N., Vajdos, F., Fee, L., Grimsley, G., and Gray, T. (1995). *Protein Sci.* **4**, 2411.
- Perutz, M.F., Rossman, M.G., Cullis, A.F., Muirhead, H., Will, G., and North, A.C.T. (1960). *Nature (London)* **181**, 416.
- Pusey, M.L. (1994). *Rev. Sci. Instrum.* **64**, 3121.
- Pusey, M.L., and Gernert, K. (1988). *J. Crystal Growth* **88**, 419.
- Reichert, E.T., and Brown, A.P. (1909). *The differentiation and specificity of corresponding proteins and other vital substances in relation to biological classification and evolution: the crystallography of hemoglobins*, Carnegie Institution, Washington DC.
- Ries-Kautt, M., and Ducruix, A. (1989). *J. Biol. Chem.* **264**, 745.
- Ries-Kautt, M., and Ducruix, A. (1991). *J. Crystal Growth* **110**, 20.
- Ries-Kautt, M., and Ducruix, A. (1992). In *Crystallization of Nucleic Acids and Proteins* (Ducruix and Giege, eds.), Chapter 9 Oxford University Press, New York.
- Saikumar, M.V., Glatz, C.E., and Larson, M.A. (1995). *J. Crystal Growth* **151**, 173.
- Salemne, F.R., Genieser, L., Finzel, B.C., Hilmer, R.M., and Wendolosky, J.J. (1988). *J. Crystal Growth* **90**, 273.
- Salemne, F.R. (1972). *Arch. Biochem. Biophys.* **151**, 533.
- Schall, C.A., Riley, J.S., Li, E., Arnold, E., and Wienczek, J.M. (1996). *J. Crystal Growth* **165**, 299.
- Schall, C.A., Wienczek, J.M., Yarmush, M.L., and Arnold, E. (1994). *J. Crystal Growth* **135**, 548.
- Shaw, D.J. (1992). *Introduction to Colloid and Surface Science*, Butterworth-Heinemann, Oxford.
- Sorenson, S.P.L. (1933). *Biochem. Z.* **258**, 16.
- Stura, E.A., and Wilson, I.A. (1992). In *Crystallization of Nucleic Acids and Proteins* (Ducruix and Giege, eds.), Chapter 5, Oxford University Press, New York.
- Sumner, J.B. (1926). *J. Biol. Chem.* **69**, 435.

- Suzuki, Y., Miyashita, S., Komatsu, H., Sato, K., and Yagi, T. (1994). *Jpn. J. Appl. Phys.* **33**, L1568.
- Takano, K.J., Harigae, H., Kawamura, Y., and Ataka, M. (1997). *J. Crystal Growth* **171**, 554.
- Veesler, S., Lafont, S., Marcq, S., Astier, J., and Boistelle, R. (1996). *J. Crystal Growth* **168**, 124.
- Vekilov, P.G., Monaco, L.A., Thomas, B.R., Stojanoff, V., and Rosenberger, F. (1996). *Acta Cryst.* **D52**, 785.
- Visuri, K., Kaipainen, E., Kivimäki, J., Niemi, H., Leisola, M., and Palo-
saari, S. (1990). *Biotechnology* **8**, 547.
- von Hippel, P.H., and Schleich, T. (1992). *Acc. Chem. Res.* **2**, 257.
- Wang, A.H.J., and Teng, M.K. (1988). *J. Crystal Growth* **90**, 295.
- Wiencek, J.M., and Darcy, P.A. (1997). *Spacebound 97 Conference Proceedings (Montreal, Canada)*, 323.
- Zeppenzauer, M. (1971). *Methods Enzymol.* **22**, 253.

This Page Intentionally Left Blank

CRYSTALLIZATION IN FOODS

Richard W. Hartel

There are many components in foods that crystallize, either partially or completely (Hartel 2001). Most important are sugars (sucrose, lactose, glucose, and fructose), ice, lipids, and starches. However, crystallization of salts, sugar alcohols, organic acids, proteins, and emulsifiers may be important in certain applications. Table 13.1 lists some of the main crystallizing components in foods with some examples of products where controlling this crystallization is important.

The crystalline structure of foods is important to product quality, texture, and stability. It is this crystalline structure, along with other structural elements (emulsions, air cells, etc.), that determines product appearance (e.g., frosted cereal coating), mechanical properties during handling (e.g., spreadability of butter), mouthfeel during consumption (e.g., smoothness of ice cream) and shelf stability (e.g., fat bloom in chocolate), as shown in Table 13.2. The nature of this crystalline structure is controlled by manipulation of product composition and conditions during processing and storage. The interrelations between product composition (formulation) and processing conditions that produce a desired microstructure are shown in Figure 13.1.

13.1. CONTROLLING CRYSTALLIZATION IN FOODS

In order to control crystallization, it is necessary to have an understanding of the phase behavior of the system, some knowledge of nucleation and growth kinetics, and the effects of both formulation and processing conditions on these kinetics. However, this is often

a difficult task in the food industry as crystallization is often extremely complex with many factors that can influence the final results. In addition, the food manufacturer does not always have access to some of the tools available for controlling crystallization due to product limitations. For example, use of certain ingredients that would modify crystallization may not be allowed under some code of identification for a product. For example, there is a Standard of Identity for chocolate (Code of Federal Regulations 1990) that specifies the ingredients that can be used. In the US, chocolate may contain cocoa butter and up to a certain level of milk fat. No other fats can be added and still have the product labeled chocolate. Thus, the ability to modify cocoa butter crystallization in chocolate is limited to milk fat ingredients. However, in compound coatings (imitation chocolates based on vegetable fats), a nucleator is often used to promote crystallization and improve throughput rates. The nucleator is typically a hardened (fully hydrogenated) vegetable oil with high melting point. It is also possible that use of a desired ingredient for controlling crystallization may produce an undesired taste or texture in the product. Thus, controlling crystallization in foods may be extremely challenging at times.

In foods, two circumstances for controlling the formation of crystals can be distinguished (Table 13.2): those where the crystals provide an element of structure in the product and those where crystallization is a separation process. In the first case, control of the correct number, size (and distribution), shape and polymorph of crystals is required to provide the desired processing characteristics, quality (texture, flavor, etc.), appearance and/or

TABLE 13.1 Typical Food Products For Which Controlling Crystallization Is Important to Quality and Shelf Life

Component	Product Categories	Product Examples
Ice	Frozen desserts	Ice cream, frozen yogurt, etc.
	Frozen foods	Meats, fruits and vegetables, entrées, etc.
Sugars	Freeze dried products	Instant coffee, dried fruits, rehydratable meals, etc.
	Confectionery products	Grained caramels, fudge, fondant, panned goods, chewing gum, etc.
	Cereals	Frosted cereals, glazed cereals
Sugar alcohols	Dairy products	Whey and milk powders
	Other	Icings, frostings, etc.
	Confectionery products	Chewing gum, sugar-free products, etc.—i.e., sorbitol
Lipids	Spreads	Butter, margarine, etc.
	Confectionery products	Chocolate, compound coatings, toffee, etc.
	Baked goods	Croissants, puffed pastries, cookies, pie crust, etc.
Salts	Other	Peanut butter, frostings, etc.
	Table salt	NaCl, salt substitutes
	Dairy products	Milk, cheese, etc.
Starches	Baked goods	Bread, cookies, cakes, crackers, etc.
	Extruded products	Snacks, crackers, etc.
Proteins	Additives	Lysine
Organic acids	Powdered additives	Citric acid, etc.
Emulsifiers	Additives	Lipid-based products, dressings, etc.

TABLE 13.2 Characteristics of Food Products For Which Controlling Crystallization Is Important

Control Number, Size, Shape, and Polymorph		
Product	Ingredient	Desired Characteristic
Caramel	Sucrose or lactose	Smooth and short texture
Fondant	Sucrose	Smooth texture
Panned confections	Sucrose	Brittle texture (hard panned) Soft texture (soft panned)
Cereal coatings	Sucrose	Appearance
Refined sugars	Sucrose, lactose, etc.	Size distribution for separation
Refined salt	NaCl	Size distribution for separation
Organic acids	Citric acid, etc.	Size distribution for separation
Bread, baked products	Starch	Texture
Frozen foods	Ice	Thawed quality
Frozen desserts	Ice	Smooth texture
Freeze concentration	Ice	Size distribution for separation
Chocolate	Cocoa butter	Texture (snap) and gloss Shelf stability to blooming
Butter	Milk fat	Hardness, spreadability
Margarine	Vegetable fats	Hardness, spreadability
Peanut butter	Vegetable fats	Texture, spreadability
Fat fractionation	Palm oil, tallow, milk fat	Size distribution for separation

shelf stability of the product. Here, the kinetics of nucleation and growth must be controlled, through proper choice of formulation and processing conditions, to give the desired crystalline microstructure. Controlling crystallization in sugar products (sugar-frosted cereals, fondant, panned candies, caramels, etc.), frozen foods (ice cream, frozen desserts, and other frozen products) and lipid-based products (tempering of chocolate, butter, margarine, shortenings, etc.) are examples of products where a certain crystal size distribution is required to give the desired attributes. For many products, the desired crystal size distribution is one that has a large number of very small crystals that provide smooth texture and excellent dissolution or melt-down properties. For example, the ice crystals in ice cream have a mean size somewhere between 35 and 45 μm (Berger 1990), with a range of sizes from 1 μm to over 100 μm . Over 10^9 crystals per liter of ice cream (Berger 1990) provide a significant cooling effect upon melting. Controlling formation of these crystals is extremely important because it is thought that we can detect ice crystals on the order

of 50 μm on our palate. However, it is unclear how this threshold detection size relates to the quantitative size distribution in ice cream. The shape of the ice crystals is also important to product texture and mouthfeel. Ice crystals in ice cream have a rather smooth, rounded surface and this allows the ice crystals to flow across each other easily to give a smooth, creamy characteristic. If the ice crystals in ice cream had jagged edges, as are often found in ice crystals in popsicles, the texture of the ice cream would be much more brittle since the crystals would not flow across one another easily. Clearly, controlling the nature of the crystalline structure in food products is crucial to the desired product attributes.

In products containing lipids, control of the crystal polymorphic form is also necessary. Lipids form different crystalline structures, or polymorphs, depending on the nature of the fat and the processing conditions. Transitions from less stable to more stable polymorphs are also dependent on composition and processing conditions. For example, tempering (or precrystallization) of chocolate is a process through which the chocolate is sequentially cooled and warmed to promote crystallization of cocoa butter into the desired polymorphic form. Controlling crystallization to produce the proper size distribution of this polymorph provides: (1) the desired contraction upon cooling (release from a mold); (2) snap or brittleness; (3) glossy surface appearance; and (4) stability to fat bloom (Hartel 1998b).

In some processes (Table 13.2), only a few crystals are desired with proper size distribution and shape for efficient separation. Refining of sugars, fractionation of fats, and freeze concentration are examples of processes where control of crystallization is necessary to provide efficient separation. In both types of products and processes, control of the crystal size distribution is important to efficient operation and production of a high-quality product.

In order to control crystallization during processing and storage, several pieces of information are required. One of the most important pieces of information required to control crystallization is the phase diagram of the system. In simple systems, the phase diagram may be quite familiar. For example, the solubility curve of sucrose in water is quite well known, as is the freezing point depression curve for water in the presence of salts and sugars. Thus, the phase diagram for the simple binary mixture of sucrose

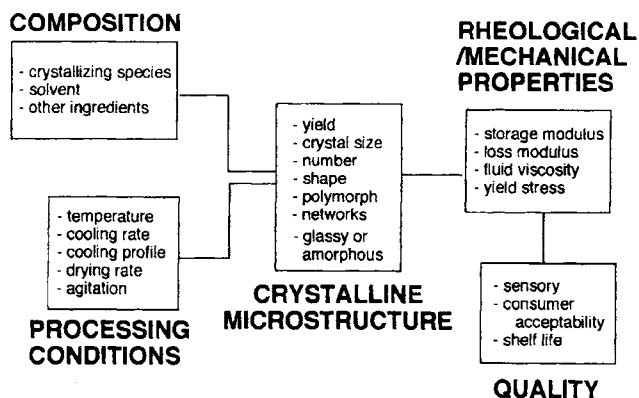


Figure 13.1 Schematic of interrelationships between composition and processing conditions on development of crystalline microstructure in foods and the subsequent quality attributes of that product. (From Hartel 2001; with permission.)

and water contains only the solubility curve and the freezing point depression curve. However, in complex food products, the influence of all other components on the phase behavior of the crystallizing species must be known, and this may be a difficult task in complex products. For example, the solubility concentration of sucrose or lactose in a caramel formulation is not easily found since the milk salts also influence solubility and the high viscosity of the system makes it difficult to perform equilibrium studies. The phase diagram gives information on the final equilibrium of the system. That is, assuming the product attains a phase equilibrium, the crystalline phase volume expected at a given temperature comes directly from the equilibrium phase boundary. The phase diagram also allows one to define the thermodynamic driving force for crystallization at any point in the process.

In some complex systems, such as mixtures of different natural fats, it is difficult to define a true thermodynamic driving force. The number and concentration of crystallizing triacylglycerols (TAG) in a mixture (for example, of cocoa butter and milk fat) may be quite large. Milk fat contains over 250 different TAG species based on chain length, degree of unsaturation and arrangement of the fatty acids on the glycerol backbone (Gresti et al. 1993), with none present at a concentration above about 4% (molar basis). As temperature is lowered to induce crystallization of milk fat, more and more different molecules join in the crystallization process. Thus, crystallization driving force for milk fat at any temperature is not easily defined. Cocoa butter is a simpler fat with only three main TAG that crystallize together. Researchers have attempted to understand cocoa butter crystallization based on the ternary phase diagram of these three components. However, this has met with limited success, in part due to the presence of the remaining minor components. In complex mixtures of natural fats like milk fat and cocoa butter, a true thermodynamic driving force for the crystallizing species has not been defined. Timms (1980) developed a pseudo-phase diagram treating milk fat and cocoa butter as two distinct entities in a binary system, although application of this type of diagram in the food industry to control crystallization has been limited.

The effects of operating conditions on crystallization kinetics must also be known to control crystallization. The kinetics of nucleation, crystal growth, and glass formation must be known to control formation of the correct number, size, shape, and polymorph of crystals. These kinetics are dependent on formulation, since many ingredients influence nucleation and growth rates, and processing conditions. Rates of heat and mass transfer during processing govern the conditions under which crystallization takes place and may dramatically influence the structure of the crystalline phase.

There are also cases in the food industry where crystallization is undesired even though the system is supersaturated in a certain component. Crystallization in such a product usually occurs during storage and leads to product defects. Table 13.3 shows examples of some products of this type. These include hard candies, some ungrained caramels, milk powders, and ice cream. In these products, crystallization of the sugars (either sucrose or lactose) leads to an undesirable texture, flavor loss, and/or appearance. The appearance of potassium tartrate in wine during storage is another example of undesired crystallization.

For example, a hard candy is produced by forming a metastable sugar glass. As long as this product is maintained below its glass transition temperature, it will be stable to sugar crystallization for a long period of time. Even though the sugar is highly supersaturated, kinetic constraints (low molecular mobility) prevent the sugar molecules from forming into the crystal lattice. Under certain storage conditions (elevated temperatures and humidities), the sugar molecules can become sufficiently mobile

TABLE 13.3 Examples of Food Products For Which Crystallization During Storage Causes Product Defects

Component	Product Categories	Product Examples
Sugar	Confectionery products	Hard candy, ungrained
Caramels, etc. —lactose, sucrose	Dairy products	Ice cream, milk powders
—fructose	Baked goods	Soft cookies, etc.
Salt —potassium bitartrate	Grape juices	Wine
—calcium lactate	Dairy	Cheese

to crystallize. At this point, the texture, appearance and flavor release of the product is no longer acceptable. A similar concern occurs in ice cream, where the unfrozen phase is supersaturated in lactose. Normally, lactose does not crystallize in ice cream, due to kinetic constraints (low mobility), to a sufficient extent to be detectable in the mouth. But again, under certain conditions (Livney et al. 1995) the lactose molecules gain sufficient mobility so that massive lactose crystallization occurs and the product has a “sandy” characteristic. Since lactose crystals dissolve slowly in the mouth, eating ice cream with lactose crystals over about 15 μm in size causes unacceptable texture changes.

Finally, storage conditions influence the rate of recrystallization that takes place after crystals have been formed and the product goes through the storage and distribution system. Ideal control of crystallization during processing can be quickly destroyed by improper storage conditions or formulation. Temperature of storage, magnitude of temperature fluctuations, and relative humidity affect the changes in crystalline structure during storage. The rates of these changes may also depend on the composition of the product. For example, stabilizers are added to ice cream to inhibit ice recrystallization during storage.

Subtle changes in the nature of the crystalline material can sometimes lead to product defects. Since many structural aspects of food products are not in equilibrium, changes in crystalline characteristics are likely to occur as the system approaches a different energy minimum. For example, cocoa butter crystals in chocolate approach a lower energy state by converting to a more stable polymorph during storage. Also, ice crystals in ice cream approach a lower surface energy state through a thermodynamic ripening process. These changes during storage are often called recrystallization and can cause significant degradation of product quality. Recrystallization has been defined as “any change in the number, size, shape, orientation, or perfection of crystals following initial solidification” (Fennema 1973). Table 13.4 shows some examples of this in the food industry.

One of the most common examples of recrystallization in foods is the coarsening of ice crystals in ice cream or any other frozen food during storage. Over time, the molecules within the ice crystals rearrange, with smaller crystals disappearing and larger ones growing. This results in larger ice crystals and the product feels coarse during consumption. This recrystallization is enhanced by the warm and fluctuating temperatures during storage in frost-free freezers. Figure 13.2 documents the changes that take place in ice crystals in ice cream that has been stored for three months at -15°C . There is a general increase in size and an overall decrease in the number of ice crystals during storage due to recrystallization mechanisms.

Another example of recrystallization in a food product is the formation of fat bloom in chocolates during long-term storage

TABLE 13.4 Examples of Recrystallization During Storage of Food Products

Component	Product Categories	Manifestation
Ice	Ice cream and frozen desserts	Increased mean crystal size and range of sizes
Sugars	Frozen foods Fondants, creams, etc.	Increased mean crystal size and range of sizes
Lipids	Margarine Chocolate	Polymorphic transformation —grainy texture or fat bloom
Starch	Compound coatings Bread, baked goods, etc.	Staling

(Hartel 1998b). Cocoa butter in fresh chocolate is not in the polymorph with lowest energy state and will gradually recrystallize into the most stable form. Under conditions where cocoa butter molecules in chocolate have sufficient mobility, they can recrystallize into this more stable polymorph. This rearrangement is often accompanied by formation of visible crystals at the surface of chocolate, which cause diffuse reflection and loss of gloss. Ultimately, formation of a whitish haze (fat bloom) on the surface occurs. Although the polymorphic transformation is not the cause of bloom in chocolate, it often accompanies bloom formation due to the mechanisms of recrystallization (Bricknell and Hartel 1998).

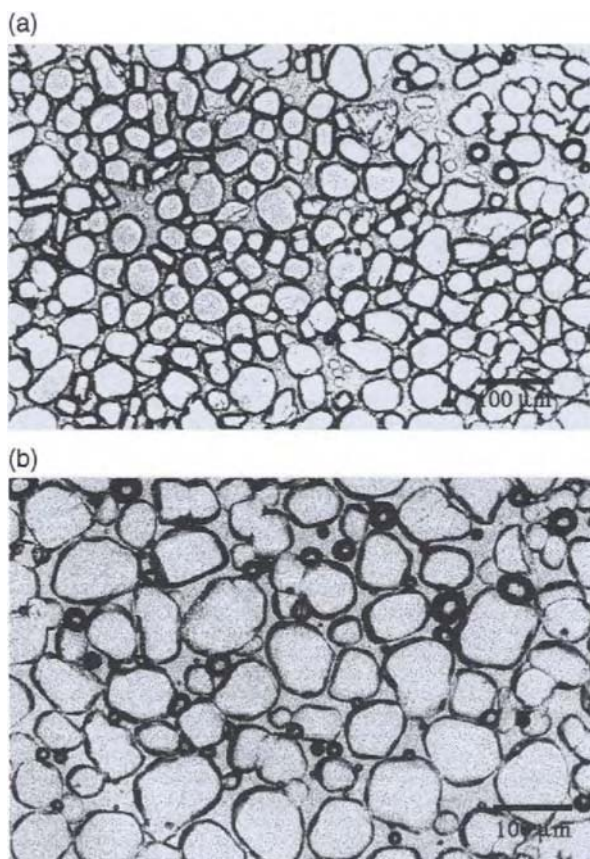


Figure 13.2 Ice crystals in ice cream (a) before and (b) after storage for three months at -15°C .

13.2. CONTROL TO PRODUCE DESIRED CRYSTALLINE STRUCTURE

13.2.1. CONTROL FOR PRODUCT QUALITY

In many food products, the desired crystalline structure provides a characteristic texture to the product. The crystals influence the texture by disrupting the continuous phase in which they are embedded. Ice cream or frozen desserts are good examples of this, where the ice crystal structure provides a certain characteristic smoothness and mouthfeel desired in the product. In these products, many small crystals of uniform shape and size are desired. If the crystals are too large, they can be detected in the mouth and the product is regarded as coarse. Crystal shape may also be important in some cases, although the effect of different shapes on product texture has not been studied in any quantified manner.

Probably the most important phenomenon for controlling the crystal size distribution is nucleation. By controlling nucleation, the desired crystalline structure can be attained. In many food products, the nucleation rate curve increases initially as driving force increases, passes through a maximum and then decreases as viscosity limitations inhibit the rate of nuclei formation. An example of this nucleation behavior was observed for citric acid by Mullin and Leci (1969). At very low temperatures, fewer crystals were formed and this correlated with the strong increase in viscosity at these conditions. This behavior has been described (Mullin 1993; Walton 1969; Van Hook and Bruno 1949) by:

$$J = A \exp \left[-\frac{16\pi\sigma_s^3 v^2}{3k^3 T^3 (\ln S)^2} + \frac{\Delta G_D}{kT} \right] \quad (13.1)$$

where σ_s is interfacial tension, v is molecular volume, k is Boltzmann's constant, T is temperature, S is supersaturation ratio, and ΔG_D is a diffusion-limited term that becomes more important as viscosity increases. This behavior applies in glass-forming systems like sugars, organic acids, glucose polymers, water, and others. At the glass transition point or zone, often defined by a glass transition temperature, T_g , molecular mobility is so low and system viscosity so high that diffusion-limited processes occur very slowly. Thermodynamically, there may be a large driving force for crystallization; however, crystallization is kinetically constrained so the system remains metastable for a very long time. If, for example, a sugar syrup is concentrated and cooled quickly, there is not sufficient time for the sugar to crystallize and a sugar glass is formed. As long as it is maintained below its T_g , the sugar glass will remain as a glass for long periods of time. This is the principle behind manufacture of hard candy.

An overlay of the crystal growth and nucleation kinetic curves (using primary heterogeneous nucleation as the mechanism of crystal formation) is shown in Figure 13.3. The point at maximum nucleation rate also corresponds to rapid crystal growth, somewhere in the middle of the crystallization zone between the equilibrium point (either solubility or melting point) and the glass transition point. At conditions both above and below this maximum, fewer nuclei are formed, and they grow more slowly. The point on this rate curve where nuclei are formed during processing of a food product is critical to the nature of the crystal size distribution generated.

If nucleation occurs at or near the peak of the nucleation rate curve, then the maximum number of crystals will be formed. To obtain many small crystals in a product, nucleation must occur at process conditions (temperature and concentrations) that correlate with this maximum rate. If nucleation takes place at some condition off the peak in the nucleation rate curve (i.e., temperature too high or too low), fewer crystals are formed, and these can grow to a

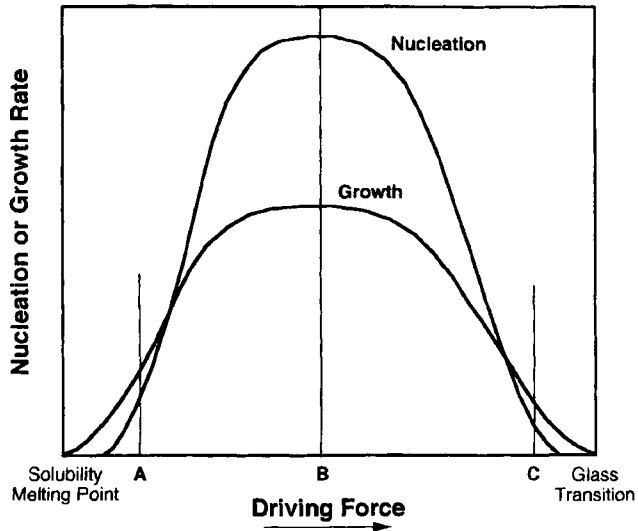


Figure 13.3 Nucleation and growth rate curves with changing driving force for crystallization. (From Hartel 2001; with permission.)

a much larger size. Comparing commercial ice cream with homemade ice cream demonstrates this principle nicely (Hartel 1998c). In commercial processes, ice cream is made in a scraped-surface freezer with liquid ammonia as refrigerant. Liquid ammonia temperatures in this process are typically around -30°C , generating a subcooling driving force (ΔT) for crystallization of about 26°C (since freezing point of ice cream mix is about -2°C and some heat is lost through the walls) at the scraped wall of the freezer. In homemade ice cream, a brine solution with temperature of only -8 to -10°C is used to provide the driving force for freezing. Clearly, the driving force is much less than in commercial systems. Thus, nucleation is slower in the homemade process and fewer crystals are formed. When these ice creams are further cooled to a storage freezer temperature of -20°C , the ice crystals in the homemade product grow to much larger size than those produced in the commercial process. The difference in texture between these products after both are stored in a freezer is readily apparent.

A comparison of typical size distributions obtained when nucleation occurs at different points on the rate curves is shown in Figure 13.4. When nucleation takes place at Point B (Figure 13.3), the maximum of the nucleation rate curve, a narrow crystal size distribution with many small crystals results. This is ideal for products that contain crystals, but where a smooth texture is still desired. Nucleation at Point A (Figure 13.3), a condition at lower driving force, results in fewer crystals being formed and they can all grow to larger size. The same distribution is obtained if nucleation occurs at Point C although the time required for completion of crystallization is much longer due to the slower growth rate. These products have a distinctly coarser crystalline structure and do not have the same desired quality. Commercial ice cream is nucleated at a point much closer to Point B (Figure 13.3) than homemade ice cream, which is closer to Point A (Figure 13.3).

Another important condition for producing many small crystals of uniform size is that nucleation takes place at one time. That is, process conditions must be set such that the entire mass of product attains the desired temperature and concentration at the same time. If the duration of nucleation lasts for any extended period of time, then a wide range of crystal sizes will be produced. The crystals that nucleate first have the opportunity to grow to

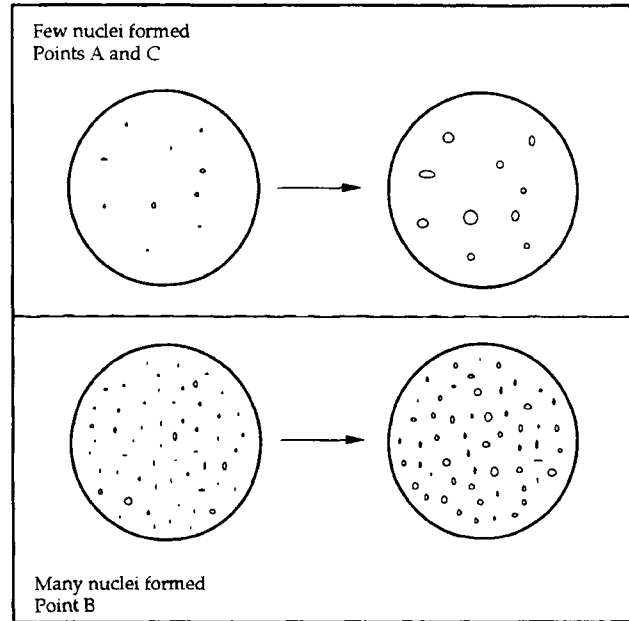


Figure 13.4 Crystal-size distributions generated by nucleation at different points on the crystallization rate curves. Points A and B correspond to points on Figure 13.3. (From Hartel 1998c; with permission.)

much larger size than those that form later in the process. Thus, process conditions that produce the maximum number of nuclei in the shortest nucleation time result in the optimal crystal size distribution. In some processes, flow conditions are not ideal so that some of the material attains supersaturated conditions well before the bulk of the mass does. In this case, the crystals that form in the regions of nonideal conditions will grow to significantly larger size than the bulk of the crystals and result in a size distribution that is skewed towards larger sizes (a log-normal type distribution). If sufficient numbers of particles are much larger than the mean, the product will be perceived as coarse or grainy.

Another way to think about controlling crystallization is in terms of a driving force that must be dissipated by the formation of crystalline structure. If the bulk of desuperaturation occurs in nucleation, the resulting average crystal size will be small. However, if only a small portion of the supersaturation is relieved during nucleation, and most of it is taken up in crystal growth, the crystals will be few in number and large in size. This is shown schematically in Figure 13.5.

For lipid products, controlling crystallization also means controlling the polymorph formed during processing. Less stable polymorphs have nucleation rate curves with maxima at sequentially lower temperatures, as shown schematically in Figure 13.6. Although less stable polymorphs (α and β') have lower melting points and higher free energies, their nucleation rates may be substantially faster than the more stable polymorphs (β). Boistelle (1988) suggests that the difference in nucleation kinetics between lipid polymorphs is due to a difference in interfacial tension. The lower stability polymorph has lower interfacial tension and thus, it nucleates more readily even though the driving force is less than that for the more stable polymorphs (see Eq. (13.1)). In fact, more stable polymorphs may not nucleate very rapidly at any temperature condition. Thus, it may be necessary to nucleate a lower-stability polymorph to get sufficient numbers of crystals and then raise the temperature slightly to promote rapid transformation to

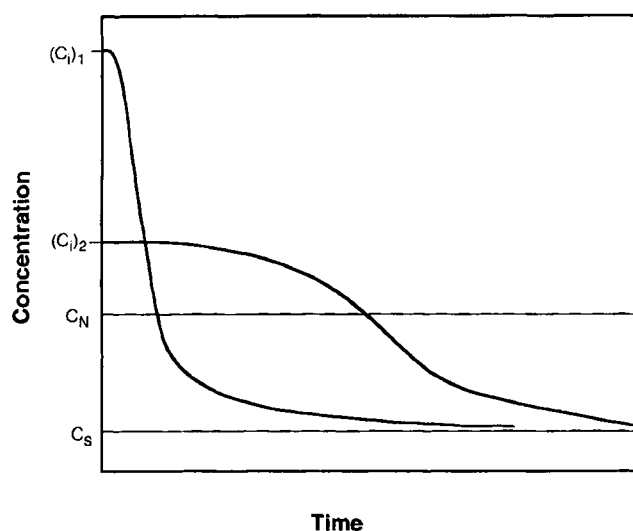


Figure 13.5 Relative rate of desupersaturation with time affects mean size of product distribution. Intense (fast) nucleation leads to many smaller crystals (Point B on figures 13.3 and 13.4), whereas slower nucleation leads to larger, wider distribution of crystal sizes (Point A on figures 13.3 and 13.4). (From Hartel 2001; with permission.)

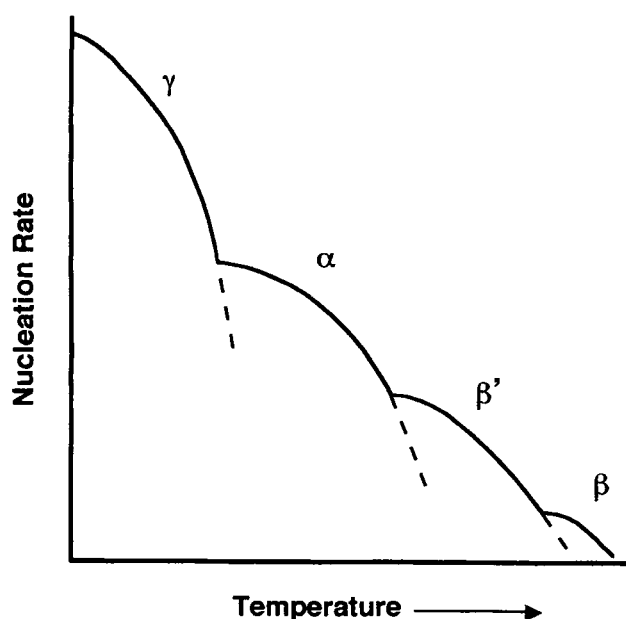


Figure 13.6 Schematic diagram of effect of temperature on nucleation rate of different lipid polymorphic forms. (From Hartel 1998b; with permission.)

the more stable, desired polymorph. This is exactly what happens during tempering of chocolate (Beckett 1988; Jovanovic et al. 1995).

In butter-making, crystallization of the milk fat occurs in the fat globules as the cream is conditioned prior to churning (Precht 1988). Upon churning and phase inversion, these milk fat crystals are dispersed into the continuous lipid phase, and they continue to grow as processing continues. Over time, these lipid crystals grow together to form a network in the continuous phase that signifi-

cantly impacts the texture of the final product. Through mechanical working, the network structure of these fat crystals can be interrupted and a softened butter produced. However, this network reforms during further storage and the hardness increases once again. Thus, both conditions of initial crystallization and subsequent recrystallization are important to the texture and quality of lipid-based products. Similar concerns are important in processing of margarines and shortening.

13.2.2. CONTROL FOR SEPARATION

In some cases, controlling crystallization to provide the most efficient separation is the desired goal. In this case, crystallization conditions that produce large mean size and a narrow distribution of sizes result in most efficient separation by filtration. Conditions that result in distributions equivalent to Point A with nucleation occurring over a narrow time period, as shown in Figure 13.4, generally produce the desired efficient separation. The primary goal in this case is to generate a population of product crystals that are similar in size and shape so that they can be easily filtered. Process conditions that give a wide size distribution result in less efficient separation.

Fractionation is an important technology for processing of such fats as tallow, palm oil, palm kernel oil, and milk fat (Hartel and Kaylegian 2001). Certain components of the raw material may have more desirable characteristics than the original material. For example, a hard fat is produced by fractionation of palm oil, which can be used as an ingredient in many applications. Often, fractionation technology is used in addition to other modification technologies (i.e., hydrogenation, interesterification). Nucleation during fat fractionation is typically controlled by cooling to the desired temperature to produce the desired nuclei. With lipids, it is important to recognize the different nucleation rates of the different polymorphs (Sato 1988), as discussed previously. However, separation of certain polymorphs may be easier than others due to desired crystal morphology, so control of the polymorph may also be required during fractionation.

Freeze concentration of aqueous solutions is often the best processing technique for providing optimal product quality in concentrated foods. Low temperature operation means that no thermal degradation reactions occur, and it is widely recognized that the flavor quality of freeze concentrated fruit juices, for example, is superior to the flavor of evaporated products. In products containing alcohol, freeze concentration is one potential technique for concentrating the aqueous phase without removal of alcohol. Ice beers are made in this way. Many different freeze concentration technologies have been developed over the years, although the method generally applied to food concentrations involves a two-step process for production of ice crystals suitable for separation. Rather than attempting to limit the production of ice, which crystallizes readily and is often difficult to control, the commercial freeze concentration unit involves generation of many small nuclei in a scraped-surface heat exchanger, which are then adiabatically ripened to large size in a separate growth tank. The resulting crystals, with mean size of 200–300 μm , are separated in a wash column with very little residual solids remaining with the melted ice.

In sugar refining, typically the nucleation step is bypassed by seeding with the appropriate crystalline material. In refining of sucrose, the seed crystals are powdered sugar produced by grinding product-sized crystals to the appropriate small size. In glucose production, a portion of the previous batch is retained in the crystallizer vessel to act as seeds, or a footing, for the next batch of refined sugars. In contrast, lactose refining typically does not use seeding to generate the desired distribution, but rather the

concentrated lactose solution is allowed to nucleate as it cools in the crystallizing tank. In all cases, however, the goal is to grow crystals uniformly up to product size through careful control of the growth conditions. After an initial seeding, or burst of nucleation in the case of lactose, no further nuclei formation is desired. If nucleation does occur, typically due to uncontrolled secondary nucleation (often called false grain in sucrose refining), a wide size distribution is the result and this causes problems in subsequent separation. Thus, careful control of nucleation (or seeding) and growth is necessary to produce the desired crystal size distribution for optimal separation.

13.3. CONTROL TO PREVENT CRYSTALLIZATION

In some products, crystallization is undesired even though the thermodynamic state is such that crystallization may occur (Hartel 1993). Products in the glassy or amorphous state, like hard candies and dried sugar (fruit or milk) powders, often fit into this category. Also, the unfrozen phase of ice cream, which is supersaturated in lactose, may crystallize during storage and cause a sandy defect in the ice cream. Other examples of products that may be supersaturated in sugars, but where crystallization is undesired, are caramel and similar ice cream toppings. In caramel, the aqueous phase contains sucrose and lactose, both of which may be supersaturated. Crystallization of lactose in caramels or ice cream toppings made with addition of whey powders or skim milk solids is a problem to many candy manufacturers. These products may be satisfactory directly after processing and packaging, but develop sufficient crystalline structure during storage to be considered a defect. The shelf life of these products is often limited by the onset of crystallization. Typically, reformulation is necessary, with reduced milk solids, to ensure stability of the product to graining of lactose crystals for the desired shelf life.

Controlling conditions to prevent crystallization generally requires one of two approaches. Either the system must have sufficiently low molecular mobility (high viscosity) that the molecules can not form into crystals or crystallization must be inhibited by the addition of other compounds. Caramels provide an excellent example of this. Prevention of crystallization in some ungrained caramels is accomplished by increased viscosity. These products are solid-like in nature and may be found on a stick, for example. They are stable to crystallization for long periods of time as long as the product remains in this highly viscous state. The lower the viscosity of the product, due primarily to either higher temperature or higher water content, the shorter the time before crystallization occurs. Crystallization in ungrained caramels may also be prevented by the addition of substantial amounts of inhibiting ingredients. The onset of nucleation of sugars is delayed substantially by the addition of ingredients such as corn syrup and other sugars (i.e., invert sugar, etc.). These products may be fluid at room temperature and even runny at elevated temperatures. However, crystallization is inhibited kinetically through proper formulation. The shelf life of products in which crystallization is undesired is often directly related to the induction time for nucleation at the storage conditions. To obtain a long shelf life through prevention of undesired crystallization, nucleation must be substantially inhibited.

13.4. FACTORS AFFECTING CONTROL OF CRYSTALLIZATION

There are a number of different factors that influence crystallization, or the prevention of crystallization, in food products. Processing conditions must be chosen for the desired effect, to either promote or prevent crystallization. These conditions depend on

the interactions of the ingredients, so formulation plays an important role in the selection of the optimal processing conditions. Once the product has been made and packaged, any changes during distribution and storage influence shelf life. Proper storage conditions are necessary to maintain the desired state of the product and allow the longest possible shelf life.

13.4.1. HEAT AND MASS TRANSFER RATES

During processing, the rates of heat and mass transfer are important to defining proper control of crystallization. The rates of heating and cooling during the process can impact crystallization as can the hold times and temperatures. If evaporation of water occurs during the process, this can impact crystallization as well. In fact, some processes require controlled evaporation (drying) to produce the desired product quality and the rate of this drying can influence crystallization. Also, agitation energy, whether intentional through forced mixing or unintentional through fluid shear forces, can promote crystallization.

Rate of cooling. The rate of cooling of a mass to a desired crystallization temperature, as in production of fondant or crystallization of grained caramel and fudge, determines the extent and type of nucleation. If the mass is cooled uniformly and rapidly to the desired processing temperature, all of the mass will crystallize at the same condition and at the same time. This leads to the maximum production of nuclei and the narrowest distribution of crystal sizes. On the other hand, if cooling is slow or nonuniform, crystallization will also be nonuniform. In regions that cool more rapidly, nucleation will take place first and these crystals will continue to grow as the rest of the mass crystallizes. The nuclei that formed first become larger than the other crystals and this may result in a coarse texture. Therefore, it is important to ensure that processes are designed so that the entire mass cools rapidly and uniformly to the desired crystallization temperature.

In lipid products, the rate of cooling affects the amount of crystalline mass, the polymorph formed and the crystal habit. The crystalline structure of a lipid product, made from a mixture of high- and low-melting components of milk fat, cooled at two different rates in an agitated, batch crystallizer and crystallized at 25°C was studied (Herrera and Hartel 2000a). After crystallization was complete, the fat slurry was poured into a mold and allowed to set overnight at 10°C. The crystals in the crystallizer slurry were smaller when the lipid melt was cooled rapidly, as shown by the optical photomicrographs in Figure 13.7. After setting of the product, the internal crystalline characteristics were significantly different, as seen in images obtained by confocal scanning laser microscopy (Figure 13.8). The nature of the crystalline mass that formed between the primary crystals (during agitation) was significantly different for the different cooling rates. These different crystalline microstructures resulted in significantly different mechanical properties (Herrera and Hartel 2000b), which lead to different textures. Clearly, the conditions under which these samples crystallized can have a large effect on the texture and quality of these products. In these particular samples, polymorphism was not an issue since milk fat forms in the β' polymorph under most conditions. In other fat systems (e.g., cocoa butter), polymorphic differences also might influence crystalline microstructure and mechanical/textural properties.

Rate of cooling also is important in systems where crystallization is undesired. For amorphous products, cooling must be sufficiently rapid that the mass passes through the crystallization zone between the solubility curve and glass transition zone before nucleation occurs. In this case, heat transfer must occur more

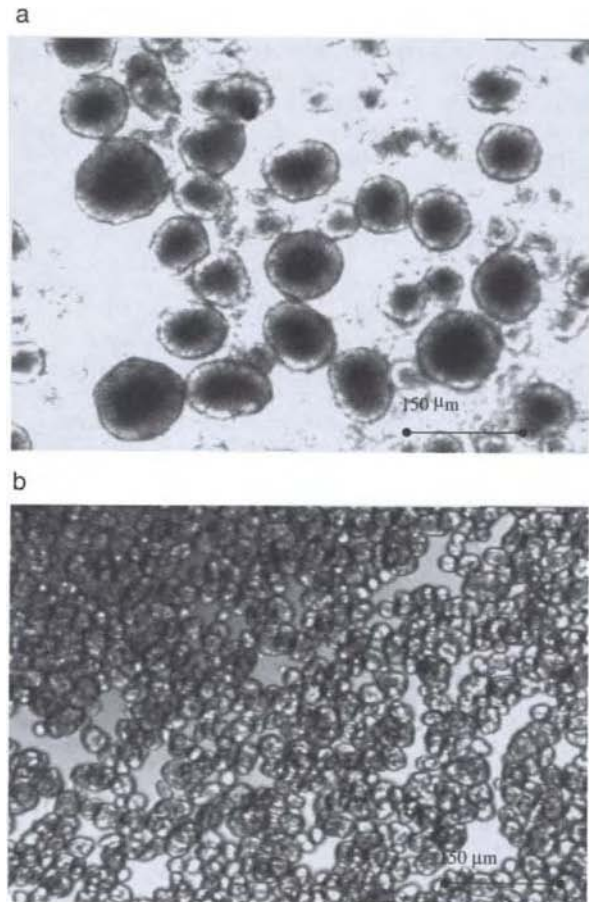


Figure 13.7 Effect of cooling rate on crystalline microstructure (polarized light microscopy) of a milk fat model system (50% high-melting and 50% low-melting component of milk fat) crystallized at 25°C and agitation rate of 200 RPM. Cooling rate: (a) 0.20°C/min; and (b) 5.50°C/min. (From Herrera and Hartel 2000c; with permission.)

rapidly than the time scale for onset of nucleation (induction time) in the product. Cooling must be sufficiently rapid so that the mass quickly reaches a point where induction times for nucleation are very long. The temperature at this point depends on formulation and other processing requirements. An example of this is forming of hard candies. Once the sugar mass has been boiled to sufficiently high temperature (low water content), it is cooled rapidly to prevent crystallization. As temperature is decreased, the mass becomes more viscous. At some intermediate temperature (50–60°C), the product is stable from crystallization for sufficiently long enough time, yet its viscosity is still low enough that the sugar mass can be worked without danger of crystallization. At this point, the mass is formed into the desired product shapes and then cooled to room temperature in a cooling tunnel to solidify into the final product (glassy state).

The intermediate temperature for forming of hard candies is critical to production of a quality product. If this temperature is too high and/or the mass is held at that temperature for too long, crystallization is likely to occur. This results in a grained product. In fact, this is exactly what is done to make a grained mint. The intermediate sugar mass is placed on a “pulling” device, which provides agitation to the mass. Usually, some powdered sugar is also added to provide seed and then the mass is agitated to dis-

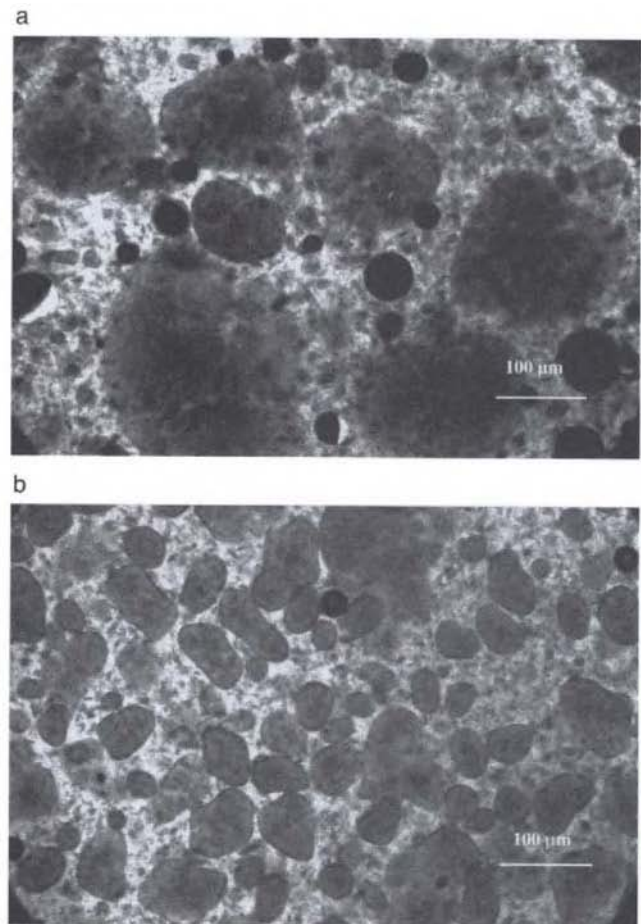


Figure 13.8 Effects of cooling rate on crystalline characteristics (dark images) of lipid mixture (50:50 high-melting and low-melting milk fat components) crystallized at 25°C (50 RPM) and then set at 10°C for 24 hours. Top photo: cooling rate 0.20°C/min. Bottom photo: cooling rate 5.50°C/min. Images taken using confocal scanning laser microscopy with Nile Blue as dye mixed in prior to crystallization. Image depth: 10 µm from surface. (From Herrera and Hartel 2000a; with permission.)

tribute the seeds and allow crystallization. After several minutes, the product is removed from the pulling machine and then formed and cut into desired shape. The sugar mass still has sufficient fluidity since, at this point, only a small portion of the sugar mass has crystallized. Since the viscosity is so high at this point, crystal growth takes a long time and the product is not fully crystallized for about 24 hours. After full crystallization, the product has a crumbly texture due to the combination of many small sugar crystals imbedded in a high viscosity matrix.

Crystallization temperature. The temperature at which crystallization occurs is also important to control of the desired crystal size distribution and product texture. As discussed previously (Figure 13.3), there is an optimal temperature for many systems where nucleation rate is highest. This optimum nucleation point is based on the balance between thermodynamic driving force (supersaturation) and mobility effects (glass transition). At this optimal temperature, the maximum number of crystals will be formed,

resulting in formation of a narrow distribution with small mean size. This is generally the desired characteristic for products with smooth texture (caramels, ice cream, frozen foods, etc.). For lipid-based products, processing temperatures must be chosen to maximize formation of the desired polymorphic form. Since rapid nucleation is rarely found for the most stable polymorphs, temperature and time conditions that allow rapid nucleation and proper polymorphic formation are necessary.

Fondant, a confectionery product used in creams and frostings, is an excellent example of how crystallization temperature can influence crystalline microstructure and textural properties. Fondant is a highly crystallized sugar product that is made by evaporating a sugar syrup to high concentration (80–90% solids), cooling it rapidly in a heat exchanger to crystallization temperature and then agitating extensively to form many small crystals. The temperature at the nucleation point is critical to formation of many nuclei, although the exact temperature at the peak of nucleation rate curve (Figure 13.3) depends on product formulation. In practice, the optimal temperature for beating is found by trial-and-error. Table 13.5 shows how beating temperature affects the size distribution of sucrose crystals in a fondant (Lees 1965). Clearly, as the beating temperature was decreased from 70 to 40°C, the percentage of small crystals increased. Although the total number of crystals formed at each condition was not measured, one would suspect that crystallization at 40°C resulted in production of the greatest number of crystals. This is why they remained small.

On the other hand, if few larger crystals are desired for efficient separation, then nucleation must occur at a point where fewer nuclei are formed. This point is at higher temperature (or lower concentration) than the maximum nucleation point. Nevertheless, it is still important that the nuclei are formed at the same time so that they all grow to about the same product size for efficient filtration.

Agitation. In products where massive nucleation is desired, it is important to provide sufficient agitation to promote maximum nucleation. Mechanical energy input enhances the nucleation process. During processing of fondant, for example, the sugar mass is cooled to the desired crystallization temperature and then worked extensively in a beater to promote massive crystallization. This results in the production of many small crystals and produces a smooth fondant. For crystallization at the same temperature, lower agitation energy resulted in larger crystals during fondant manufacture. Rapid agitation resulted in a mean size of 3.9 μm with a maximum of 9.6 μm , whereas slow agitation resulted in a mean size of 4.9 μm with a maximum of 15.0 μm (Lees 1965). In addition, the width of the distribution was wider for slow agitation.

TABLE 13.5 Effect of Crystallization Temperature on Crystal Size Distribution in Fondant Manufacture

Temperature (°C)	Crystal Size Range (%)			
	0–10 μm	10–20 μm	20–30 μm	> 30 μm
10% Glucose syrup				
70	83.2 ^a	12.2	3.6	1.1
55	89.1	9.7	1.1	1.1
40	92.3	7.4	1.1	—
25% Glucose syrup				
70	89.5	7.7	1.8	0.4
55	96.2	3.5	0.3	—
40	99.9	0.2	—	—

^aNumbers do not add up to 100% in original data.

Fondant made with 90% sucrose and 10% corn syrup in dry matter and 90% total solids. (Data from Lees 1965.)

Intensity of agitation, or the relation between micro- and macromixing, is also important in producing a crystal-size distribution suitable for efficient separation. This principle is widely recognized in many industries although it also applies in certain food processes. For example, the effect of agitation on the efficiency of separation of milk fat during fractionation by batch crystallization was studied by Patience et al. (1999). The effect of tip speed of a three-propellor agitator on filtration efficiency is shown in Figure 13.9. In this study, milk fat was crystallized at 28°C to form a crystal slurry that was subsequently separated in a pressure (5 bar) filter. Filtration curves were used to calculate a filtration resistance term. At low tip speeds, there was insufficient agitation and milk fat crystals agglomerated readily. At very high tip speed, substantial breakage or secondary nucleation took place, resulting in numerous small crystals. This size distribution did not filter very well and the resistance was extremely high. At some intermediate agitation condition in this system, agglomeration and breakage counteracted to produce a size distribution that resulted in the lowest filtration resistance (most efficient filtration). In this case, the crystals were reasonably uniform in size and were generally around 200–300 μm in size. Filtration resistance, in this case, correlated directly with the amount of liquid entrained in the filter cake. That is, more liquid entrainment occurred when the filtration resistance was high and filtration the most inefficient. It should be apparent that the choice of operating conditions plays a critical role in the efficiency of the fractionation process.

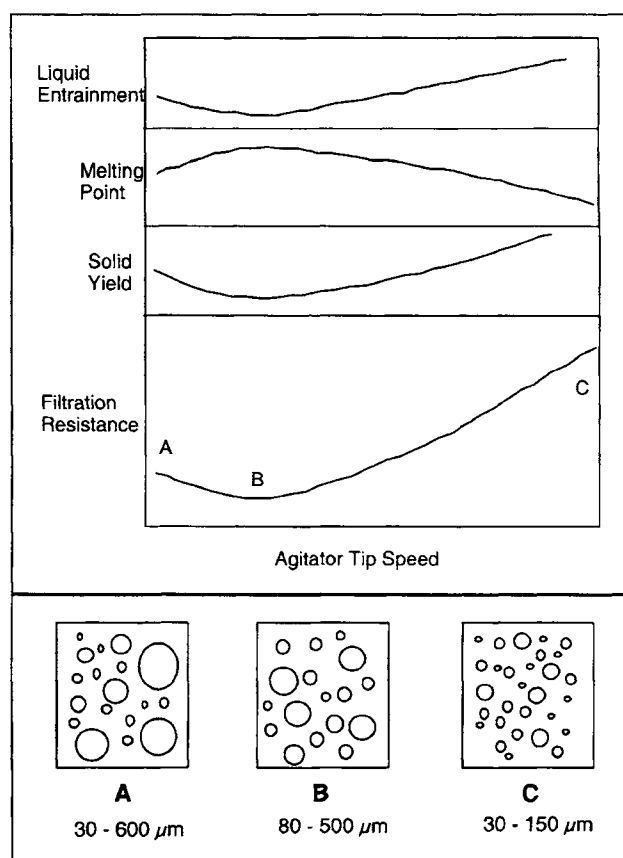


Figure 13.9 Agitation (tip speed of three-propellor agitator) affects filtration resistance and liquid entrainment in pressure filtration (5 bar) of milk fat crystals from a batch crystallizer at 28°C (Adapted from Patience et al. 1999; Hartel 2001; with permission.)

If nucleation must be avoided in a product, agitation during processing must be kept to an absolute minimum. Sometimes even the shear forces that exist as a supersaturated fluid is passed through a pipe and fittings may be sufficient to initiate nucleation.

Drying. Some food processes involve simultaneous crystallization and drying (Hartel 1995). Controlling crystallization in the sugar coating of a cereal product requires a careful balance between crystallization and drying processes since, in a sense, they are competitive processes. A similar balance is required when crystallization of sugar occurs in thin films around a panned confectionery piece (jaw breaker, sugar-coated peanut, etc.). In these processes, a concentrated sugar solution is sprayed or applied to the piece (whether a candy piece or a cereal base) under conditions where sugar crystals are formed. The film is then dried to produce a hard brittle shell in panned items or a sugar coating with desired appearance and texture. Crystallization causes a decrease in concentration in the solution phase, whereas drying causes concentration to increase as water is removed. Thus, drying influences the rate of crystallization and can significantly impact the product characteristics.

Breakfast cereal manufacturers are concerned about the appearance of their products, particularly those that should have a "frosted" appearance. In this case, a sugar syrup is applied to the cereal base to produce a thin film about 100–200 μm thick. A number of sugar crystals are introduced at this point, either through seeding from dust in the environment or induced by tumbling during the coating process. The exact source of seed crystals has not been determined. Once the film has been applied and seed crystals are present, the cereal pieces enter a dryer where water is removed from the sugar film. Careful control of crystallization and drying is needed to ensure that the desired crystalline shape for frosty appearance is attained (Ben-Yoseph and Hartel 2000). Since drying in this thin film is more rapid than crystallization, initially the sucrose concentration in the solution phase increases. In the region of a crystal imbedded in the film, the concentration initially increases since drying is rapid. At some point, the concentration in the vicinity of a growing crystal decreases as the solution desupersaturates. Over time, crystallization and drying continue until equilibrium with the environment is attained. Individual crystals grow together as the film dries, leaving a matrix of crystals surrounded by high concentration, high viscosity sucrose solution. The water content of the film reaches an equilibrium with water vapor in the surrounding air and both crystallization and drying cease. The frosty appearance of the film is derived from the characteristics of the crystalline surface, where many crystals grow together and leave a rough surface area necessary for the frosty appearance.

13.4.2. PRODUCT FORMULATION

Choice of ingredients in a product formulation is based on many factors, not simply on the necessity of controlling crystallization. In some cases, formulation may be governed by standards of identity or some other desired product characteristic (e.g., all natural). However, the impact of formulation on crystallization kinetics must be taken into account when developing processing conditions for a product. For example, the use of corn syrups in hard candy may be based on economic decisions, but corn syrup also inhibits graining of the sugar mass during both processing and storage.

One of the main factors affecting crystallization in solution systems is the water content, or total solids content. This determines supersaturation and the subsequent rate kinetics as tempera-

ture is changed. Higher solids content generally results in higher supersaturation, although this is highly dependent on the type of ingredients used. In frozen desserts, the initial water content in the mix is crucial to the nature of the crystalline state of ice. Water content influences the freezing point depression in a complex product and this determines the phase volume of ice at any given storage temperature. Higher water content generally means higher freezing point (lower solute concentrations) and more ice frozen at storage. This combination generally results in larger ice crystals, as seen in Figure 13.10 (Donhowe et al. 1991). In this case, a vanilla ice cream mix (initial total solids of 40%) was frozen under commercial conditions. The mix was diluted to 37 and 34% total solids and frozen under the same conditions. As seen in Figure 13.10, mean size and number of large crystals increased as initial water content increased (solids content decreased). This is primarily a result of the increase in ice phase volume although there may also be some effect of crystallization kinetics.

Addition of soluble components typically inhibits crystallization although the effect on supersaturation or thermodynamic driving force must also be considered. The choice of ingredients in a formulation also influences the glass transition zone. The changes in equilibrium conditions are shown in Figure 13.11 for mixtures of lactose and sucrose. Addition of lactose and sucrose in solution causes a decrease in solubility concentrations of both components, as shown by the dotted lines in Figure 13.11. Since both lactose and sucrose have the same molecular weight, both components have the same effect on freezing point depression. However, pure lactose has substantially higher glass transition temperature (about 102°C) than pure sucrose (65–70°C). Mixtures of the two components have a glass transition temperature somewhere between these two curves, depending on the relative addition levels of each. The curves shown in Figure 13.11 represent the situation for mixtures of lactose and sucrose found, for example, in typical caramels and in the unfrozen phase of ice cream under storage conditions.

Addition of other components or ingredients also can influence nucleation and growth kinetics. For example, addition of

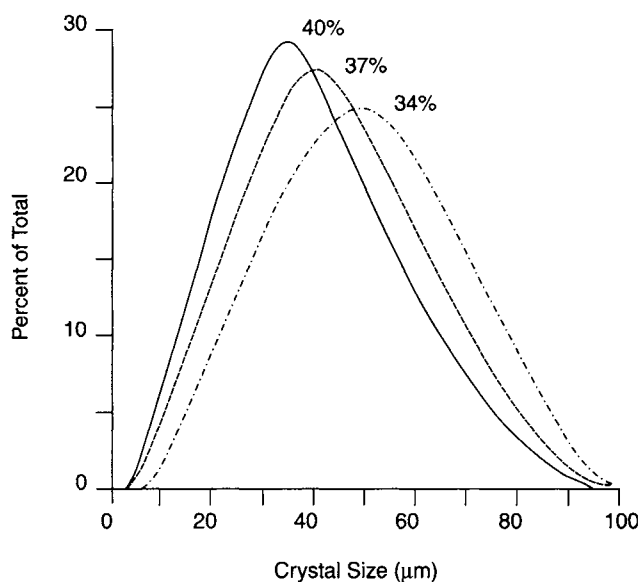


Figure 13.10 Ice crystal size distributions in ice creams made with different total solids content. The initial 40% total solids mix was diluted with water to produce mixes of 37% and 34%. Ice cream frozen in a batch freezer at constant conditions. (From Hartel 1998c; with permission.)

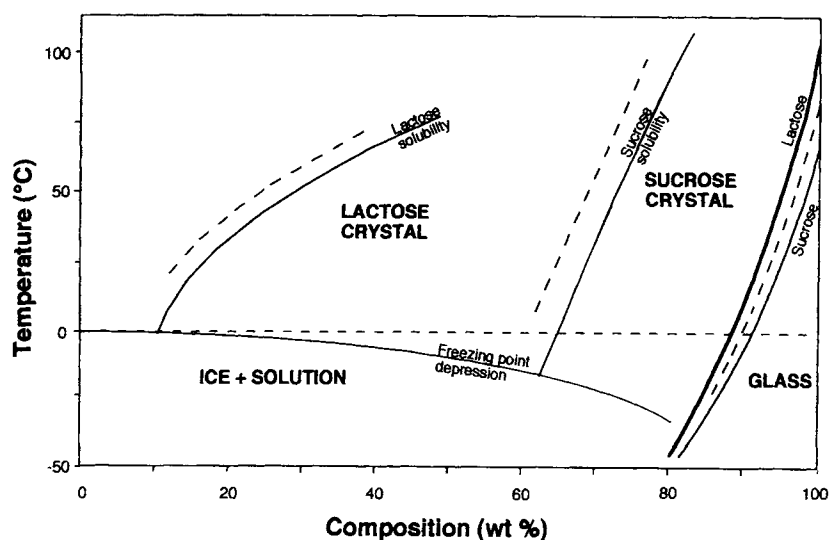


Figure 13.11 Mixtures of lactose and sucrose cause changes in phase/state behavior. Solid lines represent behavior of sucrose, dashed lines represent behavior of lactose, and dashed line represents a mixture of sucrose and lactose. (From Hartel 1993; with permission.)

corn syrup in a sugar confection helps to control sucrose crystallization. Corn syrup inhibits both nucleation and growth of sucrose (Tjuradi and Hartel 1995). Addition of over 20% corn syrup was required to see any substantial increase in induction times for onset of sucrose crystallization and much higher levels were needed to prevent nuclei formation. However, sucrose crystal growth rates were depressed at corn syrup concentrations of 10% with decreasing growth rates as corn syrup content increased. The effects of the different components (glucose polymers of different degree of polymerization, DP) on sucrose crystallization was also studied. Surprisingly, the DP of the glucose polymer had no effect on sucrose crystal growth at equivalent molar additions. Thus, one mole of glucose (DP 1) had the same inhibition effect as one mole of a long-chain polymer.

Another example of inhibition of crystallization through formulation in the food industry is the addition of milk fat to chocolate. It is widely recognized that milk fat slows the rate of cocoa butter crystallization although it is not clear if this is a nucleation or growth effect. Metin and Hartel (1997) showed that addition of 10% milk fat to cocoa butter was sufficient to slow crystallization significantly. However, this was measured using calorimetry and complete separation of nucleation from growth effects was not possible. In the chocolate industry, it is widely recognized that processing conditions for milk chocolate must be different from those for dark chocolate (no milk fat). The presence of milk fat in chocolate requires lower tempering temperatures in order to generate the same amount of nucleation (as for chocolate without milk fat).

13.4.3. POST-PROCESSING EFFECTS

Even though a product has been manufactured and packaged, it does not mean that no further changes in crystalline structure will occur. In products where crystals have been formed during processing, it is still possible, if not likely, that further changes in the crystalline structure occur during storage. It is widely recognized in some products that full crystallization is not completed for a period of time after packaging, perhaps even up to several weeks. The texture of some confectionery products, for example, is differ-

ent at the point of packaging as compared to the texture of products sold to the consumer. These changes may come about for several reasons.

It is possible that the maximum phase volume of crystalline material, or full desupersaturation of the solution, may not be attained prior to packaging. The balance between time of processing and completion of crystallization must be weighed carefully in determining process conditions. Typically, high throughput rates result in products that are not fully crystallized during processing unless crystallization kinetics are also rapid. However, as long as crystallization continues under reasonably controlled conditions after packaging, product quality will not suffer greatly. In ice cream, for example, the pumpable slurry that comes out of the scraped surface freezer (at -5 to -6°C) contains only a portion of the total ice in the final frozen product. In fact, only about half of the initial water present is frozen at this point. This intermediate product has sufficient fluidity to fill the package so that no air pockets are left. The entire package is frozen further in a hardening room until ice cream temperature reaches -18 to -20°C . Here, the amount of water frozen into ice increases to about 75–80%, depending on the formulation. Since nucleation only occurs in the scraped surface freezer, this additional ice phase volume appears as an increase in mean size of the distribution obtained from the freezer. The more crystals that are formed in the freezer, the smaller the crystals will remain after hardening.

In some frozen foods, particularly those that are frozen rapidly (using liquid nitrogen, for example), it is possible that insufficient ice has formed to relieve the temperature driving force for ice formation. Warming of the product, either in subsequent processing steps or during storage, results in continued ice formation. Growth of the existing nuclei may cause product damage as the larger ice crystals begin to break cellular structure and cause damage to the texture.

Another example of a product where crystalline changes take place after processing is butter. When butter comes off the processing line, it is still sufficiently fluid or pliable that it can be formed into the desired shape. After packaging, the butter is cooled to refrigeration temperature where further crystallization takes place.

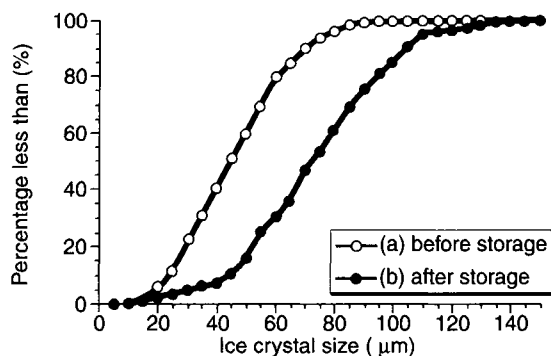


Figure 13.12 Ice crystal size distributions in ice cream (a) before and (b) after storage for three months at -15°C . Ice creams correspond to photomicrographs shown in Figure 13.2.

Lowering the temperature causes more of the butter to crystallize, which results in a significant hardening of the butter and gives the product some of its desired attributes. In general, any changes in crystal size distribution during packaging and storage must be taken into account in terms of overall product quality.

Ripening. Other changes in crystalline structure take place during storage due to a thermodynamic ripening effect, which can occur even when the crystalline phase volume does not change (Fennema 1973). Crystals in a food product are not at equilibrium even though the maximum phase volume may have been attained. That is, changes in internal energy or surface energy may still take place during storage that cause significant changes in crystal size distribution or crystalline structure. These changes may have significant impact on the qualities of the final product. Recrystallization of ice crystals in ice cream (Hartel 1998b) and frozen foods, and fat bloom in chocolates (Hartel 1998c) are two examples of this thermodynamic process.

Typically, recrystallization is promoted when a product is stored at elevated temperatures, although this depends on the product. In frozen foods, storage close to the melting point causes the most rapid recrystallization. Mobility of water and solute molecules is highest at this point and diffusion-limited processes occur rapidly. In products containing lipids, recrystallization is promoted at temperatures close to the final melting point of the fat. This usually occurs at temperatures above room temperature but it depends on the type of fat used in the product. Temperature fluctuations also affect the rate of recrystallization during storage. In general, larger thermal fluctuations lead to more rapid recrystallization although this has not been proven in every circumstance. But more importantly, recrystallization may still occur, although at a reduced rate, even though the temperature is held constant. Other factors that influence recrystallization include the state of the original crystal size distribution at the onset of recrystallization and the composition of the product. These factors influence the formation of crystalline structure during processing, but their effect on subsequent changes in crystallinity must also be considered.

Recrystallization is generally evidenced by an increase in the mean size and spread in the width of a crystal size distribution (Hartel 1998a), as seen for ice crystals in ice cream in Figure 13.12. In this case, it is also accompanied by a decrease in the number of crystals so that the total phase volume of crystalline matter remains the same. However, recrystallization also may result in a

change in the shape of crystals and/or a transformation to a more stable polymorph.

Several phenomena may occur during recrystallization. However, the underlying principle of most mechanisms of recrystallization is the thermodynamic ripening phenomenon. In many cases, it is the thermodynamic difference in equilibrium between crystals with large radius of curvature and those with small radius of curvature that leads to recrystallization. Thus, Ostwald ripening occurs due to the difference in equilibrium between large and very small crystals. In this case, the small ones disappear and the large ones grow (Figure 13.13a).

The difference in thermodynamic equilibrium between crystals of different size is defined by the Gibbs-Thomson or Ostwald-Freundlich equation (Mullin 1993). The original Kelvin equation was written to describe droplets of liquid in a vapor in terms of vapor pressures around droplets of different size. However, in crystallization studies, the vapor pressure may be related, through the solution activity, to the equilibrium concentration in solution for crystals of different size. Making the assumption that concentration can be used directly for vapor pressure gives

$$\ln \left[\frac{C(r)}{C_s} \right] = \frac{2\sigma_s v}{kTr} \quad (13.2)$$

where, $C(r)$ is the concentration in equilibrium with a crystal of size r , C_s is the concentration in equilibrium with an infinitely large crystal (or flat plane), k is the Boltzman constant, T is absolute temperature, v is molecular volume and σ_s is the interfacial tension between crystal and solution. Equation (2) assumes that the interfacial tension of a crystal in a solution is independent of crystal size and predicts that solubility concentration approaches infinity as particle size goes to zero. Since this cannot be true, Eq. (2) has been further modified (Mullin 1993) to account for surface electrical charge as particles get increasingly smaller.

The Gibbs-Thomson equation also can be written for melt systems as

$$T_0 - T(r) = \frac{2\sigma_s v T_0}{\rho(\Delta H_f)r} \quad (13.3)$$

where, T_0 is melting point of a crystal of infinite size, $T(r)$ is melting point of a crystal of size r , ρ is crystal density and ΔH_f is the latent heat of fusion for the crystallizing species.

Based on the Gibbs-Thomson equation, it is possible that conditions may occur where small crystals are in undersaturated conditions at the same time that large crystals are in supersaturated conditions. Thus, small crystals disappear and large crystals grow. However, the difference in equilibrium condition between large and small crystals based on the Kelvin equation is very small. In most systems, true Ostwald ripening is only important for crystals smaller than $1\text{--}2\text{ }\mu\text{m}$. For ice, Ostwald ripening may be important in crystals as large as $5\text{ }\mu\text{m}$. Based on approximations for the ice-sucrose system, Donhowe (1993) estimated the differences in melting point between crystals of different sizes, as shown in Figure 13.14. The line represents the difference in equilibrium melting temperature as size increases. Note that even ice crystals of $1\text{ }\mu\text{m}$ radius have only a 0.050°C difference in melting temperature as compared to an infinitely large crystal. Although these driving forces are quite small, during the long times of storage for many products, significant changes in crystal size distribution still can occur.

The rate of increase in mean crystal size depends on the mechanism that controls crystallization under these conditions

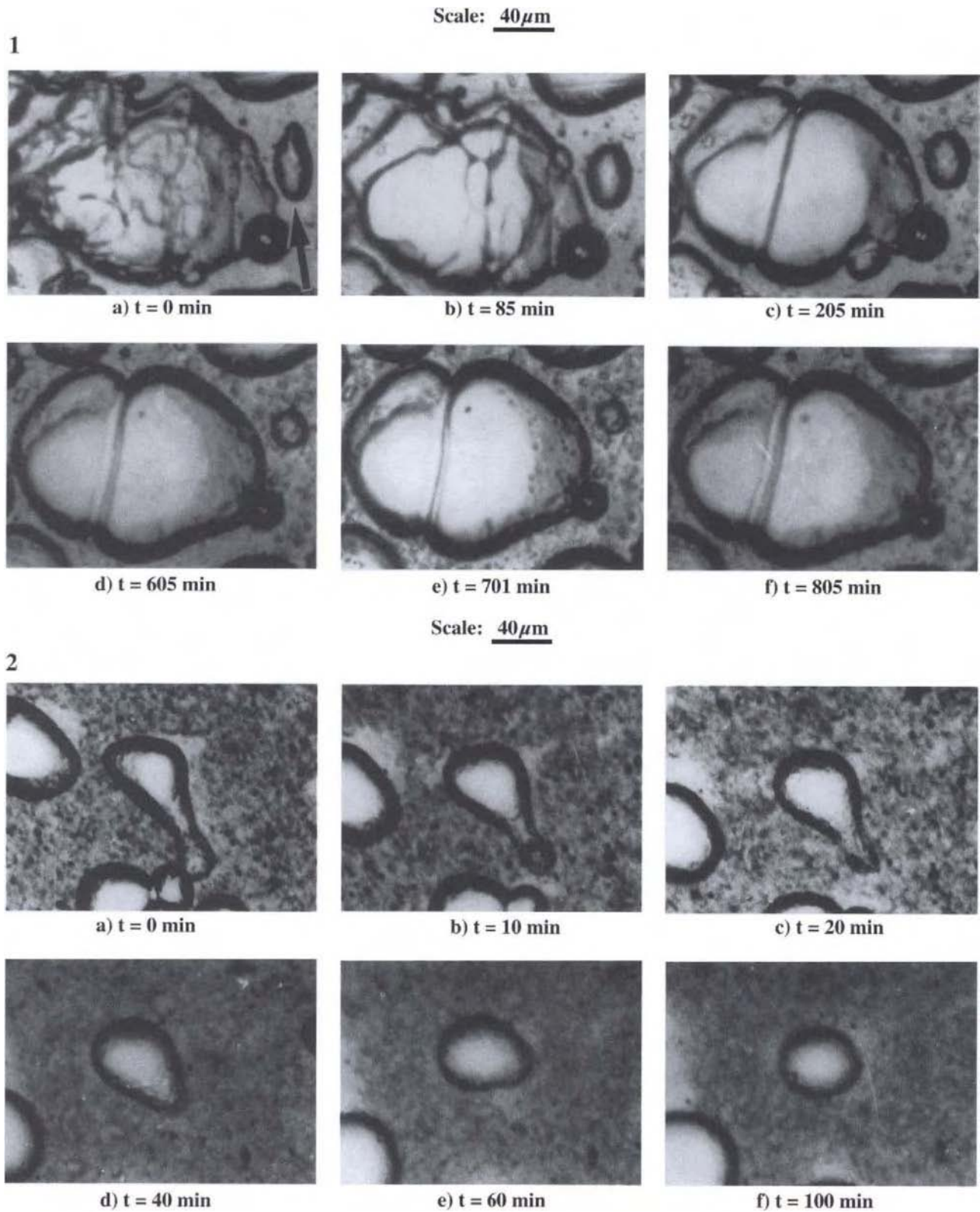
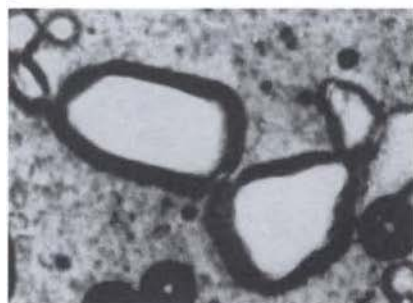


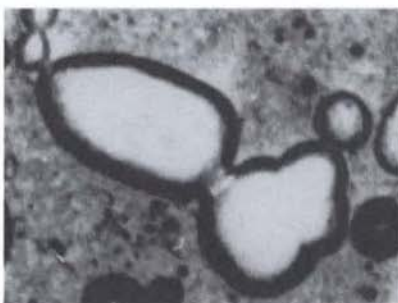
Figure 13.13 Physical mechanisms of recrystallization of ice crystals in ice cream (40% total solids) studied on a microscope slide under controlled temperature conditions: (1) Ostwald ripening: $-10.0 \pm 0.010^\circ\text{C}$; (2) Isomass rounding: $-5.0 \pm 0.010^\circ\text{C}$; (3) Accretion: $-5.0 \pm 0.010^\circ\text{C}$; and (4) Melt-refreeze: $-7.0 \pm 1.00^\circ\text{C}$ with 10 min cycles. (From Donhowe and Hartel 1996; with permission.)

Scale: 40 μ m

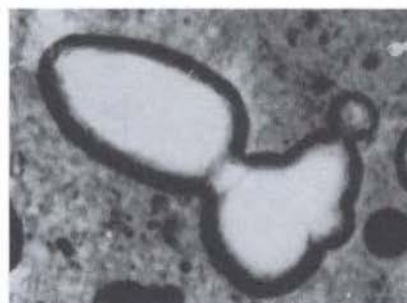
3



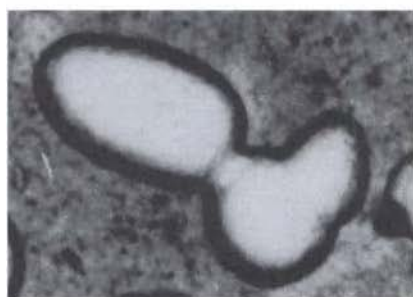
a) $t = 0$ min



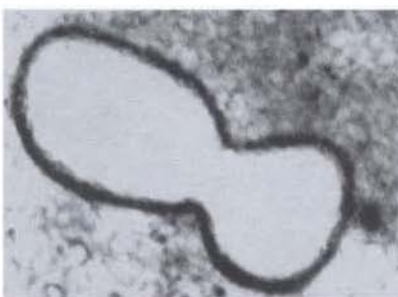
b) $t = 20$ min



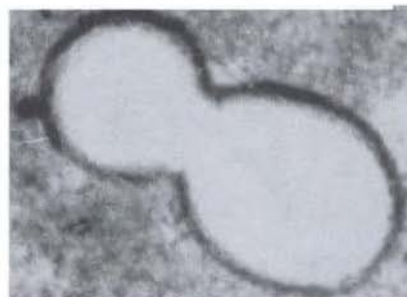
c) $t = 40$ min



d) $t = 60$ min



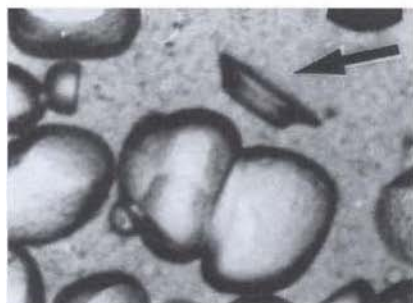
e) $t = 240$ min



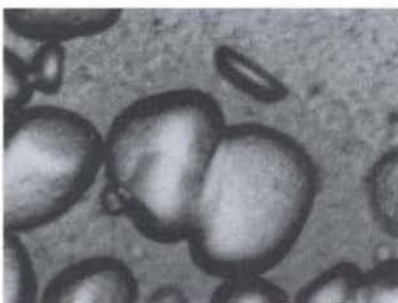
f) $t = 560$ min

Scale: 40 μ m

4



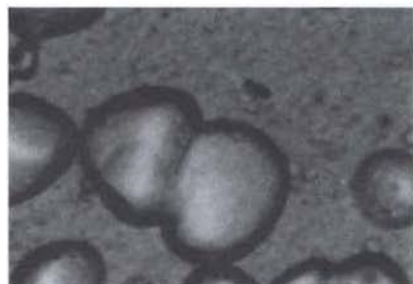
a) $T = -8^{\circ}\text{C}$, $t = 0$ min



b) $T = -6^{\circ}\text{C}$, $t = 5$ min



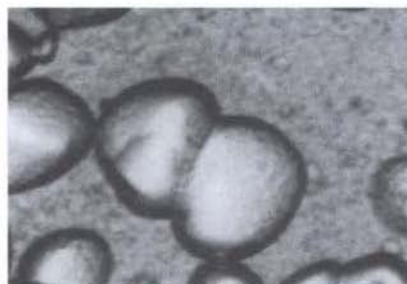
c) $T = -8^{\circ}\text{C}$, $t = 10$ min



d) $T = -6^{\circ}\text{C}$, $t = 15$ min



e) $T = -8^{\circ}\text{C}$, $t = 20$ min



f) $T = -6^{\circ}\text{C}$, $t = 25$ min

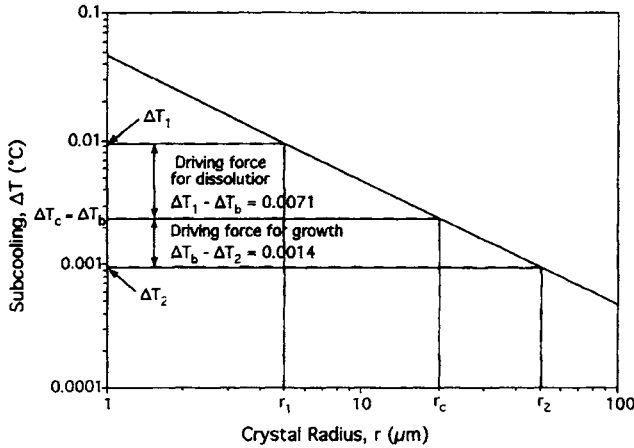


Figure 13.14 Differences in equilibrium melting temperature for ice crystals based on Ostwald ripening calculations for an ice-sucrose solution. (From Hartel 1998a; with permission.)

(Jain and Hughes 1978; Kahlweit 1975; Lifshitz and Slyozov 1961; Wagner 1961). A general asymptotic solution is given by

$$\bar{r}^n = \bar{r}_0^n + \frac{t}{\tau} \quad (13.4)$$

where, r is mean size at any time, t , r_0 is initial crystal size and n and τ are parameters that depend on the mechanism of recrystallization. When bulk diffusion of molecular species limits the rate of ripening, $n = 3$ (Lifshitz and Slyozov 1961; Wagner 1961), and when surface integration controls ripening, $n = 2$ (Jain and Hughes 1978; Kahlweit 1975). Equation (4) can be simplified for longer times to give

$$\bar{r} = \bar{r}_0 + R \left(\frac{t}{\tau} \right)^{1/n} \quad (13.5)$$

where, R represents the rate of recrystallization. The general mechanism for recrystallization processes can be determined, in part, by determining the value of n from Eq. (13.5) that matches the experimental results. For recrystallization of ice during storage of ice cream, it has been found that $n = 3$ (Donhowe and Hartel 1996). This indicates that it is the mobility of water molecules through the ice cream matrix that limits the rate of recrystallization in ice cream.

The total number of crystals decreases to balance the increase in crystal size and maintain constant crystal phase volume during recrystallization. For the case of diffusion-limited ripening, the decrease in number of crystals can be written as (Dunning 1973):

$$\frac{1}{N} = \frac{1}{N_0} \left(1 + \frac{t}{\tau} \right) \quad (13.6)$$

where, N is the number of crystals at any time, t , N_0 is the initial number of crystals and τ is the same time constant for recrystallization used in Eq. (4).

The ripening process may occur even within a single crystal of nonspherical shape. Rough edges with different radii of curvature have slightly different equilibrium energies than smooth flat surfaces and over time, these differences may be reduced as the system approaches a lower surface free energy. This process, often called iso-mass rounding (Fennema 1973), may occur in a single crystal although often there are neighboring crystals that are also involved. If there are no interactions between adjacent crystals,

isomass rounding does not lead to a change in crystal number. The phase volume of crystalline material remains the same. When rounding is the primary mechanism of recrystallization, the crystals gradually become increasingly spherical in nature (Figure 13.13b). Although this is an important mechanism of recrystallization under certain circumstances, particularly when temperature does not fluctuate substantially, there has been very little quantitative study of this mechanism of recrystallization.

Another static mechanism of recrystallization is accretion or fusion. Crystals that are very close to each other tend to grow together to form one larger crystal (Figure 13.13c). Heat and mass transfer in the region directly between the two crystals causes a bridge of crystalline material to form between them until eventually the two crystals have grown into one. This mechanism is very important in some foods, particularly those with high numbers of very small crystals situated in close proximity.

Studies on accretion have primarily focused on the joining of crystals surrounded by air, or sintering (Hobbs 1974; Kuczynski 1987). Local concentration gradients are higher in the region surrounding two adjacent crystals and this eventually leads to formation of a neck or bridge between the two crystals. Once this neck has formed, this region has high curvature and is unstable compared to the rest of the two crystals according to the Gibbs-Thomson equation. The rate at which the neck widens with time has been given as (Kuczynski 1987):

$$\frac{x^a}{r^b} = B(T)t \quad (13.7)$$

where, x is half-width of the neck at time, t , r is crystal radius, $B(T)$ is a function of temperature that incorporates physical properties of the system, and the parameters a and b depend on the mechanism of mass transport to the neck. When bulk diffusion limits the rate of mass transport, $a = 3$ and $b = 1$, whereas when surface diffusion is limiting, $a = 7$ and $b = 3$ (Kuczynski 1949).

The rate of recrystallization by accretion is also dependent on the probability that two crystals are in the same region and can form a bridge. This is a function of how tightly packed the crystals are in the product. The "coalescence frequency" has been related to the average volume of the two crystals, although the surface area has also been used to refine sintering theory. However, these theories do not fit the experimental data. Our understanding of the process of accretion recrystallization in foods is still very poor.

Despite this lack of understanding of the fundamental mechanisms, accretion is a major factor in recrystallization in some food products. Through microscopic observations, it has been shown that accretion of ice crystals is the dominant process of recrystallization when ice crystals are very small and numerous (Sutton et al. 1994). A sugar solution rapidly frozen on a microscope slide contained many small ice crystals that initially recrystallized due to accretion of these small crystals. After some time, the remaining crystals were sufficiently separated in space that accretion was no longer the main mechanism. This study clearly documented how the mechanism of recrystallization may change during the process as conditions within the product change.

Changes in ice crystal size distribution in ice cream during storage at constant temperature were studied by Donhowe and Hartel (1996). Recrystallization at constant temperature ($\pm 0.010^\circ\text{C}$) resulted in increases in mean size with time to the one-third power, demonstrating that diffusion limited this recrystallization process. Recrystallization was faster at higher temperature (-50°C) than at lower storage temperature (-200°C). Ice crystals developed a more spherical habit under these conditions with isomass rounding and accretion being the two main mechanisms of recrystallization.

Melt-refreeze. Changes in crystalline characteristics can also take place in foods due to temperature fluctuations during storage and distribution. As temperature fluctuates, the equilibrium conditions within the product also change. For example, in frozen foods under normal conditions, the amount of ice present is defined by the freezing point depression. Thus, at any storage temperature, there is an equilibrium phase volume of ice. When temperature changes, the ice must either melt or grow to maintain this equilibrium in phase volume. In some circumstances, these changes can lead to dramatic loss of product quality. Think of what happens when ice cream is left out at room temperature for long periods of time. The outer layers melt due to the thermal exposure (heat shock) and if the product is refrozen by simply placing it back in the freezer, ice crystallization is no longer controlled. The resulting product contains enormous ice crystals formed under uncontrolled conditions and the product is unacceptably coarse.

As temperature goes up, crystals either melt or dissolve to maintain the phase equilibrium at the new product temperature. When temperature goes back down again, crystalline material grows back onto the remaining crystals. The smallest crystals may eventually disappear or dissolve/melt away. Once a crystal is gone, the mass contained in that crystal is distributed among the remaining crystals and they all grow slightly larger. This assumes that no nucleation occurs as temperature decreases. As long as the temperature fluctuations are reasonably slow and of limited amplitude, nucleation is unlikely to occur within the product.

The process of cycling in phase volume with fluctuating temperatures is shown schematically in Figure 13.15. As temperature increases in frozen systems, the amount of ice present is reduced as the system strives to maintain equilibrium conditions. In solution systems, the system strives to maintain an equilibrium amount of solute in solution as defined by the solubility curve. In this case too, the amount of crystalline phase volume decreases as temperature increases due to the higher solubility. When the temperature decreases again, an increase in phase volume for both melt and solution systems occurs. However, this phase volume may be redistributed among the remaining crystals that have not melted/dissolved and result in changes in the crystal size distribution and product quality. The difference in equilibrium conditions for small crystals as compared to larger ones enhances the likelihood that small crystals will disappear first. Because of this difference in equilibrium condition, smaller crystals melt or dissolve slightly faster than larger crystals.

Donhowe and Hartel (1996) also compared recrystallization rates of ice crystals in ice cream at different amplitudes of temperature fluctuations. Above temperature fluctuations of $\pm 0.50^\circ\text{C}$, significantly faster recrystallization occurred, as compared to constant temperature conditions. Recrystallization rates were about twice as fast with temperature fluctuations of $\pm 1.00^\circ\text{C}$ compared to $\pm 0.010^\circ\text{C}$. The shape of the crystals after recrystallization at fluctuating temperatures was more jagged and uneven, whereas recrystallization at constant temperature produced a rounding effect. This was evidence that melt-refreeze and accretion were the main mechanisms of recrystallization under fluctuating temperatures.

The discussion above assumed that temperature fluctuations were sufficiently slow that the system maintained an approximate equilibrium phase volume at all times. This is probably true, in most cases, during long-term storage of foods since temperatures generally change slowly in storage facilities. In storage freezers, temperature fluctuations generally have at least a two hour cycle time and the amplitude may be about a degree. In this case, the temperature within the frozen food changes according to the laws of unsteady state heat transfer and depend on the thermal diffu-

sivity of the product. In addition, the change in latent heat caused by melting and regrowth during temperature cycling insulates the effects of external temperature fluctuations. Thus, large external temperature fluctuations often result in relatively small changes within the product (Ben-Yoseph and Hartel 1999) and the crystalline structure maintains an approximate equilibrium at the temperature within the product. A similar argument can probably be made for products stored at room temperature and experiencing normal, daily temperature fluctuations. The magnitude of these changes may be substantial, but the rate at which they occur is generally slow enough that the product maintains approximate phase volume equilibrium.

However, there may be cases where temperature fluctuations are so fast and/or the rate of melting/crystallization so slow that such an equilibrium is not maintained. In this case, less than the maximum phase volume change occurs as temperature cycles. That is, before the system can equilibrate to a reduced phase volume at high temperature, the system is already cooling and causing an increase in phase volume. This may occur in frozen foods during

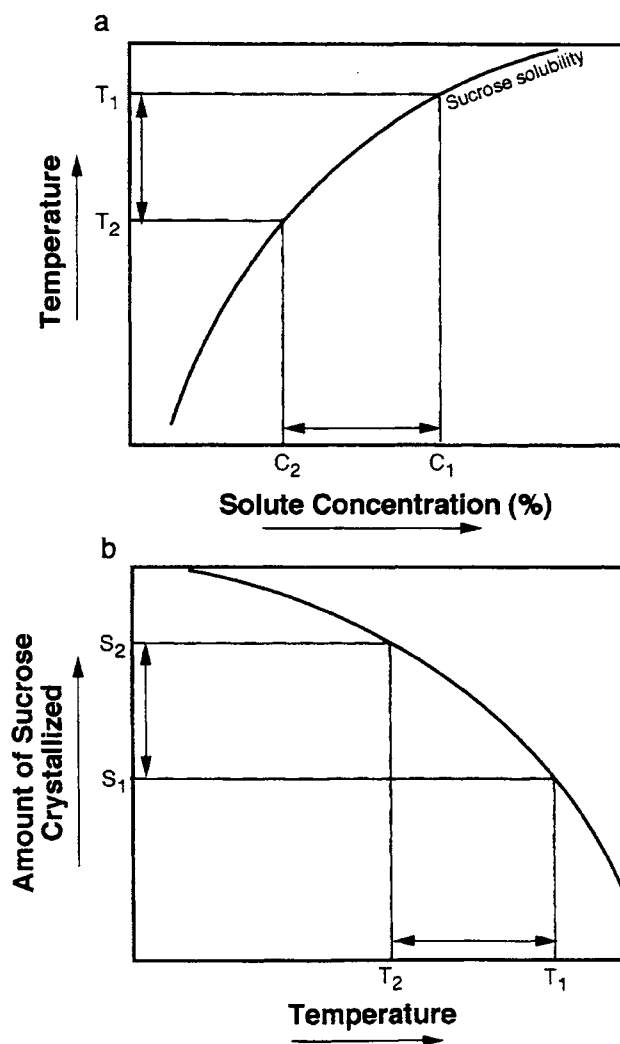


Figure 13.15 Cycling temperature (under quasi-equilibrium conditions) causes cyclic change in crystalline phase volume (shown as concentration in the solution phase) according to the equilibrium curve. (From Hartel 2001; with permission.)

heat shocking (high temperature swings), although this has not been documented.

Moisture fluctuations. Another change that may occur during storage is equilibration in moisture content. All products have an equilibrium moisture content dependent on the relative humidity of the air around it. This equilibrium may be influenced by choice of packaging material, but in many cases, there is significant moisture migration within a food product. This may arise from moisture equilibration between two components of a complex food item or through equilibration with the storage air conditions. In either case, the moisture content changes may have significant impact on the crystalline structure of a food. As a food dries out, the concentration of the remaining aqueous phase increases with a subsequent increase in supersaturation. The system then drives towards a new equilibrium between crystals and liquid to maintain the solubility concentration in solution. If the product picks up moisture from the air, crystals dissolve to maintain the equilibrium situation in solution.

Sugar glasses are notoriously hygroscopic and sorption of water can have significant detrimental effect on the shelf life of hard candy. In general, the shelf life of a hard candy is limited by moisture sorption. When a sugar glass picks up moisture, the T_g decreases in accordance with the amount of water picked up from the environment. Thus, a product that was initially stable at room temperature ($<T_g$) may become unstable as T_g falls below room temperature due to moisture sorption. Once the product is no longer in the glassy state, there are several processes that can take place to end shelf life. As soon as the product is no longer a glass, diffusion rates increase dramatically. This results in diffusional losses of flavors through the piece and loss of flavor may be a problem in some cases. Also, sufficiently high moisture content or increased temperature can cause a syrupy layer on the surface to become sticky. The “sticky point” for sugars is often defined as the condition in an amorphous mass where the viscosity is about 10^8 Pa-s (Downton et al. 1982; Wallack and King 1988), a few orders of magnitude less than the viscosity needed to attain the glassy state (10^{12} Pa-s). Any combination of temperature increase and moisture sorption that results in a decrease in viscosity to this level will cause the product to become sticky. In hard candies made with higher levels of corn syrup, this is the main concern for end of shelf life.

Hard candies made with primarily sucrose also become sticky as water is picked up from the environment. However, in this case, the amorphous sugar mass is prone to rapid crystallization or graining. At some combination of temperature and moisture uptake, the sugar mass gains sufficient mobility that the sugar molecules can rearrange and form into a crystal lattice. In fact, there are two potential causes of graining in hard candies: internal and external. Sometimes processing conditions are not controlled perfectly and a few seed crystals are present in the candy glass. These crystals are stable as long as the hard candy remains below its glass transition point. Once the temperature increases above T_g or the candy picks up sufficient moisture, these crystals can begin to grow. As they grow, they exclude colors and flavors resulting in mottled appearance and reduced flavor. Internal graining is shown schematically in Figure 13.16a. External graining occurs when the surface of the hard candy picks up sufficient moisture to initiate nucleation, as shown schematically in Figure 13.16b. Once crystallization begins, moisture in the amorphous mass migrates in through the rest of the candy and eventually the candy is crystallized throughout. This also results in loss of flavors and a mottled appearance as dyes are distributed nonuniformly at the surface of the sugar crystals. As crystallization begins, the moisture content decreases again since the equilibrium relative humidity of the

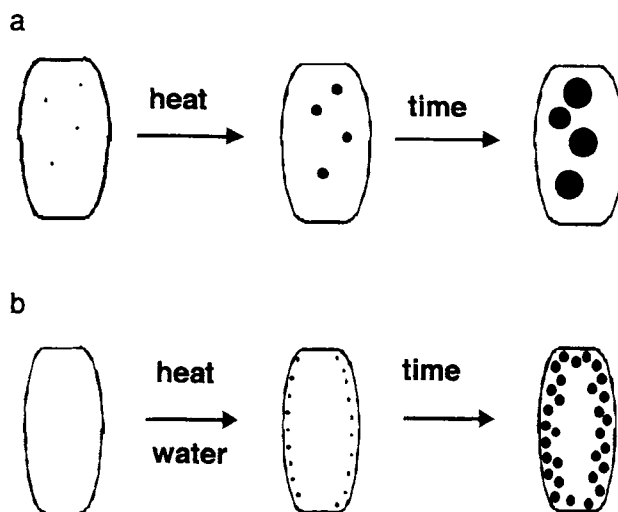


Figure 13.16 Schematic representation of physical processes for (a) internal (b) and external graining (sugar crystallization) in hard candies (sugar glass). (From Hartel 2001; with permission.)

crystallized piece is substantially lower than that of the glass (Makower and Dye 1956), and the product dries out.

One of the reasons for adding corn syrup to a hard candy formulation is to inhibit or prevent graining. Addition of 20% corn syrup reduces the likelihood of graining by increasing the induction time for nucleation (as discussed previously). Addition of 40–50% corn syrup to a hard candy generally prevents sucrose crystallization. At this level, there is not enough sucrose remaining to crystallize (lower supersaturation) and the corn syrup provides a major impediment to nuclei formation. Corn syrup components with a wide range of molecular species, including branched chain oligosaccharides, had the greatest inhibition of sucrose crystallization (Gabarra and Hartel 1998).

13.5. SUMMARY

There are many factors that influence crystallization in food products. What makes foods somewhat unique are the complexities that arise in food composition and that often we are trying to control crystallization for texture or appearance of a product and not for separation. In many products, the goal of crystallization is to generate a certain texture or appearance that makes the product acceptable. Thus, nucleating many crystals that remain small within the product itself is often the goal. There must be many crystals with small mean size and narrow distribution. The crystals also must have the proper shape and/or polymorph to enhance stability of the product during storage and distribution. However, in other types of products, crystallization is undesired even though the system is supersaturated. In these cases, techniques are used to prevent crystallization from occurring during storage, since this leads to unacceptable product quality.

ACKNOWLEDGMENT

The assistance of Daniel Donhowe, Baomin Liang, Lidia Herrera, Yi-Huang Chang, and Suzanne Smith in preparation of figures is gratefully appreciated.

REFERENCES

- Beckett, S.T. (ed.) (1988). *Industrial Chocolate Manufacture and Use*, Blackie, London.
- Ben-Yoseph, E., and Hartel, R.W. (1999). "Computer Simulation of Ice Recrystallization in Ice Cream During Storage," *J. Food Eng.* **38**(3), 309–331.
- Ben-Yoseph, E., Hartel, R.W., and Howling, D. (2000). "Three-Dimensional Model of Phase Transition of Thin Sucrose Films During Drying," *J. Food Eng.* **44**(1), 13–22.
- Berger, K.G. (1990). "Ice Cream." In *Food Emulsions*, 2nd ed. (Larsson, K., and Friberg, S.E., eds.), Marcel Dekker, New York.
- Boistelle, R. (1988). "Fundamentals of Nucleation and Growth," In *Crystallization and Polymorphism of Fats and Fatty Acids* (Garti, N., and Sato, K., eds.), pp. 189–226, Marcel Dekker, New York.
- Bricknell, J., and Hartel, R.W. (2001). "Fat Bloom in Chocolate," *J. Amer. Oil Chem. Soc.* (in press).
- Code of Federal Regulations (1990). Title 21, Chapter 1, Sections 163.123. (Dark chocolate) and 163.130 (Milk chocolate). United States Government Printing Offices, Washington, DC.
- Donhowe, D.P. (1993). "Ice Recrystallization in Ice Cream and Ice Milk," Ph.D. Dissertation, University of Wisconsin, Madison.
- Donhowe, D.P., Hartel, R.W., and Bradley, Jr., R.C. (1991). "Ice Crystallization Processes During Manufacture and Storage of Ice Cream," *J. Dairy Sci.* **74**(10), 3334.
- Donhowe, D.P., and Hartel, R.W. (1996). "Influence of Temperature on Ice Recrystallization in Frozen Desserts. I. Accelerated Storage Studies," *International Dairy J.* **6**, 1191–1208.
- Downton, G.E., Flores-Luna, J.L., and King, C.J. (1982). "Mechanism of Stickiness in Hygroscopic, Amorphous Powders," *Ind. Eng. Chem. Fund.* **21**, 447–451.
- Dunning, W.J. (1973). "Ripening and Aging Processes in Precipitates." In *Particle Growth in Suspensions* (Smith, A.L., ed.), p. 3 Academic Press, London.
- Fennema, O. (1973). "Nature of the Freezing Process." In *Low-Temperature Preservation of Foods and Living Matter* Fennema, O.R., Powrie, W.D., and Marth, E.H., eds.), p. 151, Marcel Dekker, New York.
- Gabarra, P., and Hartel, R.W. (1998). "Corn Syrup Solids and Their Saccharide Fractions Affect Crystallization of Amorphous Sucrose," *J. Food Sci.* **63**(3), 523–528.
- Gresti, J., Bugaut, M., Maniongui, C., and Bezard, J. (1993). "Composition of Molecular Species of Triacylglycerols in Bovine Milk Fat," *J. Dairy Science* **76**(7), 1850–1869.
- Hartel, R.W. (1993). "Controlling Sugar Crystallization in Food Products," *Food Technol.* **47**(11), 99–107.
- Hartel, R.W. (1995). "Crystallization and Drying During Hard Panning," *Manufact. Confect.* **75**(2), 51–57.
- Hartel, R.W. (1997). "Ice Crystallization During Manufacture of Ice Cream," *Trends Food Sci. Technol.* **7**(10), 315–320.
- Hartel, R.W. (1998a). "Mechanisms and Kinetics of Recrystallization in Ice Cream," In *Properties of Water in Foods: ISOPOW 6*, pp. 287–319, Marcel Dekker, New York.
- Hartel, R.W. (1998b). "Phase Transitions in Chocolates and Coatings." In *Phase/State Transition in Foods* (Rao, M.A., and Hartel, R.W., eds.), pp. 217–252, Marcel Dekker, New York.
- Hartel, R.W. (1998c). "Phase Transitions in Ice Cream." In *Phase/State Transition in Foods* (Rao, M.A., and Hartel, R.W., eds.), pp. 327–368, Marcel Dekker, New York.
- Hartel, R.W. (2001). *Crystallization in Foods*, Aspen Publishing, Gaithersburg, MD.
- Hartel, R.W., and Kaylegian, K.E. (2001). "Advances in Milk Fat Fractionation: Technology and Applications." In *Crystallization Processes in Fats and Lipid Systems* (Garti, N., and Sato, K., eds.), pp. 381–427, Marcel Dekker, New York.
- Herrera, M.L., and Hartel, R.W. (2000a). "Effect of Processing Conditions on Physical Properties of a Milk Fat Model System," *Microstructure, J. Amer. Oil Chem. Soc.* **77**(11), 1197–1204.
- Herrera, M.L., and Hartel, R.W. (2000b). "Effect of Processing Conditions on Physical Properties of a Milk Fat Model System," *Rheology, J. Amer. Oil Chem. Soc.* **77**(11), 1189–1195.
- Herrera, M.L., and Hartel, R.W. (2000c). "Effect of Processing Conditions on Crystallization Kinetics of a Model Milk Fat System," *J. AOCS* **77**(11), 1177–1187.
- Hobbs, P.V. (1974). *Ice Physics*, Clarendon Press, Oxford.
- Jain, S.C., and Hughes, A.E. (1978). "Ostwald Ripening and Its Applications to Precipitates and Colloids in Ionic Crystals and Glasses," *J. Material Sci.* **13**, 1611.
- Jovanovic, O., Karlovic, D., and Jakovljevic, J. (1995). "Chocolate pre-crystallization: A review," *Acta Alimentaria* **24**(3), 225–239.
- Kahlweit, M., (1975). "Ostwald Ripening of Precipitates," *Adv. Colloid Interface Sci.* **5**, 1–35.
- Kuczynski, G.C. (1949). "Self-diffusion in Sintering of Metallic Particles," *J. Metals* **1**, 169.
- Kuczynski, G.C. (1987). "Towards the Understanding of the Process of Sintering." In *Sintering '85* (Kuczynski, G.C., Uskokovic, D.P., Palmour III, H., and Ristic, M.M., eds.), p. 3, Plenum Press, New York.
- Lees, R. (1965). Factors Affecting Crystallization in Boiled Sweets, Fondants and Other Confectionery, Brit. Food Manuf. Ind. Res. Assoc., Scientific and Technical Survey No. 42, Leatherhead.
- Lifshitz, I.M., and Slyozov, V.V. (1961). "The Kinetics of Precipitation from Supersaturated Solid Solutions," *J. Phys. Chem. Solids* **10**(1/2), 35–50.
- Livney, Y.D., Donhowe, D.P., and Hartel, R.W. (1995). Influence of Temperature on Crystallization of Lactose in Ice Cream. Intern., *J. Food Sci. and Technol.* **30**(3), 311–320.
- Makower, B., and Dye, W.B. (1956). "Equilibrium Moisture Content and Crystallization of Amorphous Sucrose and Glucose," *J. Agric. Food Chem.* **4**(1), 72–77.
- Metin and Hartel (year?). "Crystallization Kinetics of Blends of Cocoa Butter and Milk Fat or Milk Fat Fractions," *J. Thermal Analysis* **47**(5), 1527–1544.
- Mullin, J.W. (1993). *Crystallization*, Butterworth, Oxford.
- Mullin, J.W., and Leci, C.L. (1969). "Some Nucleation Characteristics of Aqueous Citric Acid Solutions," *J. Crystal Growth* **5**, 75–76.
- Patience, D., Hartel, R.W., and Illingworth, D. (1999). "Crystallization and Pressure Filtration of Anhydrous Milk Fat: Mixing Effects," *J. Amer. Oil Chem. Soc.* **76**(5), 585–594.
- Precht, D. (1988). "Fat Crystal Structure in Cream and Butter," In *Crystallization and Polymorphism of Fats and Fatty Acids* (Garti, N., and Sato, K., eds.), pp. 305–361, Marcel Dekker, New York.
- Sato, K. (1988). "Crystallization of Fats and Fatty Acids." In *Crystallization and Polymorphism of Fats and Fatty Acids* (Garti, N., and Sato, K., eds.), pp. 227–266, Marcel Dekker, New York.
- Sutton, R.L., Evans, I.D., and Crilly, J.F. (1994). "Modeling of Ice Crystal Coarsening in Concentrated Disperse Food Systems," *J. Food Sci.* **59**(6), 1227.
- Timms, R.E. (1980). "The Phase Behavior of Mixtures of Cocoa Butter and Milk Fat, Lebens," *Wiss. Technol.* **13**(2), 61–65.
- Tjuradi, P., and Hartel, R.W. (1995). "Effects of Corn Syrup Oligosaccharides on Sucrose Crystallization," *J. Food Sci.* **60**(6), 1353–1356.
- Van Hook, A., and Bruno, A.J. (1949). "Nucleation and growth in sucrose solutions, Faraday Disc.," *Royal Soc. Chem.* **5**, 112.
- Wagner, C. (1961). "Theorie die Alterang von Niederschlägen durch umlösen," *Z. Elektrochem.* **65**(7/8), 581–591.
- Wallack, D.A., and King, C.J. (1988). "Sticking and Agglomeration of Hygroscopic, Amorphous Carbohydrate and Food Powders," *Biotech. Prog.* **4**(1), 31.
- Walton, A.G. (1969). "Nucleation in Liquids and Solutions," in *Nucleation* (Zettlemoyer, A.C., ed.), pp. 225–308, Marcel Dekker, New York.

Index

α -factor, 94–96

Absolute pressure control, 136

Additives

- description, 255–256
- tailor-made, 89–93

Adiabatic evaporative crystallization, 216–218

Adsorbents

- macromolecular, 143
- polymeric, 143

Adsorption, 82–86, 143

Advanced continuous control, 221–228

AFM (atomic force microscopy), 72, 280

Agglomeration, 110–111

Aggregation, 149–150

Agitated suspension crystallizers, 184–187

Agitation, 295–296

Agitators, 188–189

Air-cooled crystallizers, 133

Amino acid structures, 268–269

Amperage recorders, 137

Analytical solution of groups. *See* ASOG (analytical solution of groups)

Anemometry, laser Doppler (LDA), 192

Antisolvent crystallization (salting-out), 246

Antisolvents, 246, 251–252, 276–277

ASOG (analytical solution of groups), 14

Atomic force microscopy. *See* AFM (atomic force microscopy)

Automatic vs. manual control modes, 206

Back missing column process. *See* BMS (back missing column) process

Balance, population density. *See* Population density balance

BASF-process, 168–169

Batch crystallization, 243–244

analysis

conservation equations, 234–236

CSD (crystal size distribution) analysis

CSD control, 241–242

CSD maximums, characterization, 238

cumulative CSD method, 237–238

description, 231–232, 236. *See also*

CSD (crystal size distribution)

desupersaturation curve technique, 237

narrow CSD preparation, 241–242

thermal response technique, 236–237

description, 234

batch/semi-batch precipitators, 158

crystallizer types

description, 127–128, 133, 231.

See also Crystallizers

industrial, 233–234

laboratory, 231–233

description, 215, 231, 246–247

impact factors

batch cycle time, 238–239

CCG (constant crystal growth) model,

242–243

description, 238

external seeding, 239–241

finer destruction, 241

fouling control, 241

GRD (growth rate dispersion), 242–243

mixing, 243–244. *See also* Mixing

supersaturation profiles, 239

nomenclature, 247

operations

antisolvent crystallization (salting-out), 246

cooling crystallization, 244–245

description, 244

evaporative crystallization, 216–218, 246

seeded cooling crystallization, 244–245

unseeded cooling crystallization, 245

processes control

batch adiabatic evaporative

crystallization, 216–218

description, 215

heat transfer, indirect, 216–217

heat transfer, injection, 216

nonsolvent dilution, 218–219

temperature control, recirculating, 216

temperature control, once-through, 216

temperature control, unbalanced, 215

reference literature, 248

Batch growth, 283

Batch vs. continuous operation, 124

BCF (Burton-Cabera-Frank) model, 55–56, 147

Biochemical purity

co-crystallization, solutes and polymorphs, 260

crystal forms, 260–261

description, 258

solvent occlusion, 258–259

Bioprocessing crystallization.

See Pharmaceutical and

bioprocessing crystallization

BMS (back missing column) process, 176–177

Bonding, 35–38

Bravais lattices, 34–35

Brennan-Koppers crystal purifier, 171

Brodie purifier, 176

Bubble column crystallizer, 170

Burton-Cabera-Frank model. *See* BCF

(Burton-Cabera-Frank) model

Cabera-Vermilyea model, 81–82

Calorimeter, DSC (differential scanning

calorimeter), 78

Capacity vs. cost, 139

Cascade control, 207–208

CC (constant composition) method, 152–153

CCG (constant crystal growth) model,

242–243

CFD (computational fluid dynamic) flow

model, 191–197

Chemistry, protein

amino acid structures, 268–269

chemical modifications, 270–271

crystallization. *See* Protein crystallization

disulfide bonds as crosslinkers, 270

effectors, 270–271

glycosylation, 270–271

ionizable sidechains, 270

lipidation, 270–271

net charge, 270

peptide bonds, 269

phosphorylation, 270–271

protein concentration, 271–272

purity and homogeneity, 272–274

structure levels, 269–270

Chevron (Maruzen) process, 171

Closure model, 195

Cluster radius vs. free energy, 18

CMSMPR (continuous mixed-suspension, mixed-product removal) model, 154–155, 158–159

Co-crystallization, 260

Colloid stability, 143

Column processes, 175–177

Composition vs. processing conditions, 288

Comprehensive mixing models, 197

Computational fluid dynamic flow model.

See CFD (computational fluid dynamic) flow model

Computational mixing models, 194–195

Concentrated solutions, 5–11

Concentration units

basic concepts, 1

conversion, 2

hydrates, 2

phase diagrams, 2

type 1 (mass-mole solute/mass solvent), 1

type 2 (mass-mole solute/mass solution), 1

type 3 (mass-mole solute/volume solution), 1

Conservation equations, 234–236

Constant composition method. *See* CC

(constant composition) method

Constant crystal growth model. *See* CCG

(constant crystal growth) model

Continuous mixed-suspension, mixed-product

removal model. *See* CMSMPR

(continuous mixed-suspension,

mixed-product removal) model

Continuous plants, melt crystallization

advantages, 175

BMS (back missing column) process,

176–177

Brodie purifier, 176

column processes, 175–177

drum coolers, 175–176

four C process, 176

problems, 177

process concepts, 175–177

Sandvik-type conveyors, 177

scraped coolers, 175–176

Tsukishima Kikai (TSK) countercurrent

cooling process, 176

Continuous precipitation, 158

Continuous stirred tank removal model.

See CSTR (continuous stirred tank

removal) model

Continuous tubular precipitator, 155

Continuous vs. batch operation, 124

Controlled growth

via combined mechanisms, 147

via mass transport, 146

via surface integration, 146–147

Conversion

concentration units, 2

factors, 21

Conveyors, Sandvik-type, 177

Coolers and cooling

cooling crystallization, 244–245

cooling rates, 293–294

drum, 175–176

scraped, 175–176

Tsukishima Kikai (TSK) countercurrent

cooling process, 176

- Costs
 crystallizers, 138–139
 vs. capacity, 139
- Coulter counter, 203
- Creation methods, 18–20
- Critical growth rates, 147–148, 153
- Crosslinkers, 270
- Crystalline structure interface
 AFM (atomic force microscopy), 72
 description, 71–72
 kink sites, 71
 steps, 71
 terraces, 71
- Crystallization
 batch. *See* Batch crystallization
 crystallizers. *See* Crystallizers
 food. *See* Food crystallization
 melt. *See* Melt crystallization
 mixing. *See* Mixing
 pharmaceutical and bioprocessing. *See*
 Pharmaceutical and bioprocessing
 crystallization
 processes control. *See* Processes control
 protein. *See* Protein crystallization
- Crystallizers
 characteristics, 133
 costs, 138–139
 CSD (crystal size distribution), 118–119.
See also CSD (crystal size distribution)
 definition, 123
 description, 115, 184
 design
 agitators, 188–189
 capacity vs. cost, 139
 crystal weight distribution, 119–120
 cyclic behavior, 122–123
 definition, 115
 description, 115, 184
 feed strategies, 188
 fines removal, 120–122
 fractional crystallization, 116–117
 heat, 115–116. *See also* Heat
 melt, 188
 multiple axial flow impellers, 185
 population density balance, 118
 procedures, 133–136
 processes control, 201–202. *See also*
 Processes control
 yeilds, 116
 flow, 181–182
 instrumentation and control
 absolute pressure control, 136
 amperage recorders, 137
 description, 136–138
 discharge control, 137
 discharge lines, 137
 distributed control systems, 137
 feed-flow recording controllers, 137
 liquid level control, 136
 magma (slurry) density recorder
 controller, 136–137
 sampling systems, 137–138
 steam flow recorder controller, 137
 temperature recorders, 137
 mixing. *See* Mixing
 nomenclature, 139
 nucleation, 52–53, 117–118, 120.
See also Nucleation
 reference literature, 140
 selection
 batch vs. continuous operation, 124
 description, 115, 123
 evaluation data, 123
 scale of operation, 124
 solubility issues, 123–124
 temperature vs. solubility, 124
 types
 agitated suspension, 184–187
 air-cooled, 133
 batch type, 127–128, 133
 characteristics, 133
 description, 231
 direct contact refrigeration, 131, 133
 DTB (draft tube baffle), 129–130, 133,
 183–184, 196–197, 210–211. *See also*
 DTB (draft tube baffle) crystallizers
 FC (forced-circulation), 129, 133, 187,
 213–215
 flow sheet spray evaporator, 133
 fluidized bed, 187–188
 fluidized suspension, 128–129, 133
 growth type, 211–213
 industrial, 233–234
 laboratory, 231–233
 mechanical vapor recompression, 126
 multistage, 124–126, 213–215
 pulsed, 170
 reactive, 126–127
 spray crystallization, 132–133
 surface-cooled, 130–131, 133
 Swenson, 125–133. *See also*
 Swenson crystallizers
 teflon tube, 131–133
- Crystals
 definition, 33
 description, 33
 forms, 260–261
 growth. *See* Growth
 habit, 41–42
 imperfections, 40–41
 isomorphism, 40
 lattices. *See* Lattices
 nomenclature, 63
 polymorphism, 38–40
 reference literature, 63–65
 shape determination, 67–70
 size distribution (CSD). *See* CSD
 (crystal size distribution)
 structure and bonding, 35–38
 weight distribution, 119–120
- CSD (crystal size distribution)
 analysis
 CSD control, 241–242
 CSD maximums, characterization, 238
 cumulative CSD method, 237–238
 description, 231–232, 236
 desupersaturation curve technique, 237
 narrow CSD preparation, 241–242
 thermal response technique, 236–237
 description, 118–119
 models
 CMSMPR (continuous mixed-
 suspension, mixed-product removal),
 154–155, 158–159
 continuous tubular precipitator, 155
 growth ramp equation, 156–157
 mixing-precipitation models, 156
 MSMR (mixed-suspension, mixed-
 product removal), 154–159
 semi-batch precipitator, 155–156
 size control, 156–157
 processes control, 201–204
 CSTR (continuous stirred tank removal)
 model, 194
- Cumulative CSD (crystal size distribution)
 method, 237–238
- Cycle time, batch, 238–239
- Cyclic behavior, 122–123
- Defect sites, 76–77
- Density
 description, 20
 vs. size, 102
- Derjagun, Landau, Verwey, Overbeek.
See DLVO (Derjagun, Landau,
 Verwey, Overbeek) theory
- Design, crystallizers. *See* Crystallizers, design
- Desupersaturation curve technique, 237
- Dialysis, 282–283
- Dielectric sedimentation method, 154
- Differential Scanning Calorimeter. *See* DSC
 (Differential Scanning Calorimeter)
- Diffusion
 diffusion layer model, 56–57
 free interface, 282
 surface, 70–71
 vapor, 281–282
- Diffusivity, 22–25
- Dilute solutions (sparingly soluble species), 4–5
- Dipole moments, permanent, 13
- Direct contact refrigeration crystallizers,
 131, 133
- Direct numerical simulation model. *See* DNS
 (direct numerical simulation) model
- Disc centrifuge photosedimentometer, 154
- Discharge control, 137
- Dispersion, 108
- Distributed control systems, 137
- Distribution variables, mixing
 description, 182–184
 feed point location, 182
 particle concentration, 183–184
 product withdrawal location, 182
 turbulent kinetic energy, 182
 vessel flow field, 182
- Disulfide bonds as crosslinkers, 270
- DLVO (Derjagun, Landau, Verwey,
 Overbeek) theory, 143
- DNS (direct numerical simulation) model, 195
- Doppler anemometry, laser (LDA), 192
- Double-jet semi-batch precipitation,
 mixing-precipitation model, 151–152
- Draft tube baffle crystallizers. *See* DTB
 (draft tube baffle) crystallizers
- Drum coolers, 175–176
- Drying, 296
- DSC (differential scanning calorimeter), 78
- DTB (draft tube baffle) crystallizers, 129–130,
 133, 183–184, 196–197, 210–211
- EDAX (energy dispersive X-ray analysis), 80
- EDD (engulfment-deformation-diffusion)
 model, 150
- Effectors, 270–271
- Elastic light scattering, 154
- Electrical sensing zone method, 154
- Electrolytes
 mixtures, 8–11
 pure component strong, 8–11
 solubility effects, 275–276
- Energy dispersive X-ray analysis. *See* EDAX
 (energy dispersive X-ray analysis)
- Engulfment-deformation-diffusion model.
See EDD (engulfment-deformation-
 diffusion) model
- Enthalpy, 116

- Equilibrium, 68
- Equilibrium separation, 72–74
- Ethanol fractionation, plasma proteins, 264–265
- Evaporative crystallization, 216–218, 246
- EXAFS (extended X-ray fine structure), 79
- Experimental mixing models, 191–194
- Experimental precipitation techniques
 - CC (constant composition) method, 152–153
 - critical growth rate measurements, 153
 - description, 152
 - disc centrifuge photosedimentometer, 154
 - electrical sensing zone method, 154
 - instantaneous mixing devices, 153
 - light scattering (static or elastic), 154
 - Mie theory, 154
 - precipitate sizing, 153–154
 - sedimentation field flow fractionator, 154
- Extended X-ray fine structure. *See* EXAFS (extended X-ray fine structure)
- External seeding, 239–241
- FC (forced-circulation) crystallizers, 129, 133, 187, 213–215
- Feed
 - feed-flow recording controllers, 137
 - point location, 182
 - strategies, 188
- Feedback controllers
 - advanced control, 222–223, 228
 - automatic vs. manual control modes, 206
 - cascade control, 207–208
 - description, 204–205
 - feedforward vs. feedback control, 208–209
 - multivariable systems, 209
 - PID (three mode) controllers, 204–207
 - stability considerations, 205
 - time-delay compensation, 208
- Feedforward vs. feedback control, 208–209
- Field flow fractionator, 154
- Fines
 - destruction, 241
 - removal, 120–122
- Flow
 - description, 181–182
 - flow sheet spray evaporator, 133
 - sensors, 220–221
 - vessel flow field, 182
- Fluidized bed crystallizers, 187–188
- Fluidized suspension crystallizers, 128–129, 133
- Food crystallization
 - controlling
 - composition vs. processing conditions, 288
 - description, 287–290
 - desired crystalline structure, producing, 290–295
 - fractionation, 292–293
 - prevention of crystallization, 293
 - product quality, preservation, 290–292
 - separation, production, 292–293
 - description, 287, 303
 - impact factors
 - agitation, 295–296
 - cooling rates, 293–294
 - crystallization temperatures, 294–296
 - description, 293
 - drying, 296
 - Gibbs-Thomson equation, 298–299
 - heat and mass transfer rates, 293–296
 - melt-refreeze, 302–303
 - moisture fluctuations, 303
 - Ostwald ripening, 298–301
 - post-processing effects, 297–303
 - product formulation, 296–297
 - recrystallization, 298–301
 - ripening, 298–303
 - nucleation, 291. *See also* Nucleation
 - reference literature, 304
 - TAG (triacylglycerols), crystallizing, 288
- Fouling control, 241
- Four C process, 176
- Fractional crystallization, 116–117
- Fractionation, 292–293
- Free energy
 - barriers, 71
 - free Gibbs energy change, 143–144
 - vs. cluster radius, 18
- Free interface diffusion, 282
- Fusion enthalpy, 27
- Generalized population balance, 107.
 - See also* Population density balance
- Gibbs energy change, free, 143–144
- Gibbs-Thomson effect and equation, 141–142, 148–149, 298–299
- Glycosolation, 270–271
- GRD (growth rate dispersion), 108, 242–243
- Group contribution methods, 14
- Growth
 - description, 53–54
 - effects
 - description, 93
 - HMT (hexamethylene tetramine), 95–96
 - Jackson α -factor, 94–96
 - solvent roles, 93–94
 - growth ramp equation, 156–157
 - growth type crystallizers, 211–213.
 - See also* Crystallizers
 - kinetics
 - BCF (Burton-Cabera-Frank) model, 55–56, 147
 - controlled growth via combine mechanisms, 147
 - controlled growth via mass transport, 146
 - controlled growth via surface integration, 146–147
 - critical growth rates, 147–148
 - description, 57–58, 146
 - estimation, 60–61
 - Gibbs-Thomson effect, 148
 - measurement, 58–60
 - particle crowding effect, 148
 - Reynolds number, 146
 - screw dislocation mechanisms, 147
 - Sherwood number, 146
 - two-dimensional nucleation methods, 146–147
 - mechanisms, 280
 - nomenclature, 63
 - Ostwald ripening, 61–62.
 - See also* Ostwald ripening
 - rate effects
 - Cabera-Vermilyea model, 81–82
 - impurity adsorption isotherms, 82–86
 - limiting, 83–84
 - movement step effects, 80–82
 - non-zero growth rate behavior, 83–84
 - zero-growth rate behavior, 84–85
 - rates
 - critical, 147–148, 153
 - determination, 280
 - dispersion, 62, 108, 242–243
 - distribution, 108–110
 - reference literature, 63–65
- size dependency, 62
- theories
 - BCF (Burton-Cabera-Frank) model, 55–56, 147
 - description, 54
 - diffusion layer model, 56–57
 - two-dimensional, 54–55
- Heat
 - balance, 116
 - capacity, 26–27
 - crystallization, 28–30
 - effects, 115–116
 - enthalpy, 116
 - latent, 27–28
 - mixing, 28–30
 - solution, 28–30
 - transfer
 - indirect, 216–217
 - injection, 216
 - transfer rates, 293–296
- Heterogenous nucleation, 46–50, 144
- Hexamethylene tetramine. *See* HMT (hexamethylene tetramine)
- HMT (hexamethylene tetramine), 95–96
- Homogeneity, 272–274
- Homogeneous nucleation, 45–46, 143–144
- Hydrates, 2–3
- Ibuprofen, 263–264
- IC (interpenetrating continua) model, 195–197
- ICI-process, 168–169
- Ideal solubility, 11–13
- Impellers, 185, 195
- Imperfections, 40–41
- Impinging jet mixers, 264
- Impurities and solvents
 - biochemical, 259–260
 - chemical aspects, 86–90
 - crystal shape determination, roles
 - description, 67–68
 - equilibrium, 68
 - interplant spacings, 69
 - PBCs (periodic bond chains), 69–70
 - solid states, 68–70
 - crystalline structure interface
 - AFM (atomic force microscopy), 72
 - description, 71–72
 - kink sites, 71
 - steps, 71
 - terraces, 71
 - description, 67, 96–97
 - free energy barriers, 71
 - growth effects
 - description, 93
 - HMT (hexamethylene tetramine), 95–96
 - Jackson α -factor, 94–96
 - solvent roles, 93–94
 - growth rate effects
 - Cabera-Vermilyea model, 81–82
 - impurity adsorption isotherms, 82–86
 - limiting, 83–85
 - movement step effects, 80–82
 - non-zero growth rate behavior, 83–84
 - zero-growth rate behavior, 84–85
 - impurity incorporation factors
 - crystal lattice point defects, 72
 - crystallization rates, 75–76
 - defect sites, 76–77
 - equilibrium separation, 72–74
 - inclusion formation, 77–78
 - nonequilibrium separation, 74–78

- Impurities and solvents (*continued*)
 impurity retention mechanisms
 description, 78
 DSC (differential scanning calorimeter), 78
 EDAX (energy dispersive X-ray analysis), 80
 EXAFS (extended X-ray fine structure), 79
 optical microscopy, 78–79
 selective crystal dissolution, 78–79
 SEM (scanning electron microscopy), 79
 size vs. impurity relationship, 79
 STM (scanning tunneling microscopy), 80
 surface analysis, 79
 TGA (thermogravimetric analysis), 78
 particle size control, 255–256
 reference literature, 97–100
 solute, 259–260
 solvent occlusion, 258–259
 surface diffusion, influences, 70–71
 tailor-made additives, 89–93
- Impurity adsorption isotherms, 82–86
- Inclusion formation, 77–78
- Incrustation, 219
- Indirect heat transfer, 216–217
- Induction period, 145
- Industrial controllers
 advanced continuous control, 221–228
 batch crystallization control, 215–219.
 See also Batch crystallization
 continuous control, 221–228, 210–215
 DTB (draft tube baffle) crystallizers,
 210–211. *See also* DTB (draft tube
 baffle) crystallizers
 FC (forced-circulation) crystallizers,
 213–215
 growth type crystallizers, 211–213
 multistage crystallizers, 213–215
 objectives, 209–210
 sensors, 219–221. *See also* Sensors
- Industrial crystallizers, 233–234
- Inhomogeneity, 183
- Injection heat transfer, 216
- Inorganics, solubility
 basic concepts, 1–4
 concentrated solutions, 5–11
 definition, 1
 dilute solutions (sparingly soluble species),
 4–5
 electrolytes
 mixtures, 8–11
 pure component strong, 8–11
 hydrate calculations, 3
 salt effect, 5
 solubility products, 5
 solution thermodynamics, 7–8
- Instantaneous mixing devices, 153
- Instrumentation and control
 absolute pressure control, 136
 amperage recorders, 137
 description, 136
 discharge control, 137
 discharge lines, 137
 distributed control systems, 137
 feed-flow recording controllers, 137
 liquid level control, 136
 magma (slurry) density recorder controller,
 136–137
 sampling systems, 137–138
 steam flow recorder controller, 137
 temperature recorders, 137
- Interpenetrating continua model. *See* IC
 (interpenetrating continua) model
- Interplant spacings, 69
- Ionizable sidechains, 270
- Isomorphism, 40
- Jackson α -factor, 94–96
- Jet mixers, impinging, 264
- Kinetics
 crystal growth
 BCF (Burton-Cabera-Frank) model,
 55–56, 147
 controlled growth via combine
 mechanisms, 147
 controlled growth via mass transport, 146
 controlled growth via surface integration,
 146–147
 critical growth rates, 147–148
 description, 146
 Gibbs-Thomson effect, 148
 particle crowding effect, 148
 particle size control, 254–255
 Reynolds number, 146
 screw dislocation mechanisms, 147
 Sherwood number, 146
 two-dimensional nucleation methods,
 146–147
 melt crystallization
 description, 163–164
 purity incorporation mechanisms, 166
 temperature profiles, 165
 theoretical approaches, 164–166
 nucleation
 definition, 143
 description, 43–45, 50–52, 143
 free Gibbs energy change, 143–144
 heterogeneous nucleation, 46–50, 144
 homogeneous nucleation, 45–46, 143–144
 induction period, 145
 industrial crystallizer applications, 52–53
 investigations, 144–146
 onset of nucleation, 144–145
 primary nucleation, 143–144
 secondary nucleation, 47–50, 145–146
 stable nuclei, 145
 supersaturation, 143–146
 two-dimensional nucleation methods,
 146–147
 turbulent energy, 182
- Kink sites, 71
- Kureha double screw purifier, 171–172
- Laboratory crystallizers, 196–197, 231–233
- LaGrangian particle tracking, 196–197
- Large eddy simulation. *See* LES
 (large eddy simulation)
- Laser diffraction methods, 154
- Laser Doppler anemometry. *See* LDA
 (laser Doppler anemometry)
- Latent heat, 27–28
- Lattices
 Bravais lattices, 34–35
 description, 33–35
 imperfections, 4–41
 isomorphism, 40
 lattice planes, 35
 Miller indices, 35
 point defects, 72
 polymorphism, 38–40
 structure and bonding, 35–38
 symmetry elements, 35
- LDA (laser Doppler anemometry), 192
- LES (large eddy simulation), 195
- Level sensors, 220–221
- Light scattering
 elastic, 154
 static, 154
- Limiting, 83–84
- Lipidation, 270–271
- Liquid level control, 136
- Lysosomes, 278–279
- Macromixing, 150–151, 183–184
- Macromolecular adsorbents, 143
- Magma (slurry) density recorder controller,
 136–137
- Manual vs. automatic control modes, 206
- Maruzen (Chevron) process, 171
- Mass
 balance, 106–107
 mass-mole solute/mass solution
 concentration units, 1
 mass-mole solute/mass solvent
 concentration units, 1
 mass-mole solute/volume solution
 concentration units, 1
 transfer rates, 293–296
 transport controlled growth, 146
- Mechanical vapor recompression, 126
- Melt crystallization
 benefits, 161–162
 continuous plants
 advantages, 175
 BMS (back missing column) process,
 176–177
 Brodie purifier, 176
 column processes, 175–177
 drum coolers, 175–176
 four C process, 176
 problems, 177
 process concepts, 175–177
 Sandvik-type conveyors, 177
 scraped coolers, 175–176
 Tsukishima Kikai (TSK) countercurrent
 cooling process, 176
 definition, 161
 description, 161
 existing plants, concepts, 167
 kinetics
 description, 163–164
 purity incorporation mechanisms, 166
 temperature profiles, 165
 theoretical approaches, 164–166
 melting points, distributions, 162
 phase diagrams
 data types, 161–162
 description, 161
 methods, 161–162
 reference literature, 177–179
 solid layer crystallization
 benefits, 166–167
 description, 166
 flow diagrams, 166
 limitations, 166
 solid layer processes
 BASF-process, 168–169
 bubble column crystallizer, 170
 description, 167–171
 ICI-process, 168–169
 Proabd process, 168
 pulsed crystallizers, 170
 Sulzer falling film process,
 168–169
 tube bundle crystallization, 168
 structure, 168

- suspension crystallization
 - advantages, 167
 - limitations, 167
 - suspension processes
 - Brennan-Koppers crystal purifier, 171
 - description, 171–173
 - Kureha double screw purifier, 171–172
 - Maruzen (Chevron) process, 171
 - Newton-Chambers process, 171
 - TNO-Thijssen crystallization process, 171
 - sweating, 173–174
 - washing and rinsing, 174–175
 - Melt-refreeze, 302–303
 - Melting points, 27, 162
 - Mesomixing, 150–151
 - Metastability
 - description, 16
 - free energy vs. cluster radius, 18
 - limits, 17–18
 - stability states, 17
 - zone widths, 17–18
 - Methyldopa, 262–263
 - Micromixing, 150–152, 183–184, 197
 - Microscopy
 - optical, 78–79
 - SEM (scanning electron microscopy), 79
 - STM (scanning tunneling microscopy), 80
 - Mie theory, 154
 - Miller indices, 35
 - Mixed solvent solubility, 14–15
 - Mixed-suspension, mixed-product removal model. *See* MSMPR (mixed-suspension, mixed-product removal) model
 - Mixing
 - batch crystallization, 243–244
 - crystallizers
 - design, 184–189. *See also* Crystallizers, design
 - DTB (draft tube baffle), 183–184, 196–197. *See also* DTB (draft tube baffle) crystallizers
 - flows, 181–182
 - description, 150, 181
 - distribution variables
 - description, 182–184
 - feed point location, 182
 - particle concentration, 183–184
 - product withdrawal location, 182
 - turbulent kinetic energy, 182
 - vessel flow field, 182
 - impinging jet mixers, 264
 - inhomogeneity, 183
 - instantaneous devices, 153
 - macromixing, 150–151, 183–184
 - mesomixing, 150–151
 - micromixing, 150–152, 183–184, 197
 - models
 - CFD (computational fluid dynamic) flow, 191–197
 - closure, 195
 - comprehensive, 197
 - computational, 194–195
 - CSTR (continuous stirred tank removal), 194
 - description, 191, 197
 - DNS (direct numerical simulation), 195
 - EDD (engulfment-deformation-diffusion), 150
 - experimental, 191–194
 - IC (interpenetrating continua), 195–197
 - LaGrangian particle tracking, 196–197
 - LDA (laser Doppler anemometry), 192
 - LES (large eddy simulation), 195
 - mixing-precipitation model for double-jet semi-batch precipitation, 151–152
 - MSMPR (mixed-suspension, mixed-product removal), 104–113, 154–159, 194
 - multiphase flow, 195–197
 - PSD (particle size distribution), 192–198
 - RANS (Reynolds averaged Navier Stokes), 195–196
 - turbulence, 195
 - population density balance
 - constant growth, 108
 - random fluctuation model, 108
 - power law model parameters, 22
 - processes control, 221–222, 224–228
- Moisture fluctuations, 303
- impeller treatment, 195
- LaGrangian particle tracking, 196–197
- LDA (laser Doppler anemometry), 192
- LES (large eddy simulation), 195
- mixing-precipitation model for double-jet semi-batch precipitation, 151–152
- MSMPR (mixed-suspension, mixed-product removal), 154–159, 194
- multiphase flow, 195–197
- PSD (particle size distribution), 192–198
- RANS (Reynolds averaged Navier Stokes), 195–196
- turbulence, 195
- Navier-Stokes equations, 182–184
- rapid mixing and precipitation, 264
- reference literature, 198–199
- scale-up, 189–191
- supersaturation, 183–184
- vortex stretching, 150
- Models
 - BCF (Burton-Cabera-Frank), 55–56, 147
 - Cabera-Vermilyea model, 81–82
 - CCG (constant crystal growth), 242–243
 - CFD (computational fluid dynamic) flow model, 191–197
 - CSD (crystal size distribution)
 - CMSMPR (continuous mixed-suspension, mixed-product removal), 154–155, 158–159
 - continuous tubular precipitator, 155
 - mixing-precipitation models, 156
 - MSMPR (mixed-suspension, mixed-product removal), 154–159
 - semi-batch precipitator, 155–156
 - size control, 156–157
 - diffusion layer model, 56–57
 - mixing
 - CFD (computational fluid dynamic) flow, 191–197
 - closure, 195
 - comprehensive, 197
 - computational, 194–195
 - CSTR (continuous stirred tank removal), 194
 - description, 191
 - DNS (direct numerical simulation), 195
 - EDD (engulfment-deformation-diffusion), 150
 - experimental, 191–194
 - IC (interpenetrating continua), 195–197
 - LaGrangian particle tracking, 196–197
 - LDA (laser Doppler anemometry), 192
 - LES (large eddy simulation), 195
 - mixing-precipitation model for double-jet semi-batch precipitation, 151–152
 - MSMPR (mixed-suspension, mixed-product removal), 104–113, 154–159, 194
 - multiphase flow, 195–197
 - PSD (particle size distribution), 192–198
 - RANS (Reynolds averaged Navier Stokes), 195–196
 - turbulence, 195
 - population density balance
 - constant growth, 108
 - random fluctuation model, 108
 - power law model parameters, 22
 - processes control, 221–222, 224–228
- Mole
 - mass-mole solute/mass solution concentration units, 1
 - mass-mole solute/mass solvent concentration units, 1
 - mass-mole solute/volume solution concentration units, 1
- Molecular structures, 250
- Movement step effects, 80–82
- MSMPR (mixed-suspension, mixed-product removal) model, 104–113, 154–159, 194
- Multiphase flow model, 195–197
- Multiple axial flow impellers, 185
- Multistage crystallizers, 124–126, 213–215
- Multivariable systems, 209
- Narrow CSD (crystal size distribution) preparation, 241–242
- Navier-Stokes equations, 182–184
- Net charge, 270
- Newton-Chambers process, 171
- Nomenclature
 - batch crystallization, 247
 - crystallizers, 139
 - crystals, 63
 - growth, 63
 - nucleation, 63
 - pharmaceutical and bioprocessing crystallization, 265–266
 - population density balance, 113
 - precipitation processes, 159
 - processes control, 228
 - protein crystallization, 283–284
 - solutions and solution properties, 29–30
- Nonequilibrium separation, 74–78
- Nonsolvent dilution, 218–219
- Non-zero growth rate behavior, 83–84
- Nucleation
 - description, 43–45
 - effective rates, 108
 - food crystallization, 291
 - kinetics
 - definition, 143
 - description, 50–52, 143
 - free Gibbs energy change, 143–144
 - heterogeneous nucleation, 46–50, 144
 - homogeneous nucleation, 45–46, 143–144
 - induction period, 145
 - investigations, 144–146
 - onset of nucleation, 144–145
 - primary nucleation, 143–144
 - secondary nucleation, 47–50, 145–146
 - stable nuclei, 145
 - supersaturation, 143–146
 - two-dimensional nucleation methods, 146–147
 - nomenclature, 63
 - pharmaceutical and bioprocessing crystallization, 256–258
 - protein crystallization, 280
 - reference literature, 63–65
- Nuclei, stable, 145
- Once-through balanced temperature control, 216
- Onset of nucleation, 144–145
- Open-loop control, 224–228
- Optical isomers separation, 261–264
- Optical microscopy, 78–79

- Organics, solubility
 ASOG (analytical solution of groups), 14
 description, 11
 group contribution methods, 14
 ideal solubility, 11–13
 measurements, 15–16
 melting temperatures, 27
 mixed solvent solubility, 14–15
 permanent dipole moments, 13
 pure component phase diagrams, schematics, 12
 regular solution theory, 13–14
 Scatchard-Hildebrand theory, 14
 solubility parameters, 14
 thermodynamic concepts, 11–13
 UNIFAC (UNIQUAC function group activity), 14
 Ostwald ripening, 61–62, 141–142, 148–149, 298–301
- Particles
 concentration, 183–184
 crowding effect, 148
 LaGrangian tracking, 196–197
 size control
 additive effects, 255–256
 crystal growth kinetics, 254–255
 description, 253–254
 impurity effects, 255–256
 solvent effects, 255–256
 size distribution. *See* PSD (particle size distribution)
 PBCs (periodic bond chains), 69–70
 Peptide bonds, 269
 Periodic Bond Chains. *See* PBCs (Periodic Bond Chains)
 Permanent dipole moments, 13
 pH effects, 250–251, 274–275
 Pharmaceutical and bioprocessing
 crystallization
 applications
 description, 261
 ethanol fractionation, plasma proteins, 264–265
 ibuprofen, 263–264
 impinging jet mixers, 264
 methyl dopa, 262–263
 optical isomers separation, 261–264
 phase diagrams, 262
 rapid mixing and precipitation, 264
 biochemical purity
 co-crystallization, solutes, and polymorphs, 260
 crystal forms, 260–261
 description, 258
 solute impurities, 259–260
 solvent occlusion, 258–259
 description, 249
 nomenclature, 265–266
 nucleation, 256–258
 particle size control
 additive effects, 255–256
 crystal growth kinetics, 254–255
 description, 253–254
 impurity effects, 255–256
 solvent effects, 255–256
 reference literature, 266
 roles, 249
 seeding, 256–258
 solubility and supersaturation
 antisolvent effects, 251–252
 description, 249–250
 molecular structures, 250
 pH effects, 250–251
 salts effects, 252–253
 temperature effects, 250
 Phase diagrams, 2, 12, 161–162, 262, 278–279
 Phosphorylation, 270–271
 Photon correlation spectroscopy, 154
 Photosedimentometer, 154
 Physical and thermodynamic properties
 adsorbents, macromolecular, 143
 adsorbents, polymeric, 143
 colloid stability, 143
 DLVO (Derjagun, Landau, Verwey, Overbeek) theory, 143
 Gibbs-Thomson equation, 141–142, 148–149
 precipitation diagrams, 142–143
 solubility, 141–142
 supersaturation, 141–142
 surface chemistry, 143
 surface energy, 141–142
 Physicochemical measurements
 growth rate determination, 280
 solubility determination, 280
 PID (three mode) controllers, 204–207
 Plasma proteins, ethanol fractionation, 264–265
 Polymeric adsorbents, 143
 Polymorphism, 38–40
 Polymorphs, 260
 Population density balance
 agglomeration, 110–111
 constant growth model, 108
 density vs. size, 102
 description, 101–102, 118
 effective nucleation rates, 108
 experimental data, 108–110
 generalized population balance, 107
 growth rate
 dispersion, 108
 distribution, 108–110
 mass balance, 106–107
 MSMPR (mixed suspension, mixed product removal) model, 104–113
 nomenclature, 113
 particle size and distribution, 101–102
 random fluctuation model, 108
 reference literature, 113
 semilogarithmic population density, 112
 size-dependent crystal growth, 107–108
 size distribution measurement, 102–104
 Post-processing (food), 297–303
 Power law model parameters, 22
 Precipitate sizing, 153–154
 Precipitation processes
 aggregation, 149–150
 CSD (crystal size distribution) modeling
 CMSMPR (continuous mixed-suspension, mixed-product removal), 154–155, 158–159
 continuous tubular precipitator, 155
 growth ramp equation, 156–157
 mixing-precipitation models, 156
 MSMPR (mixed-suspension, mixed-product removal), 154–159
 semi-batch precipitator, 155–156
 size control, 156–157
 definition, 141
 description, 141, 158–159
 dielectric sedimentation method, 154
 experimental techniques
 CC (constant composition) method, 152–153
 critical growth rate measurements, 153
 description, 152
 disc centrifuge photosedimentometer, 154
 electrical sensing zone method, 154
 instantaneous mixing devices, 153
 light scattering (static or elastic), 154
 Mie theory, 154
 precipitate sizing, 153–154
 sedimentation field flow fractionator, 154
 kinetics, crystal growth
 BCF (Burton-Cabera-Frank) model, 55–56, 147
 controlled growth via combined mechanisms, 147
 controlled growth via mass transport, 146
 controlled growth via surface integration, 146–147
 critical growth rates, 147–148
 description, 146
 Gibbs-Thomson effect, 148
 particle crowding effect, 148
 Reynolds number, 146
 screw dislocation mechanisms, 147
 Sherwood number, 146
 two-dimensional nucleation methods, 146–147
 kinetics, nucleation
 definition, 143
 description, 143
 free Gibbs energy change, 143–144
 heterogeneous nucleation, 144
 homogeneous nucleation, 143–144
 induction period, 145
 investigations, 144–146
 onset of nucleation, 144–145
 primary nucleation, 143–144
 secondary nucleation, 145–146
 stable nuclei, 145
 supersaturation, 143–146
 laser diffraction methods, 154
 mixing
 description, 150
 EDD (engulfment-deformation-diffusion) model, 150
 macromixing, 150–151
 mesomixing, 150–151
 micromixing, 150–152
 mixing-precipitation model for double-jet semi-batch precipitation, 151–152
 vortex stretching, 150
 nomenclature, 159
 Ostwald ripening, 141–142, 148–149
 photon correlation spectroscopy, 154
 physical and thermodynamic properties
 adsorbents, macromolecular, 143
 adsorbents, polymeric, 143
 colloid stability, 143
 DLVO (Derjagun, Landau, Verwey, Overbeek) theory, 143
 Gibbs-Thomson equation, 141–142, 148–149
 precipitation diagrams, 142–143
 solubility, 141–142
 supersaturation, 141–142
 surface chemistry, 143
 surface energy, 141–142

- practices
 - batch precipitation, 158
 - batch/semi-batch precipitators, 158
 - CMSMPR (continuous mixed-suspension, mixed-product removal) precipitators, 154–155, 158–159
 - continuous precipitation, 158
 - description, 157–158
 - tubular precipitators, 158
- quasi-elastic light scattering, 154
- rapid mixing, 264
- reference literature, 159–169
- ultrasonic spectrometry, 154
- Pressure effects, 277
- Primary nucleation, 143–144
- Proabd process, 168
- Processes control
 - control algorithm, 203–204
 - crystallizer design, 201–202. *See also* Crystallizers, design
 - CSD (crystal size distribution), 201–204. *See also* CSD (crystal size distribution)
 - description, 201–204
- feedback controllers
 - advanced control, 222–223, 228
 - automatic vs. manual control modes, 206
 - cascade control, 207–208
 - description, 204–205
 - feedforward vs. feedback control, 208–209
 - multivariable systems, 209
 - PID (three mode) controllers, 204–207
 - stability considerations, 205
 - time-delay compensation, 208
- industrial controllers
 - advanced continuous control, 221–228
 - batch crystallization control, 215–219. *See also* Batch crystallization
 - continuous control, 210–215, 221–228
 - DTB (draft tube baffle) crystallizers, 210–211. *See also* DTB (draft tube baffle) crystallizers
 - FC (forced-circulation) crystallizers, 213–215
 - growth type crystallizers, 211–213
 - multistage crystallizers, 213–215
 - objectives, 209–210
 - sensors, 219–221. *See also* Sensors
- measurements, 202–203
- models, 221–222, 224–228. *See also* Models
- nomenclature, 228
- open-loop control, 224–228
- reference literature, 229–230
- variables
 - dynamically controlled, 201
 - equipment design, 201–202
 - manipulated, 203
- Processing vs. composition conditions, 288
- Product withdrawal location, 182
- Properties, solution. *See* Solutions and solution properties
- Protein crystallization
 - AFM (atomic force microscopy), 280
 - description, 267–269, 283
 - growth mechanisms, 280
 - nomenclature, 283–284
 - nucleation, 280
 - physiochemical measurements
 - growth rate determination, 280
 - solubility determination, 280
- protein chemistry
 - amino acid structures, 268–269
 - chemical modifications, 270–271
 - disulfide bonds as crosslinkers, 270
 - effectors, 270–271
 - glycosylation, 270–271
 - ionizable sidechains, 270
 - lipidation, 270–271
 - net charge, 270
 - peptide bonds, 269
 - phosphorylation, 270–271
 - protein concentration, 271–272
 - purity and homogeneity, 272–274
 - structure levels, 269–270
- reference literature, 284–285
- screening tools
 - batch growth, 283
 - description, 281
 - dialysis, 282–283
 - free interface diffusion, 282
 - seeding techniques, 283
 - vapor diffusion experiments, 281–282
- solubility
 - antisolvent effects, 276–277
 - description, 274
 - electrolyte effects, 275–276
 - lysosomes, 278–279
 - pH effects, 274–275
 - phase diagrams, 278–279
 - pressure effects, 277
 - soluble synthetic polymer effects, 277
 - temperature effects, 277–278
- PSD (particle size distribution), 192–198
- Pulsed crystallizers, 170
- Pure components
 - phase diagrams, schematics, 12
 - strong electrolytes, 8–11
- Purifiers
 - Brennan-Koppers crystal, 171
 - Brodie, 176
 - Kureha Double Screw, 171–172
- Purity
 - biochemical. *See* Biochemical purity
 - vs. homogeneity, 166, 272–274
- Quasi-elastic light scattering, 154
- Random fluctuation model, 108
- RANS (Reynolds averaged Navier Stokes) model, 195–196
- Rapid mixing and precipitation, 264
- Reactive crystallizers, 126–127
- Recirculating temperature control, 216
- Recrystallization, 298–301
- Reference literature
 - batch crystallization, 248
 - crystallizers, 140
 - crystals, 63–65
 - food crystallization, 304
 - growth, 63–65
 - melt crystallization, 177–179
 - nucleation, 63–65
 - pharmaceutical and bioprocessing crystallization, 266
 - population density balance, 113
 - precipitation processes, 159–169
 - processes control, 229–230
 - protein crystallization, 284–285
 - solutions and solution properties, 30–31
 - solvents and impurities, 97–100
- Refreeze-melt, 302–303
- Regular solution theory, 13–14
- Reynolds averaged Navier Stokes model. *See* RANS (Reynolds averaged Navier Stokes) model
- Reynolds number, 146
- Ripening, 141–149, 298–303
- Salt effect, 5
- Salting-out (antisolvent crystallization), 246
- Salts, 252–253
- Sampling systems, 137–138
- Sandvik-type conveyors, 177
- Scale of operation, 124
- Scale-up, 189–191
- Scanning electron microscopy. *See* SEM (scanning electron microscopy)
- Scanning tunneling microscopy. *See* STM (scanning Tunneling microscopy)
- Scatchard-Hildebrand theory, 14
- Scraped coolers, 175–176
- Screening tools
 - batch growth, 283
 - description, 281
 - dialysis, 282–283
 - free interface diffusion, 282
 - seeding techniques, 283
 - vapor diffusion experiments, 281–282
- Screw dislocation mechanisms, 147
- Secondary nucleation, 47–50, 145–146
- Sedimentation
 - dielectric methods, 154
 - field flow fractionator, 154
- Seeding
 - description, 256–258
 - external, 239–241
 - seeded cooling crystallization, 244–245
 - techniques, 283
- Selective crystal dissolution, 78–79
- SEM (scanning electron microscopy), 79
- Semi-batch precipitation, 155–156, 158
- Semilogarithmic population density, 112
- Sensors
 - description, 219
 - final control and implementation
 - description, 220
 - flow, 220–221
 - level, 220–221
 - temperature, 220
 - incrustation, 219
 - selection and installation
 - finest volume, 220
 - flow, 220
 - level, 220
 - pressure, 220
 - size distribution, 220
 - slurry density, 220
 - temperature, 219–220
- Separation, 292–293
- Shape determination, 67–70
- Sherwood number, 146
- Sidechains, ionizable, 270
- Size
 - control, 156–157
 - distribution measurement, 102–104
 - distribution sensors, 220
 - particle size control, 255–256
 - size-dependent crystal growth, 107–108
 - vs. density, 102
- Slurry density
 - recorder controllers, 136–137
 - sensors, 220

- Solid layer crystallization
 - benefits, 166–167
 - description, 166
 - flow diagrams, 166
 - limitations, 166
 - processes
 - BASF-process, 168–169
 - bubble column crystallizer, 170
 - description, 167–171
 - ICI-process, 168–169
 - Proabd process, 168
 - pulsed crystallizer, 170
 - Sulzer falling film process, 168–169
 - tube bundle crystallization, 168
 - Solid states, 68–70
 - Solubility
 - antisolvent effects, 251–252, 276–277
 - description, 249–250, 274
 - electrolyte effects, 275–276
 - inorganics
 - basic concepts, 1–4
 - concentrated solutions, 5–11
 - definition, 1
 - dilute solutions (sparingly soluble species), 4–5
 - electrolytes, mixtures, 8–11
 - electrolytes, pure component strong, 8–11
 - hydrate calculations, 3
 - salt effect, 5
 - solubility products, 5
 - solution thermodynamics, 7–8
 - lysosomes, 278–279
 - molecular structures, 250
 - organics
 - ASOG (analytical solution of groups), 14
 - description, 11
 - group contribution methods, 14
 - ideal solubility, 11–13
 - measurements, 15–16
 - melting temperatures, 27
 - mixed solvent solubility, 14–15
 - permanent dipole moments, 13
 - pure component phase diagrams, schematics, 12
 - regular solution theory, 13–14
 - Scatchard-Hildebrand theory, 14
 - solubility parameters, 14
 - thermodynamic concepts, 11–13
 - UNIFAC (UNIQUAC function group activity), 14
 - pH effects, 250–251, 274–275
 - phase diagrams, 278–279
 - physical and thermodynamic properties, 141–142
 - pressure effects, 277
 - protein crystallization, 280
 - salts effects, 252–253
 - soluble synthetic polymer effects, 277
 - temperature effects, 250, 277–278
 - vs. temperature, 124
 - Soluble synthetic polymer effects, 277
 - Solute impurities, 259–260
 - Solutions and solution properties
 - concentration units
 - basic concepts, 1
 - conversion, 2
 - hydrates, 2
 - phase diagrams, 2
 - type 1 (mass-mole solute/mass solvent), 1
 - type 2 (mass-mole solute/mass solution), 1
 - type 3 (mass-mole solute/volume solution), 1
 - definition, 1
 - description, 1
 - metastability
 - description, 16
 - free energy vs. cluster radius, 18
 - limits, 17–18
 - stability states, 17
 - zone widths, 17–18
 - nomenclature, 29–30
 - reference literature, 30–31
 - solubility, inorganics
 - basic concepts, 1–4
 - concentrated solutions, 5–11
 - definition, 1
 - dilute solutions (sparingly soluble species), 4–5
 - electrolytes, mixtures, 8–11
 - electrolytes, pure component strong, 8–11
 - hydrate calculations, 3
 - salt effect, 5
 - solubility products, 5
 - solution thermodynamics, 7–8
 - solubility, organics
 - ASOG (analytical solution of groups), 14
 - description, 11
 - group contribution methods, 14
 - ideal solubility, 11–13
 - measurements, 15–16
 - melting temperatures, 27
 - mixed solvent solubility, 14–15
 - permanent dipole moments, 13
 - pure component phase diagrams, schematics, 12
 - regular solution theory, 13–14
 - Scatchard-Hildebrand theory, 14
 - solubility parameters, 14
 - thermodynamic concepts, 11–13
 - UNIFAC (UNIQUAC function group activity), 14
 - solution properties
 - conversion factors, 21
 - density, 20
 - diffusivity, 22–25
 - power law model parameters, 22
 - viscometers, 22
 - viscosity, 20–25
 - supersaturation
 - creation methods, 18–20
 - description, 16
 - free energy vs. cluster radius, 18
 - stability states, 17
 - units, 16–17
 - thermal properties
 - description, 25–26
 - fusion enthalpy, 27
 - heat, capacity, 26–27
 - heat, crystallization, 28–30
 - heat, latent, 27–28
 - heat, mixing, 28–30
 - heat, solution, 28–30
 - melting temperatures, 27
 - Solvents and impurities
 - biochemical, 259–260
 - chemical aspects, 86–90
 - crystal shape determination, roles
 - description, 67–68
 - equilibrium, 68
 - interplant spacings, 69
 - PBCs (periodic bond chains), 69–70
 - solid states, 68–70
 - crystalline structure interface
 - AFM (atomic force microscopy), 72
 - description, 71–72
 - kink sites, 71
 - steps, 71
 - terraces, 71
 - description, 67, 96–97, 255–256
 - free energy barriers, 71
 - growth effects
 - description, 93
 - HMT (hexamethylene tetramine), 95–96
 - Jackson α -factor, 94–96
 - solvent roles, 93–94
 - growth rate effects
 - Cabera-Vermilyea model, 81–82
 - impurity adsorption isotherms, 82–86
 - limiting, 83–84
 - movement step effects, 80–82
 - non-zero growth rate behavior, 83–84
 - zero-growth rate behavior, 84–85
 - impurity incorporation factors
 - crystal lattice point defects, 72
 - crystallization rates, 75–76
 - defect sites, 76–77
 - equilibrium separation, 72–74
 - nonequilibrium separation, 74–78
 - impurity retention mechanisms
 - description, 78
 - DSC (differential scanning calorimeter), 78
 - EDAX (energy dispersive X-ray analysis), 80
 - EXAFS (extended X-ray fine structure), 79
 - optical microscopy, 78–79
 - selective crystal dissolution, 78–79
 - SEM (scanning electron microscopy), 79
 - size vs. impurity relationship, 79
 - STM (scanning tunneling microscopy), 80
 - surface analysis, 79
 - TGA (thermogravimetric analysis), 78
 - particle size control, 255–256
 - reference literature, 97–100
 - solute, 259–260
 - solvent occlusion, 258–259
 - surface diffusion, influences, 70–71
 - tailor-made additives, 89–93
- Sparingly soluble species (dilute solutions), 4–5
- Spectrometry, ultrasonic, 154
- Spectroscopy, photon correlation, 154
- Spray crystallization, 132–133
- Stability states, 17
- Stable nuclei, 145
- Static light scattering, 154
- Steam flow recorder controller, 137
- Steps, 71
- STM (scanning tunneling microscopy), 80
- Structure and bonding, 35–38
- Sulzer falling film process, 168–169
- Supersaturation
 - creation methods, 18–20
 - description, 16
 - desupersaturation curve technique, 237
 - free energy vs. cluster radius, 18
 - mixing, 183–184
 - nucleation kinetics, 143–146
 - pharmaceutical and bioprocessing
 - crystallization, 249–252
 - physical and thermodynamic properties, 141–142
 - profiles, 239
 - stability states, 17
 - units, 16–17
- Surface
 - analysis, 79
 - chemistry, 143
 - diffusion, 70–71
 - energy, 141–142

- integration controlled growth, 146–147
- surface-cooled crystallizers, 130–131, 133
- Suspension crystallization
 - advantages, 167
 - limitations, 167
 - processes
 - Brennan-Koppers crystal purifier, 171
 - description, 171–173
 - Kureha Double Screw Purifier, 171–172
 - Maruzen (Chevron) process, 171
 - Newton-Chambers process, 171
 - TNO-Thijssen crystallization process, 171
- Swenson crystallizers
 - atmospheric up-pumping reaction-type DTB (draft tube baffle), 127
 - batch (without booster), 128
 - direct-contact refrigeration, 131
 - DTB (draft tube baffle), 129
 - five-stage DTB (draft tube baffle) potash, 125
 - fluidized suspension, 128
 - single-effect recompression, 125
 - surface-cooled, 130
 - teflon tube, 132
- Symmetry elements, 35
- Synthetic polymer effects, 277
- TAG (triacylglycerols), crystallizing, 288
- Tailor-made additives, 89–93
- Teflon tube crystallizers, 131–133
- Temperature
 - control
 - once-through balanced, 216
 - recirculating, 216
 - unbalanced batch, 215
 - crystallization, 294–296
 - melting, 27
 - profiles, 165
 - recorders, 137
 - sensors, 219–220
 - solubility, 250
 - solubility effects, 277–278
 - vs. solubility, 124
- Terraces, 71
- TGA (thermalgravimetric analysis), 78
- Thermal properties
 - description, 25–26
 - fusion enthalpy, 27
 - heat
 - capacity, 26–27
 - crystallization, 28–30
 - latent, 27–28
 - mixing, 28–30
 - solution, 28–30
 - melting temperatures, 27
- Thermal response technique, 236–237
- Thermalgravimetric analysis. *See* TGA (thermalgravimetric analysis)
- Thermodynamic properties
 - adsorbents, macromolecular, 143
 - adsorbents, polymeric, 143
 - colloid stability, 143
 - concepts, 11–13
 - DLVO (Derjagun, Landau, Verwey, Overbeek) theory, 143
 - Gibbs-Thomson equation, 141–142, 148–149
 - precipitation diagrams, 142–143
 - solubility, 141–142
 - supersaturation, 141–142
 - surface chemistry, 143
 - surface energy, 141–142
- Three mode (PID) controllers, 204–207
- Time-delay compensation, 208
- TNO-Thijssen crystallization process, 171
- Triacylglycerols. *See* TAG (triacylglycerols), crystallizing
- Tsukishima Kikai (TSK) countercurrent cooling process, 176
- Tube bundle crystallization, 168
- Tubular precipitators, 155, 158
- Turbulence, 195
- Turbulent kinetic energy, 182
- Two-dimensional nucleation methods, 146–147
- Two-fluid model, 196
- Ultrasonic spectrometry, 154
- Unbalanced batch temperature control, 215
- UNIFAC (UNIQUAC function group activity), 14
- Units
 - concentration. *See* Concentration units
 - supersaturation, 16–17
- Unseeded cooling crystallization, 245
- van der Waals forces, 143
- Vapor diffusion, 281–282
- Vapor recompression, mechanical, 126
- Vessel flow field, 182
- Viscometers, 22
- Viscosity, 20–25
- Vortex stretching, 150
- X-ray
 - EDAX (energy dispersive X-ray analysis), 80
 - EXAFS (extended X-ray fine structure), 79
- Yields, 116
- Zero-growth rate behavior, 84–85
- Zone widths, 17–18

This Page Intentionally Left Blank